Santanu Banerjee
Subir Sarkar   *Editors*

Mesozoic Stratigraphy of India

A Multi-Proxy Approach

The Society of Earth Scientists
2008

Springer

Society of Earth Scientists Series

Series Editor

Satish C. Tripathi, Lucknow, India

The Society of Earth Scientists Series aims to publish selected conference proceedings, monographs, edited topical books/text books by leading scientists and experts in the field of geophysics, geology, atmospheric and environmental science, meteorology and oceanography as Special Publications of The Society of Earth Scientists. The objective is to highlight recent multidisciplinary scientific research and to strengthen the scientific literature related to Earth Sciences. Quality scientific contributions from all across the Globe are invited for publication under this series. Series Editor: Dr. Satish C. Tripathi

More information about this series at https://link.springer.com/bookseries/8785

Santanu Banerjee · Subir Sarkar
Editors

Mesozoic Stratigraphy of India

A Multi-Proxy Approach

Editors
Santanu Banerjee 🔟
Department of Earth Sciences
Indian Institute of Technology Bombay
Mumbai, India

Subir Sarkar
Department of Geological Sciences
Jadavpur University
Kolkata, India

We dedicate this book to Prof. Pradip K. Bose

Series Editor Foreword

Mesozoic sedimentary sequences of India were deposited in intra-cratonic and peri-cratonic tectonic basins, and sensitively recorded palaeoclimatic changes and ocean–land life. The pile of almost undisturbed Mesozoic sediments is punctuated by marine transgression–regression events and are most suitable for sequence stratigraphic studies. Sedimentation under the influence of tectonism, plate movement and climatic variability ended with a well-known mass extinction event leading to the demise of gigantic dinosaurs. The large parts in Central India are covered by Deccan lava flows obscuring the infratrappean geological set-up. Economic petroleum resources within Mesozoic sequences make them so important.

Owing to excellent palaeontological records, some of the basins like Kutch, Jaisalmer, Spiti and Cauvery were extensively studied. The dinosaur fossil hunting grounds of Mesozoics are a paradise for vertebrate palaeontologists. The evidence of K/Pg mass extinction and outburst of basaltic lava covering a large part of the geology of India are significant global events. The Gondwana Mesozoic sedimentary basins are another thick largely continental sediments affected by tectonism. The geological datasets obtained from Gondwana sediments are of international significance. I hope this book on the Mesozoic stratigraphy of India employing various proxies will bring out new results and open new vistas. I sincerely thank editors and contributors for bringing out this volume.

<div align="right">
Series Editor
Satish C. Tripathi
</div>

Lucknow, India

Preface and Acknowledgements

Mesozoic sedimentary rocks of India record the effects of abnormal sea level rise, greenhouse climate, intensified volcanism, hypoxia in seawater and extensive black shale deposition. Mesozoic time also witnessed the mass extinction events, the evolution of dinosaurs and the breakdown of the supercontinent Pangea, followed by the formation of Gondwana. The Mesozoic record is particularly significant for the industry as more than 75% of oil and gas formed during this time. The Mesozoic record of India has been investigated thoroughly from biostratigraphic and lithostratigraphic viewpoints in the last century. Literature survey, however, reveals significant gaps in knowledge regarding sedimentology, sequence stratigraphy, chemostratigraphy and some major geological events during the Mesozoic. This book envisages a multi-proxy approach using detailed sedimentological analysis, floral and faunal assemblage, geochemical proxies, magnetic susceptibility, stable isotopes and associated biotic events for paleoclimatic and the paleoenvironmental interpretations of the Mesozoic sedimentary record of India. The book focuses on recent findings on lithostratigraphy, chemostratigraphy, biostratigraphy, magnetostratigraphy and sequence stratigraphy of Mesozoic basins of India, including Kutch, Cauvery, Krishna-Godavari, Jaisalmer and Narmada basin and Spiti valley. The edited volume highlights the present understanding regarding stratigraphical and depositional histories of Mesozoic sedimentary basins in the backdrop of global tectono-thermal events and sea-level changes. A thorough biostratigraphic investigation of the sedimentary deposits provides high-resolution interpretations of the Mesozoic basins. A synthesis of sedimentological, palaeontological and chemical data using the multi-proxy approach provides a comprehensive understanding of the Indian Mesozoic record to the students, researchers and professionals. Information presented in this book not only benefits academicians but is also relevant for the oil and gas industry.

This book comprises 23 chapters covering most of the Mesozoic sedimentary basins in the peninsular and extra-peninsular regions of India; more than half of which are from Kutch, Cauvery and Jaisalmer basins. The first two chapters of this book present reviews of stratigraphy, sedimentation history and paleogeography of Mesozoic basins in India. The first chapter "A Review of Stratigraphy, Depositional Setting and Paleoclimate of the Mesozoic Basins of India" (Dasgupta) reviews the current understanding of the Mesozoic basins, and the second "Cretaceous Deposits

of India: A Review" (Chakraborty et al.) provides a thorough review of stratigraphy, paleoclimate and paleogeography of Cretaceous sedimentary basins. The third chapter "Radiation of Flora in the Early Triassic Succeeding the End Permian Crisis: Evidences from the Gondwana Supergroup of Peninsular India" (Ghosh et al.) presents the radiation of flora after the Permian–Triassic mass extinction event (PTME). The stratigraphy of the Kutch is debated over the years for the consideration of lithostratigraphic and chronostratigraphic aspects. In this book, we have retained both classification schemes so that scientific issues are under focuss rather than stratigraphic jargons. The fourth chapter "An Overview of the Mesozoic (Middle Jurassic to Early Cretaceous) Stratigraphy, Sedimentology and Depositional Environments of the Kachchh Mainland, Gujarat, India" (Mahender) presents a classical review on sedimentology and lithostratigraphy of the Kutch Basin. The fifth chapter "Magnetic Polarity Stratigraphy Investigations of Middle-Upper Jurassic Sediments of Jara Dome, Kutch Basin, NW India" (Venkateshwarlu) presents magentostatic data for the Jhuran Formation to constrain its age between Magneto Chrons M24 and M19 of Kimmeridgian to Tithonian. The sixth chapter "Provenance and Paleo-weathering of the Mesozoic Rocks of Kutch Basin: Integrating Results from Heavy Minerals and Geochemical Proxies" (Chaudhuri et al.) integrates geochemical data and heavy mineral assemblage of Mesozoic formations in Kutch to indicate the source of sediments. The study relates possible sources of Mesozoic sediments in the Kutch Basin to Precambrian rocks of the Aravalli craton and Nagar Parkar igneous complex. The seventh chapter "Geochemistry of Callovian Ironstone in Kutch and Its Stratigraphic Implications" (Bansal et al.) presents petrographical and mineralogical investigations of Callovian golden oolites of the Jhumara Formation of Kutch Basin, and indicate a similarity in the chemical signature of Jurassic ironstones across the globe. The eighth chapter "Oxic-dysoxic Tidal Flat Carbonates from Sadara, Pachham Island, Kachchh" (Kale et al.) presents petrographical and geochemical investigations of Bathonian to Callovian carbonates of the Kutch Basin in the Pachham Island to indicate the formation of carbonates in warm seawater during the Jurassic time. The ninth chapter "Cosmopolitan Status for *Taramelliceras kachhense* (Waagen) (Ammonoidea) from Kutch, Western India" (Roy et al.) revisits the taxonomy of the genus *Taramelliceras* from the Kutch Basin and compares with the European types to understand the palaeobiogeography. The tenth chapter "Nautiloid Biostratigraphy of the Jurassic of Kutch, India: An Exploration of Bio- and Chrono-stratigraphic Potential of Nautiloids" (Halder) presents the utility of nautiloid biozonation and proposes a biostratigraphic classification of the Jurassic succession based on nautiloids. Chapter "Taphonomic Pathways for the Formation of Bioturbated Cycles in the Early Cretaceous Wave-Dominated Deltaic Environment: Ghuneri Member, Kachchh Basin, India" (Desai and Chauhan) presents the effect of storms, erosion, sedimentation on ichnofacies and ichnoassemblage. Systematic ichnological analysis indicates 24 recurring trace fossils, categorized into fair-weather and storm-weather trace fossil ichnoassemblages. Chapter "Gastropod Biozonation for the Jurassic Sediments of Kutch and Jaisalmer Basins and Its Application in Inter-basinal Correlation" (Saha et al.) presents 12 biozones for Kutch and three biozones for Jaisalmer based on gastropod assemblage data. The authors demonstrate that like

ammonites, the gastropods can effectively be used to establish acceptable regional biostratigraphy of both Kutch and Jaisalmer Basins. Chapter "Diagenetic Controls on the Early to Late Bathonian Fort Member Sandstone of Jaisalmer Formation, Western Rajasthan" (Ahmad et al.) presents a detailed petrographic analysis of the Bathonian sandstones in the Jaisalmer basin to establish the paragenetic sequence and porosity evolution in relation to diagenetic evolution. Chapter "Seismicity Forcing Transition from Siliciclastic to Carbonate Realm in the Thaiyat-Hamira Succession of Jaisalmer, Rajasthan" (Mandal et al.) documents soft-sediment deformation layer in between Thaiyat and Hamira Members, Jaisalmer, Rajasthan and traced and relates the seismically induced deformation to global paleotectonics recorded at different countries at the Bajocian-Bathonian transition. Chapter "Biostratigraphic Implications of the Calcareous Nannofossils from the Spiti Formation at Langza, Spiti Valley", (Singh et al.) proposes a Callovian age (part of NJ12 Nannofossil Zone) to the black shale ('*Belemnites gerardi* beds') belonging to the belemnites-rich Lower Member of the Spiti Formation based on calcareous nannofossil biostratigraphy. Chapter "Records of Marine Transgressions and Paleo-Depositional Conditions Imprinted Within Cretaceous Glauconites of India" (Bansal et al.) compares the Cretaceous glauconites of India and relate them to global sea level rise, sub-oxic shallow shelves and intensive continental weathering. Chapter "Early Cretaceous Flora from the East Coast Sedimentary Basins of India: Their Chronostratigraphic and Palaeobiogeographic Significance" (Chinnappa et al.) provides precise ages of Cretaceous formations based on biostratigraphically diagnostic palynomorphs and macroflora. The study provides precise ages to the lithounits of the east coast sedimentary basins of India based on the marker taxa. Chapter "Facies and Microfacies Analysis of Kallankurichchi Formation, Ariyalur Group with an Inkling of Sequence Stratigraphy" presents a detailed facies analysis of the fossiliferous carbonate succession of late Cretaceous Kallankurichchi Formation and distinguishes two broad facies associations, wave-dominated and tide-dominated, within the succession. Chapter "Litho-Biostratigraphy and Depositional Environment of Albian-Maastrichtian Sedimentary Succession of Cauvery Basin in Ariyalur Area" (Nagendra and Nallapa Reddy) presents sedimentological analysis, sea level cycles and paleoclimatic context of the Albian-Maastrichtian sedimentary succession of the Cauvery basin. Chapter "Continental-to-Marine Transition in an Ongoing Rift Setting: Barremian-Turonian Sediments of Cauvery Basin, India" (Chakraborty et al.) presents a thorough field-based facies analysis to document fluvial-to-marine transition in a syn-rift setting during the Mesozoic breakup of east Gondwanaland. Chapter "Stratigraphy, Sedimentology and Paleontology of Late Cretaceous Bagh Beds, Narmada Valley, Central India: A Review" (Bhattacharya et al.) presents a detailed sedimentological and paleontological account of the Mesozoic sediments in the Narmada Valley region of central India. Chapter "Fluvial Architecture Modulation in Course of Aeolian Dominance: Upper Terrestrial Member, Bhuj Formation, Kutch" (Koner et al.) presents a thorough analysis of bedforms and paleohydarulic parameters within the early Cretaceous Bhuj Formation. The study documents the evolution of fluvial channel system and overall drying-up trend through time. Finally, Chapter "Mineralogical and Textural Characteristics of Red

Boles of Western Deccan Volcanic Province, India: Genetic and Paleoenvironmental Implications" (Singh et al.) presents a detailed petrographical and mineralogical analysis of the latest Cretaceous red bole beds, interlayered with Deccan Basalt in western India. The study indicates several breaks during the eruption of Deccan Basalt, which lead to the formation of volcanic paleosol at places.

We express our sincere thanks to all the authors of this book for their valuable research contributions. We are thankful to reviewers for providing critical reviews of the submitted manuscripts. Scholars who served as reviewers for this book are Subir Bera, H. N. Bhattacharya, Ajoy Bhowmick, Abhijit Chakraborty, Nivedita Chakraborty, Adrita Chaudhuri, D. K. Chauhan, Sudipta Dasgupta, Anima Mahanta, Soumik Mukhopadhyay, R. Nagendra, Suraj K. Parcha, Deo Brat Pathak, Malek Radhwani, A. Sen, D. S. N. Raju, Debahuti Mukherjee, Tathagata Roy Choudhury, Pradip Samanta and Sanjoy Sanyal. We are thankful to Sanghita Dasgupta for proofreading manuscripts for a major part of the book.

Mumbai, India   Santanu Banerjee
Kolkata, India   Subir Sarkar

Contents

About the Editors

Santanu Banerjee is a Professor at the Department of Earth Sciences, Indian Institute of Technology Bombay. He obtained a Ph.D. degree from Jadavpur University, Kolkata, in 1997. Santanu does research in sedimentology and petroleum geology. His research areas cover sedimentary facies and basin analysis, microbially induced sedimentary structures, sequence stratigraphy, recent sedimentary environments around the Gulf of Cambay for outcrop analogues of subsurface reservoirs, provenance and tectonic settings, glauconite formation in sequence stratigraphic context and Jurassic black shale in Kutch. He is the Associate Editor in Chief of the Journal of Palaeogeography. He is on the editorial board of the Arabian Journal of Geosciences, SN Applied Sciences and Journal of Earth Systems Science. He is the Vice-President of the Indian Association of Sedimentologists. He has supervised many research projects sponsored by Government agencies and oil companies. He has published more than 100 research articles in journals and edited 4 books.

Subir Sarkar is currently the Professor in the Department of Geological Sciences, Jadavpur University, Kolkata India. He obtained his Ph.D. degree from Jadavpur University in 1990. He has more than 25 years of experience in teaching and about 30 years in research. He has worked in different Proterozoic basins in India and his scientific interests are in the areas of sedimentology, sequence stratigraphy and basin analysis. With a special interest in the record of early life, he is currently studying the influence of microbial mats on Precambrian sedimentation. He is on the editorial board of the Journal of Palaeogeography. He has published more than 100 research articles in peer-reviewed national and international journals and conference proceedings. He has also published 16 book chapters and edited 4 books.

Abbreviations

ACM	Active continental margin
APWP	Apparent polar wandering path
BU	Bela Uplift
CCD	Calcite compensation depth
CEPL	Cementation porosity loss
ChRM	Characteristic Remanent Magnetization
CI	Contact index
CIA	Chemical index of alteration
CIR	Central Indian Ridge
CIW	Chemical Index of weathering
CNPS	Cretaceous Normal Polarity Superchron
COPL	Compactional porosity loss
CU	Chorad Uplift
DRM	Detrital remanent magnetization
DSDP	Deep sea drilling project
EDS	Energy dispersive spectroscopy
FA	Facies association
FAD	First appearance datum
FMS	Fort Member Sandstone
GTS	Geological time scale
HCS	Hummocky cross-stratification
HREE	Heavy rare earth element
HST	Highstand systems tract
IBF	Island Belt Fault
ICS	International commission on stratigraphy
ICV	Index of compositional variability
IGV	Intergranular volume
JMA	Jaisalmer-Mari basement arch
KG Basin	Krishna–Godavari Basin
KMF	Kutch Mainland Fault
KMU	Kutch Mainland Uplift
K-Pg boundary	Cretaceous-Paleogene boundary

KU	Khadir Uplift
LAD	Last appearance datum
LREE	Light rare earth element
Ma	Million years
MFS	Maximum flooding surface
MPS	Magnetic polarity stratigraphy
NASC	North American shale composite
NKF	North Kathiawar Fault
NPF	Nagar Parkar Fault
NRM	Natural remanent magnetization
OAE	Oceanic anoxic event
PAAS	Post-Archean Australian shale
PCA	Principal component analysis
PG Basin	Pranhita-Godavari Basin
PIA	Plagioclase index of alteration
PTB	Permian–Triassic boundary
PTME	Permian–Triassic mass extinction (PTME)
PU	Pachchham Uplift
REE	Rare earth element
RSL	Relative sea level
SB	Sequence boundary
SEM	Scanning electron microscopy
SSD	Soft sediment deformation
SWF	South Wagad Fault
SWU	South Wagad Uplift
TE	Trace element
TST	Transgressive systems tract
UCC	Upper continental crust
VGP	Virtual geomagnetic pole
VNIR	Visible-near infrared
XRD	X-ray diffraction
XRF	X-ray fluorescence

A Review of Stratigraphy, Depositional Setting and Paleoclimate of the Mesozoic Basins of India

Sanghita Dasgupta

Abstract The Indian Gondwana basins preserve a thick sedimentary deposit from Carboniferous to Cretaceous. In India, the Gondwana sediments were mainly deposited in four intracratonic basins, i.e. Pranhita-Godavari (PG), Satpura, Son-Mahanadi and Damodar essentially in a fluviatile setting. While the PG Basin preserves the most continuous sedimentary history, Mesozoic basins at the west coast, including Kutch, Barmer, Jaisalmer, Saurashtra, record sedimentation from the Jurassic period. During the Mesozoic era, there was a gradual shift in the climatic condition, which got reflected in the sedimentation pattern and fossil record. The Early Triassic sediments of the peninsular basins were deposited under warm to semi-arid climatic conditions in an essentially fluvial setting. The PG and Rewa basins record the global Triassic redbeds, having similar seasonal conditions, evidence of freshwater carbonates, along with profuse terrestrial fauna and flora. The Early Jurassic sediments of Barmer and Jaisalmer were essentially deposited in fluvio-lacustrine environment under humid climatic condition. With the advent of Middle Jurassic, limestone started depositing in the Mesozoic basins. The Middle to Late Jurassic sediments of the western coastal basins were deposited primarily in shallow marine environment. Gypsum formed under fluvio-lacustrine setting in PG and Rewa basins, while it formed under shallow marine conditions in Kutch and Jaisalmer basins. By the Early Cretaceous, oceans began to separate the major fragments of the Gondwanaland, which led to the extensive deposition of mostly marginal marine to shallow-marine sediments all along the western coastal basins of India. Whereas the Gondwana basins record a few fluvial successions, having profuse vertisol profiles. Deccan traps overlie the Mesozoic sedimentary successions of the Gondwana basins, while the Cenozoic sedimentation continues at western coastal basins. This work attempts the correlation of Mesozoic basins of India and points out areas of future research.

Keywords Depositional environment · Gondwana · Indian Mesozoic basins · Paleoposition · Stratigraphic correlation

S. Dasgupta (✉)
Department of Earth Sciences, Indian Institute of Technology Bombay, Powai, Mumbai 400076, India

1   Introduction

Gondwana supercontinent broke during ~200–60 Ma, rifted, and the fragments drifted away in many directions (McLoughlin 2001; Riley and Knight 2001; Conrad and Gurnis 2003; Jokat et al. 2003). One of the fragments—the Indian Shield, drifted approximately northward and eventually collided onto the Eurasian plate, producing the spectacular trans-continental Himalayan fold-thrust belt (Norton and Sclater 1979; Reeves and de Wit 2000; Reeves et al. 2004). The break-up and northward journey immensely affected the Indian shield in several ways, including erosion at the base of its lithosphere and the development of several structural basins (Acharyya and Lahiri 1991; Veevers and Tewari 1995; Biswas 1999; Kumar et al. 2007; Veevers 2009). Before the break-up, the Gondwana supercontinent developed several sedimentary basins along the paleo-suture zones at the end of Carboniferous. A thick succession of sedimentary rocks piled up in these basins.

Several intra-continental rift structures were formed due to supercontinent break-up and rifting which acted as locations of sedimentation in association with continued tectonic activity (Biswas 1999; Veevers 2009). The term Gondwana derived from the recognition by workers at the Indian Geological Survey in the mid- to late 19th century of a distinctive sedimentary sequence preserved in east-central India (McLoughlin 2001). The Indian Gondwana basins contain a rich record of tectonic, sedimentary, paleontological and volcanic history of the Gondwanaland (Biswas 2003; Mukhopadhyay et al. 2010; Ghosh and Sengupta 2019; Bandyopadhyay and Ray 2020). The Gondwana basins of India represent about 200 Ma of the geological record of peninsular India. The initial depressions of the basins were formed due to the sagging related to the attenuation of the crust. The Lower Gondwana sedimentation started within these pre-rift sag basins over the Proterozoic basement. Subsequently, these basins remained active due to fault-guided subsidence that provided accommodation space for the younger sediments. Different types of basins formed depending on the orientation difference between the weak zones and the stress related to the regional E-W extension (Chakraborty et al. 2003; Mukhopadhyay et al. 2010). During the Mesozoic era, the Indian subcontinent had migrated from below the 30º S latitude to near the equator (Kiessling et al. 2003; Golonka 2011; Hall 2012). Throughout the Mesozoic era, climatic conditions varied as a function of overall global climatic changes and movement of the Indian subcontinent towards the equator. In the Triassic, the exposed land extended from about 85° N to 90° S. This exposed land was called the 'Pangaea', which came into existence during the Carboniferous due to the collision between Gondwana and Laurasia (between ~330 and 320 Ma; Veevers 2004). The continent was largely assembled by the end of Permian.

This paper integrates tectonic, sedimentological and paleontological data from a range of published sources to provide a summary of the current state of knowledge concerning the changes in the depositional environments of the basin-fill successions and evolution with respect to flora and fauna, landscape and vegetation during the Mesozoic time in India. Further, this study attempts a correlation of the Mesozoic

basins. Compilation of selected references of the different Mesozoic basins of India is given in Table 1.

Table 1 A bibliography of the Mesozoic basins of India

Mesozoic Basin	Mesozoic stratigraphy	Selected references
Pranhita-Godavari	Chikiala Gangapur Kota Dharmaram Maleri Bhimaram Yerrapalli Kamthi	Goswami and Ghosh (2020), Dasgupta and Ghosh (2018), Goswami et al. (2018), Dasgupta et al. (2017), Bandyopadhyay (2011), Bandyopadhyay et al. (2010), Bandyopadhyay and Sengupta (2006), Sarkar and Chaudhuri (1992), Kutty and Sengupta (1989), Kutty et al. (1987)
Satpura	Lameta Jabalpur Bagra Denwa Pachmarhi	Sengupta et al. (2016), Ghosh et al. (2012), Dogra et al. (2010), Ghosh and Sarkar (2010), Saha et al. (2010), Prakash (2008), Ghosh et al. (2006), Wilson and Mohabey (2006), Ghosh et al. (2003, 2001), Ghosh (1997), Ghosh et al. (1995)
Rewa	Parsora Tiki Karki Pali	Bhat et al. (2018a, b), Pillai et al. (2018), Mukherjee et al. (2012), Datta (2004); Datta et al. (2004)
Kutch	Bhuj Jhuran Jhumara Jhurio	Chaudhuri et al. (2020a, b, c, d), Chaudhuri et al. (2018), Desai and Biswas (2018), Bansal et al. (2017), Mandal et al. (2016), Arora et al. (2015), Alberti et al. (2012, 2013), Biswas (2005, 1999, 1993, 1991, 1987, 1982, 1981)
Barmer	Fatehgarh Ghaggar-Hakra Lathi	Dasgupta and Mukherjee (2017), Bladon et al. (2015a, b), Dolson et al. (2015), Farrimond et al. (2015), Compton (2009)
Jaisalmer	Parh Goru Pariwar Bhadasar Baisakhi Jaisalmer Lathi	Alberti et al. (2017), Sharma and Pandey (2016), Pandey and Pooniya (2015), Pienkowski et al. (2015), Srivastave and Ranawat (2015), Mude et al. (2012), Pandey et al. (2012), Pandey and Choudhary (2010), Rai and Garg (2007), Singh (2006), Torsvik et al. (2005), Sudan et al. (2000)
Saurashtra	Wadhwan Ranipat Surajdeval Than	Khan et al. (2017), Casshyap and Aslam (1992), Aslam (1992, 1991)

2 Gondwana Basins

In peninsular India, the Gondwana sediments were mainly deposited in four intracratonic basins, i.e. Pranhita-Godavari (PG), Damodar, Satpura, and Son-Mahanadi with a distinct post-Carnian hiatus (except for the PG Basin) (Chakraborty et al. 2003). The analysis of the shape of the outcrop belt, characteristics of the basin-fill and the orientation of the associated faults relates the origin of the Gondwana basins of peninsular India to a single regional tectonic event (Chakraborty et al. 2003). The sites of basin nucleation were guided by the pre-existing zones of weakness in the Precambrian basement (Biswas 2003). Each of the major basin has been discussed below and a location map of these basins is given in Fig. 1.

2.1 Pranhita-Godavari Basin

2.1.1 Tectonics

The Pranhita-Godavari (PG) basin preserves records of repeated opening and closing of Proterozoic and Gondwana rifts (Chaudhuri et al. 2012). PG basin evolved as a NNW-SSE trending syn-rift basin. The Gondwana deposit (~4–5 km thick) is exposed as an elongated outcrop belt that is ~400 km long and ~75 km wide, surrounded by the exposures of the Proterozoic sedimentary rocks and Archean basement rocks (Biswas 2003; Chakraborty et al. 2003; Chaudhuri et al. 2012). Bouguer anomaly contours are more closely spaced near the eastern margin of the PG Gondwana basin, indicating greater accommodation of sediments towards the footwall margin of the basin over time (Narula et al. 2000; Biswas 2003; Chakraborty et al. 2003; Ghosh and Sengupta 2019). The western margin of this basin is demarcated by a number of small intrabasinal normal faults affecting the syn-rift strata. Intrabasinal normal faults are oriented at a high angle to the trend of the boundary faults. Some of these faults demarcate subordinate half-grabens within the master basin. The stratigraphically younger formations of the deposit are bound by the Godavari Valley Fault on the eastern side, which brings the upper Gondwana strata in contact with the Proterozoic rocks (Fig. 1 of Dasgupta and Ghosh 2018; Goswami and Ghosh 2020). During Permo-Carboniferous, the paleolatitudinal position (~300 Ma) of the present location of the PG Basin was below 60º S, while during Early Cretaceous (~140 Ma) the paleoposition was around 40º S (Scotese et al. 1999).

2.1.2 Stratigraphy and Lithology

The ~5 km thick, dominantly fluvial deposits that formed in the PG Gondwana Basin range in age from the Late Carboniferous to Cretaceous (Robinson 1967; Kutty et al. 1987; Kutty and Sengupta 1989; Veevers and Tewari 1995; Bandyopadhyay
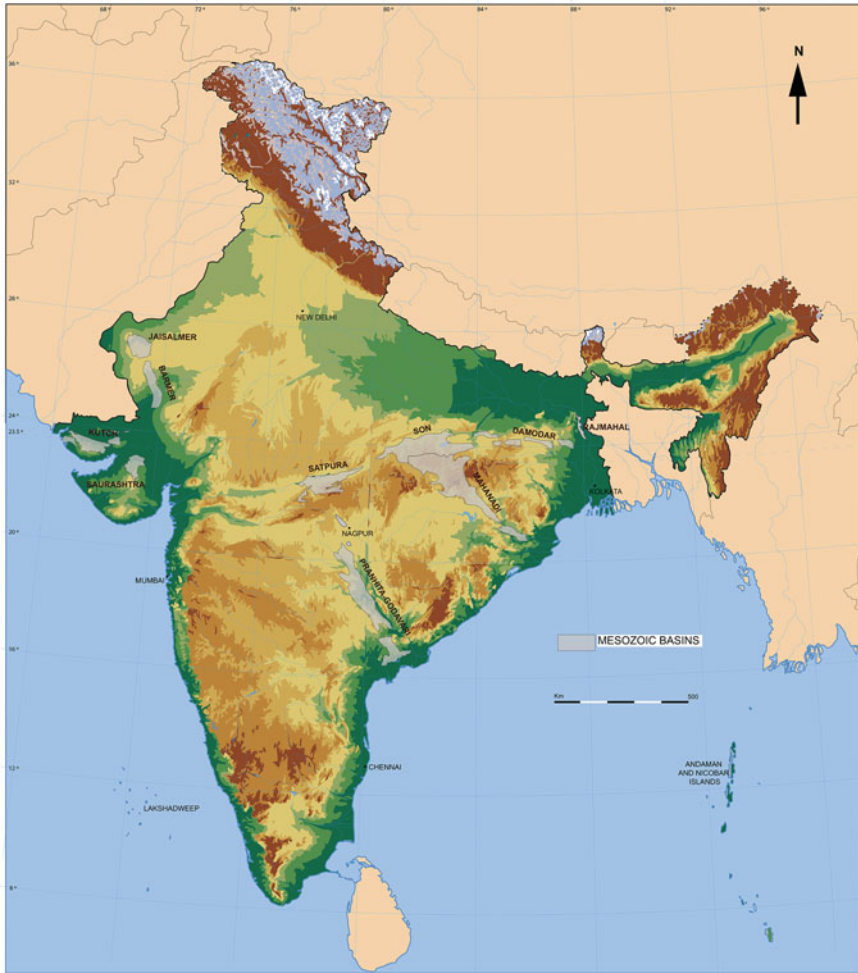
Fig. 1 Mesozoic sedimentary basins superimposed on the physical map of India (positions of sedimentary basins after Dasgupta (1975), Biswas (1991), Casshyap and Aslam (1992), Bandyopadhyay and Sengupta (1999), Farrimond et al. (2015)

2011; Dasgupta et al. 2017; Dasgupta and Ghosh 2018). Based on paleontological and lithological criteria, King (1881) subdivided the Gondwana succession into "Lower Gondwanas" and "Upper Gondwanas". He further subdivided the Lower Gondwanas into three subunits—Talchir, Barakar and Kamthi. The lower part of the succession, Late Carboniferous to Permian, contains glaciogenic conglomerates and coal-bearing strata. The Talchir Formation crops out as a narrow strip, broken at places by faults and never attaining any great thickness, along the western margin of the basin. It consists of tillites, greenish shale and sandstone (Kutty et al. 1987; Srivastava 1992). The Barakar Formation consists essentially of the coal-bearing

group of rocks that overlie the Talchir (Kutty et al. 1987; Kutty and Sengupta 1989). The 'Infra-Kamthi' Formation, as used by Bose and Sengupta (1993) was renamed as 'Kundaram Formation' by Ray (1997), and made up of shale, mudstone and thick sandstone (3–5 m). Recent observations reveal thick fault gouge (3–5 cm) of ferruginous mud at many places. The ferruginous mud shows well-preserved slickenside. The dip angle (~35°) of the fault planes (Fig. 2a) are oriented towards NE. Hence the strike of the faults is NW-SE, which coincides with the major rift faults of the PG Basin. This fault cuts across all the sedimentary strata, most likely late stage rift faults. The Kundaram Formation is overlain by the Kamthi Formation, which is composed of highly ferruginous sandstone or ironstones, numerous iron-rich concretions and purplish siltstone (Kutty et al. 1987). The Lower Gondwana is followed upwards by the Upper Gondwana formations.

The Upper Gondawanas was further subdivided into "Maleri Group", "Kota Group" and "Chikiala Group" by King (1881), and later these groups were further classified into different formations. Kutty et al. (1987) assembled the previous work and subdivided the Maleri Group of King into four conformable formations based on the lithological and faunal distinctions viz. Yerrapalli, Bhimaram, Maleri and Dharmaram, in ascending order of succession. Dasgupta and Ghosh (2018) presented the updated stratigraphic classification of the Upper Gondwanas of the PG Basin, based on a number of studies (Jain et al. 1964, 1983; Kutty 1969, 1971; Sengupta 1970, 2003; Rudra 1982; Bandyopadhyay and Rudra 1985; Kutty et al. 1987, 2007; Kutty and Sengupta 1989; Dasgupta 1993; Ray and Bandyopadhyay 2003; Bandyopadhyay and Sengupta 2006; Bandyopadhyay et al. 2010; Novas et al. 2011; Dasgupta et al. 2017). The Yerrapalli Formation (400–600 m thick) is dominantly composed of reddish brown to violet mudstones having poorly developed gypsum crystals, subordinate calcareous quartzose sandstones and smaller lenticular bodies made up of peloidal carbonate grains. The Bhimaram Formation (~400 m thick) is dominated by coarse, pebbly, clay gall bearing, yellowish brown to whitish feldspathic sandstones intercalated with a minor proportion of red mudstones. The Maleri Formation (~300–500 m thick) is a part of the Triassic redbed succession of the PG Basin. This formation is essentially composed of stratified red mudrocks, fine-grained white sandstones along with subordinate carbonate grainstones and marls (Dasgupta et al. 2017; Dasgupta and Ghosh 2018). The Dharmaram Formation (400–600 m thick) has thick basal sandstone followed upwards by a series of alternations of arkosic sandstone and mudstone beds with subordinate carbonates. The Dharmaram Formation conformably grades up to the Kota Formation, which starts with coarse, pebbly sandstone grading upwards to white fine sandstone, red clays, calcareous shales and limestones (Kutty et al. 1987; Goswami et al. 2018). Towards the northwestern part of the basin, the Gangapur Formation overlies the Kota Formation. The Gangapur Formation is made up of coarse to very coarse ferruginous sandstone with pebble bands in its lower part, succeeded by sandstones and mudstones having concretions (Kutty et al. 1987). Planar and trough cross-bedded medium- to coarse-grained sandstone units show paleocurrent direction towards the north. Towards the eastern part of the basin, the Kota Formation is overlain by the Chikiala Formation consisting of coarse to very coarse ferruginous sandstones, subordinate red clays and calcareous
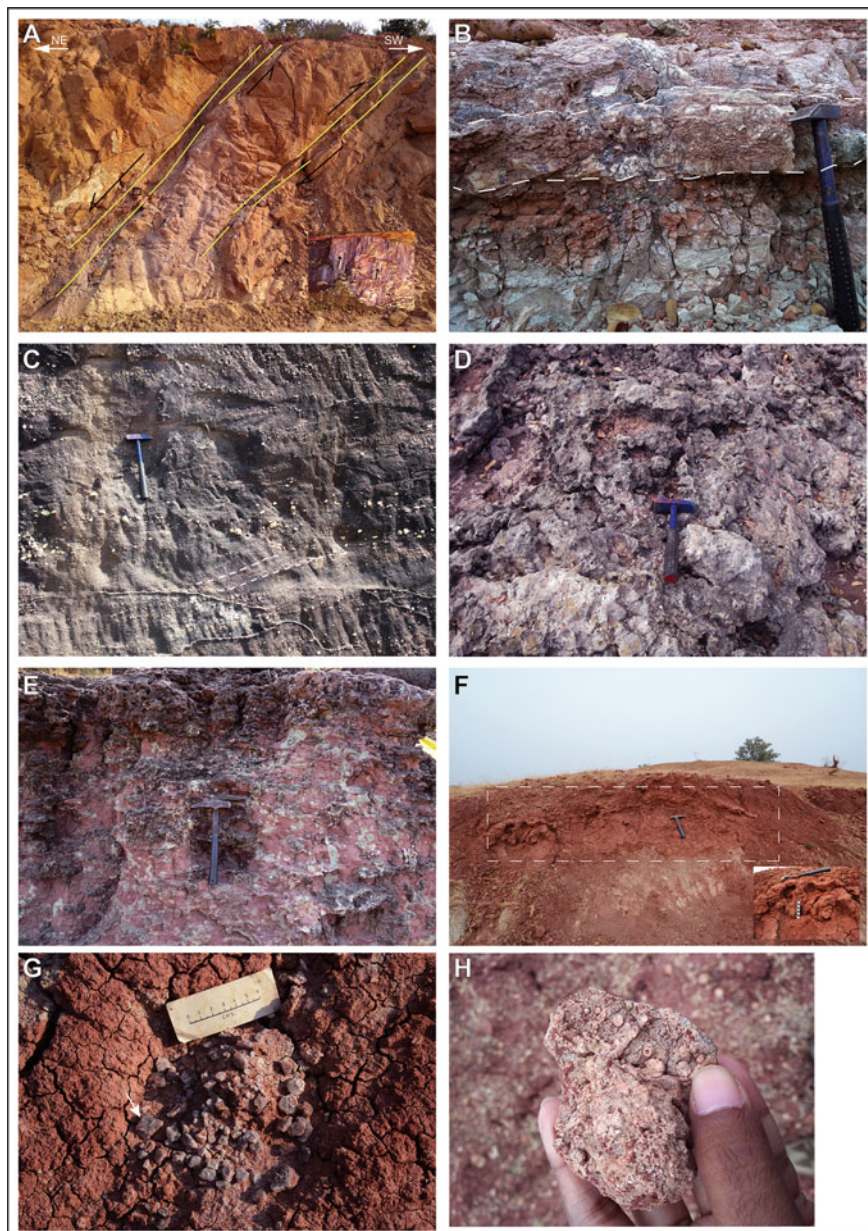
◄**Fig. 2** Field photographs showing different lithologies of the Gondwana basins. **a** Large scale normal faulting observed in the sandstone outcrop (35° towards 040°) of the Kundaram Formation (PG Basin) near Annaram bridge over Godavari river. The sense of movement has been identified from the slickensides (inset) observed in the hanging wall block (box highlighted). The fault has thick (3–5 cm) shale gouge. **b** Lithology of the Chikiala Formation (PG Basin) showing ripple laminated very fine sandstones (40–50 cm thick) and greenish clay (30–40 cm thick), separated by calcareous sandy material (10–20 cm thick, marked by dashed white line). **c** Lithology of the Pachmarhi Formation (Satpura Basin) showing cross-bedded very coarse pebbly sandstone, near Dhupgarh. The paleocurrent direction is away from the observer. **d** Plan view of hardpan of calcic vertisol of the Bagra Formation (Satpura Basin). **e** Calcic paleosol profile having red mudstone as host rock of the Lameta Formation (Satpura Basin) near Ghughura falls. Greenish-grey patches are gley. **f** A carbonate profile with rhizocretions within mudrock (area marked in dashed white box) of the Tiki Formation (Rewa Basin), near Jora village. **g** Occurrence of gypsum crystals (arrow) scattered within red mudrock of the Tiki Formation. **h** Carbonate concretion found in the red mudrock of the Tiki Formation (hammer length = 38 cm)

sandstones (Kutty et al. 1987). New findings from Chikiala Formation reveal very fine sandstones and greenish clay separated by calcareous sandy material having crystal veins (Fig. 2b). Detailed sedimentology of upper Kota, Gangapur and Chikiala formations are yet to be done.

2.1.3 Fossil Content

The fossils within the Lower Gondwana formations are discussed in detail by Ray (1999). The Permian rocks of the PG Gondwana Basin was characterized by the *Glossopteris* flora, found in the Barakar Formation (Pascoe 1959; Robinson 1967). The Kundaram Formation of this basin yields the only Permian reptilian fauna in India, which constrains the upper age of the coal-bearing Damuda Group of the Damodar Gondwana Basin as Tartarian.

The Upper Gondwanas contain a number of vertebrate fossil (amphibians, reptiles etc.) bearing zones that are important for inter basinal correlation of the strata and for assigning age. A large number of fossils have been reported from the Triassic and Jurassic formations of the PG Basin by different workers (Kutty and Sengupta 1989; Bandyopadhyay et al. 2010). These fossils mainly occur in the red mudstones, and in very rare instances in the sandstones. Based on the faunal assemblages and dispositions of the litho-units, Yerrapalli, Bhimaram, Maleri and Dharmaram formations were assigned (Anisian) early Middle Triassic, late Middle Triassic (Ladinian), (Late Carnian–Early Norian) late Late Triassic, and late Late Triassic to early Early Jurassic ages, respectively (after Jain et al. 1964; Chatterjee 1967; Kutty 1969; Sengupta 1970; Anderson and Cruickshank 1978; Kutty and Sengupta 1989; Sarkar and Chaudhuri 1992; Ray and Bandyopadhyay 2003; Bandyopadhyay et al. 2010; Bandyopadhyay 2011). Yerrapalli Formation consists of numerous fossils of fishes, amphibians, reptiles and also trace fossils (Dasgupta 1993). Apparently, no faunal assemblages have been found in the Bhimaram Formation, apart from plant fossils and few fragments of vertebrate fossils. The Maleri Formation has an exceptionally

rich vertebrate assemblage consisting of aquatic, semi-aquatic as well as terrestrial fossils. Numerous fossil vertebrates and invertebrates, and coprolites have been reported from the Maleri Formation (Jain 1983; Kutty et al. 1987, 2007; Kutty and Sengupta 1989; Bandyopadhyay and Sengupta 1999; Martin et al. 1999; Datta et al. 2004; Datta 2005; Datta and Ray 2006; Bandyopadhyay and Sengupta 2006; Nath and Yadagiri 2007; Bandyopadhyay 2011). Invertebrates are represented by unionids, while plant fossils are represented by *Dadoxylon* (Sohn and Chatterjee 1979). The Maleri vertebrate fauna is characterized by different species of fish, amphibian and reptile. The upper part of the Dharmaram Formation and the overlying lower part of the Kota Formation has been assigned an Early Jurassic age (Kutty et al. 1987; Mukhopadhyay et al. 2010; Bandyopadhyay 2011). An exceptionally rich fossil assemblage, consisting of non-marine aquatic, semi-aquatic as well as terrestrial vertebrates (fishes, reptiles, amphibians, etc.) along with invertebrates (unionids), plants and trace fossils has been reported from Dharmaram Formation (Pascoe 1959; Kutty 1971; Chatterjee and Roy Choudhury 1974; Sarkar and Chaudhuri 1992; Bandyopadhyay 2011). Very large (<15 feet) petrified wood, mainly tree trunks have been found in the Dharmaram Formation. Based on this faunal assemblage, a Hettangian age has been assigned for the upper part of the Dharmaram Formation (Bandyopadhyay and Sengupta 2006). The lower part of the Kota Formation yields fossils of sauropod dinosaurs, flying reptiles, turtles and other reptiles as well as fish, early mammals, ostracods, estherids, charophytes etc. (Kutty 1969; Yadagiri and Rao 1987; Jain 1973, 1974, 1983; Evans et al. 2002; Bandyopadhyay and Sengupta 2006; Bandyopadhyay et al. 2010; Goswami et al. 2018). Based on the faunal analysis, Sinemurian to Pliensbachian age has been assigned to the lower part of the Kota Formation. Systematic paleobotanical investigation suggests an Early to Middle Jurassic age for the Kota Formation (Chinnappa and Rajanikanth 2016a). The Gangapur Formation, overlying the Kota Formation, has been assigned Early Cretaceous age from its fossil assemblage, having abundant well-preserved leaves, macroflora and spore-pollens (Ramakrishna et al. 1985; Chinnappa and Rajanikanth 2016b). However, due to the lack of fossil content, the age of the overlying Chikiala Formation remains debatable.

2.2 Satpura Basin

2.2.1 Tectonics

The Satpura rift Basin, the westernmost Gondwana basin of peninsular India, is rhomb-shaped and elongated in ENE-WSW direction (~200 km long and ~60 km wide). The regional strike of this basin is NE-SW and the regional dip (~5°) is northerly (Chakraborty et al. 2003). Sub-vertical, ENE-WSW trending en-echelon faults, Son-Narmada South and Tapti North, with evidence of strike-slip movement, mark the longer sides of the Satpura Basin (Biswas 1999, 2003). This basin represents a pull-apart origin that developed above a releasing jog of a pre-existing transcurrent

zone as a result of sinistral displacement (Chakraborty and Ghosh 2005). The Satpura Gondwana Basin is bounded by the Mesoproterozoic Vindhyan sediments to the north, Precambrian granitic gneiss to the south and late Cretaceous Deccan Traps towards the east and the west. A thin belt of Paleoproterozoic rocks of Bijawar and Mahakoshal groups are squeezed in between the Son-Narmada North Fault (SNNF) and Son-Narmada South Fault (SNSF). The Satpura Gondwana sediments were deposited in a mega half-graben (Veevers and Tewari 1995; Biswas 1999), which later got uplifted over the Pachmarhi plateau of Central Indian Tectonic Zone (CITZ), also referred to as the Satpura Mountain Belt in central India (Mohanty 2010; Singh et al. 2015). Sediment accumulation took place under different fault-controlled subsidence regimes, with intervening tectonically static periods. The subsidence rate varied across the basin, with the thickness increasing towards the north, resulting in an asymmetric basin fill (Chakraborty and Ghosh 2005). Many tholeiitic dyke intrusions of late Cretaceous Deccan flood basalt are exposed in and around the Satpura Basin, the majority of which are aligned along the ENE-WSW trend and represent the oldest intrusive phase. Some of the dykes are seen passing into sills (Bhattacharji et al. 1996; Sheth et al. 2009). The updated geological map is given in Ghosh et al. (2012).

2.2.2 Stratigraphy and Lithology

The Satpura Gondwana intracratonic basin preserves ~5 km thick Permain to Cretaceous siliciclastic sediments (Crookshank 1936) that unconformably overlies the Precambrian basement of schist, gneiss, granites, meta-sediments, mafic and acid volcanic rocks (Ghosh and Sarkar 2010). The Satpura Basin comprises a thick sequence of Lower and Upper Gondwana sediments. The gross thickness of the lower Gondwana rocks (lower Carboniferous to upper Permian) is reported to be around 3000 m and the upper Gondwana rocks (lower Triassic to upper Cretaceous) around 2000 m thick (Peters and Singh 2001; Ghosh et al. 2012). Geological studies including sedimentology, stratigraphy, and paleontology of the Satpura Basin has been carried out by various researchers (Casshyap et al. 1993; Veevers and Tewari 1995; Mukherjee and Sengupta 1998; Bandyopadhyay and Sengupta 1999; Nandi and Raha 1998; Maulik et al. 2000; Ghosh et al. 2004, 2012 Chakraborty and Ghosh 2005, 2008; Chakraborty and Sarkar 2005; Ghosh et al. 2006; Ghosh and Sarkar 2010; Bandyopadhyay 2011; Sengupta et al. 2016). The Satpura Gondwana succession has been classified into nine lithostratigraphic units that from oldest to youngest are the Talchir, Barakar, Motur, Bijori, Pachmarhi, Denwa, Bagra, Jabalpur and Lameta formations. Bijori and Pachmarhi formations share an unconformity, so does Denwa and Bagra formations.

Distinctive lithologies characterize each of the five formations comprising the Mesozoic succession of the Satpura Basin. The preliminary study of the Pachmarhi Formation (~900 m thick) shows multistoried bodies of very coarse pebbly sandstone (Fig. 2c) with minor red (with few calcic vertisols) to grey mudstone units. The detailed sedimentological work reveals that the Denwa Formation (~600 m thick)

consists of red mudstone, heterolithic strata, fine to coarse sandstone, caliche profiles and intraformational calcirudite/calcarenite. The Bagra Formation (~400 m thick) is composed of gravelly conglomerate, pebbly sandstone, red mudstone with calcareous nodules with abundant calcic vertisols (Fig. 2d) (Ghosh and Sarkar 2010; Ghosh et al. 2012; Sengupta et al. 2016). The Bagra Formation is unconformably overlain by Jabalpur and Lameta formations (Ghosh et al. 2001; Prakash 2008). The Jabalpur Formation (~20 m thick as exposed) consists of coarse sandstone, white mudstone and thin stringers of coal (Dogra et al. 2010). The Lameta (~20–50 m thick as exposed) Formation consists of fine-grained calcareous sandstone, green sandstone, coaly shale, red mudstones, limestones, mottled nodular marl and calcic paleosol profiles (Fig. 2e) (Ghosh et al. 1995, 2001; Dogra et al. 2010; Bansal et al. 2018).

2.2.3 Fossil Content

Since no radiometric age dating has yet been carried out, fossil content was used to constrain the age of the Satpura Gondwana succession. Based on the available marine invertebrates, the Lower Gondwana succession has been designated an age from Late Carboniferous to Late Permian. The Upper Gondwana succession ranges in age from Early Triassic to Cretaceous (Ghosh et al. 2001, 2012; Ghosh and Sarkar 2010; Sengupta et al. 2016). The Upper Gondwana starts with the Pachmarhi Formation (Early Triassic) and consists of few fragmentary weathered amphibian skull bones along with the absence of *Glossopteris-Gangamopteris* flora (Bandyopadhyay and Sengupta 1999; Chakraborty and Sarkar 2005; Ghosh et al. 2012). The Denwa Formation (Middle Triassic-Anisian, Bandyopadhyay and Sengupta 1999) exhibits fossils of fishes, and vertebrate faunas of various types of amphibians, reptiles and herbivorous animals along with invertebrates-*Unionids* (Bandyopadhyay et al. 2002; Bandyopadhyay 2011; Sengupta et al. 2016). The age of the Bagra Formation is controversial. Previous workers considered this as Jurassic (Ghosh et al. 2001; Ray and Chakraborty 2002; Chakraborty and Sarkar 2005; Ghosh and Sarkar 2010; Mukhopadhyay et al. 2010; Ghosh et al. 2012). Based on the vertebrate fossil content, the Bagra Formation has been presently assigned as Cretaceous (Bandyopadhyay and Sengupta 2006; Bandyopadhyay 2011; Sengupta et al. 2016). From palynological studies, Jabalpur Formation and Lameta Formation are assigned to Early and Late Cretaceous (Maastrichtian), respectively (Dogra et al. 2010). The Jabalpur Formation includes plant fossils (Ghosh et al. 2001). The Lameta Formation exhibits semi-aquatic, aquatic communities and wood fossils represented by dinosaurs, fishes, crocodiles, gastropods, ostracods, charophytes, conifers, angiosperms (Mohabey et al. 1993; Khosla and Sahni 2000; Ghosh et al. 2003; Kar et al. 2004; Wilson and Mohabey 2006) and trace fossils (Saha et al. 2010) along with palynological evidence (Dogra et al. 2010).

2.3 Rewa Basin—A Sub-basin of the Son-Mahanadi Basin

2.3.1 Tectonics

The Son-Mahanadi Basin is a composite basin comprised of three sub-basins, namely the Rewa Basin to the north, the Hasdo-Arand Basin to the central position and the Mahanadi Basin to the south (Agarwal et al. 1993). All these three sub-basins are separated by three ridges starting from North Malwa ridge, followed southward by Manendragarh-Pratapur ridge, and then Naughata ridge (Chakraborty et al. 2003). The southwestern margin is concealed by the thick cover of Deccan Traps. The Rewa Basin is rhomb-shaped and is relatively long in the ENE-WSW direction (400 × 150 km, Chakraborty et al. 2003). Bouguer anomaly also conforms to the shape of the basin. The Rewa Basin was formed due to strike-slip motion, and the basin profile indicates fault-controlled subsidence. The overall attitude of the basin-fill strata is subhorizontal (~4–5º) with a northward dip (Chakraborty et al. 2003; Mukherjee et al. 2012). The updated geological map is given in Mukherjee and Ray (2012).

2.3.2 Stratigraphy and Lithology

The geological study of the Rewa Gondwana Basin was initiated by Hughes (1881) and subsequently followed by a number of workers such as Cotter (1917), Fox (1931, 1934), Rao and Shukla (1954), Dutta and Ghosh (1972, 1993), Raja Rao (1983), Mitra (1993), Tarafdar et al. (1993), Dutta (2002) and Shah (2004). The Gondwana sediments of the Rewa Basin is subdivided into lower and upper divisions based on the presence of *Glossopteris* and *Ptilophyllum* flora, respectively (Pascoe 1975). The sediments of the Rewa Basin comprise a basal Talchir Formation, followed by the coal-bearing Barakar Formation, and then the Mesozoic formations (Shah 2004). The Mesozoic formations start with the Pali Formation (~1000 m), which is overlain by the Parsora Formation (~400 m) in the southwestern part. Whereas it laterally grades into the sand-dominant Karki Formation (~300 m) in the north-eastern part (Mukherjee et al. 2012). These units are overlain by the mud-dominated Tiki Formation (~400 m). This, in turn, is overlain unconformably by the Hartala Formation (Shah 2004), which is characterized by typical Upper Gondwana flora of Jurassic affinity (Sahni and Rao 1956). But, according to Mukherjee et al. (2012), no lithological distinction was found between Parsora and Hartala formations. Hence the Parsora Formation constitutes the youngest member of the Rewa Gondwana succession. The Pali Formation is composed of pebbly to coarse-grained micaceous sandstone, medium- to fine-grained sandstone, moderate red, greyish green and greyish yellow coloured mudstone having incipient development of paleosol profile (Dasgupta 2009). The Karki Formation is characterized by multistoried, multilateral sheet-like beds composed of pebbly to very coarse quartzo-feldspathic sandstone. The Tiki Formation comprises subhorizontal to horizontal beds of red mudrock with paleosol profiles. Mudrocks exhibit gypsum

crystals as well as a variety of carbonates, coarse to fine-grained well-sorted quartzo-feldspathic sandstone, and sand-clay heterolithic units (Fig. 2f–3b). The Parsora Formation comprises a basal siltstone-mudstone succession followed upward by an essentially clay-rich arenaceous succession.

Sedimentological details of Pali, Karki, Tiki and Parsora formations are provided in Dasgupta (2009) and Mukherjee et al. (2012). Petrography of the sandstones, grain-size and modal analysis for these four formations reveal the dominance of quartz and k-feldspar as detrital constituents derived from the continental-block setting (Dasgupta 2009). Detailed sedimentological and paleoclimatic studies, considering process sedimentology of siliciclastics and carbonates, geochemistry of siliciclastics and stable isotope study of carbonates for all the formations are yet to be carried out for this basin.
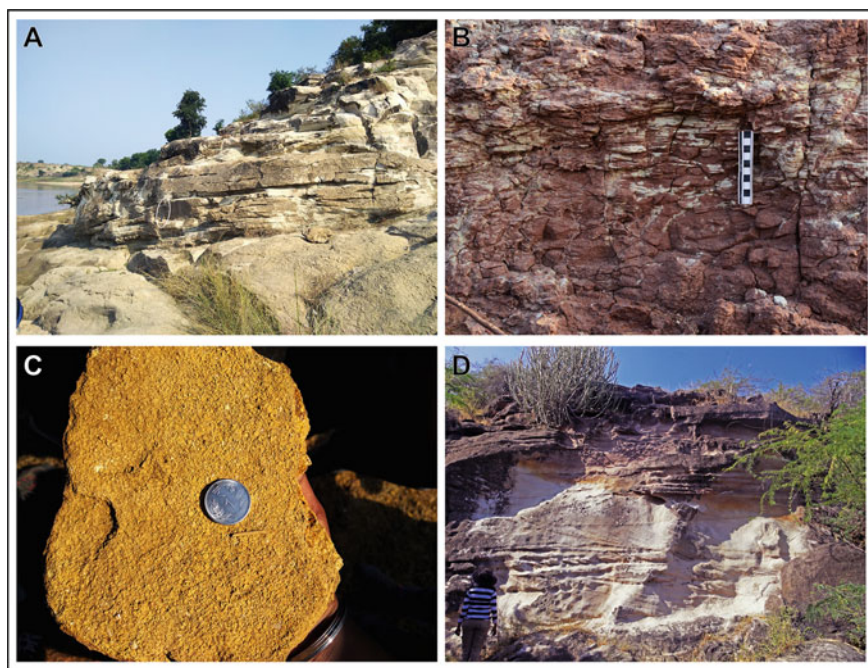
Fig. 3 Field photographs showing different lithologies of the Mesozoic basins. **a** Coarse to fine-grained, well-sorted, quartzo-feldspathic cross bedded white sandstone beds of the Tiki Formation (Rewa Basin) near Ghiyar village. **b** Fine to very fine-grained sand-clay heterolithic units of the Tiki Formation. **c** Calcareous shale having numerous trace fossils of the Jhurio Formation (Kutch Basin) near Keera dome. **d** Sandstone showing various sedimentary structures representing deltaic environment of the Bhuj Formation (Kutch Basin) near Tapkeshwari temple (hammer length = 38 cm)

2.3.3 Fossil Content

In the Upper Rewa Basin, the Pali and the Karki formations show no fossils other than large petrified woods (Mukherjee et al. 2012). However, Pillai et al. (2018) documented the evidence of *Glossopteris* flora in the Pali Formation of South Rewa Gondwana Basin. The Pali Formation is subdivided into three parts, which are again correlated with Barren measures, Raniganj and Panchet formations of the Damodar Basin (Pillai et al. 2018). The megafloral assemblage of the Pali Formation is comparable with those of non-coaliferous beds of Kamthi and Bijori formations of PG and Satpura Gondwana Basins, respectively. Lower-Middle Triassic period has been assumed for Pali and Karki formations (Mukherjee et al. 2012). The Tiki Formation consists of numerous fossils of aquatic, semi-aquatic, amphibians, reptiles of various sizes, land carnivores, mammal-like reptiles, early mammals, unionids, molluscs, petrified wood and burrow marks. The rich repository of varied vertebrate fossils of the Tiki Formation has been described by Mukherjee et al. (2012), Mukherjee and Ray (2012), Ray et al. (2016). Based on its floral and faunal content, the Tiki Formation was assigned as Upper Triassic (Carnian) (Datta 2004; Datta et al. 2004). Lungfishes and freshwater sharks have been reported from the Tiki Formation (Bhat et al. 2018a, b; Bhat and Ray 2020). Large petrified wood along with burrows are characteristics of the Parsora Formation (Lower-Middle Jurassic in age, Mukhopadhyay et al. 2010; Bandyopadhyay and Ray 2020), which overlies the Tiki Formation unconformably.

3 West Coast Mesozoic Basins

The western marginal basins developed during the later stages of the Gondwana cycle as the Indian plate separated from the rest of the Gondwanaland.

3.1 Kutch Basin

3.1.1 Tectonics

The Kutch Basin at the western continental margin of India formed by rifting initiated during the Late Triassic break-up of the Gondwanaland (Biswas 1981, 1982, 1987, 1993, 2005). The Mesozoic system of the region shows sediments ranging in age from Bathonian to Santonian. A period of non-deposition, followed by diastrophism, erosion and volcanism during the close of the Upper Cretaceous time, separates the Mesozoic and Cenozoic rocks of the Kutch Basin. The Mesozoic rocks, ranging in age from Late Triassic to Lower Cretaceous, occur noticeably in the various major uplifts, and are exposed extensively in the Kutch Mainland, Wagad, and the islands of Pachchham, Bela, Khadir, and the Chorar hills.

3.1.2 Stratigraphy and Lithology

The Mesozoic Kutch Basin preserves nearly 2500 m thick siliciclastic and carbonate sediments. The Middle Jurassic to Lower Cretaceous rocks is exposed in the highlands, while the Upper Cretaceous rocks have been noticed only in the offshore wells on Kutch continental shelf. Lithostratigraphically, the Kutch Mainland Mesozoic sediments are classified into four formations, viz., the Jhurio, Jhumara, Jhuran and Bhuj in ascending order (Biswas 1977, 1987; Chaudhuri et al. 2018, 2020a, b, c, d) on the basis of major lithologic breaks, unconformities and change over from one environment to another. The Cheriyabet Conglomerate in Khadir Island represents the base of Mesozoic succession, which passes upward to Bathonian sedimentary rocks (Biswas and Deshpande 1968) of the Jhurio Formation (~290 m thick), consisting mainly of golden oolitic limestones, shales (Fig. 3c) with minor sandstones. The overlying Jhumara Formation (~280 m thick) comprises mainly of oolitic limestones along with olive-grey laminated shales (Chaudhuri et al. 2018). Alternations between shale and wavy laminated sandstone dominate the Jhuran Formation (~350–790 m thick) (Arora et al. 2015, 2017; Chaudhuri et al. 2018). Dominantly siliciclastic Bhuj Formation (~800 m thick) is the youngest of the Mesozoic sediments consisting of glauconitic sandstones, kaolinitic claystones and shales (Fig. 3d) (Mandal et al. 2016; Bansal et al. 2017).

3.1.3 Fossil Content

The sediments of the Mesozoic formations of the Kutch Basin consist of numerous trace fossils (Desai and Biswas 2018). The Mesozoic rocks of the Jurassic age consist mainly of marine fossils and the Late Jurassic to Cretaceous rocks are devoid of marine fauna but contain numerous plant fossils. The Jhurio Formation consists of marine fossils that include brachiopods, cephalopods, pelecypods and corals (Biswas 1977). The Jhumara Formation is the richest of all in fossil content, consisting of varieties of ammonites, *Belemnites*, brachiopods, pelecypods, corals and gastropods throughout the formation. The Jhuran Formation is highly fossiliferous in the western part of the Kutch Mainland, which gradually decreases towards the east. Ammonites, *Belemnites*, pelecypods, gastropods are most common along with local corals and echinoids (Arora et al. 2015). The Bhuj Formation has few ammonites and pelecypod-rich fossiliferous bands, but is rich in plant beds. It typically exhibits Upper Gondwana flora with leaf impressions, large chunks of wood fossils and large fossilised logs (Biswas 1977; Banerji 1989; Bansal et al. 2017). The benthic faunas were examined for paleoclimatic reconstruction (Alberti et al. 2012).

3.2 Barmer Basin

3.2.1 Tectonics

The Barmer and Jaisalmer sedimentary basins are located in western Rajasthan (Roy and Pandey 1970). The Barmer Basin (∼200 km long along NNW-SSE trending, ∼50 km wide, ~6 km deep) is a failed narrow-intracratonic rift basin, separated from the Jaisalmer Basin to the north by the NE trending Devikot-Fatehgarh/Barmer-Devikot-Nachana ridge/structural high (Dolson et al. 2015; Dasgupta and Mukherjee 2017). The Barmer Basin shows exposures of Jurassic to mid-Eocene, and is linked with the Cambay Basin to the south via the poorly defined Sanchor sub-Basin (Bladon et al. 2015b). The Mesozoic Barmer rift Basin was reactivated during the early Tertiary by Deccan volcanism (Compton 2009; Mishra 2011). Displacement of the pre-Deccan/precursor-of-Deccan basaltic sill and the overlying Early Cretaceous lower Ghaggar-Hakra sandstone by the NW-trending faults indicates that the main Barmer rift extension occurred probably during the late Maastrichtian to Paleocene period (Bladon et al. 2015a; Dasgupta and Mukherjee 2017). The updated geological map of this basin has been provided in recent studies (Sharma 2007; Dolson et al. 2015; Dasgupta and Mukherjee 2017).

3.2.2 Stratigraphy and Lithology

The Barmer Basin consists of a thick accumulation of sediments from Jurassic to Eocene time. The Mesozoic succession of this basin unconformably overlies the Precambrian basement rocks of Malani Igneous Suite (Bladon et al. 2015a; Dasgupta and Mukherjee 2017). It comprises sandstone dominated Lathi Formation in the north Barmer Basin (Fatehgarh Ridge), which is unconformably overlain by the dominant sandstone succession, separated by thick packages of mudstone and siltstone of Ghaggar-Hakra Formation (Sisodia and Singh 2000; Dolson et al. 2015; Bladon et al. 2015a; Dasgupta and Mukherjee 2017). The lower unit of the Ghaggar-Hakra Formation, exposed along the unconformity, consists of basal conglomerates overlain by reddish sandstones. The Fatehgarh Formation is composed of sand, mud and phosphorite. The phosphorite is correlated with global Cretaceous upwelling (Sisodia et al. 2005) and paleosols. Sedimentological details are yet to be carried out for these Mesozoic formations of the Barmer Basin apart from the description given in Dolson et al. (2015).

3.2.3 Fossil Content

The Lathi Formation has been designated as of Early Jurassic age (Dolson et al. 2015). Based on the Aptian age proposed for the basalt underlying the Ghaggar-Hakra Formation, the deposition of this formation was suggested between Aptian

and Albian (Sharma 2007; Bladon et al. 2015a). The highly fossiliferous Fatehgarh Formation was deposited between Late Cretaceous and Paleocene time (Sisodia et al. 2005; Bladon et al. 2015a; Dolson et al. 2015). Thus, the Mesozoic sediments of the Barmer Basin represent a time span between Early Jurassic and Late Cretaceous ages, with apparently no fossil evidence reported.

3.3　Jaisalmer Basin

3.3.1　Tectonics

The Jaisalmer Basin is a pericratonic basin representing mainly the westerly dipping eastern flank of the Indus Shelf and extends over 30,000 km^2 in southwest Rajasthan with a NW-SE structural trend (Singh 2006; Sharma 2007; Alberti et al. 2017; Dasgupta and Mukherjee 2017). The shelf deepens towards the northwest across the international boundary and merges into the Sui Basin of Pakistan in the west (Pandey and Pooniya 2015). The general dip of the outcrops is gentle to flat (3°–5°) with an assemblage of en-echelon and oblique faults (Singh 2006). Tectonically, The Pokharan-Nachana high to the northeast separates the Jaisalmer Basin from the Nagaur-Bikaner basins and the Fatehgarh Fault to the south separates the same from the Barmer-Sanchor Basin (Pandey and Pooniya 2015). The basin is controlled by wrench-fault tectonics and is divided into four tectonic elements: the Mari-Jaisalmer high, Shahgarh, Miajalar and the monoclinal Kishangarh sub-basins (Sharma 2007; Pandey et al. 2010; Pandey and Pooniya 2015). The Jaisalmer Basin preserves well developed sedimentary history of Mesozoic and Cenozoic times with well-marked transgressive and regressive cycles (Singh 2006). The Mesozoic formations of the Jaisalmer Basin show a general younging and deepening trend towards the west (Torsvik et al. 2005). The Jaisalmer Basin represented the southern Tethyan margin and was situated about 23° south of the equator (Pandey et al. 2012). The basin evolved at the beginning of the Triassic with the rifting of Gondwanaland (Biswas 1982, 1991). The modified version of the geostructural units of the Jaisalmer Basin has been provided in Pandey et al. (2012).

3.3.2　Stratigraphy and Lithology

The Jaisalmer Basin preserves over 6 km thick sediments from Early Paleozoic to recent times. Lithostratigraphically, the Mesozoic sediments (~4 km thick) of the Jaisalmer Basin consist of seven formations, viz. the Lathi (Early Jurassic), Jaisalmer (Middle Jurassic), Baisakhi-Bhadasar (Late Jurassic), Pariwar (Early Cretaceous), Goru (Middle Cretaceous) and Parh (Late Cretaceous) in ascending order (Singh 2006; Pandey et al. 2010; Srivastave and Ranawat 2015; Dolson et al. 2015; Pandey and Pooniya 2015; Sharma and Pandey 2016; Alberti et al. 2017). Triassic sediment is absent in this basin. The Jurassic formations have been further classified

into different Members, which has been documented in Sudan et al. (2000), Singh (2006), Rai and Garg (2007), Pandey and Pooniya (2015) and Alberti et al. (2017). The Lathi Formation (~600 m thick) overlies the basement rocks, and is characterized by conglomerate, sandstones, siltstones and some limestones. The Jaisalmer Formation (~100–1000 m thick) is characterized by fossiliferous limestones. The Baisakhi Formation is characterized by grey and black gypsum-bearing shales, argillaceous sandstone and intraformational conglomerate. The Bhadasar Formation (~65 m thick) is characterized by ferruginous sandstone with intercalations of thin shale beds. The Pariwar Formation (~670 m thick) is characterized by sandstones and shale. The Habur Formation towards the south-eastern side of the basin, laterally separated from the Lower Goru Formation by an unconformity, is only few meters thick, and it overlies the Pariwar Formation (Singh 2006). The Goru Formation (~575 m thick) is characterized by grey shale, glauconitic sandstone and few marl beds. The Parh Formation (~350 m thick) is characterized by limestone, shale and marl. Sedimentological details of all the formations have been discussed by Sudan et al. (2000), Torsvik et al. (2005), Singh (2006), Pandey and Pooniya (2015) and Alberti et al. (2017). The Mesozoic sediments are unconformably overlain by the Cenozoic sediments.

3.3.3 Fossil Content

According to the classification based on ammonoid assemblages, Krishna (1987) assigned the ages of the then different formations of the Jaisalmer Basin. Mude et al. (2012) documented seventeen ichnofossils having paleoenvironmental significance from the Mesozoic marine sediments of the Jaisalmer Basin. A biostratigraphic correlation of the Jurassic successions of the Jaisalmer and Kutch basin has been given in Pandey et al. (2012).

The Lathi Formation exhibits abundant plant remains (Singh 2006) and calcareous nannofossils (Rai et al. 2016). Two dinosaur footprints have been reported from the Lathi Formation (Pienkowski et al. 2015). A well-diversified and moderately preserved Early Callovian nannofossil assemblage, comprising of twenty-one species has been documented (Rai and Garg 2007) and several time-diagnostic ammonites have been reported from the Jaisalmer Formation (Sharma and Pandey 2016). The Baishakhi Formation consists of ammonites and belemnites fossils along with trace fossils (Pandey and Pooniya 2015). The fossils recorded from the Bhadasar Formation are ammonites, belemnites, brachiopods, gastropods, bivalves, corals, wood fossils and trace fossils (Pandey and Pooniya 2015). Leaf impressions of Upper Gondwana, trace fossils, and large fossilised tree trunks occur in the Pariwar Formation, without any marine body fossil (Krishna 1987; Sudan et al. 2000). The Habur Formation is rich in ammonites and it is recorded as coquinoidal limestone beds (Singh 2006). The Goru Formation is characterized by both planktic and benthic foraminiferal assemblages, whereas the Parh Formation by only planktics (Singh 2006).

3.4 Saurashtra Basin

3.4.1 Tectonics

The Saurashtra Basin is NE-SW elongated and is bounded by major faults in the northern and southern boundaries (Biswas 1982; Varadarajan and Ganju 1989). It represents an Early Cretaceous pericratonic composite failed rift system (Sengor et al. 1978; Casshyap and Aslam 1992). This basin lies transversely to the west of the Aravalli orogen (Early Proterozoic) and proximal to the Cambay Basin. The western part of the Saurashtra Basin is not bounded by any major fault and the southern WSW-ENE trending fault is an extension of Narmada geofracture. The Saurashtra Basin gradually deepens towards west and is surrounded on three sides by the Gulf of Kutch, Arabian Sea and Gulf of Cambay, whereas the Gujarat alluvial plains extend to its north-eastern limit. The Precambrian basement of the basin forms an ENE-WSW trending arch which plunges towards WSW direction.

3.4.2 Stratigraphy and Lithology

The Mesozoic rocks of Saurashtra Peninsula overlie the Early Proterozoic basements and underlie the younger Deccan basalt (Casshyap and Aslam 1992). The Mesozoic sequence of the exposed area has been classified into four formations in ascending order, namely the Than (~125 m), Surajdeval (~175 m), Ranipat (~200 m) and Wadhwan (>50 m) (Casshyap and Aslam 1992). The Than Formation consists of an interbedded assemblage of sandstone, claystone, carbonaceous shale and coal (Aslam 1992). The Surajdeval Formation consists of sand dominated facies, heterolithc facies and sand matrix-supported conglomerate/pebbly (Khan et al. 2017). The Ranipat Formation consists dominantly of subarkosic sandstones, interbedded with thin shales and conglomerates (Aslam 1991; Khan et al. 2017). The uppermost Wadhwan Formation consists of pebbly, coarse to medium sandstones and mudstones with subordinate limestone (Cassyap and Aslam 1992). The paleocurrent studies suggest that the Aravalli-Delhi highlands lying 200–300 km N to NE supplied sediments for these rocks (Casshyap and Aslam 1992).

3.4.3 Fossil Content

The spores and pollen assemblage recovered from the samples from the Than Formation indicate the presence of Pteriophytes, Lycopods, Gymnosperms, Cycades, Angiosperms along with fragments of cuticles and wood, and shows that this flora is of Lower Cretaceous age (Aslam 1992). Numerous trace fossils have been identified from the Ranipat Formation associated with sandstone, siltstone and clay (Aslam 1991). The Wadhwan Formation consists lenses of fossiliferous limestone having

abundant invertebrate body fossils (Casshyap and Aslam 1992). Thus, the sediments
of the Saurashtra Basin were deposited from Late Jurassic to Early Cretaceous.

4   The Paleogeography and Paleoposition of India

India, along with the continents of southern hemisphere, was part of the supercontinent Gondwanaland (Suess 1885), that existed as a single landmass since Cambrian
till its eventual break-up in phases during Jurassic-Early Cretaceous. India, Madagascar, east Antarctica, western and northern Australia formed East Gondwana, while
South America and Africa were part of West Gondwana. These two were sutured
along the Neo-Proterozoic mobile belt of Arabia–Nubia–Ethiopia–Kenya–Mozambique (Unrug 1996). The large area of exposed land, its symmetry about the equator,
the difference in the temperature between the land and water masses, the cross-equatorial pressure gradient, and the relative positions of the exposed land and Tethys
created the paleogeographic conditions favourable to the formations of the Pangaean
mega-monsoon (Robinson 1973). No pre-Gondwana sedimentary record is preserved
in the entire interior part of Gondwanaland since unification (Mukhopadhay et al.
2010). In the Indian part, a phase of extension started in the Late Carboniferous/Early
Permian and lasted till the Early Jurassic, when four (major) discrete Gondwana
basins formed within the peninsula (Chakraborty et al. 2003).

   According to the paleogeographic reconstructions during the start of Mesozoic
era, the Indian subcontinent was in a very different orientation from the modern
position. In the Early Triassic (237 Ma) epoch, the paleoposition of India was below
30º S latitude (Mcloughlin 2001; Scotese 2002; Kiessling et al. 2003; Golonka 2011).
The N-S of modern India was then oriented towards NE-SW. During the Late Triassic
period (Carnian to Rhaetian), the western end of the Indian subcontinent was at about
20º–25º S latitude and the eastern end was at about 45º–50º S (Kiessling et al. 2003;
Golonka 2007, 2011; Metcalfe 2013). During Early Jurassic, the western end was
near 15º S latitude and the eastern end was near 35º–40º S latitude. From Middle to
Late Jurassic, the paleoposition of the Indian subcontinent was around approximately
30º S latitude but shifted its orientation (Scotese et al. 1999; Scotese 2002; Kiessling
et al. 2003; Golonka 2007, 2011; Hall 2012). By the Early Cretaceous, oceans began
to separate the major fragments of Gondwanaland, with Indian subcontinent starting
to detach from Antarctica (joined along the eastern coast of modern India), Africa
(joined along the western coast of modern India), and Australia (joined along the
eastern land side of modern India) and drift northward (Scotese et al. 1999; Scotese
2002; Kiessling et al. 2003; Golonka 2011; Hall 2012). The E-W of modern India
was oriented towards approximately N-S direction during 145–135 Ma (Reeves and
de Wit 2000; Golonka 2011) but gradually rotated in anticlockwise direction with
time. By Late Cretaceous, the Indian plate had drifted northward with its northern
and southern ends (according to modern India) near the equator and 30º S latitudes,
respectively (Kiessling et al. 2003; Hall 2012).

Gondwana began to break-up as the Indian Ocean opened up all along India's western margin during early Jurassic (with Madagascar as the connecting link between India and Africa) that led to the extensive deposits of sediments along the western coast. This included present-day offshore Bombay High area, Kathiawar and Kachchh and continued way up in Jaisalmer in India and Indus Basin, Axial Belt and Baluchistan areas in Pakistan (Mukhopadhyay et al. 2010). A marine transgression swept over the Horn of Africa during the initial break-up in the Early Jurassic, covering Triassic planation surfaces with sandstone, limestone, shale, marls and evaporites (Coltorti et al. 2007; Abbate et al. 2015). A schematic diagram showing the paleoposition of India along with the different Gondwana basins has been shown in Fig. 4.

5   Depositional Environments

This section presents depositional environments of different formations corresponding to their basins. A correlation of the different Mesozoic formations discussed is presented in Fig. 5. The Gondwana basins of India i.e. Pranhita-Godavari, Satpura, Rewa and Damodar, essentially show deposition of fluvial sediments (Robinson 1967; Kutty et al. 1987; Kutty and Sengupta 1989; Veevers and Tewari 1995; Tewari 1995; Maulik et al. 2000; Ghosh et al. 2006, 2012; Mukherjee et al. 2012; Dasgupta et al. 2017; Dasgupta and Ghosh 2018; Goswami et al. 2018; Bandyopadhyay and Ray 2020). The PG Basin records the thickest succession of Mesozoic time. The transition from the Kamthi Formation to Maleri Formation records changes in the depositional environment from sinuous channels, fluvial channel-floodplain scenario, to discontinuous ephemeral fluvial processes, accompanied by freshwater carbonate precipitating environment/spring carbonates (King 1881; Kutty et al. 1987; Dasgupta 1993, 2018; Dasgupta et al. 2017; Dasgupta and Ghosh 2018). The considerably thick Dharmaram Formation was deposited by fluvial channels while the carbonates were of freshwater in origin. The Kota Formation was characterized by very shallow water bodies where limestone-shale beds were deposited in a freshwater environment (Goswami et al. 2018; Goswami and Ghosh 2020). Thus, the climatic conditions also kept on changing from semi-arid to humid from Triassic to Jurassic period. The large-scale cross-bedded sandstone beds of the Gangapur Formation were deposited by high- velocity fluvial channels. The poorly exposed sediments of the Chikiala Formation need further investigation for paleoenvironmental interpretation.

The Early to Middle Triassic deposits of the Satpura and Rewa basin are correlatable to the Kamthi, Yerrapalli and Bhimaram formations of the PG Basin. During this time, the Satpura Basin recorded braided and anabranching river systems with climate, changing from warm, sub-humid to semi-arid conditions, as evident from the Pachmarhi and Denwa formations (Maulik et al. 2000; Ghosh et al. 2006, 2012). Preliminary studies on the Pali and Karki formations (Rewa Basin) reveal the deposition by braided river systems with fluctuation in depositional energy conditions (Mukherjee et al. 2012). The Damodar Basin has a thick siliciclastic succession
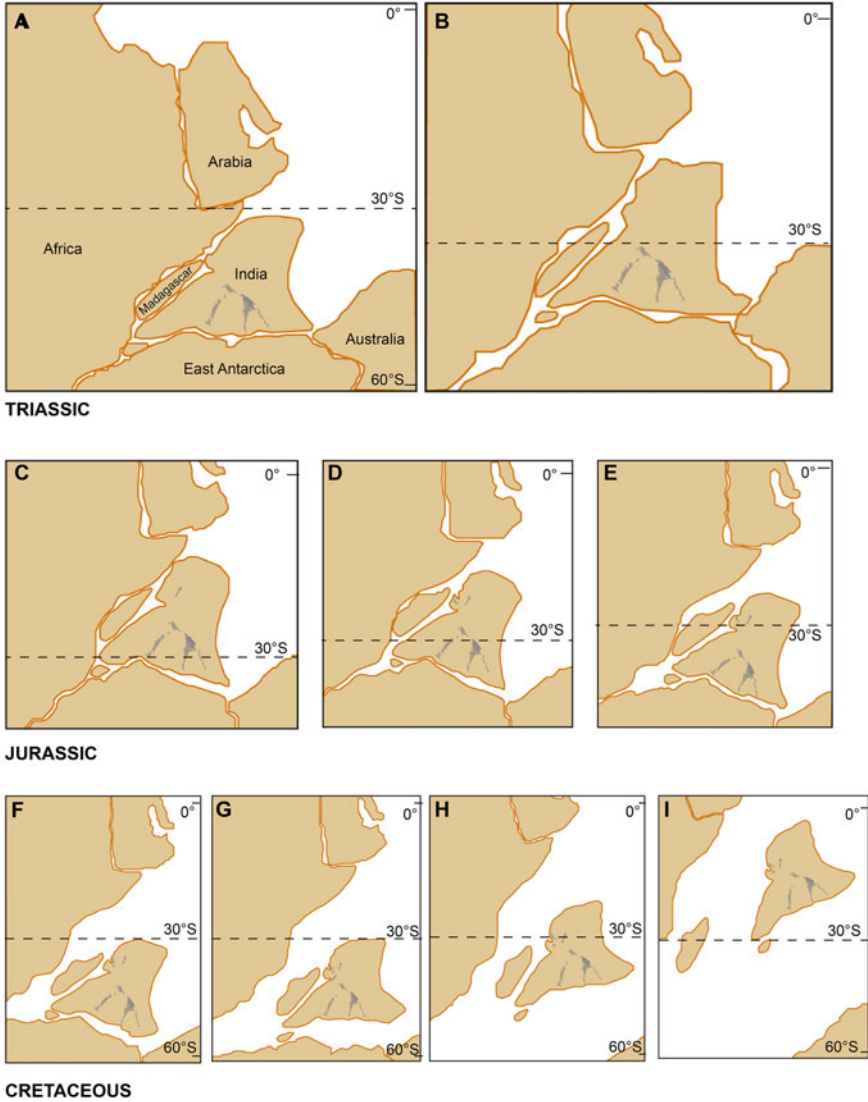
Fig. 4 Paleogeographic reconstruction of the position of Indian subcontinent along with the fragments of the Gondwanaland: **a** Early Triassic (~251–220 Ma) **b** Late Triassic (~225–202 Ma) **c** Early Jurassic (~198–178 Ma) **d** Middle Jurassic (~178–163 Ma) **e** Late Jurassic (~163–145 Ma) **f**, **g** Early Cretaceous (~135–95 Ma) **h**, **i** Late Cretaceous (~94–66 Ma) showing the different Gondwana basins of India in grey shade (Paleopositions of India adapted from Scotese et al. 1999; Mcloughlin 2001; Scotese 2002; Kiessling et al. 2003, Golonka 2007; Golonka 2011; Hall 2012; Gibbons et al. 2013)
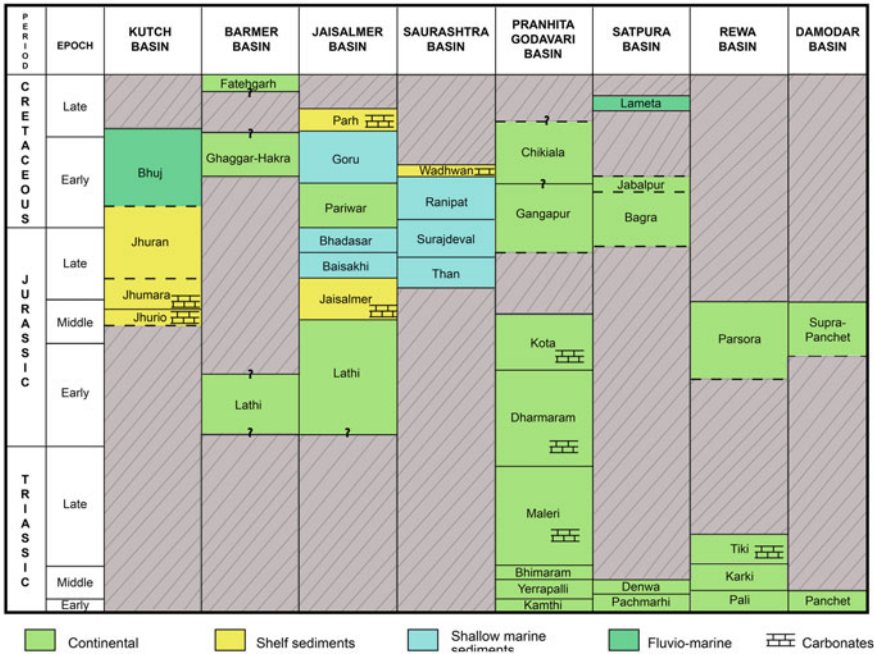
Fig. 5 Chronostratigraphic summary chart showing correlation among the Mesozoic formations of the different Mesozoic basins of India (Kutty et al. 1987; Casshyap and Aslam 1992; Ghosh et al. 2001, 2012; Prakash 2008; Mukhopadhyay et al. 2010; Mukherjee et al. 2012; Dolson et al. 2015; Alberti et al. 2017; Ghosh and Sengupta 2019; Chaudhuri et al. 2020a, b) (colour coded for type of depositional system)

(~3 km thick) of fluvio-glacial, fluvial and lacustrine sediments, though vertebrate fossils are known from only one horizon, the Early Triassic Panchet Formation (Gupta 2009). The Panchet fauna has been correlated with those of the Kamthi Formation (PG Basin). The Late Triassic Tiki Formation (Rewa Basin) is correlatable with the Maleri Formation (PG Basin) and represents the Triassic red-beds having seasonal climatic conditions. Western India is almost devoid of Triassic deposits, unlike their peninsular Gondwana sedimentary deposits, apart from Rhaetian early rift stage deposit in the Kutch Basin (Biswas 2005).

The Early Jurassic fluvial sediments of the Lathi Formation (pre-rift Barmer and Jaisalmer basins) in western India is comparable to the fluvial and freshwater derived sediments of the Dharmaram Formation (syn-rift PG Basin) of relatively humid climatic condition. The Middle Jurassic freshwater derived carbonates of the Kota Formation (PG Basin) are comparable to the upper Lathi Formation (Jaisalmer Basin). Bandyopadhyay and Ray (2020) have considered the Supra-Panchets (Damodar Basin) to be age equivalent to the high flow regime fluvial deposit of the Parsora Formation (Rewa Basin), hence of Middle Jurassic age. The pebbly sandstone rich Supra-Panchets has been interpreted as a bed-load deposit of braided

streams (Veevers and Tewari 1995). Similar shallow marine deposits, in the inner to middle shelf, have been considered for the Jhurio (Middle Jurassic) and Jhumara (Middle to Early Late Jurassic) formations of the Kutch Basin (Singh 1989; Fürsich et al. 1992, 2001; Krishna et al. 2000). The overlying Late Jurassic to Early Cretaceous Jhuran sediments deposited in outer to inner shelf environments (Arora et al. 2015, 2017). Thus, marine conditions dominated the Kutch Basin until Early Cretaceous. The deposition of Jaisalmer (marginal marine shelf condition), Baisakhi and Bhadasar formations (shallow-marine deltaic set up) took place in the Jaisalmer Basin from Middle to Late Jurassic age after marine transgression (Sharma and Pandey 2016; Alberti et al. 2017). The Mesozoic Saurashtra Basin recorded the deposition of the Than Formation (Early Late Jurassic) in a deltaic environment (Aslam 1992). A marginal shallow marine depositional condition has been considered for the overlying Surajdeval (Late Jurassic) Formation (Khan et al. 2017).

The Cretaceous rock record started with the Gangapur Formation (PG Basin), comparable with the sediments of the Bagra Formation (Satpura Basin). Bagra sediments were deposited by high gradient piedmont rivers with braided morphology, subordinate mass flow deposits (Casshyap et al. 1993) in hot, semi-arid to arid climate (Ghosh et al. 2012). The overlying sediments of the Jabalpur Formation were emplaced in warm, moist, humid climatic conditions (Prakash 2008). The sediments of Early Cretaceous Ghaggar-Hakra Formation were (Barmer Basin) deposited under a pre-rift continental setting, essentially in a fluvio-lacustrine environment (Sisodia et al. 2005; Dolson et al. 2015). Earlier researchers thought that sediments of the Late Cretaceous Lameta Formation (Satpura Basin) were deposited under a fluvio-lacustrine setting. However, recent studies suggest marginal marine depositional condition (Saha et al. 2010; Dogra et al. 2010; Bansal et al. 2018). The deposition of the Fatehgarh (Barmer Basin) sedimentary succession started from Late Cretaceous, under a syn-rift fluvio-lacustrine continental setting (Bladon et al. 2015a; Dolson et al. 2015). The absence of any marine fossils and the presence of terrestrial plant fossils suggest that the Pariwar sediments (Jaisalmer Basin) were deposited mainly under the continental setting. The Early Cretaceous Bhuj Formation (Kutch Basin) represents a fluvio-marine sequence (Mandal et al. 2016; Bansal et al. 2017; Desai and Biswas 2018). Simultaneously, marine transgression occurred throughout the Jaisalmer Basin, during which Lower Goru (Late Early Cretaceous) sediments were deposited in a marginal shallow marine condition followed by marginal marine shelf sediments of Late Cretaceous Parh Formation (Dolson et al. 2015). The sediments of Early Cretaceous Ranipat Formation (Saurashtra Basin) represent the deposition in a marginal shallow marine condition, whereas the relatively thin sedimentary succession of the overlying Wadhwan Formation suggest deposition in estuaries and shoals (Casshyap and Aslam 1992; Khan et al. 2017).

6 Discussion and Conclusions

From the depositional environments (discussed in Sect. 5) of the PG Basin, it is evident that the climatic condition gradually changed from semi-arid to humid in the continental setting during the Mesozoic era and the sediments had been derived from the Proterozoic rocks (siliciclastics and carbonates) flanking on either side of the Gondwana deposits (Dasgupta et al. 2017). In the Triassic period, the Indian subcontinent went through different phases of rifting. The Triassic formations of the Satpura Basin were deposited in a warm, sub-humid to semi-arid climate. The presence of nearly equal proportions of dravite and schorl (tourmaline varieties) in the Triassic sandstones (Pachmarhi and Denwa formations) indicate mixing from different source rocks that include granite and metasediments of the basement (Ghosh et al. 2012). The Triassic formations of the Rewa and Damodar basins were deposited under a semi-arid climate with seasonal rainfall conditions. Triassic red beds of peninsular India comprising of the Maleri, Yerrapalli, Denwa and Tiki formations from different basins can be globally comparable with formations of other Gondwana continents, namely Brazil, Argentina, South Africa, Zambia, Tanzania, Namibia, Madagascar, Western North America and Germanic basin (Kutty et al. 1987; Ray 2015).

The Jurassic Gondwana deposits of peninsular India of the PG Basin were emplaced in a fluvial setting, relatively humid climatic condition in a freshwater environment, while sediments of the Satpura Basin were deposited in hot, semi-arid to arid climate, after a long hiatus since the middle Triassic deposits. The sediments of the Rewa and Damodar basins were deposited after a long hiatus and emplaced by a higher flow regime fluvial condition. The Early Jurassic sediments of the Barmer and Jaisalmer basins were essentially deposited under fluvial and lacustrine environment. This was followed by a hiatus in the Barmer Basin, while marine transgression in the Jaisalmer Basin gave rise to sedimentary deposits of shelf to shallow-marine environmental conditions (see Sect. 5). The Jurassic sediments of the Kutch and Saurashtra basins were essentially deposited under marginal shallow-marine environment. Thus, marine conditions dominated in these basins. The climatic condition during sedimentation in the Kutch Basin, fluctuated from semi-arid hot seasonal droughts in the Middle Jurassic to subtropical humid with less prominent seasonal droughts in the Late Jurassic period (Fürsich et al. 2005; Alberti et al. 2012). Detailed petrography and geochemistry of the Jurassic Kutch Basin reveal the predominance of felsic source rocks, sediment recycling, as well as increasing tectonic stability of the basin through time (Chaudhuri et al. 2020a, b, c, d).

The Cretaceous sedimentary deposits of the PG Basin were essentially fluvial. The sediments of the Satpura Basin were emplaced in warm, moist, humid climatic conditions. There is no evidence of Cretaceous deposits in Rewa and Damodar basins. The Early and Late Cretaceous sediments of the Barmer Basin were essentially fluvio-lacustrine in nature. The Cretaceous sediments of Kutch Basin were deposited under fluvio-marine environmental conditions. The Early Cretaceous sediments of the Jaisalmer Basin were deposited under a continental setting, which was followed

by a marine transgression and the later sediments were deposited in a marginal shallow marine to marginal marine conditions. The Early Cretaceous sediments of the Saurashtra Basin were deposited under marginal marine conditions. Thus, the depositional environments and paleoclimatic conditions varied throughout the Mesozoic era.

The Gondwana succession starts with the preservation of marine fossils followed by coal deposits having plant remains. The Late Permian to Early Triassic aged rocks shows herbivorous non-mammalian therapsids (land vertebrate). The Triassic succession shows a change in the nature of fossils preserved mainly within red mudrocks. Numerous fossils of fishes, amphibians, herbivorous non-mammalian therapsids, reptiles as well as trace fossils occur at the bottom, while large plant fossils appeared gradually. Aquatic, semi-aquatic, as well as moderate sized terrestrial vertebrate fossils, reptiles, invertebrates, coprolites, ostracodes and plant fossils were found in abundance in Late Triassic. Very large (<15 feet) petrified wood, mainly tree trunks got preserved during the late Late Triassic to Early Jurassic. As the lithology changed to Jurassic limestones, sediments got enriched with rich fossils of large sauropod dinosaurs, flying reptiles, fishes, amphibians, ostracods, estherids along with remains of mammalian fauna. The Jurassic and Early Cretaceous formations of western India show preservation of marine fossils that include brachiopods, cephalopods, pelecypods, corals, ammonites *Belemnites*, pelecypods, gastropods, echinoids along with trace fossils. Drastically, there was no fossils found in Cretaceous sediments of Gondwana basins except types of plant fossils. Thus, there has been an evolution with respect to flora and fauna, landscape and vegetation along with the change in lithologies. The nature of growth rings of the Mesozoic woods was considered to understand the paleoclimate, suggesting a lesser seasonality during Triassic period, seasonal and turbulent in Jurassic period, warm environments with pronounced seasonality in Early Cretaceous period (Chinnappa and Rajanikant 2018).

Besides the above-mentioned major basins, partial records of the Mesozoic succession are known from a few places. The Cambay Basin preserves Cretaceous sediments deposited by alternating shallow-marine, brackish and deltaic environments (Mukherjee 1983; Tewari et al. 1995; Jaiswal et al. 2018). The Mesozoic succession of the Spiti Basin is characterized by carbonates, sandstones and shale containing poorly preserved *Belemnites*, brachiopods, pelecypods and ammonite fauna, deposited in marine environment (Steck et al. 1998; Singh and Jain 2007; Bhargava 2008). The Cretaceous sediments of the Cauvery Basin are composed of shale, conglomerate, clay, sandstone, and limestone which deposited in a shallow water environment (epicontinental sea) (Narasimha Chari et al. 1995; Ramkumar et al. 2004; Watkinson et al. 2007; Banerjee et al. 2016; Keller et al. 2016; Nagendra et al. 2018; Dasgupta 2019; Bansal et al. 2019b). There are reports of ammonites from Gondwana plant beds at Terani claystones (Ramkumar et al. 2004). The Mesozoic sediments of the Rajmahal Basin are characterized by carbonaceous shale, sandstone, quartzitic grit deposited under fluvio-deltaic environment with ample evidence of flora (Mukhopadhyay et al. 1986; Sakai 1989; Tripathi et al. 1990; Tiwari and Tripathi 1992; Prasad and Pundir 2017). In the east coast of India, lies the Palar and

Pennar basins. The Pennar Basin preserves thick Jurassic and Cretaceous sediments comprising carbonaceous shale, sandstone, claystone and siltstone (Saxena et al. 2012). The Cretaceous sediments of the Palar Basin are characterized by shale, clay, sandstone, ironstone, limestone and conglomerates, along with profuse Early Cretaceous plant fossils (Rajanikanth et al. 2010; Prakash et al. 2018). The Late Cretaceous Bagh Beds in the Narmada Basin are characterized by sandstones, nodular and coralline limestones deposited under initial fluvial to a transgressive tide-wave influenced estuarine and more open shallow marine settings (Bhattacharya and Jha 2014; Jha et al. 2017; Bansal et al. 2019a; Ruidas et al. 2020).

However, the interbasinal correlation is difficult at places because of the incompleteness of data in some basins. The significance of this work in the context of the current status of the different Mesozoic basins of India leads to the following conclusions.

(a) Western continental marginal basins of India are almost devoid of Triassic deposits.
(b) Long hiatus marks the boundary between Triassic and Jurassic deposits of the Satpura, Rewa and Damodar basins.
(c) Although mostly fluvio-lacustrine sedimentation has been recorded in the Gondwana basins, the climatic conditions changed from semi-arid to humid from Triassic to Cretaceous period with several fluctuations.
(d) Global Triassic redbeds within a few Gondwana deposits are significant for seasonal climatic conditions.
(e) Detailed studies on petrography, geochemistry and heavy minerals has only been carried out for Kutch Basin and partially for the Satpura Basin, which are yet to be carried out for other Mesozoic basins.
(f) The environmental interpretations of the Lameta Formation (Narmada Basin) are controversial, although continental and marginal marine conditions are inferred.
(g) Freshwater carbonates occur in the Gondwana deposits of peninsular India, which needs further study for deciphering their origin and mechanism of deposition.

References

Abbate E, Bruni P, Sagri M (2015) Geology of ethiopia: A review and geomorphological perspectives. In: Billi P (ed) Landscapes and landforms of ethiopia, pp 33–64

Acharyya SK, Lahiri TC (1991) Cretaceous palaeogeography of the Indian subcontinent; a review. Cret Res 12:3–26

Agarwal RP, Dotiwala SF, Bhoj R (1993) Structural framework of Son– Mahanadi Gondwana basin based on the study of remote sensing data. Gond Geol Mag Spec Vol Birbal Sahni Centre, National Symposium Gondwana, India, pp 207–217

Alberti M, Fürsich FT, Pandey DK (2012) The Oxfordian stable isotope record (δ18O, δ13C) of belemnites, brachiopods, and oysters from the (western India) and its potential for palaeoecologic, palaeoclimatic, and palaeogeographic reconstructions. Palaeo Palaeo Palaeo 344–345:49–68

Alberti M, Fürsich FT, Pandey DK (2013) Deciphering condensed sequences: a case study from the Oxfordian (Upper Jurassic) Dhosa Oolite member of the Kachchh Basin, Western India. Sedimentol 60:574–598

Alberti M, Pandey DK, Sharma JK, Swami NK, Uchman A (2017) Slumping in the Upper Jurassic Baisakhi Formation of the Jaisalmer Basin, western India: sign of synsedimentary tectonics? J Palaeogeogr 6:321–332

Anderson JM, Cruickshank ARI (1978) The biostratigraphy of the permian and the triassic part 5 a review of the classification and distribution of Permo-Triassic Tetrapods. Palaeontol Afr 21:15–44

Arora A, Banerjee S, Dutta S (2015) Black shale in late Jurassic Jhuran Formation of Kutch: possible indicator of oceanic anoxic event? J Geol Soc India 85:265–278

Arora A, Dutta S, Gogoi B, Banerjee S (2017) The effects of igneous dike intrusion on organic of black shale and its implications: Late Jurassic Jhuran Formation, India. Int J Coal Geol 178:84–99

Aslam M (1992) Delta plain coal deposits from the than formation of the early Cretaceous Saurashtra basin, Gujarat, Western India. Sediment Geol 81:181–193

Aslam M (1991) Trace fossils from the Ranipat sediments (Early Cretaceous), Saurashtra Basin, Gujarat, Western India. Curr Sci 61:403–405

Bandyopadhyay S, Ray S (2020) Gondwana Vertebrate Faunas of India: their diversity and intercontinental relationships. Episodes 43:438–460

Bandyopadhyay S (2011) Non-marine Triassic Vertebrates of India. In: Calvo JO, Porfiri J, Gonzalez B, Santos DD (eds) Paleontogía y dinosaurios desde América Latina. EDIUNC, Editorial de la Univ Nacional de Cuyo, Mendoza, Argentina, pp 33–46

Bandyopadhyay S, Gillette DD, Ray S, Sengupta D (2010) Osteology of Barapasaurus Tagorie (Dinosauria: Sauropoda) from the early Jurassic of India. Palaeontol 53:533–569

Bandyopadhyay S, Sengupta DP (2006) Vertebrate faunal turnover during the Triassic-Jurassic transition: an Indian scenario. In: Harris JD, Lucas SG, Kirkland JD, Milner ARC (eds) Terrestrial Triassic-Jurassic transition. New Mexico Mus Nat Hist Sci Bull 37:77–85

Bandyopadhyay S, Roychowdhury T, Sengupta DP (2002) Taphonomy of some Gondwana vertebrate assemblages of India. Sediment Geol 147:219–245

Bandyopadhyay S, Sengupta DP (1999) Middle Triassic vertebrates of India. J African Earth Sci 29:233–241

Bandyopadhyay S, Rudra D (1985) Upper Gondwana Stratigraphy, North of the Pranhita-Godavari confluence, Southern India. J Geol Soc of India 26:261–266

Banerjee S, Bansal U, Pande K, Meena SS (2016) Compositional variability of glauconites within the Upper Cretaceous Karai Shale Formation, Cauvery Basin, India: implications for evaluation of stratigraphic condensation. Sediment Geol 331:12–29

Banerji J (1989) Some Mesozoic plant remains from Bhuj Formation with remarks on the of beds. Palaeobotanist 37:159–168

Bansal U, Banerjee S, Pande K, Arora A, Meena SS (2017) The distinctive compositional evolution of glauconite in the Cretaceous Ukra Hill Member (Kutch basin, India) and its implications. Mar Pet Geol 82:97–117

Bansal U, Banerjee S, Ruidas DK, Pande K (2018) Origin and geochemical characterization of Maastrichtian glauconites in the Lameta Formation, Central India. J Palaeogeography 7:99–116

Bansal U, Banerjee S, Pande K, Ruidas DK (2019a) Unusual seawater composition of the Late Cretaceous Tethys imprinted in glauconite of Narmada Basin, Central India. Geol Mag 157:233–247

Bansal U, Pande K, Banerjee S, Nagendra R, Jagadeesan KC (2019b) The timing of oceanic anoxic events in the Cretaceous succession of Cauvery Basin: Constraints from 40Ar/39Ar ages of glauconite in the Karai Shale Formation. Geol J 54:308–315

Bhargava ON (2008) An updated introduction to the Spiti geology. J Palaeontol Soc India 53:113–129

Bhat MS, Ray S (2020) A record of new lungfishes (Osteichthyes: Dipnoi) from the Carnian (Upper Triassic) of India. Hist Biol 32:428–437

Bhat MS, Ray S, Datta PM (2018a) A new hybodont shark (Chondrichthyes, Elasmobranchii) from the Upper Triassic Tiki Formation of India with remarks on its dental histology and biostratigraphy. J Paleontol 92:221–239

Bhat MS, Ray S, Datta PM (2018b) A new assemblage of freshwater sharks (Chondrichthyes: Elasmobranchii) from the Upper Triassic of India. Geobios 51:269–283

Bhattacharji S, Chatterjee N, Wampler JM, Nayak PN, Deshmukh SS (1996) Indian intraplate and continental margin rifting, lithospheric extension, and mantle upwelling in Deccan Flood Basalt volcanism near the K/T boundary: evidence from mafic dyke swarms. J Geol 104:379–398

Bhattacharya B, Jha S (2014) Late Cretaceous diurnal tidal system: a study from Nimar Sandstone, Bagh Group, Narmada Valley, Central India. Curr Sci 107:1032–1037

Biswas SK (1977) Mesozoic rock-stratigraphy of Kutch, Gujarat. Quart J Geol Min Met Soc of India 49:1–51

Biswas SK (1981) Basin framework, palaeo-environment and depositional history of the Mesozoic sediments of Kutch Basin, Western India. Quart J Geol Min Met Soc India 53:56–85

Biswas SK (1982) Rift Basins in the Western margin of India and their hydrocarbon prospects with special reference to Kutch Basin. AAPG Bull 66:1497–1513

Biswas SK (1987) Regional tectonic framework, structure and evolution of the western marginal basins of India. Tectonophys 135:307–327

Biswas SK (1991) Stratigraphy and sedimentary evolution of the Mesozoic Basin of Kutch, Western India. In: Tandon SK, Pant CC, Casshyap SM (eds) Stratigraphy and sedimentary evolution of Western India. Gyanodaya Prakashan, Nainital, pp 74–103

Biswas SK (1993) Geology of Kutch, vol 1. KDMIPE, Dehradun

Biswas SK (1999) A review on the evolution of rift basins in India during Gondwana with special reference to western Indian Basins and their hydrocarbon prospects. Proc Indian Natl Sci Acad 65:261–284

Biswas SK (2003) Regional tectonic framework of the Pranhita-Godavari basin, India. J Asian Earth Sci 21:543–551

Biswas SK (2005) A review of structure and tectonics of Kutch Basin, Western India, with special reference to earthquakes. Curr Sci 88:1592–1600

Biswas SK, Deshpande SV (1968) The basement of Mesozoic sediments of Kutch. Bull Geol Min Met Soc India 40:7–18

Bladon AJ, Burley SD, Clarke SM, Beaumont H (2015a) Geology and regional significance of the Sarnoo Hills, Eastern Rift Margin of the Barmer Basin, NW India. Basin Res 27:636–655

Bladon AJ, Clarke SM, Burley SD (2015b) Complex rift geometries resulting from inheritance of pre-existing structures: insights and regional implications from the Barmer Basin rift. J Struct Geol 71:136–154

Bose A, Sengupta S (1993) Infra Kamthi of the central Godavari valley-petrological evidences of marine influence during the Permian. Proc Nat Acad Sci India 63:149–166

Casshyap SM, Aslam M (1992) Deltaic and shoreline sedimentation in Saurashtra Basin, Western India: an example of infilling in an early Cretaceous failed rift. J Sed Pet 62:972–991

Casshyap SM, Tewari RC, Khan A (1993) Alluvial fan origin for Bagra Formation (Mesozoic Gondwana) and tectono-stratigraphic implications. J Geol Soc India 42:262–279

Chakraborty C, Ghosh SK (2008) Pattern of sedimentation during the Late Palaeozoic, Gondwana-land glaciations: an example from the Talchir Formation, Satpura Gondwana Basin, Central India. J Earth Sys Sci 117:499–519

Chakraborty C, Ghosh SK (2005) Pull-apart origin of the Satpura Gondwana Basin, Central India. J Earth System Sci 114:259–273

Chakraborty T, Sarkar S (2005) Evidence of lacustrine sedimentation in the Upper Permian Bijori Formation, Satpura Gondwana Basin: paleogeographic and tectonic implications. J Earth Sys Sci 114:303–323

Chakraborty C, Mandal N, Ghosh K (2003) Kinematics of the Gondwana Basins of peninsular India. Tectonophys 377:299–324

Chatterjee S (1967) New and associated phytosaur material from the Upper Triassic Maleri Formation of India. Bull Geol Soc of India 4:108–110

Chatterjee S, Roy Chowdhuri TK (1974) Triassic Gondwana vertebrates from India. Indian J Earth Sci 1:96–112

Chaudhuri A, Banerjee S, Le Pera E (2018) Petrography of Middle Jurassic to Early Cretaceous sandstones in the Kutch Basin, Western India: Implications on provenance and Basin evolution. J Palaeogeography 7:2–14

Chaudhuri A, Banerjee S, Chauhan G (2020a) Compositional evolution of siliciclastic sediments recording the tectonic stability of a pericratonic rift: Mesozoic Kutch Basin, Western India. Mar Pet Geol 111:476–495

Chaudhuri A, Das K, Banerjee S, Fitzsimons ICW (2020b) Detrital zircon and monazite track the source of Mesozoic sediments in Kutch to rocks of Late Neoproterozoic and Early Palaeozoic orogenies in Northern India. Gond Res 80:188–201

Chaudhuri A, Chatterjee A, Banerjee S, Ray JS (2020c) Tracing multiple sources of sediments using trace element and Nd isotope geochemistry: provenance of the Mesozoic succession in the Kutch Basin, Western India. Geol Mag. https://doi.org/10.1017/S0016756820000539

Chaudhuri A, Banerjee S, Prabhakar N, Das A (2020d) The use of heavy mineral chemistry in reconstructing provenance: a case study from Mesozoic sandstones of Kutch Basin (India). Geol Jour. https://doi.org/10.1002/gj.3922

Chaudhuri AK, Deb GK, Patranabis-Deb S, Sarkar S (2012) Paleogeographic and tectonic evolution of the Pranhita-Godavari Valley, central India: a stratigraphic perspective. American J Sci 312:766–815

Chinnappa Ch, Rajanikanth A (2018) Mesozoic woods from India: nomenclature review and palaeoclimatic implications. Palaeoworld 27:211–225

Chinnappa Ch, Rajanikanth A (2016a) A new species of *Circoporoxylon* from Kota Formation (Jurassic), Pranhita-Godavari Basin, India and palaeobiogeography of the genus. Ameghiniana 53:675–684

Chinnappa Ch, Rajanikanth A (2016b) An integrated enquiry into the early Cretaceous floristics of the Pranhita Godavari Basin and ecological considerations. Acta Palaeobotanica 57:13–32

Coltorti M, Dramis F, Ollier CD (2007) Planation surfaces in Northern Ethiopia. Geomorphology 89:287–296

Compton PM (2009) The geology of the Barmer Basin, Rajasthan, India, and the origins of its major oil reservoir, the Fatehgarh Formation. Pet Geosci 15:117–130

Conrad CP, Gurnis M (2003) Seismic tomography, surface uplift, and the breakup of Gondwanaland: integrating mantle convection backwards in time. Geochem Geophys Geosyst 4:1031

Cotter Gde P (1917) A revised classification of the Gondwana system. Rec Geol Surv India 48:23–33

Crookshank H (1936) Geology of the northern slopes of the Satpuras between the Morand and the Sher Rivers. Mem Geol Surv India 66:217–218

Dasgupta K (1993) Some contributions to the stratigraphy of the Yerrapalli Formation, Pranhita-Godavari Valley, Deccan, India. J Geol Soc India 42:223–230

Dasgupta S (2009) Sandstone petrography and provenance determination from the upper Gondwana succession of the Rewa basin, India. Unpublished MSc thesis, Department of Geology and Geophysics, Indian Institute of Technology, Kharagpur, India, pp 1–27

Dasgupta S (2019) Implication of transfer zones in rift fault propagation: Example from Cauvery Basin, Indian East coast. In: Mukherjee S (ed) Tectonics and structural geology: Indian Context, Springer Nature, pp 313–327

Dasgupta S, Mukherjee S (2017) Brittle shear tectonics in a narrow continental rift: Asymmetric nonvolcanic Barmer Basin (Rajasthan, India). J Geol 125:561–591

Dasgupta S, Ghosh P (2018) Freshwater carbonates within a Late Triassic siliciclastic fluvial system in a Gondwana rift Basin: The Maleri Formation, India. Sediment Geol 373:254–271

Dasgupta S, Ghosh P, Gierlowski-Kordesch EH (2017) A discontinuous ephemeral stream transporting mud aggregates in a continental rift Basin: The Late Triassic Maleri Formation, India. J Sed Res 87:838–865

Dasgupta SK (1975) A revision of the Mesozoic-Tertiary stratigraphy of the Jaisalmer Basin, Rajasthan. Indian J Earth Sci 2:77–94

Datta PM (2004) A suggestion for an early Tuvalian time segment for the Tiki Formation, South Rewa Gondwana Basin, India and other correlatable continental sequences. Albertina 30(suppl):6–7

Datta PM (2005) Earliest mammal with transversely expanded upper molar from the Late Triassic (Carnian) Tiki Formation, South Rewa Gondwana basin, India. J Verteb Paleontol 25:200–207

Datta PM, Ray S (2006) Earliest lizard from the Late Triassic (Carnian) of India. J Verteb Paleontol 26:795–800

Datta PM, Das DP, Luo ZX (2004) A Late Triassic dromatheriid (Synapsida: Cynodontia) from India. Annals Carnegie Mus 73:72–84

Desai BG, Biswas SK (2018) Postrift deltaic sedimentation inwestern Kachchh Basin: insights from and sedimentology. Palaeo Palaeo Palaeo 504:104–124

Dogra NN, Singh YR, Kumar S (2010) The Lithostratigraphic status of Jabalpur and Lameta Formations and palynological constrains of the age and environment. Gond Geol Mag 25:185–194

Dolson J, Burley SD, Sunder VR, Kothari V, Naidu B, Whiteley NP, Farrimond P, Taylor A, Direen N, Ananthakrishnan B (2015) The discovery of the Barmer Basin, Rajasthan, India, and its petroleum geology. AAPG Bull 99:433–465

Dutta PK (2002) Gondwana lithostratigraphy of Peninsular India. Gond Res 5:540–553

Dutta PK, Ghosh SK (1972) Triassic sedimentation in Pali-Tiki-Parsora area, Madhya Pradesh. In: Proceedings of 49th Indian science congress, abstract volume, pp 232–233

Dutta PK, Ghosh SK (1993) The century-old problem of the Pali-Parsora-Tiki stratigraphy and its bearing on the Gondwana classification in Peninsular India. J Geol Soc India 42:17–31

Evans SE, Prasad GVR, Manhas BK (2002) Fossil lizards from the Jurassic Kota Formation of India. J Verteb Paleontol 22:299–312

Farrimond P, Naidu BS, Burley SD, Dolson J, Whiteley N, Kothari V (2015) Geochemical characterization of oils and their source rocks in the Barmer Basin, Rajasthan, India. Pet Geosci 21:301–321

Fox CS (1931) The Gondwana system and its related formations. Mem Geol Surv India 58:1–281

Fox CS (1934) Lower Gondwana coalfield of India. Mem Geol Surv India LIX

Fürsich FT, Oschmann W, Singh IB, Jaitly AK (1992) Hardgrounds, reworked concretion levels and condensed horizons in the Jurassic of Western India: their significance for Basin analysis. J Geol Soc London 149:313–331

Fürsich FT, Pandey DK, Callomon JH, Jaitly AK, Singh IB (2001) Marker beds in the Jurassic of the Kachchh Basin, Western India: their depositional environment and sequence stratigraphic significance. J Palaeontol Soc India 46:173–198

Fürsich FT, Singh IB, Joachimski M, Krumm S, Schlirf M, Schlirf S (2005) Palaeoclimate reconstructions of the Middle Jurassic of Kachchh (western India): an integrated approach based on palaeoecological, oxygen isotopic, and clay mineralogical data. Palaeo Palaeo Palaeo 217:289–309

Ghosh P (1997) Geomorphology and palaeoclimatology of some Upper Cretaceous palaeosols in central India. Sediment Geol 110:25–49

Ghosh P, Sengupta DP (2019) Geodynamics of Gondwanaland. In: Tandon SK (ed) Gupta N. Geodynamics of the Indian Plate, Evolutionary Perspectives, Springer, pp 213–232

Ghosh P, Bhattacharya SK, Jani RA (1995) Palaeoclimate and Palaeovegetation in central India during the Upper Cretaceous based on stable isotope composition of the palaeosol carbonates. Palaeo Palaeo Palaeo 114:285–296

Ghosh P, Ghosh P, Bhattacharya SK (2001) CO_2 level in the Late Paleozoic and Mesozoic atmosphere from soil carbonate and organic matter, Satpura Basin, Central India. Palaeo Palaeo Palaeo 170:219–236

Ghosh P, Bhattacharya SK, Sahni A, Kar RK, Mohabey DM, Ambwani K (2003) Dinosaur coprolites from the Late Cretaceous (Maastrichtian) Lameta Formation of India: isotopic and other markers suggesting a C_3 plant diet. Cret Res 24:743–750

Ghosh P, Sarkar S, Maulik P (2006) Sedimentology of a muddy alluvial deposit: Triassic Denwa Formation, India. Sediment Geol 191:3–36

Ghosh S, Sarkar S (2010) Geochemistry of Permo-Triassic mudstone of the Satpura Gondwana basin, central India: clues for provenance. Chem Geol 277:78–100

Ghosh S, Sarkar S, Ghosh P (2012) Petrography and major element geochemistry of the Permo-Triassic sandstones, central India: Implication for provenance in an intracratonic pull-apart Basin. J Asian Earth Sci 43:207–240

Ghosh SK, Chakraborty C, Chakraborty T (2004) Combined tide and wave influence on sedimentation of Lower Gondwana coal measures of central India: Barakar Formation (Permian), Satpura Basin. J Geol Soc London 161:117–131

Gibbons AD, Whittake JM, Mülle R (2013) The breakup of East Gondwana: Assimilating constraints from Cretaceous ocean Basins around India into a best-fit tectonic model. J Geoph Res 118:808–822

Golonka J (2007) Late Triassic and Early Jurassic palaeogeography of the world. Palaeo Palaeo Palaeo 244:297–307

Golonka J (2011) Phanerozoic palaeoenvironment and palaeolithofacies maps of the Arctic region. In: Chapter 6, Spencer AM, Embry AF, Gautier DL, Stoupakova AV, Sørensen K (eds) Arctic petroleum geology. Mem Geol Soc London 35:79–129

Goswami S, Ghosh P (2020) Evolution of sedimentation pattern in a continental rift Basin of India, between the Late Triassic and the Early Middle Jurassic: Tectonic and climatic controls. Sed Geol 405:105679. https://doi.org/10.1016/jsedgeo2020105679

Goswami S, Gierlowski-Kordesch EH, Ghosh P (2018) Sedimentology of the Early Jurassic limestone beds of the Kota Formation: record of carbonate wetlands in a continental rift basin of India. J Paleolim 59:21–38

Gupta A (2009) Ichthyofauna of the Lower Triassic Panchet Formation, Damodar Valley Basin, West Bengal, and its implications. Indian J Geosci 63:275–286

Hall R (2012) Late Jurassic-Cenozoic reconstructions of the Indonesian region and the Indian Ocean. Tectonophys 570–571:1–41

Hughes TWH (1881) Notes on the South Rewa Gondwana Basin. Rec Geol Surv India 14:126–138

Jain SL, Robinson PL, Chowdhury T (1964) A new vertebrate fauna from the Triassic of the Deccan, India. J Geol Soc London 120:115–124

Jain SL (1973) New specimens of Lower Jurassic holostean fishes from India. Palaeontology 16:149–177

Jain SL (1974) Jurassic pterosaur from India. J Geol Soc India 15:334–335

Jain SL (1983) Spirally coiled 'coprolites' from the Upper Triassic Maleri Formation, India. Palaeo 26:81–83

Jaiswal S, Bhattacharya B, Chakrabarty S (2018) High resolution sequence stratigraphy of Middle Eocene Hazad Member, Jambusar-Broach Block, Cambay Basin, India. Mar Pet Geol 93:79–94

Jha S, Bhattacharya B, Nandwani S (2017) Significance of seismites in the Late Cretaceous transgressive Nimar Sandstone succession, Son-Narmada rift Valley, Central India. Geol J 52:768–783

Jokat W, Boebel T, König M, Meyer U (2003) Timing and geometry of Early Gondwana breakup. J Geophy Res 108:2428

Kar RK, Mohabey DM, Srivastava R (2004) Angiospermous fossil woods from the Lameta Formation (Maastrichtian), Maharashtra, India. Geophytol 33:21–27

Keller G, Jaiprakash BC, Reddy AN (2016) Maastrichtian to Eocene Subsurface Stratigraphy of the Cauvery Basin and correlation with Madagascar. J Geol Soc India 87:5–34

Khan A, Aslam M, Rahman E (2017) Wave-dominated shoreline sediments in early Cretaceous Surajdeval Formation, Saurashtra Basin, Gujarat western India. Int J New Tech Res 3:74–78

Khosla A, Sahni A (2000) Late Cretaceous (Maastrichtian) ostracodes from the Lameta Formation, Jabalpur cantonment area, Madhya Pradesh, India. J Palaeontol Soc India 45:57–78

Kiessling W, Flügel E, Golonka J (2003) Patterns of phanerozoic carbonate platform sedimentation. Lethaia 36:195–226

King W (1881) Reprint 1930 geology of the Pranhita-Godavari Valley. Geol Surv India 1–161

Krishna J (1987) An overview of the Mesozoic stratigraphy of Kachchh and Jaisalmer basins. J Palaeontol Soc India 32:136–149

Krishna J, Pathak DB, Pandey B, Ojha JR (2000) Transgressive sediment intervals in the Late Jurassic of Kachchh, India. GeoRes Forum 6:321–332

Kumar P, Yuan X, Ravi Kumar M, Kind R, Li X, Chadha RK (2007) The rapid drift of the Indian tectonic plate. Nature 449:894–897

Kutty TS (1969) Some contributions to the stratigraphy of the Upper Gondwana formations of the Pranhita-Godavari Valley, Central India. J Geol Soc India 10:33–48

Kutty TS (1971) Two faunal associations from the Maleri Formations of Pranhita-Godavari Valley, Central India. J Geol Soc India 12:63–67

Kutty TS, Sengupta DP (1989) The Late Triassic Formations of the Pranhita-Godavari Valley and their vertebrate faunal succession—a reappraisal. Indian J Earth Sci 16:189–206

Kutty TS, Jain SL, Roy Chowdhury T (1987) Gondwana sequence of the northern Pranhita-Godavari Valley: its stratigraphy and vertebrate faunas. Palaeobotanist 36:214–229

Kutty TS, Chatterjee S, Galton PM, Upchurch P (2007) Basal dinosauriformes sauropodomorphs (Dinosauria: Saurischia) from the Lower Jurassic of India: their anatomy and relationships. J Paleontol 81:1552–1574

Mandal A, Koner A, Sarkar S, Tawfik HA, Chakraborty N, Bhakta S, Bose PK (2016) Physicochemical tuning of palaeogeographic shifts: Bhuj Formation, Kutch, India. Mar Pet Geol 78:474–492

Martin M, Barbieri L, Cuny G (1999) The Madagascan Mesozoic ptychoceratodontids (Dipnoi): systematic relationships and paleobiogeographical significance. Oryctos 2:3–16

Maulik PK, Chakraborty C, Ghosh P, Rudra D (2000) Meso- and macro-scale architecture of a Triassic fluvial succession: Denwa Formation, Satpura Gondwana Basin, Madhya Pradesh. J Geol Soc India 56:489–504

McLoughlin S (2001) The breakup history of Gondwana and its impact on pre-Cenozoic floristic provincialism Australian. Aust J Botany 49:271–300

Metcalfe I (2013) Gondwana dispersion and Asian accretion: tectonic and palaeogeographic evolution of eastern Tethys. J Asian Earth Sci 66:1–33

Mishra DC (2011) Gravity and magnetic methods for geological studies: principles. Integrated Explorations and Plate Tectonics. BS Publications, Hyderabad, pp 672–675

Mitra ND (1993) Stratigraphy of Pali-Parsora-Tiki formations of South Rewa Gondwana Basin and Permo-Triassic boundary problem Gondwana. Geol Mag, Spec Vol, Birbal Sahni Nat Symp India, 41–48

Mohabey DM, Udhoji SG, Verma KK (1993) Palaeontological and sedimentological observations on nonmarine Lameta Formation (Upper Cretaceous) of Maharashtra, India: their palaeoecological and palaeoenvironmental significance. Palaeo Palaeo Palaeo 105:83–94

Mohanty S (2010) Tectonic evolution of the Satpura Mountain Belt: A critical evaluation and implication on supercontinent assembly. J Asian Earth Sci 39:516–526

Mude SN, Jagtap SA, Kundal P, Sarkar PK, Kundal MP (2012) Paleoenvironmental significance of ichnofossils from the Mesozoic Jaisalmer Basin, Rajasthan, North Western India. Proc Int Acad Eco Env Sci 2:150–167

Mukherjee D, Ray S (2012) Taphonomy of an Upper Triassic vertebrate bonebed: a new rhynchosaur (Reptilia; Archosauromorpha) accumulation from India. Palaeo Palaeo Palaeo 333–334:75–91

Mukherjee D, Ray S, Chandra S, Pal S, Bandyopadhyay S (2012) Upper Gondwana Succession of the Rewa Basin, India: understanding the interrelationship of lithologic and stratigraphic variables. J Geol Soc India 79:563–575

Mukherjee MK (1983) Petroleum prospects of Cretaceous sediments of the Cambay basin, Gujarat, India. J Petrol Geol 5:275–286

Mukherjee RN, Sengupta DP (1998) New capitosaurid amphibians from the Triassic Denwa Formation of the Satpura Gondwana Basin, Central India. Alcheringa. J Palaeontol 22:317–327

Mukhopadhyay G, Mukhopadhyay SK, Roychowdhury M, Parui PK (2010) Stratigraphic correlation between different Gondwana Basins of India. J Geol Soc India 76:251–266

Mukhopadhyay M, Verma RK, Ashraf MH (1986) Gravity field and structures of the Rajmahal hills: example of the paleo-mesozoic continental margin in Eastern India. Tectonophys 131:353–367

Nagendra R, Reddy AN, Jaiprakash BC, Gilbert H, Zakharov YD, Venkateswarlu M (2018) Integrated Cretaceous stratigraphy of the Cauvery Basin, South India. Stratigraphy 15:245–259

Nandi A, Raha PK (1998) Palynoflora from Motur Formation, Satpura Basin, Madhya Pradesh. Indian Min 52:129–132

Narasimha Chari MV, Sahu JN, Banerjee B, Zutshi PL, Chandra K (1995) Evolution of the Cauvery Basin, India from subsidence modelling. Mar Pet Geol 12:667–675

Narula PL, Acharyya SK, Banerjee J (eds) (2000) Seismotectonic Atlas of India and its Environs: Kolkata, India. Geol Surv India Spec Publ 59:1–87

Nath TT, Yadagiri P (2007) A new mammal-like-reptile (Cynodontia) from Upper Triassic Maleri Formation of Pranhita-Godavari Valley, Andhra Pradesh. J Geol Soc India 69:57–60

Norton IO, Sclater JG (1979) A model for the evolution of the Indian Ocean and the breakup of Gondwanaland. J Geophys Res 84:6803–6830

Novas FE, Ezcurra MD, Chatterjee S, Kutty TS (2011) New dinosaur species from the Upper Triassic Upper Maleri and Lower Dharmaram formations of Central India. Royal Soc Edinburgh Trans 101:333–349

Pandey DK, Pooniya D (2015) Sequence stratigraphy of the Oxfordian to Tithonian sediments (Baisakhi Formation) in the Jaisalmer Basin. Vol Jurassica 13:65–76

Pandey DK, Sha J, Choudhary S (2010) Sedimentary cycles in the Calloviane Oxfordian of the Jaisalmer Basin, Rajasthan, western India. Vol Jurassica 8:131–162

Pandey DK, Choudhary S, Bahadur T, Swami N, Poonia D, Sha J (2012) A review of the Lower e lowermost Upper Jurassic facies and stratigraphy of the Jaisalmer Basin, western Rajasthan, India. Vol Jurassica 10:61–82

Pascoe EH (1975) A manual of the geology of India and Burma, vol 2. Government of India Press, Calcutta, pp 485–1343

Pascoe EH (1959) A manual of geology of India and Burma II, 3rd ed. Government of India Publications, New Delhi

Peters J, Singh SK (2001) Satpura Basin –an example of pre-rift, syn-rift and post-rift Gondwana sedimentation in India. J Geol Soc India 57:309–320

Pieńkowski G, Brański P, Pandey DK, Schlögl J, Alberti M, Fürsich FT (2015) Dinosaur footprints from the Thaiat ridge and their palaeoenvironmental background, Jaisalmer Basin, Rajastan, India. Vol Jurassica 1:17–26

Pillai SS, Agnihotri D, Gautam S, Tewari R (2018) Glossopteris flora from the Pali Formation, Johilla coalfield, South Rewa Gondwana basin, Madhya Pradesh, India: Palynological evidence for a Late Permian age. J Palaeontol Soc India 63:53–72

Prakash N (2008) Biodiversity and palaeoclimatic interpretation of Early Cretaceous flora of Jabalpur Formation, Satpura Basin, India. Palaeoworld 17:253–263

Prakash S, Ramasamy S, Varghese NM (2018) Provenance of the Gondwana sediments, Palar Basin. Southern India. Arab J Geosci 11:163. https://doi.org/10.1007/s12517-018-3494-6

Prasad B, Pundir BS (2017) Gondwana biostratigraphy of the Purnea Basin (Eastern Bihar, India), and its correlation with Rajmahal and Bengal Gondwana Basins. J Geol Soc India 90:405–427

Rai J, Garg R (2007) Early Callovian nannofossils from the Kuldhar section, Jaisalmer, Rajasthan. Curr Sci 92:816–820

Rai J, Bajpai S, Kumar R, Singh A, Kumar K, Prakash N (2016) The earliest marine transgression in western India: new insights from calcareous nannofossils from Lathi Formation, Jaisalmer Basin. Curr Sci 111:1631–1639

Ramkumar M, Stüben D, Berner Z (2004) Lithostratigraphy, depositional history and sea level changes of the Cauvery Basin, Southern India. Annales Géol De La Péninsule Balkanique 65:1–27

Raja Rao CS (1983) Coalfields of India vol III: coal resources of Madhya Pradesh, Jammu and Kashmir. B Geol Sur India Series A 45:119–129

Rajanikanth A, Agarwal A, Stephen A (2010) An integrated inquiry of early Cretaceous Flora, Palar Basin, India. Phytomorphology 60:21–28

Ramakrishna H, Ramanujam CGK, Prabhakar M (1985) Palynoassemblage of the Upper Gondwana deposits of Balhanpur area, Adilabad District, Andhra Pradesh. J Palynol 21:126–132

Rao CN, Shukla BN (1954) General report. Rec Geol Surv India 81:1–228

Ray S (1997) Some contributions to the Lower Gondwana stratigraphy of the Pranhita-Godavari Valley, Deccan India. J Geol Soc India 50:633–640

Ray S (1999) Permian reptilian fauna from the Kundaram Formation, Pranhita-Godavari Valley India. J Afr Earth Sci 29:211–218

Ray S (2015) A new Late Triassic traversodontid cynodont (Therapsida, Eucynodontia) from India. J Verteb Paleontol 35:3. https://doi.org/10.1080/02724634.2014.930472

Ray S, Chakraborty T (2002) Lower Gondwana fluvial succession of the Pench-Kanhan Valley, India: stratigraphic architecture and depositional controls. Sediment Geol 151:243–271

Ray S, Bandyopadhyay S (2003) Late Permian vertebrate community of the Pranhita-Godavari Valley India. J Asian Earth Sci 21:643–654

Ray S, Bhat MS, Mukherjee D, Datta PM (2016) Vertebrate fauna from the Late Triassic Tiki Formation of India: new finds and their biostratigraphic implications. Palaeobotanist 65:47–59

Reeves CV, de Wit MJ (2000) Making ends meet in Gondwana: Retracing the transforms of the Indian Ocean and reconnecting continental shear zones. Terra Nova 12:272–280

Reeves CV, de Wit MJ, Sahu BK (2004) Tight reassembly of Gondwana exposes Phanerozoic shears in Africa as global tectonic players. Gond Res 7:7–19

Riley TR, Knight KB (2001) Review: age of pre-break-up Gondwana magmatism. Antarctic Sci 13:99–110

Robinson PL (1967) The Indian Gondwana Formations-a review. In: 1st international symposium on Gondwana stratigraphy. International Union Geological Sciences, Argentina, pp 201–268

Robinson PL (1973) Palaeoclimatology and continental drift. In: Tarling DH, Runcorn SK (eds) Implications of continental drift to earth sciences. Academic Press, London, pp 451–476

Roy AB, Pandey S (1970) Expansion or contraction of the Great Indian Desert: proceedings. Indian Nat Sci Acad 36B:331–344

Rudra D (1982) Upper Gondwana Stratigraphy and sedimentation in the Pranhita-Godavari Valley, India. Quart J Geol Min Met Soc India 54:56–79

Ruidas DK, Pomoni Papaioannou FA, Banerjee S, Gangopadhyay TK (2020) Petrographical and geochemical constraints on carbonate diagenesis in an epeiric platform deposit: Late Cretaceous Bagh Group in central India. Carb Evap 35: 94 https://doi.org/10.1007/s13146-020-00624-2

Saha O, Shukla UK, Rani R (2010) Trace Fossils from the Late Cretaceous Lameta Formation, Jabalpur Area, Madhya Pradesh: Paleoenvironmental Implications. J Geol Soc India 76:607–620

Sahni MR, Rao CN (1956) A note on the correlation of the Parsora and Tiki Beds of Vindhya Pradesh. In: Proceedings of 20th international geological congress, Mexico, pp 95–103

Sakai H (1989) Rifting of the Gondwanaland and uplifting of the Himalayas recorded in the Mesozoic and Tertiary fluvial sediments in the Nepal Himalayas. In: Taira A, Masuda F (eds) Sedimentary facies in the active plate margin, Terra Sci Pub Com, Tokyo, pp 723–732

Sarkar S, Chaudhuri AK (1992) Trace fossils in Middle to Late Triassic fluvial redbeds, Pranhita-Godavari Valley, South India. Ichnos 2:7–19

Saxena VM, Chakraborty C, Sati GC, Mohan B, Bariak AK, Bhagwani SS (2012) Pennar Basin: a potential spot for synrift exploration. In: 9th biennial international conference and exposition on petroleum geophysics, Hyderabad

Scotese CR (2002) http://www.scotese.com, (PALEOMAP website)

Scotese CR, Boucot AJ, Mckerrow WS (1999) Gondwanan palaeogeography and palaeoclimatology. J African Earth Sci 28:99–114

Sengor AMC, Burke K, Dewey JF (1978) Rifts at high angles to orogenic belts: tests for their origin and the Upper Rhine Graben as an example. American J Sci 278:24–40

Sengupta S (1970) Gondwana sedimentation around Bheemaram (Bhimaram), Pranhita-Godavari Valley, India. J Sed Pet 40:140–170

Sengupta S (2003) Gondwana sedimentation in the Pranhita-Godavari Valley: a review. J Asian Earth Sci 21:633–642

Sengupta S, Sengupta DP, Bandyopadhyay S (2016) Stratigraphy of the Upper Gondwana formations around Sohagpur, Western Part of the Satpura Gondwana Basin, Central India. J Geol Soc India 87:503–519

Shah BA (2004) Gondwana lithostratigraphy of Peninsular India: comment. Gond Res 7:600–607

Sharma JK, Pandey DK (2016) Taxonomy of Late Bathoniane oxfordian ammonites from the Jaisalmer Basin: implications for intrabasinal litho- and biostratigraphic correlations. J Palaeontol Soc India 61:249–266

Sharma KK (2007) K-T magmatism and basin tectonism in western Rajasthan, India: results from extensional tectonics and not from Reunion plume activity. In: Foulger GR, Jurdy DM (eds) Plates, plumes, and planetary processes. GSA Spec Pap 430:775–784

Sheth HC, Ray JS, Ray R, Vanderkluysen L, Mahoney JJ, Kumar A, Shukla AD, Das P, Adhikari S, Jana B (2009) Geology and geochemistry of Pachmarhi dykes and sills, Satpura Gondwana Basin, Central India: problems of dyke-sill-flow correlations in the Deccan Traps. Contrib Min Pet 158:357–380

Singh IB (1989) Dhosa Oolite—a transgressive condensation horizon of oxfordian age in Kachchh, western India. J Geol Soc India 34:152–160

Singh J, Chandrakala K, Singh AP, Mall DM (2015) Structure and evolution of Satpura Gondwana Basin over Central Indian Tectonic Zone: inferences from seismic and gravity data. J Ind Geophy Union 19:39–54

Singh NP (2006) Mesozoic lithostratigraphy of the Jaisalmer Basin, Rajasthan. J Palaeontol Soc India 51:1–25

Singh S, Jain AK (2007) Liquefaction and fluidization of lacustrine deposits from Lahaul-Spiti and Ladakh Himalaya: Geological evidences of paleoseismicity along active fault zone. Sed Geol 196:47–57

Sisodia MS, Singh UK (2000) Depositional environment and hydrocarbon prospects of the Barmer Basin, Rajasthan, India. Nafta (Zagreb) 51:309–326

Sisodia MS, Singh UK, Lashkari G, Shukla PN, Shukla AD, Bhandari N (2005) Mineralogy and trace element chemistry of the siliceous earth of Barmer Basin, Rajasthan: evidence for a volcanic origin. J Earth Syst Sci 114:111–124

Sohn IG, Chatterjee S (1979) Freshwater ostracodes from Late Triassic coprolite in central India. J Palaeontol 53:578–586

Srivastave N, Ranawat TS (2015) An overview of Yellow Limestone deposits of the Jaisalmer Basin, Rajasthan, India. Vol Jurassica 13:107–112

Srivastava SC (1992) Permian palynological assemblages in the Godavari graben. Palaeobotanist 40:237–243

Steck A, Epard J, Vannay JC, Hunziker J, Girard M, Morard A, Robyr M (1998) Geological transect across the Tso Morari and Spiti areas: The nappe structures of the Tethys Himalaya. Eclogae Geol Helv 91:103–121

Sudan CS, Sahni AK, Sharma UK (2000) Trace fossils from the Jurassic sequence of Jaisalmer Basin, Rajasthan. J Palaeontol Soc India 45:165–171

Suess E (1885) Das Satilitz der Ende, Brand 1. Leipzig Vienna, Wien

Tarafdar P, Sinha PK, Das KP, Kundu A, Dutta DR, Rajaiya V, Parui PK, Patel MC, Thanavelu C, Ashok Kumar MK, Pillai KR, Agasty A, Dutta NK (1993) Recent advance in Post-Barakar stratigraphy in parts of Rewa Gondwana Basin. Gond Geol Mag Spec Vol 60–69

Tewari HC, Dixit MM, Sarkar D (1995) Relationship of the Cambay rift basin to the Deccan volcanism. J Geodynamics 20:85–95

Tewari RC (1995) Braided-fluvial depositional model of Late Triassic Gondwana (Mahadeva) rocks of Son-Valley, Central India: Tectonic and paleogeographic implications. J Geol Soc India 45:65–73

Tiwari RS, Tripathi A (1992) Marker assemblage-zones of spores and pollen species through Gondwana Palaeozoic and Mesozoic sequence in India. Palaeobotanist 40:194–236

Torsvik TH, Pandit MK, Redfield TF, Ashwal LD, Webb SJ (2005) Remagnetization of Mesozoic limestones from the Jaisalmer Basin, NW India. Geophys J Int 161:57–64

Tripathi A, Tiwari RS, Kumar P (1990) Palynology of the subsurface Mesozoic sediments In Rajmahal Basin, Bihar. Palaeobotanist 37:367–388

Unrug R (1996) The Assembly of Gondwana supercontinent: contrasting histories of East and West Gondwana. In: 9th Gondwana symposium Hyderabad, India, pp 989–998

Varadarajan K, Ganju JL (1989) Lineament analysis of coastal belt of peninsular India. In: Qureshy MN, Hinze WH (eds) Regional geophysical lineaments. Mem Geol Soc India 12:49–58

Veevers JJ (2004) Gondwanaland from 650–500 Ma assembly through 320 Ma merger in Pangea to 185–100 Ma breakup: supercontinental tectonics via stratigraphy and radiometric dating. Earth-Sci Rev 68:1–132

Veevers JJ (2009) Palinspastic (pre-rift and -drift) fit of India and conjugate Antarctica and geological connections across the suture. Gond Res 16:90–108

Veevers JJ, Tewari RC (1995) Gondwana master basin of Peninsular India between Tethys and the interior of the Gondwanaland province of Pangea. GSA Mem 187:1–72

Watkinson MP, Hart MB, Joshi A (2007) Cretaceous tectonostratigraphy and the development of the Cauvery Basin, Southeast India. Pet Geosci 13:181–191

Wilson JA, Mohabey DM (2006) A titanosauriform (Dinosauria: Sauropoda) axis from the Lameta Formation (Upper Cretaceous: Maastrichtian) of Nand, central India. J Verteb Paleo 26:471–479

Yadagiri P, Rao BRJ (1987) Contribution to the statigraphy and vertebrate fauna of lower Jurassic Kota Formation, Pranhita-Godavari valley, India. Palaeobotanist 36:230–244

Cretaceous Deposits of India: A Review

Nivedita Chakraborty, Anudeb Mandal, R. Nagendra, Shilpa Srimani, Santanu Banerjee, and Subir Sarkar

Abstract India offers a graceful natural laboratory for time traveling to the Cretaceous world. The present chapter attempts a review of Cretaceous geology from India heading for its stance on evolution of basin, stratigraphy, sedimentation, climate, volcanism, relative sea level, biogeography and mass extinction. It was the era when India separated from the Gondwanaland next to the South Pole and initiated the longest passage in a northward direction. Tectonic spurt and reformation steered the geography of the island continent. Margins of the land got novel shape, new ocean and bays opened up, coastlines were formed and new sedimentary basins developed at the continental margins as well as in the interior part. Later, Gondwana sedimentation was ceased. Relative sea level (RSL) was set to fluctuate at a similar pace to global transgression and regression. Sediments were deposited on the east coast, west coast, and offshore basins in response to the rise in RSL during Albian, Turonian and Campanian. A Late Cretaceous transgression in central India came from the west. The maximum fossil foraminifer diversity was in the late Cenomanian/earliest Turonian and this time-interval is corresponding with the maximum sea-level recorded during the Mesozoic. Apparently, a warm temperate humid palaeoclimate prevailed with a tendency of increasing humidity at the end of the Cretaceous. The paleotemperature graph was higher in Late Cretaceous too. India witnessed three renowned volcanic episodes during this period: Rajmahal and Sylhet flood basalts in the eastern part and Deccan volcanism in the western sector. India perhaps retained the biotic link with

N. Chakraborty (✉)
Department of Geology, Kabi Jagadram Roy Government General Degree College, Bankura 722143, West Bengal, India

A. Mandal
Department of Geology, Presidency University, Kolkata 700073, India

R. Nagendra
Department of Geology, Anna University, Chennai, Chennai 600025, India

S. Srimani · S. Sarkar
Department of Geological Sciences, Jadavpur University, Kolkata 700032, India

S. Banerjee
Department of Earth Sciences, Indian Institute of Technology Bombay, Powai, Mumbai 400076, India

Africa via Madagascar and South America till Early Cretaceous. Terrestrial vertebrates are found cosmopolitan with a lack of evidence of endemism. Besides, diversity prevailed in floral distribution pattern, as gymnosperm dominated and angiosperm appeared. The Maastrichtian sections in India report the evolution of Gondwana fauna in isolation on top of amalgamation of Laurasian taxa. The K-Pg boundary is marked by a severe loss of fauna: the disappearance of dinosaurs, ammonites, flying reptiles, scleractinian corals, belemnites and some groups of bivalves, gastropods and echinoderms; acutely affecting calcareous planktons and reef invertebrates.

Keywords Cretaceous · India · Stratigraphy · Sedimentation · Climate · Volcanism · RSL · Biogeography and Mass-Extinction

1 Background

Cretaceous (145–65 Ma), the longest period of the Phanerozoic, has always been recognized as a fascinating chapter in the geological time scale. About 60% of the Earth's known hydrocarbon deposits are from the Mesozoic, particularly from the Cretaceous (Naqvi 2005). Cretaceous was an exceptional episode of accelerated break up of Pangaea, associating with numerous rift basins formation and volcanic events (Föllmi 2012). Cretaceous was unique for its warm and equable climate too (Hay 2008). Tropical sea-surface temperatures were a few degrees higher (4–7 °C) than current days, but polar waters were usually more than 20 °C warmer (Norris et al. 2002; Jenkyns et al. 2004). Meridional and ocean to continent temperature gradients were weaker. The warmer climate was an indication of higher atmospheric levels of greenhouse gasses (Hay 2008). Much of the Tethyan carbonates released a large flux of CO_2 at the subduction zones triggering global warming (Kent and Muttoni 2008). Cerling (1991) estimated the atmospheric PCO_2 level being 2500 ppmV and 800–12,000 ppmV in the Early and Late Cretaceous, respectively. Cretaceous was almost ice-free except the Early Cretaceous winters with cool temperate forests at the poles (Scotese 2015). During the Late Cretaceous, the climate was definitely warmer than today, with no enduring polar ice caps; the average annual temperatures at the equator reached 38 °C (Chatterjee et al. 2017). It was a time of rapid seafloor spreading and the formation of new epicontinental seas (<300 m deep). Late Cretaceous (94–64 Ma) witnessed the greatest inundation of continents since Ordovician (Hancock and Kauffman 1979). Seas were calcitic with a much shallower calcite compensation depth (CCD) with respect to the present day. Cretaceous is known for ocean anoxic events, sedimentation of black-shale, ecological and evolutionary biotic changes in the seas (Rodríguez-Tovar et al. 2009). The first appearance of many Cretaceous life-forms played a key role in the impending Cenozoic world. Perhaps the most important one, at least for terrestrial life, was the first appearance of angiosperms. Seagrasses, recognized for persuading carbonate sedimentation, are generally considered to have originated in the Tethys Ocean during the Late Cretaceous (Perry and Beavington-Penney 2005). The era is notable for the extensive

growth of carbonate platforms, especially in and around the Tethyan Ocean (Schlager and Philip 1990). These platforms were favored by the rudists for their prolific growth and diversification (Gili et al. 1995). The first radiation of the diatoms took place in the Cretaceous oceans. A significant high intensity of bioturbation is reflected from the Cretaceous onwards.

2 Indian Context

Cretaceous was a period of intense tectonics placing India in a drifted position against the context of global paleogeography. India was dismembered from Gondwanaland and drifted northward as an island continent leading to many dramatic changes in basinal configurations as a result of the closure of the Gondwana rift basins as well as the emergence of new extensional structures and marginal reformation. New sedimentary basins created and evolved. A set of linear fluvial to shallow marine basins shaped east and northeast India at length. A basin opened along the present southern margin of the Himalayas and several basins along the west coast. Marginal downwarping of the southeastern coast of India led to the development of what is popularly known as the "east coast Gondwana basins" (Raju et al. 1991). Overlying the Archean Basement and isolated exposers of Upper Gondwana sediments within the Cauvery Basin on the southeast coastline, the Cretaceous succession comprises diverse fossils bearing carbonates, siliciclastics and mixed siliciclastic-carbonate sediments. On the other hand, the Cretaceous sediments within the Kutch Basin on the west coast are entirely siliciclastic. In the western part of Narmada Basin, vastly fossiliferous deposits of Cenomanian-Turonian Bagh Beds grade upwards in the Maastrichtian aged dinosaur eggshell-yielding sandy carbonates known as the Lameta Formation (Bose et al. 1986; Bansal et al. 2018). Central India witnessed a transgression approaching from the west. The Cauvery Basin and the Shillong shelf (northeast India), opened eastward while Kutch Basin opened towards the west (Acharyya and Lahiri 1991; Mandal et al. 2016). Deposits of epicontinental seas occur in the Jaisalmer region of Rajasthan confluent with the Sindhu Sea, traversing Pakistan, and in the northeastern extremity of the Indian plate in Bengal, Assam and Meghalaya (Sahni and Kumar 1974). Early Cretaceous sediments are also reported from the Gondwana rift basins, which were sites of active deposition from Permian to Jurassic. For example, in the Pranhita-Godavari graben (Gangapur Beds) and the Narmada rift zone, marginal basins on the west coast (Umia Beds), Kutch and on the east coast Athgarh Sandstone of Orissa. Early Cretaceous plant-bearing (*Ptilophyllum* flora) Upper Gondwana sediments (Terani Formation) in Cauvery Basin occur as the capping rock of the grabens during the waning and closing phase of Gondwana sedimentation. Largely Fluvio-lacustrine condition prevailed during that terminal Gondwana sedimentation. During the Cretaceous, diverse tectono-sedimentary settings ranged from active margins in a subduction zone-island arc collisional framework operating along the northern (Himalayan) and eastern (Arakan-Yoma) boundaries, extending to the Andaman-Nicobar Islands. Transgressions rushed along reactivated

rifts with the gradual spreading of epicontinental seas in downwarped areas, including continental plate margins. India subducted against Eurasia and Burma, forming island arcs in the Tethys and Indo-Pacific Oceans, which retreated temporarily. Moreover, eustatic changes throughout the period caused climatic and biotic changes. Three major volcanic episodes, encompassing more than 10 Ma, took place in eastern (Rajmahal), northeastern (Sylhet) and western (Deccan) part of India.

In summary, Early Cretaceous marks the end of Gondwana sedimentation represented in the eastern and western peri-cratonic rift basins and partly along the Narmada rift-zone (Biswas 1999). Whereas Late Cretaceous observed widespread Deccan volcanism, the collision of Indian plate with the Eurasian and the Burmese-Indonesian plates, rising of the Himalayas and closing of the Neo-Tethys Ocean (Mukhopadhyay 2010). The end of the Cretaceous suffered the well-known K-Pg (*Cretaceous*-Paleogene) erstwhile K-T (*Cretaceous*-Paleogene) mass-extinction event. The UM Shorengkew section, Meghalaya, established based on planktonic foraminiferal biostratigraphy, is reported with an iridium anomaly across the *Cretaceous*-Paleogene boundary section (Bhandari et al. 1987).

The present review article aims to revisit India during the Cretaceous for paleogeography, sedimentation, climate, sea-level, volcanism, biogeography and K-Pg mass-extinction with updated research data from peninsular, extra-peninsular and coastal part, with a focus on Cauvery Basin (southern India), Kutch Basin (western India) and Narmada Basin (central India). Authors anticipate this attempt would help in understanding the comprehensive status of the Indian sub-continent in the global backdrop during the final segment of the Mesozoic era.

3   Tectonic Orientation of Indian Plate During Cretaceous

The tectonic evolution of the Indian plate represents the longest journey of all drifting continents, about 9000 km in 160 million years (Chatterjee and Scotese 2010), with a sudden acceleration during Cretaceous (20 cm/year during latest Cretaceous at the K-Pg boundary which is maximum of the entire voyage; Chatterjee et al. 2017). The view of the Early Cretaceous paleogeography is: three large continental blocks- North America–Eurasia, South America–Antarctica-India-Madagascar-Australia, and Africa; a large open Pacific Basin; a wide eastern Tethys; and a circum-African Seaway extending from the western Tethys ("Mediterranean") region through the North and South Atlantic into the juvenile Indian Ocean between Madagascar-India and Africa (Hay et al. 1999). During the Early Cretaceous center of the Indian subcontinent was situated at 40°S and was rotated 90° clockwise with respect to the present orientation (Powell et al. 1988). In other words, India's present N-S dimension was oriented 30°–40° eastward (Hallam 1973; Markl 1974; Smith and Briden 1977; Larson 1977; Krishna 1987). The major tectonic detachment (complete) of India from the Gondwanaland was initiated rapidly. It was the second phase of Gondwana breakup history (~130 Ma); when east and west Gondwana separated into two nearly equal halves. In East Gondwana, the "Greater India" sub-continent rifted

away from the western margin of Australia, opening the central Indian Ocean from northeast to southwest by the first phase of seafloor spreading. This well-recognised rifting-volcanism event carved the eastern margin of India, creating the modern coastline (Hay et al. 1981; Khan et al. 2009). India–Sri Lanka rift might be contemporaneous with the separation of India from East Antarctica (Katz 1978; Desa et al. 2006). Apparently, it was a failed rift that was aborted around ~125 Ma. In the third phase of the Gondwana breakup, starting in Late Cretaceous time (118–84 Ma), India drifted away from Madagascar (~90 Ma) with the spreading of the Central Indian Ridge (CIR) and began to drift northward. Therefore, subduction necessarily began to take place between India and Asia to accommodate the northward journey of the Indian plate. Subduction of the Indian plate beneath the Indus Trench would give rise to the Kohistan–Ladakh (KL) oceanic Arc during the Late Cretaceous (Tahirkheli 1979). Combined evidence from geochronology, paleomagnetism, tomographic imaging, and paleontology along the Makran–Indus Suture Zone suggests that India first collided with the Kohistan–Ladakh Arc during the Late Cretaceous. The initial rifting and separation of India from the combined Australia-Antarctica continent took over 30 Ma to produce oceanic crust in the Bay of Bengal and the thinly stretched continental crust subsided to make the basement of the continental shelf. The failed third arm of aulacogen on the eastern passive margin of India acted as loci of paralic-deltaic sedimentation. The western margin of India was finally carved during the late Maastrichtian Deccan volcanism and rifting events, resulting in major hiatus in marine sedimentation at K-Pg boundary. Epicontinental sea of Tethyan margin producing basins of Kutch and Jaisalmer contain deltaic-estuarine sediments, signifying regressive facies, whereas sediment packages of east-coast basins were formed during transgressive phase (Jafar 1996).

4 Cretaceous Sedimentary Basins in India

The Cretaceous Period is represented by widely divergent sediments deposited in the different parts of India, both from outcrop and subsurface. They are widely distributed in the peninsular shield as well as confined to narrow linear belts in the Himalayas. The heterogeneous nature of Cretaceous deposits suggests the prevalence of highly diversified physical conditions in India at the time of their formation (Biswas 1999). Cretaceous rocks are widely preserved within three prime domains of India; the extra peninsula, peninsula and coastal areas (Fig. 1). South India has the best continuous exposure both on the outcrop as well as in the subsurface. Near-complete successions are also reported from Kutch, Meghalaya and NW Himalaya (Mukhopadhyay 2010).

Western and eastern continental margins have continental and offshore deposits. For example, the Cauvery, Palar, Krishna-Godavari, Pranhita-Godavari, Mahanadi basins were formed along the eastern continental margin of the Indian craton when India split away from Australia and Antarctica. Similarly, Kutch, Jaisalmer, Bombay offshore basins are all along the western margin of the Indian subcontinent. All along the periphery of the Indian landmass, deposits are found along different zones.
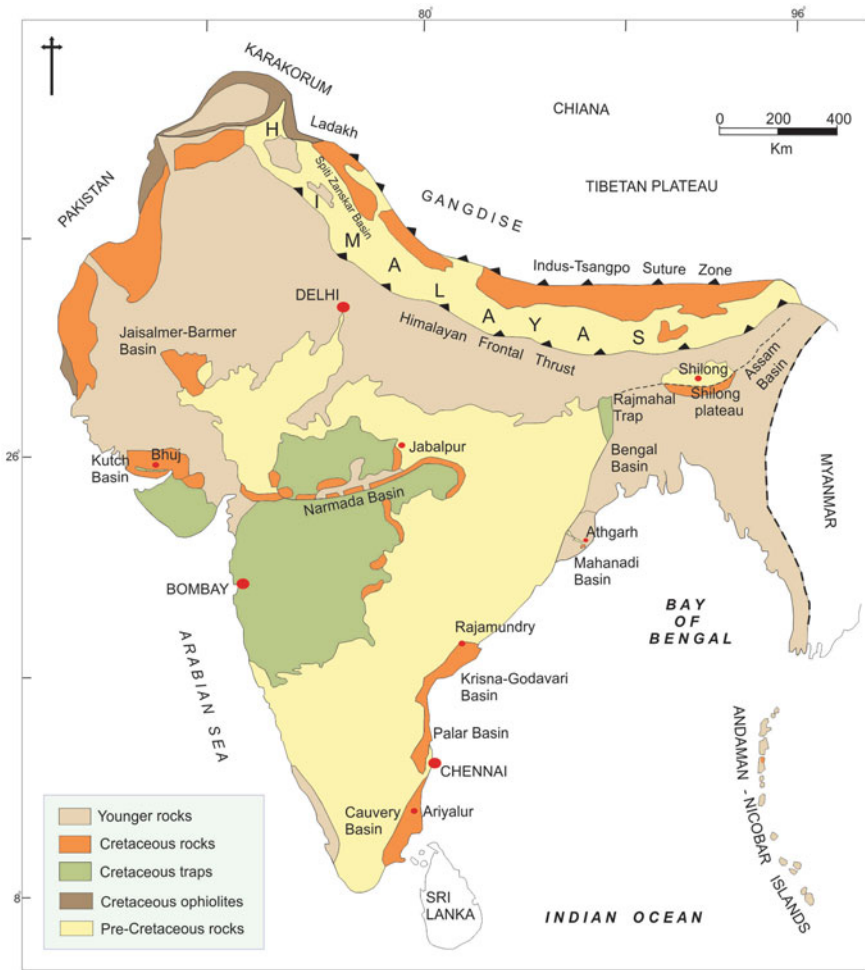
Fig. 1 Distribution of Cretaceous rocks in the Indian sub-continent (after Acharyya and Lahiri 1991)

The Late Cretaceous terrestrial sedimentary deposits occur in two distinctly separate depositional and geographical settings in peninsular India. Besides Cauvery Basin, south India, continental Late Cretaceous sedimentary beds are known to occur in association with the lava flows of Deccan volcanism in central and western India.

4.1 Southern Indian (East–Coast) Basins

Rifting of Gondwanaland during the Mesozoic resulted in the formation of several NE–SW trending basins in the Indian Precambrian crystalline basement along India's east coast (Katz 1978; Li and Powell 2001; Parson and Evans 2005). These newborn Mesozoic basins cut across the NW-trending Permian-Triassic Gondwana grabens (Sastri et al. 1981; Lal et al. 2009). This early extensional faulting during late Jurassic to earliest Cretaceous was followed by a progressive rift that seems to have continued until the end of the Turonian (Watkinson et al. 2007). Barremian to Maastrichtian sediments, along the east coast of South India, are distributed in detached outcrops (basins) parallel to the shoreline from the Gulf of Mannar to Mahanadi Basin. Cretaceous rocks of these basins are often covered by Paleogene sediments. However, the accessible outcrop and subsurface data indicate that these basins are block faulted with several narrow, longitudinal horsts and grabens (Sastri et al. 1981). The coastal areas of Cauvery, Palar, Krishna-Godavari Basin are recognized with Barremian-Aptian Upper Gondwana beds characterized by *Ptilophyllum* flora (Venkatachala 1977; Bose et al. 1990; Rajanikanth et al. 2000).

4.1.1 Cauvery Basin (Tamil Nadu–Pondicherry)

The Cauvery Basin is located in the southeastern part of the Indian peninsula between the latitudes 8°30′N and 12°30′N and longitudes 78°30′E and 80°30′E (Fig. 2a). It encompasses an area of about 25,000 km^2 on land and 30,000 km^2 offshore up to the 200 m isobaths between Pondicherry to the north and Ramanathapuram to the south and extends into the Bay of Bengal and the Gulf of Mannar (Prabhakar and Zutshi 1993; Narasimha Chari et al. 1995). The basin constitutes the southernmost sedimentary basin along the east coast of India (Fig. 2a). Cauvery Basin formed in relation to Late Jurassic-Early Cretaceous fragmentation of Gondwanaland (Powell et al. 1988). It is a NE-SW trending, pericratonic rift basin having a linear geometry with a high length (400 km) to breadth (170 km) ratio (Narasimha Chari et al. 1995). Both the margins of the basin are bounded by basin margin faults. The basin forms a high angle with the east coast margin of India and is underlain by continental crust, which has undergone a tilting during the India-Antarctica fragmentation (Narasimha Chari et al. 1995). The extension was initiated in a NW-SE direction, resulting in rifting along a preexisting older Precambrian lineament (Proto Boundary Fault, PBF) between India and Sri Lanka connecting three triple junction points (Burke and Dewey 1973). The basement faults are generally of the gravity type with a listric character. The horst-graben basin architecture results from normal faults trending parallel to the Precambrian Eastern Ghat trend (NNE-SSW). WNW-ESE and WSW-ENE trending conjugate normal faults further subdivided the Cauvery Basin into multiple sub-basins/grabens/depressions (Fig. 2b; Ramanathan 1968; Sastri et al. 1981). Cretaceous outcrops are mainly exposed in the limestone quarry, pits, and stream sections. Within the Ariyalur-Pondicherry sub-basin there are three
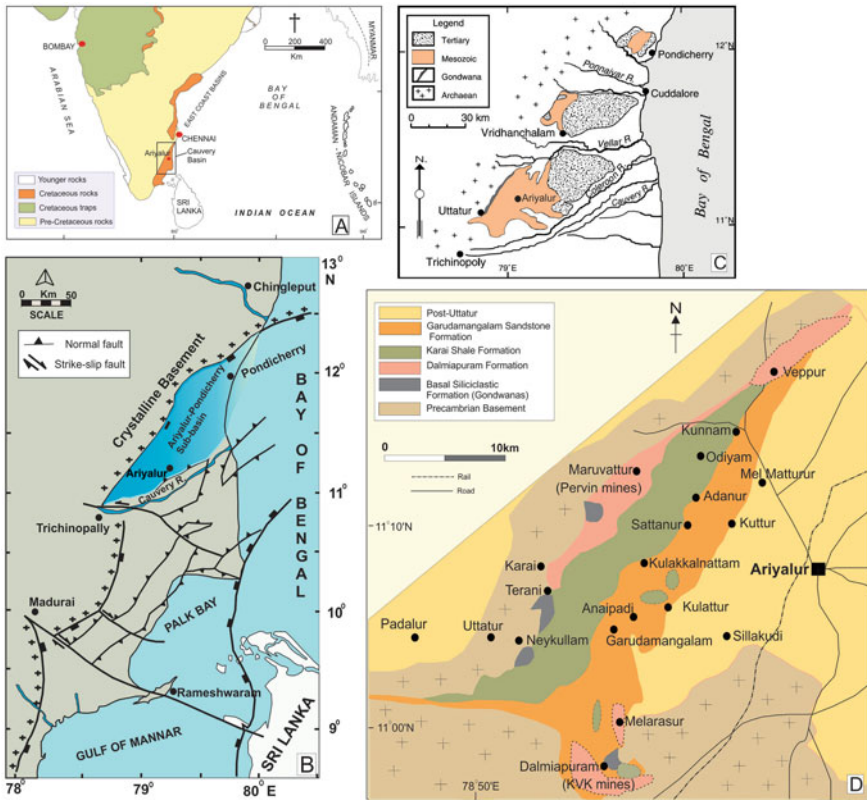
Fig. 2 Geological setting of the Cauvery Basin. **a** Map of southern India showing the position of the Cauvery Basin in the box; **b** Tectonic map of the Cauvery Basin showing the location of Ariyalur-Pondicherry sub-basin (after Sastri et al. 1981); **c** Geological map of the Ariyalur-Pondicherry sub-basin showing the onshore outcrops near Ariyalur, Vridhanchalam and Pondicherry from southwest to north (after Sastry and Rao 1964); **d** Location and lithological map of the study area (after Chakraborty et al. 2018a)

major Mesozoic-Cenozoic outcrops at Pondicherry, Vridhachalam and Ariyalur, as followed from north to southwest (Fig. 2c; Sastry and Rao 1964; Sastri et al. 1981). Among them, the Cretaceous outcrops exposed at the vicinity of Ariyalur district elucidating the Cretaceous geological history (Fig. 2d). Besides, Late Cretaceous outcrop within Cauvery Basin is exposed at Vridhachalam and Pondicherry areas.

The research was initiated on the stratigraphy of Cauvery Basin during the mid-nineteen century. Blanford (1862), Stoliczka (1871) and Kossmat (1897) were the pioneers to propose the geological frame work, stratal architecture and stratigraphical classification of Cretaceous rocks of Cauvery Basin in early 1862. After that, various workers (Tewari and Srivastava 1965; Banerji 1973; Banerji and Sastri 1979; Sundaram and Rao 1979, 1986; Banerji 1982; Chiplonkar 1985; Ramasamy and Banerji 1991) have established major lithostratigraphic units for the Cretaceous

succession in the Cauvery Basin. Foraminifera (Sastry et al. 1968; Banerji 1973; Narayanan 1977; Govindan et al. 1996; Hart et al. 2001), ammonites (Ayyasami and Banerji 1984; Chiplonkar 1985; Ayyasami 1990) and nannofossils (Kale and Phansalkar 1992) have been used for the biostratigraphic zonation and the age determination of these rocks, the majority of which have been published in the Indian literature (some of which can be quite difficult to access). Opinions, in general, amongst the workers vary and a majority of the workers proposed new terms without considering other work. An excess of stratigraphic terms and variable age for the same deposit and continuous use of them in the literature thus generate unnecessary confusion and problem in proper correlation. An approach for a more comprehensive lithostratigraphic classification of these rocks was taken by Sundaram and Rao (1986). Ramasamy and Banerji (1991) attempted a formal definition of lithological characteristics with reference to type localities/sections, though limited to the mid-Cretaceous succession. Tewari et al. (1996) proposed a revised lithostratigraphy for the Cretaceous succession in the Cauvery Basin (Table 1), followed by Watkinson et al. (2007) and Nagendra et al. (2018). However, there is still some scope for lithostratigraphic amendment, discussed in the following sections (Fig. 3).

The Cretaceous–Early Paleocene succession is exposed in the Ariyalur–Pondicherry depression of Cauvery Basin exposed in ca.1200 km^2 in Ariyalur and Perambalur district of Tamilnadu (Sastry and Rao 1964). Resting on Archean Basement in isolated pockets along the western margin of the basin, rocks of the Basal Siliciclastic Formation (Upper Gondwana equivalent) comprises the initial filling of the Cauvery Basin (Banerji 1973, 1982; Tewari et al. 1996; Chakraborty et al. 2017). Within this formation, scree-alluvial fan and channel amalgamation are restricted at the basin-margin while flood-plain presides over in the interior. These non-marine sediments (Barremian-Aptian) are exposed along the faulted block against the Archean basement and are overlain by the marine Uttatur Group, which is fossiliferous. The stratal pattern of fluvial-to-marine transition surface records a sequence boundary (Fig. 4a). The Albian to Coniacian sediments of Uttatur Group are classified into three formations from base to top: Dalmiapuram (shallow water), Karai Shale (offshore) and Garudamangalam Sandstone (marginal marine) with gradational transitions in between them and bounded by an unconformity at the top. However, both the Dalmiapuram and Karai formations show direct contact with the Archean basement in outcrop (Chakraborty and Sarkar 2018; Chakraborty et al. 2018a). The Basal Siliciclastic Formation is terrestrial in origin. Upper Gondwana plant fossils viz. *Ptillophyllum acutifolium, P. cutchense, Taeniopteris spatulata, Taeniopteris* sp., *T. lata, Dioctyozamites* sp., *Sphenopteris* sp., *Cladophlebis indica, Elatocladus plana, E. conferta, Ginkgoites cf. rajmahalensis* etc. are reported from this formation (Ramasamy and Banerji 1991). The depositional contextual shifted from continental to marine during Albian on the advent of first marine transgression along the Cretaceous eastern coast of India. A carbonate (non-rimmed) ramp platform, evolving from homoclinal to distally steepened, shaped the pre-fall shelf by depositing carbonates (Dalmiapuram Formation) while organic-rich glauconite, phosphate nodule bearing shale (Karai Shale Formation) settled in the basin center. Present authors find it irrational to divide the Karai Shale into two members, viz. Odhyium and Kunnam.

Table 1 Lithostratigraphic classification for the Cretaceous succession in the Cauvery Basin proposed by Tewari et al. (1996)

Further, it is necessary to place an unconformity between the Karai Shale and the Garudamangalam Sandstone and assign the Kulakkalnattam Sandstone and the Anaipadi Sandstone two members of Garudamangalam Sandstone Formation. It is also odd to allocate the Garudamangalam Sandstone Formation as Trichinopoly Group (Chakraborty 2016). Dalmiapuram limestone to Karai Shale transition is

Fig. 3 Stratigraphic sub-division (in outcrop and sub-surface) of the Cretaceous succession within the Cauvery Basin (after Tewari et al. 1996 and Govindan et al. 2000)
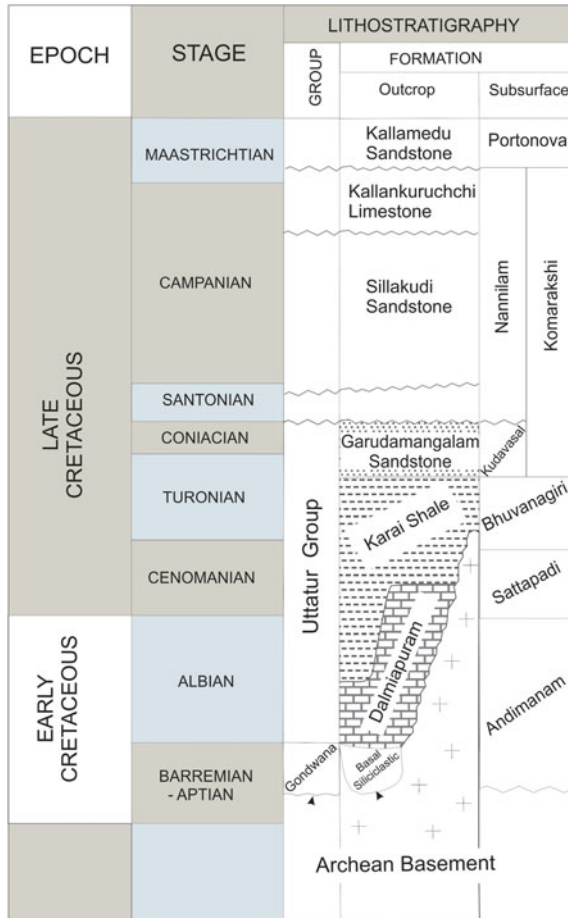
transgressive within a syn-rift tectonic regime. Basin attained its maximum depth during Karai Shale sedimentation and experienced maximum flooding. After that, the basin gradually became shallower and switched to the post-rift system. Karai shale to Garudamangalam Sandstone transitional is distinctly shallowing upward (Fig. 4b). Deposition of Mixed siliciclastic-carbonate Garudamangalam Sandstone took place in the nearshore zone in the presence of a shore-parallel river-mouth bar. The Garudamangalam Sandstone is regressive in character and represents highstand systems tract (Chakraborty et al. 2018b; Sarkar et al. 2014). The contact between the Uttatur Group and the overlying Ariyalur Group is marked by an important hiatus (Sundaram et al. 2001; Watkinson et al. 2007; Nagendra et al. 2011a, b). Ariyalur Group (Campanian-Maastrichtian) is of mixed lithology with abundant fossils. It is sub-divided into three formations: from base to top, they are Sillakkudi Sandstone, Kallankuruchchi Limestone and Kallamedu Sandstone. The base of Sillakudi shows transgressive nature while its upper part may be of deeper shelf origin (Govindan et al.
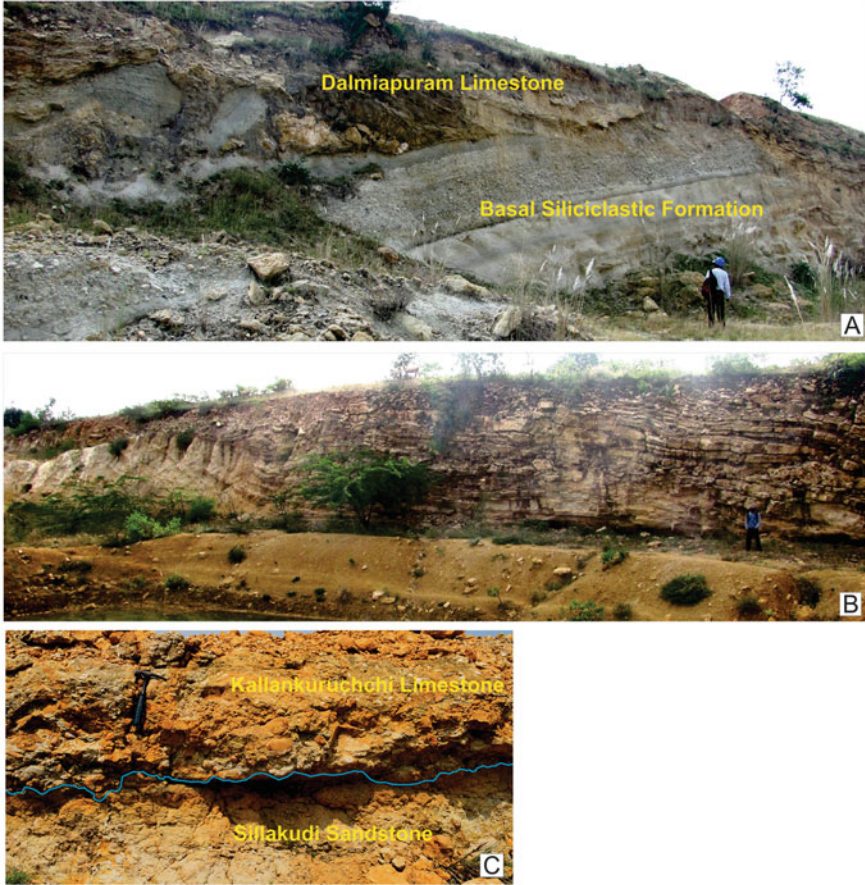
Fig. 4 Field photographs of the Cauvery Basin showing **a** fluvial (Basal Siliciclastic Formation)-to-marine (Dalmiapuram Formation) transition surface recording a sequence boundary; **b** Distinctly shallowing upward nature of the transition from the Karai Shale to the Garudamangalam Sandstone within the Uttatur Group; **c** Kallar conglomerate occurring at the base of the Kallankurichchi Limestone Formation of Ariyalur Group displaying character of transgressive lag

1996; Tewari et al. 1996). At the top of the Sillakkudi Sandstone Formation there is a marked erosion surface and the base of the Kallankurichchi Limestone Formation displays a basal conglomerate (Kallar conglomerate) (Fig. 4c). Maximum flooding is attained again within the Kallankurichchi limestone. The Kallamedu Sandstone is terrestrial (fluvial) and regressive (Watkinson et al. 2007). A major unconformity separates the Cretaceous sequence from Early Paleocene sediments (Niniyur Formation; Danian age).

4.1.2   Palar Basin (Tamil Nadu)

The Palar Basin in Tamil Nadu covers an area of about 18,300 km^2 and it is extending up to Andhra Pradesh and Karnataka. The Cretaceous succession within the basin is represented by the Upper Gondwana sequence comprising Sriperumbudur Formation (Early Cretaceous) followed by Satyavedu Sandstone beds (Late Cretaceous). The Sriperumbudur Formation is characterized by arenaceous and argillaceous rock units comprising splintery green shale, clays and sandstones with plant fossils, ironstone and limestone intercalations, while Satyavedu beds are composed of boulder beds, conglomeratic or fine sandstone (Rajanikanth et al. 2010). Acharyya and Lahiri (1991) observed that the floral and fauna1 assemblage is very similar to those from the Sivaganga Formation (Chakraborty et al. 2017) of the Cauvery Basin.

4.1.3   Krishna–Godavari Basin (Andra Pradesh)

The Krishna–Godavari (KG) Basin, covering coastal areas of Andra Pradesh and extending into the Bay of Bengal, has received much attention in recent times, being one of the most significant petroliferous basins of India, occupying an area of 28,000 km^2 on shore and 24,000–49,000 km^2 off shore. The basin has been classified as a major intra-cratonic rift within the Gondwanaland until the Early Jurassic period and it later transformed into peri–cratonic rift basin (Biswas 1993). It consists of NE-SW trending horst and grabens (Prasad and Jain 1994). The early marine incursion during late Barremian-earliest Aptian in the KG Basin compared to Albian age in Cauvery Basin suggests the opening of the east coast from north to south (Mishra et al. 2020). The Cretaceous succession within this basin comprises the lithounits, namely Gollapali Formation, Raghavapuram Shale, Tirupati Sandstone, Dudukur Limestone and Deccan traps and intertrappeans (Prasad and Pundir 1999). Marine excursion occurred during the deposition of Raghavpuram Shale. Foraminiferal record indicates deep open marine conditions during Aptian-Albian (Raju et al. 1993). Largely, a shallow marginal marine-marine environment is interpreted for the Cretaceous succession within the basin (Prasad and Pundir 1999).

4.1.4   Pranhita–Godavari Basin (Telangana)

The Pranhita–Godavari Basin (PG) is one of the largest Gondwana basins in India, embodying an almost complete succession of Gondwana rocks. The sedimentation took place during and next repeated rift activity. These sediments are exposed in and around the village Gangapur (19°16′N; 79°26′E) in Adilabad District, Telangana, India. The Cretaceous succession is represented by Chikiala Group comprising Gangapur and Chikiala formations in Central Godavari Valley and Gollapali Formation, Raghavapuram Shale, Tirupati Sandstone in the coastal Godavari Valley (Sengupta 2003). Sedimentological and faunal evidence indicate the following: marginal marine inundation during deposition of the basal Gollapilli Sandstone in

the coastal Godavari area, deposition of Raghavapuram Mudstone in a large embayment, environmental fluctuation from 'deep central bay, neritic to open gulf type', the reestablishment of a continental environment depositing the Tirupati Sandstone (Baksi 1977).

4.1.5 Mahanadi Basin (Orissa)

The Mahanadi Basin, evolved during rifting and breakup of Gondwana Land, covers a total area of 55,000 km^2, out of which about 14,000 km^2 lies in the shallow offshore area. Tectonically, Mahanadi graben represents a failed arm (aulacogen) of linked triple rift junctions related to the Gondwana breakup. The Cretaceous succession within this basin is represented by Athgarh Sandstone, trap basalts and intertrappeans (black carbonaceous shale, claystone interbeds). The Athgarh sub-basin is exposed to the north, northwest and southwest of Cuttack and Bhubaneswar city and covers an area of about 800 km^2 in the districts of Cuttack and Khurda with an estimated thickness of 400 m (Kumar and Bhandari 1973) is exposed to the north northwest and southeast of Cuttack and Bhubaneswar covering an area of about 800 km^2. The Oldest exposed sediments in onshore part of Mahanadi Basin belong to Athgarh Sandstone Formation of late Jurassic age. These sediments, directly unconformably overlying the Precambrian basement (Eastern Ghat granulites) along the western basin margin, comprise conglomerate, pebbly sandstone with intercalation of carbonaceous shale and clay. These sediments have been inferred to be deposited under fluvial conditions (Goswami et al. 2010). The Athgarh Sandstone contains a mega floral assemblage of Upper Gondwana affinity (Acharyya and Lahiri 1991; Goswami et al. 2010).

4.2 Western Indian Basins

4.2.1 Kutch Basin (Gujarat)

The Kutch Basin is situated in the westernmost part of the Indian subcontinent within Kutch district, Gujarat (22°305′N–24°30′N and 68°E–71°23′E). It is a pericratonic rift basin, initiated as a consequence of Gondwanaland breakup during the late Triassic and possesses ~3000 m thick sediments ranging in age from the Late Triassic to Early Cretaceous spreading over around 45,600 Km^2 (Biswas 1977, 1981, 1991). The Mesozoic sedimentary succession of this basin is underlain and overlain by the Precambrian Basement and the Deccan Traps (Late Cretaceous–Early Paleogene), respectively. However, in the northeastern and eastern part of the Mainland, the Mesozoic sediments are unconformably overlain by the Paleogene sediments (Biswas 1977) and at places by alluvium. The Mesozoic sediments outcrop in Kutch Mainland Uplift (KMU) defined by three east-west trending fault-bounded anticlinal ranges and in an isolated area at Wagad Uplift (WU). Apart from the Mainland the Mesozoic exposures, observed in four isolated landmasses viz. Pachchham

Uplift (PU), Khadir Uplift (KU), Bela Uplift (BU) and Chorad Uplift (CU), are surrounded by vast plains remaining submerged under water during monsoon and hence have been described as "islands" (Fig. 5; Biswas 1987, 2005). The Kateser Member (topmost unit of the Jhuran Formation) and Bhuj Formation (topmost unit of Mesozoic-Group) represent the Cretaceous sediments of the Kutch Basin (Biswas 1977). Good exposers of the Katesar Member are reached in the northwestern part of the Kutch Mainland; the river section exposed in the south of Sahera (23°47′15″: 68°55′45″) being designated as the type section. The Bhuj Formation is very well exposed from Ghuneri (East) to Bachau (West) within Kutch Mainland (Fig. 5). The Rukmawati River section (from 23°06′44″N; 69°26′43″E (~7 km east of Dahisara) comprising an almost complete succession, is the type section for Bhuj Formation (Biswas 1977). The geology of Kutch has been investigated by geoscientists for sedimentology, paleontology, ichnology, sediment geochemistry etc. (Howard and Singh 1985; Shukla and Singh 1990; Singh and Shukla 1991; Fürsich and Pandey 2003;
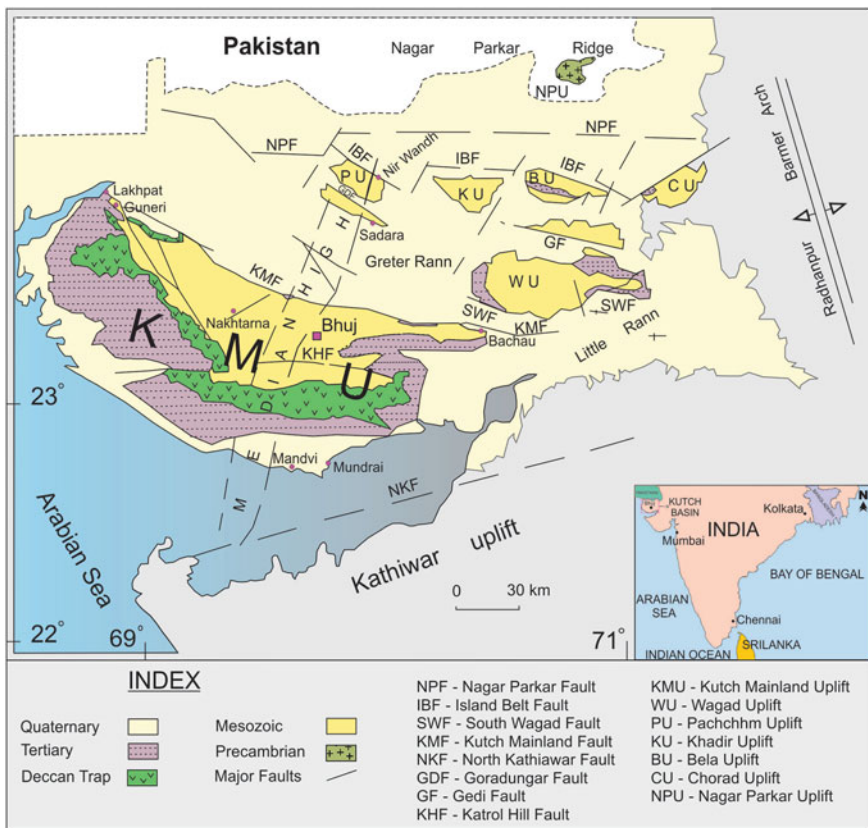
Fig. 5 Structural map of the Kutch Basin showing five major E-W trending faults (NPF, IBF, SWF, KMF and NKF) having major control on basin geomorphology (after Biswas 2005)

Desai 2013; Arora et al. 2015, 2017; Mandal 2017; Bansal et al. 2017; Chaudhuri et al. 2018, 2020a, b, c, d; Sarkar and Koner 2020; Banerjee et al. 2020). This basin, due to its hydrocarbon potential, has sought attention from oil scientists too (Biswas 1977, 1981, 1991).

The Kutch Basin formed as a segment of an embayment extending from the southern margin of Tethys to the SE direction during the Jurassic Period. The basin evolved as a result of successive rifting and recurrent movements along Precambrian tectonic trends. Following the separation from the Gondwanaland in the Late Triassic-Early Jurassic time, the basin opened up (responding to block subsidence) during the early stages of India's northward drift away from Gondwanaland (Biswas 1982, 1987, 1991). The graben was entirely covered by marine sediments during Middle Jurassic and sedimentation completed by Early Cretaceous (Biswas 1987). The basin is characterized by highlands, which are the areas of uplift and the plains (Biswas 1977). The uplifted parts are oriented E-W along five principal faults named as Nagar Parkar Fault (NPF), Island Belt Fault (IBF), South Wagad Fault (SWF), Kutch Mainland Fault (KMF) and North Kathiawar Fault (NKF) (Fig. 5; Biswas 1987). The basin platform dips (depositional slope) towards the southwest, the direction in which the embayment opens up. The platform topography was controlled by N-S-oriented Median High across parallel fault ridges demarcating the hinge zone passing through the central part of the basin and showing a perpendicular relationship with the depositional axis. The Precambrian terrain now exposed in Rajasthan, Gujarat and Pakistan defines the margins of the basin (Biswas 1987).

Stratigraphy of Kutch Basin had been addressed since long back (Wynne 1872; Waagen 1875; Spath 1924, 1927–33; Rajnath 1932; Pascoe 1959; Biswas 1977, 1981, 1991; Krishna 1987). Initially, Kutch sediments were sub-divided into two parts: lower marine unit (Early Jurassic) and upper non-marine unit (late Jurassic) based on lithostratigraphy with no identification of the Cretaceous rocks separately (Wynne 1872). Based on mineralogical and paleontological characteristics, Stoliczka (unpublished) proposed first four-fold classification for the Jurassic sediments comprising Patcham, Chari, Katrol and Umia "Groups" from base to top. Later Waagen (1875) accepted the four-fold classification scheme and further emphasized it by demarcating those units as 'ammonite assemblage zones' and assigned their ages (Patcham Group-Bathonian, Chari and Early Katrol Group-Oxfordian, Upper Katrol Group-Kimmeridgian and Umia Group-Tithonian). This classification scheme was followed by several paleontologists (Table 2, Fig. 6; Spath 1924, 1927–33; Rajnath 1932; Pascoe 1959; Krishna 1987). The pioneer workers among them was Spath (1924, 1927–33), subdividing those units into ammonite zones: Macrocephalus "Beds", Rehmani "Beds", and Anceps "Beds" etc. Later, Rajnath (1932) described 26 beds from Chari and Patcham series, redefined Umia Series and introduced a fifth unit by naming Bhuj Series, placing it on top of Umia. The "Middle Cretaceous" Bhuj "Stage" was introduced and characterized by non-marine deposit bearing plant fossils by Rajnath (1932) and adopted by many workers with minor modifications. Later, Krishna (1987) re-introduced the earlier four-fold classification, including Rajnath's Bhuj Series as 'Bhuj Member' within Umia Formation (Table 2). Mitra and Ghosh

Table 2 Lithostratigraphic classification of Mesozoic of Kutch (based on Spath 1927–33; Rajnath 1932; Krishna 1987)

Age	Spath (1927–33)	Rajnath (1932)	Krishna (1987)		
Upper Tithonian to Upper Albian	Not recognized	Bhuj series	Umia Formation	Bhuj Member	Mainly sandstone
		Umia series		Ukra Member	Mainly shale and sandstone with oolites and glauconites
				Ghuneri Member	Mainly sandstones and shale alternations
	Umia series			Umia Member	Mainly marls with oolites and glauconites
Kimmeridgian to Upper Tithonian	Katrol series	Katrol series	Katrol Formation	Mainly sandstone above and shales below	
Upper Bathonian to Oxfordian	Chari series	Chari series	Chari Formation	Mainly shales with hard ooliticlimestones bands	
Bajocian to Upper Bathonian	Patcham series	Patcham series	Patcham Formation		
Lt. Upper Triassic to Lower Jurassic	Not recognized	Not recognized	Unnamed unit	Mainly sandstone and limestones with shale interbeds (max. limestone in this unit)	
				Mainly sandstone	
Precambrian basements					

(1964) published a biostratigraphic map based on Waagen (1875) considering assemblage zones, instead of ammonite index fossil. Biswas (1971, 1977) introduced the first lithostratigraphic classification (considering the international code for stratigraphic classification—1972) with full description and intra-basinal correlation. This classification proposed four formations within Kutch Mainland, formally named as Jhurio, Jumara, Jhuran and Bhuj in ascending order (Fig. 6). Moreover, the Bhuj Formation, exclusively exposed within Kutch Mainland, is sub-divided into three members: Ghuneri/Lower Member, Ukra Member and Upper Member. Ukra Member laterally pinches out towards the eastern part of the basin, where the Lower Member is directly overlain by the Upper Member (Fig. 6).

The Katesar Member (uppermost unit of Jhuran Formation) consists of greenish-grey to yellow, internally massive to cross-bedded sandstone with minor intercalation of shales and fossiliferous hard calcareous bands of lenticular shape (Biswas 1977). The Katesar member, identified as delta front sequence, is preserved only in the NW part of Kutch Mainland (Biswas 1977). Maine body fossils like *Trigonia* and *Astarte*

AGE	FORMATION	MEMBER	LITHLOGY
		DECCAN VOLCANICS	
NEOCOMIAN-ALBIAN	BHUJ	UPPER	CROSS BEDDED SANDSTONE WITH KAOLINITIC CLAYSTONE BEDS AND SANDY IRONSRONE BANDS
		UKRA	DEVELOPED ONLY IN WEST GLAUCONITIC SANDSTONE AND SHALES,FOSSILIFEROUS
		GHUNERI OR LOWER	RHYTHMIC SEQUENCE OF SANDSTONE-SHALE-IRONSTONE BANDS ABUNDANT,PLANT FOSSILS
		DISCONFORMITY	
KIMMERIDGIAN TO TITHONIAN	JHURAN	KATESAR	CROSS BEBED SANDSTONE WITH CALC,BANDS LOCALLY FOSSILIFEROUS,DEVELOPED IN WEST ONLY
		UPPER	THINLY BEDDED SANDSTONES CALCAREOUS, FOSSILIFEROUS
		MIDDLE	MAINLY SHALES FOSSILIFEROUS
		LOWER	SHALES SANDSTONE ALTERATION, FOSSILIFEROUS
OXFOR DIAN		*DISCONFORMITY*	
CALLOVIAN	JUMARA	DHOSA OOLITE	SHALES WIT OOLITIC LIMESTONE BANDS, FOSSIL
		MIDDLE	SANDSTONE IN THE EAST, LIMESTONE WITH GOLDEN OOLITE IN THE WEST
		LOWER	OLIVE GREEN SHALES, FOSSILIFEROUS
BATHONIAN	JHURIO	UPPER	BEDDED LIMESTONE
		MIDDLE	SHALE INTERBEDDED WITH GOLDEN OOLITIC LIMESTONE
		LOWER	INTERBEDDED LIMESTONE SHALES
		PRECAMBRIAN BASEMENT	

Fig. 6 Lithostratigraphic classification for the Mesozoic succession in the Kutch Basin proposed by Biswas (1971, 1977)

are preserved within a band near the top of this member (just beside the village Umia), demarcating the contact with the overlying Bhuj Formation (Biswas 1977). The paleogeographic information regarding the Bhuj Formation is scanty and sketchy. The Bhuj Formation is dominantly composed of sandstone, subordinate shale and rarely extra-clastic conglomerate (confined almost exclusively to its unconformable base). The Bhuj Formation overlies a markedly incised unconformity on top of the Jhuran Formation (Fig. 7a) and is, in turn, overlain by the Deccan trap and/or the Paleogene rocks (Fig. 7b; Biswas 1977). Bhuj Formation was deposited in a fluvial environment

Fig. 7 Field photographs of Kutch Basin showing **a** Jhuran Formation disconformably overlain by the Bhuj Formation. Note the irregular contact between them (red solid line), very sharp everywhere and often deeply incised (maximum incision depth 8 m for scale); **b** The Bhuj Formation unconformably overlain by the Deccan trap (marked by red line)

mostly, except in the western part of its inland exposure (Biswas 1977, 1981, 1991; Bose et al. 1986, 1988). Several researchers considered the Formation entirely of marine origin based on nano fossils assemblages, trace fossils and sedimentary structures (Howard and Singh 1985; Shukla and Singh 1990). On the other hand, Biswas (1977, 1981, 1991) and Mahender (2012) recognized two fluvial intervals within the Bhuj Formation. Mandal et al. (2016) and Sarkar and Koner (2020), however, identified both marine and fluvial deposits within the Bhuj Formation. The Aptian marine incursion (following the deposition of Lower Member of Bhuj Formation) inundated the Kutch Mainland, not only its western part but also the vast area of the Kutch Mainland (up to Nadapa, 30 km NW from Bhuj). This marine interval at top of the Lower Member/Ukra Member, separated two fluvial deposits reported from the base of the Lower Member and the Upper Member (Mandal et al. 2016; Mandal 2017). In the easternmost part of the basin, the two fluvial units are juxtaposed to each other as the marine interval pinched out towards the east. From the fluvial architectural study, it has been concluded that the lower fluvial unit bears more meandering component than the upper fluvial (Mandal et al. 2016). The marine unit, along the paleo shoreline, comprises a beach-shoreface complex, a tidal delta complex and an estuary complex with tributary fluvial inputs (Mandal et al. 2016; Mandal 2017). Abundant marine body fossils like ammonites and pelycypods are reported from Ghuneri (NW of the Mainland) and restricted within the Ukra member (Biswas 1977). Continuous

Mesozoic sedimentation is terminated by Deccan lava flow at the end of Albian (Biswas 1977).

4.2.2 Jaisalmer-Barmer Basin (Rajasthan)

Jaisalmer basin is a pericratonic basin that deepens to southwest and lies on northwestern slope of Jaisalmer Mari basement arch. The basin is characterized by the eastern shelf part of the large Indus basin with a thick sedimentary sequence. The outcrop sections are similar to those of the Kutch shelf (Acharyya and Lahiri 1991). Among the Mesozoic rocks exposed in Jaisalmer Basin, sediments are represented by Pariwar, Habur, Goru and Parh formations. Pariwar Formation, unconformably underlain by the marine Bhadasar Formation of Tithonian age, is characterized by calcareous, glauconitic and arkosic sandstone, siltstone and clay. The overlying Habur Formation is composed dominantly of calcareous sandstone, limestone, sandy marl and marl bands with interfingering coquina beds (Dasgupta 1975). Goru Formation has only been designated from subsurface data. The lithology consists of a succession of shales and sandstones, often glauconitic with high clay content. These three formations deposited in a shallow marine condition. Sediments of Parh Formation consist mainly of limestone and marl. An open marine environment has been inferred for the deposition of this formation (Dasgupta 1975).

The Barmer Basin is the northernmost basin of a series of rifts that comprise the West Indian Rift System, likely to be contemporary with rifting between Madagascar and India (Dolson et al. 2015; Reeves 2014). Ghaggar-Hakra Formation of fluvial origin is exposed on the central-eastern margin of the Barmer Basin (Beaumont et al. 2018). In spite of occurrence in small outcrops around Sarnoo, the Ghaggar-Hakra Formation is regionally significant for documenting intraplate continental deposition during the early breakup of India from Gondwana. It has been reported that, the Ghaggar-Hakra Formation is likely to be the time and depositional-equivalent of the Early Cretaceous fluvial Himatnagar Sandstone of the Cambay Basin (Mukherjee 1983; Mohan 1995; Bhatt et al. 2016), the fluvial to marine Nimar Sandstone of the Narmada Basin (Ahmad and Akhtar 1990), the fluvial to coastal and deltaic Bhuj Formation of the Kutch Basin (Biswas 1987; Mandal et al. 2016) and the predominantly fluvial Dhrangadhra Group of the Than Basin in Saurasthra (Casshyap and Aslam 1992).

4.3 Eastern Indian Basins

4.3.1 Bengal-Assam Basin (West Bengal-Assam-Manipur-Nagaland)

Bengal and Assam Basins are located in the eastern part of the Indian craton where Cretaceous deposits are masked by a thick cover of Cenozoic sediments. The hydrocarbon well cores and cutting samples attributes the Cretaceous geology. The basin

is widespread, covering the plains of Bangladesh and West Bengal, and continues southward below the Bay of Bengal up to the Indian Ocean. Continental sediments with upper Gondwana flora are exposed on the surface or at shallow depths as the infratrappean Dubrajpur Formation (sandstone in lithology) and as intertrappean beds within the Rajmahal Trap basalt near the western margin of the Bengal Basin (Acharyya and Lahiri 1991). The oldest marine sediments encountered in the subsurface Bengal Basin of central West Bengal (Mishra and Singh 1997) belong to the Dhananjaypur Formation of Campanian age, assigned on the basis of planktonic foraminifera. The Formation unconformably rests on the Rajmahal Traps and are themselves overlain by the lateritic and ferruginous sandy beds of the Bolpur Formation doubtfully assigned in the lack of age diagnostic microfossils as Maastrichtian age. Bolpur and Ghatal formations consist of sandstone and shale alternations. In southwest Bengal Basin, the Early Cretaceous deposits are represented by the traps and intertrappeans overlain by the Late Cretaceous Blur and Ghana formations of the continental-brackish environment (Mukhopadhyay 2010).

Cretaceous sediments are not well exposed in the Assam Basin. On the south of the Shillong shelf, the basal Jadukata Formation comprises conglomerate often intercalated with sandstone and the overlying Mahadek Formation consist of a thick pile of glauconitic sandstones with locally developed calcareous fossiliferous horizons. The Assam-Arakan mountain range marking the eastern fringe of Bengal Basin contains Cretaceous rocks in the Disang Shale (approx. 3000 m, Late Cretaceous-Eocene) in Assam-Manipur-Nagaland region. Evans (1932) considered that the Disangs of Assam-Manipur-Nagaland and the Cretaceous-Eocene marine rocks at the southern parts of the Shillong plateau represent the geosynclinals and shelf facies of the Bengal Basin, respectively. In Meghalaya region, the Cretaceous rocks are distributed in different parts (Bhattacharya and Bhattacharya 1987). The Sylhet Trap Formation (Medlicott 1871) occurs discontinuously along the plateau margin fault in Kasi Hills and serves as the basement for the Late Cretaceous marine rocks in areas south of the Shillong Plateau.

4.3.2 Andaman Basin

The Andaman Basin is an area of 800,000 km^2 separated from the Bay of Bengal by the Andaman-Nicobar Ridge (Rodolfo 1969). Over 3000 m of sediments, ranging from Cretaceous to recent, are exposed. In the southern part of the south Andaman Islands, the igneous sequence is overlain by conglomerate and grit of the Late Cretaceous age. The conglomerate and grit are overlain by a thick pile of turbidities of Eocene-Oligocene age (Karunakaran et al. 1964a, b, 1968). However, Bandopadhyay and Carter (2017) mentioned in the updated stratigraphy that the Late Cretaceous to Paleocene succession is represented by Ophiolite group of rocks incorporating muddy carbonate, mudstone, and tuffaceous siltstone apart from other components.

4.4   Central Indian Basin

4.4.1   Narmada Basin (Madhya Pradesh)

The Mesozoic stratigraphy of the Narmada valley in central India comprises Bagh Group, Lameta Formation, Deccan Volcanics and intertrappeans. Unconformably overlying the Precambrian basement, the Bagh Group and the Lameta Formation are also referred to as infra-trappeans (Merh 1995). These two stratigraphic units, exposed as isolated patches along the Narmada region of central India, have received considerable attention for preserving the Late Cretaceous depositional history at the eastern margin of Tethys (Singh et al. 1983; Biswas 1987; Ahmad and Akhtar 1990; Srivastava and Mankar 2012, 2015; Bhattacharya and Jha 2014; Jha et al. 2017; Bansal et al. 2019, 2020). The sediments were deposited along a linear basin trending WSW-ENE, that opened westward.

The epicontinental seaway along the Narmada region formed during the Late Cretaceous global sea level rise during the northward journey of India after the breakup of Gondwana supercontinent (Tandon 2002). Although the stratigraphy of the Bagh Group has been debated over the years, the three-fold classification by Jaitley and Ajane (2013) is most widely used, according to which the Bagh Group is divided into Nimar Sandstone, Nodular Limestone and Coralline Limestone formations. Ruidas et al. (2018) used the Jaitley and Ajane (2013) classification with a modification of 'Bryozoan Limestone' in place of 'Coralline Limestone', as corals are rare within the Formation. The early, siliciclastic-dominated portion of the Bagh Group is known as the Nimar Sandstone Formation. The upper part of the Bagh Group is dominated by carbonates, consisting of Nodular Limestone and Bryozoan Limestone formations (Tandon 2000, 2002; Ruidas et al. 2018, 2020; Bansal et al. 2020). The biostratigraphy of the Bagh Group and the Lameta Formation is debated much in research records. However, recent ammonite biostratigraphic investigation confirms Cenomanian, Turonian and Coniacian ages for Nimar, Nodular Limestone and Bryozoan Limestone formations, respectively (Kumar et al. 2018). We present the salient depositional characteristics of the Upper Cretaceous deposit in the Narmada region, particularly focusing the major transgressive deposits formed during global sea-level rise during the Late Cretaceous.

Resting directly on the Precambrian basement, the thickness of the Nimar Formation varies from 15 to 150 m (Ahmad and Akhtar 1990). The early part of the Nimar Formation, consisting of conglomerate, pebbly and coarse-grained sandstone represents continental deposit (Fig. 8a). The middle and upper parts of the Nimar Formation exhibit a transgressive trend, recording a paleogeographic shift from the fluvial to storm- and tide-dominated shallow marine shelf through a mixed tidal-fluvial estuarine setting (Bose and Das 1986; Ahmad and Akhtar 1990; Bhattacharya and Jha 2014; Jha et al. 2017). Although greenish sandstone occurs within the marine-originated Nimar Formation, the presence of glauconite is yet to be confirmed (Fig. 8b).
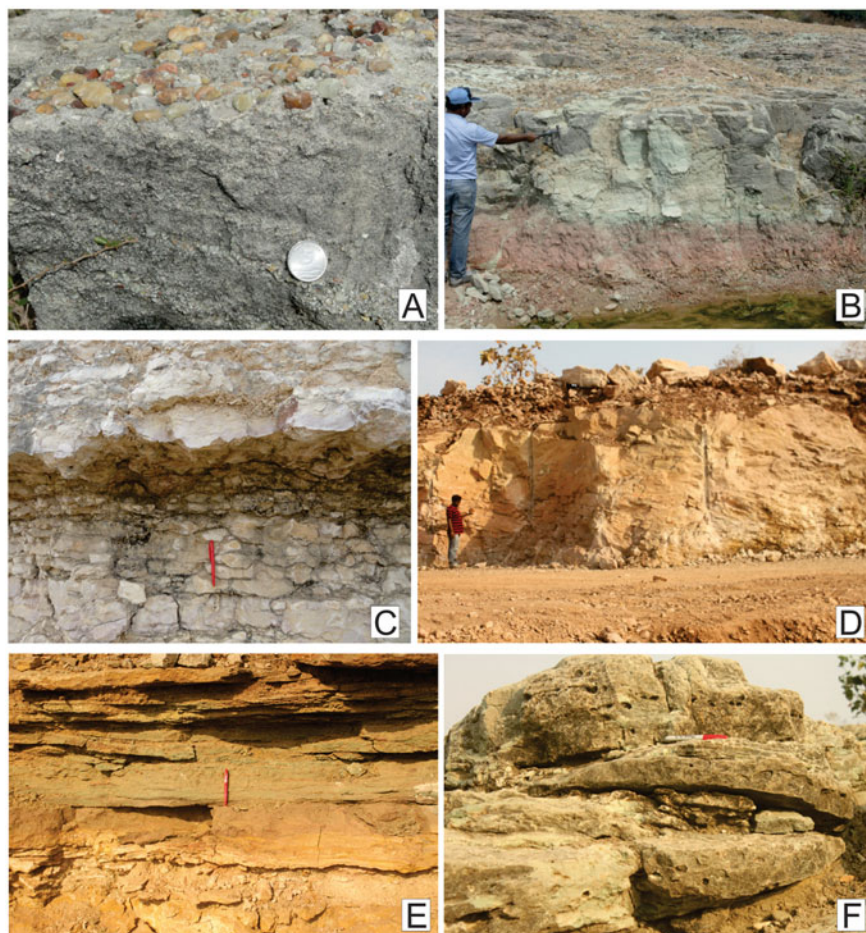
Fig. 8 Field photographs showing vertical sections of **a** Conglomerate and pebbly sandstone within the Nimar Formation; **b** Fine-grained, green sandstone within the Nimar Formation (indicated by the hammer); **c** Nodular beds; **d** Cross-stratified grainstone beds within the Bryozoan Limestone; **e** Glauconite bed within the Bryozoan Limestone; **f** Cross-stratified Lameta Formation (pen length = 14 cm, hammer length = 38 cm, coin diameter = 2.4 cm)

Conformably overlying the Nimar Formation, the Nodular Limestone (av. thickness 7 m) indicates the growth of a carbonate platform in the Narmada region. The constituent facies of the Nodular Limestone are dominated by mudstone and wackestone (Fig. 8c). The dominance of lime mudstone within the Nodular Limestone Formation indicates a low-energy depositional setting (Ruidas et al. 2018, 2020). The prolonged subaerial exposure leads to the formation of abundant pedogenic features, including root-related structures (rhizoliths), vadose silts and pisoids. The presence of conspicuous nodules within the Nodular Limestone possibly reflects the pedogenic modification, driven by root activities (Ruidas et al. 2020). Detailed

facies study infers supratidal and upper intertidal origin of the Nodular Limestone Formation (Ruidas et al. 2020).

In contrary to the fine-grained nature of the Nodular Limestone, the overlying Bryozoan Limestone Formation is coarse-grained, consisting primarily of packstone and grainstone. The thickness of the Bryozoan Limestone Formation varies from a few cm to ~5 m. A cross-stratified rudstone, occurring at the bottom part, suggests an increase in energy condition (Fig. 8d). Petrographic investigation reveals calcification, in situ brecciation, rhizoliths, alveolar-septal texture and circum granular cracks, indicating extensive meteoric diagenetic modification of the limestone (Ruidas et al. 2020). Facies study reveals early intertidal depositional conditions for the Bryozoan Limestone. A planar laminated rudstone at the top of the Bryozoan Limestone contains a glauconite bed (average thickness ~50 cm) along with abundant clastics, including quartz, feldspars and mud fragments (Fig. 8e). Bansal et al. (2020) found that similar glauconite is equivocal of Upper Cretaceous transgressive deposits in the paleo-Tethyan domain. Glauconite possibly formed exclusively in shallow hypoxic seas during the Upper Cretaceous time (see Bansal et al. 2020 and references therein).

The Late Cretaceous Lameta Formation has received the attention of many researchers for its rich faunal assemblage, which include dinosaurs, and other vertebrate fossils and palynomorphs. The lithological characteristics of the Lameta Formation (4–5 m thick) differ significantly from western to central India, varying from arenaceous, argillaceous and calcareous sandstone to arenaceous limestone (Tandon 2000). Ahmad and Akhtar (1990) reported a conformable transition from the Bagh Group to the Lameta Formation. However, Tandon et al. (1995) found an unconformable relationship between these stratigraphic units. Although the Lameta Formation underlies the Deccan Traps near Phutlibaori (southwest of Indore), it is contemporaneous with Deccan volcanics around Jabalpur (Tandon 2000). The outcrops of Lameta Formation occur in six inland basins in central and western India, viz. Nand-Dongargaon, Jabalpur, Balasinor-Jhabua, Ambikapur-Amarkantak, Sagar, and Salbardi-Belkhar inland (Srivastava et al. 2018). Larger outcrops display continental deposits, containing nests and remains of dinosaur fossils (Srivastava and Mankar 2015; Mankar and Srivastava 2015). Srivastava and Mankar (2012) reported brownish to greenish grey claystone, greenish sandstone, nodular beds and calcrete horizons within the Lameta Formation. At in Salbardi and Belkher areas inferred Lameta sediments are of fluvial and lacustrine origin. The depositional environment varied from shallow estuarine in the west (near Phutlibaori) to continental in the east (Jabalpur) (Tandon 2000; Bansal et al. 2020).

The Lameta Formation around Phutlibaori region comprises greenish, medium- to coarse-grained, internally cross-stratified, well-sorted sandstone containing glauconites. The set thickness of cross-stratification may be as high as 1 m in the early part, which decreases upward (Fig. 8f). The sandstone is bioclast-rich arkose and cemented by carbonates. The content of glauconite varies from 10 to 20% of the total sediment (Bansal et al. 2018). The occurrence of shark teeth, oyster and wood logs within the sandstones of the Lameta Formation around Phutlibaori region indicate a marginal marine depositional environment. The sedimentation possibly took

place in an E-W-oriented estuary, with progressive fluvial influence toward the east (Tandon 2000; Bansal et al. 2018). The glauconitic shallow marine and estuarine sediments of the Lameta Formation record the Maastrichtian sea level rise.

4.5 Northern Indian Basins

4.5.1 Himalayan Belt (Zanskar-Spiti-Kinnaur)

In India, the Himalayan orogenic belt extends from Kashmir in the west to Arunachal Pradesh in the east. Exposer of Cretaceous rocks and records of Cretaceous events constitute essential components of the belt. In the Himalayan domain, the late Jurassic sedimentary cycle continued uninterrupted into the Early Cretaceous, whereas the Late Cretaceous sedimentary cycle continued into the Paleogene (Mukhopadhyay 2010). In the Tethyan Belt of the Higher Himalayas (Zanskar-Spiti-Kinnaur), the Cretaceous succession is represented by Guimal and chikkim Formation overlying Spiti Formation of Jurassic age. Early Cretaceous sedimentation took place during a regressive phase depositing littoral Guimal Sandstone Formation comprising sandstone, glauconitic sandstone, silty sandstone, calcareous shale, gritty sandstone with a few pebbles. The sandstone of Guimal Formation is interpreted as proximal turbidities in Uttrakhand (Kumar et al. 1977) and Zanskar (Gaetani et al. 1983, 1986), and a shallow marine deposit in Spiti (Bhargava 2008). The Chikkim Formation of Late Cretaceous age conformably rests over the Giumal Formation. This formation is composed of limestone at the lower part representing sedimentation in shelf to the basinal environment with occasional periods of restricted circulation. The upper part of the formation is dominated by shale of outer shelf origin (Bhargava 2008).

5 Climatic Trends in India During the Cretaceous

The reconstruction of plaeoclimatic history and paleogeography of the Indian plate during the late Paleozoic-early Mesozoic is significant because of the location of India in the southern hemisphere (Clarke and Jenkyns 1999; Wilson and Norris 2001; Huber et al. 2002; Price and Hart 2002; Petrizzo and Huber 2006). Zakharov et al. (2011) studied the Paleotemperatures for the Cretaceous of India resolute on the basis of oxygen isotopic analysis of well-preserved Albian belemnite rostra and Maastrichtian bivalve shells from the Ariyalur district, southern India (Trichinopoly). The Albian (possibly late Albian) paleotemperatures for Ariyalur district are inferred to range from 14.9 to 18.5 °C for the epipelagic zone, and from 14.3 to 15.9 °C for the mesopelagic zone. Isotopic paleotemperatures interpreted as summer and winter values for near-bottom shelf waters in this area fluctuate from 16.3 to 18.5 °C and from 14.9 to 16.1 °C, respectively. These paleotemperature data are similar to those calculated from isotopic composition of middle Albian belemnites of the

middle latitude area of Pas-de-Calais in northern hemisphere but significantly higher than those calculated from isotopic composition of Albian belemnites from southern Argentina and the Antarctic and middle Albian belemnites of Australia located within the warm-temperate climatic zone. Isotope analysis of early Albian cephalopods from Madagascar shows higher paleotemperatures for summer near-bottom shelf waters (20.2–21.6 °C) in comparison with late Albian paleotemperatures calculated from southern India fossils, but similar winter values (13.3–16.4 °C); however, the latter values are higher than those calculated from early Albian ammonoids of the tropical-subtropical climatic zone of the high latitude area of southern Alaska and the Koryak Upland. The new isotopic paleotemperature data suggest that southern India and Madagascar were located apparently in middle latitudes (within the tropical-subtropical climatic zone) during Albian time. In contrast to the Albian fossils, isotope results of well-preserved early Maastrichtian bivalve shells from the Ariyalur Group are characterized by low ^{18}O values (up to −5.8) but normal $\delta^{13}C$ values, which might be a result of local freshwater input into the marine environment. The early Maastrichtian paleotemperature of the southern Indian near-bottom shelf waters was probably about 21.2 °C, and that this middle latitude region continued to be a part of tropical-subtropical climatic zone, but with the tendency of increasing humidity at the end of Cretaceous time.

Chakraborty et al. (2017) studied Barremian to Aptian sediments of Basal Siliclastic Formation (BS formation) located at three isolated outcrops: KVK mines (Dalmiapuram), Neykullam and Terani in Ariyalur district, Tamilnadu within Cauvery Basin for estimating paleoprecipitation and paleotemperatures. Calculation of rainfall (Mean annual precipitation) yield values of 844–1060 mm. The annual average of paleotemperature yielded by the studied samples is 12.5 °C (Chakraborty et al. 2017), although geophysical reconstructions suggest moderately high paleolatitude, ~60°S (Ronov et al. 1989; Hay et al. 1999). Application of weathering indices like Chemical Index of Alteration (CIA), Chemical Index of Weathering (CIW) and Plagioclase Index of Alteration (PIA) indicate a moderate degree of weathering. Overall, an apparently warm temperate humid paleoclimate is implied during the time of deposition of the studied Basal Siliclastic Formation.

Paleo-climatic reconstruction from the Early Cretaceous sediments of the Kutch Basin has been extricated solely depending on the paleosol analysis, due to absence of carbonate or shale or mega fossil deposits (Mandal 2017). Paleosol horizons are mainly preserved within fluvial succession of Early Cretaceous Bhuj Formation. High soil maturity, established from dominance of kaolinite in petrographic and mineralogical study, is reflected in A-CN-K diagram (Mandal 2017). A-CN-K diagram is in correlation with CIA, displaying higher rate of weathering of the Bhuj fluvial deposits. Well tested paleosol analysis techniques have been successfully adopted to determine paleoprecipitation rate and paleotemperature (Sheldon et al. 2002; Chakraborty 2016; Chakraborty et al. 2017; Mandal 2017). Mean annual precipitation recorded during this study vary from 417 mm/yr to 1381 mm/yr while the mean annual temperature ranged between 7°–16 °C with an average value of 12 °C (Mandal 2017). Overall a humid temperate paleoclimate is inferred (Mandal 2017).

6   Cretaceous Volcanic Episodes in India

As Gondwana began to break up during the Late Jurassic to Early Cretaceous, extensive intra-continental rifting took place in association with catastrophic flood basalt events. The Indian craton was subjected to several major rifting events during that period. On India's passage to the north during the Cretaceous, its eastern and western margins were marked by two long, linear, hot spot tracks (Duncan 1981). Kerguelen and Réunion plumes left their marks on the Indian plate during its passage over them, yielding Early Cretaceous Rajmahal–Bengal–Sylhet Province or simply as Rajmahal Province (Ray et al. 2005) in the eastern part and Late Cretaceous Deccan Volcanic Province (dated close to K-Pg boundary; Renne et al. 2015; Schoene et al. 2019; Sprain et al. 2019) in the western and central part of Peninsular India respectively (Courtillot et al. 1999). It is represented by two disconnected exposures, one on south of the Shillong Plateau in Meghalaya and the other east of the Chottanagpur Plateau in Jharkhand, termed as the Sylhet Traps and Rajmahal Traps, respectively. Evans (1964) considered Rajmahal Trap as the counterparts of the Sylhet Trap, detached about 250 km by the Dauki (/Dhauki) Fault. Based on the similarity of ages and continuity of basalt flows below younger cover (Sengupta 1966), they are considered to be part of a single volcanic province, spreading over an estimated area of >100,000 km^2. Contemporaneous flow, presumably, also occurred close to the eastern end of the Lesser Himalayan belt (Abor Volcanics) (Acharyya and Lahiri 1991). At the western margin of the mainland of Eastern India, the Cretaceous succession in the Rajmahal-Malda-Purnea-Ghalsi sub-basin began with similar volcanic flows of about 600 m thick Rajmahal Trap with Upper Gondwana intertrappean beds. The Cretaceous succession in the Rajmahal constitutes more than 15 lava flows and four to six intertrappean beds. The intertrappean sediments in the Rajmahal hills are represented by sandstone, siltstone, arenaceous clay bed, carbonaceous and siliceous shale and tuff, besides a chert bed; with their thicknesses varying from a few centimetres to about 11 m (Tripathi et al. 2013). These intertrappean beds have yielded a rich collection of fossils belonging to the *Ptilophyllum* assemblage typical of the Upper Gondwana age (Kale 2020). In terms of depositional environments, these sediments have been referred to be continental fluvio-lacustrine deposits. The Sylhet Traps (Das Gupta and Mukherjee 2006) are exposed in narrow strips between the Raibah fault in the north and the Dauki fault in the south (Baksi et al. 1987). The 245 m thick sequence of flows recorded from Cherrapunji with twenty flows and three interbedded tuffaceous horizons.

The Deccan volcanic province is one of the largest volcanic eruptions in Earth's history and has received global attention for its possible role in K-Pg mass extinction. The outpouring of the enormous continental flood basalts of the Deccan Trap, spreading over vast areas of western and central India and adjoining Seychelles, cover more than 1,500,000 km^2, with the greatest thickness of about 3.5 km along the Western Ghats escarpment (Baksi et al. 1994). Exposed over a vast contiguous area of more than half a million km^2 in the Indian Peninsula; it straddles the Dharwar craton in the south and the Aravalli–Bundelkhand craton in the north. Its eastern limits

are defined by the Pranhita–Godavari rift belt beyond which the basement of the Bhandara craton is exposed. Recent publications reveal that three distinct pulses of Deccan volcanism (phase-1, 2, and 3) of eruptions with phase-2 accounting for ~80% of the total volume (Chenet et al. 2007). The initial pulse of the eruption (phase-1) occurs in the late Maastrichtian base of C30n at ~68 Ma (Keller et al. 2016a, b), and is represented by Sarnu–Dandali volcanics in Barmer District and Mundwara volcanics in Sirohi District. The Deccan Traps occupy most of the Saurashtra peninsula and continue westwards into Kutch where they are exposed as a narrow strip between the Late Cretaceous and Eocene sedimentary sequences. Several outliers of the Traps rest upon older rocks in Madhya Pradesh (in Gwalior, Sagar, Bhopal, Ratlam, Indore, Hoshangabad, Chhindwara, Jabalpur and Khargone districts), Maharashtra (in Dhule, Nagpur, Chandrapur, Yawatmal, Beed, Solapur and Kolhapur districts) and Karnataka (in Belgaum, Bijapur and Bagalkot districts) (Kale 2020). The first phase of volcanism was small. The main pulse of volcanism occurs in chron 29R ending at the K-Pg boundary (~65 Ma) in the main Deccan volcanic province in the western and central part of the Indian shield. The main phase of Deccan volcanics accounts for about ~80% of all the traps. In Jhilmili region of central India, a planktic foraminifer assemblage of Early Danian age has been encountered above the early Deccan basaltic flow. The exposures of the last phase of Deccan volcanism have been traced eastwards to the Rajahmundry area of the Krishna–Godavari Basin and out into the Bay of Bengal. These traps were overlain by Early Danian age of planktic foraminifera (Keller et al. 2011). The main pulse of the Deccan basalts erupted very rapidly, probably within 1 Ma at the K-Pg boundary (~65 Ma), when western India laid over the Réunion hotspot now located to the east of Madagascar (Courtillot et al. 1999; Chenet et al. 2007). It was a major tectonic event producing one of the largest flood basalt provinces on the Earth's surface. The east coast volcanism is correlated to the Deccan volcanism of the west coast, which is largely continental flood basalts, whereas the Razole basalts of K-G Basin were emplaced in subaerial and submarine environments (Raju et al. 1993). Possibly the eruption happened from Keruguelen hotspots, rather than from the Reunion hotspot.

7 Relative Sea-Level Records from South and West India

The separation of Indian subcontinent from East Gondwanaland started in Late Jurassic-Early Cretaceous. As the pathways opened on both sides of the Indian Peninsula ProtoTethys, water gushed into the rifts between India and Antarctica on one side and, India and Africa on the other. Albian witnessed the first transgression during Cretaceous and as proposed by Hancock and Kauffman (1979), sea level reached its maxima during Turonian and Campanian. Consequently, considerable Mesozoic sediments were deposited on the east coast, west coast, and offshore basins.

The outcrop sediments with rich fossil assemblages reveal that the geomagnetic polarity sequence correlated with polarity chrons from C34n, the Cretaceous long normal interval, and C30n in the late Maastrichtian. The recognition of these

polarity chrons and their correlation with regional faunal assemblages established the linkage to biostratigraphic zonation in the Indian subcontinent. Smaller benthic foraminiferal assemblage was more cosmopolitan with a preponderance of Tethyan forms (Govindan and Narayanan 1980). Larger foraminifera were adapted to low-latitude, shallow-water carbonate-rich environment where seasonal influences are minimal. High-energy, neritic environments were indicated by the massive bivalve records in Maastrichtian sediments. The maximum diversity of the assemblage was in the late Cenomanian/and earliest Turonian. This interval coincides with highest sea-level recorded in the Mesozoic (Govindan et al. 1996). The presence of Tethyan foraminifer taxa; *Rotaliporagreenhornensis*, *Marginotruncanaschnee-gansi*, *Helvetoglobotruncanahelvetica*, *Dicarinellaasymetrica*, *Globotruncanitaele-vata* and *Gansserina gansseri* at this paleolatitude was significant. The flat equator-pole temperature gradient (Sellwood et al. 1994) was indicated by the presence of these faunas at 40°–45°S. In mid-Turonian Karai Formation, the planktonic foraminifera were morphologically quite distinctive; the species have pronounced keels and ornamentation. This quite distinctive paleogeographical province was restricted to the east coast basins of India and Exmouth plateau/NW Australia shelf (Hart et al. 2000). The distinctive markers of the Campanian-Maastrichtian boundary interval recorded *G. gansseri,* which was a fully tropical species, and its presence in the Cauvery Basin was possibly up to 15°–20° further south (Hart et al. 2001). The calcareous nannofossils showed a combined paleogeographical and paleoecological control over their distribution within the Uttatur Group. From the late Aptian to the late Albian, the nannoflora was of a high latitude austral setting and the late Albian onwards up to the early Turonian it gradually changed to that of middle to low latitude setting. The predominance of the sponges, algae and the small sized crustose corals refers a non-tropical origin of the reef. The formation of beach rocks in the bay of southern India indicates the water conditions were at least warm enough to permit carbonate precipitation. During the Late Cretaceous time, southern India was situated below 30° latitude in an arid, but, non-tropical, surrounded by moderately warm-ocean (Steinhoff and Bandel 2000).

India began to separate from Madagascar and Antarctica during the Coniacian/Santonian and still had a position well south of the equator. Paleogeographical reconstruction of south-eastern India during the Early to Late Cretaceous indicates that the reef growth, observed in the lower part of the Uttatur Group, took place in a region separated from its original position near the Antarctic continent but had not separated from Gondwanaland very far and moved northward. The tropical belt at this time was dominated by ruddist reefs. The faunal composition of the reefs in the Ariyalur area supports the paleoclimatic reconstruction of India, located south of the tropical belt during the Late Cretaceous. Hence, it probably resided in an arid climate below the 30° latitude, where the weather conditions had been favourable for the development of fanglomerate deposits on land and beach rocks at the coast but unfavourable for tropical reefs builders. The maximum diversity of the assemblage was in the late Cenomanian/and earliest Turonian. This interval coincident to the highest sea-level records during the Mesozoic.

The tectonic evolution and paleogeography of all central European basins were synthesized by Voigt et al. (2008). The sea level curve for the Danish and North German basins shows a mid-late Albian transgression flooding in central Europe basins, while the late Albian transgression completely flooded the Cauvery Basin, replacing shelf carbonates with organic-rich shale. As a consequence of this major transgression, the individual sub-basins evolved to a large epicontinental shelf. The post-Turonian deposits of the Cauvery Basin represent early post-rift unit that accumulated during a time of thermal subsidence consequent to rise of Marion plume. The late Aptian to mid-Albian sea level cycle (= Dalmiapuram cycle) of the Cauvery Basin shows some correspondence with the northern Gulf of Mexico. The late Turonian unconformity with a hiatus of about 2.3 Ma separates the Coniacian-Santonian sea level cycle (= Garudamangalam cycle of Raju et al. 1993) in the Cauvery Basin. This unconformity has a corresponding sub-aerial unconformity in central Europe and the northern Gulf of Mexico. However, the late Santonian regression in the Cauvery Basin has a corresponding marine flooding event in the northern Gulf of Mexico. The early Maastrichtian widespread transgression is associated with the early-late Maastrichtian sea-level cycle that has a corresponding late Albian-early Maastrichtian transgression in the northern Gulf of Mexico (Mancini et al. 1996; Mancini and Puckett 2005) and the lower boundary of this cycle is represented by a sub-aerial unconformity in western Europe (Hardenbol et al. 1998) and in the Cauvery Basin (Nagendra et al. 2011a, b). The Depositional record of Cauvery Basin was dominated by shelf carbonates in the early to mid-Albian and, by shale and sandstones throughout the Late Cretaceous. Late Albian to mid-Turonian, Coniacian and early Maastrichtian experienced the widespread occurrence of anoxic conditions.

The first marine transgression at the basin margin occurred in the late Aptian to early Albian. This is revealed by the occurrence of planktic foraminifera *H. planispira* and *H. trocoidea* along with the benthic foraminifera *Lenticulina* sp. at the uppermost contact of the Terani Formation to the overlying Dalmiapuram limestone. This faunal assemblage generally indicates a shallow neritic, open marine environment. This unit is overlain by limestone belonging to the Dalmiapuram Formation, rich in coral-algal and bryozoans with rare foraminifera indicating a warm, shallow and restricted marine environment during the early to mid-Albian. The carbonate deposition ceased abruptly during the late Albian as a result of increasing depth and clastic input (Nagendra et al. 2002b). Macrofossils, such as *Acanthoceras*sp., *Mammitesconciliatus*, *Nautilus huxleyanus*, and *Turrilitescostatus* (Kossmat 1897; Govindan et al. 1998) are abundant in the indigenous limestone beds. Marl (indigenous basinal carbonate mud) yielded few planktic and diverse benthics represented by species *Hedbergella*, *Lenticulina*, *Anomalinoides* and *Quadrimorphina,* indicating middle neritic conditions. Further deepening is evident during the late Albian to mid-Turonian as the indigenous limestone beds grades vertically into marl/limestone, wherein well preserved, diversified and abundant foraminifera, such as *Rotaliporareicheli*, *Praeglobotruncana stephani*, *P. delrioensis*, *Gavelinella plummerae*, *Gyroidinoides globosa* suggests deeper middle neritic conditions (Nagendra et al. 2002a, 2011a, b; Reddy et al. 2013). The time equivalent Karai Shale in outcrops consists

of Ammonites, Belemnites and worm tubes indicating deeper middle neritic conditions. Paleodepth attained its maxima when maximum flooding condition is achieved during the Karai Shale sedimentation (Chakraborty et al. 2018a). As a result of basin upliftment caused by the rise of Marion plume during the late Turonian (Scotese 1997), relative sea level dropped to inner neritic depths. The increased abundance of glauconite pellets from the bottom of the top TST segment accompanied by a slight increase in K_2O content reflects the role of stratigraphic condensation in glauconite evolution (Banerjee et al. 2016; Bansal et al. 2019). The paleogeography of the Karai Formation ranged from the inner shelf to the shelf-margin straddling across the maximum flooding zone heavily enriched in phosphates and glauconite pellets (Chakraborty et al. 2018a).

The *Kulakkalnattam Sandstone* (Coniacian-Santonian; exposed along Kulakkalnattam stream) of Garudamangalam Formation consists of abundant burrows characterized by *Skolithos* ichnofacies (Nagendra et al. 2010) characteristic of high energy near-shore conditions. This unit vertically grades into *Anaipadi Sandstone* (exposed along a stream near Anaipadi village), consisting of Ammonites and Mollusca shells signifying inner neritic conditions. The overlying *Saturbhugam Sandstone* (exposed at a stream section near Saturbhugam village), internally characterized by trough cross stratifications, points to a fluvial channel origin revealing sea level drop at the top of Garudamangalam Formation. Overall, the Garudamangalam Formation forms a highstand systems tract, which unveils a wide range of siliciclastic-carbonate mixing modes in a near-shore marine realm associated with the river-mouth bar. The presence of a shore-parallel river-mouth bar resulted in a restricted environment on its shore side, remained open marine on the seaward side (Sarkar et al. 2014). The Sillakkudi Formation characteristically consists of large *Inoceramus* shells along with *Skolithos* and *Ophiomorpha* burrows at the top of the unit. The lower part of the formation is represented by Kilpalvur grainstone containing glauconite pellets and calcareous nodules indicating a marine incursion into the basin. This formation yielded foraminifera, including *Globotruncana ventricosa*, *Globotruncana linneiana*, *Rosita fornicata* and *Bolivinoides strigillatus* suggesting deeper middle neritic conditions. The Kallar conglomerate between Sillakkudi and overlying Kallankurichchi Formation suggests a relative sea level drop resulting in sub-aerial exposure and development of a conglomerate bed. The Kallankurichchi Formation consists of four lithounits (Nagendra et al. 2002a), with the lower ferruginous limestone containing smaller benthic foraminifera that marks the onset of a marine transgression. The increasing abundance of foraminifera and macrofossils represented by *Gryphaea*, *Alectryonia* and *Pecten* in successively overlying arenaceous limestone is an indication of deepening bathymetry. Above the *Gryphaea* bed a layer dominated solely by *Gryphaea* shells suggests maximum paleodepth reached middle neritic depths. Drastic reduction in fossil content in the overlying upper arenaceous limestone unit signals a falling sea-level. This falling trend continued up to the end of Ottakovil Formation. The burrow structures such as *Thalassinoides* and *Ophiomorpha* in the Ottakovil Formation indicate marginal marine to littoral environment. This lithological unit (Ottakovil) marks the end of the marine phase in the basin margin area. The siliciclastic Kallamedu Formation is

internally characterized by trough cross-laminations, probably indicating deposition in a fluvial environment. The sea level curve reveals that four major transgressive and regressive cycles are imprinted in the Cretaceous rock record preserved in the Ariyalur area. The paleobathymetric trends vis-a-vis sea level changes reconstructed for the Albian to Maastrichtian reveal two major sea-level falls during late Turonian and late Maastrichtian, which correlate well with global sea level curves of Haq et al. (1987) and Miller et al. (2005). These sea-level falling events are linked to the rise of Marion hot mantle plume during the late Turonian and Reunion hot mantle plume during late Maastrichtian (Govindan 1993; Raju et al. 1993; Sundaram et al. 2001; Nagendra et al. 2002b; Watkinson et al. 2007).

Biswas (1981) proposed mega-cycle of base level change curve for the Mesozoic succession of Kutch shows a progradational pattern throughout the Cretaceous. However, a mid-interval marine transgression, during the late Aptian, has been attributed based on marine bed occurrence in the west. Mandal et al. (2016) established that the transgression had been much more extensive to inundate 80% of Kutch Mainland. The sea extended eastward as far as beyond Nadapa where the two fluvial units within the Bhuj Formation bound the marine unit juxtaposing one above the other. An explicit record of a mega-scale event of relative sea level rise is found sandwiched between two fluvial stratigraphic intervals that amalgamate only at the eastern extremity of the exposure of the Formation. A localized ~36 m-thick estuarine sequence within the type section of the Bhuj Formation recorded the minute meso-scale base level changes during that marine incursion. A granular transgressive lag often mantles the erosion surface on top of the Lower Fluvial unit.

Resting on a coarsening upward ramp, the initially fining and then coarsening upward estuarine succession is prograding, though not steadily. It was wave-dominated, but tide left imprint behind the estuary mouth bar gaining in intensity because of valley constriction. A wave-dominated barrier bar association developed under the dominant influence of shore-parallel flow of water. The progressively shoaling and resultant increase in flow shear made the top of the barrier bar a favorable site for *Ophiomorpha-Diplocraterion* burrow association to thrive. The comparatively quieter landward side of the barrier though still dominated by wave, on the other hand, turned into a habitat of *Rhyzocorallium.* However, wave dissipated rapidly and tide comparatively accentuated because of constriction of the estuary mouth. Consequently, the following association of mixed flat is repleted with tidal features like mud drapes on forests of cross-strata (Mandal et al. 2016; Mandal 2017). Its initial fining upward trend, no doubt, reflects a short spell of progradation, in relation to sediment supply from the sea. On the other hand, the trend of steady sandstone bed-thickening and coarsening upward trend in its upper part points to the next transgression again. Apparently, the rate of transgression superseded the rate of sediment accumulation. Constriction of the estuary mouth was largely removed as the relative sea level rose and wave encroachment took place. Further upward the succession continues to sandflat to mixed flat and then to mudflat eliciting reversal to progradation for a comparatively longer period. Such a long the paleocurrent direction within the estuary had been consistent, indicating landward sediment transfer. The upward passage of the mudflat to the mixed flat and then to the bayhead delta;

the transition holds a record of sediment supply from land and attests to further progradation (cf. Saha et al. 2010). However, recurrence of the same mixed flat (2) to bay-head delta transition on top of them testifies resumption of progradation after a short spell of transgression. This progradation continued till the upper fluvial terminates the estuary section as a whole. This record of meso-scale fluctuations in relative sea level presents a valuable record of local subsidence probably aided by sediment loading.

8 Biogeography and K-Pg Mass Extinction

The term 'Biogeography' focuses on the detailed study of the distribution patterns of fossils in time and space. Benthic foraminifera (calcareous microfossils), spores and pollen, are perhaps the most important groups of fossils in paleobiological and paleoenvironmental interpretation. Besides, plants and vertebrate fossils are significant in the field of paleobiogeography. Geophysical data and the established models on plate tectonics indicate isolation (for at least 35 Ma) of Indian plate before separation from Madagascar (88–90 Ma ago) till its final collision with Asia in the Early-Middle Eocene (Barron and Harrison 1980; Smith 1988; Storey et al. 1995; Prasad and Sahni 1999; Chatterjee et al. 2017). This stretched time span of isolation of landmass should have brought a radical change of pre-existing biota populations and genetic isolation should create the endemic taxa without any relation to the contemporary faunas of nearby regions. In conflict, terrestrial vertebrates of India are found cosmopolitan in nature during this time, providing no proof of endemism (Sahni 1984; Briggs 1989; Jaeger et al. 1989).

The occurrence of identical land plants between India and Australia advocates that these areas were amalgamated till late Jurassic–Early Cretaceous (McLoughlin and Pott 2009). As the continents had underway to drift apart, a barrier had been created to the dispersal of terrestrial organisms. During Early Cretaceous, the terrestrial environment was dominated by seed-bearing plants (gymnosperm) (Rajanikanth and Chinnappa 2016). During this period the flora distributed in pericratonic and intracratonic basins of India mainly consisted of *Pteridophytes, taxaleans, Bennettitaleans, ginkgoaleans, Pteridospermaleans, pentoxylaleans, Coniferaleans* (Rajanikanth and Chinnappa 2016). This Early Cretaceous flora in the eastern part of India is divided into diverse floral zonation- *Dictyozamites–Pterophyllum–Anomozamites Zonation,* (Athgarh/Pavalur/Satyavedu Formation), *Allocladus–Brachyphyllum–Pagiophyllum Zonation,* (Sriperumbudur, Gollapalli, Raghavapuram, Budavada, Vemavaram, Gangapur) and *Weichselia–Onychiopsis–Gleichenia Zonation* (Sivaganga) (Sukh-Dev 1987). In central India there was the dominance of conifers and cycadophytes and certain pteridosperms and the palynofloral assemblage includes pollen and spores of pteridophytic, bryophytic spore (e.g. *Aquitriradites*, *Triporolites*, *Cooksonites*, *Coptospora*, and spores of Schizaceaceous ferns *Cicatricosisporites* and *Contignisporites*) and gymnospermic groups (Prakash 2008). The western, central and eastern regions too enclosed plant fossils like leaf, wood, seed etc. A unique Indian flora

Pentoxylalean found in other continents addresses the evolution of the plant (Drinnan and Chambers 1985; Howe and Cantrill 2001; Taylor et al. 2009).

The Maastrichtian units are the fossil-rich horizons in India. After swapping of the Gondwana fauna with South America through biotic corridors (Chatterjee and Scotese 2010; Chatterjee et al. 2017), faunas evolved in isolation. There is a similarity of fauna of Laurasian taxa which includes discoglossid and pelobatid frogs, gobiatinae frogs, anguid lizards and eutherian mammals; these fossils are also reported from central Asia, England, Spain, France, and North America (Prasad and Rage 1995; Chatterjee et al. 2017). Incorporation of Laurasian taxa depicted as 'sweepstake' mode supported by the 'Dras–Kohistan island arc system' (Ali and Aitchison 2008; Sahni and Prasad 2008). They include some taxa of Gondwanan affinities like ranoid frogs, leptodactylid, hylid and, madtsoiid and nigerophiid snakes, pelomedusoid turtles, mesosuchian crocodiles, abelisaurid dinosaurs from Lameta Formation and Deccan intertrappean (Krause et al. 1997; Sahni and Prasad 2008; Sampson et al. 1998; Wilson et al. 2003); haramiyidan mammals (Anantharaman et al. 2006) and ostracods are of mainly endemic in character.

The marine Cretaceous succession of east coast, south India is huge repository of mega- (pelecypod, gastropods, ammonites, echinoids among the invertebrates) and micro-fossils. Stoliczka (1867, 1871) reported gastropods of four divisions: Scaphopoda, Opisthobranchia, Prosobranchia and Pulmonata and pelecypoda. The thick-shelled rudist bivalves (*Gryphea*, *Pycnodonte, Ostrea* etc.) are reported from east coast of India by Fürsich and Pandey (1999). *Inoceramus* (pelecypode) is a good index fossil of Late Cretaceous age. Ayyasami (2006), among others reported ammonites from Cauvery Basin; e.g. *Australiceras jacki*, *Eubaculites vagina*, *Mortoniceras rostratum*, *Calycoceras newboldi*, *Eucalycoceras pentagonum*, *Pseudaspidoceras footeanum* etc. Stoliczka (1873) described Echinoid *Stygmatopygus elatus* from Cenomanian rocks of the Ariyalur Group. A new species (*Gongrochanus Kier*) of Cassiduloid echinoid had been discovered by Srivastava (2003). Govindan (1972) and many other researchers worked on foraminifera (ex. *Globigerina hoterivica*, *Hedbergella planispira*, *Planomalina buxtorfi* etc.). Nagendra et al. (2011a, b) summarized the macro- and microfossils present in the Ariyalur area, Cauvery Basin.

The Bagh Beds of Narmada Basin, central India are rich in invertebrate fauna like brachiopods, echinoids, bryozoans, bivalves, gastropods and cephalopods. Total 16 species of Bivalves (e.g. *Inoceramus concentricus* Park; *I. cripssi* Mantell; *I. cuvieri* Sowerby; *I. tenuis* Mantell; *Neithea morrisi* Pictet and Renevier; *Plicatula instabilis* Stoliczka; *P. deodikari* Badve; *Modiolus typicus* Forbes; *Pholadomya elliptica* Munster; *Astarte similis* Munster; *A. sinuicostata* Badve; *Nucula baghensis* Dassarma and Sinha and *Cytheria lassula* Stoliczka (Chiplonkar 1939; Chiplonkar and Badve 1976), 8 species of Gastropods (e.g. *Turritella chikliensis* Chiplonkar and Badve; *Cerithium scalaroideum* Forbes; *Neptunia excavata* Blandford; *Gyrodes* sp. Stoliczka; Naik 2013), 2 species of Cephalopods (viz. *Placenticeras kaffrarium* and *Barroisiceras onilahyense* Basse), 7 species of Echinoids (e.g. *Dorocidaris namadica* Duncan; *Cyphosoma namadicum* Fourtau; *Echinobrissus rajnathi* Chiplonkar; *Hemiaster fourtaui* Chiplonkar; *H. holoambitatus* Chiplonkar; *H. subsimilis* Fourtau;

Salenia keatingei Fourtau) and 2 species of Brachiopods (*Acanthothyris* sp. and *Malwirhynchia subpentagonalis* Chiplonkar) have been reported from there (Bose 1884; Bardhan et al. 2002; Naik 2013). The ammonoid fossils assign Coniacian age of this formation.

The Cretaceous-Paleogene (K-Pg) mass extinction (~66 Ma) is a global extinction event eliminating approximately 80% of all species of animals leading to biotic crisis, famous for marking the end of the dinosaur era. The Deccan volcanic eruption is the longest lava flows known on the Earth (Self et al. 2008). Keller et al. (2009) revealed three phases of eruptions. This massive eruption had a pronounced impact on the environment. As the temperature reached the minimum, it lowers the primary productivity and species diversity (Keller et al. 2016a; Mateo et al. 2017). The huge phase-2 eruption during the latest Maastrichtian is directly associated with K-Pg mass extinction in India (Keller et al. 2011; Gertsch et al. 2011). It caused the rapid warming of environment (4 °C in bottom and surface waters and 8 °C on land, Mateo et al. 2017). Large amount of erupted CO_2 was leading to ocean acidification, which in turn created a major carbonate crisis and contributed to K-Pg mass extinction (Punekar et al. 2014; Keller et al. 2016a; Mateo et al. 2017). At the end of the Cretaceous two large bolide impacts occurred on the Earth's history, viz. Chicxulub crater in Yucatan Peninsula of Mexico (Hildebrand et al. 1991) and Shiva crater on the western shelf of India (Chatterjee et al. 2006). At the K-Pg boundary a significant faunal turnover occurred, marked by the disappearance of dinosaurs, ammonites, flying reptiles, scleractinian corals, belemnites, some groups of bivalves, gastropods and echinoderms. The extinction phase affected badly to the calcareous planktonic organisms, tropical reef invertebrates. The planktonic foraminiferal diversity declined by 78% and benthic species declined by 37% across the boundary.

9 Conclusions

The review of Cretaceous deposits in India leads to conclude the following.

(a) Indian plate was on accelerated velocity in Cretaceous (max. 20 cm/year in Late Cretaceous) during its northward drift from Gondwana to Asia.

(b) Margins of Indian plate reformed with the development of new sedimentary basins parallel and perpendicular to the coasts.

(c) Rise in RSL during Albian, Turonian and Campanian caused sedimentation along east and west coast. A Late Cretaceous transgression flooded central India.

(d) Climate left imprint of the greenhouse effect in sedimentation record. An overall apparently warm temperate humid paleoclimate prevailed during the entire interval, with a tendency of increasing humidity and temperature in the Late Cretaceous.

(e) Two spectacular intraplate hotspots (Réunion and Kerguelen) erupted immense flood-basalt on the two sides of the island continent; Rajmahal-Sylhet volcanism in eastern Indian and Deccan volcanism in western India.

(f) Biotic connectivity prevailed among India, Africa and South America. Lack of endemism shown by terrestrial vertebrates (Ex. Tetrapods), diversity in floral distribution pattern and appearance of angiosperm are validated.

(g) The devastating mass extinction at K-Pg boundary (~66 Ma) caused a massive faunal turnover in the history of life, marking the end of dinosaur era. It also prepared the ground for life rebound, especially for mammals and birds during the early Paleogene.

References

Acharya SK, Lahiri TC (1991) Cretaceous palaeogeography of Indian subcontinent: a review. Cret Res 12:3–12

Ahmad AHM, Akhtar K (1990) Clastic environments and facies of the Lower Cretaceous Narmada Basin, India. Cret Res 11:175–190

Ali JR, Aitchison JC (2008) Gondwana to Asia: plate tectonics, paleogeography and the biological connectivity of the Indian sub-continent from the Middle Jurassic through latest Eocene (166–35 Ma). Earth-Sci Rev 88:145–166

Anantharaman S, Wilson GP, Das Sarma DC, Clemens WA (2006) A possible Late Cretaceous "Haramiyidian" from India. J Vert Paleo 26:488–490

Arora A, Banerjee S, Dutta S (2015) Black shale in late Jurassic Jhuran Formation of Kutch: possible indicator of oceanic anoxic event? J Geol Soc India 85:265–278

Arora A, Dutta S, Gogoi B, Banerjee S (2017) The effects of igneous dike intrusion on organic geochemistry of black shale and its implications: Late Jurassic Jhuran Formation, India. Int J Coal Geol 178:84–99

Ayyasamy K (1990) Cretaceous heteromorphy ammonoid biostratigraphy of southern India. Newslett Stratigr 22:111–118

Ayyasami K (2006) Role of oysters in biostratigraphy: a case study from the Cretaceous of the Ariyalur area, southern India. Geosci J 10:237–247

Ayyasami K, Banerji RK (1984) Cenomanian-Turonian transition in the Cretaceous of southern India. Bull Geol Soc Denmark 33:21–30

Baksi AK, Barman TR, Paul DK, Farrar E (1987) Widespread early cretaceous flood basalt volcanism in eastern India: geochemical data from the Rajmahal–Bengal–Sylhet traps. Chem Geol 63:133–141

Baksi AK, Byerly GR, Chan L-H, Farrar E (1994) Intracanyon flows in the Deccan province, India? Case history of the Rajahmundry traps. Geology 22:605–608

Baksi SK (1977) Marine transgression, sedimentation and tectonics of the West Godavari coastal rocks of Andhra Pradesh. Indian J Earth Sci (S Ray) 67–94

Bandopadhyay PC, Carter A (2017) Geological framework of the Andaman–Nicobar Islands (eds) The Andaman–Nicobar Accretionary Ridge: geology, tectonics and hazards. Geol Soc London Mem 47:75–93

Banerjee S, Bansal U, Pande K, Mena SS (2016) Compositional variability of glauconites within the upper Cretaceous Karai Shale Formation, Cauvery Basin India: implications for evaluation of stratigraphic condensation. Sediment Geol 331:12–29

Banerjee S, Ghosh P, Nagendra R, Bhattacharya B, Desai B, Srivastava AK (2020) Marine and fluvial sedimentation including erosion and sediment flux in Peninsular Indian Phanerozoic Basins. Proc Indian Nat Sci Acad 86:351–363

Banerji RK (1973) Stratigraphy and micropalaeontology of the Cauvery Basin, Part 1. Exposed area. J Palaeontol Soc India 17:7–30

Banerji RK (1982) Sivaganga Formation, its sedimentology, micropalaeontology and sedimentation history. J Geol Soc India 23:450–457

Banerji RK, Sastri VV (1979) Quantification of foraminiferal biofacies and reconstruction of palaeobiogeography of the Cauvery Basin. J Geol Soc India 20:571–586

Bansal U, Banerjee S, Pande K, Arora A, Meena SS (2017) The distinctive compositional evolution of glauconite in the Cretaceous Ukra Hill Member (Kutch basin, India) and its implications. Mar Pet Geol 82:97–117

Bansal U, Banerjee S, Ruidas DK, Pande K (2018) Origin and geochemical characterization of the glauconites in the Upper Cretaceous Lameta Formation, Central India. J Palaeogeography 7:99–116

Bansal U, Pande K, Banerjee S, Nagendra R, Jagadeesan KC (2019) The timing of oceanic anoxic events in the Cretaceous succession of Cauvery basin: constraints from ^{40}Ar/^{39}Ar ages of glauconite in the Karai Shale Formation. Geol J 54:308–315

Bansal U, Banerjee S, Pande K, Ruidas DK (2020) Unusual seawater composition of the Late Cretaceous Tethys imprinted in glauconite of Narmada basin, central India. Geol Mag 157:233–247

Bardhan S, Gangopadhyay TK, Mandal U (2002) How far did India drift during the Late Cretaceous?—Placenticeras kaffrarium Etheridge, 1904 (Ammonoidea) used as a measuring tape. Sediment Geol 147:193–217

Barron EJ, Harrison CGA (1980) An analysis of past plate motions in South Atlantic and Indian oceans. In: David P, Runcorn SK (eds) Mechanisms of continental drift and plate tectonics. London, Academic Press, pp 89–109

Beaumont H, Clarke SM, Burley SD, Taylor AM (2018) Sedimentology and the facies architecture of the Ghaggar-Hakra Formation, Barmer Basin, India: implications for early Cretaceous deposition on the north-western Indian Plate margin. Depos Rec 5:53–83

Bhandari N, Shukla PN, Pandey J (1987) Iridium enrichment at the Cretaceous-Tertiary boundary at Meghalaya. Curr Sci 56:1003–1004

Bhargava ON (2008) An updated introduction of the Spiti geology. J Palaeontol Soc India 53:113–129

Bhatt NY, Solanki PM, Prakash N, Das N (2016) Depositional environment of Himmantnagar Sandstone (Lower/Middle Cretaceous): a perspective. Palaeobotanist 56:67–84

Bhattacharya A, Bhattacharya U (1987) Review of the stratigraphy and palaeontology of Upper Cretaceous sediments of northeast India. Geol Surv India Spec Publ 367–387

Bhattacharya B, Jha S (2014) Late Cretaceous diurnal tidal system: a study from Nimar Sandstone, Bagh Group, Narmada Valley, Central India. Curr Sci 107:1032–1037

Biswas SK (1971) Note on the geology of Kutch. Quart J Geol Min Met Soc India 43:223–235

Biswas SK (1977) Mesozoic rock-stratigraphy of Kutch, Gujrat. Quart J Geol Min Met Soc India 49:1–52

Biswas SK (1981) Basin framework, palaeo-environment and depositional history of the Mesozoic sediments of Kutch, Western India. Quart J Geol Min Met Soc India 53:56–85

Biswas SK (1982) Rift basins in the western margin of India and their hydrocarbon prospects with special reference to Kutch basin. AAPG Bull 66:1497–1513

Biswas SK (1987) Regional tectonic framework, structure and evolution of the western marginal basins of India. Tectonophys 135:307–327

Biswas SK (1991) Stratigraphy and sedimentary evolution of the Mesozoic basin of Kutch, western India. In: Tandon SK, Pant CC, Casshyap SM (eds) Stratigraphy and sedimentary evolution of western India. Gyanodaya Prakashan, Nainital, pp 74–103

Biswas SK (1993) Geology of Kutch, vol 1. KDM Institute of Petroleum Exploration, Dehradun

Biswas SK (1999) A review on the evolution of rift basins in India during Gondwana with special references to western Indian Basins and their hydrocarbon prospects. PINSA 65A:261–283

Biswas SK (2005) A review of structure and tectonics of Kutch basin, western India, with special reference to earthquakes. Curr Sci 88:1592–1600

Blanford HF (1862) Cretaceous and other rocks of South Arcot and Trichinopoly districts, Madras. Mem Geol Surv India 4:1–217

Bose MN, Taylor EL, Taylor TN (1990) Gondwana floras of India and Antarctica. A survey and appraisal. In: Taylor TN, Taylor EL (eds) Antarctic paleobiology. Springer, Berlin, pp 118–148

Bose PK, Das NG (1986) A Trangressive storm–and fair–weather dominant shelf sequence, Cretaceous Nimar Formation, Chakrud, Madhya Pradesh, India. Sediment Geol 46:147–167

Bose PK, Shome S, Bardhan S, Ghosh G (1986) Facies mosaic in the Ghuneri member (Jurassic) of the Bhuj Formation, western Kutch, India. Sediment Geol 46:293–309

Bose PK, Ghosh G, Shome S, Bardhan S (1988) Evidence of superimposition of storm waves on tidal currents in rocks from the Tithonian-Neocomian Umia Member, Kutch, India. Sediment Geol 54:321–329

Bose PN (1884) Geology of the Lower Narmada Valley between Nimawar and Kawant. Mem Geol Surv India 21:1–72

Briggs JC (1989) The historic biogeography of India: isolation or contact? Systematic Biol 38:322–332

Burke K, Dewey JF (1973) Plume generated triple junctions: key indicators in applying plate tectonics to older rocks. J Geol 81:406–433

Casshyap SM, Aslam M (1992) Deltaic and shoreline sedimentation in Saurashtra Basin, western India: an example of infillingin an early Cretaceous failed rift. J Sed Pet 62:972–991

Cerling TE (1991) Carbon dioxide in the atmosphere: evidence from Cenozoic and Mesozoic palaeosols. Am J Sci 291:377–400

Chakraborty N (2016) Barremian-Coniacian sediments and sequence building in the Pondicherry sub-basin of Cauvery Basin, India. Unpublished PhD thesis, Jadavpur University, Kolkata

Chakraborty N, Sarkar S, Mandal A, Mejiama W, Tawfik HA, Nagendra R, Bose PK, Eriksson PG (2017) Physico-chemical characteristics of the Barremian-Aptian siliciclastic rocks in the Pondicherry embryonic rift sub-basin, India. In: Mazumder R (ed) Sediment provenance. Elsevier, Amsterdam, pp 85–121

Chakraborty N, Mandal A, Choudhuri A, Mandal S, Sarkar S (2018a) Indigenous siliciclastic and extraneous polygenetic carbonate beds in the Albian-Turonian Karai Shale, Cauvery Basin, India. Carb Evap 33:61–576

Chakraborty N, Sarkar S, Mandal A, Mandal S, Bumby A (2018b) Microenvironmental constraint on $\delta^{13}C$ depletion: Garudamangalam Sandstone, Cauvery Basin, India. Mar Pet Geol 91:776–784

Chakraborty N, Sarkar S (2018) Syn-sedimentary tectonics and facies analysis in a rift setting: Cretaceous Dalmiapuram Formation, Cauvery Basin, SE India. J Palaeogeography 7:146–167

Chatterjee S, Scotese CR (2010) The wandering Indian plate and its changing biogeography during the Late Cretaceous-Early Tertiary period. In: Bandopadhyay S (ed) New aspects of Mesozoic biogeography. Springer, Berlin, pp 105–126

Chatterjee S, Guven N, Yoshinobu A, Donofrio R (2006) Shiva structure: a possible KT boundary impact crater on the western shelf of India. Spec Publ Museum of Texas Tech Univ 50:1–39

Chatterjee S, Scotese CR, Bajpai S (2017) The restless Indian plate and Its epic voyage from Gondwana to Asia: its tectonic, paleoclimatic, and paleobiogeographic evolution. GSA Spec Pap 529:1–147

Chaudhuri A, Banerjee S, Le Pera E (2018) Petrography of Middle Jurassic to Early Cretaceous sandstones in the Kutch Basin, western India: implications on provenance and basin evolution. J Palaeogeography 7:2–14

Chaudhuri A, Das K, Banerjee S, Fitzsimons ICW (2020a) Detrital zircon and monazite track the source of Mesozoic sediments in Kutch to rocks of Late Neoproterozoic and Early Palaeozoic orogenies in northern India. Gond Res 80:188–201

Chaudhuri A, Banerjee S, Chauhan G (2020b) Compositional evolution of siliciclastic sediments recording the tectonic stability of a pericratonic rift: Mesozoic Kutch Basin, western India. Mar Pet Geol 111:476–495

Chaudhuri A, Chatterjee A, Banerjee S, Ray JS (2020c) Tracing multiple sources of sediments using trace element and Nd isotope geochemistry: provenance of the Mesozoic succession in the Kutch Basin, western India. Geol Mag. https://doi.org/10.1017/S0016756820000539

Chaudhuri A, Banerjee S, Prabhakar N, Das A (2020d) The use of heavy mineral chemistry in reconstructing provenance: a case study from Mesozoic sandstones of Kutch Basin (India). Geol Jour. https://doi.org/10.1002/gj.3922

Chenet AL, Quidelleur X, Fluteau F, Courtillot V (2007) 40K/40Ar dating of the main Deccan large igneous province: further evidence of KTB age and short duration. Earth Planet Sci Lett 263:1–15

Chiplonkar GW (1939) Lamellibranchs from the Bagh beds. Indian Acad Sci 10:255–274

Chiplonkar GW (1985) Attempts at litho and biostratigraphic subdivision of the upper Cretaceous rocks of South India—a review. Quart J Geol Min Met Soc India 57:1–32

Chiplonkar GW, Badve RM (1976) Palaeontology of the Bagh beds. Inoceramidae. J Palaeontol Soc India 18:1–12

Clarke LJ, Jenkyns HC (1999) New oxygen isotope evidence for long-term Cretaceous climatic change in the Southern Hemisphere. Geology 27:699–702

Courtillot V, Jaupart C, Manighetti I, Tapponnier P, Besse J (1999) On casual links between flood basalts and continental breakup. Earth Planet Sci Lett 166:177–195

Das Gupta AB, Mukherjee B (2006) Geology of NW Bengal Basin. Geological Society of India, Bangalore

Dasgupta SK (1975) Revision of Mesozoic-Tertiary stratigraphy of the Jaisalmer Basin, Rajasthan. Indian J Earth Sci 2:77–94

Desa M, Ramana MV, Ramprasad T (2006) Seafloor spreading magnetic anomalies south off Sri Lanka. Mar Geol 229:227–240

Desai BG (2013) Ichnological analysis of transgressive marine tongue in prograding deltaic system: evidences from Ukra Hill Member, western Kachchh, India. J Geol Soc India 82:143–152

Dolson J, Burley SD, Sunder VR, Kothari V, Naidu B, Whiteley NP, Ananthakrishnan B (2015) The discovery of the Barmer Basin, Rajasthan, India and its petroleum geology. AAPG Bull 99:433–465

Drinnan AN, Chambers TC (1985) A reassessment of *Taeniopteris daintreei* from the Victorian Early Cretaceous: a member of the Pentoxylales and a significant Gondwana land plant. Australian J Bot 33:89–100

Duncan RA (1981) Hotspots in the Southern Oceans—an absolute frame of reference for motion of the Gondwana continents. Tectonophys 74:29–42

Evans P (1932) Tertiary successions of Assam. Trans Min GMI XXVII:155–260

Evans P (1964) The tectonic framework of Assam. J Geol Soc India 5:80–96

Föllmi KB (2012) Early Cretaceous life, climate and anoxia. Cret Res 35:230–257

Fürsich FT, Pandey DK (1999) Genesis and environmental significance of Upper Cretaceous shell concentrations from the Cauvery Basin, southern India. Palaeo Palaeo Palaeo 145:119–139

Fürsich FT, Pandey DK (2003) Sequence stratigraphic significance of sedimentary cycles and shell concentrations in the Upper Jurassic-Lower Cretaceous of Kachchh, western India. Palaeo Palaeo Palaeo 193:285–309

Gaetani M, Nicora A, Premoli SI, Fois E, Garzanti E, Tintori A (1983) Upper Cretaceous and Paleocene in Zanskar Range (NW Himalaya). Rivista Italaliana di Paleontologia e Stratigraphia 89:81–118

Gaetani M, Casnedi R, Fois E, Garzanti E, Jadoul F, Nicora A, Tintori A (1986) Stratigraphy of the Tethys Himalaya in Zanskar, Ladakh. Riv Ital Paleontol Stratigr 91:443–478

Gertsch B, Keller G, Adatte T, Garg R, Prasad V, Fleitmann D, Berner Z (2011) Environmental effects of Deccan volcanism across the Cretaceous-Tertiary transition in Meghalaya, India. Earth Planet Sci Lett 310:272–285

Gili E, Skelton PW, Vicens E, Obrador A (1995) Corals to rudists-an environmentally induced assemblage succession. Palaeo Palaeo Palaeo 119:127–136 (Chapter 1)

Goswami S, Das M, Guru BC (2010) Palaeoenvironment in the Mahanadi Basin: inferences from Mesozoic plant and ichno fossils diversity. The Ecoscan 4:07–14

Govindan A (1972) Upper Cretaceous planktonic foraminifera from the Pondicherry area, South India. Micropaleontol 18:160–193

Govindan A (1993) Cretaceous anoxic events, sea level changes and microfauna in Cauvery Basin, India. In: Proceedings of second seminar on petroliferous basins of India, vol 1. Indian Petroleum Publishers, pp 161–176

Govindan A, Narayanan V (1980) Affinities of the Cretaceous foraminifera of the east coast Indian Basin and the drifting of Indian shield. J Geol Soc India 13:269–279

Govindan A, Ravindran CN, Rangaraju MK (1996) Cretaceous stratigraphy and planktonic foraminiferal zonation of Cauvery Basin, South India. Mem Geol Soc India 37:155–187

Govindan A, Yadagiri K, Ravindran CN, Kalyanasundar R (1998) A field guide on Cretaceous sequences of Tiruchirapalli area. Cauvery Basin, India, pp 1–53

Govindan A, Ananthanarayanan S, Vijayalakshmi KG (2000) Cretaceous petroleum system in Cauvery basin, India. In: Govindan A (ed) Cretaceous stratigraphy–an update. Mem Geol Soc India, vol 46, pp 365–382

Hallam A (1973) A revolution in the earth sciences, from continental drift to plate tectonics Earth-Sci Rev 10:154–155

Hancock JM, Kauffman EG (1979) The great transgressions of the Late Cretaceous. J Geol Soc 136:175–186

Haq BU, Hardenbol J, Vail PR (1987) Chronology of fluctuating sea levels since the Triassic. Science 235:1156–1167

Hardenbol J, Thierry J, Farley MB, Jacquin T, DeGraciansky PC, Vail PR (1998) Cretaceous sequence chronostratigraphy. In: de Graciansky PC, Hardenbol J, Jacquin T, Vail PR (eds) Mesozoic and Cenozoic sequence stratigraphic framework of European Basins. SEPM Spec Publ 60:3–13

Hart MB, Bhasker A, Watkinson MP (2000) Larger foraminifera from the upper Cretaceous of the Cauvery Basin, S.E. India. Mem Geol Soc India 46:159–171

Hart MB, Joshi A, Watkinson MP (2001) Mid-Late Cretaceous stratigraphy of the Cauvery Basin and the development of the Eastern Indian Ocean. J Geol Soc India 58:217–229

Howard JD, Singh IB (1985) Trace fossils in the Mesozoic sediments Kachchh. Western India. Palaeo Palaeo Palaeo 52:99–122

Hay WW (2008) Evolving ideas about the Cretaceous climate and ocean circulation. Cret Res 29:725–753

Hay WW, Barron EJ, Sloan JL, Southam JR (1981) Continental drift and global pattern of sedimentation. Geol Runds 70:302–315

Hay WW, DeConto RM, Wold CN, Wilson KM, Voigt S, Schulz M, Wold AR, Dullo W-C, Ronov AB, Balukhovsky AN, Söding E (1999) Alternative global Cretaceous paleogeography. GSA Spec Pap 332:1–46

Hildebrand AR, Penfield GT, Kring DA, Pilkington M, Camargo A, Jacobsen SB, Bonton WV (1991) Chicxulub crater: a possible Cretaceous/Tertiary boundary impact crater on the Yucatan Peninsula, Mexico. Geology 19:867–871

Howe J, Cantrill DJ (2001) Palaeoecology and taxonomy of Pentoxylales from the Albian of Antarctica. Cret Res 22:779–793

Huber BT, Norris RD, MacLeod KG (2002) Deep-sea paleotemperature record of extreme warmth during the Cretaceous. Geology 30:123–126

Jaeger JJ, Courtillot V, Tapponnier P (1989) Palaeontological view of the ages of the Deccan Traps, the Cretaceous-Tertiary boundary, and the India-Asia collision. Geology 17:316–319

Jafar SA (1996) The evolution of marine Cretaceous Basins of India: calibration with nannofossil zones. Mem Geol Soc India 37:121–134

Jaitly AK, Ajane R (2013) Comments on Placenticerasmintoi Vredenburg, 1906 from the Bagh Beds Late Cretaceous, central India with special reference to Turonian Nodular Limestone horizon. J Geol Soc India 81:565–574

Jenkyns HC, Forster A, Schouten S, Sinninghe Damsté JS (2004) High temperatures in the Late Cretaceous Arctic Ocean. Nature 432:888–892

Jha S, Bhattacharya B, Nandwani S (2017) Significance of seismites in the Late Cretaceous transgressive Nimar Sandstone succession, Son-Narmada rift valley, central India. Geol J 52:768–783

Kale VS (2020) Cretaceous volcanism in peninsular India: Rajmahal–Sylhet and Deccan Traps. In: Gupta N, Tandon SK (eds) Geodynamics of the Indian Plate, pp 233–289

Kale AS, Phansalkar VG (1992) Nannofossil biostratigraphy of the Utatur Group, Trichinopoly District, South India. Memoire di Scienze Geologiche 43:89–107

Karunakaran C, Ray KK, Saha SS (1964a) A new probe into the tectonic history of the Andaman and Nicobar Islands. Int Geol Congr, 22nd, New Delhi, A4:45

Karunakaran C, Ray KK, Saha SS (1964b) Sedimentary environment of the formation of Andaman flysch, Andaman Islands, India. Int Geol Congr, 22nd, New Delhi, A15:222

Karunakaran C, Ray KK, Saha SS (1968) Tertiary sedimentation in the Andaman-Nicobar geosyncline. J Geol Soc India 9:32–39

Katz MB (1978) Sri Lanka in Gondwanaland and the evolution of the Indian Ocean. Geol Mag 115:237–244

Keller G, Sahni A, Bajpai S (2009) Deccan volcanism, the KT mass extinction and dinosaurs. J Biosci 34:709–728

Keller G, Bhowmick PK, Upadhyay H, Dave H, Reddy AN, Jaiprakash BC, Adatte T (2011) Deccan volcanism linked to the Cretaceouse Tertiary boundary mass extinction: new evidence from ONGC wells in the Krishna-Godavari Basin. J Geol Soc India 78:399–428

Keller G, Jaiprakash BC, Reddy AN (2016a) Maastrichtian to Eocene subsurface stratigraphy of the Cauvery Basin and correlation with Madagascar. J Geol Soc India 87:5–34

Keller G, Punekar J, Mateo P (2016b) Upheavals during the late Maastrichtian: volcanism, climate and faunal events preceding the End-Cretaceous mass extinction. Palaeo Palaeo Palaeo 441:137–151

Kent DS, Muttoni G (2008) Equatorial convergence of India and early Cenozoic climate trends. PNAS 105:16065–16070

Khan SD, Walker DJ, Hall SA, Burke KC, Shah MT, Stockli L (2009) Did Kohistan-Ladakh arc collide first with India? GSA Bull 121:366–384

Kossmat F (1897) The Cretaceous deposits of Pondicherry. Rec Geol Surv India 30:51–110

Krause DW, Prasad GVR, Von Koenigswald W, Sahni A, Grine F (1997) Cosmopolitan among Gondwana Late Cretaceous mammals. Nature 390:504–507

Krishna J (1987) An overview of the Mesozoic stratigraphy of Kachchh and Jaisalmer basins. J Paleontol Soc India 32:136–149

Kumar S, Bhandari LL (1973) Palaeocurrent analysis of the Athgarh Sandstone (Upper Gondwana), Cuttack District, Orissa. Sediment Geol 10:61–75

Kumar S, Singh IB, Singh SK (1977) Lithostratigraphy, structure, depositional environment, palaeocurrent and trace fossils of the Tethyan sediments of Malla-Johar Area, Pithoragarh-Chamoli district, Uttar Pradesh, India. J Paleontol Soc India 20:396–435

Kumar S, Pathak DB, Pandey B, Jaitly AK, Gautam JP (2018) The age of the Nodular Limestone Formation (Late Cretaceous), Narmada Basin, central India. J Earth Sys Sci 127:109. https://doi. org/10.1007/S12040-018-1017-1

Lal NK, Siawal A, Kaul AK (2009) Evolution of east coast of India–a plate tectonic reconstruction. J Geo Soc India 73:249–260

Larson R (1977) Early Cretaceous breakup of Gondwanaland off western Australia. Geology 5:57–60

Li ZX, Powell CMA (2001) An outline of the palaeogeographic evolution of the Australian region since the beginning of the Neoproterozoic. Earth-Sci Rev 53:237–277

Mahender K (2012) Mesozoic of Kachchh Basin: stratigraphic sedimentology: integrated approach. In: Key Note Address Presented at the National Level Field Workshop and Brainstorming Session on Geology of Kachchh Basin, Western India: Present Status and Future Perspectives Held from Jan 26-29 at KSKV Kachchh University, Bhuj

Mancini EA, Puckett TM, Tew BH (1996) Integrated biostratigraphic and sequence stratigraphic framework for Upper Cretaceous strata of the eastern Gulf Coastal Plain, USA. Cret Res 17:645–669

Mancini EA, Puckett TM (2005) Jurassic and Cretaceoustransgressive regressive (T-R) cycles, Northern Gulf of Mexico, USA. Stratigraphy 2:31–48

Mandal A (2017) Facies analysis and sequence-building in parts of the Lower Cretaceous Bhuj Formation, Kutch, India. Unpublished PhD thesis. Jadavpur University, Kolkata

Mandal A, Koner A, Sarkar S, Tawfik HA, Chakraborty N, Bhakta S, Bose PK (2016) Physicochemical tuning of palaeogeographic shifts: Bhuj Formation, Kutch, India. Mar Pet Geol 78:474–492

Mankar RS, Srivastava AK (2015) Salbardi-Belkher inland basin: a new site of Lameta sedimentation at the border of districts Amravati, Maharashtra and Betul, Madhya Pradesh, Central India. Curr Sci 109:1337–1344

Markl RG (1974) Evidence for the breakup of eastern Gondwanaland by the Early Cretaceous. Nature 251:196–200

Mateo P, Keller G, Punekar J, Spangenberg JE (2017) Early to Late Maastrichtian environmental changes in the Indian Ocean compared with Tethys and South Atlantic. Palaeo Palaeo Palaeo 478:121–138

McLoughlin S, Pott C (2009) The Jurrassic flora of Western Australia. GFF 131:113–136

Medlicott HB (1871) Geological sketch of Shillong Plateau. Geol Surv India Mem 7:151–207

Merh SS (1995) The Geology of Gujarat. Geological Society of India, Bangalore

Miller KG, Kominz Michelle A, Browning James V, Wright James D, Mountain Gregory S, Katz Miriam E, Sugarman Peter J, Cramer Benjamin S, Christie-Blick N, Pekar SF (2005) The Phanerozoic record of global sea-level change. Science 310:1293–1298

Mishra AK, Malarkodi N, Singh AD, Babu D, Prasad V (2020) Age of the earliest transgressive event in the Krishna-Godavari Basin, India: evidence from dinoflagellate cysts and planktonic foraminifera biostratigraphy. J Palaeogeography 9:4. https://doi.org/10.1186/s42501-019-0052-4

Mishra PK, Singh J (1997) Biostratigraphy and paleoenvironmental studies of the post-Trappean succession, Bengal Basin. Ind J Geol 69:65–82

Mitra KC, Ghosh DN (1964) A note on the Chari series around Jhura Dome, Kutch. Sci Cult 30:192–194

Mohan M (1995) Cambay Basin—a promise of oil and gas potential. J Palaeontol Soc India 40:41–47

Mukherjee MK (1983) Petroleum prospects of Cretaceous sediments of the Cambay Basin, Gujarat, India. J Pet Geol 5:275–286

Mukhopadhyay SK (2010) Paleoclimate in Asia during the Cretaceous-their variations, causes and biotic and environmental responses. IGCP project-507 Geol Surv India

Nagendra R, Nagendran G, Narasimha L, Jaiprakash BC, Reddy AN (2002a) Sequence stratigraphy of Dalmiapuram Formation, Kallakkudi Quarrye II, South India. J Geol Soc India 59:249–258

Nagendra R, Raja R, Reddy AN, Jaiprakash BC, Bhavani R (2002b) Outcrop sequence stratigraphy of the Maastrichtian Kallankurichchi Formation, Ariyalur Group, Tamil Nadu. J Geol Soc India 59:243–248

Nagendra R, Patel Satish J, Deepankar R, Reddy AN (2010) Bathymetric significance of the Ichnofossil assemblages of the Kulakkalnattam Sandstone, Ariyalur Area, Cauvery Basin. J Geol Soc India 76:525–532

Nagendra R, Kamalak Kannan BV, Sen G, Gilbert H, Bakkiaraj D, Nallapa Reddy AN, Jaiprakash BC (2011a) Sequence surfaces and paleobathymetric trends in Albian to Maastrichtian sediments of Ariyalur area, Cauvery Basin, India. Mar Pet Geol 28:895–905

Nagendra R, Nagarajan R, Bakkiaraj D, Armstrong-Altrin JS (2011b) Depositional and post depositional setting of Maastrichtian limestone, Ariyalur Group, Cauvery Basin, South India: a geochemical approach. Carb Evap 26:127–147

Nagendra R, Reddy AN, Jaiprakash BC, Gilbert H, Zakharov YD, Venkateshwarlu M (2018) Integrated Cretaceous stratigraphy of the Cauvery Basin, South India. Stratigraphy 15:245–259

Naik MK (2013) On some megainvertebrate (mollusca, echinodermata and brachiopoda) fossils from Bagh Beds, Madhya Pradesh. Rec Zool Surv India 113:137–144

Naqvi SM (2005) Geology and evolution of the Indian Plate: from Hadean to Holocene, 4 Ga to 4 Ka. Capital, New Delhi (Chapter 2)

Narasimha Chari MV, Sahu JN, Banerjee B, Zutschi PL, Chandra K (1995) Evolution of the Cauvery Basin, India from subsidence modeling. Mar Pet Geol 12:667–675

Narayanan V (1977) Biozonation of the Uttatur Group, Trichinopoly, Cauvery Basin. J Geol Soc India 18:415–428

Norris RD, Bice KL, Magno EA, Wilson PA (2002) Jiggling the tropical thermostat in the Cretaceous hothouse. Geology 30:299–302

Parson LM, Evans AJ (2005) Seafloor topography and tectonic elements of the western Indian Ocean. Phil Trans Royal Soc A363:15–24

Pascoe EH (1959) A manual of the geology of India and Burma, 3rd edn, vol II. Geol Surv India, Kolkata

Perry CT, Beavington-Penney SJ (2005) Epiphytic calcium carbonate production and facies development within sub-tropical seagrass beds, Inhaca Island, Mozambique. Sediment Geol 174:161–176

Petrizzo MR, Huber BT (2006) On the phylogeny of the late Albian genus Planomalina. J Foraminfer Res 36:233–240

Powell C, McA Roots SR, Veevers JJ (1988) Pre-breakup of continental extension in East Gondwanaland and the Early Cretaceous opening of the eastern Indian Ocean. Tectonophys 155:261–283

Prabhakar KN, Zutschi PL (1993) Evolution of the southern part of Indian east coast basins. J Geol Soc India 41:215–230

Prakash N (2008) Biodiversity and palaeoclimatic interpretation of Early Cretaceous flora of Jabalpur Formation, Satpura Basin, India. Palaeoworld 17:253–263

Prasad B, Jain AK (1994) Triassic palynoflora from the Krishna-Godavari Basin (India) and its stratigraphic significance. J Geol Soc India 43:239–254

Prasad B, Pundir BS (1999) Biostratigraphy of the exposed gondwana and cretaceous rocks of Krishna-Godavari Basin, India. J Palaeontol Soc India 44:91–117

Prasad GVR, Rage JC (1995) Amphibians and squamates from the Maastrichtian of Naskal, India. Curr Res 16:95–107

Prasad GVR, Sahni A (1999) Were there size constraints on biotic exchanges during the northward drift of the Indian plate? Proc Indian Nat Sci Acad 65A:377–396

Price GD, Hart MB (2002) Isotopic evidence for Early to mid-Cretaceous ocean temperature variability. Mar Micropal 46:45–58

Punekar J, Mateo P, Keller G (2014) Effects of Deccan volcanism on paleoenvironment and planktic foraminifera: a global survey. In: Keller G, Kerr AC (eds) Volcanism, impacts, and mass extinctions: causes and effects. GSA Spec Paper 505:91–116

Rajanikanth A, Chinnappa CH (2016) Early Cretaceous flora of India–a review. Palaeobotanist 65:209–245

Rajanikanth A, Venkatachala BS, Kumar A (2000) Geological age of the Ptilophyllum flora in India—a critical reassessment. Geol Soc India Mem 46:245–256

Rajanikanth A, Agarwal A, Stephen A (2010) An integrated inquiry of Early Cretaceous Flora, Palar Basin, India. Phytomorphol 60:21–28

Rajnath (1932) A contribution to the stratigraphy of Kutch. Quart J Geol Min Met Soc India 4:161–174

Raju DSN, Ravindran CN, Mishra PK, Singh J (1991) Cretaceous and Cenozoic foraminiferal zonal framework for the east coast sedimentary basins of India. Geosci J 12:156–175

Raju DSN, Ravindran CN, Kalyansundar R (1993) Cretaceous cycles of sea level changes in the Cauvery Basin, India—a first revision. Bull ONGC 30:101–113

Ramanathan S (1968) Stratigraphy of Cauvery Basin with reference to its oil prospects. Mem Geol Soc India 153–167

Ramasamy S, Banerji RK (1991) Geology, petrology and systematic stratigraphy of pre-Ariyalur sequence in Tiruchirapalli District, TamilNadu, India. J Geol Soc India 37:577–594

Ray JS, Pattanayak SK, Pande K (2005) Rapid emplacement of the Kerguelen plume related Sylhet traps, eastern India: evidence from 40Ar/39Ar geochronology. Geophys Res Lett 32:1–4

Reddy AN, Jaiprakash BC, Rao MV, Chidambaram L, Bhaktavatsala KV (2013) Sequence stratigraphy of late Cretaceous successions in the Ramnad sub-basin, Cauvery Basin, India. J Geol Soc India 1:78–97

Reeves C (2014) The position of Madagascar within Gondwana and its movements during Gondwana dispersal. J Africa Earth Sci 94:45–57

Renne PR, Sprain CJ, Richards MA, Self S, Vanderkluysen L, Pande K (2015) State shift in Deccan volcanism at the Cretaceous-Paleogene boundary possibly induced by impact. Science 350:76–78

Rodolfo KS (1969) Sediments of the Andaman Basin, northeastern Indian ocean. Mar Geol 7:371–402

Rodríguez-Tovar FJ, Uchman A, Martin-Algarra A (2009) Oceanic Anoxic Event at the Cenomanian–Turonian boundary interval (OAE-2): ichnological approach from the Betic Cordillera, southern Spain. Lethaia 42:407–417 (Chapter 3)

Ronov AB, Khain VE, Balukhovsky AN (1989) Atlas of lithological paleogeographical maps of the world: Mesozoic and Cenozoic of continents and oceans. USSR Academy of Sciences, Leningrad

Ruidas DK, Paul S, Gangopadhyay TK (2018) A reappraisal of stratigraphy of Bagh Group of rocks in Dhar district Madhya Pradesh with an outline of origin of nodularity of Nodular Limestone Formation. J Geol Soc India 92:19–26

Ruidas DK, Pomoni-Papaioannou FA, Banerjee S, Gangopadhyay TK (2020) Petrographical and geochemical constraints on carbonate diagenesis in an epeiric platform deposit: Late Cretaceous Bagh Group in central. Carb Evaporites 35:94. https://doi.org/10.1007/s13146-020-00624-2

Saha S, Banerjee S, Burley SD, Ghosh A, Saraswati PK (2010) The influence of flood basaltic source terrains on the efficiency of tectonic setting discrimination diagrams: an example from the Gulf of Khambhat, western India. Sediment Geol 228:1–13

Sahni A (1984) Cretaceous-Paleocene terrestrial faunas of India: lack of endemism during drifting of the Indian plate. Science 226:441–443

Sahni A, Kumar V (1974) Palaeogene palaeobiogeography of the Indian subcontinent. Palaeo Palaeo Palaeo 15:209–226

Sahni A, Prasad GVR (2008) Geodynamic evolution of the Indian plate: consequences for dispersal and distribution of biota. Mem Geol Soc India 66:203–225

Sampson SD, Witmer LM, Forster CA, Krause DW, O'Connor PM, Dodson P, Ravoavy F (1998) Predatory dinosaur remains from Madagascar: implications for the Cretaceous biogeography of Gondwana. Science 280:1048–1051

Sarkar S, Koner A (2020) Ancient rip current records and their implications: an example from the Cretaceous Ukra Member, Kutch, India. J Palaeogeography 9:10. https://doi.org/10.1186/s42501-020-00060-2

Sarkar S, Chakraborty N, Mandal A, Banerjee S, Bose PK (2014) Siliciclastic-carbonate mixing modes in the river-mouth bar palaeogeography of the Upper Cretaceous Garudamangalam Sandstone (Ariyalur, India). J Palaeogeography 3:233–256

Sastri VV, Venkatachala SBS, Narayananthe V (1981) Evolution of the East Coast of India. Palaeo Palaeo Palaeo 36:23–54

Sastry MVA, Rao BRJ (1964) Cretaceous—Tertiary boundary in south India. Proc 22nd Int Geol Cong 3:34

Sastry MVA, Rao BRJ, Mamgain VD (1968) Biostratigraphic zonation of the Upper Cretaceous Formation of Trichinopoly district, South India. Mem Geol Soc India 2:10–17

Schlager W, Philip J (1990) Cretaceous carbonate platforms. In: Ginsburg RN, Beaudoin B (eds) Cretaceous resources, events and rhythms. Springer, Dordrecht

Schoene B, Eddy MP, Samperton KM, Keller CB, Keller G, Adatte T, Khadri SFR (2019) U-Pb constraints on pulsed eruption of the Deccan traps across the end-Cretaceous mass extinction. Science 363:862–866

Scotese CR (1997) Paleomap software. Paleomap Project. http://scotese.com

Scotese CR (2015) Some thoughts on global climate change: the transition from Icehouse to Hothouse. PALEOMAP Project 21a

Self S, Jay AE, Widdowson M, Keszthelyi LP (2008) Correlation of the Deccan and Rajahmundry Trap lavas: are these the longest and largest lava flows on Earth? J Volcanol Geother Res 172:3–19

Sellwood BC, Price GD, Valdes PJ (1994) Cooler estimates of Cretaceous temperatures. Nature 370:453–455

Sengupta S (1966) Geological and geophysical studies in western part of the Bengal basin, India. AAPG Bull 50:1001–1017

Sengupta S (2003) Gondwana sedimentation in the Pranhita-Godavari Valley: a review. J Asian Earth Sci 21:633–642

Sheldon ND, Retallack GJ, Tanaka S (2002) Geochemical climofunctions from North American soils and application to paleosols across the Eocene-Oligocene boundary in Oregon. J Geol 110:687–696

Shukla UK, Singh IB (1990) Facies analysis of Bhuj Sandstone (lower Cretaceous) Bhuj area, Kachchh. J Palaeontol Soc India 35:189–196

Singh IB, Shukla UK (1991) Significance of trace fossils in the Bhuj sandstone (lower Cretaceous) Bhuj area, Kachchh. J Paleontol Soc India 36:121–126

Singh IB, Shekhar S, Agarwal SC (1983) Palaeoenvironment and stratigraphic position of green sandstone Lameta: Late Cretaceous Jabalpur area. J Geol Soc India 24:412–420

Smith AB (1988) Late Paleozoic biogeography of east Asia and palaeontological constraints on plate tectonic reconstruction. Phil Trans R Soc London Ser A326:189–227

Smith AG, Briden JC (1977) Mesozoic and Cenozoic paleocontinental maps. Cambridge

Spath LF (1924) On the Blake collection of ammonites from Kutch, India. Palaeontol Indica (G.S.I.) new ser 9, Mem 2

Spath LF (1927–33) Revision of the Jurassic cephalopod fauna of Kutch (Cutch). Palaeontol Indica (G.S.I.). New Ser 9 Mem 2 parts 1/6:1–945

Sprain CJ, Renne PR, Vanderkluysen L, Pande K, Self S, Mittal T (2019) The eruptive tempo of Deccan volcanism in relation to the cretaceous Paleogene boundary. Science 363:866–870

Srivastava AK, Mankar SR (2012) Trace fossils and their palaeoenvironmental significance in the Lameta Formation of Salbardi and Belkher area; district Amravati, Maharashtra, India. Arab J Geos 5:1003–1009

Srivastava AK, Mankar RS (2015) Megaloolithus dinosaur nest from the Lameta Formation of Salbardi area, districts Amravati, Maharashtra and Betul, Madhya Pradesh. J Geol Soc India 85:457–462

Srivastava AK, Kandwal NK, Humane SK, Humane SS, Kundal P, Khare N (2018) Record of calcareous algae from the Lameta Formation: a new insight for possible sea incursion during the Maastrichtian time. Arab J Geosci 11:14. https://doi.org/10.1007/s12517-017-3333-1

Srivastava DK (2003) A new species of Cassiduloid echinoid *Gongrochanus Kier*, 1962 from the late Cretaceous (Maastrichtian) rocks of the Ariyalur area, Tamilnadu, India. J Palaeontol Soc India 48:59–64

Steinhoff D, Bandel K (2000) Paleoenvironment significance of Early to Middle Cretaceous bioherm sequences from the Tiruchirapalli district, Tamil Nadu, southern India. Mem Geol Soc India 46:257–271

Stoliczka F (1873) Cretaceous fauna of southern India. Mem Geol Surv India, Palaeo Ind Ser VIII (3), The Echinodermata

Stoliczka F (1871) Cretaceous fauna of southern India. The Pelecypoda. Mem Geol Surv India, Palaeo Ind 3:1–537

Stoliczka F (1867) Cretaceous fauna of southern India. The Gastropoda. Mem Geol Surv India, Palaeo Ind 2:1–500

Storey M, Mahoney JJ, Sanders AD, Duncan RA, Kelley SP, Coffin SP (1995) Timing of hotspot related volcanism and the breakup of Madagascar and India. Science 267:852–855

Sukh-Dev (1987) Floristic zones in the Mesozoic formations and their relative age. Palaeobotanist 36:161–167

Sundaram R, Rao PS (1979) Lithostratigraphy classification of Uttattur and Trichinopoly Groups of Upper Cretaceous rocks of Tiruchirapalli district, TamilNadu. Misc Publ Geol Surv India 45:111–119

Sundaram R, Rao PS (1986) Lithostratigraphy of Cretaceous and Palaeocene rocks of Tiruchirapalli District, Tamil Nadu, South India. Rec Geol Surv India 115:9–23

Sundaram R, Henderson RA, Ayyasami K, Stilwell JD (2001) A lithostratigraphic revision and palaeoenvironmental assessment of the Cretaceous System exposed in the onshore Cauvery Basin, southern India. Cret Res 22:743–762

Tahirkheli RA (1979) Geology of Kohistan and adjoining Eurasian and Indo-Pakistan continents. Pakistan Geol Bull 11:1–3

Tandon SK (2000) Spatio–temporal patterns of environmental changes in Late Cretaceous sequences of central India. In: Okada H, Mateer NJ (eds) Cretaceous environments of Asia. Developments in palaeontology and stratigraphy. Elsevier, Amsterdam

Tandon SK (2002) Records of the influence of volcanism on contemporary sedimentary environments in central India. Sediment Geol 147:177–192

Tandon SK, Sood A, Andrews JE, Dennis PF (1995) Palaeoenvironments of the dinosaur-bearing Lameta Beds (Maastrichtian), Narmada valley, Central India. Palaeo Palaeo Palaeo 117:153–184

Taylor TN, Taylor EL, Krings M (2009) Paleobotany: the biology and evolution of fossil plants. Academic Press

Tewari BS, Srivastava RP (1965) On the occurrence of Globotruncana in Ariyalur stage of Trichinopoly Cretaceous. Curr Sci 34:150–151

Tewari A, Hart MB, Watkinson MP (1996) A revised lithostratigraphical classification of the Cretaceous rocks of Trichinopoly District, Cauvery Basin, Southeast India. In: Pandey J, Azmi RJ, Bhandari A, Dave A (eds) Contributions to XV Indian colloquium on micropaleontology and stratigraphy, pp 789–800

Tripathi A, Jana BN, Verma O, Singh RK, Singh AK (2013) Early Cretaceous palynomorphs, dinoflagellates and plant megafossils from the Rajmahal basin, Jharkhand, India. J Palaeontol Soc India 58:125–134

Venkatachala BS (1977) Fossil floral assemblages in the east coast Gondwana-a critical review. J Geol Soc India 18:378–397

Voigt S, Michael M, Surlik F, Walaszczyk I, Ulicny D, Cech S, Voigt T, Wiese F, Wilmsen M, Niebuhr B, Reich M, Funk H, Michalik J, Jagt JWH, Felder P, Schulp AS (2008) Cretaceous. In: McCann T (ed) The geology of Central Europe: Mesozoic and Cenozoic, vol 2, pp 923–992

Waagen W (1875) Jurassic fauna of Kuch. The cephalopoda. Mem Geol Surv India. Palaeo Indica Ser 9 Parts 1/4:1–247

Watkinson MP, Hart MB, Joshi A (2007) Cretaceous tectono-stratigraphy and the development of the Cauvery Basin, South-east India. Petrol Geosci 13:181–191

Wilson PA, Norris RD (2001) Warm tropical ocean surface and global anoxia during the mid-Cretaceous period. Nature 412:425–429

Wilson JA, Sereno PC, Srivastava S, Bhatt DK, Khoshla A, Sahni A (2003) A new abelisaurid (Dinosauria, Theropoda) from the Lameta Formation (Cretaceous, Maastrichtian) of India. Contrib Mus Paleontol 3:1–42

Wynne AB (1872) Memoir on geology of Kutch to accompany the map compiled by A.B. Wynne and F. Fedden, during the seasons of 1867–68 and 1868–1869. Mem Geol Surv India 9:1–293

Zakharov YD, Shigeta Y, Nagendra R, Safronov PP, Smyshlyaeva OP, Popov AM, Velivetskaya TA, Afanasyeva TB (2011) Cretaceous climate oscillations in the southern palaeolatitudes: new stable isotope evidence from India and Madagascar. Cret Res 32:623–645

Radiation of Flora in the Early Triassic Succeeding the End Permian Crisis: Evidences from the Gondwana Supergroup of Peninsular India

Amit K. Ghosh, Reshmi Chatterjee, Subhankar Pramanik, and Ratan Kar

Abstract Understanding the recovery of life and its radiation after the Permian–Triassic mass extinction event (PTME) that took place around 252.28 ± 0.08 Ma is a fascinating aspect of Earth science studies. In this backdrop, we have undertaken a study of the floral diversity based on plant macrofossils and megaspores from the late Permian and early Triassic sediments of the Gondwana Supergroup from Peninsular India. The early Triassic in Peninsular India is represented by the Panchet Formation that overlies the Raniganj Formation (late Permian). The outcrops of late Permian (Raniganj Formation) and early Triassic (Panchet Formation) sediments in the Tatapani-Ramkola Coalfield in Chhattisgarh State are exposed along the major rivers and their tributaries that drain the coalfield. The present work has been carried out on a Permian–Triassic section, exposed at a stream cutting (Iria Nala), in the northern part of Tatapani-Ramkola Coalfield. The macrofloral assemblage of the Raniganj Formation (late Permian) from the base of the outcrop is represented by *Schizoneura gondwanensis, Glossopteris* sp. and *Vertebraria* sp., whereas the overlying Panchet Formation (early Triassic) yielded a moderately preserved macrofloral assemblage represented by *Paracalamites* sp., *Dicroidium hughesii*, *D. zuberi*, *Desmiophyllum* sp., *Glossopteris angustifolia*, *G. communis*, *G. indica* and scale leaf of glossopterids. In addition, a megaspore assemblage hitherto unknown from the early Triassic of Tatapani-Ramkola Coalfield is recorded herein that is represented by nine species belonging to seven genera, out of which one species is new.

Keywords Early triassic · PTME · Floral radiation · Plant macrofossils · Megaspores · Tatapani-Ramkola coalfield

A. K. Ghosh (✉) · R. Chatterjee · S. Pramanik · R. Kar · R. Kar
Birbal Sahni Institute of Palaeosciences, 53 University Road, Lucknow 226007, Uttar Pradesh, India

R. Chatterjee
Department of Botany, Mrinalini Datta Mahavidyapith, Birati, Kolkata 700051, West Bengal, India

1 Introduction

Cycles in fossil diversity from the Permian–Triassic successions of Peninsular India are significant proxies to decipher the climatic scenario during that period. Permian–Triassic mass extinction (PTME) event (252.28 ± 0.08 Ma), is marked by the greatest mass extinction in the Earth's history (Erwin 1993; Shen et al. 2011). Our understanding of the Permian–Triassic Boundary (PTB) is almost exclusively based on the study of marine sediments from Europe and Asia. However, Retallack (1995) and Hallam and Wignall (1997) opined that a similar extinction event took place in the terrestrial environment as well. Nonetheless, it is yet to be established whether the extinction in the terrestrial realm was exactly synchronous to that in the marine environment (De Kock and Kirschvink 2004).

The magnitude of floral extinction and the overall change in diversity is more ambiguous, as there are no major peaks in mass extinction for plants in the fossil record. However, some plants were very much affected and got extinct at the Permian–Triassic boundary. The PTME event marks a major overturn of plant ecosystems. In the Permian, glossopterids dominated, while after the PTME, corystosperms took over the dominance.

A large (~0.9%) sudden global decrease in the stable isotope $\delta^{13}C$ coincides with the PTME; so the extinctions can be attributed to increased aridity, higher CO_2 concentration (about 2000 ppm) and a substantial rise in temperature (~8 °C), as a consequence of the eruption of Siberian Trap flood basalts (Magaritz 1989; Krull and Retallack 2000; Dolenec et al. 2001; Musashi et al. 2001; McElwain and Punyasena 2007).

Stable isotopic study reveals that the Permian–Triassic Boundary is characterized by worldwide negative $\delta^{13}C$ excursion as evidenced in marine limestones (Holser and Magaritz 1987; Baud et al. 1989; Krystyn et al. 2003), marine organic carbon (Magaritz et al. 1992; Wang et al. 1994), terrestrial organic carbon (Morante 1996; Krull and Retallack 2000; Sarkar et al. 2003; Metcalfe et al. 2009) and pedogenic carbonates (MacLeod et al. 2000).

Continental Permian and Triassic rocks are exposed in many sedimentary basins of Peninsular India, e.g., the Damodar, Son-Mahanadi and South Rewa basins. Some of the best sections of Permian and Triassic sequences are preserved in the Raniganj Coalfield (West Bengal), East Bokaro Coalfield (Jharkhand), Auranga Coalfield (Jharkhand) and Tatapani-Ramkola Coalfield (Chhattisgarh). However, in most of the outcrops, continuous sections, straddling the Permian–Triassic transition are not preserved. The basins are intra-cratonic, where the Permian rocks unconformably lie over the Precambrian basement. The topmost unit of the Permian sediments is represented by the Raniganj Formation, which in turn lies below the Panchet Formation. The contact between the Raniganj Formation of late Permian age (Lopingian) and the overlying early Triassic (Induan) Panchet Formation is either gradational or characterized by local unconformities. A similar stratigraphic framework is also evident in the East Bokaro, Auranga and Tatapani-Ramkola coalfields. Triassic floral diversity is rather poorly known in comparison to the Permian sequences in all these basins.

Based on distinct lithology, flora and fauna, the Panchet Formation is considered as the basal Triassic sequence in the continental deposits of India. From Peninsular India, geochemical and organic carbon isotope studies across the continental Permian–Triassic Boundary in Raniganj Coalfield (West Bengal), Damodar Valley Basin has been carried out (Sarkar et al. 2003). Tiwari and Vijaya (1992) reviewed the Permian–Triassic transition in Peninsular India based on marker palynological assemblages recovered from borecores. Recently, Kar and Ghosh (2018) recorded *Reduviasporonites*, a marker palynomorph from the Permian–Triassic transition of Peninsular India and attempted to demarcate the transition based on palynology. The Permian–Triassic section at Guryul Ravine, near Srinagar in Kashmir (India), has long been debatable regarding the placement of the Permian–Triassic boundary (Erwin 1993). It was earlier considered for the Permian–Triassic Global Stratotype Section and Point (GSSP) prior to the selection of Meishan D in Zhejiang Province, China (Kapoor 1996; Yin et al. 2001). At Guryul Ravine, the Lopingian (late Permian) Zewan Formation is overlain by the early Triassic Khunamuh Formation. Sequencing events across the Permian–Triassic Boundary have been identified by Algeo et al. (2007) in the Guryul Ravine section. Later on, Tewari et al. (2015b) clearly demarcated the Permian–Triassic palynological transition in the Guryul Ravine section, Kashmir, India and commented on its implications for Tethyan Gondwanan correlations.

The Triassic period marks the onset of the Mesozoic Era and extends from about 252–201 Ma (Gradstein et al. 2012). The Triassic Period is one of the least explored sequences, but in terms of evolution it is highly significant. This is one of the most significant periods in the evolution of the plant kingdom when several groups (e.g. sphenopsids, ferns, conifers) underwent morphological changes from primitive late Paleozoic forms to the first representatives of modern, derived morphologies, and adapted accordingly to withstand a new set of environmental conditions that prevailed during the Triassic.

The Triassic sediments in Peninsular India exhibit fluvio-lacustrine deposits. A complete record of the entire Triassic sequence is not known from any of the Gondwana Basins in the Indian Peninsula. The study of Triassic terrestrial flora is significant since it throws light on the onset and evolution of Mesozoic terrestrial ecosystems.

The Triassic palaeofloristics of Peninsular India is rather poorly known in comparison to the underlying Permian sequence. The South Rewa and Satpura basins occupy the heart of the Indian Peninsula. The Panchet Formation of Tatapani-Ramkola Coalfield of the South Rewa Basin is well established based on palynology (Srivastava et al. 1997; Kar and Ghosh 2018). However, the record of plant macrofossils is scanty (Saxena et al. 2019) and megaspores have not yet been reported from the Panchet Formation of Tatapani-Ramakola Coalfield. In the present contribution, these aspects have been undertaken to understand the early Triassic floral diversity.

Though in the continental Permian and Triassic deposits of Peninsular India, contributions have been made to recognize the Permian–Triassic transition based on

sporadic studies on plant macrofossils, palynomorphs and isotopic analysis; integrated study on plant macrofossils and megaspores has not yet been done. Therefore, this contribution is focused to evaluate the floral changes vis à vis the climatic changes, after the greatest mass extinction i.e. PTME in the history of planet Earth.

2 Geological Setting

In Peninsular India, the Gondwana Supergroup is composed of predominantly non-marine sequences that were deposited in several isolated outcrops and are distributed in various intracratonic basins, viz. Pranhita–Godavari, Koel-Damodar, Satpura, Narmada, Rajmahal and Son-Mahanadi basins. These sediments were deposited under a wide array of depositional environments ranging from glacial, glacio-fluvial, glacio-marine, fluvial, lacustrine to shallow- marine over a prolonged period (Mukhopadhyay et al. 2010). However, marine signatures in Indian Gondwana have also been recorded (Goswami 2008; Mukhopadhyay et al. 2010). Lithologically, the Gondwana sediments comprise of mainly conglomerates, sandstones, shales and coals of fluvial and lacustrine origin, ranging from late Carboniferous to early Cretaceous (Fox 1931; Sastry et al. 1977). The Gondwana basins of Peninsular India occur along four major linear belts: (i) Trans-Indian Basin that includes the ENE-WSW trending Satpura and Son Valley basins and E-W to WNW-ESE trending Damodar-Koel Valley basins (ii) NNW-SSE trending Wardha-Pranhita–Godavari Valley Basin (iii) NW–SE trending Mahanadi Valley Basin that swerves to WNW-ESE direction in the southernmost Talcher Coalfield and (iv) NNW-SSE trending Rajmahal Basin. However, in none of these basins the sequence is complete. These successions share the floral and faunal elements of the Gondwana strata of South America, South Africa, Australia, Antarctica, New Zealand and Madagascar (McLuoghlin 2001). The Gondwana succession of India has attracted earth scientists owing to its huge coal reserves. Earlier, various contributions have been made on the macro- and microfloral contents of the Gondwana succession (Tiwari and Tripathi 1992; Goswami and Singh 2013 and references therein). However, from the biostratigraphic point of view, palynological studies have been the most useful for relative age determination and intra- and inter- basinal correlation of the Gondwana Supergroup in Peninsular India (Tiwari and Tripathi 1992 and references therein).

In the Indian peninsular deposits, attempts have been made to trace the Permian–Triassic transition with reference to the boundary between the Raniganj and Panchet formations of the Gondwana Supergroup (Sastry et al. 1977; Sarkar et al. 2003), though the sharp contact between the two formations is not well demarcated, as the succession is mostly gradational and devoid of any marker macrofossils. Another major constrain is the lack of continuous sections, because the sections of Raniganj and Panchet formations rarely occur in stratigraphically continuous successions and are mostly confined in isolated outcrops. However, palynomorphs are mostly present throughout the Permian–Triassic succession that characterizes the change of palynoflora across the PTB.

The area of the present study, the Tatapani-Ramkola Coalfield, is the western extension of the Damodar-Koel Valley basin. It is located between 23°30´–23°55´ N latitudes and 83°00´–83°40´E longitudes in the Balrampur District of Chhattisgarh State. It is an east–west trending composite coalfield comprising a northern strip of coal-bearing rocks referred to as Tatapani Coalfield and a southern one called the Ramkola Coalfield.

The pioneering geological work in the coalfield was done way back in 1878–79 (Griesbach 1880). Thereafter, further mapping was carried out in the 1950, 60 and 70s by the Coal Wing of the Geological Survey of India (Raja Rao 1983). However, most of the work was confined to isolated pockets only, as lack of proper communication facilities was a major constraint in the development of the coalfield. Since the last three decades, the Coal Wing, GSI has carried out detailed mapping and drilling operations in different blocks of the coalfield for the estimation of sub-surface coal reserves. Palaeobotanical work was initiated in the 1970s, wherein some fragmentary plant remains were reported (Bose et al. 1977). Since 1990s, detailed palynological studies have been undertaken for stratigraphic resolution of different formations and demarcation of coal-bearing horizons (Srivastava et al. 1997; Srivastava and Kar 2001; Kar 2001, 2003, 2012; Kar and Srivastava 2003; Kar and Ghosh 2018). Studies pertaining to coal petrology have also been undertaken (Sarana 2002; Sarana and Anand-Prakash 2002; Sarana and Kar 2011). Some fructifications of late Permian age have been reported from the area (Chandra et al. 2008; Singh et al. 2011); however, a comprehensive account of plant macrofossils and megaspore assemblages especially of the early Triassic (Panchet Formation) is still lacking except the recent account of macrofossils by Saxena et al. (2019).

The topography of the coalfield is mostly flat, with minor undulations and is flanked on all sides by hillocks of Precambrian rocks. The central part is occupied by vast stretches of Upper Gondwana sediments forming ridges and low hills, which separates the coal-bearing Lower Gondwana sediments of the north and south. The Gondwana Sequence in Tatapani-Ramkola Coalfield is represented by Talchir, Karharbari, Barakar, Barren Measures, Raniganj, Panchet and Mahadeva Formations. The sediments of the Karharbari and Barren Measures formations were initially not recognized but were subsequently established by palynological studies (Kar 2003; Kar and Srivastava 2003).

3   Materials and Methods

An excellent outcrop of the sediments of Raniganj and Panchet formations has been recognized on the right bank of Iria 'nala' (stream), 5 km before Wadruf Nagar town, below the road bridge on Varanasi-Ambikapur road (Fig. 1). The basal part of the section consists of sediments of the Raniganj Formation and commences with a dark grey shale bed, followed by a thin coal layer. It is succeeded by interbedded sandstone and shale units. The sandstone is pale white in colour, micaceous, fine-grained, having well-marked ripple laminations and with thin intercalations of grey shales. The shale
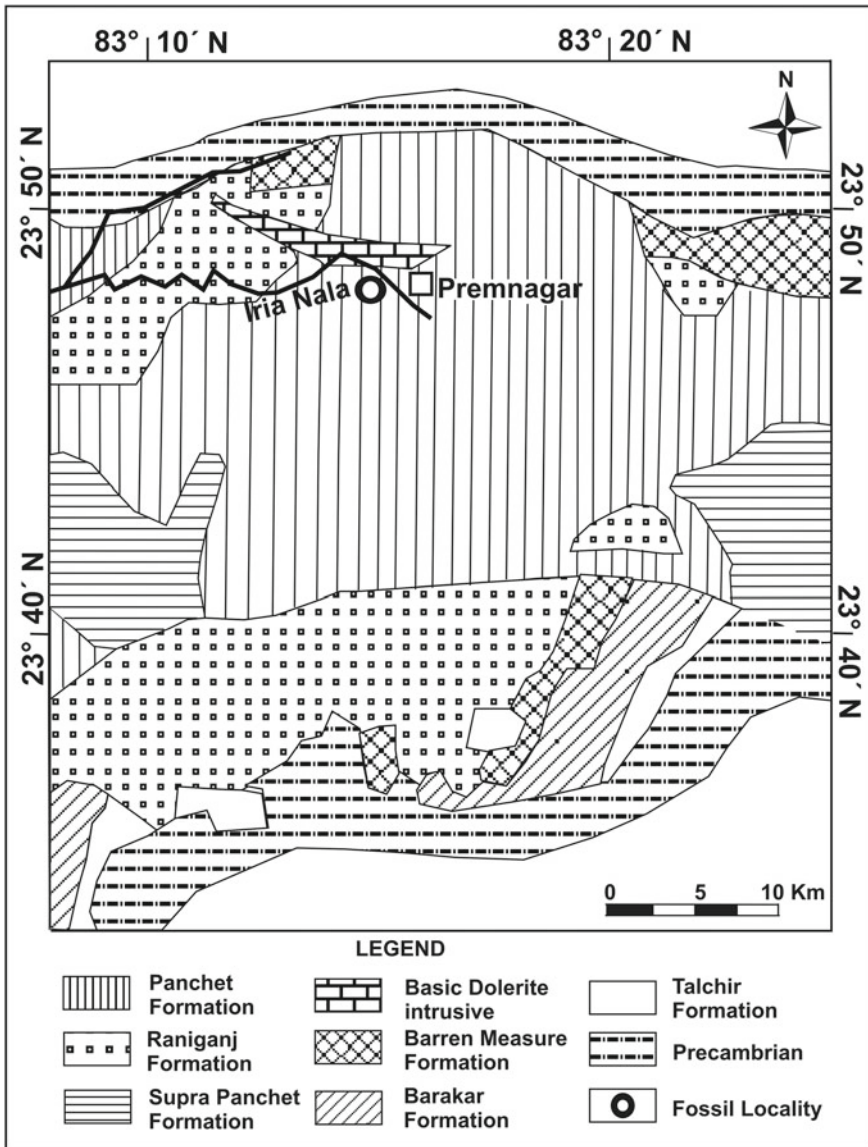
Fig. 1 Part of geological map of Tatapani-Ramkola Coalfield showing the location of the study area (modified from Raja Rao 1982)
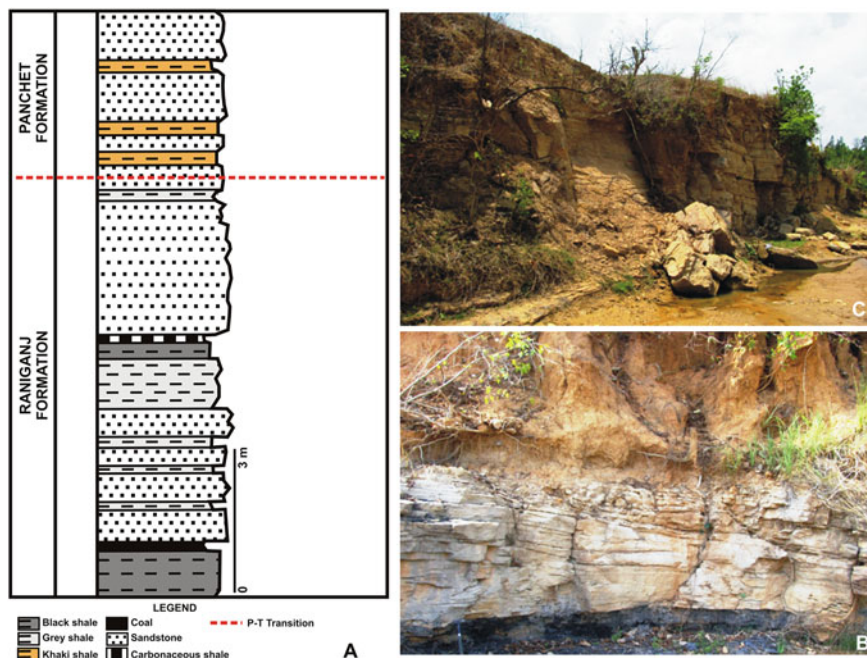
Fig. 2 **a** Litholog of the outcrop showing the transition of Raniganj and Panchet Formations (Modified after Kar and Ghosh 2018). **b** Field photograph of the outcrop showing the lithological features of the Raniganj Formation (late Permian). **c** Field photograph of the outcrop showing the lithological features of the Panchet Formation (early Triassic)

beds contain profuse impressions of plant macrofossils of late Permian affinity, and above it a sandstone-shale sequence is again exposed (Figs. 2a, b). This sandstone is dirty white in colour and coarser than the underlying layers. The overlying shale beds are khaki-green in colour and compare closely with the shales of the Panchet Formation in its type area (Figs. 2a, c). These khaki shales have yielded the plant macrofossils and megaspores.

The detailed morphographic study of the plant macrofossils was made under reflected light using a Leica Wild M420 Stereo–binocular microscope. All the macro-fossils are preserved as impressions. The macrofossils were photographed with a Nikon D2X digital camera, under strong reflected light at various angles, to obtain a clear expression of the surface features. Figured specimens are housed in the museum of the Birbal Sahni Institute of Palaeosciences, Lucknow.

Megaspores have been recovered in a dispersed state; hence to isolate them from the rock matrix the standard maceration technique (Schulze 1855; Wellman and Axe 1999; Traverse 2007) was followed. The samples were crushed and sizes of the fragments were kept roughly up to 2×2 mm in size, washed in distilled water, followed by digestion in 40% Hydrofluoric acid to remove the silica content. The process took 2–3 days, during which fresh acid was added every day with frequent

stirring. After neutralizing the acid and thorough cleaning with distilled water, it was treated with 15% Nitric acid, and kept for 2–3 days for digestion. The residue was thoroughly washed in distilled water through 150 µm meshes. The megaspores were dried and then individually picked under low power binocular microscope. These were studied and photographed in dry conditions with reflected light as well as in transmitted light. Thereafter, these were gradually treated individually with 15% Nitric acid and dilute Ammonium Hydroxide and photographs were taken in wet condition. Necessary measurements were taken both in dry and wet conditions. All the photographs were taken in Olympus microscope BX50 by (Olympus DP26 camera) using CellSens Standard. SEM study was carried out using LEO 430 after treating the single megaspore in absolute alcohol 4–5 times and in $AgNO_3$, to increase the conductivity and then finally coated with palladium.

Identification of the megaspores is largely based on gross morphological traits, such as spore shape, nature of trilete features and structural details of the wall layers. In addition, features like nexine, mesosporium, inner body, basal lamina, presence or absence of pits and cushions etc. are the required criteria for the identification of megaspores (Høeg et al. 1955; Spinner 1969). All the figured slides and SEM stubs are housed in the repository of Birbal Sahni Institute of Palaeosciences, Lucknow.

4 Results

4.1 Plant Macrofossils from the Late Permian (Raniganj Formation) and Early Triassic (Panchet Formation)

Systematic Palaeobotany
Division: Tracheophyta
Subdivision: Euphyllophytina
Class: Equisetopsida
Order: Equisetales
Family: Equisetaceae
Genus: *Schizoneura* Schimper and Mougeot
Schizoneura gondwanensis Feistmantel (Fig. 3a)

Remarks The occurrence of *Schizoneura gondwanensis* is common in the Permian sediments of Peninsular India. The present specimen from the Raniganj Formation bears a striking resemblance with the forms extensively reported from the Raniganj Formation of Peninsular India, which is characterized by leaf sheaths having prominent veins radiating from the base and running almost parallel to each other that converge towards the apex.

Genus: *Paracalamites* Zalessky
Paracalamites sp. (Fig. 3d)

Remarks This form recovered from the Panchet Formation (early Triassic) resembles equisetaceous stems assignable to the genus *Paracalamites.* Lele (1955) assigned the articulated stems under the genus *Neocalamites.* Earlier Zalessky (1932) erected the form genus *Paracalamites* that included the equisetaceous stems without leaf-sheaths and this view was supported later by Boureau (1964), Rigby (1966) and Holmes (2001).

Division: Spermatophyta
Class: Gymnospermopsida
Order: Arberiales
Family: Glossopteridaceae
Genus: *Glossopteris* Brongniart
Glossopteris sp. (Fig. 3b)

Remarks Owing to the presence of a characteristic midrib, secondary veins and meshes, this specimen from the Raniganj Formation is assignable to *Glossopteris;* however, due to the unavailability of adequate features the present specimen of *Glossopteris* cannot be safely assigned to any known species of the genus.

Glossopteris communis Feistmantel (Fig. 3f)

Remarks In gross morphological features viz. shape, angle of emergence of the secondary veins, narrow meshes, concentration of veins near the midrib and margin, the specimens resemble *Glossopteris communis* of Feistmantel (1879), Bose et al. (1977), Banerji and Bose (1977) described from the early Triassic of Peninsular India. This species recorded herein from the Panchet Formation is more common in the late Permian sediments of India; however, their size and dimensions are greater than the early Triassic forms (Chatterjee et al. 2014).

Glossopteris indica Schimper (Fig. 3g)

Remarks Feistmantel (1879) described *Glossopteris indica* from the South Rewa Basin. The presently studied specimen from the Panchet Formation bears a striking resemblance in the nature of secondary veins and architecture of meshes (i.e. broad near the midrib and narrow as well as elongated near the margin) described by Bose and Banerji (1976) from the Auranga Coalfield. Bose et al. (1977) also recovered *G. indica* from the Triassic sediments of Tatapani-Ramkola coalfield. This species is more common in the Permian sediments of other Gondwanan countries. However, recently Tewari et al. (2015a) recorded this species from the Triassic of Antarctica.

Glossopteris angustifolia Brongniart (Fig. 3e)

Remarks In venation pattern and architecture of meshes (narrow and elongated meshes) the present specimen from the Panchet Formation resembles those described by Brongniart (1828). However, the dimension of early Triassic specimens of *Glossopteris angustifloia* is comparatively reduced in comparison to the Permian sediments (Chatterjee et al. 2014). This species was also reported earlier from the early Triassic of Peninsular India (Bose and Banerji 1976; Bose et al. 1977; Banerji and Bose 1977).

Genus: *Vertebraria* Royle ex McCoy
Vertebraria sp. (Fig. 3c)

Remarks The genus *Vertebraria* recorded herein from the Raniganj Formation is often found in close association with *Glossopteris* in the Permian Gondwana. Though *Vertebraria* is a commonly occurring form in the Permian sediments of Indian Gondwana (Sen 1955; Pant 1956; Surange and Maheshari 1962; Goswami 2006) and elsewhere, so far there is a single report of *Vertebraria* by Bhowmik and Parveen (2012) from the Triassic of Nidpur, Central India.

Family: Eretmoniaceae
Genus: *Eretmonia* du Toit
Eretmonia sp. (Figs. 4a, b)

Remarks These scale leaves recovered from the Panchet Formation are characterized by rhomboidal shape with numerous veins forming polygonal meshes and are comparable to the scale leaf of glossopteridean fructification *Eretmonia* du Toit 1932. *Eretmonia* is rather uncommon in the Triassic sediments of India (Banerji et al. 1976; Pal et al. 2010) as well as other Gondwana countries. It is fairly common in the late Permian sequence (Surange and Chandra 1974; Retallack 1980; Rydberg et al. 2012).

Division: Spermatophyta
Class: Gymnospermopsida
Order: Corystospermales
Family: Corystospermaceae
Genus: *Dicroidium* Gothan
Dicroidium hughesii (Feistmantel) Lele (Figs. 4c, d, e, f)

Remarks *Dicroidium hughesii* is represented by nine specimens in the present macrofloral assemblage of Panchet Formation. *Dicroidium hughesii* is the most common species recovered from the Triassic sediments of Peninsular India. Based on the external morphologies such as size, shape of pinnules (obtuse to rounded apex with a constricted base) and odontopteroid venation pattern, the present specimens are assignable under *D. hughesii* (Pal et al. 2014). It has also been reported from India and other Gondwana countries like Australia and South Africa (Lele 1962; Pal 1984, 1985, 1990; Pal et al. 1991; Anderson and Anderson 1989; Artabe et al. 2007).

Dicroidium zuberi (Szajnocha) Archangelsky (Figs. 4g, h)

Remarks The presently studied specimens from the Panchet Formation resemble *D. zuberi* based on its characteristic features namely, pinnules with typical venation pattern characteristic of the species, e.g. 3–4 dichotomously branched primary veins concentrating at a basiscopic point. The presently described specimens resemble *D. zuberi* reported earlier from India, Australia, Antarctica, South Africa and Argentina (Archangelsky 1968; Retallack 1977; Anderson and Anderson 1983, 2008; Pal 1984; Banerji et al. 1987; Banerji and Lemoigne 1987; Escapa et al. 2011; Pal et al. 2014).

Dicroidium sp. (Fig. 4i)

Remarks Owing to the absence of adequate features and venation pattern, it is not justified to assign the specimen to any particular species of *Dicroidium* though in all available morphographic features the specimens from the Panchet Formation corroborates the generic diagnosis of the taxon. Hence, the specimen has been tentatively identified as *Dicroidium* sp.

Class: Incertae classis
Order: Incertae ordinis
Family: Incertae sedis
Genus: *Desmiophyllum* Lesquereux emend. Solms-Laubach
Desmiophyllum sp. (Fig. 4j)

Remarks The present specimens recorded from the Panchet Formation resemble the ginkgoalean leaf *Desmiophyllum* in all morphographic features. The affinity of *Desmiophyllum* is doubtful. As a matter of fact, Retallack (1981) suggested the non-committal name of *Desmiophyllum* for the strap-shaped fossil leaves with parallel venation and considered them as *incertae sedis. Desmiophyllum* has been reported from other Gondwana countries viz. Argentina, Australia, Antarctica and New Zealand (Lacey and Lucas 1981; Retallack 1983; Artabe et al. 2007; Axsmith et al. 2000; McLoughlin 2011; Holmes and Anderson 2013). Till now *Desmiophyllum* have been reported specifically from the late Triassic of India (Lele 1962; Pal et al. 1991; Pal and Ghosh 1997). This is the first report of *Desmiophyllum* from the earliest Triassic of Peninsular India.

4.2 Megaspores from the Early Triassic (Panchet Formation)

Systematic Palynology
Anteturma: Proximegerminantes Potonié
Turma: Triletes (Reinsch) Potonié
Subturma: Azonotriletes Luber
Infraturma: Laevigati (Bennie and Kidston) Potonié
Genus: *Banksisporites* Dettmann
Type Species: *Banksisporites pinguis* (Harris) Dettmann
Banksisporites sinuosus Dettmann (Figs. 5a, b)

Remarks In all the characteristic features viz. size range, shape (*amb* subcircular), granulose exine ornamentation pattern and specifically in having sinuous trilete laesurae, the present specimens resemble *Banksisprites sinuosus* described from the Rhaetian of Tasmania, Australia (Dettmann 1961). The species also has been reported by Banerji et al. (1978) from the Tiki Formation (Norian, late Triassic) of South Rewa Gondwana Basin, Central India.

Infraturma: Apiculati (Bennie and Kidston) Potonié
Genus: *Biharisporites* Potonié emend. Bharadwaj and Tiwari
Type Species: *Biharisporites spinosus* (Singh) Potonié
Biharisporites sparsus Banerji et al. (Figs. 5c, d, e)

Remarks The specimens resemble *Biharisporites sparsus* Banerji et al. (1978) described from the Tiki Formation (Norian, late Triassic) of South Rewa Gondwana Basin, Central India in having subcircular to subtraingular *amb*, conate exosporium and large mesosporium. The present species is comparable to other known species of the genus *Biharisporites* e.g., *Biharisporites maiturensis* Maheshwari and Banerji (1975) and *Biharisporites luguensis* Pal et al. (1997) recorded from the early Triassic of Peninsular India. However, all the morphographic features viz. sparsely distributed coni on the proximal surface of the megaspore and large mesosporium occupying the whole spore cavity of the present specimens conform the diagnosis of *Biharisporites sparsus* Banerji et al. (1978).

Infraturma: Muronati Potonié and Kremp
Genus: *Erlansonisporites* Potonié
Type Species: *Erlansonisporites erlansonii* (Miner) Potonié
Erlansonisporites reticulatus Singh (Figs. 5f, g)

Remarks The taxon *Erlansonisporites reticulatus* was first described by Singh (1964) from the Lower Cretaceous of Mannville Group, east-central Alberta (Canada). In all available morphological features, the present specimens resemble *Erlansonisporites reticulatus* Singh (1964) in having a trilete mark covered entirely by a strong reticulation that extends all over the spore surface.

Genus: *Ricinospora* Bergad
Type Species: *Ricinospora cryptoreticulata* Bergad
Ricinospora sp. (Fig. 6e)

Remarks This species is very rarely represented in the present megaspore assemblage and is not very well preserved. However, in all characteristic features specifically the trilete laesurae covered by coarsely spongiose wall material limited to only in the apical region, the presently recorded megaspore resembles the generic diagnosis of *Ricinospora* first described by Bergad (1978) from the Maastrichtian of south-central North Dakota, USA. The presently described taxon is not comparable to any known species of the genus.

Subturma: Lagenotriletes Potonié and Kremp
Infraturma: Trifoliati, Barbati Potonié
Genus: *Hughesisporites* Potonié
Type Species: *Hughesisporites galericulatus* (Dijkstra) Potonié
Hughesisporites orlowskae Kozur (Figs. 5h, i, j)

Remarks The presently recorded megaspores resemble *Hughesisporites orlowskae* Kozur, 1973 described from the Triassic of Germany and Poland (Kozur 1973; Marcinkiewicz 1978; Batten and Kovach 1990) in having circular *amb*, almost straight trilete laesurae and prominent ornamentation at the apical region. Recently, Neri et al. (2018) recorded the taxon from the Lower Jurassic of Rotzo Formation (Monti Lessini, northern Italy).

Hughesisporites variabilis Dettmann (Figs. 5k, l and 6a)

Remarks In all morphographic features the specimens described above resemble *Hughesisporites variabilis* Dettmann (1961) described from the Rhaetian of Tasmania, Australia. The present specimens are also very closely comparable to those of Banerji et al. (1978) reported from the Tiki Formation (Norian, late Triassic) of South Rewa Gondwana Basin, Central India.

Turma: Barbates Mädler
Genus: *Nathorstisporites hopliticus* Jung
Type Species: *Nathorstisporites hopliticus* Jung
Nathorstisporites hopliticus Jung (Figs. 6b, c, d)

Remarks This species of *Nathorstisporites* resembles *Nathorstisporites hopliticus* Jung (1958) described and illustrated by Dettmann (1961) from the Triassic of South Australia (Leigh Creek Coalfield) which is characterized by subcircular *amb*, raised trilete laesurae, spine like outgrowths those almost mask the trilete mark and granulose exine. The species also has been reported by Banerji et al. (1978) from the Triassic of Tiki Formation, South Rewa Gondwana Basin. Megaspores having affinity with *Nathorstisporites hopliticus* have been very widely recorded from Rhaetian–Hettangian sediments of Greenland (Harris 1935), Sweden (Lundblad 1956), Germany (Jung 1958), Salt Range of Pakistan (Sah and Jain 1968) and Poland (Marcinkiewicz 1971).

Genus: *Noniasporites* Maheshwari and Bajpai
Type Species: *Noniasporites harrisii* Maheshwari and Bajpai
Noniasporites harrisii Maheshwari and Bajpai (Figs. 6f, g, h, i)

Remarks In all characteristic features viz. circular *amb*, reticulate exine with low and narrow muri and presence of well-developed capilli like appendages in the proximal face this species in the present megaspore assemblage resembles *Noniasporites harrisii* described by Maheshwari and Bajpai (1984) from the late Permian of Raniganj Formation, Raniganj Coalfield (Damodar Valley Basin), West Bengal. According to Maheshwari and Bajpai (1984) their samples come from shale sequence, slightly above the Upper Kajora Coal Seam (Seam IX) exposed in the Nonia Nala Section, near Asansol. The exact stratigraphy and age of their samples is uncertain, whether it is late Permian (Raniganj Formation) or early Triassic (Panchet Formation). However, Maheshwari and Banerji (1975) commented that a number of megaspore genera continued their existence from late Permian (Raniganj Formation) to the early Triassic (Panchet Formation) in the Damodar Valley Basin.

Noniasporites triassicus sp. nov. (Figs. 6j, k, l)

Specific diagnosis—Megaspores acavate trilete, *amb* circular to subcircular, trilete laesurae wavy and raised, presence of rills near the trijuncture in the proximal face, exine granulose.

Description—Acavate trilete megaspores, mostly laterally preserved, *amb* circular to subcircular in proximo-distal view, however, in lateral view outline is broadly oval, giving a pitcher shaped appearance, equatorial diameter measuring 274–286 μm in dry state and 249–267 μm in wet condition, polar diameter measuring 280–287 μm in dry state and 289–293 μm in wet condition. After differential maceration in wet condition, there is no remarkable increase in the size of the megaspores. Trilete rays significantly wavy and highly raised, mostly masked due to the presence of rills near the trijuncture. The rill-like exoexinal projections occur in a radial orientation in the proximal side, especially in the inter-ray areas. In wet condition (after differential maceration), the exine appears smooth or laevigate excepting the proximal side. However, in dry state under reflected light as well as under SEM, the exine ornamentation is granulose. Mesosporium is indiscernible in wet conditions.

Comparison and remarks—The genus *Noniasporites* was instituted by Maheshwari and Bajpai (1984) from the Upper Permian of Raniganj Formation, Raniganj Coalfield (Damodar Valley Basin), West Bengal. The age and horizon of the taxon have been described above. *Noniasporites* Maheshwari and Bajpai (1984) is characterized by rill-like exoexinal projections in the inter-ray areas, trilete marks masked by inter-ray ornamentation and the apparent absence of mesosporium. Glasspool (2003), while reviewing the Permian Gondwana megaspores considered *Noniasporites* as a distinct genus. The presently described species resembles the generic circumscription of *Noniasporites* as attributed by Maheshwari and Bajpai (1984). It closely resembles the type species and the only known species i.e. *Noniasporites harrisii* in most of the diagnostic features; however, it differs specifically in the exoexinal ornamentation patterns. The newly instituted species is mostly laterally preserved giving a pitcher shaped appearance, whereas, *Noniasporites harrisii* Maheshwari and Bajpai (1984) is proximo-distally or obliquely preserved. Except the proximal side, the exine ornamentation of *Noniasporites harrisii* under optical microscope appears laevigate but under SEM it gives a corroded appearance. In contrast, the exine ornamentation of the present species is granulose as observed under SEM. In having these distinguishing characters, the new species *Noniasporites triassicus* has been erected.

Holotype—Fig. 6l; BSIP SEM Stub No. 1563.

Type Locality—Iria Nala Section, near Premnagar Village, Balrampur District, Chhattisgarh, Tatapani-Ramkola Coalfield, Chhattisgarh.

Age and Horizon—early Triassic, Panchet Formation.

Derivation of name—After the Triassic Period.
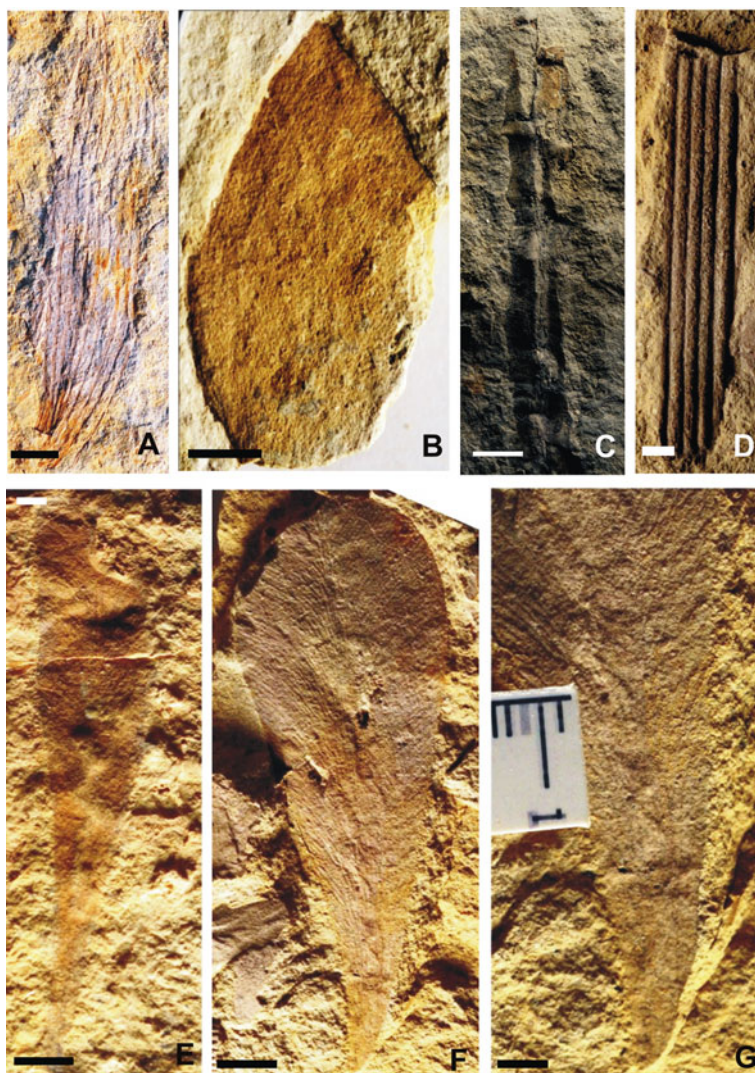
Fig. 3 **a** *Schizoneura gondwananensis* Feistmantel from Raniganj Formation of Tatapani-Ramkola Coalfield, Chhattishgarh; BSIP specimen number 8400/21. **b** *Glossopteris* sp. from Panchet Formation of Tatapani-Ramkola Coalfield, Chhattishgarh; BSIP specimen number 8400/03. **c** *Vertebraria* sp. from Panchet Formation of Tatapani-Ramkola Coalfield, Chhattishgarh; BSIP specimen number 8400/01. **d** *Paracalimites* sp. from Panchet Formation of Tatapani-Ramkola Coalfield, Chhattishgarh; BSIP specimen number 8400/09. **e** *Glossopteris angustifolia* Brongniart from Panchet Formation of Tatapani-Ramkola Coalfield, Chhattishgarh; BSIP specimen number 8400/13. **f** *Glossopteris communis* Feistmantel from Panchet Formation of Tatapani-Ramkola Coalfield, Chhattishgarh; BSIP specimen number 8400/17b. **g** *Glossopteris indica* Schimper from Panchet Formation of Tatapani-Ramkola Coalfield, Chhattishgarh; BSIP specimen number 8400/17a (Scale bar = 10 mm)

Fig. 4 a–b *Eretmonia* sp. from Panchet Formation of Tatapani-Ramkola Coalfield, Chhattishgarh. **a** BSIP specimen number 8399/12; **b** BSIP specimen number 8399/13. **C–f** *Dicroidium hughesii* (Feistmantel) Lele from Panchet Formation of Tatapani-Ramkola Coalfield, Chhattishgarh. **c** BSIP specimen number 8399/54; **d** BSIP specimen number 8400/33; **e** BSIP specimen number 8399/35; **f** BSIP specimen number 8399/55. **g–h** *Dicroidium zuberi* (Szajnocha) Archangelsky from Panchet Formation of Tatapani-Ramkola Coalfield, Chhattishgarh. **g** BSIP specimen number. 8400/35; **h** BSIP specimen number 8399/37. **i** Detached pinnule of *Dicroidium* sp. from Panchet Formation of Tatapani-Ramkola Coalfield, Chhattishgarh. BSIP specimen number 8400/21. **j** *Desmiophyllum* sp. from Panchet Formation of Tatapani-Ramkola Coalfield, Chhattishgarh. BSIP specimen number 8399/53 (Scale bar = 10 mm)
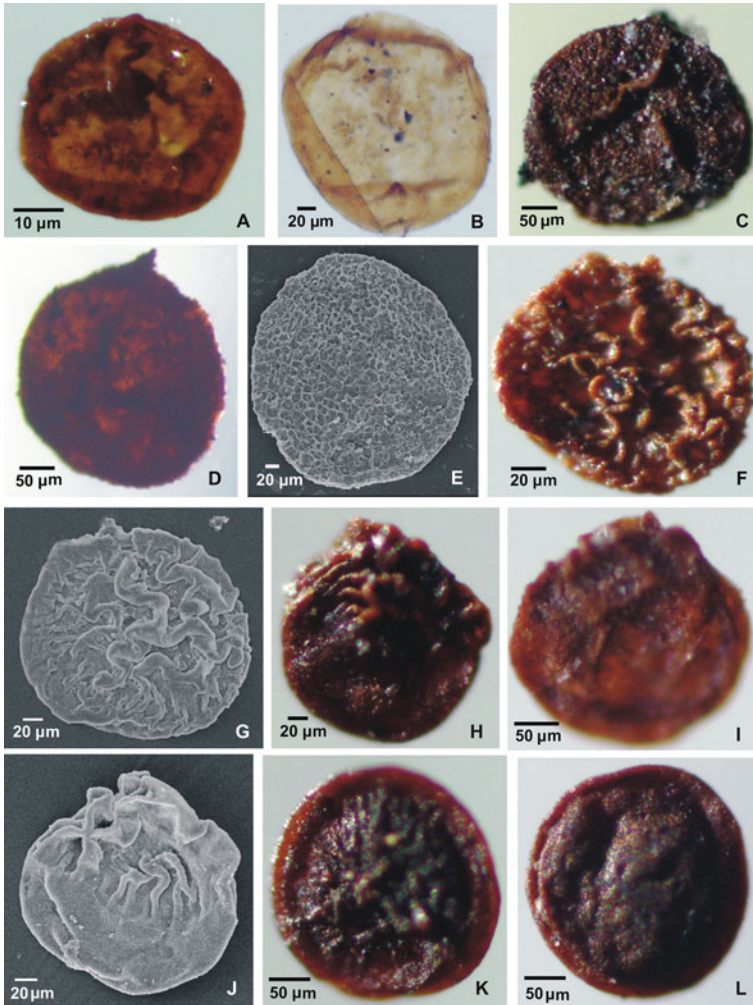
Fig. 5 **a–b** *Banksisporites sinuosus* (Harris) Dettmann **a** Megaspore in dry state showing the distinct trilete mark; **b** Megaspore in wet condition (after maceration). BSIP Slide No. 15640. **c–e** *Biharisporites sparsus* Banerji et al. **c** Megaspore in dry state showing the distinct raised trilete mark. **d** Megaspore in wet condition (after maceration). **e** SEM of the distal face of the megaspore. BSIP SEM Stub No. 15641. **f–g** *Erlansonisporites reticulatus* Singh, **f** Megaspore in dry state showing the ornamentation in the proximal face and distinct raised trilete mark. **g** SEM of the proximal face of the megaspore. BSIP SEM Stub No. 15642. **h–j** *Hugeshisporites orlowskae* Kozur, **h** Megaspore in dry state showing the proximal face with raised trilete mark. **i** Megaspore in wet condition (after maceration). **j** SEM of the proximal face of the megaspore showing sculptural elements. BSIP SEM Stub No. 15643. **k–l** *Hughesisporites variabilis* Dettmann; **k** Megaspore in dry state showing the proximal face showing the ornamentation and trilete mark. **l** Megaspore in dry state showing the distal face. BSIP Slide No. 15644
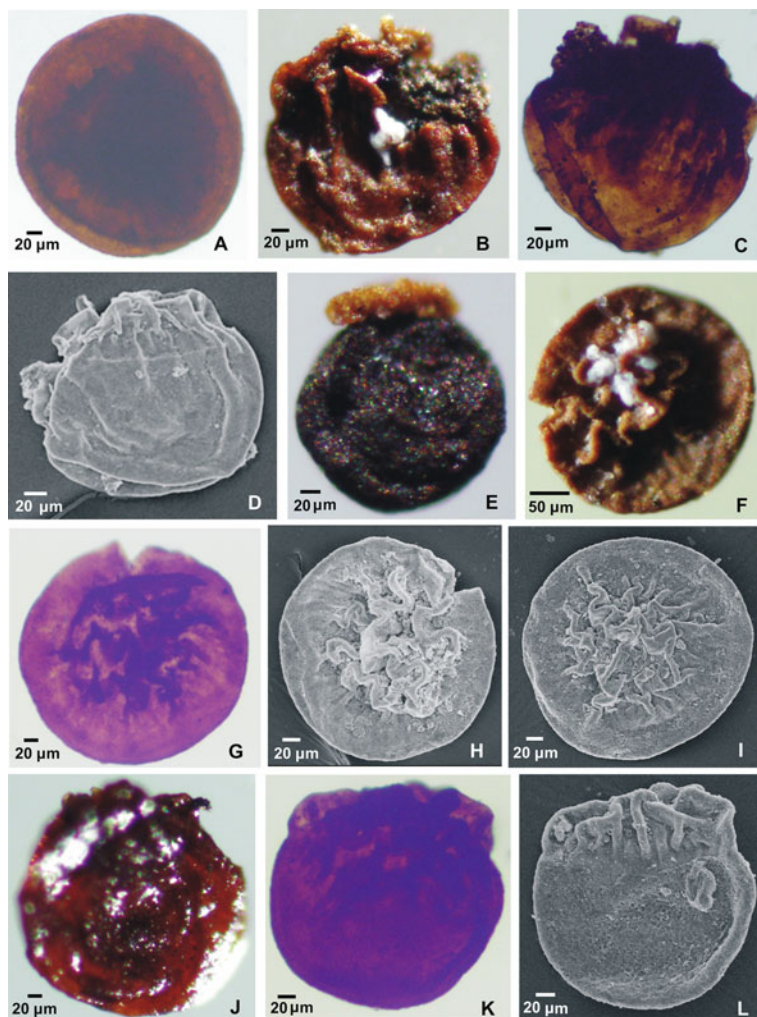
Fig. 6 a *Hughesisporites variabilis* Dettmann, Megaspore in wet condition (after maceration) BSIP Slide No. 15644; **b–d** *Nathorstisporites hopliticus* Jung, **b** Megaspore in dry state showing the proximal face with ornamentation and raised trilete mark. **c** Megaspore in wet condition (after maceration). **d** SEM of the proximal face of the megaspore showing sculptural elements. BSIP SEM Stub No. 15645. **e** *Ricinospora* sp. Megaspore in dry state showing the proximal face with ornamentation. BSIP Slide No. 15646. **f–i** *Noniasporites harrisii* Maheshwari & Bajpai, **f** Megaspore in dry state showing the proximal face with ornamentation. **g** Megaspore in wet condition (after maceration). **h** SEM of the proximal face of the megaspore showing sculptural elements. BSIP SEM Stub No. 15647. **i** SEM of another specimen showing the proximal face of the megaspore with sculptural elements. BSIP SEM Stub No. 15648. **j–l** *Noniasporites triassicus* sp. nov. (Holotype), **j** Megaspore in dry state showing the proximal face with ornamentation. **k** Megaspore in wet condition (after maceration). **l** SEM of the proximal face of the megaspore showing sculptural elements. BSIP SEM Stub No. 1563

5 Discussion

The macrofloral assemblage recorded herein from the Panchet Formation (early Triassic) of Tatapani-Ramkola Coalfield, bears a striking resemblance to the early Triassic macrofloral assemblage from the Auranga Valley, Latehar District, Jharkhand (Bose and Banerji 1976). An assemblage dominated by species of *Dicroidium,* namely *Dicroidium hughesii* and *D. zuberi* bears a striking resemblance to the early Triassic macrofloral assemblages known from other Gondwanan countries viz. Australia, Antarctica, New Zealand and Argentina (Archangelasky 1968; Retallack 1977; Anderson and Anderson 1983, 1989, 2008; Artabe et al. 2007; Escapa et al. 2011). The late Permian vegetation dominated by the glossopterids was gradually replaced by the *Dicroidium* dominated early Triassic vegetation. Late Permian holdovers, namely some species of *Glossopteris* and *Paracalamites* (Equiseatceous stems) continued up to the early Triassic. Recently Saxena et al. (2019) also recorded some plant macrofossils from the Panchet Formation (early Triassic) of Tatapani-Ramkola Coalfield that include *Paracalamites* sp., *Schizoneura gondwanensis*, *Glossopteris indica*, *G. verticilata*, *G. senii*, *G. raniganjensis*, *G. indica*, *G. taeniensis*, *Linguifolium lillieanum, Heidiphyllum elongatum, Heidiphyllum* sp., *?Autunia conferta* and *Dicroidium zuberi.*

Palynological analysis on the samples of the studied outcrop has been carried out by Kar and Ghosh (2018) and they designated four assemblage zones on the basis of dominance/sub-dominance of marker taxa. The four assemblage zones recorded, in ascending order from the base of the outcrop are—Zone I: *Striatopodocarpites-Densipollenites,* Zone II: *Striatopodocarpites-Crescentipollenites,* Zone III: *Falcisporites-Klausipollenites* and Zone IV: *Densipollenites-Lunatisporites.* Amongst these, Zone I and Zone II represent the upper Raniganj palynozones and can be correlated to the late Permian, while the assemblages of Zone III and Zone IV constitute the lower Panchet palynozones assignable to the early Triassic. Kar and Ghosh (2018) commented that the Permian–Triassic transition lies between Zone II and Zone III of the outcrop. All these palynoassemblages are comparable to the already documented palynozones known from the other Gondwana basins of Peninsular India (Tiwari and Tripathi 1992). It is very well established that throughout the world, the Permian–Triassic transition is marked by the spike of *Reduviasporonites.* This marker palynomorph of the Permian–Triassic transition has been reported by Kar and Ghosh (2018) from the same outcrop and it has been observed that their occurrence significantly enhanced from the Palynoassemblage Zone II and its maximum abundance was noticed in Palynoassemblage Zone III.

Study of fossil megaspores is very significant as it not only throws light on the evolutionary history of the land plants but can also be used in tracing the plants that are heterosporous. It has been used as a marker in biostratigraphical zonation and correlation at generic level in the Triassic succession of Europe (Kovach and Batten 1989). Triassic megaspores from Peninsular India have been reported earlier by a number of workers (Ghosh and Banerji 2007 and the references therein). Ghosh and

Banerji (2007) have established the biostratigraphic zonation based on megaspores from the Triassic sequence of Peninsular India for the correlation of different Gondwana basins. Significant contributions on Triassic megaspores from other Gondwana countries have been made by Dettmann (1961), Helby and Martin (1965), Scott and Playford (1985), Cantrill and Drinnan (1994), Lugardon et al. (2000), Macluf et al. (2010) and others.

The present contribution on the megaspores provides further addition to the knowledge of megaspores recovered from the early Triassic sequence of South Rewa Gondwana Basin. The assemblage is represented by the characteristic megaspore taxa of Triassic affinity viz. *Banksisporites sinuosus, Biharisporites sparsus, Erlansonisporites reticulates, Ricinospora* sp.*, Hughesisporites orowskae, H. variabilis, Nathorstisporites hopliticus, Noniasporites harrisii* and *N. triassicus.* Solitary new species of *Noniasporites* i.e. *N. triassicus* has been recognized in the present assemblage. Amongst the recorded megaspore taxa, the majority are known from the Triassic of Peninsular India and elsewhere. Very few species of the present assemblage have been recorded earlier from the late Permian, Jurassic and also from the early Cretaceous sediments. So, in all probabilities very few late Permian forms continued till the early Triassic, and only few early Triassic forms continued their existence up to the early Cretaceous.

It is very well known that the megaspores are basically the product of heterosporous pteridophytes. Some Triassic megaspores are characterised by the mesosporium that suggest their affinity to the Sellaginellales (Potonié 1956). Modern counterparts of *Selaginella* are usually found in areas with adequate moisture; however, some species of *Selaginella* are adapted in comparatively drier regions and are pikilohydric in nature. Therefore, probably during the early Triassic the environment was not absolutely arid; rather it was semi- arid with moderate humidity. The samples which yielded well preserved megaspores are dominated by *Dicroidium*, however; some dwarf species of *Glossopteris* e.g. *G. communis* (Chatterjee et al. 2014) and other late Permian holdovers are also present. The occurrence of *Dicroidium* in the khaki-green shale of the Panchet Formation (early Triassic) indicates a progressively drier climatic conditions in contrast to the underlying late Permian sediments.

The early Triassic experienced drier climatic conditions in comparison to the warm and humid climate during the Permian (McLoughlin et al. 1997). In contrast, the *Glossopteris* flora of late Permian was adapted to temperate, cool and moist environments (McLoughlin 1993; McManus et al. 2002). A greenhouse condition with a warmer phase prevailed during the Triassic due to the global rise of temperature. The Triassic Period also witnessed episodes of intense volcanism (Frakes et al. 1992; Retallack and Zarza 1998; Scotese et al. 1999). Chatterjee et al. (2014) opined that dwarfism was one of the strategies adapted by the early Triassic plant groups to combat the adverse conditions when there was indeed a shortage of essential nutrients in the soil, in addition to the seasonal dry climate, irregular rainfall and widespread aridity. It should be mentioned here that the Triassic genera, specifically *Lepidopteris* and *Dicroidium* possessed thick cuticles with sunken stomata since the atmosphere

during the early Triassic had a higher level of CO_2 and lower O_2 level (Berner 2006; Ward 2006; Sues and Fraser 2010).

6   Conclusions

It is evident from the present study that radiation of flora took place after the end Permian Mass Extinction Event. However, it took several million years for recovery. It is a widespread phenomenon that affected both flora and fauna of marine and terrestrial realms. As revealed from the present case study on the outcrop of late Permian to early Triassic sequence of Tatapani-Ramkola Coalfield, the late Permian vegetation dominated by glossopterids were gradually replaced by the *Dicroidium* dominated flora in the early Triassic. Some species of *Glossopteris* and associated floral elements continued up to the early Triassic. However, the dimension of *Glossopteris* leaves became comparatively smaller than the underlying late Permian sequence. Owing to wide geographical distribution and restricted geologic range, *Dicroidium* is considered as an index taxon of the continental Triassic and across the Gondwana Supergroup throughout the Triassic the *Dicroidium* flora was well diversified and prolific. Though there are reports of plant macrofossils having an affinity with *Dicroidium* from the late Permian of Middle East (Kerp et al. 2006; Hamad et al. 2008), their affinity is doubtful and yet to be resolved. However, it may be assumed that *Dicroidium* flora might have originated in the equatorial region during the late Permian and eventually became widespread in the southern hemisphere during the Triassic (Chatterjee et al. 2013). The palynological assemblage as well as the megaspore assemblage also reflects a clear evidence of floral change in the early Triassic in comparison to late Permian.

References

Algeo TJ, Hannigan R, Rowe H, Brookfield M, Baud A, Krystyn L, Ellwood BB (2007) Sequencing events across the permian-triassic boundary, guryul ravine (Kashmir, India). Palaeo Palaeo Palaeo 252:328–346

Anderson HM, Anderson JM (2008) Molteno ferns: late triassic biodiversity in southern Africa. South African national biodiversity institute. Pretoria Strelitzia 21:1–258

Anderson JM, Anderson HM (1983) Palaeoflora of Southern Africa: molteno formation (Triassic), vol 1, Part 1. Introduction, Part 2. *Dicroidium*. Balkema, Rotterdam

Anderson JM, Anderson HM (1989) Palaeoflora of southern Africa: molteno formation (Triassic), vol 2: Gymnosperms (excluding *Dicroidium*), Balkema, Rotterdam

Archangelsky S (1968) Studies on Triassic fossil plants from Argentina. IV, The leaf genus *Dicroidium* and its possible relation to *Rhexoxylon* stems. Palaeontol 11:500–512

Artabe AE, Morel EM, Ganuza DG (2007) Las floras triásicas de la Argentina. Asoc Paleontológica Argent, Publicación Espec 11:75–86

Axsmith BJ, Taylor EL, Taylor TN (2000) New perspectives on the Mesozoic seed fern order Corystospermales based on attached organs from the Triassic of Antarctica. Am J Bot 87:757–768

Banerji J, Bose MN (1977) Some Lower Triassic plant remains from Asansol region, India. Palaeobotanist 24:202–210

Banerji J, Kumaran KPN, Maheshwari HK (1978) Upper Triassic sporae dispersae from the tiki formation: megaspores from the janar nala section, South Rewa gondwana basin. Palaeobotanist 25:1–26

Banerji J, Lemoigne Y (1987) Significant additions to the Upper Triassic flora of Williams Point, Livingston Island, South Shetlands (Antarctica). Geobios 20:469–487

Banerji J, Lemoigne Y, Torres T (1987) Significant additions to the Upper Triassic flora of Williams Point, Livingston Island, South Shetland Islands, Antarctica. Series Científica INACH 36:33–58

Banerji J, Maheshwari HK, Bose MN (1976) Some plant fossils from the Gopad River Section near Nidpur, Sidhi District, Madhya Pradesh. Palaeobotanist 23:59–71

Batten DJ, Kovach WL (1990) Catalog of Mesozoic and Tertiary megaspores. Am Ass Strat Palynol Contrib Ser 24:1–227

Baud A, Magaritz M, Holser WT (1989) Permian-Triassic of the Tethys: carbon isotope studies. Geol Rundschau 78:649–677

Bergad RD (1978) Ultrastructural studies of selected North American Cretaceous megaspores of Minerisporites, Erlansonisporites, Horstisporites, and Ricinospora, n. gen. Palynology 39–51

Berner RA (2006) GEOCARBSULF: a combined model for Phanerozoic atmospheric O2 and CO2. Geochim Cosmochim Acta 70:5653–5664

Bhowmik N, Parveen S (2012) On Vertebraria Royle from Triassic of Nidpur, Madhya Pradesh. J Geol Soc India 79:618–626

Bose MN, Banerji J, Maithy PK (1977) Some fossil plant remains from Tatapani-Ramkola coalfields, Madhya Pradesh. Palaeobotanist 24:108–117

Bose MN, Banerji J (1976) Some fragmentary plant remains from the Lower Triassic of Auranga Valley, district Palamau. Palaeobotanist 23:139–144

Boureau E (1964) Traité de Paléobotanique. Sphenophyta, Noeggerathiophyta. Masson et Cie, Paris 3:544

Brongniart A (1828) Prodrome d'une histoire des végétaux fossils, Levrault, Paris. Dictionnaire Des Sciences Naturelles 57:1–223

Cantrill DJ, Drinnan AN (1994) Late Triassic megaspores from the amery group, prince Charles mountains, East Antarctica. Alcheringa 18:71–78

Chandra S, Singh KJ, Jha N (2008) First report of the fertile plant genus *Umkomasia* from the Late Permian beds in India and its biostratigraphic significance. Palaeontology 51:817–826

Chatterjee R, Ghosh AK, Kar R, Rao GMN (2014) Dwarfism and Lilliput effect: A case study on the Glossopteris from the late Permian and early Triassic of India. Curr Sci 107:1735–1744

Chatterjee S, Tewari R, Agnihotri D (2013) A *Dicroidium* flora from the Triassic of Allan Hills, South Victoria Land, Transantarctic Mountains, Antarctica. Alcheringa 37:209–221

De Kock MO, Kirschvink JL (2004) Paleomagnetic constraints on the permian-triassic boundary in terrestrial strata of the karoo supergroup, South Africa: implications for causes of the end-permian extinction event. Gond Res 7:175–183

Dettmann ME (1961) Lower mesozoic megaspores from Tasmania and south Australia. Micropaleontol 7:71–86

Dolenec T, Lojen S, Ramovs A (2001) The Permian-Triassic boundary in Western Slovenia (Idrijca Valley section): magnetostratigraphy, stable isotopes, and elemental variations. Chem Geol 175:175–190

du Toit AL (1932) Some fossil plants from the Karroo system of South Africa. Annals South African Mus 28:369–393

Erwin D (1993) The Great Paleozoic Crisis: Life and Death in the Permian. Columbia University Press

Escapa IH, Taylor EL, Cúneo R, Bomfleur B, Bergene J, Serbet R, Taylor TN (2011) Triassic floras of Antarctica: plant diversity and distribution in high paleolatitude communities. Palaios 26:522–544

Feistmantel O (1879) The fossil flora of the Lower Gondwanas–1: the flora of the Talchir–Karharbari beds. Mem Geological Surv India, Palaeontologica Indica 12:1–64

Fox CS (1931) Gondwana system and its related formations. Mem Geol Surv India 58:1–241

Frakes LA, Francis JE, Syktus JI (1992) Climate models of the Phanerozoic. Cambridge Univ Press, Cambridge

Ghosh AK, Banerji J (2007) Biostratigraphic significance of megaspores from the Triassic sequence of peninsular India. In: Sinha DK (ed) Micropaleontology: application in stratigraphy and paleoceanography. Narosa Publishing, pp 81–89

Glasspool IJ (2003) A review of permian gondwana megaspore, with particular emphasis on material collected from coals of the Witbank Basin of South Africa and the Sydney Basin of Australia. Rev Palaeobot Palynol 124:227–296

Goswami S (2006) Record of lower gondwana megafloral assemblage from lower kamthi formation of ib river Coalfield, Orissa, India. J Biosciences 31:115–128

Goswami S (2008) Marine influence and incursion in the Gondwana basins of Orissa, India: a review. Palaeoworld 17:21–32

Goswami S, Singh KJ (2013) Floral biodiversity and geology of Talcher Basin, Orissa, India during the Permian-Triassic interval. Geol J 48:36–56

Gradstein FM, Ogg JG, Schmitz MB, Ogg GM (2012) The geologic time scale 2012. Elsevier

Griesbach CL (1880) Geology of ramkola and tatapani coalfields. Mem Geol Surv India 15:129–152

Hallam A, Wignall PB (1997) Mass extinctions and their aftermath. Oxford University Press, UK

Hamad AA, Kerp H, Vörding B, Bandel K (2008) A Late permian flora with *Dicroidium* from the Dead Sea region, Jordan. Rev Palaeobot Palynology 149:85–130

Harris TM (1935) The fossil flora of Scoresby Sound east Greenland, Part 4: Ginkgoales, Coniferales, Lycopodiales and isolated fructifications. Meddelelser Om Grfnland 112:1–176

Helby R, Martin ARH (1965) Cylostrobus Gen. Nov., cones of Lycopsidean plants from the Narrabeen group (Triassic) of New South Wales. Aust J Bot 13:389–404

Høeg OA, Bose MN, Manum S (1955) On double walls in fossil megaspores, with description of Duosporites congoensis n. gen. n. sp. Nytt Mag Bot 4:101–107

Holmes K (2001) The middle Triassic megafossil flora of the basin creek formation, Nymboida Coal Measures, NSW, Australia. Part 2; Filicophyta. Proc Linnean Soc, New South Wales 123:39–87

Holmes K, Anderson HM (2013) Synthesis of the rich Gondwana Triassic megafossil flora from Nymboida, Australia. In: Tanner LH, Spielmann JA, Lucas SG (eds) The Triassic System. New Mexico Mus Nat Hist Science Bull 61:296–305

Holser WT, Magaritz M (1987) Events near the Permian-Triassic boundary. Mod Geol 11:155–180

Jung W (1958) Zur Biologie und Morphologie einiger disperser Megasporen, vergleichbarmit solchenvon Lycostrobus scotti, aus dem Rhåt-Lias Frankens. Geol Bliitterfur Nord-Bayern Bd 8:114–130

Kapoor HM (1996) The Guryul ravine section, candidate of the global stratotype and point (GSSP) of the Permian-Triassic boundary (PTB). In: Yin H (ed) The paleozoic-mesozoic boundary: candidates of the global stratotype section and point of the permian-Triassic boundary. China Univ Geosci Press, Wuhan, pp 99–110

Kar R (2001) Application of palynology in coal exploration: a case study from Tatapani-Ramkola Coalfield, Madhya Pradesh. Minetech 22:33–41

Kar R (2003) Palynological recognition of barren measures sediments (Middle Permian) from Tatapani-Ramkola Coalfield, Chhattisgarh, India. Gond Geol Mag 6:239–244

Kar R (2012) A basal Gondwana palynoflora from the glacigene sediments of Tatapani Ramkola Coalfield, India. Palaeobotanist 61:131–138

Kar R, Ghosh AK (2018) First record of *Reduviasporonites* from the Permian-Triassic transition (Gondwana Supergroup) of India. Alcheringa 42:373–382

Kar R, Srivastava SC (2003) Palynological delimitation of the coal bearing Lower Gondwana sediments in the southern part of Tatapani-Ramkola Coalfield, Chhattisgarh, India. J Geol Soc India 61:557–564

Kerp H, Hamad A, Vording B, Bandel K (2006) Typical Triassic Gondwanan floral elements in the Upper Permian of the paleotropics. GSA Bull 34:265–268

Kovach WL, Batten DJ (1989) Worldwide stratigraphic occurrences of Mesozoic and Tertiary megaspores. Palynol 13:247–277

Kozur VH (1973) Neue Megasporen aus dem Karn des Ilek-Beckens. Geol Und Paläontologische MittEn, Innsbr 3:1–12

Krull ES, Retallack GJ (2000) δ^{13}C depth profiles across the Permian-Triassic boundary: evidence for methane release. GSA Bull 112:1459–1472

Krystyn L, Richoz S, Baud A, Twitchett RJ (2003) A unique Permian-Triassic boundary section from the Neotethyan Hawasina Basin, central Oman mountains. Palaeo Palaeo Palaeo 191:329–344

Lacey WS, Lucas RC (1981) The Triassic flora of Livingston Island, South Shetland Islands. British Antarctic Surv Bull 53:157–173

Lele KM (1955) Plant fossil from Parsora in the South Rewa Gondwana Basin, India. Palaeobotanist 4:23–34

Lele KM (1962) Studies in the Indian middle Gondwana Flora–1. On *Dicroidium* from the South Rewa Gondwana basin. Palaeobotanist 10:48–68

Lugardon B, Grauvogel-Stamm L, Dobruskina I (2000) Comparative ultrastructure of the megaspores of the Triassic lycopsid Pleuromeia rossica Neuburg. Comptes Rendus L'academie Sci Ser IIA Earth Planet Sci 330:501–508

Lundblad O (1956) Zur Kenntnis süd–und mitteleuropaeischer Hydrachnellen. Arkiv För Zoologi 10:1–306

MacLeod KG, Smith RMH, Koch PL, Ward PP (2000) Timing of mammal–like reptile extinctions across the Permian-Triassic boundary in South Africa. Geology 28:227–230

Macluf C, Morbelli M, Giudice G (2010) Morphology and ultrastructure of megaspores and microspores of Isoetes sehnemii Fuchs (Lycophyta). Anais Da Academia Brasileira De Ciências 82:341–352

Magaritz M (1989) ^{13}C minima follow extinction events: a clue to faunal radiation. Geology 17:337–340

Magaritz M, Krishnamurty RV, Holser WT (1992) Parallel trends in organic and inorganic carbon isotopes across the Permian-Triassic boundary. Am J Sci 292:727–739

Maheshwari HK, Bajpai U (1984) Noniasporites, a new megaspore genus from the Upper Permian of Raniganj Coalfield. Palaeobotanist 32:113–119

Maheshwari HK, Banerji J (1975) Lower Triassic Palynomorphs from the Maitur Formation, West Bengal, India. Palaeontographica B 152:149–190

Marcinkiewicz T (1971) The stratigraphy of the Rhaetian and Liasin Poland based on megaspore investigations [Stratygrafia Retyku i Liasu w Polsce na Podstawie badan megasporowych] Prace Instytut Geologiczny (Warsaw) 65:1–57

Marcinkiewicz T (1978) Megaspore assemblages in the Keuper of Poland. In: Wodzelewska B (ed)Stratigraphy of the Keuper in Poland 87:61–84

McElwain JC, Punyasena SW (2007) Mass extinction events and the plant fossil record. Trends Ecol Evol 22:548–557

McLoughlin S (1993) Glossopterid megafossils in Permian Gondwanic non–marine biostratigraphy. In: Findlay RH, Unrug R, Banks MR, Veevers JJ (eds) Gondwana eight: assembly, evolution and dispersal. Balkema, Rotterdam, pp 253–264

McLoughlin S (2001) The breakup history of Gondwana and its impact on pre-Cenozoic floristic provincialism. Aust J Bot 49:271–300

McLoughlin S (2011) New records of leaf galls and arthropod oviposition scars in Permian-Triassic Gondwanan gymnosperms. Aust J Bot 59:156–169

McLoughlin S, Lindstorm S, Drinnan AN (1997) Gondwanan floristic and sedimentological trends during the Permian-Triassic transition: new evidence from the Amery Group, northern Prince Charles Mountains, East Antarctica. Antarct Sci 9:281–298

McManus HA, Taylor EA, Taylor TN, Collinson JW (2002) A petrified Glossopteris flora from Collinson Ridge, central Transarctic mountains: late permian or early Triassic? Rev Palaeobot Palynol 120:233–246

Metcalfe I, Foster CB, Afonin SA, Nicoll RS, Mundil R, Xiaofeng W, Lucas SG (2009) Stratigraphy, biostratigraphy and C-isotopes of the Permian-Triassic non-marine sequence at Dalongkou and Lucaogou, Xinjiang Province, China. J Asian Earth Sci 36:503–520

Morante R (1996) Permian and Early Triassic isotopic records of carbon and strontium in Australia and a scenario of events about the Permian-Triassic boundary. Hist Biol 11:289–310

Mukhopadhyay G, Mukhopadhyay SK, Roychowdhury M, Parui PK (2010) Stratigraphic correlation between different Gondwana basins of India. J Geol Soc India 76:251–266

Musashi M, Isozaki Y, Koike T, Kreulen R (2001) Stable carbon isotope signature in mid–Panthalassa shallow–water carbonates across the Permo-Triassic boundary: evidence for ^{13}C-depleted ocean. Earth Planet Sci Lett 193:9–20

Neri M, Kustatscher E, Roghi G (2018) Megaspores from the Lower Jurassic XE "Jurassic" (Pliensbachian) Rotzo Formation (Monti Lessini, northern Italy) and their palaeoenvironmental implications. Palaeobio Palaeoenv 98:97–110

Pal PK (1984) Triassic plant megafossils from the Tiki Formation, South Rewa Gondwana Basin, India. Palaeobotanist 32:253–309

Pal PK (1985) Palaeobotany and stratigraphy of the Dhaurai Hill beds, South Rewa Gondwana Basin, India. Geophytol 15:224–225

Pal PK (1990) A revision of *Dicroidium hugesii*. Sci Cult 56:295–297

Pal PK, Ghosh AK (1997) Megafloral zonation of Permian-Triassic sequence in the Kamthi Formation, Talcher Coalfield, Orissa. Palaeobotanist 46:81–87

Pal PK, Chakraborty U, Ghosh AK, Ghosh A (1991) Triassic plant megafossils from the Kamthi Formation of Talcher Coalfield, India–A new report. Indian J Earth Sci 63:119–125

Pal PK, Ghosh AK, Sannigrahi A (1997) Megaspores from the Panchet Formation of East Bokaro Coalfield, India. J Palaeontol Soc India 42:61–69

Pal PK, Srivastava AK, Ghosh AK (2010) Plant fossils of Maitur Formation: possibly the ultimate stage of Glossopteris flora in Raniganj Coalfield, India. Palaeobotanist 59:33–45

Pal PK, Ghosh AK, Kar R, Singh RS, Sarkar M, Chatterjee R (2014) Reappraisal of the genus Dicroidium Gothan from the Triassic sediments of India. Palaeobotanist 63:137–155

Pant DD (1956) On two Compressed Palaeozoic Axes. Ann Bot 20:419–429

Potonié R (1956) Synopsis der Gattungen der Sporae dispersae. I. Teil: Sporites. Beihefte Zum Geologischen Jahrbuch 23:1–103

Raja Rao CS (1983) Coalfields of India, Vol. III; Coal resources of Madhya Pradesh, Jammu and Kashmir. Bulletins of Geological Survey of India, Series A 45:75–80

Retallack GJ (1977) Reconstructing Triassic vegetation of eastern Australasia: A new approach for the biostratigraphy of Gondwanaland. Alcheringa 1:247–277

Retallack GJ (1980) Late Carboniferous to Middle Triassic megafossil floras from the Sydney Basin. Bull Geol Surv New South Wales 26:384–430

Retallack GJ (1981) Middle Triassic megafossil plants from Long Gully, near Otematata, north Otago, New Zealand. J Royal Soc New Zealand 11:167–200

Retallack GJ (1983) Middle Triassic megafossil marine algae and land plants from near Benmore Dam, southern Canterbury, New Zealand. J Royal Soc New Zealand 13:129–154

Retallack GJ (1995) Permian-Triassic life crisis on land. Science 267:77–80

Retallack GJ, Zarza A (1998) Middle Triassic paleosols and paleoclimatology of Antarctica. J Sed Res 68:169–184

Rigby JF (1966) Some Gondwana articulates from New South Wales. Symposium Floristics and Stratigraphy of Gondwanaland. Birbal Sahni Institute, Lucknow, pp 48–54

Rydberg PE, Taylor EL, Taylor TN (2012) The First Permineralized Microsporophyll of the Glossopteridales: Eretmonia macloughlinii sp. nov. Int J Plant Sci 173:812–822

Sah SCD, Jain KP (1968) Lower Mesozoic Megaspores from the Variegated Stage of Salt Range (W. Pakistan). Palaeobotanist 16:288–291

Sarana S (2002) Characterisation of organic source material from Tatapani and Ramkola coalfields, Chhattisgarh, India. Palaeobotanist 51:81–92

Sarana S, Anand-Prakash, (2002) Microconstituents and depositional environment of Lower Gondwana coals of Tatapani-Ramkola coalfield, Surguja district, Chattisgarh. J Geol Soc India 60:663–676

Sarana S, Kar R (2011) Effect of igneous intrusive on coal microconstituents: Study from an Indian Gondwana coalfield. Int J Coal Geol 85:161–167

Sarkar A, Yoshioka H, Ebihara M, Naraoka H (2003) Geochemical and organic carbon isotope studies across the continental Permo-Triassic boundary of Raniganj Basin, eastern India. Palaeo Palaeo Palaeo 191:1–14

Sastry MVA, Acharyya SK, Shah SC, Satsangi PD, Ghosh SC, Singh G (1977) Classification of Indian Gondwana sequence—a reappraisal. In: Proceedings of the 4th international Gondwana symposium, Calcutta, India, pp 502–507

Saxena A, Singh KJ, Cleal CJ, Chandra S, Goswami S, Shabbar H (2019) Development of the Glossopteris flora and its end Permian demise in the Tatapani-Ramkola Coalfield, Son-Mahanadi Basin, India. Geol J 54:2472–2494

Schulze F (1855) Bemerkungen über das Vorkommen wohlerhaltener Cellulose in Braunkohle und Steinkohle. Bericht Verhandlungen königlich–preusischen Akademie der Wissenschaften, Berlin, pp 676–678

Scotese CR, Boucot AJ, McKerrow WS (1999) Gondwanan palaeogeography and palaeoclimatology. J Africa Earth Sci 28:99–114

Scott AC, Playford G (1985) Early Triassic megaspores from the Rewan Group, Bowen Basin, Queensland. Alcheringa 9:297–323

Sen J (1955) Structure of Vertebraria. Nature 175:176

Shen SZ, Crowley JL, Wang Y, Bowring SA, Erwin DH, Sadler PM, Cao CQ, Rothman DH, Henderson CM, Ramezani J, Zhang H (2011) Calibrating the end-Permian mass extinction. Science 334(6061):1367–1372

Singh C (1964) Microflora of the Lower Cretaceous Mannville Group, east-central Alberta. Res Council of Alberta Bull 15:1–239

Singh KJ, Chandra S, Saxena A (2011) Tatapania gen nov., a possible cone of Schizoneura gondwanensis Feistmantel from the Late Permian in the Tatapani-Ramkola Coalfield. India. Palaeobotanist 60:251–263

Spinner E (1969) Preliminary studies of the megaspores from the type Formation, Quebrada del Type. La Rioja. Argentina. Pollen Spore 11:669–685

Srivastava SC, Anand-Prakash KR (1997) Palynology of Permian Triassic Sequence in Iria Nala, Tatapani-Ramkola Coalfield, India. Palaeobotanist 46:75–80

Srivastava SC, Kar R (2001) Palynological dating of some Permian outcrops from Iria Valley, Tatapani-Ramkola Coalfield, Surguja District, M.P India. Geol Surv India Spec Publ 54:97–102

Sues HD, Fraser NC (2010) Triassic life on land: the great transition. Columbia University Press

Surange KR, Chandra S (1974) Some male fructifications of Glossopteridales. Palaeobotanist 21:255–266

Surange KR, Maheshwari HK (1962) Studies in the Glossopteris Flora of India. 11. Some Observations on on Vertebraria from the Lower Gondwanas of India. Palaeobotanist 9:61–67

Tewari R, Chatterjee S, Agnihotri D, Pandita SK (2015a) *Glossopteris* flora in the Permian Weller Formation of Allan Hills, South Victoria Land, Antarctica: Implications for paleogeography, paleoclimatology, and biostratigraphic correlation. Gond Res 28:905–932

Tewari R, Pandita SK, McLoughlin S, Agnihotri D, Pillai SS, Singh V, Kumar K, Bhat GD (2015b) The Permian-Triassic palynological transition in the Guryul Ravine section, Kashmir, India: implications for Tethyan-Gondwanan correlations. Earth-Sci Rev 149:53–66

Tiwari R S, Vijaya (1992) Permo-Triassic boundary on the Indian peninsula. In: Sweet WC, Zunyi Y, Dickins JM, Hongfu Y (eds) Permo-Triassic events in the Eastern Tethys. Stratigraphy, Classification, and Relations with the Western Tethys, pp 37–45

Tiwari RS, Tripathi A (1992) Marker assemblage zones of spore and pollen species through Gondwana Palaeozoic and Mesozoic sequence in India. Palaeobotanist 40:194–236

Traverse A (2007) Paleopalynology. In: Landman N, Jones D (eds) Topics in Geobiology, Springer Verlag, Dordrecht

Wang K, Geldsetzer HHJ, Krouse HR (1994) Permian-Triassic extinction: Organic N13C evidence from British Columbia, Canada. Geology 22:580–584

Ward P (2006) Impact from the deep. Sci Am 295:64–71

Wellman C, Axe L (1999) Extracting plant mesofossils and megafossils by bulk acid maceration. In: Jones TP, Rowe NP (eds) Fossil plants and spores: modern techniques. Geological Society, London, pp 11–14

Yin H, Zhang K, Tong J, Yang Z, Wu S (2001) The global stratotype section and point (GSSP) of the Permian-Triassic boundary. Episodes 24:102–114

Zalessky MD (1932) Observations sur les vegetaux noveaux paleozoiques de Siberie. Annales dc la Societe geologique du. Nord Lille 57:111–134

An Overview of the Mesozoic (Middle Jurassic to Early Cretaceous) Stratigraphy, Sedimentology and Depositional Environments of the Kachchh Mainland, Gujarat, India

Mahender Kotha

Abstract The Mesozoic rocks in the Kachchh Basin, with their varied lithological characters and depositional facies, have been a focus of geologists' attention since the pioneering work of Wynne and Fedden in 1872–74, more than a century ago. The prolific megafauna, especially the Upper Jurassic ammonites, of the Mesozoic succession of Kachchh is well known globally that attracted paleontologists, while the wide range of condensed sections exposing Bathonian to Pleistocene drew the stratigraphers' attention. The Jurassic ammonite fauna of Kachchh is essential for its regional significance and broad provincial interest. Although an excellent volume of data is available on the Jurassic succession of India, most of that focus attention on paleontology and stratigraphy. The varied depositional, erosional, and biogenic structures present in the Mesozoic sequence of Kachchh are quite interesting. The exposed Mesozoic sequence of Kachchh Mainland consists of rocks ranging from Middle Jurassic to Early Cretaceous, is divided into four formations viz. Jhurio, Jumara, Jhuran, and Bhuj in ascending order. The Jhurio and Jumara formations, belonging to Middle Jurassic, represent a mixed carbonate–clastic sequence, while the Jhuran Formation (Late Jurassic) and Bhuj Formation (Early Cretaceous comprises an essentially clastic succession. In all, 13 lithofacies associations with varying depositional conditions are observed from the entire exposed Mesozoic succession of Kachchh Mainland. Sandstone and shales are the dominant lithologies of the succession, while the carbonate rocks occur only to the Middle Jurassic exposures. Petrographically, the sandstones belong to the predominant quartz arenite to feldspathic arenite categories, followed by a few lithic arenites, and the associated carbonate lithologies belong to a variety of types, ranging from mudstone to grainstones, and exhibit a variable microfacies character and diagenetic modifications. The present work highlights an overview of the sedimentological account of the Mesozoic succession of Kachchh Mainland and discusses the distribution of the variety of clastic and carbonate facies types and their use of the paleoenvironmental reconstruction for understanding the paleogeography of Kachchh Basin.

M. Kotha (✉)
School of Earth, Ocean and Atmospheric Sciences, Goa University, Taleigao Plateau, Panaji 403206, Goa, India
e-mail: mkotha@unigoa.ac.in; kotha.mahender@gmail.com

1 Introduction

The sedimentary basin of Kachchh (also known as Kutch), well known for its prolific megafauna, especially the Upper Jurassic ammonites, possesses a vital perspective for paleontologists, stratigraphers, and sedimentologists. The abundance of fossil faunas and the wide range of condensed sections exposing Bathonian to Pleistocene have attracted both paleontologists and stratigraphers (Fig. 1a, b). Arkell (1956) quoted this classic area as probably the most favored locality in the world for Upper
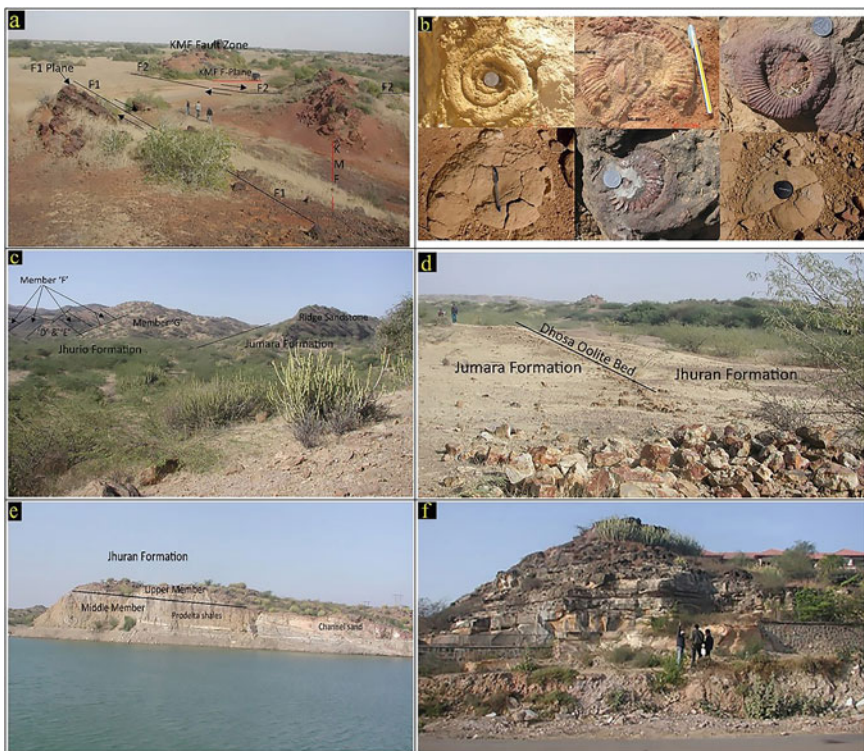
Fig. 1 Field photographs of Mesozoic outcrops: **a** Glimpse of Kutch Region and its geological importance, **b** Ammonoid fossil specimens preserved in the Mesozoic succession of Kutch, **c** Jhurio Formation as exposed at the core of the faulted Jhurio Dome, **d** Type section of Jumara Formation, northern periphery of Jumara dome. Top of Jumara Formation marked by Dhosa Oolite bed, **e** Middle (Shale) and Upper (Sandstone) members of the Jhuran Fm as seen in the Khari Nadi cliff near Rudramata temple and **f** Reference section of Bhuj Fm at Mandvi/ Lakhpat Road Junction along Ring road, opposite Prince Residency Hotel, Bhuj (coin diameter = 2.5 cm)

Jurassic Ammonites. He also pointed out that the lower part of Callovian is probably more fully developed in Kachchh than anywhere else.

The east–west aligned pericratonic sedimentary basin of Kachchh with vast plains dissected by a few low rising hills came into existence during the Late Triassic – Early Jurassic at the time of rifting of Africa and India (Biswas 1981). The basin has experienced periodic carbonate sedimentation interrupted with a vast siliciclastic deposition from Middle Jurassic to Neogene. The Mesozoic rocks are exposed in six highland areas viz. Kachchh Mainland, Wagad, Pachham, Khadir, Bela, and Chorar, whereas the Tertiary strata are exposed in the adjacent plain lands. Regional structural elements of the Kachchh Mainland consist of two parallel fault flexures along the NW–SE striking master faults (Biswas 1981, 1982, 1987, 1991). The Jurassic rocks are best developed in the northern flexure. A string of culminations observed along this flexure with depressions between them. These zones of culminations stand out in domal forms at Jara, Jumara, Nara, Keera, Jhura and Habo hills, where inliers of Middle Jurassic (relatively older) rocks, the Jhurio and Jumara formations occur at the core of these domes. The dried-up nalas, cliff sections, and road cuts provide good exposures of Mesozoic outcrops for sample collection (Mahender and Sharma 2010). While attempting to briefly review the work done earlier on stratigraphic and sedimentological aspects, this paper also presents a comprehensive account of the sedimentation history of the Mesozoic succession of Kachchh in order to understand the provenance and depositional environments.

Although the list of investigations on Kachchh is enormous, much of the available literature focuses attention mainly on the paleontology and stratigraphic aspects (Wynne 1875; Waagen 1871; Spath, 1933; Rajnath 1932, 1942; Agarwal, 1957, 1975; Ghosh, 1969; Biswas 1970, 1971, 1974, 1977, 1981, 1991; Singh and Kanjilal 1974; Krishna et al. 1983, 2000; Krishna 2017). Some of the past studies integrate the sedimentological aspects with geochemical characteristics of the Mesozoic Sediments of Kutch Basin (Shukla and Singh, 1990; Phansalkar et al. 1992; Khadkikar 1996; Dubey and Chatterjee 1997; Osman and Mahender 1997; Mahender and Sharma 2010; Ahmad et al. 2006, 2014). The detailed lithostratigraphic classification of Mesozoic of Kutch was proposed by Biswas (1977) based on detailed field studies. Some of the most recent contributions of Mesozoic of Kachchh are as follows: Mesozoic foraminiferal study (Gaur and Talib 2009; Talib et al. 2012), study of Ammonoidea assemblage of Callovian and Upper Jurassic Bivlaves (Bardhan et al. 2009, 2012), endemism and phylogeny of Bathonian–Callovian Ammonoidea (Dutta and Bardhan 2016), hydrocarbon exploration (Patil et al. 2013), possible oceanic anoxia in Jurassic (Arora et al. 2015, 2017); detrital zircon and monazite for tracking the source of Mesozoic Sediments of Kutch (Chaudhuri et al. 2020a), paleogeographic implications of glauconite composition (Banerjee et al. 2016; Bansal et al. 2017), systematics, endemism and phylogeny of Bathonian–Callovian Ammonoidea (Dutta and Bardhan 2016), Upper Jurassic soft Sediment deformation structures as a testimony to seismites (Kale et al. 2016), stable isotopic studies and its potential for paleoecologic, paleoclimatic, and paleogeographic reconstructions of Middle to Jurassic belemnites and brachiopods (Alberti et al. 2012a, b), overview of the lithostratigraphy, biostratigraphy and paleoenvironment of the Middle to Upper

Jurassic sedimentary succession (Alberti et al. 2017), oldest turritelline gastropods of Upper Jurassic (Das et al. 2018), compositional evolution of siliciclastic sediments recording the tectonic stability of a pericratonic rift during the Mesozoic Kutch Basin (Chaudhuri et al. 2018, 2020a,2020b,2020c,2020d). The present paper gives an overview of the stratigraphic sedimentology, and the depositional environments Mesozoic sequence of Kachchh Mainland.

2 Geological Background

The Mesozoic sedimentary strata, ranging in age from Middle Jurassic (Bathonian) to Early Cretaceous as exposed in Kachchh Basin is divided into four formations viz. Jhurio, Jumara, Jhuran, and Bhuj in ascending order (Biswas 1977). The Mesozoic rocks overlie the Archean basement and disconformably underlies the Late Creta-ceous basic flows of the Deccan Trap in the southern and western parts and Tertiary sediments in the eastern part of the basin. The sequence was developed due to repeated marine incursions during the Middle Jurassic to lower Cretaceous period followed by major tectonic movements and Deccan Trap volcanism in the Late Cretaceous time (Biswas 1977). The present work is based on (a) systematic sampling along selected traverses, (b) samples from cliff sections, and (c) spot sampling from specific localities presents an overview of the systematic stratigraphic sedimentology of the Mesozoic Sequence of Kachchh Mainland. The general distribution and occurrence of outcrops and their field character can be found in Mahender et al. (2008) and Mahender and Sharma (2010).

3 Systematic Stratigraphy

The Mesozoic stratigraphy of Kachchh Basin comprises strata ranging in age from Middle Jurassic (Bathonian) to Recent (Holocene) (Table 1). Mesozoic rocks, are divided into four formations viz. Jhurio, Jumara, Jhuran, and Bhuj in ascending order (Biswas 1977). The first two formations (Jhurio and Jumara) belong to the Middle Jurassic, the Jhuran Formation is Late Jurassic, and the topmost Bhuj Forma-tion belongs to an Early Cretaceous age (Biswas 1977, 2005). The Tertiary sedi-ments lie over the Trap and the Mesozoic sediments wherever the Trap is absent. A detailed description of each Mesozoic formation is given in the following paragraphs, and a summary of the generalized Mesozoic lithostratigraphic succession Kachchh mainland is presented in Table 2.

Table 1 Litho–stratigraphic classification of the Mesozoic rocks of Kutch (after Biswas 1987)

Stages	Kutch Mainland Group		Pachchham Island Group			Khadir– Bela– Chorar Islands	Eastern Kutch Group
	Formation	Member	Member		Formation		Wagad Highland
			Goradongar	Kaladongar			
Tertiary	Deccan Trap	Basalt Flows					
Maastrichtian –Danian	Deccan Trap	Basalt Flows	Recent Deposit / Miocene Shales / Palaeocene laterites				Recent Deposit
Albian	Bhuj	Upper Member: massive sandstones					
Aptian	Bhuj	Ukra Member: Green glauconitic shale/ferruginous bands with fossil.					Wagad Sandstone
Hauterivian to Barriasian	Bhuj	Ghuneri Member/ Lower Member: sandstones/shales/ferruginous bands/Shales with plant fossils.					WEST——EAST / Gamdau Member
Tithonian	Jhuran	Katesar Member: massive sandstones				Quaternary to Recent Deposits	Kanthkote Member.
Kimmeridgian	Jhuran	Upper Member : fossiliferous sandstones, shales, hard calcareous sandstones		Recent Quaternary			
Kimmeridgian	Jhuran	Middle Member: mainly shales, fossiliferous, with sandstone interbeds.					
Kimmeridgian	Jhuran	Lower Member: sandstones/shales/arena—ceous limestones with fossils					
Oxfordian		HIATUS					Wagad Sandstone

Table 1 (continued)

Age	Group	Formation	Member
Callovian	Jumara		Dhosa Oolite Member
			Gypseous Shale Member
			Ridge Sandstone Member
		Modar Hill Formation	Shelly Shale Member
		Tertiary, Quaternary and Recent	
		Gadhada Formation	Bambhanka/Gangta Bet Member
			Patasar Shale Member
		Washtawa Formation	Nara Shale Member
			Kharol Member
			Not Exposed
Aalenian–Bathonian	Jhurio	Raimalro Limestone Member	Member G: Thin bedded white Limestone and Nodular Limestone
		Gadaputa Sandstone Member	Member F: Purple sandstones / Packstones
		Goradongar Flagstone Member	Member E: Bedded rusty grainstone with golden oolites
			Member D: Gray Shales
		Goradongar Formation	Ratanpur Sandstone Member
			(Raimalro Lst. Marker)
		Khadir Formation	Hadibhadang Sandstone Member
			Hadibhadang Shale Member
			Not Exposed

Table 1 (continued)

Member C: Brick red weathering rusty grainstones with golden oolites	Middle Sandstone Member	(Leptosphinctes pebbly rudstone) Babia Cliff Sandstone Member	Cheriyabet Conglomerate Mbr.
Member B: Gray Shale	Lower Flagstone Member		? Basement
Member A: Thin bedded yellow white limestones, shales and rusty brown limestone with golden oolites.	Eomiodon Red Sandstone Member	Narewari Wandh Sandstone Member	
? ? ?	Sadara Coral Limestone Member	Dingy Hill Member ~ ? Basement	
Basement	~ ? Basement		

Kaladongar Formation

Table 2 Mesozoic Lithostratigraphy of Kachchh Mainland (adapted from Biswas 1981)

AGE	Fm	Mbr	Lithological field characteristics	Geographical extension	Type section/ typical sections
Neocomian to Albian	BHUJ (350–900mt +)(Thickening W.wards)	U	Light colored, medium to fine grained sandstone, kaolinitic claystone and sandy iron–stone bands. channel fills; X–bedded–planarand tabular, cut and fill; plant fossils, fossil wood	Exposed extensively in the mainland in two wide belts stretching from Bachau on the east to Ghuneri on the west, occupying lowlands between the hill ranges; entire city of Bhuj is located on this formation	Several reference sections of which the Rukmavati section, south of Bhuj, from Jamatara downstream up to Trap is considered as the main reference section Other impressive sections are seen in and around Bhuj and also near the Tapkeshewar Temple hill range
		M	Green glauconitic sandstones and shales, thin fossiliferous limestones and red ironstone bands containing pelecypods, gastropods and ammonites; fossil wood;	Monotonous sandy plains ribbed with cuestas formed by hard ironstone or lateritic bands, some of which are capped by Trap flows, are the typical expression of the topography where Bhuj rocks occur	
		L	Red and yellow sandstones: ferruginous, fine grained. moderately sorted; coarse grained arenites in channel fills showing fining up. X–bedded (planar) ripple marked; abundant leaf impressions. Occasional coal beds		

(continued)

Table 2 (continued)

AGE	Fm	Mbr	Lithological field characteristics	Geographical extension	Type section/ typical sections
Kimmeridgian to Neocomian	JHURAN (420 – 850 M+) (Thickening westwards)	Katesar	Greenish yellow sandstone: calcareous and ferruginous feldspathic wacke, v –med. gd; mod. to well sorted; X–bedded (planar, trough and festoon); Trigonia and Astarte sps	Exposed extensively along the southern flanks of the northern and central hill ranges in two wide E–W strips; present as inliers in the Bhuj Formation extreme east and west at the centres of domes and anticlines	Type section for most part of the formation (except Katesar member) is seen along the stream around Jhuran Village, 40 km. East of Bhuj; the upper part of the sequence(Katesar Member) is exposed along Katesar River and in Mundhan Antincline(4 km. SW of Mundhan) Other sections are seen in and around Bhuj, and in Kharinadi valley around Rudramata temple, 16 km N of Bhuj, which serves as a good reference section
		U	Mainly sandstones with subordinate shale. Sandstones: fine to med, mod. well sorted feldspathic wacke; Current bedded (tabular, festoons and herringbone), ripple marked; convolute bddg, load casts, cut and fills common. Local pelecypod and plant beds	In the central part of the Kachchh Mainland, only the Lower, Middle and lower part of the upper member are extensively exposed	
		M	Mainly grey shales with fine grained, fissile sandstone bands. Highly fossiliferous in west and sparsely so to the east; ammonites, pelecypods, belemnites; cut and fill stuctures		

Table 2 (continued)

AGE	Fm	Mbr	Lithological field characteristics	Geographical extension	Type section/ typical sections
		L	Shale/sandstone alternation. Sandstones: fine gd, mod sorted feldspathic wacke; X–bdd, ripple marked; more fossiliferous in the west		
Callovian to Oxfordian	JUMARA (280 m)	U	Greenish grey, gypseous glauconitic shales well laminated thin limestone alternations. Characteristic oolitic bands near the top. Highly fossiliferous; (mainly cephalopods, brachiopods, pelecypods and corals)	Exposed as inliers at the centre of the domal and anticlinal hills along the northern edge of the Mainland and in central Charwar Range in more or less circular and elliptical outcrops. Being soft formation, it usually gives rise to a grey undulating topography; is very widespread extending from Banni graben (subsurface) to Kachchh mainland; recognized in shelf part of the offshore and in the wells	Jumara Dome, Western Kachchh The Jhurio and Habo dome sections to the east of the type section are important reference section
		M	Base Biomicrite, middle yellow calcareous sandstone, top conglomerate. Fossiliferous with pelecypods. Represented in the west by fossiliferous limestones with golden oolites		

Table 2 (continued)

AGE	Fm	Mbr	Lithological field characteristics	Geographical extension	Type section/ typical sections
		L	Olive and grey shales with thin limestone bands, containing rich crop of fossils: ammonites, corals, brachiopods, pelecypods, belemnites etc		
Bathonian to Callovian	JHURIO (300 m)	U	Interbedded micritic and sparitic (bio- and oo-sparite) limestones with "golden oolite ", with iron–oxide coated pseudo–oolitic bands in the lower part. Fossiliferous: cephalopods, brachiopods, pelecypods etc	Widely is exposed as small inliers in three hills (Habo, Jhurio and Jumara, from east to west) along the northern margin of the Mainland Major part of the Jhurio hill is represents this formation and numerous good sections are seen in radial streams	Jhurio Hill, 38 km. North of Bhuj Others sections are seen in Habo and Jumara hills. In Habo and Jumara hills only the upper part is exposed. In Habo it crops out at three places in the northern flank of the hill south of Dhrang and Fulae. North of Jumara it is exposed in the hill adjacent to the Rann
		M	Thickly interbedded shales and limestones (mainly "golden oolites"–Oolitic intrasparrudite). Fossiliferous: brachiopods, pelecypods, cephalopods etc		
		L	Interbedded shales and limestones, with lenticular "golden oolites". Fossiliferous		

3.1 Jhurio Formation (Author: Biswas 1977; Also Known as Patcham Series)

A thick sequence of dominant limestone with interbedded shale and occasional bands of "golden oolite" and sandstone has been named as Jhurio Formation. The formation shows a change in facies, from carbonate in the west to clastics in the east.

3.1.1 Type Section

Jhurio Hill, 38 km. North of Bhuj.

3.1.2 Geographical Extension

This formation has a vast extent. It is present in the Kachchh Mainland and has been recognized in the subsurface also. The formation is exposed as small inliers in three hills (Habo, Jhurio, and Jumara, from east to west) along the Mainland's northern margin. The formation is thickest in the Jhura Dome (Fig. 1c). The hill's major part is composed of this formation and numerous good sections are seen in radial streams. In Habo and Jumara hills, only the upper part of the formation is exposed. In Habo, it crops out only at three places in the northern flank of the hill south of Dhrang and Fulae. It is also exposed in the hill adjacent to the Rann to the north of Jumara. The steeply dipping hard limestone beds form the whitish country of high relief featured by cuestas and annular valleys.
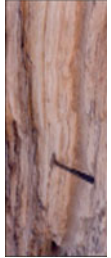
3.1.3 Lithology

The lower part comprises thin beds of yellow and grey limestones occasionally containing golden oolites, in grey shales. The middle part comprises thick beds of grey, yellow weathering shales alternated with thick beds of golden oolitic limestones. In contrast, the upper part of the formation is made up of thinly bedded white to cream coloured limestones with thin bands of golden oolites. The formation has been formally subdivided into seven informal members, named as A to G by Biswas (1977), based on the limestone, golden oolite, and shale occurrences. In Habo hill, only the topmost part of the formation is exposed. In the Jumara section, the top member is underlain by olive–grey gypseous shale with thin bands of coral bioliths equivalent to member F.

3.1.4 Lithofacies

This formation represents two lithofacies associations (Table 3), which include the quiet water subtidal carbonate association (LFA–1) and mixed siliciclastic carbonate shallow marine association (LFA–2) (Osman and Mahender 1997).

Table 3 Lithofacies association (LFA) of Mesozoic sequence of Kachchh Mainland

Age	Fm	LFA	Lithofacies name	Lithofacies characteristics	Photograph
Late Jurassic – Early Cretaceous	Bhuj	13	Bioturbated Sandstone lithofacies	Coarse grained, ferruginous sandstone with extensive bioturbation. Physical structures are partially to completely obliterate	
		12	Silty sandstone lithofacies	Well–bedded, fine to medium grained sandstone with much matrix, cross–bedded, Ripples are common	
		11	Interbedded sandstone—siltstone lithofacies	Thick fine to medium grained sandstones alternating with siltstone shale beds. The siltstone/shales beds are ferruginous	
		10	Cross–bedded sandstone association	Coarse–grained sandstone with well–developed cross bedding of various size and types	
	Jhuran	9	LFA–9. Interbedded Siltstone–Shale association	Carbonaceous, dark silty shales interbedded with fine lenticular/wavy sand beds	
		8	LFA–8. Sandstone with interlayered shale	Fine–medium grained, moderate to well sorted sandstones current bedded (tabular, festoon and herring bone types) with abundant feldspars and matrix	

Table 3 (continued)

Age	Fm	LFA	Lithofacies name	Lithofacies characteristics	Photograph
		7	LFA–7. Fossiliferous shale with thin sand/silt interbeds	Shales, grey in colour with alternating thin beds of sandstones. Shales highly fossiliferous. Fossiliferous (Ammonites, pelecypods, belemnites)	
		6	LFA–6. Interbedded shale–sandstone association	Fine grained, moderate to well–sorted sandstone, arkosic/ feldspathic wacke types, Cross–bedded, ripple marked	
Middle Jurassic	Jumara	5	LFA – 5. Cyclic shallow–water peritidal carbonate–shale association	Thin succession of shale, followed by laminated lime mudstone or peloid packstone. Cycles not regular; increasing thickness of carbonate beds with decrease in associated shale; shallow water, tidally influenced cyclic deposits;	
		4	LFA – 4. Quiet Water Lagoonal shale – carbonate association	Shale and limestone; shale gypseous, comprise chlorite and kaolinite. Limestone is fossiliferous wackestone and is dolomitized	
		3	LFA – 3. Predominantly terrigenous valley–fill association	Sandstone followed by a few conglomerate and rare shale beds. The sandstone displays herring–bone cross–stratification	

Table 3 (continued)

Age	Fm	LFA	Lithofacies name	Lithofacies characteristics	Photograph
	Jhurio	2	LFA – 2. Mixed siliciclastic carbonate shallow marine association	Varied lithology, including rippled, X–bedded sandstone, burrowed sandstone, siltstone, peloid packstone; sandstone fine–medium grained, mod. sorted exhibiting a coarsening upward sequence	
		1	LFA–1. Quiet water subtidal carbonate association	Predominantly carbonate mudstone (burrowed) with rare to common interbeds of peloid, bioclastic wackestone–packstone; beds relatively thinner, laterally, vary into lime mudstone–wackestone–packstone	

3.1.5 Boundaries

The lower boundary is not exposed in the type section. The upper contact with the overlying Jumara Formation is conformable and well–marked by the contrast of its white limestones and the green shales of the Jumara Formation. The geomorphic expression of the limestones forming high relief against the low areas of shales help to mark the boundary easily.

3.1.6 Thickness

In the type section, the thickness of the formation is 287 m. In Jumara and Habo Hills, the exposed thickness is only 70 m. (+) and 16 m. (+) respectively.

3.1.7 Paleontology

Common Fossils include Rhynchonella, Terebratula, Kachchhithyris, Allectryonia, Ostrea, Astarte, Trigonia, Belemnites, and ammonites (Macrocephalites). This formation is incredibly rich in fossils in the Jumara dome, where the shales and biostromes are packed with corals, brachiopods, pelecypods, and ammonites.

3.1.8 Age

The benthic foraminifera belongs to *Epistomina regularis – E. ghoshi* Assemblage zone, *Lenticulina dilectaformis* Partial–Range–Zone, *Tewaria Kachchhensis* partial–Range–Zone in stratotype indicate Bathonian–Callovian age (Pandey and Dave 1993). The formation was deposited in a littoral to the infra littoral environment, neritic transgressive environment.

3.2 Jumara Formation *(Author: Biswas 1971; Also Known as Chari Series)*

Monotonous grey to dark grey, laminated, rarely silty, and often calcareous shale sequence overlying the Jhurio Formation was named after its type section of Jumara Dome at the western Kachchh. The formation shows a gradual increase in thickness from east to west.

3.2.1 Type Section

Jumara Dome, Western Kachchh. The Jhurio and Habo dome sections to the east of the type section are important reference sections.

3.2.2 Geographic Extent

The formation is exposed as inliers at the center of the domal and anticlinal hills along the northern edge of the Mainland and in the central Charwar Range, in more or less circular and elliptical outcrops. Being a soft formation, it usually gives rise to a grey undulating topography. The Jumara Formation is very widespread, extending from Banni graben (subsurface) to Kachchh mainland. It has also been recognized in the shelf part of the offshore and the wells.

3.2.3 Lithology

In the type section, the formation is characterized by monotonous olive–grey, gypseous, laminated shales with thin, red ferruginous bands, alternating beds of limestone, and occasional sandstone inter–beds. It has been sub–divided into four informal members numbered I to IV based on the limestone or sandstone inter–beds dividing the continuous shale sequence (Biswas 1977). Thin fossiliferous oolitic limestone bands occur in the shales near the top of member IV, the famous "Dhosa Oolite beds" or "Stage." It is a very characteristic horizon and used as the main key bed in Mainland stratigraphy. In these sections and Chorar Range outcrops, more sandstone beds appear in the lower part. East of the type section, in the Manjal dome, the lowest exposed bed is a limestone developed locally, embracing the lower and upper parts of the members I and II.

The Jhurio and Habo dome section to the east of the type section are important reference sections. In these sections and Charwar Range outcrops, more sandstone beds appear at the lower part. East of the type section, in Manjal dome, the lowest exposed bed is a limestone, developed locally embracing the lower and upper parts of the members III and II. Further east in the Keera dome, a significant portion of the member I has been replaced by a golden–oolite–shale lithosome that resembles the middle part of the Jhurio Formation.

3.2.4 Lithofacies

Three lithofacies associations are recognizable in this formation (Table 3), which include the predominantly terrigenous valley–fill association (LFA–3), quiet water lagoonal shale—carbonate association (LFA–4) and cyclic shallow–water peritidal carbonate–shale association (LFA–5) (Osman and Mahender 1997).

3.2.5   Boundaries

The top and basal part of the formation is exposed only in Jhura, Habo, and Jumara hills. The lower boundary is defined by conformable limestone shale contact, and Dhosa Oolite Member marks the upper boundary (Fig. 1d). The contact is marked by the topmost oolitic band, which is conglomeratic and separates the unfossiliferous grey shales (of Jhuran Formation) and the green fossiliferous shales with oolite bands.

3.2.6   Thickness

The thickness of the formation (273.5 m as observed in the type section) is more or less uniform throughout the study area.

3.2.7   Paleontology

This formation is the richest of all in fossil content. Varieties of ammonites, Belemnites, brachiopods, pelecypods, corals, and gastropods are found throughout the formation. Besides mega fossils, the formation is rich in foraminifera.

3.2.8   Age

The benthic foraminifera recorded from the type area is referred to as *Tewaria kachchhensis* Partial Range–Zone, *Proteonina difflugiformis*, *Astacolus anceps* Assemblage–Zone and *Epistomina majungaensis* Range–Zone (Pandey and Dave 1993). The fossil assemblage gives an age of Callovian– Oxfordian to the formation.

3.2.9   Environment

A littoral to shallow marine circa littoral (below the wave base) environment of deposition is inferred for the formation.

3.3   Jhuran Formation (Author: Biswas 1977; Also Known as Katrol Formation)

The thick sequence of alternating beds of sandstone and shale has been named the Jhuran Formation. The Jhuran formation, defined by the underlying Dhosa Oolite Member of the Jumara Formation and the overlying non–marine sandstone of the

Bhuj Formation, is divided into four informal member—(lower, middle, upper, and Katesar members).

3.3.1 Type Section

Along the stream around Jhuran Village, 40 km east of Bhuj City and the type section for the upper part of the sequence (Katesar Member) is exposed along Katesar River and in Mundhan Anticlines (4 km. SW of Mundhan).

3.3.2 Geographic Extent

The formation is extensively exposed along the southern flanks of the northern and central hill ranges in two wide E–W strips. It is present as inliers in the Bhuj Formation at extreme east and west and in the central part of domes and anticlines. The Lower, Middle and lower part of the upper member is extensively exposed in the central part of the Kachchh Mainland, the main sections of which are better exposed (Fig. 1e) in and around Bhuj, and in Kharinadi valley around Rudramata temple, 16 km N of Bhuj, which serves as a useful reference section for the most part of the Jhuran Formation in the study area.

3.3.3 Lithology

The lower part comprises alternating yellow and red sandstone and shale beds with thin bands of hard yellow, fossiliferous, pebbly, calcareous sandstone, occasionally containing golden oolites in grey shales. The middle member in the present study area is represented by a monotonous succession of dark grey to black well–laminated shales, occasionally gypseous, weathering in olive–gray color. Thin red bands of ferruginous sandstone, micaceous siltstone, and yellow ochreous mudstone are typical in shales. The shales are unfossiliferous in the present area although they are fossiliferous in the western part. The Upper member in the present study area is represented with red and yellow, massive current bedded sandstone with intercalations of shale, siltstone, and at places, calcareous sandstone bands in the middle. The formation is uniform in lithologic character throughout, excepting the interfingering relationship between the members and the sandstone and shale beds.

3.3.4 Lithofacies

Four lithofacies type associations have been identified (Table 3) in this formation, which comprises LFA–6: Interbedded shale–sandstone association, LFA–7: Fossiliferous shale with thin sand/silt interbeds, LFA–8: Sandstone with interlayered shale, and LFA–9: Interbedded Siltstone–Shale association (Mahender and Sharma 2010).

3.3.5 Boundaries

Although it is generally conformable, a local disconformity is observed at the lower boundary of the Jhuran Formation. Jhuran shales resting over the eroded Dhosa Oolite Member. The upper contact with the overlying Bhuj Formation is gradational.

3.3.6 Thickness

The formation is thickest in the Jara–Mundhan area of NW mainland, where it is 865 m thick and thins down to the eastward to 442 m in the type Section. In the central mainland, the formation thickness is at its minimal (-380 m).

3.3.7 Paleontology

Common fossils include belemnites, ammonites, pelecypods, gastropods, and locally corals and echinoids. The irregular occurrence of plant fossils has been noted at many places in association with beds carrying marine fossils.

3.3.8 Age

Kimmeridgian to (pre–Aptian) Valangian age has been assigned by the earlier workers based on the available faunal evidence for this formation.

3.3.9 Environment

The paralic facies and the physical and biological characteristics of the sediments of different members tend to suggest a repeated paleogeographic shift from sub littoral to supra littoral environment and a continental environment in the upper part.

3.4 Bhuj Formation *(Author: Biswas 1971; Also Known as Umia/ Bhuj Series)*

A thick sequence of non–marine sandstones of uniform character constitutes the youngest formation of the Mesozoic sequence of Kachchh. The formation has been named after Bhuj. The formation is bounded by the Jhuran Formation below and the Deccan trap flows above.

3.4.1 Type Section

There are several reference sections of which the Rukmavati section, south of Bhuj, from Jamatara downstream up to Trap, is considered as the main reference section. The other impressive section of this formation can be seen around the Bhuj City (Fig. 1f) and near the Tapkeshewar Temple hill range. The formation is divided into two informal members viz. the Lower and Upper members in Kachchh mainland, whereas laterally in the west they are designated as Ghuneri (Lower) and Ukra (Upper).

3.4.2 Geographic Extent

The Bhuj rocks are exposed extensively in the mainland, occupying about 3/4th of the total Mesozoic outcrop area. The main exposures are seen in two wide belts stretching from Bachau on the east to Ghuneri on the west, occupying lowlands between the hill ranges. The entire city of Bhuj, in fact, is located on this formation. Monotonous sandy plains ribbed with cuestas formed by hard ironstone or lateritic bands, some of which are capped by Trap flows, are the typical topographic expression of Bhuj rocks. Bhuj sandstone being a good aquifer, plains on these rocks are extensively cultivated.

3.4.3 Lithology

The present study area exposes only the Lower and Upper members of the formation. The Lower Member is characterized by the cyclic repetition of ferruginous or lateritic bands, shales, and sandstones. The Upper Member consists of whitish to pale brown, massive, current-bedded, coarse-grained, well–sorted sandstones with kaolinitic shale and ferruginous band alternations at some intervals. The sandstones are pale brown to buff, soft, friable, usually current bedded (large scale tabular), fine to coarse-grained, well-sorted, loosely cemented quartz arenites, are usually micaceous, ferruginous, and/or calcareous. Some coarse-grained varieties are feldspathic arenites. Shales are grey, silty, well laminated with limonitic partings, and locally carbonaceous.

3.4.4 Lithofacies

Four lithofacies associations are described in the formation (Table 3), which includes (i) Cross–bedded sandstone association (LFA–10), (ii) Interbedded Sandstone–Siltstone association (LFA–11), (iii) Silty Sandstone with interlayered shale (LFA–12), and (iv) Bioturbated Sandstone Lithofacies association (LFA–13) (Mahender and Sharma 2010).

3.4.5   Boundaries

The formation is bounded by the planes of disconformity. The lower contact, though partly gradational at some places, show a disconformable contact. The upper boundary of the Bhuj formation is marked with the Deccan Trap flows resting on the formation's eroded undulating surface.

3.4.6   Thickness

The thickness of the formation (273 m as observed in the type section) is more or less uniform throughout the study area.

3.4.7   Paleontology

The formation, in general, is devoid of fossil fauna in the eastern part; however, in the western part, in the Ukra member, some fossils are reported. There are plenty of plant fossils reported from these rocks. The flora is typically Upper Gondwana Ptilophyllum Flora comprising *Ptilophyllum, Williamsonia, Brachyphyllum, Cladophlebis, Equisetum*, etc. besides leaf impressions, large chunks of fossil wood are seen concentrated at places.

3.4.8   Age

The lower time limit of the formation is indicated by the upper limit of the Jhuran Formation, which is the Valanginian. The hiatus due to disconformity between the formations is not known. The lowest age indicator in the Bhuj Formation is the Ukra Member, whose ammonite assemblage indicates an Aptian Age. The leaf impressions and micro–, and macrospores suggest a "Neocomian" age to these rocks.

3.4.9   Environment

Based on the lithology, the absence of fauna and rich assemblage of flora, sedimentary structures (such as large–scale cross–bedding), and marine tongues in the downward direction (in the west), the sediments can be interpreted as the products of delta deposits with distal part (delta front) towards the west and the proximal part (fluvial) to the east in the direction of land.

4 Sedimentology

4.1 Clastic Sedimentology

Sandstones, the abundant lithology of the Mesozoic sequence of Kachchh, units are well–bedded and exhibit a variety of sedimentary structures (depositional, erosional and other), including cross–bedding of various types and scales (Fig. 2a–c); varying scales of rippled bedding in sandstones indicating the shallow nature of the depositional environment (Fig. 2d, f). Large interference ripples also occur in some of the litho units (Fig. 2e). Laminated bedding with alternating fine and coarse laminae has been observed in the sequence at various localities, especially from cliff sections. Several types of trace fossils have been observed in the Middle Jurassic sequence of Kachchh from shaley units. Although the preservation of trace is fossils is better seen in argillaceous units, sandy–carbonate units also exhibit poorly preserved trace fossils such as *Rhizocorallium, Thalssinoides*, etc. The various burrow patterns observed in the succession include vertical burrows, sand-filled burrows and bioturbated horizons (Fig. 2p–r); Jointing is prominently developed in ferruginous and calcareous sandstones and sandy limestones. Two sets of joints are clearly seen, giving rise to blocks of the lithounits (Fig. 2j). At places, columnar jointing (Fig. 2k) is prominently developed in sandstones belonging to Late Jurassic to Early Cretaceous. The pattern is very similar to the columnar structures commonly observed in Basalts. Best exposures of columnar sandstone occur in and around Bhuj. Regular hexagonal columns developed perpendicular to bedding are with four to five sides are frequent. Each column is about 1–1.2 m. height and about 20–30 cm. in diameter; Iron crusts commonly occur (Fig. 2m, n) on the top of oolitic sandy beds at some localities are associated with large iron oncoids. The crusts are 2–4 cm. thick; Concretion layers (Fig. 2h) are widespread within the argillaceous limestone interbeds of Kachchh Jurassic. These beds consist of elongate, cylindrical, and irregular shaped nodules.

4.2 Paleocurrents

Cross–bedding is the most abundant and striking sedimentary structure seen at many localities of the exposed sandstones at various intervals of the sequence. The strike and dip of the cross–bedding units vary abruptly from place to place. The cross–bedding is mostly of high angle wedge type cross–stratification. Large scale planar and herringbone cross–stratification types are also observed in this rock sequence. The dip of the foreset varies from gentle (<10) at a few places to quite steep (>20) at several localities. Abrupt reversals of the direction of dips are also found. The mineral composition, grain–size changes, and their weathered surfaces define the cross–strata. The azimuth and dip of the cross–bedding data of over 200 readings recorded from various localities to calculate the vector mean direction by following the procedures of Curray (1956) indicate a paleocurrent direction towards the west
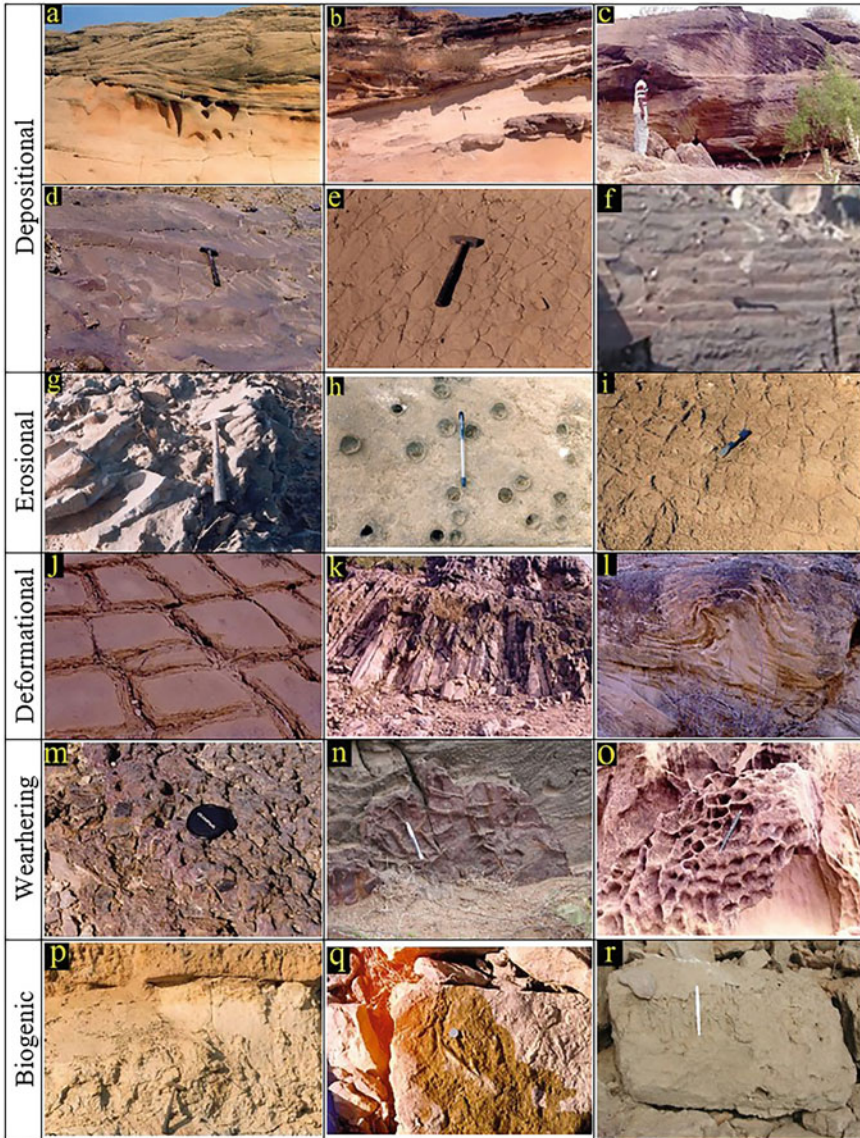
Fig. 2 Variety of Sedimentary Structures observed in Mesozoic rocks of Kachchh Mainland: **a** Large-scale, cross–bedding structure within Bhuj Formation, **b** Well developed cross-bedding exhibited by Jhuran sandstones, **c** Large-scale, composite cross-bedding structure of ferruginous sandstone, Habo Dome, **d–e** Large straight crested, slightly sinuous wave ripples shown, **g** Groove casts/marks preserved in sandstones, **h** eroded concretionary structures displaying circular, even depressions, **i** syneresis/desiccation cracks, **j** Jointing pattern (regular evenly spaced) characteristic of fossiliferous, ferruginous sandstone of Jumara Fm, **k** Columnar type jointing displayed in Bhuj sandstone, **l** Syn-sedimentary deformation exhibited by sandstone, **m**, **n** Typical outcrop surfaces formed due to weathering, **p** burrowing and bioturbation leading to complete disturbed bedding, **q** Fine-grained shaly limestone displaying burrowing and trace fossils, Jhura Hill, **q**, **r** trace fossils due to burrowing and boring by organisms (pen length = 14 cm, hammer length = 38 cm)

and southwest (from 222.89 to 246.52; Table 3). The locality wise distribution of dip azimuth and calculated vector mean data are given in Table 4.

4.3 Texture

The clastic textural attributes (viz. size, shape, sphericity, and roundness parameters) are of significant help to describe and classify the various sandstone types in addition to understand their: provenance, transporting mechanisms, and depositional environments. The grain–size distribution patterns of the representative sandstone samples exhibit, in general, a marked unimodal to bimodal nature of the rocks, which compliments the results of the paleocurrent analyses. The summary of textural parameters, as observed in the sandstones, is given in Table 5. A stratigraphic variation in the textural parameters between mixed–clastic carbonate sequence of Middle Jurassic and the predominantly clastic sequence of Late Jurassic– Early Cretaceous as observed in the sandstones can be visualized from Table 5, representing the minor changes in transportation and depositional conditions. The plotting of size data on bivariate discriminatory diagrams of Moiola and Weiser (1968) (Fig. 3a, b) shows a mixed beach to dune/river environment of deposition. However, no stratigraphic separation was observed, supporting little variation in depositional conditions.

4.4 Composition

The sandstones of Mesozoic succession, in general, are fine to medium-grained, moderate to well sorted, and cemented by quartz, hematite and Calcite (Fig. 4). Matrix occurs as crushed lithic grains, small quartz grains, and phyllosilicates and varies considerably (5–22%) or more with cement varying up to 28–41%. Cementation by quartz, hematite/ferruginous, calcite (less frequently in the Late Jurassic—Early Cretaceous). Framework grains in most sandstones are composed of detrital quartz and feldspar grains, lithic, and fossil/carbonate fragments. These sandstones can be broadly grouped into three categories viz. type 1 sandstones (quartz arenites, that are distinguished by abundant quartz, alkali feldspars with devoid of rock fragments (Fig. 4a), sub-rounded to sub–angular quartz grains with sutured contacts, monocrystalline quartz predominating over polycrystalline quartz, with heavy minerals tourmaline and rutile; type 2 sandstones (feldspathic arenites), which are characterized by moderate quartz, and moderate plagioclase feldspars and rock fragments (Fig. 4b, d); more or less similar textural characteristics of those of type1 sandstones and heavy mineral composition include tourmaline, epidote, garnet; type 3 sandstones (sub–litharenites), characterized by relatively low quartz content, moderate feldspars and rock fragments with abundant sedimentary lithic fragments cemented with quartz and poikilotopic calcite cement. While the calcite cemented type 1 and 2 sandstones (Fig. 4e–h) belong in general to Middle Jurassic, the silica cemented varieties are

Table 4 Summary of the paleocurrent analysis of cross-bedding data
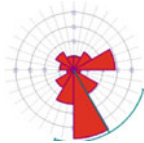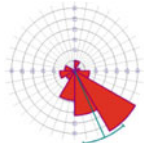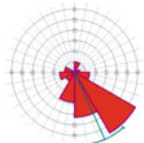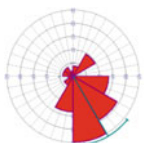
	Bhuj (around)	Jhuran	Jumara	Jhurio
Class interval (degrees)	30	30	30	30
No. of readings	98	84	69	66
Maximum %	23.80	38.30	33.30	25.00
Mean %	8.30	10.10	11.10	9.10
Standard deviation	6.05	8.24	10.24	7.79
Vector mean (degrees)	246.52	222.89	245.89	239.59
Confidence interval (degrees)	44.62	19.45	17.45	20.85
R–mag	0.27	0.55	0.62	0.49
Current rose diagrams				

Table 5 Stratigraphic variation of sandstone textural, compositional and chemical parameters

| Fm | stats | Sandstone textural parameters | | | | Framework grains | | | REE | |
		Mz	SD	Sk	KG	Qz	Fs	Rx	$\sum$REE	LR/HR
Bhuj	Mean	2.1606	0.4887	0.1934	0.9409	92.30	5.80	1.90	186.631	13.901
	σ	0.6492	0.1297	0.1755	0.5103	2.16	1.58	0.83	105.849	6.672
	Min	1.1195	0.3157	− 0.1163	0.2643	88.00	3.00	1.00	18.979	6.617
	Max	3.1697	0.7061	0.4521	1.8155	96.00	8.00	4.00	348.207	25.000
Jhuran	Mean	2.0617	0.5252	0.2660	0.9764	88.90	8.10	3.00	162.340	17.829
	σ	0.4249	0.1145	0.2455	0.3881	3.36	3.31	1.83	92.496	4.747
	Min	1.2134	0.2975	− 0.1328	0.3324	84.00	4.00	1.00	33.807	8.603
	Max	2.8685	0.6753	0.6199	1.6620	94.00	12.00	6.00	316.629	23.407
Jumara	Mean	1.6933	0.9347	0.0390	1.1260	75.55	3.81	4.41	153.04	13.56
	σ	0.8383	0.2553	0.2284	0.2219	11.98	0.58	2.10	31.14	4.78
	Min	0.4703	0.6199	− 0.2334	0.7421	67.07	3.4	2.92	117.84	8.48
	Max	2.7518	1.2801	0.2847	1.2830	84.02	4.22	5.89	222.25	25.09
Jhurio	Mean	1.9059	0.5774	0.1842	1.0584	86.43	3.86	3.30	128.90	11.095
	σ	0.8542	0.1704	0.2250	0.2110	2.03	1.55	0.70	92.51	8.299
	Min	0.3628	0.2516	− 0.1355	0.5738	85.00	2.76	2.80	29.82	8.299
	Max	2.9282	0.7514	0.5135	1.2738	87.87	4.95	3.79	341.40	31.056

Mz–Mean Size, SD– Standard Deviation, Sk–Skewness, KG– Kurtosis, Qz–Quartz, Fs–Feldspar, Rx–Rock Fragments, $\sum$REE– Total REE, LR/HR–LREE/HREE
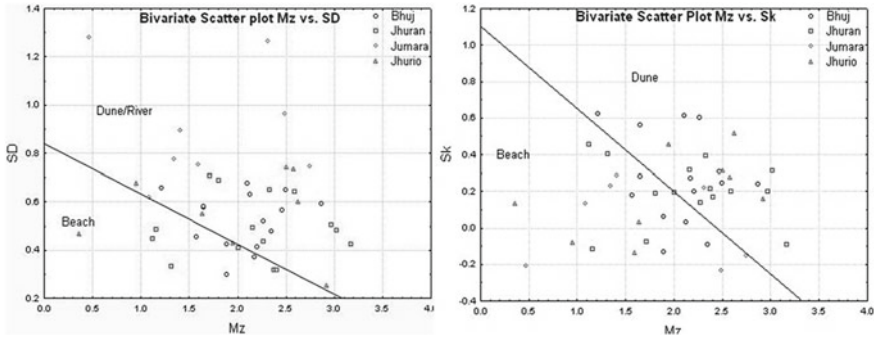
Fig. 3 Bivariate textural plots of Moiola and Weiser (1968) for discriminating depositional environments: **a** Mean–size (Mz) versus standard deviation (SD), **b** Mean–size (Mz) versus skewness (Sk)

observed only in the upper part (Late Jurassic – Early Cretaceous) of the succession. The type 3 sandstones are seen only in the Late Jurassic—Early Cretaceous (Fig. 4a–d).

4.5 Diagenesis

The detrital framework composition of sandstones of Kachchh Mainland has been altered by diagenesis, leading, in particular, to the reduction of the feldspar and unstable lithic fragments, which is supported with the presence of large matrix and cementing material (Fig. 5b, g). The significant diagenetic changes observed include the compaction, dissolution, and cementation (quartz, calcite, feldspar), resulting in reduced primary porosity. As observed in the thin sections, the sandstones, in general, are subjected to low mechanical compaction, probably just before cementation indicated by moderate packing density and the presence of the early cement. The primary porosity is primarily due to the early calcite cementation (Fig. 5h), resulting in scarce or limited quartz overgrowths. Only occasionally, the sandstones show local development of large overgrowths and chert cement. Iron oxide (hematite) cementation and feldspar cementation is ubiquitous and forms an important authigenic phase of the diagenesis of the Mesozoic sandstones. Among the carbonate cemented sandstones, two types of calcite cement are observed. The pore-filling and patchy carbonate (sparite and micrite) occur as an early diagenetic cement (Fig. 5g, h), and the large crystals of calcite (poikilotopic) probably form by neomorphism. In some Late Jurassic to Early Cretaceous samples, Ferroan dolomite and anhydrite/gypsum occur as late–stage cement.
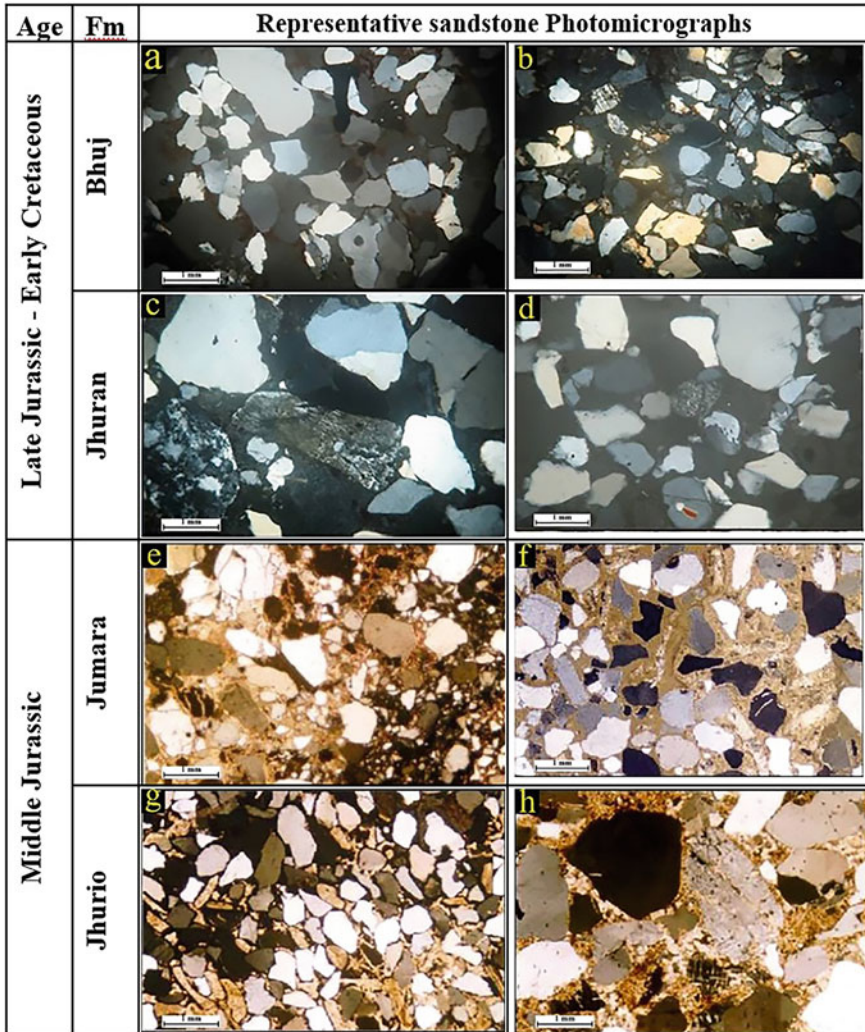
Fig. 4 Photomicrographs of representative Mesozoic sandstones of Kachchh Mainland (xpl): **a** Fine- to medium-grained, moderately-sorted sandstone, b Feldspathic arenite displaying Fe-oxide replacement, **c** Medium- to coarse-grained sandstone showing variable types of Rock fragments, **d** Fine- to medium-grained sandstone showing altered feldspar (in the centre), **e** Subangular to sub rounded, poorly sorted quartz wacke showing lithic fragments of limestone and glauconite pellet (left centre), **f** Sandstone cemented by large poikilotopic calcite crystals. Note the typical high order interference colours of calcite, **g** Subrounded to well rounded, well sorted calcite cemented quartz arenite. Matrix between the grains contain opaque iron oxide, and **h** Feldsphathic sandstone showing dissolution and alteration of feldspars and subsequent calcite cementation
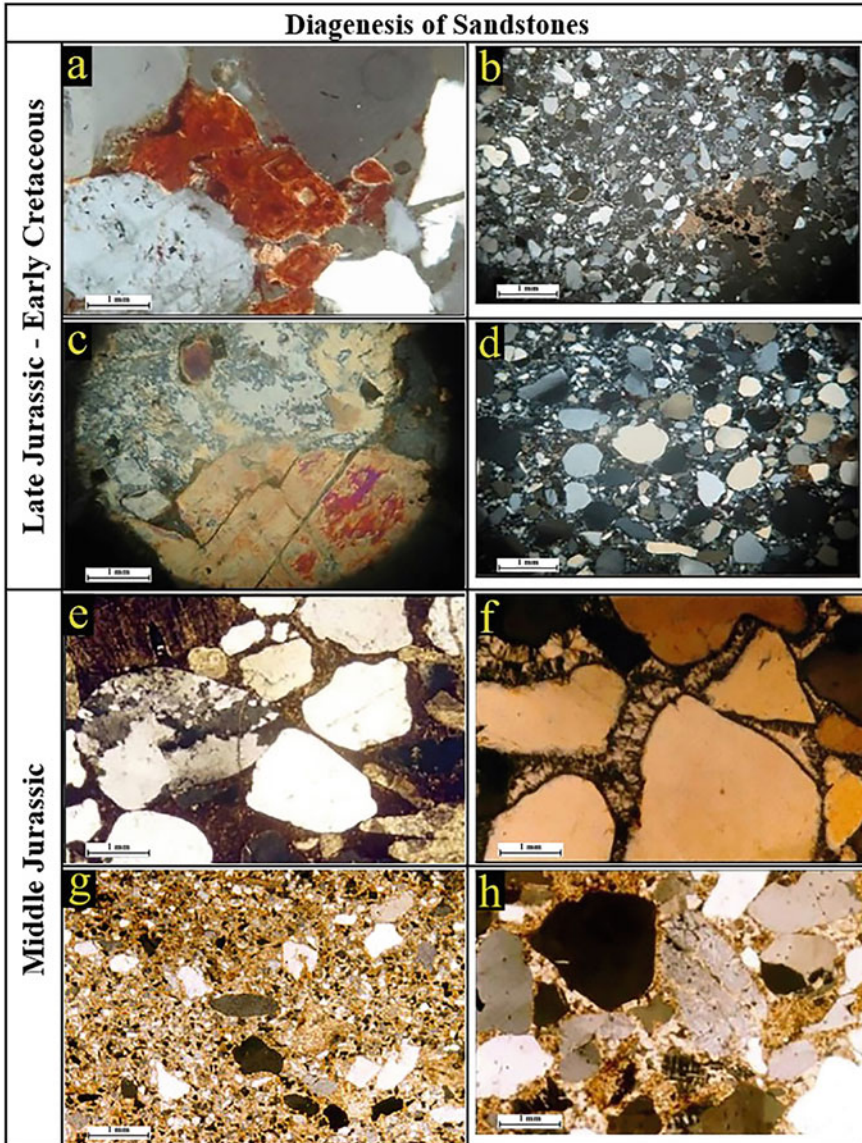
Fig. 5 Photomicrographs of the Mesozoic Sandstones displaying the various post–depositional diagenetic changes: **a** Sandstone displaying altered feldspar (lower left) and ferruginized rhomb-shaped crystals of dolomite of Jhuran Formation, **b** Fine- to medium-grained quartz wacke displaying large poikilotopic calcite cementation, **c** Gypsum/anhydrite cementation of fine sandstone, **d** Sandstone displaying Textural inversion (poorly sorted with well-rounded quartz grains) Bhuj Formation, **e** Calcarenite showing polycrystalline (composite) quartz. The sutured boundaries between crystals clearly indicate metamorphic source, **f** Sandstone displaying pore filling silica cementation in the form of isopachous fringe around quartz grains, **g** Calcarenite showing rounded quartz and chert grains together with smaller subangular to sub rounded quartz grains in a fine-grained matrix **h** Poorly sorted, quartz arenite showing grains coated with kaolinitic cement and subsequent iron oxide impregnations

4.6   Fine Clastics

The fine-grained mudrocks (shales) Mesozoic succession consists of well laminated shales, silty shales and calcareous shales of various colours and shades. The composition of the fine clastics as observed from the results of the XRD analyses comprises clay minerals (essentially of smectite, chlorite, kaolinite and illite) and silty quartz). While kaolinite is observed throughout the succession, chlorite is restricted only to the Late Jurassic to Early Cretaceous part of the succession.

5   Carbonate Sedimentology

5.1   Carbonate Allochems

The carbonate rocks (bedded/oolitic/nodular limestones) and calcareous shale units are predominantly observed only at the lower and middle part of the succession in Jhurio and Jumara formations. The limestones are hard, compact and often nodular with varied framework composition and range from clean, well–sorted packstone–grainstones to unsorted mudstone–wackestone types. The framework components observed in the carbonate rocks include a variety of carbonate allochems (pellets (Fig. 6a), ooids (Fig. 6b), intraclasts (Fig. 6c), terrigenous (Fig. 6d) and skeletal grains (Fig. 6e–l)), orthochems, including micrite and sparite with different morphological varieties, viz. microspar, sparite (Fig. 7c), fringe cement (Fig. 7i), coarse blocky mosaic, and syntaxial rim cements (Fig. 7d).

The carbonate rocks, based on texture and framework composition, are categorized into mudstones, pelletal wackestone, oolitic wackestone–packstone, molluscan packstone–grainstone and grainstone types following the Dunham (1962) classification of carbonate rocks.

5.2   Carbonate Diagenesis

Diagenesis of carbonates encompasses all the sediment processes due to physical, chemical, and biological changes immediately after deposition until realms of incipient metamorphism at elevated temperatures and pressures. Diagenesis has great relevance, especially in limestones due to their susceptibility to such modifications, which provides valuable information on the depositional and post-depositional conditions.

The carbonates of the Mesozoic sequence of Kachchh Mainland have undergone diagenetic modifications in almost all stages of diageneses. The significant diagenetic changes observed in these rocks include compaction (Fig. 7a), dissolution (Fig. 7b), cementation (Fig. 6a, b), neomorphism (Fig. 7c), micritization (Fig. 6f, 7e)
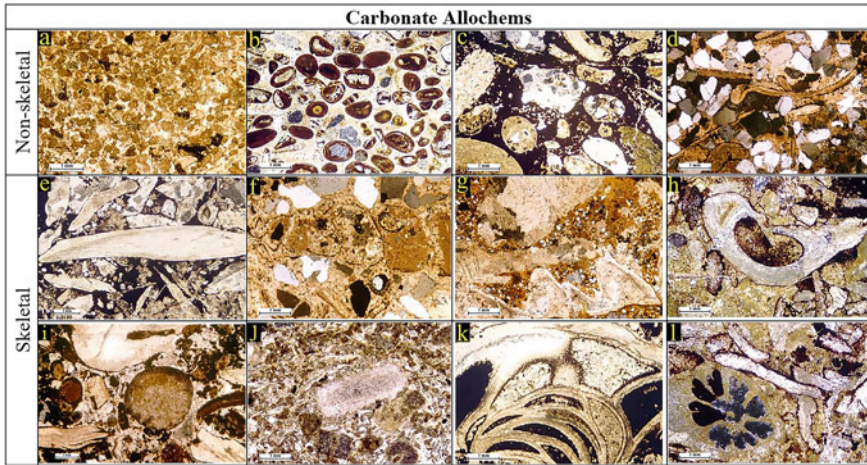
Fig. 6 Photomicrographs of Middle Jurassic carbonates displaying the different carbonate allochems with varying states of preservation (xpl): **a** Peloidal grainstone showing tight packing due to compaction, **b** Oolitic grainstone showing ooids with relatively thin cortices containing quartz and bioclasts as nuclei, **c** Lithocalstic grainstone with ferruginous cement, **d** Sandy molluscan grainstone showing casts of bivalves, algal and echinoidal bioclasts, **e** Molluscan grainstone with well-preserved bivalve showing original foliated internal structures, **f** Gastropodal wackestone with micrite-filled ghost structure of gastropod shell, **g** Brachiopod shell showing the preservation of internal structure of obliquely arranged fibres, **h** Crinoidal grainstone with large brachiopod shell fragment (cavity filled with internal sediment) with well–preserved foliated structure, **i** Echinoidal-bryozoan grainstone showing iron–oxide impregnated bioclasts (echinoid spine) suggesting replacement of bioclasts, **j** Algal-crinoidal packstone displaying the micritization of a crinoid skeletal fragment, **k** Micrite-filled internal chambers of a foraminifer displaying the aggrading neomorphism, **l** Algal wackestone with abundant silt-sized quartz and well preserved possible sponge spicule (rod-shaped) in centre and **m** Coralline-molluscan grainstone showing section of a coral and algal skeletal elements. The coral walls and septa are seen micritized (lower left)

and replacement (Fig. 6e, f). The observed diagenetic changes in these rocks include dissolution, cementation, neomorphism, micritization, replacement, and compaction. The evidence of compaction observed in these rocks include tight packing (Fig. 7a) and squeezing, bending, and even fracturing of some skeletal grains (Fig. 7e). Selective dissolution of aragonitic or high-Mg calcitic fossils and ooids are seen selectively dissolved, producing secondary (oomoldic type) porosity (Fig. 7b). Such dissolution produces secondary porosity. The Middle Jurassic carbonates, in many samples, exhibit the process of micritization wherein the carbonate allochems (skeletal and non–skeletal) are completely or partially micritized with the continuous and boring activity of algae (Fig. 6f, i, l). The replacement of the original calcite by dolomite cement (Fig. 7e) and silica (Fig. 7f) is considered a late–stage diagenetic process.
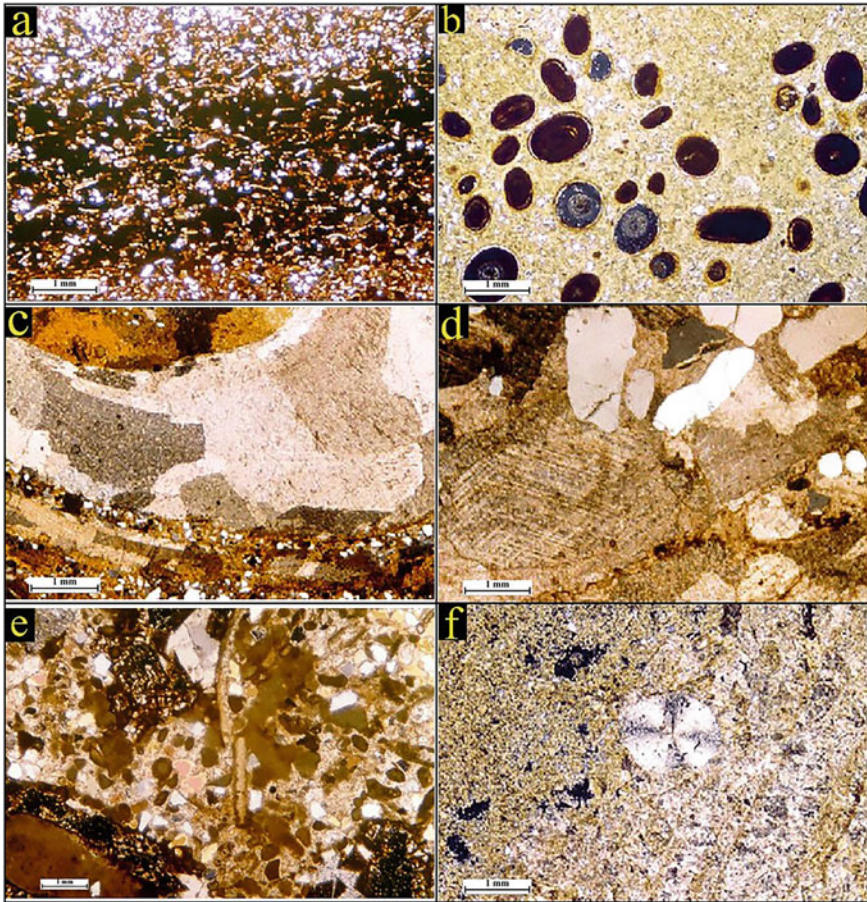
Fig. 7 Photomicrographs (xpl) displaying the various diagenetic changes of Mesozoic carbonate rocks: **a** Laminated (light and dark) ferruginous limestone with tightly compacted very thin tests/shells of bivalves **b**, **c** Replacement of original aragonitic shell fragment of mollusc by neomorphic sparry calcite. Note the ghost of primary layers in the spar (lower left), **d** Syntaxial rim cementation of echinoid skeleton, **e** Sandy–molluscan biosparite showing replacement of calcite by dolomite (dolomitization—dark patches), and **f** Silicification and chert formation in limestone

6 Depositional History

The interpretation of the environment of a litho–unit should be based on consideration of several parameters: physical (bed geometry, primary structures), lithological (petrographic, mineralogic, granulometric, textural, and diagenetic), biological (biota, trace fossils), chemical, and stratigraphic relationship, together in a process to response model. Minimal emphasis was given in the past for an integrated study to substantiate their conclusions with detailed sedimentologic observations.

6.1 Provenance

Based on the detailed petrographic and heavy mineral analyses, Chaudhuri et al. (2018) interpreted the provenance of Mesozoic sandstones resulting from two different sources, the felsic basement rocks of Nagar Parkar ridge complex in the north and the Aravalli and Delhi Super Group in the east. The paleocurrent analyses and sedimentological study of the sandstone from the present study suggesting a westerly to south paleoslope support the above indicating the movement of sediment from north and east. As observed from the thin section petrographic study, the framework composition of the sandstone suggests a mixed igneous and metamorphic source of supply of sediments. The fine to medium-grained, hard, compact sandstones containing abundant undulose quartz, lithic fragments over feldspars characterize a metamorphic source. The abundant opaque minerals and the presence of strained quartz and microcline further support the metamorphic source. The relatively coarse-grained sandstones with abundant feldspars and non–undulose quartz, inclusions of rutile in quartz suggest an igneous origin. A shift in sandstone type from Arkosic (Jumara Formation) to subarkosic (Bhuj Formation) is interpreted by Chaudhuri et al. (2018). The heavy mineral composition, consisting of rutile, ilmenite, and magnetite, suggests an acidic to a basic igneous source. QFL plots of framework composition indicated a basement up–lifted provenance of Middle Jurassic sandstones and a combined basement–uplifted and craton interior provenance for the Late Jurassic to Early Cretaceous sediments. In the present study, the plotting (Fig. 8a, b) of the Mesozoic sandstone framework compositional data on the tectonic provenance diagram (QFL) of Dickinson (1979, 1985) shows the majority of the sample falling in the recycled orogenic and craton interior provenance without much differentiation of the Middle Jurassic versus Late Jurassic–Early Cretaceous
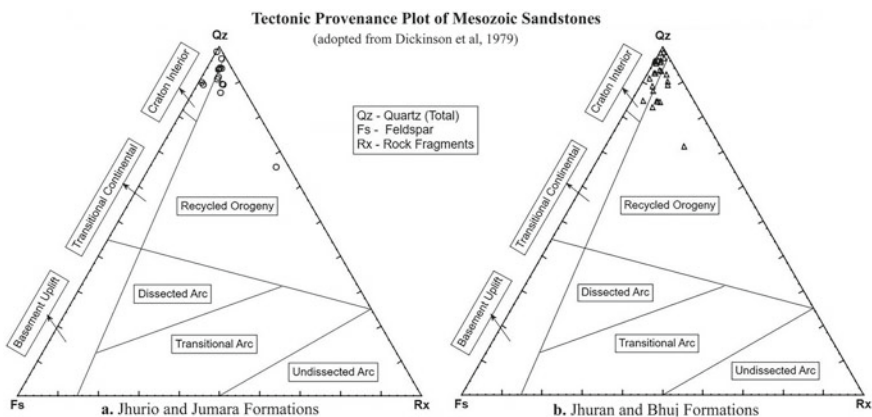
Fig. 8 Ternary QFR plots for sandstone provenance analysis (Dickinson and Suczek 1979; Dickinson 1985) for understanding the tectonic provenance of Mesozoic sandstones of Kachchh
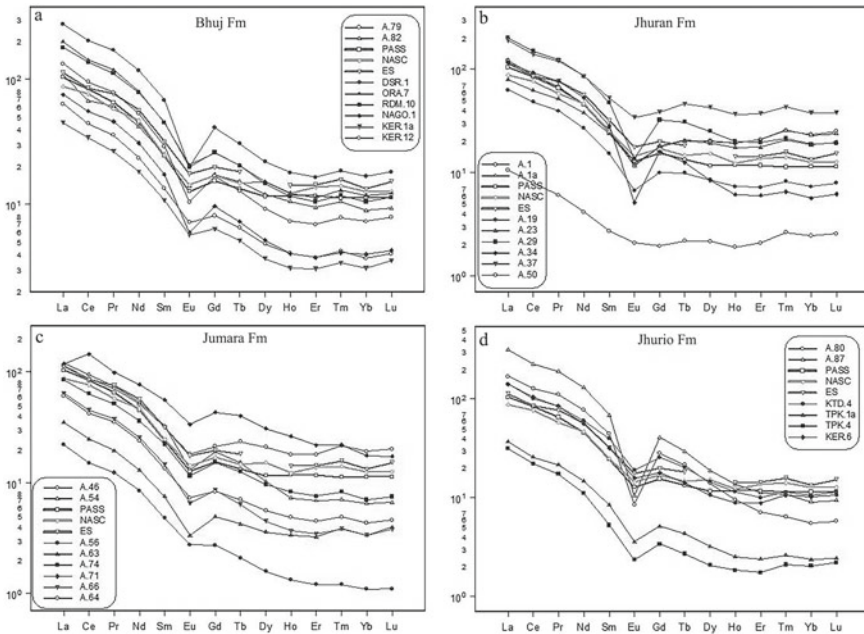
Fig. 9 Stratigraphic variation in chondrite-normalized REE plots for the data

sandstone. The rare earth element (REE) content of the rocks characterize post–Archean sediment, and the homogenization is due to erosion and transportation. The REE content of Middle Jurassic sandstones (mean from 129 to 153) is close to the crustal average. In contrast, the Late Jurassic to Early Cretaceous (Jhuran and Bhuj Formations) show a slightly higher value (above crustal average) of the total REE (Table 5). However, a greater enriched LREE and fractionated LREE and flat HREE is observed from the chondrite normalized REE patterns for the entire Mesozoic sediments (Fig. 9a–d). Although no regular vertical or spatial variation/separation is observed in the texture and composition of the sandstone when interpreted independently, the use of Canonical discriminant statistical analyses of the combined textural and mineralogical composition all the sandstones provided in differentiating the different lithological units (Fig. 10).

6.2 Depositional Environment

Most of the earlier studies on the reconstruction of the paleoenvironments of the Mesozoic stratigraphic units were qualitative and based mainly on local studies and general observations of gross lithology and ecology of fossil fauna/flora (Ghosh 1969). Subsequent studies of Krishna et al. (1983) and Howard and Singh (1985)
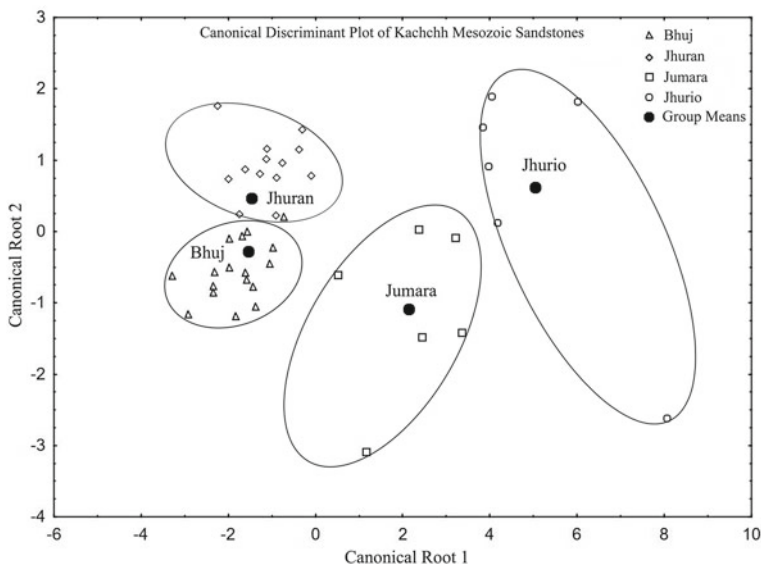
Fig. 10 Canonical discriminant plot of combined textural and framework compositional data of sandstones showing clear separation of Mesozoic formations of Kachchh Mainland

interpret the depositional environments based mainly on trace fossils with some supporting evidence from gross lithology. A comprehensive study of the basin framework, depositional processes, and environments, and the evolution based on the detailed study of the gross facies and its quantitative assessment of the basin is given by Biswas (1981). Based on a detailed study of Ammonoid fauna, shallow marine, inner to middle shelf environment of deposition has been suggested for the Middle Jurassic Jhurio and Jumara formations (Fürsich et al. 1992, 2001; Krishna et al. 2000). The vertical environment profiles of lithologic sequences indicate two distinct mega–cycles Kachchh (Biswas 1982): a transgressive, followed by a regressive cycle, with several transgressive/regressive sub–cycles and micro–cycles corresponding to the fluctuations of sea levels in unstable shelf condition. An outer to inner shelf environment of deposition for the Jhuran Formation is interpreted based on their sedimentological study (Arora et al. 2015, 2017).

The clastic textural study suggests a mixed depositional condition of fluctuating coastal beach–shallow marine environment. The average grain–size of these rocks resembles that of nearshore, beach–shallow marine sands. In general, the clastic grains are moderate to well–sorted, negative to positively skewed, and mesokurtic. According to Friedman (1967, 1969), standard deviation values of Mesozoic sandstone textures fit into the category of moderately sorted to well–sorted sand; and are similar to those of the beach sands. The depositional environments as interpreted independently from the field observation of the sedimentary structures and textural characteristics and composition of the sandstones all support each other indicating, in general, a mixed fluvial–aeolian–beach–shallow marine environment of deposition

of Mesozoic sediments. Petrographically the coarse clastics correspond to Quartz arenite and Feldspathic arenite types with little mud suggesting greater winnowing action of the depositional medium.

The mineralogical composition and sandstone in association with textural characteristics and paleocurrent data suggest their derivation from a recycled crystalline igneous and metamorphic source probably from north and east, perhaps from the Aravallis in the East and Nagar Parkar ridge in the north. Table 6 summarizes the stratigraphy and sedimentation history of the Mesozoic sequence of Kachchh Mainland.

7 Conclusions

The present integrated study of the lithofacies association with detailed clastic and carbonate sedimentology of the Mesozoic sequence of Kachchh, while substantiating the earlier interpretations, also provides additional data to interpret provenance and depositional environments.

(a) The Mesozoic sequence of Kachchh mainland represent 13 Lithofacies associations comprising various sediment characteristics with a host of sedimentary structures dominated by Cross–bedding depositional structures.
(b) The paleocurrent analyses of cross–bedding structures of sandstones support the sediment provenance source from the north (possibly Nagar Parkar massif) and east and northeast (Aravalli source).
(c) In general, the depositional environments of the Mesozoic sequence vary from a beach to shallow marine for the lower part to fluvial to shallow marine in the upper part.
(d) The Mesozoic sediments of Kachchh mainland, as indicated by their structural and petrographic textural characteristics, have been subjected to various post–depositional modifications that lead to modification of the original depositional characteristics and porosity changes.

Table 6 Summary of the Depositional Characteristics of the Mesozoic Succession of Kachchh Mainland (after Biswas 1981; Osman and Mahender 1997; Mahender et al. 2008; Mahender and Sharma 2010)

Age	Fm	Litho-facies	Bedding/ Geometry	Lithology	Dominant Structures	Biota	Texture	Clay Minerals	REE Patterns	Provenance	Environment	Probable Sea Level − 0 +
Early Cretaceous	Bhuj	LFA13 LFA12	Well Bedded (X- & planar bdd.) Blanket	Sandstone	Large scale Cross-bedding, Bioturbation, Jointing,	Plant fossils	Fine-med, Well Sorted	Kaolinite Chlorite	∑REE close to crustal average, Greater	Recycled crystalline igneous and metamorphic source of Nagar Parkar ridge in the north and Aravallis in east,	Fluvial-Upper Deltaic plains	
		LFA11 LFA10	Well Bedded (X-bedded), Blanket	Ferr. S.st, Shale, cyclic, coal beds	Soft sediment deformation	Plant & Trace Fossils	Fine to Med, V. well sorted	Kaolinite, Chlorite	Degree of Enriched LREE, Fractionated		Lr Deltaic plain (Distributary)	
Late Jurassic	Jhuran	LFA 9 LFA 8	Bedded / Tabular	S.st, minor shales	Cross-bedding, Ripple Marks,	Poorly fossiliferous	Fine, Mod Sorted	Kaolinite Chlorite	LREE and flat HREE,		Delta Front	
		LFA 7	Thin bedded / wedge	Shales, thin s.st bands	Concretions & Nodules	Marine Fossils	Fine, Mod. sorting	Illite, Chlorite Kaolinite,	Significant Negative Eu Anomaly		Pro-delta	
		LFA 6	Thin Bedded / Tabular	Sandstone & Shale		Marine Fossils	Fine, Mod. Sorting	Kaolinite, Illite			Shallow Marine to Sub-littoral	
Middle Jurassic	Jumara	LFA 5	Thin bedded	L.st & shale	Cross-bedding, Ripple marks, Trace fossils, Burrows, soft	Abundant Diverse	Non-clastic	Kaolinite Chlorite	∑REE close to crustal average, Enriched		Sub-littoral	
		LFA 4	Bedded	S.st, shale & L.st		Abundant	Fine, Mod sorted, + ve	Kaolinite chlorite	LREE over HREE, Fractionated LREE and		Sub-littoral	
		LFA 3	Well Bedded (X-bedded)	S.st, shale & conglomerate	sediment deformation, scour marks	Few (molluscs)	Medium, Well sorted + ve	Kaolinite	flat, Negative Eu Anomaly		Beach (Littoral)	
	Jhurio	LFA 2	Bedded	Shale, L.st and S.st	Boring and Burrows,	Abundant	Fine, Mod sorted, - ve	Kaolinite Chlorite			Wave zone	
		LFA 1	Thin bedded	L.st and shale	surface crusts, Trace fossils	Few	Non-clastic	Kaolinite, illite			Quiet water below wave zone	

References

Agarwal SK (1957) Kutch Mesozoic: a study of the Jurassic of Kutch with special reference to the Jhura Dome. J Palaeontol Soc India 2:119–130

Agarwal SK (1975) Kachchh mesozoic: some problems and recent contributions. Recn Res Geol 397–414

Ahmad AHM, Bhat GM, Khan AF, Saikia C (2006) Petrography, diagenesis, provenance and tectonic setting of Upper Katrol Formation (Kimmeridgian), Nakhatarana Area, Kachchh, Gujarat. J Geol Soc India 67:243–253

Alberti M, Fürsich FT, Pandey DK, Ramkumar Mu (2012) Stable isotope analyses of belemnites from the Kachchh Basin, western India: paleoclimatic implications for the Middle to Late Jurassic transition. Facies 58:261–278

Alberti M, Fürsich FT, Pandey DK (2012) The Oxfordian stable isotope record ($\delta^{18}O$, $\delta^{13}C$) of belemnites, brachiopods, and oysters from the Kachchh Basin (western India) and its potential for palaeoecologic, palaeoclimatic, and palaeogeographic reconstructions. Palaeo Palaeo Palaeo 344–345:49–68

Alberti M, Fürsich FT, Pandey DK, Mukherjee D (2017) Overview on the Middle to Upper Jurassic sedimentary succession of Gangta Bet in the Kachchh Basin, western India, with special emphasis on its lithostratigraphy, biostratigraphy, and palaeoenvironment. J Geol Soc India 89:259–270

Arkell WJ (1956) Jurassic geology of the world. Oliver and Boyd, Edinburgh

Arora A, Banerjee S, Dutta S (2015) Black shale in Late Jurassic Jhuran Formation of Kutch: Possible indicator of oceanic anoxic event? J Geol Soc India 85:265–278

Arora A, Dutta S, Gogoi B, Banerjee S (2017) The effects of igneous dike intrusion on organic geochemistry of black shale and its implications: late jurassic jhuran formation, India. Int J Coal Geol 178:84–99

Banerjee S, Bansal U, Thorat A (2016) A review on palaeogeographic implications and temporal variation in glaucony composition. J Palaeogeography 5:43–71

Bansal U, Banerjee S, Pande K, Arora A, Meena SS (2017) The distinctive compositional evolution of glauconite in the Cretaceous Ukra Hill Member (Kutch basin, India) and its implications. Mar Petrol Geol 82:97–117

Bardhan S, Chattopadhyay D, Mondal S, Das SS, Mallick S, Roy A, Chanda P (2012) Record of intense predatory drilling from Upper Jurassic bivalves of Kutch, India: implications for the history of biotic interaction. Palaeo Palaeo Palaeo 317–318:153–161

Bardhan S, Jana SK, Roy P (2009) Sexual dimorphism and polymorphism in a Callovian Phlycticeras (Ammonoidea) assemblage of Kutch, India. Geobios 43:269–281

Biswas SK (1970) Geologic and tectonic maps of Kutch. ONGC Bull 7:115–123

Biswas SK (1971) Note on the geology of Kutch. Quart J Geol Min Met Soc India 43:223–234

Biswas SK (1974) Landscape of Kutch—a morphotectonic analysis. Indian J Earth Sci 1:177–190

Biswas SK (1977) Mesozoic rock–stratigraphy of Kutch, Gujarat. Quart J Geol Min Met Soc India 49:1–52

Biswas SK (1981) Basin framework, palaeoenvironment and depositional history of the Mesozoic sediments of Kutch Basin, western India. Quart J Geol Min Met Soc India 53:56–85

Biswas SK (1982) Rift basins in the western margin of India and their hydrocarbon prospects with special reference to Kutch basin. AAPG Bull 66:1497–1513

Biswas SK (1987) Regional tectonic framework, structure and evolution of the western marginal basins of India. Tectonophys 135:307–327

Biswas SK (1991) Stratigraphy and sedimentary evolution of the Mesozoic basin of Kutch, western India. In: Tandon SK, Pant CC, Casshyap SM (eds) Stratigraphy and sedimentary evolution of Western India, Gyanodaya Prakashan, Nainital, pp 74–103

Biswas SK (2005) A review of structure and tectonics of Kutch basin, western India, with special reference to earthquakes. Curr Sci 88:1592–1600

Chaudhuri A, Banerjee S, Le Pera E (2018) Petrography of middle jurassic to early cretaceous sandstones in the Kutch Basin, western India: Implications on provenance and basin evolution. J Palaeogeography 7:2–14

Chaudhuri A, Das K, Banerjee S, Fitzsimons ICW (2020) Detrital zircon and monazite track the source of mesozoic sediments in Kutch to rocks of late neoproterozoic and early palaeozoic orogenies in northern India. Gond Res 80:188–201

Chaudhuri A, Banerjee S, Chauhan G (2020) Compositional evolution of siliciclastic sediments recording the tectonic stability of a pericratonic rift: mesozoic Kutch Basin, western India. Mar Pet Geol 111:476–495

Chaudhuri A, Chatterjee A, Banerjee S, Ray JS (2020c) Tracing multiple sources of sediments using trace element and Nd isotope geochemistry: provenance of the Mesozoic succession in the Kutch Basin, western India. Geol Mag https://doi.org/10.1017/S0016756820000539

Chaudhuri A, Banerjee S, Prabhakar N, Das A (2020) The use of heavy mineral chemistry in reconstructing provenance: a case study from Mesozoic sandstones of Kutch Basin (India). Geol Jour. https://doi.org/10.1002/gj.3922

Curray JR (1956) The analysis of two-dimensional data. J Geol 64:117–131

Das S, Saha S, Bardhan S, Mallick S, Allmon W (2018) The oldest turritelline gastropods: From the Oxfordian (Upper Jurassic) of Kutch, India. J Paleontol 92:373–387

Dickinson WR (1985) Interpreting provenance relations from detrital modes of sandstones. In: Zuffa GG (ed) Provenance of arenites. Springer, Dordrecht, pp 333–361

Dickinson WR, Suczek CA (1979) Plate tectonics and sandstone compositions. AAPG Bull 63:2164–2182

Dubey N, Chatterjee BK (1997) Sandstone of Mesozoic Kachchh basin: their provenance and basinal evolution. Indian J Petrol Geol 6:55–68

Dunham RJ (1962) Classification of carbonate rocks according to depositional texture. In: Ham WE (ed) Classification of carbonate rocks. AAPG Mem vol 1, pp 108–121

Dutta R, Bardhan S (2016) Systematics, endemism and phylogeny of Indian proplanulitins (Ammonoidea) from the Bathonian-Callovian of Kutch, western India. Swiss J Palaeontol 135:23–56

Friedman GM (1967) Dynamic process and statistical parameters compared for size frequency distribution of beach and river sands. J Sed Petrol 37:327–354

Friedman GM (1969) Depositional sedimentary environments in carbonate rocks. SEPM Spec Publ 14, Tulsa

Fürsich FT, Oschmann W, Singh IB, Jaitly AK (1992) Hardgrounds, reworked concretion levels and condensed horizons in the jurassic of western India: Their significance for basin analysis. J Geol Soc London 149:313–331

Fürsich FT, Pandey DK, Callomon JH, Jaitly AK, Singh IB (2001) Marker beds in the Jurassic of the Kachchh Basin, western India: their depositional environment and sequence–stratigraphic significance. J Palaeontol Soc India 46:173–198

Gaur KN, Talib A (2009) Middle-upper jurassic foraminifera from Jumara Hills, Kutch, India (Foraminifères du Jurassique Moyen-Supérieur des Collines de Jumara, Kutch, Inde). Rev De Micropaléontologie 52:227–248

Ghosh DN (1969) Biostratigraphic classification of Patcham–Chari sequence of Kutch. (abstract). Proc 56th Sess, Indian Sci Congress Assoc 3, p 214

Howard JD, Singh IB (1985) Trace fossils in the Mesozoic sediments of Kachchh, western India. Palaeo Palaeo Palaeo 52:99–122

Kale MG, Pundalik AS, Duraisamii RA, Karmalkar NR (2016) Soft sediment deformation structures from Khari River section of Rudramata member, Jhuran formation, Kutch: a testimony of jurassic seismites. J Geol Soc India 87:194–204

Khadikikar AS (1996) Breakup of Gondwanaland and the jurassic record of the Kachchh Basin, Gujarat, western India. Curr Sci 70:1093–1096

Krishna J, Singh IB, Howard JD, Jafar SA (1983) Implications of new data on Mesozoic rocks of Kachchh, western India. Nature 305:790–792

Krishna J, Pathak DB, Pandey B, Ojha JR (2000) Transgressive sediment intervals in the late jurassic of Kachchh, India. GeoResearch Forum 6:321–332

Krishna J (2017) The Indian Mesozoic Chronicle: Sequence Stratigraphic Approach. Springer, Singapore

Mahender K, Sharma NL (2010) Lithofacies association, clastic sedimentology and depositional environment of Late Jurassic-Early Cretaceous sequence (Jhuran and Bhuj formations) of central part of Kachchh Mainland, India. Gond Geol Mag 12:177–188

Mahender K, Rajeevan M, Sharma NL (2008) Textural and petrographic characterization and implication of diagenesis in the interpretation of provenance and depositional environment of the sandstones of the middle jurassic Jumara Formation, Kachchh Mainland, Gujarat. Int J Earth Sci Eng 11:31–43

Moiola RJ, Weiser D (1968) Textural parameters: an evaluation. J Sed Pet 38:45–53

Osman AH, Mahender K (1997) Stratigraphy and sedimentology of the Middle Jurassic (Callovo–Oxfordian) sequence of Habo Hill, Kutch District, Gujarat. J Indian Ass Sedimentol 16:103–110

Pandey J, Dave A (1993) Studies in Mesozoic foraminifera and chronostratigraphy of western Kutch, Gujarat. Palaeontographica Indica 1, ONGC

Patil DJ, Mani D, Madhavi T, Sudarshan V, Srikarni C, Kalpana MS, Sreenivas B, Dayal AM (2013) Near surface hydrocarbon prospecting in Mesozoic Kutch sedimentary basin, Gujarat, Western India—a reconnaissance study using geochemical and isotopic approach. J Petrol Sci Eng 108:393–403

Phansalkar VG, Khadkikar AS, Sudha G (1992) Sedimentary characters of the late jurassic-early cretaceous clastics near Bhuj and their environmental implications. J Indian Ass Sedimentol 11:47–53

Rajnath (1932) A contribution to stratigraphy of Kutch. Quart J Geol Min Met Soc India 4:161–174

Rajnath (1942) The Jurassic rocks of Kutch, their bearing on some problems of Indian geology. Proc 29th Indian Sci Cong Pt II:93–106

Shukla UK, Singh IB (1990) Facies analysis of Bhuj Sandstone (Lower Cretaceous) Bhuj Area, Kachchh. J Palaeontol Soc India 35:189–196

Singh CSP, Kanjilal S (1974) Some fossil Mussels from the Jurassic rocks of Habo Hill in Kutch, Gujarat, Western India. Indian J Earth Sci 1:113–125

Spath LF (1933) Revision of the Jurassic cephalopod fauna of Kachchh (Cutch). Pal Indica, Geol Surv India New Ser 9:1–945

Talib A, Gaur KN, Sisodia AK, Bhatt BA, Irshad R (2012) Foraminifera from jurassic sediments of Keera Dome, Kutch. J Geol Soc India 80:667–675

Waagen W (1871) Abstract of result of examination of the Ammonite fauna of cutch, with remarks on their distribution among the beds and probable age. Rec Geol Surv India 4:89–101

Wynne AB (1875) Memoir on the Geology of Kutch to accompany a map compiled by A.B. Wynne and F. Fedden during the sessions 1867–68 and 1868–69. Mem Geol Surv India 9:1–289

Magnetic Polarity Stratigraphy Investigations of Middle-Upper Jurassic Sediments of Jara Dome, Kutch Basin, NW India

Venkateshwarlu Mamilla

Abstract Sandstones of the Jhuran Formation in Jara Dome of Kutch Basin were investigated for Magnetic Polarity Stratigraphy (magnetostratigraphy). The Jara Dome in the Kutch Mainland exposes rocks of Jhurio and Jhuran Formations. This study is based on a collection of 100 oriented samples from 35 successive beds in the Jhuran Formation. Both thermal and AF demagnetization investigations were carried out to isolate the Characteristic Remanent Magnetization (ChRM) directions. Virtual Geomagnetic Polarity (VGP) latitudes were computed using the ChRM directions. Magnetostratigraphic column is prepared and correlated with the Geological Time Scale (GTS). The magnetostratigraphic column matches fairly with the GTS from Chron M24 to M19 (145–155 Ma). The magnetostratigraphic column exhibits the dominance of normal polarity except one single reversed polarity in the Jara dome of Kutch Basin.

Keywords Magnetostratigraphy · Kutch · Jurassic · Jhuran formation · Jara dome · Remanent magnetism

1 Introduction

The paleoposition of India after its breakup from the Gondwana and its subsequent northward journey during the Mesozoic is poorly constrained. The study of paleomagnetism and seafloor spreading (Hess 1962), expanded largely due to the availability of precise paleomagnetic data. Further, it paved the way for understanding the drift history of continents and their past positions. The apparent polar wandering path (APWP) of a lithospheric plate is prepared by connecting the paleo-positions. The record of geomagnetic polarity is well established from the present, back to the Oxfordian (Upper Jurassic), equivalent to the last 160 Ma of geological time. Three distinct episodes of reversal behavior are identified in this time interval. The oldest episode, comprising frequent reversals in the Late Jurassic and Early

V. Mamilla (✉)
CSIR-National Geophysical Research Institute, Uppal Road, Hyderabad 500007, India
e-mail: mamila_v@rediffmail.com

Cretaceous, is referred to as the M-sequence (Lowrie 2011). The youngest episode, comprising the Late Cretaceous and Cenozoic, consists of frequent reversals known as the C-sequence (Lowrie 2011). The M-sequence and C-sequence are separated by an interval of 38 Ma, called the Cretaceous Normal Polarity Superchron (CNPS), during which Earth's magnetic field did not reverse polarity. The patterns of reversals do not occur cyclically. Statistical analysis indicates that the reversals in the C- and M-sequences occur randomly, considering the time spent between opposite polarity states. During the early Jurassic break-up of Pangaea and the onset of sea-floor spreading, magnetostratigraphic confirmation of the marine polarity record is either absent or fragmentary. Marine polarity record is absent for older epochs. Consequently, despite many magnetostratigraphic investigations in ancient rocks, consistent polarity records are absent for rocks older than Upper Triassic. Extrapolation of the Geomagnetic Polarity Time Scale (GPTS) requires verifying the same polarity sequence in multiple overlapping sections, which is an essential task for paleomagnetists and biostratigraphers.

Although geology, tectonics, structure, stratigraphy, sedimentology and paleontology of the Kutch Basin are well understood, paleomagnetic data are lacking. The Kutch Basin in NW India has attracted the attention of geoscientists all over the world due to its rich fossil content, complex tectonic setting, and structural features. The preliminary paleomagnetic data on Jurassic sediments of Kutch were published by Venkateshwarlu et al. (2008). Paleomagnetic investigations of thirty magmatic bodies of Kutch provided a Virtual Geomagnetic Pole (VGP) at 33.7°N and 81.2°W (dp/dm = 5.81/9.18) (Paul et al. 2008). Venkateshwarlu et al. (2014) presented results of paleomagnetic data for twelve dyke samples that intrude into several litho units exposed in three different localities, namely, Jumara (Mainland), Kaladongar (Patcham Island) and Kantkote (Wagad, outside the Mainland). The study showed that the dykes in two of the three localities have normal directions, while the third has a reversed direction (similar to the Deccan Volcanic Province directions). The magmatic rocks of the Kutch basin were broadly contemporaneous straddling 30N–29R–29N chrons. Magmatic rocks of Kutch were possibly generated by the impact of the Réunion plume on the Kutch lithosphere under an extensional setting. Magnetostratigraphy studies were carried out on the Jumara Dome of the Kutch Basin and published by Venkateshwarlu et al. (2016). Periasamy and Venkateshwarlu (2017) provided geochemical and petrological data of rocks comprising the Jhuran Formation of Jara Dome. The objective of this study is to present the magnetostratigraphy pattern for the ammonoid-rich Middle to Upper Jurassic Kimmeridgian-Tithonian succession of the Jara Dome in Kutch Basin.

2 Geology and Sampling

The Kutch Basin is a pericratonic rift basin located in western India (Fig. 1) that came into existence after the break-up between eastern and western Gondwanaland during the late Triassic/Early Jurassic period (Biswas 1993) The east–west trending
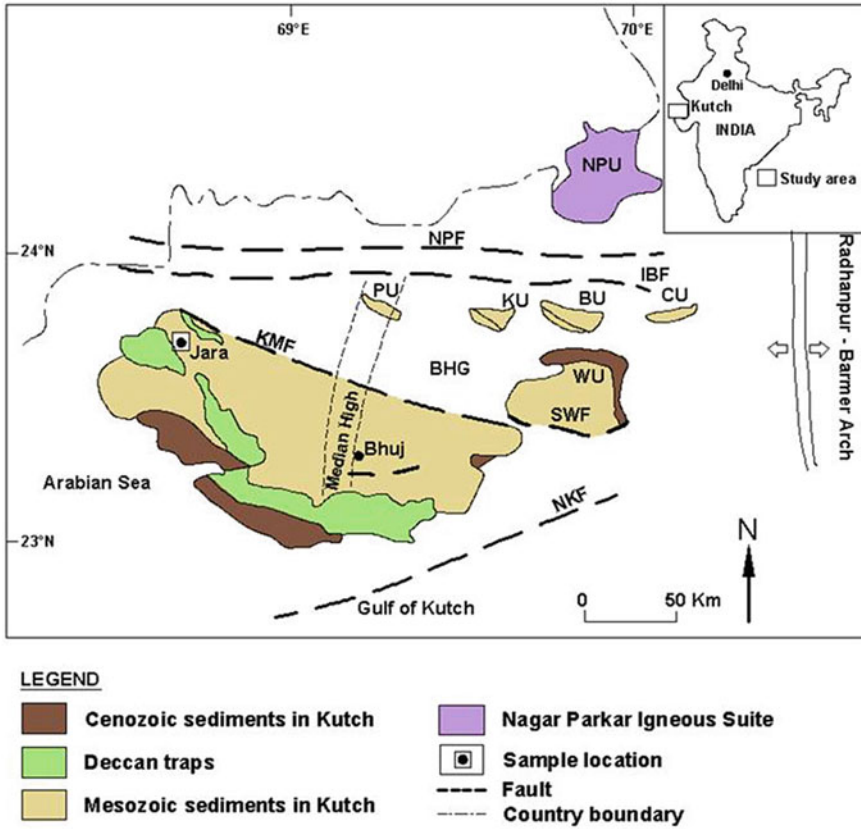
Fig. 1 Geological map showing outcrops of Mesozoic and Cenozoic rocks in Kutch Basin; black dot within rectangle indicates sample location (adapted from Biswas, 1991) (PU = Patcham Uplift; KU = Khadir Uplift; BU = Bela Uplift; CU = Chorar Uplift; WU = Wagad Uplift; NPU = Nagar Parkar Uplift; NPF = Nagar Parkar Fault; IBF-Island Belt Fault; WF = South Wagad Fault; KMF = Kutch Mainland Fault; NKF=North Kathiawar Fault; BHG = Banni Half Graben)

rift basin bounded between latitude 22°30 and 24°30 North latitude and 68° and 72° East longitude. It is confined by Nagar Parkar Fault (NPF) and North Kathiawar fault (NKF), Radhanpur-Barmer basement arch on northern, southern and eastern margins, respectively. The basin accommodates 2000–3000 m thick Mesozoic sediments ranging in age from Lower Jurassic to Lower Cretaceous, 600 m of Tertiary sediments and a thin sheet of Quaternary sediments. Major outcrops of the Mesozoic succession occur in several uplifted regions of the basin, such as Kutch Mainland, Patcham Island, Khadir Island, Bela Island, Chorar Island and Wagad uplifts (Fig. 1) which are separated by vast plains of the Great and Little Ranns and Banni plains occupied by alluvial sediments and salt pan (Biswas 1977).

The Jhuran Formation (Kimmeridgian to Middle Tithonian) consists mainly of sandstone with interbedded shale (Biswas 1977; Arora et al. 2016, 2017). It unconformably overlies the Dhosa Oolite of the Jumara Formation and is succeeded by the Bhuj Formation, with an unconformable contact in between. The present study focuses on the sandstones and shales comprising the Jhuran Formation. The stratigraphy of the Mesozoic succession of Kutch and detailed lithostratigraphic boundaries (Biswas 1977) are provided in Table 1.

The Jara Dome occurs at the western fringe of the Mainland Kutch where the Jumara, Jhuran and Bhuj Formations are best exposed. The Jhuran Formation comprises Lower, Middle and Upper and Katesar Members (Biswas 1977; Arora et al. 2016). The lithostratigraphic section of the Jhuran Formation in the Jara Dome has been prepared (Fig. 2). The study area is located around the latitude 23°43′96″N and longitude 68°56′17″E.

Table 1 Stratigraphy of the Mesozoic succession of Kutch with necessary lithological details of the Jhuran Formation (Biswas 1977)

Age		Members (Jhuran Formation)	Description
Albian to Santonian Aptian	Bhuj Formation	Katesar (Tithonian to Valangian)	Greenish grey to yellow, massive cross bedded sandstones with minor intercalations of shales, exposed only near western margin near Katesar temple
Berriasian to Barremian		Upper (Tithonian)	Predominantly arenaceous rocks. Red and yellow, massive cross bedded sandstone with intercalations of shales and sandstones. Predominantly shaley, dark grey to black shales , interbedded with ferruginous siltstones and laminated micaceous siltstone
Tithonian to Kimmeridgian	Jhuran Formation	Middle (M. Kimmeridgian to Tithonian)	Alternating yellow and red sandstones, shale beds in almost equal proportion with some yellow fossiliferous, calcareous sandstones
Oxfordian to Callovian	Jumara Formation		
Bathonian	Jhurio Formation	Lower (L. Kimmeridgian and older)	
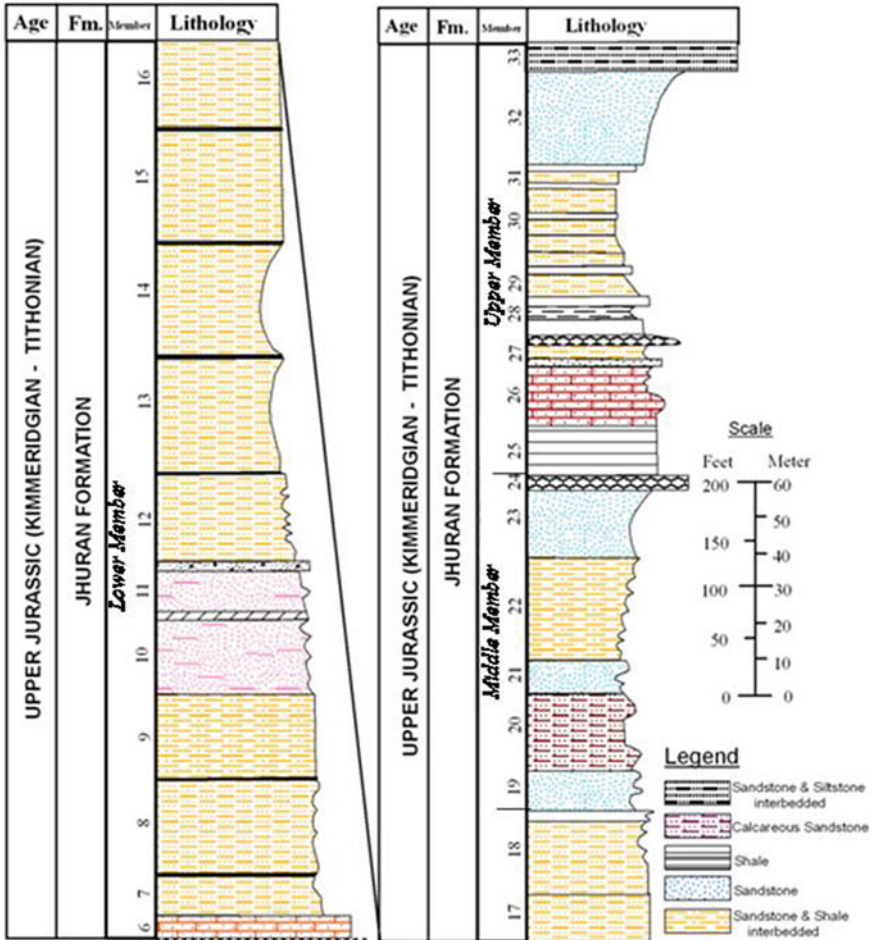
Fig. 2 Lithostratigraphic section of the Jhuran Formation in Jara Dome

3 Methods

One hundred oriented block samples of sandstones and shales of the Lower and Middle Members were collected from 35 beds in the Jara Dome (Fig. 2). Coring and cutting of all samples were carried out to prepare a total of 300 specimens of standard size (2.5 cm diameter and 2.2 cm length). Some of the samples broke into pieces during coring and transportation. Natural Remanent Magnetization (NRM) and Susceptibility measurements were done on all the specimens using JR-6 (Brno, Czechoslovakia make) spinner magnetometer and Kappa Bridge (MFK-FA, Czechoslovakia make) respectively. All the paleomagnetic and rock

magnetic measurements were carried out at Paleomagnetism laboratory, CSIR-National Geophysical Research Institute (NGRI), Hyderabad, India. The well-constrained magnetostratigraphy framework was carried out in the laboratory. About 107 specimens were selected systematically to cover all 35 beds. The specimens were subjected to Alternating Field demagnetization (AFD) studies (56 specimens) using Molspin AF demagnetizer (Molspin company, U.K make) to remove the secondary impact of magnetization and to isolate the Characteristic Remanent Magnetization (ChRM) directions. The thermal demagnetization experiment (51 specimens) was necessary to remove the secondary magnetization in these samples.

Statistical analyses were carried out using Fisher's (1953) statistics. Mean declinations (Dm) and mean inclinations (Im) were calculated using principal component analysis (PCA) of Kirschvink (1980) for the samples. Virtual geomagnetic pole (VGP) latitudes were computed for the Jara section using paleomagnetism software.

4 Results and Discussion

The magnetostratigraphic interpretations of the Jhuran Formation is based on the correlation of the reversal events with already well established GPTS in Europe and global GPTS. This correlation establishes the time estimates of the deposition of strata and also the duration of sediment deposition. The obtained magnetostratigraphic results of the Jurassic of Kutch are the new research data for the paleomagnetic records.

The NRM intensities of the samples range between 3.53×10^{-2} and 1.70×10^{-4} A/M, displaying lower remanence values. The intensity decay and orthogonal projections or Zijderveld (1967) diagrams where the vector behavior during AF demagnetization is deciphered (Fig. 3). In most of the samples, a ChRM could be isolated between 25 and 70 mT field intervals, after the elimination of a viscous component. Figure 4 shows the intensity decay and orthogonal projections where the vector behavior during thermal demagnetization is deciphered. In most of the studied samples, a low-temperature magnetization is unblocked below 300–400 °C after the removal of a viscous component at 150 °C. A stable component with a high unblocking temperature component was isolated above 300 and 580 °C, a ChRM can be identified in about 90% of the samples. Significant decay in the NRM intensity below 580 °C indicates the predominant contribution of magnetite, in addition to hematite, in some of the samples. Thermal demagnetization is much more efficient than AF for most of the specimens in this study.

The ChRM directions have been calculated using linear regression analysis. The majority of the samples show a two-component magnetization. The first component gets removed at initial steps of magnetic fields/temperatures and the stable component referred to as the characteristic remanent magnetization component, shows single polarity in northerly declinations with positive/negative inclinations (Fig. 5). The directions of both initial NRM and ChRM of the samples show a good clustering/grouping and thereby indicate that the primary magnetization rests in detrital
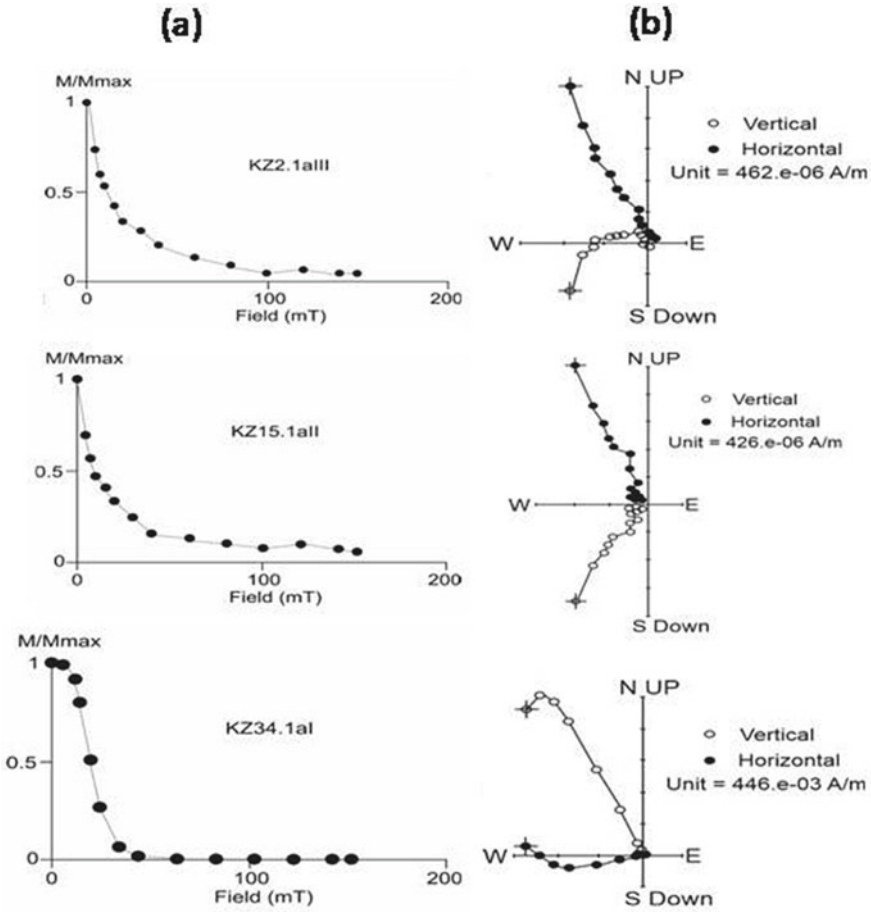
Fig. 3 Intensity decay curves (**a**) and orthogonal projections (**b**) showing vector behavior during AF demagnetization. Solid circles in orthogonal projections show vectors on to the horizontal plain and open circles show vectors on to the vertical plain

remanent magnetization (DRM). The obtained ChRM directions in this study do not show the effect of either present earth field (PEF) or Deccan effusion. All the samples/sites indicate the normal polarity except in one site where the reversed polarity was observed. Magnetostratigraphic column of the section is prepared by plotting Virtual Geomagnetic Pole (VGP) latitudes versus lithocolumn at sampling locations. Correlation of each individual magnetochronology of the section is done with the standard Geological Time Scale of Gradstein et al. (2004) and Ogg et al. (2008).

Isothermal Remanent Magnetization (IRM) studies were carried out on samples to know the remnant magnetic carrier minerals. Isothermal remanent magnetization
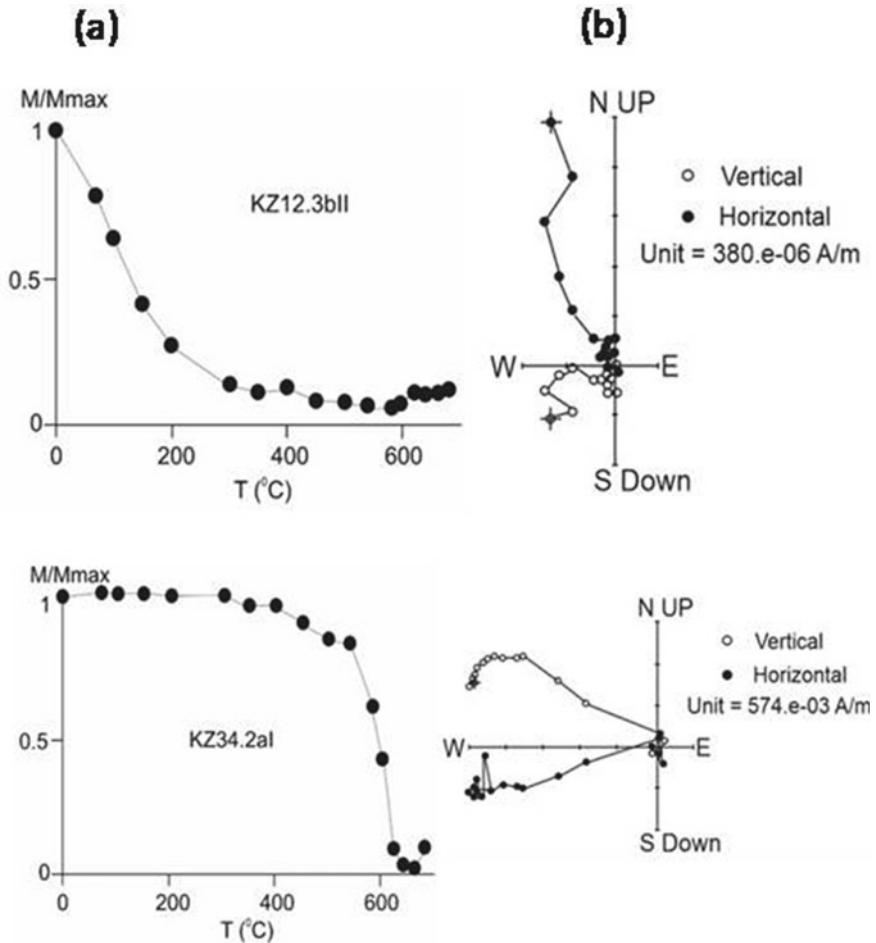
Fig. 4 Intensity decay curves (**a**) and orthogonal projections (**b**) showing vector behavior during thermal demagnetization. Solid circles in orthogonal projections show vectors on to the horizontal plain and open circles show vectors on to the vertical plain

curves reveal the presence of magnetite and hematite; the latter is the remanent carrier (Fig. 6).

Table 2 provides the paleomagnetic results from the Jara section of the Kutch Basin. The results of paleocurrent direction on the Jurassic Jara Dome sand-stones/shales of the Kutch Basin suggests that sand detritus was mostly derived from the Aravalli range situated to the northeast, east and southeast of the Kutch Basin and from the Nagar Parker massif situated to north and northwest (Periasamy and Venkateshwarlu 2015). Petrographical and geochemical studies on sediments of the Jara Dome reveal the deposition on a passive margin basin (Periasamy and
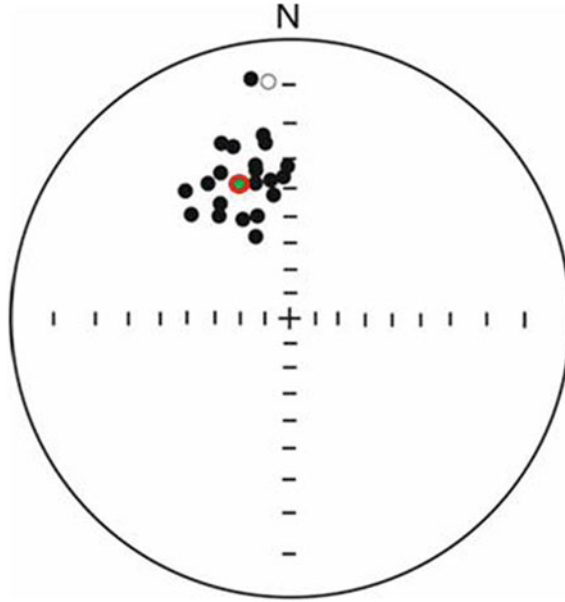
Fig. 5 Mean ChRM directions of samples. The green circle is the overall mean along with the circle of confidence level at 95% probability level in red color
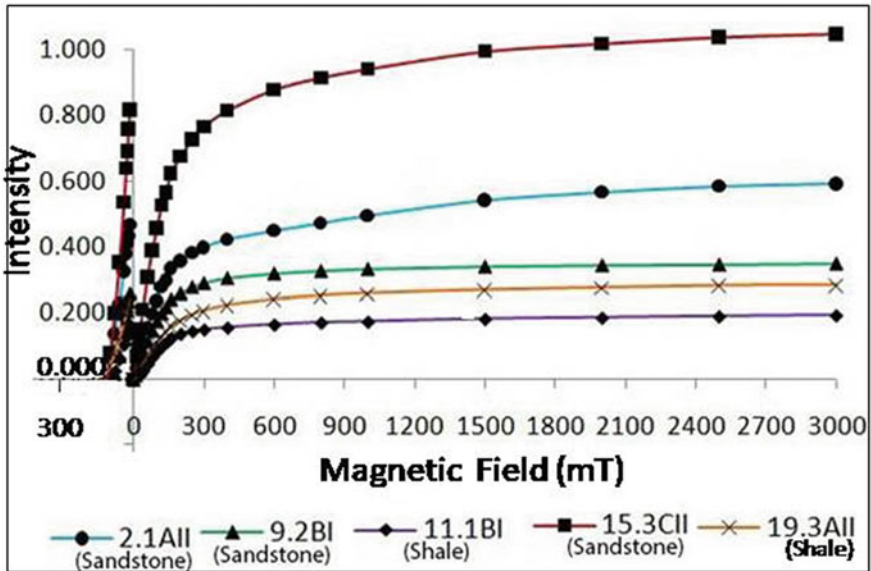
Fig. 6 Normalised IRM acquisition curves of samples of the Jhuran Formation. The sudden increase in remanence indicates the existence of low coercive minerals and unsaturated till 3T, shows the presence of hematite in samples

Table 2 Paleomagnetic results of samples in the Jara section (N/n = Total Specimen/Specimen selected for mean calculation; Dm = mean Declination; Im = mean Inclination; α95 = circle of confidence about 95% probability level; k = precision parameter; VGP Lat. = Virtual Geomagnetic Pole Latitude)

Sample No	N/n	Dm	Im	A95	k	VGP Lat
KZ2	6/4	351	8	31.8	5.38	68.5
KZ3	4/3	342	24	51.4	4.17	69.6
KZ4	6/3	338	55	34.8	13.55	67.6
KZ5	6/6	346	37	20.3	11.79	76.7
KZ6	5/4	353	42	17.4	20.18	83.6
KZ7	3/3	329	14	–	–	–
KZ8	6/6	358	36	14.3	22.69	85.8
KZ9	6/6	328	3	13.4	25.94	51.9
KZ10	5/4	352	23	–	–	–
KZ11	6/5	335	30	25.1	10.26	65.3
KZ12	6/6	339	22	18.1	14.73	66.6
KZ13	4/3	326	42	21.1	34.83	59.0
KZ14	2/2	309	83	–	–	–
KZ15	6/6	347	35	18.6	13.88	77.1
KZ16	2/2	335	47	24.1	109.71	67.1
KZ17	5/5	359	33	18.1	14.69	84.2
KZ18	5/4	355	−9	31.7	9.32	−6.3
KZ19	5/4	352	25	–	–	–
KZ20	4/4	329	39	13.6	46.14	61.4
KZ21	2/2	348	31	–	–	–
KZ22	2/2	352	37	–	–	–
KZ23	1/1	343	48	–	–	–
KZ25	2/2	310	23	–	–	–
KZ26	3/3	321	29	–	–	–
KZ29	3/3	317	36	–	–	–
KZ31	2/1	285	48	–	–	–
KZ34	2/2	273	37	–	–	–
	109/96	343	33	6.4	23.29	

Venkateshwarlu 2017; see also Bansal et al. 2017; Chaudhuri et al. 2018, 2020a, b, c, d).

5 Magnetic Polarity Stratigraphy (MPS)

Magnetic polarity stratigraphy sequence has been established by plotting the Virtual Geomagnetic Pole (VGP) latitudes against the lithocolumn prepared by measuring the thickness of the beds and projecting the lithologies of the sediments on to the column. A recent study on the Jumara Dome indicates that the magnetostratigraphy readily matches with GTS M41 and below, and exhibits the dominance of normal polarity (Venkateshwarlu et al. 2016). A plot of VGP latitudes against the lithocolumn has been prepared (Fig. 7). The figure defines a clear magnetic zonation of the sedimentary sequence at the Jara Dome and describes three magnetozones in this section representing two normal events and a reversed one.
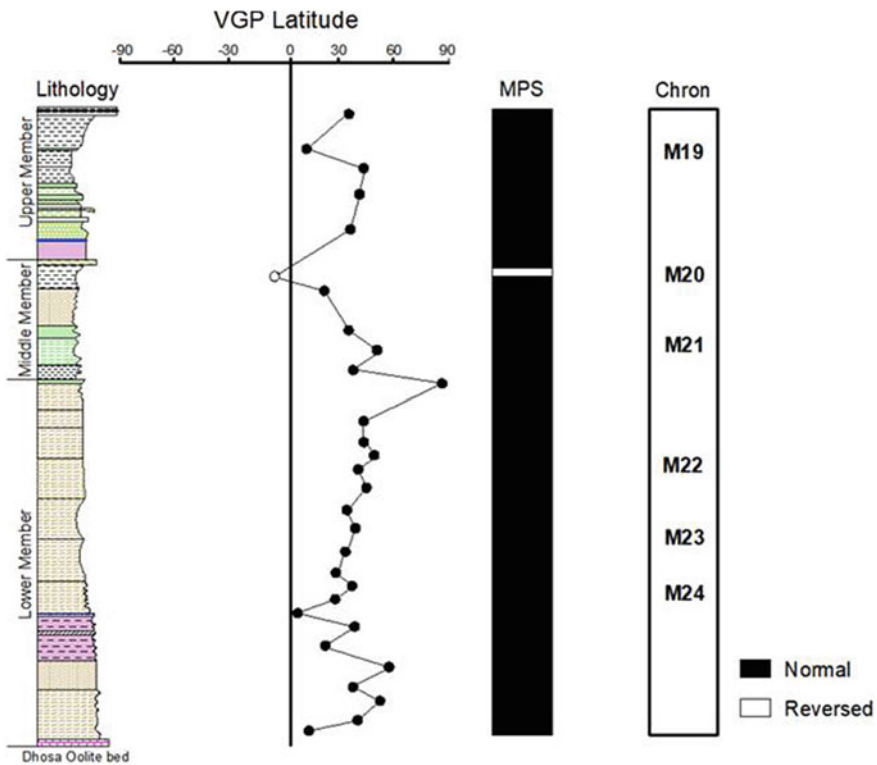
Fig. 7 Lithostratigraphic column (left) and magnetostratigraphic column for the Jhuran Formation of Jara Dome, recording primarily normal polarity, except one reversed polarity at the upper portion of the section. The magnetostratigraphic column is correlated with standard Geological Time Scale of Gradstein et al. (2004) and Ogg et al. (2008) (VGP = Virtual Geomagnetic Pole; MPS = Magnetic Polarity Stratigraphy)

Interestingly, the Jara section has recorded the normal polarity throughout the section except one reversed polarity event in the upper portion. The magnetostratigraphy column is correlated with the standard Geological Time Scale (GTS) of Gradstein et al. (2004) and Ogg et al. (2008). The Bathonian period in the GTS shows 2 to 3 major reversals, whereas the Jara section has recorded only one reversal event. However, with the available biostratigraphic data of this section, the MPS can be placed at the Kimmeridgian to Tithonian in GTS from Chron M24 to M19.

The correlation diagram of Magnetic Polarity Stratigraphy (MPS) of the Jara section in with the Standard Geological Time Scale (GTS) of Gradstein et al. (2004) and Ogg et al. (2008) is prepared (Fig. 8). The entire Kimmeridgian succession of the Jara Dome records a long normal magnetic polarity event, which correlates with the standard GTS. It belongs to the Chron M21, and below this lies the longest normal quite polarity zone in the entire Upper Jurassic period. Above this, the Tithonian succession of the Kutch Basin records one reversed and one normal event corresponding to standard GTS from chron M21 to M19. The magnetic polarity stratigraphy of the Upper Jurassic succession in the Jara Dome correlates well with the standard GTS from Magneto chrons M24 to M19. Therefore, an age span of 10 Ma (155–145 Ma) is assigned to Upper Jurassic Jhuran Formation in the Jara Dome.
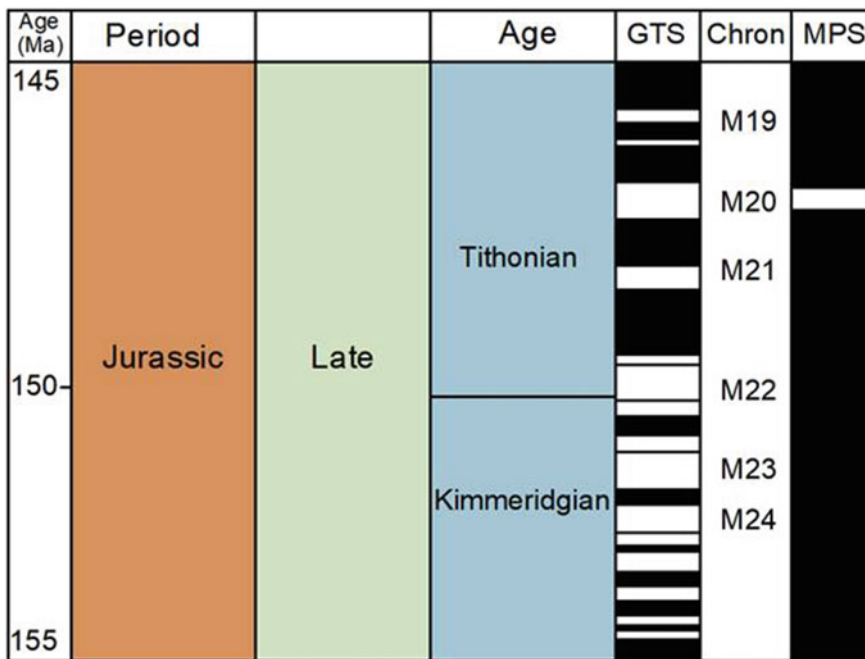
Fig. 8 Correlation of Magnetic Polarity Stratigraphy (MPS) of Jara section of the Kutch Basin with the Standard Geological Time Scale (GTS) of Gradstein et al. (2004) and Ogg et al. (2008)

However, the reversal events in GTS from M21 to M24 are not recorded in the Kutch Basin, which can be attributed to secondary disturbances like bioturbation, diagenesis or later deformation. The early Kimmeridgian/Oxfordian boundary possibly occurs within or slightly above M25. The Kimmeridgian/Tithonian boundary occurs within or slightly above M22.

Figure 9 shows the correlation diagram of the magnetostratigraphy of the Kutch Basin with the Carcabuey section of Spain and Oceanic Magnetic Anomalies. Magnetic Polarity Stratigraphy (MPS) of the Upper Jurassic outcrop sedimentary lithosection of the Jhuran Formation in the Kutch Basin correlates well with the
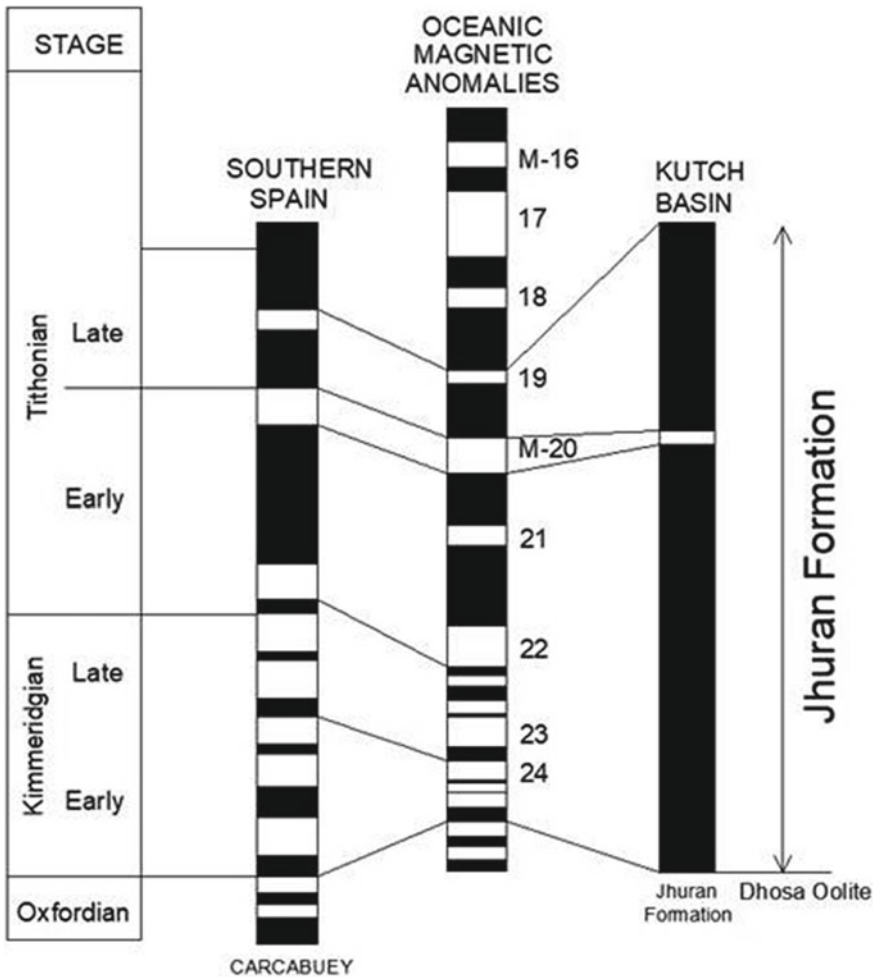
Fig. 9 Correlation of magnetostratigraphy of the Jhuran Formation in Kutch Basin with those of Carcabuey section from Spain (Ogg et al. 1984) and M-sequence of marine magnetic anomalies of Deep Sea Drilling Project (DSDP) leg 32 (Larson and Hilde 1975)

global Upper Jurassic lithosections from Carcabuey, Spain (cf. Ogg et al. 1984) and available oceanic magnetic anomalies of Deep Sea Drilling Project (DSDP) leg 32 (Larson and Hilde 1975). The famous Carcabuey section at Southern Spain represents the late Jurassic period based on paleomagnetic records (Ogg et al. 1984). Present lithosection of the Kutch Basin has retained similar imprints of the magnetic polarity stratigraphy as of Spain and oceanic magnetic anomaly with comprehensive fossil preservation. The magneto chrons are well correlated as the Jhuran Formation retained the similar magnetic signatures of Earth's Magnetic Field. Correlation to the marine magnetic chrons allows placing the precise correlation through Magneto chrons from M24 to M19 of the Jhuran section.

6   Conclusions

This paper presents the first magnetostratigraphic dating of the fossil-bearing sediments of the Jhuran Formation in the Jara Dome of the Kutch Basin. The magnetic mineralogy study reveals that the primary remanent magnetization resides in magnetite and mostly in hematite. The erected magnetic polarity stratigraphy (MPS) column indicates that the Jhuran Formation in the Jara Dome correlates well with the Standard Geological Time Scale. Based on this correlation, the MPS can be placed at Kimmeridgian to Tithonian in GTS from Magneto Chron M24 to M19.

References

Arora A, Banerjee S, Datta S (2016) Black shale in Late Jurassic Jhuran Formation of Kutch: possible indicator of Oceanic Anoxic Event. J Geol Soc India 85:265–278

Arora A, Dutta S, Gogoi B, Banerjee S (2017) The effects of igneous dike intrusion on organic geochemistry of black shale and its implications: Late Jurassic Jhuran Formation, India. Int J Coal Geol 178:84–99

Bansal U, Banerjee S, Pande K, Arora A, Meena SS (2017) The distinctive compositional evolution of glauconite in the Cretaceous Ukra Hill Member (Kutch basin, India) and its implications. Mar Petrol Geol 82:97–117

Biswas SK (1977) Mesozoic stratigraphy of Kutch, Gujarat. Quart J Geol Min Met Soc India 49:1–52

Biswas SK (1991) Stratigraphy and sedimentary evolution of the Mesozoic basin of Kutch, western India. In: Tandon SK, Pant CC, Casshyap SM (eds) Stratigraphy and sedimentary evolution of Western India. Gyanodaya Prakashan, Nainital, pp 74–103

Biswas SK (1993) Geology of Kutch—a compilation of field reports (1957–1972). KDM Institute of Petroleum Exploration, Dehradun

Chaudhuri A, Banerjee S, Le Pera E (2018) Petrography of Middle Jurassic to Early Cretaceous sandstones of the Kutch Rift Basin: implications on provenance and basin evolution. J Palaeogeography 7:2. https://doi.org/10.1186/s42501-018-0002-6

Chaudhuri A, Banerjee S, Chauhan G (2020a) Compositional evolution of siliciclastic sediments recording the tectonic stability of a pericratonic rift: Mesozoic Kutch Basin, western India. Mar Pet Geol 111:476–495

Chaudhuri A, Das K, Banerjee S, Fitzsimons ICW (2020b) Detrital zircon and monazite track the source of Mesozoic sediments in Kutch to rocks of Late Neoproterozoic and Early Palaeozoic orogenies in northern India. Gond Res 80:188–201

Chaudhuri A, Chatterjee A, Banerjee S, Ray JS (2020c) Tracing multiple sources of sediments using trace element and Nd isotope geochemistry: provenance of the Mesozoic succession in the Kutch Basin, western India. Geol Mag. https://doi.org/10.1017/S0016756820000539

Chaudhuri A, Banerjee S, Prabhakar N, Das A (2020d) The use of heavy mineral chemistry in reconstructing provenance: a case study from Mesozoic sandstones of Kutch Basin (India). Geol Jour. https://doi.org/10.1002/gj.3922

Fisher R (1953) Dispersion on a sphere. Proc Royal Soc A 217:295–305

Gradstein FM, Ogg JG, Smith AG, Bleeker W, Lourens LJ (2004) A geologic time scale. Geol Surv Canada, Miscellaneous Report 86

Hess HH (1962) History of ocean basins. In: Engel AEJ, James HL, Leonard BF (eds) Petrologic studies: a volume in honor of A.F. Buddington. Geol Soc America, Boulder CO, pp 599–620

Kirschvink JL (1980) The least squares line and plane analysis of palaeomagnetic data. Geophys J Int 62:699–718

Larson RL, Hilde TWC (1975) A revised time scale of magnetic reversals for the Early Cretaceous, Late Jurassic. J Geophys Res 80:2586–2594

Lowrie W (2011) Paleomagnetism, principles; In: Gupta HK (ed) Encyclopedia of solid earth geophysics. Springer, pp 962–963

Ogg JG, Steiner MB, Oloriz F, Tavera JM (1984) Jurassic magnetostratigraphy, 1. Kimmeridgian-Tithonian of Sierra Gora and Carcabuey, southern Spain. Earth Planet Sci Lett 71:147–162

Ogg JG, Ogg G, Gradstein FM (2008) The concise geologic time scale. Cambridge University Cambridge, New York

Paul DK, Ray A, Das B, Patil SK, Biswas SK (2008) Petrology, geochemistry and paleomagnetism of the earliest magmatic rocks of Deccan Volcanic Province, Kutch, Northwest India. Lithos 102:237–259

Periasamy V, Venkateshwarlu M (2015) Magnetic fabric studies of sandstone from Jhuran Formation (Kimmeridgian–Tithonian) of Jara dome, Kutch Basin, northwest India. Curr Sci 108:265–272

Periasamy V, Venkateshwarlu M (2017) Petrography and geochemistry of Jurassic sandstones from the Jhuran Formation of Jara dome, Kutch basin, India: Implications for provenance and tectonic setting. J Earth Sys Sci 126:44. https://doi.org/10.1007/s12040-017-0822-2

Venkateshwarlu M, Ojha JR, Pandey B, Krishna J (2008) Preliminary remanent magnetism results from the Jurassic sediments of Kutch, India. Curr Sci 95:725–727

Venkateshwarlu M, Pandey B, Papanna G, Pathak DB, Krishna J (2014) New palaeomagnetic evidences about Deccan Trap Volcanic activity from the magmatic bodies of Kutch Basin, Northwest India. J Ind Geophys Union 18:99–107

Venkateshwarlu M, Pandey B, Pathak DB, Papanna G, Krishna J (2016) Magnetostratigraphy of the Middle Jurassic Sediments from Kutch Basin, Western India. Int J Geos 7:301–310

Zijderveld JDA (1967) AC Demagnetization of Rocks: Analysis of Results. In: Runcorn SK, Creer KM, Collinson DW (eds) Methods in paleomagnetism. Elsevier, Amsterdam, pp 254–286

Provenance and Paleo-weathering of the Mesozoic Rocks of Kutch Basin: Integrating Results from Heavy Minerals and Geochemical Proxies

Angana Chaudhuri, Emilia Le Pera, Gaurav Chauhan, and Santanu Banerjee

Abstract   This study investigates the composition, tectonic setting and age of source rocks of the Mesozoic Kutch Basin, along with the extent of weathering based on heavy mineral characteristics and geochemical investigations. The Mesozoic succession, divided into Jhurio, Jhumara, Jhuran and Bhuj formations, preserves sediments deposited in the Kutch Basin from the Late Triassic to Early Cretaceous. Subangular and subrounded heavy minerals indicate mixing of first cycle and recycled input in these samples. Major oxide ratios such as SiO_2/Al_2O_3, Al_2O_3/TiO_2, K_2O/Na_2O and trace elements like Zr, Th, Sc, Th/Co, Th/Sc and La/Sc indicate dominantly felsic source. LREE enrichments and negative Eu anomalies support the predominance of felsic source rocks. The V and Ni concentrations in these sediments indicate the input from mafic sources in the older Jhurio and Jhumara formations. Weathering indices such as CIA, PIA and CIW suggest the relatively greater extent of chemical alteration for Jhumara, Jhuran and Bhuj formations in comparison to Jhurio Formation. The higher content of Hf in Jhuran and Bhuj formations suggests the input from older source rocks in younger formations, indicating erosional unroofing at the source. The concentration of Cr and Ni and ratios of Eu/Eu* and (Gd_N/Yb_N) indicate predominantly post-Archean source with inputs from older Archean rocks in younger Jhuran and Bhuj formations, and corroborate the erosional unroofing. These evidences relate possible sources of Mesozoic sediments in the Kutch Basin to Precambrian rocks of the Aravalli craton and Nagar Parkar igneous complex.

A. Chaudhuri (✉) · S. Banerjee
Department of Earth Sciences, Indian Institute of Technology Bombay, Powai, Mumbai 400076, India

S. Banerjee
e-mail: santanu@iitb.ac.in

E. Le Pera
Dipartimento di Biologia, Ecologia e Scienze della Terra, Università della Calabria, 87036 Rende, Cosenza, Italy
e-mail: emilia.lepera@unical.it

G. Chauhan
Department of Earth and Environmental Science, KSKV Kachchh University, Bhuj 370001, Gujarat, India

1 Introduction

Sedimentary rocks preserve information of their source rock, tectonic setting, paleodrainage and paleoclimatic conditions. Detailed thin section petrography of rock samples is a preliminary and routine step, especially for understanding provenance of siliciclastic sedimentary rocks (Crook 1974; Dickinson and Suczek 1979; Dickinson 1985; Zuffa 1987;Critelli and Ingersoll 1994; Le Pera et al. 2001; Critelli et al. 2003; Chaudhuri et al. 2018, 2020a). Further, the sedimentary rocks bear geochemical signatures of the source rocks (Quinby-Hunt and Wilde 1991; Ochoa et al. 2007). Major, trace, rare earth element concentrations and their ratios serve as proxies for composition, tectonic setting and age of source as well as the climate prevailing during deposition (Paikaray et al. 2008; Saha et al. 2010, 2018; Mondal et al. 2012; Armstrong-Altrin et al. 2017; Chaudhuri et al. 2020a, b). The concentration of major oxides and their ratios such as SiO_2/Al_2O_3, Al_2O_3/TiO_2, K_2O/Na_2O are useful indicators of source rock characteristics (McLennan et al. 1979; Maynard et al. 1982; Roser and Korsch 1986; Hayashi et al. 1997). Trace element ratios, such as, La/Th, La/Sc, Th/Sc, Th/Co, Ti/Zr, Sc/Cr, La/Y are also useful for provenance interpretations (Bhatia and Crook 1986; Floyd and Leveridge 1987; McLennan et al. 1993; Cullers 2002). Indices such as CIA, PIA, CIW and ICV suggest the extent of weathering of source rock and prevailing climate at source area (Nesbitt and Young 1982; Harnois 1988; Fedo et al. 1995; Cox et al. 1995).

The Kutch Basin at the western continental margin of India preserves ~3000 m of Mesozoic sediments deposited during the breakup of Gondwana and the subsequent drift of the Indian subcontinent (Biswas 1982, 1987, 2005). Several studies provided insights on provenance for the Mesozoic succession of the Kutch Basin, although based on a limited dataset (Ahmad and Bhat 2006; Ahmad et al. 2014; Periasamy and Venkateshwarlu 2017). Recently Chaudhuri et al. (2018, 2020a, b, c, d) presented sandstone petrography, single-grain heavy mineral analysis, geochemistry of trace elements, Nd isotopes in shale and geochronology of detrital zircon and monazite. However, data collected from different rock types using different methods need to be integrated. The present study aims to understand the composition, tectonic setting and age of source rocks of the Mesozoic sediments in the Kutch Basin and assess the extent of weathering at the source. This paper integrates petrographical, geochemical and geochronological data to accomplish this objective. Already published petrographic data have been considered for interpretation.

2 Geological Setting

The Mesozoic Kutch Basin formed due to the rifting of the Gondwana supercontinent (Biswas 1982, 1987, 2005). Nagar Parkar Ridge to the north, Kathiawar Uplift to the south, Radhanpur-Barmer Arch to the east and the continental shelf to the west demarcates the Kutch Basin. The vast thickness of Mesozoic sedimentary rocks of this basin crops out in several uplifts, viz., Nagar Parkar Uplift (NPU), Island Belt Uplift (IBU), South Wagad Uplift (SWU) and Kutch Mainland Uplift (KMU). The KMU is the largest uplift preserving Late Triassic to Early Cretaceous mixed siliciclastic sediments (Alberti et al. 2013).

The Mesozoic succession in the KMU comprises Jhurio, Jhumara, Jhuran and Bhuj formations in ascending order of succession (Biswas 1987) (Fig. 1). The Bathonian to early Callovian carbonates and finer siliciclastics, classified as the Jhurio Formation overlies unconformably on the Precambrian basement rocks. The younger Oxfordian sediments of the Jhumara Formation comprise argillaceous rocks at the bottom and carbonates at the top (Biswas 2005). The Kimmeridgian to Tithonian sediments of the Jhuran Formation overlies unconformably on the Jhumara Formation. The alternation between sandstone and shale makes up the overall prograding Jhuran Formation (Arora et al. 2015). The Neocomian to Albian siliciclastics of the Bhuj Formation unconformably overlie the Jhuran Formation. Although the older carbonate and finer clast-dominated formations do not show much paleocurrent
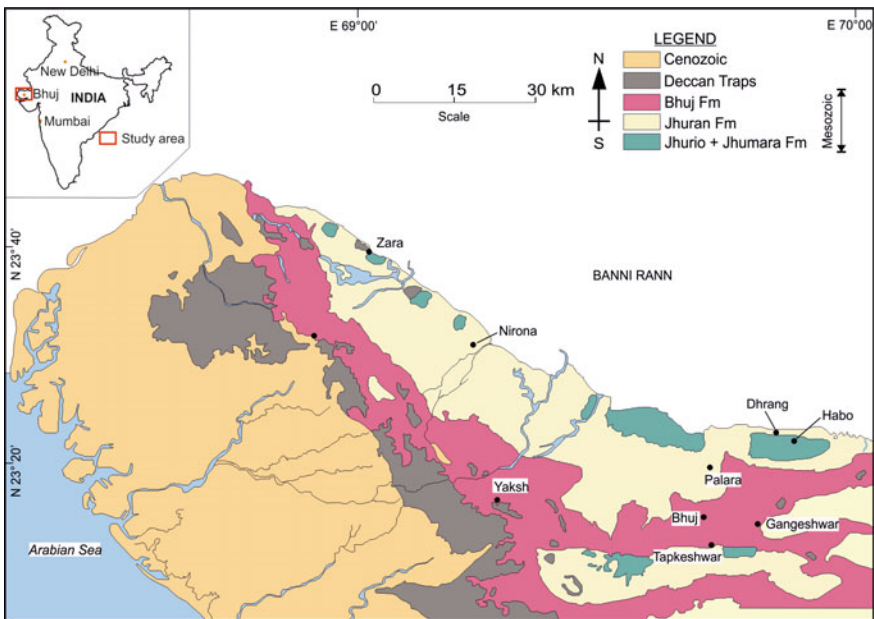
Fig. 1 Geological map of Kutch Mainland showing extent of Mesozoic and Cenozoic sedimentary rocks (adapted from Biswas 1977, 1981)

structures, the younger, siliciclastics-dominated Jhuran and Bhuj formations provide a south-westerly paleoslope (Biswas 1991, 1993, 2005; Arora et al. 2015; Mandal et al. 2016; Bansal et al. 2017; Desai and Biswas 2018).

3 Methods

Sandstone and shale samples of Jhurio, Jhumara, Jhuran and Bhuj formations were collected from outcrops at Zara, Nirona, Yaksh, Dhrang, Habo, Palara, Gangeshwar, Tapkeshwar and Bhuj. These samples were crushed and dry sieved to separate the 63–125 µm size fraction. 10 gm of each of the sieved samples was poured into a beaker. The beaker was filled with water and the sample was allowed to settle. The lighter clay minerals and water from the upper part of the beaker were decanted into a large bowl. The beaker was again filled with water and the contents were agitated by swirling. The upper part of the beaker was once again emptied in the large bowl. This process was repeated several times to concentrate the heavy minerals. The contents were then transferred to a watch glass, swirled slowly to concentrate the heavy minerals in the deepest part of the beaker. The light minerals and the extra water was siphoned off using a dropper. The dried heavy minerals were observed using Leica DM 4500P polarizing microscope attached with Leica DFC420 camera and Leica Image Analysis software (LAS-v4.6) at the Department of Earth Sciences, Indian Institute of Technology Bombay. Heavy minerals were identified using optical properties described by Mange and Maurer (2012). Sandstone samples were excluded for geochemical analysis because of both extensive cementation, that commonly results in removal of unstable framework components (e.g. Worden and Burley 2003), and the growth of authigenic phases changing the original detrital phases (e.g. Scholle and Schluger 1979; McDonald and Surdam 1984).

Shale samples were exclusively chosen for the geochemical analyses. For major oxide analyses, 0.25 g of each sample powder (<63 µm) was added to 0.75 g lithium metaborate (LiBO$_2$) and 0.50 g of lithium tetraborate (LiB$_4$O$_7$) in a platinum crucible. This mixture was fused in a muffle furnace at 1050 °C for 10 min. The temperature of the furnace was then lowered to 800 °C. The crucible was removed from the furnace, immersed in 75 ml of 1N HCl in a glass beaker and magnetically stirred for 1 h until complete dissolution of the fusion bead. This solution was transferred into a 100 ml volumetric flask. 1N HCl was added to the flask to make the volume 100 ml. 5 ml of this solution was diluted to 50 ml with distilled water for analysis using Inductively Coupled Plasma Atomic Emission Spectrometry (ICP-AES) (ARCOS, Simultaneous ICP Spectrometer by SPECTRO® Analytical Instruments GmbH, Germany) facility at the Sophisticated Analytical Instrument Facility (SAIF), Indian Institute of Technology Bombay. USGS standards, MAG-1, SBC-1, SCo-1 and SCo-2 were used for the analysis. Loss on ignition (LOI) was measured and calculated using the weight loss of 1 g of sample on heating to 950 °C.

For determining trace element (TEs) concentrations, including those of rare-earth elements (REEs), 0.05 g of each sample powder (<63 µm) was poured into individual

Savillex Teflon pressure decomposition vessels (25 ml). Ten ml of an acid mixture with $HF/HNO_3 = 7:3$ was added to each vessel. The content of the vessel was mixed thoroughly by swirling and heated at ~160 °C for 48 h. A few drops of $HClO_4$ was added to the content and evaporated at 200 °C to near dryness. Ten ml of an acid mixture with HNO_3/Milli $Q^®$ de-ionized water $= 1:1$ was added to the vessel and mixed thoroughly. The vessel was tightly closed and heated at 80 °C for 30 min. The sample solution was poured into a 250 ml volumetric flask. Five ml of 1 ng/ml [103]Rh solution was added to this flask as an internal standard. Further, Milli $Q^®$ de-ionized water was added to make the volume of content in the flask to 250 ml. Five ml of sample solution from each of the 250 ml flasks was diluted to 50 ml using Milli $Q^®$ de-ionized water for analysis by high resolution inductively coupled mass spectrometer (HR-ICP-MS) (Attom ES by Nu Instruments$^®$, UK) along with the instrument software (Attolab v.1), at CSIR-National Geophysical Research Institute (NGRI), Hyderabad. USGS standard reference materials, MAG-1, SBC-1, SCo-1 and SCo-2 were used for analysis. Chinese standard reference material, GSR-5 was used to check the accuracy of the analysis. The data processing was done using Nu Quant$^®$.

4 Results

4.1 Heavy Minerals

Sandstones of the Jhurio, Jhumara, Jhuran and Bhuj formations contain heavy minerals with both subangular and subrounded grains (Fig. 2). The most common transparent heavy minerals in these sandstones, in order of decreasing abundance, are ultrastable phases such as zircon, tourmaline, rutile (e.g. Hubert 1962), stable phases such as garnet, monazite and apatite, and less common moderately stable species such as epidote. Zircon grains are dominantly colourless or pale pink, with a few brown varieties (Fig. 2a). Tourmaline grains exhibit greenish-brown to greyish-blue colours (Fig. 2b). Rutile occurs in reddish-brown to amber-brown colours (Fig. 2c). Epidote occurs in yellow, while apatite exhibits colourless to light-grey (Fig. 2d, e). Monazite grains exhibit pale yellowish-brown colours (Fig. 2f). This diverse heavy mineral assemblage does not exhibit any significant corrosion, implying insignificant dissolution during the burial diagenesis.
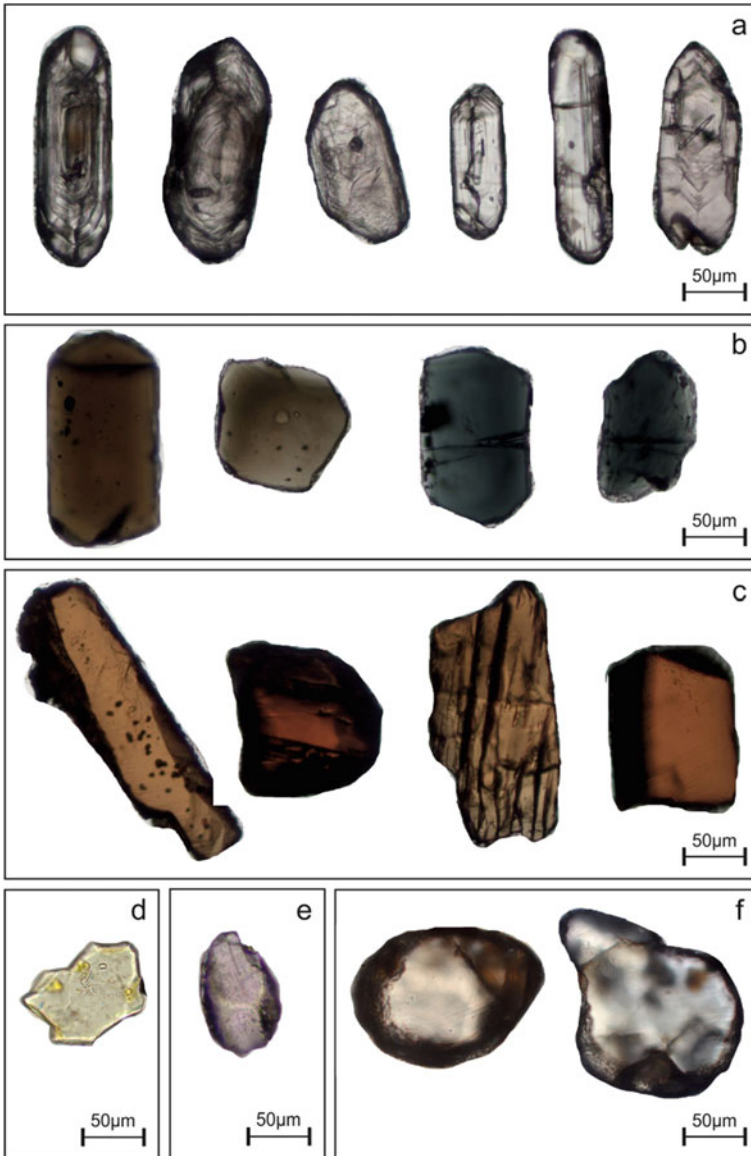
Fig. 2 Photomicrographs of transparent heavy minerals separated from sandstones (ppl)—zircon (**a**), tourmaline (**b**), rutile (**c**), epidote (**d**), apatite (**e**) and monazite (**f**)

4.2 Geochemistry

4.2.1 Major Oxides

The samples of the Jhuran Formation exhibit the lowest concentration of SiO_2 (av. 56.45%), while the samples of the Bhuj Formation show the highest concentration (av. 65.21%) (Tables 1, 2, 3 and 4). Most of the Bhuj Formation samples exhibit higher SiO_2 concentrations than the PAAS (62.80%; cf. Taylor and McLennan 1985). Al_2O_3 is the second most abundant oxide in the analysed samples. Samples of Jhumara (av. 18.98%) and Jhuran (av. 21.04%) formations exhibit average Al_2O_3 concentrations higher than the PAAS (18.90%). Samples of Jhurio (av. 11.72%) and Bhuj (av. 16.37%) formations exhibit lower concentrations than the PAAS. Samples of the Jhurio Formation exhibit the highest Fe_2O_3 content (av. 7.10%). The samples of Jhurio (av. 7.57%) and Jhumara (av. 2.23%) formations exhibit CaO concentration higher than that of the PAAS (1.30%). The samples of Jhurio, Jhumara, Jhuran and Bhuj formations exhibit average Na_2O concentrations of 0.52%, 0.39%, 0.43% and 0.34%, respectively. All the analysed samples show K_2O concentration lower than that of the PAAS (3.70%). The samples of Jhurio, Jhumara, Jhuran and Bhuj formations show average TiO_2 concentration of 0.72%, 1.23%, 1.17% and 1.09%, respectively.

Table 1 Major oxide concentration in shale samples of the Jhurio Formation

Major oxides	KU1	KU2	KU3	KU4	KU5	Avg.
SiO_2	56.47	67.59	66.04	54.26	51.07	59.09
TiO_2	0.46	0.72	0.58	0.81	1.04	0.72
Al_2O_3	7.69	10.74	9.11	14.85	16.23	11.72
Fe_2O_3	7.69	6.28	7.44	7.57	6.54	7.10
MnO	0.02	0.03	0.02	0.04	0.04	0.03
MgO	1.13	1.13	1.07	2.51	1.68	1.50
CaO	11.74	5.57	4.80	8.89	6.83	7.57
Na_2O	0.54	0.58	0.61	0.43	0.45	0.52
K_2O	2.44	2.89	2.77	2.66	2.00	2.55
P_2O_5	0.03	0.03	0.03	0.13	0.07	0.06
LOI	12.85	5.17	8.16	6.33	14.94	9.49
Total	101.05	100.74	100.61	98.48	100.89	100.35
K_2O/Na_2O	4.56	4.97	4.56	6.18	4.45	4.94
SiO_2/Al_2O_3	7.35	6.29	7.25	3.65	3.15	5.54
CIA	63.61	68.03	64.52	77.57	81.65	71.08
PIA	74.15	79.90	75.28	89.43	90.47	81.85
CIW	81.37	84.87	81.96	91.30	91.64	86.23
ICV	1.66	1.20	1.45	1.11	0.83	1.25

Table 2 Major oxide concentration in shale samples of the Jhumara Formation

Major oxides	KM1	KM2	KM3	KM4	KM5	KM6	KM7	KM8	KM9
SiO_2	54.93	55.71	59.12	57.11	56.42	61.48	53.88	57.98	59.03
TiO_2	1.20	1.20	1.21	1.34	1.49	1.05	1.26	1.15	0.88
Al_2O_3	23.52	20.72	19.64	21.02	23.48	12.13	19.83	16.54	10.04
Fe_2O_3	3.59	4.91	4.97	4.63	2.82	5.71	6.16	5.30	3.19
MnO	0.03	0.05	0.05	0.03	0.01	0.05	0.03	0.01	0.06
MgO	0.94	1.19	1.17	1.86	0.98	0.74	1.35	0.79	0.59
CaO	0.23	0.41	0.38	1.44	0.36	5.98	1.31	3.11	9.62
Na_2O	0.19	0.27	0.29	0.25	0.09	0.16	0.51	0.24	0.09
K_2O	2.18	2.20	2.38	2.65	2.27	2.51	2.63	3.49	2.49
P_2O_5	0.07	0.18	0.13	0.05	0.09	0.03	0.04	0.04	0.03
LOI	13.20	14.27	12.20	11.29	12.53	10.49	12.42	11.27	12.91
Total	100.08	101.10	101.54	101.65	100.55	100.33	99.43	99.93	98.93
K_2O/Na_2O	11.36	8.30	8.21	10.67	24.32	15.89	5.12	14.52	26.82
SiO_2/Al_2O_3	2.34	2.69	3.01	2.72	2.40	5.07	2.72	3.51	5.88
CIA	88.71	86.44	84.77	85.10	89.46	78.93	81.39	78.38	76.99
PIA	97.10	95.46	94.71	95.70	98.56	94.77	90.96	94.18	96.01
CIW	97.39	95.96	95.37	96.26	98.71	95.89	92.15	95.44	97.05
ICV	0.39	0.53	0.57	0.62	0.38	0.84	0.68	0.69	0.77

Major oxides	KM10	KM11	KM12	KM13	KM14	KM15	KM16	KM17	Avg.
SiO_2	56.18	58.18	56.63	57.28	56.48	58.50	56.87	56.02	57.16
TiO_2	1.22	1.27	1.36	1.34	1.32	1.38	1.31	0.97	1.23
Al_2O_3	21.90	17.23	20.88	20.61	18.73	21.81	19.93	14.62	18.98
Fe_2O_3	4.97	4.59	6.42	5.20	5.06	3.13	6.32	2.95	4.70
MnO	0.05	0.03	0.02	0.02	0.02	0.01	0.03	0.01	0.03
MgO	1.20	1.84	1.50	1.42	1.42	1.37	1.69	0.98	1.24
CaO	0.39	1.73	0.61	0.70	2.25	0.43	0.73	8.31	2.23
Na_2O	0.50	0.92	0.45	0.51	0.46	0.67	0.42	0.60	0.39
K_2O	2.19	2.42	2.61	2.52	2.42	2.69	2.74	2.08	2.50
P_2O_5	0.15	0.04	0.05	0.07	0.04	0.07	0.05	0.04	0.07
LOI	12.70	11.58	10.85	10.90	10.70	11.42	11.41	13.58	11.98
Total	101.46	99.82	101.38	100.57	98.91	101.46	101.48	100.15	100.51
K_2O/Na_2O	4.36	2.62	5.85	4.93	5.28	4.05	6.55	3.49	9.55
SiO_2/Al_2O_3	2.57	3.38	2.71	2.78	3.02	2.68	2.85	3.83	3.18
CIA	84.84	75.30	82.94	82.41	81.92	81.97	82.09	77.61	82.31
PIA	92.68	82.80	92.48	91.43	91.43	90.94	92.48	86.29	92.82
CIW	93.42	85.02	93.43	92.47	92.54	92.05	93.53	88.16	93.81

Table 2 (continued)

Major oxides	KM10	KM11	KM12	KM13	KM14	KM15	KM16	KM17	Avg.
ICV	0.54	0.86	0.67	0.63	0.68	0.55	0.72	0.67	0.64

4.2.2 Trace Elements

The average Sc concentration (16.6 ppm) of samples of the Jhumara Formation is comparable to the PAAS (16.0 ppm; cf. Taylor and McLennan 1985) (Tables 5, 6, 7 and 8). The average Sc content of the samples of Jhurio, Jhuran and Bhuj formations are 12.8 ppm, 13.5 ppm and 13.9 ppm, respectively. The average Zr content (177.7 ppm) of samples of Jhurio Formation is lower than the PAAS (210.0 ppm). While samples of Jhurio (av. 151.6 ppm) and Jhumara (av. 155.2 ppm) formations show V contents similar to the PAAS (150.0 ppm), the same in Jhuran (av. 125.5 ppm) and Bhuj (av. 99.6 ppm) formations exhibits lower contents than the PAAS. The average Ni content of samples of Jhurio, Jhumara, Jhuran and Bhuj formations is lower than the PAAS (55 ppm). Samples of the Bhuj Formation show higher contents of Th and Co compared to other formations. However, the Co content in the analysed samples is lesser than the PAAS (23 ppm).

4.2.3 Rare Earth Element

The average contents of the total rare earth element ($\sum$REE) of Jhurio, Jhumara, Jhuran and Bhuj formations are 121 ppm, 195 ppm, 255 ppm and 256 ppm, respectively (Tables 5, 6, 7 and 8). The chondrite-normalised REE data (cf. Boynton 1983) exhibit patterns similar to those of NASC (North American Shale Composite) and PAAS (Post Archean average Australian Shale) (cf. Haskin et al. 1968; Nance and Taylor 1976; Sun and McDonough 1989).

5 Discussion

5.1 Composition of Source Rocks

Subangular grains of heavy minerals like garnet and rutile indicate nearby source rocks and/or first-cycle input while rounded to subrounded grains of ultra-stable heavy minerals like zircon and tourmaline suggest longer transportation of grains and/or recycling processes from preexisting clastic rocks (Fig. 2). The occurrence of abraded quartz overgrowths on detrital cores of quartz in these sandstones suggests the polycyclic nature (Chaudhuri et al. 2020a, b). The presence of heavy minerals with insignificant corrosion features (e.g. Andò et al. 2012) indicates the shallow

Table 3 Major oxide concentration in shale samples of the Jhuran Formation

Major oxides	KN1	KN2	KN3	KN4	KN5	KN6	KN7	KN8	KN9	KN10
SiO_2	57.55	57.11	56.60	50.15	55.43	55.61	54.55	52.14	54.79	52.30
TiO_2	1.14	1.14	1.11	1.05	1.07	1.03	0.99	1.13	1.02	1.01
Al_2O_3	20.64	20.06	18.90	20.16	20.28	19.80	19.78	21.78	19.28	18.85
Fe_2O_3	4.93	6.35	6.70	6.91	5.83	5.26	7.17	6.19	7.23	10.54
MnO	0.04	0.06	0.07	0.10	0.04	0.04	0.05	0.05	0.07	0.07
MgO	1.18	1.23	1.27	1.79	1.41	1.26	1.38	1.47	1.69	1.38
CaO	0.63	0.72	0.67	1.18	0.70	0.69	0.97	0.97	0.97	0.50
Na_2O	0.48	0.45	0.47	0.45	0.56	0.50	0.51	0.48	0.43	0.36
K_2O	2.54	2.59	2.32	2.24	2.41	2.39	2.20	2.16	2.37	2.16
P_2O_5	0.14	0.13	0.10	0.16	0.15	0.18	0.13	0.12	0.14	0.10
LOI	12.00	12.79	12.89	14.38	13.98	13.39	13.89	15.51	13.01	12.40
TOTAL	101.27	102.63	101.11	98.57	101.86	100.16	101.61	101.99	101.00	99.68
K_2O/Na_2O	5.31	5.78	4.94	4.99	4.33	4.77	4.35	4.54	5.56	5.96
SiO_2/Al_2O_3	2.79	2.85	2.99	2.49	2.73	2.81	2.76	2.39	2.84	2.77
CIA	82.67	82.40	82.33	83.78	82.02	82.38	83.04	84.79	82.92	84.25
PIA	91.90	92.11	91.38	92.31	90.60	91.26	91.29	92.55	92.26	93.28
CIW	92.91	93.14	92.44	93.17	91.71	92.32	92.25	93.29	93.22	94.06
ICV	0.58	0.65	0.69	0.71	0.65	0.61	0.68	0.60	0.74	0.80
Major oxides	KN11	KN12	KN13	KN14	KN15	KN16	KN17	KN18	KN19	KN20
SiO_2	62.81	56.96	56.18	52.22	48.40	50.13	52.58	57.84	61.41	56.02
TiO_2	0.91	1.07	1.07	1.06	0.96	0.98	0.97	1.04	1.06	1.06
Al_2O_3	18.62	20.18	20.76	20.17	18.79	19.74	17.36	19.45	18.21	19.25
Fe_2O_3	3.43	5.90	5.31	5.17	7.34	5.66	7.00	5.18	4.88	5.24
MnO	0.03	0.04	0.04	0.04	0.07	0.04	0.06	0.04	0.05	0.05
MgO	0.88	1.26	1.38	1.53	1.96	1.30	1.32	1.37	1.41	1.40
CaO	0.48	0.57	0.61	0.52	1.63	0.57	0.92	0.87	0.91	0.83
Na_2O	0.52	0.46	0.63	0.81	0.48	0.41	0.55	0.48	0.73	0.62
K_2O	2.55	2.55	2.55	2.41	2.21	2.27	2.30	2.62	2.82	2.65
P_2O_5	0.07	0.11	0.12	0.11	0.71	0.13	0.11	0.11	0.12	0.14
LOI	8.92	12.84	13.27	15.03	17.39	16.74	16.97	13.16	8.96	11.27
Total	99.23	101.94	101.93	99.05	99.94	97.97	100.13	102.15	100.56	98.53
K_2O/Na_2O	4.87	5.52	4.05	2.98	4.63	5.59	4.14	5.47	3.89	4.25
SiO_2/Al_2O_3	3.37	2.82	2.71	2.59	2.58	2.54	3.03	2.97	3.37	2.91
CIA	80.62	82.52	81.12	80.55	82.61	83.87	80.10	81.54	77.02	79.63
PIA	90.21	91.99	89.68	88.58	91.28	92.82	89.07	91.35	86.41	88.86
CIW	91.54	93.01	90.93	89.90	92.30	93.66	90.48	92.52	88.42	90.36

(continued)

Table 3 (continued)

Major oxides	KN11	KN12	KN13	KN14	KN15	KN16	KN17	KN18	KN19	KN20
ICV	0.54	0.63	0.63	0.67	0.79	0.61	0.77	0.65	0.74	0.69

Major oxides	KN21	KN22	KN23	KN24	KN25	KN26	KN27	KN28	KN29	KN30
SiO_2	53.13	54.05	53.61	53.20	59.19	54.79	55.07	55.08	52.97	54.06
TiO_2	1.07	1.09	1.16	1.02	1.01	1.26	1.28	1.27	1.31	1.31
Al_2O_3	19.29	20.25	20.97	17.44	18.98	25.20	25.15	24.89	26.28	25.80
Fe_2O_3	7.09	5.68	5.21	7.78	5.18	2.63	2.54	2.80	2.26	3.01
MnO	0.07	0.06	0.04	0.05	0.05	0.02	0.02	0.02	0.01	0.02
MgO	1.44	1.35	1.39	1.35	1.38	0.79	0.93	0.92	0.89	0.84
CaO	0.48	0.68	0.42	0.85	1.04	0.50	0.65	0.55	0.46	0.35
Na_2O	0.53	0.62	0.59	0.59	0.51	0.18	0.30	0.31	0.29	0.30
K_2O	2.41	2.60	2.59	2.32	2.65	1.88	1.94	1.85	1.64	1.64
P_2O_5	0.13	0.18	0.15	0.09	0.12	0.08	0.07	0.08	0.07	0.08
LOI	12.58	12.47	13.00	14.92	11.58	13.10	13.53	13.84	15.66	14.16
Total	98.21	99.03	99.12	99.60	101.69	100.42	101.48	101.62	101.85	101.56
K_2O/Na_2O	4.56	4.21	4.42	3.91	5.24	10.34	6.52	5.89	5.75	5.49
SiO_2/Al_2O_3	2.75	2.67	2.56	3.05	3.12	2.17	2.19	2.21	2.02	2.10
CIA	81.59	80.66	82.26	79.61	80.72	90.53	89.09	89.11	90.64	90.36
PIA	90.55	89.54	91.34	88.42	90.64	97.48	95.92	95.67	96.31	96.08
CIW	91.72	90.86	92.40	89.92	91.94	97.68	96.25	96.01	96.55	96.34
ICV	0.72	0.66	0.62	0.81	0.67	0.32	0.35	0.35	0.31	0.33

Major oxides	KN31	KN32	KN33	KN34	KN35	KN36	KN37	KN38	KN39	KN40
SiO_2	55.71	56.85	55.27	55.69	56.13	52.90	56.93	56.61	57.68	58.33
TiO_2	1.25	1.35	1.34	1.37	1.27	1.27	1.24	1.32	1.29	1.18
Al_2O_3	22.81	23.43	23.62	23.96	24.99	23.95	21.77	23.36	22.22	17.97
Fe_2O_3	3.17	3.18	2.31	2.52	2.86	3.04	4.71	3.40	3.99	6.26
MnO	0.03	0.02	0.02	0.02	0.02	0.03	0.03	0.03	0.03	0.02
MgO	0.95	0.86	0.95	0.94	0.75	1.14	0.99	1.12	0.94	0.82
CaO	0.91	0.39	0.36	0.57	0.44	0.98	0.56	1.06	0.38	2.90
Na_2O	0.32	0.34	0.40	0.43	0.32	0.49	0.28	0.41	0.40	0.40
K_2O	1.87	1.92	1.86	1.96	1.73	1.94	2.00	1.96	2.22	1.75
P_2O_5	0.08	0.08	0.09	0.08	0.07	0.08	0.07	0.07	0.09	0.07
LOI	13.11	13.13	13.93	13.69	12.74	13.73	13.52	12.05	12.43	11.21
Total	100.20	101.56	100.16	101.23	101.31	99.54	102.10	101.38	101.65	100.91
K_2O/Na_2O	5.80	5.59	4.61	4.55	5.43	3.95	7.07	4.77	5.57	4.38
SiO_2/Al_2O_3	2.44	2.43	2.34	2.32	2.25	2.21	2.61	2.42	2.60	3.25

(continued)

Table 3 (continued)

Major oxides	KN31	KN32	KN33	KN34	KN35	KN36	KN37	KN38	KN39	KN40
CIA	88.07	87.97	87.61	87.12	89.55	86.58	87.53	87.05	85.70	81.08
PIA	95.14	94.98	94.22	93.90	95.67	93.12	95.46	94.01	93.80	91.98
CIW	95.55	95.41	94.68	94.41	95.98	93.68	95.89	94.53	94.44	93.18
ICV	0.40	0.39	0.38	0.39	0.33	0.43	0.47	0.44	0.46	0.66
Major oxides	KN41	KN42	KN43	KN44	KN45	KN46	KN47	KN48	KN49	KN50
SiO_2	63.31	59.52	60.36	62.87	59.20	59.97	57.60	55.47	56.37	56.80
TiO_2	1.29	1.34	1.32	1.34	1.32	1.39	1.30	1.42	1.18	1.16
Al_2O_3	19.17	20.66	22.05	21.63	20.72	21.55	21.97	21.85	21.93	20.99
Fe_2O_3	2.37	2.37	2.67	2.18	3.03	3.43	1.37	4.56	1.36	5.55
MnO	0.01	0.01	0.01	0.01	0.01	0.01	1.81	0.02	1.96	0.04
MgO	1.03	0.97	0.89	0.73	1.02	1.07	1.56	1.02	1.39	1.45
CaO	0.64	1.29	0.65	0.33	0.96	0.60	1.03	1.17	1.06	0.22
Na_2O	0.59	0.59	0.17	0.39	0.34	0.30	0.35	0.50	0.23	0.38
K_2O	2.00	1.99	1.98	1.99	1.99	2.12	2.32	1.89	2.17	2.48
P_2O_5	0.07	0.07	0.09	0.08	0.08	0.08	0.02	0.09	0.02	0.08
LOI	9.99	10.98	10.35	9.71	10.84	10.69	12.59	13.51	14.51	12.91
Total	100.47	99.79	100.54	101.26	99.51	101.21	101.92	101.50	102.18	102.06
K_2O/Na_2O	3.39	3.37	11.65	5.10	5.85	7.07	6.63	3.78	9.43	6.53
SiO_2/Al_2O_3	3.30	2.88	2.74	2.91	2.86	2.78	2.62	2.54	2.57	2.71
CIA	78.56	79.85	85.25	82.73	82.51	82.81	81.56	82.13	83.52	80.44
PIA	89.11	89.96	97.11	93.67	93.98	94.82	94.04	91.93	96.04	94.29
CIW	90.81	91.41	97.53	94.57	94.88	95.62	95.02	93.00	96.66	95.34
ICV	0.57	0.53	0.43	0.44	0.51	0.52	0.64	0.55	0.59	0.66

Major oxides	KN51	KN52	KN53	KN54	KN55	Avg.
SiO_2	58.26	59.20	59.53	61.12	61.37	56.35
TiO_2	1.12	1.16	1.14	1.09	1.09	1.17
Al_2O_3	20.36	20.74	20.97	19.14	19.18	21.04
Fe_2O_3	4.22	4.88	4.50	3.85	3.88	4.58
MnO	0.04	0.02	0.02	0.02	0.02	0.10
MgO	1.44	1.55	1.40	1.22	1.22	1.21
CaO	0.22	0.27	0.26	0.16	0.15	0.72
Na_2O	0.40	0.55	0.26	0.25	0.18	0.43
K_2O	2.92	2.55	2.80	2.92	2.93	2.26
P_2O_5	0.07	0.06	0.07	0.06	0.06	0.11
LOI	12.86	9.29	10.41	9.93	9.95	12.76
Total	101.91	100.27	101.36	99.76	100.03	100.72

(continued)

Table 3 (continued)

Major oxides	KN51	KN52	KN53	KN54	KN55	Avg.
K_2O/Na_2O	7.30	4.64	10.77	11.68	16.28	5.77
SiO_2/Al_2O_3	2.86	2.85	2.84	3.19	3.20	2.71
CIA	77.65	78.77	79.34	77.66	78.07	83.16
PIA	93.63	92.22	95.03	95.33	96.19	92.74
CIW	95.06	93.70	96.08	96.46	97.12	93.68
ICV	0.67	0.68	0.64	0.65	0.65	0.58

burial of sediments (e.g. Morton 1984). Heavy minerals such as epidote display a limit of persistence between 600 and 1100 m depth (e.g. Morton 1984), or between 600 and 3000 m (e.g. McBride 1985) as burial diagenesis proceeds. The geochemical analysis by Arora et al. (2017) indicated the low maturity of organic matters within the Mesozoic succession in Mainland Kutch, except near a few dike intrusions. The heavy mineral assemblage, therefore, corroborates the shallow burial nature of sediments.

In a cross-plot of TiO_2 and Al_2O_3, apart from a few samples of Jhumara and Bhuj formations which plot closer to the basalt line, data of all four formations plot in the granite + basalt field (cf. Mclennan et al. 1979; Schieber 1992) (Fig. 3). In a cross-plot of TiO_2 and Zr of Hayashi et al. (1997), most of the samples plot in the field for intermediate igneous rocks. A few samples of all the formations plot in the field for felsic igneous rocks (Fig. 4). In a cross-plot of Th versus Sc of Cullers (2002), most samples of Jhuran and Bhuj formations and nearly half of the data Jhurio and Jhumara formations bear felsic signature (Fig. 5). A few samples of Jhuran and Bhuj formations and the majority of those of Jhurio and Jhumara formations plot within the intermediate field. In a cross-plot of Th/Co versus La/Sc of Cullers (2002), all data cluster near the silicic field (Fig. 6). Most data cluster near the field marked for felsic rocks in a triangular plot of V-Ni-Th × 10 of Bracciali et al. (2007) (Fig. 7). Samples of the Jhuran and Bhuj formations plot close to the Th apex. Data of Jhurio and Jhumara formations and a few of those of the Jhuran Formation plot relatively closer to the V-Ni join. Samples of all four formations exhibit low La/Th ratios ranging from 1.59 to 3.01 (Tables 5, 6, 7 and 8). Samples of Jhurio, Jhumara, Jhuran and Bhuj formations show broadly overlapping chondrite-normalized REE patterns, with prominent LREE enrichment and negative europium anomaly (Fig. 8). These patterns are similar to those of NASC and PAAS samples. The samples of Jhuran and Bhuj formations exhibit the highest REE concentrations. All samples of Jhurio, Jhumara, Jhuran and Bhuj formations exhibit negative Eu anomalies (Eu/Eu* = Eu/($\sqrt{(Sm_N \times Nd_N)}$)), with averages of 0.66, 0.65, 0.65 and 0.55 respectively.

The presence of both rounded, as well as angular varieties of heavy minerals, indicate the presence of multiple source rocks. Chaudhuri et al. (2018, 2020a, b) report the dominance of arkoses in the sandstones of the Jhurio, Jhumara, Jhuran and Bhuj formations suggesting a significant clastic supply from felsic source rocks. The abundance of arkose, the relationship between TiO_2 and Al_2O_3, Th/Co and La/Sc

Table 4 Major oxide concentration in shale samples of the Bhuj Formation

Major oxides	KB1	KB2	KB3	KB4	KB5	KB6	KB7	KB8	KB9	KB10
SiO_2	58.85	54.54	54.61	57.67	65.69	67.55	66.99	65.64	75.75	76.76
TiO_2	1.22	1.11	1.05	1.06	1.08	1.10	1.10	1.17	0.91	0.82
Al2O3	22.77	21.23	21.14	16.73	16.40	17.13	16.44	18.03	10.80	11.21
Fe2O3	2.83	5.85	6.94	7.90	3.97	3.69	4.13	3.29	4.92	3.74
MnO	0.09	0.07	0.08	0.03	0.05	0.05	0.04	0.06	0.05	0.10
MgO	1.11	1.37	1.28	1.41	0.72	0.68	0.68	0.84	0.39	0.35
CaO	0.35	0.42	0.28	0.33	0.22	0.15	0.20	0.11	0.07	0.09
Na2O	0.18	0.14	0.20	0.10	0.28	0.29	0.30	0.32	0.21	0.44
K2O	2.76	2.41	2.38	2.86	1.99	2.09	2.01	2.16	2.93	3.19
P2O5	0.07	0.07	0.06	0.07	0.05	0.05	0.05	0.06	0.04	0.04
LOI	11.01	12.05	11.59	10.78	9.16	8.96	9.08	9.80	4.32	3.52
Total	101.25	99.26	99.61	98.95	99.61	101.75	101.01	101.47	100.40	100.25
K_2O/Na_2O	15.32	17.43	12.11	28.65	7.12	7.29	6.78	6.76	13.90	7.23
SiO_2/Al_2O_3	2.58	2.57	2.58	3.45	4.01	3.94	4.08	3.64	7.01	6.85
CIA	86.42	87.40	86.78	82.99	84.47	85.03	84.48	85.48	74.71	72.10
PIA	97.09	97.62	96.64	97.64	94.28	95.19	94.40	95.61	94.06	89.74
CIW	97.46	97.91	97.03	98.07	94.99	95.80	95.10	96.16	95.73	92.66
ICV	0.43	0.55	0.58	0.80	0.54	0.50	0.54	0.49	0.83	0.79
Major oxides	KB11	KB12	KB13	KB14	KB15	KB16	KB17	KB18	Avg.	
SiO_2	66.36	74.17	67.03	68.68	61.67	56.91	65.63	69.24	65.21	
TiO_2	0.88	1.21	0.97	0.98	1.45	1.30	1.06	1.22	1.09	
Al2O3	8.89	15.41	15.95	15.50	16.82	20.03	12.66	17.45	16.37	
Fe2O3	7.28	1.03	4.58	2.59	1.33	1.58	10.41	0.87	4.27	
MnO	0.05	0.01	0.34	0.02	0.01	0.01	0.02	0.01	0.06	
MgO	0.56	0.49	0.81	0.77	0.45	0.59	0.52	0.43	0.75	
CaO	5.35	0.12	0.29	0.39	0.05	0.07	0.08	0.10	0.48	
Na2O	0.58	0.91	0.21	0.30	0.12	0.16	0.48	0.84	0.34	
K2O	2.65	2.12	3.66	3.63	1.52	1.65	3.44	3.21	2.59	
P2O5	0.05	0.04	0.06	0.04	0.03	0.04	0.07	0.05	0.05	
LOI	7.76	6.25	6.65	7.02	18.19	17.98	5.58	7.59	9.29	
Total	100.42	101.75	100.55	99.92	101.64	100.31	99.94	101.01	100.51	
K_2O/Na_2O	4.58	2.31	17.06	12.23	12.38	10.57	7.22	3.82	10.71	
SiO_2/Al_2O_3	7.47	4.81	4.20	4.43	3.67	2.84	5.18	3.97	4.29	
CIA	65.02	79.37	77.36	75.94	89.61	90.23	73.15	77.57	81.01	
PIA	75.92	88.44	94.44	92.21	98.06	97.96	90.64	89.92	93.32	
CIW	82.33	89.99	95.76	94.07	98.24	98.14	93.21	91.76	94.69	

(continued)

Table 4 (continued)

Major oxides	KB11	KB12	KB13	KB14	KB15	KB16	KB17	KB18	Avg.
ICV	1.36	0.48	0.71	0.63	0.34	0.32	1.10	0.47	0.64

and V-Ni-Th support the dominance of felsic source rocks (Cullers 2002; López et al. 2005; Bracciali et al. 2007; Etemad-Saeed et al. 2011; Amendola et al. 2016; Armstrong-Altrin et al. 2017) (Figs. 3, 6 and 7). The relationship between TiO_2 and Al_2O_3 suggests the input from mafic sources in these sediments (Fig. 3). The intermediate igneous source rock composition, indicated by the relationship between TiO_2 and Zr contents, possibly indicates a mixing of sediments from felsic and mafic igneous rocks (Fig. 4). The relationship between Th versus Sc supports the mixing of sediments from mafic and felsic igneous rocks (Fig. 5). The fields for Jhurio and Jhumara formations plot closer to the V-Ni join in the triangular plot of V-Ni-Th and thereby corroborate the mafic input in these formations (Fig. 7). Low La/Th ratios support the predominant felsic source of sediments (Floyd and Leveridge 1987; Gu et al. 2002; Etemad-Saeed et al. 2011; Zhu et al. 2011; Yan et al. 2012). The LREE enrichment, the resemblance of the chondrite-normalized REE patterns with those of NASC and PAAS and negative Eu anomalies endorse the dominance of felsic source rocks in sediments (Fig. 8) (Kasanzu et al. 2008; Wani and Mondal 2011; Wang et al. 2015; Löwen et al. 2018; Chaudhuri et al. 2020a).

5.2 Weathering and Recycling

The degree of chemical weathering of source rocks is calculated from the chemical index of alteration (CIA) (Nesbitt and Young 1982) using the following formula (in molecular proportions)

$$CIA = [n(Al_2O_3)/(n(Al_2O_3) + n(CaO)* + n(Na_2O) + n(K_2O))] \times 100$$

The CaO content associated with calcite, dolomite and apatite is corrected to find $CaO*$ (CaO in silicates). Further, McLennan (1993) suggested if $n(CaO') < n(Na_2O)$, $n(CaO*) = n(CaO')$ else, $n(CaO*) = n(Na_2O)$ where $n(CaO') = n(CaO) - 10 \times n(P_2O_5)/3$. Samples of Jhurio, Jhumara, Jhuran and Bhuj formations exhibit average CIA values of 71%, 82%, 83% and 81%, respectively. Two other indices used to study the extent of weathering and alteration are the plagioclase index of alteration (PIA) and the chemical index of weathering (CIW). K-metasomatism during diagenesis may modify the values of CIA. Therefore, PIA and CIW are used for unbiased estimation of weathering conditions (Harnois 1988; Fedo et al. 1995).

$$PIA = [(Al_2O_3 - K_2O)/(Al_2O_3 - K_2O) + CaO* + Na_2O] \times 100$$
$$CIW = [Al_2O_3/(Al_2O_3 + CaO* + Na_2O)] \times 100$$

Table 5 Trace element concentration in shale samples from Jhurio Formation

Elements	KU1	KU2	KU3	KU4	KU5	Avg.
Sc	7.3	9.5	10.1	16.9	20.3	12.8
V	121.2	117.3	192.7	127.4	199.6	151.6
Cr	115.5	153.3	148.7	89.6	118.4	125.1
Co	9.1	16.3	11.9	13.6	13.9	13.0
Ni	30.9	36.6	42.1	27.2	39.4	35.2
Cu	17.0	22.3	21.4	29.3	33.5	24.7
Zn	31.8	44.4	86.0	43.2	51.0	51.3
Ga	9.3	12.8	12.0	13.7	20.7	13.7
Rb	63.0	86.1	79.9	118.0	100.6	89.5
Sr	254.6	159.8	240.0	619.2	168.9	288.5
Y	9.4	12.7	11.2	24.0	20.0	15.4
Zr	143.0	219.7	219.9	125.6	180.1	177.7
Nb	8.4	12.9	9.2	14.6	16.8	12.4
Cs	1.5	2.4	2.0	5.7	6.7	3.7
Ba	627.9	761.0	810.7	426.3	152.0	555.6
La	16.6	22.9	21.7	35.7	35.3	26.4
Ce	33.9	48.8	49.8	58.9	64.1	51.1
Pr	3.9	5.1	5.2	7.6	7.5	5.8
Nd	13.7	17.8	18.0	27.9	26.4	20.8
Sm	2.6	3.1	3.2	5.5	5.0	3.9
Eu	0.6	0.7	0.7	1.1	1.0	0.8
Gd	2.2	2.5	2.4	4.9	4.2	3.3
Tb	0.4	0.5	0.4	0.8	0.8	0.6
Dy	1.9	2.5	2.2	4.3	4.1	3.0
Ho	0.4	0.5	0.5	0.9	0.9	0.7
Er	1.2	1.6	1.5	2.6	2.6	1.9
Tm	0.2	0.2	0.2	0.4	0.4	0.3
Yb	1.2	1.8	1.6	2.5	2.7	2.0
Lu	0.2	0.3	0.3	0.4	0.4	0.3
Hf	4.2	6.4	6.5	3.8	5.6	5.3
Ta	0.7	0.9	0.3	1.0	0.7	0.7
Pb	14.2	17.2	32.2	13.6	18.6	19.2
Th	9.2	11.6	13.6	12.7	15.6	12.5
U	1.3	2.0	2.3	1.7	2.0	1.9
La/Th	1.8	2.0	1.6	2.8	2.3	2.1
La/Sc	2.3	2.4	2.1	2.1	1.7	2.1

Table 5 (continued)

Elements	KU1	KU2	KU3	KU4	KU5	Avg.
Th/Co	1.0	0.7	1.1	0.9	1.1	1.0
Th/Sc	1.3	1.2	1.3	0.8	0.8	1.1
$\sum$REE	78.8	108.3	107.6	153.5	155.4	120.7
(Gd_N/Yb_N)	1.4	1.2	1.2	1.6	1.3	1.3
Eu/Eu*	1.3	2.1	1.8	2.8	3.3	2.3

Samples of Jhurio, Jhumara, Jhuran and Bhuj formations exhibit average PIA values of 82%, 93%, 93% and 93% respectively. The samples exhibit average CIW values of 86%, 94%, 94% and 95%, respectively.

The index of compositional variability (ICV) proposed by Cox et al. (1995) is defined as follows.

$$ICV = (n(Fe_2O_3) + n(K_2O) + n(Na_2O) + n(CaO*)$$
$$+ n(MgO) + n(MnO) + n(TiO_2))/ n(Al_2O_3).$$

Samples of Jhurio, Jhumara, Jhuran and Bhuj formations exhibit average ICV of 1.3, 0.7, 0.6 and 0.6, respectively.

Chemical weathering and alteration of source rocks influence geochemistry and mineralogy of sedimentary rocks (Nesbitt and Young 1982; McLennan 1993; Fedo et al. 1995). Diagenesis and low-grade metamorphism lead to changes in mineralogy. However, the bulk chemical composition remains similar to that of source rock(s) (Cox et al. 1995). CIA values indicate intermediate to strong weathering for Jhurio, Jhumara, Jhuran and Bhuj formations (Fig. 9). However, a few samples of the Jhurio Formation indicate weak weathering. PIA and CIW indicate a greater degree of weathering at source than that estimated by CIA. However, all three indices show a broadly similar trend of weathering. Thus, CIA, PIA and CIW data for the studied samples indicate weak to intermediate weathering of source rocks for the Jhurio Formation. The data also indicates intermediate to strong weathering of source rocks for Jhumara, Jhuran and Bhuj formations.

Mature sediments with high clay content exhibit ICV values less than 1. It generally indicates a passive tectonic setting with recycling or intense chemical weathering of first cycle sediments (cf. Cox et al. 1995). The ICV value exceeds 1 in case of immature sediments containing a high amount of non-clay minerals. It generally indicates the first cycle deposition sourced from tectonically active regions (Cox et al. 1995; Cullers and Podkovyrov 2000; Ding et al. 2016). Therefore, the average ICV values of samples of Jhumara, Jhuran and Bhuj formations suggest recycled sediments or highly weathered first cycle sediments in a passive tectonic setting (Fig. 10). However, the average ICV values of the Jhurio Formation suggest immature sediments supplied from tectonically active sediments.

Table 6 Trace element concentration in shale samples of the Jhumara Formation

Elements	KM1	KM2	KM3	KM4	KM5	KM6	KM8	KM9
Sc	14.5	15.9	13.4	13.9	11.9	11.1	18.1	7.9
V	169.9	139.9	116.0	111.7	152.2	109.1	164.7	87.2
Cr	138.9	132.5	108.9	97.3	107.3	130.0	121.3	93.8
Co	20.3	21.3	19.5	18.8	6.4	15.9	22.3	11.9
Ni	48.1	44.2	35.1	33.4	38.2	45.2	36.4	28.0
Cu	45.4	42.4	36.6	27.8	28.8	41.9	31.1	20.9
Zn	89.2	84.3	48.2	26.8	117.9	73.3	36.3	36.5
Ga	37.4	31.2	26.1	25.5	27.4	15.8	24.8	11.6
Rb	106.2	108.0	97.0	90.7	91.4	81.6	78.7	62.9
Sr	164.9	321.9	210.7	315.9	181.4	200.7	125.8	129.2
Y	22.4	27.6	21.2	27.2	8.6	19.5	25.9	13.5
Zr	255.4	312.4	272.7	233.4	188.0	384.5	272.2	246.2
Nb	29.3	27.8	24.5	23.2	24.2	18.6	26.5	15.7
Cs	8.7	6.4	5.0	5.0	7.3	3.8	7.4	2.9
Ba	303.4	466.9	480.8	445.3	142.6	458.7	257.4	351.1
La	51.3	64.0	46.1	55.9	28.2	41.2	40.9	28.6
Ce	153.0	152.1	99.4	133.0	87.0	96.8	105.9	72.1
Pr	11.6	14.5	9.3	13.0	6.0	9.3	9.5	6.7
Nd	40.6	51.5	31.3	46.9	20.2	31.9	32.9	23.3
Sm	7.7	9.6	5.5	9.1	3.4	5.9	6.3	4.3
Eu	1.4	1.9	1.1	1.9	0.6	1.0	1.3	0.8
Gd	6.0	7.5	4.7	7.4	2.3	4.7	5.3	3.4
Tb	1.0	1.2	0.8	1.1	0.4	0.8	0.9	0.5
Dy	4.9	6.1	4.4	5.8	1.9	3.9	5.2	2.8
Ho	1.0	1.2	0.9	1.1	0.4	0.8	1.1	0.5
Er	2.7	3.4	2.6	3.0	1.2	2.3	3.2	1.6
Tm	0.4	0.5	0.4	0.4	0.2	0.3	0.5	0.2
Yb	2.8	3.5	2.8	3.0	1.5	2.5	3.6	1.7
Lu	0.5	0.6	0.5	0.5	0.3	0.4	0.6	0.3
Hf	6.0	7.2	6.2	5.5	4.4	8.8	6.4	5.8
Ta	2.3	2.2	1.9	2.0	1.8	1.6	2.1	1.2
Pb	21.4	19.1	16.2	15.1	10.6	15.9	16.7	10.8
Th	25.5	23.6	19.6	18.9	12.9	17.8	17.6	12.3
U	5.4	4.1	3.5	3.5	1.9	2.8	2.4	2.0
La/Th	2.0	2.7	2.4	3.0	2.2	2.3	2.3	2.3
La/Sc	3.5	4.0	3.4	4.0	2.4	3.7	2.3	3.6

Table 6 (continued)

Elements	KM1	KM2	KM3	KM4	KM5	KM6	KM8	KM9
Th/Co	1.3	1.1	1.0	1.0	2.0	1.1	0.8	1.0
Th/Sc	1.8	1.5	1.5	1.4	1.1	1.6	1.0	1.6
$\sum$REE	284.9	317.4	209.7	282.2	153.7	201.9	217.1	146.9
(Gd_N/Yb_N)	1.7	1.7	1.3	2.0	1.2	1.5	1.2	1.6
Eu/Eu*	0.6	0.7	0.7	0.7	0.7	0.6	0.7	0.6
Elements	KM11	KM12	KM13	KM14	KM15	KM16	KM17	Avg.
Sc	19.5	21.9	24.0	19.6	20.6	21.2	15.1	16.6
V	170.6	196.9	209.3	189.8	177.5	198.8	134.5	155.2
Cr	127.3	131.2	140.9	130.7	133.1	139.4	108.6	122.8
Co	19.0	20.7	20.7	20.0	7.4	23.2	6.8	17.0
Ni	39.3	44.7	46.3	43.4	35.3	47.6	29.3	39.6
Cu	62.2	40.1	41.2	39.5	23.8	40.1	18.8	36.0
Zn	56.6	44.2	38.4	49.3	24.9	54.1	25.8	53.7
Ga	22.2	27.2	29.8	24.1	27.2	25.7	17.8	24.9
Rb	110.2	122.7	133.4	112.1	131.1	130.5	96.7	103.5
Sr	107.3	119.6	108.9	100.4	145.9	105.0	206.9	169.6
Y	22.6	20.1	24.6	20.9	18.1	19.6	13.9	20.4
Zr	267.4	229.1	249.2	229.7	210.2	206.2	172.4	248.6
Nb	22.6	23.7	26.8	23.1	24.2	22.9	16.9	23.3
Cs	7.1	8.8	9.4	7.7	9.7	8.8	6.4	7.0
Ba	307.2	276.7	286.2	264.3	264.5	264.4	215.0	319.0
La	35.7	38.2	42.4	34.8	38.1	33.9	24.7	40.3
Ce	69.5	84.0	84.9	74.0	70.8	66.6	47.0	93.1
Pr	7.3	8.4	8.8	7.3	7.1	6.9	4.9	8.7
Nd	24.5	28.9	29.9	25.0	22.6	23.3	16.2	29.9
Sm	4.5	5.2	5.6	4.5	3.8	4.2	2.9	5.5
Eu	0.8	1.0	1.1	0.9	0.7	0.8	0.6	1.1
Gd	3.8	4.1	4.7	3.7	3.1	3.6	2.4	4.5
Tb	0.7	0.7	0.8	0.7	0.6	0.7	0.4	0.8
Dy	4.1	4.1	4.7	3.9	3.2	3.7	2.5	4.1
Ho	0.9	0.9	1.1	0.9	0.8	0.8	0.6	0.9
Er	2.8	2.7	3.2	2.7	2.3	2.5	1.8	2.5
Tm	0.4	0.4	0.5	0.4	0.3	0.4	0.3	0.4
Yb	3.1	2.9	3.4	2.9	2.6	2.7	2.0	2.7
Lu	0.5	0.5	0.6	0.5	0.4	0.4	0.3	0.4
Hf	7.9	6.8	7.4	6.9	6.4	6.1	5.1	6.5

(continued)

Table 6 (continued)

Elements	KM11	KM12	KM13	KM14	KM15	KM16	KM17	Avg.
Ta	1.8	2.0	2.1	1.8	1.7	1.8	1.4	1.8
Pb	26.1	34.6	23.4	23.3	19.1	22.1	13.2	19.2
Th	17.8	17.9	19.9	18.4	16.0	18.1	12.3	17.9
U	2.3	2.2	2.5	2.3	2.3	2.2	1.6	2.7
La/Th	2.0	2.1	2.1	1.9	2.4	1.9	2.0	2.2
La/Sc	1.8	1.7	1.8	1.8	1.8	1.6	1.6	2.6
Th/Co	0.9	0.9	1.0	0.9	2.2	0.8	1.8	1.2
Th/Sc	0.9	0.8	0.8	0.9	0.8	0.9	0.8	1.1
$\sum$REE	158.6	182.1	191.5	162.2	156.6	150.7	106.7	194.8
(Gd_N/Yb_N)	1.0	1.2	1.1	1.0	1.0	1.1	1.0	1.3
Eu/Eu*	0.6	0.7	0.7	0.6	0.6	0.7	0.7	0.7

5.3 Tectonic Setting

In a cross plot of SiO_2 and K_2O/Na_2O of Roser and Korsch (1986), the analysed shale samples plot in the passive continental margin field (Fig. 11). In a cross-plot of SiO_2/Al_2O_3 and K_2O/Na_2O of Maynard et al. (1982), the majority of the analysed samples exhibit passive margin signatures (Fig. 12). However, many samples of Jhurio, Jhumara and Bhuj formations plot at the margin of ACM (active continental margin) and PM (passive margin) fields. In the cross-plot of La/Th versus Hf of Floyd and Leveridge (1987), the majority of the samples Jhurio, Jhumara, Jhuran and Bhuj formations indicate passive margin source, while a few samples of all the formations occupy the field of acidic arc source (Fig. 13). Samples of Jhuran and Bhuj formations exhibit a distinctly higher concentration of Hf in comparison to those of Jhurio and Jhumara formations.

The concentration of major oxides and trace elements in samples of Jhurio, Jhumara, Jhuran and Bhuj formations indicate the predominantly passive margin setting (Figs. 11, 12 and 13). The offset of data points to the active continental margin field (Fig. 12) corresponds to the higher abundance of Al_2O_3 in most of shale samples.

5.4 Age of Source Rock

In a cross plot of Cr and Ni of Taylor and McLennan (1985), the majority of the analysed shale samples of Jhurio, Jhumara, Jhuran and Bhuj formations cluster in the field marked for post-Archean source rocks (Fig. 14). However, a few samples of the Jhuran Formation plot in the Late Archean field. Further, most samples of all the formations occupy the Post-Archean field in the Eu/Eu* versus (Gd_N/Yb_N) plot

Table 7 Trace element concentration in shale samples of the Jhuran Formation

Elements	KN1	KN2	KN3	KN4	KN5	KN6	KN7	KN8	KN9	KN10
Sc	15.0	16.1	10.4	17.3	16.2	16.3	18.9	18.6	10.3	19.7
V	132.8	109.9	90.1	87.2	139.9	129.4	123.5	158.9	95.4	148.3
Cr	125.8	105.0	77.9	91.9	141.3	130.9	117.8	136.0	91.9	109.5
Co	20.7	23.5	17.4	27.8	20.4	21.2	23.0	24.6	11.1	15.0
Ni	47.3	47.3	38.5	57.1	65.8	63.5	51.8	49.1	35.5	50.7
Cu	60.5	48.7	47.0	60.0	131.9	124.7	54.1	63.5	43.1	90.7
Zn	144.5	113.6	94.6	175.5	155.7	218.2	972.8	95.0	146.8	170.0
Ga	28.0	32.9	23.8	36.2	26.6	23.9	33.9	28.6	25.1	24.3
Rb	113.6	113.8	98.6	105.2	106.0	102.3	110.5	103.1	103.0	94.0
Sr	237.3	212.4	149.1	307.7	265.3	260.3	336.6	125.9	189.8	242.8
Y	28.8	32.4	27.7	47.3	29.2	32.8	38.3	31.6	30.6	45.6
Zr	191.6	258.9	269.3	308.4	227.9	309.8	233.9	189.8	204.2	171.3
Nb	21.2	23.7	21.6	28.6	20.7	20.4	23.0	21.2	20.5	18.7
Cs	6.7	6.0	5.0	5.4	8.0	6.2	6.5	6.1	6.1	6.5
Ba	572.3	617.6	586.7	398.2	776.1	768.3	597.0	461.1	503.0	534.6
La	72.1	64.2	72.0	61.2	99.7	88.8	71.5	53.3	58.4	61.1
Ce	138.2	116.5	133.5	113.5	195.6	165.8	137.3	98.8	108.3	116.9
Pr	19.4	16.6	17.4	15.6	27.5	22.7	19.5	13.5	14.3	17.2
Nd	69.9	59.8	60.8	67.2	97.8	82.2	72.6	47.6	51.1	64.8
Sm	11.4	9.4	10.1	11.8	15.5	14.6	12.0	8.3	8.8	12.5
Eu	2.0	1.8	1.5	2.5	3.0	2.6	2.4	1.7	1.7	2.7
Gd	10.8	8.0	8.9	12.2	14.4	13.0	10.4	7.7	8.3	11.5
Tb	1.4	1.2	1.2	1.7	1.9	1.8	1.6	1.2	1.2	2.0
Dy	7.3	6.9	6.5	7.8	10.4	9.8	8.4	7.0	6.6	11.6
Ho	1.3	1.2	1.2	1.3	1.8	1.8	1.5	1.3	1.3	2.3
Er	3.5	3.3	3.4	3.6	5.0	5.0	4.2	3.7	3.6	6.2
Tm	0.6	0.6	0.6	0.6	0.8	0.8	0.7	0.6	0.6	1.0
Yb	3.4	3.5	3.5	4.0	4.9	4.9	4.4	3.7	3.6	6.3
Lu	0.5	0.6	0.6	0.8	0.8	0.8	0.7	0.6	0.6	1.0
Hf	5.9	8.3	7.9	7.2	10.2	13.0	7.7	5.8	6.2	6.1
Ta	1.4	1.7	1.3	1.2	1.9	1.8	1.3	1.3	1.4	1.4
Pb	23.6	28.8	18.1	21.1	34.9	27.6	28.0	21.4	23.2	23.9
Th	25.4	24.2	34.0	22.6	33.1	39.9	23.8	22.8	23.4	25.0
U	3.5	3.5	4.3	2.6	4.7	5.6	3.9	3.4	3.5	3.6
La/Th	2.8	2.7	2.1	2.7	3.0	2.2	3.0	2.3	2.5	2.4
La/Sc	4.8	4.0	6.9	3.5	6.2	5.4	3.8	2.9	5.7	3.1

(continued)

Table 7 (continued)

Elements	KN1	KN2	KN3	KN4	KN5	KN6	KN7	KN8	KN9	KN10
Th/Co	1.2	1.0	2.0	0.8	1.6	1.9	1.0	0.9	2.1	1.7
Th/Sc	1.7	1.5	3.3	1.3	2.0	2.4	1.3	1.2	2.3	1.3
$\sum$REE	341.8	293.6	321.2	303.8	479.1	414.6	347.2	249.0	268.4	317.1
(Gd_N/Yb_N)	2.6	1.8	2.1	2.5	2.4	2.1	1.9	1.7	1.9	1.5
Eu/Eu*	0.6	0.6	0.5	0.6	0.6	0.6	0.7	0.7	0.6	0.7

Elements	KN11	KN12	KN15	KN16	KN17	KN18	KN19	KN20
Sc	15.4	12.3	15.6	15.1	16.6	17.9	15.2	15.9
V	134.9	76.4	145.2	106.4	116.3	118.9	121.7	120.9
Cr	126.3	73.2	124.2	107.4	104.7	111.7	139.9	112.7
Co	19.9	15.1	17.3	24.1	24.5	20.3	26.0	23.5
Ni	43.0	34.6	48.0	60.1	52.4	46.1	40.8	45.9
Cu	56.0	34.4	62.0	51.1	47.7	53.8	162.2	42.3
Zn	128.5	64.0	149.9	88.6	86.4	80.1	64.2	71.2
Ga	23.6	32.2	28.2	28.1	33.4	30.4	25.8	25.6
Rb	107.0	117.7	113.8	108.1	107.5	107.5	120.8	108.0
Sr	187.5	167.4	209.5	138.3	161.1	277.3	145.0	212.0
Y	26.3	40.2	27.8	38.1	45.1	40.7	28.9	30.8
Zr	205.7	287.8	156.3	234.3	223.5	244.5	312.8	285.6
Nb	20.3	24.1	19.8	21.9	23.3	21.5	22.5	22.2
Cs	5.5	6.5	8.4	5.7	6.3	5.6	5.6	4.6
Ba	544.0	590.7	397.1	550.5	515.2	620.6	687.0	637.5
La	56.8	60.3	61.2	56.4	61.9	65.3	43.8	55.1
Ce	106.5	106.6	112.2	108.0	116.8	126.0	91.8	122.1
Pr	14.7	15.4	15.9	16.1	17.0	18.0	9.7	12.6
Nd	52.1	56.8	54.4	61.5	63.8	68.7	34.1	44.3
Sm	8.5	10.1	8.0	11.4	11.7	12.6	7.0	8.6
Eu	1.6	2.1	1.6	2.3	2.4	2.5	1.6	1.8
Gd	7.9	8.8	8.4	10.0	9.7	11.6	6.5	7.3
Tb	1.1	1.5	1.1	1.6	1.7	1.8	1.1	1.2
Dy	6.1	8.4	6.5	8.6	9.4	9.1	6.0	6.5
Ho	1.1	1.5	1.2	1.5	1.6	1.6	1.2	1.3
Er	3.2	3.9	3.3	4.1	4.3	4.4	3.4	3.7
Tm	0.5	0.6	0.5	0.7	0.7	0.7	0.5	0.5
Yb	3.3	4.1	3.3	4.1	4.3	4.2	3.7	3.7
Lu	0.5	0.7	0.5	0.7	0.7	0.7	0.6	0.6
Hf	5.9	9.4	4.8	7.4	7.3	8.1	8.0	6.8

(continued)

Table 7 (continued)

Elements	KN11	KN12	KN15	KN16	KN17	KN18	KN19	KN20
Ta	1.3	1.6	1.3	1.4	1.6	1.4	1.8	1.8
Pb	23.7	23.2	26.6	26.7	25.5	23.6	35.5	17.3
Th	22.4	26.4	22.2	23.8	26.5	27.4	18.3	18.3
U	3.1	3.6	3.1	3.3	3.4	3.7	3.5	3.4
La/Th	2.5	2.3	2.8	2.4	2.3	2.4	2.4	3.0
La/Sc	3.7	4.9	3.9	3.7	3.7	3.6	2.9	3.5
Th/Co	1.1	1.7	1.3	1.0	1.1	1.3	0.7	0.8
Th/Sc	1.5	2.1	1.4	1.6	1.6	1.5	1.2	1.2
$\sum$REE	263.9	280.8	278.1	287.0	306.0	327.2	211.2	269.3
(Gd_N/Yb_N)	1.9	1.7	2.1	2.0	1.8	2.2	1.4	1.6
Eu/Eu*	0.6	0.7	0.6	0.7	0.7	0.6	0.7	0.7

Elements	KN21	KN22	KN23	KN24	KN25	KN26	KN27	KN28	KN29	KN30
Sc	10.9	11.6	10.2	11.7	15.9	16.5	15.7	14.5	16.0	16.1
V	112.0	105.9	115.7	99.2	121.9	128.2	136.2	146.6	137.6	141.5
Cr	106.4	100.2	108.1	101.7	118.2	105.8	114.5	129.2	117.0	124.9
Co	17.4	23.2	20.0	18.4	22.5	16.5	26.9	18.9	21.3	11.4
Ni	34.7	63.4	37.0	33.4	46.7	45.7	57.1	47.2	48.6	39.0
Cu	31.7	52.3	32.0	24.5	38.3	62.2	59.7	62.8	47.7	47.3
Zn	52.3	54.7	41.8	42.0	59.9	165.0	128.9	97.9	63.4	77.2
Ga	23.6	22.6	24.8	21.2	25.1	36.7	36.7	30.8	37.8	31.4
Rb	84.9	82.7	81.1	82.5	103.7	102.5	97.3	87.0	91.2	93.2
Sr	174.6	223.2	183.1	181.9	260.4	115.8	110.3	91.3	126.2	109.9
Y	17.2	20.1	17.3	21.6	33.3	28.3	26.7	22.6	26.9	26.4
Zr	207.6	224.9	217.9	392.0	333.3	220.1	220.6	211.0	216.9	237.1
Nb	20.7	19.7	20.8	23.3	26.4	25.5	25.7	26.4	28.1	25.9
Cs	4.5	2.9	4.9	2.9	4.5	6.5	6.4	5.6	6.0	5.8
Ba	340.1	452.1	314.0	505.3	694.7	361.5	367.6	335.4	382.4	395.7
La	43.7	38.8	41.4	45.2	49.2	55.2	58.9	55.0	66.3	51.9
Ce	108.1	95.1	114.6	112.0	109.6	107.6	111.0	101.8	124.5	91.3
Pr	9.7	9.9	9.3	10.8	11.1	15.0	14.8	13.7	14.8	11.7
Nd	33.2	36.6	31.9	38.4	39.8	57.4	52.5	47.2	53.2	40.7
Sm	5.9	7.2	5.6	6.9	8.0	10.0	8.9	7.6	10.0	7.1
Eu	1.1	1.5	1.1	1.4	1.9	2.1	1.8	1.5	2.0	1.4
Gd	4.7	5.9	4.5	5.4	7.4	10.3	8.7	7.3	8.9	6.7
Tb	0.7	0.9	0.7	0.9	1.2	1.3	1.2	1.0	1.3	1.0
Dy	3.9	4.9	3.8	4.8	6.6	6.7	6.2	5.6	6.3	5.7

(continued)

Table 7 (continued)

Elements	KN21	KN22	KN23	KN24	KN25	KN26	KN27	KN28	KN29	KN30
Ho	0.8	1.0	0.7	1.0	1.3	1.2	1.1	1.0	1.1	1.1
Er	2.2	2.6	2.1	2.9	3.7	3.2	3.1	2.8	3.1	3.1
Tm	0.3	0.4	0.3	0.4	0.5	0.5	0.5	0.4	0.5	0.5
Yb	2.2	2.6	2.1	3.1	3.7	3.3	3.1	2.8	3.1	3.2
Lu	0.4	0.4	0.3	0.5	0.6	0.5	0.5	0.4	0.5	0.5
Hf	4.9	5.3	5.0	9.2	7.6	6.9	7.0	6.4	7.4	7.4
Ta	1.6	1.5	1.6	3.1	2.2	1.6	1.7	1.7	2.2	1.5
Pb	15.4	14.3	15.5	13.6	21.0	25.0	23.2	23.1	26.4	19.1
Th	16.6	14.1	16.8	15.9	18.3	23.6	24.8	23.7	27.0	22.7
U	2.8	2.8	2.9	3.4	3.4	3.3	3.8	3.5	4.2	3.5
La/Th	2.6	2.8	2.5	2.8	2.7	2.3	2.4	2.3	2.5	2.3
La/Sc	4.0	3.3	4.1	3.9	3.1	3.4	3.7	3.8	4.1	3.2
Th/Co	1.0	0.6	0.8	0.9	0.8	1.4	0.9	1.3	1.3	2.0
Th/Sc	1.5	1.2	1.6	1.4	1.1	1.4	1.6	1.6	1.7	1.4
$\sum$REE	216.8	207.8	218.4	233.8	244.7	274.2	272.2	248.2	295.8	226.0
(Gd_N/Yb_N)	1.7	1.8	1.7	1.4	1.6	2.5	2.2	2.1	2.3	1.7
Eu/Eu*	0.7	0.7	0.7	0.7	0.7	0.6	0.6	0.6	0.7	0.6
Elements	KN31	KN32	KN33	KN34	KN35	KN36	KN37	KN38	KN39	KN40
Sc	13.9	17.6	4.4	15.6	15.9	15.9	15.4	20.6	12.8	7.6
V	116.2	146.6	164.1	155.1	117.7	116.2	123.4	171.4	115.9	125.5
Cr	109.1	100.1	131.1	127.0	105.5	100.8	109.6	129.4	91.0	100.7
Co	19.2	9.2	14.9	14.1	23.6	15.5	20.3	37.9	11.7	16.0
Ni	43.6	30.9	54.0	43.3	49.0	39.6	42.5	75.3	38.7	48.1
Cu	58.6	149.6	81.7	68.4	46.1	56.5	45.5	67.7	51.8	40.2
Zn	113.9	71.7	352.1	116.3	81.9	120.7	63.2	138.8	104.3	145.4
Ga	26.9	27.4	3.5	36.6	34.7	35.8	36.1	28.5	29.5	20.5
Rb	91.5	78.8	90.2	92.8	95.2	97.1	89.0	87.0	88.0	69.9
Sr	97.4	107.0	86.8	110.2	133.3	111.9	135.8	125.4	105.0	195.6
Y	21.1	32.3	23.4	25.5	23.3	29.3	29.8	47.6	28.9	12.7
Zr	238.0	231.8	176.6	193.4	236.6	279.7	239.5	237.9	223.3	218.8
Nb	23.0	22.6	21.9	24.7	25.9	27.4	27.1	23.1	23.7	20.1
Cs	4.9	5.0	5.5	6.2	6.1	6.6	5.2	5.1	5.8	2.9
Ba	420.4	450.2	304.1	339.5	399.1	396.0	398.8	388.3	427.4	220.2
La	55.8	60.1	45.4	56.2	52.2	60.6	64.0	57.8	60.8	24.5
Ce	100.6	113.1	88.8	107.2	90.2	116.1	118.5	118.3	113.7	58.5
Pr	13.1	15.6	12.5	14.4	11.2	15.5	14.1	16.7	15.4	6.2

<div align="right">(continued)</div>

Table 7 (continued)

Elements	KN31	KN32	KN33	KN34	KN35	KN36	KN37	KN38	KN39	KN40
Nd	45.6	55.6	44.9	51.8	38.9	55.4	50.6	64.4	54.5	22.1
Sm	7.6	9.6	7.9	8.8	7.1	9.1	9.6	12.6	9.3	4.4
Eu	1.4	2.0	1.7	1.9	1.4	1.8	1.9	2.8	1.9	1.0
Gd	7.1	8.8	9.5	9.5	6.8	8.0	8.6	12.8	8.6	3.6
Tb	1.0	1.4	1.2	1.2	1.0	1.2	1.3	2.0	1.3	0.6
Dy	5.0	8.3	6.4	6.2	5.0	6.6	6.2	10.3	7.3	3.0
Ho	0.9	1.6	1.1	1.1	1.0	1.1	1.2	1.9	1.3	0.6
Er	2.5	4.3	3.2	3.0	2.7	3.1	3.2	5.0	3.7	1.7
Tm	0.4	0.7	0.5	0.5	0.5	0.5	0.5	0.7	0.6	0.3
Yb	2.5	4.5	3.2	3.0	2.9	3.1	3.2	4.5	3.7	1.8
Lu	0.4	0.7	0.5	0.5	0.5	0.5	0.5	0.7	0.6	0.3
Hf	7.2	8.3	0.6	6.0	7.8	8.9	8.0	6.7	7.6	5.1
Ta	1.5	1.5	0.3	1.4	1.9	1.8	2.1	1.4	1.6	1.5
Pb	20.0	20.0	19.2	23.7	25.4	24.4	22.8	21.0	23.0	21.5
Th	25.2	21.5	21.3	23.9	23.8	27.2	24.2	20.9	22.4	13.1
U	3.8	3.6	3.5	3.7	3.8	4.0	4.2	3.8	3.6	2.6
La/Th	2.2	2.8	2.1	2.4	2.2	2.2	2.6	2.8	2.7	1.9
La/Sc	4.0	3.4	10.2	3.6	3.3	3.8	4.1	2.8	4.7	3.2
Th/Co	1.3	2.3	1.4	1.7	1.0	1.8	1.2	0.6	1.9	0.8
Th/Sc	1.8	1.2	4.8	1.5	1.5	1.7	1.6	1.0	1.7	1.7
$\sum$REE	243.8	286.4	226.8	265.0	221.4	282.7	283.3	310.4	282.5	128.6
(Gd_N/Yb_N)	2.3	1.6	2.4	2.6	1.9	2.1	2.2	2.3	1.9	1.6
Eu/Eu*	0.6	0.7	0.6	0.6	0.6	0.6	0.6	0.7	0.7	0.7
Elements	KN41	KN42	KN43	KN44	KN45	KN46	KN47	KN48	KN49	KN50
Sc	7.4	11.0	12.3	8.0	6.6	10.4	8.7	13.5	10.6	9.2
V	119.5	125.4	109.7	95.2	100.9	118.3	111.3	137.6	122.5	155.0
Cr	106.4	113.6	96.9	85.8	86.4	101.3	90.2	106.0	97.2	121.7
Co	5.8	5.5	8.1	6.4	11.2	8.1	8.3	11.7	7.9	24.3
Ni	31.9	26.7	32.6	25.0	24.2	25.5	26.6	35.1	26.8	80.2
Cu	31.2	30.0	26.1	22.4	21.6	27.0	27.4	35.4	39.5	40.3
Zn	108.2	36.0	100.0	63.2	39.6	39.9	53.5	39.3	56.6	61.3
Ga	20.9	24.6	23.8	19.2	19.6	23.5	21.5	24.9	23.6	28.2
Rb	83.7	91.6	84.6	68.2	70.1	96.6	58.5	90.0	79.0	57.0
Sr	107.8	109.7	206.5	85.8	85.1	156.8	115.7	155.8	117.2	86.8
Y	11.2	13.9	21.9	9.4	9.2	15.6	9.7	21.3	14.1	8.5
Zr	221.7	226.0	199.5	226.1	174.2	199.9	188.8	204.4	187.2	207.5

Table 7 (continued)

Elements	KN41	KN42	KN43	KN44	KN45	KN46	KN47	KN48	KN49	KN50
Nb	22.3	25.7	22.2	21.0	20.6	23.1	22.8	22.9	23.0	23.7
Cs	3.9	4.4	5.4	2.7	2.7	7.5	3.9	6.7	4.3	6.4
Ba	181.7	233.9	289.3	177.6	165.3	185.6	159.0	228.4	201.8	120.2
La	26.4	32.5	51.0	24.3	22.1	45.2	21.3	39.8	48.8	58.5
Ce	56.8	74.4	102.6	53.5	49.9	93.5	64.8	93.1	103.2	119.1
Pr	6.6	7.7	11.8	6.2	5.6	10.7	5.0	8.9	11.1	13.4
Nd	23.2	26.7	42.2	22.0	19.8	38.3	17.3	30.7	39.4	48.8
Sm	4.5	5.0	7.6	4.1	3.7	7.0	3.2	5.9	7.0	9.2
Eu	0.9	1.0	1.6	0.8	0.7	1.4	0.6	1.2	1.5	2.1
Gd	3.5	3.9	6.9	3.2	2.9	6.3	2.6	4.9	6.3	8.8
Tb	0.6	0.6	0.9	0.5	0.5	0.8	0.4	0.8	0.8	1.2
Dy	3.0	3.4	4.7	2.7	2.5	4.3	2.3	4.5	4.2	6.6
Ho	0.6	0.7	0.9	0.5	0.5	0.8	0.5	0.9	0.8	1.3
Er	1.6	1.9	2.5	1.5	1.4	2.5	1.3	2.5	2.3	4.7
Tm	0.2	0.3	0.4	0.2	0.2	0.4	0.2	0.4	0.3	0.5
Yb	1.6	2.1	2.4	1.6	1.5	2.4	1.5	2.7	2.3	3.3
Lu	0.3	0.3	0.3	0.3	0.2	0.3	0.2	0.4	0.3	0.5
Hf	5.2	5.4	4.8	5.3	4.2	4.9	4.6	4.8	4.5	4.9
Ta	1.6	2.1	1.7	1.6	1.6	1.7	1.8	1.7	1.9	1.8
Pb	15.8	16.0	14.0	14.4	13.2	12.9	13.9	16.2	15.4	17.1
Th	14.4	16.0	17.1	14.6	12.5	15.9	13.4	17.1	16.5	7.0
U	2.5	2.5	2.4	2.4	2.1	2.4	2.2	2.4	2.3	2.8
La/Th	1.8	2.0	3.0	1.7	1.8	2.8	1.6	2.3	3.0	8.4
La/Sc	3.6	3.0	4.1	3.0	3.4	4.4	2.5	2.9	4.6	6.3
Th/Co	2.5	2.9	2.1	2.3	1.1	2.0	1.6	1.5	2.1	0.3
Th/Sc	1.9	1.5	1.4	1.8	1.9	1.5	1.5	1.3	1.6	0.8
$\sum$REE	129.6	160.6	235.7	121.4	111.5	213.9	121.3	196.8	228.4	277.9
(Gd_N/Yb_N)	1.7	1.5	1.6	1.6	1.6	1.5	1.4	1.5	1.6	1.5
Eu/Eu*	0.7	0.7	0.7	0.7	0.7	0.7	0.7	0.7	0.7	0.6

Elements	KN51	KN52	KN53	KN54	KN55	Avg.
Sc	8.4	7.2	15.5	10.3	13.6	13.5
V	149.0	159.2	141.0	122.2	129.7	125.5
Cr	126.2	128.5	117.6	106.6	109.7	110.4
Co	14.9	12.4	11.3	11.6	16.9	17.3
Ni	42.5	43.9	33.5	30.5	31.5	43.6
Cu	42.8	27.3	29.8	26.8	30.3	53.1

(continued)

Table 7 (continued)

Elements	KN51	KN52	KN53	KN54	KN55	Avg.
Zn	60.2	46.7	40.0	49.7	33.1	112.0
Ga	28.5	29.8	27.3	24.8	26.0	27.3
Rb	72.3	19.7	104.0	91.8	104.6	92.4
Sr	128.2	71.7	137.6	213.0	208.0	162.2
Y	14.4	10.1	25.0	16.2	22.3	25.6
Zr	257.4	226.9	230.0	262.8	234.3	232.4
Nb	24.6	25.5	22.8	21.9	22.7	23.1
Cs	6.0	5.7	5.5	4.7	5.4	5.5
Ba	253.0	75.2	514.7	346.1	470.5	412.3
La	33.2	58.7	54.7	40.0	44.0	53.0
Ce	130.0	114.3	115.1	114.9	85.2	107.3
Pr	7.5	13.1	13.0	9.5	9.9	13.2
Nd	26.5	47.3	47.6	33.7	35.1	47.6
Sm	4.9	8.6	8.9	6.4	6.3	8.4
Eu	0.9	1.9	1.9	1.3	1.4	1.7
Gd	4.1	8.1	8.3	4.9	5.8	7.7
Tb	0.6	1.0	1.1	0.8	0.7	1.1
Dy	3.2	5.8	5.7	3.9	4.2	6.1
Ho	0.6	1.1	1.1	0.8	0.8	1.1
Er	1.7	3.2	3.1	2.1	2.5	3.2
Tm	0.2	0.5	0.4	0.3	0.4	0.5
Yb	1.7	3.1	2.9	2.2	2.6	3.2
Lu	0.3	0.4	0.4	0.4	0.4	0.5
Hf	6.1	5.3	5.4	6.1	5.6	6.5
Ta	1.8	2.1	1.8	1.7	1.7	1.6
Pb	16.3	12.1	16.4	14.7	13.9	20.6
Th	16.4	12.1	21.3	17.4	19.0	21.1
U	3.2	3.0	3.2	3.2	3.1	3.3
La/Th	2.0	4.9	2.6	2.3	2.3	2.6
La/Sc	3.9	8.1	3.5	3.9	3.2	4.1
Th/Co	1.1	1.0	1.9	1.5	1.1	1.4
Th/Sc	2.0	1.7	1.4	1.7	1.4	1.6
$\sum$REE	215.6	267.1	264.2	221.0	199.3	254.6
(Gd_N/Yb_N)	1.9	1.3	1.7	1.8	1.3	1.9
Eu/Eu*	0.6	0.6	0.7	0.7	0.7	0.7

Table 8 Trace element concentration in shale samples from Bhuj Formation

Elements	KB1	KB2	KB3	KB4	KB5	KB6	KB7	KB8	KB9
Sc	12.0	12.8	18.0	14.3	14.5	17.2	16.8	16.0	10.8
V	127.1	128.5	126.6	98.0	101.0	111.4	108.4	108.8	57.2
Cr	144.9	111.4	116.0	118.0	102.7	115.1	114.1	130.9	84.5
Co	16.1	13.7	26.6	16.4	22.9	21.3	20.5	16.5	16.1
Ni	32.2	30.6	44.6	49.6	41.1	42.2	38.3	42.9	35.9
Cu	29.5	28.7	34.8	30.4	33.9	39.0	35.1	84.9	20.4
Zn	47.1	54.1	64.1	53.1	100.0	79.0	50.7	120.8	31.6
Ga	29.5	29.3	28.1	22.6	19.0	23.6	22.5	24.2	14.0
Rb	95.3	94.2	99.0	89.6	74.4	92.5	87.4	89.3	85.8
Sr	100.2	101.8	129.3	130.4	59.1	67.9	67.3	76.2	76.4
Y	24.7	20.0	33.4	32.7	31.0	36.6	34.6	33.7	28.4
Zr	265.2	233.0	252.9	431.4	219.9	261.5	271.3	324.5	466.6
Nb	24.3	25.0	23.1	23.6	19.3	23.0	22.6	22.8	19.2
Cs	6.8	7.1	6.6	3.9	3.8	4.8	4.4	4.1	2.0
Ba	255.4	182.2	283.9	486.3	388.2	459.5	462.7	518.4	686.9
La	57.9	47.2	63.2	69.1	45.6	60.0	55.9	63.8	44.6
Ce	143.5	137.8	146.8	154.4	84.3	109.9	102.1	112.7	78.9
Pr	12.6	10.2	13.9	15.3	10.2	13.1	12.3	13.7	9.5
Nd	44.1	35.7	49.2	53.2	36.7	47.6	44.4	49.2	33.8
Sm	8.2	6.5	9.4	9.8	7.2	9.3	8.6	9.3	6.3
Eu	1.6	1.3	1.9	1.5	1.5	1.8	1.7	1.7	1.1
Gd	6.6	5.1	8.1	7.6	6.3	7.9	7.4	7.8	5.2
Tb	1.0	0.8	1.3	1.2	1.1	1.3	1.2	1.3	0.9
Dy	5.3	4.3	7.1	6.5	5.8	6.8	6.5	6.3	4.8
Ho	1.1	0.9	1.4	1.3	1.2	1.4	1.4	1.3	1.1
Er	2.9	2.4	3.9	4.0	3.4	4.0	3.9	3.7	3.1
Tm	0.4	0.3	0.5	0.6	0.5	0.5	0.5	0.5	0.4
Yb	2.8	2.4	3.9	4.5	3.3	3.8	3.8	3.5	3.1
Lu	0.5	0.4	0.6	0.8	0.5	0.6	0.6	0.6	0.5
Hf	6.2	5.7	6.2	10.1	6.2	7.6	7.8	9.4	13.2
Ta	1.9	2.2	1.9	1.8	1.2	1.7	1.7	1.8	1.3
Pb	12.4	14.1	17.1	14.9	35.4	22.3	17.9	27.4	14.6
Th	22.4	18.9	24.3	27.0	15.5	19.9	19.9	21.6	18.8
U	4.5	4.5	5.1	5.3	3.5	4.2	4.2	4.6	3.4
La/Th	2.6	2.5	2.6	2.6	2.9	3.0	2.8	3.0	2.4
La/Sc	4.8	3.7	3.5	4.8	3.2	3.5	3.3	4.0	4.1

Table 8 (continued)

Elements	KB1	KB2	KB3	KB4	KB5	KB6	KB7	KB8	KB9
Th/Co	1.4	1.4	0.9	1.6	0.7	0.9	1.0	1.3	1.2
Th/Sc	1.9	1.5	1.4	1.9	1.1	1.2	1.2	1.3	1.7
$\sum$REE	288.5	255.3	311.3	329.8	207.6	268.0	250.3	275.3	193.4
(Gd_N/Yb_N)	1.9	1.7	1.7	1.4	1.5	1.7	1.6	1.8	1.4
Eu/Eu*	0.7	0.7	0.7	0.5	0.7	0.6	0.6	0.6	0.6

Elements	KB10	KB11	KB12	KB14	KB15	KB16	KB17	KB18	Avg.
Sc	9.3	8.8	14.5	11.4	13.0	17.7	12.7	17.5	13.9
V	51.0	54.7	111.8	90.0	114.3	115.9	93.0	95.4	99.6
Cr	61.0	69.5	109.9	93.9	108.3	128.7	122.0	157.1	111.1
Co	10.6	9.1	3.4	60.3	9.6	13.8	14.6	4.1	17.4
Ni	24.6	23.9	19.2	52.6	31.8	42.1	41.5	31.5	36.7
Cu	17.0	16.7	18.2	23.1	30.7	38.5	23.4	25.2	31.1
Zn	39.8	43.1	31.9	52.1	40.3	44.5	77.2	30.8	56.5
Ga	13.6	11.3	21.3	20.8	24.5	28.3	18.0	26.7	22.2
Rb	89.3	70.8	82.5	102.3	58.0	84.1	121.7	109.1	89.7
Sr	93.9	235.4	77.9	118.1	49.6	44.3	91.7	183.2	100.2
Y	21.0	18.4	28.0	21.4	33.3	24.6	34.2	42.1	29.3
Zr	343.2	410.7	277.5	215.5	335.8	217.6	552.1	481.4	327.1
Nb	17.4	16.9	22.6	18.3	24.2	26.0	20.6	28.6	22.2
Cs	1.5	0.9	4.3	3.8	6.0	8.9	4.1	3.0	4.5
Ba	822.0	768.4	453.4	801.3	262.4	219.2	847.1	1063.3	527.1
La	41.5	59.2	52.9	40.0	62.9	61.3	52.7	83.5	56.6
Ce	74.4	107.0	99.0	91.5	107.9	114.7	96.8	148.1	112.3
Pr	9.0	12.9	11.3	9.2	12.7	11.9	11.5	17.8	12.2
Nd	32.2	45.3	40.3	33.8	44.6	41.1	41.8	62.3	43.2
Sm	5.9	7.8	7.7	6.6	7.9	7.4	7.8	11.5	8.1
Eu	1.0	0.9	1.4	1.5	1.2	1.3	1.4	2.1	1.5
Gd	4.8	5.7	6.3	5.9	6.7	5.9	7.1	9.5	6.7
Tb	0.7	0.8	1.0	0.9	1.1	1.0	1.2	1.6	1.1
Dy	3.8	3.5	5.5	4.7	5.9	5.0	6.1	7.8	5.6
Ho	0.8	0.7	1.2	0.9	1.2	1.0	1.3	1.6	1.2
Er	2.3	2.1	3.3	2.4	3.5	2.8	3.7	4.6	3.3
Tm	0.3	0.3	0.5	0.3	0.5	0.4	0.5	0.6	0.4
Yb	2.3	2.0	3.4	2.2	3.4	2.5	3.6	4.4	3.2
Lu	0.4	0.3	0.5	0.4	0.5	0.4	0.6	0.7	0.5
Hf	9.6	12.1	8.3	5.0	9.5	6.3	15.3	14.0	9.0

(continued)

Table 8 (continued)

Elements	KB10	KB11	KB12	KB14	KB15	KB16	KB17	KB18	Avg.
Ta	1.3	1.2	1.9	1.3	2.0	2.1	1.6	2.1	1.7
Pb	17.5	17.1	15.0	9.8	21.0	22.2	29.7	37.4	20.3
Th	19.2	28.0	23.2	13.7	20.4	24.2	22.2	30.2	21.7
U	2.9	3.7	4.9	4.5	4.3	4.5	5.1	6.5	4.4
La/Th	2.2	2.1	2.3	2.9	3.1	2.5	2.4	2.8	2.6
La/Sc	4.5	6.7	3.7	3.5	4.8	3.5	4.1	4.8	4.2
Th/Co	1.8	3.1	6.7	0.2	2.1	1.7	1.5	7.4	2.1
Th/Sc	2.1	3.2	1.6	1.2	1.6	1.4	1.7	1.7	1.6
$\sum$REE	179.3	248.6	234.3	200.4	259.9	256.6	236.0	356.3	255.9
(Gd_N/Yb_N)	1.7	2.3	1.5	2.1	1.6	1.9	1.6	1.7	1.7
Eu/Eu*	0.6	0.4	0.6	0.7	0.5	0.6	0.6	0.6	0.6
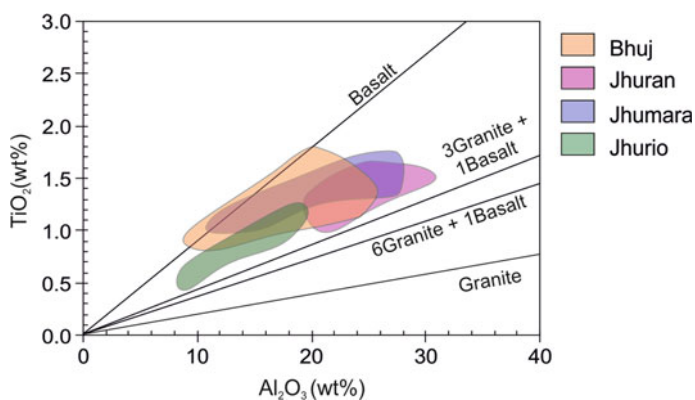
Fig. 3 Source rock discrimination based on TiO_2 versus Al_2O_3 plot (McLennan et al. 1979) for samples of Jhurio, Jhumara, Jhuran and Bhuj formations

of McLennan and Taylor (1991) (Fig. 15). However, a few samples of Jhuran and Bhuj formations occupy the Archean field.

On the basis of detrital zircon and monazite geochronology, Chaudhuri et al. (2020b) for the first time, report source rocks of Archean to Ordovician age (3300–400 Ma) located in the north and north-east of the basin contributed to the Mesozoic sedimentation in the Kutch Basin. While the majority of the age peaks indicate the dominance of post-Archean source rocks for these sediments, younger Jhuran and Bhuj formations exhibit additional older detrital zircon age peaks in the interval of 3300–2800 Ma. Chaudhuri et al. (2020c) report increasing mean T_{DM} in younger formations. Chaudhuri et al. (2020a) report zircon addition in the younger formations. The higher content of Hf in samples of Jhuran and Bhuj formations relates to the relatively high abundance of older zircon (Fig. 13). This increase in abundance of
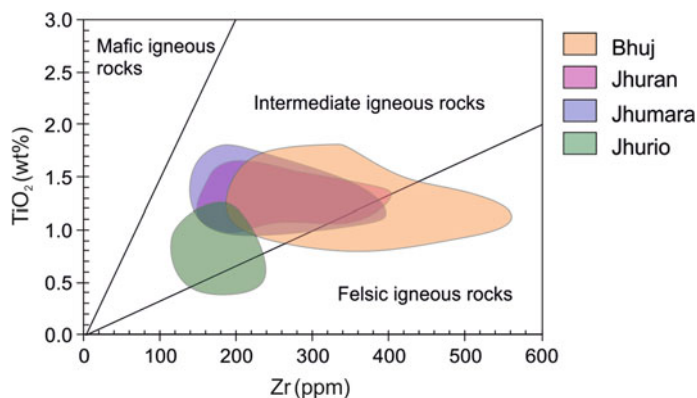
Fig. 4 Source rock discrimination based on TiO_2 versus Zr (ppm) plot (Hayashi et al. 1997) for samples of Jhurio, Jhumara, Jhuran and Bhuj formations
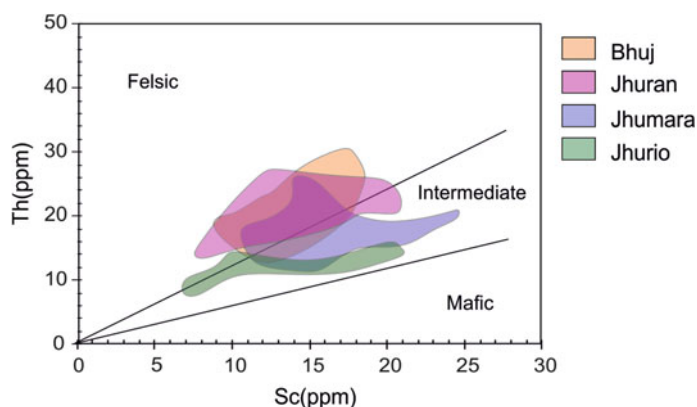
Fig. 5 Source rock discrimination based on Th versus Sc plot (Cullers 2002) for samples of Jhurio, Jhumara, Jhuran and Bhuj formations

older zircon in progressively younger formations indicates the erosional unroofing of older continental basement rocks at passive margins (Floyd and Leveridge 1987). The relationship between Cr and Ni distinguishes Early Archean, Late Archean and Post Archean source rocks (Taylor and McLennan 1985; Wronkiewicz and Condie 1987; McLennan et al. 1993; Etemad-Saeed et al. 2011; Wani and Mondal 2011). Mesozoic samples of Kutch support the predominance of the post-Archean source. Ratios of Eu/Eu* and (Gd_N/Yb_N) distinguish Archean and Post-Archean source rocks (McLennan and Taylor 1991; Armstrong-Altrin et al. 2004; Nagarajan et al. 2007; Singh 2010; Etemad-Saeed et al. 2011). The Mesozoic samples of Jhurio, Jhumara, Jhuran and Bhuj formations corroborate the dominance of post-Archean source rocks. The samples of Jhuran and Bhuj formations indicate sediments from Late Archean (Fig. 14) and Archean (Fig. 15) source rocks.
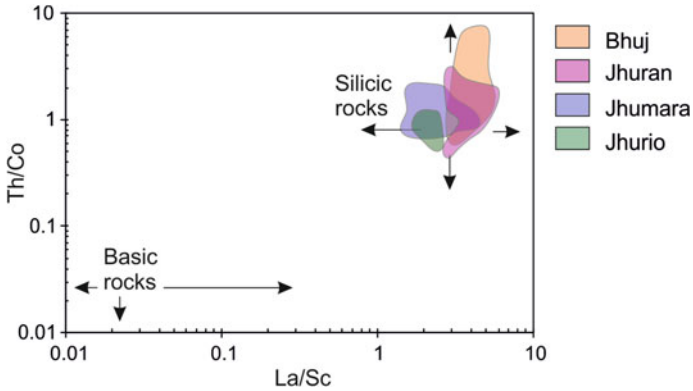
Fig. 6 Source rock discrimination based on Th/Co and La/Sc ratios (Cullers 2002) for samples of Jhurio, Jhumara, Jhuran and Bhuj formations

Fig. 7 Source rock discrimination based on V-Ni-Th × 10 plot (Bracciali et al. 2007) for samples of Jhurio, Jhumara, Jhuran and Bhuj formations
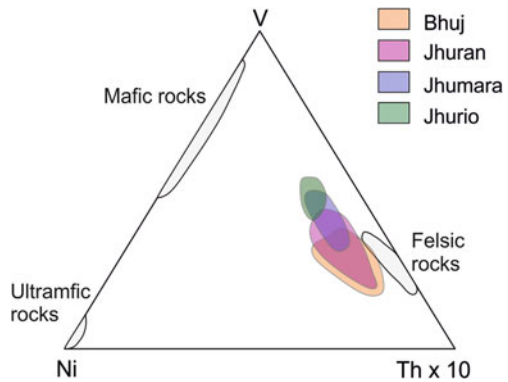
Therefore, the geochemical data broadly supports the data from detrital geochronology. Petrographical evidence, heavy minerals, geochemical and geochronological proxies, and the overwhelmingly south-westerly paleocurrent patterns indicate that the potential source rocks existed northeast and north of the Kutch Basin. These include Precambrian rocks of the Aravalli craton and Nagar Parkar igneous complex (Chaudhuri et al. 2018, 2020a, b, c).

6   Conclusions

(a)   The diversity of the heavy minerals suggests multiple source rocks with evidence of a mixed clastic supply of first-cycle and recycled sandy particles. The ultra-stable rounded heavy detrital minerals could be an indicator
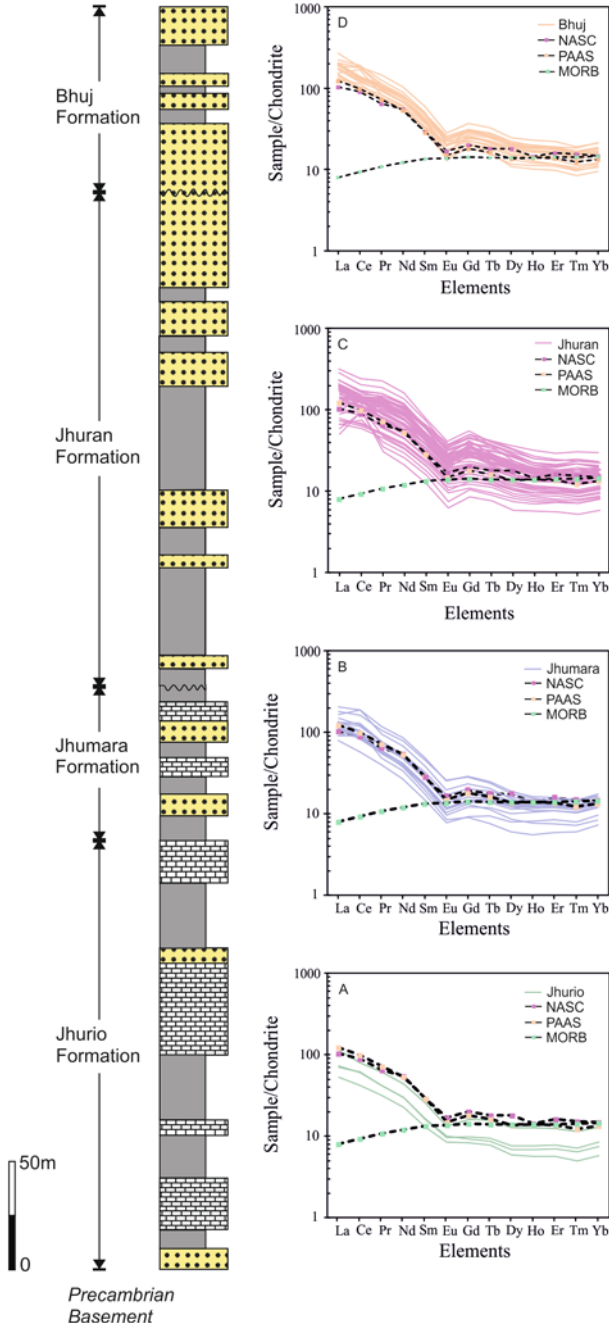
Fig. 8 Composite litholog of the Jhurio, Jhumara, Jhuran and Bhuj formations in the Kutch Mainland (adapted from Biswas 2005; Fürsich et al. 2005; Mandal et al. 2016) along with the chondrite normalised REE patterns of samples of Jhurio, Jhumara, Jhuran and Bhuj formations (solid lines), NASC, PAAS and MORB (dashed lines). Chondrite meteorite values from Boynton (1983). NASC, PAAS and MORB values are from Haskin et al. (1968), Nance and Taylor (1976) and Sun and McDonough (1989), respectively
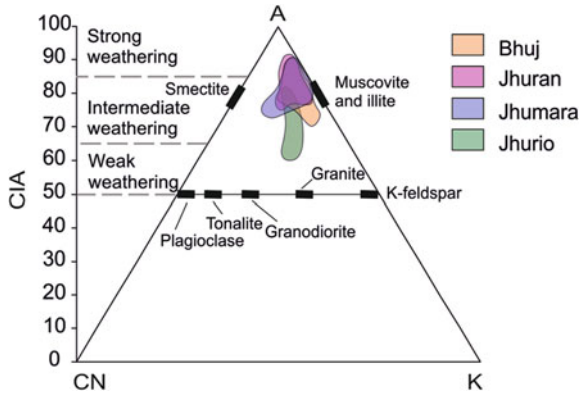
Fig. 9 A-CN-K plot (Nesbitt and Young 1982) indicating the extent of weathering for samples of Jhurio, Jhumara, Jhuran and Bhuj formations
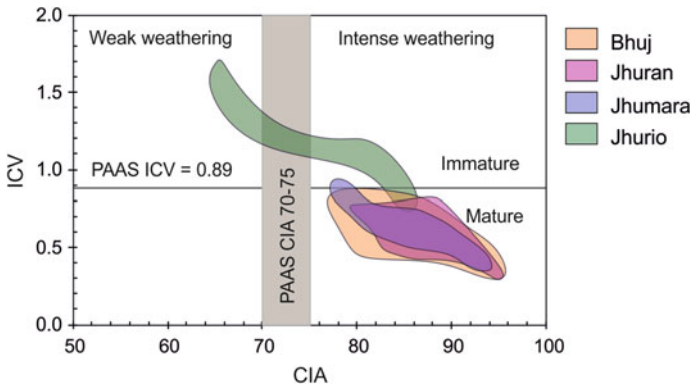
Fig. 10 CIA versus ICV indicating maturity and intensity of weathering (adapted from Long et al. 2012) for samples of Jhurio, Jhumara, Jhuran and Bhuj formations

of prolonged or intense transport other than indicators of the recycled detrital input.

(b) Major oxides (SiO_2/Al_2O_3, Al_2O_3/TiO_2, K_2O/Na_2O) and trace elements (Zr, Th, Sc, Th/Co, Th/Sc and La/Sc) suggest the dominance of felsic source rocks. The LREE enriched chondrite-normalised REE pattern and the negative Eu
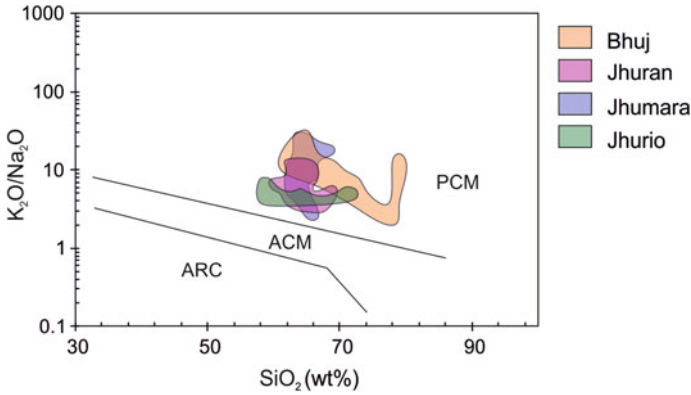
Fig. 11 Tectonic setting discrimination based on K_2O/Na_2O versus SiO_2 plot (Roser and Korsch 1986) for samples of Jhurio, Jhumara, Jhuran and Bhuj formations (PCM = Passive Continental Margin, ACM = Active Continental Margin, ARC = oceanic island arc margin)
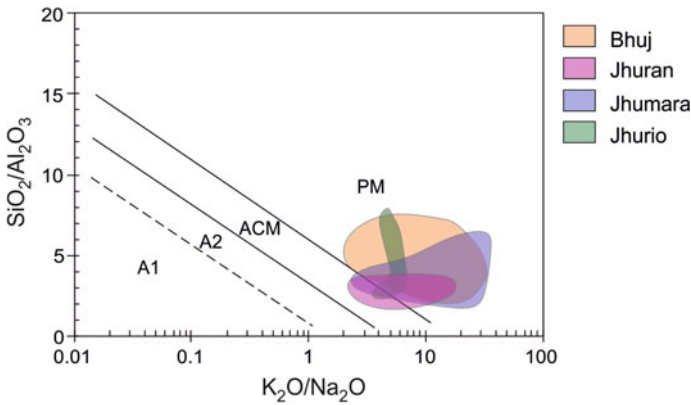
Fig. 12 Tectonic setting discrimination based on SiO_2/Al_2O_3 versus $\log(K_2O/Na_2O)$ plot (adapted from Maynard et al. 1982) for samples of Jhurio, Jhumara, Jhuran and Bhuj formations (PM = Passive continental Margin, ACM = Active Continental Margin, A1, A2 = oceanic island arc margin)

anomaly corroborate the predominance of felsic source rocks. However, the concentration of TiO_2, Al_2O_3, Zr, Th, Sc, suggest a minor mafic input in all samples. The concentrations of V and Ni highlight the presence of mafic input in the older Jhurio and Jhumara formations.

(c) Chemical index of alteration (CIA), plagioclase index of alteration (PIA) and chemical index of weathering (CIW) indicate intermediate to strong weathering of sediments in Jhumara, Jhuran and Bhuj formations and a weak to intermediate weathering for sediments in the Jhurio Formation. The Index of compositional variability (ICV) suggests mature, recycled or highly weathered
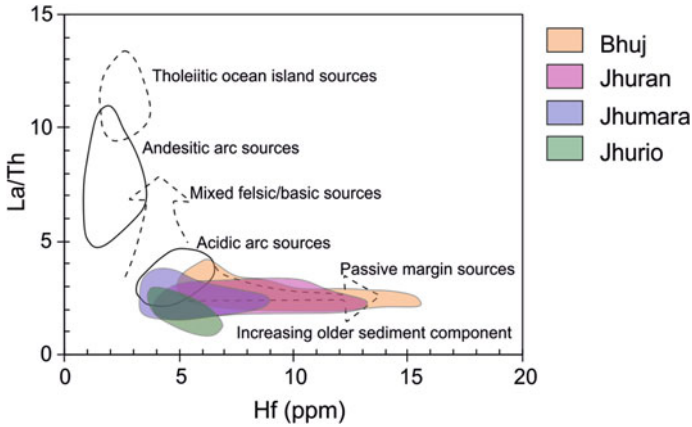
Fig. 13 Tectonic setting discrimination based on La/Th versus Hf plot (Floyd and Leveridge 1987) for samples of Jhurio, Jhumara, Jhuran and Bhuj formations
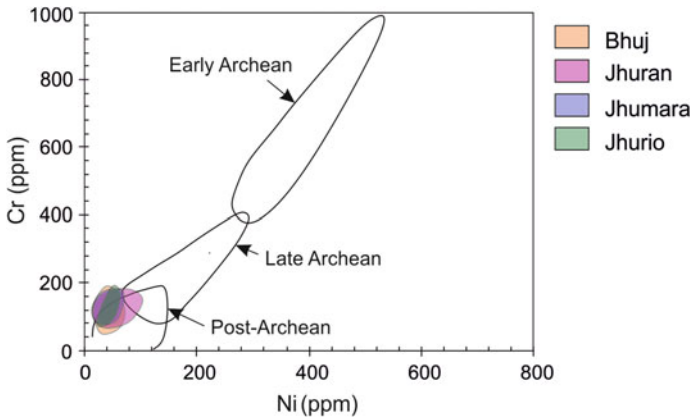
Fig. 14 Plot of Cr versus Ni (Taylor and McLennan 1985) for samples of Jhurio, Jhumara, Jhuran and Bhuj formations

first-cycle sediments in Jhumara, Jhuran and Bhuj formations and immature sediments in the Jhurio Formation.

(d) Major oxides, their ratios (SiO_2, SiO_2/Al_2O_3 and K_2O/Na_2O) and trace elements (La, Th and Hf) indicate a passive continental margin setting for the Mesozoic siliciclastic succession in Kutch Basin.

(e) The concentration of Hf in samples of Jhuran and Bhuj formations high-lights the presence of older input in younger formations suggesting erosional unroofing at the source.

(f) Concentrations of Cr and Ni and the relationship between Eu/Eu* and (Gd_N/Yb_N) indicate the dominance of post-Archean rocks at source area.
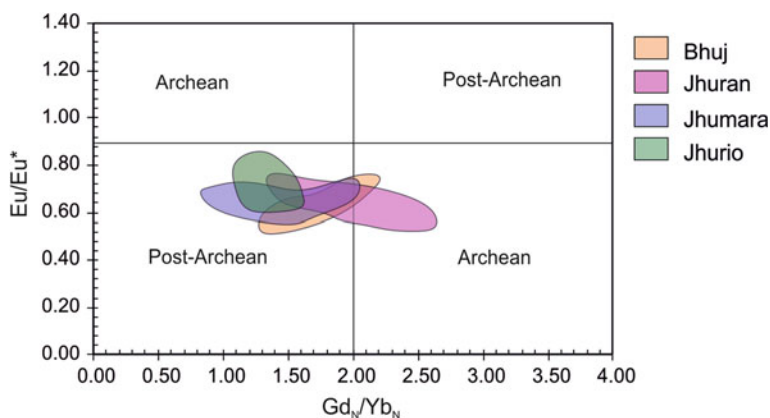
Fig. 15 Plot of Eu/Eu* versus (Gd_N/Yb_N) plot (McLennan and Taylor 1991) for samples of Jhurio, Jhumara, Jhuran and Bhuj formations

However, they also reveal older Archean or late Archean sediment input in younger Jhuran and Bhuj formations. The data corroborate the erosional unroofing, as suggested by Hf concentration. This also supports the results from detrital zircon and monazite geochronology and Nd isotopes in these sediments.

(g) Heavy mineral and geochemical characteristics of Mesozoic sediments indicate Precambrian rocks of the Aravalli craton and Nagar Parkar igneous complex as sources of Mesozoic sediments in the Kutch Basin.

References

Ahmad AHM, Bhat GM (2006) Petrofacies, provenance and diagenesis of the Dhosa Sandstone Member (Chari Formation) at Ler, Kachchh sub-basin, Western India. J Asian Earth Sci 27:857–872

Ahmad AHM, Noufal KN, Masroor AM, Khan T (2014) Petrography and geochemistry of Jumara Dome sediments, Kachchh Basin: implications for provenance, tectonic setting and weathering intensity. Chinese J Geochem 33:9–23

Alberti M, Fürsich FT, Pandey DK (2013) Deciphering condensed sequences: a case study from the Oxfordian (Upper Jurassic) Dhosa Oolite member of the Kachchh Basin, western India. Sedimentol 60:574–598

Amendola U, Perri F, Critelli S, Monaco P, Cirilli S, Trecci T, Rettori R (2016) Composition and provenance of the Macigno Formation (Late Oligocene-Early Miocene) in the Trasimeno Lake area (Northern Apennines). Mar Pet Geol 69:146–167

Andò S, Garzanti E, Padoan M, Limonta M (2012) Corrosion of heavy minerals during weathering and diagenesis: a catalogue for optical analysis. Sediment Geol 280:165–178

Armstrong-Altrin JS, Lee YI, Kasper Zubillaga JJ, Trejo Ramírez E (2017) Mineralogy and geochemistry of sands along the Manzanillo and El Carrizal beach areas, southern Mexico: implications for palaeoweathering, provenance and tectonic setting. Geol J 52:559–582

Armstrong-Altrin JS, Lee YI, Verma SP, Ramasamy S (2004) Geochemistry of sandstones from the upper Miocene Kudankulam Formation, southern India: implications for provenance, weathering, and tectonic setting. J Sed Res 74:285–297

Arora A, Banerjee S, Dutta S (2015) Black shale in late Jurassic Jhuran Formation of Kutch: possible indicator of oceanic anoxic event? J Geol Soc India 85:265–278

Arora A, Dutta S, Gogoi B, Banerjee S (2017) The effects of igneous dike intrusion on organic geochemistry of black shale and its implications: Late Jurassic Jhuran Formation, India. Int J Coal Geol 178:84–99

Bansal U, Banerjee S, Pande K, Arora A, Meena SS (2017) The distinctive compositional evolution of glauconite in the Cretaceous Ukra Hill Member (Kutch basin, India) and its implications. Mar Pet Geol 82:97–117

Bhatia MR, Crook KA (1986) Trace element characteristics of graywackes and tectonic setting discrimination of sedimentary basins. Contrib Min Pet 92:181–193

Biswas SK (1982) Rift basins in the western margin of India and their hydrocarbon prospects with special reference to Kutch basin. AAPG Bull 66:1497–1513

Biswas SK (1987) Regional tectonic framework, structure and evolution of the western marginal basins of India. Tectonophys 135:307–327

Biswas SK (1993) Geology of Kutch, vol 1. KDM Institute of Petroleum Exploration, Dehradun

Biswas SK (2005) A review of structure and tectonics of Kutch basin, western India, with special reference to earthquakes. Curr Sci 88:1592–1600

Biswas SK (1991) Stratigraphy and sedimentary evolution of the Mesozoic basin of Kutch, western India. In: Tandon SK, Pant CC, Casshyap SM (eds) Stratigraphy and sedimentary evolution of western India. Gyanodaya Prakashan, Nainital, pp 74–103

Biswas SK (1977) Mesozoic rock stratigraphy of Kachchh. Q J Geol Min Met Soc India 49:1–52

Biswas SK (1981) Basin framework, palaeo-environment and depositional history of the Mesozoic sediments of Kutch basin, western India. Q J Geol Min Met Soc India 53:56–85

Boynton WV (1983) Cosmochemistry of rare earth elements: meteorite studies. In: Hendersen P (ed) Rare earth element geochemistry. Elsevier, pp 63–114

Bracciali L, Marroni M, Pandolfi L, Rocchi S, Arribas J, Critelli S, Johnsson MJ (2007) Geochemistry and petrography of Western Tethys Cretaceous sedimentary covers (Corsica and Northern Apennines): from source areas to configuration of margins. GSA Spec Pap 420:73–93

Chaudhuri A, Banerjee S, Chauhan G (2020a) Compositional evolution of siliciclastic sediments recording the tectonic stability of a pericratonic rift: Mesozoic Kutch Basin, western India. Mar Petrol Geol 111:476–495

Chaudhuri A, Banerjee S, Le Pera E (2018) Petrography of Middle Jurassic to Early Cretaceous sandstones in the Kutch Basin, western India: implications on provenance and basin evolution. J Palaeogeography 7:2–14

Chaudhuri A, Banerjee S, Prabhakar N, Das A (2020d) The use of heavy mineral chemistry in reconstructing provenance: a case study from Mesozoic sandstones of Kutch Basin (India). Geol J. https://doi.org/10.1002/gj.3922

Chaudhuri A, Chatterjee A, Banerjee S, Ray JS (2020c) Tracing multiple sources of sediments using trace element and Nd isotope geochemistry: provenance of the Mesozoic succession in the Kutch Basin, western India. Geol Mag. https://doi.org/10.1017/S0016756820000539

Chaudhuri A, Das K, Banerjee S, Fitzsimons ICW (2020b) Detrital zircon and monazite track the source of Mesozoic sediments in Kutch to rocks of Late Neoproterozoic and Early Palaeozoic orogenies in northern India. Gond Res 80:188–201

Cox R, Lowe DR, Cullers RL (1995) The influence of sediment recycling and basement composition on evolution of mudrock chemistry in the southwestern United States. Geochim Cosmochim Acta 59:2919–2940

Critelli S, Arribas J, Le Pera E, Tortosa A, Marsaglia KM, Latter KK (2003) The recycled orogenic sand provenance from an uplifted thrust belt, Betic Cordillera, southern Spain. J Sed Res 73:72–81

Critelli S, Ingersoll RV (1994) Sandstone petrology and provenance of the Siwalik Group (northwestern Pakistan and western-southeastern Nepal). J Sed Res 64:815–823

Crook KA (1974) Lithogenesis and geotectonics: the significance of compositional variation in flysch arenites (graywackes). In: Dott RH, Shaver RH (eds) Modern and ancient geosynclinal sedimentation. SEPM Spec Publ 19:304–310

Cullers RL (2002) Implications of elemental concentrations for provenance, redox conditions, and metamorphic studies of shales and limestones near Pueblo, CO, USA. Chem Geol 191:305–327

Cullers RL, Podkovyrov VN (2000) Geochemistry of the Mesoproterozoic Lakhanda shales in southeastern Yakutia, Russia: implications for mineralogical and provenance control, and recycling. Precam Res 104:77–93

Desai BG, Biswas SK (2018) Postrift deltaic sedimentation in western Kachchh Basin: insights from ichnology and sedimentology. Palaeo Palaeo Palaeo 504:104–124

Dickinson WR (1985) Interpreting provenance relations from detrital modes of sandstones. Provenance of arenites. Springer, Dordrecht, pp 333–361

Dickinson WR, Suczek CA (1979) Plate tectonics and sandstone compositions. AAPG Bull 63:2164–2182

Ding H, Ma D, Yao C, Lin Q, Jing L (2016) Implication of the chemical index of alteration as a paleoclimatic perturbation indicator: an example from the lower Neoproterozoic strata of Aksu, Xinjiang, NW China. Geosci J 20:13–26

Etemad-Saeed NA, Hosseini-Barzi MA, Armstrong-Altrin JS (2011) Petrography and geochemistry of clastic sedimentary rocks as evidences for provenance of the Lower Cambrian Lalun Formation, Posht-e-badam block, Central Iran. J African Earth Sci 61:142–159

Fedo CM, Wayne Nesbitt H, Young GM (1995) Unraveling the effects of potassium metasomatism in sedimentary rocks and paleosols, with implications for paleoweathering conditions and provenance. Geology 23:921–924

Floyd PA, Leveridge BE (1987) Tectonic environment of the Devonian Gramscatho basin, south Cornwall: framework mode and geochemical evidence from turbiditic sandstones. J Geol Soc 144:531–542

Fürsich FT, Singh IB, Joachimski M, Krumm S, Schlirf M, Schlirf S (2005) Palaeoclimate reconstructions of the Middle Jurassic of Kachchh (western India): an integrated approach based on palaeoecological, oxygen isotopic, and clay mineralogical data. Palaeo Palaeo Palaeo 217:289–309

Gu XX, Liu JM, Zheng MH, Tang JX, Qi L (2002) Provenance and tectonic setting of the Proterozoic turbidites in Hunan, South China: geochemical evidence. J Sed Res 72:393–407

Harnois L (1988) The CIW index: a new chemical index of weathering. Sediment Geol 55:319–322

Haskin LA, Haskin MA, Frey FA, Wildeman TR (1968) Relative and absolute terrestrial abundances of the rare earths. In: Ahrens LH (ed) Origin and distribution of the elements. Pergamon, pp 889–912

Hayashi KI, Fujisawa H, Holland HD, Ohmoto H (1997) Geochemistry of ~1.9 Ga sedimentary rocks from northeastern Labrador, Canada. Geochim Cosmochim Acta 61:4115–4137

Hubert JF (1962) A zircon–tourmaline–rutile maturity index and the interdependence of the composition of heavy minerals assemblages with the gross composition and texture of sandstones. J Sed Pet 32:440–450

Kasanzu C, Maboko MA, Manya S (2008) Geochemistry of fine-grained clastic sedimentary rocks of the Neoproterozoic Ikorongo Group, NE Tanzania: implications for provenance and source rock weathering. Precam Res 164:201–213

Long X, Yuan C, Sun M, Xiao W, Wang Y, Cai K, Jiang Y (2012) Geochemistry and Nd isotopic composition of the Early Paleozoic flysch sequence in the Chinese Altai, Central Asia: Evidence for a northward-derived mafic source and insight into model ages in an accretionary orogen. Gond Res 22:554–566

López JMG, Bauluz B, Fernández-Nieto C, Oliete AY (2005) Factors controlling the trace-element distribution in fine-grained rocks: the Albian kaolinite-rich deposits of the Oliete Basin (NE Spain). Chem Geol 214:1–19

Löwen K, Meinhold G, Güngör T (2018) Provenance and tectonic setting of Carboniferous-Triassic sandstones from the Karaburun Peninsula, western Turkey: a multi-method approach with implications for the Palaeotethys evolution. Sediment Geol 375:232–255

Mandal A, Koner A, Sarkar S, Tawfik HA, Chakraborty N, Bhakta S, Bose PK (2016) Physico-chemical tuning of palaeogeographic shifts: Bhuj Formation, Kutch, India. Mar Pet Geol 78:474–492

Mange MA, Maurer H (2012) Heavy minerals in colour. Chapman and Hall, London

Maynard JB, Valloni R, Yu HS (1982) Composition of modern deep-sea sands from arc-related basins. Geol Soc London Spec Pub 10:551–561

McDonald DA, Surdam RC (1984) Clastic diagenesis. AAPG Memoir 37:1–434

McLennan SM (1993) Weathering and global denudation. J Geol 101:295–303

McLennan SM, Fryer BJ, Young GM (1979) The geochemistry of the carbonate-rich Espanola Formation (Huronian) with emphasis on the rare earth elements. Can J Earth Sci 16:230–239

McLennan SM, Taylor SR (1991) Sedimentary rocks and crustal evolution: tectonic setting and secular trends. J Geol 99:1–21

McLennan SM, Hemming S, McDaniel DK, Hanson GN (1993) Geochemical approaches to sedimentation, provenance, and tectonics. GSA Spec Pap, pp 21–21

Mcbride EF (1985) Diagenetic processes that affect provenance determinations in sandstone. In: Zuffa GG (ed) Provenance of arenites. NATO ASI Series (Series C: Mathematical and physical sciences). Springer, Dordrecht

Mondal MEA, Wani H, Mondal B (2012) Geochemical signature of provenance, tectonics and chemical weathering in the Quaternary flood plain sediments of the Hindon River, Gangetic plain, India. Tectonophys 566:87–94

Morton AC (1984) Stability of detrital heavy minerals in Tertiary sandstones of the North Sea Basin. Clay Miner 19:287–308

Nagarajan R, Armstrong-Altrin JS, Nagendra R, Madhavaraju J, Moutte J (2007) Petrography and geochemistry of terrigenous sedimentary rocks in the Neoproterozoic Rabanpalli Formation, Bhima Basin, Southern India: implications for paleoweathering conditions, provenance and source rock composition. J Geol Soc India 70:297–312

Nance WB, Taylor SR (1976) Rare earth element patterns and crustal evolution-I. Australian post Archean sedimentary rocks. Geochim Cosmochim Acta 40:1539–1551

Nesbitt HW, Young GM (1982) Early Proterozoic climates and plate. Nature 299:715–717

Ochoa M, Arribas ME, Arribas J, Mas R (2007) Significance of geochemical signatures of provenance in intracratonic rift basins: examples from the Iberian plate. In: Arribas J, Critelli S, Johnsson M (eds) Sedimentary provenance and petrogenesis: perspectives from petrography and geochemistry. GSA Spec Pap 420:99–219

Paikaray S, Banerjee S, Mukherji S (2008) Geochemistry of shales from the Paleoproterozoic to Neoproterozoic Vindhyan Supergroup: implications on provenance, tectonics and paleoweathering. J Asian Earth Sci 32:34–48

Le Pera E, Arribas J, Critelli S, Tortosa A (2001) The effects of source rocks and chemical weathering on the petrogenesis of siliciclastic sand from the Neto River (Calabria, Italy): implications for provenance studies. Sedimentol 48:357–378

Periasamy V, Venkateshwarlu M (2017) Petrography and geochemistry of Jurassic sandstones from the Jhuran Formation of Jara dome, Kachchh basin, India: implications for provenance and tectonic setting. J Earth Sys Sci 126:1–20

Quinby-Hunt MS, Wilde P (1991) The provenance of low-calcic black shales. Mineral Deposit 26:113–121

Roser BP, Korsch RJ (1986) Determination of tectonic setting of sandstone-mudstone suites using content and ratio. J Geol 94:635–650

Saha S, Banerjee S, Burley SD, Ghosh A, Saraswati PK (2010) The influence of flood basaltic source terrains on the efficiency of tectonic setting discrimination diagrams: an example from the Gulf of Khambhat, western India. Sed Geol 228:1–13

Saha S, Burley SD, Banerjee S (2018) Mixing processes in modern estuarine sediments from the Gulf of Khambhat, western India. Mar Pet Geol 91:599–621

Schieber J (1992) A combined petrographical-geochemical provenance study of the Newland Formation, Mid-Proterozoic of Montana. Geol Mag 129:223–237

Scholle PA, Schluger PR (1979) Aspects of diagenesis. SEPM Spec Pub 26

Singh P (2010) Geochemistry and provenance of stream sediments of the Ganga River and its major tributaries in the Himalayan region, India. Chem Geol 269:220–236

Sun W, McDonough WF (1989) Chemical and isotopic systematics of oceanic basalts: implications of mantle composition and processes. Geol Soc London Spec Pub 42:313–345

Taylor SR, McLennan SM (1985) The continental crust: its composition and evolution. Blackwell Scientific Publications, Oxford

Wang C, Zhang L, Dai Y, Lan C (2015) Geochronological and geochemical constraints on the origin of clastic meta-sedimentary rocks associated with the Yuanjiacun BIF from the Lüliang Complex, North China. Lithos 212:231–246

Wani H, Mondal MEA (2011) Evaluation of provenance, tectonic setting, and paleoredox conditions of the Mesoproterozoic-Neoproterozoic basins of the Bastar craton, Central Indian Shield: using petrography of sandstones and geochemistry of shales. Lithosphere 3:143–154

Worden RH, Burley SD (2003) Sandstone diagenesis: the evolution of sand to stone. In: Burley SD, Worden RH (eds) Sandstone diagenesis: recent and ancient. International Association of Sedimentologists, Blackwell Publishing, pp 1–44

Wronkiewicz DJ, Condie KC (1987) Geochemistry of Archean shales from the Witwatersrand Supergroup, South Africa: source-area weathering and provenance. Geochim Cosmochim Acta 51:2401–2416

Yan Z, Wang Z, Yan Q, Wang T, Guo X (2012) Geochemical constraints on the provenance and depositional setting of the Devonian Liuling Group, East Qinling Mountains, Central China: implications for the tectonic evolution of the Qinling Orogenic Belt. J Sed Res 82:9–20

Zhu W, Zheng B, Shu L, Ma D, Wu H, Li Y, Huang W, Yu J (2011) Neoproterozoic tectonic evolution of the Precambrian Aksu blueschist terrane, northwestern Tarim, China: insights from LA-ICP-MS zircon U-Pb ages and geochemical data. Precam Res 185:215–230

Zuffa GG (1987) Unravelling hinterland and offshore paleogeography from deep-water arenites. In: Leggett JK, Zuffa GG (eds) Deep-marine clastic sedimentology: concepts and case studies. Graham and Trotman, London, pp 39–61

Geochemistry of Callovian Ironstone in Kutch and Its Stratigraphic Implications

Udita Bansal, Santanu Banerjee, Gaurav Chauhan, Maxim Rudmin, Dipima Borgohain, and Anjali Upadhyay

Abstract A detailed study of Callovian golden oolites of Jhumara Formation from Keera dome, Kutch basin reveals a similarity in the chemical signature of Jurassic ironstones across the globe. An integrated sedimentological and stratigraphical approach involving petrographical, mineralogical, textural and geochemical analysis was carried out to understand the origin of iron ooids. X-ray diffraction analysis indicates a predominance of goethite, calcite and chamosite. Petrographic investigation reflects oolitic-grainstone microfacies originating in high-energy littoral conditions. The ooids are composed of alternate layers of chamosite and goethite over the carbonate grains, bioclasts and peloids. The geochemical analyses suggest oxidation of chamosite to goethite indicating a fluctuating redox environment from sub-oxic to oxic. The negative correlation of Fe_2O_3 (total) with Al_2O_3, SiO_2 and MgO suggest removal of Al, Si and Mg with increasing Fe. The enrichment of V, Cr, Zn, As, Pb and Th in golden oolites suggests a possible hydrothermal origin of iron. The golden oolites originate by the direct precipitation of hydrothermally-sourced Fe from seawater and accretion of Si, Al and other oxides on suspended nuclei of ooids. The origin and geochemistry of iron oolites in Kutch basin relate to the Jurassic greenhouse condition.

Keywords Jurassic · Ironstone · Golden oolite · Kutch · Chamositic ooid · Jhumara formation

U. Bansal (✉)
Senckenberg Naturhistorische Sammlungen Dresden, Königsbrücker Landstr., 01109 Dresden, Germany
e-mail: uditabansal.geo@gmail.com

S. Banerjee · D. Borgohain · A. Upadhyay
Department of Earth Sciences, Indian Institute of Technology Bombay, Powai 400076, Mumbai, India

G. Chauhan
Department of Earth and Environmental Science, KSKV Kachchh University, Bhuj 370001, Gujarat, India

M. Rudmin
Division for Geology, School of Earth Sciences & Engineering, Tomsk Polytechnic University, 634050 Tomsk, Russia

215

1   Introduction

Oolitic ironstones are prominent sedimentary rocks within transgressive deposits and condensed sections (Van Houten and Bhattacharyya 1982; Van Houten 1992; Taylor et al. 2002, Rahiminejad and Hamed 2018; Rudmin et al. 2020). The ironstone contains >15 wt% iron and >50% ferruginous ooids (Kimberley 1978; Young and Taylor 1989; Petránek and Van Houten 1997; McGregor et al. 2010; Salama et al. 2013). The oolitic (or ooidal) ironstones comprise ooids made of iron silicates such as berthierine and/or chamosite and primary/secondary goethite, hematite and/or siderite (Young 1989; Macquaker et al. 1996; Taylor et al. 2002). Ooids form in both continental and marine environments, by both biotic or abiotic processes (Young and Taylor 1989; Salama et al. 2012). Oolitic ironstones occur throughout the Phanerozoic (Petránek and Van Houten 1997; Mücke and Farshad 2005) but they are more abundant during Ordovician to Devonian and Jurassic to Palaeogene (Young 1992; Petránek and Van Houten 1997; McGregor et al. 2010; Flügel 2010; Rahiminejad and Hamed 2018). Garzanti (1993) considered a link between the stratigraphic preference of ironstone deposits and major global transgressions. Although ooids have been studied extensively, their environment of formation and origin needs further investigation (Young and Taylor 1989; Chan 1992; Young 1992; Burkhalter 1995; Heinkoop et al. 1996; Taylor et al. 2002; Flügel 2010; Salama et al. 2013).

Oolitic ironstones of Jurassic period occur at two stratigraphic levels of the Jhumara Formation; the older one is commonly known as golden oolites of Callovian age (Biswas 1977; Prasad 1993) while the younger one is Dhosa Oolite member of Oxfordian age (Ramkumar et al. 2013). While the origin and global correlation of the oolitic ironstones in the Dhosa Oolite Member have been extensively studied (Ramkumar et al. 2013) those in Callovian golden oolites are yet to be explored. The present study focuses on the Callovian ferruginous or golden oolites of the Jhumara Formation in Kutch basin and explores its stratigraphic implications. Integrated petrographical, mineralogical, textural and geochemical studies were carried out to (a) understand the origin of ferruginous ooids, (b) relate the ooid composition to prevailing physical and chemical conditions, and (c) correlate the origin of ferruginous oolites to their Jurassic equivalents across the world.

2   Geological Background

Kutch basin is a fault-bounded rift basin at the western margin of Indian craton which extends from 22°30′ to 24°30′N and 68° to 72°E (Biswas 2005; Fig. 1). The basin is bounded by Nagar-Parakar ridge, Radhampur arch and Kathiawar uplift to north, east and south respectively (Biswas 1987). The rifting initiated in the Late Triassic (Biswas 1987; Chaudhuri et al. 2018). The Jurassic sequence of the Kutch Mainland comprises Jhurio, Jhumara, Jhuran and Bhuj formations in ascending order (Biswas 1977; Arora et al. 2015; Bansal et al. 2017). The ~275 m thick (Callovian-Oxfordian)
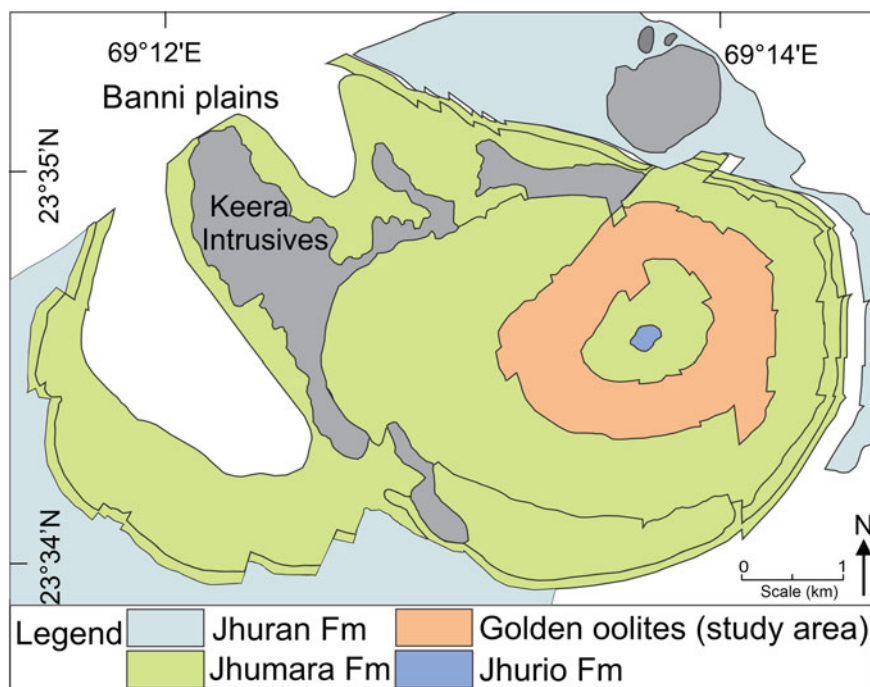
Fig. 1 Geological map of Keera dome showing the study area

Jhumara Formation is exposed as inliers in Habo, Jhurio, Jhumara and Keera domes in mainland Kutch (Biswas 1977). The Jhumara Formation is constituted by planar laminated shale, ferruginous oolite, limestone and sandstone (Biswas 1977; Prasad 1993; Fig. 2). Ferruginous oolite (also known as golden oolite) occurs within limestones and shales in both Jhurio and Jhumara formations in the Keera Dome (Biswas 1977). The present study focuses on the Callovian ferruginous/golden oolites of the Jhumara Formation, exposed in the Keera Dome. The succession in Keera Dome can be roughly sub-divided into two segments. While the lower segment consists of shale, marl, calcareous ferruginous sandstone and golden oolite, the upper part comprises of argillaceous limestone, siltstone and brown oolitic ironstone (Figs. 2 and 3a). The Jhumara Formation is capped by the Keera intrusive and is overlain by the Jhuran Formation. The entire succession is highly fossiliferous consisting of cephalopods, gastropods, bivalves, brachiopods, corals, bryozoans, crinoids, belemnites and ammonites (Biswas 1977). The golden oolites are highly bioturbated containing abundant *Ophiomorpha* burrows (Fig. 3b). The ooidal ironstones show cross-stratifications in many places (Fig. 3c). A shallow marine origin of the oolitic deposits has been inferred by the previous workers (Biswas 1977; Prasad 1993).

Jhuran Formation
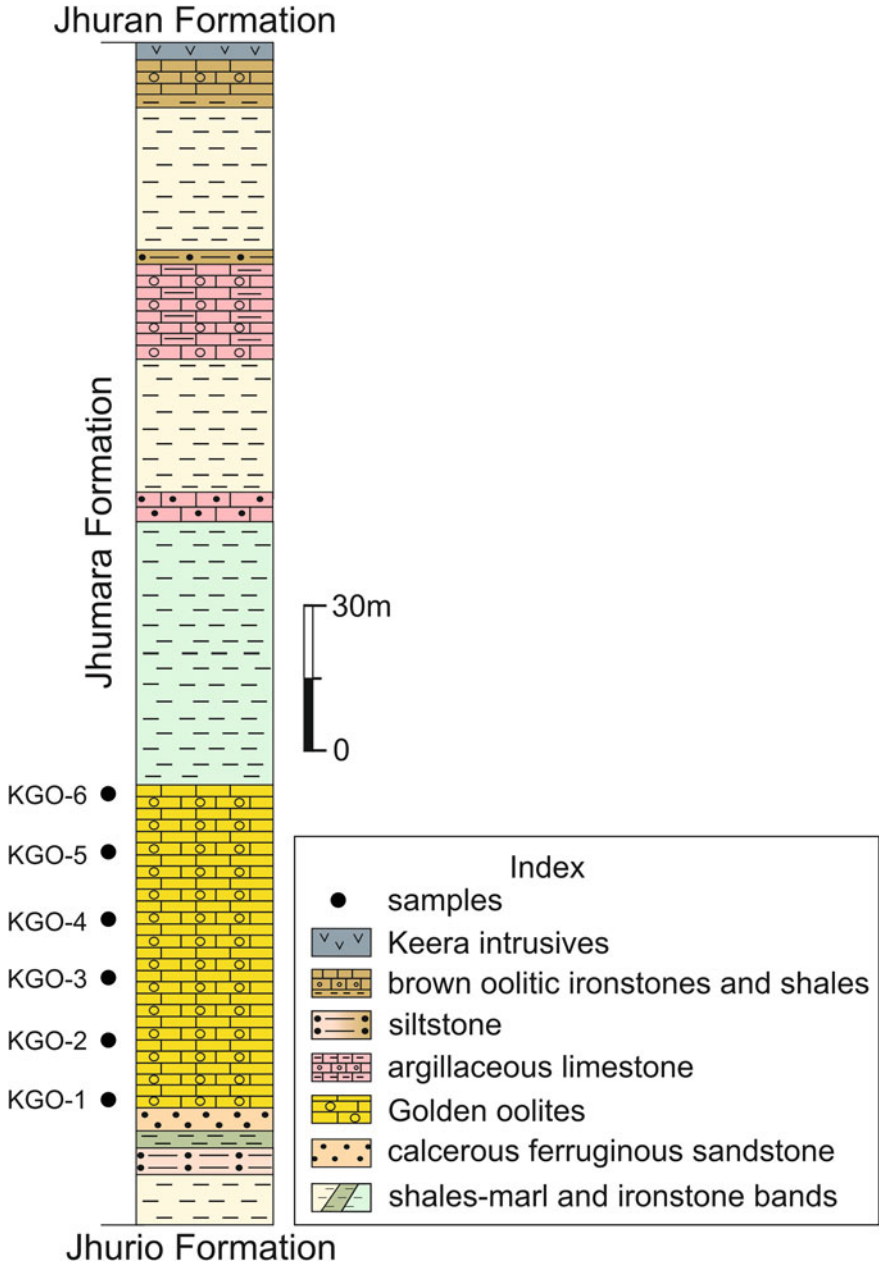
Fig. 2 Lithology of Jhumara Formation, Keera dome, Kutch basin (adapted from Prasad 1993)
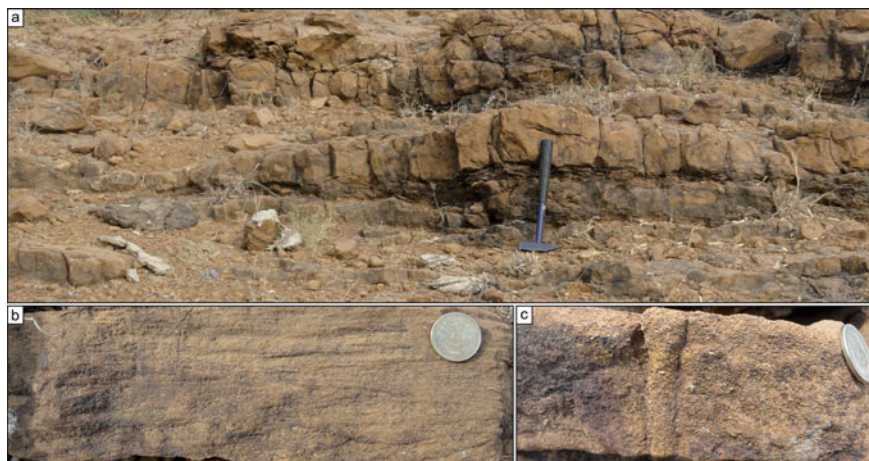
Fig. 3 Field photographs of golden oolites showing **a** oolitic grainstone beds **b** bioturbated ironstone and **c** trough cross-stratified nature (hammer length = 38 cm, coin diameter = 2.3 cm)

3 Samples and Methods

Six samples were collected from golden oolites of the Jhumara Formation at Keera dome, located 50 km NW of Bhuj. Petrographic observations were carried out using Leica DM 4500P polarizing microscope with 1.25x, 2.5x, 5x, 10x, 20x and 40x objectives at Department of Earth Sciences, Indian Institute of Technology Bombay. For the X-Ray diffraction (XRD) analysis, samples were powdered in agate mortar and scanned from 4° to 70° with a step size of 0.0130° 2θ and a scan speed of 96 s/step, using nickel filter copper radiation in an Empyrean X-Ray Diffractometer with Pixel 3D detector at Department of Earth Sciences, Indian Institute of Technology Bombay. Samples were scanned each time after removal of carbonate and separation of clays under the same instrumental setting in air-dried mode, after ethylene glycol treatment and after heating at 490 °C for 2 h. Ironstone chips for SEM-EDS study were platinum coated by sputters coater and studied by a JSM-7600F Scanning Electron Microscope at Sophisticated Analytical Instrumental Facility at Indian Institute of Technology Bombay. The chemical composition was determined by using the Camera SX-100 electron microprobe at Department of Earth Sciences, Indian Institute of Technology Bombay. Multiple points were analyzed with 1 nm beam diameter (peak: 10–20 s and background counting: 5–10 s) with accelerating voltage 15 kV, specimen current of 40 nA. All 62 data points were selected under reflected light along with the back-scattered image control. Minerals, as well as synthetic phases, were used for standards. For major oxide and trace element studies, selected six samples were powdered, made into pellets and analyzed using X-Ray Fluorescence at National Geophysical Research Institute, Hyderabad.

4 Results

4.1 Petrography

Quartz, calcite, goethite and clay minerals (chamosite) dominate the oolitic to bioclastic grainstones (Fig. 4a). Most ooids are round to ellipsoidal in shape with
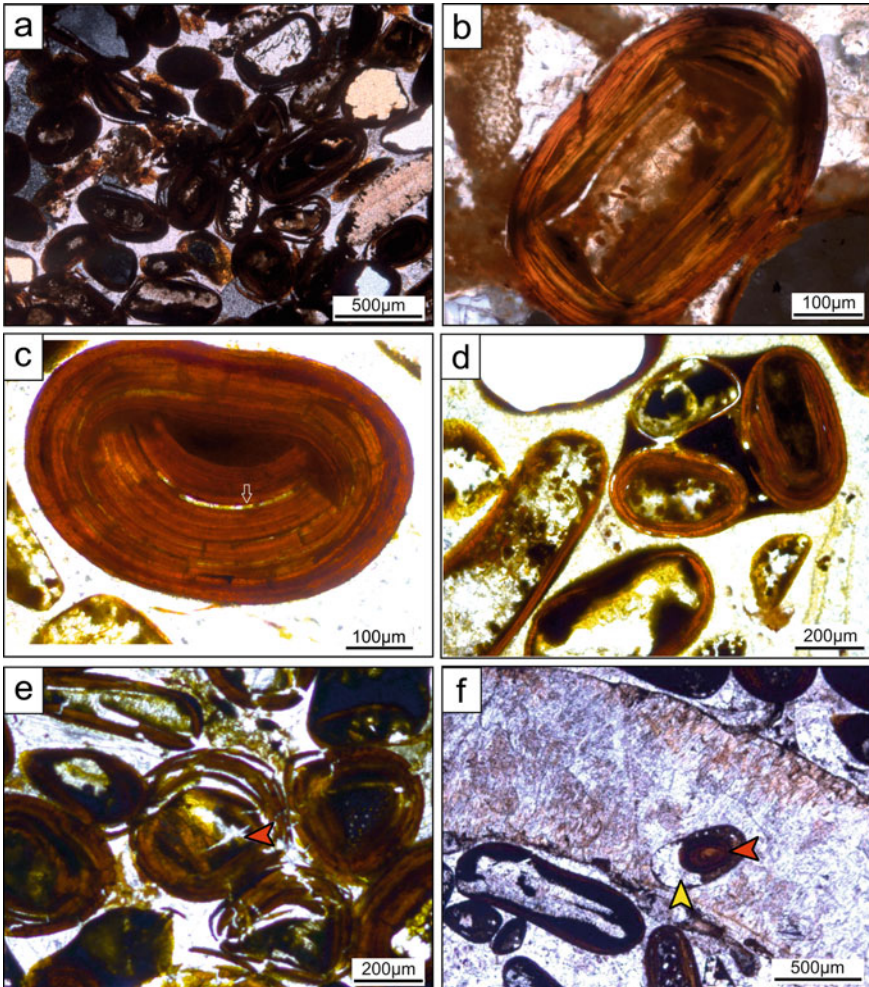
Fig. 4 Photomicrographs of golden oolites showing **a** oolitic grainstone microfacies, **b** ellipsoidal ooid with perfect concentric laminae of iron, **c** fragmented ooid with alternate light and dark laminae (marked by black arrow), **d** composite ooid composed of three ooids, **e** deformed ooid (marked by red arrow) possibly related to compaction and **f** micro-boring within bioclast filled with ooid and spar (marked by red and yellow arrows respectively)

regular concentric laminae (Fig. 4a), and alternate light and dark bands of iron-rich minerals (Fig. 4b). The size of the ooid ranges from 0.2 to 0.5 mm. A nucleus in most ooids consists of carbonate intraclast, quartz, shells fragment, peloid or broken ooid, while their cortex is composed of ferruginous phyllosilicates and/or iron (hydro-)oxides. Although most ooids are intact, a few broken or fragmented ooids are found (Fig. 4c). The broken ooid is re-coated by iron oxide with alternating light and dark laminae (Fig. 4c). Occasionally, a composite ooid comprising of 2–3 ooids may occur indicating its regrowth (Fig. 4d). Few ooids are completely deformed, and their laminae are detached from their nuclei (Fig. 4e). Secondary spar cementation is common around the ooids. Micro-borings commonly occur within the nuclei of ooids and the bioclasts (Fig. 4f). Most bioclasts show micritic envelopes. The shells are often completely replaced by either iron oxide or calcite. Interparticle porosity is mostly occupied by calcite and iron oxide cements. Calcite is equant in nature exhibiting syntaxial overgrowth. Many grains exhibit geopetal structures indicating the depositional top.

4.2 Mineralogical and Textural Study

XRD of whole rock exhibits the characteristic peaks of goethite at 4.18, 2.69, 2.45, and 1.72 Å and calcite at 3.03 Å (Fig. 5a). XRD of clay size-fraction of ooids in air-dried mode exhibits the basal reflections (001) at 14.3 Å, (002) at 7.18 Å, (003) at 4.74 Å and (004) at 3.55 Å (Fig. 5b). The peaks are sharp, intense and narrow. Upon ethylene glycolation, the (001) reflection remains stationary, while the (002) and (003) reflections exhibit negligible shifts from 7.15 Å to 7.08 Å and from 3.55 Å
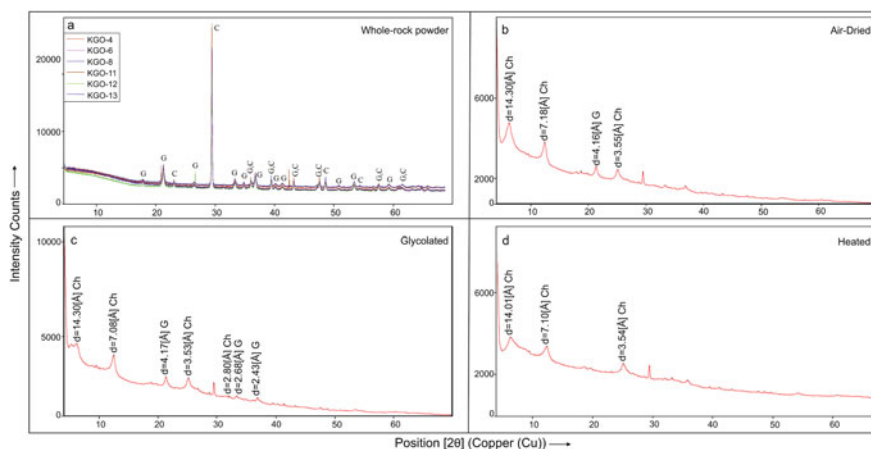
Fig. 5 X-Ray Diffractograms of **a** whole-rock powder and **b** clay size-fraction of ooids in air dried mode, **c** glycolated and **d** heated at 400 °C showing the predominance of chamosite (Ch), goethite (G) and calcite (C)
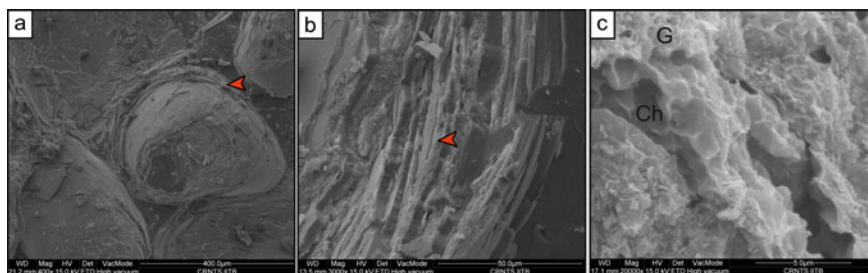
Fig. 6 SEM images of golden oolites showing **a** arrangement of ooids, **b** an enlarged view of cortex of an ooid (marked by red arrow in **a**) and **c** an enlarged view of thin lamination of an ooid (marked by red arrow in **b**)

to 3.53 Å, respectively (Fig. 5c). Peaks remain sharp and intense upon glycolation. After heating at 400 °C the (001) peak shifts to 14.01 Å, (002) peaks shifts to 7.10 Å and (004) shifts to 3.54 Å (Fig. 5d). Peaks become less intense and broad-based after heating. The systematic shift of (001) basal reflection from 14.3 Å (air-dried) to 14.01 Å (heating) and weak (002), (003) and (004) reflections indicates chamosite (Fe-rich chlorite). Subsidiary peak at 4.16 Å represent goethite (G). The oolitic grainstones, therefore, include chamosite and goethite beside calcite.

SEM investigation further reflects the growth of chamosite and goethite as very fine laminae over the ooid nuclei (Fig. 6a, b). Goethite exhibits radiating needle-like crystals over the clay mineral (Fig. 6c). EDS data of goethite exhibit the high content of Fe, with minor Si, Al and Mg (Fig. 7a). Clay minerals exhibit high contents of Fe, Si, Al, Mg and Ca, indicating chamosite (Fig. 7b). The high Ca content in the latter relates to the bioclasts.

4.3 Geochemical Analysis

Table 1 presents the major oxide of six bulk rock samples using XRF. The major oxide data of ooidal ironstones indicate their enrichment in Fe_2O_3 (total) ranging from 36.72 to 61.37% and CaO varying from 24.53 to 40.64%. The SiO_2 content of the ironstone ranges from 3.77 to 6.34%, while the Al_2O_3 content varies from 3.28 to 4.29%. The MgO content ranges from 1.0 to 1.2%. The slightly high SiO_2, Al_2O_3, and MgO contents relate to the presence of chamosite within the ooids. The studied ooidal ironstone, therefore, belongs to chamosite-type (cf. Mücke and Farshad 2005). The high P_2O_5 content (av. 0.64%) relates to phosphatic shells (cf. Mücke and Farshad 2005).

The major oxide spot analysis of Fe-bearing phases reveals two varieties. One with oxy-hydroxide phase that consists of Fe_2O_3 (total) (av. 70.41%) with minor amounts of SiO_2 (av. 3.85%), Al_2O_3 (av. 5.27%) and MgO (av. 1.23%). The average Na_2O, K_2O, P_2O_5, MnO and TiO_2 contents are insignificant (<1%) (Table 2). The other
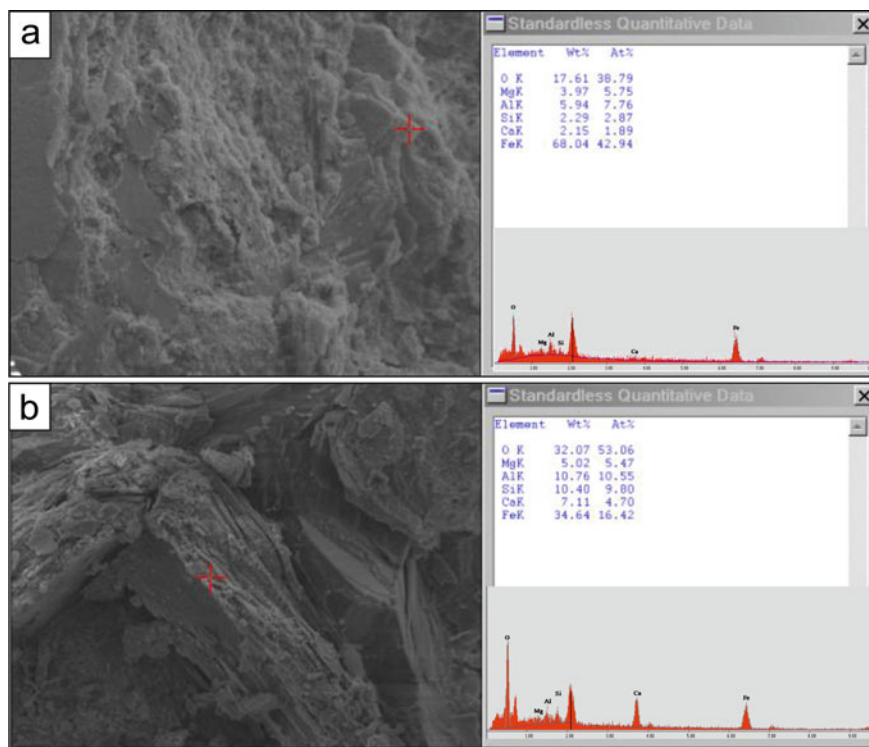
Fig. 7 EDS spectra and element composition of **a** goethite revealing high Fe and minor Si, Al, Mg and **b** chamosite reflecting high Fe, Si, Al, Mg and Ca

Table 1 Oxide weight percentage of golden oolites measured by XRF

Major oxides (%)	MgO	Al$_2$O$_3$	SiO$_2$	P$_2$O$_5$	K$_2$O	CaO	TiO$_2$	MnO	Fe$_2$O$_3$ (total)
KGO-1	1.1	4.3	4.3	0.6	0.1	24.5	0.1	0.2	60.6
KGO-2	1.2	4.2	6.3	0.3	0.2	40.6	0.1	0.1	36.7
KGO-3	1.0	4.1	4.1	0.6	0.1	24.8	0.1	0.2	61.4
KGO-4	1.1	3.3	3.8	0.5	0.1	38.1	0.1	0.2	44.2
KGO-5	1.2	3.7	4.6	0.4	0.1	34.3	0.1	0.2	48.7
KGO-6	1.2	3.4	4.4	0.5	0.1	38.0	0.1	0.2	44.2

Fe-bearing phase contains clay minerals consisting of Fe$_2$O$_3$ (total) (35.01%), SiO$_2$ (22.55%), Al$_2$O$_3$ (13.93%) and MgO (6.51%) (Table 2). The chemical composition of each phase relates closely to goethite in former and chamosite in the latter. The analysis reveals that the goethite phase dominates over the chamosite.

The Fe$_2$O$_3$ (total) content of ooids exhibits a significant negative correlation with Al$_2$O$_3$, SiO$_2$ and MgO (Fig. 8a–c). In all the plots, goethite and chamosite occupy the

Table 2 Oxide weight percentage spot analysis of golden oolites measured by EPMA

Sample/Point	Na$_2$O	MgO	Al$_2$O$_3$	SiO$_2$	P2O$_5$	K$_2$O	CaO	TiO$_2$	MnO	Fe$_2$O$_3$ (total)	Total
Goethite											
KGO-2 1/1	0.04	1.14	5.64	3.74	0.67	0.20	0.29	0.16	0.13	73.37	85.38
2/1	0.01	0.93	6.73	5.38	0.44	0.41	0.22	0.26	0.08	70.69	85.15
3/1	0.09	0.96	6.78	5.55	0.40	0.43	0.28	0.20	0.13	69.02	83.83
4/1	0.14	3.84	8.86	9.85	0.38	0.52	0.25	0.24	0.03	57.04	81.14
5/1	0.06	0.86	4.74	1.61	0.64	0.01	0.27	0.19	0.03	68.74	77.15
6/1	0.03	0.66	3.35	1.65	0.41	0.03	0.31	0.20	0.06	63.63	70.33
7/1	0.04	0.79	3.98	1.86	0.58	0.00	0.68	0.24	0.07	76.79	85.03
8/1	0.04	0.95	3.07	2.78	0.91	0.00	0.55	0.09	0.11	77.46	85.93
12/1	0.08	0.79	3.76	2.07	1.03	0.03	1.28	0.16	0.14	71.54	80.87
13/1	0.13	0.76	4.94	1.79	0.59	0.04	0.35	0.20	0.02	69.29	78.10
14/1	0.13	0.83	4.18	2.16	0.58	0.02	0.39	0.17	0.11	68.82	77.38
15/1	0.05	1.18	5.37	3.26	0.61	0.14	0.22	0.23	0.03	65.13	76.22
16/1	0.13	1.12	4.77	2.06	0.87	0.04	0.90	0.12	0.17	76.05	86.21
17/1	0.13	1.15	4.67	2.17	1.14	0.03	0.73	0.09	0.09	76.85	87.04
20/1	0.05	0.91	5.20	3.51	0.64	0.08	0.35	0.12	0.07	69.42	80.34
21/1	0.05	0.89	3.91	3.13	0.99	0.08	0.33	0.12	0.15	78.36	88.00
KGO-3 6/1	0.22	1.21	3.43	3.51	0.86	0.06	0.40	0.03	0.16	74.53	84.40
7/1	0.13	1.02	4.30	3.61	0.92	0.08	0.28	0.04	0.10	74.45	84.92
8/1	0.08	0.95	4.40	3.64	0.78	0.10	0.36	0.12	0.09	73.97	84.50
9/1	0.05	0.87	4.26	4.06	0.78	0.13	0.48	0.15	0.07	74.50	85.34
10/1	0.53	0.90	5.79	3.07	0.82	0.27	0.76	0.18	0.04	71.59	83.96
11/1	0.03	0.83	4.75	2.74	0.66	0.05	0.60	0.19	0.05	65.15	75.04
18/1	0.11	1.45	5.92	3.76	0.82	0.14	1.37	0.13	0.18	69.92	83.78
20/1	0.02	0.74	4.39	1.91	0.65	0.02	0.34	0.16	0.10	64.60	72.92
21/1	0.12	0.84	4.65	2.43	0.75	0.02	0.55	0.08	0.07	66.89	76.40
27/1	0.17	1.09	4.59	2.27	1.05	0.04	0.94	0.10	0.14	72.87	83.25
28/1	0.09	1.18	5.89	2.48	1.11	0.11	1.37	0.10	0.08	70.33	82.73
29/1	0.11	3.31	9.76	10.52	0.46	0.60	0.45	0.12	0.04	51.83	77.19
30/1	0.00	1.04	5.31	2.28	0.64	0.07	0.36	0.21	0.09	60.69	70.69
31/1	0.06	0.68	4.20	2.36	0.76	0.02	0.42	0.23	0.14	71.20	80.05
32/1	0.11	0.32	2.05	1.60	0.97	0.04	0.75	0.10	0.03	67.55	73.51
38/1	0.09	1.04	4.08	2.94	1.12	0.05	0.47	0.08	0.15	73.32	83.33
39/1	0.19	4.54	12.05	15.00	0.32	0.66	0.89	0.12	0.04	53.12	86.92
40/1	0.14	1.00	3.72	2.61	0.97	0.05	0.33	0.08	0.17	73.96	83.02
41/1	0.09	1.19	7.78	8.10	0.36	0.63	0.20	0.12	0.13	65.67	84.27
42/1	0.10	1.93	7.51	6.62	0.38	0.36	0.23	0.17	0.25	67.30	84.84

(continued)

Table 2 (continued)

Sample/Point	Na$_2$O	MgO	Al$_2$O$_3$	SiO$_2$	P$_2$O$_5$	K$_2$O	CaO	TiO$_2$	MnO	Fe$_2$O$_3$ (total)	Total
43/1	0.05	1.05	8.85	8.91	0.42	0.63	0.15	0.25	0.13	65.97	86.40
44/1	0.15	1.15	5.49	3.35	0.98	0.13	0.25	0.13	0.09	73.91	85.61
45/1	0.05	1.00	6.14	3.65	0.31	0.14	0.17	0.12	0.15	59.70	71.43
46/1	0.22	1.10	3.16	1.87	1.18	0.02	0.27	0.00	0.11	75.75	83.69
47/1	0.18	1.39	3.37	1.67	1.15	0.00	0.27	0.00	0.15	75.32	83.49
KGO-4 1/1	0.10	4.93	12.83	17.54	0.19	0.34	0.66	0.03	0.08	52.36	89.06
4/1	0.11	2.27	9.07	9.88	0.31	0.36	0.63	0.11	0.13	65.11	87.98
7/1	0.11	0.84	3.91	2.24	0.73	0.03	0.51	0.21	0.10	74.88	83.55
KGO-5 5/1	0.07	0.65	4.15	1.94	0.62	0.00	0.35	0.15	0.09	75.84	76.35
6/1	0.09	0.76	3.87	2.26	0.64	0.02	0.33	0.13	0.12	72.54	73.57
7/1	0.05	0.73	4.99	1.21	0.47	0.01	0.68	0.26	0.05	72.21	73.51
9/1	0.11	1.13	4.35	2.45	0.80	0.03	0.83	0.07	0.20	78.26	80.47
12/1	0.10	1.19	6.98	4.78	0.63	0.32	0.70	0.23	0.08	74.14	81.80
15/1	0.17	1.58	2.08	2.36	0.77	0.01	0.25	0.00	0.08	75.83	75.60
16/1	0.10	1.39	2.54	2.29	0.74	0.03	0.25	0.03	0.07	76.77	76.60
17/1	0.10	0.81	4.05	1.74	0.52	0.03	0.21	0.17	0.06	74.42	74.74
18/1	0.03	0.68	4.09	2.27	0.65	0.01	0.35	0.14	0.07	75.39	76.22
22/1	0.04	0.95	4.30	2.43	0.46	0.00	0.39	0.11	0.10	73.73	75.20
24/1	0.02	1.01	6.41	2.45	0.44	0.09	0.34	0.23	0.04	76.39	79.86
25/1	0.06	0.94	6.31	2.74	0.47	0.12	0.60	0.18	0.06	77.54	81.34
27/1	0.03	0.80	4.88	3.66	0.41	0.19	0.58	0.16	0.11	71.65	75.37
Chamosite (KGO 4-5)											
1/1	0.15	7.23	16.11	28.68	0.00	0.75	0.57	0.00	0.07	38.16	87.94
2/1	0.12	6.95	13.84	21.79	0.07	0.31	9.54	0.00	0.04	30.60	83.26
16/1	0.11	5.09	11.89	17.05	0.11	0.31	8.32	0.03	0.04	39.90	82.86
17/1	0.15	6.78	13.87	22.71	0.02	0.35	8.30	0.04	0.00	31.39	83.61

two ends of the correlation line (Fig. 8a–c). The transition of chamosite to goethite, therefore, involves the addition of Fe in latter with simultaneous removal of Si and Mg (Fig. 8). EPMA back-scattered electron (BSE) image further depicts compositional transition between chamosite and goethite layers (Fig. 9a). The X-ray mapping of Fe reveals a progressive increase of Fe$_2$O$_3$ (total) from inner to outer layers of cortex (Fig. 9b). The X-ray mapping of Ca exhibits high CaO in nuclei (Fig. 9c) consisting of calcium carbonate. The high average CaO content (6.68%) in chamosite, therefore, relates to the presence of bioclasts.

The trace elements concentrations of V, Cr, Ce, Zr, As, Cu, Sr, Y, Zn and Pb are normalized with Upper Continental Crust (UCC) (Taylor and Mclennan 1985) (Table 3). The UCC-normalized trace element data reveal that an enrichment of V,
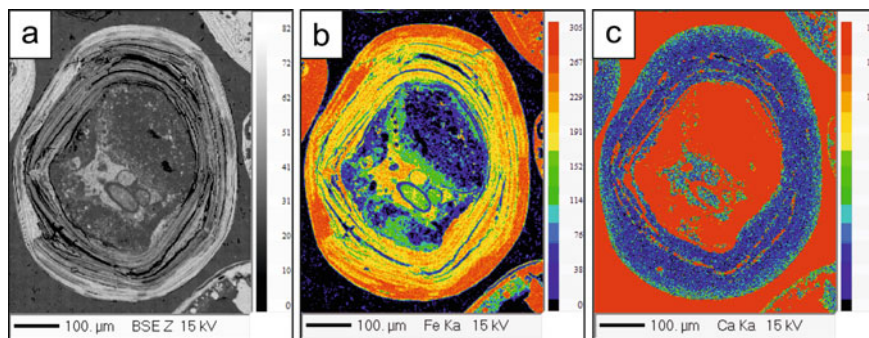
Fig. 8 EPMA (BSE) image (**a**), X-ray Fe mapping (**b**) and X-ray Ca mapping (**c**) of an ooid. Note the change in composition of ooid from chamosite to goethite
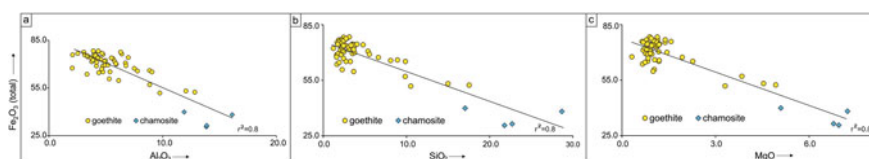
Fig. 9 Cross-plots of Fe_2O_3 (total) with (**a**) Al_2O_3, (**b**) SiO_2 and (**c**) MgO

Table 3 Trace elements concentrations of golden oolites, measured by XRF

Trace elements (ppm)	KGO-1	KGO-2	KGO-3	KGO-4	KGO-5	KGO-6
V	1240	1035	1261	900	1020	993
Cr	329	287	349	243	287	267
SO_3	847	391	936	308	360	472
Zn	218	163	206	263	222	268
As	181	90	188	110	110	133
Sr	324	412	305	486	512	647
Y	57	82	64	75	59	66
Zr	122	97	122	84	94	85
Pb	164	82	97	102	115	121

Cr, Zn, As, Y, Pb and Th in golden oolites samples while Zr is highly depleted (Fig. 10a). A cross-plot of trace elements Cr, Zn, Zr, As and Pb with Fe_2O_3 (total) reveals a significantly positive correlation (Fig. 10b). The depletion of detrital-derived Zr suggests negligible terrestrial input during the formation of oolites. High contents of V, Cr, Pb, Zn, As, Pb, Th indicates hydrothermal or volcanic origin (Baioumy et al. 2014; Garnit and Bouhlel 2017).
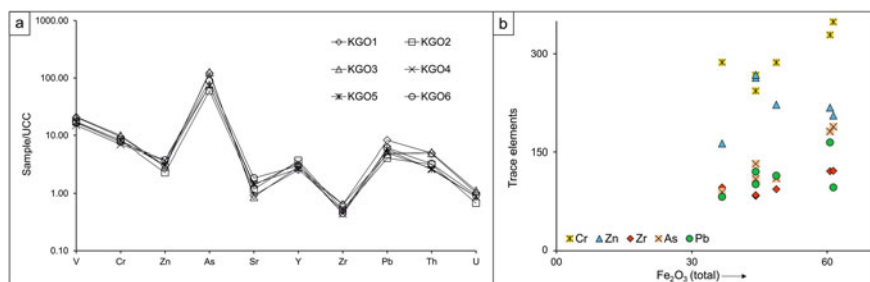
Fig. 10 UCC-normalized trace elements of samples of golden oolites (adapted from Taylor and McLennan 1985) (**a**) and a cross-plot of trace elements with Fe_2O_3 (total) revealing positive correlation (**b**)

5 Discussion

Oolitic ironstones are often related to the sea-level fluctuations, and therefore, are significant stratigraphic markers (Curial and Dromart 1998; Van Houten and Arthur 1989; Jacquin et al. 1998; Taylor et al. 2002; Reolid et al. 2008). Young (1989) and Garzanti (1993) proposed a link between the stratigraphic distribution of Phanerozoic oolitic ironstone deposits to periods of global oceanic anoxia and greenhouse climate. Recently, Rudmin et al. (2019, 2020) demonstrated a close correspondence between the occurrence of ironstones and warming events. They also found the dependence of ironstone mineralogy on redox conditions and iron influx. Most Mesozoic oolitic ironstones are chamosite-type and predominantly deposited in Early Jurassic to Middle Cenozoic (e.g. Van Houten and Bhattacharyya 1982; Boggs 2009; Mücke and Farshad 2005; Mücke 2006; Rahiminejad and Hamed 2018). The ironstones of Kutch (Keera Dome) contain ooids, rich in Fe content (~70%), with an admixture of Al_2O_3 and SiO_2 (Tables 1 and 2) and trace elements Th, Zr, Cr, P, V, As and Zn (Table 3). These oolitic ironstones are very similar to chamosite-type ironstones of Mücke and Farshad (2005).

A review of Jurassic oolitic ironstones (Table 4 and Fig. 11) suggests their deposition in a shallow marine environment, close to the palaeo-shoreline. The oolitic grainstones in Jhumara Formation, showing cross-stratifications, represent very shallow-marine depositional environment (Biswas 1977). The medium-size of ooids (0.2–0.5 mm) and co-occurrence of complete and composite ooids (broken ooids acting as nuclei for new ooids) further corroborate the littoral setting (Biswas 1977). The highly bioturbated nature of the ironstone in Jhumara Formation indicate a low rate of sediment supply. The concentric lamination and round to ellipsoidal shape of ooids suggest the accretion of Fe, Si, Al and a minor quantity of other oxides on nuclei as a result of direct precipitation from seawater (cf. Hemingway 1974; Baioumy et al. 2017; Garnit and Bouhlel 2017). The oxidizing condition of ooids corresponds well with the conversion of chamosite to goethite (Porrenga 1965; Taylor et al. 2002; Tang et al. 2018). The ooids, therefore, represent fluctuating redox conditions with initial

Table 4 Occurrence of Jurassic oolitic ironstones along with mineralogical and geochemical characterization, environment of deposition, origin of ironstones and source of iron

S. no.	Stratigraphic unit	Age	Mineralogy	Geochemical characterization	Depositional environment	Origin of ironstones/source of iron	References	Additional remarks
1	Gifhorn ooidal ironstone, Konrad shaft, Germany	Late Oxfordian	Goethite ooids, late calcite, diagenetic magnetite	High Si, Al, Fe, Ca, P	–	–	Mücke and Farshad (2005), Simon (1965)	ferruginized chamosite sub-type of Mücke and Farshad (2005)
2	Coralline beds, Southern England	Upper Oxfordian	Chamosite ooid with siderite mud	–	Offshore shelf to lagoonal	Maybe weathering product; no conclusive proof	Talbot (1974)	Very low rate of sediment supply
3	Dhosa Oolites, Kutch basin, India	Oxfordian	Ferruginous ooid with calcite in matrix or cement	–	Shallow coastal shoal	Diagenetic replacement of calcitic ooid	Ramkumar et al. (2013)	–
4	Ironstones of Iberian boundary range, Eastern Spain	Callovian-Oxfordian Boundary	Goethite with traces of kaolinite and carbonate hydroxy-apatite	–	Very shallow marine	Lateritic origin	Aurell et al. (1994)	Relative lowstand of sea level
5	Arroyofrío Bed, North-Eastern Iberian Range Spain	Middle-Upper Jurassic boundary	–	–	Shallow sub-tidal	Alteration of volcanic material	Ramajo et al. (2011)	Ephemeral high-energy events like storms and hurricanes

(continued)

Table 4 (continued)

S. no.	Stratigraphic unit	Age	Mineralogy	Geochemical characterization	Depositional environment	Origin of ironstones/source of iron	References	Additional remarks
6	Badamu Formation, Central Iran	Lower- Middle Jurassic	Quartz, calcite, hematite, chamosite	High Fe, Si, Ca	Shallow-marine nearshore	Lateritic weathering and precipitation of Fe on carbonate ooids	Rahiminejad and Hamed (2018)	Chamosite type or ferric oxide type ironstones, similar to Minette-type ironstones
7	Chorro Formation and Lorente Formation, Prebetic Zone, Betic Cordillera, Southern Spain	Middle–Upper Jurassic	Goethite, hematite, apatite	High Fe, Si, Al, P and Ca high V, Cr, Co, Ni, Zn, Y, Mo, and Pb	Shelf	Weathering of emergent carbonate shelf	Reolid et al. (2008)	–
8	Iron ooids of South-eastern Paris basin, France	Middle Callovian–Middle Oxfordian	Goethite, minor quartz, traces calcite and siderite	High Fe, minor Si and Al	Shoreface to median offshore	Primary goethite	Collin et al. (2005)	Precipitation under oxidizing conditions

(continued)

Table 4 (continued)

S. no.	Stratigraphic unit	Age	Mineralogy	Geochemical characterization	Depositional environment	Origin of ironstones/source of iron	References	Additional remarks
9	Golden Oolites, Keera Dome, Kutch basin, India	Callovian	Chamosite, goethite, minor quartz	High Fe, Si, Al, P High V, Cr, Zn, As, Pb, Th and Th/U ratio, low U, Zr	Circa-littoral, high energy and current activity		Present study	–
10	Ferruginous Oolite Formation, Tethyan Himalaya, Zanskar, North India	Callovian	Chamosite (yellow in colour) or dark chamosite/goethite ooids oxidized to limonite in places	–	Storm-controlled inner shelf coincides with Callovian sea level rise	Mixing of ferruginous grains during transgression by high energy waves	Garzanti et al. (1989)	Overlain by glauconitic Cretaceous Giumal Sandstone Formation
11	Golden Oolites, Jhura Dome, Kutch basin, India	Bathonian	Chamosite	–	Lower shoreface to transition zone	–	Patel and Patel (2015), Mishra and Tiwari (2006)	Extensive bioturbation; golden colour relates to chamosite oxidation

(continued)

Table 4 (continued)

S. no.	Stratigraphic unit	Age	Mineralogy	Geochemical characterization	Depositional environment	Origin of ironstones/source of iron	References	Additional remarks
12	Oolithe ferrugineuse, Bayeux Formation, Normandy, France	Bajocian (Middle Jurassic)	Hematite and goethite	–	Distal carbonate ramp	Microbial activity	Préat et al. (2000)	–
13	Jura mountains, North-western Switzerland	Aalenian and Bajocian	goethite, chamosite and traces of apatite and silica	–	Oxygenated marine environment above storm wave base	Biogenic origin	Burkhalter (1995)	Aerated, moderate to high-energy condition
14	Minette Basin, France	Toarcian–Aalenian (Early Jurassic)	Chamosite, goethite chlorite,		Near shore shallow marine	Pedogenic conditions and in situ ooids formed by weathering of Paris basin, reworked and deposited in Minette basin (Siehl and Thein 1989)	Mücke and Farshad (2005)	–

Table 4 (continued)

S. no.	Stratigraphic unit	Age	Mineralogy	Geochemical characterization	Depositional environment	Origin of ironstones/source of iron	References	Additional remarks
15	Cleveland Ironstone Formation Southern North Sea, UK	Early Jurassic	Chamosite, siderite replacing chamosite	High Fe, Si, Al, Mg, Ca high Th/U ratios and depleted in U, K, V, Zn, Ni, Pb, Cr and Co	Very shallow, wave environment followed by shoal-water condition	Lateritic weathering of Th-enriched kaolinitic/bauxitic clay	Mücke and Farshad (2005), Myers (1989), Young et al. (1990a), Howard (1985)	–
16	Frodingham Ironstone Formation, Southern North Sea, UK	Early Jurassic	Chamosite, quartz, siderite, framboidal pyrite and shelly material, local replacement by goethite	High Fe, Si, Al, Mg, Ca	Marine shoal isolated from land with variable degree of agitation by water currents	–	Mücke and Farshad (2005), Young et al. (1990b), Hallam (1963)	–
17	Ferguson Hill Member, west central Nevada, USA	Early Jurassic	Chamosite or berthierine and amorphous silica	–	Shallow marine carbonate environments	Possibly in situ growth as micro-concretions	Clement et al. (2020)	Iron ooids formed in a wide range of depositional environment condensed deposits

(continued)

Table 4 (continued)

S. no.	Stratigraphic unit	Age	Mineralogy	Geochemical characterization	Depositional environment	Origin of ironstones/source of iron	References	Additional remarks
18	Svedrup basin, Canadian, Arctic Archipelago	Earliest Jurassic	Ironstone with glauconites		Pro-delta to offshore shelf		Embry and Johannessen (1992)	–

Fig. 11 Global occurrences of Jurassic oolitic ironstones, as provided in Table 4 (study area marked by yellow circle)

precipitation of chamosite and later oxidation to goethite by sequestering Fe from seawater (Fig. 9a, b).

Many authors relate the high rate of Fe dissolution in seawater to the continental weathering facilitated by the warm and humid climate (Huber and Garrels 1953; Belous et al. 1964; Petránek and Van Houten 1997; Kholodov et al. 2012, 2013; 2014; Novoselov et al. 2018; Mücke 2000; Banerjee et al. 2020). However, the high amount of V, Cr, Zn, As, Pb and Th in the studied ooidal ironstones suggests a possible hydrothermal origin of iron (Kimberley 1989; Toth 1980; Choi and Hariya 1992; Sturesson et al. 2000; Baioumy et al. 2014; Afify et al. 2018; Garnit and Bouhlel 2017; Rudmin et al. 2019). The positive correlation between trace elements with Fe_2O_3 (total) content (in Kutch samples) reflects the possible hydrothermal source of the Fe in the seawater. Similar ironstone facies are reported from Bajocian Seychelles plateau (Perlmutter et al. 1995) which further supports the hydrothermal origin of iron.

The golden oolites of Kutch basin bear geochemical signatures similar to Jurassic Frodingham Ironstone Formation (UK), Cleveland Ironstone Formation (England) and Chorro and Lorente formations (Spain) (Table 4). Although, local factors, depositional settings, changes in energy regime and source of iron supply influence the compositional evolution of oolitic ironstones (James 1966; Schwarz and Germann 1993; Rahiminejad and Hamed 2018), the similar geochemical characteristics of Jurassic ironstones corresponds to warm tropical climate and sea level rise (Haq 2017).

6 Conclusions

Following are the salient conclusions of the Callovian golden oolites exposed at Keera dome:

(a) Characteristic minerals of ooidal ironstones in Jhumara Formation are chamosite, goethite, and calcite. The ooid consists of concentric layers of chamosite and goethite over a nucleus of carbonate grain or shell of organics/bioclast, peloid or quartz.

(b) The oolitic-grainstone type microfacies suggests deposition in an littoral setting with high- energy condition.

(c) The compositional variation observed in the cortex of ooid and oxidation of chamosite to goethite indicates fluctuating redox conditions from sub-oxic to oxic.

(d) Golden oolites form possibly by the direct precipitation of iron-rich minerals on nucleus accreting Fe_2O_3, SiO_2, Al_2O_3 and few other oxides. The source of Fe enrichment is possibly related to hydrothermal circulation.

(e) Ooidal ironstones of Kutch basin exhibit geochemically similar signature to those ironstones in the other parts of the world indicating a greenhouse condition.

References

Afify AM, Sanz-Montero ME, Calvo JP (2018) Differentiation of ironstone types by using rare earth elements and yttrium geochemistry—a case study from the Bahariya region, Egypt. Ore Geol Rev 96:247–261

Arora A, Banerjee S, Dutta S (2015) Black shale in late Jurassic Jhuran formation of Kutch: possible indicator of oceanic anoxic event? J Geol Soc India 85:265–278

Aurell M, Fernández-López S, Hevia G (1994) The Middle-Upper Jurassic oolitic ironstone level in the Iberian Range (Spain): eustatic implications. Geobios 17:549–561

Baioumy HM, Ahmed AH, Khedr MZ (2014) A mixed hydrogenous and hydrothermal origin of the Bahariya iron ores, Egypt: evidences from the trace and rare earth element geochemistry. J Geochem Explor 146:149–162

Baioumy H, Omran M, Fabritius T (2017) Mineralogy, geochemistry and the origin of high-phosphorus oolitic iron ores of Aswan, Egypt. Ore Geol Rev 80:185–199

Banerjee S, Choudhury TR, Saraswati PK, Khanolkar S (2020) The formation of authigenic deposits during Palaeogene warm climatic intervals: a review. J Palaeogeography 9:27. https://doi.org/10.1186/s42501-020-00076-8

Bansal U, Banerjee S, Pande K, Arora A, Meena SS (2017) The distinctive compositional evolution of glauconite in the Cretaceous Ukra Hill Member (Kutch basin, India) and its implications. Mar Petrol Geol 82:97–117

Belous C, Nikolaeva IV, Kazansky YP, Berdnikov AP, Klyarovskiy VM, Kuznetsov VP, Babin AA (1964) The Western-Siberian Iron Ore Basin. Siberian Branch of the Academy of Sciences of the USSR, Novosibirsk (in Russian)

Biswas SK (2005) A review of structure and tectonics of Kutch basin, western India, with special reference to earthquakes. Curr Sci 88:1592–1600

Biswas SK (1977) Mesozoic rock stratigraphy of Kutch, Gujarat. Quart J Geol Min Met Soc India 53:56–85

Biswas SK (1987) Regional tectonic framework, structure and evolution of the western marginal basins of India. Tectonophys 135:307–327

Boggs S Jr (2009) Petrology of sedimentary rocks, 2nd edn. Cambridge University Press, Cambridge

Burkhalter RM (1995) Ooidal ironstones and ferruginous microbialites: origin and relation to sequence stratigraphy (Aalenian and Bajocian, Swiss Jura mountains). Sedimentol 42:57–74

Chan MA (1992) Oolitic ironstone of the Cretaceous western interior seaway, east-central Utah. J Sed Petrol 62:693–705

Chaudhuri A, Banerjee S, Le Pera E (2018) Petrography of Middle Jurassic to Early Cretaceous sandstones in the Kutch Basin, western India: implications on provenance and basin evolution. J Palaeogeography 7:2. https://doi.org/10.1186/s42501-018-0002-6

Choi JH, Hariya Y (1992) Geochemistry and depositional environment of Mn oxide deposits in the Tokoro Belt, northeastern Hokkaido, Japan. Econ Geol 87:1265–1274

Clement AM, Tackett LS, Ritterbush KA, Ibarra Y (2020) Formation and stratigraphic facies distribution of early Jurassic iron oolite deposits from west central Nevada, USA. Sediment Geol 395. https://doi.org/10.1016/j.sedgeo.2019.105537

Collin PY, Loreau JP, Courville P (2005) Depositional environments and iron ooid formation in condensed sections (Callovian–Oxfordian, south-eastern Paris basin, France). Sedimentol 52:969–985

Curial A, Dromart G (1998) Apport de la sismique-reflexion et des forages a' l'analyse séquentielle et géomé- trique des corps sédimentaires et de ses encaissants: Journées scientifiques Agence Nationale de la gestion des Déchets Radioactifs, Bar-le-Duc, Atlas des Posters, pp 25–27

Embry AF, Johannessen EP (1992) T–R sequence stratigraphy, facies analysis and reservoir distribution in the uppermost Triassic–Lower Jurassic succession, western Sverdrup Basin, Arctic Canada. In: Vorren TO, Bergsager E, Dahl-Stamnes OA, Holter E, Johansen B, Lie E, Lund TB (eds) Arctic geology and petroleum potential. NPF Spec Publ 2:121–146

Flügel E (2010) Microfacies of carbonate rocks, analysis interpretation and application. Springer, Heidelberg, Dordrecht

Garnit H, Bouhlel S (2017) Petrography, mineralogy and geochemistry of the late Eocene oolitic ironstones of the jebel ank, southern tunisian atlas. Ore Geol Rev 84:134–153

Garzanti E, Haas R, Jadoul F (1989) Ironstones in the Mesozoic passive margin sequence of the Tethys Himalaya (Zanskar, Northern India): sedimentology and metamorphism. In: Young TP, Taylor WEG (eds) Phanerozoic ironstones. Geol Soc Spec Publ 46:229–244

Garzanti E (1993) Himalayan ironstones, "superplumes", and the breakup of Gondwana. Geology 21:105–108

Hallam A (1963) Observations on the palaeoecology and ammonite sequence of the Frodingham Ironstone (Lower Jurassic). Palaeontology 6:554–574

Haq BU (2017) Jurassic sea-level variations: a reappraisal. GSA Today 28:4–10

Heinkoop JM, Tsujita TC, Risk JM, Tamascik T, Mah AJ (1996) Modern iron ooids from shallow marine volcanic settings: Mahengetang, Indonesia. Geology 24:759–762

Hemingway JE (1974) Jurassic. In: Raynor DH, Hemingway JE (eds) The geology and mineral resources of Yorkshire. Yorkshire Geol Soc, pp 161–223

Howard AS (1985) Lithostratigraphy of the Staithes Sandstone and Cleveland Ironstone formations (Lower Jurassic) of north-east Yorkshire. Proc Yorkshire Geol Soc 45:261–275

Huber NK, Garrels RM (1953) Relation of pH and oxidation potential to sedimentary iron mineral formation. Econ Geol 48:337–357

Jacquin T, Dardeau G, Durlet C, de Graciansky PC, Hantzpergue P (1998) The North Sea cycle: an overview of 2nd-order transgressive/regressive facies cycles in Western Europe. In: de Graciansky PC, Hardenbol J, Jacquin T, Vail PR (eds) Mesozoic and Cenozoic sequence stratigraphy of European basins. SEPM Spec Publ 60:445–466

James HL (1966) Chemistry of the iron-rich sedimentary rocks. US Geol Survey, Prof Pap 44O-W, pp 1–61

Kholodov VN, Golubovskaya EV, Nedumov RI (2014) Origin and prospects of the Cimmerian iron ore basin in Ukraine and Russia. Lithol Miner Res 49:359–380

Kholodov VN, Nedumov RI, Golubovskaya EV (2013) Facies types of sedimentary iron ore deposits and their geochemical features: communication 2. Problems of the geochemistry of phanerozoic iron ores. Lithol Miner Res 48:14–47

Kholodov VN, Nedumov RI, Golubovskaya EV (2012) Facies types of sedimentary iron ore deposits and their geochemical features: communication 1. Facies groups of sedimentary ores, their lithology and genesis. Lithol Miner Res 47:447–472

Kimberley MM (1989) Exhalative origins of iron formations. Ore Geol Rev 5:13–145

Kimberley MM (1978) Paleoenvironmental classification of iron formations. Econ Geol 73:215–229

Macquaker JHS, Taylor KG, Young TP, Curtis CD (1996) Sedimentological and geochemical controls on ooidal ironstone and 'bone-bed' formation and some comments on their sequence stratigraphic significance. In: Hesselbo S, Parkinson DN (eds) Sequence Stratigraphy in British Geology. Geol Soc London Spec Publ 103:97–107

McGregor F, Ramanaidou E, Wells M (2010) Phanerozoic ooidal ironstone deposits–generation of potential exploration targets. Appl Earth Sci (Trans Inst Min Metall B) 119:60–64

Mishra D, Tiwari RN (2006) Lithofacies and depositional dynamics of Golden Oolite (Bathonian), Kachchh Mainland, Gujarat, India. J Asian Earth Sci 26:449–460

Mücke A (2006) Chamosite, siderite and the environmental conditions of their formation in chamosite-type Phanerozoic ooidal ironstones. Ore Geol Rev 28:235–249

Mücke A (2000) Environmental conditions in the Late Cretaceous African Tethys: conclusions from a microscopic-microchemical study of ooidal ironstones from Egypt, Sudan and Nigeria. J Afr Earth Sci 30:25–46

Mücke A, Farshad F (2005) Whole-rock and mineralogical composition of Phanerozoic ooidal ironstones: Comparison and differentiation of types and subtypes. Ore Geol Rev 26:227–262

Myers KJ (1989) The origin of the Lower Jurassic Cleveland Ironstone Formation of North-East England: evidence from portable gamma-ray spectrometry. In: Young TP, Taylor WEG (eds) Phanerozoic ironstones. Geol Soc London Spec Publ 46:221–228

Novoselov KA, Belogub EV, Kotlyarov VA, Filippova KA, Sadykov SA (2018) Mineralogical and geochemical features of oolitic ironstones from the sinara–techa deposit, kurgan district, Russia. Geol Ore Deposits 60:265–276

Patel S, Patel N (2015) Sedimentological and palaeoecological significance of the trace fossils of the Jurassic rocks of the Jhura Dome, Mainland Kachchh, western India. Vol Jurassica 23:101–140

Perlmutter MA, Brennan PA, Hook SC, Dempster K, Pasta D (1995) Global cyclostratigraphic analysis of the Seychelles Southern Shelf for potential reservoir, seal and source rocks. Sediment Geol 96:93–118

Petránek J, Van Houten FB (1997) Phanerocoic ooidal ironstones. Czech Geol Surv Spec Pap 7:1–71

Porrenga (1965) Chamosite in recent sediments of the Niger and Orinoco Delta. Geol Mijnbouw 44:400–403

Prasad S (1993) A note on the Middle Jurassic stratigraphic succession of Keera Dome, Kachchh District, Gujarat. Jour Geol Soc India 41:156–161

Préat A, Mamet B, Ridder C, Boulvain F, Gillan D (2000) Iron bacterial and fungal mats, Bajocian stratotype (Mid-Jurassic, Northern Normandy, France). Sediment Geol 137:107–126

Rahiminejad AH, Hamed ZM (2018) Synsedimentary formation of ooidal ironstone: an example from the Jurassic deposits of SE central Iran. Ore Geol Rev 95:238–257

Ramajo J, Aurell M, Gale C, Gil I, Andrés, Hevia G, Anchuela O (2011) The Middle-Upper Jurassic boundary oolitic ironstone level (Arroyofrío Bed) in northeastern Iberian Range: a genetic and depositional model. In: 28th IAS meeting of sedimentology, p 359

Ramkumar M, Alberti M, Fürsich FT, Pandey DK (2013) Depositional and diagenetic environments of the Dhosa Oolite Member (Oxfordian), Kachchh Basin, India: implications for the origin and occurrence of the ooids and their correlation with the global Fe-oolite peak. In: Ramkumar M (ed) On a sustainable future of the earth's natural resources. Springer, Berlin, Heidelberg, pp 179–230

Reolid M, Abad I, García JMM (2008) Palaeoenvironmental implications of ferruginous deposits related to a Middle-Upper Jurassic discontinuity (Prebetic Zone, Betic Cordillera, Southern Spain). Sediment Geol 203:1–16

Rudmin M, Banerjee S, Abdullayev E, Ruban A, Filimonenko E, Lyapina E, Kashapov R, Mazurov A (2020) Ooidal ironstones in the Meso-Cenozoic sequences in western Siberia: assessment of formation processes and relationship with regional and global earth processes. J Palaeogeography 9:1. https://doi.org/10.1186/s42501-019-0049-z

Rudmin M, Mazurov A, Banerjee S (2019) Origin of ooidal ironstones in relation to warming events: Cretaceous-Eocene Bakchar deposit, south-east Western Siberia. Mar Pet Geol 100:309–325

Salama W, El Aref MM, Gaupp R (2012) Mineralogical and geochemical investigations of the Middle Eocene ironstones, El Bahariya Depression, Western Desert, Egypt. Gond Res 22:717–736

Salama W, El Aref MM, Gaupp R (2013) Mineral evolution and processes of ferruginous micro-bialite accretion—an example from the Middle Eocene stromatolitic and ooidal ironstones of the Bahariya Depression, Western Desert, Egypt. Geobiology 11:15–28

Schwarz T, Germann K (1993) Ferricretes as a source of continental oolitic ironstones in northern Sudan. Chem Geol 107:259–265

Simon P (1965) Das Eisenerz des Oberen und Mittleren Korallenooliths im nördlichen Teil des Gifhorner Troges. Max Richter Festschrift, Clausthal-Zellerfeld, pp 231–255

Siehl A, Thein J (1989) Minette-type ironstones. In Young TP, Taylor WEG (eds) Phanerozoic Ironstones. Geological Society London, Special Publication, 46, pp 175–193

Sturesson U, Heikoop JM, Risk MJ (2000) Modern and Palaeozoic iron ooids—a similar volcanic origin. Sediment Geol 136:137–146

Talbot MR (1974) Ironstones in the Upper Oxfordian of southern England. Sedimentol 21:433–450

Tang D, Shi X, Jiang G, Wu T, Ma J, Zhou X (2018) Stratiform siderites from the mesoproterozoic xiamaling formation in north China: genesis and environmental implications. Gond Res 58:1–15

Taylor KG, (Toni) Simo JA, Yocum D, Leckie DA (2002) Stratigraphic significance of ooidal ironstones from the Cretaceous Western Interior Seaway: the Peace River Formation, Alberta, Canada, and the Castlegate Sandstone, Utah, USA. J Sed Res 72:316–327

Taylor SR, McLennan SM (1985) The continental crust: its composition and evolution. Blackwell Scientific Publications, London

Toth JR (1980) Deposition of submarine crusts rich in manganese and iron. GSA Bull 91:44–54

Van Houten FB, Arthur MA (1989) Temporal patterns among Phanerozoic oolitic ironstones and oceanic anoxia. In: Young TP, Taylor WEG (eds) Phanerozoic ironstones: an introduction and review. Geol Soc London Spec Publ 46:33–50

Van Houten FB, Bhattacharyya DP (1982) Phanerozoic oolitic ironstones–geologic record and facies model. Ann Rev Earth Planet Sci 10:441–457

Van Houten FB (1992) Review of Cenozoic ooidal ironstones. Sediment Geol 78:101–110

Young TP (1992) Ooidal ironstones from Ordovician Gondwana: a review. Palaeo Palaeo Palaeo 99:321–347

Young TP (1989) Phanerozoic ironstones: an introduction and review. In: Young TP, Taylor WEG (eds) Phanerozoic ironstones. Geol Soc London Spec Publ 46:ix–xxv

Young TP, Aggett JR, Howard AS (1990a) The Cleveland Ironstone formation. In: Young TP (ed) Field Guide No 9: Jurassic and Ordovician ooidal ironstones. British Sedimentological Research Group, 13th ISC, Nottingham UK, pp 1–31

Young TP, Parsons D, Aggett JR (1990b) The Frodingham ironstone. In: Young TP (ed) Field Guide No 9: Jurassic and Ordovician Ooidal Ironstones. British Sedimentological Research Group, 13th ISC, Nottingham UK, pp 32–50

Young TP, Taylor WEG (1989) Phanerozoic ironstones. Geol Soc London Spec Publ 46:1–251

Oxic-dysoxic Tidal Flat Carbonates from Sadara, Pachham Island, Kachchh

Makarand G. Kale, Ashwin S. Pundalik, Nitin R. Karmalkar, and Raymond A. Duraiswami

Abstract Sadara limestones in Goradonagar Formation of Pachham Island are dominantly intramicritic and contain bioclast, pellet, peloid, ooid; with nodular anhydrite. They exhibit intraformational chert breccia at the base, early diagenetic dolomite and predominant lime flake pebbles of intrabasinal origin in the middle, with development of algal laminated structures and desiccation cracks in the upper part; representing subtidal-intertidal-supratidal mudflat environment. Higher content of insoluble residue (av. 11.56%) and presence of illite, kaolinite, anhydrite, gypsum; indicate restricted circulation in coastal sabkha-like intertidal-supratidal zones. They exhibit higher CaO, low SiO_2, Fe_2O_3, Al_2O_3, TiO_2, K_2O and P_2O_5. Trace element composition of these sediments reveals higher Na, lower Mn, Ni, Cu, Co, Pb, U, Th, Sr contents, V/Cr and Ni/Co ratios. These signatures, together with seawater like REE pattern with low $\sum$REE + Y content, LREE depletion, positive La, Eu and negative Gd, Y, Ce anomalies, $(Nd/Yb)_{SN}$ and Y/Ho in these limestones; substantiates shallow marine oxic-dysoxic nature with an insignificant terrigenous contribution. The $\delta^{13}C$ (av. −1.06‰), $\delta^{18}O$ (av. −5.06‰), Z values (av. > 120) support the shallow marine nature of these limestones.

Keywords Intraformational lime flake conglomerate · Algal limestone · Oxic-dysoxic tidal flat · Goradongar Formation · Kachchh · Gujarat

1 Introduction

Although several studies address the paleontological and stratigraphic aspects of the Jurassic succession of Kachchh Basin, very few investigations highlight lithofacies and depositional history of the carbonate succession in Kachchh, particularly in

M. G. Kale (✉) · N. R. Karmalkar · R. A. Duraiswami
Department of Geology, Savitribai Phule Pune University, Pune 411007, India
e-mail: mgkale@unipune.ac.in

A. S. Pundalik
Department of Geology, St. Xavier's College, Mumbai, Mumbai 400001, India

the Island belt. Major and trace element composition of limestones are used extensively to illustrate the nature of seawater from which they originated, and to depict the factors responsible for syn-and post-depositional characterization of carbonates (Armstrong-Altrin et al. 2003, 2011; Nagarajan et al. 2011; Hua et al. 2013; Khelen et al. 2017; Tobia 2018; Roy et al. 2018). REE data of limestone provide insights on seawater chemistry (Piper et al. 2007; Srivastava and Singh 2019), redox conditions of the depositional environment and helps in the characterization of terrigenous input (Frimmel 2009; Zhao et al. 2009; Tanaka et al. 2007; Srivastava and Singh 2019). Stable isotope analysis of limestone provides an insight into carbonate precipitation temperature (Singh et al. 2016), isotopic composition of the ocean water (Scholle and Arthur 1980; Banerjee et al. 2006; Madhavraju et al. 2017), and robust constraints on paleoclimatic changes (Zhao and Zheng 2014). The integration of lithofacies analysis and geochemical data highlight the sedimentation history of the basin. Biswas (2016a) stressed the need of detailed research on various aspects of sedimentology of Jurassic succession of Kachchh Basin for a more precise interpretation of the depositional environment and intra-basin correlation. The present work documents sedimentary characteristics and the genetic history of Goradongar Flagstone Member of Goradonagar Formation of Pachham Island in the Sadara lithosection.

2 Geological Background

The Kachchh Basin situated on the western margin of the Indian Plate (Fig. 1a, b) is a pericratonic rift basin, that formed during the fragmentation of Gondwanaland in the Late Triassic (Biswas 1991, 2016a; Rajendran et al. 2001; Shankar 2001). The basin hosts excellent Mesozoic (1500 to 2400 m thick) and Paleogene-Neogene (550 m thick) sedimentary successions (Biswas 1977, 2016b; Arora et al. 2015; Bansal et al. 2017; Chaudhuri et al. 2018, 2020a, b, c, d). The Kachchh Basin evolved through three tectonic phases, viz. rift, late rift divergent wrench and post-rift convergent wrench; corresponding to breakup, drifting and collision of Indian plate, respectively (Biswas 2005). The rift ceased in Late Cretaceous, following trailing edge uplift prior to collision with Asian Plate; which later became a shear zone during the inversion stage after collision (Biswas 1987, 2005).

Biswas (1977) proposed the lithostratigraphic classification of Kachchh Basin, in which he recognized four units, namely the Jhurio Formation, the Jumara Formation, the Jhuran Formation and the Bhuj Formation (Fig. 1b) in the ascending antiquity. The "island" outcrops of Pachham, Khadir, Bela and Chorar, constituting the "Island Belt" (Fig. 1b), exposes the oldest sedimentary sequence from Bathonian to Callovian (Biswas 1977). The rocks exposed in Pachham island were redefined to a higher rank litho-unit, Patcham Group by Biswas (2016a), and divided it into two units, a lower Kaladongar Formation and an upper Goradongar Formation. Biswas (2016a), considered the Kaladongar Formation to be deposited in marine foreshore environment and the Goradongar Formation to be of shallow marine environment. The Goradongar Formation is divisible into lower Goradongar Flagstone Member
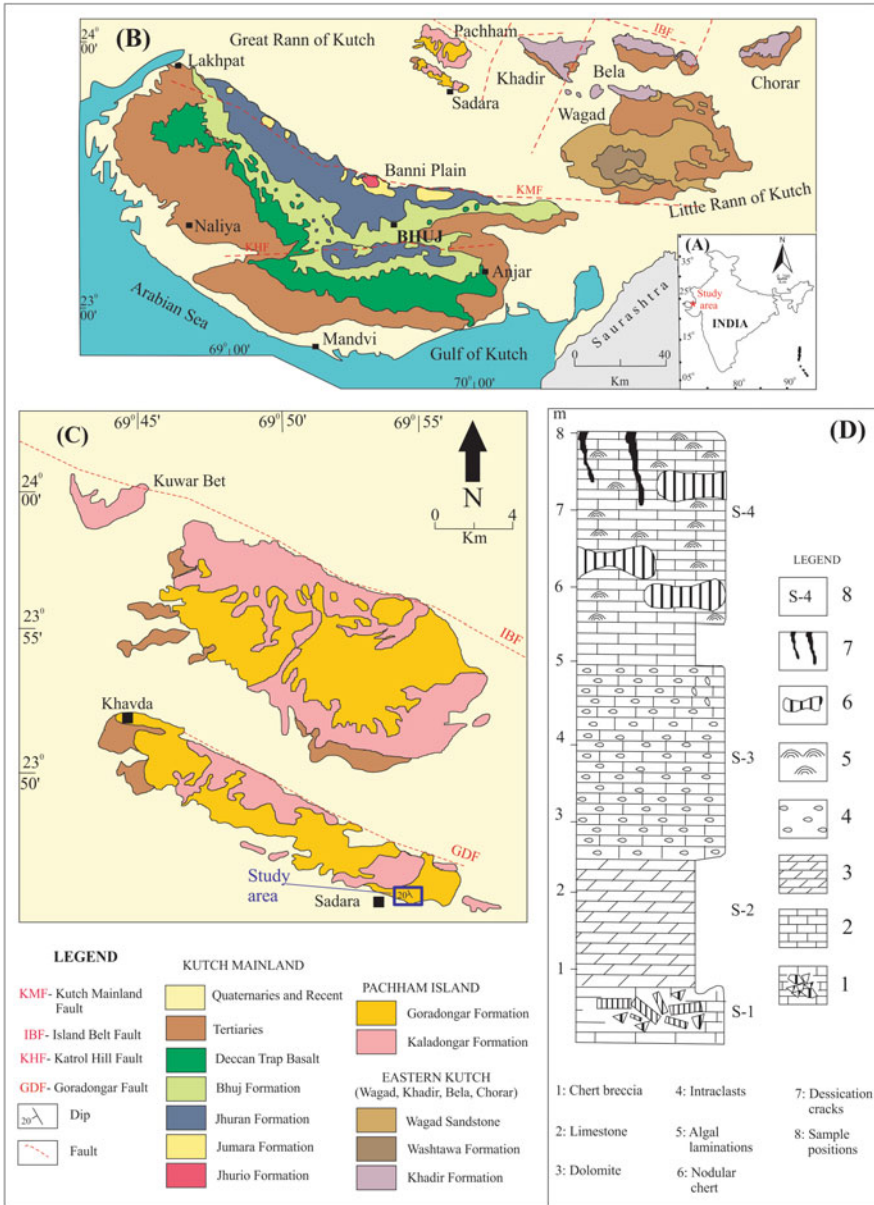
Fig. 1 **a** Outline map of India showing location of study area. **b** Regional geological map of Kutch basin (adapted from Biswas and Deshpande 1970). **c** Geological map of study area (modified after Biswas and Deshpande 1973; Patel et al. 2013). **d** Lithosection of part of the Goradongar Flagstone Member from Sadara

(interbedded shale and flaggy limestone), middle Gadaputa Member (thick sandstone) and Raimalro Member (cherty limestone) on the top. Based on lithology and macrofossil content, Agarwal and Pandey (1985) divided the 175 m thick stratigraphic column of Goradongar into thirty beds. They have attempted biozonation of Goradongar column on the basis of enclosed bivalves and cephalopods and assigned Lower to Middle Bathonian to Middle Callovian age. Pandey et al. (2013) recorded *Calliphylloceras heterophylloides* (Oppel 1856) from the basal sediments of Sadara Dome near the eastern end of Goradongar. Pandey et al. (2013) considered these basal sediments to be the oldest ammonoid-bearing horizon of the exposed Mesozoic sediments in the Kachchh Basin and assigned an Early Bajocian or older age. Patel et al. (2014) recorded forty-four ichnospecies of thirty-one ichnogenera, representing diverse ethology from the Goradongar Formation, grouped by them in five ichnoassemblages representing the *Cruziana* ichnofacies and occasionally a mixed *Skolithos-Cruziana* ichnofacies of lower shoreface to offshore environments. Joseph et al. (2016) studied the Goradongar Formation at six different localities in Patcham island for its physical as well as biogenic components, the results of which suggested two depositional regimes: lower shoreface to offshore transition and offshore for the Goradonagar Formation.

3 Methodology

The limestones were studied at two localities, namely South of Khavda and Sadara (Fig. 1c). A section of about 8 m, exposed at the northwestern part of Sadara Village was studied in detail and four samples (S-1, S-2, S-3 and S-4) were collected from Sadara lithosection (Fig. 1d). Thin polished slabs of limestone were etched in 10% HCl for ten minutes, and then subjected to staining for two to three minutes for distinguishing calcite, ferroan calcite and dolomite (Evamy 1963; Dickson 1966). The limestone samples were subjected to insoluble residue analysis following the method of Ireland (1971) and the insoluble residues were subjected to X-ray diffraction studies on Phillips X-ray diffractometer at Wadia Institute of Himalayan Geology, Dehradun, from 5° to 70° 2θ with Cu-Kα target. Four thin sections were studied in detail and volumetric compositions of different constituents were determined using a point counter. Major oxides were determined on Axios PAN Analytical XRF, while trace and rare earth element compositions were determined on Thermo X series 2 ICPMS at National Institute of Oceanography, Goa. The stable isotopic compositions of the limestone samples were carried out using a Thermo Finnigan Delta plus XP Continuous Flow Isotope Ratio Mass Spectrometer (CF-IRMS) with attached preparation device Gas Bench II and robotic sampling arm (CG-PAL), at National Geophysical Research Laboratory, Hyderabad.

4 Lithofacies Assemblage

The rocks belonging to Goradongar Flagstone Member are exposed at the north-western part of Sadara village (Fig. 1c). These are buff, yellowish to yellowish brown, fine-grained micritic limestones dipping 20° towards 240°. Sadara lithosection comprises four lithofacies namely chert breccia, laminated micritic limestone, lime flake conglomerate and algal limestone from the bottom to the top (Fig. 1d).

4.1 Chert Breccia

It is about 0.75 m thick and occurs at the lower part of Sadara lithosection (Fig. 1d). It consists of polygonal, angular to subangular clasts of fine-grained white chert with thin pink layers, in fine-grained micritic matrix (Fig. 2a). Clasts exhibit vertical as well as subhorizontal desiccation cracks filled with pale brownish clay (Fig. 2b). In places, carbonaceous clay binds these angular clasts (upper part of Fig. 2b). The chert breccia passes upwards to micritic limestone.

4.2 Laminated Micritic Dolomite

It varies in thickness from 0.50 to 1.4 m and it is represented by pale yellowish micritic limestone that exhibits parallel laminae (Fig. 2c). The thickness of lamina ranges from 2 to 5 mm and are dolomitic (Fig. 2c) in nature, as evident from acquired turquoise blue stain (Dickson 1966). The laminated micritic dolomite passes upward to intraformational lime flake conglomerate.

4.3 Intraformational Lime Flake Conglomerate

It is 2.5 m in thickness and consists of subangular to rounded, elongated flakes of pale yellowish to dark brown colored micrite, within yellowish-brown micrite; representing lime flake conglomerate (Fig. 2d). The short axis of lime flakes varies from 0.3 cm to 1.5 cm, while the long axis ranges from 0.4 cm to 4 cm (Fig. 2d). The long axes are aligned parallel to the bedding (middle part of Fig. 2d). At places (Fig. 2d), these are also seen to be at a high angle to bedding plane, thereby disturbing the lamination (right central portion of Fig. 2d). Occasionally, almost vertically oriented flakes are also noticed (upper right corner of Fig. 2d). The lime flakes are of micritic dolomite that exhibits turquoise blue stain (Fig. 2e). These lime flakes are bounded by either pinkish stained micritic calcite or turquoise blue stained dolomite matrix

◄**Fig. 2** **a** Breccia consisting of polygonal, angular to subangular clasts of fine-grained white coloured chert with thin stains of pink colour, floating in fine-grained micritic matrix. **b** Cross-sectional view of chert breccia exhibiting preferential orientation of elongated slabby clasts, bounded by pink stained calcite and carbonaceous clay (upper right and lower left portion of photo). Development of vertical as well as sub horizontal desiccation cracks within the clasts filled with pale brownish clay (coin diameter = 2.5 cm). **c** Parallel laminated micritic limestone showing turquoise blue stained ferroan dolomite. **d** Lime flake conglomerate consisting of subangular to rounded, elongated flakes of pale yellowish to dark brown coloured micrite bounded by pale yellowish brown micrite. Note the deposition of lime flakes parallel to the bedding as well as at a high angle to bedding. Imbrications of flakes are also noticed (left central part of photo) (pen length = 13.5 cm). **e** Stained slab of lime flake conglomerate showing turquoise blue stained dolomitic clasts, bounded by both turquoise blue stained dolomitic and light pink stained micritic matrix (coin diameter = 2.5 cm). **f** Algal limestone showing crenulated, semiparallel laminations with domal upwarps (coin diameter = 2.5 cm). **g** Bedding plane view of algal limestone exhibiting concentrically laminated, elongated laterally linked laminae (hammer length = 38 cm)

(Fig. 2e). The lime flake conglomerate passes upward to micritic limestones and then to algal laminated limestone (Fig. 1d).

4.4 Algal Limestone

It is 2.4 m thick and is represented by micritic limestone showing crenulated, subparallel mm scale laminations with domal upwarps (Fig. 2f). Bedding plane view of this algal limestone exhibits concentrically laminated, elongated, laterally linked laminae (Fig. 2g). This algal limestone contains irregular to subrounded granule to pebble size nodules of greyish-white chert (Fig. 2f). Micritic lime flakes are occasionally present in these algal limestones (lower left part of Fig. 2f). Desiccation cracks, both vertical as well as sub-parallel to the bedding plane, filled with sparry calcite, occur in places (Fig. 2f).

5 Mineralogy

The staining test revealed the presence of pinkish stained non-ferroan calcite in algal laminated limestone, the presence of turquoise blue stained ferroan dolomite in laminated micritic limestone (Fig. 2c) and dolomitic nature of intraclasts of lime flake conglomerate (Fig. 2d). The insoluble residue content ranges from 9.31 to 91.90% and averages to 31.36% (Table 1). The sample S-1 exhibits high content (91.90%) of insoluble residue. Microscopic investigations of insoluble residue reveal the dominance of off-white chert with pinkish stains, along with clays and few grains of quartz. X-ray diffractograms (Fig. 3) of insoluble residue revealed the presence of illite (3.35 dA°, 1.72 dA°, 2.46 dA°) as dominant clay mineral with subordinate kaolinite (2.13 dA°, 1.45 dA°), traces of quartz (1.48 dA°, 1.46 dA°, 1.38 dA°),

Table 1 Insoluble residue percentage and volume percentage composition of Sadara limestones

Sample no.	S-1	S-2	S-3	S-4	Average*
Insoluble residue analyses					
Initial weight (g)	31.28	18.89	36.33	36.38	
Insoluble residue (g)	28.75	2.28	3.38	4.85	
Calcium carbonate %	8.10	87.94	90.69	86.69	88.44
Insoluble residue %	91.90	12.06	9.31	13.31	11.56
Volume percentage composition					
Micrite	1.49	19.49	2.13	24.37	15.33
Sparry calcite	9.16	4.09	16.04	8.96	9.70
Intraclast	0.60	44.83	62.28	48.24	51.78
Bioclast	–	14.23	4.68	10.56	9.82
Peloid	–	6.99	8.89	4.30	6.73
Pellet	–	6.87	0.23	0.64	2.58
Ooid	–	0.34	0.22	0.13	0.23
Chert	74.36	–	–	–	–
Anhydrite	–	0.14	1.15	0.37	0.55
Sparry calcite veins	3.40	–	0.80	–	0.27
Ferruginous clays	4.29	0.50	–	–	0.17
Carbonaceous clays	–	–	–	4.00	1.33
Terrigenous clastics	2.27	2.21	3.46	2.30	2.66
Opaque's	0.41	0.40	0.12	0.14	0.22

*Average is of limestone samples S-2, S-3 and S-4

anhydrite (2.45 dA°, 2.46 dA°, 1.54 dA°) and rare peaks of gypsum (2.49 dA°, 1.72 dA°).

6 Microfacies

The thin section of chert breccia contains rock fragments of chert (74.36%), micritic intraclasts (0.60%), reddish-brown clay (4.29%), terrigenous clastics (2.27%), opaque's (0.41%), bounded by micrite (1.49%) and sparry calcite (9.16%) and sparry calcite veins (3.40%). In thin sections of limestone, micritic intraclast, bioclast, peloid, pellet, ooid, anhydrite, reddish-brown as well as black clay, terrigenous clastics (represented by quartz and felspars) and opaques are bounded by micritic calcite (av. 15.33%) and sparry calcite (av. 9.70%) (Table 1). Micritic intraclast (av. 51.78%) is the dominant allochemical constituent bounded by micrite; hence the rocks can be classified as intramicrite (Folk 1959) and packstone (Dunham 1962).
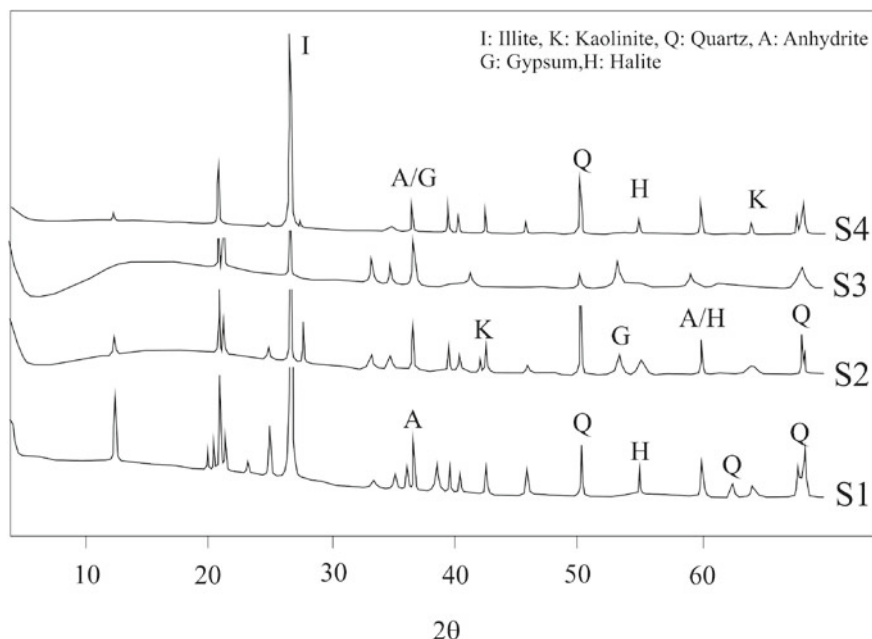
Fig. 3 X-ray diffractograms of clays separated from insoluble residue of Sadara limestones

Intraclast (av. 51.78%) range in size from 50 to >400 μm. Subrounded to rounded pale brownish micritic intraclasts float in micritic matrix (Fig. 4a). The average content of bioclast is around 10%. Bioclasts include broken fragments of mollusc, brachiopod, bryozoa, coral, foraminifera, echinoderm, sponge, ostracod and algal filament in order of decreasing abundance. Mollusc fragments include bivalve, gastropod and cephalopod. Broken bivalve shells occur as thin elongated fragments which are filled with prismatic sparry calcite (Fig. 4b). Fragment of cephalopod shows series of shell layers that consist of radiating prisms of calcite and thin smooth outer layer along with partial micritization of shell (Fig. 4c). Gastropod shell shows coiled spires, well-preserved apex, and dissolved body whorl (Fig. 4d). The chambers of the gastropod shell are filled with micrite (Fig. 4d). Elongated brachiopod fragment shows low angle fibrous/cross lamellar internal structure in which fibers are oblique to the shell wall (Fig. 4e). The longitudinal section of bryozoa exhibits partially preserved zoocia that are partially occupied by pale brownish clay (Fig. 4f). The transverse section of the wall of a coral shows fine calcitic micro-texture and septa projecting inwards from the wall (Fig. 4g). Foraminifera present are uniserial as well as biserial. Uniserial foraminifers include miliolid. Biserial foraminifer exhibits single-layered, fine-grained micro-texture of the wall, the chambers of which are filled with sparry calcite (Fig. 4h). Echinoderm plate shows fine porous microstructure in which pores are usually filled with dark brown clay (Fig. 5a). In thin section
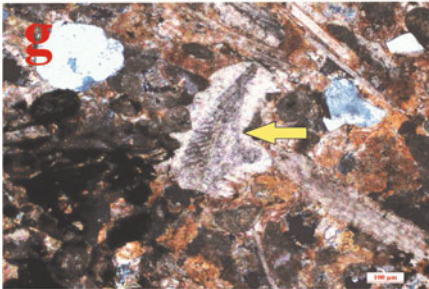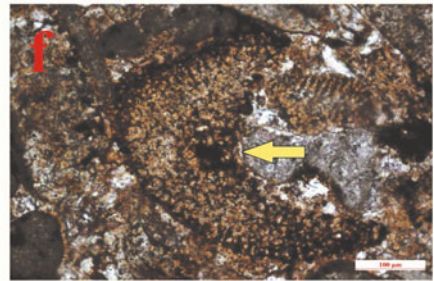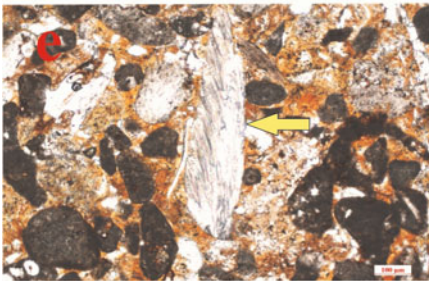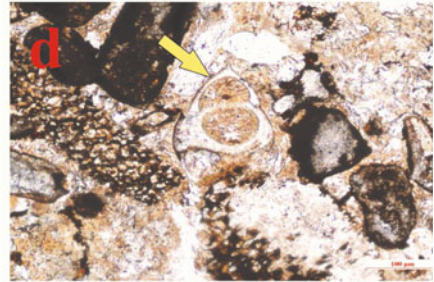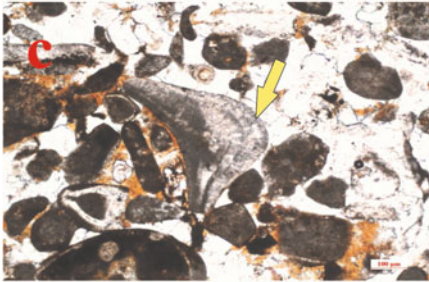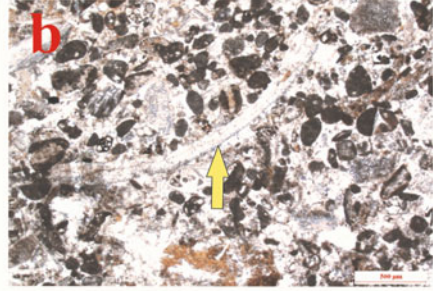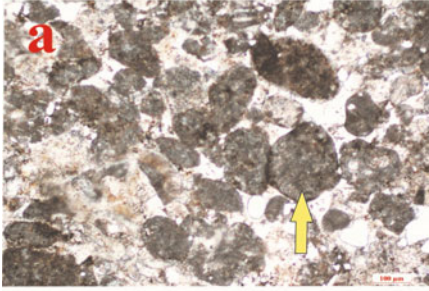
◄**Fig. 4** **a** Photomicrograph of limestone showing subrounded to rounded pale brownish micritic intraclasts in close contact with each other (central part of photo) and floating in micritic matrix in rest of the photo (S-3, PPL). **b** Thin elongated broken bivalve shell filled with prismatic sparry calcite (S-4, PPL). **c** Fragment of cephalopod showing series of shell layers that consists of radiating prisms of calcite and thin smooth outer layer, with partial micritization of shell (S-2, PPL). **d** Gastropod shell with coiled spires, well preserved apex and dissolved body whorl are present. The chambers of gastropod shell exhibit fibrous internal microstructure and are filled with pale yellowish clayey micrite (S-2, PPL). **e** Elongated inpunctate brachiopod fragment shows low angle fibrous/cross lamellar internal structure in which fibers are oblique to shell surface (S-2, PPL). **f** Longitudinal section of Bryozoa exhibits partially preserved zooecia which are partially occupied by pale brownish clay (S-2, PPL). **g** Transverse section of the wall of a coral with fine calcitic microtexture and septa projecting inwards from the wall. Micritization of coral fragment is also evident (S-2, PPL). **h** Biserial foraminifer exhibits single layered fine-grained microtexture of wall, the chambers of which are filled with sparry calcite (S-3, PPL)

of algal laminated limestone, algal septa can be seen (Fig. 5b) and micritic intraclasts rich laminae alternate with algal rich laminae (Fig. 5b). Cross-sectional view of ostracod shell shows smooth curved wall and fine prismatic internal microstructure. Elongated sponge spicule exhibits layered internal microstructure. Micritization of bioclasts is common (Fig. 4c, g). Pale brown, subrounded to oval-shaped clayey micritic pellets (av. 2.58%) and rounded peloids (av. 6.73%) occur within the limestone (Fig. 5c). Ooids exhibit alternate carbonaceous and micritic laminations around the carbonaceous clay nucleus and form aggregate (Fig. 5d). Fine-grained clayey chert fragments (S-1:74.36%) together with micritic lime intraclasts are bound by microspars of calcite and carbonaceous clay (Fig. 5e). Cracks within the chert are filled up with carbonaceous clay (Fig. 5f). Occasionally nodular anhydrite (av. 0.55%) occurs as aggregates of fine elongate anhedral crystals showing grey interference color (Fig. 5g). In places, pore-filling cement exhibiting bladed blocky sparry calcite layers alternate with concentric pale brownish clayey layers (Fig. 5h). Opaques are represented by magnetite.

7 Geochemical Studies

7.1 Major Elements

The Sadara limestones are characterized by higher CaO (av. 41.76%), moderate SiO_2 (av. 18.34%), low Al_2O_3 (av. 2.78%), Fe_2O_3 (av. 3.37%), MgO (av. 0.45%), TiO_2 (av. 0.16%), K_2O (av. 0.08%) and P_2O_5 (av. 0.09%) contents (Table 2). Exceptionally high values of SiO_2 (59.82%) characterize the sample S-1. The high SiO_2 is related with presence of clayey chert in this sample.
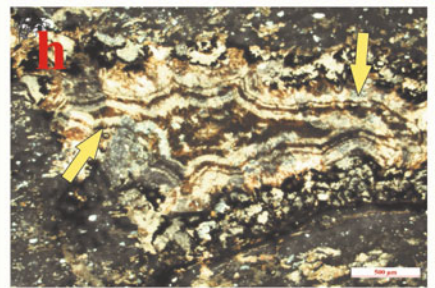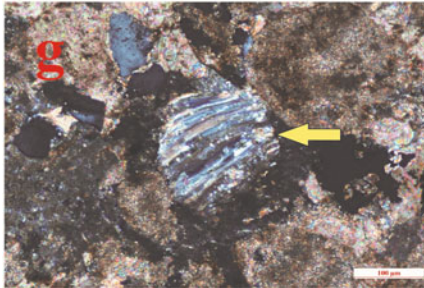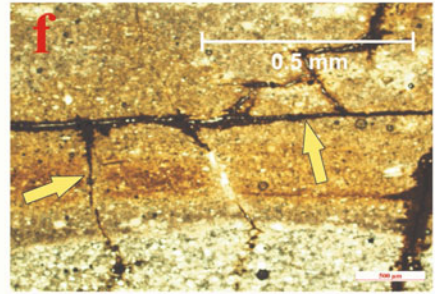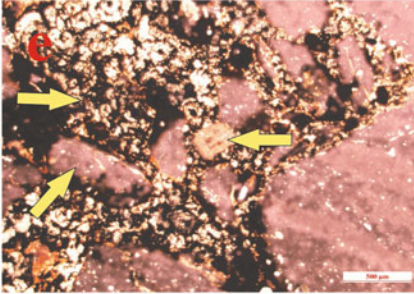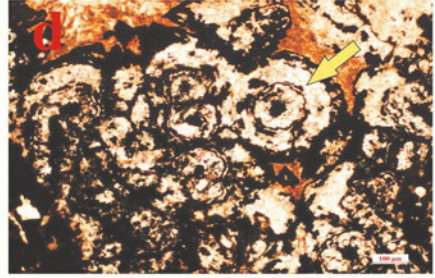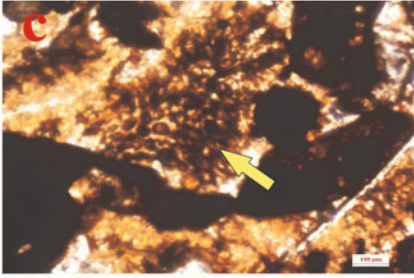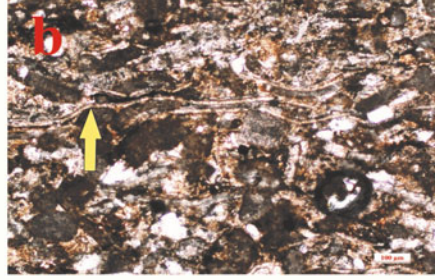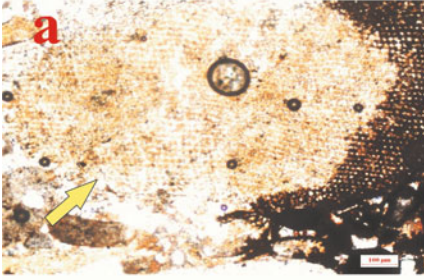
◄**Fig. 5** **a** Echinoderm plate shows fine porous microstructure, with some of the pores are filled with dark brown clayey pore fillings (S-2, PPL). **b** Algal limestone exhibiting presence of elongated algal septas. Micritic intraclast rich laminae alternate with algal rich laminae (S-3, PPL). **c** Pale brownish subrounded to oval shaped clayey micritic pellets and rounded brownish peloids bounded by pale brownish micritic matrix (S-2, PPL). **d** Aggregates of ooids bounded by pale brownish clayey micritic matrix. Note alternate carbonaceous and micritic calcite concentric laminations of ooid around the carbonaceous clay nucleus (S-1, PPL). **e** Photomicrograph of chert breccia consisting of fine-grained clayey chert fragments together with micritic lime intraclasts bounded by microspars of calcite and carbonaceous clay (S-1, PPL). **f** Presence of horizontal as well as subvertical cracks within the chert that are filled up with carbonaceous clay (S-1, PPL). **g** Nodular anhydrite exhibiting aggregates of fine elongate anhedral crystals showing grey interference colour (S-3, BCN). **h** Bladed blocky sparry calcite layers concentrically alternating with pale brownish clayey layers (S-1, BCN)

7.2 Trace Elements

Trace element distribution patterns (Fig. 6a) indicate that the limestone are characterized by high contents of Na, V, Cr, Rb, Cs; low contents of Mn, Li, Sc, Co, Ni, Cu, Zn, Ga, Sr, Zr, Mo, Ba, Pb, Th and very low contents of Be, Nb, Sn, Sb, Hf, Bi and U (Table 2).

7.3 Rare Earth Elements

The rare earth element composition of these limestones is provided in Table 3 and the PAAS normalized (cf. Piper and Bau 2013) REE patterns are exhibited in Fig. 6b. Sadara limestone show variation in Σ REE + Y from 16.03 ppm to 50.86 ppm with an average of 26.73 ppm (Table 3). The REE distribution of Sadara limestones shows slight depletion of LREE compared to HREE (Fig. 6b). Following the convention of McLennan (1989), different ratios such as Ce/Ce*, Gd/Gd* (Bau and Dulski 1996), Pr/Pr*, Y/Y* (Alibo and Nozaki 1999), and Eu/Eu* (Frimmel 2009) were calculated (Table 3). These limestones are characterized by positive anomalies of La, Gd, Eu and negative anomalies of Y and Ce (Fig. 6b, Table 3). Consistent high values of Pr/Pr* are due to the enrichment of Pr and depletion of Ce and Nd in these samples, thereby supporting negative Ce anomaly.

7.4 Stable Isotopes

The δ^{13}C ratios of these carbonates vary from −3.73‰ to 0.57‰ and averages to −1.06‰. The δ^{18}O ratios vary from −5.68‰ to −3.76‰ and averages to −5.06‰ (Table 4). Keith and Weber (1964) proposed "Z" value to discriminate between marine from fresh-water limestones for Jurassic and younger samples (assumed to

Table 2 Major oxide (wt%) and trace element (ppm) composition of Sadara limestones

	S-1	S-2	S-3	S-4	Average
SiO_2	59.82	3.26	8.23	2.42	4.64
Al_2O_3	9.87	0.26	0.66	0.35	0.42
TiO_2	0.54	0.03	0.06	0.03	0.04
Fe_2O_3	7.79	3.00	1.26	1.45	1.91
MgO	0.38	0.52	0.45	0.47	0.48
CaO	9.14	53.31	49.84	54.75	52.63
K_2O	0.11	0.05	0.11	0.06	0.07
P_2O_5	0.12	0.12	0.05	0.09	0.09
LOI	12.24	39.46	39.35	40.39	39.73
Sum	100.00	100.00	100.00	100.00	100.00
Na	371.00	223.00	371.00	223.00	297.00
Mn	4415.00	775.00	465.00	697.00	1588.00
Li	17.99	1.08	1.59	1.32	5.49
Be	1.38	0.32	0.22	0.21	0.54
Sc	13.69	2.64	2.90	2.87	5.52
V	150.00	34.53	20.01	31.79	59.08
Cr	174.40	29.59	23.50	45.13	68.16
Co	16.34	3.86	3.81	3.24	6.81
Ni	91.42	6.80	11.39	17.05	31.66
Cu	67.57	5.89	20.11	3.06	24.16
Zn	19.07	3.78	2.43	2.53	6.95
Ga	4.21	1.53	3.79	2.41	2.98
Rb	761.60	384.30	349.40	363.30	464.65
Sr	62.10	22.54	28.16	24.46	34.32
Zr	7.57	1.01	2.46	0.34	2.84
Nb	1.26	0.80	0.67	0.63	0.84
Mo	4.61	0.51	0.64	3.22	2.25
Sn	0.17	0.04	0.09	0.05	0.09
Sb	0.22	0.09	0.22	0.17	0.18
Cs	140.40	15.39	214.60	26.66	99.26
Ba	69.55	18.20	24.89	20.21	33.21
Hf	0.65	0.10	0.15	0.05	0.24
Pb	24.82	1.20	12.62	0.07	9.68
Bi	0.43	1.17	0.37	0.02	0.50
Th	9.68	2.55	4.21	2.37	4.70
U	1.53	0.59	0.96	0.84	0.98

Table 2 (continued)

	S-1	S-2	S-3	S-4	Average
U/Th	0.16	0.23	0.22	0.35	0.24
Th/Sc	0.71	0.97	1.45	0.83	0.99
Th/U	6.34	4.36	4.40	2.83	4.48
Th/Cr	0.06	0.09	0.18	0.05	0.09
Zr/Cr	0.04	0.03	0.10	0.01	0.04
Zr/Ni	0.08	0.15	0.22	0.02	0.12
Zr/Hf	11.67	9.86	16.09	6.57	11.05
Rb/Sr	12.26	17.05	12.41	14.85	14.14

be non- recrystallized rocks). The calculated Z values for Sadara limestones vary from 116.83 to 126.60 (Table 4).

8 Paleolatitude

The present-day latitude–longitude of lithosection, its age range and global apparent polar wander path (using paleomagnetic reference of Torsvik et al. 2012) has been used to determine the paleolatitude of the lithosection (van Hinsbergen et al. 2015). The inferred paleolatitude for Early Bajocian Sadara lithosection using the paleolatitude calculator of van Hinsbergen et al. (2015), falls within 25.27 to 25.23º S.

9 Discussion

9.1 Depositional Setting

The Sadara carbonates are intramicritic, with intraformational chert breccia at the base, early diagenetic dolomite and dominance of lime flake pebbles of intrabasinal origin at the middle part, with algal laminated structures and desiccation cracks in the upper part of lithosection. Therefore, these carbonates exhibit typical characteristics of subtidal-intertidal-supratidal carbonate mudflat environment (Flugel 1982; Kilibarda and Doffin 2007; Lasemi et al. 2012; Komatsu et al. 2014; James and Jones 2016). Various origins have been proposed for chert breccias, which includes syn-sedimentary breccias (Carozzi and Gerber 1978), fault breccia (Chakraborti 1980; Ghosh et al. 1981), pedogenic siliceous deposits (Ghosh et al. 1981), collapse breccias (Friedman 1997), storm wave action on the seafloor (Bouchette et al. 2001), seismic activity (Rodríguez-Pascua et al. 2000) and transported debris deposits of
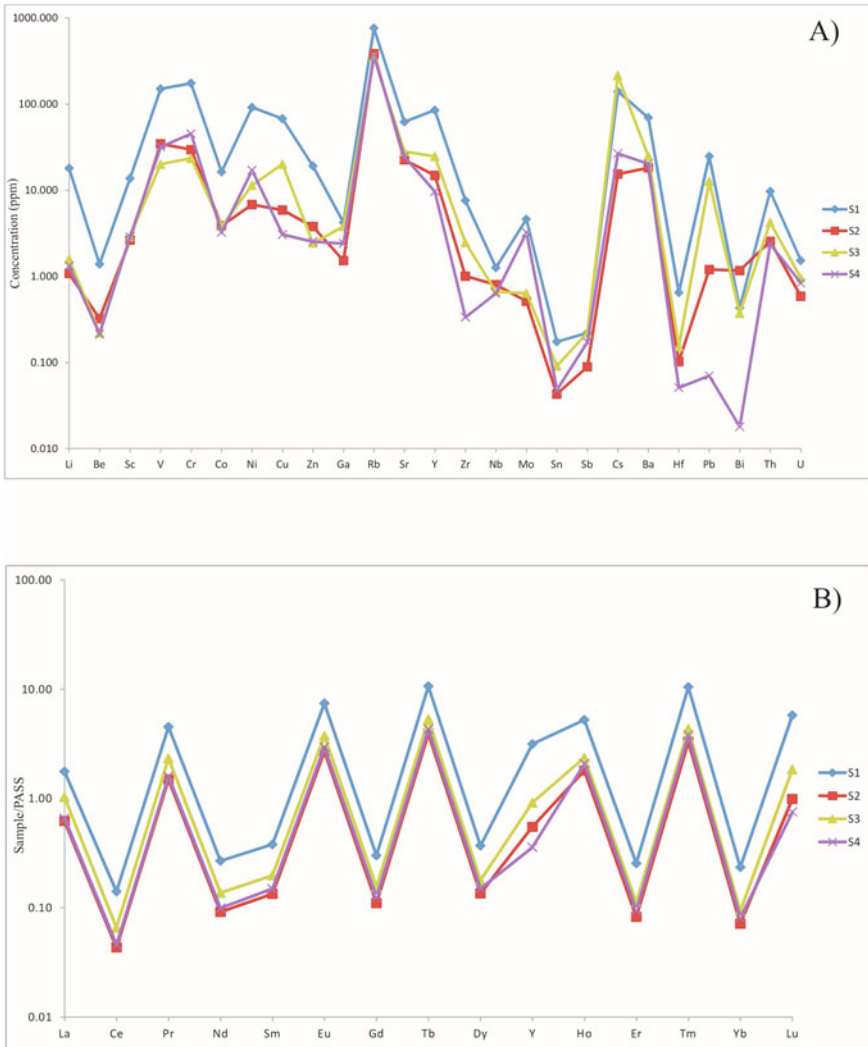
Fig. 6 a Trace element distribution pattern of chert breccia (S-1) and limestones (S-2, S-3, and S-4) from Sadara lithosection. **b** PAAS normalized rare earth element plots of breccia (S-1) and limestones (S-2, S-3, and S-4) from Sadara lithosection

syntectonogenic material that were diagenetically silicified (Kale and Patil Pillai 2011). Following Alterman and Herbig (1991), the chert breccias can be interpreted as shallow marine in origin, which are the products of incipient brecciation within the subtidal regime. James (1980) opined that brecciation and formation of polygons by force of crystallization can occur in supratidal environments. Such breccias could then be subjected to redeposition by wave action and tidal or longshore currents (Eriksson et al. 1976; Alterman and Herbig 1991). The observed polygonal

Table 3 REE + Y (ppm) composition of limestones from Sadara Lithosection (*PAAS normalized, [#]unnormalized. All REE ratios are calculated using normalized values)

	S1*	S2*	S3*	S4*	Average*	S1[#]	S2[#]	S3[#]	S4[#]	Average[#]
La	1.76	0.62	1.03	0.66	**1.02**	67.28	23.68	39.30	25.07	**38.83**
Ce	0.14	0.04	0.07	0.05	**0.07**	11.18	3.44	5.22	3.65	**5.87**
Pr	4.52	1.49	2.33	1.59	**2.48**	39.88	13.17	20.55	14.07	**21.92**
Nd	0.27	0.09	0.14	0.10	**0.15**	9.10	3.10	4.63	3.36	**5.05**
Sm	0.38	0.13	0.20	0.15	**0.21**	2.11	0.74	1.10	0.83	**1.19**
Eu	7.41	2.70	3.75	2.96	**4.21**	8.01	2.92	4.05	3.19	**4.54**
Gd	0.30	0.11	0.15	0.12	**0.17**	1.40	0.51	0.72	0.58	**0.80**
Tb	10.63	3.91	5.31	4.31	**6.04**	8.22	3.03	4.11	3.33	**4.67**
Dy	0.37	0.14	0.18	0.15	**0.21**	1.73	0.63	0.83	0.70	**0.97**
Y	0.38	0.14	0.19	0.15	**0.22**	84.98	14.84	24.68	9.64	**33.53**
Ho	5.24	1.80	2.37	2.07	**2.87**	5.19	1.78	2.34	2.06	**2.84**
Er	0.25	0.08	0.11	0.09	**0.14**	0.73	0.24	0.32	0.27	**0.39**
Tm	10.44	3.30	4.31	3.80	**5.46**	4.23	1.34	1.75	1.54	**2.21**
Yb	0.23	0.07	0.09	0.08	**0.12**	0.66	0.20	0.26	0.23	**0.34**
Lu	5.76	0.99	1.84	0.75	**2.34**	2.50	0.43	0.80	0.33	**1.01**
ΣREE + Y	48.09	15.62	22.06	17.04	**25.70**	247.19	70.05	110.66	68.83	**124.18**
La + Sm + Yb	2.38	0.82	1.32	0.89	**1.35**					
La/Lu	0.31	0.63	0.56	0.87	**0.59**					
Eu/Sm	19.54	20.23	18.98	19.85	**19.65**					
La/La*	1.60	1.68	1.82	1.65	**1.69**					
Eu/Eu*	0.34	1.96	1.99	1.94	**1.56**					
Ce/Ce*	0.15	0.12	0.11	0.12	**0.12**					
Pr/Pr*	11.04	4.07	5.18	4.19	**6.12**					
Gd/Gd*	0.04	0.04	0.04	0.04	**0.04**					
Y anomaly	1.12	0.57	0.72	0.32	**0.68**					
La/Yb	7.51	8.70	10.99	8.12	**8.83**					
Gd/Yb	1.28	1.54	1.65	1.54	**1.50**					
La/Sm	4.64	4.64	5.21	4.40	**4.72**					
Y/Ho	0.07	0.31	0.39	0.17	**0.24**					
Sm/Yb	1.62	1.88	2.11	1.84	**1.86**					
Nd/Yb	1.15	1.28	1.46	1.22	**1.28**					
Er/Nd	0.95	0.90	0.82	0.95	**0.91**					
Dy/Yb	1.57	1.89	1.90	1.85	**1.80**					

Table 4 Stable isotopic composition of limestones from Sadara lithosection

Sample no.	$\delta^{13}C_{V-PDB}$	$\delta^{18}O_{V-PDB}$	$\delta^{18}O_{SMOW}$	Z^1
S-1	−3.73	−5.68	25.01	116.83
S-2	0.57	−3.76	26.99	126.60
S-3	−1.05	−5.32	25.38	122.50
S-4	−0.05	−5.47	25.23	124.47
Average	**−1.06**	**−5.06**	**25.65**	**122.60**

[1]Z value calculation by following equation of Keith and Weber (1964): $Z = 2.048(\delta^{13}C + 50) + 0.498(\delta^{18}O + 50)$, where both $\delta^{13}C$ and $\delta^{18}O$ are expressed as ‰ PDB

flat pebble chert breccias occur locally. These exhibit desiccation cracks, ooids and are associated with intraformational lime flake conglomerate and algal limestone. These are interpreted as products of incipient brecciation of chert in shallow marine regimes (Eriksson et al. 1976; Alterman and Herbig 1991). Insoluble residue and thin sections of limestone of middle and upper parts of Sadara section reveal traces of gypsum and the presence of nodular anhydrite. Upper intertidal and supratidal environments just centimeters above mean tide level, are conducive for the formation of anhydrite and gypsum (Boggs 2009; Kilibarada and Doffin 2007). Shabafrooz et al. (2013) opined that nodular anhydrite forms in early diagenetic (synsedimentary) stage and is characteristic of sabkha facies. The laminated dolomite containing anhydrite, overlying the chert breccias, shows a close similarity with those associated with evaporites in supratidal and upper intertidal sediments of Persian Gulf and Moesian platform NE Bulgaria (Kinsman 1969; Andreeva 2015). Similar dolomite forms by replacement/dolomitization of lime mud in intertidal and supratidal environments by evaporation in shallow ponds (Woo 1999; Rameil 2008). The precipitation of anhydrite in pore waters may have increased the Mg/Ca ratio resulting in the precipitation of dolomite and therefore suggests the prevalence of arid climate (Woo 1999). The coexistence of nodular anhydrite with laminated dolomite suggest that dolomite formed under near surface, hypersaline conditions of pore waters in tidal flat settings (Woo 1999; Rameil 2008). The lime flakes or intraclasts represent clasts formed in the environment of deposition, which are generated by break up of sediments that have been partly or completely lithified on the seafloor (Flugel 1982; James and Jones 2016). Pomoni and Karakitsios (2016) consider intraclastic wackestone-packstone to be formed in shallow subtidal to intertidal moderately high energy conditions. The observed lime flakes are the result of desiccation cracks generated by drying out of lime mud during subaerial exposure. These limes flakes derived by the tearing of mud polygons were transported along with fresh sediments during the next flooding and were deposited, forming lime flake conglomerate. The deposition of flat lime flakes along the lamination as well as exhibiting imbrications is indicative of their deposition in intertidal environment (Flugel 1982; Soman and Kale 1990; Komatsu et al. 2014; Pomoni and Karakitsios 2016; James and Jones 2016). The overlying semi-parallel crenulated laminations, domal upwarps together with laterally linked hemispheroids, consisting of alternating intraclast rich laminae with algal septal rich

laminae represent the algal limestone. Alternating micritic intraclast rich layer with algal septal layers signify periodic flooding of the supratidal environment by unusually high tides (James and Jones 2016). The deposition of this lamination above the mean water level is evident from their close association with desiccation cracks. Many examples of such types of shallowing upward cycles are documented in the geologic record. Such a cycle is considered to form by periodic flooding of carbonate platforms through transgressive event (Tucker 1985). The presence of bioclasts of mollusc, brachiopod, bryozoa, coral, foraminifera, echinoderm, algal filament, ostracod and sponge in these limestones, suggest deposition in the tropical warmer shallow marine environment (Flugel 1982; James and Jones 2016). The bioclasts with micritic envelope suggest the alteration of bioclasts by microbial micritization on the seafloor or just below by endolithic algae, fungi and bacteria (Tucker and Wright 1990). The observed small pale brownish subrounded to ovoidal pellets represent fecal pellets and the comparatively big rounded peloids represent the micritized bioclast (Flugel 1982; James and Jones 2016). The observed spherical ooids with carbonaceous clay nucleus and concentric laminations of micrite are formed by accretion due to constant agitation by tidal currents, in warm shallow marine environments (James and Jones 2016). These ooids are bounded by layers of pore filling sparry calcite and alternations of bladed blocky sparry calcite with concentric pale brownish clayey layers represent meteoric phreatic cementation (Longman 1980).

High contents of insoluble residue in Sadara carbonates (av. 11.56%) are well in accordance with their algal laminated and pelmicritic nature (Flugel 1982). Illite is one of the most abundant clay minerals found in insoluble residues of carbonate rocks, and its interpretation in limestones is difficult because a diagenetic origin cannot be ruled out (Flugel 1982). In the Sadara carbonates, illite is the dominant clay mineral with minor kaolinite and is not associated with chlorite. The illite is possibly derived from preexisting Precambrian granites, under warm climate (Li et al. 2019), probably from Nagar Parkar massif in Pakistan (Jan et al. 2017; Meunier and Velde 2004). The presence of evaporite minerals such as anhydrite and gypsum within these limestones are suggestive of restricted circulation conditions (Flugel 1982; Boggs 2009).

9.2 Redox Conditions

Elemental concentrations in Phanerozoic seawater are considered as novel proxies for interpreting sea-level dynamics and paleooceanographic conditions (Coimbra et al. 2015). Trace element composition of carbonates from basinal environments can be used for paleoenvironmental and sequential analysis (Corbin et al. 2000; Vincent et al. 2006; Kamber et al. 2014; Franchi et al. 2016). High values of Na (80–240 ppm, mean 150 ppm) have been found in restricted lagoonal environments with evaporites, while early diagenetic dolomite with algal laminations and flat pebble conglomerate also yield high values of Na up to 440 ppm (Flugel 1982). The observed concentration of Na (223–371 ppm), is well in accordance with the algal and lime flake conglomeratic nature of Sadara limestone with the presence of anhydrite and early

diagenetic dolomite. U content (av. 0.98 ppm) and U/Th ratio (av. 0.24) of these limestones are low, similar to the shallow marine carbonates deposited under oxic conditions with insignificant siliciclastic contributions (Wright et al. 1984; Jones and Manning 1994; Armstrong-Altrin et al. 2003; Kamber and Webb 2001; Northdurft et al. 2004). The low Mo (av. 2.25 ppm) and V (av. 59.08 ppm) contents of these samples indicate deposition under oxidizing conditions (Jones and Manning 1994; Dypvik and Harris 2001; Hua et al. 2013; Bellanca et al. 1999). V/Cr ratio (av. 0.90) and Ni/Co ratio (av. 3.90) for these samples further suggest oxic to dysoxic bottom water conditions during deposition of these carbonates (Jones and Manning 1994; McManus et al. 2006). A low Sr (100–400 ppm) and high Sr (500–3000 ppm) content in shallow water and deep-water limestones are linked with sparry and micritic limestone types (Flugel 1982). The low Sr content (av. 34.32 ppm) in the limestones relates with meteoric water-rock interactions involving fresh-water fluids with low Sr and Mg content during diagenesis (Vincent et al. 2006). Low values of Th/Sc (av. 0.99), Zr/Cr (av. 0.04), Zr/Ni (av. 0.12), Th/U (av. 4.48) and Rb/Sr (av. 14.14) ratios suggests little terrigenous input (Qui et al. 2013; Dypvik and Harris 2001).

Several studies have demonstrated that chemically precipitated sedimentary rocks are useful proxies for the recording of REE patterns of waters from which they were precipitated (Henderson 1984; Northdurft et al. 2004; Tostevin et al. 2016). In spite that the REE concentrations in carbonates are low (Goldberg et al. 1963; Tlig and M'Rabet 1985), they are useful to differentiate the marine versus non-marine sources of REE (Frimmel 2009; Zhao et al. 2009). Carbonates precipitated in marine environment, are characterized by strong LREE depletion compared to HREE (Özyurt et al. 2020), negative Ce (Ce/Ce* < 1) anomalies accompanied by positive La, Gd and Y anomaly (Zhang and Nozaki 1998; Alibo and Nozaki 1999; Webb and Kamber 2000; Nothdurft et al. 2004; Franchi et al. 2016). The obtained low ΣREE content (av. 25.70 ppm) together with positive Eu/Eu* (1.05 < Eu* < 1.31) and La (1.05 < La* < 1.66) anomalies, negative Ce (av. 0.12), Gd (0.99 > Gd* > 1.24) anomalies and LREE depletion [(Nd/Yb)$_{SN}$ av. 1.28] supports the shallow marine origin of Sadara carbonates (Bellanca et al. 1997; Rollinson 1993; Singh et al. 2016; Allwood et al. 2010; Franchi et al. 2016). The Ce/Ce* in sedimentary rocks has been used by various workers to interpret the redox conditions in seawater at the time when REE were incorporated into marine sediment (German and Elderfield 1990; Nagendra et al. 2011; Tostevin et al. 2016). The negative Ce/Ce* (av. 0.12) anomaly of these carbonates is also an indicator of oxidation of Ce^{3+} to Ce^{4+} in marine oxidizing conditions (Nagendra et al. 2011; Tang et al. 2013; Ling et al. 2013). Several workers used elemental ratios of La/Yb, Nd/Yb, Gd/Yb, Sm/Yb, Er/Nd and Dy/Yb for quantification of REE fractionation (Frimmel 2009). High values of La/Yb, (av. 8.83), together with Nd/Yb (av. 1.28) and Sm/Yb (av. 1.86) supports LREE fractionation and enriched HREE in these sediments (Nagarajan et al. 2011; Qui et al. 2013; Sen and Mishra 2015). The Er/Nd ratio (av. 0.91) of these carbonates are suggestive of very low terrigenous input (De Barr et al. 1988; German and Elderfield 1989; Bellanca et al. 1997). The limestone samples under study exhibit a weak negative Y anomaly (av. 0.68) except one sample exhibiting positive Y anomaly (1.12), indicating retention of the marine signature by these samples (Bau and Dulski

1994). The Y/Ho (unnormalized) ratio of these samples varies from 16.37 to 4.68 and it is lower than that of PAAS (25.71) and Chondrite (28; Qui et al. 2013). Y/Ho can be used as an indicator of terrestrial contamination (Mikhalfi-Al 2008). Weak negative nature of Y anomaly and sub-chondritic Y/Ho ratio (<28) coupled with high values of Nd/Yb ratio indicates minor terrigenous particles input (Qui et al. 2013; Nagarajan et al. 2011) in near-shore environments (Zhao et al. 2009). The values of Zr, Hf, Al_2O_3 and Ce in these samples are significantly lower than that of PAAS, further, imply the minor terrigenous input (Qui et al. 2013).

Veizer and Hoefs (1976) analyzed stable isotopic composition of C and O of 170 carbonate samples and noticed a secular trend over period of ~2800 Ma. According to them, the Proterozoic dolomites are on an average heavier by ~5‰ in $\delta^{18}O$ than their coeval limestones and Precambrian carbonates are heavier in $\delta^{13}C$ at a given $\delta^{18}O$ than their Phanerozoic counterparts. The obtained $\delta^{13}C$ varying from −3.73‰ to 0.57‰ (av. −1.06‰) and $\delta^{18}O$ values varying from −5.68‰ to −3.76‰ (av. −5.06‰) lie well within the range of isotopic composition of Phanerozoic carbonates of Veizer and Hoefs (1976). The observed $\delta^{18}O$ values are negative and are suggestive of precipitation from warmer seawater (James and Jones 2016). Except for Sample S-1 (Z = 116.83), Z values for the rest of the three samples are above 120; hence they can be classified as marine limestones (Keith and Weber 1964). The paleolatitude calculation suggests that the study area during Jurassic time was located in the southern tropical region (van Hinsbergen et al. 2015), which is supported by the presence of ooids, pellets, peloids and anhydrite in these limestones (Mahboubi et al. 2010). The strong negative Ce anomaly suggests the highly alkaline nature of Jurassic seawater (Kcosis et al. 2015).

10 Conclusions

The Sadara limestones represent subtidal-intertidal-supratidal carbonate mudflat deposits on the basis of the following:

(a) The limestones are characterized by intramicritic nature with the presence of intraformational chert breccias at the base, early diagenetic dolomite in the middle part, dominance intrabasinal lime flake pebbles with development of algal laminated structures and desiccation cracks in the upper part.

(b) They have higher insoluble residue content (av. 11.56%). The presence of anhydrite in the thin section as well as its association with gypsum in the insoluble residue suggests restricted circulation conditions in coastal sabkha within intertidal and supratidal zones.

(c) The presence of bioclasts of mollusk, brachiopod, bryozoa, coral, foraminifera, echinoderm, algal filament, ostracod and sponge, as well as the presence of pellets, peloids and ooids in the thin section, suggest deposition in a warmer shallow marine environment. Bioclasts with micritic envelopes suggest microbial micritization on the seafloor representing a marine phreatic diagenetic

environment. The presence of bladed sparry calcite cement binding the ooids and its alternation with pale brownish clay is suggestive of meteoric phreatic diagenesis undergone by these sediments.

(d) The presence of higher content of Na, low content of Mn, Ni, Cu, Co, Pb, U, Th, Sr; V/Cr and Ni/Co ratios supports shallow marine oxic-dysoxic nature with an insignificant siliciclastic contribution.

(e) Low $\sum$REE content, exhibiting seawater like REE pattern with LREE depletion characterized by high values of $(La/Yb)_{SN}$, $(Nd/Yb)_{SN}$, $(Dy/Yb)_{SN}$, low values of Y/Ho, Er/Nd ratios, negative Y anomaly, Gd/Gd*, Ce/Ce*, positive La, Eu anomalies and $(Sm/Yb)_{SN}$, $(La + Sm + Yb)_{SN}$ values substantiates shallow marine nature of carbonates with insignificant terrigenous input.

(f) The $\delta^{13}C$ ($-3.73‰$ to $0.57‰$, av. $-1.06‰$), $\delta^{18}O$ ($-5.68‰$ to $-3.76‰$, av. $-5.06‰$) and Z (av. > 120) values together with paleolatitude data are suggestive of precipitation from warmer tropical seawater.

References

Agarwal SK, Pandey DK (1985) Biostratigraphy of the Bathonian-Callovian Beds of Goradongar in Patchham Island District Kachchh (Gujrat). Proc Indian Nat Sci Acad 51:887–903

Alibo DS, Nozaki Y (1999) Rare earth elements in seawater: particle association, shale-normalization, and Ce oxidation. Geochim Cosmochim Acta 63:363–372

Allwood AC, Kamber BS, Walter MR, Burch IW, Kanik I (2010) Trace elements record depositional history of an Early Archean stromatolitic carbonate platform. Chem Geol 270:148–163

Alterman W, Herbig HG (1991) Tidal flat deposits of the Lower Proterozoic Campbell Group along the southwestern margin of the Kaapvaal craton, Northern Cape Province, South Africa. J African Earth Sci 13:415–435

Andreeva PV (2015) Middle Devonian (Givetian) supratidal sabkha anhydrites from the Moesian Platform (Northeastern Bugaria). Carb Evap 30:439–449

Armstrong-Altrin JS, Verma SP, Madhavaraju J, Lee YI, Ramasamy S (2003) Geochemistry of Upper Miocene Kudankulam Limestones, Southern India. Int Geol Rev 45:16–26

Armstrong-Altrin JS, Madhavaraju J, Sial AN, Kasper-Zubillaga JJ, Nagarajan R, Flores-Castro K, Rodrigues JL (2011) Petrography and stable isotope geochemistry of the Cretaceous EI Abra Limestones (Actopan), Mexico: implication on diagenesis. J Geol Soc India 77:349–359

Arora A, Banerjee S, Dutta S (2015) Black shale in late Jurassic Jhuran Formation of Kutch: possible indicator of oceanic anoxic event? J Geol Soc India 85:265–278

Banerjee S, Bhattacharya SK, Sarkar S (2006) Carbon and oxygen isotope compositions of the carbonate facies in the Vindhyan Supergroup, central India. J Earth Sys Sci 115:113–134

Bansal U, Banerjee S, Pande K, Arora A, Meena SS (2017) The distinctive compositional evolution of glauconite in the Cretaceous Ukra Hill Member (Kutch basin, India) and its implications. Mar Petrol Geol 82:97–117

Bau M, Dulski P (1994) Evolution of Yttrium-Holmium systematics of seawater through time. In: Goldschmidt conference Edenburgh, pp 61–62

Bau M, Dulski P (1996) Anthropogenic origin of positive gadolinium anomalies in river waters. Earth Planet Sci Lett 143:245–255

Bellanca A, Masetti D, Neri R (1997) Rare earth elements in limestone/marlstone couplets from the Albian-Cenomanian Cismon section (Venetian region, northern Italy): assessing REE sensitivity to environmental changes. Chem Geol 141:141–152

Bellanca A, Masetti D, Neri R, Venezia F (1999) Geochemical and sedimentological evidence of productivity cycles recorded in Toarcian black shales from the Belluno Basin, Southern Alps, Northern Italy. J Sed Res 69:466–476

Biswas SK (1977) Mesozoic rock-stratigraphy of Kachchh, Gujarat. Quart J Geol Min Met Soc India 49:1–32

Biswas SK (1987) Regional tectonic framework, structure and evolution of Western margin basins of India. Tectonophysics 135:307–327

Biswas SK (1991) Stratigraphy and sedimentary evolution of the Mesozoic Basin of Kachchh, Western India. In: Tandon SK, Pant CC, Casshyap SM (eds) Sedimentary basins of India, Tectonic context. Gyanodaya Prakashan, Nainital, pp 74–103

Biswas SK (2005) A review of structure and tectonics of Kutch basin, western India, with special reference to earthquakes. Curr Sci 88:1592–1600

Biswas SK (2016a) Mesozoic and tertiary stratigraphy of Kachchh (Kachchh)-a review. In: Thakkar MG (ed) Recent studies in the geology of Kachchh, Geol Soc India Spec Publ, vol 6, pp 1–24

Biswas SK (2016b) Tectonic framework, structure and tectonic evolution of Kachchh Basin, Western India. In: Thakkar MG (ed) Recent studies in the geology of Kachchh, Geol Soc India Spec Publ, vol 6, pp 129–150

Biswas SK, Deshpande SV (1970) Geological and tectonic maps of Kachchh. ONGC Bull 7:115–123

Biswas SK, Deshpande SV (1973) A note on the mode of eruption of Deccan Trap lavas with special reference to Kachchh. J Geol Soc India 14:134–141

Boggs S Jr (2009) Petrology of sedimentary rocks. Cambridge University Press 600

Bouchette F, Séguret M, Moussine-Pouchkine A (2001) Coarse carbonate breccias as a result of water-wave cyclic loading (uppermost Jurassic–South-East Basin, France). Sedimentol 40:767–789

Carozzi AV, Gerber MS (1978) Synsedimentary chert breccia: a Mississippian tempestite. J Sed Pet 48:705–708

Chakraborti P (1980) A petrogenetic study of the Tirohan breccia, Karauli, Rajasthan. Indian J Earth Sci 7:57–63

Chaudhuri A, Banerjee S, Le Pera E (2018) Petrography of Middle Jurassic to Early Cretaceous sandstones in the Kutch Basin, western India: Implications on provenance and basin evolution. J Palaeogeography 7:2–14

Chaudhuri A, Banerjee S, Chauhan G (2020a) Compositional evolution of siliciclastic sediments recording the tectonic stability of a pericratonic rift: Mesozoic Kutch Basin, western India. Mar Pet Geol 111:476–495

Chaudhuri A, Das K, Banerjee S, Fitzsimons ICW (2020b) Detrital zircon and monazite track the source of Mesozoic sediments in Kutch to rocks of Late Neoproterozoic and Early Palaeozoic orogenies in northern India. Gond Res 80:188–201

Chaudhuri A, Chatterjee A, Banerjee S, Ray JS (2020c) Tracing multiple sources of sediments using trace element and Nd isotope geochemistry: provenance of the Mesozoic succession in the Kutch Basin, western India. Geol Mag. https://doi.org/10.1017/S0016756820000539

Chaudhuri A, Banerjee S, Prabhakar N, Das A (2020d) The use of heavy mineral chemistry in reconstructing provenance: a case study from Mesozoic sandstones of Kutch Basin (India). Geol J. https://doi.org/10.1002/gj.3922

Coimbra R, Immenhauser A, Oloriz F, Rodriguez-Galiano V, Chica-Olmo M (2015) New insights into geochemical behaviour in ancient marine carbonates (Upper Jurassic Ammonitico Rosso): novel proxies for interpreting sea-level dynamics and palaeoceanography. Sedimentol 62:266–302

Corbin JC, Person A, Iatzoura A, Ferre B, Renard M (2000) Manganese in pelagic carbonates: indication of major tectonic events during the geodynamic evolution of a passive continental margin. Palaeo Palaeo Palaeo 156:123–138

De Baar HJW, German CR, Elderfield H, Van Gaans P (1988) Rare earth element distributions in anoxic waters of the Cariaco Trench. Geochim Cosmochim Acta 52:1203–1219

Dickson JAD (1966) Carbonate identification and genesis as revealed by staining. J Sed Pet 36:491–505

Dunham RJ (1962) Classification of carbonate rocks according to depositional texture. AAPG Mem 1:108–121

Dypvik H, Harris NB (2001) Geochemical facies analysis of fine-grained siliciclastics using Th/U, Zr/Rb and Zr + Rb/Sr ratios. Chem Geol 18:131–146

Eriksson KA, Truswell JF, Button A (1976) Paleoenvironmental and geochemical models from an Early Proterozoic carbonate succession in South Africa. In: Walter MR (ed) Stromatolites, pp 635–643

Evamy BD (1963) The application of a chemical staining technique to a study of dedolomitization. Sedimentol 2:164–170

Flugel E (1982) Microfacies analysis of limestones. Springer, Berlin, Heidelberg, p 633

Folk RL (1959) Practical petrographical classification of limestones. AAPG Bull 43:1–38

Franchi F, Turetta C, Cavalazzi B, Corami F, Barbieri R (2016) Trace elements and REE geochemistry of Middle Devonian carbonate mounds (Maider Basin, Eastern Anti-Atlas, Morocco): implications for early diagenetic processes. Sediment Geol 343:56–71

Friedman GM (1997) Dissolution collapse breccias and paleokarst resulting from dissolution of evaporite rocks, especially sulfates. Carb Evap 12:53–63

Frimmel HE (2009) Trace element distribution in Neoproterozoic carbonates as palaeoenvironmental indicator. Chem Geol 258:338–353

German CR, Elderfield H (1989) Rare earth elements in Saanich Inlet, British Columbia, a seasonally anoxic basin. Geochim Cosmochim Acta 53:2561–2571

German CR, Elderfield H (1990) Application of the Ce anomaly as a paleoredox indicator: the ground rules. Paleoceanography 5:823–833

Ghosh DB, Soni MK, Nair KKK, Munshi MM (1981) Stratigraphy and sedimentation of the Vindhyans in the lower Narmada valley. Misc Publ Geol Surv India 108:182–188

Goldberg ED, Koide M, Schmitt RA (1963) Rare earth distributions in the marine environment. J Geophy Res 68:4209–4217

Henderson P (1984) Rare earth element geochemistry. Elsevier, Amsterdam 510

Hua G, Yuansheng D, Lian Z, Jianghai Y, Hu H (2013) Trace and rare earth elemental geochemistry of carbonate succession in the Middle Gaoyuzhuang Formation, Pingquan Section: Implications for Early Mesoproterozoic ocean redox conditions. J Palaeogeography 2:209–221

Ireland HA (1971) Insoluble residues. In: Carver RA (ed) Procedures in sedimentary petrology, pp 479–498

James NP (1980) Shallowing upward sequences in carbonates. In: Walker RG (ed) Facies models, Geosci Canada Reprint Ser 1:109–120

James NP, Jones B (2016) Origin of carbonate sedimentary rocks. John Wiley, UK 466

Jan MQ, Agheem MH, Laghari A, Anjum S (2017) Geology and petrography of the Nagar Parkar igneous complex, Southeastern Sind, Pakistan: the Kharsar body. J Geol Soc India 89:91–98

Jones B, Manning DAC (1994) Comparison of geochemical indices used for the interpretation of palaeoredox conditions in ancient mudstones. Chem Geol 111:111–129

Joseph JK, Patel SJ, Bhatt NY (2016) Stratigraphy and depositional environment of sediments of the Goradongar Formation, Goradongar Range, Patcham Island, Kachchh. In: Thakkar MG (ed) Recent studies in the geology of Kachchh, Geol Soc India Spec Publ, vol 6, pp 32–45

Kale VS, Patil Pillai S (2011) A reinterpretation of two Chert breccias from the Proterozoic Basins of India. J Geol Soc India 78:429–445

Kamber BS, Webb GE (2001) The geochemistry of late Archaean microbial carbonate: implications for ocean chemistry and continental erosion history. Geochim Cosmochim Acta 65:2509–2525

Kamber BS, Webb GE, Gallagher M (2014) The rare earth element signal in Archaean microbial carbonate: information on ocean redox and biogenicity. J Geol Soc 171:745–763

Kcosis L, Gheerbrant E, Mouflih M, Cappetta H, Ulianov A, Chiaradia M, Bradep N (2015) Gradual changes in upwelled sea water conditions (redox, pH) from the late Cretaceous through early Paleogene at the NW coast of Africa: -ve Ce anomaly trend recorded in fossil bioapatite. Chem Geol 421:44–54

Keith ML, Weber YN (1964) Carbon and oxygen isotopic composition of selected limestone and fossils. Geochim Cosmochim Acta 8:1787–1816

Khelen AC, Manikyamba C, Ganguly S, Singh TD, Subramanyam KSV, Ahmad SM, Reddy MR (2017) Geochemical and stable isotope signatures of Proterozoic stromatolitic carbonates from the Vempalle and Tadpatri formations, Cuddapah Supergroup, India: implications on paleoenvironment and depositional conditions. Precam Res 298:365–384

Kilibarada Z, Doffin J (2007) Mudcracks, bird's-eye, and anhydrite in intertidal/ supratidal late Silurian Kokomo limestone, Indiana. Proc Indiana Acad Sci 116:1–10

Kinsman DJ (1969) Modes of formation sedimentary associations and diagnostic features of shallow water and supratidal evaporites. AAPG Bull 53:830–840

Komatsu T, Naruse H, Shigeta Y, Takashima R, Maekawa T, Dang HT, Dinh TC, Nguyen PD, Nguyen HH, Tanaka G, Sone M (2014) Lower Triassic mixed carbonate and siliciclastic setting with Smithian–Spathian anoxic to dysoxic facies, an Chau Basin, northeastern Vietnam. Sediment Geol 300:28–48

Lasemi Y, Jahani D, Amin-Rasouli H, Lasemi Z (2012) Ancient carbonate tidalites. In: Davis RA, Dalrymple RW (eds) Principles of tidal sedimentology. Springer, Heidelberg, Germany, pp 567–607

Li P, Zhang C, Guo Z, Deng C, Ji X, Jablonski NG, Wu H, Zhu R (2019) Clay mineral assemblages in the Zhaotong Basin of southwestern China: implications for the late Miocene and Pliocene evolution of the South Asian monsoon. Palaeo Palaeo Palaeo 516:90–100

Ling HF, Chen X, Li D, Wang D, Shields-Zhou GA, Zhu MY (2013) Cerium anomaly variations in Ediacaran–earliest Cambrian carbonates from the Yangtze Gorges area, South China: implications for oxygenation of coeval shallow sea-water. Precam Res 225:110–127

Longman MW (1980) Carbonate diagenetic textures from near surface diagenetic environments. AAPG Bull 64:461–487

Madhavaraju J, Löser H, Scott RW, Sandeep S, Sial AN, Ramasamy S (2017) Petrography, geochemistry and stable isotopes of carbonate rocks, Lower Cretaceous Alisitos Formation, Los Torotes section, Baja California. Mexico Revis Mex de Cien Geológ 34:63–77

Mahboubi A, Moussavi-Harami R, Carpenter S, Aghaei A, Collins LB (2010) Petrographical and geochemical evidences for paragenetic sequence interpretation of diagenesis in mixed siliciclastic-carbonate sediments: Mozduran Formation (Upper Jurassic), south of Agh-Darband, NE Iran. Carb Evap 25:231–246

McLennan SM (1989) Rare earth elements in sedimentary rocks: influence of provenance and sedimentary processes. Rev Mineral Geochem 21:169–200

McManus J, Berelson WM, Severmann S, Poulson RL, Hammond DE, Klinkhammer GP, Holm C (2006) Molybdenum and uranium geochemistry in continental margin sediments: paleoproxy potential. Geochim Cosmochim Acta 70:4643–4662

Meunier A, Velde B (2004) The geology of illite. In: Meunier A, Velde B (eds) illite. Springer, Berlin, Helidelberg, pp 63–143

Mikhalfi-Al AS (2008) Rare earth elements in modern coral sands: an environmental proxy. Environ Geol 54:1145–1153

Nagarajan R, Madhavraju J, Armstrong-Altrin JS, Nagendra R (2011) Geochemistry of Neoproterozoic limestones of the Shahabad Formation, Bhima Basin, Karnataka, southern India. Geosci J 15:9–25

Nagendra R, Nagarajan R, Bakkiaraj D, Armstrong-Altrin JS (2011) Depositional and post-depositional setting of Maastrichtian limestone, Ariyalur Group, Cauvery Basin, South India: a geochemical appraisal. Carb Evap 26:127–147

Nothdurft LD, Webb GE, Kamber BS (2004) Rare earth element geochemistry of Late Devonian reefal carbonates, canning basin, Western Australia: confirmation of a seawater REE proxy in ancient limestones. Geochim Cosmochim Acta 68:263–283

Oppel A (1856) Dei Juraformation Englands Frankreichs und Südwestlichen Deutschlands. Abdruck des Würternbergen naturwissen-schaflichen Jahreshefte 12–14:1–857

Özyurt M, Kırmacı MZ, Al-Aasm I, Hollis C, Taslı K, Kandemir R (2020) REE characteristics of Lower Cretaceous Limestone Succession in Gümüşhane, NE Turkey: implications for Ocean Paleoredox conditions and diagenetic alteration. Minerals 10:1–25

Pandey B, Pathak D, Krishna Jai (2013) *Calliphylloceras Heterophylloides* (Oppel, 1856) from the basal most Jurassic succession of Sadhara dome, Kachchh, India. J Palaeontol Soc India 58:61–65

Patel SJ, Joseph JK, Bhatt NY (2013) Sequence stratigraphic analysis of the mixed siliciclastic-carbonate sediments (Middle Jurassic) of the Patcham island, Kutch, Western India: an ichinological approach. Geol Soc India Spec Publ 1:57–77

Patel SJ, Joseph JK, Bhatt NY (2014) Ichnology of Goradonger Formation, Goradongar Hill Range, Patcham Island, Kachachh, Western India. J Geol Soc India 84:129–154

Piper DZ, Bau M (2013) Normalized rare earth elements in water, sediments, and wine: identifying sources and environmental redox conditions. Am J Analytic Chem 4:69–83

Piper DZ, Perkins RB, Rowe HD (2007) Rare-earth elements in the Permian Phosphoria formation: paleo proxies of ocean geochemistry. Deep-Sea Res II 54:1396–1413

Pomoni FA, Karakitsios V (2016) Sedimentary facies analysis of a high-frequency, small-scale, peritidal carbonate sequence in the Lower Jurassic of the Tripolis carbonate unit (central western Crete, Greece): long-lasting emergence and fossil laminar dolocretes horizons. J Palaeogeography 5:241–257

Qui Z, Wang QC, Yan DT (2013) Geochemistry of the Middle to Late Permian limestones from the marginal zone of an isolated platform (Laibin, South China). Sci China Earth Sci 56:1688–1700

Rajendran K, Rajendran CP, Thakkar M, Tuttle MP (2001) The 2001 Kachchh (Bhuj) earthquake: coseismic surface features and their significance. Curr Sci 80:1397–1405

Rameil N (2008) Early diagenetic dolomitization and dedolomitization of Late Jurassic and earliest Cretaceous platform carbonates: a case study from the Jura Mountains (NW Switzerland, E France). Sediment Geol 2:70–85

Rodríguez-Pascua MA, Calvo JP, De Vicente G, Gómez-Gras D (2000) Soft-sediment deformation structures interpreted as seismites in lacustrine sediments of the Prebetic Zone, SE Spain and their potential use as indicators of earthquake magnitudes during the Late Miocene. Sediment Geol 135:117–135

Rollinson H (1993) Using geochemical data: evaluation, presentation, interpretation. Pearson Education Ltd, Essex, London 352

Roy A, Chakrabarti G, Shome D (2018) Geochemistry of the Neoproterozoic Narji limestone, Cuddapah Basin, Andhra Pradesh, India: implication on palaeoenvironment. Arab J Geosci 784:1–13

Scholle PA, Arthur MA (1980) Carbon isotope fluctuations in Cretaceous pelagic limestones: potential stratigraphic and petroleum exploration tool. AAPG Bull 64:67–87

Sen S, Mishra M (2015) Geochemistry of Rohtas limestone from Vindhyan Supergroup, Central India: evidences of detrital input from felsic source. Geochem Int 53:1107–1122

Shabafrooz R, Mahboubi A, Moussavi-Harami R, Amiri-Bakhtiar H (2013) Facies analysis and sequence stratigraphy of the evaporite bearing Sachun Formation at the type locality, South East Zagros Basin. Iran. Carb Evap 28:457–474

Shankar R (2001) Seismotectonics of Kachchh rift Basin and its bearing on the Himalayan Seismicity. ISET J Earthquake Tech 38:59–65

Singh AK, Tewari VC, Sial AN, Khanna PP, Singh NI (2016) Rare earth elements and stable isotope geochemistry of carbonates from the melange zone of Manipur ophiolitic Complex, Indo-Myanmar Orogenic Belt, Northeast India. Carb Evap 31:139–151

Soman GR, Kale MG (1990) Sedimentological studies of Penganga limestones from Wani area, District Yeotmal, Maharashtra. Geol Surv India Spec Publ 28:369–383

Srivastava VK, Singh BP (2019) Depositional environments and sources for the middle Eocene Fulra Limestone Formation, Kachchh Basin, western India: evidences from facies analysis, mineralogy, and geochemistry. Geol J 54:62–82

Tanaka K, Akagawa F, Yamamoto K, Tani Y, Kawabe T, Kawai T (2007) Rare earth element geochemistry of Lake Baikal sediment: its implication for geochemical response to climate change during the last glacial/interglacial transition. Quat Sci Rev 26:1362–1368

Tang HS, Chen YJ, Santosh M, Zhong H, Yang T (2013) REE geochemistry of carbonates from the Guanmenshan Formation, Liaohe Group, NE Sino-Korean Craton: implications for seawater compositional change during the Great Oxidation Event. Precam Res 227:316–336

Tlig S, M'Rabet A (1985) A comparative study of the Rare Earth element (REE) distributions within the lower Cretaceous dolomites and limestones of Central Tunisia. Sedimentol 32:897–907

Tobia FH (2018) Stable isotope and rare earth element geochemistry of the Baluti carbonates (Upper Triassic), Northern Iraq. Geosci J 22:975–987

Tostevin R, Shields GA, Tarbuck GM, He T, Clarkson MO, Wood RA (2016) Effective use of cerium anomalies as a redox proxy in carbonate-dominated marine settings. Chem Geol 438:146–162

Torsvik TH, Van der Voo R, Preeden U, Mac Niocaill C, Stenberger B, Doubrovine PV, van Hinsbergen DJ, Domeir M, Gaina C, Tohver E, Meerut JG (2012) Phanerozoic polar wander, paleogeography and dynamics. Earth Sci Rev 114:325–368

Tucker ME (1985) Shallow marine carbonate facies and models. Geol Soc London Spec Publ 18:147–169

Tucker ME, Wright VP (1990) Carbonate sedimentology. Blackwell Scientific Publications, Oxford, London, Edinburgh, Melbourne 482

van Hinsbergen DJ, de Groot LV, van Schaik SJ, Spakman W, Bijl PK, Sluijs A, Langereis, CG, Brinkhuis H (2015) A paleolatitude calculator for paleoclimate studies. PloS One 10. https://doi.org/10.1371/journal.pone.0126946

Veizer J, Hoefs J (1976) The nature of O^{18}/O^{16} and C^{13}/C^{12} secular trends in sedimentary carbonate rocks. Geochim Cosmochim Acta 40:1387–1395

Vincent B, Rambeau C, Emmanuel L, Loreau JP (2006) Sedimentology and trace element geochemistry of shallow-marine carbonates: an approach to paleoenvironmental analysis along the Pagny-sur-Meuse Section (Upper Jurassic, France). Facies 52:69–84

Webb GE, Kamber BS (2000) Rare earth elements in Holocene reefal microbialites: a new shallow seawater proxy. Geochim Cosmochim Acta 64:1557–1565

Woo KS (1999) Cyclic tidal successions of the middle Ordovician Maggol Formation in the Taebaeg area, Kangwondo, Korea. Geosci J 3:123–140

Wright J, Seymour RS, Shaw HF (1984) REE and neodymium isotopes in conodont apatite. Variation with geological age and depositional environment. GSA Spec Pap 196:325–340

Zhang J, Nozaki Y (1998) Behavior of rare earth elements in seawater at the ocean margin: A study along the slopes of the Sagami and Nankai troughs near Japan. Geochim Cosmochim Acta 62:1307–1317

Zhao YY, Zheng YF, Chen F (2009) Trace element and strontium isotope constraints on sedimentary environment of Ediacaran carbonates in southern Anhui, South China. Chem Geol 265:345–362

Zhao MY, Zheng YF (2014) Marine carbonate records of terrigenous input into Paleotethyan seawater: geochemical constraints from Carboniferous limestones. Geochim Cosmochim Acta 141:508–531

Cosmopolitan Status for *Taramelliceras kachhense* (Waagen) (Ammonoidea) from Kutch, Western India

Pinaki Roy, Sunipa Mandal, Sayak Sur, and Sharadindu Layek

Abstract Individual organisms within extant species, including cephalopods, vary morphologically (size, shape and colour), physiologically, behaviourally and demographically. This was no different for the extinct ammonoids, which are well known for intra-specific variation in conch shape, ornamentation, ontogeny as well as the morphology of the suture line. The ammonoides, like other molluscs, sometimes exhibit wide morphological intra-specific variation of their shells. Although this phenomenon is of greatest importance, it has rarely been investigated and quantified in large samples. The present work thrives on revisiting the taxonomy of the genus *Taramelliceras* del Campana from Kutch, western India. For that purpose, morphometric analysis has been performed using multivariate data available from the present collection as well as the earlier topotypes. A comparison has been made with the European types to understand the palaeobiogeography of the present species *Taramelliceras kachhense* (Waggen).

Keywords Cosmopolitan · *Taramelliceras* · Ammonoidea · Upper jurassic · Morphometric analysis · Taxonomy · Kutch · India

1 Introduction

The present study encompasses taxonomic revision of the species described by Spath (1927–33) under the genus *Taramelliceras* Del Campana. The subfamily Taramelliceratinae belonging to the family Oppelidae was recorded and described by Spath (1927–33) from the Jurassic (Upper Oxfordian – Kimmeridgian) sediments, Kutch, Gujarat, India. However, the study of ammonoids, mainly those forms resembling *Taramelliceras* fauna was first introduced by Waggen (1875). Since the early works

P. Roy (✉)
Department of Geology, Durgapur Government College, Kazi Nazrul University, Durgapur, West Bengal, India
e-mail: pinakieroy@gmail.com

S. Mandal · S. Sur · S. Layek
Department of Geological Sciences, Jadavpur University, Kolkata, West Bengal, India

of Waggen (1875) and Spath (1927–1933) on ammonoids, which mostly lack strati-graphic precision, no serious studies were made until recently of Kimmeridgian ammonoids from Kutch, India. Altogether 13 species had been described and cate-gorized separately by Spath (1927–33) for the Kutch assemblage under the genus *Taramelliceras* del Campana: *Taramelliceras kachhense, T. compsom, T. transito-rium, T. planifrons, T. akher* sp nov., *T.* aff. *holbeini, T. neriforme, T. gibbosum, T. subkobyi, T.* sp. ind, *T. pseudoflexuosum, T. succedense, T. franciscanum.* Spath (1927–1933) mentioned close similarities between *T. kachhense* and *T.* cf. *compsum* and both were described from the Middle Kimmeridgian of Kutch.

In the present endeavor, while revisiting the type specimens (Spath 1927–33, mostly of GSI) along with their comparative study with recent collections. The aforementioned species have been synonymized under *Taramelliceras kachhense* (Waggen 1875). Since all 13 species, described by Spath (1927–33), belongs to a single stratigraphic level within the Kimmeridgian stage, the present study thrives on invoking unnecessary subjective splitting, and the minor morphological differences have been redesignated as intraspecific variations. Despite the good preservation of the type materials, a number of morphological details e.g. shape and size important for the systematic placement of the taxon have not been properly taken recourse. However, the re-examination the type materials of *Taramelliceras* (Spath 1927–33) reveals their morphometrical homologies with present collections and it re-affirm the same contention.

The topotypes, as well as the type specimens, were derived from the argilla-ceous to arenaceous carbonate sediments of the Jhuran Formation (Kimmeridgian to Tithonian) of the Kutch basin exposed near Ler at about 29 km southeast of Bhuj (Fig. 1). Baudouin et al. (2011) described *Taramelliceras compsum* (Oppel) from Acanthicum zone of upper Kimmeridgian of Mt. Crussol (Ardèche, France) and addressed ontogenetic variability and sexual dimorphism within the species. The intrinsic studies were conducted with a specific focus on the Upper Jurassic ammonite genus *Taramelliceras* del Campana from Kutch, encompassing the Jhuran
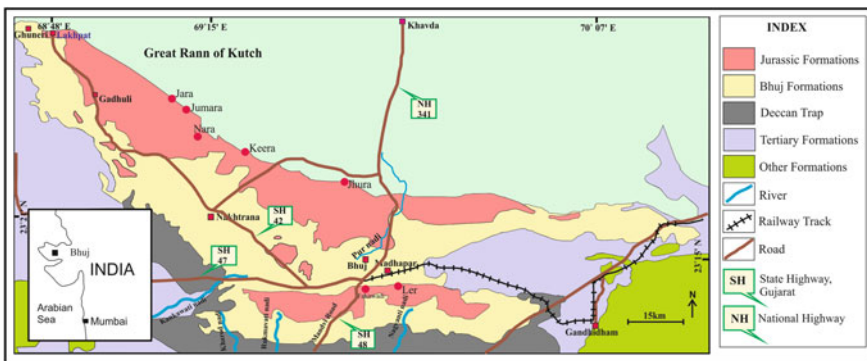
Fig. 1 Locations of fossil collections, shown on a Geological Map of Kutch, western India

Formation. The morphological variations have been analysed in the light of sexual dimorphism (Callomon 1963; Roy 2011) and population dynamics.

The present study of *Taramelliceras kachhense* has been emphasized on the following diagnostic features: **a** Involute discoidal shell **b** Smooth inner whorls with sparse clavi at the ventro-lateral margin **c** Keel at the venter disappears as it reaches the adult stage of growth. The present study has also attempted a multivariate analysis to test the congruency of clubbing 13 species of Spath (1927–33) into *T. kachhense,* besides, it strived to find similarities between the two species *T. kachhense* and *T. compsum* that ensues cosmopolitan status for *T. kachhense.*

2 Geological Setting

The ammonite bearing beds occur in Kimmeridgian to Tithonian of the Kutch basin. The pericratonic basin situated at the western margin of the Indian plate (Biswas 1981); controlled by three major faults, viz., northern margin of the basin is bounded by the subsurface ridge of Nagarparkar; Radhanpur Arch is present in the Eastern margin and in the southern part Kathiawar uplift (Biswas 1981, 2016). A general consensus is that the Jurassic succession in Kutch developed in a marine realm (Biswas 1977, 1981; Howard and Singh 1985; Krishna et al. 1983; Fursich et al. 1991, 2001; Fursich and Pandey 2003). The basin opened up with the initial fragmentation of Gondwana during the Middle Jurassic and sedimentation began soon due to repeated transgression and regression events (Biswas 1977). The southward extension of the Tethyan Ocean between Africa and India formed a small arm of Gulf of Madagascar (Fürsich et al. 2001; Fürsich and Pandey 2003; Shome 2009). In the south, the Gulf of Kutch separates Kutch Mainland and the Kathiawar uplifts. The basin was predominantly filled with fine- to coarse-grained siliciclastics except for the substantial amount of carbonate sediments in the Bajocian-Callovian. The most striking feature of the Kutch Mainland basin architecture is the occurrence of an NNE-SSW oriented meridional high, a basement ridge across the middle of the E-W rift system (Biswas 2016). The regional structure consists of three parallel, NW–SE trending anticlines. The Jurassic rocks are best developed in the central anticline (Wynne 1872; Nath 1932), situated towards the north of the Mainland. These anticlines are superimposed by a set of zones of culmination that crop out as topographical domes, as at Jara, Jumara, Keera and Jhura in the north and Ler-Hamundra in the east of the Mainland. To the west of the Median high, the basin was deeper, accommodating a considerably thicker pile of sediment than on the east. The highlands are tilted fault blocks and sub-basin between them are half-graben (Biswas 1981). The highlands have been produced by a series of parallel east to west quasi vertical, marginal faults which follow the major trend of the Precambrian granitic basement. The domal outcrops are disturbed by the Deccan Trap volcanic intrusion. Jurassic sediments in Kutch basin, ranging in age from Bathonian to Aptian, are subdivided into four major divisions, namely Jhurio, Jumara, Jhuran and Bhuj formations (Biswas 1977; Krishna 1984; Arora et al. 2015, 2017;

Bansal et al. 2017; Chaudhuri et al. 2018, 2020a,2020b,2020c,2020d). Among these the Jhurio and Jumara Formations are present as inliers and are surrounded by the younger Jhuran Formation. The Jhuran Formation is divisible into four distinct members, viz. the Lower, Middle (also known as Rudramata Shale Member), Upper and Katesar members (Table 1). The youngest Katesar Member is exposed only in the western part of the basin. In the remaining part of the basin, the Katesar Member and the top part of the Upper Member are eroded and represented by a regional unconformity. The Upper Jurassic (i.e. Kimmeridgian to Tithonian) Jhuran Formation is approximately 400–750 m thick (Table 1); and is underlain by the Dhosa Oolite Member of the Jumara Formation, separated by a late middle Oxfordian-early Kimmeridgian disconformity (Krishna et al. 1983; Desai and Patel 2009; Alberti et al. 2013; Biswas 2016; Chaudhuri et al. 2018, 2020a,2020b,2020c,2020d). The Kimmeridgian-Tithonian sediments of Jhuran Formation consist of sandstones that become increasingly silty and shaley westward. The specimens of the present study have been collected from Ler, southeast of Bhuj encompassing the late Early to Late Kimmeridgian age (Krishna et al. 1996), which is exposed as the Lower Member of the Jhuran Formation in Kutch Mainland (Biswas 2016 and references therein). It mainly comprises alternating sandstone and shale of equal proportions intervened

Table 1 Stratigraphic nomenclature of the Jurassic sediments of Kutch in the studied section adopted from Biswas (1977)

Neocomian	Bhuj		Ghuneri	Rhythmic sequence of sandstone-shale-ironstone
	Disconformity			
	Jhuran		Katesar	Cross bedded sandstone with calcareous bands locally fossiliferous
Kimmeridgian to Tithonian			Upper	Thinly bedded sandstones calcareous, fossiliferous
			Middle	Predominantly fossiliferous shales
			Lower	Fossiliferous Shale, sandstone alternation
Oxfordian	Jumara		Dhosa oolite	Shales with oolitic limestone bands, fossils

by several fossiliferous sandstones. But top of the Lower Member is characterised by marl with large sized belemnites.

3   Materials and Methods

The well-developed sequence of the Lower Member of the Jhuran Formation crops out in the area between the Jumara and Jara domes and at the base of the Jara-Mara Cliff in the western part of Kutch Mainland and Ler, Jawaharnagar in the eastern part (Fig. 1). Selected local and regional marker beds were traced across the sections for a closed-spaced lithostratigraphic correlation. For a regional understanding, the sections were correlated with the type section in the eastern part of the basin. The ammonite fossil assemblages were studied on bedding surfaces as well as in bedding sections for collecting the following data: (1) shape and size components (2) ornamental characteristics, and (3) degree of involution along with other parameters.

A comprehensive high-resolution collection of fossil specimens, systematic study and faunal elements along with their distribution encompassing the Lower Member of the Jhuran Formation from Ler section near Bhuj in the Kutch district, Gujarat have been carried out. The shape and size of faunal elements and compositions through the successive beds have been quantified from 24 specimens of the present collection (housed in the Department of Geology, Durgapur Government College, Durgapur, West Bengal) and 12 GSI specimens. The morphological attributes like shell diameter, umbilical diameter, whorl height and whorl width of each specimen were estimated by using Digital Vernier calipers (dimensions of the specimens are given in Annexure 1). Morphometric and multivariate analyses were erected by using calculation of a variety of frequency and richness measures for determining the distinctive characteristics from variant taxa through PAST software (ver. 2.17c; Hammer et al. 2001); based on distance measures and landmarks for a proper understanding of ontogenetic and intra-specific differences.

4   Systematic Description

Class **Cephalopoda** Cuvier 1797
  Order **Ammonoidea** Zittel 1884
  Suborder **Ammonitina** Hyatt 1889
  Superfamily **Haploceratacea** Zittel 1884
  Family **Oppelidae** Douvillé 1890
  Subfamily **Taramelliceratinae** Spath 1927–33
  Genus *Taramelliceras* Spath 1927–33
  Type species:- *Ammonite trachinotus* Oppel (1863)
  Taramelliceras kachhense **(Waagen)**

Figures 2, 3, 4, 5, 6).

1875	*Oppelia kachhense*, Waagen p. 55, plate 10, Fig. 4
1893	*Ammonites* (*Oppelia*) *kachhensis* (Waagen): Oldham, p. 222
1903	*Oppelia* (*Neumaryia*) *cachensis* (Waagen); Uhlig, p.41
1912	*Oppelia kutchensis* Waagen; Smith (a), p. 714
1913	*Oppelia kachhensis* (Waagen); Smith (c), p. 422
1924	*Neumaryiceras kachhense* (Waagen), Spath, p. 113
1927–33	*Taramelliceras* cf. *compsum* (Oppel), p. 137, plate 18, Fig. 10
1927–33	*Taramelliceras* aff. *holbeini* (Oppel), Spath, p. 138, plate 14, Fig. 14
1927–33	*Taramelliceras* aff. *franciscanum* (Fontannes), Spath p. 139, plate 15, Fig. 9
1927–33	*Taramelliceras pseudoflexuosum* (Favre), Spath p. 141, plate 18, Fig. 2a–b
1927–33	*Taramelliceras transitorium*, Spath p. 142, plate 14, Fig. 8
1927–33	*Taramelliceras planifrons*, Spath p. 143, plate 14, Fig. 9a–b; plate 18, Fig. 5; plate 19, Fig. 2
1927–33	*Taramelliceras subkobyi*, Spath p. 146, plate 15, Fig. 8; plate 17, Fig. 8a–b
1927–33	*Taramelliceras akher*, Spath p. 135, plate 19, Fig. 4a, b
1927–33	*Taramelliceras nereiforme* Spath plate 16, Figs. 11a, b; 12a, b; plate 19, Figs. 3a, b

Description [Macroconch]: Shell large; the gigantic specimen of *T. kacchense* reported by Spath (1927–33, plate 18, Fig. 1) has a diameter of 162 mm with about last half whorl is occupied by body chamber. Adult phragmocone diameter is ranging between 80–110 mm. Shell is involute at the inner whorls and becomes evolute at the adult phragmocone (U/D = 0.15–0.3). Compressed shell (W/H = 0.45–0.9) shows elliptical to subtrapezoidal whorl section.

Innermost whorl smooth with the rounded periphery, only a few traces of transversely elongated tubercles occur near the ventral area at the diameter of 20 mm (see Spath 1927–33, plate 19, Fig. 3a, b). Though some variants still have smoothly arched periphery at the diameter of 40 mm and ventro-lateral tubercles appear at the last quarter of the whorl (Spath 1927–33, plate 16, Fig. 12a, b). However, the smooth stage varies and may not always be biological; most of the specimens, including types and additional topotypes are internal moulds. Therefore, weakly developed ribs may be completely obliterated, thus exhibiting the impression of smooth inner whorls, as shown by some inflated varieties with highly ornamented inner whorls. Weak falcoid primaries appear at the umbilical seam at the diameter of about 15–30 mm. They are bifurcating at mid-lateral and secondaries continue up to the ventro-lateral margin where they form strong tubercles. At the adult phragmocone stage, ribbing becomes weak or obsolete, though in finely costate varieties, ribbing continues till the end and ribbing becomes uniformly thicken and distant at latter whorls. In either of the cases, adult phragmocone with smooth or ribbed inner lateral, ventro-lateral and mid-ventral tubercles continue till to the end.

Venter is rounded and characterized by almost circular whorl section in inner whorls. Traces of transversely elongated tubercles present on the mid venter at about
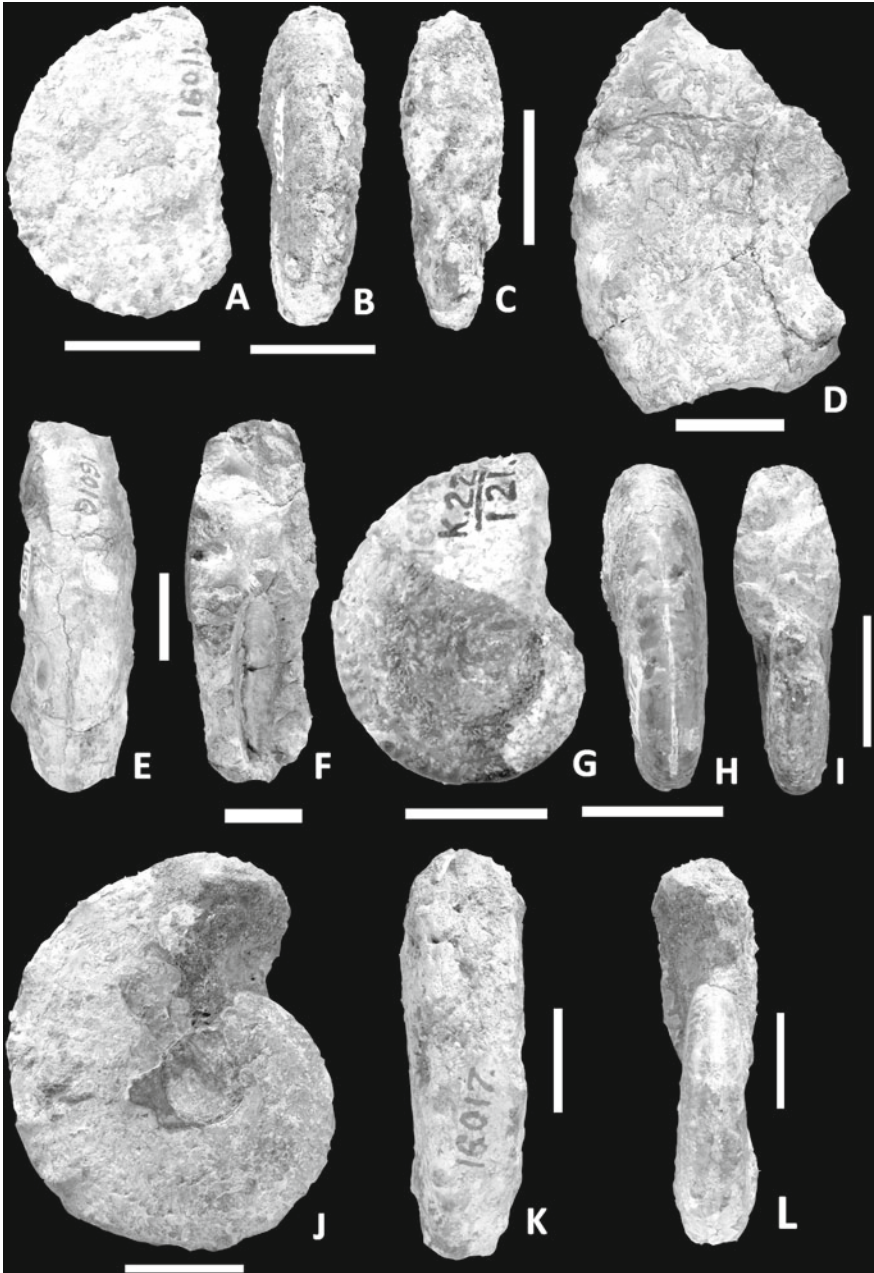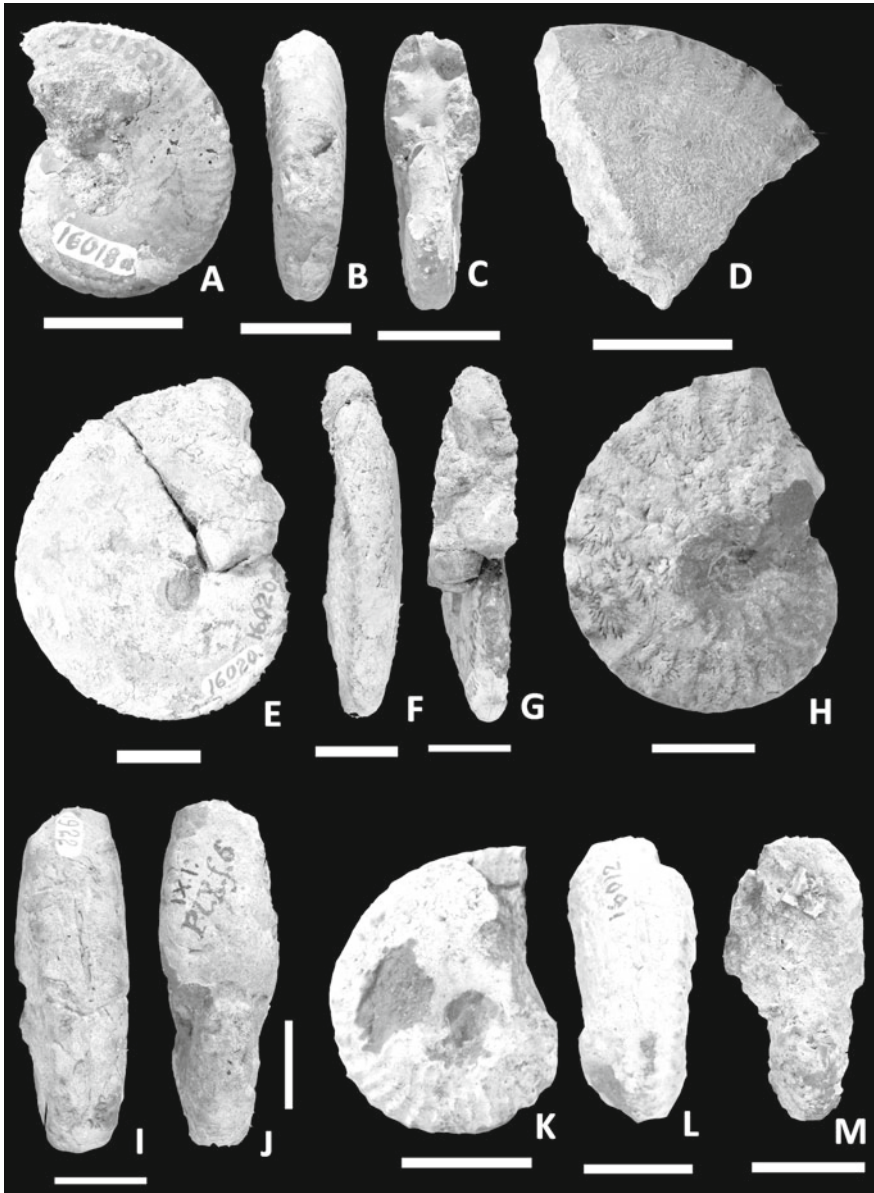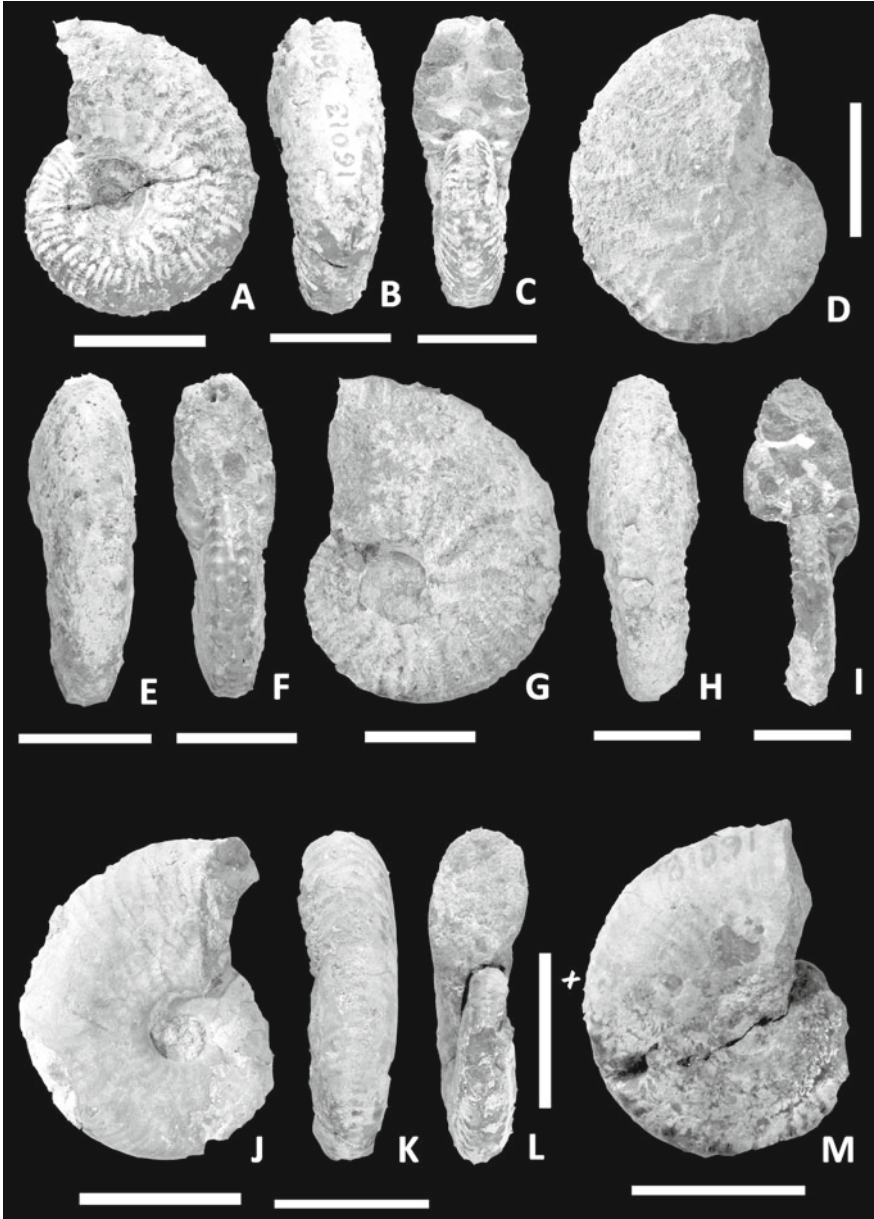
◄**Fig. 2** Photographs of *Taramelliceras kachhense* (Waagen). **A**, lateral; **B**, ventral and **C**, apertural views of incomplete microconch, GSI Type specimen no. 16011 from Middle Kimmeridgian of Fakirwadi. **D**, lateral; **E**, ventral; and **F**, apertural views of incomplete, fragmentary macroconch GSI Type specimen no. 16016 from Middle Kimmeridgian of Kutch (locality labeled as unrecorded). **G**, lateral; **H**, ventral and **I**, apertural views of completele macroconch, GSI Type specimen no. 16017 from Middle Kimmeridgian (locality labeled as unrecorded). **J**, lateral; **K**, ventral and **L**, apertural views of incomplete macroconch, GSI Type specimen no. 16017 from Middle Kimmeridgian of Kutch (locality labeled as unrecorded) (white bar = 2 cm)

20 mm diameter. Venter becomes gradually wider and tri-tuberculate in later phragmocone with one row of mid-ventral and two rows of ventro-lateral tubercles. At the adult phragmocone, venter becomes tabulate, though varieties with broadly rounded venter are also common. Mid-ventral tubercles, though continue, become distant and irregular in appearance. Inflated varieties with prominent mid-ventral tubercles at first transversely elongated and become clavate at adult phragmocone.

The umbilicus is wide in inner whorls and little occluded in latter phragmocones. In adult phragmocone, it becomes wider, subject to egression of whorls. The umbilical seam is steep with a sharp margin all through the ontogeny. However, some variants have a high umbilical wall with a rounded margin.

The suture of all the forms of *Taramelliceras* with flexuous ribbing is more or less the same. There are five lateral lobes, the first one being by far the largest. The siphonal lobe is very short, divided into two short branches. The external saddle is also short and divided by a small secondary lobe; the first lateral saddle very longer than all the others (see Fig. 7).

Description [Microconch]: The authors have eight specimens, including six GSI Type specimens. Among those only one specimen (GSI Type No. 16018a) is nearly complete with the original shell preserved. Shell is relatively involute in comparison to early phragmocone (U/D = 0.35 in D = 36 and 0.25 in D = 70) and compressed (W/H = 0.61–0.091) with elliptical whorl section.

Ribbing is not very distinct or absent in inner whorls up to a diameter of 6 mm. After that, weak primary ribs appear near the umbilical seam. Primary ribs are coarse, dense and form strongly elongated bullae near the umbilical margin in some variants. Primaries bifurcate at the mid-lateral and secondary ribs continue over the venter. Ribbing becomes coarse at later phragmocone at about 20 mm diameter, where secondaries form tubercles near the ventro-lateral margin; however, some variants at the same stage of growth do not form any ventro-lateral tubercles and ribbing continues over the venter. Though in some variants ventro-lateral tubercles appear haphazardly, especially at the late stage of growth. At the later part of adult phragmocone as well as at the body chamber, there is mid-ventral tubercles that continue up to the preserved end.

Venter is rounded at an early stage of growth and becomes tabulate or widely rounded at late phragmocone. In the body chamber, ribbing continues over the rounded venter and they form mid-ventral tubercles in most of the specimens. However, specimens without mid-ventral clavi are also there.

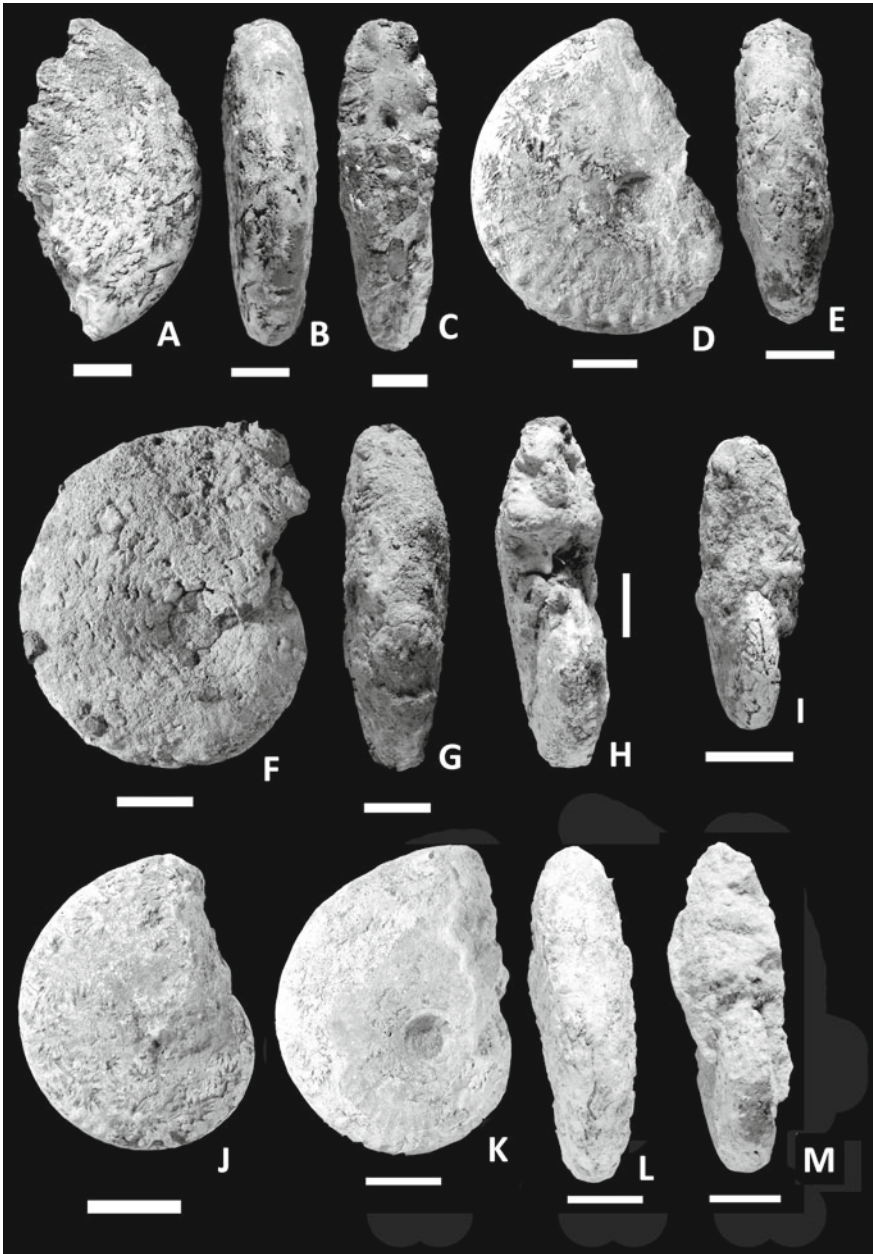**Fig. 3** Photographs of *Taramelliceras kachhense* (Waagen). **A**, lateral; **B**, ventral and **C**, apertural views of incomplete macroconch, GSI Type specimen no. 16018a from Middle Kimmeridgian of Fakirwadi. **D**, lateral view of an incomplete fragmentary macroconch, GSI Type specimen no. 16019 from Middle Kimmeridgian of Fakirwadi. **E**, lateral; **F**, ventral and **G**, apertural views of completely septate macroconch, GSI Type specimen no. 16020 from Middle Kimmeridgian of Fakirwadi. **H**, lateral; **I**, ventral and **J**, apertural views of incomplete microconch, GSI Type specimen no. 1922 from Middle Kimmeridgian of East of Ler. **K**, lateral; **L**, ventral and **M**, apertural views of completely septate microconch, GSI Type specimen no. 16012 from Middle Kimmeridgian of Fakirwadi (Katrol Bed of Spath 1928) (white bar = 2 cm)

◄**Fig. 4** Photographs of *Taramelliceras kachhense* (Waagen). **A**, lateral; **B**, ventral and **C**, apertural views of incomplete microconch, GSI Type specimen no. 16013 from Middle Kimmeridgian of Ler (Spath 1928). **D**, lateral; **E**, ventral and **F**, apertural views of an incomplete, fragmentary microconch, GSI Type specimen no. 16014 from Middle Kimmeridgian of Ler (Spath 1928). **G**, lateral; **H**, ventral and **I**, apertural views of completely septate microconch GSI Type specimen no. 16015 from Middle Kimmeridgian of Ler (Spath 1928). **J**, lateral view of incomplete GSI Type specimen no. 16018a from Middle Kimmeridgian of Fakirwadi (Spath 1928). **K**, ventral; **L**, apertural and **M**, lateral views of partly preserved microconchiate body whorl (body chamber starts with "X" mark; GSI Type specimen no. 16018 from Middle Kimmeridgian of Fakirwadi (Katrol Bed of Spath 1928) (white bar = 2 cm)

The umbilicus is wide, with a high umbilical wall and rounded edge throughout the ontogeny.

The suture is same as that of macroconch (Fig. 7).

Discussion: Spath redescribed *T. kachhense* with 60 specimens which include four specimens of *Oppelia kachhense* Waagen (1875). Spath himself showed intraspecific variations and compared *T. kachhense* with other species from Europe as well as the species found in Kutch.

T. cf. *compsum* of Spath (1927–33, plate 18, Fig. 10) from Middle Kimmeridgian, though locality uncatalogued, probably from Fakirwadi or Ler is 113 mm in diameter and is still inflated comparing to *T. kachhense*. The sectional view figured by Spath (1927–33, plate 18, Fig. 10) has wider and flattened periphery same as that of *T. kachhense* (p. 14, Fig. 12 of Spath 1927–33).

T. aff. *holbeini* (plate 14, Fig. 14 of Spath, 1927–33) from Katrol beds, Lower or Middle Kimmeridgian is still septate at 97 mm diameter and it is "transitional" to the typical form of *T. kachhense* (plate 8, Fig. 2) as mentioned by Spath (1927–33), "This variety of *T. kachhense* has similar fine ribbing as *T.* aff. *holbeini*". According to Spath (1927–33) *T. holbeini* differs from *T. kachhense* by having smaller umbilicus in early stage of ontogeny. But the present study involving a large sample size reveals variation in the degree of involution from early stage of growth.

The ventral view of *T.* aff. *franciscanum* described by Spath (1927–33, plate 15, Fig. 9) shows same wider periphery as in *T. kachhense*. Two imperfect specimens with an inflated section as mentioned by Spath (1927–33) are transitional to European *T. compsum* and *T. holbeini* (Oppel). But in the present endeavour degree of inflation also varies considerably and Spath's *T.* aff. *franciscanum* falls within the range of variability.

T. planifrons from Middle Kimmeridgian is similarly larger specimen (Spath 1927–33, plate 14, Fig. 9) with wider periphery. Spath (1927–33) while comparing young specimens of his *T. planifrons* with European *O. pugilis* stated that "minute tubercles are at first transversely elongated" (p. 143) on the other hand in the description of inner whorls of *kachhense* group of species he stated that "on the median line of the ventral area there are traces of transversely elongated tubercles" (p. 135). So, it suggests that both *T. kachhense* and *T. planifrons* which Spath (1927–33) described from Kutch, shows same ornamentation in inner whorls as well. The suture of both is also similar, as exemplified by Spath (1927–33).

Fig. 5 Photographs of *Taramelliceras kachhense* (Waagen). **A**, lateral; **B**, ventral and **C**, apertural views of completely septate specimen no. T/LR/3 from middle sandstone ridge of Ler. **D**, lateral and **E**, ventral views of a completely septate specimen no. T/LR/4 from middle sandstone ridge of Ler. **F**, lateral; **G**, ventral and **H**, apertural views of completely septate specimen no. TR/LR/9 from middle sandstone ridge of Ler. **I**, apertural and **J**, lateral views of completely septate specimen no. T/LR/1 from middle sandstone ridge of Ler. **K**, lateral; **L**, ventral and **M**, apertural views of an incomplete specimen no. T/LR/7 from East of Ler below middle sandstone ridge (white bar = 2 cm)
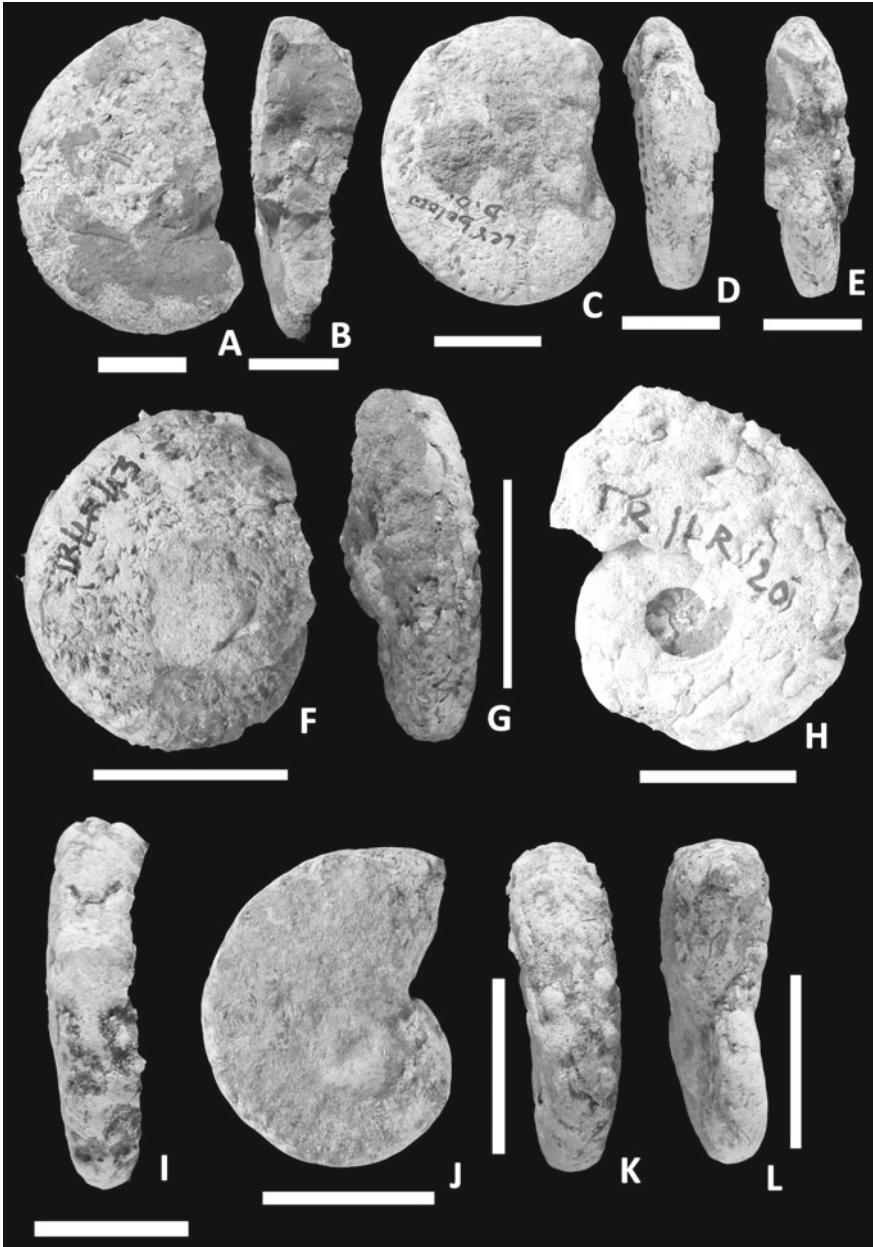
Fig. 6 Photographs of microconchiate forms of *Taramelliceras kachhense* (Waagen). **A**, lateral and **B**, apertural views of incomplete specimen no. T/LR/2 from middle sandstone ridge of Ler. **C**, lateral; **D**, ventral and **E**, apertural views of a completely septate specimen no. TR/LR/19 from Ler, Lower sandstone ridge. **F**, lateral and **G**, ventral views of completely septate specimen no. TR/LR/13 Ler, Lower sandstone ridge. **H**, lateral and **I**, ventral views of completely septate specimen no. T/LR/3 from Ler, Lower sandstone ridge. **J**, lateral; **K**, ventral and **L**, apertural views of completely septate specimen no. TR/LR/15 from middle sandstone ridge of Ler (white bar = 2 cm)
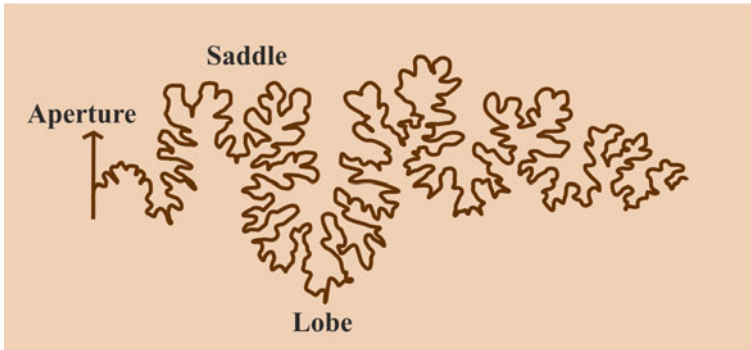
Fig. 7 Sutural pattern of *Taramelliceras kachhense*, showing very short siphonal lobe, short external saddle and large first lateral saddle

Spath (1927–33) compared the inflated forms of *T. subkobyi* with *T. franciscanum* (Fontanes) and on the other hand, he argued that those forms are connected by intermediate forms with *T. holbeini* and *T. kachhense*. But as in some varieties of *T. kachhense* (Spath 1928, plate 14, Fig. 6; plate 17, Fig. 3a, b) shows involute inner whorls, smooth and arched ventral area and at the same time thick, coarser and distant ribbing at the adult growth stage.

T. taurimontanus described by Bonnot et al. (1999, plate 3, Figs. 10–11) from Upper Callovian Athleta Zone of Dizon area, France has stronger ribbing all throughout ontogeny than in *T. kachhense.*

Caracuel et al. (2006) described *T. (T.) subcalliceram* (Gemmellaro) from Lower Kimmeridgian of South East Spain. It has compressed shell, flat venter and closely spaced falcoid secondaries. Ribbing comparatively prominent than in *T. kachhense* and it continues till to the end of the adult body chamber. They also described *T. cf. trachinotum* (Oppel) from the same horizon and locality, which is larger than *T. subcalliceram* and has a stronger ribbing pattern. Both primaries and secondaries continue up to the adult body whorl unlike *T. kachhense.* Both *T. cf. trachinotum* and *T. kachhense* have closely spaced secondaries, but in case of *T. cf. trachinotum,* bifurcation occurs above the mid flank.

Strongly ornamented forms of Spath (1927–33) which have similarities in having identical smooth innermost whorls and ribbing pattern in later phragmocone stage but microconchs are strongly tuberculate and tuberculation continues till to the end. In macroconchs however, tuberculation ceased to develop on body chamber.

T. akher of Spath (1927–33) characterized by "low whorls and very strong and prominent ornamentation" as in Waagen's (1875) *O. trachynota* and both of them are transitional to the "most robust varieties of *T. kachhense*, with more distantly and more coarsely costate inner whorls" as asserted by Spath (1927–33, p. 136). Spath (1927–33) mentioned that the inner whorls of holotype *T. gibbosum* are "intermediate in costation" between "finely ribbed" *T.subflexuosum* and the coarser varieties of *T. kachhense. T. gibbosum* has similar inflated outer whorls characterized by strong and

curved primary ribs, prominent mid-ventral calvi as in *T. akher*. As claimed by Spath (1927–33) "*T. akher* is as close to *T. gibbosum* as to *T. kachhense*" (p. 136). This supports the contention that both *T. akher* and *T. gibbosum* closely resemble each other and are similar to inner whorls of macroconchiate *T. kachhense*.

T. cf. *succedens*, from Middle Kimmeridgian of Fakirwadi has the body chamber with preserved diameter of −70 mm. As mentioned by Spath *T.*cf. *succedens* "apparently do not differ from those of other forms of the *kachhense* group here discussed notably of *T. gibbosum* (Spath 1927–33; plate 14, Fig. 10)". *T. pseudoflexuosum* of Spath (1927–33, plate 18, Fig. 2) shows fine to coarse ribbing during ontogeny and is merely finely costate variety of *T. gibbosum* which is again intermediate between ltivariate dataset along and *T. kachhense*; so, it is also microconchiate variety of *T. kachhense*. *T. transitorium* from Jhuran Formation, Middle Kimmeridgian has similar flexuose ribbing and tri-tuberculate periphery as in *T. akher* and strong ribbing persists up to the preserved end. As mentioned by Spath (1927–33, p. 142) there are many transitional forms "between *T. transitorium* and *Taramelliceras* of Kachhense-Compsa type". This also supports its inclusion as microconch of *T. kachhense*. *T. nereiforme* from Middle Kimmeridgian of Fakirwadi is smaller in size and ribs are relatively strong and have tuberculate periphery which continue up to the preserved end. It exhibits similar sutural patterns as well as has raised tubercles at mid ventral, like other microconchiate forms of *Taramelliceras* from Kutch. So, it has been included within *T. kachhense*.

Because of many similarities of Spath's plethora of species, stratigraphic contemporaneity and geographic contiguity prompted us to club all of 13 Spath's species into a highly variable and strongly dimorphic species *T. kachhense*. The present contemplation has also been supported by the following morphometric analysis of multivariate data. So, it can be believed that present revised *T. kachhense* is a long ranging species which reached its acme only during the Middle Kimmeridgian.

5   Data Analysis

Principal Component Analysis (PCA) has been performed with the multivariate data, which are acquired from the present specimens as well as GSI types to support the aforementioned connotation. The present study has also been included the data of European *T. compsum* available from Baudouin et al. (2011) (see Annexure 1). Multivariate dataset along with linear measurements, which are required for PCA, have been put into the PAST software (ver. 2.17c) (Hammer et al. 2001). It is a procedure for finding hypothetical variables or components that account for as much of the variance in the given multidimensional data as possible (Hotelling 1933; Jackson 1991; Reyment and Jöreskog 1993; Jolliffe 2002). For the morphometric analysis using PCA four variables are considered: shell diameter, umbilical diameter, whorl height and whorl width.

6 Results and Discussion

A simple x–y plot taking shell diameter along x-axis and log of umbilical diameter along y-axis shows overlapping ellipsoids of the 3 groups of data and juvenile forms plotted in close proximity, whereas adult forms are plotted wide apart with respect to the above two variables (Fig. 8). Principal component analysis (PCA) of the independent variable (shell diameter, umbilical diameter, whorl width and whorl height) reduced the multidimensional plots into two-dimensional plots with respect to two orthogonal axes which are principal component axes. Here the plot shows minimum scatter and the ellipsoids (95% confidence ellipsoid) are trending to stretched unidirectionally (Fig. 9). The scree plot of the four components related to shell morphometry along x-axis and their eigen values along the y-axis depicts minimum variance for

Fig. 8 X–Y plot taking shell diameter along the X-axis and log of umbilical diameter along the Y-axis. Black dots encircled by black ellipsoid are present collection; Blue squares encircled by blue ellipsoid are GSI type specimens and Red plus encircled by red ellipsoid are European specimens
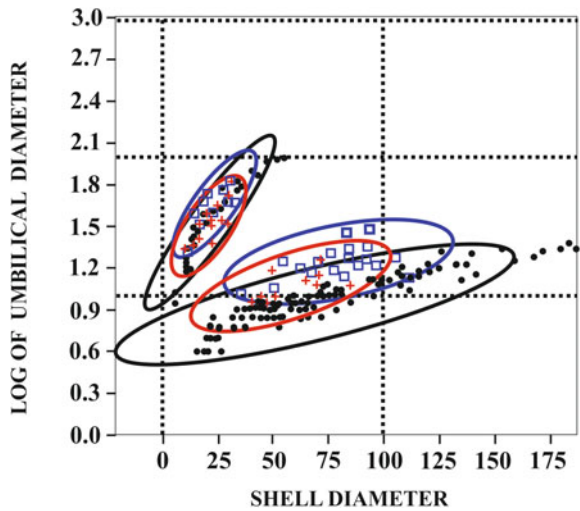
Fig. 9 PCA scatter plot along with 95% confidence ellipsoids showing similar variance and positive covariance within variables. Colour index are same as in Fig. 8
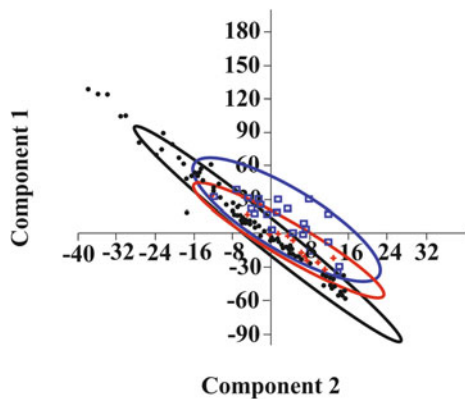
Fig. 10 Scree plot of the four components along X-axis and their Eigen values along Y axis
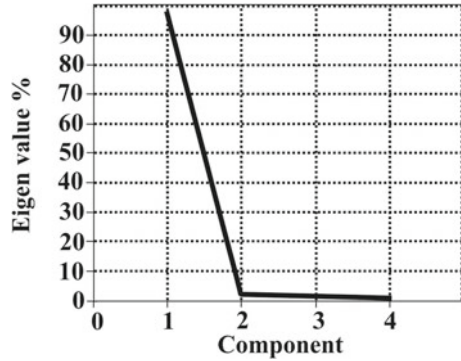
the three-component and the maximum variance for the first component. It becomes almost straight for three components, which suggests that variation exists within the different variables due to shell diameter that is an ontogenetic constraint (Fig. 10).

7 Conclusions

PCA clearly depicts congruency in morphometric aspects not only among the 13 species earlier described by Spath (1927–33) but also between Kutch species *T. kachhense* and Sub-Mediterranean species *T. compsum* described by Baudouin et al. (2011). The Kutch species shows wide temporal distribution from upper part of Early Kimmeridgianto Middle Kimmeridgian. Similarly, *T. compsum* first appear in Europe in lower part of Acanthicum zone and it extends upto Lower Tithonian (Hybonotum zone). *T. compsum* has a wide ornamental variation though morphometrically all the variants show a similar ontogenetic pattern. Even they included *T.* cf. *compsum* described by Spath (1927–33) in its synonymy list. So, it can be inferred that *T. kachhense* is only a geographic variant of *T. compsum* and it ranges from Kimmeridgian to Tithonian. Variation in ornamentation in ammonoids has different functional attributes like protective, buoyancy regulation, sexually selected feature etc. (for detail see Kennedy and Cobban, 1976 and references therein). Keels and clavi are mainly meant for regulating drag force, specially to cope up with nektonic behavior. In compressed ammonoid, like *Taramelliceras,* keel is replaced by mid ventral nodes and sometimes accompanied by ventro-lateral tubercles, clavi and ventral features may show intraspecific variability and which is common within the *Taramelliceras* species as described by Spath (1927–33) from Kutch. So, all the studies and quantified assessment derived out from multivariate analysis attest the congruency of clubbing 13 species of Spath (1927–33) into *T. kachhense,* besides, the utmost attempts to find similarities between the two species *T. kachhense* and *T. compsum* that evinces cosmopolitan status for *T. kachhense.*

Annexure 1

Materials and Dimensions:

Specimen no		D	U	W	H	Locality and Horizon
GSI Type						
16018B	Ph	72.00	18.00	27.00	35.00	Fakirwadi, Middle Kimmeridgian
		40.00	9.00	10.00	22.00	
16018A	Ph	42.00	9.00	14.00	22.00	Fakirwadi, Middle Kimmeridgian
16,011	Ph	50.00	15.00	14.00	23.00	Fakirwadi, Middle Kimmeridgian
16,012	Ph	47.00	9.00	23.00	24.00	Fakirwadi, Middle Kimmeridgian
16,013	Ph	45.00	10.00	19.00	23.00	Ler, Middle Kimmeridgian
		70.00		30.00	33.00	
16,014	Ph	51.00	10.00	17.00	26.00	Ler, Middle Kimmeridgian
16,015	Ph	65.00	13.00	22.00	32.00	Ler, Middle Kimmeridgian
16,016	Ph	100.00		30.00	53.00	Unlocalised, Middle Kimmeridgian
		48.00	9.00	15.00		
16,017	Ph	71.00	14.00	17.00	33.00	Unlocalised, Middle Kimmeridgian
16,019	Ph			20.00	39.00	Fakirwadi, Middle Kimmeridgian
16,020	Ph	85.00	12.00	25.00	45.00	Fakirwadi, Middle Kimmeridgian
1922	Ph	70.00	12.00	22.00	35.00	East of Ler, Middle Kimmeridgian
Present collection						

(continued)

Specimen no		D	U	W	H	Locality and Horizon
T/LR/4	Ph	90.00	17.50	25.00	49.50	Ler, Middle Sandstone ridge
T/LR/5	Ph	96.00	21.00	29.50	48.00	Ler, Middle Sandstone ridge
T/LR/2	Ph	66.50	11.00	20.00	39.50	Ler, Middle Sandstone ridge
T/LR/3	Ph	109.50	19.00	32.50	62.00	Ler, Middle Sandstone ridge
T/LR/1	Ph	63.50	10.00	22.00	32.00	Ler, Middle Sandstone ridge
T/LR/6	Ph	64.50	8.50	16.00	37.50	Ler, Middle Sandstone ridge
T/LR/21	Ph	80.00	20.00			Ler, Middle Sandstone ridge
T/LR/7	Ph	83.50	13.50	25.50	46.50	East of Ler, Middle Sandstone ridge
T/LR/8	Ph	53.00	10.00	18.00	29.00	East of Ler, Middle Sandstone ridge
T/LR/9	Ph	90.00	15.50	26.00	45.50	Ler, Middle Sandstone ridge
T/LR/12	Ph	68.00	9.50	22.00	34.00	Ler, Middle Sandstone ridge
T/LR/15	Ph	42.00		14.50	19.00	Ler, Middle Sandstone ridge
T/LR/13	Ph	36.00	12.50	12.00	17.00	Ler, Lower Sandstone ridge
T/LR/11	Ph	39.00	10.50	12.50	19.50	Ler, Middle Sandstone ridge
T/LR/D/1	Ph	90.00	20.00	32.00	41.50	Ler, Middle Sandstone ridge
T/LR/D/2	Ph	97.00	21.00	31.50	48.50	Ler, Middle Sandstone ridge
T/LR/D/3	Ph	89.00	19.00	29.5	47.00	Ler, Middle Sandstone ridge
T/LR/D/4	Ph	84.00	14.00	25.5	45.00	Ler, Middle Sandstone ridge
TR/LR/17	Ph	83.00	19.00	28.50	46.00	Ler, Lower Sandstone ridge
TR/LR/18	Ph	86.00	17.50	24.00	47.50	Ler, Lower Sandstone ridge
TR/LR/20	Ph	41.50	12.50	14.00	19.50	Ler, Lower Sandstone ridge

(continued)

Specimen no		D	U	W	H	Locality and Horizon
TR/LR/19	Ph	55.00	16.50	13.50	22.50	Ler, Lower Sandstone ridge
T/LR/D/7	Ph	63.50	14.00	26.00	46.50	Ler, below Middle Sandstone ridge
T/LR/D/8	Ph	53.00	9.00	18.00	29.00	Ler, below Middle Sandstone ridge
European specimens						
Crl028		64.00	9.00	-	36.00	Ardèche, France
Crl021		65.00	9.00	-	37.00	Ardèche, France
Crl140a		69.00	10.00	-	39.00	Ardèche, France
Crl029		72.00	8.00	-	41.00	Ardèche, France
Crl035b		68.00	10.00	-	36.00	Ardèche, France
Crl035a		77.00	11.00	-	42.00	Ardèche, France
Crl019		59.00	10.00	20.00	32.00	Ardèche, France
Crl016		48.00	9.00	-	26.00	Ardèche, France
Crl017		45.00	7.00	14.00	25.00	Ardèche, France
Crl018		45.00	8.00	15.00	23.00	Ardèche, France
Cru069		37.00	7.00	-	21.00	Ardèche, France
Crl078		41.00	7.00	-	20.00	Ardèche, France
Crl092		33.00	11.00	-	-	Ardèche, France
Crl098		28.00	9.00	-	-	Ardèche, France
Cru058		34.00	11.00	-	-	Ardèche, France
Cru060		37.00	12.00	-	-	Ardèche, France
Cru061		17.00	5.00	-	-	Ardèche, France
Cru022		38.00	13.00	-	-	Ardèche, France
Crl117		37.00	12.00	-	-	Ardèche, France
Cru035b		22.00	6.00	-	-	Ardèche, France
Cru53c		20.00	4.00	-	-	Ardèche, France
Crl012		23.00	7.00	-	-	Ardèche, France
Crl053		35.00	11.00	-	-	Ardèche, France

References

Alberti M, Fürsich FT, Pandey DK (2013) Deciphering condensed sequences: a case study from the Oxfordian (Upper Jurassic) Dhosa Oolite member of the Kachchh Basin, western India. Sedimentol 60:574–598

Arora A, Banerjee S, Dutta S (2015) Black shale in late jurassic Jhuran formation of Kutch: possible indicator of oceanic anoxic event? J Geol Soc India 85:265–278

Arora A, Dutta S, Gogoi B, Banerjee S (2017) The effects of igneous dike intrusion on organic geochemistry of black shale and its implications: late jurassic Jhuran formation, India. Int J Coal Geol 178:84–99

Bansal U, Banerjee S, Pande K, Arora A, Meena SS (2017) The distinctive compositional evolution of glauconite in the Cretaceous Ukra Hill Member (Kutch basin, India) and its implications. Mar Pet Geol 82:97–117

Baudouin C, Boselli P, Bert D (2011) The oppeliidae of the acanthicum zone (Upper Kimmeridgian) from Mount Crussol (Ardèche, France): ontogeny, variability and dimorphism of the genera Taramelliceras and Streblites (Ammonoidea). Rev Paléobiologie, Genève 30:619–684

Biswas SK (1977) Mesozoic rock-stratigraphy of Kutch, Gujarat. Quart J Geol Min Met Soc India 49:1–51

Biswas SK (1981) Basin framework, palaeo-environment and depositional history of the Mesozoic sediments of Kutch basin, western India. Quart J Geol Min Met Soc India 53:56–85

Biswas SK (2016) Mesozoic and tertiary stratigraphy of Kutch (Kachchh)–a review. In: Thakkar MG (ed) Recent Studies on the Geology of Kachchh, Spec Publ Geol Soc India, vol 6, pp 1–24

Bonnot A, Marchand D, Neige P (1999) Les Oppelidae (Ammonitina) de l'horizon à Collotiformis (Callovien supérieur, zone à Athleta) de la région dijonnaise (Côte-d'Or, France). Annal Paléont 85:241–263

Callomon JH (1963) Sexual dimorphism in jurassic ammonites. Transact Leices Lit Phil Soc 57:21–56

Caracuel JE, Sandoval J, Martín-Martín M, Estévez-Rubio A, Martín-Rojas I (2006) Jurassic biostratigraphy and paleoenvironmental evolution of the Malaguide complex from Sierra Espuña (Internal Betic Zone, SE Spain). Geobios 39:25–42

Chaudhuri A, Banerjee S, Le Pera E (2018) Petrography of middle jurassic to early cretaceous sandstones in the Kutch basin, western India: implications on provenance and basin evolution. J Palaeogeography 7:2–14

Chaudhuri A, Banerjee S, Chauhan G (2020) Compositional evolution of siliciclastic sediments recording the tectonic stability of a pericratonic rift: Mesozoic Kutch Basin, western India. Mar Petrol Geol 111:476–495

Chaudhuri A, Das K, Banerjee S, Fitzsimons ICW (2020) Detrital zircon and monazite track the source of Mesozoic sediments in Kutch to rocks of Late Neoproterozoic and Early Palaeozoic orogenies in northern India. Gond Res 80:188–201

Chaudhuri A, Chatterjee A, Banerjee S, Ray JS (2020) Tracing multiple sources of sediments using trace element and Nd isotope geochemistry: provenance of the Mesozoic succession in the Kutch Basin, western India. Geol Mag. https://doi.org/10.1017/S0016756820000539

Chaudhuri A, Banerjee S, Prabhakar N, Das A (2020) The use of heavy mineral chemistry in reconstructing provenance: a case study from Mesozoic sandstones of Kutch Basin (India). Geol J. https://doi.org/10.1002/gj.3922

Desai BG, Patel SJ (2009) Upper Callovian-Middle Oxfordian belemnite assemblage from Jara dome, Western Kachchh. J Geol Soc India 74:343–356

Fürsich FT, Pandey DK (2003) Sequence stratigraphic significance of sedimentary cycles and shell concentrations in the upper jurassic-lower cretaceous of Kachchh, western India. Palaeo Palaeo Palaeo 193:285–309

Fürsich FT, Oschmann W, Jaitly AK, Singh IB (1991) Faunal response to transgressive-regressive cycles: example from the jurassic of western India. Palaeo Palaeo Palaeo 85:149–159

Fürsich FT, Pandey DK, Callomon JH, Jaitly AK, Singh IB (2001) Marker beds in the Jurassic of the Kachchh Basin, western India: their depositional environment and sequence-stratigraphic significance. J Palaeont Soc India 46:173–198

Hammer Ø, Harper D, Ryan PD (2001) PAST: paleontological statistic software package for education and data analysis. Paleontological Association (Computer software)

Hotelling H (1993) Analyses of a complex of statistical variables into principal components. J Edu Psycho 24:417–441

Howard JD, Singh IB (1985) Trace fossils in the Mesozoic sediments of Kachchh, western India. Palaeo Palaeo Palaeo 52:99–122

Jackson JE (1991) A user's guide to principal components. Wiley, New York

Jolliffe IT (2002) Principal component analysis, 2nd edn. Springer, New York

Kennedy WJ, Cobban WA (1976) Aspects of ammonite biology, biogeography, and biostratigraphy. Palaeont Asso Spec Pap 17:1–94

Krishna J, Pathak DB, Pandey B (1996) Quantum refinement in the Kimmeridgian ammonoid chronology in Kachchh (India). GeoRes 1(2):195–204

Krishna J (1984) Current status of jurassic stratigraphy of Kachchh, western India. Int Symp J Strat Erlangen 3:731–742

Krishna J, Singh LB, Howard J, Jafer SA (1983) Implications of new data on the Mesozoic rocks of Kachchh, western India. Nature 305:790–792

Nath R (1932) A contribution to the stratigraphy of Kutch. Quart J Geol Mine Met Soc India 4:161–174

Reyment RA, Jöreskog E (1993) Applied factor analysis in the natural sciences. Cambridge University Press, Cambridge, UK

Roy P (2011) Stratigraphy, phylogenetic systematics and evolutionary palaeobiology of the family Oppelidae Douvillé (Ammonoidea) and related ancillary taxa from the Jurassic of Kutch, western India. Unpublished PhD thesis, Jadavpur University

Shome S (2009) Systematics, palaeobiogeography and evolution of the Upper Jurassic (Kimmeridgian-Tithonian) ammonites of Kutch, western India. Unpublished PhD thesis, Jadavpur University

Spath LF (1927–1933) Revision of the jurassic cephalopod fauna of Kachh (Cutch). Palaeontologia Indica, New Series 9

Waagen W (1873–1875) Jurassic fauna of Kutch. The Cephalopoda. Palaeontologia Indica, Series 9

Wynne AB (1872) Geology of Kutch. Mem Geol Surv India 8(9):1–289

Nautiloid Biostratigraphy of the Jurassic of Kutch, India: An Exploration of Bio- and Chrono-stratigraphic Potential of Nautiloids

Kalyan Halder

Abstract   The Jurassic-Cretaceous ammonites have been overwhelmingly used for biostratigraphic classification and correlation globally. Nautiloids often accompany ammonites in the contemporaneous deposits of the Tethyan Realm. However, they have never been used for biostratigraphy. Nautiloids are present through the Jurassic succession of Kutch, India, although with lower diversity and abundance than ammonites. Here, a biostratigraphic classification of the Jurassic succession based on nautiloids is presented. Four formal nautiloid biozones are erected along with some subzones. The zonation is compared to the available ammonite zones for Kutch and the Sub-Mediterranean Province from Europe. Based on important changes in the nautiloid faunal composition, some biohorizons are established. Nautiloid zones, in spite of their relative coarseness, and biohorizons, are capable of demarcating the chronostratigraphic boundaries, such as stages and substages. Precise demarcation of such boundaries is possible with nautiloids in the absence of clarity from ammonites. Hence, an integration of information from both the cephalopod faunas in establishing biostratigraphy is suggested here.

Keywords Nautiloid · Jurassic · Patcham Formation · Chari Formation · Kutch · biostratigraphy · chronostratigraphy

1   Introduction

The Mesozoic biostratigraphy maps the overwhelming presence of ammonites – their remarkable diversity and abundance, wide dispersal and rapid evolution. Ammonites

---

The original version of this chapter was revised: The Table 1 has been formated correctly. The correction to this chapter is available at https://doi.org/10.1007/978-3-030-71370-6_24

K. Halder (✉)
Department of Geology, Presidency University, 86/1 College Street, Kolkata 700073, India
e-mail: kalyan.geol@presiuniv.ac.in

provide biostratigraphers with index fossils facilitating precise temporal correlation between distant regions. Ammonite biohorizons, the smallest indivisible biostratigraphic intervals based on ammonites, have been erected locally and used successfully in large-scale correlation (Cariou and Hantzpergue 1997).

Nautiloids, in contrast to their celebrated cousin ammonites, were commonly considered as biostratigraphically inert, having conservative morphology, and low diversity and abundance. Biostratigraphic classification and correlation of the Mesozoic strata were attempted based on several organisms other than ammonites such as brachiopods, echinoderms, foraminifers, ostracodes, calcareous nannofossils, etc., which include even benthic groups (Cariou and Hantzpergue 1997). Nautiloids were not used for such analyses except for a handful of occasions from the Paleozoic (Evans et al. 2014 and references therein). Evans et al. (2014) reviewed the potential of nautiloids from different geological periods and observed that they could be used for biostratigraphic classification and correlation, especially where other more reliable markers are absent or rare. Branger (2004), although did not attempt a nautiloid biozonation, found that most of the Middle Jurassic nautiloids he reported from western France were restricted to one or two ammonite zones. This indicates their biostratigraphic usefulness. Geographic distribution of nautiloids was restricted to the Tethys Realm during the Mesozoic. Within this realm, however, several genera were quite widespread. Cichowolski (2003) observed that while nautiloid genera were pandemic, the species were mostly endemic. Halder (2000), however, found some relatively widespread species.

The Jurassic succession of Kutch is famous for its ammonite fauna. Pioneers of the study of the Mesozoic cephalopods from Kutch described a few nautiloids based on very few specimens as subsidiary faunas to the ammonites. Waagen (1873) described six species based only on fourteen specimens. Spath (1927-1933), when revising Waagen's work, recognised twelve species with the addition of only nineteen specimens. Recent taxonomic revisions of the Jurassic nautiloids from Kutch revealed that species diversity of this group is not very meagre although much less than contemporary ammonites (Bardhan et al. 1994; Halder and Bardhan 1996a, b, 1997; Halder et al. 1998; Halder 2000, 2002). Certain species are also quite abundant. Halder (2002) reported sixteen species of Jurassic nautiloids from Kutch based on about two hundred specimens.

In the course of taxonomic revision of the Jurassic nautiloids from Kutch it has been observed that in spite of relatively less diversity and abundance compared to the contemporaneous ammonites, their distribution records rapid enough evolution that warrants biostratigraphic utility, contradicting popular belief. The Jurassic nautiloids even included a fleeting genus *Cymatonautilus* Spath, 1927, an index taxon of the latest Early to Middle Callovian (Halder and Bardhan 1996a). The genus dispersed rapidly within this period through all the provinces of the Tethyan Realm. Biostratigraphic classification of the Jurassic succession of Kutch based on ammonites has been attempted since 1873, first by Waagen, followed by Spath (1927). Several other biostratigraphic classifications have been proposed by many later researchers (e.g. Mitra et al. 1979; Krishna and Cariou 1986; Bardhan and Datta 1987; Jana et al. 2005; Roy et al. 2007; Krishna et al. 2011; Bardhan et al. 2012; Talib et al. 2017).

   This paper is devoted to explore the biostratigraphic potential of the Jurassic nautiloids from Kutch. Biostratigraphy of the Jurassic rocks exposed in the mainland Kutch is erected here based on nautiloids. The classification is compared and correlated with the available recent ammonite biostratigraphy of Kutch to evaluate its potential. A correlation with the standard European Submediterranean Province biostratigraphic scheme is also done. The stage and substage boundaries that this rock succession traverses are also delineated based on nautiloid faunal distribution.

2   Material and Methods

Sixteen species of nautiloids previously described from the Jurassic succession of the mainland Kutch (Halder 2002) are used for the establishment of the biostratigraphic scheme. The type area of this zonal scheme is the well-known section exposed near the village Jumara (23°40´N, 69°03´E) in western Kutch, from where most of the specimens were gathered. Other specimens were collected from some other well-known localities such as Jara (23°42´N, 69°02´E), Keera (23°34´N, 69°14´E), Jhura (23°24´N, 69°34´E) and Habo (23°22´N, 69°52´E) domes.

   Assemblage biozones and subzones are erected based on the pattern of the stratigraphic distribution of nautiloids. The boundaries between zones and subzones are placed where characteristics of the faunal assemblages change. The units are formally named based on the most abundant/characteristic nautiloid species of the assemblage. The nautiloid biostratigraphy is compared with well-established ammonite schemes for Kutch (Roy et al. 2007; Bardhan et al. 2012; Talib et al. 2017; Roy et al. 2019). Roy et al. (2007) dealt with the lower part (Bathonian) of the exposed section at Jumara, whereas Bardhan et al. (2012) discussed the Callovian part from the Kutch mainland. The paper by Talib et al. (2017) was based on the section from Keera, which presented somewhat different biostratigraphy and included the upper part (Oxfordian) of the succession. However, the Oxfordian part is easily correlatable – litho- and bio-stratigraphically – with that at Jumara at a very high resolution. Roy et al. (2019) also contributed to the understanding of the upper part of the succession. The nautiloid biostratigraphy is also correlated with the standard ammonite zonation of Europe from the Submediterranean Province (Cariou and Hantzpergue 1997; Schweigert 2015).

   Biohorizons, which refer to boundaries having no thickness and representing significant changes in biostratigraphic character (Murphy and Salvadore 2020), are demarcated based on nautiloids. The biohorizons are used here for the emplacement of zone boundaries. It may be pertinent to mention that ammonite biohorizons, as referred by Cariou and Hantzpergue (1997), mean the smallest biostratigraphic intervals. In spite of the fact that the International Commission on Stratigraphy (ICS) unequivocally discourages such use of biohorizon (Murphy and Salvadore 2020) it remains in vogue among biostratigraphers (Callomon 2003; Roy et al. 2007; Krishna et al. 2011; Bardhan et al. 2012; Dutta and Bardhan 2016). Here, I use the term in the connotation that the ICS recommends.

A systematic description of one of the species, *Paracenoceras waageni*, which was described as a new species in Halder (2002), is included here because this is an unpublished material.

3 Nautiloid Biozonation

The succession comprising the Patcham Formation and the Chari Formation, as exposed in the type area Jumara and other localities, is subdivided into four assemblage biozones, which are *Procymatoceras pictonicum*, *Paracenoceras calloviense*, *Pseudaganides aganiticus* and *Paracenoceras hexagonum* in stratigraphic ascending order. The lowest biozone is further subdivided into two subzones - *Procymatoceras pictonicum* and *Paracenoceras prohexagonum*. The *Paracenoceras calloviense* Assemblage Biozone is further subdivided into three subzones, which are *Paracenoceras jumarense*, *P. kumagunense-P. dorsoexcvatum* and *P. waageni*. The biozones are described below with reference to the type section. The zonal species and other members of the assemblages are mentioned. A range-chart of the sixteen nautiloid species with reference to the biozones is provided in Fig. 1. The correlatable ammonite zones of Kutch and the European Submediterranean Province are also indicated (Table 1).

3.1 Procymatoceras pictonicum *Assemblage Biozone*

The basal part of the succession at Jumara comprises varied limestones. The lowermost bed is an alternation between coral-rich rudstone and white lime-mud rich wackestone (Datta 1992). *P. pictonicum* Tintant, 1970 is a common component of the fossil cephalopods in this basal bed. Other nautiloids are rare here and represented in my collection only by a juvenile specimen of *Paracenoceras prohexagonum* Spath, 1935 and an individual of *Paracenoceras calloviense* (Oppel, 1858) (Fig. 1). This bed is overlain by a thick unit of white wackestone at Jumara, which is followed up by a brown packstone to grainstone containing ooids and bioclasts (Datta 1992). These two beds did not yield many nautiloid specimens except an immature specimen of *P. pictonicum* from the former. A small fragment, doubtfully referred to this species, is collected from the lower part of the overlying zone at Keera (Fig. 1). The zone comprising these three beds is defined based on this species. A subzone for the basal coral-rich limestone is erected also based on this species, which is the most dominant nautiloid here. A subzone comprising the rest two beds is erected based on *Paracenoceras prohexagonum* that continued to the lowermost bed of the overlying biozone (Fig. 1). This biozone is referred to the Upper Bathonian (discussed later).

The *P. pictonicum* Subzone is correlatable with the Triangularis Zone based on ammonites, whereas the *P. prohexagonum* Subzone is equivalent to the Chrysoolithicus Subzone and lower part of the Madagascariensis Subzone (Roy
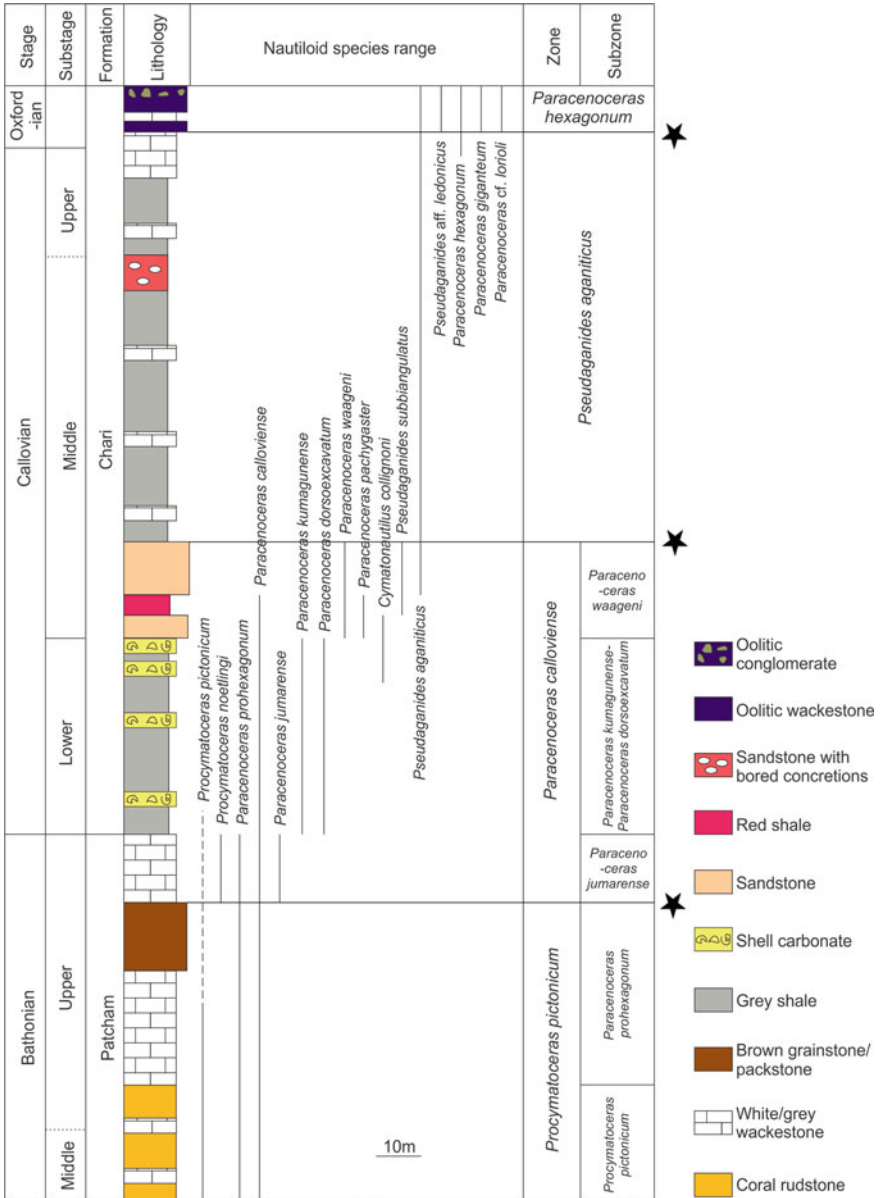
Fig. 1 Biozonation of the Bathonian-Oxfordian succession of Kutch mainland based on nautiloids. Stratigraphic ranges of nautiloid species are shown. Doubtful occurrence is demarcated by broken line. Biohorizons are indicated by stars. Stage and substage boundaries are indicated; those not supported by nautiloid data are dotted

Table 1 Correlation chart of nautiloid biozonation with that of ammonites from Kutch and Submediterranean Europe

Zonation of Kutch mainland			Ammonite zones of Submediterranean Province, Europe (#)	Substage
Nautiloid zonation (This study)		Ammonite zonation (*)		
Zone	Subzone	Zone	Subzone	
Paracenoceras hexagonum				Planula	Upper Oxfordian
				Bimammatum	
				Bifurcatus	
		Helenae-Maya	Kranaus	Transversarium	Middle Oxfordian
			Helenae		
			Maya	Plicatilis	
			Semirugosum	Paturattensis	Lower Oxfordian
				Minax	
Pseudaganides aganiticus		Lamberti?		Lamberti	Upper Callovian
		Athleta		Athleta	
		Reissi	Aberrans	Coronatum	Middle Callovian
			Reissi		

(continued)

Table 1 (continued)

Zonation of Kutch mainland		Ammonite zonation (*)		Ammonite zones of Submediterranean Province, Europe (#)	Substage
Nautiloid zonation (This study)					
Zone	Subzone	Zone	Subzone		
Paracenoceras calloviense	*Paracenoceras waageni*	Anceps	Indicus	Anceps	Lower Callovian
			Opis		
			Anceps		
	Paracenoceras kumagunense- Paracenoceras dorsoexcavatum	Formosus	Semilaevis	Gracilis	
			Formosus		
			Diadematus	Bullatus	
			Transitorius		
	Paracenoceras jumarense	Chrysoolithicus	Madagascariensis	Discus	Upper Bathonian
Procymatoceras pictonicum	*Paracenocers prohexagonon*		Chrysoolithicus	Retrocostatum	
	Procymatoceras pictonicum	Triangularis			

Sources of ammonite zones: *= Roy et al. (2007), Bardhan et al. (2012), Talib et al. (2017), Roy et al. (2019); #= Cariou and Hantzpergue (1997), Schweigert (2015)

et al. 2007; Dutta and Bardhan 2016) of Kutch (Table 1). The Blanazense Subzone of the Retrocostatum Zone from the Submediterranean European scheme is correlatable with the *P. pictonicum* Subzone (Mangold and Rioult 1997; Schweigert 2015). The Hannoveranus Subzone and the lower part of the Discus Zone, i.e. the Hollandi Subzone, roughly correspond to the *P. prohexagonum* Subzone (Mangold and Rioult 1997; Schweigert 2015) (Table 1).

3.2   Paracenoceras calloviense *Assemblage Biozone*

P. calloviense is the most abundant species of nautiloid in Kutch (Halder 2002). It appeared already in the basal bed in the Jumara succession and continues through almost to the top of this biozone (Fig. 1). The lowermost bed of this zone – a massive white wackestone – is also the top unit of the Patcham Formation. This bed marks a significant increase in nautiloid species diversity and abundance. Hence, its base is demarcated by a biohorizon. There are *Paracenoceras jumarense* (Waagen, 1873), *P. prohexagonum* and *Procymatoceras noetlingi* (Halder and Bardhan, 1997) apart from *P. calloviense* in this bed (Fig. 1). *P. jumarense* is quite abundant here along with the zonal species (Halder 2002). It is also restricted to this bed (Fig. 1). It demarcates the *P. jumarense* Subzone. This subzone is equivalent to the upper part of the ammonite based Madagascariensis Subzone of Kutch (Roy et al. 2007; Dutta and Bardhan 2016) and the Discus Subzone of Tethyan Submediterranean Europe (Mangold and Rioult 1997; Schweigert 2015) (Table 1). This subzone represents the uppermost part of Bathonian (discussed later).

A distinct change in the litho-character demarcates the beginning of the Chari Formation (Fig. 1). A thick shale succession interspersed with thin bands of bioclastic packstones (shell carbonate) occurs at the lower part of this formation (Datta 1992). Shell carbonate bands become more frequent in the upper part of this argillaceous unit (Fig. 1). A similar litho-unit is found in coeval parts of the succession in other localities of Kutch except Keera, where golden-coloured oolitic limestone is found to alternate with shale and shell carbonates. Two nautiloids – *Paracenoceras kumagunense* (Waagen, 1873) and *P. dorsoexcavatum* (Parona and Bonarelli, 1895) – are recorded from this unit along with *P. calloviense* (Fig. 1). *P. kumagunense-P. dorsoexcavatum* Subzone is erected based on these species, which corresponds to the ammonite-based Formosus Zone of Kutch (Bardhan et al. 2012; Talib et al. 2017) (Table 1). There are two zones—Bullatus and Gracilis—in the Submediterranean Europe in this interval (Thierry et al. 1997) (Table 1). This subzone represents the Lower Callovian (discussed later).

Two sandstone units pierce the shale-dominated shale-limestone alternation motif of the Chari Formation at its middle part (Personal observation). A highly fossiliferous red shale occurs in between the two sandstone bodies. *P. calloviense* disappears after this shale unit (Fig. 1). This sandstone-dominated part of the Chari Formation accommodates a diverse nautiloid fauna and constitutes a subzone. *Cymatonautilus collignoni* Tintant, 1970 that appears in the upper part of the underlying subzone

continues to the lower part of this one (Fig. 1). *Paracenoceras pachygaster* (Tintant, 1981) is restricted to the lower part of it and does not continue in the upper sandstone unit (Fig. 1). The genus *Pseudaganides* Spath, 1927 appears in this subzone and eventually becomes abundant in the overlying biozone. *Pseudaganides subbiangulatus* (d'Orbigny, 1850) is the oldest species of this genus in Kutch and is restricted to this subzone, whereas *Pseudaganides aganiticus* (Schlotheim, 1820) appears in the upper sandstone unit (Fig. 1). However, *Paracenoceras waageni* n. sp. is present throughout this part and defines this subzone (Fig. 1). This species is quite common especially in the upper part of the subzone where *P. calloviense* is absent. The *P. waageni* Subzone is equivalent to the ammonite-based Anceps Zone of Kutch (Bardhan et al. 2012; Krishna et al. 2011; Talib et al. 2017) (Table 1). This zone is also present in the Submediterranean Province (Thierry et al. 1997; Schweigert 2015) (Table 1). The subzone is referred to the lower part of the Middle Callovian (discussed later).

3.3 Pseudaganides aganiticus *Assemblage Biozone*

The upper part of the Chari Formation except the top litho-unit is characterised by alternation between shale and white/grey wackestone (Datta 1992). A fine-grained narrow red sandstone bed containing limestone concretions, which bear lithophagid borings, punctuates this part of the succession at its middle. A thin white wackestone bed marks the top of this part (Fig. 1). Similar lithologically correlatable units with minor variations are there in other localities (personal observation). *Pseudaganides aganiticus* is present through the whole of this part of the succession. A biozone is erected comprising the upper litho-units of the Chari Formation except the topmost bed based on this species. This is the sole nautiloid species found in most parts of this zone (Fig. 1), however, in moderate abundance (Halder 2002). *Paracenoceras hexagonum* (Sowerby, 1826) appears near the top of this zone. A biohorizon characterised by the sudden fall in nautiloid species diversity demarcates the base of this zone (Fig. 1). This zone subsumes three ammonite zones of Kutch—Reissi, Athleta and Lamberti (Bardhan et al. 2012; Roy et al. 2019) (Table 1). It is broadly correlatable to the Coronatum, Athleta and Lamberti Zones of the Submediterranean Europe (Thierry et al. 1997; Schweigert 2015) (Table 1). This zone contains the upper part of the Middle Callovian, the whole of the Upper Callovian and a part of the Lower Oxfordian (discussed later).

3.4 Paracenoceras hexagonum *Assemblage Biozone*

The top of the Chari Formation is characterised by an admixture of white and oolitic wackestones that alternate with grey shale (Datta 1992). This is known as the Dhosa Oolite, which is laterally persistent through the whole of the Kutch mainland. The topmost part of this unit is a conglomeratic hardground. *P. hexagonum*

is the most common nautiloid in the Dhosa Oolite unit. A biozone is established based on this species. A biohorizon demarcates the base of it, which is characterised by the sudden appearance of several nautiloid species after the monotony of the underlying zone (Fig. 1). *Paracenoceras giganteum* (d'Orbigny, 1825), *Paracenoceras* cf. *lorioli* (Loesch, 1914) and *Pseudaganides* aff. *ledonicus* (Loriol, 1903) appear here in the Dhosa Oolite and occur in subordinate numbers to *P. hexagonum* (Personal observation). The zone can be correlated with ammonite-based Helenae-Maya Zone established at the Keera dome (Talib et al. 2017) (Table 1). In the Tethyan Europe, there are several ammonite zones that belong to this time interval (Cariou et al. 1997; Schweigert 2015) (Table 1). The zone represents the major part of the Oxfordian (discussed later).

4   Systematic Paleontology

Subclass Nautiloidea Agassiz, 1847
Order Nautilida Agassiz, 1847
Family Paraceoceratidae Spath, 1927
Genus *Paracenoceras* Spath, 1927
Type species *Nautilus hexagonus* Sowerby, 1826 by OD.
Paracenoceras waageni n. sp.
(Fig. 2).

Etymology The specific name is after W. Waagen, the pioneering researcher on the cephalopods from the Jurassic of Kutch.

Type locality Jumara, Kutch.

Stratigraphic and geographic distribution Chari Formation, Middle Callovian from Jumara, Jara and Keera.

Type material Holotype—FI 10127, internal mould, mostly body chamber; paratypes—FI 10125, body chamber and part of phragmocone, shell mostly preserved; FI 10146, phragmocone, internal mould.

Other material 16 specimens; mostly internal moulds, some covered with shell; mostly body chambers.

Repository Specimens are reposited in the Paleontology Laboratory of the Department of Geology, Presidency University, Kolkata.

Measurements Table 2.

Diagnosis Shell inflated, widening rate high, section subtrapezoidal to subrectangular; flanks and venter flat in adulthood, venter commonly very wide, ventrolateral margin angular; umbilicus small, surface smooth.

Description Large, quite inflated shell (max. W/H= 1.48), a few specimens slightly higher than wide (min. W/H= 0.79); shell very rapidly widening in later ontogeny; umbilicus small, umbilical wall steep, convex in early ontogeny, umbilical shoulder rounded; flanks arched in juvenile stage, flat later, in body chamber lower part of flanks bulged while upper part just below venter slightly sulcate; ventrolateral
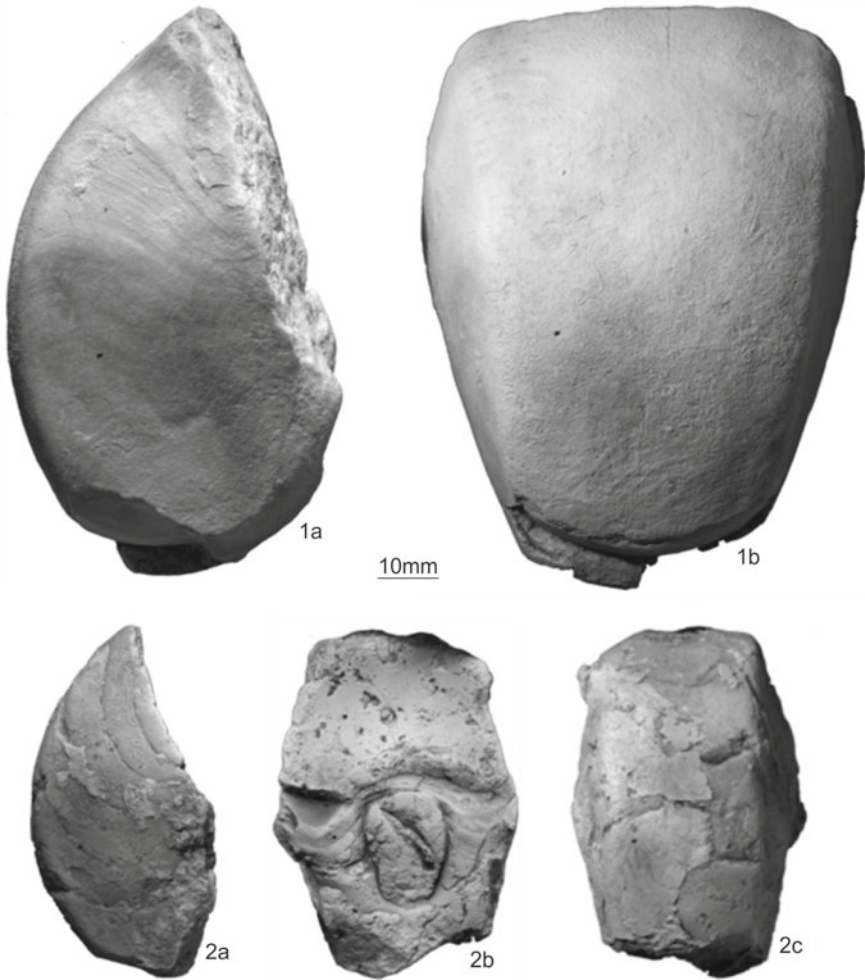
Fig. 2 *Paracenoceras waageni* n. sp. (1) FI 10127, the holotype; lateral (1a) and ventral (1b) views. (2) FI 10146, one of the paratypes; lateral (2a), apertural (2b) and ventral (2c) views

margins rounded in early stage, prominent and angular later, in latest part of body chamber angularity diminishes, angularity of ventrolateral margin varies intraspecifically to a certain extent; venter rapidly widening, flat to only slightly sulcate in body chamber, convex in early stage; aperture generally depressed, quite wide, subtrapezoidal to subrectangular; maximum width just above umbilical shoulder; septa moderately concave; suture with broad prominent lateral and ventral lobes intervened by narrowly rounded ventrolateral saddle; siphuncle central; surface smooth, characterised by only growth lirae with deep hyponomic sinus at mid-venter, one faint longitudinal line occasionally found along mid-venter.

Table 2 Measurements of selected specimens of *Paracenoceras waageni* n. sp

Specimen no.	Shell Diameter (D) mm	Shell Width (W) mm	Shell height (H) mm	Ventral width (VW) mm	Dorso-ventral height (h) mm
FI 10125	134	76	70	60	47
FI 10127	100c	79	69	65	40
FI 10128	97	66	60	51	37
FI 10136	71	53	43	44	–
FI 10140	60	52	36	32	31
FI 10143	54	34	30	21	–
FI 10146	62c	39	34	26	27

Discussion The present species is comparable in all aspects to *P. calloviense* except having a more inflated shell than the latter. The species in its early stage is barely distinguishable from *P. calloviense*; their differences appear later. Both, in juvenile, are involute with arched flanks and venter, and rounded ventrolateral and umbilical shoulders. The flanks and the venter, in both, become flat in the adult stage. *P. waageni* n. sp., however, has a flatter venter than that of *P. calloviense*. The ventrolateral margin in *P. calloviense* never becomes so angular as that in the present species. In *P. calloviense*, it becomes more prominent in later stages, and especially near end-phragmocone sometimes gets angulation, which dies down in the body chamber. In the present species, angulation is more prominent from a late ontogeny and persists well in the body chamber only to diminish near the matured peristome margin. But the main difference between these two species lies in their W/H ratio. Although considerably variable in both, this ratio is generally close to 1 in *P. calloviense* with a slight bias towards inflation, whereas distinctly greater than 1 in the present form. This difference becomes more obvious in later stages. The suture is comparable between the present species and the microconch of *P. calloviense* whereas the macroconch of the latter has a more flexuous pattern with deeper lateral lobes.

5 Discussion

5.1 Evaluation of Biostratigraphic Potential of Nautiloids

The nautiloid biozonation appears to be relatively coarser than that based on ammonites. For example, the nautiloid-based *P. kumagunense-P. dorsoexcavatum* Subzone is equivalent to the ammonite-based Formosus Zone, which is subdivided into four subzones (Table 1). Similarly, the overlying *P. waageni* Subzone is correlatable to a whole ammonite zone, the Anceps Zone, which is divided into three subzones

(Table 1). The *P. aganiticus* Zone subsumes three ammonite zones (Table 1). The nautiloid zonation, when compared to the standard European biostratigraphic classification based on ammonites (Mangold and Rioult 1997; Thierry et al. 1997; Cariou et al. 1997; Schweigert 2015), also proved coarser (Table 1). In spite of this coarseness, nautiloid biostratigraphy exhibits that most of the zone and subzone boundaries coincide with those erected based on ammonites. This means that the broad pattern of faunal turnover for both groups of cephalopods is similar. Hence, nautiloids can be of use as a subsidiary fauna to ammonites in biostratigraphy (also see Evans et al. 2014). An integrated biostratigraphy combining both the faunas can be more useful than one based only on ammonites, especially at places where the latter group of fossils is absent or rare.

Paracenoceras calloviense, the most abundant nautiloid species in Kutch, is geographically and temporally widespread (Halder 2000, 2002). Although it penetrates the Upper Bathonian Stage in Kutch a broad Callovian time can be ascribed to a litho-unit based on its presence. In contrast to *P. calloviense*, several species of nautiloids in Kutch exhibit a temporally restricted occurrence (Fig. 1), suggesting their biostratigraphic potential. However, some of them are endemic. For example, *Paracenoceras jumarense* is endemic to Kutch (Bardhan et al. 1994; Halder 2000, 2002) and *Procymatoceras noetlingi* is endemic to the Indian subcontinent (Halder and Bardhan 1997; Halder 2000, 2002). Some other species, such as *P. prohexagonum*, are endemic to the Indo-Madagascan Province (Halder et al. 1998; Jain 2019). There are other species such as *Procymatoceras pictonicum* and *Pseudaganides aganiticus* that appear earlier in Kutch than in Europe. However, several other species are useful in inter-provincial correlation and delineation of chronostratigraphic boundaries (discussed later).

Temporal distribution of nautiloids in the Kutch basin records some important biohorizons that demarcate sudden changes in faunal diversity and composition, facilitating demarcation of the zone boundaries (Fig. 1). The base of the *P. calloviense* Zone marks an important shift in the dominance pattern of nautiloids in Kutch stratigraphy along with an increase in species diversity. The oldest nautiloid zone of Kutch, the *Procymatoceras pictonicum* Zone, contains a low-diversity fauna. The zonal species is much more abundant here than other co-occurring nautiloids. *Procymatoceras* Spath, 1927, a genus closely related to *Cenoceras* Hyatt, 1884, the root stock of all the post-Triassic nautiloids (Tintant 1970; Halder 2002), while continues to the overlying *P. jumarense* Subzone the genus *Paracenoceras* Spath, 1927 rose into prominence with higher specific diversity and abundance (Fig. 1). This conforms to the global pattern of nautiloid evolution. *Cenoceras*-like forms with a relatively round whorl section and non-sulcate venter traversed by nearly straight suture line, characterise the entire Lower Jurassic globally (see Kummel 1956). *Paracenoceras*, with trapezoidal outline and commonly sulcate venter, having distinctly lobed suture at the venter, became the most diverse genus in the Callovian-Oxfordian. *Pseudaganides* Spath, 1927 is contemporaneous to *Paracenoceras* and also quite diverse (Kummel 1956; Marchand and Tintant 1973). The reign of *Paracenoceras-Pseudaganides* continues until *Cymatoceras* Hyatt, 1884 and *Eutrephoceras* Hyatt, 1894 took over mainly during the Cretaceous (Kummel 1956). In Kutch, however, another biohorizon

demarcates the sudden disappearance of *Paracenoceras* in the upper Middle-Upper Callovian at the base of the *Pseudaganides aganiticus* Zone only to reappear in the Oxfordian at the *Paracenoceras hexagonum* Zone (Fig. 1). The disappearance of *Paracenoceras* appears to be a local phenomenon and possibly linked to the shallowing of the basin. The parasequence that represents this part of the stratigraphy of Kutch mainland (Datta 1992) indicates a regressive phase. The shallow basin did not allow nautiloids other than *Pseudaganides* to thrive. It may be pertinent to mention here that nautiloids are extremely rare in the Jhura and the Habo domes, the eastern part of the mainland basin, except in the Dhosa Oolite Member. The eastern side of the Kutch basin represents the shoreward direction. The Dhosa Oolite Member is the evidence of transgression in the basin and represents an MFS (Fürsich et al. 1992; Krishna et al. 2011) that allowed nautiloids to invade this shallower part of the basin. The biohorizon that demarcates the boundary between the *P. aganiticus* Zone and the *P. hexagonum* Zone (Fig. 1) is characterised by the reappearance of *Paracenoceras* in high diversity facilitated by the deepening of the basin.

5.2 Delineation of Stage Boundaries

The distribution pattern of nautiloids in the Kutch mainland illustrates that this cephalopod can facilitate the delineation of stage boundaries. *Procymatoceras noetlingi* was known only from the Upper Bathonian Polyphemus Limestone of Pakistan (Noetling 1897) before it was reported from Kutch (Halder and Bardhan 1997; Halder 2002). *Paracenoceras prohexagonum* was known only from definite Upper Bathonian rocks of Somalia (Spath 1935). The latter has recently been reported from contemporaneous level of Ethiopia (Jain 2019). Their disappearance from Kutch along with *Paracenoceras jumarense*, which is endemic to Kutch, marks the end of the Bathonian Epoch (Table 1). The Upper Bathonian, however, has been conclusively established based on ammonites such as *Epistrenoceras* Bentz, 1928, which is an index of the Bathonian (Kayal and Bardhan 1998; Roy et al. 2007). Recently, the presence of unequivocal Middle Bathonian ammonites from the mainland deposits, including Jumara, has been reported (Roy et al. 2007; Jain 2014). Nautiloid data is inadequate to support this (Fig. 1). *Paracenoceras dorsoexcavatum* was known from the Lower Callovian of France (Tintant 1984; Halder 2000; Branger 2004). Its appearance marks the beginning of the Callovian in Kutch also (Fig. 1). It is accompanied here by *P. kumagunense*, an endemic Indo-Madagascan species (Halder 2000, 2002) (Fig. 1). The boundary between the Bathonian and the Callovian is demarcated by the disappearance of ammonites such as *Oxycerites* cf. *orbis* (Giebel, 1852), *Macrocephalites madagascariensis* Lemoine, 1911, *M*. *chrysoolithicus* (Waagen, 1873), *Kheraiceras* cf. *hannoveranum* Roemer, 1911 and *Sivajiceras congener* (Waagen, 1875) and appearance of *Macrocephalites formosus* (Sowerby, 1840) *Sivajiceras paramorphum* (Waagen, 1875) and *Choffatia recuperoi* (Gemmellaro, 1873) (Roy et al. 2007; Dutta and Bardhan 2016).

Cymatonautilus spp. has a wide paleobiogeographic distribution including areas of "subboreal" northern Tethys (Tintant 1981, 1987; Halder and Bardhan 1996a) within a short geological time straddling the boundary between the Early and the Middle Callovian (Fig. 1). The boundary between the Lower and the Middle Callovian is demarcated by the disappearance of several macrocephalitid ammonites like *Macrocephalites formosus*, *M. semilaevis* (Waagen, 1873) and the appearance of *Reineckeia anceps* (Reinecke, 1818) (Bardhan et al. 2012; Talib et al. 2017).

Demarcation of the boundary between the Middle and the Upper Callovian in Kutch cannot be done with the present set of data on nautiloids because the species that disappeared or appeared there are either endemic or known by longer temporal ranges (Fig. 1). However, the appearance of large, spine-bearing, evolute ammonite *Peltoceras* Waagen, 1871 spp. including the zonal species *P. athleta* (Phillips, 1829) characterises the beginning of the Upper Callovian (Talib et al. 2017; Dutta and Bardhan 2016; Roy et al. 2019).

The boundary between the Callovian Stage and the Oxfordian Stage is commonly placed below the Dhosa Oolite Member (Roy et al. 2012, 2019; Pandey et al. 2015; Talib et al. 2017). Talib et al. (2017) placed the Callovian-Oxfordian boundary between the litho-units Kr-6 and 7 based on the disappearance of *Pachyceras lelandeanum* (d'Orbigny, 1847) in the lower unit and appearance of *Peltoceras* (*Peltoceras*) *semirugosum* Waagen, 1875 in the overlying unit. Pandey et al. (2015) recorded changes in the ammonite composition of the family Aspidocertidae Zittel, 1895 along the Callovian-Oxfordian boundary. They found that *Peltoceras* and *Metapeltoceras* Spath, 1931 are restricted to the Callovian of Kutch as also in Europe while *Euaspidoceras* Spath, 1931 is most diverse in the Oxfordian. In contrast, Roy et al. (2019) found that *Peltoceras* continues to the Lower Oxfordian of Kutch. However, all these authors placed the Callovian-Oxfordian boundary below the Dhosa Oolite unit.

A narrow white wackestone, often with secondary gypsum partings, lies below the Dhosa Oolite unit (Fig. 1) in all the studied localities. This bed yielded only a handful of fossils. Ammonites from this bed are often fragmentary or represented by only juvenile inner whorls; hence, difficult to identify with confidence. Still, typical Callovian ammonites are represented here by *Peltoceras* spp. including *P. athleta*, hecticoceratin genera *Putealiceras* Buckman, 1922, *Sublunuloceras* Spath, 1928 and *Brightia* Rollier, 1922, and shivajiceratin *Obtusicostites* Buckman, 1921 (Waagen 1873–1875; Spath 1927–1933; Roy et al. 2012, 2019; Roy 2014; Dutta and Bardhan 2016). Hence, a Late Callovian age is generally assigned to this bed (e.g. Roy et al. 2012, 2019). Consequently, the Callovian-Oxfordian boundary is placed above this unit (Roy et al. 2012, 2019). However, juvenile specimens of ammonites, only at their first or second whorls, seem to represent an admixture of Callovian forms mentioned above and *Mayaites* Spath, 1924 and *Perisphinctes* Waagen, 1869-like forms of distinct Oxfordian affinity (Personal observation). In the course of this investigation, I have discovered an unambiguous specimen of the nautiloid *Paracenoceras hexagonum*, the type species of the genus, from this bed. This species is a characteristic nautiloid of the Lower and the Middle Oxfordian from western Europe (see Halder and Bardhan 1996b; Halder 2000). It is also known

from contemporaneous stratigraphy of Saudi Arabia (Tintant 1987), Egypt (Douvillé 1916), Somalia (Abbate et al. 1974) and Ethiopia (Ficarelli 1968). The ammonite assemblage suggests that the boundary between the Callovian and the Oxfordian passes through this limestone unit below the Dhosa Oolite Member. The presence of the nautiloid *P. hexagonum* conclusively elucidates that this unit straddles the Callovian-Oxfordian boundary (Fig. 1, Table 1).

There are controversies regarding the age of the Dhosa Oolite Member. For instance, Fürsich et al. (2001) indicated its age as the Early Oxfordian. Talib et al. (2017), based on the ammonite fauna from Keera, reported an Early to Middle Oxfordian age (see also Krishna et al. 2011). Roy et al. (2012), based mainly on ammonites from several sections of Kutch, established that the Dhosa Oolite represents the whole of the Oxfordian Stage. Its top about 50cm thick portion is conglomeratic, richly oolitic and rich in fossil content. This is a condensed layer (Fürsich et al. 1992; Pandey et al. 2009) yielding a diverse assemblage of fossils. Ammonites occurring within the boulders and in the matrix represent a time-averaged fauna (e.g. Pandey et al. 2015; see Roy et al. 2012 for a discussion). Nautiloids, represented by five species in the Dhosa Oolite, also come mainly from this top part. While *P. hexagonum* was known from the Lower-Middle Oxfordian of Europe and Africa *P. giganteum* was reported from the Upper Oxfordian of France (see Halder 2000). *Pseudaganides ledonicus* was known from the Middle-Upper Oxfordian of France and Switzerland (Marchand and Tintant 1973). The co-occurrence of these nautiloids lends support to an age range of the Dhosa Oolite Member from the Early to the Late Oxfordian (Fig.1, Table 1).

6   Conclusion and Remarks

(a)   The Jurassic succession of Kutch comprising the Patcham Formation and the Chari Formation is classified based on the nautiloid fauna, primarily with reference to the section exposed at Jumara. Four biozones are erected. Two of the zones are further subdivided into subzones.

(b)   It has been observed that the classification is relatively coarser than that based on contemporaneous ammonites. It is no surprise because the exemplary biostratigraphic potential of the Mesozoic ammonites has been proved for a long time. Ammonites are observed to show temporal precision to a scale of 100ka (e.g. Callomon 2003). The relative coarseness of the biozonation is also true for all other contemporaneous fossil organisms (e.g. Cariou and Hantzpergue 1997; Talib et al. 2017).

(c)   The relative coarseness is no deterrent to the establishment of nautiloid zones, especially because there are several nautiloid taxa of short temporal ranges and/or wide geographic ranges (see also Branger 2004). Nautiloids also exhibit a more or less similar pattern of faunal turnover with the ammonites.

(d) Nautiloids can be fruitfully utilised in delineating the stage and the substage boundaries. The Callovian-Oxfordian boundary in Kutch is precisely demarcated with the help of a geographically widely distributed nautiloid species. It further demonstrates the biostratigraphic potential of nautiloids.

References

Abbate E, Ficcarelli G, Pirini Radrizzani C, Salvietti A, Torre D, Turi A (1974) Jurassic sequences from the Somali coast of the Gulf of Aden. Rivista Italiana di Paleontologia e Stratigrafia 80:409–478

Bardhan S, Datta K (1987) Biostratigraphy of Jurassic Chari Formation: A study in Keera Dome, Kutch, Gujarat. J Geol Soc India 30:121–131

Bardhan S, Halder K, Jana SK (1994) Earliest sexual dimorphism in Nautiloidea from the Jurassic of Kutch, India. Neues Jahrbuch für Geologie und Paläontologie Abhandlungen 193:287–309

Bardhan S, Dutta R, Chanda P, Mallick S (2012) Systematic revision and sexual dimorphism in *Choffatia* (Ammonoidea: Perisphinctoidea) from the Callovian of Kutch, India. Palaeoworld 21:29–49

Branger P (2004) Middle Jurassic Nautiloidea from western France. Rivista Italiana di Paleontologiae Stratigrafia 110:141–149

Callomon JH (2003) The Middle Jurassic of western and northern Europe: its subdivisions, geochronology and correlations. Geol Surv Denmark and Greenland Bull 1:61–73

Cariou É, Hantzpergue P (Co-ord.) (1997) Biostratigraphie du Jurassique ouest-européen et méditerranéen. zonations parallèles et distribution des invertébrés et microfossiles. Bull Centre Rech Elf Explor Prod Mém 17

Cariou É, Enay R, Atrops F, Hantzpergue P, Marchand D, Rioult M (1997) Oxfordien. Ch. 9 In: Cariou É and Hantzpergue P. (Co-ord.) Biostratigraphie du Jurassique ouest-européen et méditerranéen, zonations parallèles et distribution des invertébrés et microfossiles. Bull Centre Rech Elf Explor Prod Mém 17:79–86

Cichowolski M (2003) The nautiloid genus *Cymatoceras* from the Cretaceous of the Neuquin and Austral basins, Argentina. Cret Res 24:375–390

Datta K (1992). Facies, fauna and sequence: an integrated approach in the Jurassic Patcham and Chari Formations, Kutch, India. Unpublished PhD thesis, Jadavpur University, Kolkata

Douvillé H (1916) Les terrains secondaires dans le massif du Moghara à l'Est de l'isthme de Suez. Mémoire de l'Académie des Sciences, Paris 54:1–184

Dutta R, Bardhan S (2016) Systematics, endemism and phylogeny of Indian proplanulitins (Ammonoidea) from the Bathonian-Callovian of Kutch, western India. Swiss J Palaeontol 135:23–56

Evans DH, King AH, Histon K, Cichowolski M (2014) Nautiloid cephalopods - a review of their use and potential in biostratigraphy. Denisia 32:7–22

Ficcarelli G (1968) Fossili Giuresi della serie sedimentaria del Nilo Azurro meridionale [Jurassic fossils from the sedimentary series of the southern Blue Nile]. Rivista Italiana di paleontologia e Stratigrafia 74:23–50

Fürsich FT, Oschmann W, Singh IB, Jaitley AK (1992) Hardground, reworked concretion levels and condensed horizons in the Jurassic of western India: their significance for basin analysis. J Geol Soc 149:313–331

Fürsich FT, Pandey DK, Callomon JH, Jaitly AK, Singh IB (2001) Marker beds in the Jurassic of the Kutch basin, Western India: their depositional environment and sequence-stratigraphic significance. J Palaeontol Soc India 46:173–198

Halder K (2000) Diversity and biogeographic distribution of Jurassic nautiloids of Kutch, India, during the fragmentation of Gondwana. J African Earth Sci 31:175–185

Halder K (2002) Jurassic nautiloids of Kutch, western India: a study on their systematics, palaeoecology and evolution. Unpublished PhD thesis, Jadavpur University, Kolkata

Halder K, Bardhan S (1996a) The fleeting genus *Cymatonautilus* (Nautiloidea): New record from the Jurassic Chari Formation, Kutch, India. Canadian J Earth Sci 33:1007–1010

Halder K, Bardhan S (1996b) The Oxfordian (Upper Jurassic) nautiloid fauna of Kutch, western India. Neues Jahrbuch für Geologie und Paläontologie Abhandlungen 201:17–32

Halder K, Bardhan S (1997) On some new Late Bathonian paracenoceratids (Nautiloidea) from Kutch, India and their evolutionary and biostratigraphic implications. Neues Jahrbuch für Geologie und Paläontologie Monatshefte 1997:543–561

Halder K, Jana SK, Bardhan S (1998) Ornamental polymorphism in *Paracenoceras prohexagonum* (nautiloidea) from the Jurassic Chari sequence, Kutch, Gujarat. Indian Min 52:89–94

Jain S (2014) The Arkelli Chronozone: a new early Middle Bathonian standard ammonite zone for Kachchh, western India (southern Jurassic Tethys). Zittelliana A 54:91–135

Jain S (2019) First Bathonian (Middle Jurassic) nautiloid *Paracenoceras* Spath from Ethiopia. J African Earth Sci 149:84–96

Jana SK, Bardhan S, Halder K (2005) Eucycloceratin ammonites from the Callovian Chari Formation, Kutch, India. Palaeontol 48:883–924

Kayal A, Bardhan S (1998) *Epistrenoceras* Bentz (Ammonoidea) from the Middle Jurassic of Kutch (western India): a new record and its chronostratigraphic implication. Canadian J Earth Sci 35:931–935

Krishna J, Cariou É (1986) The Callovian of western India: new data on the biostratigraphy, biogeography of the ammonites and correlation with Western Tethys (submediterranean Province). Newslett Strat 17:1–8

Krishna J, Pandey B, Pathak DB (2011) Current Status of the Jurassic ammonoid stratigraphic framework in the Indian Subcontinent with focus on the tectonically controlled regional transgressive – regressive couplets. Mem Geol Soc India 78:140–176

Kummel B (1956) Post-Triassic nautiloid genera. Bulletin of the Museum of Comparative Zoology at Harvard College 114, Cambridge, Massachussets

Mangold C, Rioult M (1997) Bathonien. Ch. 7 In: Cariou É. and Hantzpergue P. (Co-ord.) Biostratigraphie du Jurassique ouest-européen et méditerranéen. zonations parallèles et distribution des invertébrés et microfossiles. Bull. Centre Rech. Elf Explor Prod Mém 17:55–62

Marchand D, Tintant H (1973) Étudie statistiques sur *Pseudaganides aganiticus* (Schlotheim) et diverses espèces voisines. Bull Sci Bourgogne 28:111–169

Mitra KC, Bardhan S, Bhattacharya D (1979) A study of Mesozoic stratigraphy of Kutch, Gujarat, with special reference to rock-stratigraphy and bio-stratigraphy of Keera dome. Bull Indian Geol Ass 12:129–143

Murphy MA, Salvadore A (eds) (2020) International Stratigraphic Guide - An abridged version. International Commission on Stratigraphy

Noetling F (1897) Fauna of the Kellaways of Mazat Drik. Palaeontologia Indica Memoir 16:1–22

Pandey DP, Fürsich FT, Sha JG (2009) Interbasinal marker intervals - a case study from the Jurassic basins of Kutch and Jaisalmer, western India. Sci China Ser D: Earth Sci 52:1924–1931

Pandey DK, Alberti M, Fürsich FT (2015) Ammonites of the genera *Peltoceras* Waagen, 1871, *Metapeltoceras* Spath, 1931, and *Euaspidoceras* Spath, 1931 from the Upper Callovian and Oxfordian of Kachchh, western India, and their biostratigraphic potential. J Palaeontol Soc India 60:1–26

Roy A, Bardhan S, Das S, Mondal S, Mallick S (2012) Systematic revision and palaeobiogeography of *Perisphinctes* Waagen (Ammonoidea) from the Oxfordian of Kutch, India: stratigraphic and evolutionary implications. Palaeoworld 21:167–192

Roy A, Banerjee S, Bardhan S (2019) Peltoceratinae (Ammonoidea) from the Upper Callovian-Lower Oxfordian of Kutch, India: systematic revision and biostratigraphic implication. Geobios 56:1–22

Roy P (2014) Callovian-Oxfordian hecticoceratins from western India: their biostratigraphic and palaeobiogeographic Implications. J Palaeogeography 3:174–206

Roy P, Bardhan S, Mitra A, Jana SK (2007) New Bathonian (Middle Jurassic) ammonite assemblages from Kutch, India. J Asian Earth Sci 30:629–651

Schweigert G (2015) Ammonoid biostratigraphy in the Jurassic. Chapter 14. In: Klug C, Korn D, De Baets K, Kruta I, Mapes RH (eds) Ammonoid Paleobiology: From Macroevolution to Paleogeography. Topics Geobiol 44:389–402

Spath LF (1927-1933) Revision of the Jurassic cephalopod fauna of Kachh (Cutch). Palaeontologia Indica, New Series 9

Spath LF (1935) Jurassic and Cretaceous Cephalopoda. The Mesozoic palaeontology of British Somaliland. Geol Palaeontol British Somaliland 2:205–228

Talib A, Jain S, Irshad R (2017) Integrated benthic foraminiferal and ammonite biostratigraphy of Middle to Late Jurassic sediments of Keera dome, Kachchh, western India. In: Kathal PK, Nigam R, Talib A (eds) Advanced Micropaleontology, Scientific Publishers, pp 71–81

Thierry J, Cariou É, Elmi S, Mangold C, Marchand D, Rioult M (1997) Callovien. Ch. 8 In: Cariou É. and Hantzpergue P. (Co-ord.) Biostratigraphie du Jurassique ouest-européen et méditerranéen. zonations parallèles et distribution des invertébrés et microfossiles. Bull. Centre Rech. Elf Explor Prod. Mém. 17:63–78

Tintant H (1970) Les "Nautiles à côtes" du Jurassique. Annales de Paléontologie (Invertébrés) 55:53–96

Tintant H (1981) Un cas de parallélisme évolutif synchrone chez les Nautiles à côtes du Jurassique. Boletim Sociedade Geológica de Portugal 22:63–69

Tintant H (1984) Exemples de nanisme spécifique chez les Nautiloidés du genre *Paracenoceras* au Jurassique moyen. Géobios, Mémoire Spécial 8:403–410

Tintant H (1987) Les Nautiles du Jurassique d'Arabie Saoudite. Géobios, Mémoire Spécial 9:67–129

Waagen W (1873-1875) Jurassic fauna of Kutch. The Cephalopoda. Palaeontologia Indica, Series 9

Taphonomic Pathways for the Formation of Bioturbated Cycles in the Early Cretaceous Wave-Dominated Deltaic Environment: Ghuneri Member, Kachchh Basin, India

Bhawanisingh G. Desai and Suruchi Chauhan

Abstract The Early Cretaceous Ghuneri Member (Bhuj Formation) in the Kachchh Basin represents deposition in a wave-dominated deltaic environment. It is characterized by asymmetrical bioturbated cycles of low to high bioturbated sandstone units. Systematic ichnological analysis of the Ghuneri Member across Kachchh basin indicates twenty-four recurring trace fossils categorized in fair-weather and storm-weather trace fossil ichnoassemblages. Fair-weather ichnoassemblages consist of shallow tier *Gyrochorte, Lockeia* and *Planolites*, middle tier *Paleophycus, Polykladichnus*, *Rhizocorallium*, *Rosselia*, *Taenidium*, and deep tier *Chondrites*. Storm-weather ichnoassemblage comprises of middle to deep tier *Arenicolites, Diplocraterion, Psilonichnus Skolithos, Ophiomorpha*, and *Thalassinoides* along with occasional escape traces of *Conichnus conicus*. Based on ichnofabric analysis, five categories are delineated, namely (a) low bioturbated ichnofabric, (b) structureless sand ichnofabric, (c) bioturbated top ichnofabric, (d) high bioturbated units with glossifunguites ichnofacies surface and (e) amalgamated bioturbated unit ichnofabric. These ichnofabrics occur in cyclic order representing the taphonomic pathways for the genesis of bioturbation cycles in Early Cretaceous wave-dominated deltaic environment of Kachchh Basin.

Keywords Ichnology · Mesozoic · Kachchh basin · Wave-dominated delta · Ichnofabric · Cyclic bioturbation

B. G. Desai (✉) · S. Chauhan
School of Petroleum Technology, Pandit Deendayal Petroleum University, Raisan Village, Gandhinagar 382007, Gujarat, India

S. Chauhan
Department of Earth and Environmental Science, KSKV Kachchh University, Bhuj 370001, Gujarat, India

1   Introduction

Taphonomic processes, an important aspect of the ichnofabric analysis, is responsible for preserving trace fossils in sediments record (Bromley 1990). The resulting ichnofabric summarizes the effect of environmental parameters and taphonomic filters. The diverse ichnofabric developed in the shallow marine environment is a result of numerous governing factors. Similarly, alternative and contrasting hydrodynamics conditions in shallow marine depositional environment yields diverse trace fossil assemblage in a sequence represented by a mixed *Skolithos* and *Cruziana* Ichnofacies. However, such diversity has to pass the primary fossilization barrier before they are preserved in rock records. The ensuing trace fossils, although originally diverse, may preserve fewer traces after it passes through the fossilization barrier. Thus, the taphonomic analysis along with ichnofabric analysis is a helpful method for quantitative estimates of penecontemporaneous sea-floor erosion and stratigraphic incompleteness (Wetzel and Aigner 1986).

In deltaic environments, ichnology helps in distinguishing specific influence of the wave, river or tide and the stress factors applied by them. Among the three classical end-members of the deltaic system, the wave-dominated delta is least stressful, offering fully marine mixed *Skolithos* and *Cruziana* ichnofacies elements (MacEachern et al. 2005; Buatois and Mángano 2011; Desai and Biswas 2018). However, wave-dominated deltaic settings frequently experience repeated storm events interrupting fair-weather conditions. Hence, complex and overprinted ichnofabric are the result of fair-wave conditions alternating with storm events. A systematic analysis of such ichnofabric helps in differentiating paleoenvironmental processes.

The Late Jurassic to Middle Cretaceous sediment of Kachchh basin represents three episodes of deltaic phases, of which the most prominent and well exposed is the Early Cretaceous Bhuj Delta (Desai and Biswas 2018). The purpose of the research is to understand taphonomic pathways for the genesis of bioturbated cycles in a wave-dominated deltaic environment. The Early Cretaceous Ghuneri Member (Bhuj Formation) of the Kachchh basin offers a unique opportunity to discuss the genesis and taphonomic pathways of bioturbated cycles.

2   Geological Setting

The pericratonic rift basin of Kachchh is contiguous to the petroliferous south Indus basin. It evolved during the Late Triassic break-up of Gondwanaland. The rifting occurred on the pre-existing Delhi trend, with the basin forming between Nagar Parkar rift shoulder in north and southern peninsula in the south. The combined offshore-onshore Kachchh basin is approximately 71,000 km^2 in area with Mesozoic basin-fill reaching a maximum thickness in the depocentre. The basin-fill sediments are categorized as syn-rift and post-rift sediments. The post-rift basin fill is dominated
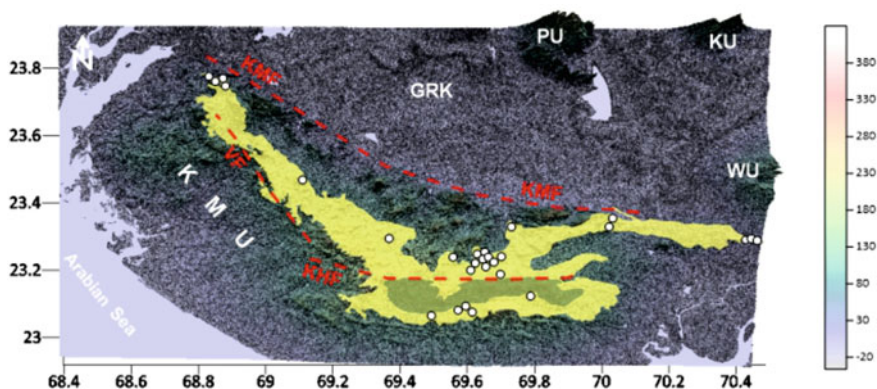
Fig. 1 Generalized digital elevation map of the Kachchh basin, with overlay of Bhuj Formation (Yellow color). Circles represents studied sections of Ghuneri Member. PU = Patcham Uplift, KU = Khadir Uplift, WU = Wagad Uplift, GRK = Great Rann of Kachchh, KMU = Kachchh mainland Uplift, KMF = Kachchh mainland Fault, KHF = Katrol Hill faults

by deltaic sedimentation (Desai and Biswas 2018). The basin has a thick succession of Mesozoic strata (+3000 m; Biswas 1977, 2016), followed by a thin sequence of Tertiary sediments (+900 m; Biswas 1977, 2016). The Mesozoic sediments are exposed in the form of six discontinuous domal areas: (a) Kachchh Mainland, (b) Pachham Island, (c) Khadir Island, (d) Bela Island, (e) Chorar Island and (f) Wagad (Fig. 1). These are major uplifts forming highlands that are separated by vast covered plain. In the Mainland Kachchh, rocks belonging to Bajocian to Albian (Biswas 1977; Table 1) are exposed in the form of two E-W chains of "Domes." Namely (1) the Northern Flexure Zone and (2) the Katrol Hill range. Lithostratigraphically, these comprise of four formations in ascending order, viz. Jhurio, Jumara, Jhuran and Bhuj (Biswas 1977; Table 1). The lithostratigraphy of the Mesozoic sediments is summarized in Table 1.

The Bhuj Formation constitutes of youngest Mesozoic sedimentary formation dominated by the huge thickness of marine to non-marine sandstones. The formation occupies 3/4th of the total Mesozoic outcrops in Kachchh Mainland and extends from Bhachau town in the east to Ghuneri village in the west (Biswas 1977). The formation is divisible into three distinct members, viz. (1) Ghuneri Member, (2) Ukra Member and (3) Upper Member. Lithostratigraphically (Table 1), Bhuj Formation represents the Bhuj deltaic deposit, divisible into three members, of which the lower Ghuneri Member represents the highly bioturbated, wave-dominated deltaic depositional environment. This is followed upward by an Aptian transgression, representing the Ukra Member (Desai 2013, 2016a; Bansal et al. 2017), and topped by a major regressive phase, representing the Upper Member.

The type section of the Ghuneri Member is situated in the western Kachchh, near the Ghuneri Village (Fig. 1). These sediments start from shale and grades up into different sandstones. It is characterized by highly bioturbated ferruginous medium to coarse-grained cross-bedded sandstones alternating with ferruginous micaceous

Table 1 Updated and modified litho-statigraphic classification of the Mesozoic rocks of Kachchh (after Biswas 2016)

Stages	Kutch Mainland Group		Pachchham Island Group		Eastern Kutch Group		
			Member		Formation	Khadir- Bela- Chorar Islands	Wagad Highland
Tertiary	Formation	Member	Goradongar	Kaladongar			
Maastrichtian - Danian	Deccan Trap	Basalt Flows					
Albian	Bhuj Formation	**Upper Member:** massive sandseones					
Aptian		**Ukra Member:** Green glauconitic shale/ferruginous bands with fossil.					
Hauterivian to Barriasian		**Ghuneri Member/ Lower Member:** sandstones/shales/ferruginous bands/Shales with plant fossils.					
	Jhuran Formation	**Katesar Member:** massive sandstones					Recent Deposit
Tithonian		**Upper Member:** fossiliferous sandstones, shales, hard calcareous sandstones				Recent Deposit	
Kimmeridgian		**Middle Member:** mainly shales, fossiliferous, with sandstone interbeds.				WEST------- EAST Gamdau Member	Wagad Sandstone
		Lower Member: sandstones/shales/arena--ceous limestones with fossils				Kanthkote Member.	Wagad Sandstone
	HIATUS					Quaternary to Recent Deposits	Patasar Shale Member
Oxfordian	Jumara Formation						Nara Shale Member
		Dhosa Oolite Member				Bambhanka/ Gangta Bet Member	
Callovian		Gypseous Shale Member	Recent Deposit Miocene Shales Paleocene laterites		Tertiary, Quaternary & Recent		Kharol Member
		Ridge Sandstone Member.				Ratanpur Sandstone Member	
		Shelly Shale Member	Modar Hill Formation	Recent Quaternary	Modar Hill Formation		Not Exposed
	Jhurio Formation	**Member G:** Thin bedd. White L.st. & Nod. L.st.	Raimalro Limestone Member		Goradongar Formation	(Raimalro Lst. Marker) Hadibhadang Sandstone Member	
		Member F: Purple sandstones / Packstones	Gadaputa Sandstone Member				
		Member E: Bedded rusty grainstone with golden oolites	Goradongar Flagstone Member			Hadibhadang Shale Member	Khadir Formation
Aalenian-Bathonian		**Member D:** Gray Shales					
		Member C: Brick red weathering rusty grainstones with golden oolites	Middle Sandstone Member Lower Flagstone Member	(Leptosphinctes pebbly rudstone) Babia Cliff Sandstone Member	Kaladongar Formation	Cheriyabet Conglo-merate Mbr. ? Basement	
		Member B: Gray Shale	Eomiodon Red Sandstone Member	Narewari Wandh Sandstone Member			
		Member A: Thin bedded yellow white limestones, shales and rusty brown limestone with golden oolites.	Sadara Coral Limestone Member	Dingy Hill Member			
		???		?			
		Basement	? Basement	Basement			

Note: columns "Gadhada Formation" and "Washtawa Formation" span the Eastern Kutch Group region, with "Recent Deposit", "Nara Shale Member", "Kharol Member", and "Not Exposed" appearing under the Wagad Highland / Washtawa Formation.

laminated fine-grained sandstone with minor shales. The Ghuneri Sandstones are differentiated from the underlying Jhuran formation (Katesar member) sandstones by the presence of ferruginous hard bands (Biswas 1977) and by highly bioturbated sandstones occurring with low bioturbated sandstone/siltstone in the asymmetrical cyclic order (Desai 2016a) (Fig. 2).

Several trace fossils are reported from the Bhuj Formation. However, the published work lacks stratigraphic details and are generalized for the entire formation. Kumar et al. (1982) listed *Arenicolites, Lockeia, Planolites, Thalassinoides*, and Calianassa Burrows from the Bhuj Formation near Bhuj City. Casshyap et al. (1983) reported three trace fossils, i.e., *Planolites, Skolithos*, and *Thalassinoides*, indicating a littoral marginal marine environment. However, it lacked stratigraphic details. Krishna et al. (1983) reported seven trace fossils that include *Thalassinoides, Skolithos, Chondrites, Ophiomorpha, Rhizocorallium, Aulichinites, Cylindrichnus* from Umia Formation (top part equivalent to Ghuneri Member of Bhuj). Howard and Singh (1985) described *Rhizocorallium, Ophiomorpha Thalassinoides, Skolithos, Chondrites, Gyrochorte, Monocraterion, Teichichnus, Cylindrichnus*, and *Medousichnus* from their shaly horizons. Singh and Shukla (1991) reported highly bioturbated
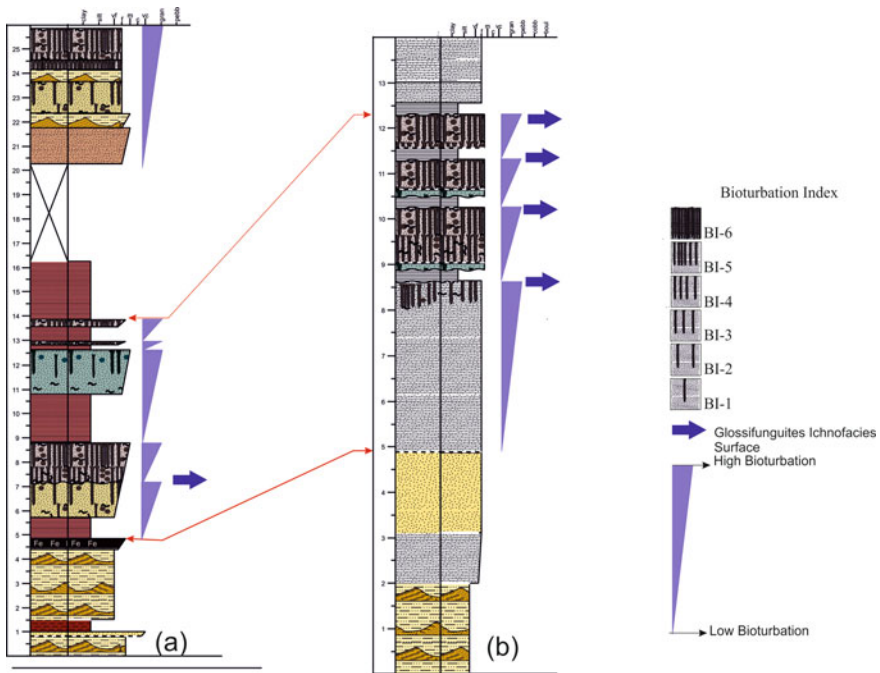
Fig. 2 Representative litholog of the Ghuneri Member showing asymmetrical bioturbational cycles **a** Lower part of the Ghuneri Member near the Katesar Member, the base of the Ghuneri Member is 5 m below the lowest bed. **b** Section showing development of correlatable bioturbational cycle in section exposed in Bhuj City. Note the multiple level development of *Glossifunguites* ichnofacies surface

horizons along with, *Rhizocorallium, Diplocraterion, Thalassinoides*, inclined sand-filled burrows, and sand-filled burrows from Rukhamavati section south of Bhuj. Patel et al. (2008) reported *Asteriacites quinquefolius*, a resting trace of starfish from the lower part of the Bhuj Formation (=Ghuneri Member) from the central Mainland. Recently, two significant trace fossil-rich horizons are reported that includes the occurrence of Ichnogenus *Balanoglossites* Magdefrau 1932 corresponding to *Glossifunguites* Ichnofacies surface (Desai and Saklani 2012). Moreover, a unique equilibrium trace fossils *Conichnus conicus* is also reported from the Ghuneri Member (Desai and Saklani 2015).

3 Methodology

The Ghuneri Member was systematically mapped in both strike and dip direction and logged for their detailed sedimentological and ichnological data along with Stratigraphic correlation in various parts of the Kachchh Basin (Fig. 2). The procedure for mapping and correlation, followed is (a) general reconnaissance of the area, (b) selection of several closely spaced sections (3) delineation of local marker beds and bands, (4) delineation of regional marker bands and (5) regional correlation. Apart from several small and large sections, the type sections and reference sections designated by Biswas (1977) and several other workers were also re-logged for facilitating easy correlation (Fig. 2).

Logging of Ichnological data included (a) ichnotaxa identification, (b) tiering position, (c) cross-cutting relations of the trace fossils and (d) abundance and diversity of the ichnotaxa. Wherever possible serial sectioning was done to understand the tiering of the trace fossils. The ichnological data was collected systematically bed-by-bed and transferred on the stratigraphic column. Ichnofabric analysis on the bioturbated beds from various sections was done following methods suggested by Ekdale and Bromley (1983), Miller and Smail (1997) and Taylor et al. (2003).

4 Results

Twenty-four recurring trace fossils are identified from twenty-eight sections of the Ghuneri Member exposed in the Basin; recurring trace fossils are listed in Table 2. Systematic analysis of these trace fossils, their tier positions and feeding strategies along with their classification in r-selective or K-Selective trace makers are summarized in Table 2.

Table 2 List of recurring trace fossils occurring in the Ghuneri Member along with their averaged tier position, feeding strategy of trace makers, their abundance in the Ghuneri Member and their opportunistic (r-selective or K selective strategy)

Sr. No.	Trace fossil	Figure No.	Tier position	Feeding	Abundance	r-Selective or K-Selective
1	*Arenicolites variabilis* Fursich, 1974	Figure 3a	Middle	Suspension feeding	Abundance	r-Selective
2	*Balanoglossites triadicus* Mägdefrau, 1932	Figure 3b	Shallow	Suspension feeding	Common	K-Selective
3	*Balanoglossites ramosus* Knaust, 2008	–	Shallow	Suspension feeding	Common	K-Selective
4	*Chondrites intricatus* Brongniart, 1823	Figure 3c	Deep	Mixed suspension feeding and chemosymboisis	Common	K-Selective
5	*Conichnus conicus* (Männil 1966)	Figure 3f	Shallow	Filter feeding	Common	r-Selective
6	*Diplocraterion bicalvatum* Miller, 1875	Figure 3d-i	Middle	Suspension feeding	Abundance	r-Selective
7	*Diplocraterion Parallelum* Torell, 1870	Figure 3d-ii	Middle	Suspension feeding	Abundance	r-Selective
8	*Gyrochorte comosa* Heer, 1865	Figure 3e	Shallow	Deposit feeding	Abundance	r-Selective
9	*Gyrolithes isp* Saporta, 1884	Figure 3j	Middle	Deposit feeding	Common	r-Selective
10	*Lockeia siliquaria* James, 1879	Figure 3g	Shallow	Deposit feeding	Rare	K-Selective
11	*Monocraterion tentaculatum* Torell, 1870	Figure 3h	Middle	Suspension feeding	Rare	K-Selective
12	*Ophiomorpha nodosa* Lundgren, 1891	Figure 3i	Deep	Suspension feeding	Abundance	r-Selective
13	*Palaeophycus tubularis* Hall, 1847	Figure 4a	Middle	Suspension feeding	Abundance	r-Selective
14	*Planolites beverleyensis* Billings, 1862	Figure 4b	Shallow	Deposit feeding	Common	r-Selective
15	*Polykladichnus irregularis* Fursich, 1981	Figure 4c	Middle	Suspension feeding	Abundance	K-Selective

Table 2 (continued)

Sr. No.	Trace fossil	Figure No.	Tier position	Feeding	Abundance	r-Selective or K-Selective
16	*Psilonichnus tubiformis* (Fursich 1981)	Figure 4d	Deep	Deposit feeding	Abundance	r-Selective
17	*Rhizocorallium jenense* Zenker, 1836	Figure 4e	Middle	Suspension feeding	Common	K-Selective
18	*Rossellia rotatus* MacCarthy, 1979	Figure 4f	Middle	Detritus feeding	Common	K-Selective
19	*Skolithos linearis* Haldeman, 1840	Figure 4g	Deep	Suspension feeding	Abundance	r-Selective
20	*Skolithos verticalis* Hall, 1943	Figure 4g	Deep	Suspension feeding	Abundance	r-Selective
21	*Taenidium serpentinum* Brady, 1947	Figure 4h	Middle	Detritus feeding	Common	K-Selective
22	*Teichichnus rectus* Seilacher, 1955	Figure 4i	Middle	Deposit feeding	Rare	r-Selective
23	*Thalassinoides suevica* Rieth, 1932	Figure 4j	Deep	Mixed deposit and suspension feeding	Abundance	r-Selective
24	*Thalassinoides paradoxica* Woodward, 1830	–	Deep	Mixed deposit and suspension feeding	Abundance	r-Selective

4.1 Tiering and Key Bioturbators

Balanoglossites, *Conichnus*, *Gyrochorte*, *Lockeia* and *Planolites* characterize shallow tier suites in Ghuneri Member. Among these, Ichnogenus *Balanoglossites* forms a complex, unlined burrow system (Knaust 2008). Although, it commonly occurs in carbonates of Ordovician and onwards. However, it also occurs in clastic firmground substrate in Cretaceous of Bhuj Formation (Desai and Saklani 2012) and modern fine-grained sands from Intertidal lagoon of Mandvi Area, Kachchh (Patel and Desai 2009). Ichnospecies of *Balanoglossites* occurs as a part of the *Glossifunguites* Ichnofacies surfaces common in the lower part of the Ghuneri Member (Desai and Saklani 2012). Similarly, *Conichnus* is an equilibrium trace fossil that maintains equilibrium with the aggrading sediment surface (Desai and Saklani 2015). In Ghuneri Member *Conichnus* occurs as an isolated occurrence in poorly bioturbated sandstones, except in one section where it occurs as a community of thirteen adult specimens. Thus, the opportunistic (r-selective) deposit-feeding trace makers (*Gyrochorte*, *Lockeia* and *Planolites)* dominates the shallow tier suites. The Middle tier is composed of *Arenicolites, Diplocraterion, Monocraterion, Palaeophycus, Polykladichnus, Rhizocorallium, Rosselia, Taenidium* and *Teichichnus.* The Middle tier trace fossils are mixed opportunistic and climax community examples forming

mixed suspension, detritus feeding trace makers. While, the Deep tier is composed of Opportunistic suspension-feeding trace makers of *Chondrites, Ophiomorpha, Skolithos, Thalassinoides along with deposit feeding Psilonichnus.* The Ghuneri Member tiering analysis indicates that the middle tier is most diverse, followed by deep tier and shallow tier is the least diverse, though, their diversity does not vary significantly.

Our analysis of shallow tier in Ghuneri Member indicates (a) timing, lateral extend and availability of colonization window, (b) substrate conditions, and (c) intra-specific competition as key controlling factors.

Key bioturbators in the shallow tier are highly mobile, active and prey-seeking organisms that produce abundant structures (Bromley 1996), the preservation of shallow tier trace fossils is primarily dependent on the availability of suitable substrate. In case deltaic or wave-dominated shoreface environments, the colonization in shifting sands during high-energy periods is not possible. The organisms, colonize same substrate during less energetic periods, this is known as Colonization window (Pollard et al. 1993; Bromley 1996). In addition to the availability of colonization window, rate of sediment reworking by individual organism also influences, for example, *Donal variabilis* reworks sediment in a few hours (Thayers 1983). Thus, preservation of tiers depends on availability of colonization window and rate of sediment reworking in that window. Higher rate of sediments will tend to destroy earlier formed tiers. Thus, depleted shallow tier trace fossils diversity in Ghuneri Member reflects limitation on either colonization window or erosion of the shallow tier. In the lower part of Ghuneri Member, the preservation of *Glossifunguites* Ichnofacies surface in Ghuneri Dome (Desai and Saklani 2012) supports the erosion of the substrate followed by substrate consistency change. In the younger stratigraphic section of Ghuneri member exposed in western and central part of the Kachchh Basin, the limited occurrence of colonization window controls the resulting tiering profile (Fig. 2).

Based on the trace fossils and their interpreted trace makers, polychaetes worms are considered as key bioturbators for the middle tier in the Ghuneri Member. Such trace makers are initially immobile, but when faced with competition, may shift to mobile mode. Thus, the middle tier offers diverse examples of trace maker's adaptability, for example, with small-scale aggradation of sediments, the *Diplocraterion* changes its burrow position forming protrusive speriten. In shallow marine polychaetes community, amensalism also plays an important role in structuring the benthic trace maker community (Levinton 1977; Bromley 1996). Thus, the intraspecific competition among the key bioturbators seriously affects the middle tier trace maker community. In Present study, suspension-feeding trace makers dominate the middle tier, except for events bed of *Gyrolithes* and *Taenidium,* occurring in in central part of basin (Bhuj city). These points towards the intra-specific competition like amensalism as responsible for excluding deposit-feeders from the middle tier. Dominance of suspension feeding catches the settling organic matter/nutrient. This causes overexploitation of nutrients by deposit feeders, leading to depletion of nutrient in sediments. This forces the deposit feeders to abandoned the area because of presence of suspension feeders. In Similar example Woodin (1977) describes the

burrowing suspension-feeding polychaetes inhibited the growth of deposit-feeding organism and excluded them.

The deep tier community in Ghuneri Member is dominated by large bioturbators capable of creating three-dimensional burrow systems (e.g. *Ophiomorpha, Thalassinoides*). These are opportunistic and mobile bioturbators quickly adapting to the changing environmental conditions by modifying their burrows systems. Desai (2016b) provides a classic example of such burrow modification because of environmental factors from Pleistocene age sequences of 'Shankhodhar Sand Clay Member' of Dwarka Formation, in Gulf of Kachchh. In Dwarka Formation, trace makers of *Ophiomorpha* burrows modified their burrows for storing the food, for brooding and for escaping the predators and the external environmental factors like high-energy, salinity change rarely affected the trace makers.

4.2   Bioturbated Cycles

Wave-dominated shallow marine environment experiences alternating and contrasting hydrodynamic energies, frequently because of storms. Degree of bioturbation in sedimentary sequence especially in deltaic environment is dependent on other associated factors including density of organisms, the temperature of water, presence or absence of Keystone species, type of activity and tiering (Bromley 1996). In the case of total bioturbation in sediments, it is assumed that the rate of bioturbation exceeds the rate of sediment action. However, the rate of bioturbation in-turn depends on the type and sediment reworking speed of trace makers (Thayers 1983). Nevertheless, incomplete bioturbation implies stress factors involving changes in sedimentation rate, oxygen variation, salinity variation, colonization widow availability (Bromley 1996; Buatois and Mángano 2011). Such environmental variations are common in the deltaic environment, and results in incomplete bioturbation (e.g. ichnofabric of Jhuran Delta, see Desai and Biswas 2018). Wave-dominated delta is considered to be the least stressful of all deltas and consist of impoverished *Skolithos* ichnofacies (Buatois and Mángano 2011). The predominant stress factor is the frequency of the storms. Lateral mapping of the bioturbated sequences and ichnofabric analysis across the Kachchh basin reveals two distinct trace fossil suites, namely (a) fair-weather ichnoassemblage and (b) storm-weather ichnoassemblage (Figs. 3 and 4).

Fair-weather Ichnoassemblage: The Fair-weather ichnoassemblage is composed of mixed suspension and deposit-feeding ichnoassemblages characteristic of low energy conditions, especially components of *Cruziana* ichnofacies. In case of the Ghuneri Member, Shallow tier *Gyrochorte, Lockeia*, dominates the Fair-weather ichnoassemblage and *Planolites*, Middle tier *Palaeophycus, Polykladichnus*, *Rhizocorallium*, *Rosselia*, *Taenidium*. The fair-weather suites of the deep tier are dominated by *Chondrites*.

Storm-weather ichnoassemblage: The Storm-weather ichnoassemblage consist of trace makers characteristics of high-energy conditions and includes middle
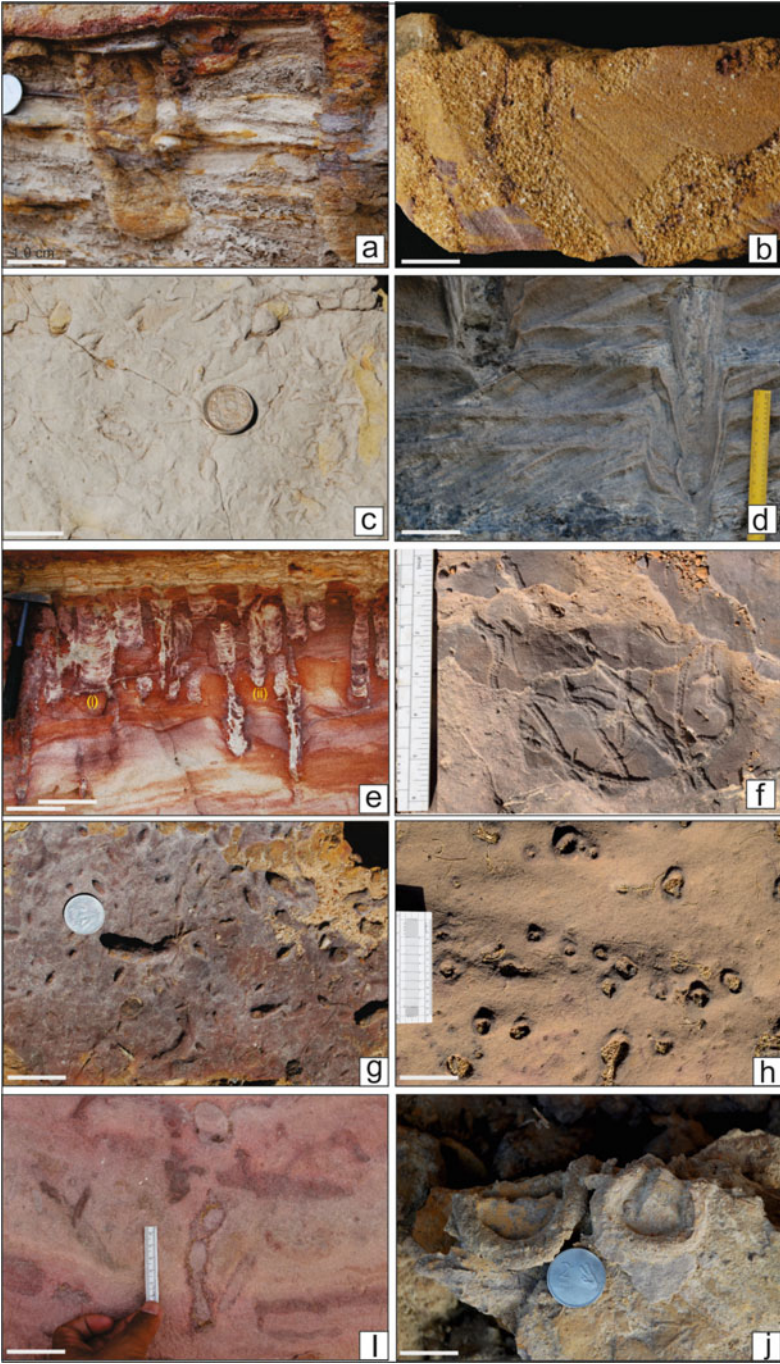
◄**Fig. 3** Trace fossils within the Ghuneri Member of Bhuj Formation, Kachchh Basin (Scale indicates 2 cm) **a** *Arenicolites variabilis* from the upper part of the Ghuneri Member, Ghuneri Dome, **b** *Balanoglossites* showing unlined burrows filled with coarse-grained sediments, **c** Plan view of the *Chondrites* occurring as dendritic burrows in the fine-grained siltstones, Ghuneri Dome **d** *Diplocraterion bicalvatum* (i) and *Diplocraterion parallelum* (ii) formed from top of the colonization surface, note the lower part of the sediments are non-bioturbated. **e** *Gyrochorte comosa* from the siltstone of middle Ghuneri Member **f** *Conichnus conicus* in medium to coarse-grained sandstone **g** *Laevicyclus* developed at the base of the fine-grained sandstone, suggesting cast of the lower substrate. **h** Bedding plane view of the lined *Monocraterion* in the medium-grained sandstone **i** Cross sectional view of the *Ophiomorpha* burrows in the fine-grained sandstones **j** Plan view of the trace fossil *Gyrolithes* burrows formed in event beds of the Ghuneri Member

to deep tier *Arenicolites, Diplocraterion, Psilonichnus Skolithos, Ophiomorpha*, and *Thalassinoides* along with occasional occurrence of escape and equilibrium *Conichnus conicus.* The trace makers are highly mobile, opportunistic elements of Skolithos ichnofacies. Shallow tier is nearly absent in the storm-weather ichnoassemblage.

In Kachchh basin, several asymmetrical bioturbated cycles are common in the Ghuneri Member (Fig. 2), each of the cycle is composed of a complete transition from zero bioturbation to incomplete bioturbation to total bioturbation units (Desai 2016a). These cycles are well exposed and laterally consistent from the west of Ghuneri Dome to Kas Hills in the east.

5   Taphonomic Pathways in the Formation of Bioturbated Cycles

Six Taphonomic pathways are delineated each with the unique identity of the genesis of the process. These are (a) type-1—low bioturbated ichnofabric, (b) type-2—ichnofabric of structureless sand, (c) type-3—incomplete bioturbated top ichnofabric; (d) type-4—bioturbated units with *Glossifunguite*s ichnofabric, (e) type-5—firmground bypass ichnofabric; (f) type-6—amalgamated bioturbated unit with resumed colonization (Figs. 3, 4, 5, 6, 7, 8, 9 and 10).

5.1   Type-1 Low Bioturbated Ichnofabric

Lined burrows in structureless medium-grained sandstones comprising of post-storm opportunistic colonization overprinting low bioturbated fair-weather ichnoassemblage characterize this type of ichnofabric (Fig. 5). Typical trace fossils found well preserved are fair-weather *Polykladichnus irregularis,* along with thickly lined *Skolithos linearis* (Fig. 4g). The bioturbation index across the cross-section of sedimentary bed is (BI-1 or 2), while the bedding-plane bioturbation index is BPBI of 2

Fig. 4 Trace fossils within the Ghuneri Member of Bhuj Formation **a** *Paleophycus tubularis* in the ferruginous sandstone, **b** *Planolites beverleyensis* developed as shallow tier, preserved as Hypichnial burrows. **c** Well developed *Polykladichnus irregularis* unit sandwiched between coarse-grained non-bioturbated sandstones, suggesting availability of the colonization surface **d** *Psilonichnus tubiformis* showing typical Y shaped burrows filled with different material, South of Bhuj. **e** *Rhizocorallium jenense* formed in the fine to medium-grained sandstone, **f** bedding plane view showing extensive development of the *Rosselia rotatus*, note the concentric laminations **g** Crowded development of *Skolithos* in the medium-grained sandstones **h** oblique sectional view of *Taenidium serpentinium* showing well developed speriten structures **i** *Teichichnus rectus* showing burrow and speriten at the base of the burrow **j** well developed horizontal network of the *Thalassinoides* in the coarse-grained sandstones (coin diameter ~2.3 cm, pen length = 14 cm)
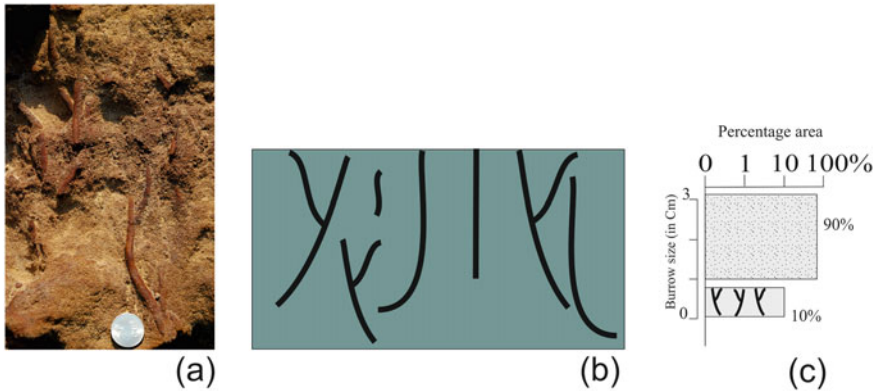
Fig. 5 Type-1 ichnofabric showing low bioturbated (BI-1) units containing fair-weather *Polykladichnus*. **a** Field photograph showing mud lined Polykladichnus (coin = 2.4 cm); **b** representative tier diagram; **c** ichnofabric constituent diagram
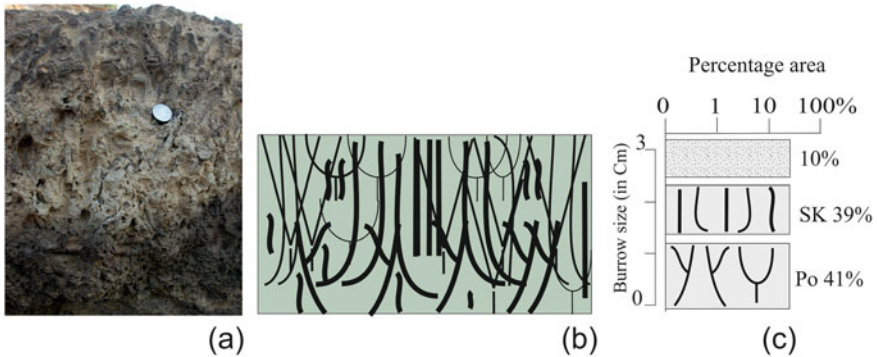
Fig. 6 Highly bioturbated type-2 ichnofabric showing bioturbated (BI-5) units. **a** Field photograph showing highly bioturbated medium-grained sandstones (coin = 2.4 cm); **b** representative tier diagram **c** ichnofabric constituent diagram

(i.e. 0–10%), comprises of even distribution of different shape traces. The ichnofabric is represented by simple tiering style made by shaft producers. The tiering profile comprises of deep tier characterized by the permanent dwelling, suspension and filter-feeding organisms. Crowded populations of vertical burrows are often attributed to the work of opportunistic organism (Vossler and Pemberton 1988). However, the present ichnofabric represents low Bioturbation of the burrow, indicating, depositional condition and colonization substrate were of shifting nature and might be experiencing adverse conditions, forcing the organism to line the burrow thickly. The ichnofabric is interpreted to represent high-energy condition with a higher rate of sedimentation.
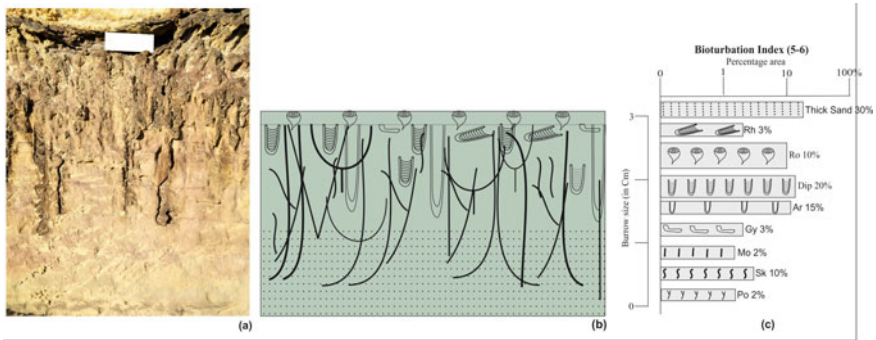
Fig. 7 Ichnofabric representative of incomplete bioturbation (type-3), bioturbation restricted only in the top part of the sedimentary units. **a** Field photograph showing highly bioturbated medium-grained sandstone; **b** representative tier diagram showing tier position **c** ichnofabric constituent diagram showing sequence of colonization
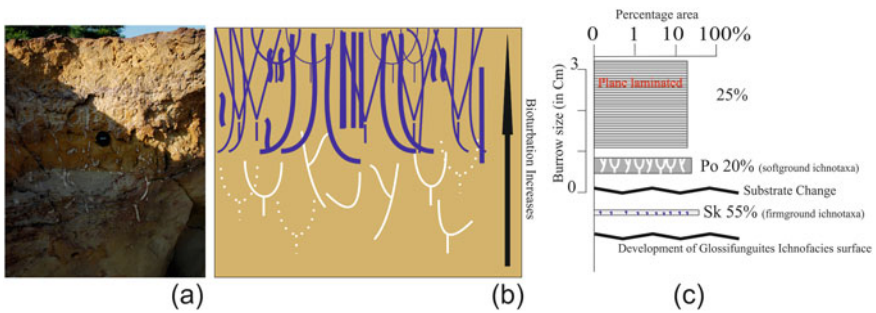
Fig. 8 Bioturbated units associated with *Glossifunguites* ichnofacies surface (type-4) showing substrate change from softground to firmground and increase of bioturbation towards top of the unit; **a** field photograph showing white contrasting burrow fill in unlined burrow indicative of firmground; **b** representative tier diagram showing changes in substrate and increase in bioturbation; **c** ichnofabric constituent diagram showing sequence of events
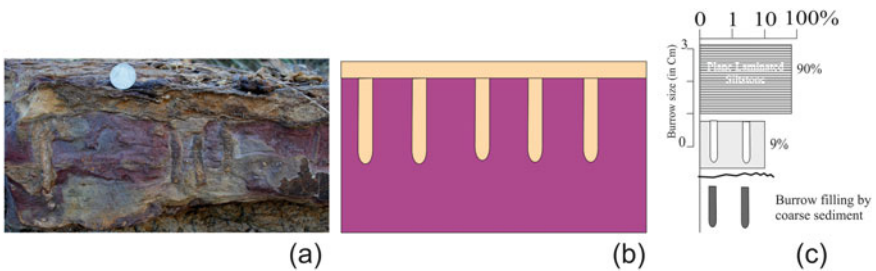
Fig. 9 Firmground bypass ichnofabric showing development of *Skolithos linearis*; **a** field photograph (coin diameter = 2.4 cm); **b** representative tier diagram; **c** ichnofabric constituent diagram
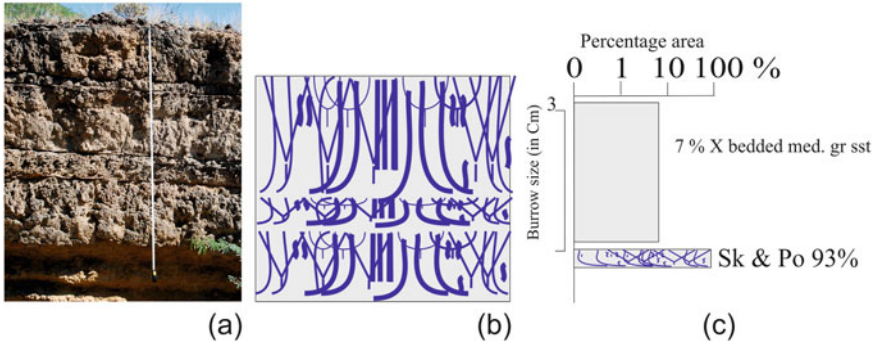
Fig. 10 Amalgamated highly bioturbated (BI-6) unit showing development of overcrowded *Skolithos* burrows; **a** field photograph; **b** representative tier diagram; **c** ichnofabric constituent diagram

5.2 Type-2 Ichnofabric of Structureless Sand

Highly bioturbated medium-grained sandstones characterize this type of ichnofabric. Typical trace fossils found in type-2 ichnofabric are storm-weather suites of *Arenicolites variabilis, Skolithos linearis, Ophiomorpha nodosa* and *Thalassinoides paradoxicus* overprinting fair-weather *Rosellia rotatus*, *polykladichnus irregularis,* and *Rhizocorallium jenese*. The bioturbation index of the ichnofabric is (BI-5), and the bedding plane bioturbation index comprises of BPBI of 4 (i.e. 40–60%) (Fig. 6). The ichnofabric is represented by multiple colonization with simple tier. The tiering profile of the ichnofabric consists of (1) medium-tier characterized by a permanent dwelling, filter-feeding organism. (2) Deep tier dwelling burrows of suspension-feeding. In storm-dominated deltas, well-developed fair-weather suites get over-printed by deeper tier storm-weather suites. Such conditions are result of post-storm colonization under favourable condition including little erosion. Erosion played an important role for the formation of type-2 ichnofabric, as the middle tier fair weather trace fossils were still well preserved and are overprinted by storm-weather suites, a typical indicator of short-term colonization window.

5.3 Type-3 Incomplete Bioturbated Top Ichnofabric

This type of ichnofabric is characterized by a high degree of bioturbation preserved only in the top part of the thick-bedded sandstone units (Fig. 7). Typical trace fossils include *Arenicolites variabilis*; *Diplocraterion bicalvatum, Diplocraterion parallelum*, *Gyrochorte comosa, Monocraterion tentaculatum, Skolithos linearis; Polykladichnus irregularis* and *Rhizocorallium jenense*. Thinly bedded units are colonized by *Rosselia rotates*. The main character of this ichnofabric is that the degree of the

Bioturbation increases towards the bed top and reaches bioturbation index of (BI 5–6). The average depth of bioturbation is about 70 cm. The bedding plane bioturbation index of the top of the bed comprises of even distribution of different shape traces with BPBI of 4 (i.e. 40–60%). The ichnofabric is represented by multiple colonization with simple tier. Such type of ichnofabric results from long term availability of colonization window for r-selected trace makers and its preservation is secured by renewed storm) deposits (Buatois and Mángano 2011; Fig. 71, p. 127).

5.4　Type-4 Bioturbated Units with Glossifunguites Ichnofabric

The ichnofabric consists of softground and firmground ichnology separated by a *Glossifunguites* Ichnofacies surface (Fig. 8). In the central part of the Basin (Bhuj area), five bioturbated cycles end with *Glossifunguites* ichnofacies surfaces (GIS). However, such cycles are also common across the basin, but in varying number (Fig. 2). The characteristics of GIS vary laterally but can be summarized as (a) formation of erosional or omission surface, (b) different trace fossils across the surface, (c) presence of firmground trace fossils and omission surface suites (Fig. 8) and (d) presence of thick ferruginous layer. In some sections, the erosional surface is pronounced, and the erosional undulations are up to 20 cm thick. In pre-Omission surface suites, *Polykaldichnus* and *Gyrolithes isp* are common. Other example includes occurrences of *Balanoglossites triadicus; B. ramosus,* in association with tear-shaped *Gastrochaeonolites* boring (Desai and Saklani 2012). The tiering profile of the ichnofabric consists of (1) shallow tier characterized by a permanent dwelling, suspension-feeding organism overprinted by (2) Shallow tier dwelling burrows of filter-feeding (Fig. 8). The top part of the bioturbated unit represents *Glossifunguites* ichnofacies surface ichnofabric is characterized by (1) simple colonization with tier replacement, (2) moderate bioturbation (BI = 4) and (3) Low ichnotaxa diversity. Such types of contrasting trace fossils association, characterized by omission and post-omission trace fossil suite along with sharp walled, unlined burrows, passively filled with contrasting sediments than host rock are characteristic features of *Glossifunguites* ichnofacies (MacEachern et al. 1992). Thus, the ichnofabric records replacement of firmground, opportunistic, trace fossil (*Balanoglossites*) belonging to omission suite by hardground trace fossils (*Gastrochaenolites* borings) of the post-omission suite. The type of emplacement of the trace fossil suggests that there was a significant change in substrate condition, with background trace fossils comprised of *Polykladichnus irregularis,* with rare *Arenicolites* and *Rhizocorallium* in softground substrate. This softground trace represented pre-omission suite overprinted by dense crowding of S*kolithos linearis.* These were seen to be crosscutting pre-omission suites. The emplacement of *Skolithos* represents a change of substrate to firmground condition representing omission suite traces. This omission suite is followed later by erosion of the top layer and ferruginization. Such types of ichnofabric are typical

of the shifting substrate with frequent exposure, similar to intertidal zone environment. Similar pre-omission and omission suites were also reported from the recent intertidal zone of Mandvi, Gulf of Kachchh (Desai and Patel 2008; Patel and Desai 2009).

5.5   Type-5 Firmground Bypass Ichnofabric

This type of ichnofabric is characterized by thickly lined burrows in fine-grained siltstones (Fig. 9). In this ichnofabric, only *Skolithos linearis* is documented. The bioturbation index of the ichnofabric is (BI-1), and the bedding plane bioturbation index comprises of even distribution of different shape traces with BPBI of 2 (i.e. 0–10%). The ichnofabric is represented by simple colonization. The traces are passively filled with coarse-grained sediments.

In contrast, the coarse-grained unit shows sediments with cryptic laminations with erosional base and flute marks. The unit top contains thinly ripple-laminated units. The ichnofabric occurs in the distal part of the Basin. This ichnofabric is interpreted to be representing a "firmground bypass" where the strata surface does not show any overall environmental shift. The burrows seem to have formed in firmground substrate of subtidal environment, probably below normal wave base; this was later filled by sediments deposited on account of storm action.

5.6   Type-6 Amalgamated Bioturbated Unit with Resumed Colonization

This ichnofabric is similar to the type-2. However, it differs in having multiple stacked highly bioturbated units (BI-6) units (Fig. 10). The bioturbation occurs in multiple stacked units in which thin (5 cm) and thick (80 cm) alternates and have a sharp erosional base. The grain sizes of these units are moderately sorted, medium to coarse-grained units. The bioturbation is restricted to the bedform only and does not extend into the underlying units. The ichnofabric is characterized by dense overcrowding of the *Skolithos* burrows (Fig. 9a). It indicates low energy condition necessary for colonization of suspension feeders. The nature of the bedform restricted bioturbation indicates that the sedimentation was probably cyclic with periods of sedimentation followed by colonization period with low energy conditions. This ichnofabric was commonly observed in the proximal part of the Basin.

6 Discussion and Conclusions

Ichnology of the shallow marine environment in deltaic systems is governed by several factors, including the availability of colonization window, presence of opportunistic organisms and preservation potential of the substrate during high-energy regimes (Pemberton et al. 1992). The resulting ichnofabric preserves a limited snapshot of the processes after passing through the fossilization barrier. Thus, the taphonomic process has strong control over the ichnofauna colonizing high-energy regime (Buatois and Mángano 2011).

In Ichnological analysis of the deltaic system, colonization window and changes in substrate conditions governs the resulting fully or partially bioturbated the substrate. Seasonal fluctuation governing the delta lobe allows months' time for the colonization window giving rise to total bioturbation (bioturbation index of 3–5). Moreover, during storms events or high sedimentation and high-energy regimes, colonization window timing is short, leading to partial bioturbation. Thus, ichnofabric analysis of Ghuneri Member offers insight into the taphonomic process involved in the formation of cyclic bioturbated units.

Six types of bioturbated units are identified namely (a) Type-1 Low bioturbated ichnofabric; (b) Type-2 Ichnofabric of structureless sand; (b) Type-3 incomplete bioturbated top ichnofabric; (c) Type-4 Bioturbated units with *Glossifunguites* ichnofabric; (d) Type-5 Firmground bypass ichnofabric; (e) Type-6 Amalgamated bioturbated unit with resumed colonization. Studies show storms frequently defaunate and erode the substrate, opportunistic organisms can recolonize such substrate (Frey and Goldring 1992; Pemberton et al. 1992). Additionally, completely bioturbated units dominated by opportunistic trace fossils like *Skolithos* suggest a flourishing and recolonizing community. Thus, as a result, re-colonization also produces highly bioturbated units.

In the present case, an ideal bioturbation cycle starts with low bioturbation units represented by Type-1 ichnofabric. Low bioturbated units imply that despite high-energy regime stress and limited timing of colonization window opportunistic organisms were able to colonize the substrate; however, they could not flourish. Similar environments are also common in Type-3 ichnofabric where the bulk of the sediment thickness is poorly bioturbated, and the top is highly bioturbated. For example, in the study area (e.g. Ghuneri Dome, Kodki George, and Bhuj Sections) the top 20–25 cm of the thick non-bioturbated units (~ 3–4 m) are colonized by *Diplocraterion* colony, the maximum depth of *Diplocraterion* reaching maximum up to 25 cm. Such colonization indicates rapid deposition with frozen colonization window surface (Figs. 3d and 4c). Howard (1978) suggested that during rapid deposition, organism have little time for sediment reworking and have to be in equilibrium with the aggrading substrate. Thus, the organism reworks and bioturbated only the top of the beds. In wave-dominated settings, preservation of such surfaces also indicates absence or negligible rate of erosion, helping in the preservation of depositional surfaces. High bioturbation ichnofabric like Type-2 are prefect examples of slow deposition, especially in cases where the rate of bioturbation exceeds the rate of sedimentation,

causing total bioturbation (Bromley 1990). Such ichnofabric in a storm affected wave environment suggest either the ichnofabric was generated during inter-storm periods or complete reworking of storm beds with increased tiering depths of storm trace fossil suites completely overprinting the fair-weather suites. Such conditions are only possible in case of very long-term opening of the colonization window with suitable substrate conditions. In high-energy regimes, prospering opportunistic organisms will produce dense or highly bioturbated Skolithos ichnofabric (Pemberton et al. 1992).

In a deltaic environment, shifting of lobes, abandonment or changes in the sedimentation rate produces substrate change usually from softground substrate to firmground substrate. This change to firmground causes changes in the infaunal community. In the present case of Ghuneri Member, several levels of Glossifunguites ichnofacies surface are delineated (e.g. Type-4, and Type-5), of which the type-4 is a classic example of the Glossifunguites ichnofacies surface across which firmground and hardground ichnofauna are developed. At Ghuneri Dome, two levels of Firmground *Balanoglossites* are well developed (Desai and Saklani 2012). Lateral mapping suggested the same stratigraphic unit shows well-developed *Glossifunguites* ichnofacies surfaces. It can be correlated from Ghuneri Dome (west) to Bhuj City Area (Central) and up to Kas Hill/ Jhawarnagar section (east) of the Basin. Type-4 is most common, and the Glossifunguites ichnofacies surface is also associated with moderate erosion. Type-5 is locally and patchily developed and indicative of firmground-bypassed sediments; however, in this case, the erosion is not prominent. Type-6 shows Amalgamation of the high bioturbated horizons (BI-5–6) where the sediments are bioturbated. Complete reworking of the sediments indicates the existence of the timing and extent of the colonization window remained opened for very long term. The trace making community was keeping pace with the combined effect of the depositional and erosional process. In this case, the fair-weather suit will get completely overprinted by storm-weather suites and the opportunistic trace makers will recolonize the substrate. Amalgamated bioturbated units also indicate a flourishing and thriving community of opportunistic organism that have adopted in high-energy stressed environment.

Thus, in the Ghuneri Member, cyclic development of the bioturbated horizons indicates the fluctuating effect of storms, erosion, and a higher rate of sedimentation and availability of colonization window.

(a)   The wave-dominated deltaic system of Ghuneri Member is represented by twenty-four recurring ichnospecies forming two distinct trace fossil suites namely (a) fair-weather suite and (b) storm-weather suite.
(b)   Fair-weather suites are represented by climax community of essentially K-selective species having mixed feeding strategy.
(c)   An opportunistic community of r-selective species having suspension-feeding mode represents storm-weather suites.
(d)   The Ghuneri Member is represented by asymmetrical bioturbated cycles; an ideal cycle ranges from low bioturbation units to high bioturbation units, and are commonly associated with Glossifunguites ichnofacies surface.

References

Bansal U, Banerjee S, Pande K, Arora A, Meena SS (2017) The distinctive compositional evolution of glauconite in the Cretaceous Ukra Hill Member (Kutch basin, India) and its implications. Mar Petrol Geol 82:97–117

Biswas SK (1977) Mesozoic rock-stratigraphy of Kutch, Gujarat. Quart J Geol Min Met Soc India 49:1–51

Biswas SK (2016) Mesozoic and tertiary stratigraphy of Kutch (Kachchh)—a review. In: Thakkar MG (ed) Recent studies on the geology of Kachchh. Spec Publ Geol Soc India 6:1–24

Bromley RG (1990) Trace fossils-biology. Taphonomy, London, Unwin Hyman

Bromley RG (1996) Trace fossils-biology, taphonomy and applications, 2nd edn. Chapman & Hall, London

Buatois LA, Mángano MG (2011) Ichnology: organism-substrate interactions in space and time. Cambridge University Press, Cambridge

Casshyap SM, Dev P, Tewari RC, Raghuvanshi AKS (1983) Ichnofossils from Bhuj formation (Cretaceous) as paleoenvironmental parameters. Curr Sci 52:73–74

Desai BG (2013) Ichnological analysis of transgressive marine tongue in prograding deltaic system: evidences from Ukra Hill Member, Western Kachchh, India. J Geol Soc India 82:143–152

Desai BG (2016a) Ichnological events associated with evolution of Kachchh Rift Basin, Western India. In: Thakkar MG (ed) Recent studies on the geology of Kachchh. Spec Publ Geol Soc India 6:114–128

Desai BG (2016b) Ichnological analysis of the Pleistocene Dwarka Formation, Gulf of Kachchh: tracemaker behaviors and reworked traces. Geodin Acta 28:21–36

Desai BG, Biswas SK (2018) Post rift deltaic sedimentation in western Kachchh basin: insights from ichnology and sedimentology. Palaeo Palaeo Palaeo 504:104–124

Desai BG, Patel SJ (2008) Trace fossil assemblages (Ichnocoenoses) of the tectonically uplifted Holocene shorelines, Kachchh, Western India. J Geol Soc India 71:527–540

Desai BG, Saklani RD (2012) Significance of the trace fossil Balanoglossites Mägdefrau 1932 from the Lower Cretaceous Ghuneri member (Bhuj formation) of the Ghuneri dome, Kachchh, India. Swiss J Palaeontol 131:255–263

Desai BG, Saklani RD (2015) Palaeocommunity dynamics and behavioral analysis of Conichnus: Bhuj Formation (Lower Cretaceous), Kachchh-India. Ichnos 22:43–55

Ekdale AA, Bromley RG (1983) Trace fossils and ichnofabric in the Kjølby Gaard Marl, uppermost Cretaceous, Denmark. Bull Geol Soc Denmark 31:107–119

Frey RW, Goldring RG (1992) Marine event beds and recolonization surfaces as revealed by trace fossil analysis. Geol Mag 129:325–335

Howard JD (1978) Sedimentology and trace fossils. In: Basan P (ed) Trace fossil concepts. SEPM Short Course 5:13–47

Howard JD, Singh IB (1985) Trace fossils in the Mesozoic sediments of Kachchh Western India. Palaeo Palaeo Palaeo 52:99–122

Knaust D (2008) Balanoglossites Mägderfrau 1932 from the Middle Triassic of Germany: part of a complex trace fossil probably produced by burrowing and boring polychaetes. Paläontologische Zeitschrift 82:347–372

Krishna J, Singh IB, Howard JD, Jafar SA (1983) Implications of new data on Mesozoic rocks of Kachchh, western India. Nature 305:790–792

Kumar A, Bartarya SK, Bisht K (1982) Distribution of trace fossils in the Mesozoic rocks of Kutch, India. Neues Jahrbuch für Geologie Palaontologie Montashefte 1:36–40

Levinton JS (1977) Ecology of shallow water deposit-feeding communities, Quisset Harbor, Massachusetts. In: Coull BC (ed) Ecology of marine benthos. University of South Carolina Press, Columbia, pp 191–227

MacEachern JA, Raychaudhuri I, Pemberton SG (1992) Stratigraphic applications of the Glossifunguites Ichnofacies: delineating discontinuities in the rock record. SEPM Core Workshop 17:169–198

MacEachern JA, Bann KL, Bhattacharya JP, Howell CD (2005) Ichnology of deltas: organism responses to the dynamic interplay of rivers, waves, storms and tides. In: Bhattacharya JP, Giosan L (eds) River deltas: concepts, models and examples. SEPM Spec Publ 83:49–85

Miller MF, Smail SE (1997) A semiquantitative field method for evaluating bioturbation on bedding planes. Palaios 12:391–396

Patel SJ, Desai BG (2009) Animal-sediment relationship of the crustaceans and polychaetes in the intertidal zone around Mandvi, Gulf of Kachchh, Western India. J Geol Soc India 74:233–259

Patel SJ, Bhatt NY, Desai BG (2008) *Asteriacites quinquefolius*-asteroid trace maker from the Bhuj formation (Lower Cretaceous) of the Mainland Kachchh. Western India. J Geol Soc India 71:129

Pemberton SG, MacEachern JA, Ranger MJ (1992) Ichnology and event stratigraphy: the use of trace fossils in recognizing tempestites. In: Pemberton SG (ed) Application of ichnology to petroleum exploration: a core workshop. SEPM Core Workshop 17:1–85

Pollard JE, Goldring R, Buck SG (1993) Ichnofabrics containing *Ophiomorpha*: significance in shallow-water facies interpretation. J Geol Soc India 150:149–164

Singh IB, Shukla UK (1991) Significance of trace fossils in the Bhuj sandstone (Lower Cretaceous), Bhuj area, Kachchh. J Palaeontol Soc India 36:121–126

Taylor A, Goldring RG, Gowland S (2003) Analysis and application of ichnofabrics. Earth-Sci Rev 60:227–259

Thayer CW (1983) Sediment-mediated biological disturbance and the evolution of marine benthos. In: Tevesz MJS, McCall PW (eds) Biotic interactions in recent and fossil benthic communities. Springer, Boston, pp 479–625

Vossler SM, Pemberton SG (1988) *Skolithos* in the Upper Cretaceous Cardium Formation: an ichnological example of opportunistic ecology. Lethaia 21:351–362

Wetzel A, Aigner T (1986) Stratigraphic completeness: tiered trace fossils provide a measuring stick. Geology 14:234–237

Woodin SA (1977) Algal 'gardening' behaviour by nereid polychaetes: effects on soft-bottom community structure. Mar Biol 44:39–42

Gastropod Biozonation for the Jurassic Sediments of Kutch and Jaisalmer Basins and Its Application in Interbasinal Correlation

Sandip Saha, Shiladri S. Das, and Subhronil Mondal

Abstract Kutch and Jaisalmer are the two western Indian basins having similar Jurassic marine sediments and associated rich fossil assemblages. The Jurassic successions of both basins are thick and well-developed, and lithostratigraphically are highly comparable with each other. Stratigraphically, the Jurassic rocks of both basins have been subdivided into various ammonite-based biostratigraphic units, which provide fine-scale stratigraphic division from the Late Bajocian to the latest Tithonian as well as precise interbasinal correlations. In spite of so much detail, still, some time units lack any proper ammonite biozones due to sedimentary hiatus. Recently, diverse gastropod assemblages are emerging from various stratigraphic sections of both basins. Like ammonites, the gastropods can effectively be used to establish more acceptable regional biostratigraphy of both basins because of their basinal endemism. Based on these collections, for the present study, 12 biozones for Kutch and three biozones for Jaisalmer have been proposed. These proposed gastropod assemblage data and the existing ammonite biozonations for both basins have been used for correlation between these two basins. In many cases, our proposed gastropod biozones based on coeval gastropod assemblage distributions at different levels helps to fine-tune the preexisting ammonite-based biozones, most-specifically for the Middle Jurassic (Bajocian, Middle Bathonian, and Early Callovian). However, the scarcity of gastropods from most of the stratigraphic levels of Jaisalmer Basin made the same comparison difficult for other intervals.

Keywords Gastropoda · Lithostratigraphy · Biostratigraphy · Stratigraphic correlation · Western india

S. Saha · S. S. Das
Geological Studies Unit, Indian Statistical Institute, Baranagar, Kolkata 700108, India

S. Mondal (✉)
Department of Earth Sciences, Indian Institute of Science Education and Research (IISER) Kolkata, Mohanpur 741246, West Bengal, India
e-mail: subhronil.m@gmail.com

Department of Geology, University of Calcutta, Ballygunge, Kolkata 700019, India

333

1 Introduction

Kutch and Jaisalmer—two neighboring western Indian basins—are famous for their thick, well-developed Mesozoic sedimentary successions (Biswas 1977; Mitra et al. 1979; Krishna 1987; Das 2008; Fürsich et al. 2013; Pandey et al. 2009, 2014). Both basins originated from rifting of the Gondwana super plate (Indian-African plate region); rifting occurred perhaps near the Late Triassic (Biswas 1991). Due to repeated marine transgression-regression cycles, the Tethys sea flooded both basins simultaneously during the Early Jurassic (Pliensbachian) (Rai and Jain 2013), and a thick pile of Mesozoic sediments deposited in both basins. Consequently, Mesozoic marine sediments filled in these basins are very similar, representing coastal, estuarine, and shallow to mid-shelf environments (Fürsich et al. 1992), ranging in age from the Triassic up to the Early Cretaceous (Krishna 1987). Here, we focus on the Jurassic System of both basins for their excellent stratigraphic sections, yielding diverse shallow marine taxa, including the stratigraphically significant ammonites (Krishna 2017).

Jurassic sediments in Kutch Basin range in ages from the Pliensbachian to the latest Tithonian, while in Jaisalmer, it ranges from the Early (older than Bajocian) to Late (latest Tithonian) Jurassic (Biswas 1977; Fürsich and Oschmann 1993; Rai and Jain 2013; Fürsich et al. 2013). Pandey et al. (2009) identified four marker beds within the Jurassic sedimentary succession of both basins, and these common marker beds indicate a common control in the sedimentation history. The deposition of Jurassic sediments in both basins initiated with non-marine sediments followed by marine settings (Fürsich et al. 2013). The Bathonian sediments in both basins are characterized by shallow-marine mixed siliciclastics-carbonates (Pandey et al. 2009), while the Callovian sediments are largely fine-grained siliciclastics (Fürsich et al. 1991, 1992; Fürsich and Oschmann 1993). A period of peak transgression in the Oxfordian is marked by the iron-rich oolitic sediments (Fürsich et al. 1991; Fürsich and Oschmann 1993), present in both basins. The overlying Kimmeridgian rocks are fine- to coarse-grained siliciclastics in nature, whereas the Tithonian rocks show characteristic near-shore facies (Fürsich et al. 1991, 1992; Fürsich and Oschmann 1993), which are present in both basins.

Because of good lithostratigraphic homogeneities, as mentioned above, interbasinal comparisons for the Jurassic rocks have been attempted by a few authors (Krishna 1987; Pandey et al. 2009, 2012). However, the most effective way of this interbasinal comparison is fossils: faunal homogeneity of both basins is temporally controlled by time-diagnostic ammonites, based on which regional biostratigraphic correlations during the Jurassic have been done (Waagen 1873–1875; Spath 1927–1933; Krishna 1987; Bardhan and Datta 1987; Prasad 2006; Prasad et al. 2007; Pandey et al. 2014 and many others). The development of Jurassic ammonite biozonations of both basins is characterized by their commonly present species or assemblages as a whole. Each ammonite zone is based on bed-by-bed collections under possible stratigraphic precision and the zonal boundaries are marked as time boundaries through intra-basinal correlations (Krishna 2017). Apart from ammonites, other

fossils groups like foraminifera, brachiopods, and ostracods are also used in the biostratigraphic correlations (Pandey and Dave 1993; Talib and Gaur 2008; Khosla et al. 2009; Andreu et al. 2012; Jain 2012; Mukherjee 2015 and many others), only with limited success.

In the present contribution, we propose several gastropod-based biozones for both basins by plotting newly emerging diverse gastropod assemblages discovered from various stratigraphic levels and geographic locales of both basins. Like ammonites, characteristic provincialism and a significant degree of endemism of the Jurassic gastropods of Kutch and Jaisalmer basins can effectively be used to establish finer refinement of regional biostratigraphy within and between the subprovinces, as endemic molluscan taxa are restricted within the subprovinces (Kauffman et al. 1993). More importantly, these newly emerging gastropod assemblages are associated with many time-diagnostic ammonite species. Therefore, the stratigraphic distributions of these gastropod genera could be ascertained without a doubt. The final aspect of our work is to use these gastropod assemblage data against the existing ammonite biozonation of the two basins to correlate these basins based on our newly proposed gastropod-based biozonation scheme. The addition of gastropods (including endemic taxa) in the biostratigraphic scheme of the Jurassic sediments of both Kutch and Jaisalmer basins may improve the resolution of the biozonation.

2 Lithostratigraphy of Kutch and Jaisalmer Basins

For a better understanding of the biostratigraphic distribution of gastropods in both basins, the knowledge of detail lithostratigraphy in both local sections and the regional settings is a prerequisite. The general lithologies for both basins as well as details of studied locations from where most of the present gastropod specimens were systematically collected are discussed below.

2.1 Kutch Basin

The Mesozoic sediments of the Kutch Basin are exposed in three parallel anticline belts standing out as structural as well as topographical domes roughly along the NW–SE direction (Fig. 1; Wynne 1872). Recently, Biswas (2016) recognized three distinct lithostratigraphic domains i.e. Mainland Group, Pachham Group, and Eastern Kutch Group, based on their distinctive lithological association. In the mainland of Kutch, the major exposures of the Mainland Group of rocks are present at six domes: Mundhan-Lakhapar, Jara, Jumara, Keera, Jhura, and Habo, from west to east (Fig. 1). Besides these domes, the Mesozoic sediments are also exposed in the Patcham, Khadir, Bela, Chorad "islands", and Wagad Highland. The Pachham Group is represented by the rocks exposed in Patcham "island" and the rocks exposed in the
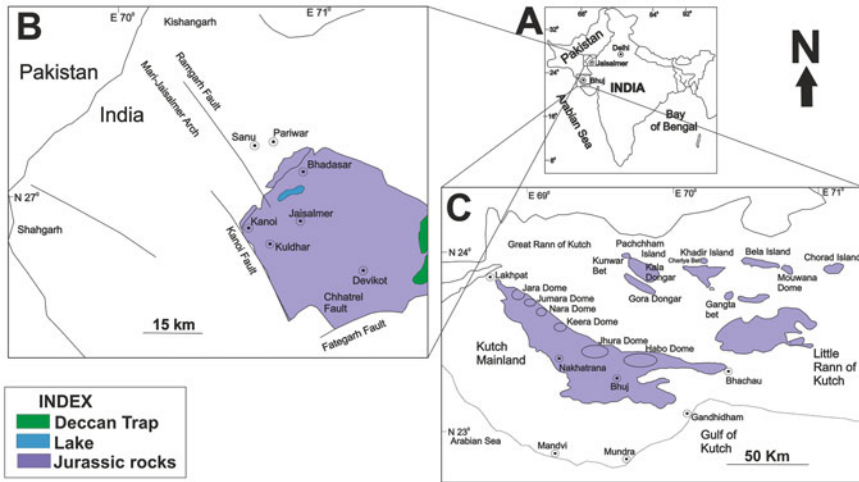
Fig. 1 **a** An outline map of India showing two western Indian basins, i.e. Kutch and Jaisalmer. **b**, **c** Simplified maps of the Jaisalmer (**b**) and Kutch (**c**) basins showing major Jurassic exposures. Modified after Fürsich et al. (2014) and Pandey et al. (2014)

rest "islands" (Khadir, Bela, and Chorad islands) and Wagad Highland are denoted as the Eastern Kutch Group (Fig. 1; Biswas 2016).

In Pachham Island, the Kaladongar Formation is the oldest stratigraphic unit of Kutch, having the Lower to Middle Jurassic age, comprises of a thick sequence of conglomerate, sandstone, and shale, and can be subdivided into three members: Dingy Hill, Narewari Wandh Sandstone, and Babia cliff Sandstone (Tables 1 and 2; Biswas 1977, 2016; Fürsich et al. 2013). A marker bed, i.e. Leptospinctes-bearing Pebbly Rudstone occurring in the top of the Babia cliff Sandstone Member (Table 2). The Middle Jurassic (Bathonian) rocks of Goradongar Formation, overlying the Kaladongar Formation, have a sequence of Goradondar Yellow Flagstone Member, Gadaputa Sandstone Member, and Raimalro Limestone Member in ascending order (Biswas 2016). Modar Hill unit was previously considered as a member within the Goradongar Formation, but Biswas (2016) upgraded this unit as formation. This formation overlying the Raimalro Limestone Member and comprises the grey, silty, fossiliferous shale bed at the lower part. The upper part of the Moder Hill Formation is not exposed.

The Mainland stratigraphic sequence of Kutch has been divided into four lithos-tratigraphic units: the Jhurio (Jhura), Jumara, Jhuran, and Bhuj formations in ascending order (Table 1; Biswas 2016). The Jhurio Formation is uncovered only in Habo, Jhurio, and Jumara domes and is characterized by Golden Oolite beds (Biswas 2016). The Formation is equivalent to Kaladongar and Goradongar formations of Pachham Island Group. The Lower to Middle Jurassic (?Aalenian-Bathonian) Jhurio Formation, which indicates marine transgression in the lower part and maximum flooding surface in the upper part, can be subdivided into seven members (Biswas

Table 1 Biostratigraphic correlation of the Jurassic successions of the Kutch and Jaisalmer basins based on ammonite-based biozonation. Modified after Krishna (1987), Krishna and Pathak (1991), Krishna and Ojha (1996), Krishna et al. (1996, 2000), Prasad (2006), Shome et al. (2004), Jana et al. (2005), Roy et al. (2007), Prasad et al. (2007), Alberti et al. (2011), Pandey et al. (2012, 2014), Sharma and Pandey (2016), and Roy et al. (2019). Here "No ammonites" denotes that the time interval is devoid of any ammonite species and "No zones" specifies the time interval cannot be subdivided into ammonite biozones

Kutch basin				Jaisalmer basin		
Age	Formation		Biozone	Formation	Biozone	Age
Late Tithonian	Jhuran		*Corongoceras*	Bhadasar	*Himalayites*	Late Tithonian
			Denseplicatus			
Early Tithonian			Communis			Early Tithonian
			Natricoides		Kobelliforme	
			Virgatosphinctoides			
			Pottingeri			
Late Kimmeridgian			Katrolensis	Baisakhi		Late Kimmeridgian
Middle to Late Kimmeridgian			Bathyplocus		No zones	Middle Kimmeridgian
			Intermedius			
Early Kimmeridgian			Alterneplicatus			Early Kimmeridgian
			No ammonites		No ammonites	
Late Oxfordian	Jumara	Washtawa	Bifarcatus		*Dichotomoceras*	Late Oxfordian
Middle Oxfordian			Plicatilis-Transversarium		*Mayaites*	Middle Oxfordian
				Jaisalmer		
Early Oxfordian			Cordatum		Semirugosus	Early Oxfordian
			Mariae			
Late Callovian			Lamberti		*Properisphintes*	Late Callovian
			Athleta			

(continued)

Table 1 (continued)

Kutch basin				Jaisalmer basin		
Age	Formation		Biozone	Formation	Biozone	Age
Middle Callovian			Reissi		Gigantea	Middle Callovian
			Anceps			
Early Callovian			Subkossmatia opis			Early Callovian
	Modar Hill		Formosus			
Late Bathonian	Jhurio	Goradongar	Chrysoolithicus		Congener	Late Bathonian
			Triangularis			
Middle Bathonian			Procerites		Clydoniceras sp.	Middle Bathonian
			Arkelli			
Early Bathonian			No ammonites		No ammonites	Early Bathonian
			Zigzag			
Late Bajocian		Kaladongar	Leptosphinctes sp.		No ammonites	Late Bajocian

Table 2 The proposed gastropod biozones using different biozonation concept (following Murphy and Salvador 1999 and Backman et al. 2012) for the Jurassic successions in the Kutch and Jaisalmer basins based on gastropods. Biostratigraphic correlations between these two basins based on these gastropod-based biozones along with lithofacies are shown. Here "No gastropods" indicates that no such gastropods have been recorded from that time interval; "No zones" specifies the time interval cannot be subdivided into gastropod biozones and "NA" signifies the time interval is lack of any biozonation schemes due to the absence of gastropods

Jaisalmer basin					Kutch basin				
Formation	Member	Age	Scheme for biozonation	Proposed gastropod zone	Scheme for biozonation	Proposed gastropod zone	Age	Member	Formation
Bhadasar	Kolar Dungar	Tithonian	No zones	No zones	Cross-over abundance zone	*Chartronella*	Tithonian	Katesar Upper	Jhuran
Baisakhi	Lanela	Late Kimmeridgian	NA	No gastropods	NA		Kimmeridgian	Middle (Rudramata Shale)	
	Ludharwa	Middle Kimmeridgian							
	Rupsi	Early Kimmeridgian						Lower	
		Late Oxfordian	No zones	No zones	Range and abundance zone	*Turritella*	Late Oxfordian	Dhosa Oolite	Jumara
	Basal	Early to Middle Oxfordian	No zones	No zones	Range and abundance zone	*Eucyclus*	Early to Middle Oxfordian		Washtawa
Jaisalmer	Jajiya								

(continued)

Table 2 (continued)

Jaisalmer basin				Kutch basin					
Formation	Member	Age	Scheme for biozonation	Proposed gastropod zone		Scheme for biozonation	Age	Member	Formation
	Kuldhar	Late Callovian	NA	No gastropods	*Adeorbisina*	Assemblage zone	Late Callovian	Gypsiferous Shale	
		Middle Callovian	No zones	No zones	*Buckmanina*	First appearance and abundance	Middle Callovian	Ridge Sandstone	
		Early Callovian	Range zone	*Pleurotomaria*		Range zone	Early Callovian	Shelly Shale	
			No zones	No zones	*Pictavia*	Top common			Modar Hill

(continued)

Table 2 (continued)

Jaisalmer basin					Kutch basin				
Formation	Member	Age	Scheme for biozonation	Proposed gastropod zone	Proposed gastropod zone	Scheme for biozonation	Age	Member	Formation
	Bada Bag	Late Bathonian	NA	No gastropods	*Leptomaria*	Top common	Late Bathonian	Thin bedded White Lst. & Nod. Lst. / Raimalro Limestone	Jhurio / Goradongar
					Riselloidea	Abundance zone			
	Fort	Middle Bathonian	Range zone	*Pietteia*		First appearance and base common	Middle Bathonian	Purple Sandstone/Packstone / Gadaputa Sandstone	
								Bedded rusty grainstone with golden oolite / Goradongar Yellow Flagstone	
		Early Bathonian	NA	No gastropods	No gastropods	NA	Early Bathonian	Gray Shales	
	Joyan	Bajocian	No zones	No zones	No gastropods	NA	Bajocian	(Leptosphinctes-bearing Pebbly Rudstone) Babia Cliff Sandstone	Kaladongar
	Hamira		NA	No gastropods					
Lathi	Thaiat		Abundance zone	*Nerinea*	*Turbinea*	Cross-over abundance zone		Narewari Wandh Sandstone	
	Odania		NA	No gastropods	*Katosira*	Range zone		Dingy Hill	

1991, 2016). The Jumara Formation, overlying the Jhurio Formation, is comprised of mainly shale with interbeds of thin marlite, sandstone, and siltstone, and has been assigned the Callovian- Early Oxfordian age (Biswas 2016). The Jumara Formation has been sub-divided into four members: Shelly Shale, Ridge Sandstone, Gypseous Shale, and Dhosa Oolite (Biswas 2016). The Dhosa Oolite Member is characterized by greenish, glauconitic, oolitic limestone, and glauconitic shale inter-beds and also marks the maximum flooding surface in Early Oxfordian age followed by a Middle Oxfordian-Early Kimmeridgian hiatus (Krishna et al. 2009; Biswas 2016). But the presence of Late Oxfordian sedimentary successions in the Mainland of Kutch has been recently described by us from the Jhura dome (see Das et al. 2018, 2019), which shorten the interval of hiatus, i.e. Early Kimmeridgian. The contact boundary between the Jumara Formation and the overlying Jhuran Formation lies above the Dhosa Oolite Member. The Upper Jurassic (Kimmeridgian to Tithonian) Jhuran Formation represents the shale/sandstone alternation with thin-bedded hard calcareous sandstones and has four members: the Lower, Middle (also Rudramata Shale Member), Upper and Katesar (Table 2; Biswas 2016; Desai and Biswas 2018; Chaudhuri et al. 2018, 2020a, b, c, d). In the western part of the mainland, three Tithonian fossiliferous bands, i.e. Trigonia Ridge sandstone, three ammonite-rich oolitic limestone bands, and the *Gryphaea* band occur towards the middle and upper part of the sequence (Desai and Biswas 2018). The top part of the Mesozoic sequence, i.e. Bhuj Formation (Lower Cretaceous) is marked by thick non-marine (fluvio-deltaic) brown and pink sandstone with bioturbated ferruginous beds (Biswas 1977, 2016). The Bhuj Formation is exposed in two wide belts: (1) in the central part of the Kutch mainland, and (2) in the western fringe of the mainland (Desai 2013). In the western Kutch, the Bhuj Formation has been subdivided into three members: Ghuneri (Lower), Ukra, and Upper (Desai 2013; Biswas 2016). The Ukra Member is absent in the Eastern and Central Kutch.

In the Eastern Kutch, the Khadir Formation includes the oldest beds of the sequence and is dominantly arenaceous. The Khadir Formation can be subdivided into three members: Cheriyabet Conglomerate, Hadibhadang Shale, and Hadibhadang Sandstone. The Callovian to Oxfordian rocks of Gadhada Formation, overlying the Hadibhadang Sandstone Member of the Khadir Formation, is divided into two members, i.e. the lower Ratanpur Sandstone and the upper Bambhanka/Ganta Bet (Biswas 2016). The Washtawa Formation and Wagad sandstones are part of the Wagad Highland, which ranges from the Callovian to the Kimmeridgian in age (Biswas 2016). The top part of Wagad sandstones is not exposed here. The Washtawa Formation, which ranges from the Middle Callovian to the Oxfordian, comprises of thickly bedded, cross-laminated sandstone, and shale with occasional thin fossiliferous limestone bands (Biswas 1977; Shome and Bardhan 2005). The Wagad Sandstone, ranging from the Oxfordian to Kimmeridgian, has two distinct marine and non-marine parts and can be subdivided into three members: Patasar Shale, Kanthkote, and Gamdau (Biswas, 2016). The upper non-marine part indicated a deltaic environment of deposition in the Eastern Wagad section and the lower marine part is represented by the fossiliferous gypseous shale interlamination with fine-grained sandstones (Biswas 1977, 2016).

2.2 Jaisalmer Basin

The Jaisalmer Basin is tectonically divided into four structural units and the Mesozoic sediments are best exposed along the Mari-Jaisalmer Arch spreading NW-SE over the central part of the basin (Das Gupta 1975; Pandey et al. 2009). The Mesozoic rocks of the Jaisalmer Basin have been divided into four lithostratigraphic units: Lathi, Jaisalmer, Baisakhi, and Bhadesar formations, in ascending order (Table 1; Das Gupta 1975; Prasad 2006; Pandey et al. 2012, 2014). The Lathi Formation is the lowermost Early to Middle Jurassic stratigraphic unit of the Jaisalmer Basin. The rock type of the formation is mainly sandstone and has been subdivided into two members: lower Odania and upper Thaiat (Table 2; Das Gupta 1975). The overlying Jaisalmer Formation comprises of mainly calcareous sediments, ranging from the Bajocian up to the Oxfordian, and can be sub-divided into five members: Hamira, Joyan, Fort, Bada Bag, and Kuldhar (Table 2; Das Gupta 1975). Kachhara and Jodhawat (1981) later recognized the Jajiya Member, as the topmost member of the Jaisalmer Formation.

The Baisakhi Formation, which overlies the Jaisalmer Formation is marked by the shales with buff-coloured sandstone, has been divided into three members: Rupsi, Ludharwa, and Baisakhi (Das Gupta 1975). Later, Prasad (2006) proposed the Lanela Member for thin siltstone and fine-grained sandstone unit, which is previously known as Baisakhi Member, exposed at the south of the village Lanela and Pandey et al. (2014) introduced one new member i.e. Basal Member within the Baisakhi Formation. Thus, Basal, Rupsi, Ludharwa, and Lanela are the four members within the Baisakhi Formation (Table 2) and range in age from the Oxfordian to the Early Tithonian (Prasad 2006; Pandey et al. 2014; Pandey and Pooniya, 2015). The topmost formation of the Jaisalmer basin, i.e. the Bhadesar Formation, overlies the Baisakhi Formation, and is represented by fossiliferous limestone followed by ferruginous sandstone with thin intercalation of clay beds, and is of Tithonian to possible Lower Cretaceous age (Pandey et al. 2014). At the base of the formation, a sandy to gritty calcareous conglomerate bed is exposed near the cliff of the Bhadesar ridge (Pandey et al. 2012). Das Gupta (1975) subdivided the formation into two members, i.e. Kolar Dungar and Mokal (Table 2).

2.3 Interbasinal Correlations

Lithostratigraphically these two basins are similar in many aspects, indicating a common control in depositional settings. The lowermost Bajocian stratigraphic unit of the Jaisalmer Basin, i.e. Lathi Formation, is similar to the Kaladongar Formation of Kutch Basin in having similar Rudstone marker beds. The major Bajocian units of these two basins are marked by the first marine transgression. The Goradongar Yellow Flagstone Member (Early to Middle Bathonian) within the Goradongar Formation

of the western Kutch Basin has similar sediment composition and primary sedimentary structures with the middle part of the Fort Member (Jaisalmer Formation) of the Jaisalmer Basin (Table 2; Pandey et al. 2009). The Late Bathonian Raimalro Limestone Member is characterized by trough cross-bedded, sandy packstone to grainstone with a mega-ripple surface, matching with the time-equivalent basal part of Kuldhar Member (Jaisalmer Formation) comprising cross-bedded, fine-grained sandstones to ooid-packstone, topped by mega-ripple surface. The Callovian sediments in Kuldhar Member of the Jaisalmer Basin are highly correlated with the sediments of the Jumara Formation of the neighboring Kutch Basin (Krishna 1987; Pandey et al. 2012).

The Jajiya Member of Jaisalmer Formation is characterized by ooid- bearing rudstones and an Oxfordian in age (Pandey et al. 2014; Sharma and Pandey 2016) has been highly comparable with the Oxfordian Dhosa Oolite Member of Kutch Basin (Pandey et al. 2009, 2012; Alberti et al. 2011). The Baisakhi Formation of Jaisalmer and the Jhuran Formation of Kutch appear similar to us, with alternating beds of shales and sandstones. Kolar Dungar Member of Bhadasar Formation (Jaisalmer Basin) is represented by ferruginous sandstone with thin intercalation of clay beds while the equivalent Upper Member of Jhuran Formation in Kutch Basin consists of sandstone which is occasionally oolitic and laminated shale (Das Gupta 1975; Das 2002).

Also, these two basins are well-known for their numerous fossiliferous horizons, similar shell beds, cyclic sedimentation, and comparable stratigraphic units within the Jurassic successions (e.g. Fürsich et al. 1991, 1992, 2013; Fürsich and Oschmann 1993). The oldest Bajocian members of both basins i.e. Dingy Hill Member of Kutch and Odania Member of Jaisalmer are marine but having non-marine occurrence in case of the Odania Member (Desai 2012; Pandey et al. 2012; Fürsich et al. 2013). In Jaisalmer, the marine condition of Odania Member is characterized by some trace fossils, whereas fossils like gastropods, nannofossils, etc. are recorded from the marine condition in the Kutch Basin (Pandey et al. 2012; Fürsich et al. 2013). The widespread hardgrounds (synsedimentary-cemented layers) throughout the Jaisalmer Basin from east to west indicate excellent marker horizons of the Late Bathonian rocks. In comparison, marker hardgrounds are not developed in the equivalent Late Bathonian Jhurio Formation of the neighboring Kutch basin (for detail, see Pandey et al. 2018). In the Callovian sequence of Kutch Basin, Fe-oolitic grainstones shoal deposits formed a thick succession in the Jumara Formation of Keera Dome (Biswas 2016). But in Jaisalmer, no shoal deposits are recorded. The glauconitic ammonite bands occur in the basal part of the Jhuran Formation of the western Mainland of Kutch, indicating sediments of maximum flooding zone (Krishna et al. 2009; Fürsich et al. 2013; Biswas 2016) while it is absent in the Jaisalmer Basin (Pandey et al. 2014).

3   Jurassic Biostratigraphy of Kutch and Jaisalmer Basins

3.1   Kutch Basin

In the Kutch Basin, the best fossiliferous (includes nannoplankton, corals, sponges, bivalves, gastropods, ammonites, brachiopods, foraminifera, ostracods, and many other fossils) sections are situated in the central anticline, i.e. in the Mainland among three parallel anticlines (for details see Mitra et al. 1979; Das 2004). In the Kutch Mainland, the Jhurio (Raimarlo Limestone Member) and Jumara (Dhosa Oolite Member) formations are particularly highly fossiliferous and include several fossils (Das 2004). The other major fossiliferous formations and members are Dingy Hill Member and Narewari Wandh Sandstone Member of Kaladongar Formation; Goradondar Yellow Flagstone Member and Gadaputa Sandstone Member of Goradongar Formation; Jhuran Formation and Umia Ammonite Beds of Jhuran Formation (Fürsich et al. 2013). In Eastern Kutch, Washtawa Formation (equivalent to Jumara Formation) and Wagad Sandstone are the major fossiliferous units (Shome and Bardhan 2005).

Waagen (1873–1875) and Spath (1927–1933) made the early attempts in subdividing the Jurassic sedimentary rocks of the Kutch Basin based on ammonites. Their schemes have been followed by the other workers (e.g. Krishna 1987; Bardhan and Datta 1987; Prasad 1998). Later, by using newly collected ammonites, many workers further subdivided the preexisting biostratigraphic units based on their stratigraphic positions (Mitra et al. 1979; Agrawal and Pandey 1985; Krishna and Pathak 1991; Krishna and Ojha 1996; Krishna et al. 1996, 2000; Jain and Pandey 2000; Alberti et al. 2011; Pandey et al. 2012, 2014; Jain 2014; Pandey and Pathak 2015), and morphological and phylogenetic analyses (Shome et al. 2004; Jana et al. 2005; Roy et al. 2007; Roy et al. 2019). Based on all these works, until now, a total of 26 biozones so far have been identified in Kutch. Despite all these attempts, several time units still could not be assigned by their respective biozones and index fossils (Table 1). For example, the Bajocian and the upper Early Bathonian is still lacking any proposed ammonite biozone. The same is true for the lower part of the Early Kimmeridgian time unit.

Apart from these ammonite-based studies, other fossils groups have also been used to achieve the same but only with limited success. For example, some attempts have been made to use foraminifera to establish biozones (Pandey and Dave 1993; Talib and Gaur 2008). Similar attempts have been made by using brachiopods (Mukherjee et al. 2003) and ostracods (Khosla et al. 2009; Andreu et al. 2012). However, the spatio-temporal distribution of benthic foraminifera, as well as ostracods, is controlled mainly by the environmental parameters rather than their temporal evolutionary patterns (Garg and Singh 1986; Fürsich et al. 2013). Andreu et al. (2012) accepted that the present ostracod used in regional biostratigraphy zonation in the basin is not accurate.

3.2 Jaisalmer Basin

The Jaisalmer Formation (Fort, Bada Bag, Kuldhar, and Jajiya members) is the most fossiliferous unit during the Jurassic and the major fossils are cephalopods, brachiopods, bivalves, gastropods, microfaunas, etc. (Pandey et al. 2012, 2014). Thaiat Member (gastropods, bivalves, trace fossils, corals, woods, etc.) of the Lathi Formation, Rupsi Member (cephalopods, brachiopods, bivalves, microfaunas, corals, etc.) of the Baisakhi Formation and Kolar Dungar Member (cephalopods, brachiopods, and broken gastropods, bivalves, etc.) of the Bhadasar Formation are the other fossiliferous members within the Jurassic sedimentary succession of the Jaisalmer basin (Pandey et al. 2014; Sharma and Pandey 2016).

The early attempts to mark the Lower to Upper Jurassic succession of the Jaisalmer Basin based on ammonites were made by Kachhara and Jodhawat (1981) and Jodhawat (1984). Since then, other authors subdivided this time slices based on ammonites (Krishna 1987; Pandey and Krishna 2002; Prasad 2006; Prasad et al. 2007; Jain and Garg 2012). Finally, Pandey et al. (2012) summarized stratigraphic distributions of different ammonite zones proposed by earlier workers (Kachhara and Jodhawat 1981; Jodhawat 1984; Krishna 1987; Prasad 2006; Prasad et al. 2007). Based on all these works, until now, 19 ammonite biozones with zonal index species have been established (Table 1). However, no such ammonite biozone has been so far proposed from the Bajocian and the Early Bathonian time units. Like Kutch Basin, the lower part of the Early Kimmeridgian also lacks any proposed ammonite biozone in Jaisalmer.

3.3 Interbasinal Correlations

Krishna (1987), first compared the ammonite-based biozones of the Jaisalmer Basin with the adjacent Kutch Basin. His ammonite-based biostratigraphic and lithostratigraphic studies in both basins gave the finest time resolution for most of the Mesozoic rocks, which improve the understanding of time boundaries, and intra and interbasinal correlations. In recent years, many diverse ammonite assemblages have been recorded from different stratigraphic sections from Jaisalmer, which further improved the biostratigraphic scheme of that basin (Prasad 2006; Prasad et al. 2007). Based on these works, Pandey et al. (2014) summarized the biostratigraphic distribution of ammonites from the Lower to Upper Jurassic sediments of the Jaisalmer Basin and compared broadly with the neighboring Kutch Basin. Pandey et al. (2014) documented the Oxfordian genera such as *Peltoceratoides* Spath 1924, *Mayaites* Spath 1924, *Epimayaites* Spath 1928, *Dhosaites* Spath 1928, *Paryphoceras* Spath 1928, *Klematosphinctes* Buckman 1922, and *Dichotomoceras* Buckman 1922 (Kachhara and Jodhawat 1981; Krishna 1987; Prasad 2006) from the Jajiya Member of Jaisalmer, which is equivalent to the Dhosa Oolite Member in Kutch. Recently, few

workers (e.g. Sharma and Pandey 2016; Roy et al. 2019) enhanced the biostratigraphy of the Jurassic rocks of both Kutch and Jaisalmer basins by incorporating newly described ammonite species (see below).

The oldest ammonite was recorded from Kutch in Late Bajocian of age (Singh et al. 1982), while, in Jaisalmer, it is of Middle Bathonian age (Prasad et al. 2007) (Table 1). The Late Bajocian time unit of the Kutch Basin is represented by the *Leptosphinctes* sp. biozone (Singh et al. 1982; Krishna 1987). The Zigzag zone of lower Early Bathonian sediments in Kutch includes *Parkinsonia* Bayle 1878, *Siemiradzkia* Hyatt 1900, *Berbericeras* Roman 1933, *Zigzagiceras* Buckman 1922, *Telermoceras* Arkell 1952, etc. (Pandey and Pathak 2015) whereas no such ammonites have been described from the Early Bathonian sediments of Jaisalmer Basin. In Kutch, the Middle Bathonian sedimentary succession is dominated by *Kamptokephalites* Buckman v, *Prohecticoceras* Spath 1928, *Gracilisphinctes* Buckman v, *Clydoniceras* Blake 1905, *Procerites* Siemiradzki 1898, etc. and is demarcated as Arkelli and *Procerites* biozones respectively (Krishna 1987; Fürsich et al. 1994, 2013; Prasad et al. 2007; Roy et al. 2007; Jain 2014). In comparison, one single species of the genus *Clydoniceras* have been reported from the Middle Bathonian horizons of Jaisalmer and is known as the *Clydoniceras* sp. zone (Prasad et al. 2007). The Late Bathonian successions of both basins are subdivided into two ammonite zones—Triangularis and Chrysoolithicus zone in Kutch, and Triangularis and Congener zone in Jaisalmer (Table 1; Krishna 1987; Roy et al. 2007). In the Early Callovian, macrocephalitids (*Macrocephalites* Zittel 1884) dominated in both basins and subdivided the time unit into Formosus and *Subkossmatia opis* (Sowerby) biozones (Krishna 1987; Pandey et al. 2010). The sedimentary successions of the Middle Callovian are characterized by eucycloceratids (*Eucycloceras* Spath 1924, *Subkossmatia* Spath 1924, etc.) and reineckeiids (*Reineckeia* Bayle 1878, *Reineckeites* Buckman 1922, *Collotia* Grossouvre 1917, and many others) from both basins and the time unit subdivided into two zones (Table 1; Krishna 1987; Mukherjee et al. 2003; Jana et al. 2005; Fürsich et al. 2013; Pandey et al. 2014). The ammonoid zones identified in the Late Callovian part of the Kutch Basin are Athleta and Lamberti (Roy et al. 2019 and references therein), whereas, in Jaisalmer, the Late Callovian has been marked by only one zone, i.e. *Properisphinctes* (Table 1; Kachhara and Jodhawat 1981).

For the Oxfordian interval of the Upper Jurassic, four distinct biozones (i.e. Mariae, Cordatum, Plicatilis-Transversarium, and Bifurcatus) (Alberti et al. 2011; Fürsich et al. 2013; Roy et al. 2019) have been identified in the Kutch Basin, whereas the equivalent units in Jaisalmer have been subdivided into three (i.e. Semirugosus, *Mayaites*, and *Dichotomoceras*) biozones; the index genera are *Perisphinctes* Waagen 1869 (subgenera *Kranaosphinctes* Buckman 1922, *Dichotomosphinctes* Buckman 1922, *Dichotomoceras*, and others), *Mayaites*, *Epimayaites*, *Dhosaites*, *Paryphoceras*, and *Peltoceratoides* (Table 1; Kachhara and Jodhawat 1981; Krishna 1987; Prasad 2006; Alberti et al. 2011; Pandey et al. 2012, 2014; Fürsich et al. 2013; Roy et al. 2019) for both basins. The overlying Kimmeridgian strata have two common taxa occurring in both basins—*Katroliceras* Spath 1924 and *Torquatisphinctes* Spath 1924 (Krishna et al. 1996) and has been subdivided into four (Alterneplicatus, Intermedius, Bathyplocus, and Katrolensis Zone) and two (Alterneplicatus and

Katrolensis) biozones, respectively, for Kutch and Jaisalmer (Krishna and Pathak 1991; Krishna et al. 1996, Pandey and Krishna 2002; Fürsich et al. 2013). The latest Jurassic (Tithonian) strata of both basins have been divided into six biozones: Pottingeri, Virgatosphinctoides, Natricoides (coeval biozone Kobelliforme for Jaisalmer), Communis, Denseplicatus and *Corongoceras* (*Himalayites* for Jaisalmer) (Table 1; Krishna and Pathak 1991; Krishna et al. 2000; Pandey and Krishna 2002; Shome et al. 2004; Shome and Bardhan 2009 and references therein).

4 The Proposed Biozones Based on Gastropod Assemblages

Recently, new gastropod assemblages are emerging from various stratigraphic levels and geographic locations from both the basins (Das Gupta 1975; Pareek et al. 1977; Jodhawat 1984; Pandey and Choudhary 2007; Pandey et al. 2012, 2014; Sharma and Pandey 2016 for Jaisalmer Basin; Das et al. 1998, 1999, 2005, 2018, 2019; Jaitly et al. 2000; Jaitly and Szabo 2002, 2007; Das 2004, 2007, 2008; Szabo and Jaitly 2004; Alberti et al. 2013 for Kutch Basin), which are also associated with many important time-diagnostic ammonite species. These works, supplemented by the vast collections made by one of us (SSD), encouraged us to revise the established ammonite biozones for the Jurassic stratigraphy of both Kutch and Jaisalmer basins by using newly collected gastropods taxa. Finally, between-basin comparisons are made based on these gastropod assemblages. For doing so, we have used the concept of range zone, assemblage zone, and abundance zone for biostratigraphic distribution of gastropod assemblages and divided each stratigraphic interval into different zones, following Murphy and Salvador (1999). Gastropod distribution against the ammonite biozonation shows that many gastropod species have short temporal ranges and many of them are found in great numbers at certain levels. It is tempting us to propose several new zones based on gastropod data. Some gastropod genera are represented by few specimens at their first appearance and some show cross-over in abundance between two taxa. For this purpose, we also use the concepts, cross-over abundance, and base and top common, following Backman et al. (2012), for biostratigraphic zonation.

4.1 Kutch Basin

Gastropods are ubiquitous throughout the Jurassic sediments of Kutch, although Jhurio and Jumara formations are virtually the repositories of marine Jurassic life. Gastropods are abundant, diverse, and exceptionally well preserved. Based on stratigraphic positions and distributions of gastropods, 12 biozones comparable with ammonite zones have been shown in Table 2. The Early Bathonian and Kimmeridgian horizons of Kutch are devoid of any gastropods taxa, so no such biozones have

been proposed for these two horizons. All the gastropod zones established in the present endeavor are given below:

***Katosira* and *Turbinea* zones (Bajocian)**: In Kutch, the top part of the Babia Cliff Member of the Kaladongar Formation (Late Bajocian) is demarcated by the *Leptosphinctes* sp. biozone (Singh et al. 1982; Krishna 1987) and the remaining lower members (Dingy Hill and Narewari Wandh Sandstone members) are devoid of any ammonite biozone. We, here, based on gastropod assemblages, subdividing these lower members of the Kaladongar Formation into two gastropod zones: *Katosira* and *Turbinea* zones (Table 2). The *Katosira* (Family Zygopleuridae) zone is characterized by the range of the species *Katosira bajocensis* (newly collected, provisionally described species; detailed systematic description is under preparation), collected from sandstone siltstone sequence at Kuar bet belonging to the Dingy Hill Member of Kaladongar Formation. Other species from the same zone are *K.* sp. 2 Das 2004 and *Pseudomelania* sp. Das 2004 (Table 3).

The *Turbinea* zone (Family Nerineidae) is marked by the peak abundance of *Turbinea khadirensis* Jaitly and Szabo 2007 and *Pseudomelania (Oonia)* sp. Das 2004 (Table 3). These two species are collected from the Narewari Wandh Sandstone Member of Patcham Island. Bivalves and trace fossils from the same zone where these two gastropod specimens are recorded indicate the Bajocian age. This zone also indicates the cross-over abundance zone for both of those dominant taxa.

***Pietteia* zone (Middle Bathonian)**: The Middle Bathonian sedimentary succession in Kutch is divided into two ammonite zones, i.e. the Arkelli and *Procerites* zone, in ascending order (Table 1; Jain 2014). We, here, propose the entire Middle Bathonian as *Pietteia* zone (Family Aporrhaidae). This zone is marked by the first appearance of *Pietteia sadharaensis* Jaitly and Szabo 2007 from the Goradongar Yellow Flagstone Member, and associated ammonites indicate the typical Middle Bathonian age. This zone also includes *Bhujnerita bhattii* Jaitly and Szabo 2002, *Neritopsis (Neritopsis) benoisti* Cossmann 1900, *Pseudomelania calloviensis* Hébert and Deslongchamps 1860, *Ampullospira brevispira* Fischer 2001, etc. Most of the species are represented by fragments, although *P. sadharaensis* are almost complete and more abundant than others. *P. sadharaensis* ranges from the Middle Bathonian to Upper Oxfordian (Jumara Formation) (Jaitly and Szabo 2007) and this zone is defined by the first appearance and base common of the species, *P. sadharaensis.*

***Riselloidea* and *Leptomaria* zones (Late Bathonian)**: The *Riselloidea* zone is equivalent to the Triangularis biozone of the lower part of the Late Bathonian in Kutch. The zone is indicated by the genus *Riselloidea* Cossmann 1909 (Family Trochidae) and altogether four species are recorded: *Riselloidea tagorei* Das et al. 1999 (as index fossils)*, R. elongata* Das et al. 1999, *R. pileiformis* Jaitly et al. 2000, and *R. biarmata* Münster 1844. These four species, along with *Onkospira kutchensis* Das et al. 1999; *Helicacanthus chanda* Das et al. 1999, and *Emarginula karuna* Das et al. 1999 are restricted within this early Late Bathonian zone (Das et al. 1999) (Table 3). Among them, *R. tagorei* shows abundant association along with *Macrocephalites triangularis* Spath 1928, the index ammonite species of this zone. The zone is characterized by the abundance of the genus *Riselloidea*. Other genera, like, *Colpomphalus* Cossmann 1916; *Proconulus* Cossmann 1918; *Neritopsis* Grateloup

Table 3 The proposed gastropod biozones and their component taxa from the Bajocian up to the latest Tithonian in the Kutch and Jaisalmer basins. Zone-wise gastropods distribution against the ammonite biozonation shows the temporal range of each gastropod species and the species distribution pattern in both the basins. Here "No gastropods" indicates that the time interval is devoid of any gastropod specimens and "No zones" specify that the zone contains gastropod specimens but we cannot assign any particular zones for that time. Asterisk (*) indicates the index taxa of the respective zones

Jaisalmer basin			Kutch basin		
Age	Zones	Major gastropods	Major gastropods	Zones	Age
Tithonian	No zones	Gastropod fragments	Chartronella lakhaparaensis*, C. mundhanensis, Euspira lakhaparaensis, Talantodiscus sp., Obornella lakhaparaensis	Chartronella	Tithonian
Kimmeridgian	No gastropods	No gastropods	No gastropods	No gastropods	Kimmeridgian
Late Oxfordian	No zones	Nerineid gastropods	Turritella jadavpuriensis*, T. jhuraensis, T. amitava, Bathrotomaria gangtaensis, Euspira jhuraensis, Gyrodes mahalanobisi, Leptomaria daityai, Leptomaria cf. pseudoumbilicata, Bathrotomaria buddhai, Paracerithium sp., Ampullina sp.	Turritella	Late Oxfordian
Early to Middle Oxfordian	No zones	Turriform; gastropod fragments	Eucyclus tramauensi*, E. laevijugatus, Bathrotomaria gangtaensis, B. densireticulata, B. prasantai, Obornella granulata, Pleurotomaria (Indomaria) purba, P. rajnathi, Ilerdus aff. pyrenaeus	Eucyclus	Early to Middle Oxfordian

(continued)

Table 3 (continued)

Jaisalmer basin			Kutch basin		
Age	Zones	Major gastropods	Age	Zones	
Late Callovian	No gastropods	No gastropods	Late Callovian	*Adeorbisina*	*Adeorbisina* sp.*, *Ringicula* sp., *Palaeohydatina* sp., *Pygotrochus* sp., *Amphitrochus angulatus, Ataphrus (A.) kaladongarensis, Bourgetia saemanni, Discohelix* cf. *sapho, Globularia michelini, Naricopsina cornelia, Omphaloptycha* sp., *P.(I.) bhakriensis*
Middle Callovian	No zones	Gastropod fragment	Middle Callovian	*Buckmanina*	*Buckmanina bhakriensis*, Procunulus* sp., *Trochopsidea bajirensis, Calliostoma* sp., *Bourgetia saemanni, Discohelix* cf. *sapho, Globularia michelini, Naricopsina cornelia, Omphaloptycha* sp., *Pleurotomaria (Indomaria) bhakriensis*
Early Callovian	*Pleurotomaria*	*Pleurotomaria* sp.*	Early Callovian	*Pleurotomaria*	*Pleurotomaria (P.) keeraense*, Pygotrochus* sp., *Spinigera compressa, Trochactaeomina ventricosa, Bourgetia saemanni, Discohelix* cf. *sapho, Naricopsina cornelia, Kosmomphalus reticulates, Ataphrus (Ataphrus) belus, A. (A.) orbis, Bathrotomaria calloviana, B. siebereri, B. tiwari, Colpomphalus jumarense, Hayamia bajocensis, H. subsulcosa*

(continued)

Table 3 (continued)

Jaisalmer basin			Kutch basin		
Age	Zones	Major gastropods		Zones	Age
	No zones	Gastropod fragment	Ampullospira (Pictavia) bajocensis*, A. (Pictavia) cf. pyramidata, A. (P.) lorierei, A. (P.) tanganyicensis, Globularia michelini, Naricopsina cornelia, Omphaloptycha sp., Pleurotomaria (Indomaria) bhakriensis, Kosmomphalus reticulates, Spingera compressa, Trochactaeonina ventricosa, Hayamia subsulcosa	Pictavia	
Late Bathonian	No gastropods	No gastropods	Leptomaria asurai*, L. simplex, ?Onkospira praecursor, Neridomus involuta, B. kachchhensis, Obornella wuerttembergensis, Lamelliphorus cf. ornatissimus, Hayamia bajocensis, Emarginula (Tauschia) jumarensis, Colpomphalus jumarense	Leptomaria	Late Bathonian
			Riselloidea tagore*, R. pileiformis, R. biarmata, Amphitrochus angulatus, Helicacanthus chanda, O. kutchensis, Emarginula karuna, Hayamia bajocensis, Neritopsis (Neritopsis) patchamensis, Globularia khadirensis, Colpomphalus jumarense	Riselloidea	
Middle Bathonian	Pietteia	Pietteia sp.*, Ampullina sp. A, Amphitrochus sp., Ptygmatis sp., Ampullina sp. B	Pietteia sadharaensis*, Bhujnerita bhattii, Neritopsis (Neritopsis) benoisti, Pseudomelania calloviensis, Ampullospira brevispira	Pietteia	Middle Bathonian

Table 3 (continued)

Jaisalmer basin			Kutch basin		
Age	Zones	Major gastropods		Zones	Age
Early Bathonian	No gastropods	No gastropods	No gastropods	No gastropods	Early Bathonian
Bajocian	No zones	Turreted gastropod	No gastropods	No gastropods	Bajocian
	No gastropods	No gastropods	*Turbinea khadirensis**, *Pseudomelania (Oonia)* sp.	*Turbinea*	
	Nerinea	*Nerinea* sp.*, *Pseudomelania* sp., *Volutilithes* sp.	*Katosira bajocensis**, *K.* sp., *Pseudomelania* sp.	*Katosira*	
	No gastropods	No gastropods			

1832; *Hayamia* Kase 1980; *Globularia* Swainson 1840, have their first appearance here, while the genus *Turbinea* Pchelintsev 1965 and *Pseudomelania* Fischer 1886 continue from the lower horizons, although they are rare (Jaitly and Szabo 2007).

The *Leptomaria* zone is equivalent to the upper part of the Late Bathonian Chrysoolithicus biozone in Kutch and is marked by the appearance of several pleurotomariid genera: *Leptomaria* Eudes-Deslongchamps 1864; *Bathrotomaria* Cox 1956; *Anodomaria* Szabo 1980 and *Obornella* Cox 1959. Their representative species are *Leptomaria asurai* Das et al. 2005 (Index species); *L. simplex* Jaitly et al. 2000; *L.* sp. Jaitly et al. 2000; *Bathrotomaria waageni* Das et al. 2005; *B. reticulata* Sowerby 1821; *B. siebereri* Jaitly et al. 2000*; B. kachchhensis* Jaitly et al. 2000; and *Obornella wuerttembergensis* Sieberer 1908 (Table 3). Among them, *L. asurai* appeared in the previous zone but shows great abundance in this zone and is described from the upper Late Bathonian units of Jumara dome from where the zonal index ammonite species *Macrocephalites chrysoolithicus* (Waagen) has been described. This zone is defined by the top common of the species *L. asurai*. Few other genera like *Proconulus*, *Hayamia*, etc., which appeared early in the previous horizons, also continued (Das et al. 1999).

Pictavia **and** *Pleurotomaria* **zone (Early Callovian)**: The *Pictavia* zone (Family Ampullinidae) is equivalent to the Formosus zone and is described by six species of the subgenus *Pictavia* Cossmann 1925: *Ampullospira* (*Pictavia*) *bajocensis* Orbigny 1852; *A.* (*Pictavia*) cf. *pyramidata* Morris and Lycett 1851; *A.* (*P.*) *lorierei* Orbigny 1852; *A.* (*P.*) *tanganyicensis* Cox 1965; *A.* (*P.*) aff. *tanganyicensis* Cox 1965 and *A.* (*P.*) sp. Szabo and Jaitly 2004 (Table 3). The index species *A.* (*P.*) *bajocensis* first appeared in the previous *Leptomaria* zone but became very abundant in this zone, indicating the top common biozonation scheme for this interval. The associated ammonites (*Macrocephalites semilaevis* Spath 1928*, M. dimerus* Waagen 1875, etc.) of the horizon from where the specimens are collected indicate the lower Early Callovian age. Few other species, like *Kosmomphalus reticulates* Fischer 2001; *Naricopsina cornelia* Laube 1868; *Spinigera compressa* Orbigny 1850; *Bourgetia saemanni* Oppel 1856 and *Trochactaeonina ventricosa* Orbigny 1852 (Szabo and Jaitly 2004; Jaitly and Szabo 2007), are also recognized from this zone.

The *Pleurotomaria* zone is characterized by the first appearance of the genus *Pleurotomaria* Defrance 1826 (Family Pleurotomariidae) along with *Pygotrochus* Fischer 1885, and *Discohelix* Dunker 1848. *Pleurotomaria (Pleurotomaria) keeraense* Das 2008 is the only species which is restricted within the stratigraphic range of this zone and indicates the late Early Callovian age. The zone is defined by the range of the species *P. (P.) keeraense*. Many other associated species are also present within this zone (see Table 3). *K. reticulates*; *N. cornelia*; *S. compressa*; *B. saemanni*; and *T. ventricosa* (Szabo and Jaitly 2004; Jaitly and Szabo 2007) of the previous zone are also prolonging their range up to this zone.

Buckmanina **zone (Middle Callovian)**: The *Buckmanina* zone of Kutch is marked by the first appearance of the genus *Buckmanina* Cossmann 1920 (Family Trochidae). This record comes from both Anceps and Reissi zone of Jana et al. (2005), which is Middle Callovian in age based on the time diagnostic ammonites species. The index species, *Buckmanina bhakriensis* Das 2004, shows abundance and is restricted within

the Middle Callovian zone. Other associated genera are *Bathrotomaria*, *Anodomaria, Procunulus* Cossmann 1918, *Trochopsidea* Wenz 1938, and *Calliostoma* Swainson 1840 (Table 3). The first appearance and abundance of *Buckmanina bhakriensis* is the main characteristic of this zone.

Adeorbisina zone (**Late Callovian**): This zone is characterized by the assemblages of three taxa: *Adeorbisina* sp. Jaitly et al. 2000; *Ringicula* sp. Jaitly and Szabo 2007; and *Palaeohydatina* sp. Jaitly and Szabo 2007 (Table 3). The lithology of the horizon where the species are distributed as well as the associated ammonites indicate the Late Callovian age within the Jumara Formation. The genus *Adeorbisina* Greco 1899 (Family Ataphridae) shows a global occurrence during the Middle Jurassic and is marked as an index genus of this zone (Paleobiology Database). Other existing genera are *Bathrotomaria, Pygotrochus, Kosmomphalus, Pleurotomaria, Ampullospira, Globularia*, etc.

Eucyclus zone (**Early and Middle Oxfordian**): The Early to Middle Oxfordian horizon of Kutch is characterized by the four species of *Eucyclus* Eudes-Deslongchamps 1860 (Family Eucyclidae) (Tables 2 and 3). They are *Eucyclus tramauensis* Alberti et al. 2013; *E. laevijugatus* Quenstedt 1884; *E.* aff. *laevijugatus* Quenstedt 1884; and *E.* sp. Among them, the index species *E. tramauensis* is very abundant and restricted within the range of this zone. The zone is specified by the range and abundance of the species *E. tramauensis*. Based on ammonites, this time horizon is divided into three biozones; in comparison, only one gastropod biozone so far can be established (Tables 1 and 2). Most of the collections are made from the Dhosa Oolite Member and Dhosa Conglomerate Bed, which also comprise several ammonites pointing to the Early to Middle Oxfordian age. Besides, many genera like *Bathrotomaria, Ataphrus, Bourgetia*, *Discohelix, Hayamia, Leptomaria, Obernella, Anodomaria,* and *Indomaria* and their several species are also recorded from that horizon (Alberti et al. 2013 and references therein).

Turritella zone (**Late Oxfordian**): This zone within the Dhosa Oolite Member is equivalent to the Bifarcatus zone and comprises of a rich, distinct and dominant assemblage of *Turritella sensu stricto*, *T. jadavpuriensis* Mitra and Ghosh 1979 (Das et al. 2018). Here, gastropods are represented by 12 new genera, including *Turritella* (Bardhan et al. 2021). The assemblage, other than *T. jadavpuriensis*, includes 25 species and the most common species among them are as follows: *T. amitava* Das et al. 2018, *T. jhuraensis* Mitra and Ghosh 1979, *Gyrodes mahalanobisi* Das et al. 2019, *Euspira jhuraensis* Das et al. 2019, *Leptomaria daityai* Das et al. 2005, *Bathrotomaria buddhai* Das et al. 2005, *Paracerithium* sp. (newly collected species and provisionally described by us), and *Ampullina* sp. (newly collected species and provisionally described by us). This time interval is marked by the range and abundance of the species *T. jadavpuriensis*.

Chartronella zone (**Tithonian**): The genus *Chartronella* Cossmann 1902 (Family Paraturbinidae) made its first appearance in the uppermost Jurassic horizons of Kutch and represented by two species, *C. mundhanensis* Das and Bardhan 2010 and *C. lakhaparaensis* Das and Bardhan 2010 (Table 3). The zone is designated by the crossover abundance between these two *Chartronella* species. The associated ammonites taxa of both species mark the range of the genus as well as the range of this zone

up to the Jurassic—Cretaceous System boundary (Shome et al. 2004 and references therein). Ammonites biostratigraphy indicates six biozones, while we can propose only one based on gastropods taxa (Tables 1 and 2). Two other species, i.e. *Obornella lakhaparaensis* Das 2007 and *Talantodiscus* sp. (newly collected species and provisionally described by us) also show their occurrences in this Tithonian zone of Kutch.

4.2 Jaisalmer Basin

The gastropods of the Jaisalmer Basin are not as rich as found in Kutch Basin. A recent collection of some gastropods, along with previously published literature from Jaisalmer (Supplementary Table 1) prompted us to propose a new biozonation based on gastropod data. A detailed systematic study of those gastropod species is under preparation. The distribution of gastropods recorded from the Lower to Upper Jurassic sediments of the Jaisalmer Basin is shown in Tables 2 and 3 (also, Supplementary Table 1). Like Kutch, any gastropod biozone for the Early Bathonian and Kimmeridgian horizons of Jaisalmer have not been proposed due to devoid of any gastropods taxa. This also applies in the case of Late Bathonian and Late Callovian horizons of that basin.

Nineazone **(Bajocian)**: This Bajocian succession of Jaisalmer is known only by the abundance of the genus *Nerinea* Defrance 1825 (Family Nerineidae). Along with *Nerinea*, two more genera, i.e. *Volutilithes* Swainson 1831 and *Pseudomelania* are also co-occurring in this zone and are represented by one species each (Table 3). This zone is devoid of any ammonite, but the presence of the typical Bajocian coral, *Isastraea bernardiana* (d'Orbigny), in the upper part of the zone indicates that the upper age limit of the zone should be Bajocian (Pandey et al. 2012). The upper part of the zone also consists of shell concentrations with nerineid gastropods and bivalves along with characteristics coral (Pandey et al. 2012, 2014).

Some turreted gastropods have been found from the Bajocian Joyan Member of Jaisalmer Formation (Pandey et al. 2014), but the specimens are not well preserved. Therefore, we could not assign any separate gastropod biozone for this member (Table 2).

Pietteiazone **(Middle Bathonian)**: The *Pietteia* zone (Family Aporrhaidae) is characterized by the species *Pietteia* sp. collected from the Fort Member of Jaisalmer Formation (Tables 2 and 3). The species is restricted within this time interval, which is also supported by the previously published literature and designated the zone as a range zone. The genus *Ptygmatis* Sharpe 1850 which occurs here, has not so far been recorded from the Jurassic sediments of Kutch. On the other hand, two more genera, i.e. *Amphitrochus* Cossmann 1907 and *Ampullina* Bowdich 1822, which are described here, appeared in the Kutch basin in the Late Bathonian and Oxfordian horizons, respectively (Table 3). The stratigraphic position of this zone is above the Bajocian Joyan Member and the lower Late Bathonian Bada Bag Member and associated ammonite, *Clydoniceras* sp. indicates Middle Bathonian age.

Pleurotomaria **zone (Early Callovian)**: This zone is marked by the first appearance of the genus *Pleurotomaria* from the Kuldhar Nala section of Jaisalmer (Tables 2 and 3). The presence of associated ammonites suggests the Early Callovian age for the present zone. The range of the index species *Pleurotomaria* sp. restricted within this zone and specified the zone as Range zone.

Single gastropod fragment and some turriform gastropods (Sharma and Pandey 2016) have been recorded from the Middle Callovian and Early to Middle Oxfordian successions of Jaisalmer, respectively. We failed to assign any generic affinity for those gastropods due to poor preservation, so the time units are devoid of any gastropod biozone (Tables 2 and 3). Likewise, the Late Oxfordian sedimentary succession in Jaisalmer is represented by the presence of nerineid gastropods along with other taxa like ammonites, bivalves, and brachiopods, etc. (Pandey et al. 2012, 2014). The nerineid gastropods of this horizon are aligned on hard bedding planes and it is very difficult to collect them. Therefore, we could not assign any gastropod biozone for this Late Oxfordian time unit (Table 3). The same is also true for the Tithonian Bhadasar Formation, where we have found some broken specimens (Table 3).

4.3 Interbasinal Correlation Based on the New Scheme

The stratigraphic distributions of gastropod genera in two basins are provided in Table 3. As evident, gastropods are mostly present in Kutch Basin from the Bajocian to the Tithonian, based on which 12 gastropod zones have been proposed (Table 2). In contrast, the Jurassic succession of the Jaisalmer Basin contains less number of gastropod specimens. Consequently, many of the gastropods zones cannot be recognized in the Jaisalmer basin due to the lack of proper zonal gastropods. In the present study, an attempt has been made to correlate biozones from the Jurassic sediments between these two basins (Tables 2 and 3). Age-wise comparisons of biozones are provided below.

In both basins, the oldest Jurassic gastropods came from the Bajocian. For this time bin, we established *Katosira* and *Turbinea* zones in the Kutch Basin and recognized *Katosira bajocensis* and *Turbinea khadirensis* as index fossils, respectively, for these zones (Table 2). The equivalent time interval in the Jaisalmer Basin has been divided into *Nerinea* gastropod zone based on the index genus *Nerinea* (Table 2). At Jaisalmer, the index genus *Nerinea* comes from the Thaiat Member, which has been largely correlated with the Narewari Wandh Sandstone Member of Kutch Basin (Pandey et al. 2009, 2014). Narewari Wandh Sandstone Member has *Turbinea* biozones. Both members have similar lithology, i.e. cross-bedded calcareous sandstone (Fürsich et al. 2013; Pandey et al. 2014). Even the index genera—*Turbinea* in Kutch and *Nerinea* in Jaisalmer—belong to the same family, i.e. Nerineidae (Tables 2 and 3). Therefore, the *Nerinea* zone in Jaisalmer can precisely be correlated with the *Turbinea zone* in the neighboring Kutch Basin by their characteristic lithology and faunal content. Because of the cementing nature of most of the Odania Member

in Jaisalmer, outcrops are very limited. The upper part of the Odania Member is condensed with concretions (occasional), wood fragments, and tree trunks. This member is highly comparable with Dingy Hill Member in Kutch from where the genus *Katosira* is recorded. Both members have marine sediments but the Odania Member does not contain fossils.

The Early Bathonian sediments of both basins are devoid of any gastropod specimens (Table 3). Therefore, it was not possible to propose any gastropod-based biozone for this interval. The sedimentary successions of the Middle Bathonian in Kutch Basin are noticeable by the first appearance of *Pietteia sadharaensis* from the Goradongar Yellow Flagstone Member, and based on this, the *Pietteia* biozone for this time unit is proposed. The same genus *Pietteia* is also present in the Middle Bathonian Fort Member of the Jaisalmer Basin (Table 3). Therefore, the Middle Bathonian sedimentary successions of both basins are highly comparable. Like the Early Bathonian, the Jaisalmer Basin is devoid of any time-diagnostic gastropod from the Late Bathonian, therefore barring from raising any gastropod zone (Table 3). However, in Kutch, two gastropod biozones, *Riselloidea* and *Leptomaria* zones, have been proposed for this time unit.

The Early Callovian sequence of the Kuldhar Nala section in Jaisalmer Basin also shows a correlation with the Early Callovian sequence of the Jumara Formation in Kutch by the presence of the index genus *Pleurotomaria* in both the basins (Table 3). The biozone scheme is the same for the Early Callovian sequence of both basins and indicated by the range of the respective index species of the zone. From the Middle Callovian up to the Oxfordian, the absence of proper zonal gastropod fossils in Jaisalmer once again barred us from proposing any biozone for these intervals. In comparison, these time units in Kutch Basin are well established by several gastropod zones—*Buckmanina* zone for the Middle Callovian, *Adeorbisina* zone for the Late Callovian, *Eucyclus* zone for the Early to Middle Oxfordian, and *Turritella* zone for the Late Oxfordian (Table 2). Therefore, no interbasinal comparisons were possible. These discrepancies in gastropod distributions in Jaisalmer related to transgression-regression: a lesser amount of sediments deposit, habitat restriction due to marine regression and distinct facies change, e.g. from a carbonate sedimentary regime in the Bathonian to a siliciclastic regime in the Callovian, can be related to the disappearance of gastropod distributions in Jaisalmer (pers. obser.).

The Kimmeridgian time unit in both basins has no gastropods (Table 3). Few fragmentary gastropod specimens are recorded from the Kimmeridgian unit in Kutch Basin. Due to poor preservation, we could not assign any particular genus for those gastropod specimens, and no such gastropod zones were determined for this time unit. Once again, the Jaisalmer Basin does not have any Tithonian gastropods, although the equivalent horizons in Kutch Basin have been assigned as *Chartronella* zone (Table 2); therefore, it was not possible to correlate these two basins using gastropod-based biozone.

5   Discussion and Conclusions

Kutch and Jaisalmer are the two adjacent sedimentary basins situated at the western margin of the Indian plate, having similar Jurassic sediment deposits and associated diverse fossil assemblages. Due to many transgression-regression couplets, both basins were inundated, preserving several common litho and biostratigraphic marker horizons. Because of this cyclic sedimentary depositional pattern observed in both basins, the same environments came out repeatedly and were occupied with taxa of the same generic but different species composition (Fürsich et al. 2001; Pandey et al. 2010). Based on these litho and biostratigraphic similarities, many authors tried to correlate these two basins using the established ammonite-based biozones supplemented by lithofacies characters (Krishna 1987; Pandey et al. 2009, 2012, 2014). Ammonite-based biostratigraphy provides fine-scale stratigraphic division and helps in establishing a regional and intercontinental correlation with other areas (Bardhan et al. 2002; Jana et al. 2005; Roy et al. 2019).

However, there are several problems in performing this interbasinal correlation. For example, the Jurassic sedimentary successions of the Jaisalmer Basin are less complete than the Kutch Basin (Pandey et al. 2009, 2014; Biswas 2016), which may be due to its shelf basin structure. In comparison, the Kutch Basin is a rift basin, and characteristically is more open and allowing greater accommodation space (Pandey et al. 2009). As a consequence, sediments deposited in the Jaisalmer Basin during transgressive events are not much thick (maximum up to 1 m) than the neighboring Kutch Basin (rarely 10–15 m; Fürsich et al. 2001; Pandey et al. 2012). Moreover, the deposited sediments in the Jaisalmer Basin may frequently be interrupted by the phase of erosion (Fürsich et al. 2001). This might also explain why the Jaisalmer Basin is less fossiliferous than the neighboring Kutch Basin. Some Jurassic time units lack any characteristic ammonite fossils, barring from classifying these time units into corresponding ammonite biozones. Therefore, although ammonites are good for zonal correlation, other independent schemes are required for further verification and classification, but the use of other fossils groups like foraminifera, brachiopods, ostracods, etc., are very limited in success. Here, we propose an independent biozone scheme based on gastropods. Gastropods, whenever present in these basins, are abundant and, like ammonites, show basinal endemism.

Based on the newly gastropod-based biozonation scheme, we so far established 12 gastropod biozones against 26 ammonites biozones in the Kutch Basin and three gastropod biozones against 19 biozones in Jaisalmer (Tables 2 and 3). These established gastropod biozones from various stratigraphic sections of both the basins reveal the existence of coeval biozones at a certain level in the Kutch and Jaisalmer basins. However, at least for the lower part of the Jurassic, gastropod-based biozones are effective in fine-tuning the preexisting ammonite-based biozones and using it to correlate the two basins; the same may not be true for the latter part of the Jurassic. Here, we discuss time-wise comparisons of gastropod biozones in these basins in the context of the existing ammonite-based biozones to highlight the importance of our present contribution.

The Late Bajocian time unit of Kutch Basin is demarcated by the *Leptosphinctes* sp. biozone (Singh et al. 1982; Krishna 1987), but lack of any proposed ammonite biozone in Jaisalmer (Table 1), made difficult for interbasinal correlation for this interval. Here, we have subdivided the Bajocian time unit into two gastropod biozones—*Katosira* and *Turbinea* zones in Kutch, and one, i.e. *Nerinea* zone in Jaisalmer. As discussed above, the *Turbinea* and *Nerinea* biozones are paleontologically and lithostratigraphically similar. Therefore, they can be considered for fine-scale within-basin correlation. This is an important contribution of the present work.

Unfortunately, for the Early Bathonian, no gastropods are present in both basins (Table 3). This is also true for ammonoids in case of Jaisalmer Basin, but one biozone i.e. Zigzag zone has been proposed for lower Early Bathonian sediments of Kutch Basin (Table 1). This may be because of regression mainly due to a drop in sea levels. The younger Middle Bathonian time interval has comparable gastropod biozone (i.e. *Pietteia*) in both basins (Tables 2 and 3), allowing correlation between two basins. However, the absence of any ammonite species in Jaisalmer Basin, except *Clydoniceras* sp., from this time interval made it difficult for proper time-dependent correlation of the Middle Bathonian horizons of these basins, and our proposed gastropod biozone offers an excellent solution of this problem.

For the Late Bathonian, although two gastropod biozones (i.e. *Riselloidea* and *Leptomaria*) have been proposed for Kutch, the absence of any gastropod species from the Jaisalmer Basin barred any interbasinal correlation. This time interval of both basins is subdivided into two ammonite zones—Triangularis and Chrysoolithicus zone in Kutch, and Triangularis and Congener zone in Jaisalmer (Table 1) and this ammonite-based biozonation scheme is more preferable for the Late Bathonian succession. The underlying Fort Member and overlying Kuldhar Member in Jaisalmer both contain gastropod fossils, so the absence of gastropods in the intermediate Bada Bag Member (Late Bathonian) may be due to the preservation artefacts. The Early Callovian time interval, however, can be correlated between two basins based on the proposed gastropod biozone, *Pleurotomaria* (Tables 2 and 3). The proposed gastropod biozone increases the finer refinement of the preexisting ammonites based biozonation. The Middle to Late Callovian, once again, shows a complete absence of gastropods fossils (except single gastropod fragment

from Middle Callovian) in the Jaisalmer Basin barred any interbasinal comparison, although the same time interval has several established biozones in the Kutch Basin (Tables 2 and 3). The ammonite rich Middle to Late Callovian time units has been remarkably resolved and refined in both basins into several ammonites zones (Four zones: Anceps, Reissi, Athleta, Lamberti for Kutch and three zones: Anceps, Gigantea, *Properisphintes* for Jaisalmer).

The Early to Middle Oxfordian time interval of both basins has been subdivided into three distinct ammonite biozones (i.e. Mariae, Cordatum, and Plicatilis-Transversarium for Kutch Basin and Semirugosus, *Mayaites*, and *Dichotomoceras* for Jaisalmer Basin) (Table 1). In gastropod biostratigraphy, only one zone, i.e. *Eucyclus* zone, has been proposed for Kutch and no such zones have been preferred for Jaisalmer due to the proper zonal gastropods. The diverse ammonite-rich lithofacies may suggest this gastropods inconsistency of this time interval (pers. obs.) and characteristic ammonite-based biozonation scheme may refine this time units. One gastropod zone (*Turritella* zone) has been identified for the Late Oxfordian interval of Upper Jurassic in the Kutch Basin, is equivalent to the Bifarcatus ammonite zone. Few nerineid gastropods are recorded from the Late Oxfordian sedimentary succession of Jaisalmer but not collectible due to alignment within the hard bedding planes. So, the time unit is lack of any gastropod biozones but contain *Dichotomoceras* ammonite zone. The ammonite-based biostratigraphy is the only choice for interbasinal corrections of this time interval.

In ammonite-based biostratigraphy, the Kimmeridgian time unit in both basins is subdivided by several ammonite biozones except the lower part of the Early Kimmeridgian (Table 1). In comparison, the time unit is barren with respect to gastropods, only except a few fragmentary specimens recorded from Kutch (pers. obs.). Therefore, biozonation of this interval based on gastropods cannot be performed and the classic ammonite-based scheme is the only viable option. During the Early Oxfordian, sediments were deposited very rapidly due to transgression. As evidence in this event, several tiny ammonite species are discovered from the Kimmeridgian horizons of Kutch. This may be the cause of this rarity in gastropods fossils during this time interval. After this transgression event, a complete erosion occurs in the sequence, which is termed as Middle Oxfordian-Early Kimmeridgian "submarine gap" by Krishna et al. (2009). Due to this, a large stratigraphic gap occurs in the Mainland of Kutch in between Dhosa Oolite Member of Jumara Formation and the Lower Member of Jhuran Formation. On the other hand, the presence of anoxia in Kutch- Jaisalmer Sea during this Oxfordian- Kimmeridgian boundary (Mukherjee 2015) possibly create a stressful environment that became very unfavorable for gastropods.

The Tithonian time unit in Kutch has been well-known by six ammonite biozones but based on gastropods, only one biozone is proposed. The marine Tithonian part is mainly restricted in the mainland of Kutch and contains few sparse specimens of gastropods. The index genus *Chartronella* of this time unit, ranging from the Early Tithonian up to the Jurassic–Cretaceous System boundary, is very abundant. Thus, only one gastropod biozone so far established for the Tithonian time unit. This time interval in both basins has been best studied and resolved based on ammonites, which have resulted in the whole Tithonian unit into six ammonite zones (see Table 1).

Supplementary Table 1

Stratigraphic distribution of Jurassic gastropods along with precise lithology of the horizons from the Jaisalmer Basin. Associated ammonite biozonation are also mentioned. The table is based on Das Gupta (1975), Pareek et al. (1977), Jodhawat (1984), Pandey and Choudhary (2007), Pandey et al. (2006, 2010, 2012, 2014), Pandey and Pooniya (2015), and Sharma and Pandey (2016), supplemented by additional collections (marked as *) made by us. "No ammonites" and "No gastropods" indicate time interval devoid of any ammonite and gastropod species, respectively. "No zones" states the time interval cannot be subdivided into ammonite biozones

Formation	Member	Age	Ammonite zone	Index ammonites	Gastropods	Lithology and geographic locality of gastropods bearing horizons
Bhadasar	Kolar Dungar	Late Tithonian	Himalayites	Himalayites aff. seideli	Unidentified broken gastropods	Sandstone and limestone exposed at about 1 km north of the Bhadasar ridge section
			Denseplicatus	Virgatosphinctes denseplicatus		
		Early Tithonian	Communis	Virgatosphinctes communis	Unidentified gastropod fragments*	Limestone exposed at Bhadasar ridge (both sides of the road towards Krishnagarh*)
			Kobelliforme	Hildoglochiceras kobelliforme		
			Virgatosphinctoides	Katroliceras virgatosphinctoides		
			Pottingeri	Katroliceras pottingeri		
Baishaki	Lanela	Late Kimmeridgian	Katrolensis	Katroliceras katroliceras	No gastropods	
	Ludharwa	Middle Kimmeridgian	No zones	Torquatisphinctes aff. alterneplicatus, Pachysphinctes aff. major, P. bathyplocus, Aulacosphinctes,		
	Rupsi	Early Kimmeridgian	Alterneplicatus	Torquatisphinctes aff. alterneplicatus		
			No ammonites	No ammonites		
		Late Oxfordian	Dichotomoceras	Dichotomoceras spp.	Nerineid gastropods*	Limestones present in the north of the Rupsi village
	Basal					

(continued)

(continued)

Formation	Member	Age	Ammonite zone	Index ammonites	Gastropods	Lithology and geographic locality of gastropods bearing horizons
Jaisalmer	Jajiya	Middle Oxfordian	*Mayaites*	*Mayaites* spp.	Turriform gastropods; unidentified gastropod fragments*	Oolitic limestone exposed at Jajiya river section, Jajiya scarp and about 1 km west of Kuldhar nala-section*
		Early Oxfordian	Semirugosus	*Peltoceratoides semirugosus*		
	Kuldhar	Late Callovian	*Properisphintes*	*Properisphintes* sp.	No gastropods	
		Middle Callovian	Gigantea	*Collotia gigantea*	Unidentified gastropod fragment*	Silty marls with oolitic limestone present about 4 km northwest of Kuldhar River Section*. Also about 2 km east of Kudhara Abandoned village*
			Anceps	*Reineckeia anceps*		
		Early Callovian	*Subkossmatia opis*	*Subkossmatia opis*	*Pleurotomaria* sp.*	Limestone show in the Kudhar Nala Section and Kudhar River Section*
			Formosus	*Macrocephalites formosus*	Unidentified gastropod fragment*	Silty marls with oolitic limestone exposed at the Kudhar River bed* (near the Kuldhar Abandoned well)
	Bada Bag	Late Bathonian	Congener	*Sivajiceras congener*	No gastropods	
			Triangularis	*Macrocephalites triangularis*		

(continued)

(continued)

Formation	Member	Age	Ammonite zone	Index ammonites	Gastropods	Lithology and geographic locality of gastropods bearing horizons
	Fort	Middle Bathonian	Clydoniceras sp.	Clydoniceras sp.	Turriform and turbinate gastropods. Pietteia sp.*, Ampullina sp. A*, Amphitrochus sp.*, Ptygmatis sp.*, and Ampullina sp. B*	Limestone at Fort Wall Section
					Pietteia sp.*, Ampullina sp. A*	Limestone at Fort Hill Section
		Early Bathonian	No ammonites	No ammonites	No gastropods	
	Joyan	Bajocian			Turreted gastropods	Limestone and sandstones exposed at about 4 km southeast of Jaisalmer and about 2 km north of the Jaisalmer Fort*
	Hamira				No gastropods	
Lathi	Thaiat				Nerineid gastropods; Nerinea sp.*, Volutilithes sp.*, and Pseudomelania sp.*	Sanstone at the southeast of the Thaiyat Village and near the Thaiyat Stop* (Right side of the Jaisalmer-Jaipur road)

(continued)

(continued)

Formation	Member	Age	Ammonite zone	Index ammonites	Gastropods	Lithology and geographic locality of gastropods bearing horizons
					Nerinea sp.*, *Volutilithes sp.*	Limestone present near the Thaiyat Stop* (Right side of the Jaisalmer-Jaipur road)
	Odania				No gastropods	

References

Agrawal SK, Pandey DK (1985) Biostratigraphy of the Bathonian-Callovian Beds of Gora Dongar in Pachchham"Island", district Kachchh (Gujarat). Proc Indian Natl Sci Acad 51:887–903

Alberti M, Pandey DK, Fürsich FT (2011) Ammonites of the genus *Peltoceratoides* Spath, 1924 from the Oxfordian of Kachchh, western India. N Jb Geol Paläont Abh 262:1–18

Alberti M, Nützel A, Fürsich FT, Pandey DK (2013) Oxfordian (Late Jurassic) gastropods from the Kachchh Basin, western India. N Jb Geol Paläont Abh 270:275–300

Andreu B, Colin JP, Singh J (2012) Middle and Upper Jurassic ostracods from western Kachchh, Gujarat, India: Biostratigraphy and palaeobiogeography. Gond Res 22:1110–1124

Arkell WJ (1951–1958) Monograph of English Bathonian Ammonites. Palaeontol Soc Monogr. London, Palaeontogr Soc:viii+264

Backman J, Raffi I, Rio D, Fornaciari E, Pälike H (2012) Biozonation and biochronology of Miocene through Pleistocene calcareous nannofossils from low and middle latitudes. Newsl Stratigr 45:221–244

Bardhan S, Datta K (1987) Biostratigraphy of Jurassic Chari Formation: a study in Keera Dome, Kutch, Gujarat. J Palaeontol Soc India 30:121–131

Bardhan S, Sardar SK, Jana SK (2002) The Middle Jurassic *Kheraiceras* Spath 1924 from the Indian Subcontinent. In: Summesberger H, Histon K, Daurer A (eds) Cephalopods-Present and Past. Abh Geol B-A 57:265–277

Bardhan S, Saha S, Das SS, Saha R (2021) Paleoecology of naticid–molluscan prey interaction during the Late Jurassic (Oxfordian) in Kutch, India: evolutionary implications. J Paleontol. https://doi.org/10.1017/jpa.2021.24

Bayle E (1878) Atlas I, Fossiles principaux des terrains. Memo pour servir a I'explication de la Carte Geolog detail France 4:158

Biswas SK (1977) Mesozoic rock stratigraphy of Kutch. Quart J Geol Min Met Soc India 49:1–2

Biswas SK (1991) Stratigraphy and sedimentary evolution of the Mesozoic basin of Kutch, western India. In: Tandon SK, Pant CC, Casshyap SM (eds) Sedimentary basins of India: tectonic context. Gyanodaya Prakashan, Nainital, pp 74–103

Biswas SK (2016) Mesozoic and tertiary stratigraphy of Kutch (Kachchh)–a review. In: Thakkar MG (ed) Recent studies on the geology of Kachchh. Spec Pub Geol Soc India 6:1–24

Blake JF (1905) Fauna of the Cornbrash. Monogr Palaeontol Soc, London 1–106

Bowdich E (1822) Elements of conchology including the fossil genera and the animals. Part 1, Univalves. Treuttel & Würtz, London, p 83

Buckman SS (1909–1930) Yorkshire Type Ammonites, vol 1–2, Type Ammonites, vol 3–7. Wheldon & Wesley, London, p 541

Chaudhuri A, Banerjee S, Le Pera E (2018) Petrography of Middle Jurassic to Early Cretaceous sandstones in the Kutch Basin, western India: implications on provenance and basin evolution. J Palaeogeogr 7:2–14

Chaudhuri A, Banerjee S, Chauhan G (2020a) Compositional evolution of siliciclastic sediments recording the tectonic stability of a pericratonic rift: Mesozoic Kutch Basin, western India. Mar Pet Geol 111:476–495

Chaudhuri A, Das K, Banerjee S, Fitzsimons ICW (2020b) Detrital zircon and monazite track the source of Mesozoic sediments in Kutch to rocks of Late Neoproterozoic and Early Palaeozoic orogenies in northern India. Gond Res 80:188–201

Chaudhuri A, Chatterjee A, Banerjee S, Ray JS (2020c) Tracing multiple sources of sediments using trace element and Nd isotope geochemistry: provenance of the Mesozoic succession in the Kutch Basin, western India. Geol Mag. https://doi.org/10.1017/S0016756820000539

Chaudhuri A, Banerjee S, Prabhakar N, Das A (2020d) The use of heavy mineral chemistry in reconstructing provenance: a case study from Mesozoic sandstones of Kutch Basin (India). Geol Jour. https://doi.org/10.1002/gj.3922

Cossmann M (1900) Rectifications de nomenclature. Revue Critique de Palaeozoologie 4:42–46

Cossmann M (1907) Le Barrémien supérieur à faciès urgonien de Brouzet-les-Alais (Gard). Description des gastropodes et pélécypodes. Mém Soc géol France, 15:42

Cossmann M (1909) Essais de paléoconchologie comparée, 8. The author and de Rudeval, Paris, p 248

Cossmann M (1918) Essais de paléoconchologie comparée, 11. The author, Paris, p 388

Cossmann M (1921) Essais de paléoconchologie comparée, 12. The author, Paris, p 348

Cossmann M (1924) Essais de paléoconchologie comparée, 13. Presses Universitaires de France, Paris, p 345

Cox LR (1956) A new genus of Mesozoic Pleurotomariidae. Proc Malacol Soc London, 32:79

Cox LR (1959) Diagnoses of two new genera of Mesozoic Pleurotomariidae. Proc Malacol Soc London, 33:235

Cox LR (1965) Jurassic Bivalvia and Gastropoda from Tanganyika and Kenya. Bull br Mus Nat Hist Supp 1:213

Das SS (2002) Two new pleurotomariid (Gastropoda) species, including the largest *Bathrotomaria*, from the Berriasian (Early Cretaceous) of Kutch, western India. Cret Res 23:99–109

Das SS (2004) New assemblage of the Mesozoic gastropod faunas of Kutch, western India–a study of systematics, palaeobiogeography and evolution. Unpublished PhD thesis, Jadavpur University

Das SS (2007) Record of a new species of Obornella Cox 1959 (Gastropoda) from the Tithonian of Kutch, western India. J Asian Eart Sci 30:207–212

Das SS (2008) Gastropod diversity patterns and evolutionary tempo during the early rifting phase (Jurassic) of the Kutch Basin. J Palaeontol Soc India 53:9–18

Das SS, Bardhan S (2010) Evolution and extinction of Chartronella (Gastropoda): acase study from the uppermost Jurassic of Kutch, India. In:Abstract Volume of 17th International Congress of Unitas Malacologica (World Congress of Malacology) 18–24 July 2010, Phuket, Thailand. Trop Nat Hist, Suppl 3:124

Das SS, Lahiri TC, Bardhan S (1998) A life's window from the Middle Jurassic of Kutch, Gujarat—a new assemblage of gastropods. Geol Surv India News 29:21–22

Das SS, Bardhan S, Lahiri TC (1999) The Late Bathonian gastropod fauna of Kutch, western India—a new assemblage. Paleontol Res 3:268–286

Das SS, Bardhan S, Kase T (2005) A new pleurotomariid gastropod assemblage from the Jurassic sequence of Kutch, western India. Paleontol Res 9:329–346

Das SS, Saha S, Bardhan S, Mallick S, Allmon WD (2018) The oldest turritelline gastropods: from the Oxfordian (Upper Jurassic) of Kutch, India. J Paleontol 92:373–387

Das SS, Mondal S, Saha S, Bardhan S, Saha R (2019) Family Naticidae (Gastropoda) from the Upper Jurassic of Kutch, India and a critical reappraisal of taxonomy and time of origination of the family. J Paleontol 93:673–684

Das Gupta SK (1975) A revision of the Mesozoic-Tertiary stratigraphy of the Jaisalmer Basin, Rajasthan. Indian J Earth Sci 2:77–94

Defrance MJL (1825) Nériné. Dictionnaire des Sciences Naturelles, Tome 34. Levrault, Strasbourg-Paris 462-464

Defrance MJL (1826) In: Blainville HMDe, Manuel de malacologie et de conchyologie: Levrault, Paris:1–664

Desai BG (2012) Trace fossils from Kaladongar Formation exposed in Kuar Bet, Patcham Island, Kachchh Basin, India. J Palaeontol Soc India 57:53–59

Desai BG (2013) Ichnological analysis of transgressive marine tongue in the prograding delta system: evidences from Ukra Hill Member, western Kachchh, India. J Geol Soc India 82:143–152

Desai BG, Biswas SK (2018) Postrift deltaic sedimentation in western Kachchh Basin: insights from ichnology and sedimentology. Palaeo Palaeo Palaeo 504:104–124

Dunker W (1848) Ueber die in der Molasse bei Günzburg unfern Ulm vorkommenden Conchylien und Pflanzenreste. Palaeontographica (1846–1933):155–168

Eudes-Deslongchamps E (1860) Observations concernant quelques gastéropodes fossiles des terrains jurassiques. Bull Soc Linn Normandie 5:119–148

Eudes-Deslongchamps E (1863–1869) Notes Paléontologiques. Le Blanc-Hardel, Caen and Savy, Paris, p 392

Fischer P (1880–1887) Manuel de conchyliologie et de paléontologie conchyliologique. Savy, Paris, p 1369

Fischer JC (2001) Study of the gastropods. In: Fischer JC, Le Nindre IM, Manivit J, Vaslet D Jurassic gastropod faunas of central Saudi Arabia. GeoArabia 6:63–100

Fürsich FT, Oschmann W (1993) Shell beds as tools in basin analysis: the Jurassic of Kachchh, western India. J Geol Soc 150:169–185

Fürsich FT, Oschmann W, Jaitly AK, Singh IB (1991) Faunal response to transgressive-regressive cycles: example from the Jurassic of western India. Palaeo Palaeo Palaeo 85:149–159

Fürsich FT, Oschmann W, Singh IB, Jaitly AK (1992) Hardgrounds, reworked concretion levels and condensed horizons in the Jurassic of western India: their significance for basin analysis. J Geol Soc India 149:313–331

Fürsich FT, Pandey DK, Callomon JH, Oschmann W, Jaitly AK (1994) Contribution to the Jurassic of Kachchh, western India. II. Bathonian stratigraphy and depositional environment of the Sadhara Dome, Pachchham Island. Beringeria 12:95–125

Fürsich FT, Pandey DK, Callomon JH, Jaitly AK, Singh IB (2001) Marker beds in the Jurassic of the Kachchh Basin, western India: Their depositional environment and sequence-stratigraphic significance. J Palaeontol Soc India 46:173–198

Fürsich FT, Alberti M, Pandey DK (2013) Stratigraphy and palaeoenvironments of the Jurassic Rocks of Kachchh: field guide. Beringeria Spec Iss 7:1–174

Garg R, Singh SK (1986) *Singhamina* and *Tandonina*, new foraminiferal genera–evidence for Discorbid lineage from the Middle Jurassic of Jaisalmer, western Rajasthan, India. J Palaeontol Soc India 31:52–62

Grateloup JPS (1832) Description of a new kind of shell, called Neritopsis. Proc Iinneenne Bordeaus Soc 5:125–131

Greco B (1899) Fauna della zona a Lioceras opalinum Rein. sp. di Rossano in Calabria. Paleontogr Ital. 4:93–139

Grossouvre AD (1917) Étude sur le groupe des Peltoceras toucasi et transversarium. Note sur des fossiles nouveaux rares ou peu connus de l'Est de la France. Vesoul 53–65

Hébert M, Eudes-Deslongchamps E (1860) Mémoire sur les fossiles de Montreuil-Bellay (Maine-et-Loire), 1st partie. Céphalopodes et Gastéropodes. Bull Soc Linn Normandie 5:153–240

Hyatt A (1900) Cephalopoda. Zittel, KA: Text book of Palaeontology 502–592

Jain S (2012) Integrated biostratigraphy and palaeoenvironment of the Middle Jurassic sediments at Kuldhar (Jaisalmer), Western India. J Palaeontol Soc India 57:1–41

Jain S (2014) The Arkelli Chronozone: a new early middle Bathonian standard ammonite zone for Kachchh, western India (southern Jurassic Tethys). Zitteliana A54:91–135

Jain S, Pandey DK (2000) Middle Jurassic ammonite biozonation in Kachchh, western India. Bull India Geol Ass 33:1–12

Jain S, Garg R (2012) Biostratigraphic implications of the record of genus *Himalayites* from the Late Tithonian sediments of Jaisalmer, western India. J Palaeontol Soc India 57:105–111

Jaitly AK, Szabó J (2002) *Bhujnerita* (Neritidae), a new gastropod genus from the Kachchh Jurassic (western India). Fragm Palaeont Hung 20:49–52

Jaitly AK, Szabó J (2007) Contributions to the Jurassic of Kachchh, western India. The gastropod fauna. Part III: further Caenogastropoda and Opisthobranchia. Fragm Palaeont Hung 24:77–82

Jaitly AK, Szabó J, Fürsich FT (2000) Contributions to the Jurassic of Kachchh, western India. VII. The gastropod fauna. Part I. Pleurotomarioidea, Fissurelloidea, Trochoidea and Eucycloidea. Beringeria 27:31–61

Jana S, Bardhan S, Halder K (2005) Eucycloceratin ammonites from the Callovian Chari Formation, Kutch, India. Palaeontology 48:883–924

Jodhawat RL (1984) A study of Bivalvia from the Jurassic beds of Jaisalmer, Rajasthan. Unpublished PhD thesis, University of Rajasthan, Jaipur

Kachhara RP, Jodhawat RL (1981) On the age of Jaisalmer Formation. Indian Colloq Micropaleontol Stratigraphy, Rajasthan, India, p 247

Kase T, Maeda H (1980) Early Cretaceous Gastropoda from the Chosi district, Chiba Prefrecture, central Japan. Trans & Proc Palaeonta Soc Japan, New Ser, 118:291–324

Kauffman EG, Sageman BB, Kirkland JI, Elder WP, Harries PJ, Villamil T (1993) Molluscan biostratigraphy of the Cretaceous Western Interior Basin, North America. In: Caldwell WGE, Kauffman EG (eds) Evolution of the Western Interior Basin. Geol Ass Canada Spec Pap 39:397–434

Khosla SC, Jakhar SR, Kumari M (2009) Atlas of the Middle Jurassic ostracods from western India. Palaeontol Soc India, pp 1–167

Krishna J (1987) An overview of the Mesozoic stratigraphy of Kachchh and Jaisalmer basins. J Palaeontol Soc India 32:136–149

Krishna J (2017) The Indian Mesozoic chronicle. Springer, Singapore

Krishna J, Pathak DB (1991) Ammonoid biochronology of the Upper Jurassic Kimmeridgian stage in Kachhchh, India. J Palaeontol Soc India 36:1–13

Krishna J, Ojha JR (1996) The Callovian ammonoid chronology in Kachchh (India). GeoRes Forum 1(2):151–166

Krishna J, Pathak DB, Pandey B (1996) Quantum refinement in the Kimmeridgian ammonoid chronology in Kachchh (India). GeoRes Forum 1(2):195–204

Krishna J, Pandey B, Ojha JR, Pathak DB (2000) Ammonoid-foraminifer zonal integration in the Jurassic of Kachchh, India. Bull ONGC 37:9–21

Krishna J, PandeyB Ojha JR, Pathak DB (2009) Reappraisal of the age framework, correlation, environment and nomenclature of Kachchh Mesozoic lithostratigraphic units in Wagad. J Sci Res 53:1–20

Laube GC (1868) Die Gastropoden der braunen Jura von Balin. Denkschr. Kaiserl. Akad. Wiss, 28:1–28

Mitra KC, Bardhan S, Bhattacharya D (1979) A study of Mesozoic stratigraphy of Kutch, Gujarat with special reference to rock-stratigraphy of Keera dome. Bull Indian Geol Assoc 12:129–143

Mitra KC, Ghosh DN (1979) Jurassic Turritellas from Kutch, Gujarat. Quart J Geol Min Met Soc India 51:119–122

Morris J, Lycett J (1851) A monograph of the Mollusca from the Great Oolite, Chiefly from Minchinhampton and the Coast of Yorkshire. Part 1, Univalves. Palaeontogr. Soc., London:viii + 130

Mukherjee D (2015) Diversity dynamics of the Jurassic Brachiopod fauna of Kachchh and Jaisalmer Basins, India. J Palaeontol Soc India 60:1–9

Mukherjee D, Bardhan S, Datta K, Ghosh DN (2003) The terebratulid *Kutchithyris* (Brachiopoda) from the Jurassic sequence of Kutch, western India-revisited. Paleontol Res 7:111–128

Murphy MA, Salvador A (1999) International stratigraphic guide-an abridged version. Episodes 22:255–271

Oppel A (1856) Die Juraformation Englands, Frankrechs und des südwestlichen Deutschland. Jahresh. Ver. vaterl. Naturkd. Württemberg, 12, p 121

Orbigny Ad' (1850–60) Pale´ontologie francaise, terrains jurassiques. Tome. 2, Gastropodes, 621 p., atlas, pls. 235–428. Masson, Paris

Pandey J, Dave A (1993) Studies in Mesozoic Foraminifera and chronostratigraphy of Western Kutch, Gujarat. Palaeontogr Indica 1:1–221

Pandey B, Krishna J (2002) Ammonoid biostratigraphy in the Tithonian (Late Jurassic) of Jaisalmer, western India. Geophytol 30:17–25

Pandey DK, Choudhary S (2007) Sequence stratigraphic framework of Lower to lower Middle Jurassic sediments of the Jaisalmer Basin, India. Beringeria 37:121–131

Pandey B, Pathak DB (2015) Record of Early Bathonian ammonoids from Kachch, India: biostratigraphic and paleobiogeographic implications. J Palaeontol Soc India 60:33–44

Pandey DK, Pooniya D (2015)Sequence stratigraphy of the Oxfordian to Tithonian sediments (Baisakhi Formation) in the Jaisalmer Basin. Vol Jurassica 13:65–76

Pandey DK, Fürsich FT, Sha J (2009) Interbasinal marker intervals—a case study from the Jurassic basins of Kachchh and Jaisalmer, western India. Sci China Ser D Earth Sci 52:1924–1931

Pandey DK, Sha J, Choudhary S (2010) Sedimentary cycles in the callovian-oxfordian of the Jaisalmer Basin, Rajasthan, western India. Vol Jurassica 8:131–162

Pandey DK, Choudhary S, Bahadur T, Swami N, Sha J (2012) A review of the Lower—lowermost Upper Jurassic lithostratigraphy of the Jaisalmer Basin, western Rajasthan, India-an implication on biostratigraphy. Vol Jurassica 10:61–82

Pandey DK, Fürsich FT, Alberti M (2014) Stratigraphy and palaeoenvironments of the Jurassic Rocks of the Jaisalmer Basin: field guide. Beringeria Spec Iss 9:1–111

Pandey DK, Fürsich FT, Alberti M, Sharma JK, Swami N (2018) Recurrent hardgrounds and their significance for intra-basinal correlations: a case study of upper Bathonian rocks from the western margin of the Indian craton. J Palaeogeogr 7:14. https://doi.org/10.1186/s42501-018-0013-3

Pchelintsev VF (1965) Murchisoniata Mezozoia Gornogo Kryma. [Mesozoic Murchisoniata of the Crimean highlands]. Nauka, Moskva, p 216

Prasad S (1998) Ammonite biozonation of the Middle-Late Jurassic sediments with special reference to Keera and Jara Dome, Kachchh District, Gujarat. J Palaeontol Soc Ind 52:25–40

Prasad S (2006) Ammonite biostratigraphy of Middle to Late Jurassic rocks of Jaisalmer Basin, Rajasthan, India. Mem Geol Surv India 52:1–146

Prasad S, Jain RL, Srivastava MS (2007) Record of Middle Jurassic (Bathonian) ammonite genus *Clydoniceras* Blake from Jaisalmer Basin, western Rajasthan. J Palaeontol Soc India 69:53–56

Pareek HS, Rao M, Laul VP (1977) First record of Golden Oolite from Badesar Formation, Jaisalmer Basin, Rajasthan. Curr Sci 46:302–303

Quenstedt FA (1881–1884) Petrefaktenkunde Deutschlands. Band 7. Gastropoden. Leipzig (Fues), p 867

Rai J, Jain S (2013) Pliensbachian nannofossils from Kachchh: implications on the earliest Jurassic transgressive event on the western Indian margin. Zitteliana 53:105–120

Roman F (1933) Note sur le Bathonien infe´rieur du Djebel-es-Sekika pre‘s Nemours (De´part. d'Oran). Bull. Soc. géol. France, 5:59–73

Roy P, Bardhan S, Mitra A, Jana SK (2007) New Bathonian (Middle Jurassic) ammonite assemblages from Kutch, India. J Asian Earth Sci 30:629–651

Roy A, Banerjee S, Bardhan S (2019) Peltoceratinae (Ammonoidea) from the upper Callovian–lower Oxfordian of Kutch, India: systematic revision and biostratigraphic implication. Geobios 56:1–30

Sharma JK, Pandey DK (2016) Taxonomy of late Bathonian-Oxfordian ammonites from the Jaisalmer Basin: implications for intrabasinal litho-and biostratigraphic correlations. J Palaeontol Soc India 61:249–266

Sharpe D (1850) On the secondary district of Portugal which lies on the North of the Tagus. Quart J Geol Soc 6:135–195

Shome S, Bardhan S (2005) Record of a new species of Erymnoceras Hyatt, 1900 (Ammonoidea) from the Middle Jurassic of eastern Kutch, India and its stratigraphic and evolutionary significance. J Asian Earth Sci 25:679–685

Shome S, Bardhan S (2009) The genus *Umiaites* Spath, 1931 (Ammonoidea) from the Tithonian (Late Jurassic) of Kutch, western India. Palaeontologia Electronica 12:1–10

Shome S, De S, Roy P, Das SS (2004) Ammonites as biological stopwatch and biogeographical black box—a case study from the Jurassic-Cretaceous boundary (150 Ma) of Kutch, Gujarat. Curr Sci 86:197–202

Sieberer X (1908) Die Pleurotomarien des schwa¨bischen Jura. Palaeontographica 54:1–68

Siemiradzki JV (1898–1999) Monographic description of the ammonite group Perisphinctidae. Palaeontographia 45:69–296

Singh CSP, Jaitly AK, Pandey DK (1982) First report of some Bajocian-Bathonian (Middle Jurassic) ammonoids and the age of the oldest sediments from Kachchh, Western India. Newsl Stratigr 11:37–40

Spath LF (1924) On the Blake collection of ammonites from Kachh (India). Palaeontol Indica, Geol
  Surv Ind, New Ser 9:1–129
Spath LF (1927–1933) Revision of the Jurassic cephalopod fauna of Kachh (Cutch). Palaeontol
  Indica, Geol Surv India, New Ser 9:1–945
Swainson W (1831) Zoological Illustrations or original figures and description of new, rare or
  interesting animals. Baldwin & Cradock, London 2:46–85
Swainson W (1840) A Treatise on Malacology; or, Shells and Shell-Wsh. London, p 419
Szabó J (1980) Lower and Middle Jurassic gastropods from the Bakony Mountains (Hungary).
  Part II., Pleurotomariacea and Fissurellacea (Archaeogastropoda). Annls hist-nat Mus natn Hung
  72:49–71
Szabó J, Jaitly AK (2004) Contributions to the Jurassic of Kachchh, western India. VIII. The
  gastropod fauna. Part II: Discohelicidae, Neritomorpha, Caenogastropoda. Fragm Palaeont Hung
  22:9–26
Talib A, Gaur KN (2008) Foraminiferal composition and age of the Chari Formation, Jumara Dome,
  Kutch. Curr Sci 95:367–373
Waagen W (1869) Die Formenreihe des Ammonites subradiatus: Versuch einer paläontologischen
  Monographie. R. Oldenbourg
Waagen W (1873–1875) Jurassic fauna of Kutch. The Cephalopoda. Mem Geol Surv India.
  Palaeontol Indica Ser 9, 1:1–27
Wenz W (1938–1944) Teil 1: Allgemeiner Teil und Prosobranchia. In: OH Schindewolf, ed.,
  Handbuch der Paläozoologie, Band 6, Gastropoda. Borntraeger, Berlin:xii + 1639
Wynne AB (1872) Memoir on the Geology of Kutch. Mem Geol Surv India 9:1–293
Zittel KA (1884) Cephaloda. Handbuch der Palaontologie 1:329–522

Diagenetic Controls on the Early to Late Bathonian Fort Member Sandstone of Jaisalmer Formation, Western Rajasthan

Faiz Ahmad, A. H. M. Ahmad, and Sumit K. Ghosh

Abstract Petrographic analysis, Scanning Electron Microscopy (SEM) and X-ray diffraction (XRD) were used to examine the various diagenetic controls on reservoir quality of the Fort Member Sandstone (FMS), Jaisalmer Formation in western Rajasthan. Diagenetic processes include mechanical compaction, cementation, pressure solution and dissolution of framework grains. The main diagenetic cements are carbonate, ferruginous, silica cement and authigenic clays. Cements occur as coatings around the detrital grain boundaries, pore fillings and pore linings. Compaction and cementation are common factors responsible for the reduction of porosity and permeability. The dissolution of detrital feldspar grains was the main drive for porosity enhancement in the FMS. The corroded contacts between successive carbonate phases and quartz grains, followed by the dissolution of carbonate cements were also responsible for the secondary porosity. The main porosity preservation in the FMS is due to scattered patches of carbonate cement, which prevented the compactional collapse of the framework. The relationship between the intergranular volume (IGV) and cement volume indicates a minor role of compaction in destroying the primary porosity. The widespread occurrences of carbonate cement suggest that the FMS lost a significant amount of primary porosity at an eodiagenetic stage. In addition to carbonate, authigenic clays like chlorite and kaolinite occur as pore-filling and pore-lining cements. The pore-filling chlorite resulted in a considerable loss of porosity, while the pore-lining chlorite may have helped in retaining the porosity by preventing the precipitation of syntaxial silica overgrowths. Paragenetic sequences are established to understand the pathways of diagenetic evolution and their impact on reservoir quality of the FMS.Please check and confirm if the authors and their respective affiliations have been correctly identified. Amend if necessary.Confirmed the respective authors affiliations and correctly identified.

F. Ahmad · A. H. M. Ahmad (✉)
Department of Geology, Aligarh Muslim University, Aligarh 202002, India
e-mail: ahmahmad2004@yahoo.com

Present Address:
S. K. Ghosh
Wadia Institute of Himalayan Geology (WIHG), 7 Kalimandir Enclave, G M S Road, Dehradun 248001, India

1   Introduction

The relationship between diagenesis and reservoir quality is well recognized and much of our awareness about the sandstone diagenesis has advanced from studies comprising reservoir property evolution and quality prediction (Wilson and Stanton 1994; Jeans 2000; Quasim et al. 2019). The reservoir quality of sandstone can be critically influenced by the detrital compositions, which modify the pathway of both physical and chemical diagenesis (Bloch 1994). Variations in intra-formational detrital composition can cause significant diversity in reservoir quality. Compositional changes respond to variations in climate, depositional setting and especially provenance. Parameters influencing the reservoir quality are framework composition, texture and physico-chemical processes. Porosity controls the quality of oil and gas reserves. These properties, in turn, are controlled by the primary depositional texture and post-depositional processes during burial diagenesis. The final geometry of pore structure, grain orientation and packing, and the degree of cementation and clay fillings of pore spaces are also controlled by the burial diagenesis (Slatt 2006).

Recently, the Rajasthan Shelf is upgraded to category-1 (producing) basin due to the latest commercial discoveries in the Barmer-Sanchor Basin, which increases the possibilities of finding potential hydrocarbons in other adjoining basins too. Various geological aspects such as lithostratigraphy, biostratigraphy, sedimentology and petrography have already been studied in the Jaisalmer Basin and the publications include lithostratigraphy (Oldham 1886; Pareek 1984), tectonic framework (Ghosh 1952), biostratigraphy (Richter-Bernberg and Schott 1963), geophysical investigations (Rao 1972), depositional environment (Pandey et al. 2012; Bhat and Ahmad 2013; Ahmad et al. 2017a), tectono-provenance (Ahmad et al. 2019), diagenetic evolution (Mahendra and Banerji 1990; Ahmad et al. 2017b). However, the impact of diagenesis on reservoir quality is poorly known. Ahmad et al. (2017b) investigated the diagenetic evolution of the Fort Member Sandstone (FMS) and established the features of mesodiagenetic stages. This present study is based on the comprehensive fieldwork and measured litho-sections of FMS to provide details about the diagenetic evolution of Fort Member in space and time. The purpose of this study is to evaluate the potential controls on FMS diagenesis by petrographical and mineralogical analysis.

2   Geological Setting

Rajasthan peripheral foreland basin covers (Fig. 1a), 1,20,000 km^2 areas. It occurs on the west of the Aravalli Craton up to the Pakistan border (Biswas et al. 1993). It is a
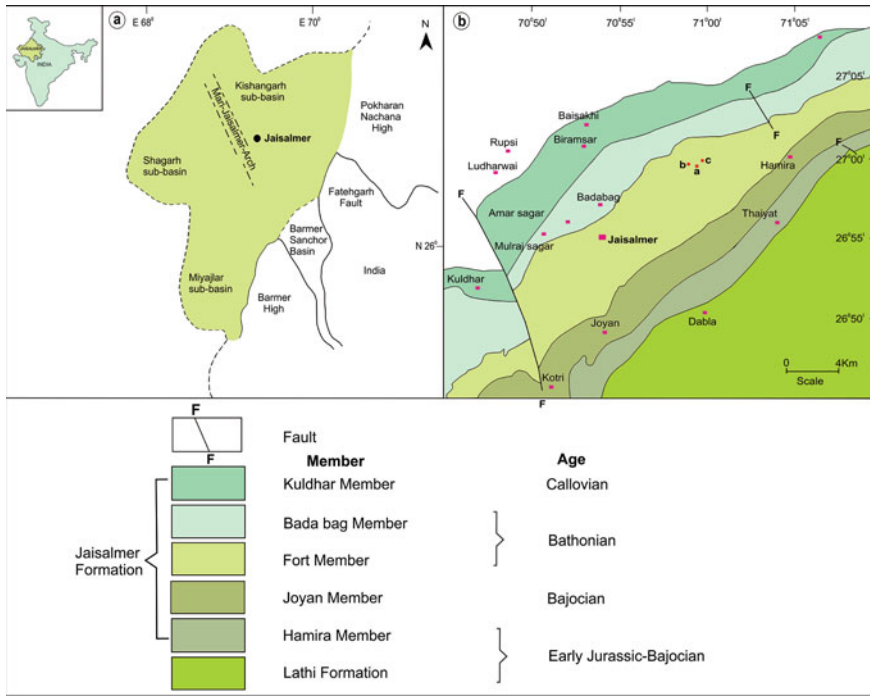
Fig. 1 **a** Tectonic map of the Jaisalmer Basin (after Biswas 1982; Misra et al. 1993); **b** Geological map of the Jaisalmer Formation, western Rajasthan, showing the study area (after Jodhawat and Kachhara 2000)

part of the Indus foreland basin and is divided into four sub-basins (Fig. 1a): Jaisalmer basin (JB) on the northwestern slope of the Jaisalmer-Mari basement arch (JMA), Bikaner-Nagaur (BN) basins on the northeast, Shahgarh-Miajlar (SM) basin southwest and Barmer-Sanchor (BS) basins south of the arch. The raised JMA extends through the central part of the basin with a NW-SE trend and separates the Kishangarh sub-basin in the north from the Shahgarh sub-basin in the south. The Mesozoic sediments of the Jaisalmer Basin begin with non-marine fluvial, deltaic or lacustrine sediments followed by marginal marine sediments, which in turn followed by a sequence of several non-marine, marginal marine and fully marine deposits (Mahender and Banerji 1989; Pandey et al. 2006a, b; Ahmad et al. 2017a). The rocks of Jaisalmer Basin are underlain by Precambrian igneous/metamorphic rocks and are important due to the fossiliferous nature (Pandey et al. 2010, 2012), hydrocarbon reserves and building stones. The Mesozoic sequence of Jaisalmer Basin consists of Lathi, Jaisalmer, Baisakhi and Bhadasar formations in ascending order and is represented by a succession of shale, siltstone, sandstone and limestone (Oldham 1886; Swaminathan et al. 1959). The Jurassic sequence of Jaisalmer Basin consists of six facies associations: (i) cross-bedded, medium- to coarse-grained sandstone, (ii) cross-bedded to thinly laminated fine-grained sandstone and siltstone, (iii) silty marl,

(iv) calcareous mud- to grainstone and sandy rudstone, (v) thinly laminated carbonaceous shale and (vi) conglomerate. These facies associations represent fluvial, floodplain, lacustrine, protected marginal marine, and shoreface to shelf environments (Pandey et al. 2012). The Jaisalmer Formation consists of 300 m thick sequences of golden-brown fossiliferous limestone, sandstone and siltstone. Jaisalmer Formation (Fig. 1b) is divided lithostratigraphically into Hamira, Joyan, Fort, Badabag, Kuldhar and Jajiya Members in ascending order of succession (Kachhara and Jodhawat 1981).

The best exposure of studied Fort Member Sandstone occurs along the escarpments of the Jaisalmer Fort. It comprises of fine- to medium-grained sandstone, oolitic sandy, bioturbated and fossiliferous limestone and cross-bedded sandy limestone (Mahendra and Banerji 1990; Ahmad et al. 2017a, 2019). The carbonate-rich part is highly fossiliferous and containing shell fragments of brachiopod, bivalves, gastropods, echinoids, corals, bryozoans, and foraminifers. Pandey et al. (2006a, b) distinguished four facies assemblages in Fort Member i.e. well-sorted, fine-grained sandstone; mixed siliciclastic-carbonate; fossiliferous, bioturbated, mixed carbonate-siliciclastics and cross-bedded packstone to grainstone facies. These facies associations show non-marine to brackish water sediments, which in turn replaced by fully marine conditions. Pandey et al. (2012) recorded a shallowing of the marine basin from below to above the fair-weather wave-base, with increasing water energy, with occasional storm actions (Pandey et al. 2012). On the basis of inter-basinal correlation of marker beds (Pandey et al. 2009), the stratigraphic position of the Fort Member is placed above the late Bajocian coral-bearing horizon of Joyan Member. The record of *Clydoniceras* (Prasad et al. 2007; Pandey et al. 2012) assigns an Early-Middle/Early-Late Bathonian age for the Fort Member.

3   Materials and Methods

The present study is based on measurement of three well-exposed lithostratigraphic sections of the Fort Member of Jaisalmer Formation: (1) near Jaisalmer Fort (Lat. 26° 92′ 97″ Log. 70° 92′ 05″), (2) near Shive Madi Darbaar (Lat. 26° 94′ 82″ Log 70° 89′ 41″) and (3) along Jaithwai road (Lat. 26° 99′12″ Log. 70° 95′ 66″). Forty representative sandstone samples were collected from the measured lithostratigraphic sections (Fig. 2) for modal analysis. Detrital and diagenetic components, pore type as well as textural attributes were determined by counting 250–400 points in each of thin sections. The point counting was carried out by using polarizing microscope (Laborlux 11 Pol 8) at Department of Geology, AMU, Aligarh, using both Gazzi-Dickinson (Dickinson 1970; Ingersoll et al. 1984) and standard methods to minimize the dependence of rock composition in grain size (Ingersoll et al. 1984).

Thin-section petrography, SEM and XRD were used to examine composition, texture, compaction, porosity, clay minerals and nature of cements. The morphology and textural relationships among minerals were examined in six, gold-coated samples using a JEOL JSM 6400 scanning electron microscope (SEM) equipped with an Energy Dispersive X-ray microanalyses (EDAX) under an accelerating voltage of
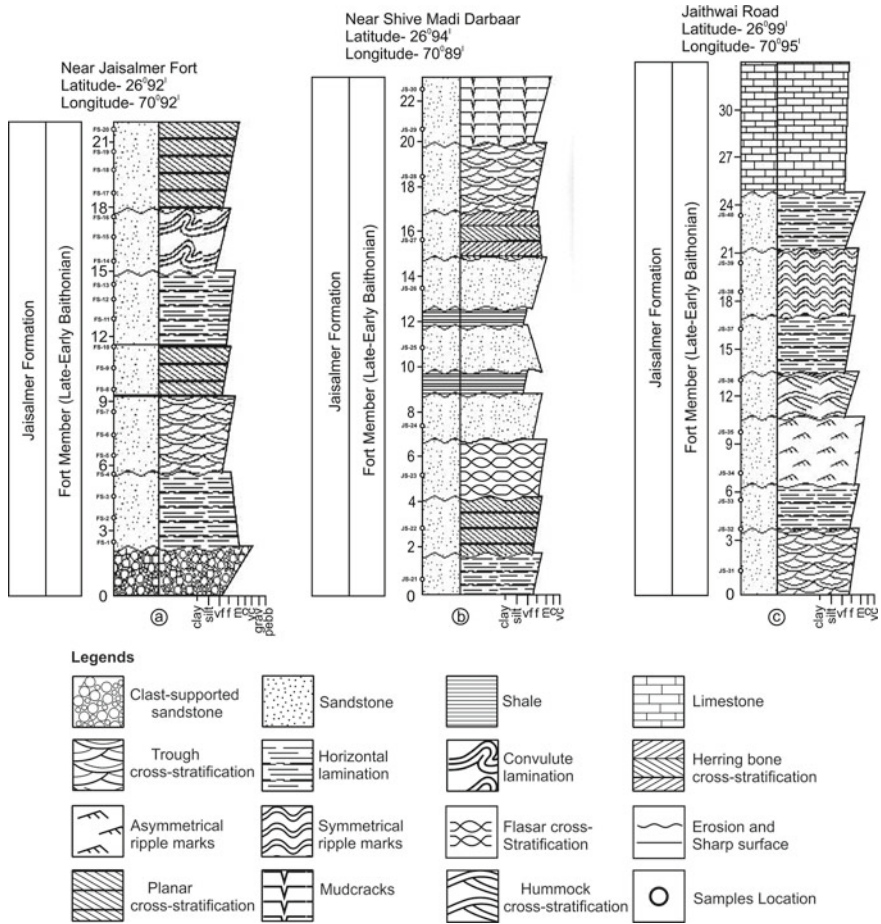
Fig. 2 Lithostratigraphic successions of the Fort Member, Jaisalmer Formation, western Rajasthan, at different localities **a** Near Jaisalmer Fort **b** Near the Shive Madi Darbaar near the Jaisalmer Fort **c** At Jaithwai Road near the Jaisalmer Fort

10 kV, at University Sophisticated Instrument Facility (USIF), AMU. SEM was used to observe the cement morphology, pore geometry, paragenetic relationships, textural attributes, clay cements, micro-porosity and secondary porosity of the sandstone samples. XRD analyses were performed using a JEOL (6400) diffractometer [Cu-Kα (λ = 1.54Å)] source at scan speed 1°/min, step size of 0.05°, and 2θ in the range 0° to 80° were opted. Clay mineralogy and clay crystallinity were studied by XRD analysis.

4 Results

4.1 *Framework Composition and Texture of the Sandstone*

The studied sandstone is predominantly composed of sub-angular to sub-rounded, fine- to medium-grained, moderate- to well-sorted grains. The sub-angular nature is found especially among the smaller grains, whereby the large grains show rounded nature (Fig. 3a). Detrital quartz (Q) is the major framework constituent. Both monocrystalline as well as polycrystalline quartz are found with dominance of the former type that commonly shows small, abraded overgrowths, which suggests their reworked, secondary cycle origin (Fig. 3b, c). Sub-angular to angular feldspar (F) content is 11%, which includes both potash- and plagioclase feldspar. The potash feldspar being more abundant than plagioclase feldspar (Fig. 3d, e). A few feldspar grains alter to clay or exhibit a honeycombed (dissolution) texture, while other
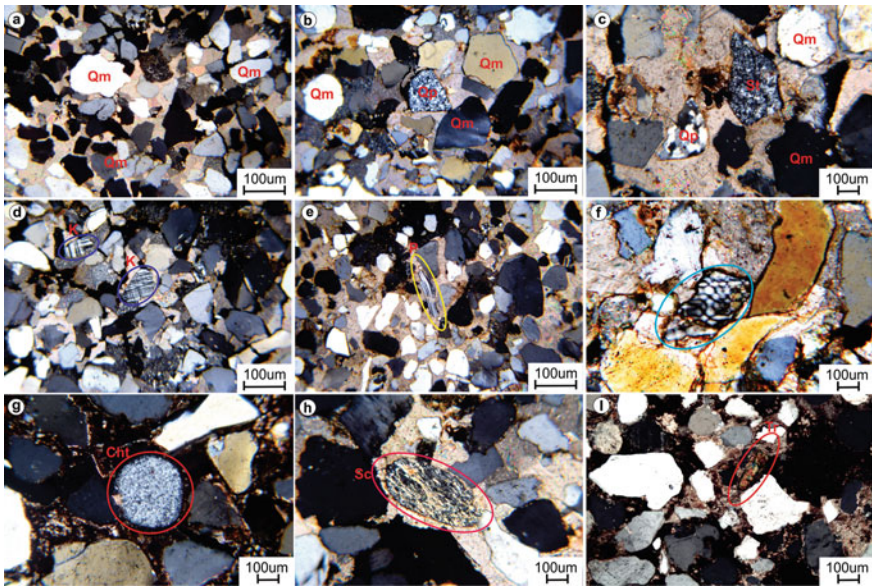
Fig. 3 Photomicrographs (under crossed polars), showing main framework grains of the FMS **a** monocrystalline quartz (Qm) are fine- to medium-grained, subangular to subrounded, moderately to well sorted and with early carbonate cementation; **b** Polycrystalline quartz (Qp) and monocrystalline quartz (Qm) grained are fine- to medium-grained, subangular to rounded, moderately to well sorted; **c** monocrystalline quartz (Qm), polycrystalline quartz (Qp) and siltstone (St) are subangular to subrounded with early carbonate cement prevented further mechanical compaction; **d** K-feldspar (K) grains with quartz detritals are well cemented with carbonate; **e** Plagioclase grain (P) and quartz are subangular to subrounded, carbonate engulfing the detrital grains; **f** honey texture of feldspar, **g** Chert (Cht) with quartz grains and iron oxide corroding the carbonate and quartz grain at their margin, **h** Schist (Sc), grain surrounded quartz grains with carbonate cement, **i** detrital Tourmaline (Tr) enclosed by moderately to well sorted quartz grains cemented by the iron oxide cement

Fig. 4 Ternary plot of FMS shows the classification and modal composition according to the McBride (1963) classification scheme
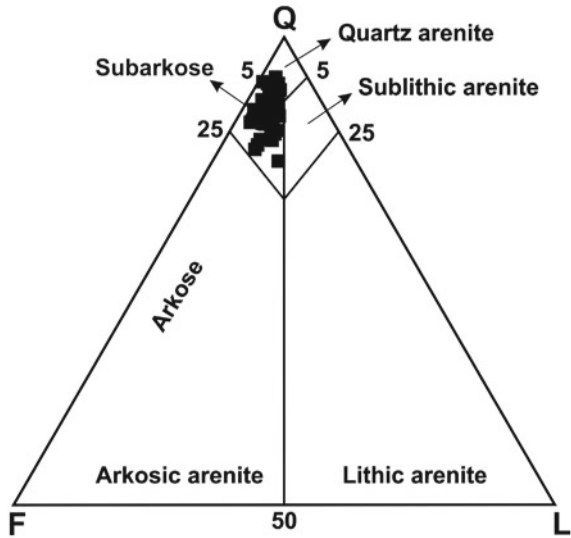
grains are partially replaced by carbonate cement (Fig. 3f). Lithic fragments include chert, shale, siltstone, schist and phyllite grains (Fig. 3c, h). Bioclasts (brachiopods, gastropods, corals and ostracods) are also observed in thin section. Heavy minerals form a minor constituent and include zircon, rutile, tourmaline and apatite minerals (Fig. 3i). The FMS of the Jaisalmer Basin is dominated by subarkose with minor quartz arenite field (Fig. 4).

4.2 Diagenetic Processes

The main diagenetic processes in the studied sandstone are mechanical compaction, cementation, and precipitation of authigenic clays, as well as the generation of secondary porosity through the dissolution of detrital and diagenetic constituents.

4.2.1 Compaction

The sandstones show low to moderate mechanical compaction during the burial as evidenced by the commonness of floating contacts (Fig. 5a). Few grains show point and long contacts (Fig. 5b). The abundance of floating contacts with very low contact index values (average 1.3%) reveals that the FMS has gone through low to moderate degree of mechanical compaction. The effect of moderate mechanical compaction is further established by the presence of minor bending of the flexible muscovite grains (Fig. 5c). Rearrangement of the detrital grains in the rock texture results in the increased number of long contacts (Fig. 5b), and brittle grain fracturing to a lesser
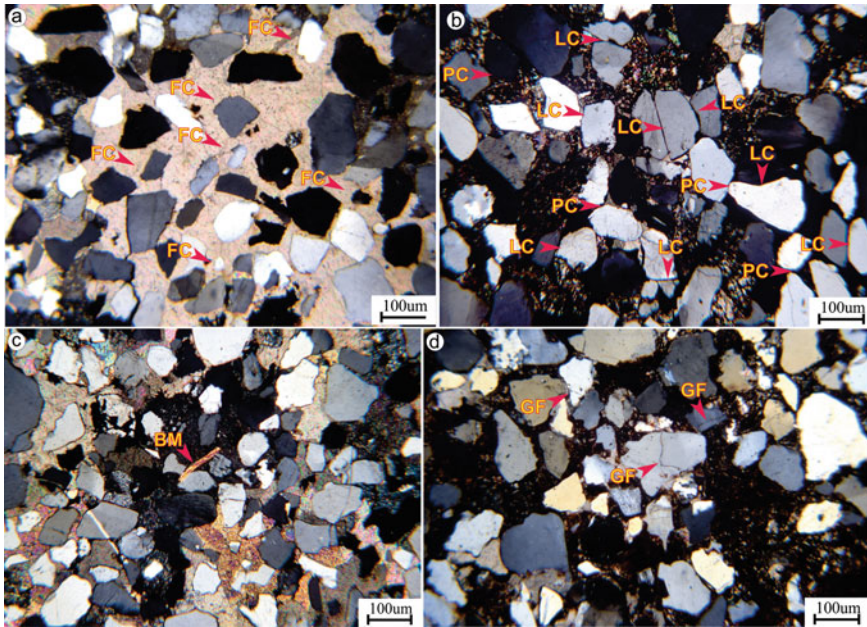
Fig. 5 Photomicrographs (under crossed polars) of FMS compaction **a** floating contact (FC) between grains indicating less mechanical compaction and early carbonate cementation; **b** point contact (PC) and long contact (LC) between quartz grains indicating moderate mechanical compaction and early carbonate cementation replaced by ferruginous cement; **c** Ductile deformation of mica grain due to mechanical compaction result in porosity reduction; **d** grains fracturing (GF) in detrital quartz grain due to compaction, resulted in the enhancement of permeability

extent (Fig. 5d). The lowest degree of mechanical compaction is observed in FMS with pre-compaction carbonate cements which stabilized the rock texture in the early diagenetic stage, preventing further compaction (Fig. 5a). In general, the FMS was less affected by the mechanical compaction, which is related to its shallow depth of burial and local precipitation of early carbonate cements.

4.2.2 Cementation

Cementation is a vital diagenetic process. Due to the fact that cement lithifies sedimentary deposits and fills up pore spaces, it has a negative effect on reservoir properties. Various types of cements are present in the FMS, which includes carbonate, ferruginous and minor silica cement in the form of silica overgrowth and authigenic clay minerals.
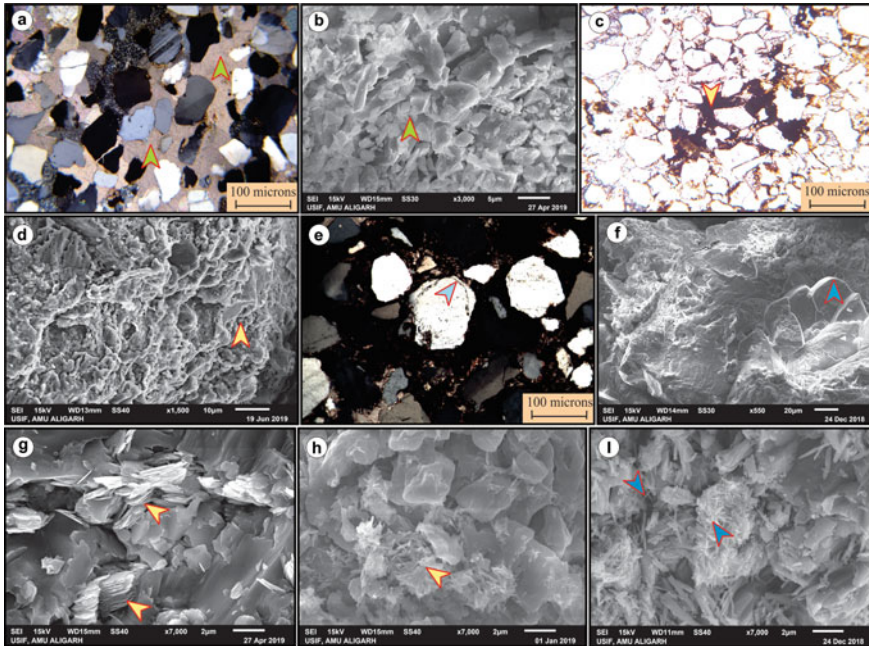
Fig. 6 Photomicrographs and SEM of the FMS **a** Carbonate cement occur as pore filling in intergranular pore resulting in reduction of porosity (under crossed polars), **b** SEM showing carbonate cements occur in pore spaces and reducing porosity, **c** Iron cement occur as pore filling and coating around detrital grains resulting in reduction of porosity (in plane polarized light), **d** SEM image showing iron oxide cement, **e** Photomicrograph showing syntaxial silica overgrowth occur as pore occluding cement and decreasing porosity and permeability (under crossed polars), **f** SEM are showing silica overgrowth, **g** book stack of kaolinite occurred as pore-filling material; **h**, **i** chlorite engulfing the pore spaces between the detritals preventing the precipitation of silica overgrowth

Carbonate Cement (CCT)

CCT is the most dominant cement in FMS, ranging from 3 to 31%, with an average of 18.9%. It occurs as crystalline poikilotopic, pore fillings and blocky patches, which partly or totally replace the detrital feldspar and quartz grains mainly around periphery (Fig. 6a). Few quartz and feldspar grains are corroded and replaced by CCT. The carbonate cement tends to corrode the quartz grain margins to produce irregular-shaped grains and most of the feldspar grains are replaced by the carbonate cements (Fig. 6a).

CCT plays a dominant role in the porosity evolution of sandstone (Alaa et al. 2000). The presence of oversized pore-filled CCT might be due to the destruction and leaching of labile framework grains, possibly feldspars, which indicate that they postdate the dissolution of feldspar or lithic fragments. CCT before compaction increased the compressive strength of sediments during the early diagenesis and inhibited compaction dramatically, but the primary pores are also filled and get

destroyed by CCT in the early stages. While it destroys the primary porosity but also dissolves the detrital mineral grains to form secondary porosity, so it has a positive effect on the reservoir quality of the sandstone. Furthermore, fine- to medium crystalline CCT are also seen in the studied sample and identified by using SEM (Fig. 6b).

Ferruginous Cement (FCT)

FCT is the second most dominating cementing material, ranging from 0 to 21.7%, with an average of 3.2%. It occurs as a coating around detrital grains, localized patches and extensive pore filling (Fig. 6c, d). In a few samples, quartz grains are corroded and enveloped by FCT. This is because of release of iron oxide through the disintegration of unstable ferromagnesian minerals during weathering and pedogenic processes. Thin iron-coating on detrital grains is perhaps inherited from the source rock. The corroded quartz grains indicate the presence of earlier carbonate cement which was replaced by FCT (Fig. 7c). The patchy distribution of FCT suggests either aborted cementation or dissolution during the uplift. Destruction and corrosion of labile framework grains (most probably feldspars) is the reason behind oversized cement. FCT seems to occur early in the diagenetic sequence before appreciable compaction (Fig. 6c) and overlapping silica growths (Fig. 6e).

Silica Cement (SCT)

The SCT ranges nil to 5.7% (average 1.9%) and occurs mainly as partial to complete syntaxial overgrowths around detrital monocrystalline quartz grains (Fig. 6e, f). The boundary between the overgrowths and detrital core is either poorly defined or demarcated by the thin clay coatings/cements rim which separates the detrital quartz from the secondary silica cement (Fig. 6e, 8e). Quartz overgrowths are most abundant in deeply buried sandstone and also in sandstones with clean quartz surfaces compared to sandstone with widespread grain-coating chloritic cements. Silica overgrowths reduced the intergranular porosity and are detrimental for reservoir quality in the study area.

4.2.3   Clay Mineral

The clay minerals range from nil to 3.2% with an average of 0.3% in FMS (Table 1). Diagenetic clay minerals exhibit a wide variety of morphology and types. Kaolinite appears to be the abundant clay mineral being present in almost all analyzed, with a few samples having illite and chlorite as the dominant clay mineral phase (Fig. 8).
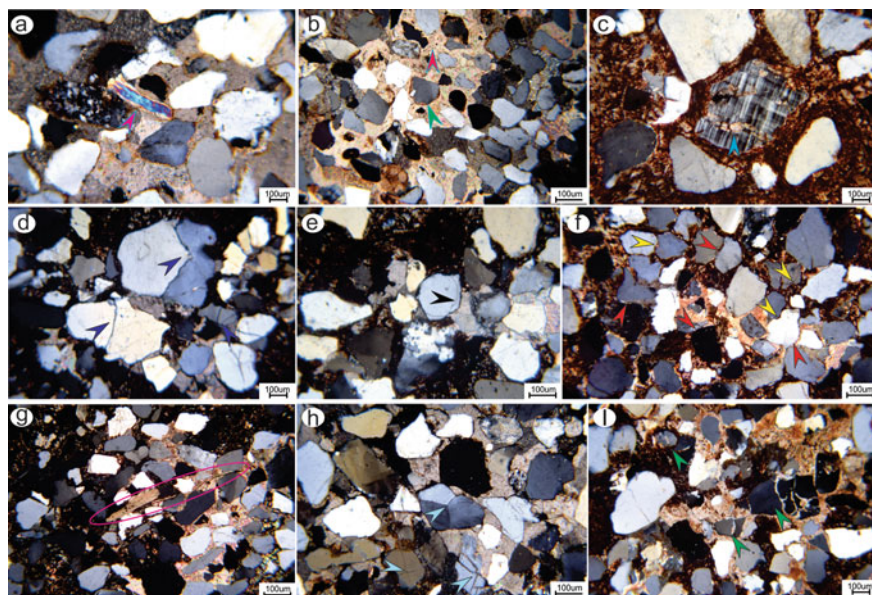
Fig. 7 Photomicrographs (under crossed polars) showing burial diagenesis: **a** muscovite (red arrow) is indicating less mechanical compaction, grains coating and early carbonate cementation in eodiagenesis stage; **b** fine- to medium-grained quartz (green arrow) coated with carbonate cement (red arrow); **c** dissolution of K-feldspar grain with carbonate and carbonate replaced by ferruginous cement and corrode the detrital grains; **d** Grain fracturing (black arrow) in detrital quartz grain due to compaction occur in mesodiagenesis stage; **e** silica overgrowth (black arrow) in the form of overgrowth; **f** suture contact (red arrow) and concave-convex contact (yellow arrow) developed between the detrital grains indicate of the pressure solution; **g** deformation of muscovite grain (red ellipsoid spherical) due to mechanical compaction and rearrangements of quartz grains occurred in mesodiagenesis stage; **h** triple junction (arrow) are developed in mesodiagenesis stage; **i** detrital grains (green arrow) are corroded by carbonate cement at their margin and carbonate cement dissolve the quartz grain

Kaolinite

Kaolinite in studied sandstone is authigenic and includes both cements and replacement of silicate framework grains and appears as pore fillings. It represents a precursor to illite. Kaolinite is present in most of the samples examined by SEM but usually in low proportions. Kaolinite is characterized by the typical booklet-like alignment of the crystal plates (Fig. 6g). It fills pores space, both primary as well as secondary ones, between grains. Kaolinite formation is dependent on sufficient porosity and permeability to allow migration of interstitial pore water of an acidic pH. The porosity and permeability, on the other hand, also provide ample space for crystal growth and presence of K-feldspar and/or muscovite as source of Al and Si.
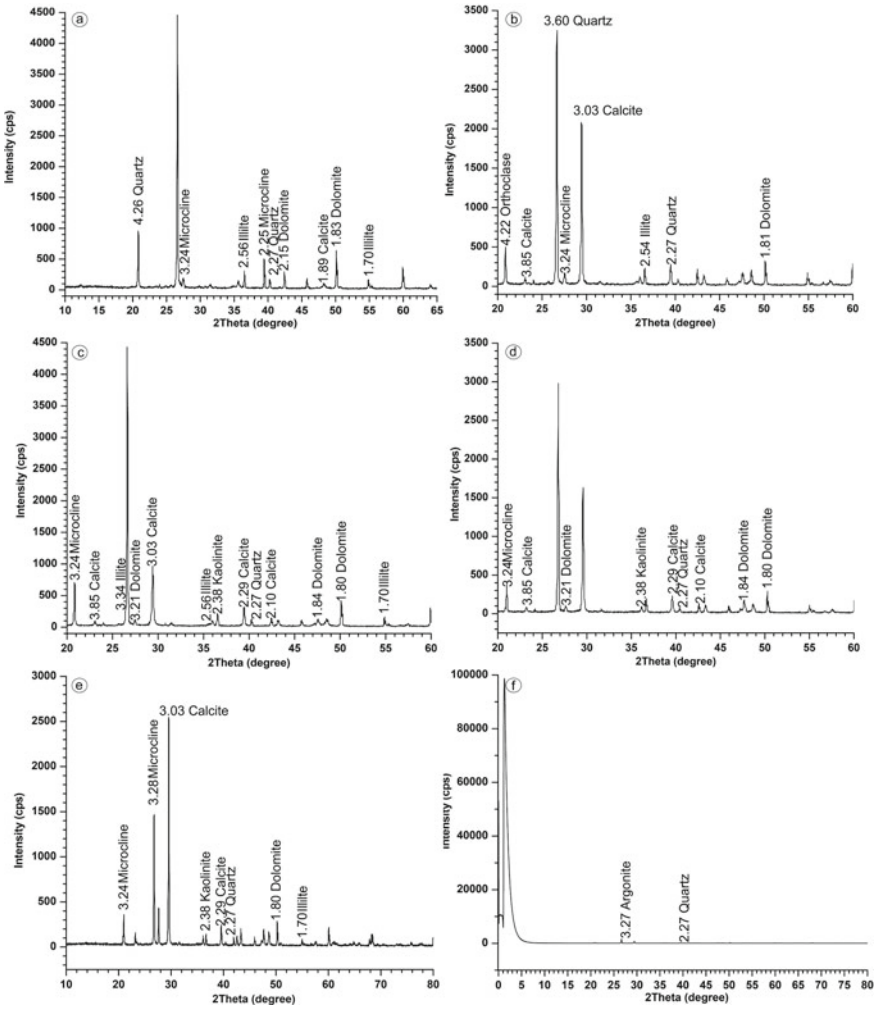
Fig. 8 X-ray diffraction (XRD) analysis of clay minerals identified in the analyzed FMS

Illite

It occurs as tangential grain coating, pore fillers and common authigenic clay mineral in the Fort Member Sandstone. Illite is fibrous in nature and occurs throughout the FMS. It forms hair- or thread-like crystal that have replaced or intergrown with authigenic or detrital clay.

Table 1 Percentages of cement and void spaces of the FMS, Jaisalmer Formation, western Rajasthan

| S. no | Detrital grain | Cements | | | | | Total cements | Existing optical porosity (EOP) | Intergranular volume (IGV) | Compactional porosity loss (COPL) | Cementation porosity loss (CEPL) | Icompact |
		Silica	Iron	Carbonate	Clay	Matrix						
FS-1	74.28	0.53	14.09	7.47	0.00	0.43	22.09	3.20	25.72	25.96	16.36	0.61
FS-2	74.05	0.71	4.05	7.14	0.00	0.48	11.90	13.57	25.95	25.72	8.84	0.74
FS-3	81.22	0.00	5.91	7.13	0.00	2.09	13.04	3.65	18.78	32.28	8.83	0.79
FS-4	68.76	2.95	12.77	8.25	0.00	0.39	23.97	6.88	31.24	20.01	19.17	0.51
FS-5	59.96	3.01	9.77	16.54	0.00	0.38	29.32	10.34	40.04	8.28	26.90	0.24
FS-6	59.03	1.94	10.29	12.62	0.00	0.00	24.85	16.12	40.97	6.83	23.16	0.23
FS-7	59.86	4.36	6.42	19.50	0.00	0.00	30.28	9.86	40.14	8.12	27.82	0.23
FS-8	75.23	0.00	21.70	3.07	0.00	0.00	24.77	0.00	24.77	26.89	18.11	0.60
FS-9	62.67	2.10	3.45	19.64	0.00	2.25	25.19	9.90	37.33	12.24	22.11	0.36
FS-10	77.78	5.79	0.93	10.65	0.00	0.00	17.36	4.86	22.22	29.29	12.28	0.70
FS-11	62.37	1.27	1.90	25.16	0.00	0.42	28.33	8.88	37.63	11.81	24.98	0.32
FS-12	64.74	2.61	4.48	19.59	0.00	0.00	26.68	8.58	35.26	15.04	22.67	0.40
FS-13	71.43	0.56	0.00	25.49	0.00	0.00	26.05	2.52	28.57	23.00	20.06	0.53
FS-14	61.48	2.32	0.00	27.15	0.00	0.00	29.47	9.05	38.52	10.55	26.36	0.29
FS-15	64.83	2.36	1.18	20.43	0.59	0.00	24.56	10.61	35.17	15.17	20.83	0.42
FS-16	62.47	3.27	1.01	26.45	0.00	0.00	30.73	6.80	37.53	11.96	27.06	0.31
FS-17	66.83	1.21	0.00	21.79	0.00	0.00	23.00	10.17	33.17	17.70	18.93	0.48
FS-18	66.51	0.95	0.00	28.03	0.00	0.00	28.98	4.51	33.49	17.30	23.96	0.42
FS-19	59.18	0.00	5.38	31.01	0.00	0.00	36.39	4.43	40.82	7.06	33.82	0.17
FS-20	62.66	4.43	0.00	28.16	0.00	0.00	32.59	4.75	37.34	12.22	28.61	0.30

(continued)

Table 1 (continued)

| S. no | Detrital grain | Cements | | | | | Total cements | Existing optical porosity (EOP) | Intergranular volume (IGV) | Compactional porosity loss (COPL) | Cementation porosity loss (CEPL) | Icompact |
		Silica	Iron	Carbonate	Clay	Matrix						
JS-21	62.76	0.00	5.72	22.87	0.00	0.59	28.59	8.06	37.24	12.36	25.06	0.33
JS-22	70.50	1.30	0.49	19.77	0.00	0.49	21.56	7.46	29.50	21.99	16.82	0.57
JS-23	65.20	1.15	3.63	21.61	0.00	0.76	26.39	7.65	34.80	15.65	22.26	0.41
JS-24	63.23	3.20	1.67	20.06	0.00	0.14	24.93	11.70	36.77	13.02	21.69	0.38
JS-25	70.41	2.21	2.04	19.05	1.36	0.00	24.66	4.93	29.59	21.88	19.26	0.53
JS-26	64.27	2.87	1.23	23.82	3.29	0.00	31.21	4.52	35.73	14.42	26.71	0.35
JS-27	71.90	1.90	0.80	16.00	2.10	0.00	20.80	7.30	28.10	23.50	15.91	0.60
JS-28	79.43	1.26	0.00	16.00	0.00	0.00	17.26	3.31	20.57	30.76	11.95	0.72
JS-29	74.16	1.38	0.99	19.92	0.00	0.00	22.29	3.55	25.84	25.84	16.53	0.61
JS-30	72.20	1.36	0.56	20.45	0.00	0.00	22.37	5.42	27.80	23.83	17.04	0.58
JS-31	78.26	2.17	1.01	15.22	0.00	0.00	18.41	3.33	21.74	29.72	12.94	0.70
JS-32	73.27	3.17	0.57	14.61	0.57	1.47	18.91	6.34	26.73	24.94	14.20	0.64
JS-33	70.74	2.14	1.01	21.06	1.77	0.38	25.98	2.90	29.26	22.25	20.20	0.52
JS-34	64.92	1.02	0.00	26.44	0.34	0.00	27.80	7.29	35.08	15.27	23.55	0.39
JS-35	71.50	3.05	0.89	18.70	0.64	0.00	23.28	5.22	28.50	23.08	17.91	0.56
JS-36	70.71	3.03	0.00	15.32	0.00	0.00	18.35	10.94	29.29	22.21	14.27	0.61
JS-37	70.68	2.19	0.85	19.22	0.00	0.49	22.26	6.57	29.32	22.19	17.32	0.56
JS-38	70.85	1.36	0.00	20.51	1.69	0.00	23.56	5.59	29.15	22.37	18.29	0.55
JS-39	70.05	2.41	1.72	18.93	0.86	0.00	23.92	6.02	29.95	21.49	18.78	0.53
JS-40	63.29	0.63	1.90	23.42	1.05	0.00	27.00	9.70	36.71	13.10	23.47	0.36

Chlorite

Identified by the typical euhedral and pseudo-hexagonal crystal or plate that is arranged in different forms and patterns such as rosette and cluster (Fig. 6h, l). Chlorite cement typically grows as a radial coating over detrital grain composed of euhedral, interlocking plates that typically shield detrital grains from subsequent diagenetic processes. XRD analysis of the clay fraction from 12 samples corroborates the presence of chlorite, which is supported by the SEM analysis (Fig. 6h, l). In some samples, chlorite is also present as a grain-coating on kaolinite.

4.2.4 Matrix (Mx)

In the studied sandstone, it ranges from 0 to 2.2%, with an average of 0.2% (Table 1). Some thin sections show silty to clayey matrix. Most of the matrix material is syn-depositional pore fillers. The matrix also influences the diagenetic process by supplying Fe and reducing porosity and permeability.

4.2.5 Dissolution

The dissolution of authigenic minerals or grains can enhance secondary porosity (Ehrenberg 1990; Shalaby et al. 2014). Dissolution is evident from the presence of secondary porosity, possibly as a result of partial or complete dissolution of detrital feldspars, lithics fragments and quartz grains. Within the FMS, dissolution primarily affects feldspar and lithic fragments. Corroded contacts between quartz grains and CCT point towards the generation of secondary intra-particle porosity. Petrographic observations of the FMS indicate that the dissolution of the unstable grains began in the early diagenetic stage, which produced pore space for secondary cementation. Some of the pore spaces were protected by clay coats and remained open. Another dissolution episode occurred in the late diagenetic stage and dissolved authigenic minerals to produce secondary porosity. Presences of secondary pore spaces indicate that the feldspar and CCT dissolution might have occurred at a later diagenetic stage.

5 Discussion

5.1 *Diagenetic History*

Diagenetic features caused by coeval processes can be grouped in different types viz. eodiagenesis, mesodiagensis and telodiagensis (Pettijohn et al. 1987; Morad et al. 2012). Eodiagenesis is the stage, wherein the chemistry of pore water is controlled

by depositional water, at the burial depth < 2.0 km and temperature <70 °C. Mesodi-agenesis is mediated by evolved formation waters, where at the burial depth > 2.0 km and temperature >70 °C.

5.1.1 Processes During Eodiagenetic Stage

During this shallow burial stage, principal processes operating is mechanical compaction, carbonate cementation, the formation of clay minerals such as kaoli-nite, illite and smectite and dissolution of the unstable grains (Fig. 7a, b). In the FMS, point and long contacts are formed between detrital grains during eodiagen-esis stage (Fig. 5a, b). Plagioclase dissolution probably contributed to the formation of eogenetic kaolinite and smectite (Fig. 7c). Compaction, on the other hand, is primarily responsible for the significant loss in primary porosity. The eodiagenetic cements observed in the FMS are crystalline poikilotopic carbonate, blocky, fibrous and grain-coating types (Fig. 7b, d).

5.1.2 Processes During Mesodiagenesis Stage

Processes during this stage are burial, compaction, cementation, dissolution and mineral replacement (Chilingarian and Wolf 1988). The key factors that affect meso-diagenetic stage are increased temperature and pressure, coupled with the change in pore-water compositions. Physical and chemical compaction, dissolution, recrys-tallization, precipitation, and replacement of minerals, pressure solution, and frac-turing (Fig. 7d) are the processes that operated during burial. Subsequently, silica overgrowths and replacements of feldspar as well as other mineral replacement along with alteration of the clay mineral (i.e., smectite to illite, sericite or chlorite, kaolinite to illite or sericite) dominate the burial diagenetic changes (Fig. 7e). Silica cement is the major diagenetic process that controls the porosity and permeability in sandstone (McBride 1989; Bjorlykke and Egeberg 1993). Silica overgrowth mainly found near sites of intergranular crystals and occlude pores in the sandstones due to dissolution of feldspar (Hawkins 1978), pressure solution (Bjorlykke et al. 1986; Houseknecht 1988; Dutton and Diggs 1990; Walderhaug 1994), replacement of quartz and feldspar by carbonate (Burley and Kantorowicz 1986) and precipitate from the transforma-tion of clay minerals such as smectite to illite and mixed layer illite-smectite, due to an increase of burial depth and temperature (Hower et al. 1976; Rodrigo and Luiz 2002; Worden and Morad 2003). For every mole of K-feldspar altered to kaolinite two moles of silica are released and made available for cement (Siever 1957)

Subsequently, during mesodiagenetic stage, point and long contacts between grains get transformed to concavo-convex contacts and finally to sutured contacts giving rise to the formation of triple junction; muscovite flakes became bent and deformed (Fig. 7 f, g, h). Intergranular dissolved pores resulting from the dissolution of quartz grains are observed in the FMS in the mesodiagenetic stage (Fig. 7i). This process is related to the maximum pH (>8) and temperature (>70 °C) with alkaline

conditions (Knauss and Wolery 1988). According to Liu et al. (2015), quartz dissolution occurs during late mesodiagenesis because with the deepening of diagenesis, the organic acid gets destroyed with weakened decarboxylation effect and diminishing of H$^+$ in the fluid. All of which made the digenetic environment change from acid to alkaline. The creation of porosity in sandstone by the dissolution of quartz is limited in the studied sandstone (Fig. 7i). The reaction of organic acids with feldspar or rock fragments created secondary pore space. It is also created due to the fracturing of the detrital feldspar, rock fragments, and muscovite grains. The precipitation of CCT during the late mesodiagenetic stage filled in the primary porosity and consequently reduced the secondary porosity.

Mesodiagenesis produced observable amounts of FCT and silica overgrowth and as a consequence, reduced the porosity and permeability in the studied sandstone considerably (Fig. 7c–f). In case of the studied sandstone, three porosity-reducing diagenetic processes were observed: (1) mechanical compaction, (2) authigenic mineral cementation, and (3) formation of the authigenic clay minerals. However, during the later stage of diagenesis feldspar dissolution (Fig. 7c) by CCT and FCT led to a significant increase in secondary porosity.

5.2 Porosity, Compaction and Intergranular Volume

The wet-packed original porosity of the sandstone was investigated as about 40% volume (Beard and Weyl 1973; Atkins and McBridge 1992). Porosity is attributed to three classes: primary intergranular porosity (a), secondary porosity caused by dissolution (b), and by grain fracturing (c). Evidence of porosity reduction during burial by mechanical and chemical compaction and cementation are observed in thin section. The existing optical porosity (EOP) of fine- to medium-grained, moderately- to well-sorted FMS ranges from nil to 16.1% (average 6.9%) with intergranular volume (IGV) from 18.8 to 40.9% (average 31.6%; Table 1). In the studied sandstone, secondary porosity is mainly produced by the dissolution of the detrital grains, mostly feldspar (Fig. 7c). An insignificant proportion of secondary porosity is produced by grain fracturing (Fig. 7i).

Compaction can be additionally assessed from the study of grain contacts (Pettijohn et al. 1987). The FMS has been subjected to compaction, both mechanical and chemical. Various types of grain contacts, bending of mica grains and grain fracturing supports mechanical compaction in sandstone (Fig. 7d, g; Table 2). Grain contacts are classified as floating, point, long, concave-convex, and sutured (Figs. 5a, b and 8f). The average percentage of contact types are floating—69.2%, point (tangential)—21.8%, long (straight)—4.2%, concavo-convex (embayed)—2.3% and sutured (serrated)—2.2% (see Table 2). The dominance of floating and point contacts indicate that the FMS had suffered the least pressure solution due to either shallow burial or by early cementation. Grain to grain dissolution (concavo-convex, sutured), as observed mostly in the quartz detritals indicates the chemical compaction. Further, it

Table 2 Percentages of various types of grain to grain contacts of the FMS, Jaisalmer Formation, western Rajasthan

S no.	Types of contacts					Number of contacts per grain					Total number of contacts	Contact index (CI)
	Floating	Point	Long	Concave-Convex	Suture	0	1	2	3	≥4		
FS-1	67.50	16.67	7.50	5.00	3.33	42.68	24.39	21.95	6.10	4.88	57.32	1.85
FS-2	43.33	15.56	18.89	16.67	5.56	37.50	33.93	17.86	7.14	3.57	62.50	1.69
FS-3	59.01	32.30	2.48	3.73	2.48	51.24	34.71	10.74	2.48	0.83	48.76	1.37
FS-4	63.97	16.91	6.62	5.88	6.62	48.76	38.84	9.92	1.65	0.83	51.24	1.31
FS-5	73.48	17.68	3.31	1.10	4.42	69.89	20.45	7.39	1.70	0.57	30.11	1.42
FS-6	86.00	2.00	4.00	3.00	5.00	89.13	10.14	0.72	0.00	0.00	10.87	1.07
FS-7	72.16	25.00	1.70	0.00	1.14	72.02	20.83	4.17	2.38	0.60	27.98	1.38
FS-8	46.60	42.41	5.24	4.71	1.05	41.53	40.98	12.02	4.92	0.55	58.47	1.40
FS-9	72.58	20.97	1.61	1.61	3.23	64.86	29.73	4.05	1.35	0.00	35.14	1.19
FS-10	89.90	6.73	2.40	0.48	0.48	78.67	18.00	3.33	0.00	0.00	21.33	1.16
FS-11	84.98	9.86	3.76	0.94	0.47	77.29	18.36	3.38	0.97	0.00	22.71	1.23
FS-12	55.08	42.37	2.54	0.00	0.00	47.79	34.56	12.50	5.15	0.00	52.21	1.44
FS-13	82.83	15.15	0.00	1.01	1.01	70.71	25.25	3.03	1.01	0.00	29.29	1.17
FS-14	64.95	33.51	1.55	0.00	0.00	50.00	32.95	12.50	4.55	0.00	50.00	1.43
FS-15	76.79	19.64	1.79	1.79	0.00	60.33	32.23	6.61	0.83	0.00	39.67	1.21
FS-16	80.95	17.01	1.36	0.68	0.00	72.56	22.56	4.88	0.00	0.00	27.44	1.18
FS-17	42.65	41.18	11.76	4.41	0.00	29.90	46.39	15.46	7.22	1.03	70.10	1.47
FS-18	74.63	22.44	0.49	1.95	0.49	66.05	22.33	10.70	0.93	0.00	33.95	1.37
FS-19	95.27	3.55	0.59	0.59	0.00	75.36	23.19	1.45	0.00	0.00	24.64	1.06
FS-20	60.77	20.77	11.54	4.62	2.31	57.81	24.22	10.94	4.69	2.34	42.19	1.65

(continued)

Table 2 (continued)

S no.	Types of contacts					Number of contacts per grain					Total number of contacts	Contact index (CI)
	Floating	Point	Long	Concave-Convex	Suture	0	1	2	3	≥4		
JS-21	92.02	5.63	0.94	0.47	0.94	84.85	13.85	0.43	0.43	0.43	15.15	1.17
JS-22	50.00	41.49	7.45	1.06	0.00	41.44	40.54	15.32	2.70	0.00	58.56	1.35
JS-23	87.07	8.62	1.72	0.00	2.59	80.80	15.20	4.00	0.00	0.00	19.20	1.21
JS-24	88.65	7.80	0.71	1.42	1.42	80.13	16.67	3.21	0.00	0.00	19.87	1.16
JS-25	77.27	7.58	4.55	7.58	3.03	68.06	30.56	1.39	0.00	0.00	31.94	1.04
JS-26	90.72	5.15	1.03	1.03	2.06	81.48	16.67	0.00	0.93	0.93	18.52	1.25
JS-27	81.08	11.49	3.38	0.68	3.38	74.07	20.37	1.85	3.70	0.00	25.93	1.36
JS-28	85.95	10.27	2.16	0.00	1.62	75.71	21.90	2.38	0.00	0.00	24.29	1.10
JS-29	67.53	12.99	1.30	9.09	9.09	47.25	50.55	2.20	0.00	0.00	52.75	1.04
JS-30	28.79	57.58	12.12	0.00	1.52	22.62	50.00	20.24	7.14	0.00	77.38	1.45
JS-31	80.49	17.56	1.95	0.00	0.00	84.18	9.69	6.12	0.00	0.00	15.82	1.39
JS-32	39.19	45.95	6.76	2.70	5.41	30.53	44.21	20.00	4.21	1.05	69.47	1.45
JS-33	89.80	8.84	0.68	0.00	0.68	84.62	12.18	2.56	0.00	0.64	15.38	1.29
JS-34	60.51	25.48	5.10	3.82	5.10	41.48	48.91	7.42	1.75	0.44	58.52	1.21
JS-35	45.71	40.00	11.43	1.43	1.43	55.78	36.05	7.48	0.68	0.00	44.22	1.20
JS-36	41.18	39.22	3.92	1.96	3.73	28.00	66.67	5.33	0.00	0.00	72.00	1.07
JS-37	70.37	23.70	2.22	0.74	2.96	65.07	23.97	9.59	0.00	1.37	34.93	1.39
JS-38	69.72	23.85	3.67	0.92	1.83	58.91	32.56	6.98	1.55	0.00	41.09	1.25
JS-39	61.22	34.69	2.04	0.00	2.04	46.15	47.69	4.62	1.54	0.00	53.85	1.14
JS-40	68.46	21.54	5.38	3.08	1.54	60.54	36.05	2.72	0.68	0.00	39.46	1.10

also results in an increased number of contacts per grain. Both types of compaction results in the loss of porosity and permeability.

The contact index (CI) (see Appendix 1) is the average number of contacts a grain has with its neighboring grains (Pettijohn et al. 1987). It also gives an idea about the degree of compaction of the sediments. The average CI for FMS shows a low (1.3%) value, indicating minor effect of compaction. The percentage of framework grains having contacts with no grain, one grain, two grains, three grains and ≥ 4 grains are 60.4, 29.7, 7.4, 1.9 and 0.5%, respectively (Table 2). The high percentage of floating, point and long contacts with a low CI indicates that the studied sandstone has gone lower degree of compaction.

Packing proximity (Pp) (see Appendix 1) is represented as the percentage of grain to grain contacts in a traverse. The packing proximity (Pp) parameter of the FMS ranges from 10.9 to 77.3%, with an average 39.6%. Contact strength (Cs) (Fuchtbauer 1967) (see Appendix 1) in studied sandstone ranges from 1.0 to 1.9% with an average of 1.3%. The consolidation factor (Cf) (Fuchtbauer 1967) values of the FMS ranges from 14.4 to 65.4% (average 36.8%). Weight Contact Packing (Hoholick et al. 1982), (see Appendix 1) values in FMS ranges from 1.1 to 3.7% and average 1.9% (Table 3).

The bivariate plots were made to see the relationship of contact index (CI) with mineralogical parameters and other compactional parameters (Fig. 9). In the FMS, contact index (CI) increases with increasing percentages of quartz grain. However, the correlation coefficient between the parameters is close to nil ($r = 0.02$) (Fig. 9a), indicating less mechanical compaction. The contact index (CI) versus weight contact packing plot suggests a direct and good relationship ($r = 0.04$) between the two parameters (Fig. 9b). Packing proximity (Pp) values show a weak relationship with contact index (CI), with negligible correlation ($r = 0.16$) (Fig. 9c). This implies that the average number of contacts per grain increase with increasing packing proximity (Pp). The consolidation factor (Cf) shows a positive relationship with contact index (CI) ($r = 0.09$) (Fig. 9d). This implies that contact index (CI) increases with the increase of consolidation factor (Cf).

Compaction in sandstone can be identified by IGV, the sum of remaining primary pore spaces, volume of pore-filling cements and depositional matrix (Paxton et al. 2002). It is important to understand the relative effects of compaction and cementation on overall sandstone porosity loss. Based on the assumption that sandstone start with original porosity of 40%, can be achieved by determining the volume of cement and the IGV. The IGV of moderately- to well-sorted FMS ranges from 18.8 to 40.9% (av. 31.6%). Floating and point contacts are abundant in the studied sandstone, which indicates high IGV. A plot of IGV versus cement volume (Fig. 10) indicates that the cementation played a key role than mechanical compaction in destroying the primary porosity in the FMS. The values of IGV and EOP do not show a regular increasing or decreasing trends (Fig. 11). It is also evident that samples with high values of total cement have high IGV (Fig. 11). The high IGV values suggest that low mechanical compaction has been taken place just before cementation.

Further, to investigate the influence of compaction to porosity loss, the relationship between cementation porosity loss (CEPL) and compactional porosity loss (COPL) has been used (see Appendix 1). The cross-plot of COPL versus CEPL shows that the

Table 3 Percentages of compactional parameters of FMS, Jaisalmer Formation, western Rajasthan

S. no.	Packing proximity	Contact strength	Consolidation factor	Weight contact packing
FS-1	57.32	1.49	38.40	2.24
FS-2	62.50	1.73	40.60	3.72
FS-3	48.76	1.21	51.00	2.03
FS-4	51.24	1.53	47.40	2.77
FS-5	30.11	1.33	52.60	2.02
FS-6	10.87	1.86	27.80	2.10
FS-7	27.98	1.10	46.80	1.47
FS-8	58.47	1.21	65.40	2.07
FS-9	35.14	1.24	17.60	1.85
FS-10	21.33	1.33	47.80	1.25
FS-11	22.71	1.34	52.00	1.35
FS-12	52.21	1.06	34.80	1.50
FS-13	29.29	1.12	24.20	1.37
FS-14	50.00	1.04	53.00	1.38
FS-15	39.67	1.15	28.80	1.38
FS-16	27.44	1.11	35.80	1.26
FS-17	70.10	1.28	24.20	2.07
FS-18	33.95	1.12	53.80	1.45
FS-19	24.64	1.25	36.00	1.09
FS-20	42.19	1.47	43.40	2.22
JS-21	15.15	1.29	48.00	1.26
JS-22	58.56	1.17	30.00	1.71
JS-23	19.20	1.33	28.40	1.53
JS-24	19.87	1.31	33.60	1.41
JS-25	31.94	1.67	20.00	2.20
JS-26	18.52	1.44	23.00	1.46
JS-27	25.93	1.39	39.60	1.77
JS-28	24.29	1.27	44.80	1.41
JS-29	52.75	1.60	27.60	3.17
JS-30	77.38	1.19	24.80	2.17
JS-31	15.82	1.10	49.80	1.23
JS-32	69.47	1.24	28.00	2.66
JS-33	15.38	1.13	33.20	1.21
JS-34	58.52	1.35	52.60	2.44
JS-35	44.22	1.26	24.20	2.06

(continued)

Table 3 (continued)

S. no.	Packing proximity	Contact strength	Consolidation factor	Weight contact packing
JS-36	72.00	1.33	21.20	3.71
JS-37	34.93	1.20	38.40	1.80
JS-38	41.09	1.21	30.80	1.69
JS-39	53.85	1.11	14.40	1.71
JS-40	39.46	1.32	38.40	1.82
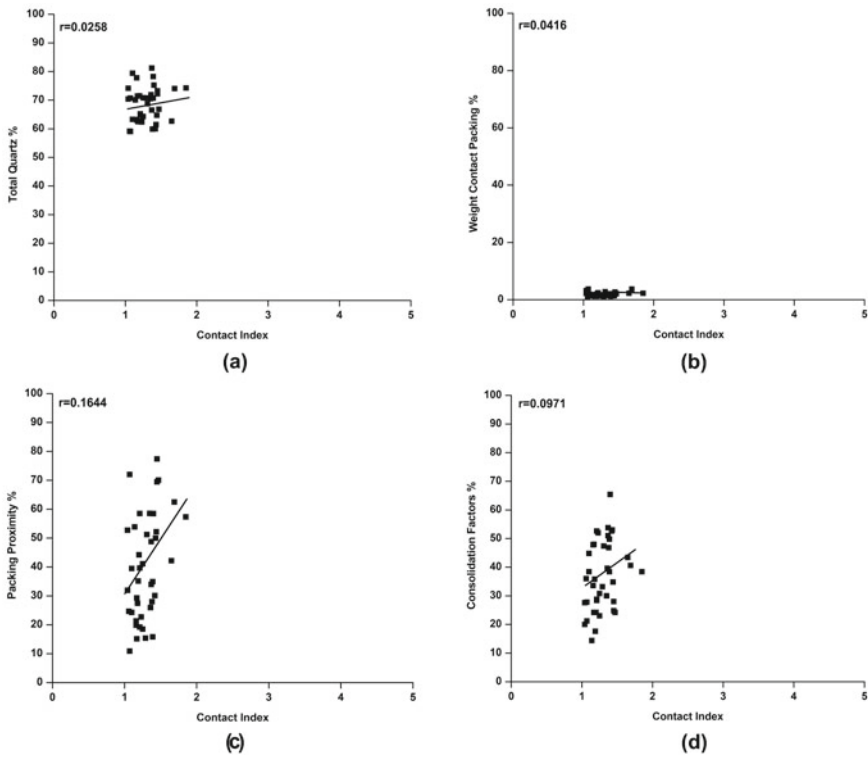
Fig. 9 Cross-plots showing relationship of Contact Index (CI) with **a** detrital quartz and **b, c, d** compactional parameters

porosity loss is mainly due to cementation and less due to compaction (Fig. 12). There is an increasing trend in the values of COPL with depth of burial but the CEPL shows an irregular trend (Fig. 11). The Icompact (see Appendix 1) is a measure of the role of compaction, played in porosity loss. A value of 1.0 implies that porosity loss is due to compaction and 0.0 indicates porosity loss due to cementation. The average Icompact value in the studied sandstone is 0.48, indicating the major role of cementation
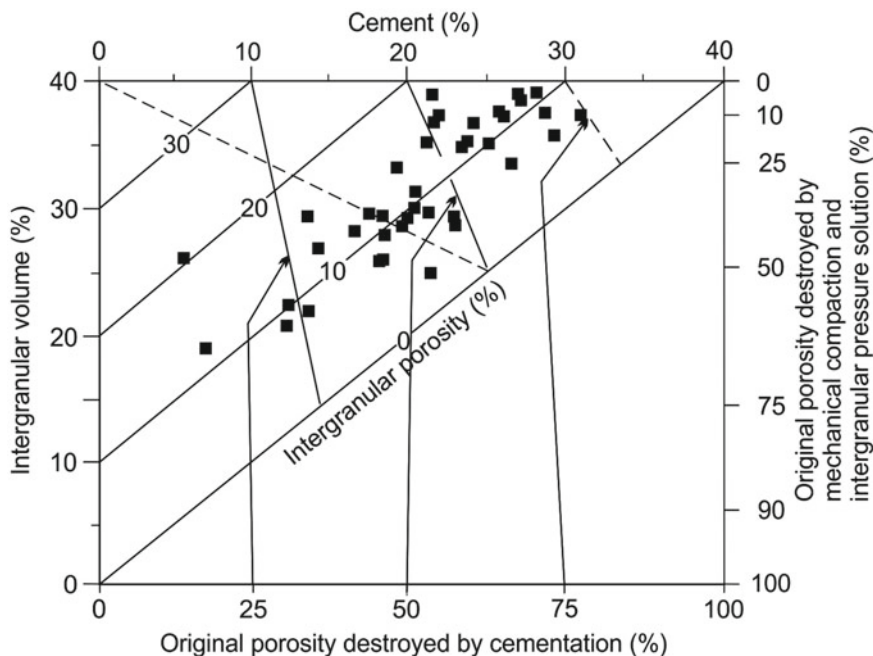
Fig. 10 Houseknecht (1987) diagram showing the relationship between intergranular volume (IGV) and total cement, correlating the primary porosity reduction with cementation and compaction

towards the porosity reduction. In the present case, it seems compaction has played an insignificant role in the porosity loss. On the contrary, the early cementation has played a significant role for porosity loss, while on the other hand, it also prevented the further compaction of sandstone, thus preserving the unfilled pores as primary porosity.

5.3 Paragenetic Sequence

The relative timing of the major diagenetic events in the analyzed sandstone samples of the Fort Member was inferred from the textural relationship (Fig. 13). The diagenetic features include compaction, cementation and precipitation of authigenic minerals, dissolution and grain replacement and generation of secondary porosity. Diagenesis of the FMS begins with early mechanical compaction as evidenced by grain rearrangement, packing and different types of contact and fracturing of detrital grains. However, early carbonate cementation prevented the effects of mechanical compaction. The presence of adequate floating grains in the FMS indicates a negligible effect of pressure solution may be due to either shallow burial or early cementation. But the presence of a few numbers of concavo-convex and sutured contacts of
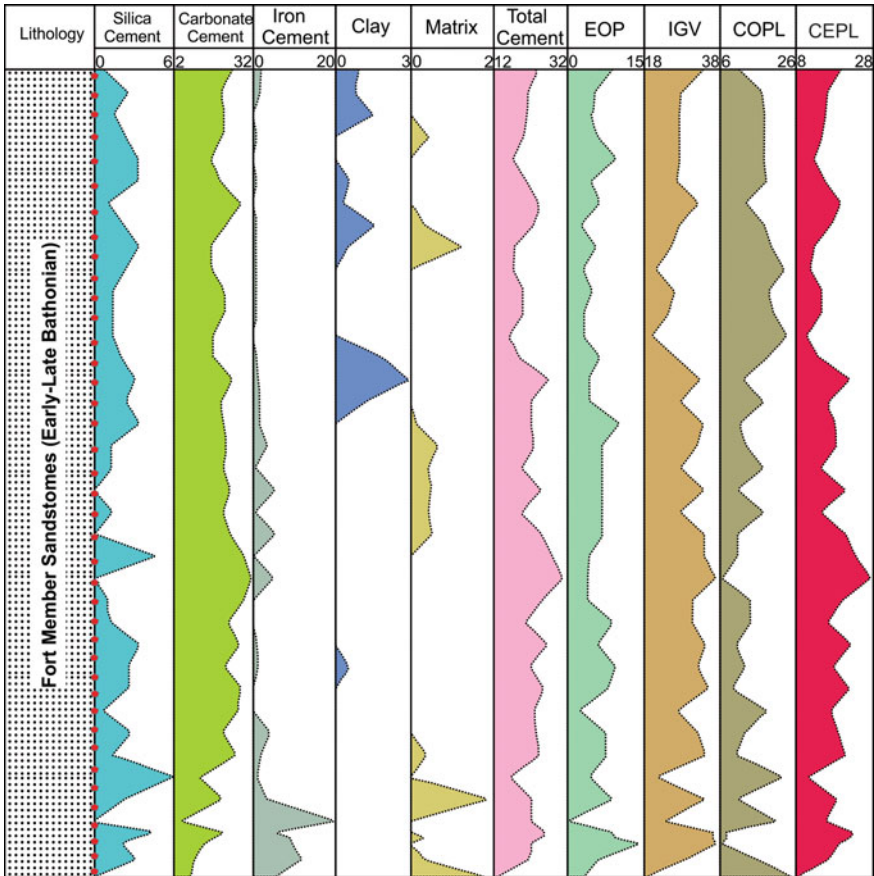
Fig. 11 Vertical variation of diagenetic phases controlling reservoir quality in the Fort Member Sandstone (FMS), Jaisalmer Formation

detrital quartz grains suggests post-early cementation compaction. The dissolution of feldspar and grain replacement occurs in eodiagenesis stage along with clay precipitation as a replacement product from feldspar and mica. During mesodiagenesis, small amount of silica cement present in the form of syntaxial overgrowth on quartz grain, are precipitated, followed by iron cementation. Among the various cements, carbonate was the first to be precipitated, filling the interparticle pore spaces. The boundaries of quartz grains are corroded by CCT and some of the detrital grains are also replaced by CCT, which further gets enveloped by FCT in mesodiagenesis stage. The potential sources of carbonate cements include mud rocks and underlying carbonate rocks, the corroded quartz grains indicate the presence of earlier CCT and silica overgrowth which was replaced by FCT in mesodiagenesis stage (Fig. 6e). The dissolution of quartz also results in intragranular pores (Fig. 7c). Kaolinite is present as an early replacement product of feldspar in the studied sandstone. Illite occurs as
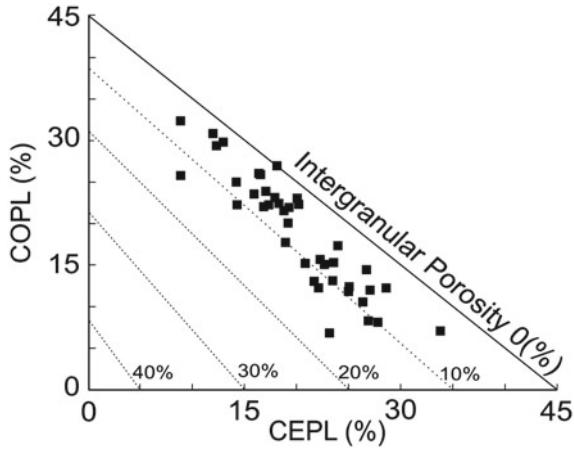
Fig. 12 Cementational porosity loss (CEPL) vs compactional porosity loss (COPL) for the FMS (after Lundegard 1992), indicating that the porosity loss was more due to the cementation and less by compaction

Fig. 13 Simplified paragenetic sequence of the FMS based on petrographic and SEM studied. Note that this is a schematic diagram, comprising data from the study area. The dashed line indicates relative time during diagenetic stages

fibrous form that forms during late diagenesis by the transformation from kaolinite or other early diagenetic clays. The dissolution of CCT results in the generation of secondary porosity during the mesodiagenesis stage. The CCT also encompasses the residual kaolinite locally, suggesting that the precipitation of CCT took place during eodiagenetic and mesodiagenetic stages. Overall diagenetic processes of the FMS indicate shallow to intermediate burial conditions.

6 Inducing Factors on the Reservoir Quality

6.1 Textural and Compositional Controls on Reservoir Quality

The FMS is composed of moderately- to well-sorted, fine- to medium-sand-sized sediments. Fine sand-sized varieties commonly have a lower initial permeability than those consisting of coarse grains (Shepherd 1989). The FMS had a relatively low initial permeability during the deposition. In addition, the mineral composition of rocks has an important influence on subsequent diagenetic processes, such as compaction (Ramm 2000; Bjørlykke 2014), which influences the reservoir quality. The average feldspar (K-feldspar and plagioclase) content of FMS is ~11%. The feldspar, altered to authigenic clay minerals and negatively affect the porosity and permeability. The presence of mica flakes leads to comparatively rapid loss porosity through ductile deformation during progressive burial. The textural and mineralogical compositions of the FMS are susceptible to affect the reservoir quality.

6.2 Diagenetic Controls on Reservoir Quality

Commonly, the compaction and cementation were responsible for the reduction of porosity and permeability. Mechanical compaction in the FMS includes bending of flexible mica flakes, rearrangement and reorientation of detrital grains, resulting in increasing point, long, concavo-convex contacts, and fracturing of grains. Cumulatively it causes the reduction of primary porosity during eodiagenetic stage. Concavo-convex and sutured contacts developed in the studied sandstone as a result of chemical compaction in the mesodiagenetic stage.

Cementation in the FMS appears to have been initiated with carbonate followed by ferruginous, siliceous and various type clay minerals. All these have played an important role in the reduction of porosity and permeability. The precipitation of CCT is primarily responsible for blocking the pore throats at the early stages of diagenesis, leading to reduction of both porosity and permeability. However, when it occurs as patches, it hinders the effects of mechanical compaction due to early cementation, and as a consequence, the reduction in permeability is less prominent. It also results in dissolution related secondary porosities. Thus, the CCT has different impacts on reservoir quality depending upon its mode of occurrences.

The FCT shows a negative impact on the porosity and permeability of the FMS owing to their occurrence in patches, filling pore spaces, veinlets and microconcretion. Silica overgrowths played a subordinate role in reducing the porosity and permeability of the FMS, by occluding pore throats. The limited role of silica cement could be attributed to the chlorite coating, which inhibits the precipitation of silica overgrowths. The clay minerals in the sandstone occur as rims around detrital grains

and/or as pore-filling and pore-lining cements, blocking pore throats and as a consequence, reduce porosity and permeability. Authigenic illite precipitate as fibrous or filamentous form during late diagenesis causes the reduction of the permeability of sandstone (Seemann 1979).

Dissolution is the main factor for the development of secondary porosity in the FMS. Some intragranular, inter-granular and oversized pores are related to dissolution. The dissolution of feldspar grains generates the secondary porosity. Secondary porosity is developed by the dissolution of feldspar, other unstable detrital grains and early carbonate cements, which has a significant contribution in improving the reservoir quality. Fracturing in detrital grains caused by mechanical compaction is significant, which enhances the permeability of reservoir quality of FMS.

7　Conclusions

The Fort Member Sandstone is composed of sub-angular to sub-rounded and moderately- to well-sorted grains of fine- to medium sand-sized material. Minerologically it is quartz arenitic to subarkosic in nature with a variable amount of porosities. The diagenetic processes affecting the reservoir quality include mechanical compaction, cementation by carbonate cement, ferruginous cement, silica cement, authigenic clay minerals and dissolution. The mechanical compaction and early cementation reduced the primary porosity considerably. The presence of early carbonate cement has played an important role in the reservoir quality of FMS by slowing down the effects of mechanical compaction and, in consequence, facilitating the creation of secondary porosity by dissolution. The presence of chlorite coating had a positive impact on permeability retention in the FMS by preventing the silica overgrowths.

The potential of the FMS to act as a reservoir is determined by examining the porosity loss in the sandstone by compaction or cementation during diagenesis. The plot of COPL versus CEPL and IGV vs cement volume suggests that FMS has reduced porosity significantly by cementation. The early cementation has resulted in high IGV. On the other hand, the EOP and secondary porosity, generated during late stages of diagenesis, promote the FMS to act as a potential reservoir. Therefore, this study helps us to recognize the differences in the conduits of diagenetic evolution and to assess their impact on the reservoir quality as a whole. Further, the study enables us to evaluate the potential as well as the heterogeneity of the FMS as a probable reservoir rock to guide forthcoming hydrocarbon exploration and to look for similar reservoirs rocks in Jaisalmer Basin.

Appendix 1

Contact Index (CI) = the average number of contacts per grain irrespective of nature of contacts.

Packing Proximity (Pp) = is expressed as percentage of grain to grain contacts in a traverse:

$$Pp = \frac{q}{n} * 100$$

where **q** is the number of grain to grain contact and **n** is total number of grains.

Contact Strength (Cs) = is quantified by following formula:

$$Cs = \frac{a + 2b}{a + b}$$

where **a**, is the number of point contact and **b**, is the number of all other contacts including long, concavo-convex and sutured contacts.

Consolidation Factor (Cf) = is expressed as:

$$Cf = \frac{F + 2T + 3L + 4C + 5S}{500} * 100$$

where F, T, L, C and S are the percentages of floating, tangential, long, concavo-convex and sutured contacts respectively

Weight Contact Packing (WCP) $= \frac{a+2b+4c+8d+16e}{a+b+c+d+e}$

where is floating contact (a), point contact (b), long contact (c), concave convex contact (d) and sutured contact (e).

Intergranular Volume (IGV) = Sum of remaining primary pore spaces, volume of pore filling cements and depositional matrix (Paxton et al. 2002). This is equivalent to the term "pre-cement primary porosity" and the term minus-cement porosity commonly found in earlier publications.

Compactional Porosity Loss (COPL) = amount of original porosity lost by compactional processes (expressed as a percentage of the original rock volume).

$$(COPL) = Pi\left\{ \frac{(100 - Pi) * IGV}{100 - IGV} \right\}$$

where Pi is the initial depositional porosity (=40%) and IGV is intergranular volume (sum of remaining primary pore spaces, volume of pore filling cements and depositional matrix (Paxton et al. 2002).

Cementational Porosity Loss (CEPL) = amount of original porosity lost by precipitation of intergranular cement (expressed as a percentage of the original rock

volume).

$$(CEPL) = (Pi - COPL) \times \frac{Tc}{IGV}$$

where Tc is total cement and IGV is intergranular volume.

$$Icompact = \frac{COPL}{COPL + CEPL}$$

References

Ahmad F, Ahmad AHM, Quasim MA (2017a) Diagenetic features of Jurassic Fort Member Sandstone, Jaisalmer Formation, Western Rajasthan. J Geol Soc India 90:273–282

Ahmad F, Quasim MA, Ghaznavi AA, Khan Z, Ahmad AHM (2017b) Depositional environment of the Fort Member of the Jurasic Jaisalmer Formation (western Rajasthan, India), as revealed from lithofacies and grain-size analysis. Geol Acta 15:153–167

Ahmad F, Quasim MA, Ahmad AHM, Ghaznavi AA, Khan Z, Albroot M (2019) Factors influencing detrital mineralogy and tectono-provenance of Fort Member Sandstone, Jaisalmer Formation, Western Rajasthan, India. J Geol Soc India 93:392–398

Alaa M, Salem S, Morad S (2000) Diagenesis and reservoir quality-evolution of fluvial sandstones during progressive burial and uplift evidence from the Upper Jurassic Boipeba Member, Reconcavo Basin, Northeast Brazil. AAPG Bull 84:1015–1040

Atkins JE, McBridge EF (1992) Porosity and packing of Holocene river, dune and beach sands. AAPG Bull 76:339–355

Beard DC, Weyl PK (1973) Influence of texture on porosity and permeability of unconsolidated sand. AAPG Bull 57:349–369

Bhat GM, Ahmad AHM (2013) Temporal facies and diagenetic evolution of the mixed siliciclastic-carbonate Jajiya Member (Callovian–Oxfordian), Jaisalmer Formation, West India. Vol Jurassica 11:147–162

Biswas SK (1982) Rift basins in western margin of India and their hydrocarbon prospects with special reference to Kutch Basin. AAPG Bull 66:1497–1513

Biswas SK, Bhasin AL, Ram J (1993) Classification of Indian sedimentary basin in the framework of Plate tectonics. In: Dave A, Garg P, Pandey J, Maithani A, Thomas NJ, Biswas SK (eds) Proceeding Second seminar on Petroliferous Basins of India. Indian Petroleum Publishers, Dehradun, pp 1–46

Bjørlykke K (2014) Relationships between depositional environments, burial history and rock properties. Some principal aspects of diagenetic process in sedimentary basins. Sediment Geol 301:1–14

Bjorlykke K, Egeberg PK (1993) Quartz cementation in sedimentary basins. AAPG Bull 77:1538–1548

Bjorlykke K, Aagaard P, Dypvik H, Hastings AS, Harper DS (1986) Diagenesis and reservoir properties of Jurassic sandstones from the Haltenbanken area, offshore mid-Norway. In: Spencer AM, Holter E, Cambell CJ, Hanslien PHH, Nysæther E, Ormaasen EG (eds) Habitate of hydrocarbons of the Norwegian Continental Shelf. Graham and Trotman, London, pp 275–276

Bloch S (1994) Effects of detrital mineral composition on reservoir quality. In: Wilson MD (ed) Reservior quality assessment and prediction in clastic rocks, vol 30. SEPM short course, pp 161–182

Burley SD, Kantorowicz JD (1986) Thin section and SEM textural criteria for the recognition of cement-dissolution porosity in sandstones. Sedimentol 33:587–604

Chilingarian G, Wolf K (1988) Diagenesis I. Elsevier, Amsterdam, Netherlands

Dickinson WR (1970) Interpreting detrital modes of greywacke and arkose. J Sed Res 40:695–707

Dutton SP, Diggs TN (1990) History of quartz cementation in the Lower Cretaceous Travis Peak Formation, East Texas. J Sed Pet 60:191–202

Ehrenberg SN (1990) Relationship between diagenesis and reservoir quality in sandstones of the Garn Formation, Haltenbanken Mid-Norwegian Continental Shelf. AAPG Bull 74:1538–1558

Fuchtbauer H (1967) Influence of different type of diagenesis on sandstone porosity. Seventh World Petroleum Congress Mexico Proceeding 2:353–369

Ghosh PK (1952) Western Rajputana-its tectonics and minerals including evaporites. Bull Nat Inst Sci Ind 1:101–130

Hawkins PJ (1978) Relationship between diagenesis, porosity reduction and oil replacement in Late Carbonifereous sandstone reservoirs, Bothamsall oil field, E. Midlands. J Geol Soc London 135:7–24

Hoholick JD, Metarko TA, Potter PE (1982) Weight contact packing-improved formula for grain packing of quartz arenites: the Mount Geol 19:79–82

Houseknecht DW (1987) Assessing the relative importance of compaction processes and cementation to reduction of porosity in sandstones. AAPG Bull 71:633–642

Houseknecht DW (1988) Intergranular pressure solution in four quartzose sandstones. J Sed Pet 58:228–246

Hower J, Eslinger EV, Hower ME, Perry EA (1976) Mechanism of burial metamorphism of argillaceous sediments, 1-mineralogical and chemical evidence. AAPG Bull 87:725–737

Ingersoll RV, Bullard TF, Ford RL, Grimm JP, Pickle JD, Sares SW (1984) The effect of grain size on detrital modes: a test of the Gazzi-Diclcinson point-counting method. J Sed Pet 54:103–116

Jeans CV (2000) Mineral diagenesis and reservoir quality–the way forward: an introduction. Clay Min 35:3–4

Jodhawat RL, Kachhara RP (2000) Modiolus zonation of the Jaisalmer Formation, Rajasthan. ONGC Bull 37:207–211

Kachhara RP, Jodhawat RL (1981) On the age of Jaisalmer formation, Rajasthan, India. In: Proceedings of IX Indian Colloquium on Micropalaeontology and Stratigraphy, pp 235–247

Knauss KG, Wolery TJ (1988) The dissolution kinetics of quartz as a function of pH and time at 70 C. Geochim Cosmochim Acta 52:43–53

Liu JK, Peng J, Shi Y, Bao ZF, Sun YL, Liu XM, Zhang Z (2015) The genesis of the quartz dissolution in tight sand reservoirs and its impact on pore development: a case study of Xujiahe Formation in the transitional zone of Central-Southern Sichuan Basin. Acta Petrolei Sinica 36:1090–1097

Lundegard PD (1992) Sandstone porosity loss. A 'big picture' view of the importance of compaction. J Sed Pet 62:250–260

Mahender K, Banerji RK (1989) Textural study and depositional environment of sand grains from rocks of Jaisalmer Formation, Jaisalmer District, Rajasthan, India. J Geol Soc India 33:228–242

Mahendra K, Banerji RK (1990) Petrography, diagenesis and depositional environment of Middle Jurassic Jaisalmer Carbonates, Rajasthan, India. Indian J Earth Sci 17:194–207

McBride EF (1963) A classification of common sandstones. J Sed Res 33:664–669

McBride EF (1989) Quartz cement in sandstones. A review. Earth-Sci Rev 26:69–112

Misra PC, Singh NP, Sharma DC, Upadhyay H, Karoo AK, Saini ML (1993) Western Rajasthan basin: lithostratigraphy of Indian Petroliferous Basins, Document II. KDMIPE, ONGC, Dehradun, pp 1–6

Morad S, Jk Ketzer, De Ros LF (2012) Linking diagenesis to sequence stratigraphy. IAS Spec Publ 45:1–536

Oldham RD (1886) Preliminary note on the geology of northern Jaisalmer. Rec Geol Surv India 19:157–160

Pandey DK, Sha J, Choudhary S (2006a) Depositional environment of Bathonian sediments of the Jaisalmer Basin, Rajasthan, western India. Progress in Natural Science (Special issue of IGCP 506 on the Jurassic Boundary Events). Beijing 16:163–175

Pandey DK, Sha J, Choudhary S (2006b) Depositional history of the early part of the Jurassic succession on the Rajasthan Shelf, western India. In: Progress in Natural Science (Special issue of IGCP 506 on the Jurassic Boundary Events) Beijing, vol 16, pp 176–185

Pandey DK, Fürsich FT, Sha J (2009) Interbasinal mark intervels. A case study from the Jurassic of Kachch and Jaisamer Western India. Sci China Ser D-Earth Sci 52:1924–1931

Pandey DK, Sha J, Choudhary S (2010) Sedimentary cycles in the Callovian-Oxfordian of the Jaisalmer Basin, Rajasthan, Western India. Vol Jurassica 8:131–162

Pandey DK, Choudhary S, Bahadur T, Swami N, Sha, J (2012) A review of the Lower lowermost Upper Jurassic lithostratigraphy of the Jaisalmer Basin, western Rajasthan, India-an implication on biostratigraphy. Vol Jurassica 10:61–82

Pareek HS (1984) Pre-quaternary geology and mineral resources of northwestern Rajasthan. Mem Geol Surv India 115:1–99

Paxton ST, Szabo JO, Ajdukiewiez JM, Klimentidis RE (2002) Construction of an intergranular volume compaction curve for evaluating and predicting compaction and porosity loss in rigid grain sandstone reservoirs. AAPG Bull 76:2047–2067

Pettijohn FJ, Potter PE, Siever R (1987) Sand and sandstone. Springer, New York

Prasad S, Jain RL, Srivastava MS (2007) Record of middle Jurassic (Bathonian) ammonite genus Clydoniceras Blake from Jaisalmer Basin. western Rajasthan. J Geol Soc India 69:53–56

Quasim MA, Ghosh SK, Ahmad AHM (2019) Petrography and diagenetic evolution of the Proterozoic Kaimur Group sandstones, Son Valley, India: implication towards reservoir quality. In: Mondal MEA (ed) Geological evolution of the precambrian Indian shield. Springer, pp 515–550

Ramm M (2000) Reservoir quality and its relationship to facies and provenance in Middle to Upper Jurassic sequences, northeastern North Sea. Clay Mineral 35:77–94

Rao VR (1972) Subsurface stratigraphy, tectonic setting and petroleum prospects of the Jaisalmer area, Rajasthan, India. In: Proceedings of the IV symposium of development in petroleum resources of Asia and the far east, vol 41. Camberra, Australia, Series, pp 366–371

Richter-Bernberg G, Schott W (1963) Jurassic and Cretaceous at the western border of Gondwana Shield in India, and the stratigraphy of oil possibilities. Proceedings of the Second Symposium on the Development of Petroleum Resources of Asia and the Far East, Mineral Resource Development Series 1:230–236

Rodrigo DL, Luiz FDR (2002) The role of depositional setting and diagenesis on the reservoir quality of Devonian sandstones from the Solimones Basin, Brazilian Amazonia. Mar Pet Geol 19:1047–1071

Seemann U (1979) Diagenetically formed interstitial clay minerals as a factor in Rotliegand sandstone Reservoir Quality in the Dutch Sector of the North Sea. J Petrol Geol 1:55–62

Shalaby MR, Hakimi MH, Abdullah WH (2014) Diagenesis in the Middle Jurassic Khatatba Formation sandstones in the Shoushan Basin, northern Western Desert, Egypt. Geol Jour 49:239–255

Shepherd RG (1989) Correlations of permeability and grain size. Ground Water 27:633–638

Siever R (1957) Pennsylvanian sandstones of the Eastern Interior coal basin. J Sed Res 27:227–250

Slatt RM (2006) Stratigraphic reservoir characterization for petroleum geologists, geophysicists, and engineers. Elsevier, Amsterdam

Swaminathan J, Krinshnamurthy JG, Verma KK, Chandiak GJ (1959) General geology of Jaisalmer area, Rajasthan. In: Bangkok (ECAFE, UN) Proceedings of the symposium of development in petroleum resources of Asia and the Far East, Mineral Resources Development Series, p 10

Walderhaug O (1994) Temperatures of quartz cementation in Jurassic sandstones from the Norwegian continental shelf—evidence from fluid inclusions. J Sed Res 64:311–323

Wilson MD, Stanton PT (1994) Diagenetic mechanisms of porosity and permeability reduction and enhancement. In: Wilson MD (ed) Reservoir quality assessment and prediction in clastic rocks, vol 30. SEPM Short Course, pp 59–118

Worden RH, Morad S (2003) Clay minerals in sandstones: controls on formation, distribution and evolution. In: Worden RH, Morad S (eds) Clay mineral cements in sandstones, vol 34. IAS Spec Publ, pp 3–41

Seismicity Forcing Transition from Siliciclastic to Carbonate Realm in the Thaiyat-Hamira Succession of Jaisalmer, Rajasthan

Sunipa Mandal, Pinaki Roy, and Sharadindu Layek

Abstract This paper addresses a Soft Sediment Deformation (SSD) layer in between the Thaiyat and the Hamira Members, Jaisalmer, Rajasthan and traced it physically beyond a distance of 75 km. A drastic change in the depositional system across the SSD layer has been worked out. A microtidal siliciclastic back-barrier lagoon was the site of deposition of the Thaiyat Member. The barrier bar advanced landward and accreted shore-parallel. Occasionally storm sands were delivered from the sea. Biotic diversity had been highly restricted, and tracks-trails dominated the trace fossil record. Paleocurrent direction had been shore-normal. In the post-deformation phase, an open marine shelf frequented by storms was established. Calcrudite and calcarenite deposition rate episodically enhanced enormously. Biotic diversity enlarged drastically and suspension feeders dominated the depositional scenario. Paleocurrent orientation turned dominantly shore-parallel. This likely seismically-induced deformation in the intervening period is correlated to global paleotectonics recorded at different countries at the Bajocian-Bathonian transition.

Keywords Soft sediment deformation event · Depositional system · Thaiyat-Hamira contact · Bajocian-Bathonian transgression · Supercontinent fragmentation

1 Introduction

Soft sediment deformation structures (SSDs) are the only features that can only help us to record past seismicity, but there is no SSD which is distinctive for seismicity (Seilacher 1969; Cita and Ricci Lucchi 1984; Owen and Moretti 2011). SSDs are created by multiple causes and a particular SSD can be created by multiple processes. Wave pounding, overloading, oversteepening, overhanging (biogenic), undercutting

S. Mandal (✉) · S. Layek
Department of Geological Sciences, Jadavpur University, Kolkata, West Bengal, India
e-mail: sunipam@gmail.com

P. Roy
Department of Geology, Durgapur Government College, Durgapur, West Bengal, India

and seismicity are the various causes of SSD formation (Owen 1987; Seth et al. 1990; Bose et al. 1997, 2001; Montenat et al. 2007; Moretti and Ronchi 2011; Sarkar et al. 2014). Sediment, once laid, is stable and does not undergo deformation unless it is disturbed. A 2-layer sedimentary system with contrasting viscosity is inherently prone to deformation; still it needs a driving force to deform (Van Loon 2009; Van Loon and Su 2013; Sarkar et al. 2014). A wide spatial extension of a SSD layer may be a good evidence for seismicity (Seth et al. 1990; Moretti and Van Loon 2014). Sharp facies transition across such a SSD layer help further to recognize past seismicity (Sarkar et al. 2014; Liesa et al. 2016). Facies transition implies change in the depositional regime as a consequence of alteration of paleoenvironmental condition. This paper presents a laterally extensive SSD layer at the contact between the Thaiyat and the Hamira members in Jaisalmer, Rajasthan, India across which the depositional system changed altogether and interprets it as a seismic product (Fig. 1a, b). The objective of this paper is to understand the role of seismicity on sediment depositional system.

2 Geological Background

The Jurassic Jaisalmer succession in western Rajasthan, India, is well known for numerous fossiliferous horizons, shell beds and well-preserved trace fossils. Condensed horizons, reworked concretions, hardgrounds, and cyclic sedimentation and lateral thickening and thinning of stratigraphic units within the Jurassic succession (e.g. Blanford 1877; Oldham 1886; Das Gupta 1975; Krishna 1983; Singh 1989; Fürsich et al. 1991, 1992, 2013, 2017, 2018; Biswas et al. 1993; Fürsich and Oschmann 1993; Kulkarni et al. 2008; Pandey et al. 2010). The Jaisalmer basin is pericratonic and its evolutionary history dates back as far as the Permian time (Datta 1983; Krishna 1987). During inception, it has a syngenetic evolutionary history with other Mesozoic basins of western India, as all of them had formed during one rifting event that separated India from the African continent (break-up of Gondwana Super-continent). Gradual northerly movement of the Indian plate, a very low gradient extensive shallow shelf had formed along its western margin, which received a huge amount of carbonate deposit especially during the Jurassic (Subbotina et al. 1960). Several phases of marine transgression and regression were witnessed. At the peak of the first transgression during the late Bajocian all the basins engendered by this rifting were inundated (Singh et al. 1982; Pandey and Fürsich 1994; Pandey and Choudhary 2007). However, carbonate platform geometry had altered considerably in the course of multiple events of transgressions and regressions; not all of them were of global-scale. The Bouguer anomaly data clearly defines highs and lows distributed over western Rajasthan. Devikot-Pokran-Nachna uplift delimits the Jaisalmer basin in the east. Fatehgarh fault isolates it from the Barmer basin in the southern part and basement ridges bound the basin on the south-west. The basin, nonetheless, opened towards northwest and merged with the Indus shelf (Singh 2006). The basin development was controlled by mainly faults (Datta 1983). The regional tectonic map documents the Jaisalmer basin-fill as an arcuate belt extending overall in northeast
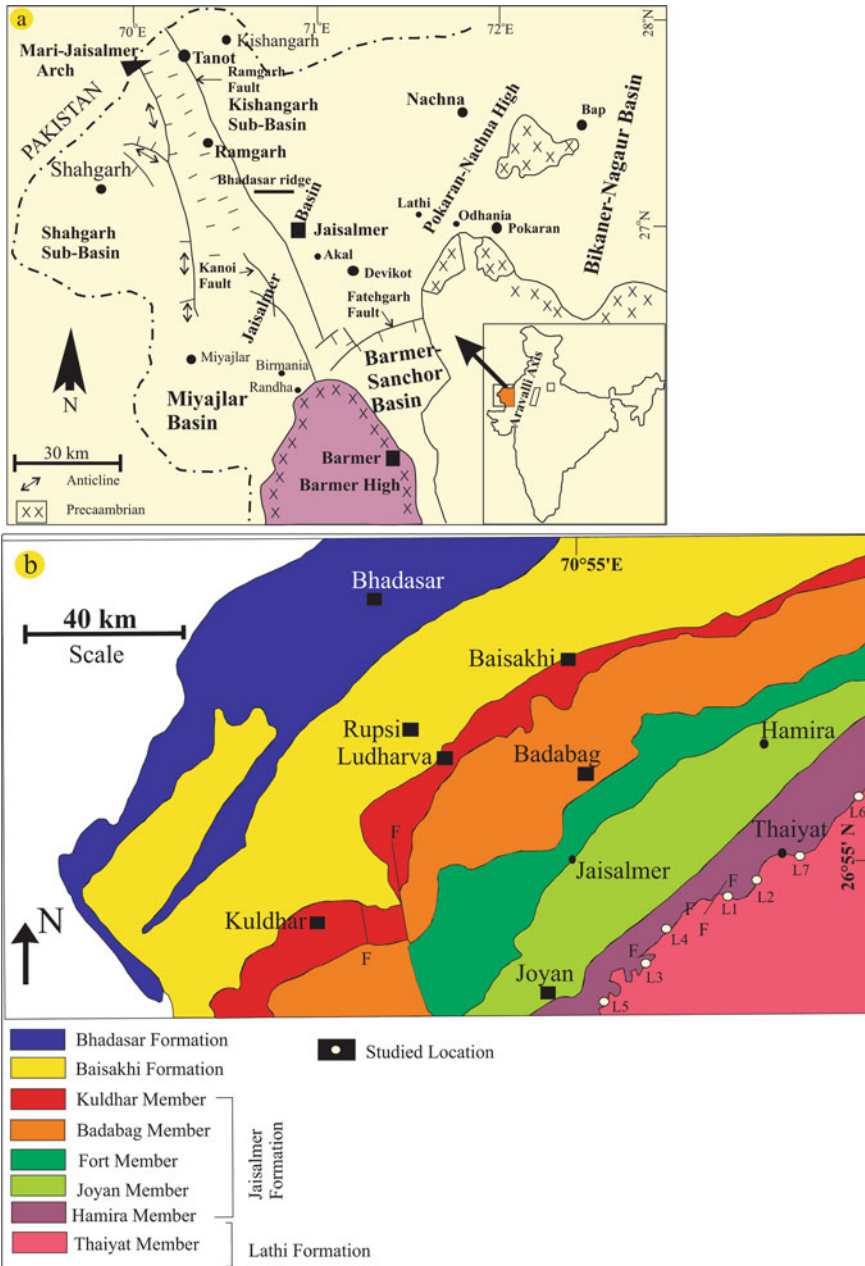
Fig. 1 Enlarge view of the area showing major tectonic elements and their respective ages, indicated within the studied area (map of western India within inset and studied sections demarcated by orange colour) (modified after Mishra et al. 1993) (**a**). Geological map (modified after Dave and Chatterjee 1996) showing distribution of exposures of the Lathi and Jaisalmer Formations in the study area. The map highlights the major faults, the formations and distribution of SSDs exposed in studied stretch (**b**)

to southwest direction (Mitra et al. 1993). The general dip of beds is, in general, gentle to flat (3° to 5°) with a minor system of en-echelon and oblique faults. A broad plunge of the beds towards north-west is manifested by the arcuate trend. The structural trends in Jaisalmer basin are mainly NNW-SSE or roughly NW-SE, corresponding to the Precambrian Dharwarian trend along with NE-SW trending Aravalli ranges. The Jaisalmer basin is differentiated from North to South into four geotectonic blocks. Despite this differentiation, the basement configuration overall had a westerly and north-westerly slope. The Precambrian igneous (Malani Igneous Suite—rhyolite/granite) and metamorphic rocks (phyllite and schist) constitute the basement for the sedimentary successions in the western Rajasthan. The Jaisalmer basin came to existence after the Mesozoic times incorporating four subbasins separated from each other by basement horsts. The subbasins are named as: (a) a median northwest–southeast trending raised Mari-Jaisalmer arch, (b) a synclinal Shahgarh sub-basin in the southwest, (c) the Kishangarh sub-basin in the north and northeast, and (d) the Miyajlar sub-basin in the south (Rao 1972; Sinha et al. 1993; Pandey et al. 2014) (Fig. 1a). The lowermost formation in the Jaisalmer Basin is the Lathi Formation of Triassic–Jurassic age and was initially designated as Lathi Beds by Oldham (1886) after the village Lathi on the Pokaran–Jaisalmer road. The proposed stratigraphic scheme of Oldham (1886) was modified substantially by Das Gupta (1975), Garg and Singh (1983) and Krishna (1987) who grouped the beds into the entirely siliciclastic Lathi Formation. The lower Member of the Lathi Formation is designated as the Odhania Member (Das Gupta 1975) and the upper Member as the Thaiyat Member. The Odhania Member is interpreted as fluvial (Das Gupta 1975; Fürsich et al. 1992; Bonde 2010) and the Thaiyat Member is interpreted as marginal marine (Das Gupta 1975). Initiation of marine transgression is implied. The Odhania Member and the overlying Thaiyat Member, collectively form an overall fining-upward succession. The Jaisalmer Formation, overlying the Lathi Formation, ranges in age from possible Bajocian to Oxfordian (Pandey and Fürsich 1994; Prasad 2006) and forms a major part of the marine Mesozoic succession of Rajasthan. The basal part of this formation is represented by the Harima Member (Das Gupta 1975; Garg and Singh 1983). The estimated thickness of the Hamira Member of Jaisalmer Formation is 30–35 m (Das Gupta 1975) (Fig. 1b). Rai et al. (2016) reported from the Thaiyat Member calcareous nannofossils, like *Lotharingius velatus* and *Carinolithus magharensis* that were allotted to the Late Bajocian by Fernández-López et al. (2009). These authors also recorded existence of calcareous nannofossil, *Watznaueria barnesiae*, immediately underneath the limestone at the base of the Hamira Member and suggested its age to be Late Bajocian. Nevertheless, Tiraboschi and Erba (2010) fixed the date of advent of the same species at Earliest Bathonian, while Mattioli and Erba (1999) placed it within the NJT11 biozone comparable to ammonite biozone, Zigzag, of the same Earliest Bathonian age. It is thus reasonable to assume that the contact between the Thaiyat Member and the Hamira Member belonged to the transition between the Bajocian and the Bathonian. The Jaisalmer Formation represents a deposit of marine transgressive phase after the deposition of fluvio-deltaic Lower Jurassic Lathi Formation that opened in the WNW-ESE trending rifted graben-basin in the area (Das Gupta 1975; Torsvik et al. 2005).

3   Below the SSD Level

Up to 90 m from the SSD level downward, the Thaiyat Member is entirely silici-clastic. At the lowermost level, grey shale dominates. The shale beds alternate with thin laterally pinching sheets of sandstone (Fig. 2a, b). The shale beds are compar-atively thicker, measuring up to 80 cm, and the average thickness of associated sandstone is around 35 cm. The sandstone interbeds are internally either massive or planar laminated. The massive beds are discernibly poorly sorted, but the planar laminated ones are relatively better sorted. This shale-sandstone interbed is inter-mittently incised by sandstone bodies with concave-up bases and flat tops (Fig. 2c). These sandstone bodies are very poorly sorted, and more often than not, incorporate wood fragments (Fig. 2d). The sandstone beds have an exposure width of around 90 cm and their maximum thickness measures up to 1.3 m. Internally, the sandstone beds are generally massive and only locally cross-stratified. The cross-strata gradu-ally become well pronounced away from the massive units. The cross-sets measure up to 65 cm in thickness. Only a few cross-strata yielded paleocurrent direction towards NW.

At the mid-level, amidst the shale-sandstone interbeds, the frequency of occur-rence of sandstone increases and the shale turns reddish in colour (Fig. 2e). The sandstones are, in contrast to the previously described sandstones, fine-grained and well sorted, but they differ among themselves in body geometry, internal structures and thickness. The most common type has channel-form filled by trough cosets (Fig. 2f). The cross-sets reduce in thickness upward within each coset; the maximum cross-set thickness and coset thickness are 4.7 cm and 35 cm, respectively. The foresets are draped by mud (Figs. 2f and 3a). Reactivation surfaces are common in occurrence within the sets (Fig. 2f). The orientation of these cross-strata is towards WSW (Fig. 2f). There are lenticular and flaser bedded sandstones and siltstones (Fig. 3b). Within lenticular bedded sandstones, the sand ripples are often starved and detached from adjacent ones (Fig. 3c). Besides, there are laterally pinching sheet sandstones that often have minute gutters and other sole marks, like prod marks and flutes (Fig. 3d). The sole marks are showing shore-normal paleocurrent, while flutes are oriented in landward direction (Fig. 3e, j). Internally these beds are massive or parallel laminated. Hummocky cross-stratifications of average wave length around 25 cm are present at places (Fig. 3f–h). The bed-tops are often corrugated with ripples that have straight or broadly sinuous crests, locally bifurcated (Fig. 3i, k, l). These beds are overall graded.

Grazing marks, such as, *Planolites* and *Taenidium* are common on top of many of the beds (Fig. 4a). The ichnoassemblage also includes *Rhizocorallium irregulare* (Fig. 4b, c, k). Numerous tellinacean bivalve traces and Radulichnus gastropod traces are locally present (Fig. 4j, k). Associated trace fossils are *Gyrochorte*, *Planolites*, *Syringomorpha*, *Taenidium* and *Ancorichnus* (Fig. 4d). At places, turreted gastropod (Nerineid) shells are oppositely oriented, disregarding their size variation (Fig. 4e). Besides nerineid gastropods, heterodont bakevellid bivalves, *Trigonia* and *Eomiodon*
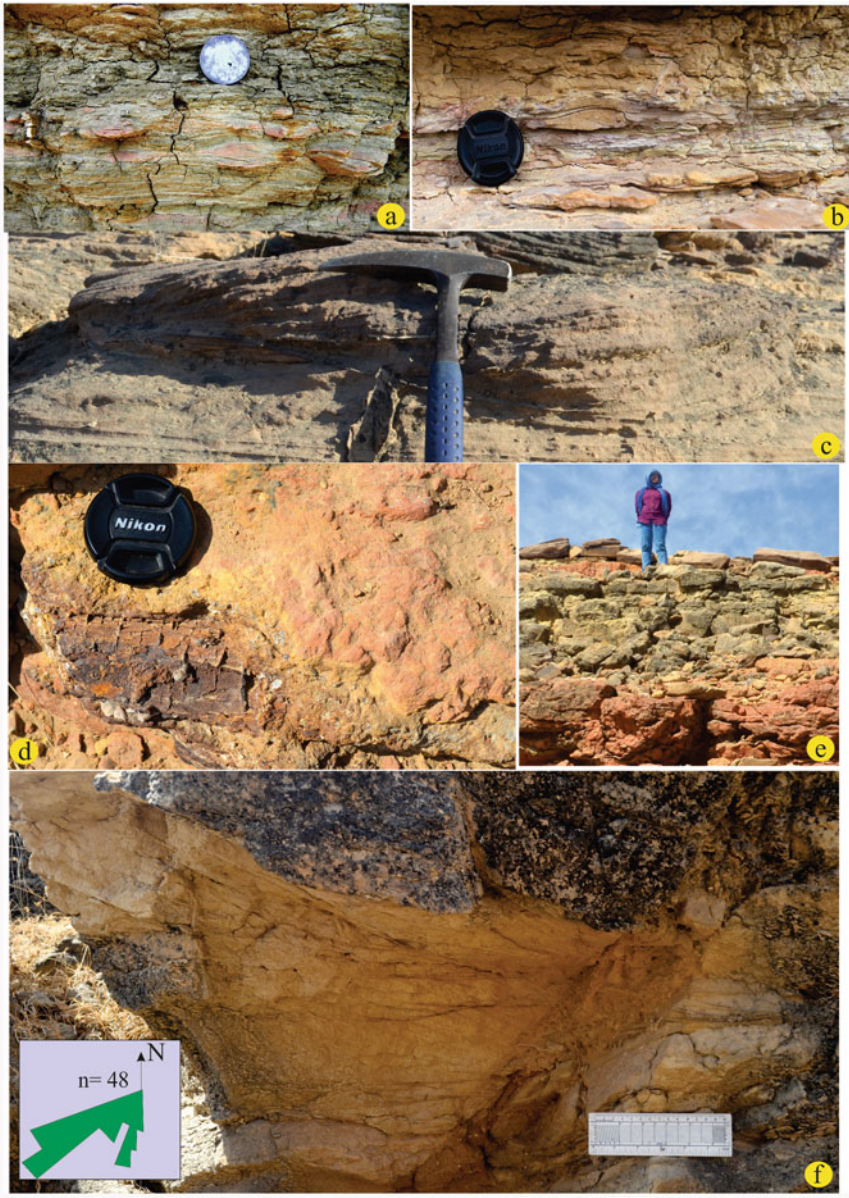
Fig. 2 The shale beds alternate with thin sheets of sandstone that pinches laterally (**a**). Sand-shale alternating layer showing straight crested wave ripple (**b**). The poorly sorted sandstone bodies with concave-up bases and flat tops (**c**). The plan view of poorly sorted channel sandstone bearing wood fragments (**d**). Interbedded shale-sandstone beds showing gradual increasing trend of sand contents and shale turn reddish in colour (**e**). Foresets of trough cross-strata with mud drapes and showing reactivation surfaces; rose diagrams derived from trough cross-stratified sandstone showing sea ward direction (**f**)

Fig. 3 Thick-thin lamina alternating attesting the periodic fluctuations in flow velocity (**a**). Flaser and lenticular bedded siltstone and sandstone (**b**). Linsen or lenticular bedding encapsulating numerous silty starved ripples within the dark coloured shale (**c**). The sandstone beds showing lateral persistence and amalgamation to form thick sandstone units (**d**). Shale interbedded siltstone with sandstone and the sandstone beds have sharp lower contact with gutter and the gutter itself with stepped margins (**e**). Hummocky cross-stratified sandstone (**f**). Chevron cross-stratified sandstone (**g**). Hump back dune infested sandstone (**h**). Sinuous to almost straight crested ripple forms with asymmetric nature (**i**). Palaeoflow directions from the gutter showing shore-normal whereas flute casts residing at the base of the sandstone beds denoting landward direction (**j**). Alternating storm and fair-weather product (**k**). Festoon shaped small scale trough cross strata showing ripple or small dune migration (**l**)
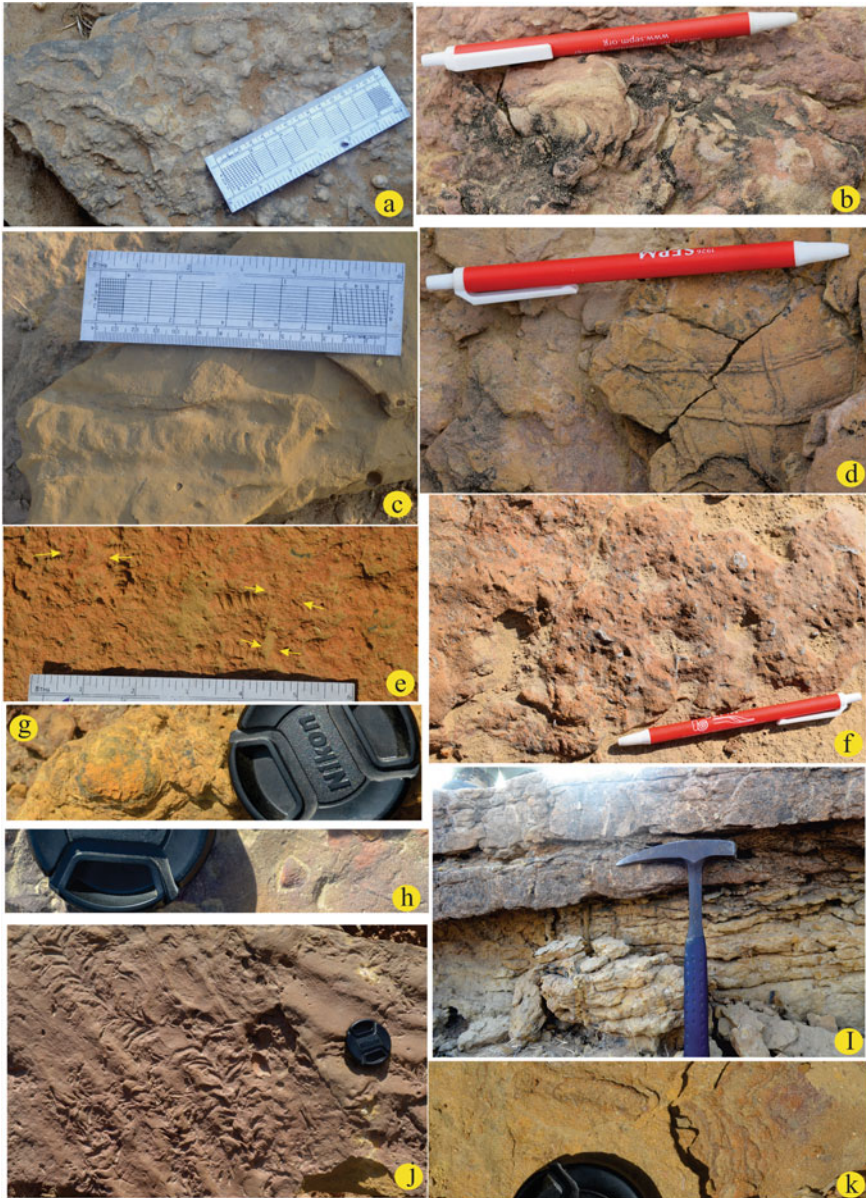
Fig. 4 Bedding plane surface marked by *Taenidium* trace imprints (**a**). Burrows containing concave up geometry showing distinctly irregular burrow walls and marked by *Rhizocorallium irregulare* (**b** and **c**). Bedding plane surface showing *Gyrochorte* trace imprints (**d**). Occurrence of nerineid gastropods fossils in the Thaiyat Member showing opposite direction and marked by yellow arrow head (**e**). Coarse grained sandstone of Thaiyat Member containing gastropods and bivalves (**f**, **g** and **h**). Intensely bioturbated beds with vertical to subvertical burrows point to skolithos (**i**). Vertical burrows containing trace imprints by *Hillichnus lobosensis* in plan view (**j**). *Rhizocorallium* trace marks in plan view (**k**)

are also present (Fig. 4f–h). Rootlets are locally present on top of some beds. Vertical burrows are locally present and that includes *Hillichnus lobosensis* (Fig. 4i, j).

At top occurs large-scale tabular and sigmoidal cross-strata in medium-grained and well-sorted sandstone (Fig. 5a, b). The cross-set thickness is around 52 cm. The tabular cross-strata are oriented in ENE ward direction, but the sigmoidal cross-strata are at a high angle to them (Fig. 5d). Reactivation surfaces are common in occurrence
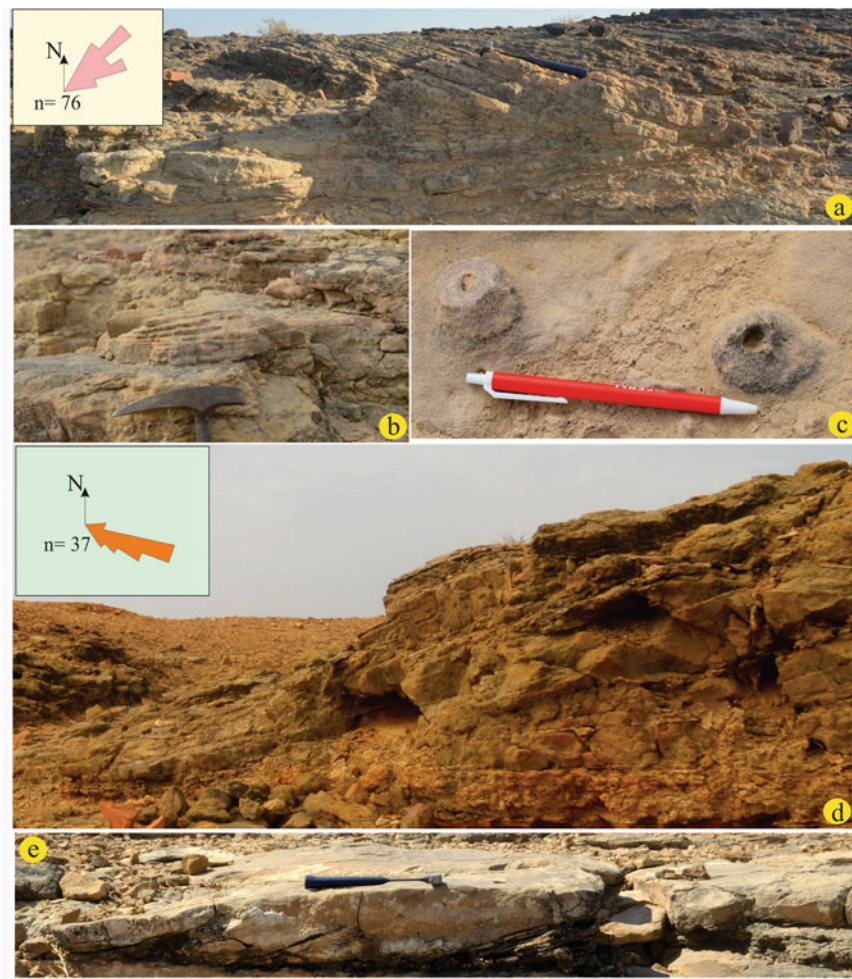
Fig. 5 Large scale tabular cross-stratified sandstone; Rose diagram derived from the paleocurrent direction of tabular cross-stratified sandstone indicating ENE direction (**a**). Sigmoidal cross-stratified sandstone (**b**). Bioturbated beds showing vertical to subvertical burrows (*Ophiomorpha*) and filled by sand in case of wider but narrower burrows filled by mud (**c**). Sigmoidal cross-stratified sandstone showing high angle orientation with tabular cross strata and representing the shore parallel orientation (**d**). Reactivation surfaces in sigmoidal cross-stratified sandstone (**e**)

(Fig. 5e). Locally there are *Ophiomorpha* and *Diplocraterion* burrows are present within this sandstone (Fig. 5c)

3.1 Interpretation

The predominant muddy lithology suggests that the Thaiyat Member overlying the Odhania Member of fluvial origin (Das Gupta 1975; Fürsich et al. 1992; Bonde 2010), was deposited in a low-energy restricted coastal setting. Fossils, like nereneid gastropods, bakevellid bivalves, *Trigonia*, *Eomiodon* suggest lagoonal environment (Aberhan et al. 2002). Trace fossils like *Rhyzocorallium*, *Hillichnus lobosensis* strongly supports this contention (Pazos and Fernández 2010; Ekdale and Ekdale 2018). The restriction was presumably imposed by a barrier bar for which the large-scale cross-stratified well-sorted sandstone at the top of the Member is a fit candidate. The tabular cross-strata in this sandstone record progressive encroachment of the barrier bar upon the lagoon, whereas the sigmoidal cross-strata at a high angle to them provide the accretionary direction of the bar (Kumar and Sanders 1974; Chaudhuri and Howard 1985; Kumar 2006). The presence of *Diplocraterion* and *Ophiomorpha* burrows tell-tales exposure of the barrier bar to a high energy of deposition. Progressive reduction in the frequency of occurrence of sandstone interbeds suggests sand delivery mainly from the sea. Mud drapes on foresets of dunes and ripples, lenticular and flaser bedding identify tide as the driver of sediment into the back-barrier lagoon (de Raaf and Boersma 1971; Terwindt and Breusers 1972; de Raaf et al. 1977; Terwindt 1988; Bose and Chaudhuri 1990; Sarkar et al. 2016). However, straight-crested ripples on some sandstone beds indicate that waves locally and temporarily touched the depositional surface. The sheet sandstones with current structures at the sole and overall grading inside are likely to have deposited from occasional storm-driven flows waning rapidly through time. The sole marks indicate shore-normal paleocurrent, while flute orientation indicates landward delivery of the storm sands. Vertical *Skolithos* burrows are suggestive of high salinity and temperature fluctuations. The deeper the burrows, greater was the protection received by the burrowers (Howard and Singh 1985). Intricate grazing marks in close association suggest a slow rate of sedimentation.

The fining downward trend suggests retrogradation. Sand supply generally dwindled landward. However, the channels filled with poorly sorted and coarser sandstone close to the bottom of the measured section possibly record occasional encroachment of floodwater from the nearby river into the lagoon. Sea-ward paleocurrent direction strongly corroborates this contention.

4 SSD Level

This is a stratigraphic level characteristically populated by soft sediment deformation structures at the top of the Thaiyat Member and immediately under the Hamira Member. It is present all over a distance of more than 75 km (Fig. 6a, b). Its upper surface is sharp and planar everywhere, although its thickness varies between 70 and 150 cm as the deformation generally disappears gradually. Amongst the wide varieties, the most commonly occurring deformation structure is convolute fold. All the convolute folds have, as usual, broad troughs and sharp peaks, but their dimensions are widely variable; some are unitary, most others are multilobated (Fig. 7a–c; Seilacher 1969; Sims 1973, 1975; Allen 1977, 1982; Field et al. 1982; Moretti and Ronchi 2011). Some convolutes are sharply truncated by younger load structures (Fig. 7 d–f; Owen et al. 2011). Droplet structures with broadly rounded bottoms and constricted tops often occur between adjacent convolutes (Fig. 7g, h; Potter and Pettijohn 1963; Nagtegaal 1965; Dżułyński and Walton1965; Seilacher 1969; Lowe 1975; Allen 1982; Owen 1987, 2003; Van Loon 2009; Suter et al. 2011). Convolute folds are, at places, associated with muddy flame structures, of maximum measured
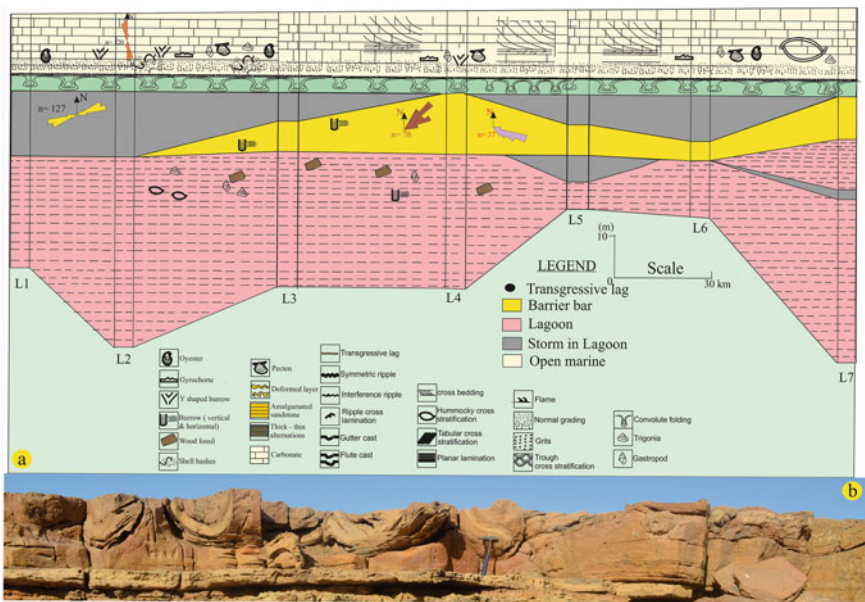
Fig. 6 Fence diagram showing the regional correlation of seismic belt (SSD layer) from detailed study of all locations (marked in Fig. 1) in between Lathi and Jaisalmer Formations and attesting back-barrier lagoonal system gave way to open marine shelf, pointing to change over from siliciclastic into carbonate depositional system, tide dominance gave way to strong wave agitation, with shore-normal paleocurrent turned shore-parallel along with faunal change-over in diversification (**a**). Occurrence of thick conspicuous laterally persistent SSDs variations in between Thaiyat and Hamira Members (**b**)
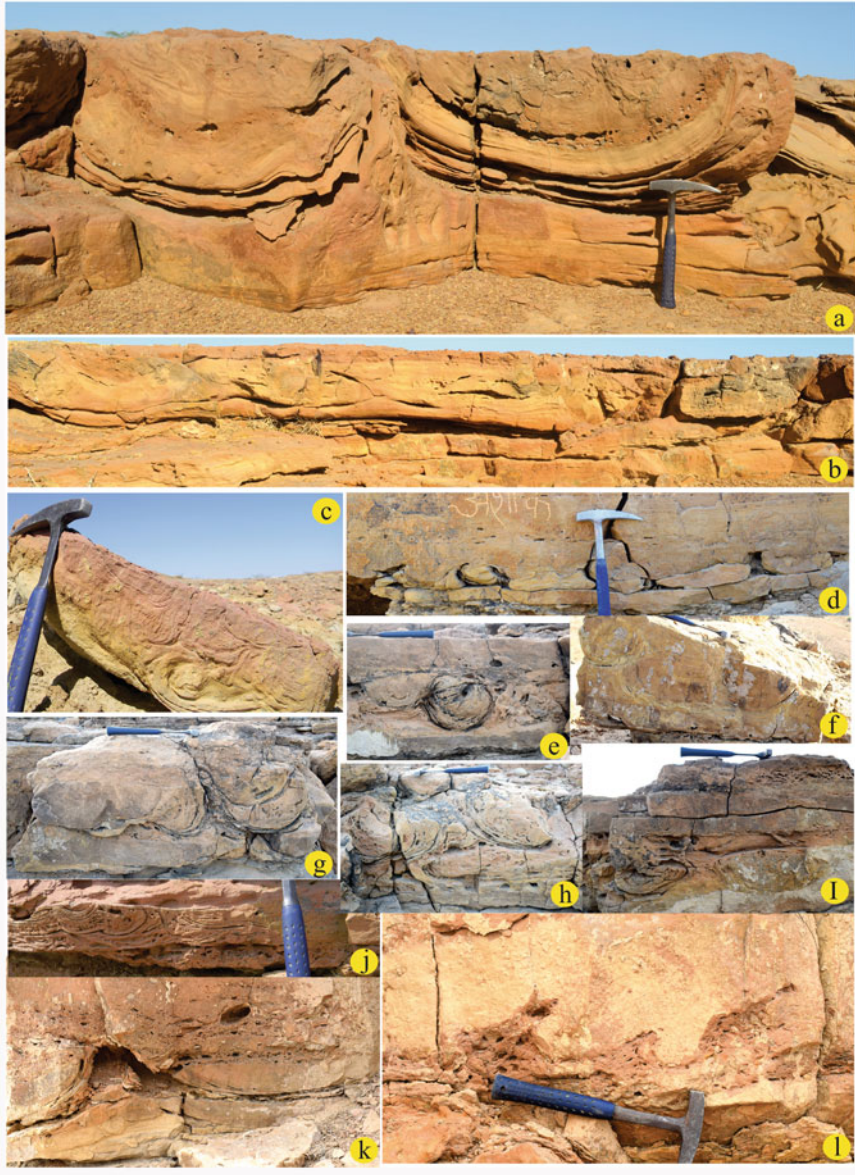
Fig. 7 Soft-deformational structures (SSDs) along the boundary between two Formations (Lathi and Jaisalmer Formations) as imprint of tectonic jerking: Convolute folds showing broad trough with sharp peaks (**a** and **b**). Multi-lobated convolute (**c**). Load structures (**d** and **e**). Some older convolutes showing sharp truncation by younger load structures (**f**). Convolute folds with muddy flame structure (**g**). Droplets (**h**). Imbricated convolute and water escape structure (**i**). Contorted laminae (**j**). Brecciated structures showing matrix supported clast and twisted clast in flame (**k** and **l**)

length 1 m (Fig. 7i). At places, the SSD level is characterized by intricately contorted laminate (Fig. 7j). At a few other places, breccias occupy the SSD level partially or completely (Fig. 7k). The lithological composition of the clasts is similar to that of the matrix in between them. The breccia bodies are of irregular shape and their clasts can be traced into the unbrecciated mass surrounding them. Locally there are small-scale faults with or without the accompaniment of massive sandstone above (Fig. 7k, l).

4.1 Interpretation

The above observations strongly suggest that liquefaction and fluidization of sediment took place closely following each other. It is also apparent that destabilization of sediment took place, in some cases, in closely timed pulses. The deformation is generally ductile in nature all over the long stretch of distance. However, the breccias and microfaults make brittle deformation apparent locally. Some breccia clasts are bent, indicating their softness during derivation.

5 Above the SSD Level

Up to 20 m above on the SSD level, the Hamira Member is entirely carbonate, but it rests on a thin blanket of siliciclastic granules, matrix-free and well sorted (Fig. 8a, b). Thin (15 cm on average) planar laminated or low angle cross-stratified calcarenite alternate with thick (45 cm on average) normally graded calcarenite of tabular geometry. In the latter, the grading is coarse-tailed, being depicted by vertical distribution of shells, mainly of bivalves (Fig. 8c). The majority of disarticulated bivalve shells are concave-up in attitude (Fig. 8d, e). The graded calcarenite beds are up to 45 cm in thickness but often amalgamate. From about 1.1 m above the granular sheet, the graded calcarenite is increasingly replaced by comparatively finer-grained calcarenite beds of sheet-like geometry. Internally these beds are wavy parallel-laminated (Fig. 8f, g, 9d–g and 10a, b). Large-scale Hummocky cross-strata (HCS) are readily discernible in some of them (Fig. 8f, h). The average wave length of the HCS is around 1.7 m. The HCS beds have sharp bases sculpted by gutter casts. These beds are also overall graded and may have mud-clast concentration at their bases (Fig. 9c). The basal part of the HCS beds may be massive in some cases. These beds also tend to amalgamate together in older levels but get separated from each other by fine-grained marl beds in younger levels (Fig. 8i, j and 9b). These marl beds are mostly massive or crudely planar laminated. Under both the graded beds and the HCS beds, the gutters are oriented parallel to the paleoshore-line (Figs. 8f and 9a). Besides bivalve shells (*Ostrea*, *Trigonia*, *Nucula*, *Pecten, Pholadomya, Ceratomya, Homomya* and *Modiolus)*, fossils of brachiopod (Rhynchonellid), cephalopod, bryozoa and gastropods (Turritellid and Nerineid) of wide

Fig. 8 Thaiyat Member terminated against transgressive lag (marked by sheet body geometry and well sorted) on which Hamira Member overlies (**a**). Occurrence of tree logs with transgressive lags (**b**). Coarse-tailed grading with vertical distribution of shells (**c**). Disarticulated bivalve shells with concave up orientation (**d** and **e**). Occurrences of prod marks, flutes within the hummocky cross-stratified sandstone bed surfaces; rose diagram measured from flute cast bearing hummocky cross-stratified calcarenite (**f**). Planar laminated thick calcarenite (**g**). Hummocky cross-stratified calcarenite (**h**). Amalgamated hummocky cross-stratified calcarenite (**i**) Clast bearing Storm product (**j**). Trigonia bearing calcarenite in Hamira Mamber (**k**)
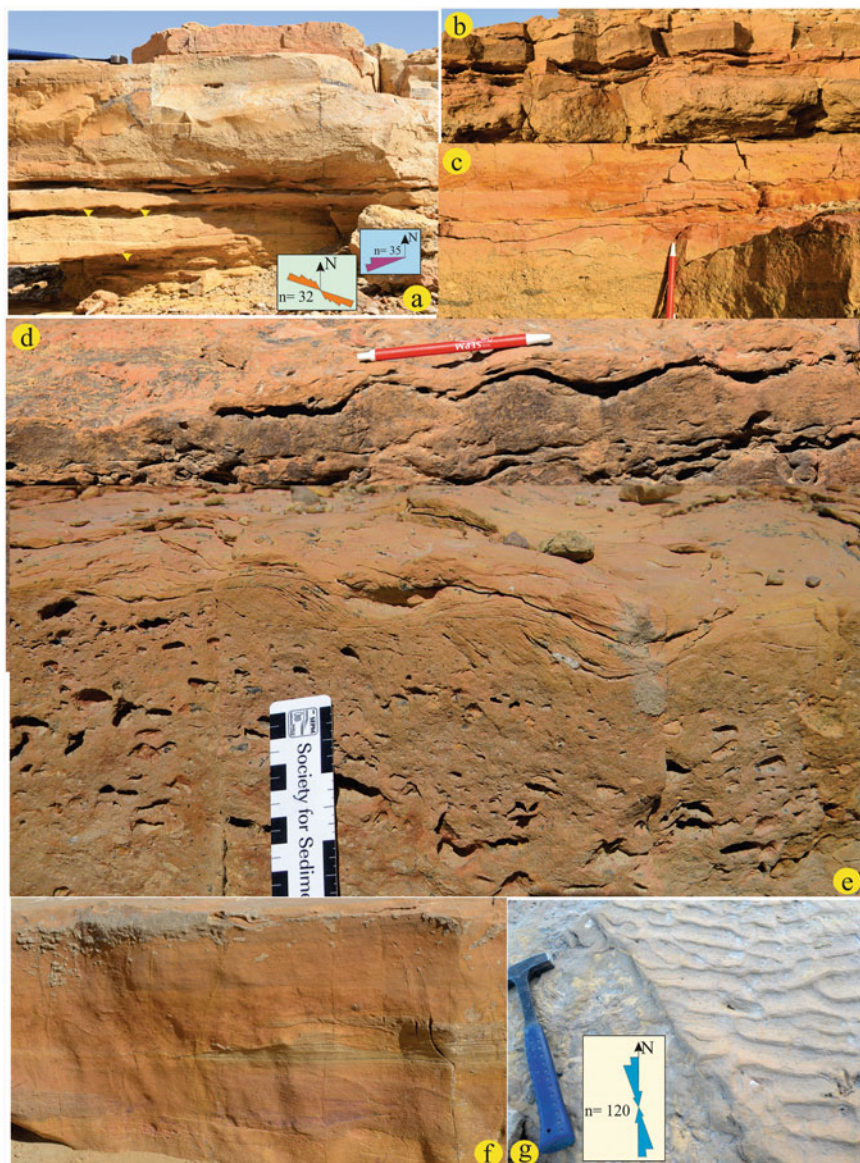
Fig. 9 Alternating occurrence of storm calcarenite and fair-weather marl; Gutter marked by yellow arrow head and rose diagram depicted from gutter infested storm bed showing shore parallel orientation (**a**). The calcarenite beds showing lateral persistence and amalgamation to form thick sandstone units (**b**). Occurrence of clast within storm bed (**c**). Wave ripple in fair-weather product (**d**). Clast bearing calcarenite internally characterized by hump back dune showing ripple drifting (**e**). Chevron cross-stratified calcarenite (**f**). Bifurcating wave ripple showing orientation of palaeo-shoreline trend NNW-SSE (**g**)
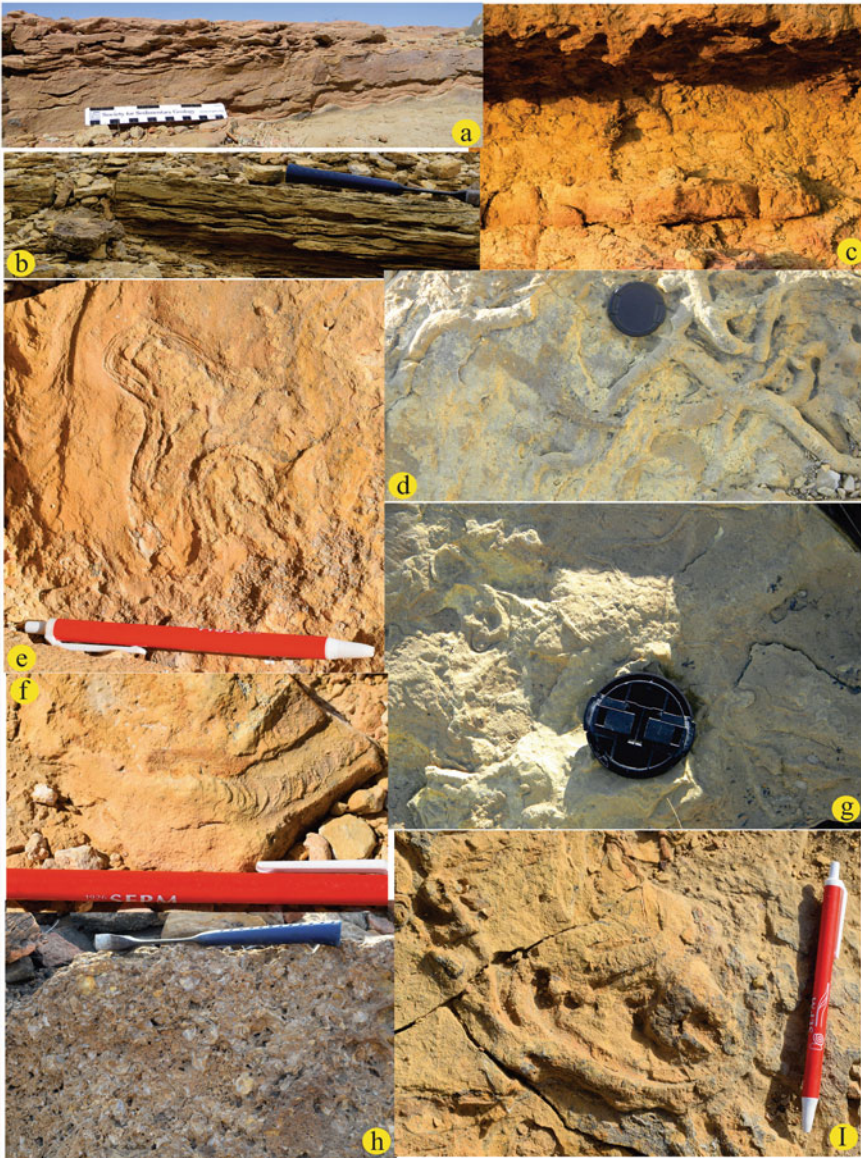
Fig. 10 Wave ripple in fair-weather product (**a** and **b**). Alternate storm and fair-weather product showing abundance of vertical burrows (Skolithos-*Psilonichnus*) and their appearance in storm deposits (**c**). Horizontal to subhorizontal *Thalassinoids* burrows by stenohaline gastropods, bivalves and worms (**d**–**g**). Oyster bearing bed (**h**). Trace imprints marked as meniscate burrow (**i**)

species variation are important constituents of the limestone concerned (Figs. 8k and 10h). Burrows of suspension feeders, *Skolithos, Ophiomorpha* and *Psilonichnus* and *Thalassinoides dominate* the basal 20 m of the Hamira Member (Fig. 10c–g, i).

5.1 Interpretation

On top of the entirely siliciclastic Thaiyat Member, the succession of the carbonate rocks of the Hamira Member, rich in marine fossil population of stenohaline biotic community, clearly records rapid marine transgression leading to the establishment of an open shelf (Das Gupta 1975; Torsvik et al. 2005). The thin sheet of siliciclastic granules at the base of Hamira Member is then the likely transgressive lag, an erosional residue of the underlying siliciclastic sediments, as erosion far exceeded deposition (Cattaneo and Steel 2003). Carbonate sedimentation initiated when the depositional rate outdid the rate of erosion. Opening of the shoreline presumably enhanced wave action and storms frequented the coast (Dalrymple et al. 1992, 2012; Yang et al. 2005; Fan et al. 2012). The likely products of storm deposition are the graded beds and the HCS beds, again with overall grading. The current structures at the sole of these beds indicate high erosional activity of the sediment-driving flow before the initiation of storm deposition. The overall grading within the beds records gradual waning of their parent flows. The HCS records operation of wave-cum-current combined flows (Harms et al. 1975, 1982; Arnott and Southard 1990). The dominant concave-up orientation of bivalve shells strongly suggests deposition from suspension. The common amalgamation of storm beds in the lower part of the section indicates shallow shelf deposition. Fairweather beds are little preserved under strong storm action in the proximal part (Aigner 1982, 1985; Bose and Das 1986; Bose and Chanda 1986). The gradual reduction in the amalgamation of storm beds up the Hamira succession is thus attributable to deposition away from the shoreline. The intervening marl beds are thus interpreted as the fair-weather products as comparatively weaker downwelling storms failed to reach the offshore depositional site. The nearly shore-parallel orientation of the gutters at the soles of the carbonate storm beds presumably records geostrophic flow under the enhanced influence of Coriolis force (Swift et al. 1979, 1987; Leckie and Krystinik 1989; Duke 1990; Sarkar et al. 2002).

6 Discussion

The top 90 m of the Bajocian predominantly siliciclastic Thaiyat Member, Jaisalmer, Rajasthan, India was deposited in a back-barrier lagoon. The barrier bar migrated landward apparently slowly. The resultant slow retrogradational stratigraphic trend is explained most readily by the subsidence of the basin created by rifting. The retrogradation further indicates that the rate of subsidence, even though slow it had

been in absolute term, exceeded the rate of sedimentation. Between the periodic tidal inrushes, temperature and salinity fluctuations dictated burrowers to dig deeper into the lagoon floor. Yet, the slow rate of sedimentation and the muddy nature of sediment helped abundant preservation of animal trails and tracks. The seaward orientation of tidal cross-strata points to strong tidal asymmetry, the ebb being stronger than the flood. Storm waves occasionally brought in high gradient changes in the depositional energy spectrum. The orientation of flutes indicate that storm sands were delivered from the sea landward. However, oscillatory flow at the penultimate stage of storm deposition oriented turreted gastropod shells both ways, land and seaward. The tabular cross-strata indicate that the barrier bar advanced landward. Nonetheless, the orientation of its sigmoidal cross-strata indicates the direction of accretion of the bar had been, more or less, parallel to the paleoshoreline.

The topmost part of the Thaiyat Member bears soft sediment deformation (SSD) structures traced beyond 75 km. The level depicts a single event of deformation affecting a wide area simultaneously. The nature of deformation varies widely, presumably because of lateral variation in consistency of the contemporary sediments. Liquefaction and fluidization as well as ductile and brittle deformation took place almost simultaneously.

The Thaiyat Member is terminated by a sheet of transgressive lag. Open marine shelf deposition followed the Hamira Limestone Member. The paleoshoreline was wave-dominated and frequented by storms. Coarse-tail grading in well-preserved bivalve shells in the basal beds records rapid deposition from temporally waning flows during storm downwelling. At the comparatively higher stratigraphic position of the Hamira Member sheet-like HCS beds become the more common type of storm beds depicting combined operation of wave and current on comparatively lighter density flows. Storm beds amalgamated frequently at the lower part of the Member, but increasingly alternated with fair-weather marl, since weaker storms failed to reach the depositional site. Further transgression, at a slower rate, is depicted in basal 20 m of the Hamira Member. The current structures at the soles of the storm beds record nearly shore-parallel sediment movement, apparently under the influence of Coriolis force.

The depositional regime before and after the deformation event affecting a wide region evidently underwent a sea change. The restricted marginal marine setting represented by the Thaiyat Member turned into a storm-infested open shelf of the Hamira Member. Dominant tide influence of pre-deformation setup gave way to wave-domination in the post-deformation setup. Shore-normal paleocurrent gave way to shore-parallel paleocurrent. Lithology drastically altered from siliciclastic mudstone-sandstone to calcrudite-calcarenite. Highly restricted fossil species changed to a wide spectrum of species. The slow rate of deposition changed to that of rapid depositional events. In consequence, the fossil preservation rate enhanced drastically. Well-preserved assemblage of animal tracks and trails gave way to burrows of vertical attitude (Fig. 6). The deformational event, in all probability, was seismically induced. Hallam (2001) predicted an increase in plate compression enough to cause about 50 m of plate subsidence and such subsidence readily explains the relative sea level rise noted at the contact between the Thaiyat and the Hamira Members.

It is also a significant coincidence that the transgression at the Bajocian-Bathonian transition has a globally widespread record (Jacquin et al. 1998). Surlyk (1991) recorded a major transgressive event in Greenland at this juncture. Legaretta and Uliana (1996) also recognized a late Bajocian major transgression in Argentina. Hallam (1988) depicted a contemporary transgression in his reconstruction of the global sea level curve through time. It is thus reasonable to assume that the Bajocian-Bathonian transgression at Jaisalmer a result of global plate tectonics. An alternative explanation for global transgression could be large-scale melting of polar icecaps. However, there is a general consensus that the Jurassic world generally lacked major icecaps (Frakes et al. 1992; Hallam 1993), with perhaps some minor ephemeral exceptions in the northern hemisphere, only during the Late Jurassic time (Sellwood et al. 2000). Hence the balance of evidence prompts a correlation of the seismically-induced transgression at the transition between the Thaiyat and the Hamira Members with an event of supercontinent fragmentation.

7 Conclusions

This Soft Sediment Deformation (SSD) layer at the contact between the Bajocian Thaiyat Member and the Bathonian Hamira Member, over a distance beyond 75 km in Jaisalmer, Rajasthan was seismically induced. A sea change in depositional set-up took place between the pre- and post-deformation stages: (a) Back-barrier lagoonal system gave way to open marine shelf, (b) siliciclastic depositional system abruptly transited into carbonate depositional system, (c) tide dominance gave way to strong wave agitation, (d) slow rate of sedimentation changed to episodic rapid deposition, (e) abundance of tracks and trails gave way to profusion of vertical burrow system, (f) shore-normal paleocurrent turned shore-parallel, (g) faunal diversification enhanced sharply, (h) euryhaline invertebrate community was replaced by stenohaline community. A rapid transgression accompanied the deformation. The Bajocian-Bathonian transgression has been traced in different parts of the world, in both the northern and southern hemispheres. In general absence of icecaps in the Early and Middle Jurassic world, this transgression across the globe is correlated with supercontinent fragmentation.

References

Aberhan M, Busser R, Heinrich W-D, Schrank E, Schultka S, Sames B, Kriwet J, Kapilima S (2002) Palaeoecology and depositional environments of the Tendaguru beds (Late Jurassic to Early Cretaceous, Tanzania). Mitt Mus Nat kd Berl Geowiss Reihe 5:19–44

Aigner T (1982) Calcareous tempestites: storm-dominated stratification in upper muschelkalk limestones (Middle Triassic, SW-Germany). In: Einsele G, Seilacher A (eds) Cyclic and event stratification. Springer, pp 180–198

Aigner T (1985) Storm depositional systems. Lecture notes in earth sciences. Springer, Berlin

Allen JRL (1977) The possible mechanics of convolute lamination in graded sand beds. J Geol Soc London 134:19–31

Allen JRL (1982) Sedimentary structures: their character and physical basis, vol II. Elsevier, New York

Arnott RWC, Southard JB (1990) Exploratory flow-duct experiments on combined-flow bed configurations, and some implications for interpreting storm-event stratification. J Sed Petrol 60:211–219

Biswas SK, Bhasin AL, Ram J (1993) Classification of Indian Sedimentary Basin in the framework of Plate tectonics. In: Biswas SK, Dave A, Garg P, Pandey J, Maithaoni A, Thomas NJ (eds) Proceeding second seminar on petroliferous basins of India, vol 1. Indian Petroleum Publishers, Dehradun, pp 1–46

Blanford WT (1877) Geological notes on the Great Indian Desert between Sind and Rajputana. Rec Geol Surv India 10:10–21

Bonde SD (2010) A new genus of podocarpaceous wood from the Lathi Formation (Early Jurassic) of Rajasthan, India. Geophytol 38:19–24

Bose PK, Chanda SK (1986) Storm deposits and hummocky cross-stratification: a geological viewpoint. Quart J Geol Min Met Soc India 58:53–68

Bose PK, Das NG (1986) A transgressive storm- and fair-weather wave dominated shelf sequence: Cretaceous Nimar Formation, Chakrud, Madhya Pradesh, India. Sediment Geol 46:147–167

Bose PK, Chaudhuri AK (1990) Tide versus storm in epeiric coastal deposition: two Proterozoic sequences, India. Geol J 25:81–100

Bose PK, Banerjee S, Sarkar S (1997) Slope–controlled seismic deformation and tectonic framework of deposition of Koldaha Shale, India. Tectonophys 269:151–169

Bose PK, Sarkar S, Chakraborty S, Banerjee S (2001) Overview of the Meso to Neoproterozoic evolution of the Vindhyan basin, central India. Sed Geol 141:395–419

Cattaneo A, Steel RJ (2003) Transgressive deposits: a review of their variability. Earth-Sci Rev 62:187–228

Chaudhuri AK, Howard JD (1985) Ramgundam Sandstone; a Middle Proterozoic shoal-bar sequence. J Sed Petrol 55:392–397

Cita MB, Ricci Lucchi F (eds) (1984) Seismicity and sedimentation (Special Issue). Mar Geol 55:1–493

Dalrymple RW, Zaitlin BA, Boyd R (1992) Estuarine facies models: conceptual basis and stratigraphic implications. J Sed Petrol 62:1130–1146

Dalrymple RW, Mackay DA, Ichaso AA, Choi KS (2012) Processes, morphodynamics, and facies of tide-dominated estuaries. In: Davis R Jr, Dalrymple R (eds) Principles of tidal sedimentology. Springer, Dordrecht, pp 79–107

Das Gupta SK (1975) A revision of the Mesozoic-Tertiary stratigraphy of the Jaisalmer Basin, Rajasthan. Ind J Earth Sci 2:77–94

Datta AK (1983) Geological evolution and hydrocarbon prospects of Rajasthan Basin, India. Petrol Asia J 93–100

Dave A, Chatterjee TK (1996) Integrated Foraminiferal and Ammoniod biostratigraphy of Jurassic sediments in Jaisalmer basin, Rajasthan. J Geol Soc Ind 47:477–490

De Raaf JFM, Boersma JR (1971) Tidal deposits and their sedimentary structures. Geol Mijnbouw 50:479–504

De Raaf JFM, Boersma JR, van Gelder A (1977) Wave generated structures and sequences from a shallow marine succession. Lower Carboniferous County Cork, Ireland. Sedimentol 24:451–483

Duke WL (1990) Geostrophic circulation or shallow marine turbidity currents? The dilemma of paleoflow patterns in storm-influenced prograding shoreline systems. J Sed Petrol 60:870–883

Dżułyński S, Walton EK (1965) Sedimentary features of Flysch and Greywackes. Elsevier, Amsterdam

Ekdale EG, Ekdale AA (2018) *Hillichnus lobosensis*, an unusually complex trace fossil of burrowing bivalves from the Paleogene of southern California, USA. Palaeo Palaeo Palaeo 493:119–125

Fan Y, Lin SJ, Held IM, Yu Z, Tolman HL (2012) Global ocean surface wave simulation using a coupled atmosphere–wave model. J Climate 25:6233–6252

Fernández-López SR, Pavia G, Erba E, Guiomar M, Henriques MH, Lanza R, Mangold C, Olivero D, Tiraboschi D (2009) Formal proposal for the Bathonian GSSP (Middle Jurassic) in the Ravin Du Bès Section, Bas-Auren, SE France. Swiss J Geosci 102:271–295

Field ME, Gardner JV, Jennings AE, Edwards BD (1982) Earthquake induced sediment failures on a 0.25° slope, Klamath River delta. Calif Geol 10:542–546

Frakes LA, Francis JE, Syktus JI (1992) Climate modes of the phanerozoic: the history of the earth's climate over the past 600 million years. Cambridge University Press

Fürsich FT, Oschmann W (1993) Shell beds as tools in basin analysis: the Jurassic of Kachchh, Western India. J Geol Soc London 150:169–185

Fürsich FT, Oschmann W, Jaitly AK, Singh IB (1991) Faunal response to transgressive–regressive cycles: example from the Jurassic of Western India. Palaeo Palaeo Palaeo 85:149–159

Fürsich FT, Oschmann W, Singh IB, Jaitly AK (1992) Hardgrounds, reworked concretion levels and condensed horizons in the Jurassic of western India: their significance for basin analysis. J Geol Soc London 149:313–331

Fürsich FT, Alberti M, Pandey DK (2013) Stratigraphy and palaeoenvironments of the Jurassic Rocks of Kachchh—field guide. Bering Spec Iss 7:1–174

Fürsich FT, Alberti M, Pandey DK (2017) Behavioural variants of the trace fossil Gyrochorte. Zittel 89:13–21

Fürsich FT, Uchman A, Alberti M, Pandey DK (2018) Trace fossils of an amalgamated storm-bed succession from the jurassic of Kachchh Basin, India: the significance of time averaging in ichnology. J Palaeogeography 7:14–31

Garg R, Singh SK (1983) Distinctive Bathonian agglutinated Foraminifera from Jaisalmer, western Rajasthan, India. J Palaeontol Soc India 28:118–133

Hallam A (1988) A re-evaluation of Jurassic eustasy in the light of new data and the revised Exxon curve. In: Wilgus CK, Hastings BS, Kendall CG StC, Posamatir HW, Ron CA, van Wagner JC (eds) Sea-level changes—an integrated approach. SEPM Spec Publ 42:261–273

Hallam A (1993) Jurassic climate as inferred from the sedimentary and fossil record. Phil Trans R Soc London B 341:287–296

Hallam A (2001) A review of the broad pattern of the Jurassic sea-level changes and their possible causes in the light of current knowledge. Palaeo Palaeo Palaeo 167:23–37

Harms JC, Southard JB, Spearing DR, Walker RG (1975) Depositional environments as interpreted from primary sedimentary structures and stratification sequences. SEPM Short Course 2:1–161

Harms JC, Southard JB, Walker RG (1982) Structures and sequences in clastic rocks. SEPM Short Course 9:8–51

Howard JD, Singh IB (1985) Trace fossils in the Mesozoic sediments, Kachchh, western India. Palaeo Palaeo Palaeo 5:99–122

Jacquin T, Dardeau G, Durlet C, de Graciansky PC de, Hantzpergue P (1998) The North Sea cycle: an overview of 2nd order transgressive/regressive facies cycles in western Europe. In: de Graciansky PC, Hardenbo J, Jacquin T, Vail PR (eds) Mesozoic and Cenozoic sequence stratigraphy of European Basins. SEPM Spec Publ 60:445–466

Krishna J (1983) Callovian-Albian ammonoid stratigraphy and palaeobiogeography in the Indian sub-continent with special reference to the Tethys Himalaya. Him Geol 11:43–72

Krishna J (1987) An overview of the Mesozoic stratigrapgy of the Kachchh and Jaisalmer basins. J Palaeont Soc India 32:136–149

Kulkarni KG, Borkar VD, Petare TJ (2008) Ichnofossils from the Fort Member (Middle Jurassic), Jaisalmer Formation, Rajasthan. J Geol Soc Ind 71:731–738

Kumar N (2006) Modern and ancient barrier sediments: New interpretations based on stratal sequence in inlet-filling sands and on recognition of nearshore storm deposits. Ann New York Acad Sci 220:245–340 (Chapter 1)

Kumar N, Sanders JE (1974) Inlet sequence: a vertical succession of sedimentary structures and textures created by the lateral migration of tidal inlets. Sedimentol 21:491–532

Leckie DA, Krystinik LF (1989) Is there evidence for geostrophic currents preserved in the sedimentary record of inner to middle-shelf deposits. J Sed Res 59:862–870

Legarreta L, Uliana MA (1996) The Jurassic succession in west-central Argentina: strata patterns, sequences and palaeogeographic evolution. Palaeo Palaeo Palaeo 120:303–330

Liesa CL, Rodríguez-López JP, Ezquerro L, Alfaro P, Rodríguez-Pascua MÁ, Lefuente P, Arlegui L, Simón JL (2016) Facies control on seismites in an alluvial-aeolian system: the Pliocene dunefield of the Teruel half-graben basin. Sediment Geol 344:237–252

Lowe DR (1975) Water escape structures in coarse grained sediments. Sedimentol 22:157–204

Mattioli E, Erba E (1999) Synthesis of calcareous nannofossil events in Tethyan Lower and Middle Jurassic successions. Rivista Italiana Di Paleontol Stratigr 105:343–376

Mishra PC, Singh NP, Sharma DC, Kakaroo AK, Upadhyay H, Saini ML (1993) Lithostratigraphy of Indian petroliferous basins, document ii west Rajasthan basins. KDMIPE, ONGC Publication 1–123

Mitra P, Mukherjee MK, Mathur BK, Bhandari SK, Qureshi SM, Bahukhandi GC (1993) Exploration and hydrocarbon prospect in Jaisalmer Basin, Rajasthan. In: Biswas SK, Pandey J, Dave A, Maithani A, Garg P, Thomas NJ (eds) Proceedings of second seminar on petroliferous basins of India, vol 2. Indian Petroleum Publishers, Dehradun, pp 235–284

Montenat C, Barrier P, Ott d′Estevou P, Hibsch C (2007) Seismites: an attempt at critical analysis and classification. Sediment Geol 196:5–30

Moretti M, Ronchi A (2011) Liquefaction features interpreted as seismites in the Pleistocene fluvio-lacustrine deposits of the Neuquén Basin (Northern Patagonia). Sediment Geol 235:200–209

Moretti M, Van Loon AJ (2014) Restriction to the application of 'diagnostic criteria' for recognising ancient seismites. J Palaeogeography 3:162–173

Nagtegaal PJC (1965) An approximation to the genetic classification of non-organic sedimentary structures. Geol Mijnbouw 44:347–352

Oldham RD (1886) Preliminary notes on the geology of Northern Jaisalmer. Rec Geol Surv India 19:157–160

Owen G (1987) Deformation processes in unconsolidated sands. In: Jones ME, Preston RMF (eds) Deformation of sediments and sedimentary rocks. Geol Soc London Spec Publ 29:11–24

Owen G (2003) Load structures: gravity-driven sediment mobilization in the shallow subsurface. In: Van Rensbergen P, Hillis RR, Maltman AJ and Morley CK (eds) Subsurface sediment mobilization. Geol Soc London Spec Publ 216:21–34

Owen G, Moretti M (2011) Identifying triggers for liquefaction-induced soft-sediment deformation in sands. Sediment Geol 235:141–147

Owen G, Moretti M, Alfaro P (2011) Recognising triggers for soft-sediment deformation: current understanding and future directions. Sediment Geol 235:133–140

Pandey DK, Fürsich FT (1994) Bajocian (Middle Jurassic) age of the Lower Jaisalmer Formation of Rajasthan, western India. Newslett Strat 30:75–81

Pandey DK, Choudhary S (2007) Sequence stratigraphic framework of Lower to lower Middle Jurassic sediments of the Jaisalmer Basin, India. Bering 37:121–131

Pandey DK, Sha J, Choudhary S (2010) Sedimentary cycles in the Callovian-Oxfordian of the Jaisalmer Basin, Rajasthan, western India. Vol Jurassica 8:131–162

Pandey DK, Fürsich FT, Alberti M (2014) Stratigraphy and palaeoenvironments of the Jurassic rocks of the Jaisalmer Basin—field guide. Beringia Spec Issue 9:1–111

Pazos PJ, Fernández DE (2010) Three-dimensionally integrated trace fossils from shallow-marine deposits in the Lower Cretaceous of the Neuquén Basin (Argentina): Hillichnus agrioensis isp. nov. Act Geol Pol 60:105–118

Potter PE, Pettijohn FJ (1963) Paleocurrents and basin analysis. Springer, Berlin

Prasad S (2006) Ammonite biostratigraphy of Middle to Late Jurassic rocks of Jaisalmer Basin, Rajasthan, India. Mem Geol Surv Ind 52:1–146

Rai J, Bajpai S, Kumar R, Singh A, Kumar K, Prakash N (2016) The earliest marine transgression in Western India: new insights from calcareous nannofossils from Lathi Formation, Jaisalmer Basin. Cur Sci 111:1631–1639

Rao RV (1972) Subsurface stratigraphy, tectonic setting and petroleum prospects of the Jaisalmer area, Rajasthan, India. Procs IV Symp Dev Petrol Res Asia and Far East. Camberra, Australia 41:366–371

Sarkar S, Chakraborty S, Banerjee S, Bose PK (2002) Facies sequence and cryptic imprint of sag tectonics in late Proterozoic Sirbu Shale, central India. In: Altermann W, Corcoran P (eds) Precambrian sedimentary environments: a modern approach to ancient depositional systems. IAS Spec Publ 33:369–382

Sarkar S, Choudhuri A, Banerjee S, Van Loon AJ, Bose PK (2014) Seismic and non-seismic deformation structures in the Proterozoic Bhander Limestone, Central India. Geologos 20:89–103

Sarkar S, Choudhuri A, Mandal S, Eriksson PG (2016) Microbial mat-related structures shared by both siliciclastic and carbonate formations. J Palaeogeography 5:278–291

Seilacher A (1969) Fault-graded beds interpreted as seismites. Sedimentol 13:155–159

Sellwood WB, Valdes PJ, Price GD (2000) Geological evolution of multiple general circulation model stimulations of Late Jurassic palaeoclimate. Palaeo Palaeo Palaeo 156:147–160

Seth A, Sarkar S, Bose PK (1990) Synsedimentary seismic activity in an immature passive margin basin (Lower member of the Katrol Formation, Upper Jurassic, Kutch, India). Sediment Geol 68:279–291

Sims JD (1973) Earthquake-induced structures in sediments in Van Norman Lake, San Fernando, California. Science 182:161–163

Sims JD (1975) Determining earthquake recurrence intervals from deformational structures in young lacustrine sediments. Tectonophys 29:141–152

Singh CSP, Jaitly AK, Pande DK (1982) First report of some Bajocian-Bathonian (Middle Jurassic) ammonoids and the age of the oldest sediments from Kachchh, Western India. Newslett Strat 11:37–40

Singh IB (1989) Dhosa Oolite—a transgressive condensation horizon of Oxfordian age in Kachchh, western India. J Geol Soc Ind 34:152–160

Singh NP (2006) Mesozoic lithostratigraphy of Jaisalmer Basin, Rajasthan. J Palaeont Soc Ind 51:53–56

Sinha AK, Yadav RK, Qureshi SM (1993) Status of exploration in South Shahgarh Sub-basin of Jaisalmer Basin, Rajasthan. In: Biswas SK (ed) Proceedings of second seminar on petroliferous basins of India, vol 2. Indian Petroleum Publishers, pp 285–333

Subbotina NN, Datta AK, Srivastava BN (1960) Foraminifera from the Upper Jurassic deposits of Rajasthan (Jaisalmer) and Kachchh, India. Bull Geol Min Metal Soc India 23:1–48

Surlyk F (1991) Sequence stratigraphy of the Jurassic Lowermost Cretaceous of east Greenland. AAPG Bull 75:1468–1488

Suter F, Martínez JI, Vélez MI (2011) Holocene soft-sediment deformation of the Santa Fe–Sopetrán Basin, northern Colombian Andes: evidence for pre-Hispanic seismic activity? Sed Geol 235:188–199

Swift DJP, Freeland GL, Young RA (1979) Time and space distribution of megaripples and associated bedforms, Middle Atlantic Bight, North American Atlantic Shelf. Sedimentol 26:389–406

Swift DJP, Hudelson PM, Brenner RL, Thompson P (1987) Shelf construction in a foreland basin: storm beds, shelf sand-bodies, and shelf slope depositional sequences in the Upper Cretaceous Masaverde Group, Book Cliffs, Utah. Sedimentol 34:423–457

Terwindt JHJ (1988) Palaeo-tidal reconstructions of inshore tidal depositional environments. In: Boer PL, Gelder de A van, Nio SD (eds) Tide-influenced sedimentary environments. Reidel, Dordrecht, pp 233–263

Terwindt JHJ, Breusers HNC (1972) Experiments on the origin of flaser, lenticular and sand-clay alternating bedding. Sedimentol 19:85–98

Tiraboschi D, Erba E (2010) Calcareous nannofossil biostratigraphy (Upper Bajocian-Lower Bathonian) of the Ravin Du Bès Section (Bas Auran, Subalpine Basin, SE France): evolutionary trend of *Watznaueria barneside* and new findings of "*Rucinolithus*" morphotypes. Geobios 43:59–76

Torsvik TH, Pandit MK, Redfield TF, Ashwal LD, Webb SJ (2005) Remagnetization of Mesozoic limestones from the Jaisalmer basin, NW India. Geophys J Int 161:57–64

Van Loon AJ (2009) Soft-sediment deformation structures in siliciclastic sediments: an overview. Geolog 15:3–55

Van Loon AJ, Su DC (2013) Deformed stromatolites in marbles of the Mesoproterozoic Wumishan Formation as evidence for synsedimentary seismic activity. J Palaeogeography 2:390–401

Yang BC, Dalrymple RW, Chun SS (2005) Sedimentation on a wave-dominated, open-coast tidal flat, southwestern Korea: summer tidal flat—winter shoreface. Sedimentol 52:235–252

Biostratigraphic Implications of the Calcareous Nannofossils from the Spiti Formation at Langza, Spiti Valley

Abha Singh, Nazim Deori, D. K. Pandey, Rajesh Singh Shekhawat, and Poonam Verma

Abstract Calcareous nannofossil biostratigraphy has been attempted for the first time on black shale of the Lower Member of the Spiti Formation exposed in Langza area, Spiti Valley, Himachal Pradesh. Ammonites and dinoflagellate cysts biostratigraphy usually assign the age of the Spiti Formation as Oxfordian to Tithonian. The present study provides an older, Callovian age (part of NJ12 Nannofossil Zone) to the black shale ('*Belemnites gerardi* beds') belonging to the belemnites-rich Lower Member of Spiti Formation based on biostratigraphic ranges of *Ansulasphaera helvetica*, *Lotharingius hauffii, Watznaueria contracta and Watznaueria ovata.* Reworking of nannofossil taxa has also been reported by the sporadic occurrences of *Carinolithus magharensis* (LAD in Bathonian) in a few samples. The rare occurrence of *Faviconus multicolumnatus* (FAD in Oxfordian) in the uppermost fossiliferous sample indicates the leaking of this taxa from the younger horizons.

Keywords Calcareous nannofossils · Spiti Formation · Callovian · Langza · Spiti valley

A. Singh (✉) · P. Verma
Birbal Sahni Institute of Palaeosciences, 53, University Road, Lucknow 226007, Uttar Pradesh, India
e-mail: abha.maurya@gmail.com

N. Deori
Department of Earth and Environmental Sciences, K.S.K.V. Kachchh University, Bhuj, Gujarat, India

D. K. Pandey
Department of Geology, School of Earth, Biological and Environmental Science, Central University of South Bihar, Gaya 824236, Bihar, India

R. S. Shekhawat
Department of Geology, University of Rajasthan, Jaipur 302004, Rajasthan, India

1 Introduction

The Spiti Valley, Himachal Pradesh is well known for its excellent exposures of Neoproterozoic to Cretaceous sediments of the Tethyan Himalaya (Bhargava 2008). Among them, the predominantly marine Jurassic and Cretaceous sequences, represented by Spiti, Giumal and Chikkim formations are well exposed in the Spiti valley near Kaza area (Fig. 1). Earlier researchers have reported exceptionally rich invertebrate fossil fauna, especially the ammonites from Spiti and Giumal formations (Strachey 1851; Arkell 1956; Oppel 1863; Blanford 1865; Stoliczka 1865; Uhlig 1903, 1910a, b, Srikantia 1981; Krishna et al. 1982; Krishna 1983; Pathak 1993; Pathak and Krishna 1993; Pathak 1997, 2007; Bhargava and Bassi 1998; Lukeneder et al. 2013; Pandey et al. 2013, 2018 Pandey and Pathak 2015). In the last few years, the Spiti Formation is getting more attention of the researchers because of the presence of black shale for its hydrocarbon potential and redox implications.

The first ammonoid collection from the Spiti Formation was done by Greisbach (1891). Stoliczka (1865) recognized three distinct litho-units in the Spiti Formation (i) lower part representing dark splintery shale containing mostly belemnites, other fossils being rare (ii) middle part characterized by friable dark shale with concretions yielding ammonoids and (iii) upper part of grey shale, sandy to silty interbeds and
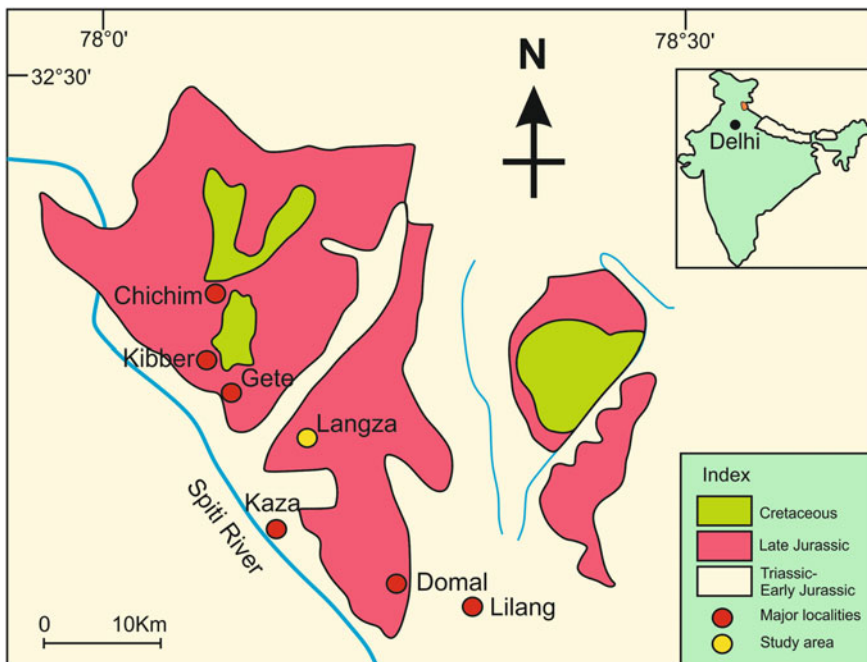
Fig. 1 Geological map showing Mesozoic rock outcrops in and around Kaza area, Spiti Valley, Himachal Pradesh (adapted from Hayden 1904)

sparse fossils. These three divisions were later named as *Belemnites gerardi* beds, Chidamu beds and Lochambel beds in ascending order by Diener (1895). Pathak (1993) followed the three-fold division of the Spiti Formation, but used Lower, Middle and Upper members which very well coincide with the three-fold division of Diener (1895).

Further, Arkell (1956) used Uhlig's ammonoid collection for his study and assigned Lower Oxfordian age to *'Belemnites gerardi* beds' (Lower Spiti Shale), Lower Tithonian age to 'Chidamu beds' (Middle Spiti Shale) and Upper Tithonian-Valanginiana age to 'Lochambel beds' (Upper Spiti Shale). The Spiti Formation exposed in Malla-Johar area was dated Oxfordian-Valanginian based on ammonites (Krishna et al. 1982; Krishna 1983). Jain et al. (1984) assigned Kimmeridgian-Tithonian age to a major part of the Spiti Formation of Kumaun area based on five successive dinoflagellate cysts assemblages. Ammonite biostratigraphic studies by Pathak (1993, 1997) and Pathak and Krishna (1993) from the Spiti Formation exposed in and around Chichim and Gete villages in the Spiti valley area, near Kaza also suggested Oxfordian to Tithonian age. However, Cariou et al. (1996) have suggested Callovian age to the Lower Member ('Belemnites gerardi beds') of the Spiti Formation.

The biostratigraphic potential of calcareous nannofossils is quite high in the Lower and Middle Jurassic, due to their rapid evolutionary rate, and common and continuous occurrence in sediments. The objective of this study is to present calcareous nannofossil biostratigraphy to precisely date the lower part of the Spiti Formation (*'Belemnites gerardi* beds'), which is hitherto devoid of ammonoids, except one record published by Cariou et al. (1996).

2 Lithostratigraphic Framework

The Paleozoic–Mesozoic succession of the Spiti valley in the Tethyan Himalaya of Himachal Pradesh is considered as the deformed remnants of the northern continental margin of the Indian subcontinent. It is the largest marine sedimentary basin among the other synclinoria basin in the Tethyan Himalaya. The sedimentary succession of ~12,000 m thick consists dominantly of limestone, shale, siltstone and dolomite. The altitude of exposures varies from 3500 to 5000 m above the mean sea-level in the area. The succession was first referenced by Gerard (1827); subsequently worked by Hayden (1904, 1908) and Diener (1912). Further, detailed work on geological and paleontological aspects was done by many workers (Srikantia 1981; Bagati 1990; Gaetani and Garzanti 1991; Bhargava and Bassi 1998; Srikantia and Bhargava 1998; Myrow et al. 2003). The detailed lithostratigraphic framework of the Spiti valley was proposed by Bhargava (2008). He classified the sedimentary successions of the Spiti Basin into nine groups and twenty-four formations (Fig. 2). In chronostratigraphic order the groups are as follows- (i) Himanta Group, (ii) Sanugba Group, (iii) Kanawar Group, (iv) Kuling Group, (v) Tamba Kurkur Group, (vi) Sanglung Group, (vii) Nimoloksa Group, (viii) Kioto Group and (ix) Lagudarsi Group. In all the groups,

Group	Formation	Lithology	Age
Lagudarsi	Chikkim	Limestone, Shale	Albian-Campanian/Early Maastrichtian (Bertle and Suttner 2005, Bhargava and Bassi 1998)
	Giumal	Sandstone	Berriasian-Aptian (Lukeneder et al. 2013, Pandey and Pathak 2015)
	Spiti	Shale	Callovian-Tithonian (Pathak 2007, Cariou et al. 1996, Present study)
——————————— Unconformity ———————————			
Kioto	Tangling	Limestone, Dolomite	Late Triassic-Early Jurassic
	Para	Limestone, Dolomite	Late Rhaetian
Nimoloksa	Nunuluka	Sandstone, Siltstone, Limestone	Late Norian-Early Rhaetian
	Alaror	Shale, Siltstone, Limestone	Late Norian
	Hangrang	Limestone, Dolomite	Middle Norian
	Rangrik	Shale, Sandstone, Limestone	Early-Middle Norian
Sanglung	Rongtong	Dolomite, Limestone	Middle-Late Carnian
	Rama	Shale, Sandstone, Limestone	Early-Middle Carnian
Tamba Kurkur	Chomule	Limestone	Ladinic-Early Carnian
	Kaga	Shale, Sandstone, Limestone	Ladinian
	Mikin	Limestone	Induan-Anisian
——————————— Unconformity ———————————			
Kuling	Gungri	Shale	Dzulfian-? Early Dorashamian
	Gechang	Sandstone	Asselian-?Sakmarian
——————————— Unconformity ———————————			
Kanawar	Ganmachidam	Conglomerate, Sandstone, Shale	Late Carboniferous
	Po	Shale, Sandstone	Visean-?Serpukhovian
	Lipak	Limestone, Sandstone, Shale	Givetian-Tournaisian
	Muth	Sandstone	Early Devonian
——————————— Unconformity ———————————			
Sanugba	Takche	Limestone, Sandstone, Shale	Ashgill-? Wenlockian
	Thango	Conglomerate	Early Ordovician
——————————— Unconformity ———————————			
Haimanta	Kunzam La	Sandstone, Shale, Limestone	Early-Middle Cambarian
	Batal	Sandstone, Siltstone, Shale	Ediacaran-Early Cambarian

Fig. 2 Lithostratigraphic succession of the Spiti Valley (adapted from Bhargava 2008)

Lagudarsi is the youngest Group and further sub-divided into Spiti, Giumal and Chikkim formations in ascending order.

The Spiti Formation is 200 m thick succession, showing sharp and uncon-formable contact with the underlying Kioto Formation extending from Spiti Valley in Himachal Pradesh to the west to Malla Johar region in Uttarakhand to the east (Bertle and Suttner 2005). It continues up to Thakkhola region in Nepal. The Forma-tion comprises belemnite-rich grey to black shale having concretions, usually devoid of fossil nucleus in the Lower Member. The Middle Member show sharp reduction of belemnites and it is rich in ammonites with frequent occurrence of concretions having

fossil in nucleus (locally known as "Saligram"). The Upper Member is characterized by a decrease in the number of concretions and an increase in silt content with the frequent intercalations of hard bands. Ammonite biostratigraphy assigns Oxfordian to Tithonian age for this member (Pathak 1997, 2007; Pandey et al. 2013).

The Giumal Formation is 150 m thick. It lies conformably over the Spiti Formation exposed near Gete village situated about 20 km east of Kaza, Spiti Valley, Himachal Himalaya (Pandey and Pathak 2017). The Formation overlies sharply on the poorly cemented Spiti Formation. It comprises a succession of glauconitic sandstones, silty sandstones, calcareous shale and poorly sorted, rounded, subrounded to subangular coarse-grained sandstone, cemented by authigenic silica, ferruginous material and pigmentary glauconite (Bhargava 2008). The lithological characters and the presence of bivalve shells in the bottom part indicate a shallow marine environment of deposition. However, turbidity current related deposits characterize the deeper part of the basin (Bhargava 2008). Based on Ammonite genera *Berriasella*, *Odontodicoceras* and *Neocomites* from the lowermost part (Pathak 1997) and *Deshayesites*, *Cleoniceras*, *Colombiceras*, *Australiceras* etc. from the upper part (Lukeneder et al. 2013; Pandey and Pathak 2015), the age of Giumal Formation is assigned as Berriasian to Aptian.

The Chikkim Formation is exposed as thick cliff in the Chichim Village. At the type section, its thickness is about 150 m overlying the Guimal Formation (Bertle and Suttner 2005). It is further sub-divided into two Members

(a) Limestone Member: It comprises bluish-grey to greyish-blue argillaceous dolomitic limestone and also contains a few siliciclastic, shale bands and sporadic dark grey pyritic limestone.

(b) Shale Member: It lies conformably over the Lower Limestone Member; it consists of grey to ash grey colored silty shale, shaly limestone, marl, and fine silty beds.

The palaeo-depositional environment varies from shelf to basin accompanied by intervals of limited circulation in the Lower Limestone Member. The Upper Shale Member represents deposition in the outer shelf (Bhargava and Bassi 1998). The Limestone Member is assigned Cenomanian to Turonian age based on various species of *Globotruncana* (Kohli and Sastri 1956). Bertle and Suttner (2005) redesignated the Limestone Member as Lower Chikkim Member and assigned an Albian age on the basis of occurrence of *Biticinella breggiens* and *Planomalina buxforti* in the basal part of the formation. The Cenomanian/Turonian boundary was marked encompassing the OAE 2 event, 26 m above from the base of the Chikkim Formation (Bertle and Suttner 2005). Bertle and Suttner (2005) further redesignated the Shale Member as Upper Chikkim Member and assigned to Campanian age on the basis of rotaliids, *Globotruncana elevata, G. stuartiformis, G. stuarti,* and *G. gansseri*. They related the co-occurrence of *G. elevate* and *G. gansseri* to reworking. Bhargava and Bassi (1998) provided the age of the member range up to Campanian/Early Maastrichtian.

3 Materials and Methods

Sampling was done for calcareous nannofossils study from the section exposed on the way from Kaza to Langza. Beautiful black splintery shales were exposed along a Nala (rivulet cutting) near a small bridge (Fig. 3). Twenty black shale samples were collected from the Lower Member or *'Belemnites gerardi'* beds' of the Spiti Formation. Samples 1–16 were collected continuously at regular intervals moving upstream in the nala (N32º 16′ 04″: E78º 04′ 44″). Sample nos. 17 (N32º 15′ 35″:

Fig. 3 Litholog of the studied section along with the field photograph (length of sample packet = 21 cm)
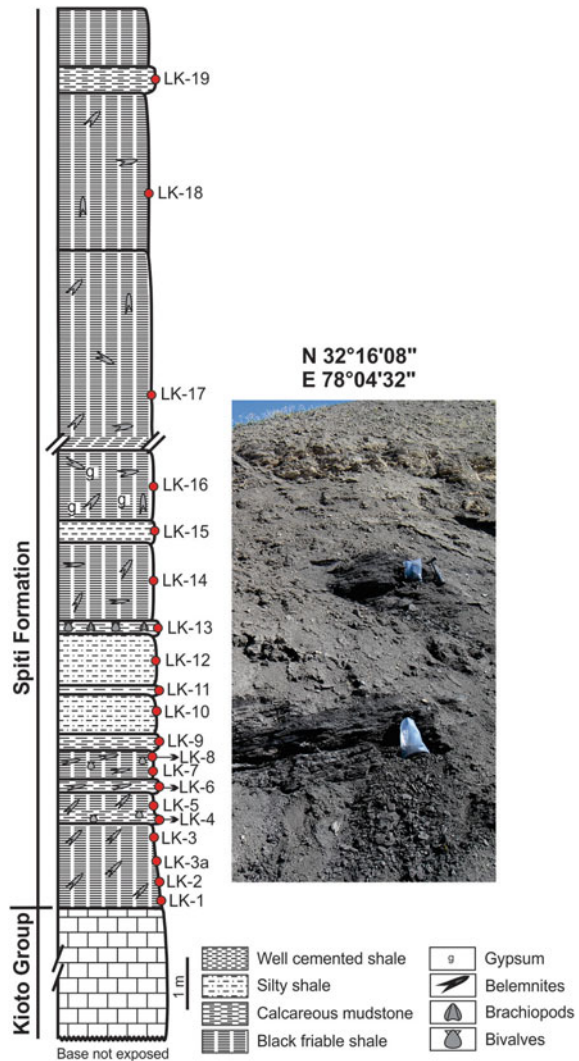
E78º 05′ 20″), 18 and 19 (N32º 14′ 44″: E78º 06′ 33″) were collected along rode cuttings.

For the qualitative estimation of nannofossils, smear-slides of all 20 samples were examined under a polarized microscope (Leica DM 2500 P) at a magnification of 1000X. The abundance of selected nannofossil taxa on each slide was estimated using the following criteria: V = very abundant, >10 specimens per field of view (fov); A = abundant, 1–10 specimens per fov; C = common, 1 specimen per 2–10 fov; F = few, 1 specimen per 11–50 fov; R = rare, 1 specimen per 51–200 fov. For the preservation of nannofossil assemblages, codes used are: G = Good, little evidence of etching or overgrowth; M = Moderate, specimens exhibit some etching and/or overgrowth; P= Poor, specimens are severely etched or exhibits overgrowth.

The bibliographic references of the species used in this study can be found in Bown (1998) and nannotax3 website. The numerical ages (in Ma years) were taken from nannotax3 website. The studied slides are housed in the museum of Birbal Sahni Institute of Palaeosciences, Lucknow (India) vide 16586–16605.

4 Biostratigraphy

The distribution and illustrations of the recorded nannofossils from Langza section are presented below (Figs. 4, 5). Highly productive, moderately preserved and fairly diversified nannofossil assemblage characterizes from sixteen productive samples (LK 1-16). The assemblage includes *Ansulasphaera helvetica*, *Axopodorhabdus cylindratus*, *Biscutum sp.*, *Carinolithus magharensis*, *Cyclagelosphaera margerelii*, *Ethmorhabdus gallicus*, *Faviconus multicolumnatus*, *Lotharingius hauffii*, *Stephanolithion bigotii*, *Watznaueria barnesiae*, *Watznaueria britannica*, *Watznaueria contracta*, *Watznaueria fossacincta*, *Watznaueria manivitiae*, *Watznaueria ovata*, *Zeugrhabdotus erectus* and two unidentified forms. The total range of *Ansulasphaera helvetica* (FAD-NJ12a, 166.4 Ma, Bathonian; LAD-NJ13, 163.8 Ma, Callovian, Bown and Cooper 1998) along with the presence of *Stephanolithion bigotii* (FAD-NJ13, 164.8 Ma, Callovian, Bown and Cooper 1998), *Watznaueria ovata* (FAD-166.07 Ma, Callovian, Grün and Zweili 1980) and *Lotharingius hauffii* (LAD-NJ12a, 165.55 Ma, Callovian, Bown and Cooper 1998), *Watznaueria contracta* (LAD-NJ12a. 165.55 Ma, Callovian, Bown and Cooper 1998) suggests a Callovian age (part of NJ12 Nannofossil Zone) to the assemblage recorded from the Lower Member (‘*Belemnites gerardi* beds’) of the Spiti Shale Formation (Fig. 6). The presence of Carinolithus magharensis (LAD-Bathonian, 167.2 Ma, Mattioli and Erba 1999) suggests reworking. The occurrence of Faviconus multicolumnatus (FAD-NJ15b, 157.9 Ma, Oxfordian, Bown and Cooper 1998) in LK-16 (productive sample in the upper part of succession) along with the marker nannofossils of Callovian age indicates that it leaked from the younger horizon (Fig. 4).
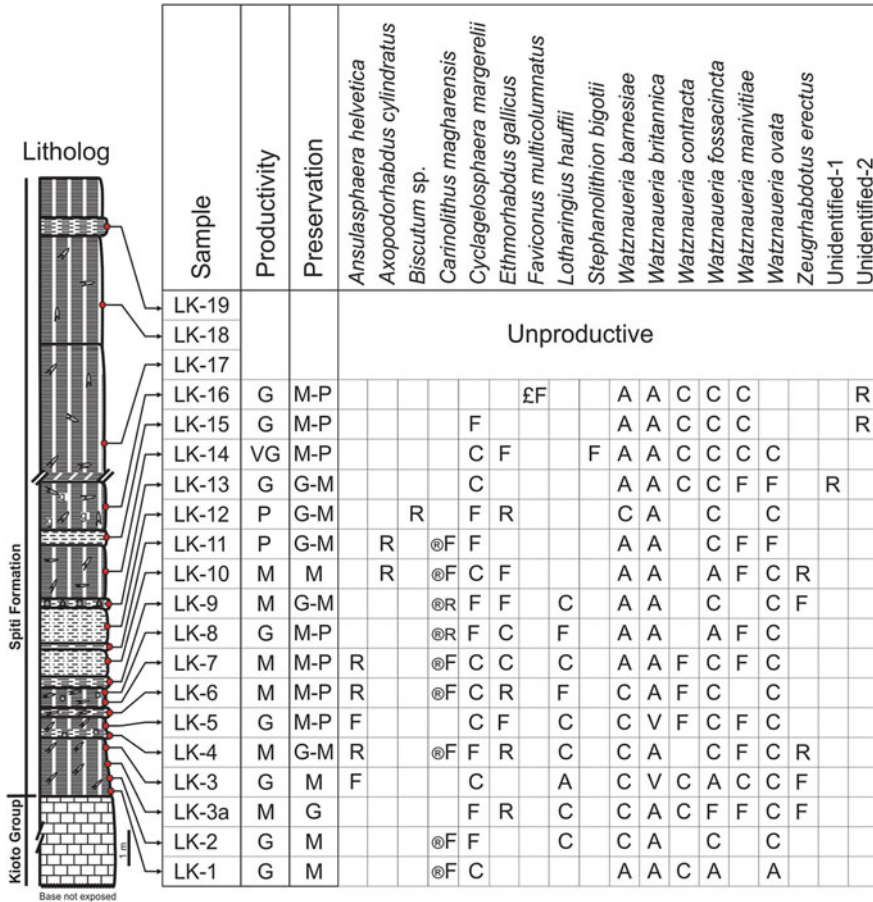
Fig. 4 Semi-quantitative distribution of nannofossils taxa recorded from studied section (®—indicates reworked taxa, £—indicates leaked taxa, V = Very abundant, A = Abundant, C = Common, F = Few, R = Rare, G = Good, M = Moderate, P = Poor)

Sample	Productivity	Preservation	Ansulasphaera helvetica	Axopodorhabdus cylindratus	Biscutum sp.	Carinolithus magharensis	Cyclagelosphaera margerelii	Ethmorhabdus gallicus	Faviconus multicolumnatus	Lotharingius hauffii	Stephanolithion bigotii	Watznaueria barnesiae	Watznaueria britannica	Watznaueria contracta	Watznaueria fossacincta	Watznaueria manivitiae	Watznaueria ovata	Zeugrhabdotus erectus	Unidentified-1	Unidentified-2
LK-19											Unproductive									
LK-18																				
LK-17																				
LK-16	G	M-P							£F			A	A	C	C	C				R
LK-15	G	M-P					F					A	A	C	C	C				R
LK-14	VG	M-P					C	F		F		A	A	C	C	C	C			
LK-13	G	G-M					C					A	A	C	C	F	F		R	
LK-12	P	G-M		R			F	R				C	A	C		C				
LK-11	P	G-M		R	®F		F					A	A	C	F	F				
LK-10	M	M		R	®F		C	F				A	A	A	F	C	R			
LK-9	M	G-M			®R		F	F		C		A	A	C		C	F			
LK-8	G	M-P			®R		F	C		F		A	A	A	F	C				
LK-7	M	M-P	R		®F		C	C		C		A	A	F	C	F	C			
LK-6	M	M-P	R		®F		C	R		F		C	A	F	C		C			
LK-5	G	M-P	F				C	F		C		C	V	F	C	F	C			
LK-4	M	G-M	R		®F		F	R		C		C	A		C	F	C	R		
LK-3	G	M	F				C			A		C	V	C	A	C	C	F		
LK-3a	M	G					F	R		C		C	A	C	F	F	C	F		
LK-2	G	M			®F		F			C		C	A		C		C			
LK-1	G	M			®F		C					A	A	C	A		A			

5 Discussion

Ammonites have been worked out in detail from the Spiti Shale Formation for the biostratigraphy and dating of the Mesozoic sequences of the Spiti Valley. Earlier, several workers have assigned Oxfordian to Valanginian age to the Spiti Formation (Pascoe 1959; Krishna et al. 1982; Krishna 1983; Pathak and Krishna 1993). Krishna et al. (1982) proposed a two-fold classification for the Spiti Formation and divided it into Lower Spiti and Upper Spiti. The Lower Spiti yields abundant belemnites, whereas the Upper Spiti has given rise several ammonites in addition to some belemnites, bivalves, brachiopods, etc. (including middle and upper members of Pathak 1993). Jain et al. (1984) reported five dinoflagellate

cyst assemblages from the Spiti Shale Formation of Kumaun area and assigned Kimmeridgian–Tithonian age to the major part of the formation. Pathak and Krishna (1993) recognised following ammonoid assemblage; *Mayaites, Epimayites* (Oxfordian),? *Torquatispinctes, Pachysphinctes, Subdichotomoceras, ?Taramelliceras, Streblites* (Kimmeridgian), *Aulacosphinctoides* and *Hildoglochiceras* assemblages (Early Tithonian), *Virgatosphinctes* and *Himalayites* assemblages (Late Tithonian) and *Neocosmoceras* and *Odontodiscoceras* assemblages (Berriiasian-Valanginian). Pathak (1997) recognized the Kimmeridgian Stage and recorded Kimmeridgian-Tithonian boundary on the basis of the temporal distribution of *Pachysphinetes linquiferus, P. granti, Torquatisphinctes torquatus, Katroliceras* cf.

Figure plate showing calcareous nannofossils:
1a, 1b — *Ansulasphaera helvetica*
2a, 2b — *Axopodorhabdus cylindratus*
3a, 3b — *Biscutum* sp.
4, 5 — *Carinolithus magharensis*
6 — *Cyclagelosphaera margerelii*
7 — *Ethmorhabdus gallicus*
8 — *Faviconus multicolumnatus*
9 — *Lotharingius hauffii*
10 — *Lotharingius hauffii*
11 — *Stephanolithion bigotii*
12a, 12b — *Watznaueria barnesiae*
13 — *Watznaueria britannica*
14 — *Watznaueria britannica*
15 — *Watznaueria britannica*
16 — *Watznaueria britannica*
17 — *Watznaueria contracta*
18 — *Watznaueria contracta*
19 — *Watznaueria contracta*
20 — *Watznaueria fossacincta*
21 — *Watznaueria manivitiae*
22 — *Watznaueria ovata*
23 — *Watznaueria ovata*
24 — *Zeugrhabdotus erectus*
25 — Unidentified-1
26 — Unidentified-2

◄**Fig. 5** Photomicrographs of calcareous nannofossils under cross-polarized light. **1a–b** *Ansulasphaera helvetica* Grün and Zweili (1980) (BSIP slide no.-16589, 63.2/19.4), **2a–b** *Axopodorhabdus cylindratus* (Noël 1965) Wind and Wise *in* Wise and Wind (1977) (BSIP slide no.-16590, 84.1/17.2), **3a–b** *Biscutum sp. (*BSIP slide no.-16591*, 84.6/15.2), **4–5** *Carinolithus magharensis* (Moshkovitz and Ehrlich 1976) Bown (1987) (4- BSIP slide no.-16590, 62.2/19.1; 5- BSIP slide no.-16586, 87.2/18.0), **6** *Cyclagelosphaera margerelii* Noël (1965) (BSIP slide no.-16586, 90.0/18.0), **7** *Ethmorhabdus gallicus* Noël (1965) (BSIP slide no.-16588, 78.8/16.8), **8** *Faviconus multicolumnatus* Bralower *in* Bralower et al. 1989 (BSIP slide no.-16595, 61.2/17.2), **9–10** *Lotharingius hauffii* Grün and Zweili *in* Grün et al. 1974 (9- BSIP slide no.-16587, 90.1/17.0; 10- BSIP slide no.-16586, 76.9/12.0), **11** *Stephanolithion bigotii* Deflandre 1939 *bigoti* Medd (1979) (BSIP slide no.-16593, 73.1/17.0), **12a–b** *Watznaueria barnesiae* (Black *in* Black and Barnes 1959) Perch-Nielsen 1968 (BSIP slide no.-16586, 63.0/12.0), **13–16** *Watznaueria britannica* (Stradner 1963) Reinhardt 1964 (13- BSIP slide no.-16586, 68.8/12.0; 14- BSIP slide no.-16588, 69.5/17.8; 15- BSIP slide no.-16586, 60.2/12.0; 16- BSIP slide no.-16589, 83.1/17.0), **17–19** *Watznaueria contracta* (Bown and Cooper 1989) Cobianchi et al. (1992) (17- BSIP slide no.-16593, 70.1/17.0; 18- BSIP slide no.-16592, 90.0/17.0; 19- BSIP slide no.-16588, 88.8/16.8), **20** *Watznaueria fossacincta* (Black 1971) Bown *in* Bown and Cooper 1989 (BSIP slide no.-16586, 62.8/12.0), **21** *Watznaueria manivitiae* Bukry 1973 (BSIP slide no.-16589, 62.8/19.6), **22–23** *Watznaueria ovata* Bukry 1969 (22- BSIP slide no.-16586, 60.0/12.0; 23- BSIP slide no.-16588, 64.6/16.5), **24** *Zeugrhabdotus erectus* (Deflandre *in* Deflandre and Fert 1954) Reinhardt 1965 (BSIP slide no.-16589, 82.6/19.8), **25** *Unidentified-1* (BSIP slide no.-16592*, 90.5/17.0*), **26** *Unidentified-2 (*BSIP slide no.-16594*, 70.6/17.2) (scale bar = 2 μm in each photomicrograph)*

pottingeri, Hybonoticeras hybonotum, Aspidiceras ephiceroides, A. subwynnei, and *Taramelliceras* sp.

Vijaya and Kumar (2002) recorded palymnomorphs from the Spiti Shale Formation and recognized three Assemblage Zones and assigned age from Oxfordian to Berriasian. Assemblage zone 1 and 2 corresponds to the lower and upper part of the Spiti Shale B and Assemblage zone 3 corresponds to the upper part of the Spiti Shale C. While the Spiti Shale A was devoid of palynomorphs which correspond to the Lower Member of Pathak (1993). Further, Pathak (2007) indicated hiatus from Late Callovian—Early Oxfordian and suggested that the age range of the lower part of the Spiti Formation is not older than middle Oxfordian. Furthermore, Pandey et al. (2013) recognized four distinct ammonoid assemblages within all the three members*, Pachysphinctes* Assemblage 1 (Late Kimmeridgian), *Aulacosphinctoides* Assemblage 2 (basal Tithonian), *Virgatosphinctes* Assemblage 3 (Early Tithonian) and *Himalayaintes* Assemblage 4 (Late Tithonian). The ages were assigned by correlating the ammonoid assemblages with zones/assemblages of the Indian subcontinent and standard Tethyan scheme (Cariou and Hantzpergue 1997). Cariou et al. (1996) assigned Callovian age to the Lower Member of the Spiti Formation based on records of ammonite genera *Idiocyclocers*, *Kinkeliniceras*, *Hubertoceras*, *Obtusicostites* and *Grossouvevera* from this Member at Langza Section i.e., present study area.

The present nannofossil biostratigraphical work carried out from the Lower Member of the Spiti Formation, which has recently yielded one specimen of *Epimayaites* (Oxfordian) in the upper part of Lower Shale Member of the Spiti Formation (Pandey DK et al. under preparation). The recorded nannofossil assemblage from the lower and middle parts of the succession (upper part of succession
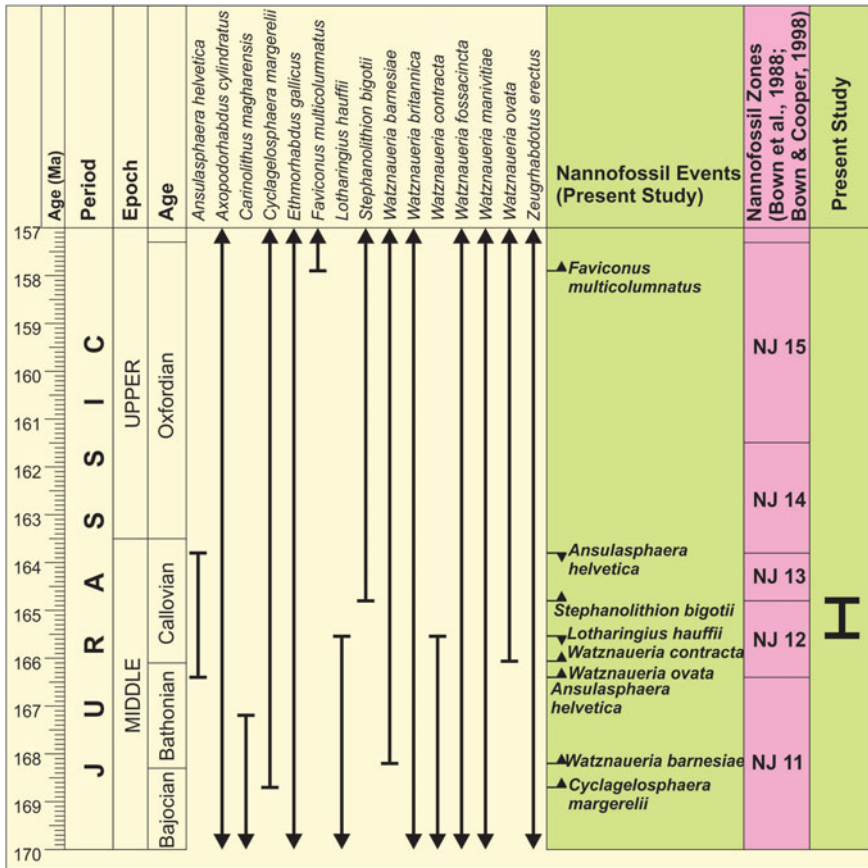
Fig. 6 Calcareous nannofossils stratigraphic ranges and events recorded in the present study and its calibration with standard nannofossil zonation scheme for age assignment

unproductive for nannofossils) suggests the Callovian (part of NJ 12 Zone of Bown et al. 1988) age. Thus, on the basis of present calcareous nannofossil records and previous fossil studies, the stratigraphic range of the Spiti Formation can be considered as Callovian to Tithonian, which is well supported by ammonite record (Cariou et al. 1996). It appears that the older part of the Lower Member of the Spiti Formation is missing in other sections (Chichim, Gete, Diumal etc.) or needs further careful investigations.

6   Conclusions

The present study signifies the potential of nannofossil studies for biostratigraphy and demonstrates its extensive use for dating the marine successions devoid or having rare occurrence of ammonoids, which are the basic chronostratigraphic markers during the Mesozoic. The ammonoid poor lower part of the Lower Member of the Spiti Formation is precisely dated as Callovian (part of NJ 12 Nannofossil Zone) based on the nannofossil assemblage recorded from it.

References

Arkell WJ (1956) Jurassic geology of the world. Oliver and Boyd, Edinburgh

Bagati TN (1990) Lithostratigraphy and facies variation in the Spiti Basin (Tethys), Himachal Pradesh, India. Him Geol 1:35–47

Bertle RJ, Suttner TJ (2005) New biostratigraphic data from the Chikkim Formation (Cretaceous, Tethys Himalaya, India). Cret Res 26:882–894

Bhargava ON (2008) An updated introduction to the Spiti geology. J Palaeontol Soc India 53:113–129

Bhargava ON, Bassi UK (1998) Geology of the Spiti-Kinnaur, Himachal Himalaya. Mem Geol Surv India 124:1–210

Black M (1971) Coccoliths of the Speeton Clay and Sutterby Marl. Proc Yorks Geol Soc 38:381–424

Black M, Barnes B (1959) The structure of Coccoliths from the English Chalk. Geol Mag 96:321–328

Blanford H (1865) Paleontology of Niti in the northern Himalayas; being descriptions and figures of the Paleozoic and secondary fossils collected by colonel Richard Strachey RE Jurassic. Military Orphan Press, Calcutta, Cutter

Bown PR (1987) Taxonomy, evolution, and biostratigraphy of Late Triassic-Early Jurassic calcareous nannofossils. Spec Pap Palaeont 38:1–118

Bown PR, Cooper MKE (1989) New calcareous nannofossils from the Jurassic. J Micropalaeontol 8:91–96

Bown PR (ed) (1998) Calcareous nannofossil biostratigraphy. British Micropalaeontological Soc Publ Ser, Chapman and Hall, London

Bown PR, Cooper MKE (1998) *Jurassic*. In: Bown PR (ed) Calcareous nannofossil biostratigraphy. British Micropalaeontological Society Publication Series, Chapman and Hall, London, pp 34–85

Bown PR, Cooper MKE, Lord AR (1988) A calcareous nannofossil biozonation scheme for the early to mid Mesozoic. Newsl Stratig 20:91–114

Bralower TJ, Monechi S, Thierstein HR (1989) Calcareous nannofossil zonation of the Jurassic-Cretaceous boundary interval and correlation with the geomagnetic polarity timescale. Mar Micropaleontol 14:153–235

Bukry D (1969) Upper Cretaceous coccoliths from Texas and Europe. Univ Kans Paleontol Contrib Article 51 (Protista 2):1–79

Bukry D (1973) Phytoplankton stratigraphy, Deep Sea Drilling Project Leg 20, Western Pacific Ocean. Initial Reports DSDP 20:307–317

Cariou E, Enay R, Almeras Y (1996) Newly discovered Callovian ammonite fauna in the Himalayan SPITI shales at Spiti and compared chronostratigraphy of Middle and Upper Jurassic succession in Spiti and Central Nepal (Thakkhola) areas. CR Acad Sci 322(II):861–868

Cariou E, Hantzpergue P (eds) (1997) Biostratigraphie du Jurassique ouest-européen et méditerranéen: zonations parallèles et distribution des invertébrés et microfossils. Bulletin du Centre Recherches Elf Exploration Production Mémoire 17

Cobianchi M, Erba E, Pirini-Radrizzani C (1992) Evolutionary trends of calcareous nannofossil genera *Lotharingius* and *Watznaueria* during the Early and Middle Jurassic. Memorie di Scienze Geologiche 43:19–25

Deflandre G (1939) Les stéphanolithes, représentants d'un type nouveau de coccolithes Jurassique supérieur. Comptes Rendus Hebdomadaires des Séances de l'Académie des Sciences, Paris 208:1331–1333

Deflandre G, Fert C (1954) Observations sur les coccolithophoridés actuels et fossiles en microscopie ordinaire et électronique. Ann de Pale 40:115–176

Diener C (1895) Ergebnisse einer geologischen expedition in den Zentral Himalaya von Johar, undes and Painkhand. Denkschr Kaiserl Akad Wiss 62:533–608

Diener C (1912) The Triassic of the Himalaya. Mem Geol Surv India 36:207–358

Gaetani M, Garzanti E (1991) Multicyclic history of the northern India continental margin (northwestern) Himalaya. AAPG Bull 75:1427–1446

Gerard A (1827) On the Valley of the Satluj River. Trans R Asiat Soc London 1:1–343

Griesbach CL (1891) Geology of the Central Himalayas. Mem Geol Surv India 23:1–232

Grün W, Zweili F (1980) Das kalkige Nannoplankton der Dogger-Malm-Grenze im Berner Jura bei Liesberg (Schweiz). Jb Geol B-A 123:231–341

Hayden HH (1904) The geology of Spiti with parts of Bashahr and Rupshu. Mem Geol Surv India 36:1–129

Hayden HH (1908) A sketch of the geography and geology of the Himalaya Mountains and Tibet. The Geology of the Himalaya, Part 4. Government of India Press

Jain KP, Garg R, Kumar S, Singh IB (1984) Upper Jurassic dinoflagellate biostratigraphy of the Spiti Shale (Formation), Malla Johar area, Tethys Himalay, India. J Palaeontol Soc India 29:67–83

Kohli G, Sastri VV (1956) On the age of the Chikkim series. J Palaeontol Soc India 1:199–201

Krishna J (1983) Callovian-Albian ammonoid stratigraphy and paleobiogeography in the Indian subcontinent with special reference to the Tethys Himalaya. Him Geol 11:43–72

Krishna J, Kumar S, Singh IB (1982) Ammonite stratigraphy of the Spiti Shale (Upper Jurassic), Tethys Himalaya, India. Neues Jahrb Geol P-A 10:580–594

Lukeneder A, Suttner TJ, Bertle RJ (2013) New ammonoid taxa from the Lower Cretaceous Giumal Formation of the Tethyan Himalaya (Northern India). Palaeontology 56:991–1028

Mattioli E, Erba E (1999) Synthesis of calcareous nannofossil events in Tethyan lower and middle Jurassic successions. Riv Ital Paleontol S 105:343–376

Medd AW (1979) The Upper Jurassic coccoliths from the Haddenham and Gamlingay boreholes (Cambridgeshire, England). Eclogae Geol Helv 72:19–109

Moshkovitz S, Ehrlich A (1976) Distribution of Middle and Upper Jurassic calcareous nannofossils in the northeastern Negev, Israel and in Gebel Maghara, northern Sinai. Bull Geol Surv Israel 69:1–47

Myrow PM, Hughes NC, Paulsen TS, Williams IS, Parcha SK, Thompson KR, Bowring SA, Peng SC, Ahluwalia AD (2003) Integrated tectonostratigraphic analysis of the Himalaya and implication for its tectonic reconstruction. Earth Planet Sc Lett 212:433–441

Noël D (1965) Sur les Coccolithes du Jurassique Européen et d'Afrique du Nord. Éditions du Centre National de la Recherche Scientifique, Paris

Oppel A (1863) Palaeontologische Mittheilungen IV, Ueber ostindische Fossilreste aus den secundären Ablagerungen von Spiti und Gnari-Khorsum in Tibet. Palaeontologische Mittheilungen Museum Bayerische Staatsammlung, Stuttgart 1:267–288

Pandey B, Pathak DB (2015) Status of the Indian Early Cretaceous ammonoid record in light of recent observations in the Spiti Valley, Himachal Himalaya. Him Geol 36:1–8

Pandey B, Pathak DB (2017) The biostratigraphic implication of Olcostephanus Neumayr, 1875 (ammonoidea) from the Lower Cretaceous Giumal Formation, Spiti Valley, Tethys Himalaya, India. Cret Res 70:244–251

Pandey B, Pathak DB, Jaitly AK (2018) A new ammonite Geticeras gen. nov. from the Lower Valanginian (Lower Cretaceous) of the Spiti Valley, Tethys Himalaya, India. Him Geol 39:115–120

Pandey B, Pathak DB, Krishna J (2013) Preliminary remarks on new ammonoid collection from freshly exposed succession of the Spiti Formation between Lidang and Giumal, Spiti Valley, Himachal Himalaya, India. Him Geol 34:124–134

Pascoe EH (1959) A manual of the geology of India and Burma. Geol Surv India 2:585–1343

Pathak DB (1993) The first record of the ammonite genus *Hybonoticeras* from Himalaya and its biostratigraphic significance. Newslett Stratigr 28:121–124

Pathak DB (1997) Ammonoid biostratigraohy of the Spiti Shale Formation in the Spiti Himalaya, India. J Geol Soc India 4:207–221

Pathak DB (2007) Jurassic/Cretaceous boundary in the Spiti Himalaya, India. J Palaeontol Soc India 52:51–57

Pathak DB, Krishna J (1993) Preliminary remarks on the biostratigraphic relevance of the ammonoid collection from the Spiti Shale Formation, Tethys Himalaya, India. Him Geol 4:207–221

Perch-Nielsen K (1968) Der Feinbau und die Klassifikation der Coccolithen aus dem Maastrichtien von Danemark. Biologiske Skrifter. K Dansk Vidensk Selsk 16:1–96

Reinhardt P (1964) Einige Kalkflagellaten-Gattungen (Coccolithophoriden, Coccolithineen) aus dem Mesozoikum Deutschlands. Monatsber Deutsch Akad Wiss Berlin 6:749–759

Reinhardt P (1965) Neue Familien für fossile Kalkflagellaten (Coccolithophoriden, Coccolithineen). Monatsber Deutsch Akad Wiss Berlin 7:30–40

Srikantia SV (1981) The lithostratigraphy, sedimentation and structure of the Proterozoic-Phanerozoic of the Spiti Basin in the Higher Himalaya of Himachal Pradesh, India. In: Sinha AK (ed) Contemporary geoscientific research in the Himalaya, Dehradun, pp 31–48

Srikantia SV, Bhargava ON (1998) Geology of Himachal Pradesh. Geol Soc India, Text Book Ser 9

Stoliczka F (1865) Geological section across the Himalayan mountain range from Wangtu Bridge on the river Sutlej to Sungdeo with an account of formations in Spiti accompanied by a revision of all known fossils from that district. Mem Geol Surv India 5:1–153

Strachey R (1851) On the geology of the part of the Himalayan mountains and Tibet. J Geol Soc London 7:292–310

Stradner H (1963) New contributions to Mesozoic stratigraphy by means of nannofossils. In: Proceedings of sixth world petroleum congress, Section 1 paper, vol 4, pp 167–183

Uhlig V (1903) The fauna of the Spiti shales. Mem Geol Surv India 15:1–132

Uhlig V (1910a) The Fauna of the Spiti Shales. Mem Geol Surv India Ser 15(4):133–306. Palaeontologica Indica, Calcutta

Uhlig V (1910b) The Fauna of the Spiti Shales. Mem Geol Surv India Ser 15(4):307–395. Palaeontologica Indica, Calcutta

Vijaya Kumar S (2002) Palynostratigraphy of the Spiti Shale (Oxfordian-Berriasian) of Kumaun Tethys Himalaya, Malla Johar area, India. Rev Palaeobot Palyno 122:143–153

Wise SW, Wind FH (1977) Mesozoic and Cenozoic calcareous nannofossils recovered by DSDP Leg 36 drilling on the Falkland Plateau, south-west Atlantic sector of the Southern Ocean. Init. Rep. DSDP 36:269–491

Records of Marine Transgressions and Paleo-Depositional Conditions Imprinted Within Cretaceous Glauconites of India

Udita Bansal, Santanu Banerjee, and Dipima Borgohain

Abstract This study presents a comparison of geological and geochemical characteristics of the Cretaceous glauconites of the Cauvery, Kutch, Narmada and Meghalaya basins and relates them to depositional conditions, sedimentation rate and substrate. Glauconites within the Ukra Hill Member and the Karai Shale formations originated in middle and outer shelf environments, respectively. While glauconites within the Bryozoan Limestone, Mahadek and the Lameta formations formed in shallow marine environments. Glauconite formed either by the alteration of faecal pellet, K-feldspar, quartz and mica grains, or as infillings within the bioclasts. Across the formations, glauconites forming within fecal pellets are found to be 'highly-evolved' to 'evolved', while those occurring within the tiny pores of bioclasts are 'slightly-evolved'. Glauconites within the Ukra Hill Member and the Bryozoan Limestone, Lameta and the Mahadek formations contain higher K_2O (av. ~7.17%) because of their formation within K-feldspar, than those formed in the condensed zone deposits of the Karai Shale Formation (av. ~6.00%). Therefore, the maturation of glauconite depending on both sedimentation rate and the substrate composition. The Fe_2O_3 (total) content of glauconites is high in the Ukra Hill Member (24.79%) and Karai Shale Formation (24.17%), moderate in the Bryozoan Limestone (17.17%) and Lameta formations (16.01%), and low in the Mahadek Formation (6.67%). While the high Fe_2O_3 (total) of glauconite in the Karai Shale Formation is possibly related to upwelling, a large influx of continental weathering products during the Cretaceous supplied the Fe in the Ukra Hill Member. However, the restricted mobility of Fe ions in more oxygenated environments resulted in low Fe_2O_3 (total) contents of glauconites in the Bryozoan Limestone and Lameta formations. Chloritization reduced the original Fe_2O_3 (total) content of glauconite in the Mahadek Formation. Glauconites in the Ukra Hill Member largely follow the evolution trend of the 'pseudomorphic replacement' theory. The origin of glauconites in the Karai Shale is

U. Bansal · S. Banerjee (✉) · D. Borgohain
Department of Earth Sciences, Indian Institute of Technology Bombay, Powai, Mumbai 400076, India
e-mail: santanu@iitb.ac.in

U. Bansal
Senckenberg Naturhistorische Sammlungen Dresden, Königsbrücker Landstr., 01109 Dresden, Germany

best explained by a combination of 'layer lattice' and 'verdissement' theories. Glauconites in the Bryozoan Limestone, Lameta and the Mahadek Formation are best explained by the 'replacement' theory. Glauconites formed in profusion on shallow shelves across the world. The Cretaceous glauconites of India bear the global sea level rise signatures, sub-oxic shallow shelves and intensive continental weathering under hot and humid climate.

Keywords Cretaceous · Glauconite · Transgressive system tracts · Shallow marine · Global sea-level

1 Introduction

Authigenic glauconite generally suggests a low rate of sedimentation and it commonly occurs within marine transgressive deposits and condensed zones (Odin and Matter 1981; Amorosi 1995, 1997; Amorosi and Centineo 2000; Amorosi et al. 2012; Chattoraj et al. 2009, 2018; Banerjee et al. 2012a, b, 2016a, b, 2020a, b; Bansal et al. 2017, 2018, 2020a; Rudmin et al. 2017, 2019). The abundance and compositional evolution of glauconite within a sedimentary deposit, therefore, provide crucial information related to sedimentation rate, depositional setting, sea-level changes and paleoclimate (Odin and Matter 1981; Amorosi 1995, 1997; Giresse and Wiewióra 2001; Hesselbo and Huggett 2001; Meunier and El Albani 2007; Banerjee et al. 2008, 2012a, b, 2015). Several studies document a greater abundance as well as higher K_2O content of glauconites forming close to the maximum flooding surface compared to those in the rest of the sequence (Amorosi 1995, 1997, 2012; Giresse and Wiewióra 2001; Banerjee et al. 2012a, b, 2016a, b; Chattoraj et al. 2009, 2016; Boukhalfa et al. 2020). Widespread glauconite and phosphorite deposits characterize condensed zone deposits of the Cretaceous passive margin basins across the world, which is related to the unusually high sea level (Burnett 1980; Bremner 1981; Glenn and Arthur 1988; Jiménez-Millán et al. 1998; Delamette 1989; Garzanti et al. 1989; Glenn et al. 1994; Parrish et al. 2001; Amorosi et al. 2012; Banerjee et al. 2016a; 2019; Jafarzadeh et al. 2020).

Glauconite occurs in profusion in most of the Mesozoic basins in India (Rathore et al. 1999; Mishra and Sen 2001; Tewari et al. 2010; Desai 2013; Banerjee et al. 2016a; Bansal et al. 2017, 2018, 2020a). However, these glauconites are yet to be distinguished in terms of chemical and mineralogical compositions. Stratigraphic and depositional implications of these glauconites are yet to be compared. The objectives of this study are (a) to compare mineralogical and chemical characteristics of the Cretaceous glauconites in the Mesozoic basins of India and to relate the compositional variation to factors like evolutionary path, depositional conditions, sedimentation rate and substrate and (b) to consider the formation of glauconite in the global context of the Cretaceous greenhouse climate.

2 Methodology

Rock samples were collected from the exposures of the Karai Shale Formation (around Karai and Maruvattur villages) in the Cauvery basin, Ukra Hill Member (Ghuneri village) in the Kutch basin, Bryozoan Limestone Formation (Ratitalai section) and Lameta Formation (Phutlibaori area) in Narmada Basin and Mahadek Formation along the Cherrapunjee-Therria road section in Khasi Hills (near Um Sohrynkew River Section), Meghalaya Basin (Fig. 1). The precise stratigraphic position of the samples is marked in graphic logs (Fig. 2). Petrographic observations on thin sections of glauconitic rocks were carried out using Leica DM 4500P polarizing microscope at the Department of Earth Sciences, Indian Institute of Technology Bombay (IIT Bombay) using both transmitted and reflected light. Glauconite pellets were separated from the rock samples for geochemical and mineralogical analysis. The samples were soaked in water, treated with anhydrous Na_2CO_3 powder and H_2O_2 solution and were kept on a hot plate for 15–20 min. Later the mixture was cooled,
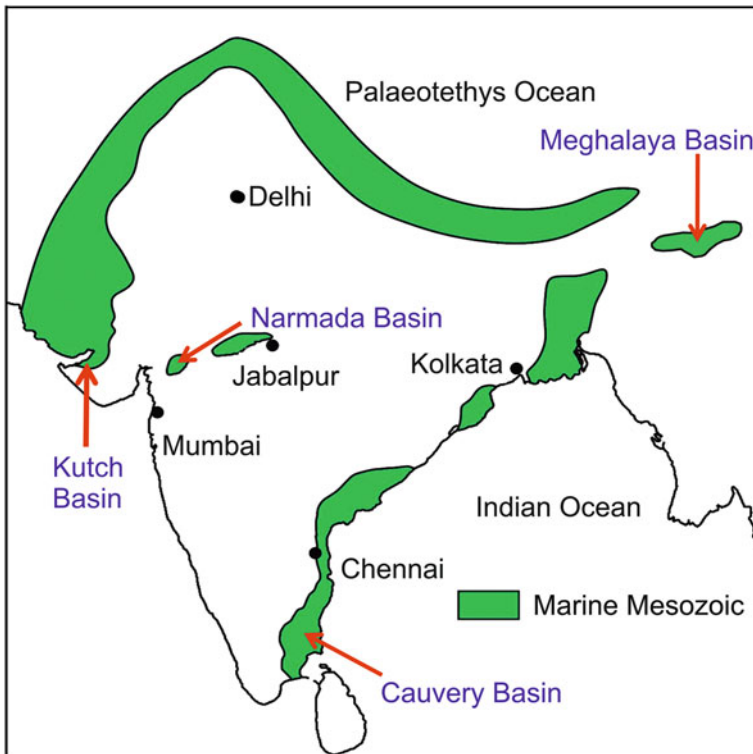
Fig. 1 Schematic map showing marine Mesozoics in India (adapted from Valdiya 2016) indicating locations of study areas (red arrows)
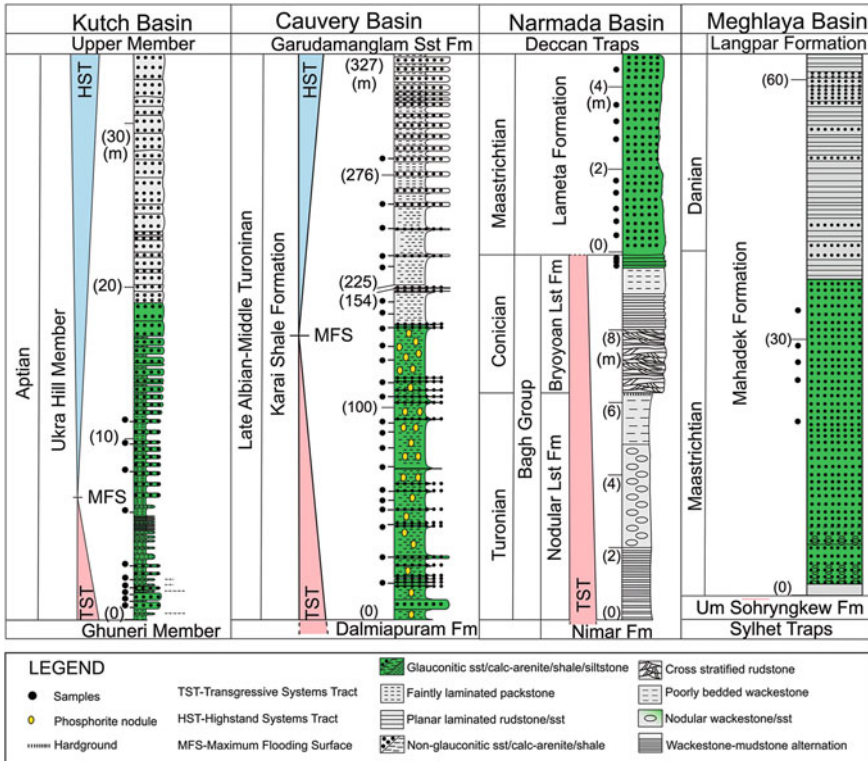
Fig. 2 Graphic logs showing the stratigraphy of glauconite within the Ukra Hill Member and the Karai Shale, Bryozoan Limestone, Lameta and the Mahadek formations. The sequence stratigraphic context has been shown for the Ukra Hill Member (from Bansal et al. 2017) and Karai Shale Formation (Banerjee et al. 2016a)

washed and dried. Glauconite pellets were concentrated using Franz magnetic separator (LB-1) with 15° slope and 15° lateral tilt and 1.5–1.8 A current at the Department of Earth Sciences, IIT Bombay. Glauconite pellets were separated from the rock matrix using a Zeiss Stemi 2000 stereo zoom microscope. The powdered samples were scanned from 4° to 30° with a step size of 0.026° 2θ and with a scan speed of 96 s/step, using nickel filter copper radiation in an Empyrean X-Ray Diffractometer with Pixel 3D detector at the Department of Earth Sciences, IIT Bombay. The samples were scanned every time after air-drying, treatment with ethylene glycol and finally after heating at 400 °C, under the same instrumental setting. Cleaned glauconite pellets were mounted on stubs, coated with platinum for 200 Å thicknesses by sputters coater and examined in secondary electron imaging (SEI) mode. Micro-textural details of glauconite samples were studied using a JSM-7600F Scanning Electron Microscope at IIT Bombay. The chemical composition of glauconite pellets and their substrates were investigated using a Cameca SX 5 Electron Probe Micro Analyzer at

the Department of Earth Sciences, IIT Bombay with accelerating voltage 15 kV, specimen current of 40 nA and beam diameter of 1 µm (peak: 10–20 s and background counting: 5–10 s). Minerals as well as synthetic phases were used as standards. All the data points were selected under the reflected light along with the BSE image control.

3 Glauconite Occurrences in Mesozoic Basins

3.1 Glauconite in the Kutch Basin

3.1.1 Stratigraphy and Depositional Environment

Glauconite occurs within the Aptian Ukra Hill Member of the Bhuj Formation in the Kutch Basin. The ~34 m-thick glauconitic succession within the Ukra Hill Member conformably overlies the Ghuneri Member, and it occurs exclusively at the western end of the Mesozoic outcrops in the Kutch Mainland (Biswas 1977; Rathore et al. 1999). Glauconite occurs at the lower part of the Ukra Hill Member, consisting of intercalation of shale and sandstone (Fig. 3a), while it is absent at the upper sandy part. The Member is highly fossiliferous at the lower part including ammonite, belemnite,
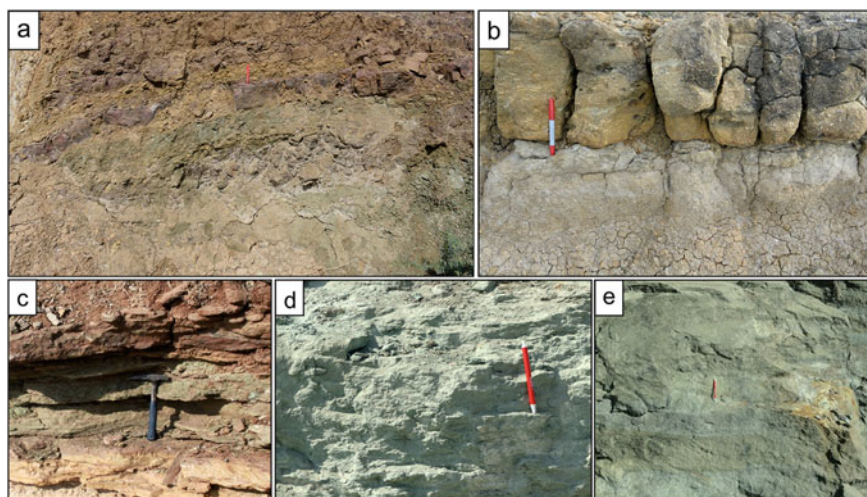
Fig. 3 Field photographs showing **a** green shale and sandstone contact in the Ukra Hill Member, **b** sharp contact of glauconitic shale with overlying calc-arenites in the Karai Shale Formation, **c** glauconitic bed in the Bryozoan Limetsone Formation, Bagh Group, **d** green sandstones of the Lameta Formation and **e** glauconitic sandstone of the Mahadek Formation (marker pen length = 14 cm, hammer length = 30 m)

bivalve and gastropod and fossil wood. The presence of belemnite fossils *Neohibolithes ewaldi* and *Tetrabelus seculus* suggests an Aptian age for the Ukra Hill Member (Desai 2013). Desai (op. cit.) suggested a middle shelf to near-shore transition on the basis of ichnofabrics (*Psilonichnus*, *Teredolite* and *Gyrolithes- Rhizocorallium*). Bansal et al. (2017, 2018, 2020a) considered a transgressive systems tract culminating into a maximum flooding surface (MFS) at the basal glauconite-rich, shaley part of the Ukra Hill Member. This is followed upward by the shallowing-upward, glauconite-free, sandstone-dominated deposits, passing conformably into the Upper Member of the Bhuj Formation. The maximum concentration of glauconite pellets (72%) occurs near the top of the transgressive systems tract (Bansal et al. 2017, 2018, 2020a).

3.1.2 Types of Glauconite

Glauconite occurs in two different modes within the Ukra Hill Member, as glauconite pellets with no trace of substrate (Fig. 4a) and as replacement along K-feldspar, quartz and mica grains (Bansal et al. 2017, 2018, 2020a). Glauconite forms by the dissolution and further replacement of substrate. Most glauconite pellets are spherical to sub-spherical and sometimes elliptical. They exhibit dark olive green colour and are weakly pleochroic. The average diameter of a spherical pellet is ~230 µm while the long axis of the elliptical glauconite is ~335 µm. Glauconite formed by the replacement of quartz appears rounded with an average diameter of ~160 µm. It occurs as linear and stringers along the cleavage planes of K-feldspars, with an average length 200 µm. The glauconite formed within mica exhibit distinct vermicular shape (av. length ~320 µm and av. width ~235 µm). Under cross-polars the pellets show pinpoint extinction and high order interference colours.

3.1.3 Chemico-Mineralogical Characteristics

X-Ray diffractograms of the glauconite pellets in air-dried mode exhibits prominent basal reflections (001) and (003) at 10.05 Å and at 3.32 Å respectively (Fig. 5a). The $11\bar{2}$ reflection is present at 3.6 Å while the 112 reflection is absent. The (001) peak shifts towards 10.1 Å while the $11\bar{2}$ reflection disappears upon glycolation and heating of the sample at 400 °C. The peaks show broad base and appear asymmetrical in air-dried sample, but become sharp, intense and symmetrical on glycolation and heating. The minor peak of illite at 5.0 Å accompanies glauconite in all modes of scanning. The negligible shift of 10 Å as well as narrow and symmetrical nature of peaks indicates minimal expandable layers (cf. Thompson and Hower 1975). Further, the absence of 112 and $11\bar{2}$ (upon glycolation) reflections corroborates negligible (~10%) expandable layers. The FEG-SEM image exhibiting lamellar structure within glauconite grains corroborate the 'highly evolved' nature (Fig. 6a; Wigley and Compton 2007; Bansal et al. 2017, 2018, 2020a).
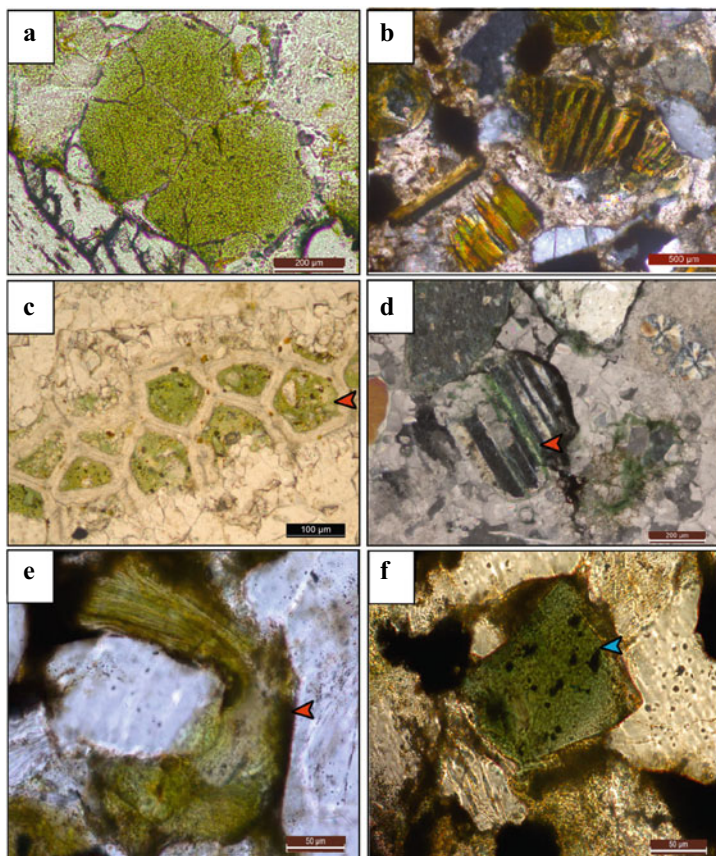
Fig. 4 Photomicrographs showing **a** completely evolved glauconite pellet within the Ukra Hill Member, **b** glauconite formed by replacement along the mica grains exhibiting vermiform appearance within the Karai Shale Formation, **c** glauconite infillings within bryozoan aperture (marked by red arrow) within the Bryozoan Limestone Formation, **d** glauconite replacement along the cleavages of K-feldspar grain within the Lameta Formation, **e** deformed glauconite (marked by red arrow) formed after the replacement of mica grain within the Mahadek Formation and **f** chloritization of glauconite within the Mahadek Formation (marked by blue arrow)

The detailed geochemical data of glauconite is provided in Bansal et al. (2017, 2018, 2020a). The average K_2O content of glauconite is 7.12%, indicating it's 'evolved' nature. The Fe_2O_3 (total) content of glauconite (av. 24.79%) is high. The average Al_2O_3, SiO_2 and MgO contents are 9.72%, 48.73% and 2.60% respectively. The K_2O and Fe_2O_3 (total) contents of glauconite decreases in diagenetically altered rims and cracks of glauconite pellets (Bansal et al. 2017, 2018, 2020a). The broad scatter of data within a cross-plot between K_2O and Fe_2O_3 (total) defines the significant role of stratigraphic condensation in glauconite maturation (Bansal et al. 2017,

2018, 2020a, Fig. 7). However, the marginal rise in the K_2O content of glauconite pellets reflects a minor time-dependent fixation of K.
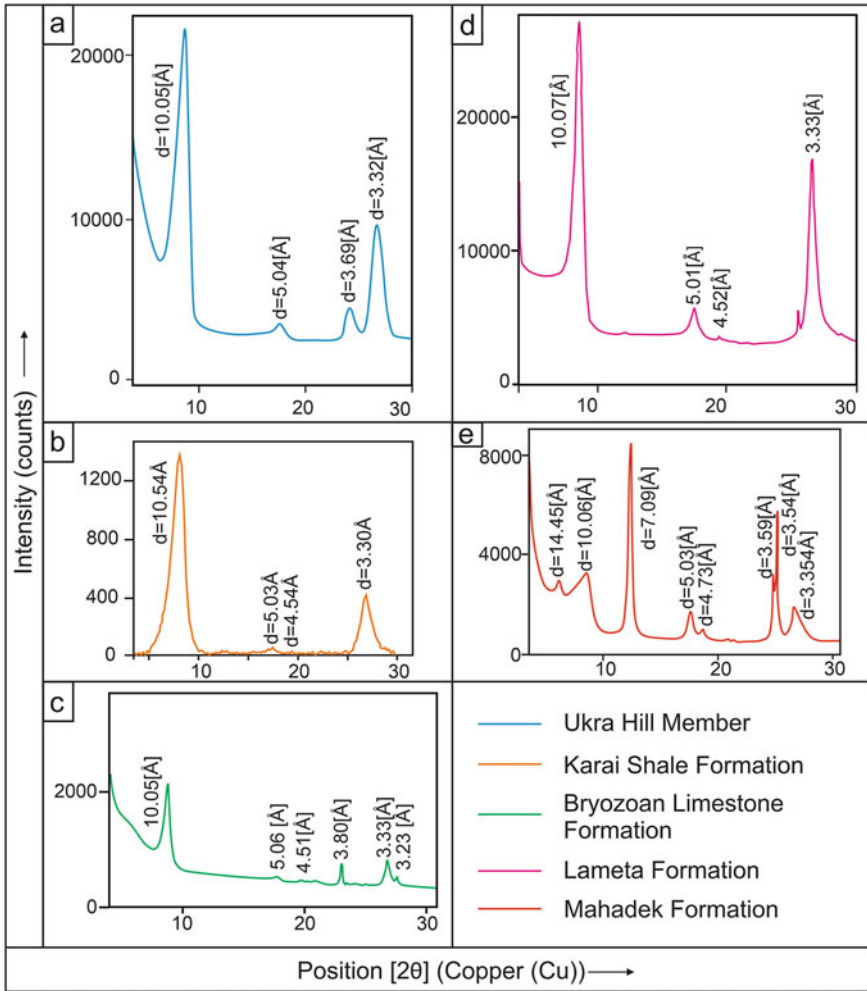
Fig. 5 XRD diffractograms of glauconite pellets under air-dried mode **a** Ukra Hill Member, **b** Karai Shale Formation, **c** Bryozoan Limestone Formation, **d** Lameta Formation and **e** Mahadek Formation
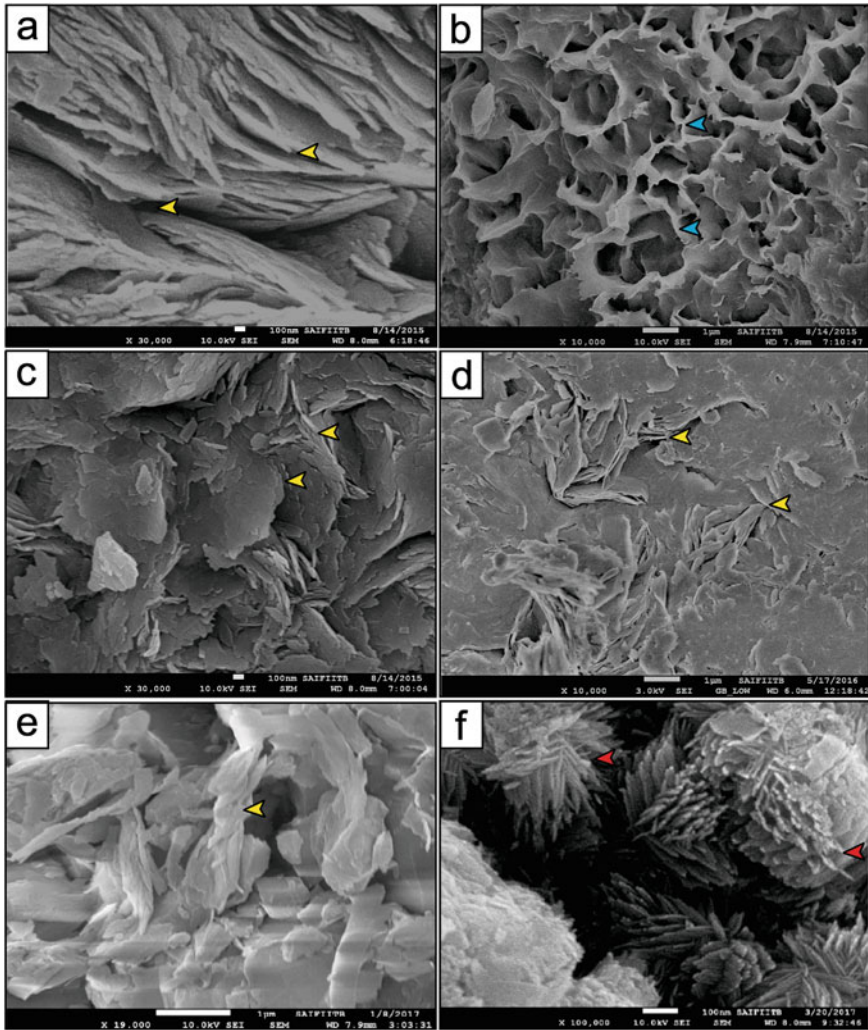
Fig. 6 FEG-SEM image of glauconite pellets showing lamellar structure (marked by yellow arrows) in the Ukra Hill Member (**a**), Bryoyoan Limestone Formation (**c**), Lameta Formation (**d**) and Mahadek Formation (**e**) which is characteristic of 'highly-evolved' variety of glauconite. Blue arrows mark the rosette structure in the Karai Shale Formation (**b**) indicating 'evolved' stage of maturation. The flower like structures marked by yellow arrows represent chlorite in Mahadek Formation (**f**)
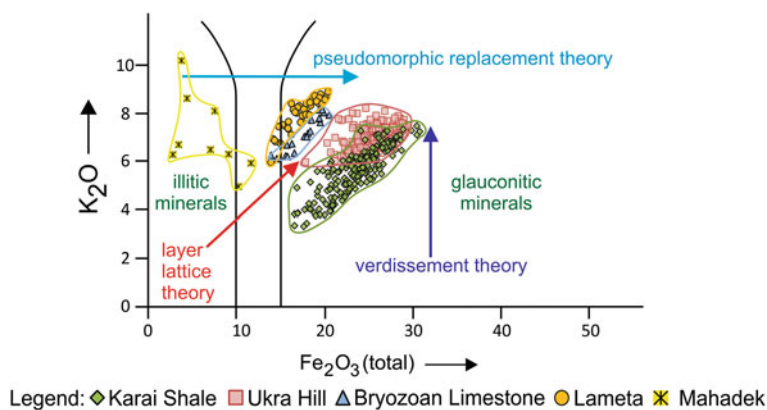
Fig. 7 The relationship between K$_2$O and Fe$_2$O$_3$ (total) within the studied glauconites, showing clusters. Evolutionary trends supporting layer lattice theory, verdissement theory and pseudomorphic replacement theory are presented by red, purple and blue arrows respectively

3.2 Glauconite in Cauvery Basin

3.2.1 Stratigraphy and Depositional Environment

The Late Albian-Middle Turonian Karai Shale Formation conformably overlies the Dalmiapuram Formation and passes over to the Garudamangalam Sandstone Formation (Fig. 2; Watkinson et al. 2007; Sarkar et al. 2014; Banerjee et al. 2016a). The ca. 410 m thick Karai Shale Formation consists of glauconitic shale with locally developed phosphorite nodules, intercalated with thin beds of calc-arenite at the lower and middle parts (Figs. 2, 3b). The upper part of the Formation primarily consists of grey shale and thick calc-arenite, and is devoid of glauconite. Age-diagnostic foraminifera (*Praeglobotruncana helvitica, Hedbergella planispira, Whiteinella archaeocretacea*, Rotalipora suite), belemnites (in the bottom part) and ammonites (at the top) provide the Late Albian-Middle Turonian age for the Karai Shale (Hart et al. 2001; Sundaram et al. 2001; Nagendra et al. 2011). The ^{40}Ar/^{39}Ar dating of glauconites provides an absolute age ranging from 100.3 ± 0.7 Ma to 92.6 ± 0.6 Ma for the glauconitic lower to middle parts of the Karai Shale (Bansal et al. 2019). The glauconitic interval of the Karai Shale corresponds to the OAE1d and OAE2 events in the equivalent offshore deposits (Bansal et al. 2019). The glauconites formed in the outer shelf depositional environment (Nagendra et al. 2011; Banerjee et al. 2016a). The lower and middle parts of the Karai Shale exhibit transgressive trend, while the upper part shows shallowing upward trend (Fig. 2; Banerjee et al. 2016a). The concentration of glauconite increases within the transgressive deposits and is up to 60% near the maximum flooding surface.

3.2.2   Types/Modes of Glauconite

Three principal types of glauconite occur in the Karai Shale, as glauconite pellets (faecal origin), as glauconitic infillings within the bioclasts and as replacement along the mica grains appearing as vermiforms (Fig. 4b; Banerjee et al. 2016a). Most glauconite pellets are rounded and are pleochroic from yellow green to brown green. The average diameter of rounded pellets is ~550 µm. Sometimes, the pellets are elliptical with the long axis of ~650 µm. Glauconite pellets frequently exhibit cracks that taper down from the periphery to the center. Glauconitic infillings occur within the foraminiferal chambers, ostracoda carapace, bryozoan apertures and algal voids (Banerjee et al. 2016a). The average diameter of the glauconitic infilling varies from ~20 µm in algae and bryozoan to ~650 µm (length) in ostracoda. The calcareous tests of these bioclasts do not exhibit any dissolution. Glauconite display distinct cleavages perpendicular to the long axis of mica grains (Fig. 4b). The average length of these glauconites is ~650 µm, whereas its maximum width is ~150 µm, giving it a vermicular appearance (Fig. 4b).

3.2.3   Chemico-Mineralogical Characteristics

X-Ray diffractograms of glauconite pellets exhibit basal (001) and (003) reflections at 10.5 Å and 3.3 Å respectively. The $11\bar{2}$ and 112 reflections are absent. Upon glycolation, the (001) peak shifts from 10.5 Å to 9.5 Å (Fig. 5b). The peaks are asymmetrical and broad-based in air-dried mode, but become sharp and symmetrical on glycolation. The peak remains stationary after heating at 400 °C. The glycolation of glauconite samples reveals minor kaolinite at 7.2 Å (Banerjee et al. 2016a, b). The slight shift of 10 Å peak after glycolation indicates ~10–15% expandable layers, described as the 'disordered' glauconite, corresponding to ~6.5% K_2O content (evolved stage of maturation) and 1.42 FWHM (full width at half maximum value) value (Thompson and Hower 1975; Odom 1984; Amorosi et al. 2007; Banerjee et al. 2016a). The FEG-SEM study of glauconite reveals rosette structures confirming the 'slightly-evolved' to 'evolved' stage of maturation (Fig. 6b).

Detailed geochemistry of glauconite is discussed in Banerjee et al. (2016a). The average K_2O content is high in glauconite pellets (6.23% in cores) and glauconite vermiform (6.26% in unaltered zones), while it is low in the infillings (4.59%). The first two varieties belong to 'evolved' and the last one belongs to 'slightly evolved' maturation. The Fe_2O_3 (total) content of glauconite is high (av 24.17%). The average MgO, SiO_2 and Al_2O_3 contents are 2.88%, 51.74% and 9.25%, respectively. The K_2O and Fe_2O_3 (total) content remains high in cores of glauconite pellets and vermiforms than in rims and altered wedge-shaped zones respectively (cf. Banerjee et al. 2016a). The relationship between K_2O and Fe_2O_3 (total) of glauconites reflects moderately good correlation and substrate-specific compositional variation (Banerjee et al. 2016a).

3.3 Glauconite in Narmada Basin

3.3.1 Stratigraphy and Depositional Environment

Glauconite occurs at two different stratigraphic levels, Coniacian and Maastrichtian, within the Mesozoic succession of the Narmada Basin. Glauconite occurs at the top of the Bagh Group of rocks, consisting of the Nimar, Nodular Limestone and the Bryozoan Limestone formations. Resting conformably over the siliciclastic Nimar Formation (Bose and Das 1986), the ~10 m thick carbonate-dominated part of the Bagh Group comprises of the Turonian Nodular Limestone Formation at the bottom and the Coniacian Bryozoan Limestone Formation at the top (Fig. 2; Kumar et al. 2018; Bansal et al. 2020a; Ruidas et al. 2020). Glauconite occurs within a 40 to 60 cm thick, planar laminated rudstone at the top of the Bryozoan Limestone containing abundant siliciclastic sand and mud fragments (Fig. 3c). The glauconitic rudstone of the Bryozoan Limestone Formation represents the top part of a transgressive deposit (Fig. 2; Bansal et al. 2020a).

The Lameta Formation at the western part of the Narmada Basin (Phutlibaori area) (Fig. 2) is represented by a ~4 to 5 m thick, trough cross-bedded, medium- to coarse-grained, friable and well-sorted glauconitic sandstone (Fig. 3d; Tandon 2000; Bansal et al. 2018). The sandstone is highly fossiliferous, containing abundant oysters, gastropods, shark teeth and fossilized wood logs. While the Lameta Formation in the study area indicates deposition in an estuarine environment, its equivalents in the eastern part of the basin are of continental deposits (D'Emic et al. 2009; Kumar and Tandon 1977, 1978, 1979; Pascoe 1959; Tandon 2000).

3.3.2 Types/Modes of Glauconite

Glauconite within the Bryozoan Limestone Formation occurs as replacement along K-feldspar grains, as glauconitic infillings within the bryozoan zooecial aperture (Fig. 4c), and rarely within the echinoid spines and ostracoda carapace (Bansal et al. 2020a). The glauconite forms initially as streaks along cleavages and fractures of K-feldspars, developing into linear and interconnected stringers (~150 μm). Many of the evolved glauconites leave no relics of substrate. The tests of the bryozoa remain intact, while their pores are filled with glauconite. The average diameter of glauconitic infilling within the bryozoan tests ranges from 40 μm to 250 μm. Glauconite of both varieties exhibit high relief and are pleochroic from light to olive green. Glauconite shows high third order (dark green) interference colour and pitted texture.

Glauconite within the Lameta Formation principally forms by the replacement of K-feldspars along cleavages and fractures (Fig. 4d; Bansal et al. 2018). The linear and interconnected glauconitic stringers in the Lameta Formation may extend to ~400 μm in length and ~50 μm in width. Both K-feldspar and glauconite grains of the Lameta Formation are later replaced partially by calcite (Bansal et al. 2018).

3.3.3 Chemico-Mineralogical Characteristics

X-Ray diffractograms of glauconite pellets in the Bryozoan Limestone Formation exhibit prominent basal reflections (001) at 10.0 Å, (020) at 4.51 Å, (003) at 3.32 Å whereas the 11$\bar{2}$ and 112 reflections are absent (Fig. 5c). The sharp, intense and narrow peaks remain static in all modes of scanning. The unmoved peaks on glycolation and heating indicate minimum inter-stratification, corresponding to ~10% expandable layers of 'evolved' to 'highly-evolved' types of glauconite with ~8% K_2O (Thompson and Hower 1975; Odom 1984; Bansal et al. 2020a). The FEG-SEM study of the glauconite reveals lamellar structure, which corroborates the 'highly-evolved' stage of maturation (Fig. 6c; Wigley and Compton 2007; Bansal et al. 2020a).

Detailed geochemical characterization of glauconite within the Bryozoan Limestone Formation is provided in Bansal et al. (2020a). The K_2O content of glauconite ranges from 6.13% to 8.16%, indicating 'evolved' to 'highly-evolved' maturation (Odin and Matter 1981; Amorosi 1997; Bansal et al. 2020a). The average Fe_2O_3 (total) content of glauconite is moderate (17.17%). The average contents of MgO, SiO_2 and Al_2O_3 content of glauconites are 3.78%, 51.34% and 9.19%, respectively. The high K_2O (total) content of glauconite is consistent with its origin by the replacement of K-feldspar.

XRD of glauconite samples of the Lameta Formation in all types of scanning exhibit well-developed basal reflections (001) and (003) at 10.0 Å and 3.3 Å, respectively and (020) reflection at 4.5 Å (Fig. 5d). The peaks remain sharp, narrow and intense. A poorly-developed peak of illite co-exists at 5.0 Å. The narrow and symmetrical peaks and the static (001) reflection indicate negligible expandable layers (~10%) (Thompson and Hower 1975), corresponding to the 'highly-evolved' glauconite, with ~7.5% K_2O content (Odom 1984). The glauconite exhibits lamellar structure under FEG-SEM, which further confirms the 'highly-evolved' nature (Wigley and Compton 2007; Bansal et al. 2018).

The K_2O content of glauconites in the Lameta Formation varies from 5.99% to 8.29%, indicating 'evolved' to 'highly-evolved' stage of maturation (Odin and Matter 1981; Amorosi 1997). The Fe_2O_3 (total) content of glauconite is moderate, varying from 13.29% to 18.90%. The average MgO, SiO_2 and Al_2O_3 contents of glauconite are 4.19%, 52.82% and 10.35% respectively. The high K_2O content of glauconite relates to the addition of K^+ ions from K-feldspar substrate. The high MgO, SiO_2, Al_2O_3 contents of glauconite in the Lameta Formation is related to Deccan volcanism (Bansal et al. 2018).

3.4   Glauconite in Meghalaya Basin

3.4.1   Stratigraphy and Depositional Environment

The well-exposed Late Maastrichtian Mahadek Formation rests directly on the Bottom Conglomerate and/or Jadukata Formation in the east Khasi Hills region, near the Um Sohryngkew River section in Meghalaya basin (Tewari et al. 2010). The ~30 m thick Mahadek Formation comprises medium- to coarse-grained, cross-stratified glauconitic sandstones which gradationally passes over to shales, marls and limestones of the early Paleocene Langpar Formation, Jaintia Group (Tewari et al. 2010). The Formation contains well-preserved gastropods, ammonoids, echinoids and mollusks (Tewari et al. 2010). The moderately-sorted glauconitic sandstone consists of ~40% quartz, ~25% feldspar, ~30% rock fragments (>5%) indicating its lithic characteristic. The presence of cross-stratification suggests a littoral environment. The glauconite in the Mahadek Formation represents the flooding of the Tethyan shelf during the Cretaceous (Tewari et al. 2010).

3.4.2   Types/Modes of Glauconite

Glauconite primarily occurs as replacement along K-feldspar and mica and occasionally within quartz grains. Glauconite exhibits pleochroism from light brown to light green and high third-order green to dark green interference colour under cross-polars. The incipient glauconite within K-feldspars occurs as linear and stringers along the cleavage planes, with length ~150 μm. The glauconite formed by the replacement along the mica grains appears deformed (Fig. 4e). It replaces the quartz grains along the periphery. Chlorite often replaces the glauconite completely while retaining the original shape of the latter (Fig. 4f).

3.4.3   Chemico-Mineralogical Characteristics

XRD of glauconite samples in the Mahadek Formation reveals the basal (001) and (003) reflections at 10.06 Å and at 3.35 Å respectively. The peaks of glauconite are broad-based and asymmetrical in air-dried mode (Fig. 5e). On glycolation, the (001) reflection breaks into two peaks at 10.3 Å and at 10.07 Å. On heat treatment, the peaks shift to 10.2 Å and appear relatively sharp, intense and symmetrical. The well-developed peaks (in air-dried mode) at 14.45 Å, 7.09 Å, 4.73 Å and 3.54 Å indicate the presence of chlorite, while a strong peak at 3.59 Å represents kaolinite (Fig. 5e). Within the Mahadek Formation, the glauconite exhibit both lamellar and rosette (flower) structures (Fig. 6e, f). While the lamellar structure indicates the 'evolved' nature of glauconite, rosette structure relates to the presence of chlorite (Fig. 6e, f).

The high avg. K_2O content (7.26%) indicates an 'evolved' nature of glauconite. The average Fe_2O_3 (total) (6.67%) and MgO (1.45%) contents of glauconite are

lower than other present studied formations. The average SiO_2 content of glauconite is 48.53%. Glauconite in the Mahadek Formation contains high K_2O and low Fe_2O_3 (total), similar to many Precambrian equivalents (Dasgupta et al. 1990; Deb and Fukuoka 1998; Bandopadhyay 2007; Ivanovskaya et al. 2006; Banerjee et al. 2008, 2015, 2016a; Bansal et al. 2020b). The exceptionally high average Al_2O_3 content in some of the glauconite (29.80%) relates to its chloritization. Recently, Bansal et al. (2020b) reported a similar conversion of glauconite to chlorite in the Precambrian Rabanpalli Formation, Bhima basin, India. A high thermal maturation induced by the Sylhet Traps, surrounding the Mahadek Formation, possibly facilitated the transformation of glauconite to chlorite.

4 Discussion

4.1 Comparison of Mineralogical and Textural Characteristics of Glauconite

Glauconite forms either within the shales and/or sandstones in the Mesozoic basins of India except in the case of the Bryozoan Limestone Formation, where it occurs within the planar laminated rudstone of a carbonate deposit. Glauconite forms mostly within the detrital K-feldspar grains and within pores of bioclasts, while calcitic skeletons are not affected by the glauconitization process. Glauconite occurs in close association with phosphorite deposits in the Karai Shale Formation.

XRD diffraction patterns reveal the characteristic peaks of glauconite and the subsidiary peaks of illite or kaolinite, except in the Mahadek Formation (Fig. 5). The negligible shift of peak upon glycolation and heating at 400 °C indicates a minimum interstratification in these glauconites (Thompson and Hower 1975). The broad, asymmetrical peaks of glauconites in the Karai Shale correspond to 10–15% expandable layers (Banerjee et al. 2016a), while sharp and symmetrical peaks in glauconites of the Ukra Hill Member, Bryozoan Limestone Formation and the Lameta Formation indicate less than 10% expandable layers (Bansal et al. 2017, 2018, 2020a). The X-ray diffractional parameters reveal a mixture of glauconite, chlorite and kaolinite in the Mahadek Formation.

Textural studies of glauconites using FEG-SEM further corroborate the XRD results. Glauconite in the Karai Shale reveals rosette structure while those in the Ukra Hill Member, Bryozoan Limestone Formation and the Lameta Formation exhibit lamellar structure. The lamellar and rosette structure corresponds to a 'highly-evolved' and 'evolved' stage of evolution respectively (Fig. 6; Odin and Matter 1981). Glauconite within the Mahadek Formation reveals both lamellar and rosette structures (Fig. 6e, f). While the lamellar structure relates to the 'evolved' stage of glauconite maturation, the rosette structure of glauconite in the Mahadek Formation corresponds to chlorite.

4.2 Origin and Evolution of Glauconite

Three popular theories explain the origin of most glauconites, viz. 'layer lattice', 'verdissement' and 'pseudomorphic replacement'. The glauconite forming within a degraded smectite or illite, with simultaneous increase of K_2O and Fe_2O_3 (total) supports the layer lattice theory (Burst 1958a, b; Hower 1961). As per 'verdissement theory', the glauconite precipitates initially as a K-poor glauconitic smectite within the pores of bioclasts/faecal pellets, which is followed by subsequent dissolution and recrystallization of substrate, accompanied by an increase of the K_2O content at a constant Fe_2O_3 (total) (Odin and Matter 1981). The 'pseudomorphic replacement theory' envisages the formation of glauconite by the dissolution and replacement of the original substrate, in which the K_2O content remains constantly high (Banerjee et al. 2015, 2016a, b). The evolutionary trends of glauconite, supporting each theory, are different (Fig. 7).

Glauconite formed within quartz, K-feldspar and mica grains in the Ukra Hill Member. The glauconite exhibits high K_2O and variable Fe_2O_3 (total), hence the evolutionary trend supports the 'pseudomorphic replacement' theory. The glauconitization took place in a pore-water environment highly charged with a_{K+} and a_{Si+} (cf. Banerjee et al. 2008, 2015; Bansal et al. 2017, 2018, 2020a). Marginally high K_2O content in the most evolved variety of glauconite within the Ukra Hill Member is possibly related to the long-term fixation of K^+ into glauconite structures, because of the low rate sedimentation (Bansal et al. 2017, 2018, 2020a).

Within the Karai Shale Formation, the glauconite forming within the faecal pellet, K-feldspar, quartz and mica are highly mature, while those forming within the tiny pores in bryozoan, algae, and foraminifera are less evolved. Faecal pellet is enriched with the required ions for the formation and evolution of glauconite. Therefore, glauconites forming within them are of evolved variety (Banerjee et al. 2016a). Glauconitization in the Karai Shale Formation involved by two stages, the initial precipitation of low-K and moderate-Fe glauconite (such as in 'verdissement' theory) and its subsequent maturation by the addition of K and Fe (supporting 'layer lattice' theory). The glauconite formation within mica involved the second stage, i.e., simultaneous incorporation of K and Fe along with the removal of Si and Al.

Glauconite formed by the replacement of K-feldspar grains in the Bryozoan Limestone Formation and the Lameta Formation. Glauconite in the Mahadek Formation formed by the replacement of both K-feldspar and mica grains. The consistently high K_2O content of glauconite and detailed petrographic and textural evidence corroborate the 'pseudomorphic replacement' trend in these cases (Banerjee et al. 2015, 2016a; Bansal et al. 2017, 2018). Glauconite alters to chlorite in places within the Mahadek Formation.

4.3 Depositional and Sequence Stratigraphic Implications of Glauconite

The depositional setting of glauconite within the Mesozoic successions varies considerably (Table 1). While glauconite forms within middle shelf to nearshore environment in the Ukra Hill Member, those occurring within the Karai Shale represent outer shelf deposits (Bansal et al. 2017). On the contrary, glauconite formed in littoral deposits within the Bryozoan Limestone and the Mahadek Formation (Tewari et al. 2010; Bansal et al. 2020a). Within the Lameta Formation, the glauconite formed

Table 1 Physical, mineralogical and chemical comparison of glauconites within Cretaceous successions in India and their stratigraphic relevance

	Ukra Hill Member	Karai Shale Formation	Bryozoan Limestone Formation	Lameta Formation	Mahadek Formation
Age	Aptian	Late Albian-Middle Turonian	Coniacian	Maastrichtian	Late Maastrichtian
Background lithology	Shales and sandstone	Shales and calc-arenite	Planar laminated rudstone	Sandstone	Sandstone
Phosphorite	Absent	Present	Absent	Absent	Absent
Mode of occurence	Pellets and replacement along feldspar, quartz and mica grains	Pellets, infillings within bioclasts and vermiforms	Replacement of feldspars and infillings within bioclasts	Replacement of feldspar	Replacement of feldspars, mica and quartz
XRD	Glauconite with minor illite	Glauconite with minor kaolinite	Glauconite with minor illite	Glauconite with minor illite	Glauconite, chlorite and kaolinite
SEM	Lamellar	Rosette	Lamellar	Lamellar	Lamellar and rosette (chlorite)
Av. K_2O (%)	7.12	6.00	7.15	7.15	7.26
Av. Fe_2O_3 (%)	24.79	24.17	17.17	16.01	6.67
Av. MgO (%)	2.60	2.88	3.78	4.19	1.45
Av. SiO_2 (%)	48.73	51.74	51.34	52.82	48.53
Av. Al_2O_3 (%)	9.72	9.25	9.19	10.35	29.80
Depositional environment	Middle shelf to near shore	Outer shelf	Littoral	Estuarine	Littoral
Systems tracts	TST	TST	TST	Unknown	Unknown

in estuarine depositional condition (Bansal et al. 2018). Glauconite rarely forms within a carbonate sequence (Banerjee et al. 2016a). Within the mixed siliciclastic-carbonate Cenozoic sequence of Kutch, the glauconite formed exclusively within the argillaceous limestones and shales, while it is completely absent in pure carbonates (Banerjee et al. 2012a, b, 2020a, b; Chattoraj et al. 2009, 2016). Although glauconite occurs within the Bryozoan Limestone Formation, it forms mostly by the replacement of detrital K-feldspar (Bansal et al. 2020a). Glauconite occurs exclusively within the planar laminated rudstone, primarily consisting of allochthonous carbonate particles, detrital feldspar and quartz grains.

Glauconite forms close to the maximum flooding surface (MFS) in the Karai Shale Formation and the Ukra Hill Member. In both cases, the concentration of glauconite pellets increase from the bottom of the transgressive systems tracts to the maximum flooding surface. The K_2O content of these glauconites is always high (>6%), corresponding to the 'evolved' to 'highly evolved' stage of maturation. Therefore, the stratigraphic condensation determines the maturation and abundance of these glauconites. However, in the Ukra Hill Member, glauconite contains higher K_2O than that in the Karai Shale, because of its formation within K-feldspar substrate.

The K_2O content is high within the littoral and estuarine-originated glauconite of Bryozoan Limestone, Mahadek and Lameta formations respectively. The high K_2O content of these glauconites correspond with the K-feldspar substrate, and is unrelated to the stratigraphic condensation. This study, therefore, confirms that maturation of glauconite, estimated by its K_2O content, not only depends on sedimentation rate, but also on the composition of substrate, as indicated in few studies (Bansal et al. 2017, 2018, 2020a). Therefore, the K_2O content of glauconite, forming within K-feldspar substrate, is not a reliable indicator of stratigraphic condensation.

4.4   Relationship Between Fe_2O_3 (Total) Content and Depositional Conditions

The average Fe_2O_3 (total) content of 'evolved' glauconite increases from the Lameta Formation (16.01%) to the Ukra Hill Member (24.79%) through Bryozoan Limestone Formation (17.20%) and Karai Shale Formation (24.23%). The amount of Fe_2O_3 (total) content depends on the availability of Fe and redox conditions of the depositional environment (El Albani et al. 2005; Banerjee et al. 2016a; Tang et al. 2017). Seawater contains negligible Fe, which is insufficient for the formation of glauconite on the seafloor. The Fe content of glauconite is, therefore, mostly derived by continental weathering, upwelling or submarine volcanism (Banerjee et al. 2016b, 2020a).

The glauconitic segment of the Karai Shale formed within the outer shelf. The Fe content of the glauconite is unlikely to be derived from land. Therefore, the high Fe_2O_3 (total) content may be related to upwelling. Fe is available in upwelling zones of modern oceans, on the outer shelf or in a slope environment (Cook and Marshall

1981). The co-occurrence of phosphatic and glauconitic sediments within the Karai Shale Formation is consistent with modern upwelling zones (Burnett 1980; Bremner 1981; Glenn and Arthur 1988; Glenn et al. 1994; Parrish et al. 2001).

The formation of glauconite in the Ukra Hill Member, Bryozoan Limestone Formation, Lameta Formation and Mahadek Formation was possibly facilitated by a large flux of continental weathering products, related to the warm and humid climatic conditions during the Cretaceous. Although Fe was available within the shallow seas, the weakly suboxic depositional conditions restricted mobility of Fe ions into the glauconite structure resulted in a moderate Fe_2O_3 (total) content of glauconites within Bryozoan Limestone and Lameta formations (Banerjee et al. 2016a; Bansal et al. 2018, 2020a).

4.5 Glauconite Formation in the Context of Cretaceous Transgressions in India

The occurrences of glauconite within the Mesozoic basins of India correspond to four major transgressions. The glauconite within the Aptian Ukra Hill member in the Kutch basin records the oldest transgression at the western margin of India. Glauconite-phosphorite deposits within the Late Albian-Middle Turonian Karai shale in the Cauvery Basin records the next transgression at the eastern margin of India. The glauconite within the Bryozoan Limestone and the Lameta Formation in the Narmada Basin correspond to transgression during Coniacian and Maastrichtian respectively. The glauconite bed within the Mahadek Formation of Meghalaya basin records the Late Maastrichtian transgression. The Cretaceous glauconites of India, therefore, correspond well with the major global sea level rises.

Haq (2014) reported long periods of consistently high sea-level rise throughout the Cretaceous. Increasing supply of nutrients and enhanced productivity led to the formation of oxygen-depleted shallow shelves during the Cretaceous (Ozaki and Tajika 2013). A consistently high sea-level rise in Cretaceous and the warm, humid climate facilitated the formation of glauconite in less oxygenated shallow seas (Banerjee et al. 2016a; Bansal et al. 2020a). Recently, Bansal et al. (2020a) reviewed the maximum occurrence of late Cretaceous glauconites all along the Tethyan margin, suggesting a high abundance of glauconite in Cenomanian, Turonian, Coniacian, Campanian and Maastrichtian consecutively. The global sea-level increase during the Cretaceous is, therefore, well-recorded within the glauconite-bearing Aptian to Maastrichtian transgressive sequences of India (Fig. 8).

Fig. 8 Glauconite formation in relation to the global second order sea-level curve of Haq (2014). Double headed arrows representing the approximate age range of glauconite
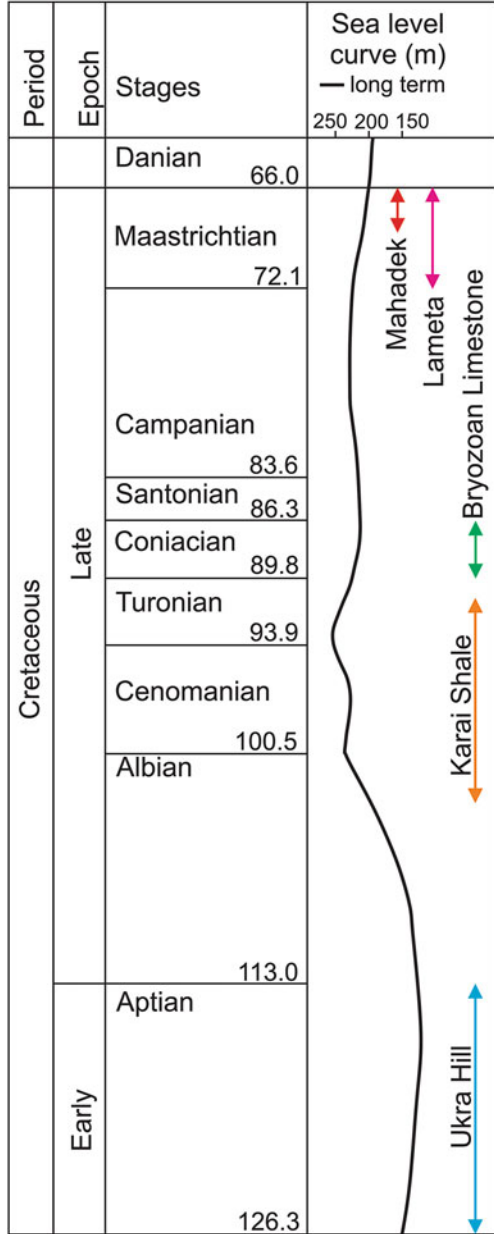
5 Conclusions

The study of the Cretaceous glauconites of India led to the following conclusions.

(a) Glauconites formed within faecal pellet, K-feldspar, quartz and mica are 'evolved' to 'highly evolved', while those formed within the tiny pores in bryozoans, algae, and foraminifera are 'slightly-evolved'. The composition of glauconite, therefore, varies depending on the substrate characteristics.

(b) The composition of the Mesozoic glauconites follows different evolutionary trends. The origin of glauconite in the Karai Shale Formation is best explained by a combination of 'layer lattice' and 'verdissement' theories. Glauconites in the Ukra Hill Member mostly follow the evolution trend of the 'pseudomorphic replacement' theory, while a few of the glauconite bears the signature of long-term fixation of K_2O. Glauconites within Bryozoan Limestone, Lameta and Mahadek formations follow the trend of 'pseudomorphic replacement' theory.

(c) The Fe_2O_3 (total) of glauconite in the Karai Shale Formation is possibly related to upwelling. A large flux of continental weathering products supplies the Fe (total) content of glauconite the Ukra Hill Member, Bryozoan Limestone Formation and the Lameta Formation. The low Fe_2O_3 (total) content of glauconite in Bryozoan Limestone and Lameta formations is related to the restricted mobility of Fe ions into the glauconite structure. The low Fe_2O_3 (total) and high Al_2O_3 contents in glauconite of the Mahadek Formation are related to chloritization.

(d) Glauconite formed in the passive margin basins of India in response to the global sea-level rise, warm and humid climate and sub-oxic depositional redox condition in shallow seas during the Cretaceous. Glauconites in the Mesozoic basins of India recorded marine transgressions during Aptian, Late Albian-Middle Turonian, Coniacian and Maastrichtian.

References

Amorosi A (1995) Glaucony and sequence stratigraphy: a conceptual framework of distribution in siliciclastic sequences. J Sed Res 65:419–425

Amorosi A (1997) Detecting compositional, spatial, and temporal attributes of glaucony: a tool for provenance research. Sediment Geol 109:135–153

Amorosi A (2012) The occurrence of glaucony in the stratigraphic record: Distribution patterns and sequence-stratigraphic significance. In: Morad S, Ketzer JM, De Ros LF (eds) Linking diagenesis to sequence stratigraphy, vol 45. IAS Special Publication, pp 37–54

Amorosi A, Centineo MC (2000) Anatomy of a condensed section: the lower Cenomanian glaucony rich deposits of Cap Blanc-Nez (Boulonnais, Northern France). In: Glenn CR, Prévôt-Lucas L, Lucas J (eds) Marine authigenesis: from global to microbial, vol 66. SEPM Special Publication, pp 405–413

Amorosi A, Sammartino I, Tateo F (2007) Evolution patterns of glaucony maturity: a mineralogical and geochemical approach. Deep-Sea Res II 54:1364–1374

Amorosi A, Guidi R, Mas R, Falanga E (2012) Glaucony from the Cretaceous of the Sierra de Guadarrama (Central Spain) and its application in a sequence-stratigraphic context. Int J Earth Sci 1:415–427

Bandopadhyay PC (2007) Interpretation of authigenic vs. allogenic green peloids of ferric clay in the Proterozoic Penganga Group, southern India. Clay Mineral 42:471–485

Banerjee S, Jeevankumar S, Eriksson PG (2008) Mg-rich ferric illite in marine transgressive and highstand systems tracts: examples from the Paleoproterozoic Semri Group, central India. Precam Res 162:212–226

Banerjee S, Chattoraj SL, Saraswati PK, Dasgupta S, Sarkar U (2012a) Substrate control on formation and maturation of glauconites in the Middle Eocene Harudi Formation, western Kutch, India. Mar Petrol Geol 30:144–160

Banerjee S, Chattoraj SL, Saraswati PK, Dasgupta S, Sarkar U, Bumby A (2012b) The origin and maturation of lagoonal glauconites: a case study from the Oligocene Maniyara Fort Formation, western Kutch, India. Geol J 47:357–371

Banerjee S, Mondal S, Chakraborty PP, Meena SS (2015) Distinctive compositional characteristics and evolutionary trend of Precambrian glaucony: example from Bhalukona Formation, Chhattisgarh basin, India. Precam Res 271:33–48

Banerjee S, Bansal U, Thorat A (2016a) A review on palaeogeographic implications and temporal variation in glaucony composition. J Palaeogeography 5:43–71

Banerjee S, Bansal U, Pande K, Meena SS (2016b) Compositional variability of glauconites within the Upper Cretaceous Karai Shale Formation, Cauvery Basin, India: implications for evaluation of stratigraphic condensation. Sediment Geol 331:12–29

Banerjee S, Farouk S, Nagm E, Roy Choudhury T, Meena SS (2019) High Mg-glauconite in Campanian Duwi Formation of Abu Tartur Plateau, Egypt and its implications. J African Earth Sci 156:12–25

Banerjee S, Choudhury TR, Saraswati PK, Khanolkar S (2020a) The formation of authigenic deposits during Palaeogene warm climatic intervals: a review. J Palaeogeography 9:27. https://doi.org/10.1186/s42501-020-00076-8

Banerjee S, Ghosh P, Nagendra R, Bhattacharya B, Desai B, Srivastava AK (2020b) Marine and fluvial sedimentation including erosion and sediment flux in peninsular indian phanerozoic basins. Proc Indian Nat Sci Acad 86:351–363

Bansal U, Banerjee S, Pande K, Arora A, Meena SS (2017) The distinctive compositional evolution of glauconite in the Cretaceous Ukra Hill Member (Kutch basin, India) and its implications. Mar Petrol Geol 82:97–117

Bansal U, Banerjee S, Ruidas DK, Pande K (2018) Origin and geochemical characterization of Maastrichtian glauconites in the, Central India. J Palaeogeography 7:99–116

Bansal U, Pande K, Banerjee S, Nagendra R, Jagadeesan KC (2019) The timing of oceanic anoxic events in the Cretaceous succession of Cauvery basin: constraints from ^{40}Ar/^{39}Ar ages of glauconite in the Karai Shale Formation. Geol J 54:308–315

Bansal U, Banerjee S, Pande K, Ruidas D (2020a) Unusual seawater composition of the Late Cretaceous Tethys imprinted in glauconite of Narmada basin, central India. Geol Mag 157:233–247

Bansal U, Banerjee S, Nagendra R (2020b) Is the rarity of glauconite in Precambrian Bhima Basin in India related to its chloritization? Precam Res 336:1–14

Biswas SK (1977) Mesozoic stratigraphy of Kutch. Quart J Geol Min Met Soc India 49:1–52

Bose PK, Das NG (1986) A Transgressive storm-and fair-weather wave dominated shelf sequence: Cretaceous Nimar Formation, Chakrud, Madhya Pradesh, India. Sediment Geol 46:147–167

Boukhalfa K, Soussi M, Ozcan E, Banerjee S, Tounekti A (2020) The Oligo-Miocene silici-clastic foreland basin deposits of northern Tunisia: stratigraphy, sedimentology and paleogeography. J Afr Earth Sci 170:2. https://doi.org/10.1016/j.jafrearsci.2020.103932

Bremner JM (1981) Sediments on the continental margin off south west Africa between latitudes 171 and 251 south. Bull Joint Geol Surv/Univ Cape Town 10:1–233

Burnett WC (1980) Apatite-glauconite associations off Peru and Chile: palaeo-oceanographic implications. J Geol Soc India 137:757–764

Burst JF (1958a) "Glauconite" pellets: their mineral nature and applications to stratigraphic interpretations. AAPG Bull 42:310–327

Burst JF (1958b) Mineral heterogeneity in 'glauconite' pellets. American Mineral 43:481–497

Chattoraj S, Banerjee S, Saraswati PK (2009) Glauconites from the late Palaeocene Early Eocene Naredi Formation, western Kutch and their genetic implications. J Geol Soc India 73:567–574

Chattoraj SL, Banerjee S, Saraswati PK, Bansal U (2016) Origin, depositional setting and stratigraphic implications of Palaeogene glauconite of Kutch. Spec Publ Geol Soc India 6:75–88

Chattoraj SL, Banerjee S, van der Meer F, Champati Ray PK (2018) Application of visible and infrared spectroscopy for the evaluation of evolved glauconite. Int J Appl Earth Obs 64:301–310

Cook PJ, Marshall JF (1981) Geochemistry of iron and phosphorus-rich nodules from the east Australian continental shelf. Mar Geol 41:205–221

Dasgupta S, Chaudhuri AK, Fukuoka M (1990) Compositional characteristics of glauconitic alterations of K-feldspar from India and their implications. J Sed Pet 60:277–281

Deb SP, Fukuoka M (1998) Fe-illites in a Proterozoic deep marine slope deposit in the Penganga Group of the Pranhita Godavari Valley: their origin and environmental significance. J Geol 106:741–749

Delamette M (1989) Trace fossil assemblages from the Albian phosphate-rich sandstones of the Helvetic shelf (Western Alps). Cret Res 10:207–219

D'Emic MD, Wilson JA, Chatterjee S (2009) The titanosaur (Dinosauria: Sauropoda) osteoderm record: review and first definitive specimen from India. J Vert Paleontol 29:165–177

Desai BG (2013) Ichnological Analysis of transgressive marine tongue in prograding deltaic system: evidences from Ukra Hill Member, western Kachchh, India. J Geol Soc India 82:143–152

El Albani A, Meunier A, Fursich F (2005) Unusual occurrence of glauconite in a shallow marine lagoonal environment. Terra Nova 17:537–544

Garzanti E, Haas R, Jadoul F (1989) Ironstones in the Mesozoic passive margin sequence of the Tethys Himalaya (Zanskar, Northern India): sedimentology and metamorphism. Geol Soc Spec Publ 46:229–244

Giresse P, Wiewióra A (2001) Stratigraphic condensed deposition and diagenetic evolution of green clay minerals in deep water sediments on the Ivory Coast-Ghana Ridge. Mar Geol 179:51–70

Glenn CR, Arthur MA (1988) Petrology and major element geochemistry of Peru margin phosphorites and associated diagenetic minerals: authigenesis in modem organic rich sediments. Mar Geol 80:231–267

Glenn CR, Föllmi KB, Riggs SR, Baturin GN, Grimm KA, Trappe J, Abed AM, GalliOliver C, Garrison RE, Ilyan A, Jehl C, Rohrlich V, Sadaqah RM, Schidlowski M, Sheldon RE, Siegmund H (1994) Phosphorus and phosphorites: sedimentology and environments of formation. Eclogae Geol Helv 87:747–788

Haq BU (2014) Cretaceous eustasy revisited. Global Planet. Change 113:44–58

Hart MB, Joshi A, Watkinson MP (2001) Mid-Late Cretaceous stratigraphy of the Cauvery Basin and the development of the Eastern Indian ocean. J Geol Soc India 58:217–229

Hesselbo SP, Huggett JM (2001) Glaucony in ocean-margin sequence stratigraphy (Oligocene–Pliocene, Offshore New Jersey, USA; ODP Leg 174A). J Sed Res 71:598–606

Hower J (1961) Some factors concerning the nature and origin of glauconite. Am Mineral 46:313–334

Ivanovskaya TA, Gor'kova NV, Karpova GV, Pokrovskaya EV (2006) Layer silicates (glauconite, illite, and chlorite) in terrigenous rocks of the Arymash Formation (Olenek Uplift). Lith Miner Res 6:601–623

Jafarzadeh M, Roy Choudhury T, Taheri A, Banerjee S, Jafarian A (2020) Glauconite within Albian-Cenomanian Aitamir Formation, Kopet-Dagh Basin, northeastern Iran: origin and implications for Cretaceous seawater. Arabian J Geosci. https://doi.org/10.1007/s12517-020-05920-8

Jiménez-Millán J, Molina JM, Nieto F, Nieto L, Ortiz PAR (1998) Glauconite and phosphate peloids in Mesozoic carbonate sediments (Eastern Subbetic Zone, Betic Cordilleras, SE Spain). Clay Miner 33:547–559

Kumar S, Tandon KK (1977) A note on the bioturbation in the Lameta beds. Jabalpur area, MP. Geophytol 7:135–138

Kumar S, Tandon KK (1978) Thalassinoides in the Mottled Nodular Beds, Jabalpur area, MP. Curr Sci 47:52–53

Kumar S, Tandon KK (1979) Trace fossils and environment of deposition of the sedimentary Succession of Jabalpur, Madhya Pradesh. J Geol Soc India 20:103–106

Kumar S, Pathak DB, Pandey B, Jaitly AK, Gautam JP (2018) The age of the nodular limestone formation (late cretaceous), Narmada Basin, central India. J Earth Syst Sci 127:1–7

Meunier A, El Albani A (2007) The glauconite–Fe-illite–Fe-smectite problem: a critical review. Terra Nova 19:95–104

Mishra UK, Sen S (2001) Dinosaur bones from Meghalaya. Curr Sci 80:1053–1056

Nagendra R, Kamalak Kannan BV, Sen G, Gilbert H, Bakkiaraj D, Nallapa Reddy A, Jaiprakash BC (2011) Sequence surfaces and paleobathymetric trends in Albian to Maastrichtian sediments of Ariyalur area, Cauvery Basin, India. Mar Petrol Geol 28:895–905

Odin GS, Matter A (1981) De glauconiarium origine. Sedimentol 28:611–641

Odom EI (1984) Glauconite and celadonite minerals. In: Bailey SW (ed) Micas: reviews in mineralogy and geochemistry 13. MSA, Washington DC, pp 554–572

Ozaki K, Tajika E (2013) Biogeochemical effects of atmospheric oxygen concentration, phosphorus weathering, and sea-level stand on oceanic redox chemistry: implications for greenhouse climates. Earth Planet Sci Lett 373:129–139

Parrish JT, Droser ML, Bottjer DJ (2001) A Triassic upwelling zone: the Shublik Formation, Arctic Alaska, U.S.A. J Sed Res 71:272–285

Pascoe E (1959) A manual of the geology of India and Burma, 3rd ed, Part 2. Govt of India Press, Calcutta, pp 485–1343

Rathore SS, Prabhu BN, Vijan AR, Vic KC, Misra KN (1999) K/Ar age of Ukra glauconites from the Kutch Basin, India. Proc Indian Acad Sci (Earth and Planet Sci) 108:49–55

Rudmin M, Banerjee S, Mazurov A (2017) Compositional variation of glauconites in Upper Cretaceous-Paleogene sedimentary iron-ore deposits in South-eastern Western Siberia. Sediment Geol 355:20–30

Ruidas DK, Pomoni-Papaioannou FA, Banerjee S, Gangopadhyay TK (2020) Petrographical and geochemical constraints on carbonate diagenesis in an epeiric platform deposit: Late Cretaceous Bagh Group in central. Carb Evaporites 35:94. https://doi.org/10.1007/s13146-020-00624-2

Rudmin M, Mazurov A, Banerjee S (2019) Origin of ooidal ironstones in relation to warming events: cretaceous-Eocene Bakchar deposit, south-east Western Siberia. Mar Petrol Geol 100:309–325

Sarkar S, Chakraborty N, Mandal A, Banerjee S, Bose PK (2014) Siliciclastic-carbonate mixing modes in the river-mouth bar palaeogeography of the Upper Cretaceous Garudamangalam Sandstone (Ariyalur, India). J Palaeogeography 3:233–256

Sundaram R, Henderson RA, Ayyasami K, Stilwell JD (2001) A lithostratigraphic revision and palaeoenvironmental assessment of the Cretaceous System exposed in the onshore Cauvery Basin, southern India. Cret Res 22:743–762

Tandon SK (2000) Spatio-temporal patterns of Environmental changes in Late Cretaceous sequences of Central India. In: Okada H, Mateer NJ (eds) Cretaceous environments of Asia, developments in palaeontology and stratigraphy, vol 17. Elsevier, pp 225–241

Tang D, Shi X, Ma J, Jiang G, Zhou X, Shi Q (2017) Formation of shallow water glaucony in weakly oxygenated Precambrian ocean: an example from the Mesoproterozoic Tieling Formation in North China. Precam Res 294:214–229

Tewari VC, Lokho K, Kumar K, Siddaiah NS (2010) Late Cretaceous Paleogene basin architecture and evolution of the Shillong shelf sedimentation, Meghalaya, northeast India. J Indian Geol Cong 2:61–73

Thompson GR, Hower J (1975) The mineralogy of glauconite. Clays Clay Miner 23:289–300

Valdiya KS (2016) The making of India: geodynamic evolution. Springer

Watkinson MP, Hart MB, Joshi A (2007) Cretaceous tectonostratigraphy and the development of the Cauvery Basin, Southern India. Petrol Geosci 13:181–191

Wigley R, Compton JS (2007) Oligocene to Holocene glauconite–phosphorite grains from the Head of the Cape Canyon on the western margin of South Africa. Deep-Sea Res II 54:1375–1395

Early Cretaceous Flora from the East Coast Sedimentary Basins of India: Their Chronostratigraphic and Palaeobiogeographic Significance

**Ch. Chinnappa, Pauline Sabina Kavali, A. Rajanikanth,
Mercedes di Pasquo, and M. E. C. Bernardes-de-Oliveira**

Abstract Macrofloristic or microfloristic zonation of Mesozoic successions, with or without independent marine–biostratigraphic age constraints, is extensively utilized in sedimentary basin analyses worldwide. However, precise macrofloral or palynological demarcation of the non-marine Mesozoic successions remains elusive in India. This uncertainty stems from several factors, including unfossiliferous deposits in critical stratigraphic intervals. However, marine fauna (ammonoids, foraminifers) have been well documented from the Mesozoic sequences of India and offer a unique correlation interface. We attempt to establish tie-points between these fauna and the macro and microflora from the East Coast sedimentary basins of India, which include the Cauvery and Palar basins of Tamilnadu, Krishna-Godavari and Pranhita-Godavari basins of Andhra Pradesh and Mahanadi Basin of Orissa. They offer considerable potential to achieve an integrated correlation to establish a higher time resolution. The early Cretaceous lithounits in these basins provide a long-ranging Neocomian-Aptian age. This work aims to provide precise ages to these formations based on biostratigraphically diagnostic taxa, especially palynomorphs and macroflora. These ages are supported by correlation with reports of coeval marine fossils such as ammonoids, foraminifers and dinoflagellates wherever available. Thus, based on

Ch. Chinnappa
Department of Botany (PG), Andhra Loyola College, Vijayawada 52008, Andhra Pradesh, India

P. S. Kavali (✉)
Birbal Sahni Institute of Palaeosciences, 53 University Road, Lucknow 226007, UP, India
e-mail: kpauline_sabina@bsip.res.in

A. Rajanikanth
Ushodaya Apartments, Tarnaka, Hyderabad 500017, India

M. di Pasquo
Laboratorio de Palinoestratigrafía y Paleobotánica, CICYTTP-CONICET (Consejo de Investigaciones Científicas y Tecnológicas), Dr. Materi y España SN, E3105BWA Diamante, Entre Ríos, Argentina
e-mail: medipa@cicyttp.org.ar

M. E. C. Bernardes-de-Oliveira
Instituto de Geociências, Universidade de São Paulo, IGc/USP. Rua do Lago 562, CEP.
05508-080, São Paulo, SP, Brazil
e-mail: maryeliz@usp.br

the marker taxa precise ages have been assigned to the lithounits of the east coast sedimentary basins. Palaeobiogegraphic studies indicate that latitudinal control on climate was a more important factor in delineating the paleofloristic realms. The development of the angiosperms took place around the Neocomian and their diversification around Aptian-Turonian. Marine routes were established along the margins of the southern continents.

Keywords Early Cretaceous · Macroflora · Palynoflora · Biostratigraphy · East Coast sedimentary basins

1 Introduction

The east coast sedimentary basins of India are differentiated geomorphologically and segmented tectonically into Cauvery, Palar, Krishna-Godavari, Mahanadi and Pranhita-Godavari Basins and they are distributed in Tamil Nadu; Andhra Pradesh and Orissa (Fig. 1a–f). These sedimentary basins represent a known range of stratigraphic units encompassing the Mesozoic-Cenozoic time span. The Early Cretaceous well-represented litho-units are the Sriperumbudur Formation of Palar Basin, Kovandankurichchi and Terani formations of Cauvery Basin in Tamil Nadu, Budavada, Vemavaram (Krishna Depression), Golapalli and Raghavapuram formations (Godavari Depression) of Krishna–Godavari Basin and Gangapur/Chikiala formations of Pranhita–Godavari Basin in Andhra Pradesh and Athgarh Formation of Mahanadi Basin in Orissa.

The Early Cretaceous east coast sedimentary basins of India are well known for their fossiliferous rocks (Rajanikanth 1996; Chinnappa and Rajanikanth 2016, 2018). Feistmantel (1877a, b, c, 1879), for the first time, described the fossil flora represented by pteridophytes and gymnosperms and compared them with Rajmahal and Jabalpur flora. He established the term 'mixed flora' to refer to a mixture of floral components from Rajmahal and Jabalpur and suggested an Early Jurassic age. Seward and Sahni (1920), Sahni (1928) and Sahni (1931) revised the fossil floras of India proposing major taxonomic changes and incorporating many new taxa. These authors also suggested a Jurassic age to the plant assemblages bearing sediments of the east coast. However, its upper limit was extended to the late Jurassic, which was accepted for many years (Suryanarayana 1954; Ramanujam 1957; Gopal et al. 1957; Mahabale and Satyanarayana 1979; Adyalkar and Rao 1963; Kar and Sah 1970).

Subsequent studies based on fauna and flora (macro and micro) and tectonics, suggested a new paradigm reassigning those plant assemblages of 'Upper Gondwana' sediments to the Early Cretaceous (Spath 1933; Bhalla 1969; Rajeshwar Rao and Ramanujam 1979; Ramanujam and Rajeshwar Rao 1980; Sastri et al. 1981; Rajeshwar Rao et al. 1983; Ramakrishna et al. 1985; Venkatachala and Sinha 1986; Prabhakar 1987; Venkatachala and Rajanikanth 1988; Rajanikanth 1996, 2009; Prasad and Pundir 1999; Rajanikanth et al. 2000). However, none of these studies provided the precise ages and a long-ranging Neocomian-Aptian age is considered.
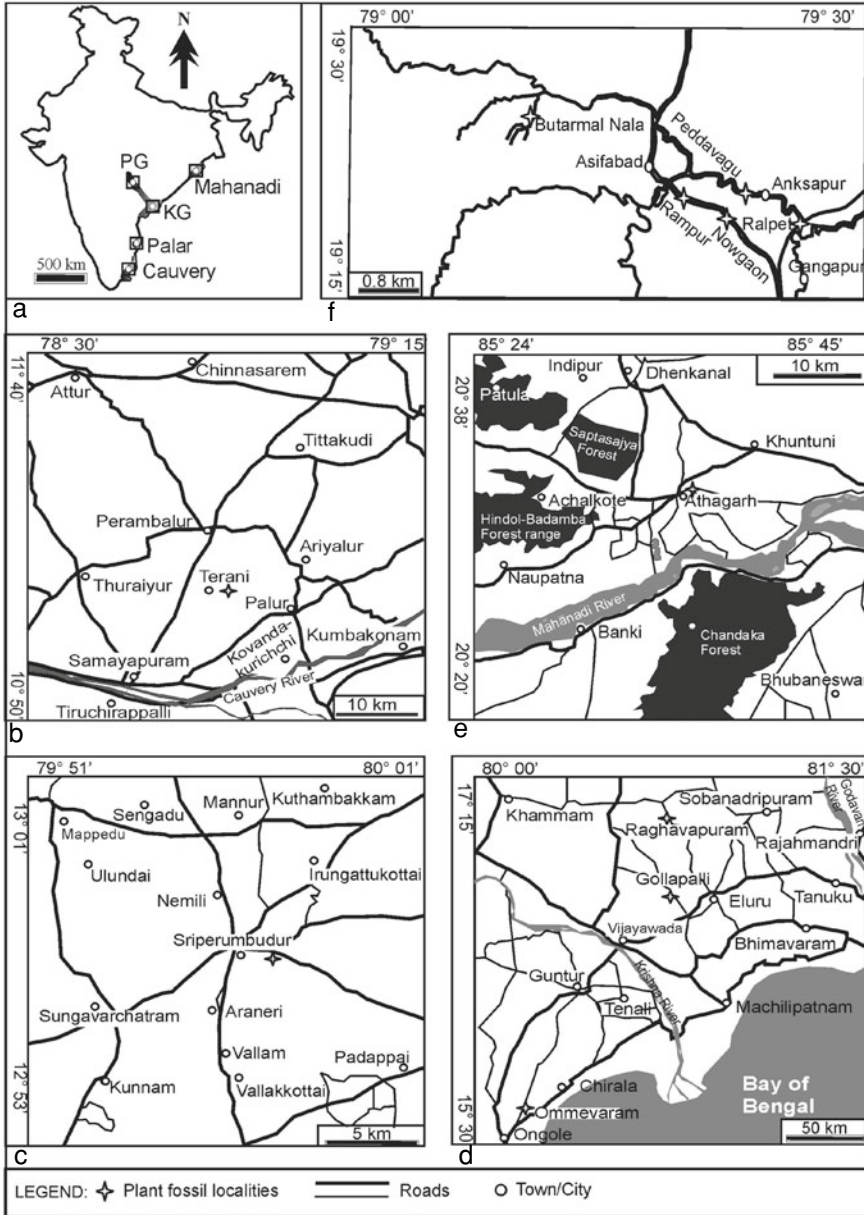
Fig. 1 **a** Location map showing east coast sedimentary basins of India; **b–f** maps showing the early Cretaceous outcrops in different basins (**b** Cauvery Basin, **c** Palar Basin, **d** Krishna–Godavari Basin, **e** Mahanadi Basin, **f** Pranhita–Godavari Basin)

Therefore, the present work aims to determine the precise age for the various Early Cretaceous sedimentary units in the east coast of India based on the availability and the newly obtained micro-and macro floral evidence and their correlation with faunal entities.

2 Evolution of East Coast Sedimentary Basins

The east coast of India is defined by the rifted passive margin that evolved in response to the continental rifting and seafloor spreading processes between India, Antarctica and Australia that occurred during the Late Jurassic to early Cretaceous period (Sastri et al. 1981; Powell et al. 1988; Lal et al. 2009). Subsurface and gravity magnetic data reveal that the east coast of India has evolved through four major tectonic stages (Lal et al. 2009).

The pre-breakup history of the Gondwanaland constitutes the first stage in the tectonic evolution of sedimentary basins of the east coast of India. The reconstruction of Gondwanaland suggests the juxtaposition of Enderby Land and Mac Robertson Land of Antarctica against east coast of India (Smith and Hallam 1970; Katz 1978; Lawver and Scotese 1987; Yoshida et al. 1992; Agarwal and Pandey 1999). The initial breakup of eastern and western Gondwanaland marks the beginning of the rift phase and the second stage of evolution. The development of a rift is linked to the volcanic outbreak during 198–173 Ma in South Africa from Mozambique to Natal Sea (Cox 1992) and Antarctica (Encarnacion et al. 1996). Nevertheless, the final breakup and development of the Indian Ocean took place around 152 Ma as evidenced by seafloor magnetic anomaly M-22 in Somali and Natal basins (Veevers and Tewari 1995). The Cauvery Basin was first to initiate deposition around magnetic anomaly M-22 as a result of rifting of Africa-Antarctica (Mozambique rift) and development of Natal Basin between Africa—India (with Madagascar)—Antarctica (Veevers and Tewari 1995; Lal et al. 2009). The Palar Basin came into existence around the same time as a result of rifting between India and Antarctica (Biswas et al. 1993).

The next phase of the evolution was marked by the extension of India-Western Australia rift further in a southwesterly direction up to Krishna-Godavari Basin (Lal et al. 2009). The basin came into existence along the East Coast around 144 Ma due to NNE-SSW, NE-SW, and E-W faulting, resulting in the upliftment of basement ridges of the Peninsular Gneissic complex and Eastern Ghats Mobile Belt. This crustal extension in KG Basin was an oblique one with Nayudupeta High acting as a pivot, resulted in the formation of horsts and grabens in Krishna-Godavari Basin (Prabhakar and Zutshi 1993; Rao 2001; Radhakrishna et al. 2012). The Mahanadi Basin also came into existence during this time. Oblique extension of India-Western Australia rift, followed by asymmetric seafloor spreading mark final stage of rifting (Ramana et al. 1994), which resulted in transpression at India-Sri Lanka and Antarctica junction. This led to the development of a transcurrent fault (NNW-SSE) along which Antarctica moved southward (Lal et al. 2009). The evolution of east coast of

India resulted in the development of the margins under passive margin conditions during the later period.

The Pranhita-Godavari is an intracratonic rift basin and it preserves records of repeated opening and closing of Proterozoic and Gondwana rifts. The basin opened at *c.* 1700 Ma. The stability of the craton was disrupted when the first major cratonic rift nucleated at *c.* 1620 Ma (Chaudhuri et al. 2012). Rifting along the PGR took place in a NW-trending Precambrian belt, which witnessed episodic tectonism (Mitra 1994). Gondwana sedimentation commenced with crustal sagging in the early Permian during pre-breakup crustal distension followed by episodic rifting in late Permian–Cretaceous time (Biswas 2003). Pre-rift sagging formed the initial basin, which evolved into an interior fracture, and intracratonic rift basin (Casshyap et al. 1993; Biswas 2003). This was followed by the repeated cycles of syn-rift-fluvial sedimentation during the early to late rift stages. Early Cretaceous Chikiala and Gangapur sediments were deposited during the late rifting.

3 Materials and Methods

The macro-and microfloral data available in published literature were consulted (Tables 1 and 2). Stratigraphically significant taxa were used to construct their first and last appearance datum. The scheme of zonation pattern and stratigraphic ranges of various spore-pollen were primarily after Morgan et al. (2002) and Tripathi (2008). Similarly, the macro-floral zonation was adopted from the Douglas (1969) sensu lato Cantrill and Webb (1987).

Additionally, new data were also generated from the outcrop sections of Krishna-Godavari and Pranhita-Godavari basins of Raghavapuram and Gangapur formations, respectively. Some of the significant and well-preserved palynomorphs and megafossils were photographed (Figs. 2 and 3). The techniques used to isolate the spore pollen from the sediments followed a general maceration technique, practiced by palynologists.

4 Chronostratigraphic Implications

4.1 Cauvery Basin

The Cauvery Basin (Fig. 1b) is a pericratonic basin, located along the south-eastern coast of India, developed during the breakup of Gondwana in the Late Jurassic (Rangaraju et al. 1993). The basin extends over 50,000 km^2 both on land and offshore up to 2000 m bathymetry. More than 6000 m pile of sediments ranging from Permian to Holocene is well preserved in the basin. The Cauvery Basin is composed of six half-graben blocks trending in NE-SW separated by horsts. The exposed Cretaceous

Table 1 Distribution of macroflora in various Early Cretaceous basins of East Coast of India (*Data source* Rajanikanth and Chinnappa (2016); present study; Legend: CA—Cauvery, PL—Palar, KG—Krishna-Godavari, PG—Pranhita-Godavari, MH—Mahanadi, Ter—Terani, Sri—Sripermbudur, Vem—Vemavaram, Gol—Golapalli, Rag—Raghavapuram, Gan—Gangapur, Ath—Athagarh)

Basin	CA	PL	KG					PG	MH
Stratigraphic Unit	Ter	Sri	Bud	Vem	Gol	Rag	Gan	Ath
Plant Taxa									
Pteridophytes									
Equisetaceae									
Equisetites rajmahalensis Oldham and Morris									+
Equisetites sp.	+							+	+
Neocalamites sp.								+	
Marattiaceae									
Marattiopsis macrocarpa (Oldham and Morris) Seward and Sahni	+				+	+			+
Osmundaceae									
Cladophlebis acutipennis Oishi									+
C. daradensis Bose and Banerji									+
Cladophlebis denticulata (Brongniart) Seward								+	+
C. indica (Oldham and Morris) Feistmental	+							+	+
C. kathiawarensis Roy									+
C. medlicottiana (Oldham) Pascoe						+			+
C. longipennis Sewrad					+				+
C. srivastavae Gupta	+								+
Cladophlebis sp.	+			+	+	+		+	+
Todites indicus (Oldham and Morris) Bose and Sah		+			+				+
Gleicheniaceae									
Gleichenia bosahii (Bose) Pant and Srivastava					+			+	+
G. nordenskioldii Heer						+		+	+
G. rewahensis Feistmantel								+	
Gleichenia sp.								+	+
Dipteridaceae									
Hausmannia buchii Andreae								+	
Hausmannia sp.								+	+
Matoniaceae									
Matonidium sp.									+
Phlebopteris athgarhensis Jain									+
P. polypodioides Brongniart									+

(continued)

Table 1 (continued)

Basin	CA	PL	KG				PG	MH
Stratigraphic Unit	Ter	Sri	Bud	Vem	Gol	Rag	Gan	Ath
Phlebopteris sp.								+
Cyatheaceae								
Protocyathea cyatheoides (Unger) Feistmental	+							
P. trichinopoliensis Feistmantel	+							
Dicksoniaceae								
Coniopteris sp.								+
Onychiopsis psilotoides (Stopes and Webb) Ward						+	+	+
Onychiopsis sp.								+
ICP								
Actinopteris sp.	+						+	
Sphenopteris specifica (Feistmantel) Roy					+			
S. tiruchirapalliense Sukh-Dev and Rajanikanth	+							
Sphenopteris sp.	+			+	+		+	+
Rhizomopteris ballii Feistmantel								+
R. sahnii Gupta								+
Rhizomopteris sp.	+							
Gymnosperms								
Pteridosperms								
Thinnfeldia feistmantelii Lele				+		+		
T. vemavaramensis n. sp.	+	+		+		+		
Thinnfeldia sp.		+		+			+	
Pachypteris gangapurensis Sukh-Dev and Rajanikanth							+	
P. specifica Feistmental								+
Pachypteris sp.								+
Pachypteris indica (Oldham and Morris) Bose and Roy				+	+	+	+	+
Cycadales								
Morrisia dentata (Rao and Jacob) Bose and Banerji	+	+		+		+		

Table 1 (continued)

Basin	CA	PL	KG					PG	MH
Stratigraphic Unit	Ter	Sri	Bud	Vem	Gol	Rag		Gan	Ath
M. rajmahalensis (Feistmental) Bose and Banerji					+				
Nilsoniopteris sp.								+	+
Taeniopteris kutchensis Bose and Banerji								+	
T. lata Oldham and Morris	+								
Taeniopteris longifolium Sukh-Dev and Rajanikanth								+	
Taeniopteris spatulata McClelland	+	+	+	+	+	+		+	+
Taeniopteris sp.						+			
Bennettitales									
Anomozamites amarjolense Sharma et al.		+		+					
A. fissus Feistmantel	+			+					+
A. haburensis Bose and Banerji	+								
A. jungens Feistmantel				+					
Anomozamites sp.	+					+		+	
Bucklandia sp.					+	+		+	
Cycadolepis indica Gupta						+			
Cycadolepis sp.				+					
Cycadites rajmahalensis Oldham									+
Cycadites sp.								+	
Dicyozamites falcatus Medlicott and Blanford	+	+	+	+		+			
D. feistmantelii Bose and Bano	+	+	+	+	+	+			
D. gondwanensis Sukh-Dev and Rajanikanth								+	
D. hallei Sahni and Rao				+					
D. indicus Feistmantel		+	+	+	+				
D. ommevaramensis sp. nov.				+					
D. sahnii Gupta and Sharma						+		+	
Dictyozamites sp.								+	
Otozamites acutifolius Feistmantel				+					
O. bengalensis Schimper		+		+		+		+	+
O. exhislopi Bose				+					
O. goldlaei Brongniart	+							+	

Table 1 (continued)

Basin	CA	PL	KG				PG	MH
Stratigraphic Unit	Ter	Sri	Bud	Vem	Gol	Rag	Gan	Ath
O. gondwanensis Bose				+				
O. imbricatus Feistmantel				+				
O. vemavaramensis Bose and Jain		+		+		+	+	
Otozamites sp.			+	+		+	+	
Pseudocycadeoidea indicus Aiyangar and Jacob	+							
Pterophyllum braunianum Goppert					+			
P. distans Morris			+			+	+	+
P. footeanum Feistmantel	+			+				+
P. incisum Sahni and Rao				+				
P. kingianum Feistmantel					+			+
P. medlicottianum Oldham and Morris							+	
P. morrisianum Oldham					+			
Pterophyllum sp.	+	+		+	+			+
Ptilophyllum acutifolium Morris	+	+	+	+	+	+	+	+
P. cutchense Morris	+			+	+	+	+	+
P. deodikarii Mahabale and Satyanarayana					+			
P. heterophylla sp. nov.				+				
P. indicum Jacob and Jacob								+
P. oldhamii Jacob and Jacob								+
Ptilophyllum cf. *distans* (Feistmantel) Jacob and Jacob				+		+	+	
Ptilophyllum cf. *institacallum* Bose					+			
Ptilophyllum cf. *amarjolense* Bose					+			
Ptilophyllum cf. *gladiatum* Bose and Sukh-Dev					+			
Ptilophyllum cf. *horridum* Roy					+		+	
Ptilophyllum cf. *jabalpurense* Jacob and Jacob					+			
P. raghdevapurense Mahabale and Satyanarayana						+		
P. rarinervis (Feistmantel) Bose and Kasat	+	+		+		+	+	
P. sahnii Gupta and Sharma						+		+
P. tenerrimum Feistmantel					+			

Table 1 (continued)

Basin	CA	PL	KG				PG	MH
Stratigraphic Unit	Ter	Sri	Bud	Vem	Gol	Rag	Gan	Ath
Ptilophyllum sp.							+	
Williamsonia blandfordii Feistmantel					+			
W. indica Seward					+			
W. kakadbhitensis Pandya and Sukh-Dev					+			
Zamites sp.				+			+	+
Ginkgoales								
Baiera sp.								+
Ginkgoites crassipes Fiestmantel		+		+		+		
G. feistmantelii Bose and Sukh-Dev						+		
Ginkgo cf. *biloba* Linnaeus						+		
Ginkgo sp.		+				+		
Coniferales								
Allocladus bansaensis Sukh-Dev and Zeba-Bano		+					+	
Araucarites cutchensis Feistmantel	+	+		+	+	+	+	+
A. fibrosa Sukh-Dev and Bose		+			+			
A. macropteris Feistmantel		+			+	+		+
A. minutus Bose and Maheshwari	+	+		+				+
A. nipaniensis Sing								+
A. raghavapurensis n. sp.						+		
A. sehoraensis Bose and Maheshwari								+
Araucarites sp.						+	+	+
Brachyphyllum expansum (Sternburg) Seward			+	+				+
B. feistmantelii (Halle) Sahni			+			+		
B. regularis Borkar and Chiplonkar	+				+			+
B. rhombicum Feistmantel		+	+			+		+
B. sehoraensis Bose and Maheshwari							+	
B. theraniense Sukh-Dev and Rajanikanth	+							
Brachyphyllum sp.	+			+	+	+	+	
Cheirolepis cf. *muensterii* Schimper					+			
Coniferocaulon rajmahalense Gupta							+	+
Coniopteris sp.								+

(continued)

Table 1 (continued)

Basin	CA	PL	KG					PG	MH
Stratigraphic Unit	Ter	Sri	Bud	Vem	Gol	Rag	Gan	Ath
Conites sessilis Sahni		+		+		+		
Conites sriperumaturensis Sahni		+					+	
Conites sp.				+		+	+	
Desmiophyllum indicum Sahni				+				
Echinostrobus sp.					+			
Elatocladus andhrii Chinnappa and Rajanikanth							+	
Elatocladus bosei Maheshwari and Kumaran							+	
Elatocladus confertus Seward and Sahni		+			+	+	+	+
E. heterophylla Halle	+						+	
E. jabalpurensis (Feistmantel) Sahni		+		+			+	+
E. kingianus Bose et al.							+	
E. loyolii Chinnappa and Rajanikanth				+				
E. plana (Feistmantel) Seward	+	+		+	+	+	+	+
E. sehoraensis Maheshwari and Kumaran							+	
E. tenerrimus (Feistmantel) Sahni	+	+		+				+
E. vemavaramensis Pandya et al.				+				
Elatocladus sp.				+				+
Pagiophyllum feistmantelii Halle				+				+
P. gollapallensis Pandya and Sukh-Dev					+			
Pagiophyllum cf. *grantii* Bose and Banerji					+			+
Pagiophyllum marwarensis Bose and Sukh-Dev	+						+	
Pagiophyllum cf. *marwarensis* Bose and Sukh-Dev						+	+	
P. ommevaramensis Chinnappa and Rajanikanth				+				
P. rewaensis Bose and Sukh-Dev							+	
P. peregrinum Lindley and Hutton							+	+
P. spinosum Sukh-Dev and Rajanikanth							+	
Pagiophyllum sp.				+			+	+
Torreyites constricta (Feistmantel) Seward and Sahni		+		+				

Table 1 (continued)

Basin	CA	PL	KG					PG	MH
Stratigraphic Unit	Ter	Sri	Bud	Vem	Gol	Rag		Gan	Ath
T. sitholeyi Ganju								+	
Woods (Coniferales)									
Araucarioxylon agathioides (Kräusel and Jain)						+			
Araucarioxylon amraparense Manik and Srivastava								+	
A. rajmahalense Sahni		+							
A. trichinopoliense Varma		+							
Araucarioxylon sp.		+							
Baieroxylon cicatricum Muralidara Rao and Ramanujam								+	
Platyspiroxylon parenchymatosum Muralidara Rao and Ramanujam								+	
Podocarpoxylon parthasarathyi Manik and Srivastava		+						+	
Podocarpoxylon sp.		+				+			
Cupressinoxylon alternans Sahni						+			
C. coromandelinum Sahni		+							
Angiosperms									
cf. *Potamogeton* sp.						+			
Sahniophyllum indica								+	
cf. *Trapa* sp.						+			

system of the Cauvery Basin represents a marine sequence, rich in faunal assemblages ranging from Albian to Maastrichtian. The Lower Cretaceous sediments are exposed as isolated outcrops, and they include Kovandankurichchi and Terani formations (Nagendra et al. 2019). These formations were previously considered as the members of the Sivaganga Formation (Tewari et al. 1996).

4.1.1 Kovandankurichchi Formation

The Kovandankurichchi Formation (Nagendra et al. 2019) was previously known as Kovandankurichchi Conglomerate Member of the Sivaganga Formation (Tewari et al. 1996). This formation is named after Kovandankurichchi Village (78° 56′ E; 10° 56′ N). The type section of the unit is located at 78° 55′ E; 10° 52′ N in the Kovandankurichchi Quarry II. The Kovandankurichchi Formation is the oldest sedimentary unit of the Cretaceous system in and around Ariyalur where it is ~175 m thick and is mappable (Sundaram and Rao 1986; Sundaram et al. 2001). It is also traced in stream sections, well cuttings and trenches up to the region south of Perali.

Table 2 Distribution of microflora in various Early Cretaceous basins of East Coast of India (Venkatachala and Rajanikanth 1987; Prasad and Pundir 1999; Goswami et al. 2006; 2008, Mehrotra et al. 2010; Present study; for legend refer Table 1)

Basin	CA	PL	KG			PG	MH
Stratigraphic unit	Ter	Sri	Vem	Gol	Rag	Gan	Ath
Plant Taxa							
Bryophytes							
Aequitriradites spinulosus		+	+			+	
A. verrucosus		+				+	
Aequitriradites sp.	+						+
Cooksonites minor						+	
C. variabilis	+	+	+	+	+	+	
Coptospora cauveriana	+	+			+		
C. cutchensis		+				+	
Coptospora sp.		+				+	
Coronatispora perforata		+					
Coronatispora sp.					+		
Corrugatisporites sp.	+						
Distalanulisporites verrucatus		+					
Foraminisporis assymetricus						+	
F. dailyi		+		+		+	
F. wonthaggiensis				+		+	
Rouseisporites dakshinii	+						
R. muricatus	+						
R. reticulatus	+						
Staplinisporites caminus		+				+	
Triporoletes reticulatus		+					
Pteridophytes							
Alsophyllidites grandis				+			
Appendicisporites cristatus		+					
A. erdtmanii		+					
A. sellingii			+		+		
Appendicisporites sp.	+	+					
Baculatisporites baculatus			+		+		
B. rotundus						+	
Baculatisporites sp.	+						
Biformaesporites baculosus		+					
Biformaesporites sp.						+	
Biretisporites potoniae	+	+			+		

Table 2 (continued)

Basin	CA	PL	KG			PG	MH
Stratigraphic unit	Ter	Sri	Vem	Gol	Rag	Gan	Ath
B. spectabilis	+	+				+	
Biretisporites sp.		+					
B. paucipunctatus	+						
B. praeclarus							+
Camerozonosporites rudis						+	
Ceratosporites acutus	+						
C. couliensis		+				+	
C. equalis	+	+		+		+	
Ceratosporites sp.	+						
Cicatricosisporites abacus		+					
C. augustus		+				+	
C. australiensis	+	+	+	+	+	+	
C. brevilaesuratus	+						
C. dorogensis						+	
C. gangapurensis						+	
C. goniodontos		+					
C. hallei		+				+	
C. hughesi	+	+	+	+	+	+	
C. imbricatus						+	
C. ludbrookiae	+	+	+		+	+	
C. mohrioides		+				+	
C. pseudotripartitus	+						
C. verrumuratus						+	
Cicatricosisporites sp.	+	+			+	+	
Cingulatisporites formosus	+						
Cingulatisporites sp.	+						
Cingutriletes clavus	+						
Clavifera sp.	+						
Conbaculatisporites densibaculatus	+		+		+		
Concavissimisporites kutchensis		+					
C. punctatus				+		+	
C. variverrucatus				+	+	+	
Concavissimisporites sp.	+		+		+		

Table 2 (continued)

Basin	CA	PL	KG			PG	MH
Stratigraphic unit	Ter	Sri	Vem	Gol	Rag	Gan	Ath
C. cooksoniae	+	+	+	+	+	+	
C. crenatus		+					
C. dettmannii		+					
C. glebulentus	+	+	+	+	+	+	
C. multimuratus	+	+	+			+	
C. problematicus		+					
C. psilatus						+	
Contignisporites sp.	+	+			+		
Crybelosporites punctatus						+	
C. striatus					+		
C. stylosus		+	+		+		
Crybelosporites sp.					+		
Cupanieidites reticularis	+						
Cyathieacidites tectifera					+		
Cyathidites asper			+			+	
C. australis	+	+	+	+	+	+	+
C. cutchensis			+				
C. ghuneriensis						+	
C. jurassicus			+				
C. minor	+	+	+				
C. pseudopunctatus			+				
C. punctatus			+				
C. rajmahalensis			+				
C. trilobatus			+				
Cyathidites sp.	+		+		+		
Deltoidospora diaphana				+			
D. juncta		+				+	
Deltoidospora sp.	+		+		+		
Densoisporites microregulatus				+			
D. velatus	+	+	+	+	+		
Densoisporites sp.		+				+	
Dictyophyllidites crenatus					+		
D. pectinataeformis	+						

(continued)

Table 2 (continued)

Basin	CA	PL	KG			PG	MH
Stratigraphic unit	Ter	Sri	Vem	Gol	Rag	Gan	Ath
D. venkatachalai		+					
Dictyophyllidites sp.						+	
Dictyotosporites complex		+		+			
D. filosus						+	
Distaverrusporites margaritatus	+						
Echinatisporis varispinosus		+					
E. vembanii		+					
Foveosporites sahnii						+	
Foveosporites sp.		+					
Foveotricolporites brevicolpatus	+						
Foveotriletes crassipunctatus			+		+		
F. subtriangularis		+					
Foveotriletes sp.	+						
Gleichinidites circinidites				+			
G. senonicus		+	+			+	
Gleichinidites sp.	+	+				+	+
Impardecispora adilabadensis						+	
I. apiverrucata		+				+	+
I. croassus						+	
I. decora	+						
I. indica							+
I. marylandensis		+					
I. purverulentus			+		+		
I. tribotrys			+		+		
I. trioreticulosa		+	+		+		
Impardecispora sp.					+		+
Ischyosporites crateris		+	+		+	+	
I. punctatus		+		+		+	
I. pusillus						+	
Ischyosporites sp.	+		+				+
Klukisporites areolatus		+				+	
K. foveolatus		+		+		+	
K. kallameduensis	+						

Table 2 (continued)

Basin	CA	PL	KG			PG	MH
Stratigraphic unit	Ter	Sri	Vem	Gol	Rag	Gan	Ath
K. scaberis	+		+	+	+	+	+
K. supinicus	+						
K. variegatus							+
Kraeuselisporites sp		+					
Kuylisporites lunaris						+	
Kuylisporites sp.						+	
Laevigataletes sp.			+				
Laevigatazonaletes sp.			+				
Laevigatimonoletes sp.			+				
Laevigatisporites sp.			+				
Lematatriletes mesozoicus							
Leptolepidites major						+	
L. verrucatus		+		+			
Leptolepidites sp.	+		+				
Liratosporites sp.			+				
Lycopodiacidites asperatus						+	
Lycopodiacidites sp.							+
Lycopodiumsporites austroclavidites	+	+	+		+	+	
L. crassimacerius	+					+	
L. crassireticulatus			+		+		
L. eminulus	+	+	+		+		
L. regulatus	+		+		+		
L. reticulum	+		+		+	+	
L. trambauensis		+					
Lycopodiumsporites sp.		+	+		+		
Lygestepollenites balmei					+		
Matonisporites cooksonii		+					
M. discoidalis		+					
M. phlebopteroides		+				+	
Matonisporites sahnii		+					
Matonisporites sp.		+	+		+		
Metamonoletes haradensis		+				+	
Metamonoletes sp.						+	

Table 2 (continued)

Basin	CA	PL	KG			PG	MH
Stratigraphic unit	Ter	Sri	Vem	Gol	Rag	Gan	Ath
Microfoveolatosporites atbertonensis	+						
M. punctata	+						
Microfoveolatosporites sp.		+					
Monolites indicus		+				+	
Monolites sp.		+					
Murospora florida			+		+		+
M. mesozoica		+					
Murospora sp.							+
Neoraisticka limbata	+						
N. neozealandica					+	+	
N. rallapetensis						+	
N. truncatus		+	+			+	
Neoraistrickia sp.	+						
Ornamentifera echinata		+				+	
O. granulosa			+		+		
Ornamentifera sp.	+				+	+	
Osmundacidites singhii		+					
O. wellmanii	+	+	+			+	+
Osmundacidites sp.	+						
Pilosisporites sp.		+					
Playfordiaspora cancellosa						+	
Plicifera minutus	+	+					
P. senonicus			+	+	+		
Plicifera sp.	+					+	
Polycingulatisporites clavus						+	
P. reduncus		+		+		+	
P. trabeculatus							
Polycingulatisporites sp.	+						
Polypodiisporites multiverrucosus						+	
Polypodiisporites sp.	+						
Reticulatazonalesporites sp.			+				
Reticulatisporites sp.			+				
Retitriletes austroclavatidites				+			

Table 2 (continued)

Basin	CA	PL	KG			PG	MH
Stratigraphic unit	Ter	Sri	Vem	Gol	Rag	Gan	Ath
R. circolumenus				+			
R. eminulus				+			
R. facetus							
Schizosporis coromandelensis	+						
S. regulatus		+				+	
S. reticulata							+
Schizosporis sp.							+
Schizaeoisporites eocaenicus	+						
Sestrosporites pseudoalveolatus		+		+		+	
Staplinisporites caminus			+		+		
Steriosporites antiquasporites	+		+			+	
S. bimmatus	+						
Steriosporites sp.	+						
Striatella balmei				+			
Taurocusporites segmentatus		+		+			
Taurcusporites sp.		+					
Thymospora sp.			+		+		
Todisporites crassus		+					
T. major							+
T. minor				+			
T. rotundiformis		+					
T. grandiverrucosus	+						
T. orikkaiensis		+					
T. rugosus	+						
T. tuberculiformis		+				+	
T. verrucosus	+		+		+		
Triletes sp.					+		
Undulatisporites pannuceus		+					
U venkatachalai						+	
Undulatisporites sp.	+						
Verrucosisporites rotundus		+					
Verrucosisporites sp.		+					
Gymnosperms							

(continued)

Table 2 (continued)

Basin	CA	PL	KG			PG	MH
Stratigraphic unit	Ter	Sri	Vem	Gol	Rag	Gan	Ath
Abietineaepollenites ellipticus			+				
A. robustus			+				
Abiespollenites triangularis						+	
Abiespollenites sp							+
Alisporites grandis	+	+	+			+	
A. ovalis		+				+	+
A. rotundus		+				+	
Alisporites sp.	+		+		+		+
Andreisporites mariae	+						
Apiculatasporites sp.			+				
Apiculatimonoletes sp.			+				
Apicultaletes sp.			+				
Araucariacites australis	+	+	+			+	+
A. ghuneriensis						+	
A. indicus				+	+		
Bhujiasporites sp.			+		+		
Bulosporites triangularis	+						
Bulosporites sp.		+					
Callialasporites crassimarginatus						+	
C. enigmaticus						+	
C. dampieri	+	+	+		+	+	+
C. discoidalis		+				+	
C. doeringii						+	+
C. minus						+	
C. monoalasporus	+		+		+		
C. radisaccus						+	
C. reticulatus		+				+	
C, segmentatus	+	+	+		+	+	
C. triletus	+	+	+		+	+	
C. trilobatus	+	+	+	+		+	+
Callialasporites sp.					+		
Cedripites cretaceus		+	+				
C. nudis			+			+	+

(continued)

Table 2 (continued)

Basin	CA	PL	KG			PG	MH
Stratigraphic unit	Ter	Sri	Vem	Gol	Rag	Gan	Ath
Classoidites glandis						+	
C. glanris						+	
Classopollis belloyensis						+	
C. classoides	+	+	+		+	+	
Classopollis indicus							+
C. meditriangulus	+						
C. obidesensis	+					+	
C. pflugii						+	
C. simplex						+	
C. torosus			+				
Classopollis sp.	+	+					
Complexiopollis complicatus					+		
Complexiopollis sp.					+		
Coniatisporites telata					+		
Coniavisporites minimolivisus						+	
Crassimonoletes surangei						+	
Crassimonoletes sp.							+
Cycadopites couperi						+	+
C. crassimarginis						+	
C. fragilis						+	
C. gracilis		+				+	
C. granulatus						+	
C. nitidus						+	
C. sakrigaliensis		+					
Cycadopites sp.	+						+
Cyclusphaera intacta	+						
Dacrycarpites australiensis		+				+	
Engelhardtiapollenites sp.	+						
Ephedripites multicostatus	+						
Erdtmannipollis sp.					+		
Florinites sp.			+				
Granuloperculatipollis flavatus			+				
G. mundus	+					+	

Table 2 (continued)

Basin	CA	PL	KG			PG	MH
Stratigraphic unit	Ter	Sri	Vem	Gol	Rag	Gan	Ath
G. subcircularis			+				
G. triletus			+				
Inaperturopollenites dubius					+		
Inaperturopollenites sp.	+						
Indusiisporites microsaccatus			+				
Intratriporopollenites sp.	+						
Laricoidites communis		+					
L. indicus			+			+	
Laricoidites sp.						+	
Microcachryidites antarcticus	+	+	+	+	+	+	
Monosulcites ellipticus						+	
M foveolatus	+						
Odontochitina operculata					+	+	
Perinopollenites elatoides	+						
Periplecosporites sp			+				
Phyllocladidites inchoatus		+					
Pityosporites sp.			+				
Platysaccus bhardwajii						+	
P. densus		+				+	
P. indicus						+	
P. queenslandi						+	
Platysaccus sp.			+			+	
Podocarpidites alareticulosus			+				
P. cristiexinus			+				
P. ellipticus	+	+	+		+	+	+
P. grandis			+				
P. major		+				+	
P. microsaccatus	+						
P. minisulcus		+				+	
P. multesimus	+		+		+		
P. novus							+
P. rarus			+				
P. typicus			+				

Table 2 (continued)

Basin	CA	PL	KG			PG	MH
Stratigraphic unit	Ter	Sri	Vem	Gol	Rag	Gan	Ath
Podocarpidites sp.		+	+		+		+
podocarpites austricus						+	
Podosporites raoi			+				
P tripakshii		+	+	+	+	+	+
Podosporites sp.			+				
Psilospora lata						+	
P. parva	+						
Ramanujamiaspora reticulata			+				
Regulatisporites sp.					+		
Scabraatephanocolpites pentaaperturites	+						
Setosisporites sp.			+				
Singhipollis rudis			+				
S. triletus			+				
Spheripollenites psilatus	+						
S. scabratus	+	+					
Spheripollenites sp.		+					
Straiatriporites cauveriana	+						
Striatotuberculatisporites sp.			+				
Triporopollenites minimus	+						
T. rugatus	+						
Triporopollenites sp.	+						
Ulmipollenites arcuatus	+						
U. regulatus	+						
U. tetraporites	+						
Venustaesporites sp.		+					
Verrutricolporites distinctus	+						
Victorisporites ornatus	+						
V tetraporoides	+						
Vitreisporites pallidus	+	+				+	
Vitreisporites sp.							+
Angiosperms							
Asteropollis asteroides					+		
Cearipites nudis						+	

Table 2 (continued)

Basin	CA	PL	KG			PG	MH
Stratigraphic unit	Ter	Sri	Vem	Gol	Rag	Gan	Ath
Clavainaperturites ornatus	+						
Clavatipollenites hughesii					+		
Clavatricolporites leticiae					+		
Constantinisporis jacquei	+						
C. sulcatus	+						
Hymenozonotriletes mesozoicus		+					
Krutzipites annalatus	+						
L reticulatus					+		
Monulcipollenites foveolatus	+						
Myrtaceidites eugeniioides	+						
M. mesonesus	+						
M. parvus	+						
Polybrevicolpites sp.					+		
Polycolpites sp.					+		
Proteacidites amolosexinous	+						
Proteacidites cauverii	+						
Proteacidites decorus	+						
Psilatricolporites operculatus	+						
P pseudolaevigatus	+						
P vridhachalamensis	+						
Pterospermopsis sp.	+						
Racemonocolpites facilis					+		
R ramonus					+		
Retisyncolporites cauveriensis	+						
Rousea georgensis					+		
Scabratriporites simpliformis	+						
Spinizonocolpites echinatus					+		
Striatopollis simplus	+						
Striatricolporites conspicus	+						
Triatripollenites minutus	+						
Tricolpites americana	+						
T. crassimarginatus	+						
T. georgensis					+		

Table 2 (continued)

Basin	CA	PL	KG			PG	MH
Stratigraphic unit	Ter	Sri	Vem	Gol	Rag	Gan	Ath
T. gillii	+						
T. microreticulatus	+						
T. pannosus	+						
T. pausifoveolatus	+						
T. pilosus	+						
T. reticulatus	+						
T. triangularis	+						
Tricolpopollenites globularis	+						
Triorites sp.	+						
Tubulifloridites lilleie					+		
Turonipollis helmegii	+				+		
Vacuopollis pyramis	+						

Banerji (1982) reported isolated outcrops of this member in Virudhachalam. The Kovandankurichchi Formation rests on an unconformity with underlying Archaean basement. The Terani Formation unconformably overlies the Kovandankurichchi Formation (Table 3). The Kovandankurichchi is a conglomerate with feldspar, sub-angular to sub-rounded quartz, boulders, cobbles and clasts derived from Archean Gneiss (Govindan et al. 1998; Nagendra et al. 2019).

Fossil content and age: The outcrops of this unit are devoid of plant fossils. However, subsurface counterparts contain Barremian foraminifer *Globigerina boteriveca* (Govindan et al. 1996; Rajanikanth et al. 2000).

4.1.2 Terani Formation

The Terani Formation is named after the well-exposed in Terani Clay Mine located near Karai Village (Banerji 1982; Ramasamy and Banerji 1991). The type section is located at 78° 54′ E; 11° 07′ N in the Terani clay mine. These beds generally occur as isolated patches in and around Karai along the western border of the sedimentary basin. The Formation is about 60 m thick and is well-exposed in the Terani Clay Mine.

The Terani Formation rests on an unconformity with underlying Kovandankurichchi Formation and it is unconformably overlain by the Dalmiapuram Formation Albian-Cenomanian age. The Terani Formation consists of two members: the Terani Claystone Member with sandstone intercalations at the base, and the Terani Gritty Ferruginous Sandstone Member at the top (Table 3). These sediments consist of quartzose and feldspathic, gritty and ferruginous sandstones with intercalated claystones (Nagendra et al. 2019).
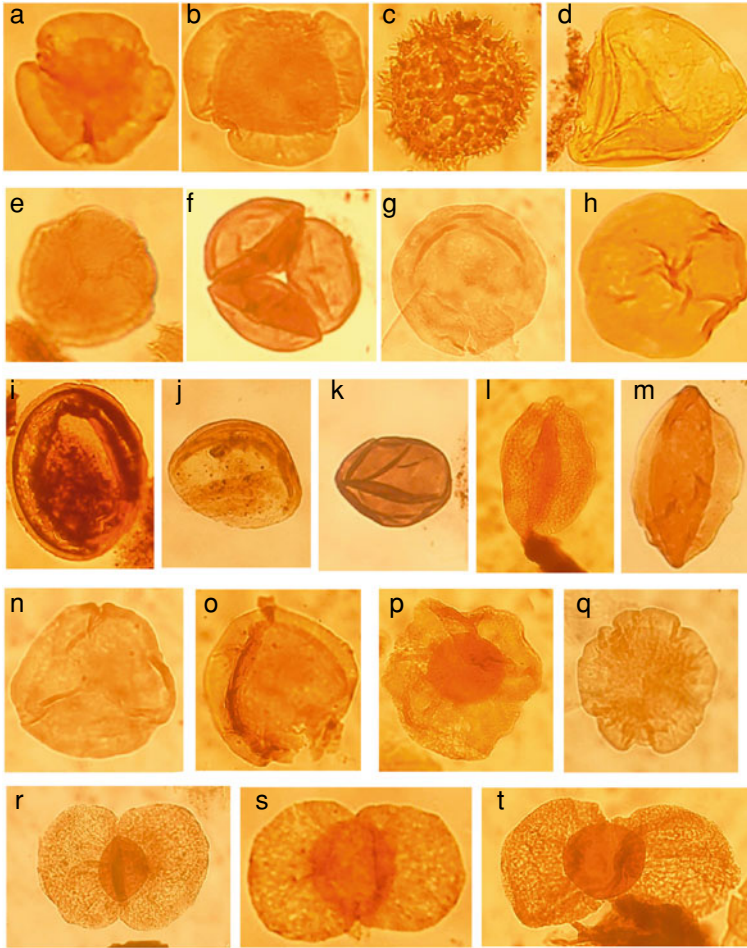
Fig. 2 Representative photographs under microscope showing Cretaceous spores and pollen (all photographs were captured under 500 × magnification). **a**, **b** *Callialasporites trilobatus* (Balme) Sukh Dev 1961 (1. BNIM 20 EF: P.57.3, 2. BNIM 23 A.44.4). **c** *Neoraistrickia neozealandica* Couper (BNIM 8, X.60.2). **d** *Cyathidites australis* Couper 1953? (CH 42, P.44.2). **e** *Camerozonosporites rudis* (Leschik 1955) Claus 1960 (BNIM 28, V.57.4). **f**, **j** cf. *Classopollis* (**6.** CH.44, N.36.3; **10.** Ch.47, F.62.1). **g** *Classopollis simplex* (Danze-Corsin and Laveine 1963) Reiser and Williams 1969 (BNIM 57, R.25). **h**, **n** *Foraminisporis dailyi* (Cookson and Dettman) Dettman 1963 (**8**. BNIM 17, T.23.2; **14**. BNIM 63, S.62.3). **i** *Balmeiopsis limbatus* (Balme) Archangelsky (CH 39, W.36.4). **k** *Inaperturopollenites dubius* (Potonie and Venitz 1934) Thompson and Pflug 1953 (CH 48, F.48). **l** *Cycadopites granulatus* (De Jersy) De Jersy 1964 (BNIM 70, R.44.3). **m** *Cycadopites crassimarginis* (De Jersy) De Jersy 1964 (BNIM 40, G.30.2). **o** *Callialasporites dampieri* (Balme) Sukh Dev 1961 (BNIM 6, N.54.1). **p** *Playfordiaspora cancellosa* (BNIM 59, U.55). **q** *Callialasporites minus* (Tralau) Guy 1971 (BNIM 74, M.46.3). **r** *Platysaccus queenslandi* De Jersy 1962 (BNIM 73, Q.45). **s**, **t** *Podocarpites astrictus* Haskel 1968 (**19**. BNIM 14, F.33.1; **20**. BNIM 53, N.36.3)
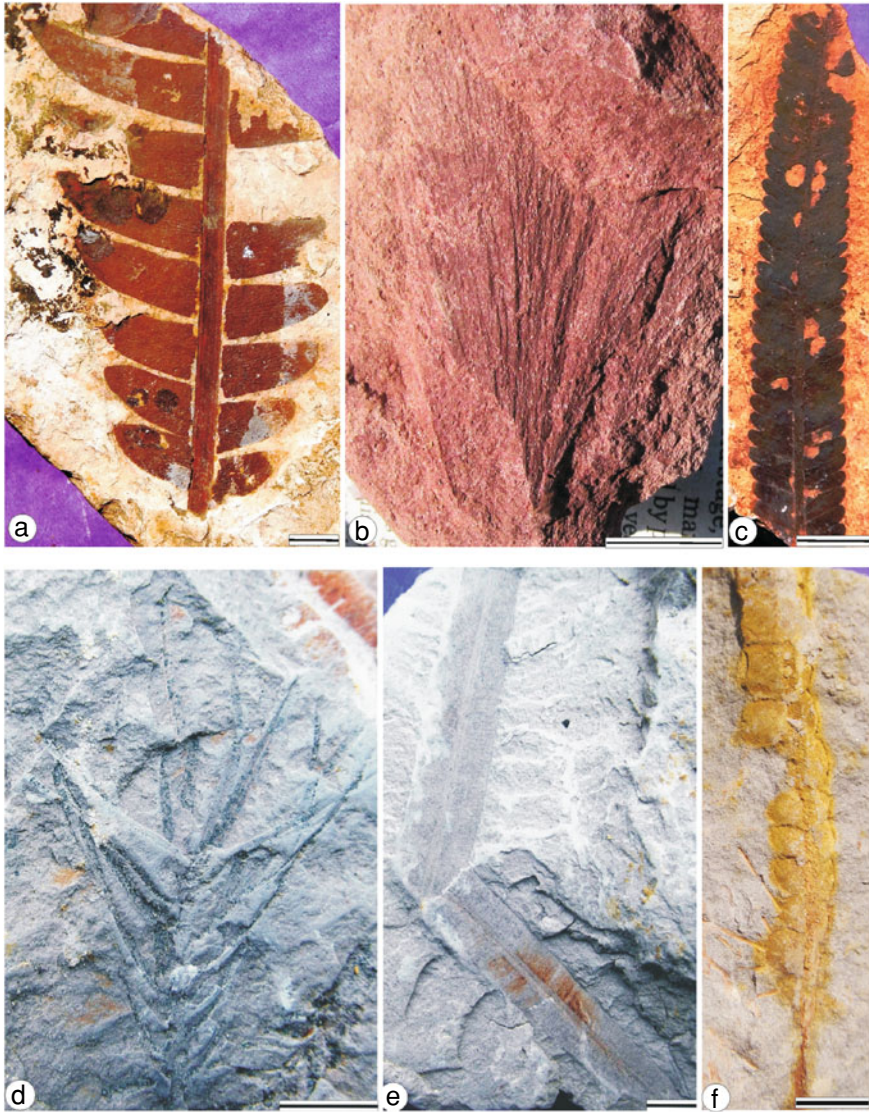
Fig. 3 Photographs showing representative Cretaceous macroflora (scale bar = 1 cm unless and otherwise mentioned). **a** *Dictyozamites ommevaramensis* Chinnappa et al. 2015 (BSIP Specimen no. 40164). **b** *Ginkgo* sp. **c** *Ptilophyllum rarinervis* (Feistmantel) Bose and Kasat 1972 (BSIP Specimen no. 40262). **d** *Torreyites sitholeyi* Ganju 1947 (BSIP Specimen no. 40647) (Scale 0.5 cm). **e** *Taeniopteris spatulata* (McClelland) Bose and Banerji 1981 (BSIP specimen no. 40601) (Scale 0.5 cm). **f** *Anomozamites* sp.

Table 3 Generalised stratigraphy (Early Cretaceous) of Cauvery Basin (*after* Nagendra et al. 2019)

Lithounit	Lithology	Age
Dalmiapuram	Marl bedded limestone	Albian
Terani	Coarse gritty and ferruginous sandstone Claystone with sandstone intercalations	Neocomian
Kovandankurichchi	Conglomerate with inversely graded fanglomerate	
Archaean	————unconformity——— Granite Gneiss and other metamorphic rocks	Archaean

Fossil content and age: The Terani Claystone Member contains well-preserved plant fossils (Feistmantel 1879; Gopal et al. 1957; Ayyasami and Gururaja 1977; Jeyasingh and Sudharsan 1985; Maheshwari 1986; Sukh-Dev and Rajanikanth 1988a), whereas the shale and clay layers of the Terani Gritty Ferruginous Sandstone Member contain arenaceous foraminifera (Banerji 1982; Sastri et al. 1963). The plant fossils from the unit include members of *Equisetum, Marattiopsis, Cladophlebis, Protocyathea, Actinopteris, Sphenopteris*, *Thinnfeldia, Taeniopteris, Morrisia, Anomozamites*, *Otozamites*, *Dictyozamites, Pterophyllum*, *Ptilophyllum, Brachyphyllum, Araucarites, Ginkgo, Elatocladus* and *Torreyites*. This assemblage is provisionally referred to the Zone C of Douglas (1969) or *Phyllopteroides serreta* zone of Cantrill and Webb (1987), based on microflora.

Palynology from the surface deposits of this unit is not known. However, well-preserved palynofloras from sub-surface sediments (Rao and Venkatachala 1971; Venkatachala et al. 1972; Venkatachala 1973, 1974; Venkatachala and Sharma 1974; Venkatachala and Rajanikanth 1987) yielded spores such as *Cooksonites variabilis* and *Crybelosporites stylosus.* But in the absence of *Pilosisporites notensis* and *Coptospora paradoxa* the assemblage is referable to upper *Pilosisporites notensis-Crybelosporites striatus* zones (Morgan et al. 2002) of Aptian to early Albian age. The presence of planktonic foraminifera, including *Hedbergella trocoidea, H. planispira* and *H. delrioensis*, support an Aptian-early Albian age (Reddy et al. 2013).

4.2 Palar Basin

The Palar Basin (Fig. 1c), named after the river Palar covers an area of about 18,300 km^2 in Tamil Nadu and it extends up to Andhra Pradesh and Karnataka. The basement is composed of an Archean metamorphic complex overlain by the fluvio-glacial deposits of early Permian (Lower Gondwana) that in turn overlain by the early Cretaceous sediments. The Precambrian rocks of the Southern Granulite Terrain (SGT) and the rocks belonging to the Eastern Ghat Mobile Belt (EGMB) limit the basin in the west. While the Nayudupetta High separates the Palar from the Pennar basin in the north, the Sri Lanka massif limits the basin in the south. Towards east, the basin extends into offshore, having nearly 33,000 km^2 area up to 200 m isobath

and more than 95,000 km^2 area in the deepwater (Rangaraju et al. 1993; Bastia and Radhakrishna 2012). The Lower Cretaceous unit represented by the Sriperumbudur Formation comprises the sedimentary filling of the basin.

4.2.1 Sriperumbudur Formation

The litho-unit was previously known as Sriperumbudur Beds (Feistmantel 1879) named after the homonymous town (79° 56′ E; 12° 58′ N). The outcrop thickness of the formation may be up to 600 m in thickness. It is characterized by arenaceous and argillaceous rocks comprising splintery green shale, clays and sandstones with ironstone intercalations and contains marine intercalations (Murthy and Sastri 1961). The unit is unconformably overlying either the Precambrian basement or Precambrian boulder beds and green shales. The formation is overlain by the Upper Cretaceous Satyavedu Formation (Table 4).

Fossil content and age: The early Cretaceous floristics of the Sriperumbudur Formation are known through plant macrofossils, mostly preserved in the form of leaves (Feistmantel 1879; Seward and Sahni 1920; Sahni 1928, 1931; Suryanarayana 1953, 1954). These are represented by species of *Cladophlebis*, *Taeniopteris*, *Dictyozamites* and *Pterophyllum*, *Ginkgoites*, *Araucarites* and *Conites*. Jeyasingh and Kumarasamy (1994a) reported a winged seed *Pityospermum nathorst*. This assemblage is comparable to the Zone B of Douglas (1969) and *Phyllopteroides laevis* zone of Cantrill and Webb (1987).

Several species of pycynoxylic woods belonging to the conifers were also reported, which include *Cupressinoxylon coromandelinum*, *Mesembrioxylon* (*Podocarpoxylon*) sp. (Sahni 1931), *M.* (*Podocarpoxylon*) *thirumangalense* (Suryanarayana 1953), *Araucarioxylon giftii*, *Araucarioxylon rajivii* (Jeyasingh and Kumarasamy 1994b), *Araucarioxylon mosurense* (Jeyasingh and Kumarasamy 1995).

Palynology of the sediments was studied by Ramanujam and Varma (1977, 1981) and Varma and Ramanujam (1984). The spore-pollen assemblage is characterised by the presence of *Foraminisporis dailyi*, *Aequitriradites spinulosus* and *Cooksonites variabilis*. In the absence of *Crybelosporites striatus* or any younger zonal index

Table 4 Generalised stratigraphy (Early Cretaceous) of Palar Basin (after Murthy and Sastri 1961)

Lithounit	Lithology	Age
Satyavedu	Coarse boulder beds, conglomerate, compact fine grain sandstone ——transgressive overlap——	Late Cretaceous
Sriperumbudur	Splintery grey and greenish shales, dark clays, partly gypseous interbedded with sandstones and thin bands of ironstones and limestones ————unconformity————	Early Cretaceous
?Talchir	Boulder beds and greenish shales	Permian

species the assemblage is assigned to *Foraminisporis wonthaggiensis-Pilosisporites notensis* zones (Morgan et al. 2002) of Hauterivian to Aptian age. The presence of arenaceous foraminifera and dinoflagellate cysts also suggests similar age assignments, however, with slight variation from Valanginian to Barremian (Basavaraju et al. 2016).

4.3   Krishna-Godavari (KG) Basin

The Krishna-Godavari Basin (KGB) is an extensive deltaic plain formed by two large east coast rivers—Krishna and Godavari in the state of Andhra Pradesh and the adjoining areas of Bay of Bengal in which these rivers discharge their water. The KGB is a proven petroliferous basin located along the east coast of India (Fig. 1d). Its onland part covers an area of 15,000 km^2 and occupies an area of 25,000 km^2 up to 1000 m isobaths in offshore. The basin contains about 5 km thick sediments with several cycles of deposition, ranging in age from late Carboniferous to Pleistocene. The basement faults defining the series of horst and grabens, are aligned NE-SW along the Precambrian eastern Ghat trend (Sastri et al. 1981; Rao 2001).

The Lower Cretaceous sediments are exposed towards the western and northwestern fringes of the basin. These sediments are distributed in two depressions, namely Godavari and Krishna (Sastri et al. 1981; Venkatachala and Sinha 1986). Gollapalli and Raghavapuram formations comprise the sedimentary filling of the former, while Budavada and Vemavaram formations make up the latter. The Golapalli and Ragahavapuram formations in Godavari depression are considered homotaxial to the Budavada and Vemavaram formations, respectively, and are considered as facies variants (Sastri et al. 1981).

4.3.1   Godavari Depression

Gollapalli Formation

The Gollapalli Formation was previously known as Gollapalli Sandstone (King 1880), named after the village Gollapalli (16° 44′ N: 80° 55′ E). The type section of the Formation is designated at Gollapalli village (16° 53′ N: 80° 55′ E). In the type of section, it exhibits white to pale white and light brown sandstone with siltstone parting. The unit crops out in Gollapalli, Nuzvid, Ravacherla, Somavaram, Musnure, Nehrunagaram, the Sudikonda-Adamili areas and west of the Dwaraka Tirumala. It is best developed in the type section and Somavaram hill, where it reaches up to several meters thickness. The Gollapalli Formation rests unconformably on Permian sediments of the Chintalapudi/Kamthi Formation. It is overlain unconformably by the Raghavapuram Formation. The sediments in the Gollapalli Formation are characterized by hard, red brown, ferruginous to conglomeratic to coarse-grained sandstone at the base in Somavaram, Musnure and Nehrunagaram. Brown ferruginous claystone,

siliceous shale, shaly sandstone and purple sandstone comprises the middle segment of the Formation, which crops out at Sudikonda-Adamili and Somavaram hill. The sediments at Gollapalli area exhibits white to pale white compact sandstone with siltstone parting at the top part.

Fossil content and Age: A few plant mega-fossils are known from the Golla-palli Formation (Feistmantel 1877a, 1879; Pandya and Sukh-Dev 1990; Prasad and Pundir 1999). These plant fossils include members of *Cladophlebis, Gleichenia, Marattiopsis, Onychiopsis, Todites, Pachypteris, Taeniopteris, Morrisia, Dictyozamites, Ptilophyllum, Brachyphyllum, Pagiophyllum, Araucarites* and *Elatocladus.* The plant fossils are preserved as impressions on sandstone. The macrofossil assemblage is dominated by the bennettitaleans and it is closely comparable to that of the Berriasian Zone A of Douglas (1969).

Spore-pollen assemblages are absent in outcrops of the Gollapalli Formation. However, Prasad and Pundir (1999) reported a rich assemblage of spore-pollen from the bore core sections of the formation. The spore-pollen assemblage includes important marker taxa such as *Aequitriradites spinulosus*, *Foraminisporis wonthaggiensis*, *F*. *dailyi* and *F*. *assymetricus.* The absence of *Pilosisporites notensis* or younger zonal indices suggests the upper age limit for this litho-unit as Barremian. This spore-pollen assemblage is attributable to the upper *Foraminisporis wonthaggiensis* zone (Morgan et al. 2002) of late Neocomian (Hauterivian to Barremian) age (Tripathi 2008). The dinoflagellate cysts from the surface and subsurface sediments of the Gollapalli Formation concurs with Neocomian age (Prasad and Pundir 1995, 1999). The differences on the age assignments by means of the paleobotany and palynological assemblages relate to the poor preservation of fossil assemblages in this unit.

Raghavapuram Formation

The Raghavapuram Formation is originally known as the Raghavapuram shale (King 1880) named after the village Raghavapuram (17° 02′ N: 81° 22′ E). Its type section is designated in a hillock about 2 km east of the village (17° 13′ N; 81° 19′ E). It is characterized by white to light gray claystone with ferruginous concretion partings. The unit is distributed around Raghavapuram, Musnure-Nehrunagaram area and at the western margin of the Dwaraka Tirumala town (16° 57′ N; 81° 17′ E). It is best developed in the type section and west of the Dwaraka Tirumala hill where it reaches 75 m and 80 m thickness, respectively. In Musnure-Nehrunagaram area, the unit is up to 4.5 m thick with sediments made up of clay, silt and sandstone.

The Raghavapuram Formation rests on an unconformity with the underlying conglomeratic grit and sandstone of the Gollapalli Formation. The Raghavapuram Formation is overlain unconformably by the Tirupati Sandstone (Table 5). The sediments exposed at Raghavapuram and Dwaraka Tirumala comprises two distinct lithologies. The lower part of the section (40 m) is characterized by white to pale brown shales and claystones, containing thin beds of medium-grained glauconitic

Table 5 Generalised stratigraphy (Early Cretaceous) of KG Basin (after Sastri et al. 1981)

Lithounit	Lithology	Age
Tirupati/Pavalur	Purple red-light brown sandstone/clay and caleritic sandstone	Late Cretaceous
Raghavapuram/Golapalli/ Vemavaram/Budavada	White pale-reddish earthy shale, red ferruginous claystone, light buff-grayish white glauconitic sandstone/shale containing carbonaceous matter ————unconformity———- Coarse-grained feldspathic sandstone, alternating calcareous claystone	Early Cretaceous
Chintalapudi/Kamthi		Permian

sandstone (Sastri et al. 1981). The upper part comprises reddish to purple shale and claystone beds with thin bands of red ferruginous claystone.

Fossil content and age: Feistmantel (1879) published the first reference to plant mega-fossils from the Raghavapuram Formation along with the other Early Cretaceous sedimentary units. Since that time, several authors described fossil foliage and other kinds of plant mega-fossils (Baksi 1967, 1968; Mahabale and Satyanarayana 1979; Prasad and Pundir 1999; Chinnappa et al. 2015). These plant fossils were primarily known from the type locality of the formation. Conifers and ginkgos dominate plant macro-fossil assemblages. Ferns and fern-like foliages, cycadeoids, ginkgoaleans and several taxa of uncertain systematic position are also recorded (Chinnappa and Rajanikanth 2018). The abundance of ginkgos from this unit suggests a possible correlation with Zone C of Douglas (1969) or *Phyllopteroides serreta* zone of Cantrill and Webb (1987). Interestingly, the formation also yielded some unidentified angiosperm fossils, which are comparable to the monocots (Chinnappa 2016). The known and acceptable records of monocotiledonean fossils are from the Aptian onwards (Friis et al. 2011).

Spore-pollen assemblages from the outcrops of the type section are poorly known except from one section exposed at Dwaraka Tirumala having rich assemblages (Prasad and Pundir 1999). However, spore-pollen assemblages from the sub-surface samples of the formation are well documented (Sharma et al. 1977; Venkatachala and Sinha 1986; Mehrotra et al. 2010, 2012). Palynomorph assemblages obtained from the Raghavapuram Formation yielded *Cooksonites variabilis*, *Foraminisporis dailyi*, *Crybelosporites striatus* and *Clavatipollenites* sp., but *Coptospora paradoxa* is absent. The palynomorph suites are thus referable to the upper *Pilosisporites notensis-Crybelosporites striatus* Zones of Morgan et al. (2002) of Aptian-early Albian age. The presence of ammonite genus *Acanthohoplites* and bivalve *Anopeae constrica* (Arkel et al. 1957; Crame and Kelly 1995) and index planktic foraminifera, *Ticinella bejaouensis, Hedbergella trocoidea, H. gorbachikae* and *Microhedbergella miniglobularis* (Raju and Reddy 2016; Raju 2017) in the Raghavapuram Formation support the age assignments.

4.3.2 Krishna Depression

Budavada Formation

The Budavada Formation is originally known as Budavada sandstone (Foote 1879), named after the village Budavada (15° 84′ N; 80° 14′ E) located about 41 km north of Ongole in Prakasam District, Andhra Pradesh. The formation is distributed around Budavada and Inkollu located at 40 km north of Ongole. The Inkollu area shows limestone and sandstone with abundant ammonites and molluscans. Small exposures of the unit also occur in Yendluru situated 10 km west of Ongole. Here, the formation is characterized by sandstone with fragmentary plant fossils.

The Budavada Formation is characterized by white-pale and light brown sandstone beds with siltstone partings/sandstone beds and it rests on an unconformity with underlying Permian sediments of the Chintalapudi/Kamthi Formation. The Formation is unconformably overlain by the Vemavaram Formation (Table 5).

Fossil content and age: Plant fossils from this litho-unit is poor. Plant taxa consist of *Taeniopteris, Dictyozamits, Otozamites, Ptilophyllum* and *Pterophyllum* with altogether seven species. The marine fossils known from the Budavada Unit include ammonites *Pascocites budavadensis*, *Gymnoplites simplex* and associated foraminifera, bryozoans, lamellibranchs, gastropods and brachiopods, which suggest an Early Cretaceous age (Spath 1933; Bhalla 1969; Sastri et al. 1977). Palynoflora is not known from this unit, and it is considered homotaxial to the Golapalli Formation of Hauterivian-Barremian age (Sastri et al. 1981).

Vemavaram Formation

The Vemavaram Formation, previously known as Vemavaram shale (Foote 1879) named after the village Vemavaram (currently known as Ommevaram-15° 41′ N; 80° 09′ E) is located 19 km north of Ongole in Prakasam District, Andhra Pradesh and about 8 miles inland from the coast. The formation, however, does not have any designated type section. The formation is distributed in and around the Ommevaram Nagalauppalapadu, Prasangulapadu, Rachapudi and Uppugonduru and it is also exposed 22 km away from the south of the Kandukuru.

The Vemavaram Formation rests on an unconformity with the underlying sandstone layer of the Budavada Formation and it is overlain unconformably by the Pavaluru Formation. The Vemavaram Formation is characterized by medium to coarse-grained clay and lateritic sandstones. The Formation is composed primarily of shales containing carbonaceous matter.

Fossil content and age: The Vemavaram Formation is well known for its rich plant fossils and marine fauna. The plant fossils were largely reported from in and around the village Vemavaram (Feistmantel 1879; Bose and Jain 1967; Jain 1968; Vagyani 1984, 1985; Pandya et al. 1990; Chinnappa et al. 2014, 2015). Sporadic reports are known from other areas (Vagyani and Zutting 1986; Vagyani and Jamane 1988). The plant fossils from the unit include members of *Cladophlebis, Sphenopteris,*

Pachypteris, Thinnfeldia, Taeniopteris, Morrisia, Anomozamites, *Otozamites, Dicty-ozamites, Pterophyllum, Ptilophyllum, Cycadolepis, Brachyphyllum, Pagiophyllum, Araucarites, Elatocladus, Torreyites, Harrisiophyllum* and *Conites*. These plant fossils are preserved as impressions on grey to white-coloured shale.

Rich assemblages of spore-pollen were documented from both the outcrop and sub-surface (Ramanujam 1957; Kar and Sah 1970; Rao and Venkatachala 1971; Sharma et al. 1977; Venkatachala and Sinha 1986). The significant spore-pollen taxa include *Aequitriradites spinulosus*, *Cooksonites variabilis*, *Cicatricosisporites australiensis*, and *Contignisporites cooksoniae* etc. The fossil fauna known from this Unit include ammonites *Holcodiscus* cf. *prezianus, H*. cf. *caillandiamus*, *Hoplites* cf. *borowae*, *H*. cf. *beskidensis*, *H*. *cadazzianus*, *Lytocerus* sp., *Pascocites budavadensis*, *P. crassus*, *Gymnoplites simplex* and associated lamellibranchs, and brachiopods, which suggests an Early Cretaceous age (Spath 1933). The phytoplankton assemblage correlates the subsurface sediments of the Vemavaram Formation with the Raghavapuram Formation (Sharma et al. 1977).

4.4   Pranhita-Godavari (PG) Basin

The Pranhita-Godavari Basin is an intra-cratonic Gondwana rift basin (Fig. 1f), named after the two well-known rivers of Peninsular India—Pranhita and Godavari. The basin is trending NW-SE, located in the eastern part of Peninsular India, and extends up to the east (Lakshminarayana 1996). The thickness of the deposits in the basin is ~3000 m dated from late Carboniferous/early Permian to Cretaceous (Biswas 2003). The Gondwana sediments seem to have deposited on block-faulted Proterozoic basins that evolved due to repeated sagging along SW and NE faults. A thick, almost uninterrupted sequence of Permo-Triassic and partly Jurassic and Cretaceous sediments of mainly continental origin overlie the Proterozoic sediments. The Lower Cretaceous sediments in the basin are represented by the Gangapur Formation/Chikiala Formation.

4.4.1   Gangapur Formation/Chikiala Formation

The Gangapur Formation was named after the village Gangapur (19° 16′ N; 79° 26′ E), exposing the contact between Gangapur beds (King 1880) and the underlying Kota beds (Kutty 1969). The sedimentation in the Gangapur/Chikiala Formation took place during the early Cretaceous after renewed rift activity (Biswas 2003). The thickness of the Gangapur Formation ranges from 100 to 250 m, whereas the Chikiala Formation is about 275 m thick (Lakshminarayana 1996). The formation is characterized by coarse ferruginous sandstone beds with many pebble bands succeeded by an alternating sequence of sandstones and mudstones or silty mudstone (Table 6). These sediments are exposed around the village Gangapur in Adilabad district of Telangana. The formation extends from north of Nowgaon (19° 20′ N, 79° 24′ E) to the west of

Table 6 Generalised stratigraphy of Pranhita-Godavari Basin (after Lakshminarayana 1996)

Lithounit	Lithology	Age
Deccan Traps	Infra/intertrappean beds: limestone, clay and sandstone	Late Cretaceous/Paleogene
Gangapur/Chikiala	Coarse ferruginous sandstone, greywhite-pinkish mudstone and silty mudstone/shale ————unconformity—— *Upper*: Sandstone, siltstone and claystone *Middle*: Limestone *Lower*: Conglomeratic sandstone, siltstone trough cross-stratified sandstone	Early Cretaceous
Kota		?Jurassic

village Gangapur (19° 16′ N; 79° 26′ E) and in the east up to Dharmaram and Paikasigudem (Kutty 1969).

Although, both the Gangapur and Chikiala formations are known to overlie the Kota Formation unconformably, the relationship between the Gangapur and Chikiala formations is unclear. Flora and fauna are absent in the Chikiala Formation, whereas the Gangapur Formation yielded a well preserved Early Cretaceous flora (Bose et al. 1982; Sukh-Dev and Rajanikanth 1988b; Chinnappa and Rajanikanth 2016). The Upper Gondwana sequences are covered by the Deccan Traps (Lakshminarayana 1996).

Fossil content and age: Abundant and well-preserved leaf, cone and shoot macrofossils are present along bedding planes particularly within siltstone/mudstone facies of the Gangapur Formation (Feistmantel 1877c; Bose et al. 1982; Rajeshwar Rao et al. 1983; Ramakrishna and Muralidhara Rao 1986, 1991; Ramanujam et al. 1987; Muralidhara Rao and Ramakrishna 1988; Pal et al. 1988; Sukh-Dev and Rajanikath 1988b; Manik and Srivastava 1991; Chinnappa and Rajanikanth 2016). The macroflora contains around two species of seed-ferns belonging to the single genus *Pachypteris*, about twenty five species of conifers referred to *Araucarites, Elatocladus*, *Brachyphyllum*, *Pagiophyllum*, *Conites*, *Harrisiophyllum*, *Torreyites* and *Taxites,* and ten to twelve species of ferns assigned to *Sphenopteris*, *Cladophlebis*, *Coniopteris*, *Hausmannia, Gleichenia* and *Marattiopsis*) and thirteen or fourteen species of bennettitaleans placed under *Ptilophyllum, Dictyozamites, Pterophyllum* and *Taeniopteris.* The presence of *Taeniopteris daintreei* in the Gangapur assemblage suggests its relation to Zone B and C of Douglas (1969). However, the presence of a monocot fossil leaf in the Gangapur assemblage (Chinnappa 2016) limits the older age connotation to the Barremian. The monocot fossil leaves were not known from the early part of the Neocomian (Friis et al. 2011). Therefore, the assemblage is likely referable to the Zone C of Douglas (1969) or *Phyllopteroides serreta* zone of Cantrill and Webb (1987).

Apart from a rich and diverse macroflora, the formation also yields a rich assemblage of spore-pollen (Ramanujam and Rajeshwar Rao 1979, 1980; Bose et al. 1982; Rajeshwar Rao et al. 1983; Prabhakar 1987; Ramakrishna and Ramanujam 1987;

Ramakrishna et al. 1985). Palynomorph assemblages from the Gangapur Formation yielded *Aequitriradites spinulosus*, *Foraminisporis wonthaggiensis*, *F. assymetricus* and *Cooksonites variabilis*, but lacks *Dictyotosporites speciosus* and *Crybelosporites striatus*. The palynomorph suites are thus referable to the upper *Foraminisporis wonthaggiensis-Pilosisporites notensis* Zones of Morgan et al. (2002), which indicates Barremian-Aptian age. The Gangapur sediments were deposited during the syn-rift stage of the second Gondwana sedimentation cycle around the Aptian time period (Raju 2017).

4.5   Mahanadi Basin

The Mahanadi Basin (Fig. 1e) is named after the river Mahanadi which flows through the states of Chhattisgarh and Odisha. The basin covers a total area of 55,000 km^2 out of which about 14,000 km^2 lies in the shallow offshore area. Geographically, the shallow offshore part of the basin lies off the coast of Andhra Pradesh and Orissa. The 85° E ridge occurring to the south of Lake Chilka forms the approximate southwestern limit of the basin. The onland part of the basin is limited to northwest and west by Precambrian outcrops belonging to the Indian Shield. Towards northeast, it merges into the North East Coast region (NEC) with Bengal Basin lying further northeast. Onshore Mahanadi Basin is located in the State of Orissa. The Lower Cretaceous sediments in the Mahanadi Basin are exposed in Athgarh Basin and Chhatrapur Outlier.

The Athgarh basin is named after the village Athgarh near Cuttack, Orissa (Blandford et al. 1859) situated between the 20° 15′ and 20° 33′ N and 85° 35′ and 85° 50′ E. The sediments are exposed to the north, northwest and southwest of Cuttack and Bhubaneswar city and cover an area of about 800 km^2 in the districts of Cuttack and Khurda with an estimated thickness of 400 m (Kumar and Bhandari 1973). The river Mahanadi divides the basin into two unequal southern and northern parts. The basin includes sediments belonging to Lower Permian and Cretaceous. The Lower Cretaceous sediments in the basin are represented by the Athgarh Formation.

4.5.1   Athgarh Formation

The Athgarh Formation (Sandstone) constitutes the northernmost exposure of coastal Gondwana and was first studied by Blandford et al. (1859) followed by Ball (1877). This formation with an estimated thickness of 400 m rests unconformably over Eastern Ghats granulites and at places on the Permian rocks (Kumar and Bhandari 1973; Tiwari et al. 1987). The formation is exposed near the western margin of the basin and mainly consists of white to grey hard sandstones with intercalations of lenticular greyish white to pinkish clays and carbonaceous shales (Table 7). Fossil bearing horizons of the unit are known from Naraj, Jagannath Prasad and Talbast (Cuttack district, Orissa).

Table 7 Generalised stratigraphy of Mahanadi Basin (after Tiwari et al. 1987)

Lithounit	Lithology	Age
Recent	Alluvium, laterite	Holocene
Athgarh	Dolerite intrusive	Early Cretaceous
Talchir	sandstone with intercalation of shale and clays ————unconformity—— Pale green splintery shale	Permian

Fossil content and age: Feistmantel (1877b) reported plant fossils for the first time from the Athgarh Formation, and later many workers (Adyalkar and Rao 1963; Jain 1968; Pandya and Patra 1968; Patra 1973a, b, 1980, 1982, 1989, 1990; Patra and Patnaik 1974; Patra and Sahoo 1992, 1995a, b, 1996; Goswami et al. 2006, 2008) have documented floral assemblages characterized by *Marattiopsis, Phlebopteris, Cladophleis, Eboracia, Hausmannia, Cycadopteris, Onychiopsis, Anomozamites, Ptilophyllum, Araucarites and Brachyphyllum.* The spore-pollen assemblages reported from this unit corresponds to the Zone C of Douglas (1969) or *Phyllopteroides serreta* zone of Cantrill and Webb (1987).

The rich palynomorph assemblages were known from the Athgarh Formation (Venkatachala and Rajanikanth 1987; Goswami et al. 2006, 2008). The assemblages include a stratigraphically significant *Aequitriradites spinulosus*, *Coptospora verrucosa* and *Pilosisporites notensis.* In the absence of *Cooksonites variabilis* or younger age indices, the assemblage corresponds to lower *Pilosisporites notensis* Zone of Morgan et al. (2002). The lower age limit of the formation is extended to the Barremian based on *Coptospora verrucosa* (Tripathi 2008).

5   Biostratigraphic Comparison

The occurrence of chronostratigraphically significant taxa in the Early Cretaceous sedimentary basins of the east coast of India enables us to establish reasonable ages of the stratigraphic units (see Venkatachala and Rajanikanth 1987). Ages are determined on the basis of biostratigraphically diagnostic taxa, especially palynomorphs and floral zones (Table 8). Marine faunal species are considered wherever available. The Australian palynozonal scheme of Morgan et al. (2002) improved from the classic one of Helby et al. (1987) has been used herein as is referred by other Indian workers (Vijaya 1999; Vijaya and Bhattacharji 2002).

The Kovandankurichchi and Terani formations of the Cauvery Basin are attributed to the Barremian– early Albian. The Kovandakurichhi Formation is assigned to the Barremian based on the presence of the foraminifer *Globigerina boteriveca* (Govindan et al. 1996; Rajanikanth et al. 2000). The Terani Formation is correlated to the *Pilosisporites notensis* Zone of Aptian to early Albian in age due to the marker spore-pollen taxa *Cooksonites variabilis, Crybelosporites stylosus.* Despite the absence of *Pilosisporites notensis* and *Coptosporapa radoxa*, this age is supported

Table 8 Age determination based on integrated correlation of marine and terrestrial floras and fauna from the Early Cretaceous sediments of East Coast of India (*Data source* Macroflora-Rajanikanth and Chinnappa 2016 and references therein, Present study; Microflora—Venkatachala and Rajanikanth 1987; Prasad and Pundir 1999; Goswami et al. 2006, 2008; Mehrotra et al. 2010; Present study; Ammonoids, Dinoflagellates and Foraminifera-Sastri et al. 1963; Baksi 1966; Mamgain et al. 1973; Singh and Ghosh 1977a, b, c; Shah et al. 1977; Prasad and Pundir 1999)

Age	Basin	Litho-unit	Significant Foraminifera	Significant Ammonoids	Significant Dinoflagellates	Significant Macroflora	Significant Palynoflora	Palynozones
Barremian	Cauvery	Kovandan-kurichchi	*Globigerina boteriveca*					
Aptian-early Albian		Terani	*Hedbergella trocoidea H. planispira H. delrioensis*	*Gymnoplites simplex, P. crassus, Inoceramus* sp.		*Taeniopteris spatulata, Dicyozamites falcatus, Ptilophyllum acutifolium, Pagiophyllum marwarensis*	*Cooksonites variabilis, Crybelosporites stylosus*	Upper *Pilosisporites notensis- Crybelosporites striatus*
Hauterivian-Aptian	Palar	Sriperum-budur	*Bathysiphon taurivensis, Pelosina comolsnata, Ammodiscus cretaceous, Haplophragoides dickinesnii, H. concave, H. footei, H. indicus Spiroplctamina indica*	*Pascoites crassus*	*Gochteodinia villosa, Neldinopsis kostromiensis, Ctenidodinium elegantulim*	*Pachypteris gangapurensis, Dicyozamites falcatus, Ptilophyllum acutifolium, Ginkgoites crassipes*	*Foraminisporis dailyi, Aequitriradites spinulosus, Cooksonites variabilis*	*Foraminisporis wonthaggiensis- Pilosisporites notensis*
late Neocomian (Hauterivian-Barremian)	Krishna-Godavari	Gollapalli	*Animobaculitis, sp., Animodiscoides sp., Haplophragoides*		*Odontochitina oprculata, Oligosphaeridium complex, Systematophora aereolata*	*Sphenopteris specifica Pterophyllum braunianum Ptilophyllum acutifolium Elatocladus confertus*	*Aequitriradites spinulosus, Foraminisporis wonthaggiensis, F. dailyi, F. assymetricus*	Upper *Foraminisporis wonthaggiensis*

(continued)

Table 8 (continued)

Age	Basin	Litho-unit	Significant Foraminifera	Significant Ammonoids	Significant Dinoflagellates	Significant Macroflora	Significant Palynoflora	Palynozones
Aptian-early Albian		Raghava-puram	Ammobaculates fishri, A. loboso, A. sahnii, Haplophragmoides concave, H. chapmani, Ticinella bejaouensis, Hedbergella trocoidea, H. aptiana, H. gorbachikae, Microhedbergella miniglobularis	Acantholoplites, Bernrites	Odontochitina oprculata, Mudrongia australis, Cyclonephelium distinctum, Diconodium pusillum, Cribroperidinium edwardsii, Oligosphaeridium complex	Marattiopsis macrocarpa, Ginkgoites crassipes, G. feistmantelii, Palm like leaves	Cooksonites variabilis, Foraminisporis dailyi, Crybelosporites stratus, Clavatipollenites sp.	Pilosisporites notensis-Crybelosporites striatus
late Neocomian (Hauterivian–Barremian)		Budavada	Dentalina sp., Lenticulina sp., Frondicularia sp., Pseudopolymorphina sp.	Pascocites budavadensis, Gymnoplites simplex		Taeniopteris, Dictyozamits, Otozamites, Ptilophyllum, Pterophyllum		Upper Foraminisporis wonthaggiensis
Aptian-early Albian		Vemavaram		Holcodiscus cf. prezianus, H. cf. caillandiamus, Hoplites cf. borovvae, H. cf. beskidensis, H. cadaczianus, Lytocerus sp., Pascocites budavadensis, P. crassus, Gymnoplites simplex		Thinnfeldia feistmantelii, Anomozamites amarjolense, Otozamites acutifolius, Pagiophyllum feistmantelii	Aequitriradites spinulosus, Cooksonites variabilis, Cicatricosisporites australiensis, Contignisporites cooksoniae	Pilosisporites notensis-Crybelosporites striatus

Table 8 (continued)

Age	Basin	Litho-unit	Significant Foraminifera	Significant Ammonoids	Significant Dinoflagellates	Significant Macroflora	Significant Palynoflora	Palynozones
Barremian-Aptian	PG	Gangapur/Chikiala				*Gleichenia bosahii, Hausmannia buchii, Onychiopsis psilotoides, Taeniopteris daintreei, Sahniophyllum indica*	*Aequiradites spinulosus, Foraminisporis wonthaggiensis, F. assymetricus, Cooksonites variabilis*	Upper *Foraminisporis wonthaggiensis-Pilosisporites notensis*
Aptian	Mahanadi	Athgarh				*Equisetites rajmahalensis, Todites indicus, Onychiopsis psilotoides, Pachypteris indica, Araucarites cutchensis*	*Aequiradites spinulosus, Coptospora verrucosa, Pilosisporites notensis,*	Lower *Pilosisporites notensis*

by the planktic foraminifera, such as *Hedbergella trocoidea, H. planispira* and *H. delrioensis* (Reddy et al. 2013).

The Palar Basin includes the Early Cretaceous Sriperumbudur formation. A Hauterivian to Aptian age is considered for this litho-unit based on the presence of *Foraminisporis dailyi*, *Aequitriradites spinulosus* and *Cooksonites variabilis*. It lacks younger zonal indices *Crybelosporites striatus*. The presence of Barremian arenaceous foraminifera and dinoflagellate cysts supports such age assignments (Basavaraju et al. 2016).

The Krishna-Godavari basin includes the Early Cretaceous Golapalli/Budavada formations and Raghavapuram/Vemavaram formations. The Golapalli/Budavada formations represent older sediments and they are assigned the Hauterivian—Barremian age, based on the important spore-pollen marker taxa such as *Aequitriradites spinulosus*, *Foraminisporis wonthaggiensis*, *F. dailyi* and *F. assymetricus*. The absence of *Pilosisporites notensis* or younger zonal indices suggests the upper age limit for this litho-unit as Barremian. The presence of Neocomian dinoflagellate cysts from the Gollapalli Formation provides additional support for the Barremian age (Prasad and Pundir 1995, 1999). The Raghavapuram/Vemavaram formations represent younger sediments and they include important spore-pollen marker taxa such as *Cooksonites variabilis*, *Foraminisporis dailyi*, *Crybelosporites straitus* and *Clavatipollenites* sp. The ammonite genus *Acanthohoplites* (constrained by an $^{40}Ar/^{39}Ar$ date of 114.9 ± 0.4 Ma near the top of the *Parahoplites nutfieldiensis* Zone) and the bivalve *Anopeae constrica* (Arkel et al. 1957; Crame and Kelly 1995) and an index planktic foraminifera *Ticinella bejaouensis, Hedbergella trocoidea, H. gorbachikae* and *Microhedbergella miniglobularis* (Raju and Reddy 2016; Raju 2017) in the Raghavapuram Formation confirm such age assignments.

The significant marker taxa from the Gangapur Formation include *Aequitradites spinulosus*, *Foraminisporis wonthaggiensis*, *F. assymetricus* and *Cooksonites variabilis*, but lacked *Dictyotosporites speciosus* and *Crybelosporites striatus*. Palynomorph assemblages from the Athgarh Formation include *Aequitradites spinulosus*, *Coptosporaverrucosa* and *Pilosisporites notensis*, and lacks *Cooksonites variabilis* or younger age indices. Based on the available marker palynomorphs both the Gangapur and Athgarh formations of PG Basin and Mahanadi basins respectively are assigned Barremian-Aptian in age.

6 Palaeobiogeographic Control on Eastern Indian Palaeoflora

The Indian subcontinent was united with the other Gondwanan continents throughout the early Mesozoic (Fig. 4). However, the united Indo-Madagascar plate began to separate from mainland Africa in the Jurassic when the breakup of Gondwana started. India drifted northwards, separated from Australia and Antarctica in the Early Cretaceous, from Madagascar in the early Late Cretaceous. The Indo-Pakistan plate had

Fig. 4 Paleobiogeographic map of the Early Cretaceous showing the position of Indian subcontinent (after Chinnappa and Rajanikanth 2018; Legend: An—Antarctica, Au—Australia, Ma—Madagascar, Af—Africa, SA—South America)

contact with Africa in the Senonian and possibly made initial contact with Asia at the end of the Cretaceous (Metcalfe 2001). The global sea-level in the Late Cretaceous pushed India into lengthy isolation from other landmasses (Fitzgerald 2002; Briggs 2003; Khan and Srivastava 2006; Underwood et al. 2011).

The peak of construction of the southern and largest portion of the Kerguelen Plateau in the southern Indian Ocean may have been simultaneous with the eruption of the formerly adjacent Rajmahal Traps of eastern India at ~118 Ma in the mid-Aptian (Baksi et al. 1987; Coffin et al. 2002). This episode probably contributed to the broad carbon isotope excursion that characterizes the late Aptian (Wignall 2001; Tripathi 2008; Gradstein et al. 2012).

Early Cretaceous paleodiversity changes of terrestrial and marine biotas of East Coast Cauvery, Palar, Krishna-Godavari, Pranhita-Godavari and Mahanadi sedimentary basins of India (Tables 2 and 3; see Venkatachala and Rajanikanth 1988; Rajanikanth and Chinnappa 2016) together with well-preserved floras in the Rajmahal, Kutch and Jabalpur basins (see Tiwari and Tripathi 1992; Rajanikanth and Chinnappa 2016) give support to this dynamic paleogeographic evolution of

India and the changes of land-sea configuration. Cretaceous palaeobiogeographic configurations were proposed by Srivastava (1978, 1983), Herngreen et al. (1996) and McLoughlin (2001).

Herngreen et al. (1996) summarized the Early Cretaceous–Cenomanian flora, marked by strong provincialism, delimited by ecological and geographical differences (Figs. 5 and 6). The large Trisaccates Province in Southern Hemisphere embraces Antarctica, southern South America, southern Africa, Australia and New Zealand and India (Tables 4 and 5). Two subprovinces are recognized in the
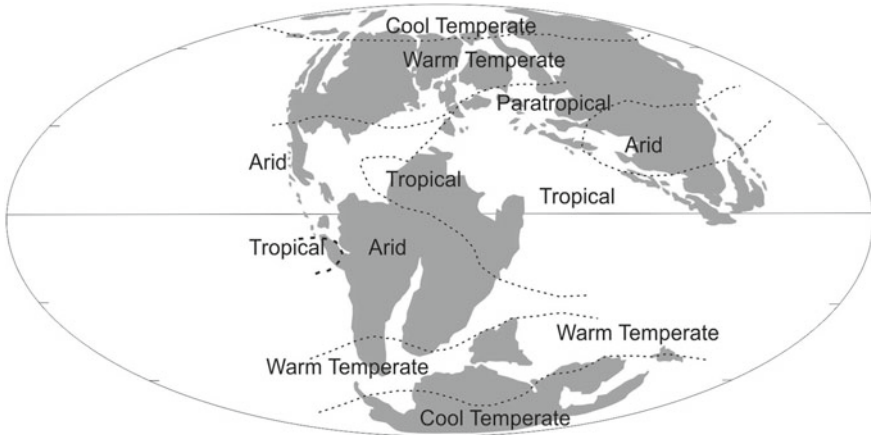
Fig. 5 Paleobiogeographic map of the Early Cretaceous showing the climatic zones (modified after Chinnappa and Rajanikanth 2016)
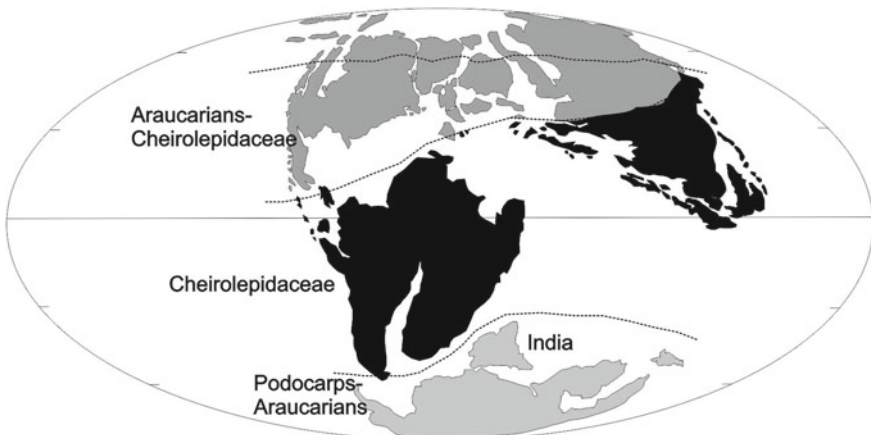
Fig. 6 Paleobiogeographic map of the Early Cretaceous showing the vegetation provincialism (modified after Chinnappa and Rajanikanth 2016) (top grey: Araucarian-Cheirolepidaeace Province; middle black: Cheirolepidaeace Province; bottom grey: Podocarps-Araucarian Province

Neocomian-Aptian, the *Cyclusphaera–Classopollis* subprovince extended in Africa and southern South America, and the *Murosporaflorida* subprovince of Australia and India (Herngreen et al. 1996). They are characterized by great abundance and diversity of bryophytes, lycophytes and pteridophytes (BLT) together with gymnospermous podocarpacean and cheirolepidiacean and various types from araucariacean and monosulcate pollen of Cycadophyta. Instead, trisaccate pollen grains are variably present across the province in the *M. florida* subprovince in which species of *Murospora* are present and *Cyclusphaera* are absent, whereas the inverse occurs in the other subprovince. In this sense, Cantrill and Poole (2012) indicated that within these two provinces, the microflora exhibits important regional variations like the abundance of *Microcachrydites antarcticus* typically up to 25% of the palynoassemblages in Australia whereas it is less than 10% in Antarctica.

McLoughlin (2001) outlined four floristic subprovinces or regions of endemism within southern Gondwana, supported by macro- and micro-fossil data. These included southeastern Australia-New Zealand, northern Australia-India, southern South America–Antarctic Peninsula, and South Africa, which by this time had separated from the supercontinent. The Early Cretaceous vegetation of Australia was characterised by ferns and lycopods and by the Aptian ginkgophytes had become common, yet cheirolepidiacean conifers remained in low abundance (Dettmann 1994). In the northern Australia–India subprovince, palynofloras were more diverse relative to that further south, bearing Bennetitalean, ferns and more abundant Cheirolepidiacean conifers comparatively to the southeastern Australia–New Zealand subprovince, in which Araucariaceae predominated (Dettmann 1994).

Beyond the endemisms across Gondwana, the terrestrial connection of the western to easternmost parts of southern Gondwana during the early Cretaceous is corroborated based on the common occurrence of numerous gymnosperms and BLT plant fossils and palynomorphs of the Barremian-Aptian deposits from eastern India (Tables 9, 10 and 11; see Venkatachala and Rajanikanth 1988; Tiwari and Tripathi 1992; Tripathi 2008). Among them, *Ptilophyllum* and *Taeniopteris* and spores like *Aequitriradites spinulosus*, *Foraminisporis wonthaggiensis*, *F. assymetricus* and *Cooksonites variabilis* and pollen grains of *Callialasporites, Classopollis, Cycadopites, Podocarpidites* are documented in two regions which are distantly extreme such as southern Argentina (Volkheimer and Quattrocchio 1981; Quattrocchio et al. 2006; del Fueyo et al. 2007) and Australia (e.g. McLoughlin 2001; McLoughlin and Kear 2010; Cantrill and Poole 2012). On the other hand, Schrank (2010) documented palynoassemblages composed of dominant or abundant pollen produced by Cheirolepidiaceae (*Classopollis*) and Araucariaceae (*Araucariacites*) and trisaccate podocarpaceous pollen in Tanzania. Although, the absence of *Murospora* and *Cyclusphaera* proves the existence of local differences despite the proximity of this region with eastern India, in which the trisaccate pollen is absent or quite rare (e.g. Tiwari and Tripathi 1992; Tripathi 2008).

Sporadic records of angiospermic pollen from Upper Aptian and Albian strata are known from the eastern and southern parts of India and they are identified as angiospermid pollen aff. *Clavatipollenites* from the intertrappean beds of Rajmahal

Table 9 Comparative analysis of the common macroflora from southern Gondwana (*Data source* **Antarctica**—Cantrill 1992, 1995, 1996, 1997, 1998, 2000; Cantrill and Nichols 1996; Cantrill and Falcon-Lang 2001; Cantrill and Nagalingum 2005; **Australia**—Douglas 1969, 1973; Drinnan and Chambers 1986; McLoughlin et al. 1995, 2000, 2002; McLoughlin 1996; **South America**—Del Fueyo et al. 2007)

Continent name	India	South America	Antarctica	Australia
Plant Taxa				
Pteridophytes				
Cladophlebis denticulata	+		+	
Coniopteris indica	+			+
Phyllopteroides laevis	+			+
Sphenopteeris patagonica	+	+		
Todites williamsoni	+	+		
Gymnosperms				
Carnoconites cranwellii	+		+	+
Dicyozamites falcatus	+		+	
Pachypteris indica	+		+	+
Ptilophyllum acutifolium	+	+		+
P. angustus	+	+		
P. antarcticum	+	+		
P. cutchense	+			+
P. gladiatum	+			+
P. tenerrimum	+			+
Taeniopteris daintreei	+		+	+
T. spatulata	+			+
Elatocladus confertus	+		+	
E. plana	+			+
Wnged seed	+			+

Basin (Tiwari and Tripathi 1992). This is congruent with the presence of mono-cotiledonean plant fossils in the Aptian-Albian Raghavapuram Formation (Chinnappa 2016). In southern Argentina, oldest pollen of angiosperms *Asteropollis* sp., *Clavatipollenites hughesii* Couper, *Retimonocolpites* sp. and *Tricolpites* sp. is known from Hauterivian–Barremian (Archangelsky and Archangelsky 2002, 2004; Quattrocchio et al. 2006). This suggests the global development of the angiosperms around the Neocomian, and in the Aptian-Turonian their spread and diversification occurred in terrestrial landscapes (see McLoughlin 2001; Archangelsky et al. 2009; McLoughlin and Kear 2010; Cantrill and Poole 2012).

In marine environments, Neocomian dinoflagellate cysts in the Gollapalli Formation and foraminifers of *Hedbergella* and *Ticinella* and ammonoids of *Acanthohoplites* in eastern India reveals that marine routes of cool-water paleoenvironments

Table 10 Comparative analysis of the common microflora from southern Gondwana (*Data source* **Antarctica**—Dettmann and Thomson 1987; Keating et al. 1992; Torres et al. 1997; Hathway et al. 1999; Hathway and Riding 2001; **Australia**—Kemp 1976; Backhouse 1978, 1988; Burgur 1976, 1980; Dettmann et al. 1992; Sajjadi and Playford 2002a, b; **South America**—Del Fueyo et al. 2007; **Africa**—Schrank 2010)

Continent name	India	South America	Africa	Antarctica	Australia
Plant Taxa					
Bryophytes					
Aequitriradites spinulosus	+	+			+
A. verrucosus	+	+			+
Cooksonites variabilis	+				+
Foraminisporis assymetricus	+	+			+
F. dailyi	+	+		+	+
F. variomatus	+	+			
F. wonthaggiensis	+	+			+
Staplinisporites caminus	+	+			
Triporoletes laevigatus	+				+
T. radiatus	+				+
Triporoletes reticulatus	+	+		+	
Pteridophytes					
Appendicisporites erdtmanii	+	+			
Baculatisporites comaumensis	+	+		+	+
Biretisporites potoniae	+	+	+		
B. spectabilis	+		+		+
Ceratosporites equalis	+	+		+	+
Cicatricosisporites australiensis	+	+		+	+
C. hughesi	+	+	+	+	+
C. ludbrookiae	+	+		+	+
C. pseudotripartitus	+				+
Concavissimisporites penolaensis	+	+			+
C. potoniei			+		
C. punctatus	+	+	+		
C. subverrucosus	+				
C. variverrucatus	+	+			
Contignisporites cooksoniae	+	+		+	+

<div align="right">(continued)</div>

Table 10 (continued)

Continent name	India	South America	Africa	Antarctica	Australia
C. fornicatus	+	+		+	+
C. glebulentus	+	+			+
C. multimuratus	+			+	+
Crybelosporites punctatus	+	+			+
C. striatus	+	+		+	+
C. stylosus	+	+		+	+
Cyathidites asper	+	+		+	
C. australis	+	+	+	+	+
C. concavus	+				+
C. minor	+	+		+	+
C. punctatus	+	+			+
Deltoidosporites juncta	+	+			
Densoisporites microregulatus	+		+		
D. velatus	+		+	+	
Dictyophyllidites crenatus	+	+			+
Dictyotosporites complex	+	+			+
Gleichinidites circinidites	+	+		+	+
G. senonicus	+	+		+	+
Ischyosporites crateris	+				+
I. punctatus	+			+	+
Klukisporites scaberis	+	+		+	+
Leptolepidites major	+	+	+		+
L. verrucatus	+	+	+	+	+
Lycopodiacidites asperatus	+	+			+
Lycopodiumsporites austroclavidites	+				+
L. circolumens	+				+
L. eminulus	+				+
L. trambauensis	+				+
Matonisporits cooksonii	+	+		+	+
M. dubius	+				+
Nepraisticka limbata	+				+
N. neozealandica	+				+

(continued)

Table 10 (continued)

Continent name	India	South America	Africa	Antarctica	Australia
N. truncatus	+	+	+	+	+
Ornamentifera echinata	+	+			
O. granulosa	+				+
Osmundacidites singhii	+				+
O. wellmanii	+	+	+		+
Pilosisporites parvispinosus	+				+
Polycingulatisporites reduncus	+		+		+
Retitriletes austroclavatidites	+	+		+	
R. circolumenus	+				+
Ruffordiaspora australiensis	+	+	+		
Sestrosporites pseudoalveolatus	+	+		+	+
Staplinisporites caminus	+		+	+	
Steriosporites antiquasporites	+			+	+
S. bimmatus	+				+
Todisporites minor	+	+	+		
Triletes tuberculiformis	+	+		+	+
Verrucosisporites rotundus	+				+
Gymnosperms					
Alisporites grandis	+	+	+	+	
Andreisporites mariae	+				+
Araucariacites australis	+		+	+	
A. indicus	+				+
Callialasporites dampieri	+	+	+	+	
C. discoidalis	+				
C. doeringii	+				+
C. segmentatus	+	+	+		
C. triletus	+		+		+
C. trilobatus	+	+	+	+	
Classoidites glanris	+				+

(continued)

Table 10 (continued)

Continent name	India	South America	Africa	Antarctica	Australia
Classopollis chateaunovii	+	+		+	
C. classoides	+	+			
Classopollis indicus	+				+
C. simplex	+	+			
C. torosus	+	+	+		
Cycadopites gracilis	+				+
C. nitidus	+			+	
Cyclusphaera radiata	+			+	
Dacrycarpites australiensis	+		+	+	
Ephedripites multicostatus	+				+
Microcachryidites antarcticus	+	+		+	+
Monosulcites ellipticus	+				+
Phyllocladidites inchoatus	+				+
Podocarpidites ellipticus	+	+	+	+	+
P. grandis	+				+
P. multesimus	+	+	+		+
Podosporites raoi	+				+
Vitreisporites pallidus	+	+		+	+
Angiosperms					
Asteropollis asteroides	+	+		+	+
Clavatipollenites hughesii	+	+		+	
Cupuliferoidaepollenites parvulus	+	+			
Myrtaceidites eugeniioides	+			+	
Retimonocol[pites peroreticulatus	+				+
Rousea georgensis	+			+	+
Tricolpites gillii	+			+	
T. variabilis	+				+

were established approximately following the margins of the continents of southern South Argentina, Antarctica, South Africa, Arabian Plate and Australia (Krishna 1988) across the Barremian-Aptian/Albian interval (e.g. Musacchio 1981; Krishna 1988; Bulot 2007; Al-Husseini 2013). Ichthyosaur and diverse shark assemblages documented in lower Cenomanian glauconitic mudstones of the Karai Formation (Banerjee et al. 2016; Bansal et al. 2019) in Cauvery Basin (Underwood et al.

Table 11 Correlation of the Early Cretaceous lithounits of east coast sedimentary basins of India based on the present study

Era	Age		Spore-pollen zones of Morgan et al. (2002)		Cauvery Basin	Palar Basin	KG Basin	PG Basin	Mahanadi Basin
Early Cretaceous	Albian		*Phimopollenites pannosus*						
			Coptospora paradoxa	upper					
				lower					
			Crybelosporites striatus				Raghavapuram/ Vemavaram Fm.		
	Aptian		*Pilosisporites notensis*	upper	Terani Fm.			Gangapur/ Chikiala Fm.	Athgarh Fm.
				lower					
	Barremian		*Foraminisporis wontheggiensis*	upper	Kovandan-kurichchi Fm	Sripernumbudur Fm.	Golapalli/ Budavada Fm.		
	Neocomian	Hauterivian		lower					
		Valanginian	*Ruffordiaspora australiensis*						
		Berriasian							

2011), together with previous scarce records known from the late Albian are considered endemic fauna known from high paleolatitudes elsewhere. They are absent in Tethyan areas and indicates a cool-water paleoenvironment for the marine vertebrate assemblage.

Therefore, it seems that the marine corridors in Gondwana were not barriers that have affected the paleobiogeographic distribution of the floras during the Barremian-Aptian (Table 11). Although more punctual barriers could have influenced local paleoenvironments and biotas, the latitudinal control on climate was a more important factor delineating the paleofloristic realms (Herngreen et al. 1996; McLoughlin 2001; Hay and Floegel 2012).

7 Conclusions

Early Cretaceous floras have been the subject of intensive study, preliminarily from the viewpoint of taxonomic descriptions and revisions. Subsequent works dealt with assigning ages to those assemblages. This work attempts to provide reasonably precise ages based on the integration of macrofloral and palynological data with faunal data. Marine fauna (ammonoids, foraminifers) have been well documented from the Mesozoic sequences of India and offer a better resolution of age constraints. Dinoflagellate records have also been used wherever available. Based on this integrated correlation, a higher time resolution could be established to the Early Cretaceous formations of the east coast sedimentary basins. An Aptian-Albian

age is assigned to the Terani Formation; Hauterivian-Aptian age to the Sriperumbudur Formation; Hauterivian-Barremian age to the Gollapalli and Budavada formation; Aptian-early Albian age to the Raghavarpuram and Vemavaram formations; Barremian-Aptian age to the Gangapur/Chikiala Formation and Aptian age to the Athgarh Formation. The Kovandankuruchi and Budavada formations are devoid of any botanical entities but have been dated on the basis of marine fauna as Barremian based on the occurrence of foraminifer-*Globigerina boteriveca* and Hauterivian-Barremian based on ammonoids such as *Pascocites budavadensis*, *Gymnoplites simplex* respectively.

Palaeobiogeographic studies indicate latitudinal control on climate was a more important factor delineating the paleofloristic realms. The study shows terrestrial connections between the western to easternmost parts of southern Gondwana during the early Cretaceous based on numerous gymnosperms and BLT plant fossils and palynomorphs of the Barremian-Aptian deposits from eastern India that are shared with the two subprovinces of the Trisaccates Province. Development of the angiosperms took place around the Neocomian and their diversification around Aptian-Turonian. East India records sporadic angiospermic pollen aff. *Clavatipollenites* from the Upper Aptian and Albian intertrappean beds of Rajmahal Basin, and monocotiledonous plant fossils from the Aptian-Albian Raghavapuram Formation.

Marine routes along the margins of the continents of southern South Argentina, Antarctica, South Africa, Arabian Plate, India and Australia across the Barremian–Aptian/Albian interval is envisaged by the presence of dinoflagellate cysts, foraminifers and ammonoids.

References

Adyalkar PG, Rao CN (1963) Some new plant fossils from the Athagarh Stage, Upper Gondwanas, Orrisa. Rec Geol Surv India 92:319–322
Agarwal PK, Pandey OP (1999) Was there an intracontinental rift between India and Sri Lanka? J Geol Soc India 54:237–249
Al-Husseini M (2013) Antarctica's glacio-eustatic signature in the Aptian and late Miocene–Holocene: implications for what drives sequence stratigraphy. GeoArabia 18:17–52
Archangelsky S, Archangelsky A (2002) Palinología estadística en el Cretácico de la Cuenca Austral, Plataforma Continental Argentina. I. Seis perforaciones del área de Magallanes. Revista del Museo Argentino de Ciencias Naturales, Nueva Serie 4:25–34
Archangelsky S, Archangelsky A (2004) Cretácico estadística en el Cretácico de la Cuenca Austral, Plataforma Continental Argentina. I. Seis perforaciones del a´rea de Magallanes. III. Discusiones y conclusiones. Revista del Museo Argentino de Ciencias Naturales, Nueva Serie 6:245–255

Archangelsky S, Barreda V, Passalia MG, Gandolfo M, Prámparo M, Romero E, Cúneo R, Zamuner A, Iglesias A, Llorens M, Puebla GG, Quattrocchio M, Volkheimer W (2009) Early angiosperm diversification: evidence from southern South America. Cret Res 30:1073–1082

Arkel WJ, Kummel B, Wright CW (1957) Mesozoic Ammonoidea. In: Arkel WJ, Furnish WM, Kummel B, Miller AK, Moore RC, Schindewolf OH, Sylvester-Bradley PC, Wright CW (eds) Treatise on invertebrate paleontology, Part L, Mollusca 4: Cephalopda, Ammonoidea. Geol Soc America and the University of Kansas Press, Lawrence, pp 80–436

Ayyasami K, Gururaja MN (1977) Plant fossils from East Coast Gondwana beds of Tamil Nadu with note on their age. J Geol Soc India 18:398–400

Backhouse J (1978) Palynological zonation of the Late Jurassic and early Cretaceous palynology of the Yerragadee Perth Basin, Western Australia. Geol Surv West Australia Bull 7:1–53

Backhouse J (1988) Late Jurassic and early Cretaceous palynology of the Perth Basin, Western Australia. Geol Surv West Australia Bull 135:1–128

Baksi AK, Barman TR, Paul DK, Ferar E (1987) Widespread early Cretaceous flood basal volcanism in eastern India: geochemical data from the Rajmahal-Bengal-Sylhet traps. Chem Geol 63:133–141

Baksi SK (1966) On the foraminifera from Raghavapuram mudstone, west Godavari district, Andhra Pradesh. Bull Geol Min Met Soc India 37:1–19

Baksi SK (1967) On new occurrence of *Gingoites feistmantelii* Bose & Sukh Dev (1958) from the coastal Gondwana of South India. Curr Sci 36:580

Baksi SK (1968) Fossil plants from Raghavapuram Mudstone, West Godavari District, A.P. Palaeobotanaist 16:206–215

Ball V (1877) On the Athgarh Sandstones near Cuttack. Rec Geol Surv India 10:63–68

Banerji RK (1982) Sivaganga Formation, its sedimentology and sedimentation history. J Geol Soc India 23:450–457

Banerjee S, Bansal U, Pande K, Meena SS (2016) Compositional variability of glauconites within the Upper Cretaceous Karai Shale Formation, Cauvery Basin, India: implications for evaluation of stratigraphic condensation. Sediment Geol 331:12–29

Bansal U, Pande K, Banerjee S, Nagendra R, Jagadeesan KC (2019) The timing of oceanic anoxic events in the Cretaceous succession of Cauvery Basin: constraints from 40Ar/39Ar ages of glauconite in the Karai Shale Formation. Geol J 54:308–315

Basavaraju MH, Jaiprakash BC, Chidambaram L, Ayyadurai M (2016) Biostratigraphy and depositional environments of subsurface sediments in Well Arani-A, Palar Basin. J Geol Soc India 88:407–420

Bastia R, Radhakrishna M (2012) basin evolution and petroleum prospectivity of the continental margins of India. Elsevier, Amsterdam

Bhalla SN (1969) Foraminifera from the type Raghavapuram Shale, east Coast Gondwanas, India. Micropalaentol 15:61–84

Biswas SK (2003) Regional tectonic framework of the Pranhita-Godavari Basin, India. J Asian Earth Sci 21:543–551

Biswas SK, Bhasin AL, Jokhan R (1993) Classification of Indian sedimentary basins in the framework of plate tectonics. In: Biswas SK, Alak D, Garg P, Pandey J, Maithani A, Thomas NJ (eds) Proceedings of the second seminar on petroliferous basins of India, vol 1. Indian Petroleum Publishers, Dehradun, pp 1–46

Blandford WT, Blandford HF, Theobald WM (1859) On the geological structure and relations of the Talcher coalfield in the district of Cuttack. Mem Geol Surv India 1:33–88

Bose MN, Jain KP (1967) Otozamites vemavaramensis sp. nov. from the Upper Gondwana of the East Coast of India. Palaeobotanist 15:14–315

Bose MN, Kutty TS, Maheshwari HK (1982) Plant fossils from Gangapur Formation. Palaeobotanist 30:121–142

Briggs JC (2003) The biogeographic and tectonic history of India. J Biogeogr 30:381–388

Bulot LG (2007) Endémisme et cosmopolitisme des faunes d'ammonites de la plaque arabique au Crétacé moyen (Aptien - Turonien). In: Bulot LG, Ferry S, Grosheny D (eds) Relations entre les

marges septentrionale et méridionale de la Téthys au Crétacé [Relations between the northern and southern margins of the Tethys ocean during the Cretaceous period]. Carnets de Géologie 02:49–55

Burgur D (1976) Some early Cretaceous plant microfossils from Queensland. Bureau Min Res Geol Geoph Bull 160:1–23

Burgur D (1980) Palynological studies in the lower Cretaceous of Surat Basin, Australia. Bureau Min Res Geol Geoph Bull 189:1–106

Cantrill DJ (1992) Araucarian foliage from the Lower Cretaceous of southern Victoria, Australia. Int J Plant Sci 153:622–645

Cantrill DJ (1995) The occurrence of the fern Hausmannia Dunker (Dipteridaceae) in the Cretaceous of Alexander Island, Antarctica. Alcheringa 19:243–254

Cantrill DJ (1996) Fern thickets from the Cretaceous of Alexander Island, Antarctica containing Alamatus bifarius Douglas and Aculea acicularis sp. nov. Cret Res 17:169–182

Cantrill DJ (1997) Hepatophytes from the Early Cretaceous of Alexander Island, Antarctica: systematics and paleoecology. Int J Plant Sci 158:476–488

Cantrill DJ (1998) Early Cretaceous fern foliage from President Head, Snow Island, Antarctica. Alcheringa 22:241–258

Cantrill DJ (2000) A Cretaceous (Aptian) flora from President Head, Snow Island, Antarctica. Palaeontographica Abt B 253:153–191

Cantrill DJ, Webb JA (1987) A reappraisal of *Phyllopteroides* Medwell (Osmundaceae) and its stratigraphic significance in the Lower Cretaceous of eastern Australia. Alcheringa 11:59–85

Cantrill DJ, Nichols GJ (1996) Taxonomy and palaeoecology of Early Cretaceous (late Albian) angiosperm leaves from Alexander Island, Antarctica. Rev Palaeobot Palynol 92:1–28

Cantrill DJ, Falcon-Lang HJ (2001) Cretaceous (late Albian) coniferales of Alexander Island, Antarctica. 2. Leaves, reproductive structures and roots. Rev Palaeobot Palynol 115:119–145

Cantrill DJ, Nagalingum NS (2005) Ferns from the Cretaceous of Alexander Island, Antarctica: implications for Cretaceous phytogeography of the Southern Hemisphere. Rev Palaeobot Palynol 137:83–103

Cantrill DJ, Poole I (2012) The origin of southern temperate ecosystems. In: Cantrill DJ, Poole I (eds) The vegetation of Antarctica through geological time. Cambridge University Press, pp 249–307

Casshyap SM, Tewari RC, Srivastava VK (1993) Origin and evolution of intracratonic Gondwana basins and their depositional limits in relation to Narmada-Son lineament. In: Casshyap SM, Valdiya KS, Khain VE, Milanovsky EE, Raza M (eds) Rifted Basins and Aulacogens. Gyanodaya Prakashan, Nainital, pp 183–200

Chaudhuri AK, Deb GK, Patranabis-Deb S, Sarkar S (2012) Paleogeographic and tectonic evolution of the Pranhita-Godavari Valley, Central India: a stratigraphic perspective. American J Sci 312:766–815

Chinnappa Ch (2016) Contribution to plant ecosystem of early Cretaceous sequences of east coast, India—floral diversification and ecological implications. PhD thesis, Andhra University, Visakhapatnam

Chinnappa Ch, Rajanikanth A (2018) Floristics and plaeoecological implications of the early Cretaceous sequences of Krishna-Godavari basin, east coast of India. Geobiodiversita 40:259–281

Chinnappa Ch, Rajanikanth A, Rao YV (2014) Floral diversity and implications in palaeoenvironment of Vemavaram Formation (Krishna Depression), Krishna-Godavari Basin, Andhra Pradesh, India. Palaeobotanist 63:63–78

Chinnappa Ch, Rajanikanth A, Rao YV (2015) Early Cretaceous plant diversity and ecology in the Krishna-Godavari Basin, East Coast. J Palaeontol Soc India 60:73–96

Chinnappa Ch, Rajanikanth A (2016) An integrated enquiry into the early Cretaceous floristics of the Pranhita Godavri Basin and ecological considerations. Acta Palaeobotanica 57:13–32

Coffin MF, Pringle MS, Duncan RA, Gladczenko TP, Storey RD, Müller RD, Gahagan LA (2002) Kerguelen hotspot magma output since 130 Ma. J Petrol 43:1121–1140

Cox KG (1992) Karoo igneous activity and the early stages of the breakup of Gondwanaland. Geol Soc London Spec Publ 68:137–148

Crame JA, Kelly RA (1995) Composition and distribution of the inoceramid bivalve genus Anopaea. Palaeontol 38:87–103

Del Fueyo GM, Villar de Seoane L, Archangelsky A, Guler V, Llorens M, Archangelsky S, Gamerro JC, Musacchio EA, Passalia MG, Barreda VD (2007) Biodiversidad de las Paleofloras de Patagonia Austral durante el Cretácico Inferior. Asociación Paleontológica Argentina. Publicación Especial 11, Ameghiniana 101–122

Dettmann ME (1994) Cretaceous vegetation: the microfossil record. In: Hill RS (ed) History of the Australian Vegetation. Cambridge University Press, Cambridge, pp 143–170

Dettmann ME, Thomson MRA (1987) Cretaceous palynomorphs from the James Ross Island area, Antarctica—a pilot study. British Antarctic Surv Bull 77:13–59

Dettmann ME, Molnar RE, Douglas JG, Burger D, Fielding C, Clifford HT, Francis J, Jell P, Rich T, Wade M, Rich PV, Pledge N, Kemp A, Rozefelds A (1992) Australian Cretaceous terrestrial faunas and floras: biostratigraphic and biogeographic implications. Cret Res 13:207–262

Douglas JG (1969) The Mesozoic floras of Victoria, Parts 1 and 2. Mem Geol Surv Victoria 28:1–310

Douglas JG (1973) The Mesozoic Floras of Victoria: Part 3. Geol Surv Victoria Mem 29:1–185

Drinnan AN, Chambers TC (1986) Flora of the lower cretaceous Koonwarra fossil beds (Korumburra Group), South Gippsland, Victoria. Australasian Ass Palaeontol Mem 3:1–77

Encarnacion J, Flemming TH, Elliot DH, Eales HV (1996) Synchronous emplacement of Ferrer and Karoo dolerites and the early break up of Gondwana. Geology 24:535–538

Feistmantel O (1877a) Jurassic (Liassic) flora of the Rajmahal group from Golapalli (near Ellore), south Godavari district. Mem Geol Surv India, Palaeontol Indica Ser 2:63–190

Feistmantel O (1877b) Notes on fossil floras in India–IX. On some fossil plants from the Athgarh sandstones. Rec Geol Surv India 10:68–70

Feistmantel O (1877c) Notes on fossil floras in India. Rec Geol Surv India 10:73–74

Feistmantel O (1879) The fossil flora of Upper Gondwanas, Outliers on the Madras Coast. Mem Geol Surv India, Palaeontol Indica Ser 2:191–224

Fitzgerald P (2002) Tectonics and landscape evolution of the Antarctic plate since the break up of Gondwana, with an emphasis on the West Antarctic rift system and the transantarctic mountains. Royal Soc New Zealand Bull 35:453–469

Friis EM, Crane PR, Pedersen KR (2011) Early Flowers and Angiosperm Evolution. Cambridge University Press

Foote RB (1879) On the geological structure of the Eastern coast from latitude 150 Northward to Masulipatam. Mem Geol Surv India 16, Pt 1

Gopal V, Jacob C, Jacob K (1957) Stratigraphy and palaeontology of the Upper Gondwana of the Ramnad District on the East Coast. Rec Geol Surv India 84:477–496

Goswami S, Singh KJ, Chandra S (2006) Palaeobotany of Gondwana basins of Orissa State, India: A bird's eye view. J Asian Earth Sci 28:218–233

Goswami S, Meena K, Das M, Guru BC (2008) Upper Gondwana Palynoflora of Mahanadi Master Basin, Orissa, India. Acta Palaeobotanica 48:171–181

Govindan A, Ravindran CN, Rangaraju MK (1996) Cretaceous stratigraphy and planktonic foraminiferal zonation of Cauvery Basin, South India. Mem Geol Soc India 37:155–187

Govindan A, Yadagiri K, Ravindran CN, Kalyanasundar R (1998) A field guide on Cretaceous sequences of Tiruchirappalli Area, Cauvery Basin, India. ONGC, Chennai, pp 1–53

Gradstein FM, James G, Ogg JG, Hilgen FJ (2012) On the geologic time scale. Newslett Strat 45:171–188

Hathway B, Riding JB (2001) Stratigraphy and age of the Lower Cretaceous Pedersen Formation, northern Antarctica Peninsula. Antarctic Sci 13:67–74

Hathway B, Duane AM, Cantrill DJ, Kelley SP (1999) 40AR/39Ar geochronology and palynology of the Cerro Negro Formation, South Shetland Islands, Antarctica: a new radiometric tie for Cretaceous terrestrial biostratigraphy in the Southern Hemisphere. Australian J Earth Sci 46:593–606

Hay WW, Floegel S (2012) New thoughts about the Cretaceous climate and oceans. Earth-Sci Rev 115:262–272

Helby R, Morgan R, Patridge AD (1987) A palynological zonation of the Australian Mesozoic. Mem Ass Australasian Palaeontol 4:1–94

Herngreen GFW, Kedves M, Rovnina LV, Smirnova SB (1996) Chapter 29C. Cretaceous palynofloral provinces: a review. In: Jansonius J, McGregor DC (eds) Palynology: principles and applications. Am Ass Strat Palynol Found 3:1157–1188

Jain KP (1968) Some plant remains from the Upper Gondwana of East Coast, India. Palaeobotanist 16:151–154

Jeyasingh DEP, Kumarasamy D (1994a) Occurrence of Pityospermum Nathorst in the Sriperumbudur Formation, Tamil Nadu. Curr Sci 67:305

Jeyasingh DEP, Kumarasamy D (1994b) Araucarioxylon from the Sriperumbudur Formation, Upper Gondwana, Tamil Nadu, India. Geophytol 24:43–48

Jeyasingh DEP, Kumarasamy D (1995) An unusual pycnoxylic wood from a new Upper Gondwana locality in Tamil Nadu, India. Rev Palaeobot Palynol 74:163–192

Jeyasingh DEP, Sudhersan C (1985) Fertile pinnules of Marattiopsis Schimper from the Sivaganga beds of Ramanathapuram District, Tamil Nadu. Curr Sci 54:197–199

Kar RK, Sah SCD (1970) Palynological investigation of the Gondwana outcrop from Vemavaram with remarks on the age of the beds. Palaeobotanist 18:103–117

Katz MB (1978) Sri Lanka in Gondwanaland and the evolution of the Indian Ocean. Geol Mag 115:237–244

Keating JM, Spencer-Jones M, Newham S (1992) The stratigraphical paalynology of the Kotick point and Whisky Bay formations, Gustav Group (Cretaceous), James Rose Island. Antarctic Sci 4:279–292

Kemp EM (1976) Palynological observations in the Officer Basin, Western Australia. Min Res Geol Geophys Bull 160:23–68

Khan AM, Srivastava SK (2006) The paleogeographic significance of *Aquilapollenites* occurrences in Pakistan. J Earth Sys Sci 28:251–258

King W (1880) Upper Gondwana and other formations of the Godavari district. Mem Geol Surv India 16:195–252

Krishna J (1988) Biological evidence for better appreciation of Indian Gondwana. Palaeobotanist 36:268–284

Kumar S, Bhandari LL (1973) Palaeocurrent analysis of the Athgarh Sandstone (Upper Gondwana), Cuttack District, Orissa. Sediment Geol 10:61–75

Kutty TS (1969) Some contributions to the stratigraphy of the Upper Gondwana Formations of the Pranhita-Godavari Valley, Central India. J Geol Soc India 10:33–48

Lakshminarayana G (1996) Stratigraphy and structural framework of the Gondwana sediments in the Pranhita-Godavari Valley, Andhra Pradesh. Gondwana Nine, Geol Surv India, pp 311–330

Lal NK, Siawal A, Kaul AK (2009) Evolution of east coast of India—a plate tectonic reconstruction. J Geol Soc India 73:249–260

Lawver LA, Scotese CR (1987) A revised reconstruction of Gondwanaland. In: Mckenzie D (ed) Gondwana six: structure, tectonics and geophysics. Geophys Monograph 40:17–23

Mahabale TS, Satyanarayana T (1979) Upper Gondwana plant fossils from East Godavari District in Andhra Pradesh, India. Geophytol 9:65–82

Maheshwari HK (1986) Thinnfeldia indica Feistmantel and associated plant fossils from Tiruchirapalli District, Tamil Nadu. Palaeobotanist 35:13–21

Mamgain VD, Sastry MVA, Subbaraman JV (1973) Report of ammonites from Gondwana plant beds at Terani, Tiruchirapalli District, Tamil Nadu. J Geol Soc India 14:198–200

Manik SR, Srivastava SC (1991) Conifer woods from new sites of Gangapur Formation, India. Acta Biologica Szeged 37:45–55

McLoughlin S (1996) Early Cretaceous macrofloras of Western Australia. Rec Western Australian Mus 18:19–65

McLoughlin S (2001) The breakup history of Gondwana and its impact on pre-Cenozoic floristic provincialism. Aust J Botany 49:271–300

McLoughlin S, Kear BP (2010) The Australasian Cretaceous scene. Alcheringa 34:197–203

McLoughlin S, Drinnan AN, Rozefelds AC (1995) The Cenomanian flora of the Winton Formation, Eromanga Basin, Queensland. Mem Queensland Museum 38:273–313

McLoughlin S, Tosolini AM, Drinnan AN (2000) Revision of an Early Cretaceous macroflora from the Maryborough Formation, Maryborough Basin, Queensland, Australia. Mem Queensland Museum 42:483–503

McLoughlin S, Tosolini AM, Nagalingum NS, Drinnan AN (2002) The Early Cretaceous (Neocomian) flora and fauna of the lower Strzelecki Group, Gippsland Basin, Victoria, Australia. Mem Australasian Ass Paleontol 26:1–144

Mehrotra NC, Shanmukhappa M, Babu R, Kumar M, Alpana Singh, Singh BD, Kapoor PN (2012) Development of palynology in fossil fuel exploration in India with emphasis on recent significant contribution from Western-Offshore, Krishna-Godavari Basin and Frontier areas. Proc Indian Nat Sci Acad 78:457–473

Mehrotra NC, Venkatachala BS, Kapoor PN (2010) Palynology in hydrocarbon Exploration: high Impact Palynological studies in western Offshore and Krishna-Godavari basins. J Geol Soc India 75:364–379

Metcalfe I (2001) Warm Tethys and cold Gondwana: East and SE Asia in Greater Gondwana during the Phanerozoic. In: Weiss RH (ed) Contributions to geology and palaeontology of Gondwana. In honour of Helmut Wopfner Kölner Forum Für Geologie und Paläontologie, pp 333–348

Mitra ND (1994) Tensile resurgence along fossil sutures: a hypothesis on the evolution of Gondwana Basins of Peninsular India. In: Proceedings of the second symposium on petroliferous basins of India, KDM Institute of Petroleum Exploration, Oil and Natural Gas Commission, Dehradun, pp 55–62

Morgan R, Rowett AI, White MR (2002) Biostratigraphy. The Petroleum Geology of South Australia, Volume 5 Great Australian Bight

Muralidhar Rao G, Ramakrishna H (1988) Torreyites sitholeyi, a new record from the Gangapur Formation of Andhra Pradesh. Curr Sci 57:203–204

Murthy NGK, Sastri VV (1961) Foraminifera from the Sriperumbudur beds near Madras. Indian Min 14:214–215

Musacchio E (1981) South American Jurassic and Cretaceous foraminifera, ostracoda and charophyta of Andean and Sub-andean regions. In: Volkheimer W, Musacchio EA (eds) Cuencas Sedimentarias del Jurásico y Cretácico de América del Sur. Buenos Aires, pp 461–49

Nagendra R, Reddy AN, Jaiprakash BC, Gilbert H, Zakharov YD, Venkateshwarlu M (2019) Integrated Cretaceous stratigraphy of the Cauvery Basin, South India. Stratigraphy 15:245–259

Pal AK, Datta M, Basu PK, Shome S, Ghosh SC (1988) Cone bearing shoots of Elatocladus Halle from Gangapur Formation (Lower Cretaceous) of Andhra Pradesh, India. Curr Sci 57:141–142

Pandya KL, Patra BP (1968) A note on the occurrence of some Ptilophyllum species at Jagannath Prasad, Puri District, Orissa. Prakruti, Utkal University. J Sci 5:31–33

Pandya N, Srivastava VB, Sukh-Dev (1990) A new conifer fossil from Vemavaram (early Cretaceous), Andhra Pradesh, India. Geophytol 20:74

Pandya N, Sukh-Dev (1990) Fossil flora of Gollapalli Formation. Palaeobotanist 38:147–154

Patra BP (1973a) Notes on some Upper Gondwana plants from the Athgarh Sandstones, District Cuttack, Orissa. Palaeobotanist 20:325–333

Patra BP (1973b) On the occurrence of Otozamites sp. in the Athagarh Sandstones at Naraj, District Cuttack, Orissa. Curr Sci 42:477–478

Patra BP (1980) Some ferns from the east coast Gondwana of Orissa with a note on its age. In: Proceedings of the 3rd Indian Geological Congress, Poona, pp 57–68

Patra BP (1982) Contribution to Jurassic–Cretaceous Palaeobotany of India. Unpublished PhD thesis, Utkal University

Patra BP (1989) Sagenopteris sp. a rare plant remains from the East Coast Upper Gondwana Athagarh Sandstone, Cuttack District, Orissa. J Geol Soc India 33:271–275

Patra BP (1990) Palaeofloristics of the Athagarh Sandstone, Orissa. In: Proceedings of seminar cum workshop. IGCP, 216, 245 Chandigarh, pp 64–67

Patra BP, Patnaik S (1974) Some Upper Gondwana plants from Athgarh Sandstone at Naraj, Cuttack District, Orissa. Publications of Centre of Advanced Studies in Geology, Punjab University, Chandigarh 10:25–30

Patra BP, Sahoo NK (1992) Plant megafossils from Athgarh Formation near Bouda, Cuttack District, Orissa. Geophytol 22:127–132

Patra BP, Sahoo NK (1995a) Some observations on the occurrence of Cycadophytes and Bennettitales in the East Coast Upper Gondwana Athagarh sandstone, Cuttack and Khurda Districts of Orrisa, India. Palaeobotanist 44:139–151

Patra BP, Sahoo NK (1995b) A reappraisal of geology and palaeobotany of the Athagarh Sandstone, Orrisa, India. Geophytol 25:17–26

Patra BP, Sahoo NK (1996) Megafloral Assemblage of the Athagarh Sandstone and its comparison with other East Coast Upper Gondwana floras of India. Gondwana Nine, Oxford and IBH Publishing Company Private Limited, New Delhi 1:109–122

Powell CM, Roots SR, Veevers JJ (1988) Pre-breakup continental extension in east Gondwanaland and the early opening of the eastern Indian Ocean. Tectonophys 155:261–283

Prabhakar M (1987) Palynology of the Upper Gondwana deposits of Rampur area, Pranhita-Godavari Basin, Andhra Pradesh, India. J Palaeontol Soc India 32:114–121

Prabhakar KN, Zutshi PL (1993) Evolution of southern part of Indian east coast basins. J Geol Soc India 41:215–230

Prasad B, Pundir BS (1995) Palynostratigraphy and source rock evaluation of Gondwana and Cretaceous sediments of Krishna-Godavari and Cauvery basins. Part-1. Palynological studies of exposed Gondwana and Cretaceous sediments of Krishna-Godavari. KDMIPE report (unpublished), pp 1–35

Prasad B, Pundir BS (1999) Biostratigraphy of the exposed Gondwana and Cretaceous rocks of Krishna-Godavari Basin, India. J Palaeontol Soc India 44:91–117

Quattrocchio ME, Martínez MA, Pavisich AC, Volkheimer W (2006) Early Cretaceous palynostratigraphy, palynofacies and palaeoenvironments of well sections in northeastern Tierra del Fuego, Argentina. Cret Res 27:584–602

Radhakrishna M, Srinivasa Rao G, Nayak S, Bastia R, Twinkle D (2012) Early Cretaceous fracture zones in the Bay of Bengal and their tectonic implications: constraints from multi-channel seismic reflection and potential field data. Tectonophys 522:187–197

Rajanikanth A (1996) Diversification and evolution of early Cretaceous east coast flora of India. Palaeobotanist 45:121–131

Rajanikanth A (2009) Status of coastal Gondwana—a floristic perspective. In: Jayappa KS, Narayana AC (eds) Coastal environments-problems and perspectives. IK International, New Delhi, pp 264–275

Rajanikanth A, Chinnappa Ch (2016) Early Cretaceous flora of India—a review. Palaeobotanist 65:209–245

Rajeshwar Rao PV, Ramanujam CGK (1979) The genus Contignisporites from the Lower Cretaceous, Gangapur beds of Adilabad District, A.P. Geophytol 9:139–143

Rajanikanth A, Venkatachala BS, Kumar A (2000) Geological age of the Ptilophyllum flora—a critical reassessment. In: Govindan A (ed) Cretaceous stratigraphy—an update. Mem Geol Soc India 46:245–266

Rajeshwar Rao PV, Ramanujam CGK, Verma YNR (1983) Palynology of the Gangapur beds, Pranhita-Godavari Basin, Andhra Pradesh. Geophytol 13:22–45

Raju DSN (2017) New evidences on age dating and paleoenvironments of Cretaceous sequences in the Krishna-Godavari basin (KGB), India. ONGC Bull 52:1–44

Raju DSN, Reddy AN (2016) Why there is substantial diachroneity in biostratigraphic dating of Cretaceous sediments in the KG and Cauvery basins-an appraisal. ONGC Bull 51:119–134

Ramakrishna H, Muralidhar Rao G (1986) Pterophyllum medlicottianum from the Gangapur Formation of Andhra Pradesh. Curr Sci 55:1199–1200

Ramakrishna H, Ramanujam CGK (1987) Palynoflora from Gangapur beds at Moar in Adilabad District, Andhra Pradesh. Indian J Earth Sci 14:64–72

Ramakrishna H, Muralidhar Rao G (1991) Conites sripermaturensis from the Gangapur Formation, A.P. J Swamy Botanical Club 8:113–114

Ramakrishna H, Ramanujam CGK, Prabhakar M (1985) Palynoassemblage of the Upper Gondwana deposits of Balhanpur area, Adilabad District, Andhra Pradesh. J Palynol 21:126–132

Ramana MV, Nair RR, Sarma KVLNS, Ramprasad T, Krishna KS, Maria D'cruz, Subramanyam C, Paul John, Subramanyam AS, Chandra Shekhar DV (1994) Mesozoic anomalies in the Bay of Bengal. Earth Planet Sci Lett 121:469–475

Ramanujam CGK (1957) Microfossils from carbonaceous shale near Vemavaram (Jurassic) in the east coast Gondwanas of India. J Indian Botan Soc 36:181–197

Ramanujam CGK, Rajeshwar Rao PV (1979) Palynological approach to the study of some Upper Gondwana clays at Ralpet near Asifabad in Adilabad District of Andhra Pradesh. Geol Surv India Misc Publ:45–60

Ramanujam CGK, Rajeshwar Rao PV (1980) Palynological evidence for the age of some Upper Gondwana deposits in Adilabad District of Andhra Pradesh. Proceedings of the IV International Palynological Conference, Lucknow, pp 386–391

Ramanujam CGK, Varma YNR (1977) Palynological evidence for the age of Sriprumbudur beds near Conjeevaram, Tamil Nadu. J Geol Soc India 18:429–435

Ramanujam CGK, Varma YNR (1981) Hilate spores from the upper Gondwana deposits of Palar basin, Tamil Nadu. Palaeobotanist 28(29):308–315

Ramanujam CGK, Muralidhar Rao G, Ramakrishna H (1987) Floristic and stratigraphic significance of the megafloral assemblage of Gangapur Formation in Andhra Pradesh. Gond Geol Mag 2:1–5

Ramasamy S, Banerji RK (1991) Geology, petrography and systematic stratigraphy of the pre-Ariyalur sequence in Tiruchirappalli district, Tamil Nadu, India. J Geol Soc India 37:577–594

Rangaraju MK, Aggarwal A, Prabhakar KN (1993) Tectonostratigraphy, structural styles, evolutionary model and hydrocarbon prospects of Cauvery and Palar Basins, India. In: Biswas SK, Dave A, Garg P, Pandey J, Maithani A, Thomas NJ (eds) Proceedings of the second seminar on petroliferous basins of India, Indian Petroleum Publishers, Dehradun, pp 371–388

Rao GN (2001) Sedimentation, stratigraphy and petroleum potential of Krishna-Godavari Basin, east coast of India. AAPG Bull 8:623–1643

Rao VR, Venkatachala BS (1971) Upper Gondwana marine intercalations in peninsular India. Annu Geol Department Aligarh Muslim Univ 5(6):353–389

Reddy AN, Jaiprakash BC, Rao MV, Chidambaram L, Bhaktavatsala KV (2013) Sequence stratigraphy of Late Cretaceous successions in the Ramnad Sub-basin, Cauvery Basin, India. Geol Soc India Spec Publ 1:78–97

Sahni B (1928) Revisions of Indian fossil plants Pt. 1 Coniferales (a. impressions & incrustations). Mem Geol Surv India. Palaeontologia Indica n. Ser 11:1–49

Sahni B (1931) Revision of Indian fossil plants: Parts II-Coniferales (b. Petrifications). Mem Geol Surv India. Palaeontologia Indica n. series 11:51–124

Sajjadi F, Playford G (2002a) Systematic and stratigraphic palynology of Late Jurassic-earliest Cretaceous strata of the Eromanga Basin, Queensland, Australia: Part one. Palaeontographica Abteilung B 261:1–97

Sajjadi F, Playford G (2002b) Systematic and stratigraphic palynology of Late Jurassic-earliest Cretaceous strata of the Eromanga Basin, Queensland, Australia: Part Two. Palaeontographica Abteilung B 261:99–165

Sastry MVA, Acharyya SK, Shah SC, Satsangi PP, Ghosh SC, Raha PK, Singh G, Ghosh RN (1977) Stratigraphic lexicon of Gondwana formations of India. Geol Surv India Misc Publ 36:1–99

Sastri VV, Chandra A, Pant SC (1963) Foraminifera from Raghavapuram shale near Tirupati, Andhra Pradesh, India. Rec Geol Surv India 92:311–314

Sastri VV, Venkatachala BS, Narayanan V (1981) The evolution of the East Coast of India. Palaeo Palaeo Palaeo 36:23–54

Shah SC, Singh G, Raha PK, Acharyya SK (1977) Description of Gondwana units- Sriperumbudur Formation. In: Sastry MVA, Acharyya SK, Shah SC, Satsangi PP, Ghosh SC, Raha PK, Singh G, Ghosh RN (eds) Stratigraphic lexicon of Gondwana formations of India, Geol Surv India Misc Publ 36:88–92

Schrank E (2010) Pollen and spores from the Tendaguru Beds, Upper Jurassic and Lower Cretaceous of southeast Tanzania: palynostratigraphical and paleoecological implications. Palynology 34:3–42

Seward AC, Sahni B (1920) Indian Gondwana plants: a revision. Mem Geol Surv India, Palaeontologia Indican Ser 7:1–41

Sharma KD, Jain AK, Venkatachala BS (1977) Palynology of the Early Cretaceous sediments from the subsurface of the Godavari-Krishna Basin, Andhra Pradesh, south India. In. Venkatachala BS, Sastri VV (eds) Proceedings of the IV Colloquim on Indian Micropalaeontology and Stratigraphy, pp 110–124

Singh G, Ghosh RN (1977a) Description of Gondwana units- Budavada Sandstone. In: Sastry MVA, Acharyya SK, Shah SC, Satsangi PP, Ghosh SC, Raha PK, Singh G, Ghosh RN (eds) Stratigraphic lexicon of Gondwana formations of India, Geol Surv India Misc Publ 36:27–28

Singh G, Ghosh RN (1977b) Description of Gondwana units-Raghavapuram Shale. In: Sastry MVA, Acharyya SK, Shah SC, Satsangi PP, Ghosh SC, Raha PK, Singh G, Ghosh RN (eds) Stratigraphic Lexicon of Gondwana Formations of India, Geol Surv India Misc Publ 36:75–76

Singh G, Ghosh RN (1977c) Description of Gondwana units-Vemavaram Shale. In: Sastry MVA, Acharyya SK, Shah SC, Satsangi PP, Ghosh SC, Raha PK, Singh G, Ghosh RN (eds) Stratigraphic lexicon of Gondwana formations of India. Geol Surv India Misc Publ 36:94–95

Smith AG, Hallam A (1970) The fit of southern continents. Nature 225:139–144

Spath LF (1933) Revision of the Jurassic Cephalopod fauna of Cutch (Kutch). Mem Geol Surv India, Palaeontologia Indica Series 9:1–945

Srivastava SK (1978) Cretaceous spore-pollen floras: a global evaluation. Biol Mem 3. Palaeopalynol Ser 5:1–130

Srivastava SK (1983) Cretaceous phytogeographic provinces and palaeogeography of the Indian plate based on palynological data. In: Maheshwari HK (ed) Cretaceous of India: Palaeoecology. Palaeogeography and time boundaries, Indian Ass Palynostratigraphers, Lucknow, pp 141–157

Sukh-Dev, Rajanikanth A (1988a) The Sivaganga formation: fossil flora and stratigraphy. Geophytol 18:186–205

Sukh-Dev, Rajanikanth A (1988b) The Gangapur: fossil flora and stratigraphy. Geophytol 18:1–27

Sundaram R, Rao PS (1986) Lithostratigraphy of Cretaceous and Paleocene rocks of Tiruchirappalli district, Tamil Nadu. Rec Geol Surv India 115:9–23

Sundaram R, Henderson RA, Ayyasami K, Stilwell JD (2001) A lithostratigraphic revision and paleoenvironmental assessment of the Cretaceous System exposed in the onshore Cauvery Basin, southern India. Cret Res 22:743–762

Suryanarayana K (1953) Mesebrioxylon tirumangalense, a new species from the Sripermatur Group near Madras. J Indian Bot Soc 32:159–164

Suryanarayana K (1954) Fossil plants from the Jurassic rocks of the Madras Coast, India. Palaeobotanist 3:87–90

Tewari A, Hart MB, Watkinson MP (1996) A revised lithostratigraphic classification of the Cretaceous rocks of the Trichinopoly District, Cauvery Basin, and Southeast India. Contributions XV Indian Colloquium of Micropaleontology and Stratigraphy, pp 789–800

Tiwari RS, Tripathi A (1992) Marker assemblage zones of spore and pollen species through Gondwana Palaeozoic-Mesozoic sequence in India. Palaeobotanist 40:194–236

Tiwari RS, Tripathi A, Dutt AB, Mukhopadhyay A (1987) Palynological dating of olive green shales underlying the Athgarh sandstone in Mahanadi Basin. Curr Sci 56:1150–1153

Torres T, Barale G, Meon H, Philippe M, Thevenard F (1997) Cretaceous floras from Snow Island (South Shetland Island, Antarctica) and their biostratigraphic significance. Geological Evolution and process, The Antarctic Region, pp 1023–1028

Tripathi A (2008) Palynochronology of Lower Cretaceous volcano-sedimentary succession of the Rajmahal Formation in the Rajmahal Basin, India. Cret Res 29:913–924

Underwood CJ, Goswami A, Prasad GVR, Verma O, Flynn JJ (2011) Marine vertebrates from the 'middle Cretaceous (early Cenomanian) of South India. J Vert Paleontol 31:539–552

Vagyani BA (1984) On the occurrence of Desmiophyllum indicum Sahni from Vemavaram. In: Proceedings of 5th Indian geophytological conference, Paleobotanical Society, Lucknow, pp 362

Vagyani BA (1985) Occurrence of Ginkgoites crassipes (Feistmental) Seward from the Jurassic of Andhra Pradesh. Curr Sci 54:705–706

Vagyani BA, Zutting MP (1986) Occurrence of Pterophyllum distans Morris from Uppugunduru, Andhra Pradesh. Geophytol 16:133

Vagyani BA, Jamane MR (1988) Genus Dictyozamites Oldham from Uppugunduru, Prakasam District, Andhra Pradesh. Geophytol 18:87

Varma YNR, Ramanujam CGK (1984) Palynology of some upper Gondwana deposits of Palar basin, Tamil Nadu, India. Palaeontographica B 190:37–86

Veevers JJ, Tewari RC (1995) Gondwana Master Basin of Peninsular India Between Tethys and the Gondwana Province of Pangea. GSA Mem 187:1–72

Venkatachala BS (1973) Palynological evidence on the age of Cuddalore Sandstone. Geophytol 3:145–149

Venkatachala BS (1974) Palynological zonation of the Mesozoic and Tertiary subsurface sediments in the Cauvery Basin. Asp Appr of Indian Palaeobot, pp 476–494

Venkatachala BS, Sharma KD (1974) Palynology of the Cretaceous sediments from the subsurface of Vridhachalam area, Cauvery Basin. Geophytol 4:153–183

Venkatachala BS, Rajanikanth A (1987) Stratigraphic implication of "late Gondwana" floras in the East Coast. Palaeobotanist 36:183–196

Venkatachala BS, Rajanikanth A (1988) Stratigraphic implication of "late Gondwana" floras in the East Coast. Palaeobotanist 36:183–196

Venkatachala BS, Sharma KD, Jain AK (1972) Palynological zonations of Jurassic-Lower Cretaceous sediments in the sub-surface of Cauvery Basin. In. Ghosh AK et al (eds) Proc Sem Palaeopalynol Indian Stratigr, Botany Department, Calcutta University, pp 172–188

Venkatachala BS, Sinha RN (1986) Stratigraphy, age and palaeoecology of Upper Gondwana equivalents of the Krishna-Godavari Basin, India. Palaeobotanist 35:22–31

Vijaya (1999) Palynological dating of the Neocomian–Aptian succession in the Indian Peninsula. Cret Res 20:597–608

Vijaya, Bhattacharji TK (2002) An Early Cretaceous age for the Rajmahal traps, Panagarh area, West Bengal: palynological evidence. Cret Res 23:789–805

Volkheimer W, Quattrocchio M (1981) Distribución estratigráfica de los palinomorfos jurásicos y cretácicos en la faja andina y áreas adyacentes de América del Sur austral con especial consideración de la Cuenca Neuquina. Comité Sudamericano del Jurásico y Cretácico: Cuencas sedimentarias del Jurásico y Cretácico de América del Sur, 2:407–444, Buenos Aires

Wignall PB (2001) Large igneous provinces and mass extinctions. Earth-Sci Rev 53:1–33

Yoshida M, Funaki M, Vitannage PW (1992) Proterozoic to Mesozoic East Gondwana: the juxtaposition of India, Sri Lanka and Antarctica. Tectonics 11:381–391

Facies and Microfacies Analysis of Kallankurichchi Formation, Ariyalur Group with an Inkling of Sequence Stratigraphy

Shilpa Srimani, Sunipa Mandal, and Subir Sarkar

Abstract The fossiliferous carbonate succession of late Cretaceous Kallankurichchi Formation rest over siliciclastic Sillakuddi Formation of the Ariyalur Group, Cauvery Basin. Detailed sedimentary facies analysis shows that the rock assemblage is broadly divisible in two associations, viz., (1) Wave-dominated and (2) Tide-dominated. A distinct 'thin muddy facies' (15 cm) is demarcated the boundary between these two associations. With a thin tidal deposit at its base, the wave dominated basinward facies association (transgressive system tract/TST) is overlain by the muddy facies, likely to be the maximum flooding surface (MFS). This surface is followed by shallowing upward succession (highstand systems tract/HST) dominated again by tidal features. Petrographic study shows that this part is replete with quartz flux strongly suggests progressive shift of paleogeography from basinward to shoreward part. The faunal distribution varies throughout the formation incorporates echinodermata, varieties of foraminifers, brachiopods, cephalopods and bivalves (*Gryphea* and *Inoceramus*).

Keywords Sedimentary facies analysis · Microfacies · Fossiliferous Kallankurichchi Formation · Wave and tide dominated association · Maximum flooding surface · TST and HST

1 Introduction

This paper addresses the carbonate succession in the late Cretaceous Kallankurichchi Limestone Formation. This carbonate succession of marine origin rests on a siliciclastic Sillakuddi Formation of shallow marine origin (Bakkiaraj et al. 2010; Sundaram et al. 2001; Watkinson et al. 2007; Madhavaraju et al. 2002). Transgression of the sea evidently took place prior to carbonate sedimentation. Yet, a conglomerate at the contact between the two formations is stated to be related to an unconformity and warrants a relook about its stratigraphic status. This paper, however, ignores the local fluxes of siliciclastics of highly immature texture, on the western basin margin.

S. Srimani (✉) · S. Mandal · S. Sarkar
Department of Geological Sciences, Jadavpur University, Kolkata 700032, India

The Kallankurichchi Limestone, famously rich in varied kinds of marine fossils, that leaves little doubt for its shelf origin (Nagendra et al. 2011a; Ramkumar 1999; Ramkumar et al. 2004; Nallapa Reddy et al. 2013). Sedimentary structures led Ramkumar (2006) to recognize a single storm event within this carbonate Formation. Fürsich and Pandey (1999), while considering shell concentrations, interpreted deposition under very shallow water, but below the fair-weather wave base. Nagendra et al. (2011b) concluded from their geochemical studies that deposition of the carbonate sediments took place in a dysoxic zone. Quite a bit of confusion thus remains about the paleogeography and paleoenvironment of deposition of this Formation, and water depth variation through time during its sequence development. To resolve the issue this paper undertakes a process-related sedimentary facies analysis and a microfacies analyses tied to the macrofacies.

2   Geological Background

The southernmost peri-cratonic Cauvery (rift) Basin, trending NE-SW along the eastern margin of India (Fig. 1a). The basin-margins are delimited by faults (Fig. 1b; Sundaram et al. 2001). The Cretaceous rocks are exposed in discontinuous patches within mines and on river banks along the south eastern Coromondal coast of India (Fig. 1b). The best vertical sections are in the limestone mines at different stratigraphic levels around Dalmiapuram and Ariyalur. The Kallankurichchi Limestone, under specific focus here, is exposed in a number of mines in the latter locality. This limestone Formation is underlain by Sillakuddi Sandstone unconformably and regionally passes upward into Ottakovil Sandstone of shallow marine origin (Nagendra and Nallapa Reddy 2017). On the basis of foraminiferal fossil population Hart et al. (1999) suggested Campanian-Early Maastrichtian age for the Kallankurichchi Limestone. The thick fossil population within the Kallankurichchi Limestone include *Gryphea*, *Inoceramus*, Oyster, Bryozoa, Echnoid, Brachiopod, *Ammonite* and varied kinds of foraminifera. Not only the Kallankurichchi Limestone, but also the entire Ariyalur Group which it belongs to, is very rich in invertebrate fossils. Seminal work of Blandford (1862) and Stoliczka (1867, 1871) on them was followed by several workers (Chiplonker and Tapaswi 1976, 1979; Chiplonker and Ghare 1977; Chiplonker 1985; Radulović and Ramamoorthy 1992; Guha and Nathan 1996; Nagendra et al. 2001, 2002, 2011b, 2018). Physical attributes of carbonate rocks of this Formation have received only perfunctory treatment so far (Fürsich and Pandey 1999; Ramkumar et al. 2004). A state-of-art facies analysis and a micro-facies analysis are done for understanding the mode of evolution of the Formation.

Kallankurichchi Limestone Formation; F: Fault
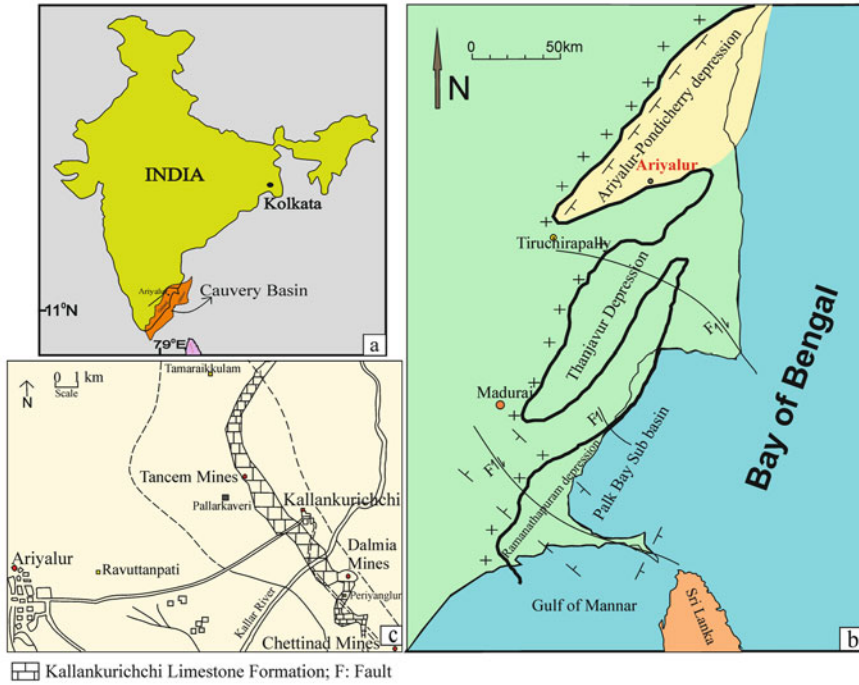
Fig. 1 Map of India showing the locations of Cauvery Basin (**a**); tectonic background of Pondicherry sub-basin basin margins delimited by faults (**b**) (modified after Sundaram et al. 2001); studied locations of the Kallankurichchi Limestone Formation (**c**)

3   Materials and Methods

Field data has been collected observing the lithofacies and their physical relationship and macrofossil content from mine areas (Fig. 1c). Numerous samples are collected systematically, vertically as well as laterally from the 50 m thick succession. Friable samples were handled with extra care during collection and transportation. Sampling is done to represent complete petrographic profile. Thin sections are prepared from collected rock samples and studied thoroughly under microscope to obtain microfacies data. Field studies along with microscopic observation are attempted towards understanding depositional textures.

4   Facies Analysis

This late Cretaceous Limestone is not bereft of primary physical attributes, although grain-size variation cannot be viewed from the angle of flow regime because of shell enrichment. Together the broad lithologic variation, primary sedimentary structures

and vertical intra-bed variation in fossil concentration are used to designate facies. The rock assemblage representing the Kallankurichchi Limestone is broadly divisible in two, viz. (1) Wave-dominated association and (2) Tide-dominated association. Before delving into the carbonate facies analysis, it is deemed necessary to have a brief look into the conglomerate that underlies the limestone succession (Fig. 2).

4.1   Basal Conglomerate

The Kallankurichchi Limestone is floored by a siliciclastic conglomerate. This conglomerate is well sorted, made of well-rounded clasts of varied composition (Fig. 3a). The clasts are traceable to the Sillakuddi Sandstone and the Precambrian metamorphosed basement (Fig. 3b, c). The conglomerate is non-recurrent in occurrence, tabular in geometry and about 45 cm in thickness. The clasts have an average diameter 4 cm. Sand grade matrix is present between the clasts, but remains confined to the top part of the conglomerate body.

Interpretation

At the contact between the fluvial siliciclastic below and the marine carbonate rocks above, the well-sorted and clast-supported conglomerate is a good candidate for transgressive lag (Posamentier et al. 1988; Catuneanu 2006; Yang 2007; Catuneanu et al. 2011; Sarkar and Koner 2020). High roundness of the clasts elicits prolonged reworking. Sharpness of both the bottom and the top contacts of the conglomerate bed further corroborate the contention. The interstitial matrix at the upper part of the bed had probably infiltrated from above on relative decline in the vigour of transgression.

4.2   Facies Association I

4.2.1   Facies 1A, Tidal Channel Facies

This calcarenite facies remains confined to the base of the measured succession and has broad lenticular geometry (Fig. 4a). The lenses measured ca. 2.5 m in outcrop width and maximum individual bed thickness 65 cm. The facies is characterized by oppositely oriented cross-strata in vertically adjacent beds (Fig. 4b). The cross-sets vary in thickness between 40 and 32 cm.

Interpretation

Apparent paleocurrent reversal in successive beds tell-tales flood-ebb tide alternations. Within the wave-dominated association this facies appears a bit out-of-place. However, this facies occurs only at the base of the measured succession and its lenticular in geometry, suggests deposition took place within channels. It seems that
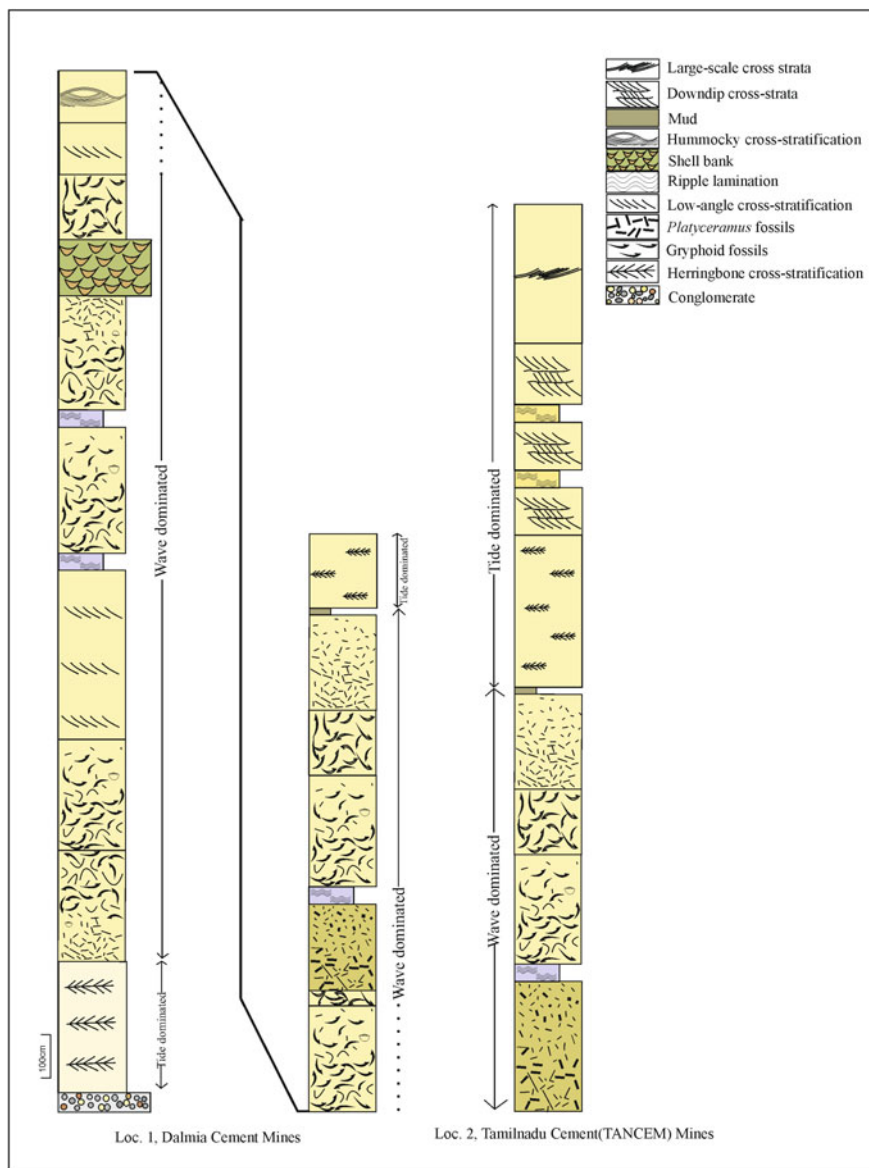
Fig. 2 Litholog of the Kallankurichchi Limestone Formation, broadly divisible into wave-dominated and tide-dominated association
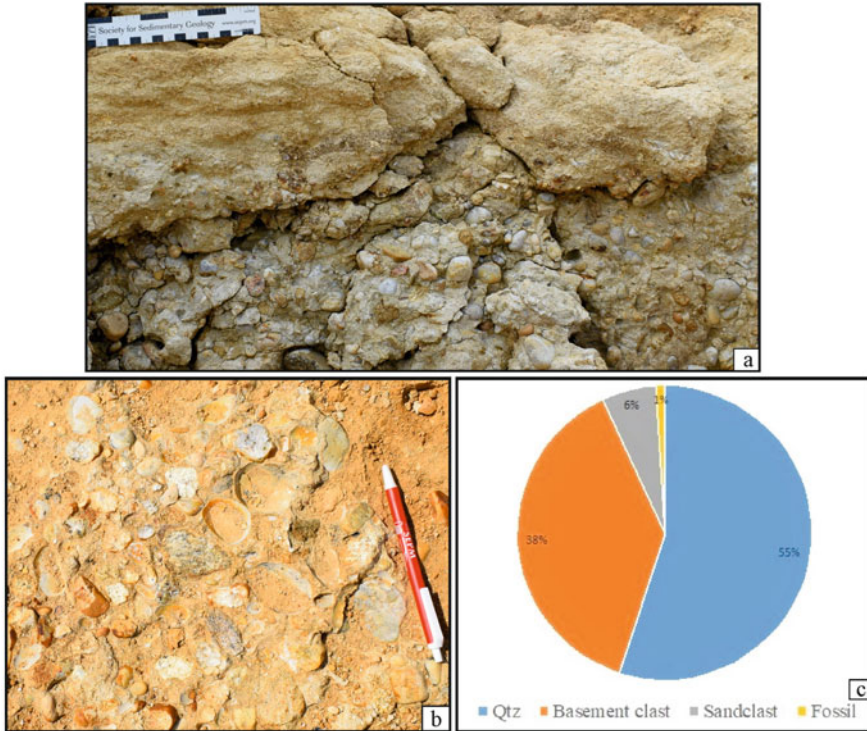
Fig. 3 Basal conglomerate is made up of well sorted and well-rounded clasts (**a**) of varied composition (**b**) and percentage (**c**)

when the transgression began, in the shallowest part of the basin, tide got accentuated within channel restrictions, while wave tended to dissipate. With progression of transgression, as the water depth increased, wave probably gained over tide and had cast greater influence on sedimentation. The herringbone cross-stratification arising from the paleocurrent reversibility implies that the tidal regime had been, more or less, symmetrical.

4.2.2 Facies 1B, Graded Storm Facies

These facies units are thick, measuring from 3 to 5 m. The beds are tabular in geometry. The beds have sharp bases, while their tops are comparatively less sharp. Internally the beds are graded and this grading is manifested in vertical distribution of fossils. In some beds the dominant fossils are of *Gryphea* (Fig. 4c) and in others they are of *Platyceramus* (Fig. 4d). In the latter case the elongated bioclasts are distinctly haphazard in orientation. The majority of *Gryphea* shells in these beds are also haphazard in orientation (Fig. 4c).
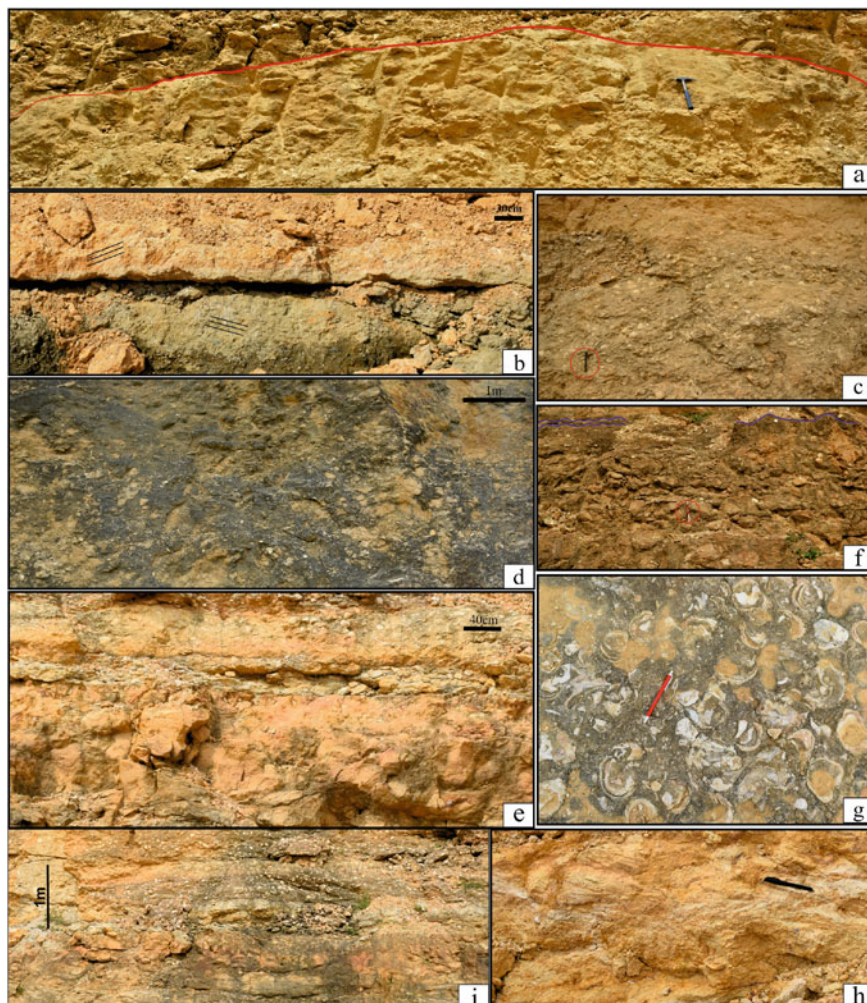
Fig. 4 Lenticular body-geometry of the lowermost calcarenite facies (**a**); oppositely oriented cross-strata in vertically adjacent beds (**b**); *Gryphea* (**c**) and *Platyceramus* (**d**) dominated graded storm facies. Note the haphazard orientation of the clasts; Sheet-like rippled facies (**e**) showing nodularity (scale encircled with red color) (**f**); Shell bank facies. Note the concave-up nature of most of the shells and shell cavities are filled with grey colored lime-mud (**g**); Chevron (**h**) and hummocky cross-stratified facies (**i**)

Interpretation

The grading indicates deposition from suspension and hence transportation of sedimentary load in a density current. Despite that the grading itself suggests that the sediment driving flow had been light enough in density to allow larger clasts to settle first. Chaotic orientation of the elongated *Platyceramus* fragments suggests

turbulence in the flow immediately prior to deposition. Formidable thickness of the beds indicates enhanced rate of deposition from individual flows, hardly ever achievable in fair-weather processes. In all probability, these beds were laid by down welling induced by storms (cf. Harms et al. 1975; Bose et al. 1988; Walker and Plint 1992; Banerjee 2000; Banerjee and Jeevankumar 2007; Sarkar and Koner 2020). It is reasonable to assume that storms significantly enhanced the rate of delivery of organic particles (Kumar and Sanders 1976; Wilson 2012).

4.2.3 Facies 1C, Rippled Facies

This facies is distinctly finer-grained with respect to the immediately preceding facies of inferred storm origin with which it alternates. It overall appears as typically sheet-like in geometry (Fig. 4e) and nodular in nature (Fig. 4f). Close inspection reveals cross-laminae within the nodules. Average thickness of the facies units bounded below and above by storm beds is around 40 cm. The cross-lamina sets within them are around 3–6 cm thick. The cross-lamina set boundaries appear erosional and concave-up in orthogonal sections.

Interpretation

Comparatively finer grain-size and smaller structural elements with respect to those of adjacent storm beds help to identify this facies as a fair-weather product. The facies presumably depict ripple migration. A steep depositional energy gradient seems to be implied by vertical transitions from this facies to the adjacent facies of inferred storm origin and vice versa. However, the cross-laminae indicate that the facies was deposited in an agitated condition, may not be as much agitated as during storm. Geometry of the cross-set boundaries in orthogonal sections suggest wave origin of the ripples created by this agitation (De Raaf et al. 1977). In temporal alternations with storm beds, this facies is inferred to be fair weather origin.

4.2.4 Facies 1D, Shell Bank Facies

This carbonate facies with conspicuous enrichment in well preserved *Gryphea* shells of average diameter 14 cm is a rudstone in Dunhum's (1962) terminology. It overlies the storm beds, either graded or cross-stratified. Shell concentration varies laterally; in fact, it alternately decreases and increases. Grey colored lime-mud admixed with shell hash fill the space between the shells and within the shell cavities (Fig. 4g). The bed geometry is highly irregular. The beds have sharp top where shell concentration is high, but gradational at bottom everywhere. The shells are generally concave-up in attitude, but exceptions are also there (Fig. 4g).

Interpretation

Frequent good preservation of a large number of thick and relatively heavy shells of *Gryphea*, and that too in living concave-up condition suggests the shell concentration

is a result of in situ growth, in other words, colonization. Random orientation of some shells is always explicable with bioturbation. Distinct lateral variation in shell density without any apparent taphonomic control probably reflects deliberate choice of living organisms about spots to flourish. Indistinct lower surfaces of the beds in contrast to their upper surfaces agree with this contention of in situ growth. Exclusive occurrence of this *Gryphea* colonization on top of storm beds is possibly because of enhanced production rate of these sedentary organisms at the aftermath of storms.

4.2.5 Facies 1E, Chevron and Hummocky Cross-Stratified Facies

This facies includes all large-scale cross-stratified rocks except those bearing herringbone cross-strata. In the majority of cases the cross-strata in this facies are chevronlike and a few are hummocky cross-stratified (HCS; Ramkumar 2006). The chevron cross-stratified beds are, in general, tabular in geometry and their bed thickness is nowhere less than 50 cm (Fig. 4h). The hummocky cross-stratified beds are, on the other hand, sheet-like in geometry, measuring around 95 cm in thickness (Fig. 4i).

Interpretation

This facies, with chevron cross-strata or with HCS, appears to be dominantly wave affected. The thick chevron cross-stratified beds appear to record vertical up building of bedforms over duration much longer than fair-weather waves. The HCS implies wave-current combined flow (Greenwood and Sherman 1986; Nøttvedt and Kreisa 1987; Tinterri 2011). The large spacing of HCS also points to waves larger than usual short period fair weather waves (Swift et al. 1983). Hence storm down-welling as the sediment-driving mechanism is implied (Harms et al. 1975; McCrory and Walker 1986; Bose et al. 1988).

4.2.6 Facies 1F, Muddy Facies

This facies is conspicuous for its deep grey color and muddy nature and laterally persistent (Fig. 5), despite its thinness (15 cm). Its base is slightly and broadly undulated, while its top is flat. This facies occurs at the top of the wave-dominated facies association and is non-recurrent.

Interpretation

The fine-grained nature suggests deposition in a quieter area. Deposition in a deeper shelf is interpreted (see later). The body geometry of the facies suggests limited erosion at its base. This facies occurring at the contact between the two facies associations and does not have any hall mark for either wave or tide. For the justification of the preferred inclusion of this in facies association II (see below).

Fig. 5 Thin laterally persistent muddy facies with broadly undulated base (arrowed) above the wave dominated association

4.3 Facies Association II

4.3.1 Facies 2A, Small-Scale Herringbone Cross-Stratified Facies

This facies characterized by herringbone cross-strata overlies the muddy facies 1F. The cross-strata appear in reverse orientation across bed surfaces (Fig. 6a). The cross-sets are about 14–16 cm in thickness. The forests bear distinctive mud drapes
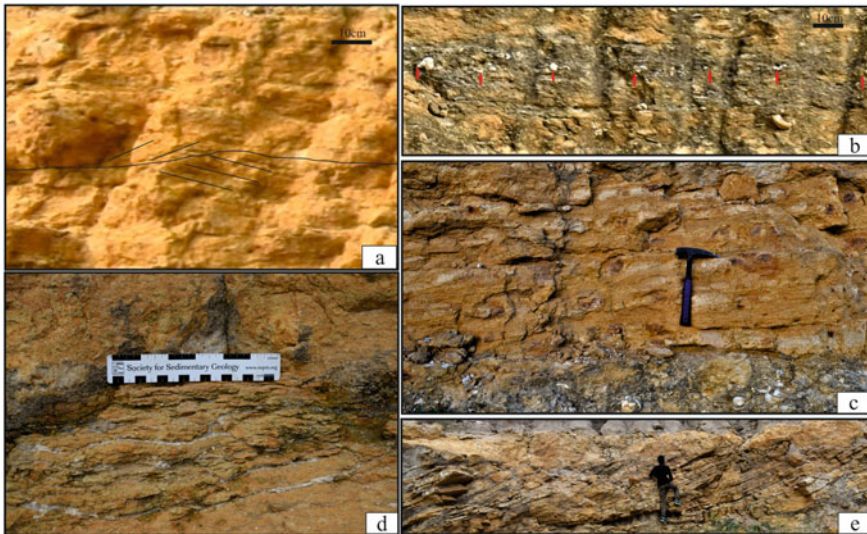
Fig. 6 Small-scale herringbone cross-stratified facies with mud drapes (**a**); broadly undulated set boundaries are, at places, demarcated by shell concentrations (arrowed) (**b**); down-dip cross-stratified facies. Note the geometry also changes laterally (from steep to gentle) (**c**); rippled facies (**d**); large-scale cross-stratified facies. Note the lateral change of forest geometry (**e**)

(Fig. 6a). Shell fragments remain scattered within the cross-sets. The broadly undulated set boundaries are, at places, well demarcated by shell concentrations (Fig. 6b). The entire facies body compromised of multiple such cross-sets is about 3.5 m in thickness. This is non-recurrent in the Kallankurichchi Limestone stratigraphy.

Interpretation

The paleogeography appears to be tide-dominated, although shell concentrations along some cross-set boundaries are inferred as wave winnowed lag deposits (Fig. 6b). The mud drapes on forests and bimodal, if not bipolar, cross-strata orientations are distinctive finger prints of tide (Bose et al. 1997; Eriksson and Simpson 2000; Eriksson et al. 2006; Mandal et al. 2019). The fossil content, as mentioned before, identifies this tidal facies as of a shelf. The small-scale of cross-strata speaks of relatively weakly agitated environment. The depositional site thus seems to be away from the shoreline, at a distal position.

4.3.2   Facies 2B, Down-Dip Cross-Stratified Facies

This facies rests on the preceding facies unit and recurs further upward. Large-scale low angle cross-strata confine small-scale steeper cross-strata between every pair of them. Both the sets dip in the same direction (Fig. 6c). Set thickness of the small-scale cross-strata is, on average, 8–9 cm and that of the larger-scale cross-strata averages 21 cm. The smaller-scale cross-strata bear mud drapes. Cross-strata geometry also changes laterally, cyclically from steep to gentle and to steep again (Fig. 6c).

Interpretation

The mud drapes suggest that the carbonate particles were transported under influence of tide. The down-dip cross-strata suggest flow-parallel elongation of bedforms that resulted. These bedforms identified as longitudinal tidal bars are inferred to have originated on a shelf (Reading 1996; Prothero and Schwab 2013), presumably at relatively shallower part of the shelf with respect to the preceding facies.

4.3.3   Facies 2C, Rippled Facies

This facies is distinctly finer grained than the immediately preceding facies with which it alternates (Fig. 6d). It is sheet-like in geometry. The ripple forms are preserved being wrapped around by thin mud drapes.

Interpretation

The mud drapes were possibly formed during tidal slackening phases and ripples migrated during periods intervening them. Alternating with the immediately preceding facies, this facies seems to have deposited in the same paleogeography as the former. Most probably, this facies formed in the interbar region.

4.3.4 Facies 2D, Large-Scale Cross-Stratified Facies

This facies is at the top of the measured carbonate succession. It is non-recurrent and represented by a single large cross-set (Fig. 6e) of preserved thickness ranging up to 2.3 m. The forests change geometry laterally from steep to gentle and to steep again (Fig. 6e). While the foreset is steepest, the toeset is shortest and the gentlest forsets are accompanied by longest toesets. The forests are draped by mud.

Interpretation

This facies is interpreted as proximal to the shore. The mud drapes on top of the forests and cyclical change in the cross-stratification geometry are distinctive signatures of tide. The cross-strata geometry changes presumably record cyclical transitions between spring and neap tide (Collinson et al. 2006; Reading 1996). Their foreset steepness and toeset lengths varied presumably with cyclically changing velocity of the parent flow (Bose et al. 1997; Sarkar et al. 1999).

5 Microfacies Analysis

5.1 Facies 1A

The facies 1A is carbonate sandstone with a subordinate, but locally substantial, admixture of detrital population, mainly quartz, some feldspar and very few biotite grains (Fig. 7a). However, in this facies, confined to the basal few metres of the measured succession, the siliciclatic population dwindles away rapidly upward (Fig. 7b). The carbonate clastic population is either intraclasts with or without bioclasts within them and bioclasts alone. Significant presence of intraclasts warrants the name intramicrite for the rock in the bottom level but gradually changes into intrasparite at the topmost level of the tidal section (Folk 1959, 1962). The intraclasts are brown in color. Almost all the carbonate clastic grains bear micritic rims around themselves, only at the uppermost level of this tide-imprinted section, isopachous needle-shaped carbonate cement crystals take their place (Fig. 7c). In the lower part of the same section blocky cement occurs preferably at the underside of clastic grains. No such preference for blocky cement occurrence is observed in the upper level. In the latter case there is always a conspicuous ferruginous coat between the 1st generation isopachous cement and the 2nd generation blocky cement (Fig. 7d). The isolated bioclasts have a wide range in length, while the intraclasts occupy the lower segment of this range.

Interpretation

At the onset of carbonate deposition, at the shallowest part of the sea tide amplitude probably increased within constriction of channels while wave dissipated rapidly and that may be the reason for the presence of tide signatures at the bottom section of the
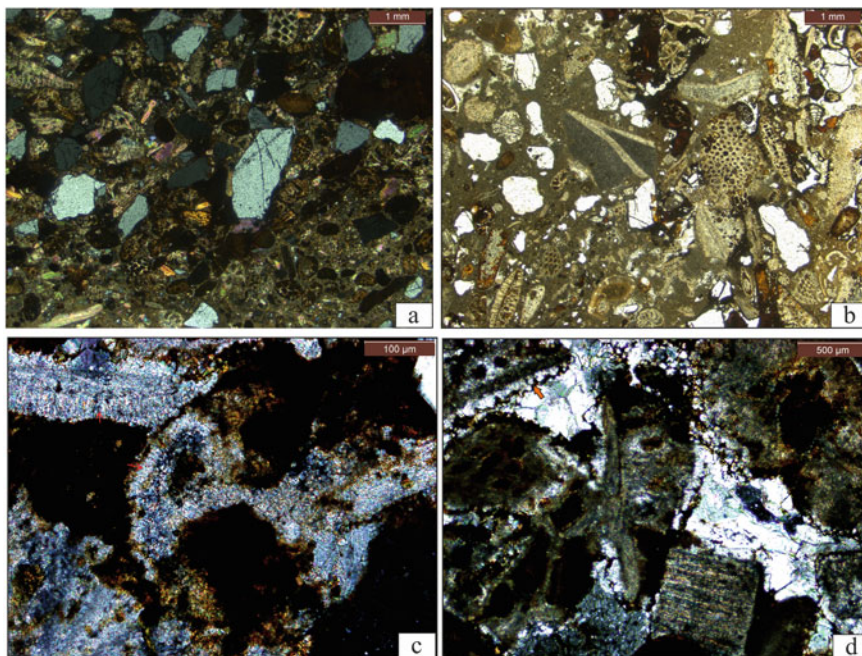
Fig. 7 Calcareous sandstone with detrital population of quartz, feldspar and biotite (**a**) rapidly dwindles away rapidly upward (**b**); needle-shaped carbonate cements crystals around carbonate clasts (**c**); Ferruginous coat between two generation cements (**d**)

wave-dominated association. Herringbone cross-strata imply that the tide had been, more or less, symmetric. Intramicritic composition at the lower level and intrasparitic composition in the upper part of facies 1A imply progressive increase in the tidal flow intensity with the shift of paleogeography seaward. This seaward paleogeographic shift through time is strongly corroborated by upward decrease in size and frequency of occurrence of siliciclastic grains (Fig. 7b). At the shallowest part of the paleo-geography the intraclasts were derived presumably from the banks of the migratory tidal channels, although intramicritic composition of the rock indicates low energy of tide. Preferred cement accumulation at the underside of the grains suggests vadose origin of the cement at the bottom part (Adams and Mackenzie 1998; Scholle 1978). This fact is compatible with the shallowness of this bottom part; probably emer-gence took place as the channels shifted away. With seaward paleogeographic shift tide might have been accentuated to winnow out lime mud and eliminated the possi-bility of emergence of the depositional surface and marine phreatic 1st generation isopachous cement rimmed the clasts (Adams and Mackenzie 1998; Scholle 1978); intermicritic thus changes upward to intrasparite composition of the rock. Empty pore spaces were later filled by 2nd generation blocky cement.

5.2 Facies 1B to 1E

Facies 1B to 1E are intrasparite; drusy growth in cement is commonplace (Fig. 8a). Within shelter pores, under shells, especially under convex-up pelecypod valves, the cement patches are larger (Fig. 8b). Syntaxial cement selectively grown around echinoid plates or spines is also common in occurrence (Fig. 8c). Intraparticle pores within the shells are, however, generally biomicrite. Gryphea-rich shell banks or the basal part of graded storm beds fit the term rudstone (cf. Dunhum 1962). Bryozoan zooycea are often partially filled by heavily iron-stained biomicrite, while the rest of the pores are filled by blocky calcispars (Fig. 8d). Both the fresh-looking, apparently indigenous, bioclasts are generally admixed with almost equal number of intraclasts with or without bioclasts embedded within them. Large shells generally retain their delicate primary texture, but smaller shells embedded within intraclasts often have their shell walls replaced by calcite cement. The intraclasts are brown in color. All the clasts bear micritic rims. Most of them have rounded edges (Fig. 8e), but some have delicate protrusions. Steinkerns are locally found (Fig. 8f). Within some intraclasts long shell fragments have lime mud attached delicately on one side. In some such intraclasts borings pass through both the shells and the mud attached to them (Fig. 8g). In some borings the infilling matches exactly with the sediment hosting them, in some other they are different and in the rest the infilling is partly or fully calcite spar cement (Fig. 8h). Some shells are broken and the same blocky calcite cement fills the fractures as well as the intraparticle pores outside.

Interpretations

Intrasparite fabric points to winnowing out of fines in agitated environment, even during fairweather. The fines were, however, retained in protected microenvironments of intraparticle pores. Some imported clasts might have their intraparticle pores filled at their original sites of deposition. Since millions of crystals constituting the echinoid grains together behaved as single grains, syntaxial cement grew around them on the consideration of lower energy consumption (Adams and Mackenzie 1998). The shell-bank rudstones on top of storm beds do not reflect high energy sediment transport as they are products of colonization by *Gryphea* during virtual sedimentation hiatuses. In contrast, rudstone at the base of graded storm beds reflects high energy influx. Micritic rims around all the clasts strongly suggest final deposition within the photic zone (Adams and Mackenzie 1998). The micritic rims helped to retain characteristic shapes of bioclasts whose shells have been dissolved. Some shells are well retained, while others got dissolved – this fact points to difference in primary shell mineralogy (Adams and Mackenzie 1998). Presumably shells of metastable mineralogy dissolved, but the low Mg-calcite shells escaped dissolution (Bathurst 1972; James and Choquette 1983). Abundance of intraclasts bears evidence of strong erosional nature of the sediment-driving flows. Intraclasts with delicate projections suggests that the flows eroded firm or even hardgrounds (Ramkumar 1996). Presence of boring cutting through both sediment and bioclast without any deflection corroborates this contention (Fig. 8g). Borings filled by sediment suggests a short time gap
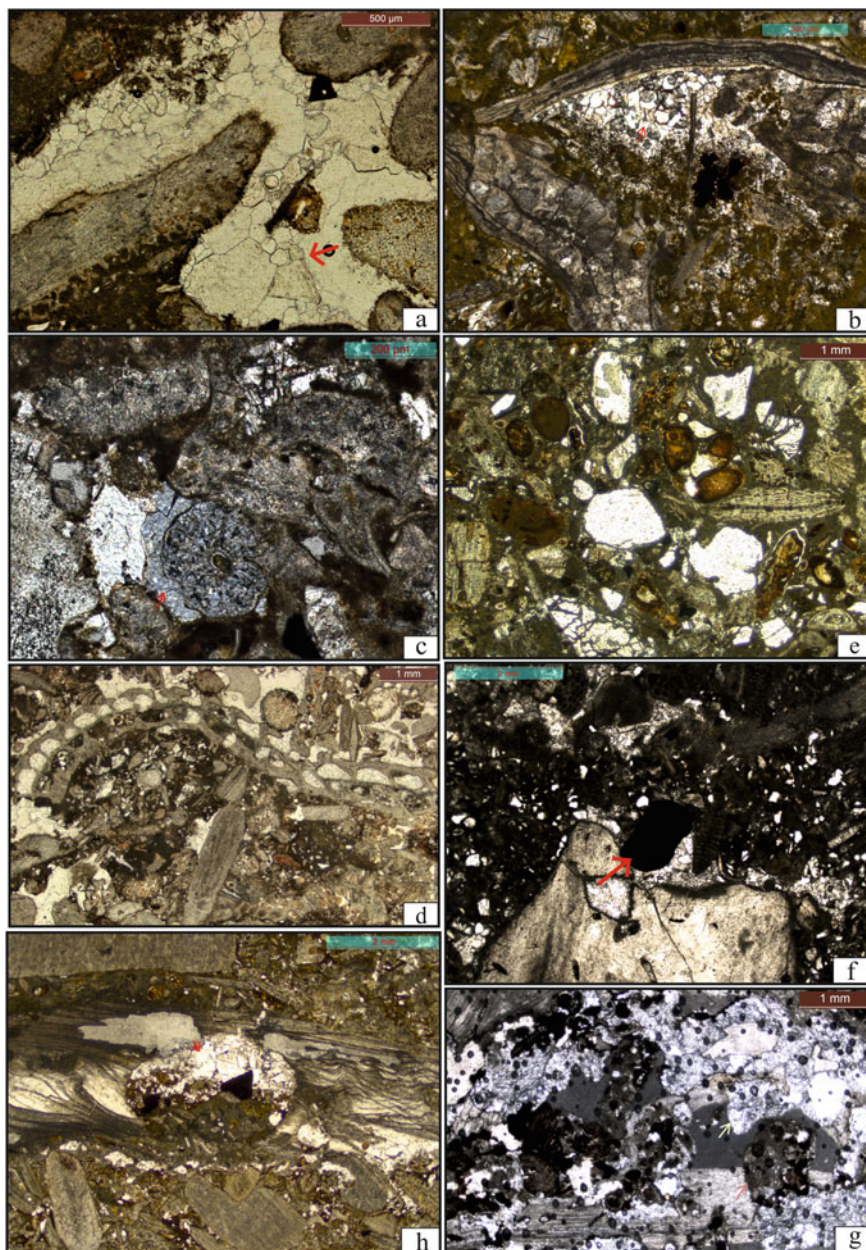
Fig. 8 Drusy growth in cement (**a**); shelter pores in Intrasparite (**b**); syntaxial cement selectively grown around echinoid plates (**c**); bryozoan zooycea filled up by heavily iron-stained biomicrite (**d**); brown rounded intraclasts bear micritic rims (**e**); steinkerns (**f**); boring passes through shells and mud (**g**) and they are filled with host sediment and spar cement (**h**)

between boring and its infilling than when the borings are filled by cement; a biostratinomic sequence like filling by host sediment-filling by younger sediment-filling partially by younger sediment-filling by cement alone, can be drawn. The steinkerns indicate that the mud that infilled shell cavity was already cemented prior to transporting ion to the present depositional site. Hardground formation is evident and that reflects overall low sedimentation rate and sporadic (Bromley 1968; Molenaar and Zijlstra 1997). Contrasting degree of preservation of shells suggests difference in shell mineralogy. The micritic cement and the isopachous needle-shaped cement around grains are probably marine, but the blocky cement is inferred to be burial in origin. Continuation of the same cement within fractures on shells corroborates this contention.

5.3   Facies 1F

Facies 1F is intramicritic or biomicritic limestone depending upon the volume percentage of intraclasts (Folk 1959, 1962). Cement is confined to intraparticle and shelter pores (Fig. 9a). Remarkable is absence of micritic rims around clasts. Another remarkable feature of this facies is almost intact preservation of very long isolated and delicate strips of encrusting bryozoa, twisted and folded with little breakage (Fig. 9b). With respect to other facies in the wave-dominated association another feature is exceptional in this facies is silicification of bioclasts, especially of echinoids.

Interpretation

In this muddy facies clasts are virtually floating within mud matrix. Some shelter pores and intraparticle remained empty till they were filled by late diagenetic cement, seemingly of burial origin as in other members of the Association I. Shells of primary aragonitic mineralogy were preferably selected for diagenetic silicification presumably because their constituent crystals were not enlarged through dissolution and
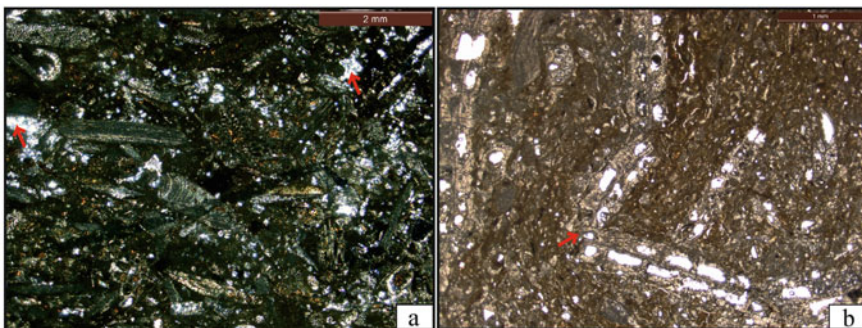
Fig. 9   Confinement of cement to pores (**a**); Intact preservation of long delicate strips of encrusting bryozoa, twisted and folded with little breakage (**b**)

re-precipitation in order to gain stability. The sediment thus appears to be a mudflow product. Viscosity of the flow, however, allowed long strips of bryozoa to sustain despite frequent twists and folding. The matrix probably frozen rapidly and caused rapid cessation of the flow. Rapid burial presumably ruled out as microbial boring present around the intraclasts or bioclasts. Because of finer grain-size this facies, with respect to all other facies in Association I, seems to have deposited at comparatively deeper shelf.

5.4 Facies 2A to 2D

Facies 2A to 2D is very rich in bioclasts, although there is also a subordinate population of intraclasts with or without bioclasts. Packing is usually very tight. The rock is biomicritic at places (Fig. 10a), biosparite elsewhere (Fig. 10b); the lateral transition appears a bit irregular in thin section. Micritic cement around clasts is a common feature. Spaces left by dissolution of shells are small sparry calcite cement. Drusy cement in biomicritic rock fills shelter and intraparticle pores. Drusy cement is commonplace in interparticle pores in biosparitic rocks. These cements are all blocky in nature. Intraclasts are all brown in color, darker than the micritic groundmass. Within one such intraclast, a steinkern is even deeper brown in color (Fig. 10c). Many of the shells are bored repeatedly (Fig. 10d). In contrast to facies Association I, all the facies within this Association contain substantial proportion of detrital grains, such as, quartz, feldspar and granite fragments (Fig. 10e). Some brown oxidized mudclast bears multiple cracks. The crack-filling cement is different from the blocky cement within interparticle pores outside. All the facies of the Association II incorporate substantial amount of detrital grains.

Interpretations

Degrading neomorphism in form of micritic rims, of supposed microbial origin, around all the clasts strongly suggest deposition within the photic zone, presumably on the shelf as suggested by the fossil population. The herringbone cross-strata, the mud drapes on cross-strata, lateral change in the geometry of the cross-strata— all tell-tale tidal action. The lateral transitions between biosparite and biomicrite are indicative of temporal variation in flow intensity, biomicrite belonging to the slackening phase of tide. Repeated borings on bioclasts and transportation of the shells with empty boring suggests that the shells remained exposed for considerable period of time at source (Fig. 10d). In contrast, some shells arrived at the final depositional site with their borings filled (Fig. 10f). Leaving aside facies 2C, the facies Association II succession reveals steady upward increase in the size and frequency of occurrence of detrital grains.
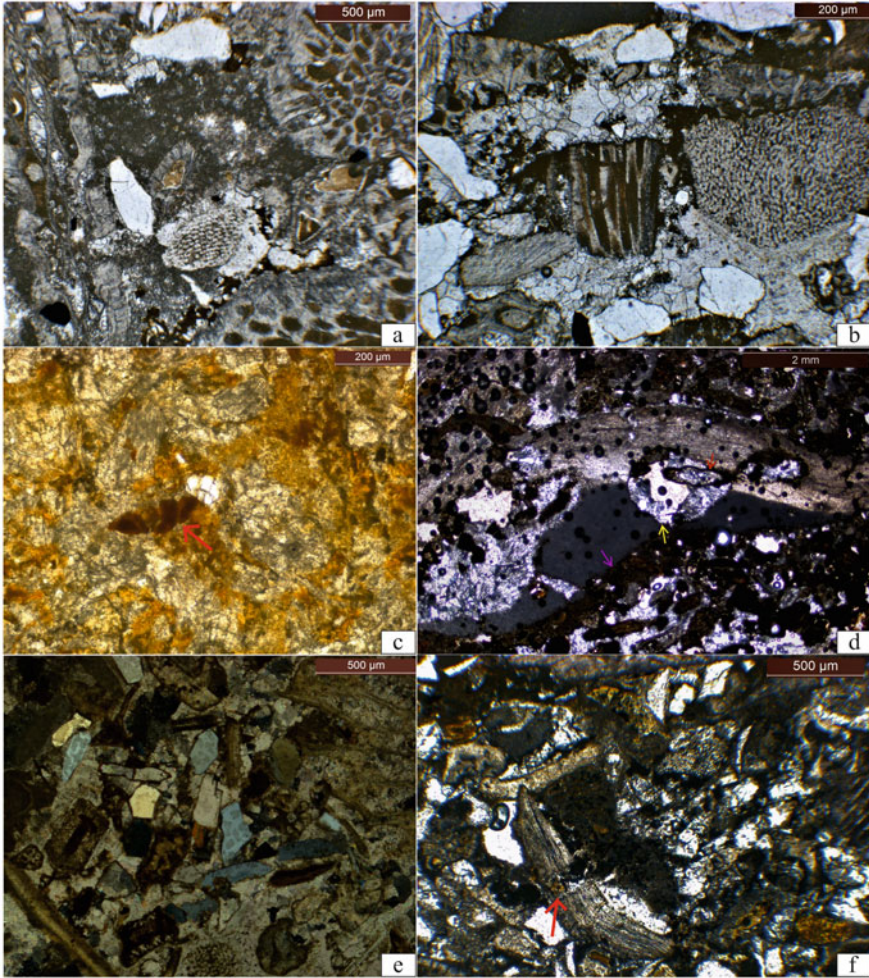
Fig. 10 Biomicritic (**a**) and biosparite (**b**) within facies 2A to 2D; Brown color intraclasts with steinkern (**c**); bored shells (**d**); substantial proportion of detrital grains within this association (**e**); earlier filled borings (**f**)

6 Detrital Quartz Distribution

Away from the basin-margin detrital quartz occurs generally sparingly. Systematic measurements of frequency of occurrence (Fig. 11) reveal an interesting pattern of variation in the vertical section. From the base of the measured section quartz grains have been detected upward up to about 5 m. The frequency of occurrence of quartz grains decrease upward. Quartz grains are detected again at a level around 30 m from the base of the measured succession, immediately above the non-recurrent muddy
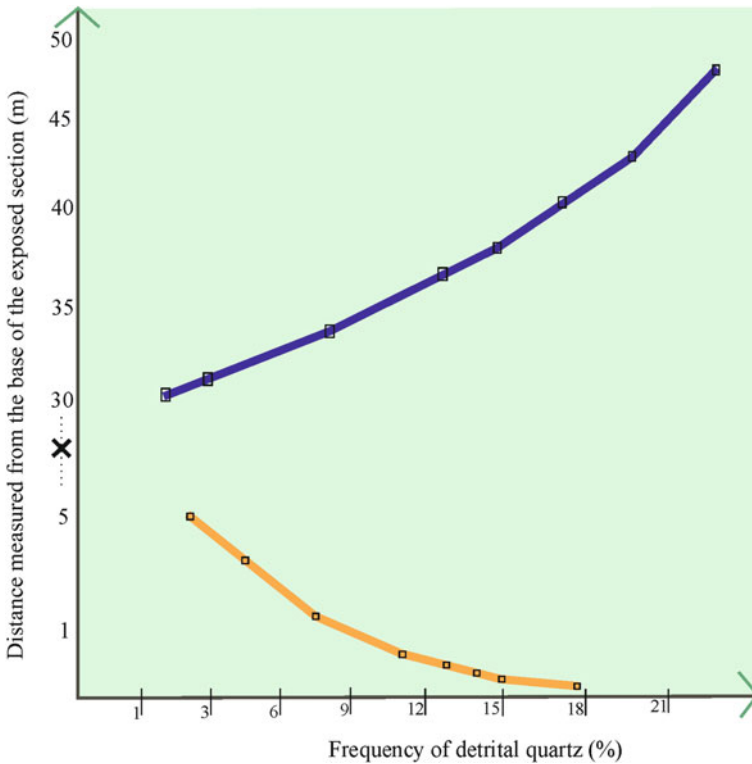
Fig. 11 Variation in frequency of occurrence of detrital quartz grains along the vertical stratigraphic section. Note the occurrence of quartz grains maximum in the lower and upper part of the tide dominated section

facies unit. From this level upward both median size and frequency of occurrence of quartz grains increase rapidly, more rapidly than their decreasing trend at the base of the measured succession. The non-recurrent very large-scale cross-stratified facies at the very top of the studied stretch is fairly rich in quartz, though not exceeding 50%. From the top of the muddy facies the succession is preserved up to about 19 m.

7   Sequence Stratigraphy

From the top of the well sorted siliciclastic conglomerate identified as transgressive lag, decrease in size and frequency of land-derived detrital grains strongly suggests progressive shift of paleogeography basinward. Further upward passage into a 25 m-thick vertical zone barren of detrital grains suggests further progressive deepening of the sea (Fig. 12). Paleogeographic shift further basinward is an imperative. This contention about progressive basin deepening is further corroborated by
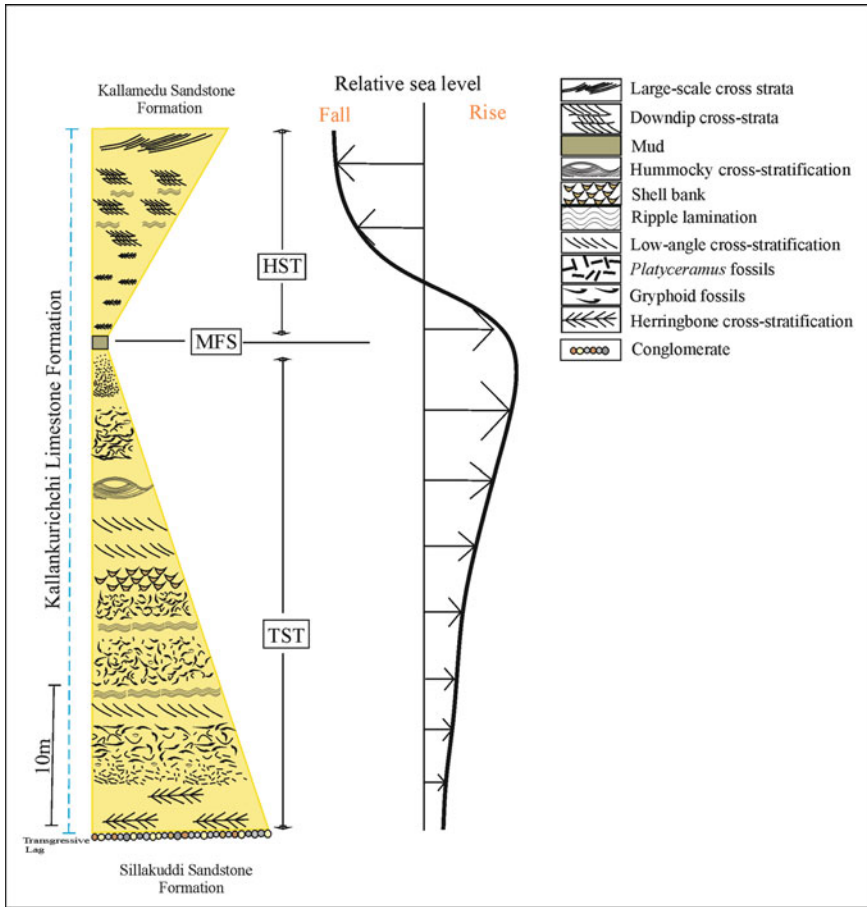
Fig. 12 Representative section of Kallankurichchi Formation showing systems tracts. The transgressive system tracts (TST) overlain by highstand system tracts (HST) with a maximum flooding (MFS) in between

placement of the only muddy facies on top of the quartz-barren zone likely to be the maximum flooding surface (MFS). From the putative transgressive lag to the muddy facies may, therefore, reasonably be recognized as a Transgressive Systems Tract (TST). The sea encroached inland through narrow fault-bounded valleys. At the land-margin narrower valleys and coves between promontories tide had been accentuated at the expense of wave. With progressive deepening of the basin, wave became progressively dominant.

From top of the muddy facies quartz influx increases and detrital quartz grain-size also increases rapidly upward. The mode of sequence development resembles what is expected in Highstand Systems Tract (HST). Tide regained its strength and outdid wave action in leaving their signature in sediments.

8 Faunal Distribution

The Kallankurichchi Limestone is very rich in bivalve fossils, particularly *Gryphea* and *Inoceramus*. Besides, there also occur bryozoa, dominantly the encrusting variety, echinoderms, varieties of foraminifers, brachiopods and cephalopods in order of decreasing abundance. However, the former two are the most conspicuous by far under unaided eye. The faunal distribution here covers on these two conspicuous groups of bivalves.

The basal tide-dominated part of the older facies association displays any conspicuous faunal population, though representatives of both the communities are present. However, thin their populations are they are thoroughly admixed. At about 4 m above the base of the measured succession the *Inoceramus* dominates. Thereafter, up the section, there are successive alternate zones of clear domination of either *Gryphea* or *Inoceramus*. At about 14 m above the base of the measured succession there is an exceptional concentration of *Cataceramus*, a genus of *Inoceramus*. In this connection it is to be mentioned that *Platyceramus* is the most common genus of *Inoceramus* present within this succession, while the commonly occurring *Gryphea* genera are 60 and 35%. Only in the muddy facies on the very top of the Association I they are replaced by Bryozoa and Echinoid. Above this facies, nonetheless, supremacy of *Inoceramus* and *Gryphea* is resumed. However, they could not be traced under unaided eye in the very large-scale cross-stratified facies on the very top of the Facies Association II. Immediately underneath this facies a thin layer of high concentration of *Gryphea* terminates the faunal succession of this Kallankurichchi Limestone.

9 Conclusions

The Kallankuruchi Limestone Formation, famously rich in marine fossils, built up on the siliciclastic Sillakuddi Formation following a major transgression of the sea. A well sorted conglomerate characterized by well-rounded pebbles of granite and sandstone, and lack of marine fossils except at its top makes strong erosion under prolonged to-and-fro wave motion evident before the onset of carbonate deposition. In the constricted intracratonic basin tide had dominated initially. Ere long it gave way to wave as the relative sea level continued to rise. In consequence both the fair weather and storm deposits alternated, although the latter largely escaped reworking by fair weather waves because of basin constriction. The restricted basinal setting favored growth of colonies of sedentary bivalves and bryozoa in profusion with addition of other marine invertebrates, like brachiopods and ammonites. Terrigenous influx steadily dwindled through time. The Transgressive Systems Tract culminated with a thin carbonate mudstone with well-preserved very delicate long chains of encrusting bryozoa as a dominant constituent. The Highstand Systems Tract on top of the Maximum Flooding Surface is again replete with tidal features, similar biotic elements and terrigenous quartz flux.

References

Adams AE, MacKenzie WS (1998) A color Atlas of carbonate sediments and rocks under the microscope. WS Manshon Publishing

Bakkiaraj D, Nagendra R, Nagarajan R, Armstrong-Altrin JS (2010) Geochemistry of siliciclastic rocks of Sillakkudi Formation, Cauvery Basin, southern India: Implications for provenance. J Geol Soc India 76:453–467

Banerjee S (2000) Climatic versus tectonic control on storm cyclicity in Mesoproterozoic Koldaha Shale, central India. Gond Res 3:521–528

Banerjee S, Jeevankumar S (2007) Facies and depositional sequence of the Mesoproterozoic Rohtas Limestone: eastern Son valley, India. J Asian Earth Sci 30:82–92

Bathurst RGC (1972) Carbonate sediments and their diagenesis. Developments in sedimentology, vol 12. Elsevier, Amsterdam

Blanford HF (1862) On the Cretaceous and other rocks of the South Arcot and Trichinopoly districts. Mem Geol Surv India 4:1–217

Bose PK, Chaudhuri AK, Seth A (1988) Facies, flow and bedform patterns across a storm dominated inner continental shelf: Proterozoic Kaimur Formation, Rajasthan, India. Sediment Geol 59:276–293

Bose PK, Majumder R, Sarkar S (1997) Tidal sandwaves and related storm deposits in the transgressive Protoproterozoic Chaibasa Formation, India. Precam Res 84:63–81

Bromley RG (1968) Burrows and boring in hardgrounds. Dansk Geol Foren Meddr 18:247–250

Catuneanu O (2006) Principles of sequence stratigraphy. Elsevier, Amsterdam

Catuneanu O, Galloway WE, Kendall CGSC, Miall AD, Posamentier HW, Strasser A, Tucker ME (2011) Sequence stratigraphy: methodology and nomenclature. Newsl Stratigr 44:173–245

Chiplonkar GW (1985) Attempts at litho- and biostratigraphic subdivision of the Upper Cretaceous rocks of South India—a review. Quart J Geol Min Met Soc India 57:1–32

Chiplonkar GW, Ghare MA (1977) Serpulid and barnacle borings on south Indian Cretaceous fossils from Trichinapoly district, Tamil Nadu. Biovigyanam 3:193–204

Chiplonkar GW, Tapaswi PM (1976) Bivalvia from the Upper Cretaceous of Trichinopoly district, South India. Part 1, Inoceramidae. Recent Res Geol 3:87–123

Chiplonkar GW, Tapaswi PM (1979) Biostratigraphy, age and affinities of the bivalve fauna of the Cretaceous of Tiruchirapalli District, South India. Misc Publ Geol Surv India 45:137–164

Collinson JD, Mountney N, Thompson DB (2006) Sedimentary structures, 3rd edn. Terra Publishing, Harpenden

DeRaaf JFM, Boersma JR, Van Gelder A (1977) Wave-generated structures and sequences from a shallow marine succession, Lower Carboniferous, County Cork, Ireland. Sedimentol 24:451–483

Dunhum RJ (1962) Classification of carbonate rocks according to depositional textures. AAPG Mem 1:108–121

Eriksson KA, Simpson EL (2000) Quantifying the oldest tidal record: the 3.2 Ga Moodies Group, Barberton Greenstone Belt, South Africa. Geology 28:831–834

Eriksson KA, Simpson EL, Mueller W (2006) An unusual fluvial to tidal transition in the Mesoarchean Moodies Group, South Africa: a response to high tidal range and active tectonics. Sediment Geol 190:13–24

Folk RL (1959) Practical petrographic classification of limestones. AAPG Bull 43:1–38

Folk RL (1962) Spectral subdivision of limestone types. AAPG Mem 1:62–84

Fürsich FT, Pandey DK (1999) Genesis and environmental significance of Upper Cretaceous shell concentrations from the Cauvery Basin, southern India. Palaeo Palaeo Palaeo 145:119–139

Greenwood B, Sherman DJ (1986) Hummocky cross-stratification in the surf zone: flow parameters and bedding genesis. Sedimentol 33:33–45

Guha AK, Nathan DS (1996) Bryozoan fauna of the Ariyalur Group (Late Cretaceous), Tamil Nadu and Pondicherry, India. Palaeontologia Indica, Monograph, Geol Surv India, New Series, vol XLIX

Harms JC, Southard JB, Spearing DR, Walker RG (1975) Depositional environments as interpreted from primary sedimentary structures and stratification sequences, Dallas. SEPM Short Course 2:1–161

Hart M, Joshi A, Watkinson M (1999) Palaeoecology and Stratigraphical setting of the Kallankuruchchi Limestone Formation (U. Cretaceous), S.E. India. European Palaeontol Ass Workshop, Abstract Vol, Lisboa, pp 47–51

James NP, Choquette PW (1983) Diagenesis 6. Limestones—the sea floor diagenetic environment. Geos Canada 10:1–18

Kumar N, Sanders JE (1976) Characteristics of shoreface storm deposits; modern and ancient examples. J Sed Res 46:145–162

Madhavaraju J, Ramasamy S, Mohan SP, Asir G (2002) Ooids in Sillakkudi Formation of Ariyalur Group of Tiruchirapalli Cretaceous, Tamil Nadu: implications for origin and depositional environment. J Geol Soc India 60:317–322

Mandal S, Choudhuri A, Mondal I, Sarkar S, Chakraborty PP, Banerjee S (2019) Revisiting the boundary between the Lower and Upper Vindhyan, Son valley, India. J Earth Sys Sci 128:222. https://doi.org/10.1007/s12040-019-1250-2

McCrory VLC, Walker RG (1986) A storm and tidally influenced prograding shoreline Upper Cretaceous Milk River Formation of southern Alberta, Canada. Sedimentol 33:47–60

Molenaar N, Zijlstra JJP (1997) Differential early diagenetic Low-Mg calcite cementation and rhythmic hardground development in Campanian-Maastrichtian chalk. Sediment Geol 109:261–281

Nagendra R, Bhavani R, Dinakaran V, Reddy AN, Jaiprakash BC (2001) Outcrop sequence stratigraphy of Kallankurichchi Formation of Velliperijnjiyam mine, and its correlation with TANCEM mine, Ariyalur Group, Tamil Nadu. Indian J Petrol Geol 10:23–36

Nagendra R, Kamalak Kannan BV, Sen G, Gilbert H, Bakkiaraj D, Nallapa Reddy A, Jaiprakash BC (2011a) Sequence surfaces and paleobathymetric trends in Albian to Maastrichtian sediments of Ariyalur area, Cauvery Basin, India. Mar Petrol Geol 28:895–905

Nagendra R, Nagarajan R, Bakkiaraj D, Armstrong-Altrin JS (2011b) Depositional and post-depositional setting of Maastrichtian limestone, Ariyalur Group, Cauvery Basin, South India: a geochemical appraisal. Carb Evap 26:127–147

Nagendra R, Raja R, Nallapa Reddy A, Jaiprakash BC, Bhavani R (2002) Outcrop sequence stratigraphy of the Maastrichtian Kallankurichchi Formation, Ariyalur Group, Tamil Nadu. J Geol Soc India 59:243–248

Nagendra R, Nallapa Reddy A (2017) Major geologic events of the Cauvery Basin, India and their correlation with global signatures—a review. J Palaeogeography 6:69–83

Nagendra R, Nallapa Reddy A, Jaiprakash BC, Gilbert H, Zakharov YD, Venkateshwarlu M (2018) Integrated Cretaceous stratigraphy of the Cauvery Basin, South India. Stratigraphy 15:245–259

Nallapa Reddy A, Jaiprakash BC, Rao MV, Chidambaram L, Bhaktavatsala KV (2013) Sequence stratigraphy of Late Cretaceous successions in the Ramnad Sub-basin, Cauvery Basin, India. Geol Soc India Spec Publ 1:78–97

Nøttvedt A, Kreisa RD (1987) Model for the combined-flow origin of hummocky cross-stratification. Geology 15:357–361

Posamentier HW, Jervy MT, Vail PR (1988) Eustatic controls on clastic deposition: I. Conceptual framework. In: Wilgus CK, Hastings BS, Kendall CGStC, Posamentier HW, Ross CA, van Wagoner JC (eds) Sea level changes: an integrated approach. SEPM Spec Publ 42:109–240

Prothero DR, Schwab F (2013) Sedimentary geology: an introduction to sedimentary rocks and stratigraphy, 3rd edn. WH Freeman

Radulović V, Ramamoorthy K (1992) Late Cretaceous (Early Maastrichtian) brachiopods from South India. Senckenb Lethaea 72:77–89

Ramkumar M (1996) Occurrence of hardgrounds in the Kallankurichchi Formation (Lower Maestrichtian), Ariyalur Group, Tiruchy District, South India and their significance. Indian J Petrol Geol 5:83–97

Ramkumar M (1999) Lithostratigraphy, depositional history and constraints on sequence stratigraphy of the Kallankurichchi Formation (Maestrichtian), Ariyalur Group, South India. Geologki Anali Balkanskoga Poluostrva 63:19–42

Ramkumar M (2006) A storm event during the Maastrichtian in the Cauvery basin, south India. Annales Géologiques De La Péninsule Balkanique 67:35–40

Ramkumar M, Stüben D, Berner Z (2004) Lithostratigraphy, depositional history and sea level changes of the Cauvery basin, South India. Annales Géologiques De La Péninsule Balkanique 65:1–27

Reading HG (1996) Sedimentary environments: processes, facies and stratigraphy, 3rd edn. Blackwell Publishing

Sarkar S, Koner A (2020) Ancient rip current records and their implications: an example from the Cretaceous Ukra Member, Kutch, India. J Paleogeogr 9:10. https://doi.org/10.1186/s42501-020-00060-2

Sarkar S, Mazumder R, Bose PK (1999) Changed bedform dynamics: some observations from Proterozoic Chaibasa formation, India. J Indian Ass Sedimentol 18:31–40

Scholle PA (1978) Carbonate rock constituents, textures, cements, and porosities. AAPG Mem 27:1–245

Stoliczka F (1867) Cretaceous fauna of southern India. The Gastropoda. Mem Geol Surv India, Palaeontologia Indica 2:1–500

Stoliczka F (1871) Cretaceous fauna of southern India. The Pelecypoda. Mem Geol Surv India, Palaeontologia Indica 3:1–537

Sundaram R, Henderson RA, Ayyasami K, Stilwell JD (2001) A lithostratigraphic revision and paleoenvironmental assessment of the Cretaceous System exposed in the onshore Cauvery Basin, southern India. Cret Res 22:743–762

Swift DJP, Figueiredo AG, Freeland GL, Oertel GF (1983) Hummocky cross-stratification and megaripples; a geological double standard? J Sed Res 53:1295–1317

Tinterri R (2011) Combined flow sedimentary structures and the genetic link between sigmoidal- and hummocky-cross stratification. GeoActa 10:43–85

Walker RG, Plint AG (1992) Wave- and storm-dominated shallow marine systems. In: Walker RG, James NP (eds) Facies models: response to sea level change. Geol Ass Canada, pp 219–238

Watkinson MP, Hart MB, Joshi A (2007) Cretaceous tectonostratigraphy and the development of the Cauvery Basin, Southern India. Geol Soc London Spec Publ 13:181–191

Wilson JL (2012) Carbonate facies in geologic history. Springer, Berlin

Yang W (2007) Transgressive wave ravinement on an epicontinental shelf as recorded by an Upper Pennsylvanian soil-nodule conglomerate-sandstone unit, Kansas and Oklahoma, U.S.A. Sediment Geol 197:189–205

Litho-Biostratigraphy and Depositional Environment of Albian-Maastrichtian Sedimentary Succession of Cauvery Basin in Ariyalur Area

R. Nagendra and A. Nallapa Reddy

Abstract Cretaceous sequences of the Cauvery Basin serve as an analogue to understand the subsurface successions. In this area, the distribution of hydrocarbon reservoir and source rock facies was profoundly influenced by relative sea level changes amplified by rifting and related tectonic activities. Of particular interest are the outcrop sedimentary strata exposed in and around Ariyalur area of Tamil Nadu that emulate subsurface strata. The first marine transgression close to Aptian/Albian boundary at the western margin of the basin terminates the syn-rift tectonic phase. Two regional tectonic episodes of global significance, driven by the activity of mantle plumes, are well documented in the basin. A major basinal uplift during late Turonian caused by Marion hot mantle plume resulted in widespread subaqueous volcanism in the southern part of the Cauvery Basin. This uplift also led to relative sea level (RSL) fall of about 100 m in Cauvery Basin, in tune with the global sea level fall, and an unconformity of a magnitude of 2.3 Ma. This volcanic episode also resulted in Madagascar detachment from India. The reunion mantle plume that led to Deccan volcanism in central India resulted in the E-SE tilt of the Cauvery Basin during upper Maastrichtian (CF1-CF3 zones). This tilt caused a sea level fall of about 80 m and lateral withdrawal of shoreline by about 50 km developing a major erosional unconformity ranging in the magnitude of ~1.8–30 Ma. The magnitude of the RSL corresponded well with global sea level fall. This sea level fall caused widespread development of canyon features in the Cauvery Basin, resulting in differential subaqueous erosion. The globally significant ocean anoxic events viz. OAE-1b, OAE-1d, OAE-2 and OAE-3 are fairly discernible in the Cauvery Basin. The new isotopic palaeotemperature data suggests that southern India and Madagascar were located apparently in middle latitudes within the tropical-subtropical climatic zone during Albian and early Maastrichtian. The magnitude of hiatus across K-T boundary varying from 0 to 30 Ma is estimated based on planktic foraminifera for subsurface sections.

R. Nagendra (✉) · A. Nallapa Reddy
Department of Geology, Anna University, Chennai 600025, India
e-mail: geonag@gmail.com

A. Nallapa Reddy
CG (Rtd) RGL, ONGC, Chennai 600025, India

The magnetostratigraphy of outcrop sediments reveals 13 magnetozones in the Late Cretaceous sedimentary strata.

Keywords Cauvery basin · Cretaceous · Geological events · Ariyalur · Paleogeogeography · Biostratigraphy · Magnetostratigraphy

1 Introduction

The pericratonic Cauvery Basin, located along the south-eastern coast of India, developed during the breakup of Gondwana in the Late Jurassic-Early Cretaceous (Rangaraju et al. 1993; Nagendra et al. 2018). This basin records four major tectonic phases during its evolution including (1) an early sheared rift extensional faulting that initiated during Late Jurassic/Early Cretaceous, (2) end-phase rifting that established during the late Aptian and which resulted in a marine transgression (Reddy et al. 2013), (3) late Turonian basinal uplift caused by the Marion plume activity (Raju et al. 2005) resulted in widespread volcanic intrusions in the southern part of the basin that was linked to the separation of Madagascar from India, and (4) major eastward tilt of the basin was linked to the Deccan volcanic rise in central India and which led to a major sea level fall and lateral withdrawal of the sea by about 50 km (Raju et al. 1993). These major tectonic events profoundly influenced relative sea level changes and the distribution of hydrocarbon reservoirs and source rock facies in the Cauvery Basin (Reddy et al. 2013). Over the past four decades, the Cauvery Basin has been the center of exploration activities for limestone in Tamil Nadu where Cretaceous sediments are exposed in isolated outcrops, mines, and quarries exposed along the western margin of the Archaean basement. Drilling of exploratory deep wells revealed nearly 7 km thick sedimentary successions ranging in age from Late Jurassic to Recent, with two-thirds deposited in the Cretaceous. Inland outcrops, late Aptian through Maastrichtian marine deposits, are divided into the Kovandankurichi Formation, Terani Formation, and the Uttatur, Trichinopoly, and Ariyalur Groups (Fig. 1). Low-angle unconformities and conglomerate beds mark interruptions in sediment deposition (Nagendra et al. 2011). The lithostratigraphic framework and geologic history of the Cauvery Basin based on the integration of published research, including biostratigraphy, magnetostratigraphy and sequence stratigraphic records. In addition, we aim to standardize the various stratigraphic classifications with updated nomenclatures and link currently disparate surface and subsurface data through age and paleo-environmental correlations. The results have applications for petroleum exploration in the Cauvery Basin as well as for academic research and future investigations of yet unexplored hydrocarbon deposits.

2 Rifting Process and Basin Evolution

The initiation of the Cauvery Basin along the eastern passive margin of India and consequent sedimentation relates to the fragmentation of eastern Gondwana and opening up of the Indian Ocean, which began in Late Jurassic (~160 Ma ago)
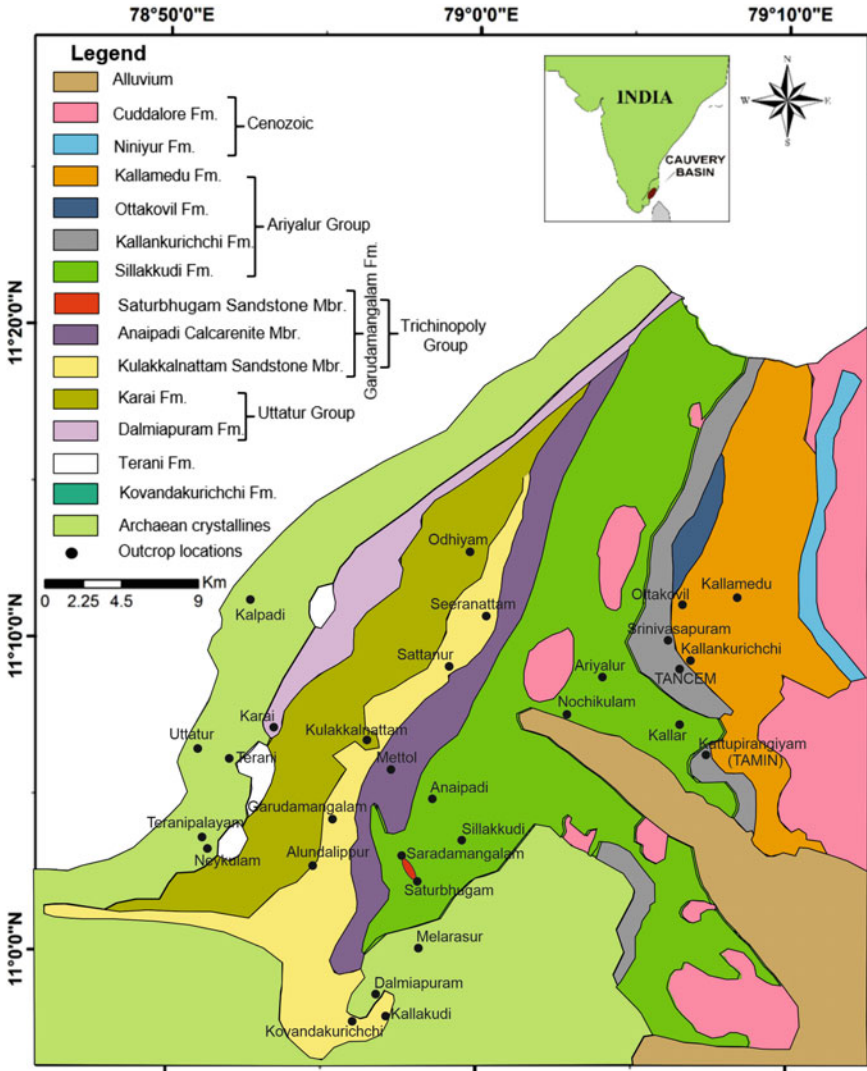
Fig. 1 Geological map showing outcrops of Cretaceous formations of the Cauvery Basin around Ariyalur area, south India

(Rangaraju et al. 1993). The early sheared rift extensional faulting initiated during Late Jurassic/Early Cretaceous (Scotese 1997), and was followed by a progressive rift that seems to have continued until the end of the Turonian (Watkinson et al. 2007). The end of the syn-rift phase in Lower Cretaceous (late Aptian 112 Ma) is inferred primarily on the basis of chronology of various events, the breakup unconformity and first marine transgression at the western basin margin (Reddy et al. 2013).

The Cauvery Basin consists of six half-graben blocks trending in NE-SW separated by horsts. The exposed Cretaceous system of the Cauvery Basin consists of a complete marine sequence, rich in faunal assemblages ranging from Albian to Maastrichtian. The non-marine syn-rift sediments are represented by four isolated outcrops (Teranipalyam, Kalpadi, Neykulam and Terani) along the western margin of the Ariyalur area. The Archaean basement is characterized by structural highs and lows, evidenced by strong tectonic activity affecting the basin since its inception. Four major tectonic and sedimentary phases are recorded. (1) The first is taphrogenic rifting and associated block movement along the dominant NE-SW trend during Upper Jurassic-Lower Cretaceous, resulting in morphotectonic humps and deep slopes. (2) Post-rift thermal subsidence during Albian to Maastrichtian led to deepening of the basin, accommodating thick marine carbonates and clastics. A significant uplift caused by Marion hot mantle plume ca. 88–90 Ma, resulted in widespread volcanism in the southern part of the Cauvery Basin. The detachment of Madagascar from India is also linked to this volcanic episode (Keller et al. 2016). Post uplift event, subsidence rate rapidly increased and basin experienced deep marine conditions. (3) Eastward and southeastward tilt of the basin during late Maastrichtian-Paleocene and resultant relative sea level fall due to Deccan volcanism (67.4–65.3 Ma) caused by reunion hot mantle plume, and as a result sediment depocentres migrated basin wards, filling the canyon features developed consequent to the relative sea level fall. (4) The last phase, spanning Eocene to Miocene, signifies coastal progradations/deltaic sedimentation through a series of marine transgression and regressions in response to the oscillatory tectonic movements. Watkinson et al. (2007) revealed that continental lacustrine and alluvial sediments, classified as basal siliciclastic (Chakraborty et al. 2017) were deposited during rift-related extension in the Cauvery Basin. The continued extension facilitated the inundation of marine waters into the most landward parts of the Cauvery Basin. Watkinson et al. (2007) considered that the terminal point of rift-related extension in the mid-Turonian marks the end of syn-rift stage, and the main subsidence mechanism after this was dominantly thermal re-equilibration of the lithosphere. However, we feel that the Turonian uplift of the basin cannot be related to rift tectonics, as the entire basin was under deep marine conditions at the time of the rise of Marion hot mantle plume (Courtillot et al. 1988; Raju et al. 1994; Reddy et al. 2013). Lambiase (1990) considered two approaches for marking the terminal syn-rift in passive margin basins viz. (1) end of major rift tectonics and (2) end of continental/fluvial sediment deposition. Therefore, we prefer to adopt the second approach to marking syn-rift top in the Cauvery Basin. The facies transition between fluvial and marine deposition can be observed in the uppermost Terani Formation exposed in Neykulam quarry. The marine sediments yielded planktic foraminifera *Hedbergella trocoidea*, *Hedbergella planispira*, *Hedbergella delrioensis,* and broken ammonite fossils, suggesting late Aptian to Early Albian, indicating that the top of syn-rift fill is close to Aptian/Albian boundary (Reddy et al. 2013). In the Cauvery Basin, the syn-rift fill can be subdivided based on lithological content into early syn-rift phase, which is predominantly fluvial and lacustrine deposits and late syn-rift phase consisting of shelf carbonates and marine shale (Reddy et al. 2013).

The east coast basins of India, mainly the Cauvery and Krishna-Godavari basins, are comparable with central European basins, such as the Danish, North German and North Sea basins and the northern Gulf of Mexico, because of the similarity in their tectonic evolution, stratigraphy and sea level trends (Nagendra et al. 2011). The sedimentary units of the Cauvery Basin are similar to those of the central European basins. However, central European basins experienced compression tectonics during the Late Cretaceous (Santonian-Maastrichtian), while the Cauvery Basin remained a passive margin basin throughout.

3 Lithostratigraphy

Lithostratigraphy orders layers of different rocks into easily identifiable units that can be regionally correlated and reflect the same or similar depositional environments, such as beds of shale, sands, limestones or conglomerates that can be traced over some geographic distance. However, lithostratigraphic units are time transgressive as they reflect specific depositional environments and cannot be used for age correlation, except in the broadest sense (e.g. Lower, Middle and Upper Cretaceous or substages). Blanford (1862) published the first lithostratigraphic study of the Cauvery Basin. Between 1943 and 1990s a series of publications concentrated on outcrops and sections exposed by mining (e.g. Banerji 1982; Krishnan 1943; Ramanathan 1968; Nair 1974; Sastri et al. 1963, 1977; Ramasamy and Banerji 1991; Sundaram and Rao 1979, 1986; Tewari et al. 1996a). Through this time, authors modified earlier stratigraphic framework studies. During the past 15 years, the authors re-investigated all available mines, quarries and outcrop sections to integrate and developed a comprehensive lithostratigraphic and biostratigraphic scheme (Tables 1a, 1b).

3.1 Kovandankurichi Formation

The informally labeled Kovandankurichi Conglomerate Member of Tewari et al. (1996b) is raised to formation status by Nagendra et al. (2018) and renamed the Kovandankurichi Formation (Table 1b) following the guidelines of the International Stratigraphic Guide (Murphy and Salvador 1999). The Kovandankurichi Formation is the oldest (possibly Berriasian) sedimentary unit of the Cretaceous system in and around Ariyalur, where it reaches a thickness of 175 m (Sundaram et al. 2001; Table 1b) and has a mappable extent. This Formation is named after Kovandankurichi Village and is best exposed at its type section in the Kovandankurichi Quarry II where it overlies basement rocks (Sundaram and Rao 1986) (Fig. 2). The Kovandankurichi is a conglomerate with inversely graded fanglomerate features. The clasts comprise buff-coloured feldspar, sub-angular to sub-rounded quartz, boulders, cobbles and

Table 1a Lithostratigraphic classifications of the Cretaceous succession of Cauvery Basin in Ariyalur area by different workers

Blanford (1862)	Krishnan (1943)			Ramanathan (1968)							Nair (1974)				Sundaram and Rao (1979)			
	Age	Stage	Description of fossil	Era	Period	Epoch	Age	Formation	Approx. Thickness (m)	Lithostratigraphy	Series	Stages	Group	Formation	Age	Group	Formation	Unit
Trichinopoly Group — Sandy clays and shale with infiltered Kankar and sands of shell limestone	Maastrichtian to Danian	Niniyur	White sandy limestones and sandstones with *Nautilus danicus, Lyria formosa, codakia percrassa, Stylina parvula*.	Cretaceous			Neocomian to Albian (Time Transgressive)	Trichinopoly	600	Calcareous, coarse grained conglomerates, gritty sandstone with bands of sandy limestone, yellowish brown clays towards north alternating bands of shell limestone and conglomeratic sandstone in the lower part and shell limestones, argillaceous limestones & sandy clays in the upper part, known only in outcrops.	Maastrichtian	Ariyalur		Kallamedu Sandstone	Ariyalur		Kallamedu	Sandstone
		Ariyalur	Upper: Strata containing *Siderolites and Lepidorbitoides*			Turonian to Upper Senonian								Kallankurichi			Kallankurichi	Limestone with fossils
	Senonian		Lower: Pale sands and clays with *Pachydiscus egertoini, P. Otacodersis, Brahmaites brahma, Baculites vagina Rostellaria palliata, Macrodon japeticum, Gryphaea vesicularis, Alectryonia ungalata, Stigmatophygus elatus*							Greenish grey to yellowish brown gypseous clays with thin fossiliferous argillaceous limestone bands in the south and gypseous clays, argillaceous limestones and fossiliferous coarse conglomerates towards north.	Upper Cretaceous	Campanian	Upper Cretaceous / Trichinopoly	Sillakkudi			Sillakkudi	Fossiliferous sandstone
									700			Santonian		Trichinopoly			Anaipadi	Upper sandstone dominant
												Coniacian		Paravay			Kulakkalnattam	Lower shale dominant
Uttatur Group — Fine silts, calcareous shales and sandy clays frequently concretionary tinted with ocherous matter. Limestone bands in the lower part and grit in the upper part including coral reef at its base.	Turonian	Trichinopoly	Upper: Sandstones, clay with *Placenticenus tamulicum, Schloenbachia dravidica, Heteroceras indicum, Fasciolaria rigida*.				Neocomian to Albian (Time Transgressive)	Uttatur		Argillaceous to arenaceous limestone interbedded with yellowish brown marl & succeeded by bedded argillaceous coral rag limestone marls, clays of fore reef facies known in outcrops near Dalmiapuram and along western margin at the basin (M) met with in subcrops in Pattukota well black carbonaceous shale at the base.	Lower Cretaceous	Turonian		Maruvattur clay				Southern Uttatur clay
			Lower: Sandstones, clays and shell limestone with *Pachydiscus peramplus, Schloenbachia (Prionocyclus) serraticarinatus, Trigonia trichinopolitensis, Protocardium hillanum*.									Cenomanian	? Uttatur	Kullakkudi Limestone			Nothern section / Kunnam / Odhiyam / Maruvattur	
	Upper most Albian to Cenomanian	Uttatur	Upper: Sandy beds with *Mammites conciliatus, Acanthoceras newboldi, Nautilus huxleyanus*.			Upper Jurassic to Cretaceous	Bathonian to Neocomian	Upper Gondwana	400	Ferruginous sandstone friable with clayey micaceous sandstone & soft grey clays in the northern part, boulder beds interbedded with ferruginous grit and clays in the south near Sivaganga.		Albian		Karai shale			Upper Gondwana	
Uttatur plant beds			Middle: Clays with *Acanthoceras cf. coleroonense, Turrilites costatus, Alectryonia carinata*.										Upper Jurassic to Aptian	Upper Gondwana	Lower Cretaceous? Upper Jurassic?		Upper Gondwana	
			Lower: Basalt, limestone and coal rag with clays above with *Turrilites bergeri, Schloenbachla inflata, Stoliczkaia dispar, Belemnites and Hamites armatus*.	Azoic			Precambrian			Granite gneiss, banded gneiss charnockite, pegmatites, dunites, cryztalline limestone, cordierite garnet, sillimanite gneisses.		Archaean			Precambrian		Charnockite	

pebbles derived from Archean Gneiss (Govindan et al. 1998). The Terani Formation unconformably overlies the Kovandankurichi Formation.

Table 1b Lithostratigraphic classifications of the Cretaceous succession of Cauvery Basin in Ariyalur area

Sastri et al. (1977)			Sundaram & Rao (1986)		Banerji (1982); Ramasamy & Banerji (1991)	Tewari et al. (1996a)			This study			
Age	Formation	Lithology				Group	Formation	Member	Stage	Group	Formation	Member
Late Cretaceous	Upper Ariyalur	Cross-bedded, friable sandstone near base. Greenish-purple sandstone intercalated with claystone and biostromal limestone	Kallamedu Sandstone Formation	Kallamedu Member	Ariyalur Formation	Ariyalur	Kallamedu	Ottakovil Sandstone	Maastrichtian	Ariyalur	Kallamedu Formation (200 m)*	
				Ottakovil Member				Dherani Sandstone			Ottakovil Formation (200m)*	
			Kallankurichchi Formation				Kallankurichchi	Dalmia Biostromal limestone			Kallankurichchi (44 m)*	Upper arenaceous limestone
				Upper Sandstone Member				TANCEM Limestone				Gryphaea limestone
			Sillakkudi Formation / Lower Limestone Member				Sillakkudi	Sandstone Member				Lower arenaceous limestone
								Killi paluvar / Member Grainstone				Ferruginous limestone
												Kallar Conglomerate
	Lower Ariyalur	Lower part-variegated clayey sandstone, conglomerate, siltstone Middle part-fossiliferous calcareous limestone Top part-argillaceous fossiliferous limestone.	The lower bedsof upper Sandstone Member in the Malway Saradamangalam section		Break in marine sedimentation not recognised	Garudamangalam		Fluvial sandstone & silty sandstone with feldspar pebbles not given a formal name	Campanian	Trichinopoly	Sillakkudi Formation (60 m)*	
					Kulattur Member		Garudamangalam	Anaipadi Sandstone	Coniacian- Santonian		Garudamangalam	Saturbhugam Sandstone
	Trichinopoly	Calcareous-gritty and conglomeratic sandstone with sandy limestone bands, gypseous claystone alternating bands of shelly limestone and conglomeratic limestone in lower part.	Anaipadi Formation		Anaipadi Member							Anaipadi Calcarenite (246m)*
			Kulakkalnattam Formation		Kottarai Member			Kulakkalnattam Sandstone				Kulakkalnattam Sandstone
			Karai Formation		Lower clay Member		Karai					Maruvattur Claystone
	Uttatur	Greenish-grey to yellowish-brown gypseous claystone and thin fossiliferous limestone, gypseous claystone, coarse conglomerate and argillaceous limestone.			Upper sandy clay Member	Uttatur		Odhiyam Sandstone	Late Albian-Middle Turonian	Uttatur	Dalmiapuram (236 m)*	Marl (ML) / Odhiyam Sandstone
			Kunnam & Odhiyam Member									Karai Formation (410m)*
Early Cretaceous	Dalmiapuram	Reefoidal limestone and black shale; in subsurface, Lower Cretaceous sequence consists of shale, sandstone and minor limestone.	Upper limestone, marl and clay Member	Not recognised	Recognised in part as lower clay Member	Dalmiapuram	Dalmiapuram	Kallakudi Siltstone				Marl bedded limestone (MBL)
					Upper limestone Member			Kallakudi Sandstone				
			Lower conglomerate Member (part)					Dalmiapuram Limestone				Coral limestone (CAL)
			Middle grey shale Member		Lower grey shale Member			Grey siltstone				
	Sivaganga Upper Gondwana	Coarse-gritty & pebbly sandstone	Not recognised		Upper clay & sandstone Member	Gondwana	Sivaganga	Kovandankurichchi Siltstone	Neocomian		Terani (60)*	Terani gritty ferrruginous sandstone / Terani claystone with sandstone intercalation
			Lower conglomerate Member (Part)		Lower conglomerate Member			Kovandankurichchi Conglomerate			Kovandankurichchi Formation (175m)*	
Archaean		Granite, gneiss and other metamorphic rocks					Archaean		Archaean		Gneisses, charnockite and granulites	

Fig. 2 Lithology, magnetic polarity, depositional environment and sequence stratigraphic elements across the Cretaceous succession of Cauvery Basin in Ariyalur area

3.2 Terani Formation

The Barremian-Aptian Terani Formation is about 60 m thick and is well-exposed in the Terani Clay Mine located near Karai Village (Ramasamy and Banerji 1991) (Fig. 1, Table 1b). The Terani Formation underlies the Dalmiapuram Formation, with an unconformable contact between the two. The Terani Formation consists of two members: The Terani Claystone Member with sandstone intercalations at the base, and the Terani Gritty Ferruginous Sandstone Member at the top. These sediments consist of quartzose and feldspathic, gritty and ferruginous sandstones with intercalated claystones (Tables 1a, 1b). The sandstone contains pebbles and

boulders of igneous (gneiss) rock. The Terani Claystone Member contains rare and poorly preserved plant fossils of *Ptilophyllum acutifolium.* Whereas the shale and clay layers of the Terani Gritty Ferruginous Sandstone Member contain planktic foraminifera *Hedbergella trocoidea, H. planispira* and *H. delrioensis*, and ammonites in Neykulam quarry, indicating Late Aptian-Early Albian age (Reddy et al. 2013; Nagendra et al. 2018).

3.3　Uttatur Group

The Uttatur Group consists of the Dalmiapuram and Karai formations, which are time equivalent but lithologically dissimilar (Tables 1a, 1b). These two formations were deposited during the Albian through middle Turonian (Chiplonkar 1985; Raju et al. 1993) and overlie the Terani Formation. These two formations are unconformably overlain by Garudamangalam Formation of the Trichinopoly Group. The geology and stratigraphy of the Dalmiapuram region have been studied by many researchers (Gowda 1964; Rama Rao 1956; Sundaram and Rao 1979; Ramasamy and Banerji 1991), who separated the Dalmiapuram Formation into three members: Coral Algal Limestone (CAL), Marl Bedded Limestone (MBL), and Marl Member (ML) in ascending order. These sedimentary facies developed during syn-sedimentary tectonics within the Dalmiapuram Formation (Chakraborty and Sarkar 2018). The Karai Formation consists of variegated shales associated with gypsum veins, phosphatic nodules and abundant belemnite guards. Phosphatic nodules, locally known as "Uttatur potatoes", are normally encased in chalky surfaces. The lateral facies equivalent of the upper Karai Formation is known as the Odhiyam Sandstone and Maruvattur Claystone Members exposed at Odhiyam and Maruvattur respectively (Figs. 1 and 3).

3.4　Trichinopoly Group

The Trichinopoly Group consists of the Garudamangalam Formation in the Ariyalur area. The contact between the Garudamangalam and overlying Sillakkudi Formation is unconformable. Sundaram et al. (2001) and Tewari et al. (1996a) divided the Garudamangalam Formation into three members: Kulakkalnattam Sandstone, Anaipadi Calcarenite and Saturbhugam Sandstone Member in ascending order of succession (Tables 1a, 1b). The Kulakkalnattam Sandstone Member is extensively burrowed by *Skolithos, Ophiomorpha,* and *Thalassinoides.* The Anaipadi Calcarenite Member consists of concretionary siltstone, mudstone and fine-grained micaceous sandstone in the lower part and well-sorted calcareous medium to coarse sandstone in the upper part with scattered bivalves and sporadic lenticular interbeds of sandy coquina (Sundaram et al. 2001). Fossil wood concretions are common

Fig. 3 Field photographs showing Boulder bed; the oldest sedimentary sequence Kovandankurichi Formation overlying the basement, VP mine **a** Terani clay-plant beds, Terani Formation continental origin **b** Contact between basement rock (below) and Coral algal limestone **c** Kulakkalnattam Sandstone contact with Karai Shale (below), Garudamangalam Formation **d** Bedded marl with intercalations of grey shale, VP mine, Dalmiapuram Formation **e** (hammer length in a and e = 38 cm; pen length in d = 14.5 cm; outcrop height in Fig. b = 2.2 m; men for scale in **c**

in stream channel outcrops near Saturbhugam. The overlying Saturbhugam Sandstone Member consists of fluvial sandstones and silty sandstones with re-worked pebbles and cobbles (Sundaram and Rao 1986). Large-scale trough cross-bedding (less than 3 m thick) in the sandstone member is indicative of a fluvial channel fill. To the northeast and down-dip, the Kulakkalnattam Sandstone laterally grades into the Anaipadi Calcarenite facies. Four facies associations are identified in the Garudamangalam Formation by Sarkar et al. (2014). These facies associations with genetically different components indicate deposition occurred in the nearshore zone (Sarkar et al. 2014). Chakraborty et al. (2018a) reported instances of excessive depletion of $d^{13}C$ in carbonate cement within the calcareous Garudamangalam Sandstone Formation (Fig. 3).

3.5 *Ariyalur Group*

The Ariyalur Group is represented by the Sillakkudi, Kallankurichchi, Ottakovil, and Kallamedu formations in ascending stratigraphic order (Sundaram and Rao 1986) (Table 1b). At the base, the Sillakkudi Formation is dominated by sandstones that are well exposed in the Mettol and Nochikulam areas (Fig. 1). Sedimentological studies indicate that the sandstones are mineralogically and texturally immature and poorly sorted. An abundance of feldspar, especially plagioclase, indicates rapid deposition from a nearby granite/gneiss source. The Sillakkudi Formation is characterized by clastic sediments with a carbonate fraction in the Kilpalvur area. The sediments consist of off-white to buff-coloured, coarse-grained, texturally immature, poorly sorted, friable to hard sandstone with occasional calcareous cement. The presence of glauconitic pellets in the sandstones suggests deposition during a transgressive episode at paleo water depths of 30–60 m (Nagendra et al. 2001). The presence of angular grains indicates transport was from a nearby source (Nagendra et al. 2001). The Sillakkudi sandstone underlies the Kallar Conglomerate Member, which is exposed in stream sections near Kallar and in the Dalmia mine section (Figs. 1 and 2). Orange to yellow pebbles with abundant sub-angular to angular, pink to white pebbles and cobbles characterize the conglomerate bed, which is non-calcareous and indicative of sub-aerial deposition that marks a hiatus during the late Campanian. The Kallar Conglomerate is considered to be the upper member of the Sillakkudi Formation.

The Kallankurichchi Formation and its three members are characterized by marine carbonates and conformably overlie the Sillakkudi Formation (Fig. 2). The lowermost Ferruginous Limestone (FL) Member consists of fine- to medium-grained massive biomicrite, rich in benthic foraminifera. Above the FL Member is the Lower Arenaceous Limestone (LAL) Member marked by yellowish, massive, compact limestone rich in silica. Overlying the LAL is the *Gryphaea* Limestone (GL) Member, identified by its reddish-brown color and fine to medium-grained carbonate. At the top is the Upper Arenaceous Limestone (UAL) Member, marked by a high terrigenous influx. The Ottakovil Formation contains mollusks, bryozoans and rare burrows. The lower contact with the Kallankurichi Formation is conformable, whereas the upper contact with the overlying Kallamedu Formation is unconformable. The Kallamedu Formation contains cross-bedded sandstones indicative of fluvial channel deposits that mark the end of the Cretaceous in the Ariyalur area (Nagendra et al. 2002) (Fig. 4).

4 Biostratigraphy and Paleoenvironment

Biostratigraphy is based on fossils present in rock layers and sediments and is the most commonly used method for relative age dating in geological studies. Age control is based on short-lived species, evolution and extinction (first and last appearances)

Fig. 4 Field photographs showing Karai Shale (left) and Oyster bed (right) (**a**), *Thalassinoides* trace fossil on Kulakkalnattam Sandstone (**b**), A 18 m long trunk of petrified conifer tree trunk, Sattanur within Trichinopoly Group (**c**), *Placentice tamulicum* Ammonite exposure at Karumbayam village (**d**), Coquina bed in Anaipadi Calcarenite (**e**), Sandstone outcrop, Ottakovil Fm. (**g**), Fluvial sandstone exposure of Kallamedu Fm. (hammer length = 38 cm, pen length = 14 cm)

that are unique bio-events with proven coeval regional and/or global occurrences. Biostratigraphy thus provides reliable relative age control in any environment globally, independent of the nature of sediment deposition or paleo-environment. In this study, biostratigraphic age control is based on both macro and microfossils, including ammonites, belemnites, brachiopods, mollusks, calcareous nannofossils and foraminifera. These fossils also provide information on paleo-environment (e.g., near-shore, shelf, slope, and deep) and paleoecology (e.g., warm, cool, oxic, dysoxic, anoxic, degree of salinity etc.) (Saraswati and Srinivasan 2016).

The oldest lithostratigraphic unit, the Kovandankurichi Formation, is devoid of fauna and flora, and thus age dating is unavailable. *Ptilophyllum acutifolium,* a plant fossil of Barremian–Aptian age, is reported from a shale horizon of the Terani Formation (Mamgain et al. 1973; Venkatarengan et al. 1993; Sundaram et al. 2001). The upper sandstone member of the Terani Formation yielded planktic foraminifera, including *Hedbergella trocoidea, H. planispira* and *H. delrioensis*, suggestive of a late Aptian-early Albian age (Reddy et al. 2013). The occurrence of planktic

foraminifera and ammonite fragments marks the first marine transgression in the basin margin (Table 2). The presence of poorly preserved, low diversity foraminifera in the Terani Formation suggests brackish, low salinity waters indicative of estuary to restricted bay environments. It is also possible that the low salinity waters may have resulted from tidal wave incursions into a freshwater basin. Based on the planktic foraminiferal assemblages, an Early Cretaceous (Late Aptian-Early Albian) age is assigned to the Terani Gritty Ferruginous Sandstone Member (Fig. 2).

The lower Coral Algal Limestone Member of the Dalmiapuram Formation, Uttatur Group, is rich in algae and contains *Parachaetetes asvapattii, Sporolithon* sp., *Lithothamnion* sp., *Lithophyllum* sp*., Pseudoamphiroa propria, Neomeris cretaceae,*

Table 2 Lithological description and depositional environment of the Cretaceous succession of Ariyalur area, Cauvery Basin

Ma	Stratigraphic Group/ Formation/ Member		Lithological description	Biota	Depositional environment
66.0		Kallamedu Formation (300 m) +	Thick sandstone, inter-bedded with sandy claystone, sands are white to grey, friable fine- to medium- grained, moderately to well-sorted, well-preserved, cross bedding structure.	Dinosaurian femur bones- *Titanosaurus*. Gonoid fishes, amphibians, turtles, crocodiles.	Fluvial
	ARIYALUR GROUP / Kallankurechchi Formation (44 m)*	Ottakovil Formation (60 m) +	White grey to pale yellowish, medium-to coarse-grained sandstone with calcite cement.	Echinoids, *Stigmatopygus, Lopha, Ichnofossil- Thalassinoides*. Calcareous nannoplankton- *Arkhangelskiella cymbiformis, Broarodosphaera bigelowii, Ceratolithus acudeus,Chiastozygus litterarius, Cyclagelosphaera deflandrei, Cribrosphaerella chrengergii, Cribrosphaera* sp.*, Eiffelithus gorkae, E. parallelus, E. turriseiffeli, Microrhabdulus unodasus, Macula decussata, M. staurophora, M. swastika, Petrobrasiella? Bownii Prediscosphaera cretacea, P. spinosa, Stradneria cremulata, Staurolithites crux, Zygodiscus minimus* and *Z.spiralis*	Marginal marine to upper shoreface
		Upper arenaceous limestone (UAL)	Poor in both macro and microfossils with rich terrigenous input.	Bivalves, *Terebratula,Gavelinella plummerae, Cibicides* sp., *Orbitoides* spp.,	Middle neritic
		Gryphaea limestone (GL)	Reddish fine- to medium-grained, massive, rich in lime content. *Gryphaea, Alectryonia* and *Exogyra* are abundant.	Bryozoa, rudist bivalves, *Terebratula, Gryphaea*, ammonites, inoceramids. Foraminifera- *Lepidorbitoids,Siderolites, Lingulogavelinella Cibicide* sp., *Gavelinella plummerae, Osangularia* sp.,*Cibicides harperi, Gavelinella* spp., *Textularia.* sp.,	
		Lower arenaceous limestone (LAL)	Yellowish, massive, highly compacted, rich in silica content, associated with microfossils.	Inoceramids, ammonites, *Terebratula, Bryozoa-Onychocellid* & *Rectoporina kulumerensis.*Bivalves- *Pecten sarumensis, Schloenbachia.* Foraminifera- *Cibicides* sp. *Lingulogavelinella, Gavelinopsis bembix, Osangularia* sp.,*Textularia* sp., *Gavelinella plummerae, Gyroidinoides* sp.,	
72.1		Ferruginous limestone (FL)	Fine- to medium-grained, massive biomicrite.	*Gavelinopsis.*sp. *Quinqueloculina* sp., *Cibicides* sp., *Gavelinella danica, Gavelinella* spp. *Gavelinopsis bembix,Gyroidinoides* sp., *Alabaminia dorsoplana, Gavelinella plummerae, Gryphaea, Lopha.*	
		Kallar Conglomerate	Conglomerates-unconformity surface.		
83.6	TRICHINOPOLY GROUP / Garudamangalam Fm.	Sillakkudi Formation (600 m)	White buff color, medium- to coarse grained sandstone, poorly-sorted, friable to hard, calcareous.	Gastropod shells, ammonites-*Kossmaticeras theobaldinum* and *Placenticeras tamulicum.* Foraminifera *Bolivinoides decorates.* Ichnofossils-*Skolithos, Ophiomorpha* and *Thalassinoides.*	Continental Middle shelf conditions below wave Forming part of transgressive episode
		Saturbhugam Sandstone	Coarse-grained reddish white sandstone with well preserved current bedding structures-fluvial sandstone	—	Fluvial
91.1		Anaipadi Calcarenite (264 m)*	Sandstone with of wood fragments, gastropods shells and ferruginous calcareous sandstone. Silty concretion.	Gastropod shells and ammonites such as *Kossmaticeras theobaldianum* and *Placenticeras tamulicum*	Middle neritic
		Kulakkalnattam Sandstone (230 m)*	Fine- to coarse-grained, sandstone, texturally immature poorly sorted, enriched in calcite cement.	*Skolithos, Ophiomorpha, Thalassinoides horizontalis, Thalassinoides suevicus, Planolites beverlyensis* and *Palaeophycus tubularis.*	Foreshore -Estuarine to inter tidal flat
	UTTATUR GROUP / Dalmiapuram Formation (236 m) *	Marl (ML) / Karai Formation (410 m)+	Yellow in colour, compact,friable, massive and highly ferruginised. The fabric resembles that of wackestone. MC-Claystone OS-Sandstone with glauconite and gypsum Shale- Gypsiferous mudstone, shale claystone and siltstone with phosphatic nodules.	*Praeglobo-truncana delri-oensis* and *P. Stephani, Anomalinoides, Gavelinella plummerae, Gyroidinoides globosa, Lenticulina* and *Quadrimorphina.* Belemnites, ammonites and worm tubes. *Rotalipora, Preaglobotruncana, Whiteinella* and *Hedbergella, Planomalina buxtorfi, Rotalipora reicheli, Praeglobotruncana stephani,* and *Hedbergella portsdownensis*	Deep shelf / Outer neritic zone
		Marl bedded limestone (MBL)	Cyclic deposition of limestone/marl. White to greyish brown in color. Grey todark grey, poorly fissile, silty, calcareous shale with mica, pyrite, smectite clay.	*Acanthoceras* sp., *Mammites concilianus, Nautilus huxleyanus* and *Turrilites costatus,* Foraminifera- *Rotalipora gandolfi, Rotalipora brotzeni,Praeglobotruncana stephani, P. delrioensis,Hedbergella planispira* and *Globigerinelloides benoensis* and Dinoflagellate Cysts- *Odontochitina costata, Epelidosphaeridia spinosa, Cyclonephelium* cf. *C. vannophorum,Dioxya* sp., *Kiokansium snituberculatum, Ovoidinium verrucosum* and *Batioladinium micropodium.*	Deep shelf
113		Coral algal limestone (CAL)	Massively bedded, hard, compact, variegated coral reefoidal limestone with pink to flesh red color giving a mottled appearances, dissolution vugs and cavity.	Algae- *Parachaetetes asvapattii, Sporolithon* sp., *Lithothamnion* sp., *Lithophyllum* sp.*,Pseudoamphiroa propria, Neomeris cretaceae* and *Agardioliopsis cretaceae.* Bryozoans, coral fragments and foraminifera.	Shallow marine
	Terani Formation (60 m)+	Terani gritty ferruginous sandstone	Coarse gritty sandstone- quartzwacke to lithic graywacke.	*Hedbergella trochoidea, H. planispira, H. delrioensis*	Littoral
		Terani Claystone with sandstone intercalations	Claystone (kaolinite) with intervening medium to coarse-grained friable, ferruginous sandstone.	*Ptilophyllum acutifolium*	Fluvial to lacustrine
	Kovandankurichchi Formation (175 m)*		Boulder conglomerates / fanglomerate.	—	Continental/ fluvial
	Gneisses, charnockite and granulites		Gneiss, charnokites, granulites.		Plutonic

Salpingoporella verticelata and *Agardioliopsis cretaceae,* which are indicative of an Albian age (Mishra et al. 2004) (Table 2). In addition, bryozoans, rare coral fragments and foraminifera are present (Mishra et al. 2004). Marine cephalopods, such as *Acanthoceras* sp., *Mammites conciliatus*, *Nautilus huxleyanus* and *Turrilites costatus,* are abundant in the Marl Bedded Limestone Member (Kossmat 1897; Govindan et al. 1998). The basal part of the Marl Bedded Limestone Member contains lenticular grey shale layers immediately overlying the Coral Algal Limestone. The age of the gray shale is well constrained based on planktic foraminifera and dinoflagellates. The latest Albian age is indicated for the gray shale of the Kallakkudi mine based on dinoflagellate index species *Odontochitina costata, Epelidosphaeridia spinosa, Cyclonephelium* cf. *C. vannophorum, Dioxya* sp.*, Kiokansium unituberculatum, Ovoidinium verrucosum* and *Batioladinium micropodium* (Nagendra et al. 2002) (Table 2). A latest Albian age is also indicated by moderately well-preserved planktic foraminiferal index taxa, including *Rotalipora gandolfi, Rotalipora brotzeni, Praeglobotruncana stephani, P. delrioensis, Hedbergella planispira* and *Globigerinelloides bentonensis* (Caron 1985) and corroborates the age assigned based on dinoflagellates (Nagendra et al. 2002, 2013).

The lower part of the Marl Bedded Limestone yielded the planktic foraminiferal index species *Rotalipora reicheli.* In contrast, the upper part of the Marl Limestone Member contains index species *Praeglobotruncana delrioensis* and *P. stephani*, which suggests a Cenomanian to mid-Turonian age (Table 2). The benthic foraminifera *Anomalinoides, Gavelinella plummerae, Gyroidinoides globosa*, *Lenticulina,* and *Quadrimorphina* are common in both the Marl Bedded Limestone and the Marl Limestone member. Similar foraminiferal assemblages of *Rotalipora, Preaglobotruncana, Whiteinella* and *Hedbergella* (Govindan et al. 1996) are documented from the Karai Formation, in addition to belemnites, ammonites and worm tubes. The presence of the planktic foraminifera *Planomalina buxtorfi*, *Rotalipora reicheli*, *Praeglobotruncana stephani*, and *Hedbergella portsdownensis* (Nagendra et al. 2013) suggests a late Albian to middle Turonian age. Ferruginous material infills the chambers of the foraminifers and other fossils tests in the mudstone-wackestone facies of the lithostratigraphic units in the Dalmiapuram Formation. This suggests sediment deposition occurred in a low energy environment marked by diagenetic alteration (Nagendra et al. 2002).

The Kulakkalnattam Sandstone of the Garudamangalam Formation, Trichinopoly Group, contains characteristic ichnofossils, such as *Skolithos, Ophiomorpha* and *Thalassinoides* (Table 2). The Anaipadi Calcarenite Member contains abundant gastropod shells and ammonites, such as *Kossmaticeras theobaldianum* and *Placenticeras tamulicum,* which indicate a Coniacian-Santonian age (Ayyasami and Jagannatha Rao 1978). The overlying Sillakkudi Formation, Ariyalur Group, includes inoceramids and gastropod shells. Rasheed and Ravindran (1978) recorded the presence of the benthic foraminifera *Bolivinoides decoratus* and based on this species assigned a Campanian age. Well-preserved ichnofossils of *Ophiomorpha* and *Thalassinoides* occurs at the upper part of this formation (Table 2). The Kallankurichi Formation contains smaller benthic foraminifera, including *Gavelinopsis bembix, Gyroidinoides globosa, Lingulogavelinella* and *Cibicides.* The presence of planktic

foraminifera *Globotruncana linneiana, G. aegyptiaca* and *G. arca* indicate an early Maastrichtian age. Similarly, Tewari et al. (1996a, b) assigned an early Maastrichtian age based on the larger foraminifera *Siderolites.* Recently Malarkodi et al. (2017) reported *Lepidorbitoides* and *Siderolites* from Lower Kallankurichchi Formation, confirming early Maastrichtian age. Macrofossils represented by mollusks, such as *Gryphaea, Alectryonia,* and *Pecten,* as well as bryozoans are abundant in this formation. A diverse assemblage of late Maastrichtian calcareous nannoplankton is reported from the Ottakovil Formation, including *Arkhangelskiella cymbiformis, Braarudosphaera bigelowii, Ceratolithoides aculeus, Chiastozygus litterarius, Cyclagelosphaera deflandrei, Cribrosphaerella ehrenbgergii, Cribrosphaera* sp., *Eiffellithus gorkae, E. parallelus, E. turriseiffeli, M. staurophora, M. swastica, Petrobrasiella? bownii, Prediscosphaera cretacea, P. spinosa, Stradneria crenulata, Staurolithites crux, Zygodiscus minimus* and *Z. spiralis* (Rai and Ramkumar 2007).

Diverse vertebrate fossils are reported from the Kallamedu Formation, including ganoid fishes, amphibians, turtles, crocodiles, and dinosaurs that suggest a Late Cretaceous link between India and other Gondwanan landmasses. Teeth of abelisaurid dinosaurs, known previously from the Middle Jurassic of South America and the Late Cretaceous of Africa, Madagascar, and central and western India, support a pan-Gondwanan distribution for these groups of theropod dinosaurs. Of greatest significance, however, is the discovery of a *Simosuchus*-like notosuchian crocodile outside of Madagascar (Prasad et al. 2013). This report of the first Indian *Simosuchus*-like notosuchian crocodile further strengthens the idea that a link existed between India and Madagascar during the Late Cretaceous. Vertebrate dispersal most likely was facilitated via the Seychelles block, Amirante Ridge, and Providence Bank (Ali and Aitchison 2008).

5 Ichnofossils

Ichnofossils are relatively well preserved in Kulakkalnattam Sandstone, Anaipadi Calcarenite, Sillakkudi Sandstone and Ottakovil Sandstone units. The Kulakkalnattam Sandstone Member of the Garudamangalam Formation is intensely burrowed and well-preserved ichnofossils were used to reconstruct a paleobathymetry using the model of Seilacher (1967). Frey and Pemberton (1985) have constructed ichnofacies that are representative of environmental gradients. They illustrate eight ichnofacies spanning from the rocky coast to the deep abyssal environment. In semi-consolidated substrates, Frey and Pemberton (1985) report an abundance of vertical burrows with both smooth and reinforced walls with 'U'-, 'J'-, 'Y'-, and 'T'-shaped structures that are characteristic of foreshore, moderate to high energy conditions (Seilacher 1967; Frey and Goldring 1992; Reddy et al. 1992; Sathyanarayana et al. 1999). The ichnological study on the Kulakkalnattam Sandstone Member by Nagendra et al. (2010) revealed the dominant occurrence of vertical burrows in association with horizontal burrows. The vertical burrows are predominantly represented by *Ophiomorpha nodosa* and *Skolithos linearis,* which

are produced by suspension-feeding animals and preserved in full relief (Table 2). These structures are part of the *Skolithos* ichnofacies of Frey and Pemberton (1985). Abundant biogenic structures indicate moderate to high energy conditions and a shifting substrate exploited by opportunistic burrowing animals in foreshore environments. Alternatively, the Kulakkalnattam Sandstone has a fine-grained, immature grain texture and is bioturbated with well-preserved horizontal structures of deposit-feeding communities. These communities are dominated by cylindrical, branched, large-sized three-dimensional horizontal burrows of *Thalassinoides horizontalis* and *Thalassinoides suevicus,* and un-branched horizontal burrows indicative of *Planolites beverlyensis* and *Palaeophycus tubularis* (Table 2). Horizontal structures of *Planolites* and *Palaeophycus* were formed a few centimeters below the sediment-water interface where their producers lived, suggesting an unconsolidated substrate in a moderate to low energy sub-tidal environment. In the Kulakkalnattam sandstone, abundant bioturbation obscures the physical sedimentary structures. Ichnofossils in the Kulakkalnattam Sandstone Member are represented by the *Skolithos* ichnofacies, which were probably made by crustaceans, polychaetes, etc. in shallow marine environments. The *Skolithos* ichnofacies indicates, moderate to high energy conditions and un-consolidated shifting substrate. Petrography reveals poorly sorted grains that are free floating, angular to sub-angular. Sediment characteristics and biogenic (feeding/dwelling) activity suggest normal salinity in a fully marine foreshore-shoreface environment during the deposition of the Kulakkalnattam Sandstone Member (Nagendra et al. 2010). The Ottakovil Formation contains macrofossils, including echinoids and bivalves along with few burrowing trace fossils of *Thalassinoides* and *Ophiomorpha,* which are characteristic of the *Skolithos* ichnofacies and indicative of high energy conditions. This formation marks the terminal marine Cretaceous in the Ariyalur area (Tewari et al. 1996a).

6 Sequence Stratigraphy

The sequence stratigraphic concepts followed in this work are based on the concepts of Vail et al. (1977) and Van Wagoner et al. (1988). Outcrop sections are widespread and include locations in Terani, Karai, Kallakkudi quarry, Kovandankurichi mines, Melarasur, Kulakkalnattam, Anaipadi, Saradamangalam, Garudamangalam, Seeranattam, Karumbayam, Sillakkudi, Kallankurichchi TANCEM mines, TAMIN mines, GRASIM mines and Srinivasapuram limestone quarries, Ottakovil, and Kallamedu (Tewari et al. 1996a; Nagendra et al. 2001, 2002, 2011) (Fig. 1). Wherever the lithological contacts were missing, the succession of lateral vertical facies transition i.e. in space and time (stratigraphic and environmental) was determined based on lithology and biostratigraphy regiment, to ascertain the nature of the contact. Seven sequence boundaries and seven second/third order sequences are identified (Table 1b; Nagendra et al. 2011).

The oldest sedimentary unit overlying the granitic basement is the Kovandankurichi Formation with fanglomerate facies (Govindan et al. 1998). This unit

is overlain by the Terani Formation of fluvial to littoral origins (Banerji 1982). The contact between the Archaean basement and Kovandankurichi Formation forms the sequence boundary-1 (SB1) and the upper contact with the Terani Formation forms the sequence boundary-2 (SB2), based on lithofacies and sedimentary environments (Fig. 2). The Terani Claystone with sandstone intercalations is characterized by the occurrence of *Ptilophyllum acutifolium.* It is conformably overlain by the Terani Gritty Ferruginous Sandstone Member, consisting of foraminifera and ammonite shells. This surface top likely represents the sequence boundary-3 (SB3), which separates non-marine from marine facies. The SB3 merges with the transgressive surface (TS), which marks the first marine transgression at the basin margin (Fig. 2). This surface closely coincides with the Aptian/Albian boundary (Reddy et al. 2013).

The Dalmiapuram and Karai formations of the Uttatur Group, successively developed in a marine environment during the Albian to middle Turonian and overlie the Terani Formation. The para-conformable contact lies between the Terani Formation and the Coral Algal Limestone Member of the Dalmiapuram Formation. The abrupt termination of the Coral Algal Limestone is inferred to represent a drowning surface, which occurred due to clastic input and relative rise in sea level (Nagendra et al. 2002). The upper surface of the Karai Formation has an unconformable relationship with the overlying Garudamangalam Formation and represents upper sequence boundary-4 (SB4) (Nagendra et al. 2002, 2011). The SB4 represents a hiatus of about 2.10 Ma that developed as a result of basin uplift caused by the rising Marion hot mantle plume during late Turonian (Nagendra et al. 2002, 2011; Raju et al. 2005).

The Garudamangalam Formation overlies the SB4. The relative sea level (RSL) fall during the late Santonian produced fluvial channel deposits as part of the high-stand system tract (HST) , and is represented by the Saturbhugam Sandstone; the erosion surface at the top of this sandstone is the sequence boundary-5 (SB5) (Nagendra et al. 2011; Reddy et al. 2013). The base of the Kallar Conglomerate, which overlies the Saturbhugam Sandstone, delineates an unconformity surface and forms the sequence boundary-6 (SB6) (Fig. 2). The conglomerate was developed after weathering and erosion of the exposed Sillakkudi sandstones. The base of the Ferruginous Limestone is a transgressive surface marked by the presence of smaller benthic foraminifera, indicating marine flooding at the base of the Kallankurichchi Formation. The transgressive systems tract consists of the Ferruginous Limestone, Lower Arenaceous Limestone and the *Gryphaea* Limestone. The stacking patterns of these three members represent a retrogradational parasequence corresponding to intermittent flooding events (Fig. 2) (Nagendra et al. 2002). Macro- and microfossil assemblages and the frequency and preservation of microfossil tests indicate a deepening water depth up section. The *Gryphaea* Limestone Member, which is very rich in macrofossils, represents one of the best developed maximum flooding surfaces (MFS) in the area (Fig. 2). The MFS is sharp, located between the *Gryphaea* Limestone and the Upper Arenaceous Limestone, and corresponds to the upper surface of the *Gryphaea* shell bed. Abundant large-sized *Gryphaea* shells suggest a tranquil environment. High silica content and reduced micro- and macro-fossil abundance suggest shallowing towards the top of the Upper Arenaceous Limestone, which represents a HST. The shallowing trend continues into the Ottakovil Formation,

which marks the end of the marine phase, which terminated due to major sea level fall caused by the eastward tilt of the basin. This tilt is attributed to the rise of the Reunion mantle plume and Deccan eruptions causing uplift in central India (Raju et al. 1993; Jaiprakash et al. 2016; Nagendra and Reddy 2017). The top of the Ottakovil Formation is interpreted as the sequence boundary-7 (SB7).

7 Relative Sea Level Changes

Voigt et al. (2008) synthesized the tectonic evolution and paleogeography of all central European Basins. The sea level curve for the Danish and North German basins shows a mid-late Albian transgression flooding in central Europe basins, while the late Albian transgression completely flooded the Cauvery Basin, replacing shelf carbonates with organic-rich shale. As a consequence of this major transgression, the individual sub-basins formed as one large epicontinental shelf area. The post-Turonian deposits of the Cauvery Basin represent an early post-rift unit that accumulated during a time of thermal subsidence consequent to rise of Marion plume. The Late Aptian to mid-Albian sea level cycle (=Dalmiapuram cycle) of the Cauvery Basin shows some correspondence with the northern Gulf of Mexico. The late Turonian unconformity with a hiatus of about 2.3 Ma separates the Coniacian-Santonian sea level cycle (= Garudamangalam cycle of Raju et al. 1993) in the Cauvery Basin. This unconformity has a corresponding sub-aerial unconformity in central Europe and the northern Gulf of Mexico. However, the late Santonian regression in the Cauvery Basin has a corresponding marine flooding event in the northern Gulf of Mexico. The early Maastrichtian widespread transgression is associated with the early-late Maastrichtian sea level cycle that has a corresponding late Albian-early Maastrichtian transgression in the northern Gulf of Mexico (Mancini and Puckett 2005) and the lower boundary of this cycle is represented by a sub-aerial unconformity in western Europe (Hardenbol et al. 1998) and in the Cauvery Basin (Nagendra et al. 2011). Throughout the Upper Cretaceous, the Cauvery Basin was dominated by deposition of shale and sandstones with shelf carbonates in the early to mid-Albian. Late Albian to mid-Turonian, Coniacian and early Maastrichtian experienced the widespread occurrence of anoxic conditions. The first marine transgression at the basin margin occurred in the late Aptian to early Albian. This is revealed by the occurrence of planktic foraminifera *H. planispira* and *H. trocoidea* along with the benthic foraminifer *Lenticulina* spp. in the uppermost part of the Terani Formation. This faunal assemblage generally indicates a shallow neritic, open marine environment. This unit is overlain by limestone belonging to the Dalmiapuram Formation, which is rich in coral-algal and bryozoans with rare foraminifera indicating a warm, shallow and restricted marine environment during the early to mid-Albian. The carbonate deposition ceased abruptly during the late Albian as a result of increasing depth and clastic input (Nagendra et al. 2002). Macrofossils, such as *Acanthoceras* sp., *Mammites conciliatus*, *Nautilus huxleyanus*, and *Turrilites costatus* (Govindan et al. 1998; Kossmat 1897) are abundant in the bedded limestone. Marl yielded

few planktic and diverse benthic represented by species *Hedbergella*, *Lenticulina*, *Anomalinoides* and *Quadrimorphina,* indicating middle neritic conditions. Further deepening is evident during the late Albian to mid-Turonian as the bedded limestone grades vertically into marl/limestone, wherein well preserved, diversified and abundant foraminifera, such as *Rotalipora reicheli*, *Praeglobotruncana stephani*, *P. delrioensis*, *Gavelinella plummerae*, *Gyroidinoides globosa* suggests deeper middle neritic conditions (Nagendra et al. 2002, 2011; Reddy et al. 2013). The time equivalent Karai Shale Formation in outcrops consists of Ammonites, Belemnites and worm tubes indicating deeper middle neritic conditions. Paleodepth attained its maximum at the end of Dalmiapuram/Karai Formation. As a result of basin uplift caused by the rise of Marion plume (Raju et al. 2005) during the late Turonian (Scotese 1997), relative sea level dropped to inner neritic depths (Fig. 2). The increased abundance of glauconite pellets from the bottom to the top TST accompanied by slight increase in K_2O content reflects the effect of stratigraphic condensation on the evolution of glauconite (Banerjee et al. 2016). The paleogeography of the Karai Shale Formation ranged from inner shelf to the shelf-margin straddling across the maximum flooding zone heavily enriched in phosphates and glauconites pellets (Banerjee et al. 2016; Chakraborty et al. 2018b). The Kulakkalnattam sandstone unit (Coniacian-Santonian) of Garudamangalam Formation unconformably overlies the Karai Shale Formation. This sandstone consists of abundant burrows characterized by *Skolithos* ichnofacies (Frey 1973; Pemberton et al. 1992) characteristic of high energy nearshore conditions. The presence of poorly marked sandstones indicates their deposition under wave base. This unit vertically grades into Anaipadi Sandstone Member, which consists of Ammonites and Mollusk shells signifying inner neritic conditions. The overlying Saturbhugam Sandstone Member, characterized by cross laminations, points to a fluvial channel origin and revealing sea level drop at the end of Santonian (Garudamangalam Formation). The Garudamangalam Sandstone Formation forms a highstand systems tract, which unveils a wide range of siliciclastic-carbonate mixing modes in a nearshore marine realm associated with river-mouth bar. The presence of a shore parallel river-mouth bar resulted in a restricted environment on its shore side, remained open marine on the seaward side (Sarkar et al. 2014). The Sillakkudi Formation overlies the Garudamangalam Formation. This formation characteristically consists of large *Inoceramus* shells along with *Skolithos* and *Ophiomorpha* burrows at the top of the unit. The lower part of the formation is represented by Kilpalvur grain stone containing glauconites pellets and calcareous nodules indicating a marine incursion into the basin. This formation yielded foraminifera, including *Globotruncana ventricosa*, *Globotruncana linneiana*, *Rosita fornicata* and *Bolivinoides strigillatus,* suggesting deeper middle neritic conditions (Rasheed and Ravindran 1978). The Kallar conglomerate between Sillakkudi and overlying Kallankurichchi formations suggests a relative sea level drop resulting in subaerial exposure and development of a 1.5 m thick conglomerate bed. The Kallankurichchi Formation consists of four litho units (Nagendra et al. 2002) with the lower ferruginous limestone containing smaller benthic foraminifera that marks the onset of a marine transgression. The increasing abundance of foraminifera and macrofossils

represented by *Gryphaea*, *Alectryonia* and *Pecten* in successively overlying arenaceous limestone and *Gryphaea* limestone is an indication of deepening bathymetric conditions. Above the *Gryphaea* bed a layer dominated solely by *Gryphaea* shells suggests maximum paleodepth reached to middle neritic depths. Drastic reduction in fossil content in the overlying upper arenaceous limestone unit signals a falling sea level. This falling trend continued up to the end of Ottakovil Formation, which overlies Kallankurichchi Formation. The burrow structures such as *Thalassinoides* and *Ophiomorpha* in the Ottakovil Formation indicate marginal marine to littoral environment. This lithological unit (Ottakovil) marks the end of the marine phase in the basin margin area. The Kallamedu Formation overlies the Ottakovil Formation and is characterized by cross-laminations indicating deposition in a fluvial environment. The sea level curve reveals that four major transgressive and regressive cycles are imprinted in the Cretaceous rock record preserved in the Ariyalur area. The T-R cycles divide the Cretaceous succession into four 2nd/3rd order sequences, and the maximum surfaces define the sequence boundaries. The paleo- bathymetric trends *vis-a-vis* sea level changes reconstructed for the Albian to Maastrichtian (Dalmiapuram through Ottakovil Formation) reveal two major sea level falls during late Turonian and late Maastrichtian, which correlate well with global sea level curves (cf. Haq et al. 1987; Miller et al. 2005; Vail et al. 1977). These sea level falls are linked to the rise of Marion hot mantle plume during the late Turonian and Reunion hot mantle plume during late Maastrichtian (Ramanathan 1977; Courtillot et al. 1988; Govindan 1993; Raju et al. 1993; Sundaram et al. 2001; Nagendra et al. 2002; Watkinson et al. 2007) (Fig. 2). Rich shale perhaps resulted from the expansion of oxygen-depleted conditions at the depositional surface. There are also gamma-ray log evidences to suggest that the presence of high organic content due to anoxic conditions at Coniacian-Santonian level in this basin (oil well sections) probably correlates with global episodes of OAE-3 (Bomou et al. 2013) (Fig. 5). These low oxygen levels coincide well with the local peaks of transgressive cycles in the Cauvery Basin (Govindan 1993).

8   Cretaceous Climate

Bowen (1961) recorded the paleotemperature 21.4–22.4 °C using the biogenic calcite equation of Epstein et al. (1953) based on oxygen-isotopic composition of *Belemnites* fibula (=*Parahibolites blanfordi*) (Doyle 1985) samples collected from the basal limestone and clays, belonging to the latest Aptian-Coniacian, Uttatur Group. After publication of a paper by Bowen (1961), additional data on stable isotope composition of Cretaceous carbonates from central and southern India (Ayyasami 2006; Ghosh et al. 1995), as well as on diversity of Cretaceous foraminifera of the Cauvery Basin (Govindan and Narayanan 1980) were used to infer that Late Cretaceous foraminiferal faunas of the Cauvery Basin, in contrast to the Early Cretaceous fauna, are composed of tropical elements of Tethyan affinity. Within the fluvial package (Basal Siliciclastic), Chakraborty et al. (2017) anticipated that paleoclimate
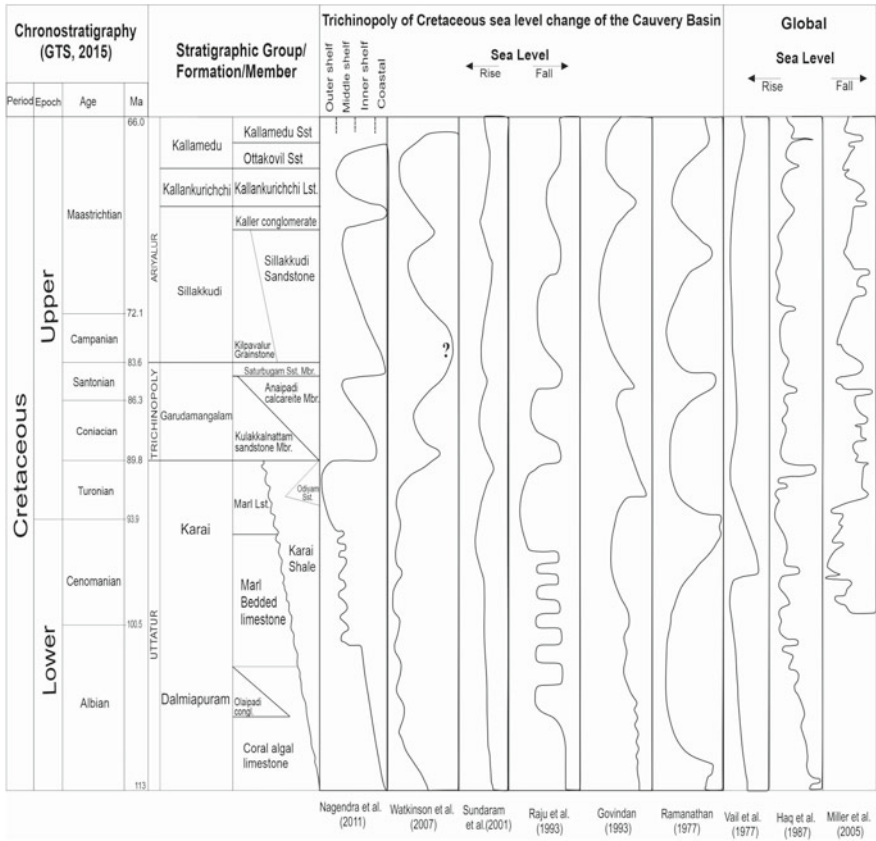
Fig. 5 Paleobathymetric curves of Cretaceous sediments based on outcrops around Ariyalur area and their correlation to global sea level curves (adapted from Nagendra et al. 2011)

was reasonably humid, with estimated rate of precipitation around 1000 mm/year, and moderate weathering intensity. Average annual temperature (around 12.5 °C, nonetheless, had possibly been moderate due to the high Barremian-Aptian paleoclimate of the depositional site. Das Gupta et al. (2007) recorded the paleotemperature of 21 °C–23 °C and 28 °C–29 °C, respectively on the basis of oxygen-isotopic composition of benthic and planktic foraminifera for lower Cenomanian to upper Turonian portion of the Karai Formation of the Cauvery Basin. Zakharov et al. (2011) studied the paleotemperature trends for the Cretaceous of India and Madagascar, which have been determined on the basis of oxygen isotope analysis. Well-preserved Albian *Belemnite rostra* and Maastrichtian bivalve shells from the Cauvery Basin, southern India, and Albian nautiloid, ammonoids and cephalopods from the Mahajang Province, Madagascar were analyzed for oxygen isotopes. The Albian (possibly Late Albian) paleotemperatures for the Cauvery Basin are inferred to range from 14.9 to 18.5 °C for the epipelagic zone, and from 14.3 to 15.9 °C for the

mesopelagic zone, based on analyses of 65 samples; the isotopic paleotemperature interpreted as summer and winter values for near-bottom shelf waters in this area fluctuate from 16.3 to 18.5 °C and from 14.9 to 16.1 °C, respectively. The mentioned paleotemperatures are very similar to those calculated from the isotopic composition of middle Albian belemnites of the middle latitude area of Pas-de-Calais in northern hemisphere but significantly higher than those calculated from the isotopic composition of Albian belemnites from southern Argentina and the Antarctic and middle Albian belemnites of Australia located within the warm-temperate climatic zone. The isotopic analysis of early Albian cephalopods from Madagascar shows somewhat higher paleotemperature for summer near-bottom shelf waters in this area (20.2–21.6 °C) in comparison with late Albian paleotemperature calculated for fossils from the Cauvery Basin, but similar winter values (13.3–16.4 °C); however, the latter values are somewhat higher than those calculated from early Albian ammonoids of the tropical-subtropical climatic zone of the high latitude area of southern Alaska and the Koryak Upland (Zakharov et al. 2011). The new isotopic paleotemperature data suggests that Cauvery Basin and Madagascar were located apparently in middle latitudes (within the tropical-subtropical climatic zone) during Albian time. In contrast to the Albian fossils, isotope results of well-preserved early Maastrichtian bivalve shells from the Ariyalur Group of strata of the Cauvery Basin are characterized by lower $\delta^{18}O$ (up to $-5.8‰$ in PDB) but normal $\delta^{13}C$ ratios, which might be a result of local freshwater input into the marine environment (Zakharov et al. 2011). The data suggest that the early Maastrichtian paleo-temperature of the southern Indian near-bottom shelf waters was probably about 21.2 °C. This middle latitude region continued to be a part of tropical-subtropical climatic zone, but with the tendency of increasing of humidity at the end of Cretaceous time.

9 Oceanic Anoxic Events

Oceanic anoxic events (OAEs) were episodes of widespread marine anoxia during which substantial amounts of organic carbon were buried on the ocean floor under oxygen-deficient bottom waters (Turgeon and Creaser 2008). The globally significant oceanic anoxic events viz. OAE-1b, OAE-1d, OAE-2 and OAE-3 (Cronin et al. 2010) are fairly discernible in the Cauvery Basin (Fig. 5). The first marine transgression in uppermost Terani Formation in the outcrops at the basin margin closely denotes Aptian/Albian boundary (Reddy et al. 2013). The expansion of this level in the subsurface of the basin contains organic-rich shale, which probably characterizes OAE-1b. The organic lean grey shale at the basal part of the marl bedded limestone (late Albian-Cenomanian) exposed in mine sections along the western margin of the basin closely correlates with OAE-1d. The extension of these litho units in the subsurface contains well preserved black/dark grey shale in the late Albian intervals in many exploratory wells drilled in the basin (Govindan 1993; Nagendra and Reddy 2017). These shale units deposited through OAE-1d show very high gamma counts

suggesting excellent potential as source rock, and are logged in different sub-basins of the Cauvery Basin (Fig. 6).

The next event of organic-rich sedimentation through late Cenomanian-Early Turonian correlates well with major transgression and global oceanic anoxic event OAE-2. The high concentration of dark-coloured, pyritized agglutinated foraminifera, presence of small calcareous benthic foraminifera viz. *Lenticulinids, Gavelinellids* indicates ecological stress induced by anoxic depositional conditions (Govindan 1993; Nagendra and Reddy 2017). Late Cenomanian-early Turonian is also characterized by world-wide anoxic conditions (Schlanger and Jenkyns 1976). The preservation of this organic-rich shale perhaps resulted from the expansion of oxygen-depleted conditions at the depositional surface. The ^{40}Ar/^{39}Ar plateau ages of Glauconite samples are consistent with the biostratigraphic age of Late Albian
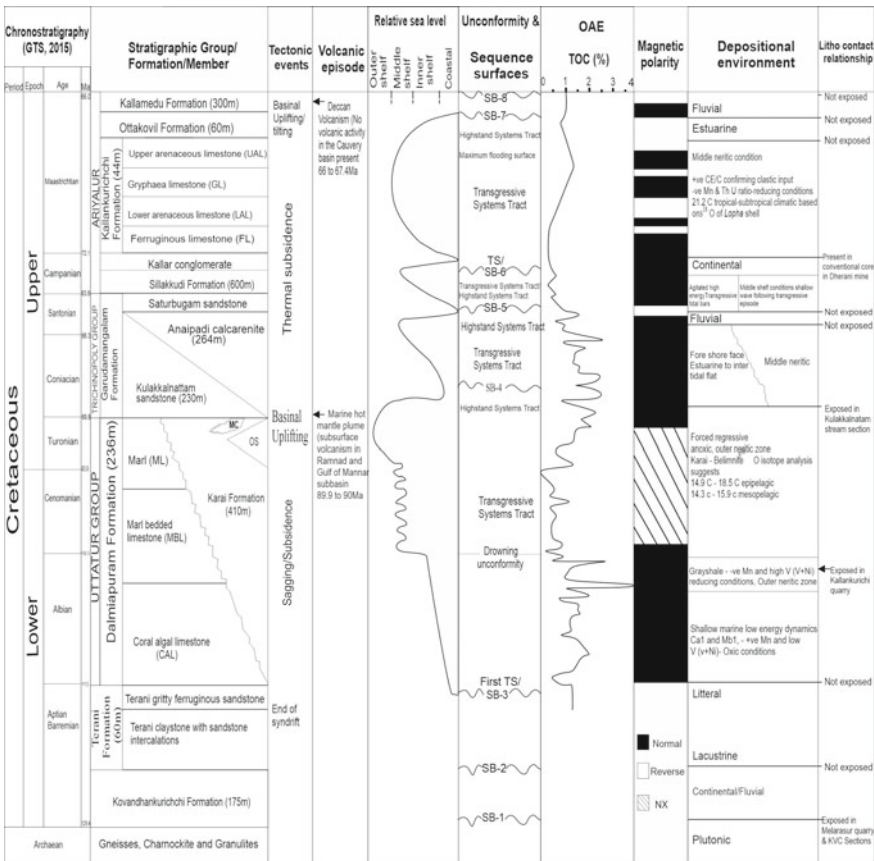
Fig. 6 Tectonic events, episodes, relative sea-level oscillations, sequence stratigraphic surfaces, total organic carbon (TOC) contents, depositional environments across the Cretaceous succession of Cauvery Basin (modified after Nagendra and Reddy 2017)

to Middle Turonian of Karai Formation (Bansal et al. 2019) There are also gamma ray log evidences to suggest that the presence of high organic content due to anoxic conditions at Coniacian-Santonian level in this basin probably correlates with global episodes of OAE-3 (Bomou et al. 2013) (Fig. 6). These low-oxygen levels coincide well with the local peaks of transgressive cycles in the Cauvery Basin (Govindan 1993).

10 Paleomagnetism

India began its separation and drifted northward from the supercontinent Gondwana during the middle Cretaceous, approximately 100 my ago (Chatterjee et al. 2017). By the Late Cretaceous, India separated from Australia and Africa and continued northward towards Asia. During the late Maastrichtian, prior to the Deccan Trap eruptions, uplift in southern India resulted in sedimentation in the adjacent nascent Indian Ocean. Among all the Gondwana continents, India moved at a relatively high rate of 20–25 cm/year (Poornachandra Rao and Bhalla 1981). India collided with the Eurasian plate about 55 Ma ago, which resulted in the rise of the Himalayan mountain chain. The rapid northward movement of the Indian plate is recorded in marine magnetic anomalies, such as the Rajmahal-Sylhet Traps and the Deccan Traps. The geochronology is well established for the Deccan and Malwa Traps, but less so for the Rajmahal Traps. The Rajmahal Traps yield a $^{40}Ar/^{39}Ar$ age of 117 ± 1 Ma (Baksi et al. 1987). No recent analyses with improved methods have been done. Hence the error bar is likely significantly larger for ages determined 30-40 years ago. The major phase of the Deccan Trap eruptions occurred during magnetochron C29r and has recently been dated based on U-Pb geochronology (Zircons) to span from 66.288 ± 0.027 Ma to 65.552 ± 0.026 Ma, which encompasses the Cretaceous-Paleogene boundary (Schoene et al. 2015). U-Pb geochronology for the Deccan Traps greatly improves earlier age estimates based on $^{40}Ar/^{39}Ar$ dating of 65.5 ± 2.5 Ma (Vandamme et al. 1991). $^{40}Ar/^{39}Ar$ geochronology of the Malwa Plateau (Northern Deccan Traps) based on plateau ages of multiple samples recently yielded an age of 67.12 ± 0.044 Ma, which shows that these eruptions started during magnetochron C30n preceding the main Deccan Traps eruptions (Schöbel et al. 2014). Paleomagnetic studies on the Rajmahal, Malwa and Deccan volcanic episodes indicate the drift of the Indian plate during the Early and Late Cretaceous. During the Early Cretaceous eruptions of the Rajmahal Traps (~117 $\pm$ 1 Ma, Aptian) the Indian subcontinent was situated at paleolatitude 43º S. By the latest Cretaceous (late Maastrichtian), the Malwa and Deccan Traps were deposited at a paleolatitude of 30º S. Magnetic polarity stratigraphy of the Cenomanian-Maastrichtian outcrops in the Cauvery Basin is reviewed to construct a composite magnetic polarity scale that helps understand the continental drift history. Outcrop samples from 29 locations in the vicinity of the Ariyalur district were treated for thermal demagnetization (100–700 °C) after measuring their natural remanent magnetization. The calculated declinations and inclinations of the Characteristic Remanent Magnetism (ChRM) components were

used to derive the paleolatitudes of the virtual geomagnetic pole of outcrops (Papanna et al. 2014). The constructed magnetic polarity scale for the Cenomanian–Maastrichtian sediments of the Cauvery Basin is correlated with the standard Geological Time Scale (Gradstein et al. 2004; Ogg et al. 2008). The composite magnetic polarity scale of the Dalmiapuram, Karai, Garudamangalam, Kallankurichchi, Ottakovil, and Kallamedu formations comprise 13 magnetozones, 7 normal and 6 reversal events, which correlate to chron C34n to chron C30n. The Cauvery Basin was located in the southern latitude during the late Cretaceous. Isothermal remanent magnetisation measurements indicate that the remanence carrier is hematite which resides in these sediments.

11 Discussion

Over 60 surface exposures, mines and quarries have been investigated in the Ariyalur area of the Cauvery Basin. These investigations were often based on multiple disciplines, and only limited studies employed an integrated multidisciplinary approach to evaluate the sum of the age and the paleo-environment. A concerted effort was employed to review and evaluate these outcrops from the Cretaceous (Barremian-Aptian to Maastrichtian) of the Ariyalur area of the Cauvery Basin based on an interdisciplinary approach that integrates multiple stratigraphic schemes ranging from lithostratigraphy, biostratigraphy, and sequence stratigraphy. Diverse multiple biostratigraphic schemes employed in relative age correlations include ammonites, larger foraminifera, benthic foraminifera, planktic foraminifera, ichnofossils, dinoflagellates and nannofossils. The results of this study provide a direct calibration of lithologic, biostratigraphic and sequence stratigraphic events for the Aptian to Maastrichtian and paleomagnetic polarity events for the Cenomanian-Maastrichtian interval (Fig. 2).

Lithological observations of various outcrop sections reveal 8 lithostratigraphic formations and 5 members (Fig. 2). The inversely graded fanglomerate, previously recognized as the informal Boulder bed, is hereby raised to formation status and is named the Kovandankurichi Formation, which is an excellent regional lithostratigraphic marker. Likewise, the Kallar conglomerate, which is present in the upper Sillakkudi Formation, permits easy regional correlation. A subtle unconformity across the Terani and Dalmiapuram formations (Aptian/Albian) and major unconformities across the Karai and Garudamangalam formations (late Turonian), Sillakkudi and Kallankurichchi formations (late Campanian) have equivalents in the adjoining Krishna-Godavari Basin (Raju and Reddy 2016). Good preservation of very small planktic foraminifera, including *Hedbergella trocoidea, H. planispira* and *H. delrioensis*, yield important age control for the Aptian Terani Formation and for recognizing the first marine transgression at the western margin of the basin (Reddy et al. 2013). However, the relative abundance of these species is lower in the upper sandstone layers of the Terani Formation. This marine transgression event of the Terani Formation is a corollary to the terminal phase of syn-rift tectonics in the

Cauvery Basin. The Karai Formation, which is exposed at the basin margin, contains diverse assemblages of ammonites, foraminifera and radiolarian. This formation consists predominantly of shale facies with abundant calcareous benthic foraminifera suggesting deposition in >150 m water depth (Nagendra et al. 2013). The age equivalent of this shale facies in the shallow neritic environment is the Dalmiapuram Formation, which consists of algal and bryozoan limestone at the bottom, a marl-bedded limestone in the middle, and marl at the top. The age ranges from early Albian to middle Turonian (Nagendra et al. 2011; Reddy et al. 2013) and marks a major transgressive cycle (Fig. 2) (Nagendra et al. 2002; Raju and Reddy 2016). The transgressive phase was terminated by rapid basin uplift caused by the rising Marion hot mantle plume (Nagendra et al. 2011; Reddy et al. 2013). The basin uplift led to a major unconformity with a hiatus of about ~2 Ma (=late Turonian) and is regionally correlatable in east coast basins of India (Raju et al. 2005).

Well-preserved dinoflagellates in the gray shale at the base of marl-bedded limestone yielded index taxa *Odontochitina costata, Epelidosphaeridia spinosa, Cyclonephelium cf. C. vannophorum, Dioxya* sp., *Kiokansium unituberculatum, Ovoidinium verrucosum* and *Batioladinium micropodium* (Nagendra et al. 2002). The index planktic foraminifer taxa recorded are *Rotalipora gandolfi, Rotalipora brotzeni, Praeglobotruncana stephani, P. delrioensis, Hedbergella planispira* and *Globigerinelloides bentonensis.* Index taxa of both fossil groups suggest a latest Albian age (Caron 1985; Nagendra et al. 2002, 2013). This age date significantly improves the calibration of OAE 1d in the Cauvery Basin (Nagendra and Reddy 2017).

In the Kulakkalnattam Sandstone Member of the Garudamangalam Formation, the presence of low diversity but well-preserved ichnofossil assemblages marks a significant paleo-ecological event. These assemblages coincide with a rapid relative sea level fall from deep outer neritic to inner neritic depth, which was likely caused by basin uplift during the late Turonian (Fig. 2) (Nagendra et al. 2011). The fossil assemblage consists of *Skolithos, Ophiomorpha, Thalassinoides, Planolites* and *Paleophycus,* which are characteristic of the *Skolithos* and *Cruziana* ichnofacies that represent typical shoreface, moderate to high energy environments (Nagendra et al. 2010). Marine carbonates with mudstone and wackestone facies dominate the Kallankurichchi Formation, which consists of four limestone units differentiated by their characteristic content. These limestones were deposited during a major transgressive-regressive (T–R) cycle. The *Gryphaea* unit is enriched in mollusks, *Gryphaea, Alectryonia,* and *Pecten* and bryozoans and represents a well-marked MFS (Nagendra et al. 2002). This unit also contains well preserved larger benthic foraminifera, particularly the *Lepidorbitoides-Siderolites* assemblage (Malarkodi et al. 2017) and planktic foraminifera *Globotruncana aegyptiaca*, *G. linneiana* and *G. arca*, which suggest zone CF6 of the late early Maastrichtian (Li and Keller 1998a, b; Keller et al. 2016; Nagendra et al. 2018). The Ottakovil Formation contains rare burrows and a diverse nannoplankton assemblage (=*Gansserina gansseri* Zone) indicative of the late Maastrichtian (=CF5-3) (Rai and Ramkumar 2007; Nagendra et al. 2011, 2018). Keller et al. (2016) identified planktic foraminifera characteristic of zones CF5 to CF3 in Cauvery Basin deep wells (ONGC); therefore, it may be

noted that this age interval should also be present in outcrop sections. The marine phase ends at the top of this formation in the Ariyalur area of the Cauvery Basin. The determination of paleolatitudes for the Cauvery Basin from the Cenomanian through the Maastrichtian was based on the magnetic polarity time scale. Thirteen magnetozones comprising 7 normal and 6 reversal events were recognised for the Marl bedded limestone of Dalmiapuram, Karai, Garudamangalam, Kallankurichchi, Ottakovil and Kallamedu formations (Fig. 2). These polarity events corroborate well with chron C34n to chron C30n of the Geologic Time Scale of Gradstein et al. (2004). This permits us to infer a low (?) southern latitude during the Late Cretaceous period for the Cauvery Basin. Integration of lithological contacts, the succession of vertical facies (stratigraphic and environmental) and biostratigraphy demarcate seven sequence boundaries and seven second/third order sequences (Nagendra et al. 2011; Reddy et al. 2013). Major sea level fall during the late Turonian, late Santonian and late Maastrichtian correlate well with global sea level falls (Vail et al. 1977; Haq et al. 1987; Miller et al. 2005; Haq 2014) Late Turonian and late Maastrichtian sea level fall is linked to the rise of Marion and Reunion mantle plumes, respectively (Raju et al. 1993; Courtillot et al. 1988; Nagendra et al. 2002). Paleotemperatures for the Dalmiapuram and Karai formations (upper Albian) and Kallankurichchi Formation (lower Maastrichtian) were determined using oxygen isotope analyses based on cephalopods, belemnites and *Lopha* shells. The calculated paleotemperatures range from 14.3 to 18.5 °C for the late Albian Karai Shale and between 19.8 and 21.2 °C for the Kallankurichchi Formation. These paleotemperatures are consistent with known paleotemperature data obtained from Albian cephalopods from the Pas-de-Calais area (21.9–22.8 °C) and Normandy (19.3–22.8 °C) (Zakharov et al. 2006). The isotopic paleotemperature data suggests that southern India and Madagascar were located in middle latitudes during the Albian with temperatures equivalent to the present day tropical-subtropical climatic zone.

12 Conclusions

(a) The evolution of the Cauvery Basin and subsequent sedimentation along eastern passive margin of India is attributed to the fragmentation of eastern Gondwana and opening up of the Indian Ocean, which began in Late Jurassic-Early Cretaceous. The exposed Cretaceous system of the Cauvery Basin consists of a complete marine sequence, rich in faunal assemblages, ranging from Albian to Maastrichtian. A plausible lithostratigraphic framework and standardized stratigraphic nomenclatures based on a review of published classifications systems. Informally named Kovandankurichi conglomerate (Lower Cretaceous) to be renamed as the Kovandankurichi Formation.

(b) The Cretaceous-Paleogene sections of the Cauvery Basin are closely related to the rifting and drifting phases of peninsular India. A major basin uplift caused by Marion hot mantle plume *ca*.88–90 Ma, resulted in widespread volcanism

in the southern part of the Cauvery Basin. Madagascar detachment from India is also linked to this uplift.

(c) The east, southeast tilting of the basin during Late Maastrichtian due to Deccan volcanism caused by reunion hot mantle plume, led to relative sea level fall (~80 m) and canyon development. Major unconformity of a magnitude 0–30 Ma straddles the K-Pg (KTB) boundary. The sediment depocentres migrated eastwards owing to the lateral withdrawal of sea by 50 km. Eocene to Miocene signifies coastal progradation/deltaic sedimentation through a series of marine transgression and regressions in response to the oscillatory tectonic movements.

(d) In the Cauvery Basin, the early syn-rift fill can be subdivided based on lithological content into syn-rift phase which is predominantly fluvial and lacustrine deposits and late syn-rift phase, consisting of shelf carbonates and marine shale. The marine sediments yielded planktic foraminifera *H. trocoidea*, *H. planispira* and broken ammonite fossils, suggesting late Aptian to earliest Albian, indicating that the top of syn-rift fill is close to Aptian/Albian boundary.

(e) The paleobathymetry reconstructed for the Albian to Maastrichtian (Dalmiapuram through Ottakovil Formation) reveals two major sea level falls during late Turonian and late Maastrichtian, which correlate well with global sea level curves. These sea level falls are linked to the rise of Marion mantle plume during the Late Turonian and reunion mantle plume during Late Maastrichtian.

(f) The deposition of organic-rich sediments during Late Aptian- Early Albian (OAE-1b) late Albian (OAE 1d), late Cenomanian-early Turonian (OAE-2) times in the Cauvery Basin is explained by the expansion of an oxygen-depleted condition due to major transgressive episodes.

(g) Uplift and eastward tilting of the basin can be linked to the rise of reunion hot spot, which caused Deccan volcanic activity in central India. This tectonic activity led to a vertical sea level fall, and lateral withdrawal of sea by about 50 km during late Maastrichtian. The fall in sea level and eastward tilting jointly triggered major canyon activities in the Cauvery Basin, causing differential erosion across the K-Pg boundary.

(h) The isotopic paleotemperature of southern India and Madagascar were located apparently in middle latitudes (within the tropical-subtropical climatic zone) during Albian time. In contrast to the Albian fossils, isotope results of well-preserved Early Maastrichtian bivalve shells from the Ariyalur Group of strata in the Cauvery Basin are characterized by lower $\delta^{18}O$ ratios but normal $\delta^{13}C$ ratios, which might be a result of local freshwater input into the marine environment. The data suggest that the early Maastrichtian paleo-temperature of the southern Indian near-bottom shelf waters was probably about 21.2 °C, and that this middle latitude region continued to be a part of tropical-subtropical climatic zone, but with the tendency of increasing of humidity at the end of Cretaceous time. The geomagnetic polarity sequence may be correlated with polarity chrons from C34n, the Cretaceous long normal interval, through C30n in the Late Maastrichtian.

(i)   The record of *Lepidorbitoides-Siderolites* of late Campanian-Maastrichtian suite in this basin is well known and compared with European type assemblages. Smaller benthic foraminifera assemblage is more cosmopolitan with a preponderance of Tethyan forms. In mid-Turonian, the planktonic foraminifera are morphologically quite distinctive; the species are pronounced keels and ornamentation. This quite distinctive paleogeographical province appears to be restricted to the east coast basins of India and Exmouth plateau/NW Australia shelf. The ichnofossil traces of the Kulakkalnattam Sandstone Member (Garudamangalam Formation) represented by the *Skolithos* ichnofacies suggest crustaceans and polychaetes burrows in a shallow marine environment.

(j)   The distinctive markers of the Campanian-Maastrichtian boundary interval, such as *G. gansseri* are recorded from the Cauvery Basin. *G. gansseri* was a fully tropical species, and its presence in the Cauvery Basin is possibly up to 15°–20° further south. During Middle and Upper Cretaceous time, the southern Indian region was situated below 30° latitude in an arid, but, non-tropical, surrounded by moderately warm Ocean.

(k)   Seven 2nd/3rd order depositional sequences are recognized within the Cretaceous sedimentary succession of the Ariyalur area, Cauvery Basin.

References

Ali JR, Aitchison JC (2008) Gondwana to Asia: plate tectonics, paleogeography and the biological connectivity of the Indian sub-continent from the Middle Jurassic through latest Eocene (166-35 Ma). Earth Sci Rev 88:145–166

Ayyasami K (2006) Role of oysters in biostratigraphy: a case study from the Cretaceous of the Ariyalur area, Southern India. Geos J 10:237–247

Ayyasami K, Jagannatha Rao BR (1978) On the possible faunal break at the contact of Trichinopoly and Ariyalur Groups in the Cretaceous succession of Tiruchirappalli District, Tamil Nadu. Proc VII Indian Colloq Micropal and Strati 3–4

Baksi AK, Ray Barman T, Paul DK, Farrar E (1987) Widespread early Cretaceous flood basalt volcanism in eastern India: Geochemical data from the Rajmahal Bengal-Sylhet traps. Chem Geol 63:133–141

Banerjee S, Bansal U, Pande K, Mena SS (2016) Compositional variability of glauconites within the upper Cretaceous Karai Shale Formation, Cauvery Basin, India: implications for evaluation of stratigraphic condensation. Sediment Geol 331:12–29

Banerji RK (1982) Sivaganga Formation, its sedimentology and sedimentation history. J Geol Soc India 23:450–457

Bansal U, Pande K, Banerjee S, Nagendra R, Jagadeesan KC (2019) The timing of oceanic events in the Cretaceous succession of Cauvery Basin: Constraints from 40Ar/39Ar ages of Glauconite in the Karai Shale Formation. Geol J 54:308–315

Blanford HF (1862) Cretaceous and other rocks of South Arcot and Trichinopoly districts, Madras. Mem Geol Surv India 4:1–217

Bomou B, Adatte T, Tantawy A, Mort HP, Fleitmann D, Huang Y, Föllmi KB (2013) The expression of the Cenomanian-Turonian oceanic anoxic event in Tibet. Palaeo Palaeo Palaeo 369:466–481

Bowen R (1961) Oxygen isotope paleotemperature measurements on Cretaceous Belemnoidea from Europe, India and Japan. J Paleontol 35:1077–1084

Caron M (1985) Cretaceous planktic foraminifera. In: Bolli HM, Saunders JB, Perch-Nielsen K (eds) Plankton stratigraphy. Cambridge University Press, pp 17–86

Chakraborty N, Sarkar S (2018) Syn-sedimentary tectonics and facies analysis in a rift setting: Cretaceous Dalmiapuram Formation, Cauvery Basin, SE India. J Palaeogeography 7:146–167

Chakraborty N, Sarkar S, Mandal A, Mejiama W, Tawfik HA, Nagendra R, Bose PK, Eriksson PG (2017) Physico-chemical Characteristics of the Barremian-Aptian Siliciclastic Rocks in the Pondicherry Embryonic Rift Sub-basin India. In: Mazumder R (ed) Sediment provenance: influences on compositional change from source to sink. Elsevier, pp 85–121

Chakraborty N, Sarkar S, Mandal A, Mandal S, Bumby A (2018a) Microenvironmental constraint on δ^{13}C Depletion: garudamangalam sandstone, Cauvery Basin, India. Mar Petrol Geol 91:776–784

Chakraborty N, Sarkar S, Mandal A, Choudhuri A, Mandal S (2018b) Indigenous siliciclastic and extraneous polygenetic carbonate facies in the Albian-Turonian Karai Shale, Cauvery Basin, India. Carb Evap 33:561–576

Chatterjee S, Scotese CR, Bajpai S (2017) The restless Indian plate and its epic voyage from Gondwana to Asia: its tectonic, paleoclimatic, and paleobiogeographic evolution. GSA Spec Pap 529:1–147

Chiplonkar GW (1985) Attempts at litho- and biostratigraphic sub-divisions of the upper Cretaceous rocks of South India—a review. Q J Geol Min Met Soc India 57:1–32

Courtillot V, Feraud G, Maluski H, Vandamme D, Moreau MG, Besse J (1988) Deccan flood basalts and the Cretaceous/Tertiary boundary. Nature 333:843–846

Cronin TM, Hayo K, Thunell RC, Dwyer GS, Saenger C, Willard DA (2010) The medieval climate anomaly and little Ice Age in Chesapeake Bay and the North Atlantic Ocean. Palaeo Palaeo Palaeo 297:299–310

Das Gupta K, Saraswati PK, Kramar U, Ravindran CN, Stüben D, Berner Z (2007) Oxygen isotopic composition of Albian-Turonian foraminifera from Cauvery Basin, India: evidence of warm sea-surface temperature. J Geol Soc India 69:390–396

Doyle P (1985) 'Indian' belemnites from the albian (lower Cretaceous) of James Ross Island, Antarctica. British Ant Surv Bull 69:23–34

Epstein S, Buchsbaum R, Lowenstam HA, Urey HC (1953) Revised carbonate-water isotopic temperature scale. GSA Bull 64:1315–1326

Frey RW (1973) Concepts in the study of biogenic sedimentary structures. J Sediment Petrol 43:6–19

Frey RW, Pemberton SG (1985) Biogenic structures in out-crops and cores: I: Approaches to ichnology. Bull Can Petro Geol 33:72–115

Frey RW, Goldring R (1992) Marine event beds and recolonization surfaces as revealed by trace fossil analysis. Geol Mag 129:325–335

Ghosh P, Bhattacharya SK, Jani RA (1995) Palaeoclimate and palaeovegetation in central India during the Upper Cretaceous based on stable isotopic composition of the palaeosol carbonates. Palaeo Palaeo Palaeo 114:285–296

Govindan A (1993) Cretaceous anoxic events, sea level changes and microfauna in Cauvery Basin, India. In: Proceedings of second seminar on petroliferous Basins of India, vol 1. Indian Petroleum Publishers, pp 161–176

Govindan A, Narayanan V (1980) Affinities of the Cretaceous foraminifera of the east coast Indian Basin and the drifting of Indian shield. J Geol Soc India 13:269–279

Govindan A, Ravindran CN, Rangaraju MK (1996) Cretaceous stratigraphy and planktonic foraminiferal zonation of Cauvery Basin, South India. Mem Geol Soc India 37:155–187

Govindan A, Yadagiri K, Ravindran CN, Kalyanasundar R (1998) A field guide on Cretaceous sequences of Tiruchirappalli Area, Cauvery Basin, India 1–53. Oil & Natural Gas Corporation Limited, Chennai

Gowda SS (1964) The foraminifera of the South Indian Cretaceous-Eocene. Eclogae Geol Helv 57:213–299

Gradstein F, Ogg J, Smith A (2004) A geological time scale 2004. Cambridge University Press, London

Haq BU, Hardenbol J, Vail PR (1987) Chronology of fluctuating sea levels since the Triassic. Science 235:1156–1167

Haq BU (2014) Cretaceous eustasy revised. Global Planetary. Change 113:44–58

Hardenbol J, Thierry J, Farley MB, Jacquin T, De Graciansky PC, Vail PR (1998) Cretaceous sequence chronostratigraphy. In: de Graciansky PC, Hardenbol J, Jacquin T, Vail PR (eds) Mesozoic and cenozoic sequence stratigraphic framework of European Basins. SEPM Spec Publ 40:3–13

Jaiprakash BC, Venkatesh P, Maya VP, Gilbert H, Selvin SP (2016) Biochron and tectonic framework for the origin of KTB Canyon in Nagapattinam sub-basin, Cauvery Basin. Proc Indian Nat Sci Acad 82:905–921

Keller G, Jaiprakash BC, Reddy AN (2016) Maastrichtian to Eocene subsurface stratigraphy of the Cauvery Basin and correlation with Madagascar. J Geol Soc India 87:5–34

Kossmat F (1897) The Cretaceous deposits of Pondicherry India. Rec Geol Surv India 30:51–110

Krishnan MS (1943) Geology of India and Burma, 6th edn. CBS Publishers, New Delhi

Lambiase JJ (1990) A model for tectonic control of lacustrine stratigraphic sequences in continental rift Basins. In: Katz BJ (ed) Lacustrine Basin exploration a case studies and modern analogs, AAPG Mem 50:265–276

Li L, Keller G (1998a) Maastrichtian climate, productivity and faunal turnovers in planktic foraminifera of South Atlantic DSDP Sites 525A and 21. Mar Micropaleontol 33:55–86

Li L, Keller G (l998b) Diversification and extinction in Campanian-Maastrichtian planktic foraminifera of North–Western Tunisia. Eclogae Geologicae Helvetiae 91:75–102

Malarkodi N, Özcan E, Venkataraman D, Suresha Gowda SC, Nagaraja PKT, Osmanyücel Ali (2017) Lepidorbitoides (Foraminifera) from the lower Maastrichtian Kallankurichchi Formation, Cauvery Basin, India: Morphometry and paleobiogeography. Cret Res 77:143–157

Mamgain V, Sastry MVA, Subbaraman JV (1973) Report of ammonites from Gondwana plant beds at Terani, Trichinopoly, Cauvery Basin. J Geol Soc India 14:189–200

Mancini EA, Puckett TM (2005) Jurassic and Cretaceous transgressive regressive (T-R) cycles, Northern Gulf of Mexico, USA. Stratigraphy 2:31–48

Miller KG, Kominz Michelle A, Browning James V, Wright James D, Mountain Gregory S, Katz MirIam E, Sugarman Peter J, Cramer Benjamin S, Christie-Blick N, Pekar SF (2005) The phanerozoic record of global sea level change. Science 310:1293–1298

Mishra PK, Rajanikanth A, Jauhri AK, Kishore S, Singh S (2004) Albian limestone building algae of Cauvery Basin South India. Curr Sci 8711:1516–1518

Murphy MA, Salvador A (1999) International stratigraphic guide–an abridged version. Episodes 22:255–271

Nagendra R, Reddy AN (2017) Major geological events of the Cauvery Basin, India and their correlation with global signatures—a review. J Palaeogeogr 6:69–83

Nagendra R, Bhavani R, Dinakaran V, Reddy AN, Jaiprakash BC (2001) Outcrop sequence stratigraphy of Kallankurichchi Formation of Velliperijnjiyam mine, and its correlation with TANCEM mine, Ariyalur Group, Tamil Nadu. Ind J Petrol Geol 10:23–36

Nagendra R, Nagendran G, Narasimha K, Jaiprakash BC, Reddy AN (2002) Sequence stratigraphy of Dalmiapuram Formation, Kallakkudi Quarry-II, South India. J Geol Soc India 59:249–258

Nagendra R, Patel SJ, Deepankar R, Reddy AN (2010) Bathymetric significance of the ichnofossil assemblages of the Kulakkalnattam Sandstone, Ariyalur area, Cauvery Basin. J Geol Soc India 76:525–535

Nagendra R, Kamalakkannan BV, Sen G, Bakkaiaraj H, Reddy AN, Jaiprakash BC (2011) Sequence surfaces and paleobathymetric trends in Albian to Maastrichtian sediments of Ariyalur area, Cauvery Basin, India. Mar Petrol Geol 28:895–905

Nagendra R, Sathiyamoorthy P, Reddy AN, Gilbert H, Jaiprakash BC (2013) Stratigraphic status, age and paleobathymetry of the Grey Shale Member of the Dalmiapuram Formation, Cauvery Basin, India. J Arab Geos 7:4133–4144

Nagendra R, Reddy AN, Jaiprakash BC, Gilbert H, Zakharov YD, Venkateswarlu M (2018) Integrated Cretaceous stratigraphy of the Cauvery Basin, South India. Stratigraphy 15:245–259

Nair KM (1974) Carbonates in Cauvery Basin, South India, seminar on carbonate rocks of Tamil Nadu, geological society of Tamil Nadu, pp 45–62

Ogg JG, Ogg G, Gradstein FM (2008) The concise geologic time scale. Cambridge University Cambridge, New York

Papanna G, Venkateshwarlu M, Periyasamy V, Nagendra R (2014) Anisotropy of magnetic susceptibility (AMS) studies of Campanian-Maastrichtian sediments of Ariyalur Group, Cauvery Basin, Tamil Nadu, India: An appraisal to paleocurrent directions. J Earth Sys Sci 123:351–364

Pemberton SG, Frey RW, Ranger MJ, Maceachern J (1992) The conceptual framework of ichnology. In: Pemberton SG (ed) Applications of ichnology to petroleum exploration. SEPM Core Workshop, vol 17, pp 4–29

Poornachandra Rao GVS, Bhalla MS (1981) Paleomagnetism of Dhar traps and drift of the subcontinent during the Deccan volcanism. Geophys J Royal Astro Soc 65:155–164

Prasad GVR, Verma O, John JF, Anjali G (2013) A new Late Cretaceous vertebrate fauna from the Cauvery Basin, South India: Implications for Gondwanan paleobiogeography. J Vertebr Paleontol 33:1260–1268

Rai J, Ramkumar M (2007) Calcareous nannofossils from Ottakovil Formation (Late Maastrichtian), Cauvery Basin, South India. (Abstract.). XXI Indian Colloquium on Micropaleontology and Stratigraphy, pp 144–145

Raju DSN, Ravindran CN, Kalyanasundar R (1993) Cretaceous cycles of sea level changes in the Cauvery Basin, India—a first revision. ONGC Bull 30:101–113

Raju DSN, Jaiprakash BC, Ravindran CN, Kalyanasundar R, Ramesh P (1994) The magnitude of hiatus and sea level changes across the K T boundary in Cauvery and Krishna Godavari Basin. J Geol Soc India 44:301–315

Raju DSN, Jaiprakash BC, Ravindran CN, Kalyanasundar R, Ramesh P (2005) The magnitude of hiatus and sea level changes across K/T boundary in Cauvery and Krishna-Godavari Basins. Indian Ass Petrol Geol Spec Publ 1:104–113

Raju DSN, Reddy AN (2016) Why there is a substantial dichroneity in biostratigraphic dating of Cretaceous sediments in the Krishna-Godavari Basin and Cauvery Basin—a review. ONGC Bull 51:119–134

Ramanathan S (1968) Stratigraphy of the Cauvery Basin with reference to its oil prospects. In: Cretaceous-Tertiary Formations of South India. Mem Geol Soc India 2:153–167

Ramanathan RM (1977) Depositional systems and thrust area for exploration in Cauvery Basin. ONGC Bull 24:53–69

Rama Rao L (1956) Recent contribution to our knowledge of the Cretaceous rocks of South India. Proc Indian Acad Sci, Sec B 44:185–245

Ramasamy S, Banerji RK (1991) Geology, petrography and systematic stratigraphy of the pre-Ariyalur sequence in Tiruchirappalli district, Tamil Nadu, India. J Geol Soc India 37:577–594

Rangaraju MK, Agarwal A, Prabhakar KN (1993) Tectono-stratigraphy, structural style, evolutionary model and hydrocarbon prospects of the Cauvery and Palar Basins of India. Indian Petrol Publ Dehradun 1:371–398

Rasheed DA, Ravindran CN (1978) Foraminiferal biostratigraphic studies of the Ariyalur Group of Tiruchirappalli Cretaceous rocks of Tamil Nadu state. In: Proceedings of VII Indian Colloquium on Micropal and Strati, pp 321–326

Reddy AN, Nayak KK, Gogoi D, Sathyanarayana K (1992) Trace fossils in cores of Kopili, Barail and Tipam sediments of Upper Assam Shelf. J Geol Soc India 40:253–257

Reddy AN, Jaiprakash BC, Rao MV, Chidambaram L, Bhaktavatsala KV (2013) Sequence stratigraphy of late Cretaceous successions in the Ramnad Sub-Basin, Cauvery Basin, India. Geol Soc India Spec Publ 1:78–97

Saraswati PK, Srinivasan MS (2016) Micropaleontology: principles and applications. Springer, Switzerland

Sarkar S, Chakraborty N, Mandal A, Banerjee S, Bose PK (2014) Siliciclastic-carbonate mixing modes in the river-mouth bar paleogeography of the Upper Cretaceous Garudamangalam Sandstone (Ariyalur, India). J Paleogeogr 3:233–256

Sastri VV, Chandra A, Pant SC (1963) Foraminifera from Raghavapuram shales near Tirupati, Andhra Pradesh. Rec Geol Surv India 92:311–314

Sastri VV, Raju ATR, Sinha RN, Venkatachala BS, Banerji RK (1977) Biostratigraphy and evolution of the Cauvery Basin, India. J Geol Soc India 18:355–377

Sathyanarayana K, Reddy AN, Banerjee S, Krishna M (1999) Ichnology and facies interpretation of subsurface sediments of Krishna-Godavari basin. Indian J Petrol Geol 8:91–102

Schlanger SO, Jenkyns HC (1976) Cretaceous oceanic anoxic events: causes and consequences. Geol Mijnbouw 55:179–184

Schöbel S, de Wall H, Ganerod M, Pandit MK, Rolf C (2014) Magnetostratigraphy and [40]Ar-[39]Ar geochronology of the Malwa plateau region (Northern Deccan traps), central western India; significance and correlation with the mail Deccan large igneous province sequences. J Asian Earth Sci 89:28–45

Schoene B, Samperton KM, Eddy MP, Keller G, Adatte T, Bowring SA, Khadri SFR, Gertsch B (2015) U-Pb geochronology of the Deccan Traps and relation to the end-Cretaceous mass extinction. Science 34:182–184

Scotese CR (1997) Paleomap software. Paleomap project. http://scotese.com

Seilacher A (1967) Bathymetry of trace fossils. Mar Geol 5:413–428

Sundaram R, Rao PS (1979) Lithostratigraphic classification of Uttatur and Trichinopoly group of rocks in Trichinopoly district, Tamil Nadu. Geol Surv India Misc Publ 45:11–119

Sundaram R, Rao PS (1986) Lithostratigraphy of Cretaceous and Paleocene rocks of Tiruchirappalli district, Tamil Nadu. Rec Geol Surv India 115:9–23

Sundaram R, Henderson RA, Ayyasami K, Stilwell JD (2001) A lithostratigraphic revision and paleo-environmental assessment of the Cretaceous System exposed in the onshore Cauvery Basin, Southern India. Cret Res 22:743–762

Tewari A, Hart MB, Watkinson MP (1996a) A revised lithostratigraphic classification of the Cretaceous rocks of the Trichinopoly District, Cauvery Basin, and Southeast India. Contrib XV Indian Colloquium of Micropal and Strati, pp 789–800

Tewari A, Hart MB, Watkinson MP (1996b) Foraminiferal recovery after the mid-Cretaceous oceanic anoxic events, OAE in the Cauvery Basin, southeast India. In: Hart MB (ed) Biotic recovery from mass extinction events. Geol Soc London Spec Publ 102:237–244

Turgeon SC, Creaser RA (2008) Cretaceous oceanic anoxic event 2 triggered by a massive magmatic episode. Nature 454:323–327

Vail PR, Mitchum RM, Thompson S (1977) Seismic stratigraphy and global changes of sea level, part 3 relative changes of sea level from coastal onlap. In: Payton CE (ed) Seismic stratigraphy: applications to Hydrocarbon exploration. AAPG Mem 26:63–81

Vandamme D, Courtillot V, Besse J, Montigany R (1991) Paleomagnetism and age determinations of the Deccan traps (India); results of a Nagpur–Bombay traverse and review of earlier work. Rev Geophys 29:159–190

Van Wagoner JC, Posamentier HW, Mitchum RM, Vail PR, Sarg JF, Loutit TS, Hardenbol J (1988) An overview of the fundamentals of sequence stratigraphy and key definitions. In: Wilgus CK,

Hastings BS, Kendall CG St C, Posamentier HW, Ross A, Van Wagoner JC (eds) Sea level changes: an integrated approach. SEPM Spec Publ 42:39–45

Venkatarengan R, Rao GN, Prabhakar KN, Singh DN, Awasthi AK, Reddy PK (1993) Lithostratigraphy of Indian petroliferous Basins. Document VIII, Krishna Godavari Basin, KDMIPE, ONGC, Dehradun

Voigt S, Michael, M, Surlik F, Walaszczyk I, Ulicny D, Cech S, Voigt T, Wiese F, Wilmsen M, Niebuhr B, Reich M, Funk H, Michalik J, Jagt JWH, Felder P, Schulp AS (2008) Cretaceous. In: McCann T (ed) The geology of Central Europe: Mesozoic and Cenozoic, vol 2, pp 923–992

Watkinson MP, Hart MB, Joshi A (2007) Cretaceous tectonostratigraphy and the development of the Cauvery Basin, Southern India. Geol Soc London Spec Publ 13:181–191

Zakharov YD, Smyshlyaeva OP, Popov AM, Shigeta Y (2006) Isotopic composition of late mesozoic organogenic carbonates of far east (oxygen and carbon isotopes, palaeoclimatic events and their global correlation). Vladivostok: Izdatel'stvo "Dalnauka", 204 p (in Russian)

Zakharov YD, Shigeta Y, Nagendra R, Safronov PP, Smyshlyaeva OP, Popov AM, Velivetskaya TA, Afanasyeva TB (2011) Cretaceous climate oscillations in the southern paleolatitudes: new stable isotope evidence from India and Madagascar. Cret Res 32:623–645

Continental-to-Marine Transition in an Ongoing Rift Setting: Barremian-Turonian Sediments of Cauvery Basin, India

Nivedita Chakraborty, Subir Sarkar, and R. Nagendra

Abstract Study of Cretaceous (Barremian-Turonian) sediments within the Ariyalur-Pondicherry sub-basin, Cauvery Basin, India mirrors the deposition of fluvial-to-marine transition in a syn-rift setting during the Mesozoic breakup of east Gondwanaland. Within the investigated interval, fluvial Basal Siliciclastic Formation (Upper Gondwana equivalent), overlying the Archean Basement, is succeeded by the marine Dalmiapuram Formation (shallow water) and the Karai Shale Formation (offshore). However, both the marine formations demonstrate the lithocontact with the basement locally. Process-based sedimentary facies analysis identifies nine facies associations categorized in non-marine, shallow marine and deep marine super associations, cumulatively comprising forty sedimentary facies. Facies associations vary in its lithology, primary sedimentary structures, stratal geometry and pattern, paleoucrrent direction, as well as in grain size and sorting. The present study reveals the depositional processes ensued across the environmental continuum of mountain front to the ocean. Basal Siliciclastic sediments are restricted in isolated outcrops, along the western margin of the basin. Within this formation, scree-alluvial fan and channel amalgamation are restricted at basin-margin while flood-plain governs in basin-interior. The depositional contextual shifted from continental to marine during Albian on the advent of marine transgression along the eastern passive margin of India. A carbonate (non-rimmed) ramp platform, evolving from homoclinal to distally steepened, shaped the pre-fall shelf by depositing carbonates (Dalmiapuram Formation) while, organic-rich glauconite, phosphate nodule bearing shale (Karai Shale Formation) settled in the basin center. The fluvial-to-marine transition surface records a sequence boundary with the overlying formations reflecting relative sea level change. Limestone to shale conversion is gradational in accord with

N. Chakraborty (✉)
Department of Geology, Kabi Jagadram Roy Government General Degree College, Bankura 722143, West Bengal, India
e-mail: nivedita.jugeo@gmail.com

S. Sarkar
Department of Geological Sciences, Jadavpur University, Kolkata 700032, India

R. Nagendra
Department of Geology, Anna University, Chennai 600025, India

the pronounced retrogradational trend. However, the basal part of the Dalmiapuram Formation displays a shallowing upward trend (aggradational or progradational). The maximum flooding condition is achieved during the Karai Shale sedimentation at the crowning of transgression.

Keywords Continental-to-marine transition · Facies · Sequence stratigraphy · Rift basin · Cretaceous · Cauvery basin

1 Prologue

Continental to marine transition is recurrent in the rock record, covering both Precambrian and Phanerozoic era. Many case studies have been documented on environmental amend in global sedimentary basins (Fedo and Cooper 1990; Bose and Chakraborty 1994; Simpson et al. 2002; Veiga et al. 2007; Gani et al. 2015; Mazumder et al. 2015; Chakraborty et al. 2017). However, incessant exposure of continental to marine sediments is atypical; especially in case of rift setting in passive margin. Besides, process-based considerate of sedimentary successions of such contextual facies analysis, paleogeography, stratigraphic architecture in sequence stratigraphic context is approximately insignificant, barring a few (Bhattacharya et al. 2018; Dillinger and George 2019; Higgs et al. 2019). However, considerable interest has been employed recently on re-evaluating the depositional systems of passive margins, consistent and reachable mainstay of hydrocarbon exploration success worldwide (Levell et al. 2010). Reportedly, the passive margin post-rift sequences are estimated to host approximately 35% of all giant oil field discoveries (Mann et al. 2003).

Cauvery Basin is a hydrocarbon producing pericratonic rift basin located along the east coast passive margin of South India. Barremian-Turonian (Cretaceous) succession of the Ariyalur-Pondicherry sub-basin, built up during the rifting phase of the Cauvery Basin (Watkinson et al. 2007; Nagendra and Reddy 2017), is an epitome example to investigate the depositional processes effective across a spectrum of environments ranging from mountain front to ocean. Resting on the Archean crystalline basement continental Basal Siliciclastic Formation (Chakraborty et al. 2017), which researchers considered as Upper Gondwana equivalent (Barremian–Aptian), is followed by the shallow marine Dalmiapuram Formation (Albian-Cenomanian) and the deep marine Karai Shale Formation (Albian-Turonian) at the top of the studied sequence (Chakraborty et al. 2018a; Watkinson et al. 2007). The Barremian-Turonian interval records a continuous deposition within onshore rift basin and their equivalent in subsurface (Govindan et al. 2000; Figs. 1, 2).

In the present study, the continental alluvial fan-axial channel-floodplain system and the marine shelf (inner to outer) deposits together afford to examine a classical fluvio-marine transition during syn-rift stage of a sedimentary basin and its response to sea-level change. A high-resolution sedimentary facies analysis of the Barremian-Turonian succession has been carried out to interpret the depositional environments and paleogeographic distribution of the rocks. This study reveals interplay of multiple depositional agents within a spectrum of flow conditions. Moreover,
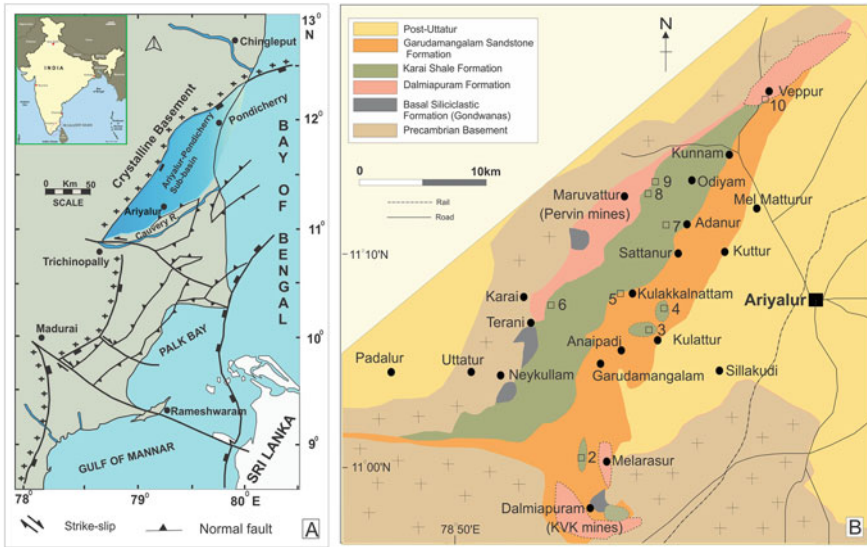
Fig. 1 Tectonic map of the Cauvery rift basin showing the location of Ariyalur-Pondicherry sub-basin (Position of Cauvery Basin on the Indian map within inset) (**a**). Location and lithological map of the study area (**b**)

Fig. 2 Stratigraphic sub-division of the Lower-Upper Cretaceous succession in the study area in outcrop and sub-surface
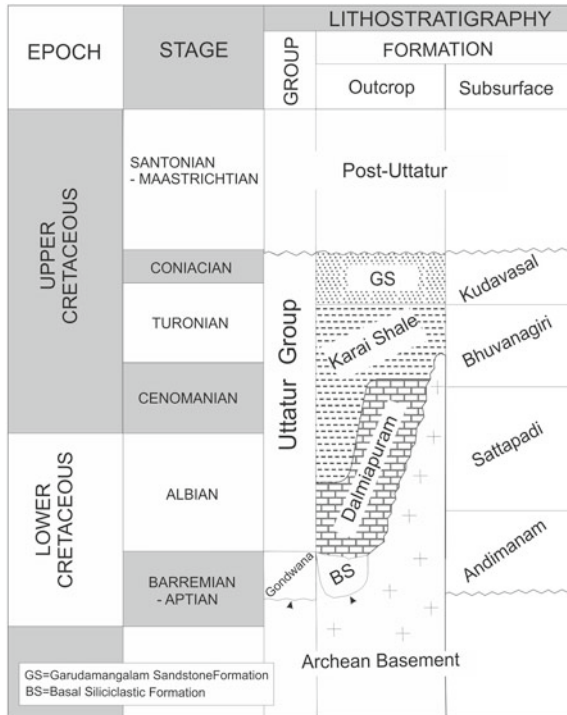
the study targeting lithological successions of Barremian to Turonian age outcropping in and around Ariyalur (Tamil Nadu), Cauvery Basin bears a considerable potential to future hydrocarbon exploration in continental shelf, syn-rift zones and deep-water deposits within this basin in addition to other basin-fills along south-eastern passive margin of India.

2 Geological Setting

The Late Jurassic-early Cretaceous rifting of East Gondwanaland separated India from Australia-Antarctica, opened up the Indian Ocean and, formed a number of NE-SW trending basins along the eastern passive margin of India (Powell et al. 1988; Watkinson et al. 2007). Cauvery Basin is the southernmost basin among that population of rift basins. (Nagendra et al. 2011). The Cauvery Basin has evolved due to crustal extension between India and Sri Lanka as a result of the breakup of the East Gondwana (Premarathne, 2020). The basin is located in the south-eastern part of Peninsular India between 8° 30′ N and 12° 30′ N and 78° 30′ E and 80° 30′ E (Fig. 1a; Narasimha Chari et al. 1995). Cauvery Basin houses commercially viable oil and natural gas deposits both onshore and offshore. The Indian side of the Cauvery Basin extends over 62,500 km^2 onshore and offshore up to 200 m isobath. The basin is a block-faulted pericratonic failed rift basin comprising horst-graben basin architecture (Sastri et al. 1973, 1981; Nagendra and Reddy 2017). Rift-related extension generated a series of linked half-graben basins separated from each other by subsurface (basement) ridges, which includes Ariyalur-Pondicherry sub-basin (Ariyalur-Pondicherry Depression) in the north (Sastri et al. 1979; Chakraborty et al. 2017) (Fig. 1a). This study deliberated with the Barremian-Turonian succession exposed in the southern sector of the Ariyalur-Pondicherry sub-basin in and around Ariyalur and Perambalur district, Tamil Nadu (Fig. 1b).

3 Stratigraphy

Resting on the Archean basement the Basal Siliciclastic Formation (Upper Gondwana sediments) exposed as isolated pockets. These non-marine sediments (Barremian-Aptian) are invariably faulted against the Archean basement during the initial phase of rifting and are overlain by the Uttatur Group (Fig. 2). Bounded by two unconformities, the Albian to Coniacian sediments of the Uttatur Group, within the Cauvery Basin, comprises three formations: from base to top, they are Dalmiapuram, Karai Shale and Garudamangalam Sandstone with gradational transitions in between them (Fig. 2). However, the outcrops of both the Dalmiapuram and Karai Shale formations show direct contact with the Archean basement (Chakraborty and Sarkar 2018; Chakraborty et al. 2018a). The Karai Shale Formation was earlier divided into two members (Odhyium and Kunnam), one is clayey and the other is sandy (calcarenite).

The two lithologies, however, alternate many times in vertical section to debase their suitability as criteria for stratigraphic classification. Unavoidable confusion arose as some authors placed the sandy member at the base and others at the top of the Formation (Sundaram and Rao 1986; Ramkumar et al. 2004). Present authors disagree with the existing oversimplification of lithostratigraphy but prefer to explain the dilemma in light of paleogeographic distribution and sedimentation dynamics through space and time (Chakraborty et al. 2018a). The floral and palynological assemblages assign a Barremian-Aptian age for the Basal Siliciclastic Formation (Singh and Venkatachala 1988; Garg et al. 1988; Ramasamy and Banerji 1991; Venkatachalapathy and Ragothaman 1995; Bou Dagher-Fadel et al. 1997), which has been interpreted as of fluvial origin (Banerji 1983; Chakraborty et al. 2017). The marine origin of the fossil-rich Dalmiapuram and Karai Shale formations is apparent from the records of the macro- and micro-fauna (Ayyasamy 1990; Venkatachalapathy and Ragothaman 1995; Banerji et al. 1996; Tewari et al. 1996b; Hart et al. 2001; Sundaram et al. 2001; Mishra et al. 2004) and isotopic characters of the diagenetically unaltered sediments (Fig. 3; Chakraborty and Sarkar 2018; Chakraborty et al. 2018b). The benthic assemblage within the Karai Shale Formation indicates an open marine depositional condition with a bathymetry of 100–200 m (Nagendraa et al. 2013). The presence of authigenic glauconite within Karai Shale corroborates its offshore origin (Banerjee et al. 2016). Sedimentation of organic-rich shale perhaps resulted from the expansion of oxygen-depleted conditions at the depositional surface (Nagendra and Reddy 2017). The Karai Shale Formation is overlain by post-rift Garudamangalam Sandstone of marginal marine setting, which marks end of Uttatur Group (Sarkar et al. 2014). This study focusses upon the Barremian-Turonian succession within the Ariyalur-Pondicherry sub-basin in and around Ariyalur, incorporating the Basal Siliciclastic, Dalmiapuram (Carbonate-Marl) and Karai Shale formations (mixed siliciclastic-carbonate).

4 Facies Analysis

The sedimentary facies analysis is applied based on lithology, sedimentary structures, body geometry, thickness and association. Diagnostic features of forty distinguished sedimentary facies constituents of Basal Siliciclastic (entirely siliciclastic), Dalmiapuram (Carbonate and Marl) and Karai formations (mixed siliciclastic-carbonate) are summarized (Table 1; Figs. 4, 5, 6, 7). The distribution of the four studied formations in outcrop has been shown in Fig. 8. The facies are grouped into nine facies associations in relation to sedimentary dynamics and paleogeography.

Fig. 3 Litholostratigraphic, δ¹³C stratigraphic and sequence stratigraphic context of the studied succession (modified after Chakraborty et al. 2018b)
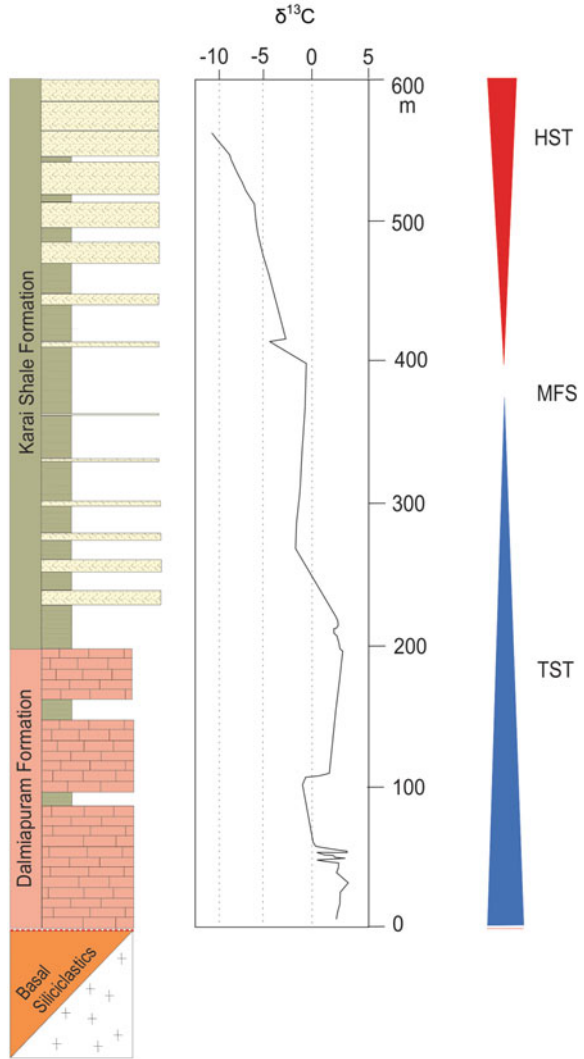
4.1 Non-marine Facies Associations

On the floor of the Ariyalur-Pondicherry sub-basin of Cauvery Basin, resting above the Archean basement with non-conformable contact, the Basal Siliciclastic (Gondwana sediments) represents the non-marine facies associations and is well exposed in three mine sections at KVK mine, Dalmiapuram and clay mines, Neykulam and Terani villages (Fig. 5a, 8). Exposures are sparse, not exceeding 70 m in thickness. Breccias-conglomerates and pebbly sandstones constitute the major part and coarse

Table 1 Summary of facies associations, description and interpretation of each facies

Description	Interpretation
Non-marine super facies association	
FA 1. Scree Cone	
1A. This facies is characterised by clast supported wedge-shaped breccia attaining bed thickness up to 75 cm and stacked one above another unless locally interleaved by facies 1B. The tops of the breccia beds are irregular and jagged if underlain by the sandstone beds (1B); some sub-vertical clasts have their basal portions extending down into the underlying sandstone laminae. The breccia clasts are sharply angular. In size they are generally of pebble grade, but may reach up to the boulder grade of maximum measured length of 45 cm. These clasts are mostly traceable into the local Archean basement (granite gneiss and amphibolites). They are generally haphazardly oriented, but in mutual contact with each other, though their interstitial spaces are filled by smaller granule-rich sand of the same composition. In one instance, the relationship between two large clasts is such that one seems to have landed on the other, breaking it and pushing it downward. Tabular clasts are, at places, found reclining on inclined surfaces of the breccia beds	Scree or rock fall deposit formed at steep basin-margin localities (Selley 1965). Clast angularity reflects little bed load transport. Tabular clasts reclining on breccia bed-surfaces possibly reflect some degree of sliding of those clasts along inclined scree-slopes
1B. This facies is composed of sandstone interspersed with breccias beds of the facies 1A; together give rise to wedge-shaped bodies, of maximum thickness around 8 m. The sandstone is poorly sorted, massive, with thin beds not exceeding 15 cm, and laterally impersistent; measured outcrop width up to 1.5 m. The top parts of the beds may locally bear planar laminae, but at places are ruptured and eroded out around breccia clasts that intruded into them from above. In comparison to sandstone bed-tops, their bases are broadly smooth tending to retain the configuration of the underlying breccia bed surfaces	Making drastic alteration of sedimentation dynamics without any change in the inferred basin-margin palaeogeography, the sandstone beds were possibly deposited as hill-wash during rain storms (Bose et al. 2008). These generally massive beds indicate rapid deposition and their tendency to retain primary configuration of underlying surfaces specifies to the settling of sand grains dominantly from suspension

(continued)

Table 1 (continued)

Description	Interpretation
1C. Basinwards the facies 1A–1B combination gives way to the non-recurrent conglomerate facies 1C, generally clast-supported. These beds are, more or less, tabular in geometry and around 80 cm thick. Clasts are distinctly bimodal both in size and shape without any apparent correlation with composition. The comparatively larger clasts, smaller though with respect to the clasts of facies 1A, are angular and tabular in shape, while the smaller clasts are well rounded, often highly spherical. No compositional preference is apparent between the two size populations. Although the beds are internally massive, the long axes of the larger tabular clasts within them are dominantly aligned parallel to the bed	Identified as scree apron (Bose et al. 2008) since the facies, appearing to skirt the postulated scree cone, found only at the interpreted down-slope fringe. Without any correlation with clast composition textural inversion present within the facies indicating sediment supply from dual sources. The angular larger clasts had a proximal source, possibly the scree cone upslope while the better rounded smaller clasts possibly came from a relatively distal source
FA 2. Alluvial Fan	
2A. This facies constitutes conglomerates, dominantly matrix-supported. Most have lenticular geometry with bases of conglomerate beds being flat and their tops convex-upward. Their thickness maxima range up to ~1.25 m. With respect to clast composition they do not differ significantly from the breccias, although their maximum clast size is reduced to 8 cm. Internally, the beds are massive, clasts floating haphazardly within fine grained matrix; some clasts protrude above the bed surface	Debris flow that underwent sudden freezing of matrix with expulsion of fluid (Blair and McPherson 1994). Where the flow viscosity did not allow the clasts to sink, they protruded above the flow surface
2B. These lenticular conglomerates are matrix to clast-supported, but reverse graded in coarse-tailed fashion and have maximum bed thickness of ~1 m. These conglomerates also generally have convex upward bed geometry, although a few have scoured bases. In one instance this conglomerate was found channelized. The maximum clast size of this facies is comparable to that of the preceding facies	Inferred as modified grain flow (Middleton and Hampton 1976). Reverse grading manifests collision between clasts and freezing of the flow through clast-clast interlocking
2C. This facies comprises convex-upward conglomerate bodies, clast-supported in the basal part of the beds but gradually turn matrix-supported upward and may eventually even become sandy. Both the bed-bounding surfaces are sharp. The pebbly lower part of these bodies is generally massive, but may also bear crudely defined cross-strata. Maximum cross-set thickness and maximum clast-size recorded in this facies are around 8 cm and 9 cm respectively	This facies appears to be sieve deposits manifesting freezing bedforms, possibly because water readily percolated away through the porous sediment (Todd 1989). As the flow waned sand infiltrated on top of the bedforms

(continued)

Table 1 (continued)

Description	Interpretation
2D. These conglomerates, generally, though not always, encased by pebbly sandstone (facies 2F), are tabular in geometry, but locally have small scours at their bases. The maximum clast length is measured up to 8 cm. No grading was observed, but tabular clasts are dominantly bed-parallel and locally imbricated	These conglomerate units may have been deposited from a more fluidal sheet-flow (Bose et al. 2008), the basal scours manifesting initial turbulence
2E. The conglomerates characterizing this facies occupy the deepest part of the channel forms, thereby showing concave upward bases and flat tops. Multiples of such beds, not exceeding 60 cm in total thickness, may amalgamate. Pebble size, however, decreases upward through such a stack, the maximum recorded clast-size 10 cm	Deposited most probably from strong turbulent flows preferably along the channel thalwegs
2F. This facies is characterized by pebbly sandstone, locally crudely trough cross-stratified. The cross-sets do not exceed 15 cm in thickness while their co-sets range up to 50 cm. The pebbles generally concentrate along foreset bases and cross-set boundaries	The upward passage of the conglomerates to cross-stratified pebbly sandstone clearly manifests progressive decline in flow shear
2G. The cross-stratified facies 2F is generally overlain by the dominant planar laminated sandstone. Being channel-confined, exposure width of this facies bodies does not exceed 3 m and their thicknesses range up to 22 cm. In a few other instances, however, facies 2G gives way upward to small ripples, not exceeding 3 cm in height, and draped by a thin film of mud	The upward switch of cross-strata into planar lamination or ripple forms draped by mud, records instances of flooding
FA 3. Axial channel	
3A. The channel-fills are often multi-storeyed, each storey generally having massive sandstone at the base. the maximum thickness of the individual channel-fills measures up to 2.5 m	The massiveness of the facies attests to rapid deposition presumably because of hydraulic jump induced by sharp decrease in gradient at the fan base
3B. The facies is characterized by coarse-grained planar laminated sandstone resting on channel base within each storey of channel fill unit	This facies is thought to have formed either as linguoid bars or cross-channel bars (Miall 1996)
3C. This facies comprises large scale cross-stratified sandstone overlying the preceding facies	Probably manifests bar-top reworking during low water stage
3D. Facies 3C is followed by comparatively finer grained ripple laminated sandstone	

(continued)

Table 1 (continued)

Description	Interpretation
3E. The channel-fill mosaic is locally disrupted by this facies characterised by isolated wedge-shaped or broadly tabular and rust-coloured granular sandstone bodies, internally devoid of structure	This facies stands out as aberrant within the association and possibly owes its origin to intermittent massflows. Seismicity, overloading and undercutting are the most likely mechanism to trigger such flows
FA 4. Flood-plain	
4A. This facies is characterised by trough cross-stratified, poorly sorted and coarse-grained, though pebble-free sandstone. They exhibit broadly lenticular body geometry with concave-up bases and maximum thickness around 1.85 m	River channel deposit (Long 2011)
4B. This facies comprises trough cross-stratified sandstone beds having flat bases and convex-up tops, and also bear thin silty mudstone partings inclined at a high angle to the orientation of the associated trough cross-strata. The cross-set thickness is, on average, 16 cm although it discernibly decreases upward within individual co-sets	Inferred as point bar (Chung et al. 2005); inclined mud laminae were presumably deposited during successive floods
4C. These coarse-grained sandstones have planar erosional bases and internal planar laminae, and may be slightly convex upward. They have tabular body geometry and measure up to ~1.4 m in thickness	Linguoid or cross-channel bars on the channel-floor
4D. Some sandstone bodies, distinctly finer grained, thinner (<3 cm) and sheet-like in geometry, are generally found inter-bedded with comparatively thicker (>23 cm) mudrocks. They are typically planar laminated, but may have small ripples on top of them. Presence of rootlets and burrows is noted	Interpreted as of overbank crevasse-splay origin. The sand-laden water spilled over from the fixed channels (Farrell 2001) during floods had possibly given rise to sheet flows. Later reworking might have generated the ripples on the bed-tops
4E. This facies is composed of darker shale characterised by planar laminae manifested in thin silt stringers. Rootlet marks occur locally on bed-tops and burrows, often compressed, within the beds. Mudrock beds are comparatively thicker (>40 cm) and darker in colour. Under the microscope they reveal crinkled carbonaceous laminae, stray rafted over-sized sand grains and disseminated pyrite	Presumably deposited farther away from the river channels. Curled mat fragments at certain levels suggest episodic deposition. Pyrite presumably precipitated during early diagenesis because of mat decomposition
4F. Dark grey carbonate mudstone, broadly lenticular and substantially thick (~70 cm), occurs rarely within encasing mudrock. Dark carbonaceous, often curled fragments concentrate preferably in the lower part of these argillaceous bodies	Possibly formed in isolated lakes or ponds in close association with overbank sediments, where prolonged evaporation helped to precipitate calcite

(continued)

Table 1 (continued)

Description	Interpretation
4G. This granule-rich facies is non-recurrent, distinctly coarser grained, tabular in shape and internally massive. It maintains a uniform thickness of over 25 cm. This facies has a sharp base and less distinct top contact	Deposition possibly took place from waning sediment gravity flow
4H. This facies is characterised by light grey coloured fine grained thick shale attaining thickness up to 5 m	Inferred as overbank deposit
4I. This facies is identified by intermittent occurrence of medium to fine-grained, poorly sorted sandstones of lenticular geometry	Interpreted as shoestring channels (Bridge 2006)
Shallow marine super facies association	
FA 5. Sea-margin	
5A. The breccia bodies are strongly wedge-shaped, and consist of chaotically arranged angular blocks of calcarenite, as if, tumbled down one above another, with the largest one measured ~1.45 m long. The smaller limestone breccias clasts are interlaminated and constitute the only remnant of the interlaminated Facies 5B, as stated above. In their midst sparsely distributed are clast traceable to the Archean basement or the basal siliciclastics (non-marine facies association). These breccia bodies rest directly on the Archean basement or basal siliciclastics and shale. The contact at their base is stepped and not as smooth as it is under Facies 6C. The facies is non-recurrent	Rock-fall or scree deposit (Bose et al. 2008; Chakraborty and Sarkar 2018; Shanmugam 2015). The stepped nature of this facies base manifests the block faulting

(continued)

Table 1 (continued)

Description	Interpretation
5B. This facies skirts round the scree fan, strongly wedge-shaped, about 30 m in width and maximum thickness of ~4.5 m. The clasts are predominantly of calcarenite. The pebbles are well rounded, almost of uniform size, averaging around 45 cm in diameter. They are in mutual contact and interstitial spaces are filled mostly by sparry calcite. This facies rests directly on the basement	Apron around the base of the basin-margin scree (Burchette 1988). The apron must have been affected by strong current running along the sea coast as manifest in good roundness and size sorting of the clasts and the sparry cement between them
FA 6. Shoreface	
6A. Large-scale cross-stratified biosparite and intrasparite alternating with small-scale cross-stratified biosparite and biomicrite. The large-scale cross-strata, locally displaying chevron shape, possess set-thickness up to 22 cm while the smaller scale cross-stratified variety attains bedform-height about 12 cm. In both the varieties, bioclasts tend to concentrate along foreset bases. Bioclasts belong to bivalves, coral, echinoid and encrusting bryozoan	Wave-affected, at least locally, bar-interbar system (Chakraborty and Sarkar 2018; Sarkar et al. 2014)
6B. Pink-colored massive biomicrite alternating with significantly coarse-grained yellowish massive or graded biomicrite. Upward transition from the latter is generally gradational and looks planar where sharper. The reverse transition isalways sharp and irregular with minute load casts. The former locally displays bird's eye structure. The bioclasts belong mainly to bivalves, algae and corals. Micritized rims around bioclasts are common. Some detrital quartz and feldsparare also present. This facies laterally passes into the preceding facies	Lagoon-like confined waterbody, possibly behind the bar-interbar system. The pink limestone appears to be indigenous, while the yellowish coarse-grained sediment is of a storm wash-over origin (Sarkar et al. 2014). Bird's eye structures were possibly formed because of gas accumulation, implying shallow depth of deposition
6C. Non-recurrent massive biometric limestones having laterally uniform thickness around 25 cm. Bioclasts are dominantly of small thin bivalve shells; also fragments of echinoids, foraminifers and algae. Siliciclastics, silt-sized, are also sparsely distributed. This facies grades laterally into the next facies with deleting content of siliciclastic grains	Deposited on the shelf, marking the initiation of carbonate sedimentation, beneath the storm wave base (Schieber et al. 2007; Seidler and Steel 2001)
FA 7. Shallow Shelf	

Table 1 (continued)

Description	Interpretation
7A. Non-recurrent dark-colored shale interspersed with paper-thin planar stringers of calcarenite containg shell hash. Laterally it grades into the facies 6C. The maximum attaining thickness is ~2.5 m. Glauconite is noted in its comparatively lighter colored part, however pyrite is common in occurrences within its darker part	Deposition apparently took place in the deepest part of the inland sea, dysoxic to anoxic in nature
7B. Wedge-shaped and locally distinct convex-up bodies of matrix-supported limestone conglomerate in which the clasts float within fine-grained matrix, even may protrude above the bed surface. The limestone pebbles are generally rounded, so are sandstone shale fragments, but basement clasts are more often, not. The maximum pebble length recorded is 8 cm. The clasts are mostly traceable to the preceding facies association, but a few others are derived from the Archean basement and the basal siliciclastic sediments. All the clasts are chaotically arranged and oriented. This facies rests on the previous association	Deposition apparently took place on the shelf through mass transport. The clasts are transported in suspension within matrix. Some clasts are even buoyed up above the bed surface. Deposition took place apparently as the matrix froze instantaneously. Debris flow (Bose and Sarkar 1991) mechanism had possibly been the dominant transport mechanism
7C. This facies of variable clast size is also matrix-supported, sheet-like in geometry, internally massive or normally graded. Bed thickness varies, ranging up to 1.87 m, however more commonly 25–50 cm. Occasionally ripples occur on bed tops, and flute casts, groove casts and gutter casts at their soles. This facies also succeeds the preceding association	Deposition apparently took place on the shelf, beneath the stormwave-base. This facies is also a mass-flow product, turbidite, transporting particles in auto-suspension with help of internal turbulence
7D. This micritic limestone is sheet-like in geometry and occurs in between different couplets of above-mentioned mass-flow facies 6C and 6D. Their basal contacts are gradational but upper contacts are sharp. It contains moulds of bivalve shells, and fragments of coral, echinoid, crinoid and bryozoan bearing micritic rims	This facies deposited in between the mass-flow events on the shelf, beneath the storm wave base in an inland sea that possibly had not much depth
7E. Intramicritic limestone internally characterized by cross-strata of 6–7 cm set thickness, but reducing up section as the facies passes upwards into the next facies. The cross-strata are separated from each other in vertical section by micritic limestone with average thickness of 2.5 cm. Thin drapes of micritic limestone also occur on some foresets, rarely in double (Bhattacharya et al. 2018). The cross-strata orientation is bipolar-bimodal. The facies contains numerous fragments of corals, echinoid, crinoid and bryozoan	Tidal shelf broadened enough to have its tide synchronized with oceanic tide to create tidal bedforms of significant heights. Double mud drapes bear tell-tale evidence for deposition in permanently submerged area. Bipolar-bimodal cross-strata orientation reveals, more or less, symmetrical ebb and flood

(continued)

Table 1 (continued)

Description	Interpretation
7F. This facies differs from the preceding facies only in scale of cross-strata (2–3 cm) and thickness of interspersed micritic laminae (3.5 cm). This facies is predominantly rich in small bivalve shells, micritized along their rims	Deposition took place in a comparatively deeper shelf setting in comparison to that where the preceding facies was deposited
Deep marine super facies association	
FA 8: Storm dominated muddy shelf	
8A. This facies, predominantly calcarenitic (packstone) in composition, attains ca. 4.6 m maximum thickness possessing laterally persistent tabular or sheet-like beds. The individual calcarenite beds achieve thicknesses up to 75 cm where they amalgamate, but reduce down to 22 cm in individual cases. Grey shale interbeds, often iron-stained, never exceed a thickness of 10 cm. Base of calcarenites often bears gutters (average width 9 cm and depth 4 cm). The beds internally characterized by partly developed tempestite sequences, massive basal parts, otherwise being planar laminated, wavy laminated and hummocky cross-stratified (width c. 22 cm, height c. 10 cm) followed by locally wave rippled (width c. 10 and height c. 6 cm) bed-tops. The rock contains plentiful broken shell hash, a few granite fragments and some feldspar and quartz grains, fragile algal flakes and micritic rims around shell clasts. The non-carbonate clasts appear to be angular/sub-angular but with irregular nibbled boundaries. The interstitial spaces are filled by fine-grained carbonate matrix	Product of meteorological storm-induced flow in open shelf setting. An extraneous source for deposition can be recognized to a waning current event
8B. This facies (maximum thickness 4.35 m) is characterized by interbedded calcarenite and grey shale. Shale:calcarenite ratio within this facies is 40:60. The shale beds have an average thickness of 16 cm displaying only internal laminations. The calcarenite beds possess characteristics almost similar to their counterparts in facies 7A except in having a thickness that ranges from 12 to 25 cm, and in not being amalgamated. Internally the beds are wavy laminated. Small hummocks (width c. 15 cm, height c. 8 cm) are also encountered occasionally. Top surfaces of the calcarenite beds are wave rippled (width c. 8.5 cm, height c. 5 cm). Gutters (width c. 5 cm, height c. 3.5 cm) are present at the bases of the beds	Palaeogeographic shift towards the inner shelf is inferred. Shales are indigenous sediments, suspension fall out between storm events. Calcarenite bed constituents are interpreted in the same way as their respective counterparts in the preceeding facies

Table 1 (continued)

Description	Interpretation
8C. Repeatedly alternating shale and calcarenite differentiate this facies which attains a thickness of up to 3.2 m. The ratio of shale to calcarenite is around 70:30. The shale contains millimetre-thick planar fine silt inter-laminae. The shale laminae often incorporate millimetre-thick, darker and wrinkled shaley wisps of length about 8 cm. Calcarenite beds are characteristically thinner (>5 and <10 cm) than the alternating shale beds (thickness >25 cm). Calcarenite and shale are internally equivalent to previous facies. The graded sequence within calcarenite beds distinctly incomplete differing facies 7A and 7B. Hummocks (width c. 10 cm, height c. 6 cm) and wave ripples (width c. 6.5 cm, height c. 3 cm) are smaller in dimension. Gutters (width c. 3 cm, height c. 1.5 cm), smaller too, maintain a consistent trend to their counterpart in other facies	Deposition presumably took place in a more distal part of the depositional basin in affinity to outer shelf, however within the storm wave base. The beds of contrasting lithologies are interpreted genetically in the same way as their counterparts in the preceding facies
8D. This unique facies is characterized by lenticular amalgamated non-recurrent calcarenite bed package (stack of five beds) with maximum recorded thickness of 1.86 m and, common presence of pebble–sized basement clasts and fossil woods. Sorting is very poor. The beds are internally: (a) massive ($7D_1$) with very sharp flat base and convex–up top bearing chaotically floating basement clasts within it; (b) cross–stratified ($7D_2$) with their fore-sets often defined by basement clasts and mega ripples on bed top; and (c) differentiated with comparatively larger and chaotically arranged clasts occuring in the lower parts of the bed type, but smaller and clasts orientated to bed-parallel are found in the upper parts	Product of a mega-event infering a highly unsteady nature for the flows, much more vigorous than normal meteorological storms. Calcarenite sediments were probably delivered from the coastal zone in rapidly succeeding ebbs. As the flow eventually waned, deposition is thought to have finally dominated over erosion
FA 9: Deeper shelf/shelf margin	
9A. The single constituting facies of this association is characterised by greenish grey-coloured shale, attaining thickness up to 18.5 m, characteristically contains millimetre-thick planar fine silt inter-laminae. These siltstone laminae are internally massive or planar laminated. Their bases are sharp, while their tops may be slightly undulated. Under the microscope they are almost arkosic in composition. Plagioclase feldspars are very common and fresh compared to other varieties of feldspar. The beds are laterally extensive (~12–15 m). Calcarenites of this facies occur as single beds or as a bed set of 3–4 beds. Individual bed thickness is c.a 25 cm. The cross-strata orientation within this facies (SSE) significantly shows high angle relationship with that of the preceding facies (WWS). The shale is rich in fossils including abundant belemnites, bivalves and ammonites and, phosphate nodules, glauconite pellets. Compositionally the shale is kaolinite to montmorillonite containg TOC ranging from 0.75–1.35 (Chakraborty et al. 2018a, 2018b)	Deposition probably took place in the distal most part, favourable for chemogenic precipitation under euxinic conditions within maximum flooding zone/condense zone. The shale is the indigenous products of the basin, indicative of low-energy condition. The silt inter-layers are likely to have been derived from continental sources. The calcarnite bed-set are inferred as shallow bottom–current sand/contourite (Viana et al. 1998) or product of ocean bottom currents or contour currents
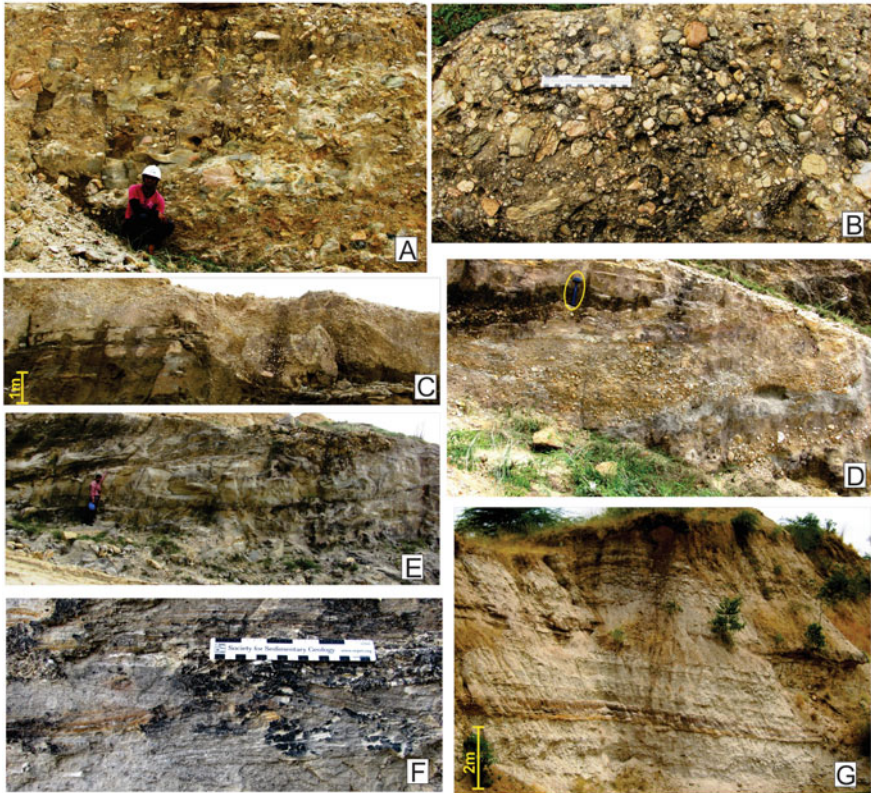
Fig. 4 Non-marine super association. Jagged boundary between massive hillwash sandstone, facies 1B and scree breccia, facies 1A overlying it (**a**). Clast supported conglomerate showing bimodality. Note that, smaller clasts are better rounded in facies 1C (**b**). Flow transformation between reverse graded conglomerate (unconfined flow in facies 2B) and massive conglomerate (confined flow in facies 2A) (**c**). Cross-stratified conglomerate conceding gradationally upward into sandstone (sieve deposit, facies 2C) (**d**). Large channel fills general view of facies 3A (**e**). Trough cross-stratified channel fill sandstones at Neykulam (facies 4A) (**f**). Internally planar laminated shale dominated succession at Terani (facies 4H) (**g**) (men for scale)

sandstone the rest of the concerned facies associations at KVK mine section, Dalmiapuram (FA 1-3). Mud is relegated merely to clay cutans around detrital grains, thin stringers and minor interstitial matrix. At Neykulam, sandstone and mudstone beds alternate in roughly equal proportions to comprise the section. In contrast, shale dominates at Terani, with fine-grained sheet and channel-form sandstone, and lenticular granular sandstone interbeds. Facies association 4 comprises Neykulam and Terani lithosections.
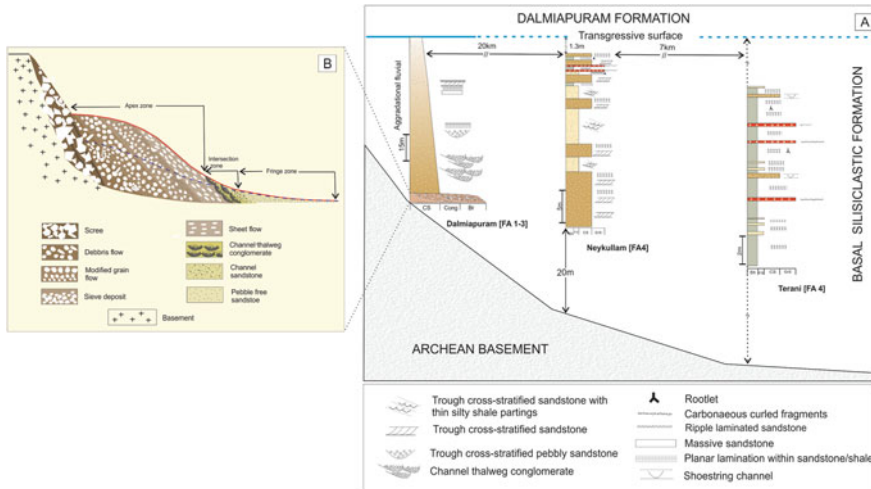
Fig. 5 Lithologs with sedimentary structures in the three studied locations within the Basal Siliciclastic Formation (**a**). Paleogeographic modelling of basin-margin facies associations (FA 1-2) within the formation at Dalmiapuram (**b**)

FA 1: Scree Cone

This is a coarse-grained association, dominated by breccia (Facies 1A) interspersed with thin sandstones (Facies 1B) and conglomerates (Facies 1C). Repeated alternations of facies 1A and 1B give rise to wedge-shaped bodies (Fig. 4a). The individual breccia beds are also wedge-shaped and stacked one above another showing jagged base and typically angular shaped basement derived vertical to sub-vertical clasts. The conglomerate facies 1C, found only at the down-slope fringe of this association shows distinctly bimodal clasts representing textural inversion (Fig. 4b; Pettijohn 1975).

Interpretations

FA1 is presumed to have been closest to the basin-margin (Fig. 5b). Considering its direct occurrence on the basement and other characteristics, this facies is identified as a scree or rock fall deposit at steep basin-margin (Selley 1965). The thin and laterally impersistent sandstone beds of facies 1B are possibly deposited as hill-wash during rains (Bose et al. 2008). These sandstone beds sparsely interspersed with the scree deposits, obviously make a drastic alteration of sedimentation dynamics. Within the bimodal clast composition of facies 1C, the angular larger clasts presumably have a proximal source, possibly the scree cone upslope. On the contrary, the better-rounded smaller clasts possibly have come from a relatively distal source, possibly being driven along the base of the scree cones. Since this facies skirted the scree cone, it is identified as an apron deposit. Lateral shift of the flow in response to scree fan progradations explains the tabular geometry of the conglomerate.
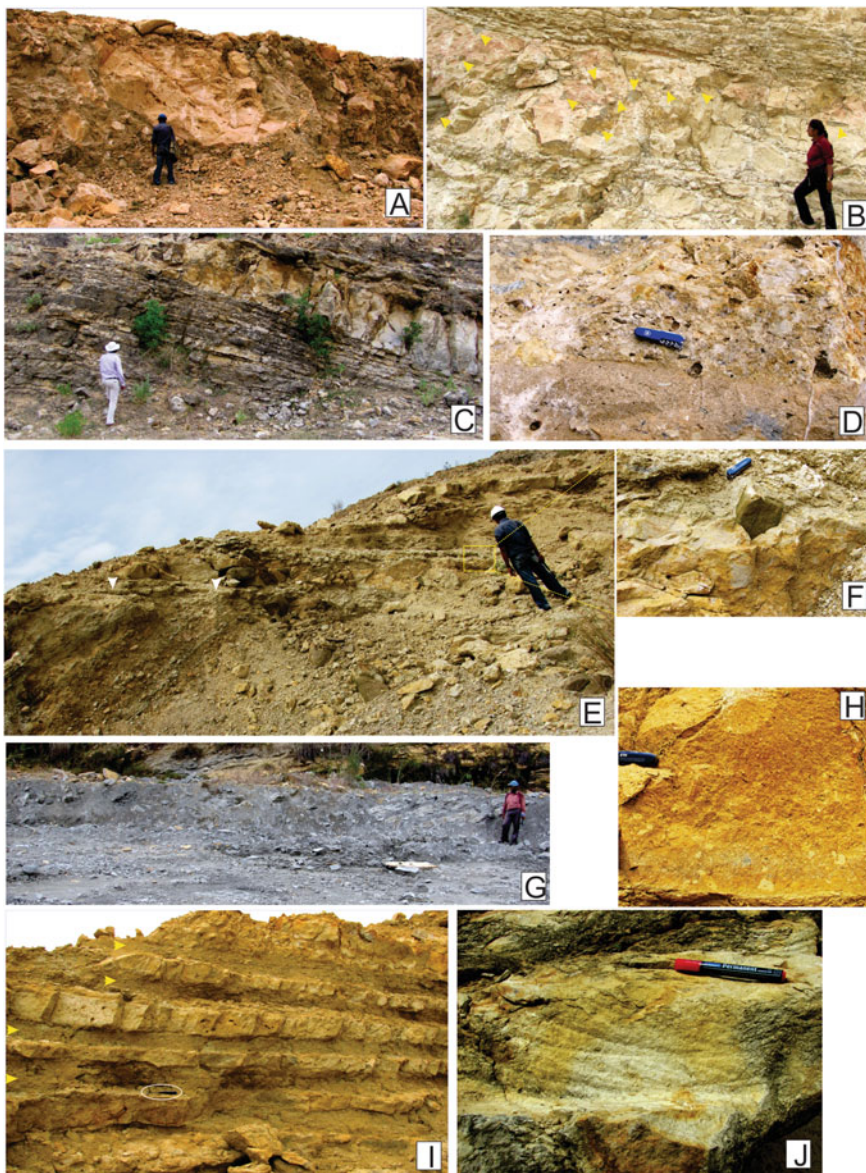
Fig. 6 Shallow marine super association. Unsorted boulder megabreccias with haphazardly oriented clasts (Facies 5A) (**a**). Pebbly conglomerate showing basement clasts (Facies 5B) (**b**). Large-scale cross-stratified bio-intrasparite alternating with sheet-like small-scale cross-stratified bed sets of biosparite, intrasparite and biomicrite within Facies 6A (**c**). Heterolithic limestone comprising pink-colored massive biomicrite alternating with significantly coarse-grained yellowish massive or graded biomicrite (Facies 6B) (**d**). Non-recurrent massive biometric limestone having laterally uniform thickness overlying the Basal Siliciclastic Formation (white arrows; Facies 6C) (**d**). Matrix-supported large pebbly limestone conglomerate with chaotically arranged clasts protruding bed top within facies 7B (**f**). Dark-colored shale interspersed with paper-thin planar stringers of calcarenite (Facies 7A). Internally normally graded shallow water turbidite beds (Facies 7C). Micritic limestone (marl) deposited in between the mass-flow events (Facies 7D). Trough cross-stratified intramicritic limestone showing thin drapes of micritic limestone (Facies 7E) (men for scale)

FA 2: Alluvial Fan

At the apex zone of this association, lithology varies from sandy conglomerate to pebbly sandstone of lenticular geometry in which the clasts are distinctly less angular than those within the breccias (Fig. 5b). The conglomerates are dominantly matrix-supported (Facies 2A) and internally massive, having clasts floating randomly within fine-grained matrix. However, some lenticular conglomerates are matrix to clast-supported, but reverse graded in coarse-tailed fashion (Facies 2B) (Fig. 4c). There are instances of flow transformation in space (Fig. 4c). Some convex-upward conglomerate bodies are clast-supported in the basal part, but, gradually turn matrix-supported upward and may eventually become sandy (Facies 2C; Fig. 4d). Still other conglomerates, the fourth variety within this association and are encased by pebbly sandstone, are tabular in geometry, but locally have small scours at their bases (Facies 2D).

At the base of this association, there are juxtaposition of mutually cross-cutting small channel bodies (not exceeding 3 m width in exposure and 1.5 m in thickness) and filled by clast-supported conglomerate (Facies 2E) at base, and dominant sandstone above which are massive, planar laminated, cross-stratified and locally rippled (Fig. 5b). Pebbly sandstone, locally crudely trough cross-stratified (Facies 2F) is the other common constituent. The cross-stratified facies is often overlain by planar laminated sandstone (Facies 2G). However, facies 2G gives way upward to small ripples and draped by a thin film of mud.

Interpretations

This facies association occurring away from the basin-margin in lateral contiguity of scree cone represent an alluvial fan. At the fan apex, conglomerates representing facies 2A are interpreted as the product of debris flow (Blair and McPherson 1994; Chakraborty et al. 2017). While conglomerates of facies 2B have been interpreted as modified grain flow (Middleton and Hampton 1976). Characteristic properties of facies 2C appear to be of sieve deposits manifesting freezing bed forms (Todd 1989). Facies 2D is possibly product of a fluidal sheet-flow, the basal scours manifesting initial turbulence (Bose et al. 2008). At the base of alluvial fan, well below the level
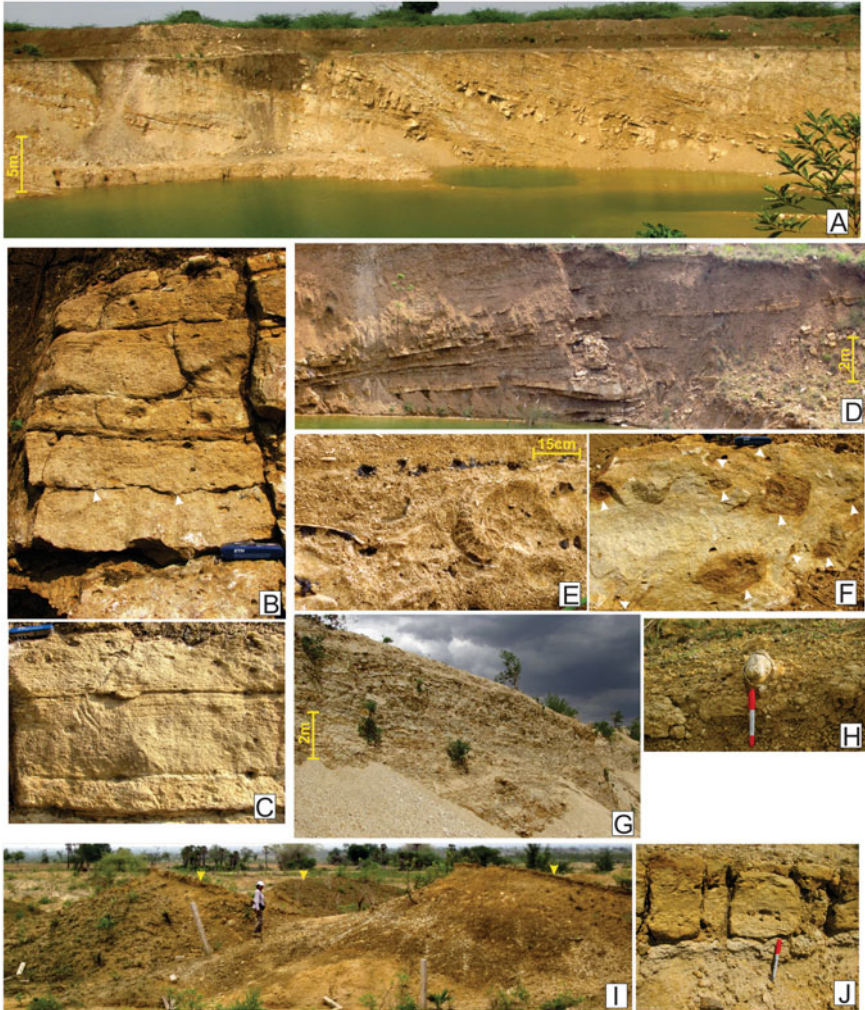
Fig. 7 Deep marine super association. Laterally persistent calcarenite beds showing sheet-like geometry (**a**), amalgamation of beds showing gutters at base (**b**) and internally showing partly developed tempestite sequence (**c**) within facies 8A. Facies 8B comprising interbedded calcarenite and shale (**d**). Facies 8D constituting mega fossil fragments (**e**) and chaotically floating basement clasts within it (**f**). Facies 9A consisting of greenish grey coloured shale with fine planar silt inter-laminae (**g**), abundant in phosphate nodules (**h**) and constituting very rare laterally extensive sheet like calcarenite (**i**) occurring as a bed set of three to four beds (**j**)
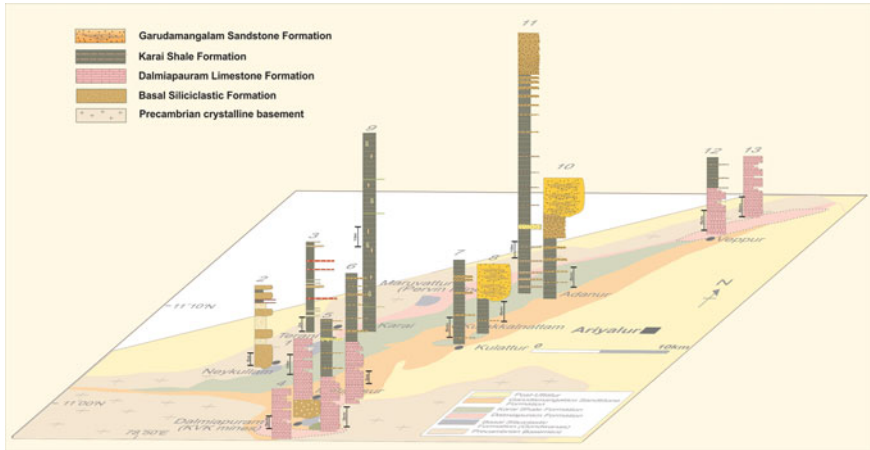
Fig. 8 Litho-sections constructed at studied locations showing lithostratigraphic relations in space and time within the study area

of intersection between the groundwater table and the fan surfaces, the conglomerates (facies 2E) are deposited along the channel thalwegs. The upward passage of these conglomerates to cross-stratified pebbly sandstone (facies 2F) clearly manifests progressive decline in flow shear. On the other hand, the upward passage of cross-strata (facies 2F) to planar lamination (Facies 2G) or ripple forms draped by mud (Facies 2G), rare though, records instances of flooding.

FA 3: Axial Channel

This association occurs in lateral contiguity with the FA1 and FA2 (Fig. 5b). Rapid avulsions categorized the channels of this association that seldom carries pebbles (Fig. 4e). The dominant sandstone lithology is characterized by a mosaic of channel-fill bodies. The channel-fills are often multi-storeyed, each stage having massive sandstone at the base (Facies 3A), followed by planar laminated sandstone (Facies 3B) and large-scale cross-stratified sandstone (Facies 3C) above, and locally ripple laminated sandstone (Facies 3D) on top.

Interpretations

This association is inferred to have accumulated at the base of the basin-margin slope amidst a network of river channels. Facies 3A indicates rapid deposition presumably because of hydraulic jump induced by a sharp decrease in gradient at the fan base. Facies 3B is formed either as a linguoid bar or cross-channel bar (Miall 1996). Overlying facies 3C and being comparatively finer-grained, facies 3D probably manifests bar-top reworking during low water stage. Declining flow strength is reflected in the vertical sequences of sedimentary structures within the channel-fill sections. Significant diversion in the orientation of cross-strata between this and the preceding fan associations suggests that the river had been axial running along the base of the fan

complex (Chakraborty et al. 2017). The widest span of paleocurrent data and internal characters of this fluvial channel deposit collectively suggests braided nature of the river (Chakraborty et al. 2017).

FA 4: Flood-Plain

Within this association, at Neykulam lithosection, repeated alternations between shale and sandstone beds or bed-sets with rare interventions of significantly calcareous beds characterise the assemblage. Facies 4A is internally characterised by poorly sorted trough cross-stratified sandstone (Fig. 4f). However, the other cross-stratified sandstone (facies 4B), comparatively finer-grained with muddy siltstone partings is inclined in direction at a high angle to the troughs. The coarse-grained planar laminated sandstone (facies 4C) rests on major erosion surfaces. The fine-grained sandstone (Facies 4D) is interbedded with shale. Rootlets occur on top of the beds and burrows are present within the beds within this facies. Facies 4E is characterised by dark shale. There are dark grey coloured carbonate mudstones (Facies 4F). The non-recurring granular facies (Facies 4G) is an obvious aberration in the fine-grained motif of this facies association. It comprises inordinately coarser grain-size, internal massiveness with bases sharper than their tops.

The lithosection at Terani is shale-dominated (Fig. 4f). The most dominant among them is light grey coloured shale (Facies 4H). Next in order in abundance is a shale-sandstone interbedded unit comparable to facies 4D (Neykulam). The shale-dominated motif of the section is disrupted by the intermittent occurrence of medium to fine-grained, poorly sorted sandstones of lenticular geometry (Facies 4I). The rarest, though conspicuous, facies is of reddish granule-rich beds, sheet-like in geometry with the frequent presence of gutters (look-alike facies 4G).

Interpretations

Within the floodplain association, Facies 4A is likely to be river channel deposit (Long 2011) while, facies 4B is inferred as point bar (Chung et al. 2005). Facies 4C is possibly formed as linguoid or cross-channel bars on the channel-floor. Facies 4D is probably of overbank crevasse-splay origin. The sand-laden water spilled over from the fixed channels (Farrell 2001) during floods had possibly given rise to sheet flows. The presence of rootlets and burrows corroborates the overbank origin of the facies. Facies 4E is presumably deposited farther away from the river channels. Abundant occurrence of crinkled carbonaceous laminae of possible microbial mat origin (Schieber et al. 2007) elicits even slower rate of sedimentation. Facies 4F is possibly generated in isolated lakes or ponds. Facies 4G is probably the product of rapid deposition from wining sediment gravity flow. The flow driving the granules had initially been intensely turbulent, as manifested in gutters present at sole of the beds. General massiveness of this facies, nonetheless, indicates high sediment load in the flows. The orientation of the gutters making a distinct angle to the channel-filling trough cross-strata suggests derivation of these granular materials from basin-flanks presumably during episodic high energy events. The thinness of this facies beds at Terani is supportive of the contention that Terani was farthest from the basin-margin. Facies 4H, being the most dominating at Terani likely to be over bank

deposit. Facies 4I manifests deposition within shoestring channels (Bridge 2006). Vertical stacking of such channel sandstones within the background of overbank fines suggests tendency of channels to anastomose (Makaske 2001).

4.2 Shallow Marine Facies Associations

Marine sedimentation was initiated within the Cauvery Basin during the earliest Albian and deposited limestone of the Dalmiapuram Formation on a restricted shelf environment, punctuated thereafter with rift-related tectonics (Chakraborty and Sarkar 2018). The limestone Formation, directly overlying Archean crystalline basement in many places and non-marine Basal Siliciclastic (FA 1-4) locally, is well exposed at Kovandankurichchi (VP) mines of Dalmiapuram Cements and at Veppur and Melarasur abundant mines. Two facies association with their constituting facies, described below, comprises the carbonate platform in relation to paleogeographical allocation.

FA 5: Sea-margin

Facies association 5 comprises two distinguished facies (Table 1). Facies 5A, proximately overlying the basement with intensely irregular and stepped boundary, is distinctly wedge-shaped unsorted boulder mega-breccia with a polymodal angular clast with variable composition (Archean granite gneiss, amphibolite, basal siliciclastics and carbonates) (Fig. 6a). Facies 5B, befalling in association with the preceding facies, as well as in contact with the basement, is characterized by wedge-shaped, poorly-sorted, clast-supported, pebbly breccias (Fig. 6b). Clast composition and characteristics are similar to the preceding facies.

Interpretation

Within the sea-margin association, facies 5A is inferred as a product of rock-fall at the base of steep fault scarp (Bose et al. 2008; Shanmugam 2015). Facies 5B is being deposited as slope aprons spreading over the preceding facies, as well as on the fault scarps (Burchette 1988; Bose et al. 2008).

FA 6: Shoreface

Facies association 6 consists of three distinguished facies (Table 1). Facies 6A is composed of large-scale (ca. 20 cm high), locally chevron cross-stratified, convex-up-topped and flat-based lenticular bio-intra-sparite beds, with large shell fragments, alternating with sheet-like small scale cross-stratified to rippled beds of biosparite, intrasparite and biomicrite with a thickening-upward trend (Fig. 6c). Facies 6B is composed of fine-grained, pink colored, massive biomicrite alternating with coarse-grained yellowish massive or graded biomicrite (Fig. 6d). The first lithotype comprising an abundance of fenestrae with "bird's eye" structures, native presence of algal fragments and poor skeletal fragments with micritic rims whereas the second lithotype of facies 6B contains plentiful broken shell fragments The non-recurrent,

thin, sheet-like, massive biomicritic limestone facies (Facies 6C; Fig. 6e, marked by white arrow) occurs draping the directly underlying Archean basement/Basal Siliciclastic with sharp, but planar basal contact, displaying small shells and abundant silt-sized siliciclastic particles "floating" within a micritic matrix.

Interpretations

Within the shoreface association facies 6A is a shallow marine wave-affected, at least locally, bar-inter-bar system (Sarkar et al. 2014; Chakraborty and Sarkar 2018). The first lithotype of heterolithic facies 6B is interpreted as sediments of a lagoon-like water body, whereas the second lithotype indicates occasional storm washover events (Sarkar et al. 2014). The presence of bar-interbar system (Facies 6A) in instantaneous association also supports the view and non-cyclicity has been observed within the sediment of Facies 6B. The non-recurrent facies 6C indicates a single basin-wide marine transgressive event during the Albian (Watkinson et al. 2007; Nagendra et al. 2011) deposited below the storm wave-base.

FA 7: Shallow Shelf

This association is composed of six distinguished facies (Table 1). The biomicritic limestone (Facies 6C) laterally grades basin wards into non-recurrent, dark-colored shale interspersed with paper-thin planar stringers of calcarenite (Facies 7A) containing abundant glauconite and pyrite (Fig. 6g). Facies 7B is made up of matrix-supported, ungraded, massive limestone conglomerate, having lenticular geometry, with flat base and convex-up top (Fig. 6e), with clast composition similar to the preceding facies, and displaying basement clasts "floating" and protruding within a micritic groundmass Fig. 6f. Facies 7C is composed of locally graded sheet-like calcarenite beds attaining variable thickness (20 cm–1.9 m), very sharp bases bearing sole marks (flute casts, gutters in places and rarely groove casts) and relatively less sharp tops (Fig. 6h). The beds (thickness >70 cm) possess a partly developed Bouma sequence (graded/massive bedding followed by ripples). Under microscope, this facies appears as intra-biomicrite Facies 7D, characterized by thin sheet-like laterally persistent, homogeneous or slightly planar laminated marls in between the beds of Facies 6B and 6C with a sharper top than their bases (Fig. 6i, marked by yellow arrow). Facies 7E is characterized by medium-scale (6–7 cm high), trough cross-stratified calcarenite with flat base and convex-up top, comprising large broken shell fragments and micritic rims around shells (Fig. 6j). The pattern of cross-stratification within the beds changes laterally, from steep to gentle, showing high-angle directional variation in successive beds and, locally, herringbone cross-strata are also present, exhibiting a bipolar-bimodal paleocurrent pattern (NNW–SSE). The gentle cross-strata are often draped by mud. Facies 7F is composed of comparatively thin sheet-like beds of small-scale cross-stratified calcarenite. Facies 7E and 7F together show a slightly undulatory contact with the underlying mass flow-marl packages (Facies 7B-D).

Interpretations

Facies 7A represents basinal fines in a low-energy restricted shelf under reducing conditions, possibly where the depositional basin achieved its maximum depth below storm wave-base (Seidler and Steel 2001; Schieber et al. 2007). Facies 7B and 7C have been interpreted as a product of debris flow (Bose and Sarkar 1991; Chakraborty et al. 2017) and carbonate turbidites respectively. Facies 7D has been inferred as indigenous shelf mud deposited during interludes between mass-flow events. Deposition of facies 7E is interpreted as occurring on a shallow tidal shelf while facies 7F possibly deposited in a comparatively deep tidal shelf. Together, both the facies, have been interpreted as a tidal bar–interbar complex (Bose et al. 1997; Sarkar et al. 2014).

4.3 Marine Facies Associations

Shallow shelf-originated Dalmiapuram Formation is conformably overlain by deeper-shelf marine sediments of Karai Shale Formation, a mixed siliciclastic–carbonate formation. However, at places the Albian-Turonian formation directly rests on the Archean basement (Chakraborty and Sarkar 2018). Exposures of the Karai Shale are present at the Pervin mines near Maruvattur village, stream rivulets known as the "badland area" (Nagendraa et al. 2013) near east of Karai village and road cut sections regionally isolated from each other. The organic- rich shale comprises two components; authigenic shale and allogenic calcarenites (Fig. 7a). Two facies associations, constituting five facies comprise the Karai Shale Formation.

FA 8: Storm dominated muddy shelf

This association comprises four sedimentary facies. Facies 8A, predominantly calcarenitic in composition, is repetitive in occurrence and often amalgamated (Fig. 7b). The beds are laterally persistent, tabular or sheet-like in geometry. Despite internal overall grading the beds display partly developed tempestite sequences, may have massive basal parts, otherwise being planar laminated, wavy laminated and hummocky cross-stratified and the bed-tops are locally wave rippled (Fig. 7c). Base of the beds, often sculpted with gutters, are sharper than their tops. Sorting of the rock is upright. The rock bears numerous broken shell fragments. Facies 8B is characterized by interbedded calcarenite and grey shale (Fig. 7d). The shale beds display only planar lamination while the calcarenite beds possess characteristics almost similar to their counterparts in facies 8A except in having a lesser thickness (Table 1). Gutters and load casts present locally at the sole of the beds. Repeatedly alternating shale and calcarenite comprise Facies 8C with a greater shale: calcarenite ratio and characteristically thinner calcarenite beds (Table 1). Both the components have internal character similar to their counterparts in former facies. In the absence of a basal massive part and/or planar lamination, internally the calcarenites are characterized by wavy laminations or small hummocks and may be wave rippled on top. Facies 8D comprising a lenticular amalgamated calcarenite bed package of five beds stacked

one above another, is strikingly distinctive because of its unique, non-recurrent occurrence. This laterally persistent facies, encased below and above by facies 8C stands out macrofossil fragments (Fig. 7e), gigantic basement clast constituents (Fig. 7f) and fossil wood fragments. Internally the facies may be sub-divided into three subfacies: massive ($8D_1$), cross-stratified ($8D_2$) and differentiated ($8D_3$) (Chakraborty et al. 2018a). The beds have sharp bases sculpted with gutters and very poorly sorted.

Interpretations

Facies 8A is inferred to have been an allogenic meteorological storm deposit within the muddy shelf (Banerjee 2000; Sarkar et al. 2002a, b; Fan et al. 2004; Blomeier et al. 2011). Allogenic sediments were presumably derived from the 'carbonate factory' on the shallow shelf of the underlying Dalmiapuram Formation and carried to the shale depositing deeper part of the shelf, with meteorological storms having been the transporting agent (Chakraborty et al. 2018a). The bottom-truncated, partly developed tempestite sequence present within calcarenites of facies 8B indicates a paleogeographic shift towards the inner shelf. The absence of amalgamation of the calcarenite beds within this facies also supports this contention. The shales are interpreted as low-energy suspension deposits, laid down between the storm events. The absence of bottom-truncation in relatively thin calcarenite beds of facies 8D indicates deposition in a distal part of the basin. Paleogeography is interpreted as of outer shelf affinity but within the storm wave base. The unique bed sets of facies 8D (calcarenite bed set) is related to a regional event in obvious. The three sub-facies of this facies have been interpreted as deposition through instantaneous freezing of a viscous flow ($8D_1$), product of the traction current ($8D_2$) and deposition due to vertical settling of calcarenite sand under temporally waning energy conditions ($8D_3$) respectively. Sedimentary flow dynamics indicates that the deposit is product of a mega event origin like a tsunami rather than meteorological storm, flash flood, mass flow or accentuated tide deposits (Sarkar et al. 2011; Chakraborty et al. 2018a).

FA 9: Deeper shelf/shelf margin

This association is constituted by only one facies (9A) characterized by commonly greenish grey-coloured organic-rich shale containing thin silt inter-laminae (Fig. 7g). The profusion of phosphate nodules (Fig. 7h) and glauconite pellets within this facies is significant. Gypsum is locally present within fractures. Belemnite guards are present abundantly along with bivalves and ammonites. Locally compressed horizontal burrows are present. This shale is almost devoid of calcarenite beds, except for a few, characterized by sheet-like bed geometry (Fig. 7i). The calcarenite beds showing gradational basal contacts with the underlying shale are internally characterized by trough cross-stratifications at their lower parts and ripples at the top (Fig. 7j).

Interpretation

Facies 9A is inferred to be deposited in the distal most part of the basin in the deeper shelf to shelf-margin paleogeography. The shale beds are the indigenous products of the basin. The abundance of phosphate and glauconite within this facies

is an indicative of maximum flooding (Odin and Matter 1981; Watkinson et al. 2007; Banerjee et al. 2012a, b, 2015, 2016; Bansal et al. 2019). The allogenic cross-stratified calcarenite beds have been interpreted as products of ocean bottom current or contour current (Viana et al. 1998; Chakraborty et al. 2018a). Remarkable high angle relationship between cross-strata orientation within this facies and that of the preceding facies corroborates the interpretation that calcarenite beds of this facies are shore parallel while that of the storm-induced beds are deposited along the slope.

5   Discussion

5.1   Paleogeographic Distribution and Stratigraphic Architecture

Facies associations along the linear exposer belt within the Ariyalur-Pondicherry sub-basin reveals deposition of Cretaceous sediments across continent to marine transition from the mountain front to the ocean. The paleogeography traversed from scree cone-alluvial fan to axial river channel and its adjacent flood plains comprising the continental (fluvial) depositional system within the Basal Siliciclastic Formation (Fig. 9a). The lithological spectrum includes breccia/conglomerate, sandstone and shale, but they are distributed in selective associations over the three isolated exposures in quarries at Dalmiapuram, Neykulam and Terani villages (Figs. 5, 8). An alluvial fan assemblage followed by extraordinarily thicker fluvial channel sandstone bodies through conglomerate-sandstone couplet depicts substantial increment in water discharge and channel depth. The internal structures of this fluvial channel deposit collectively bear documentation of a braided river system. Rapid lateral shifting and avulsions suggest a low rate of accommodation space creation (Fig. 10). At Neykulam quarry section, this sedimentary unit is comprised of alternations between sandstone and shale, the former being much abundant than the latter and devoid of conglomerate (Fig. 5a). The low-sinuosity River at Dalmiapuram presumably branched up into high sinuosity channels at Neykulam. All the features present indicate a meandering river system. The absence of overbank deposits in the previously described Dalmiapuram lithosection and their substantial presence in the Neykulam lithosection indicates relatively higher rate of accommodation space generation in the latter site (Bridge 2006). The deposit at Terani section is dominated by shale, sandstone being a subordinate component (Fig. 5a). The dominance of overbank fines encasing isolated river channels is indicated, ensuring maintenance of an extended accommodation space (Fig. 10; Chakraborty 2016). Thus, the paleogeography spectacle distinguishable spatial variation, as an alluvial fan assemblage in steep slopes of faulted basin margin of Dalmiapuram changes to distal fringes of an alluvial-fan followed by a braided river in low gradients of this same area. The river pattern changes to meandering at Neykulam (basin intermediate) and seizures to fixed isolated channels at Terani, the basin interior part (Fig. 10). Syn-tectonic
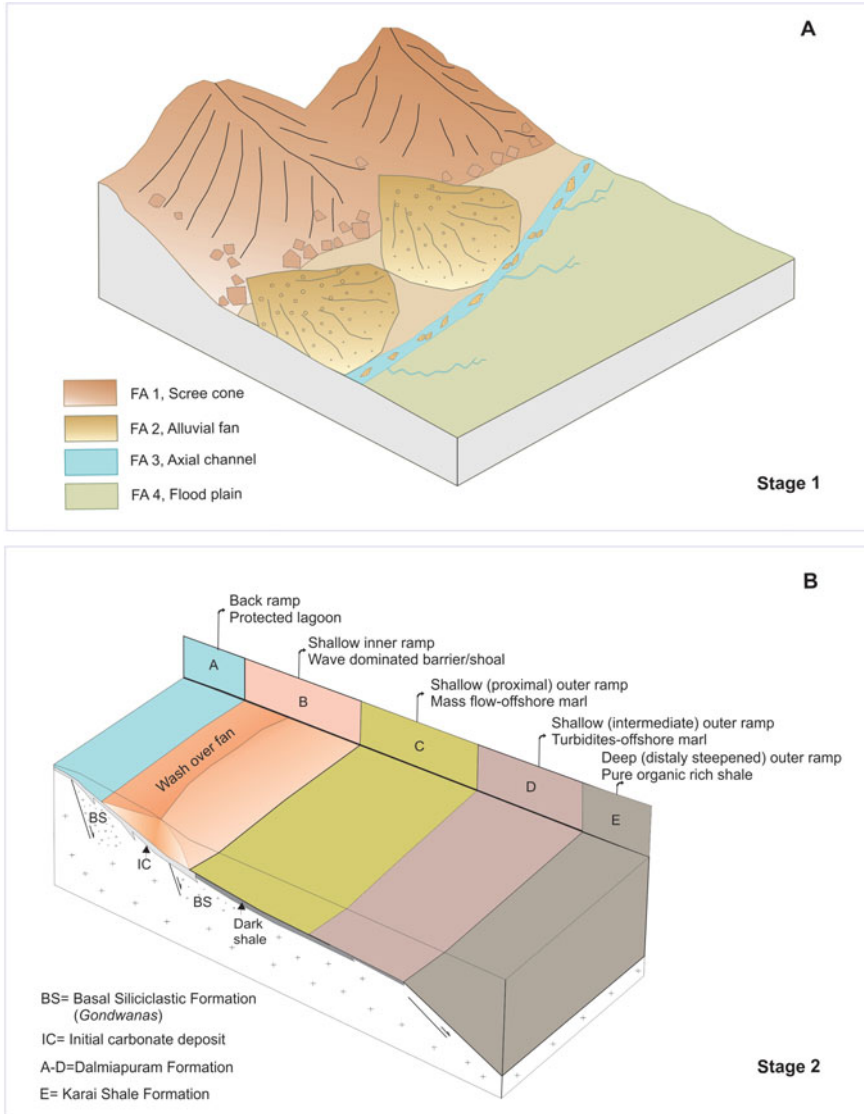
Fig. 9 Palaeogeographic and depositional modelling of the studied succession within the rift basin-fill. Stage 1 depicts deposition of initial non-marine siliciclastics (BS Formation) (**a**). Stage 2 illustrates development of marine succession; development of shallow marine carbonate platform (Dalmiapuram Formation) and deposition of deep marine shale (Karai Shale) (**b**)

Terani	High Accomodation Setting	• Abundant overbank deposit • Encasing lenticular channel Sandstone bodies • Fixed river channels		*Facies Mosaic*
Neykullam	Medium Accomodation Setting	• Overbank deposit subordinate • Pointbar and crevasses splay bodies present • Meandering of rivers evident		*Facies Prosaic*
Dalmiapuram	Low Accomodation Setting	• Overbank deposit absent • Channels amalgamate • Rivers braided		*Facies Mosaic*

Stratigraphic architecture — Basin subsidence rate increasing

Fig. 10 Low to high accommodation space from basin margin to basin interior in accord to the rate of subsidence within the Basal Siliciclastic Formation

interference is acme at Dalmiapuram, located at the basin margin, while it is occasional at other studied outcrops (Fig. 5; Watkinson et al. 2007; Chakraborty et al. 2017). The granular sandstone is possibly the product of these occasional tectonic pulses. The stratigraphic record indicates that the rate of base profile rise had been slow at Dalmiapuram, moderate at Neykulam and rapid at Terani areas. The rate of base profile rise distinctly varied between the places (Chakraborty 2016).

The transition between the terrestrial (fluvial) to shallow marine system is sharp and significant. As the sea flooded the early Albian coast, the fluvial system drowned and a carbonate platform developed across the shelf (Fig. 9b). The type of carbonate platform recognised in the Dalmiapuram Formation is a non-rimmed ramp (land-attached). A carbonate ramp, as originally conceived, is a gently sloping surface, generally <1° on which high-energy shoreline environments pass gradually into deeper water with no noticeable change in slope (Ahr 1973). Read (1982, 1985) divided ramps into two categories; they may be homoclinal low gradient platforms smoothly merging into the basinal plain or may be distally steepened, maintaining low gradient character of the platform in the shallower part of the seas. In case of the Dalmiapuram Formation the carbonate platform evolved from a homoclinal ramp near the shore to distally steepen towards the basin. In the inland sea, on the low gradient ramp, wave action dominated, developing a wave affected bar-interbar complex (facies 6A, Table 1) at the shoreface and a restricted shelf lagoon with outer-margin washover fan at its back (facies 6B). The orientation of the carbonate ramp is hard to deduce, since sedimentary structures which might reveal paleoslope or paleocurrent directions are very rare or not preserved. Field observation (few paleocurrent data available from the indigenous facies) indicates a transport direction possibly towards southwest, which is consistent with the paleocurrent data obtained from the storm-induced calcarenite beds (reworked from the shelf's *carbonate factory* by along-slope currents) within the overlying Karai Shale. The

wave features viz. chevron cross-stratification, wave ripple and, facies organization suggest homoclinal ramp geometry for the carbonate succession of Dalmiapuram Formation on the shoreface. Tectonically induced (intrabasinal) slope transformed the nature of the ramp from homoclinal to distally steepen away from the shore and guided deposition of mass flows and turbidites. Dark shale, containing organic matter, pyrite and glauconite, deposited at the deepest part of the Dalmiapuram inland sea. Dalmiapuram limestone to Karai shale transition is overall retrogradational. However, the basal part of the Dalmiapuram Formation displays a shallowing upward trend, ideal for a carbonate ramp succession. Gradually the basin was filled up. The presence of huge carbonate blocks at the basin-margin hinge zone possibly signifies the widening of the basin to a significant extent (Chakraborty and Sarkar 2018). The presence of wave features attests to this statement and implied that the basin depth did not alter much. Rapid supply of sediments during basin-widening had apparently offset the effect of continuing basin subsidence, thereby indicating an initial trend of aggradation or progradation in the carbonate platform. On reducing of syn-tectonic disturbance, massflows declined, rate of sedimentation, decreased and once rate of subsidence outpaced rate of sedimentation allowing the deepening trend to extend.

There is variation in the distribution pattern of different sedimentary facies within the shallow shelf originated Dalmiapuram Formation spatially. The presence of bar-interbar complexes, both wave- and tide-dominated, is present at Veppur and Dalmiapuram lithosections, while it is restricted in occurrence at Melarasur limestone mine. Shoreface association is entirely preserved exclusively at Dalmiapuram section. Within this association a thin non-recurrent limestone marks the initiation of carbonate deposition directly over the basement (Archean granite gneiss/non-marine siliciclastics). This sheet-like limestone facies laterally grades into a darker shale in the deeper part of the basin. Overlying the limestone bed a wave affected barrier bar-interbar system developed at basin margin. A lagoon formed behind the bar-interbar system. During high-energy condition, storm wash over waves debouch coarse sediments within lagoon mud. The complete presence of breccia/mass-flow facies assemblage is dominant at Dalmiapuram Formation, substantial at Veppur outcrop but infrequent at Melarasur limestone quarry. The breccia occurs at the faulted basin edge (hinge zone) while mass flow units befall away from the basin periphery in repetition with indigenous offshore marl, amid the inferred turbidites at the farthest away. Tidal bar–interbar system comprises the topmost stratigraphic level of the carbonate formation. A panel diagram over ca. 55 km reveals the irregular topography of the Archean basement, characterized by structural highs and lows (Nagendra and Reddy 2017), as well as variation in accommodation space, enhancing variability in the distribution of carbonate facies (Fig. 12 in Chakraborty and Sarkar 2018).

The Dalmiapuram Formation overlying the Karai Shale Formation with llithological changeover from limestone to shale undoubtedly indicates deepening in the depositional framework. The facies types identified within the Karai Shale Formation are distributed in a range of paleogeography from storm dominated muddy shelf to deeper shelf/shelf margin. Mud depositing marine shelf was, however, often

interrupted by carbonate event beds, which were driven by three different agents under a set of conditions (Chakraborty et al. 2018a). The temporally distributed among them are the meteorological storms that evince deposition from occasional waning wave-cum-current combined flow. Storm reworks the shallow shelf carbonates of the Dalmiapuram Limestone and calcarenite beds up to the storm wave base within the comparatively deeper muddy shelf, especially in the proximal area. Further below shale is deposited at the outer shelf/shelf margin, recorded towards the distal sector of the basin. Chemogenic precipitation took place under maximum flooding circumstance (Chakraborty et al. 2018a). Within the deep marine shale, a couple of calcarenite bed-set are driven when ocean-bottom current impinged at the shelf-margin during the time of maximum deepening.

5.2 Sequence Stratigraphic Context

This study demonstrates the transition of continental (fluvial) sedimentation to marine associations (shallow to deep) up the stratigraphic column and thereby suggests an inclusive retrogradational stacking pattern. In the stratigraphy record, the fining-upward succession is applied to establish transgressive sequences, and construed as a signature of progressive deepening (Bourgeois 1980; Emery and Myers 1996). The research results reveal some hidden information of sea level rise, so far overlooked.

Resting between a basal nonconformity on top surface of the Archean basement and a transgressive surface at the base of the Dalmiapuram Formation, the Basal Siliciclastic Formation comprised the initial filling of the Cauvery rift basin representing as isolated fluvial units, resting on pre-fall shelf deposit (the pre-rift Basement) (Figs. 2, 9). The Dalmiapuram Formation, the lowermost unit of the Uttatur Group, recorded the first widespread marine carbonate deposition during the early Cretaceous transgression onto the east-coast of India. Carbonate sedimentation over a widespread carbonate ramp platform, initiated on a shallow shelf environment. was perturbed thereafter with syn-rift tectonics (Fig. 9). However, carbonate sedimentation was initiated prior to this interruption. Chakraborty and Sarkar (2018) recognized the facies package (Figs. 6a–c, 7A; Table 1) as the early syn-tectonic record of carbonate deposition. The suite was locally preserved and its constituents were sparse in thickness but stratigraphically significant, recording a rapid marine transgression. Without the evidence of accompanying tectonics, the transgression probably was induced by the eustatic sea level rise (Vail et al. 1977; Haq et al. 1987). Carbonate deposition, however, continued even after the tectonic disturbance, but the character of sediments changed (Chakraborty and Sarkar 2018). At the peak of transgression, the shale onlapped the Archean basement. The progressive deepening promoted the retrogradational trend, setting off open marine, deep-water conditions and the deposition of Karai Shale across the basin. Ultimately, maximum flooding condition was achieved at a certain stage, during the shale sedimentation, and attained the maximum paleodepth. This marine flooding of the basin was, however, probably

an effect of the major global flooding events during Albian and Turonian (Hardenbol et al. 1998), amplified by continued major tectonic subsidence of the rift basin between Albian and Coniacian (Narasimha Chari et al. 1995; Nagendra and Reddy 2017). The later phase of Karai Shale was marked by a regressive trend, gradationally passing over to the overlying Garudamangalam Sandstone of the Uttatur Group (Fig. 3; Chakraborty et al. 2018a, b).

6 Conclusions

The conclusions of this study are as follows.

(a) The Cretaceous (Barremian-Turonian) sediments of the onshore Ariyalur-Pondicherry sub-basin of Cauvery Basin, provides an insight of continental-marine transition within a rift basin formed during the Gondwanaland fragmentation.

(b) High-resolution sedimentary facies identifies the paleogeographic distribution of rocks from the mountain front to the ocean.

(c) The continental (fluvial) deposit, Basal Siliciclastic (Barremian-Aptian) occurs within isolated outcrops along the western margin of the basin. Within this non-marine segment, scree-alluvial fan and channel amalgamation at basin-margin depicts a low accommodation stage while basin-interior flood-plain amalgamation indicates high accommodation stage in sequence-building.

(d) The depositional paradigm shifted from continental to marine with the advent of marine flooding along the south-east Indian passive continental margin during Albian.

(e) Overlying the pre-fall shelf (the basement), a widespread carbonate ramp platform, evolving from homoclinal to distally steepened, deposited limestone of the Dalmiapuram Formation. The organic-rich shale was deposited in the basin (Karai Shale Formation).

(f) Limestone to shale transition was gradational in accord with the pronounced transgressive trend and a maximum flooding condition was archived within the Karai Shale sedimentation during the deeper water conditions.

References

Ahr WM (1973) The carbonate ramp-an alternative to the shelf model. Gulf Coast Assoc. Geol Soc Trans 23:221–225

Ayyasamy K (1990) Cretaceous heteromorphy ammonoid biostratigraphy of Southern India. Newslett Stratigr 22:111–118

Banerjee S (2000) Climatic versus tectonic control on storm cyclicity in Mesoproterozoic Koldaha Shale, central India. Gond Res 3:521–528

Banerjee S, Chattoraj SL, Saraswati PK, Dasgupta S, Sarkar U (2012a) Mineralogy and geochemistry of lagoonal glauconites and their implications on origin and maturation: oligocene Maniyara Fort Formation, western Kutch, India. Geol J 47:357–371

Banerjee S, Chattoraj SL, Saraswati PK, Dasgupta S, Sarkar U (2012b) Substrate control on formation and maturation of glauconites in the Middle Eocene Harudi Formation, western Kutch India. Mar Petrol Geol 30:144–160

Banerjee S, Mondal S, Chakraborty PP, Meena SS (2015) Distinctive compositional characteristics and evolutionary trend of Precambrian glaucony: example from Bhalukona Formation, Chhattisgarh Basin, India. Precam Res 271:33–48

Banerjee S, Bansal U, Pande K, Meena SS (2016) Compositional variability of glauconites within the Upper Cretaceous Karai Shale Formation, Cauvery Basin, India: implications for evaluation of stratigraphic condensation. Sediment Geol 331:12–29

Banerji RK (1983) Evolution of the Cauvery Basin during Cretaceous. In: Maheswari HK (eds) Cretaceous of India. Proceedings of the symposium on cretaceous of india: paleoecology, paleogeography and time boundaries, Lucknow, India, pp 22–39

Banerji RK, Ramasamy S, Malini CS, Singh D (1996) Uttatur group redefined. J Geol Soc India 37:213–229

Bansal U, Pande K, Banerjee S, Nagendra R, Jagadeesan KC (2019) The timing of oceanic anoxic events in the Cretaceous succession of Cauvery basin: constraints from ^{40}Ar/^{39}Ar ages of glauconite in the Karai Shale Formation. Geol J 54:308–315

Bhattacharya B, Bhattacharjee J, Banerjee S, Bandopadhyay S, Adhikary K (2018) Early Permian transgressive-regressive cycles: sequence stratigraphic reappraisal of the coal-bearing Barakar Formation, Raniganj Basin, India. J Earth Sys Sci 127:1–29

Blair TC, McPherson JG (1994) Alluvial fans and their natural distinction from rivers based on morphology, hydraulic processes, sedimentary processes, and facies assemblages. J Sed Res A64:450–489

Blomeier D, Dustria A, Forke H, Scheibner C (2011) Environmental change in the early Permian of NE Svalbard: from a warm-water carbonate platform (Gipshuken Formation) to a temperate, mixed siliciclastic-carbonate ramp (Kapp Starostin Formation). Facies 57:493–523

Bou Dagher-Fadel MK, Banner FT, Whittaker JE (1997) The early evolutionary history of planktonic foraminifera. Chapman and Hall, London

Bose PK, Sarkar S (1991) Basinal autoclastic mass flow regime in the Precambrian Chanda Limestone Formation, Adilabad, India. Sediment Geol 73:299–315

Bose PK, Chakraborty PP (1994) Marine to fluvial transition: proterozoic Upper Rewa Sandstone, Maihar, India. Sediment Geol 89:285–302

Bose PK, Banerjee S, Sarkar S (1997) Slope-controlled seismic deformation and tectonic framework of deposition: Koldaha Shale, India. Tectonophys 269:151–169

Bose PK, Sarkar S, Mukhopadhyay S, Saha B, Eriksson P (2008) Precambrian basin-margin fan deposits: Mesoproterozoic Bagalkot Group, India. Precam Res 162:264–283

Bourgeois J (1980) A transgressive shelf sequence exhibiting hummocky cross stratification. The Cape Sebastian Sandstone (Upper Cretaceous), south western orogen. J Sed Pet 50:681–702

Bridge JS (2006) Fluvial facies models. In: Posamentier H, Walker RG (eds) Facies models revisited, vol 84. SEPM Special Publication, pp 85–170

Burchette TP (1988) Tectonic control on carbonate platform facies distribution and sequence development: miocene, Gulf of Suez. Sediment Geol 59:179–204

Chakraborty N (2016) Barremian-Coniacian sediments and sequence building in the Pondicherry sub-basin of Cauvery Basin, India. Ph.D. thesis, Jadavpur University, Kolkata

Chakraborty N, Sarkar S, Mandal A, Mejiama W, Tawfik HA, Nagendra R, Bose PK, Eriksson PG (2017) Physico-chemical characteristics of the Barremian-Aptian siliciclastic rocks in the Pondicherry embryonic rift sub-basin, India. In: Mazumder R (ed) Sediment provenance: influences on compositional change from source to sink. Elsevier, pp 85–121

Chakraborty N, Sarkar S (2018) Syn-sedimentary tectonics and facies analysis in a rift setting: cretaceous Dalmiapuram Formation, Cauvery Basin, SE India. J Palaeogeography 7:146–167

Chakraborty N, Mandal A, Choudhuri A, Mandal S, Sarkar S (2018a) Indigenous siliciclastic and extraneous polygenetic carbonate beds in the Albian-Turonian Karai Shale, Cauvery Basin, India. Carbo Evap 33:561–576

Chakraborty N, Sarkar S, Mandal A, Mandal S, Bumby A (2018b) Microenvironmental constraint on $\delta^{13}C$ depletion: Garudamangalam Sandstone, Cauvery basin, India. Mar Pet Geol 91:776–784

Chung GS, Lee JY, Yang DY, Kin JY (2005) Architectural elements of the fluvial deposits of meander bends in midstream of the Yeongsan River, Korea. J Korean Earth Sci Soc 26:809–820

Dillinger A, George AD (2019) Syn-rift sequence development in a fault-controlled embayment (Early Permian Irwin River Coal Measures, Northern Perth Basin, Western Australia). Sedimentol 66:2828–2873

Emery D, Myers KJ (1996) Sequence stratigraphy. Blackwell Science, Oxford

Fan D, Li C, Wang P (2004) Influences of storm erosion and deposition on rhythmites of the Upper Wenchang Formation (Upper Ordovician) around Tonglu, Zhejiang Province, China. J Sed Res 74:527–536

Farrell KM (2001) Geomorphology, facies architecture, and high-resolution, non-marine sequence stratigraphy in avulsion deposits, Cumberland Marshes, Saskatchewan. Sediment Geol 139:93–150

Fedo CM, Cooper JD (1990) Braided fluvial to marine transition: the basal Lower Cambrian Wood Canyon Formation, Souther Marble Mountains, Mojave Desert, California. J Sed Pet 60:220–234

Gani MR, Ranson A, Cross DB, Hampson GJ, Gani ND, Sahoo H (2015) Along-strike sequence stratigraphy across the Cretaceous shallow marine to coastal-plain transition, Wasatch Plateau, Utah, U.S.A. Sediment Geol 325:59–70

Garg R, Ateequzzaman K, Jain KP (1988) Jurassic and lower cretaceous dinoflagellate cysts with some remarks on the concept of upper Gondwana. Palaeobotanist 36:254–267

Govindan A, Ananthanarayanan S, Vijayalakshmi KG (2000) Cretaceous petroleum system in Cauvery basin, India. In: Govindan A (ed) Cretaceous stratigraphy–an update, vol 46. Mem Geol Soc of India, pp 365–382

Hardenbol J, Thierry J, Farley MB, Jacquin T, De Graciansky PC, Vail PR (1998) Mesozoic and Cenozoic sequence chronostratigraphic framework of European basins. In: De Graciansky PC, Hardenbol J, Jacquin Th, Vail PR (eds) Mesozoic and cenozoic sequence stratigraphy of European basins, vol 60. SEPM Special Publication, pp 3–14

Haq BU, Hardenbol J, Vail PR (1987) Chronology of fluctuating sea levels since the Triassic. Science 235:1156–1167

Hart MB, Joshi A, Watkinson MP (2001) Mid-Late cretaceous stratigraphy of the Cauvery basin and the development of the Eastern Indian Ocean. J Geol Soc India 58:217–229

Higgs KE, Browne GH, Sahoo TR (2019) Reservoir characterisation of syn-rift and post-rift sandstones in frontier basins: an example from the Cretaceous of Canterbury and Great South basins, New Zealand. Mar Pet Geol 101:1–29

Levell B, Argent J, Doré AG, Fraser S (2010) Passive margins: overview. In: Vining BA, Pickering SC (eds) Petroleum geology: from mature basins to new, Geol Soc London, pp 823–830

Long DGF (2011) Architecture and depositional style of fluvial systems before land plants: a comparison of Precambrian, early Paleozoic, and modern river deposits. In: North C (ed) From river to rock record: the preservation of fluvial sediments and their subsequent interpretation, vol 97. SEPM Special Publication, pp 37–61

Makaske B (2001) Anastomosing rivers: a review of their classification, origin and sedimentary products. Earth-Sci Rev 53:149–196

Mann P, Gahagan L, Gordon MB (2003) Tectonic setting of the world's giant oil and gas fields. AAPG Mem 78:15–105

Mazumder R, Van Kranendonka MJ, Altermann W (2015) A marine to fluvial transition in the Paleoproterozoic Koolbye Formation, Turee Creek Group, Western Australia. Precam Res 258:161–170

Miall AD (1996) The geology of fluvial deposits: sedimentary facies, basin analysis and petroleum geology. Springer, New York

Middleton GV, Hampton MA (1976) Subaquous sediment transport and deposition by sediment gravity flows. In: Stanley DJ, Swift DJP (eds) Marine sediments, transport and environmental management. Wiley, New York, pp 197–219

Mishra PK, Rajnikanth A, Jauhri AK, Kishore S, Singh SK (2004) Albian limestone building algae of Cauvery Basin, South India. Curr Sci 87:1516–1518

Nagendra R, Reddy AN (2017) Major geologic events of the Cauvery Basin, India and their correlation with global signatures-a review. J Palaeogeography 6:69–83

Nagendra R, Kamalak Kannan BV, Sen G, Gilbert H, Bakkiaraj D, Nallapa Reddy AN, Jaiprakash BC (2011) Sequence surfaces and paleobathymetric trends in Albian to Maastrichtian sediments of Ariyalur area, Cauvery Basin, India. Mar Pet Geol 28:895–905

Nagendraa R, Sathiyamoorthy P, Pattanayak S, Reddy AN, Jaiprakash BC (2013) Stratigraphy and paleobathymetric interpretation of the cretaceous Karai Shale formation of Uttatur Group, Tamil Nadu, India. Strat Geol Corr 21:675–688

Narasimha Chari MV, Sahu JN, Banerjee B, Zutschi PL, Chandra K (1995) Evolution of the Cauvery Basin, India from subsidence modeling. Mar Pet Geol 12:667–675

Odin GS, Matter A (1981) De glauconiarium origine. Sedimentol 28:611–641

Pettijohn FJ (1975) Sedimentary rocks, 3rd edn. Harper and Row, New York

Powell C, McA Roots SR, Veevers JJ (1988) Pre-breakup of continental extension in East Gondwanaland and the Early Cretaceous opening of the eastern Indian Ocean. Tectonophys 155:261–283

Premarathne U (2020) Burial and thermal history of The Cauvery Basin, Sri Lanka: a basin modeling approach. J Geol Soc of Sri Lanka 21:33–45

Ramasamy S, Banerji RK (1991) Geology, petrology and systematic stratigraphy of pre-Ariyalur sequence in Tiruchirapalli District, Tamil Nadu, India. J Geol Soc India 37:577–594

Ramkumar M, Stuben D, Berner Z (2004) Lithostratigraphy, depositional history and sea level changes of the Cauvery Basin, southern India. Annales Geologiques de la Peninsule Balkanique 65:1–27

Read JF (1982) Carbonate platforms of passive (extensional) continental margins: types, characteristics and evolution. Tectonophys 81:195–212

Read JF (1985) Carbonate platform facies models. AAPG Bull 69:1–21

Schieber J, Bose PK, Eriksson PG, Banerjee S, Sarkar S, Altermann W, Catuneanu O (2007) Atlas of microbial mat features preserved within the siliciclastic rock record. Elsevier, Amsterdam

Shanmugam G (2015) The landslide problem. J Palaeogeography 4:109–166

Sarkar S, Chakraborty S, Banerjee S, Bose PK (2002a) Facies sequence and cryptic imprint of sag tectonics in the late Proterozoic Sirbu Shale, Central India. IAS Spec Publ 33:369–381

Sarkar S, Banerjee S, Chakraborty S, Bose PK (2002b) Shelf storm flow dynamics: insight from the Mesoproterozoic Rampur Shale, Central India. Sediment Geol 147:89–104

Sarkar S, Bose PK, Eriksson PG (2011) Neoproterozoic tsunamiite: upper Bhander Sandstone, Central India. Sediment Geol 238:181–190

Sarkar S, Chakraborty N, Mandal A, Banerjee S, Bose PK (2014) Siliciclastic-carbonate mixing modes in the river-mouth bar palaeogeography of the Upper Cretaceous Garudamangalam Sandstone (Ariyalur, India). J Palaeogeography 3:233–256

Simpson EL, Dilliard KA, Rowell BF, Higgins D (2002) The fluvial-to-marine transition within the post-rift Lower Cambrian Hardyston Formation, Eastern Pennsylvania, USA. Sediment Geol 147:127–142

Sastri VV, Sinha RN, Singh G, Murti KVS (1973) Stratigraphy and tectonics of sedimentary basins on east coast of peninsular India. AAPG Bull 57:655–678

Sastri VV, Raju DSN, Venkatachala BS, Acharyya SK (1979) Sedimentary Basin Map of India. Stratigraphic correlation between sedimentary basins of the ESCAP Region. Mineral Resource Development Series, United Nations, New York

Sastri VV, Venkatachala SBS, Narayananthe V (1981) Evolution of the east coast of India. Palaeo Palaeo Palaeo 36:23–54

Seidler L, Steel R (2001) Pinch-out style and position of tidally influenced strata in a regressive–transgressive wave-dominated deltaic sandbody, Twentymile Sandstone, Mesaverde Group, NW Colorado. Sedimentol 48:399–414

Selley RC (1965) Diagnostic characters of fluviatile sediments of the Torridonian Formation (Precambrian) of Northwest Scotland. J Sed Res 35:366–380

Singh HP, Venkatachala BS (1988) Upper jurassic-lower Cretaceous spore-pollen assemblages in the peninsular India. Palaeobotanist 36:168–176

Sundaram R, Rao PS (1986) Lithostratigraphy of Cretaceous and Palaeocene rocks of Tiruchirapalli District, Tamil Nadu, South India. Rec Geol Surv India 115:9–23

Sundaram R, Henderson RA, Ayyasami K, Stilwell JD (2001) A lithostratigraphic revision and palaeoenvironmental assessment of the Cretaceous System exposed in the onshore Cauvery Basin, southern India. Cret Res 22:743–762

Tewari A, Hart MB, Watkinson MB (1996b) Foraminiferal recovery after the mid Cretaceous oceanic anoxic events (OAEs) in the Cauvery Basin, southeast India. In: Hart MB (ed) Biotic recovery from mass extinctions events, vol 102. Geol Soc London Special Publication, pp 237–244

Todd SP (1989) Sream-driven, high-density gravelly traction carpets: possible deposits in the Trabeg Conglomerate Formation, SW Ireland and some theoretical considerations of their origin. Sedimentol 36:513–530

Vail PR, Mitchum RM, Thompson S (1977) Seismic stratigraphy and global changes of sea level, part 3: relative changes of sea level from coastal onlap. In: Seismic stratigraphy–applications to hydrocarbon exploration, vol 26. Mem AAPG, pp 63–82

Veiga GD, Spalletti LA, Flint SS (2007) Anatomy of a fluvial lowstand wedge: the Avilé Member of the Agrio Formation (Hauterivian) in central Neuquén Basin (northwest Neuquén province), Argentina. In: Nicholls G, Williams E, Paola C (eds) Sedimentary processes, environments and basins: a tribute to peter friend, vol . IAS Spec Publication, pp 341–365

Venkatachalapathy R, Ragothaman V (1995) A foraminiferal zonal scheme for the mid-Cretaceous sediments of the Cauvery Basin, India. Cret Res 16:415–433

Viana AR, Faugeres JC, Stow DAV (1998) Bottom current controlled sand deposits: a review of modern shallow to deep-water environments. Sediment Geol 115:53–80

Watkinson MP, Hart MB, Joshi A (2007) Cretaceous tectono-stratigraphy and the development of the Cauvery Basin, South-east India. Petrol Geosci 13:181–191

Stratigraphy, Sedimentology and Paleontology of Late Cretaceous Bagh Beds, Narmada Valley, Central India: A Review

Biplab Bhattacharya, Kalyan Halder, Suparna Jha, Prantik Mondal, and Rupsa Ray

Abstract The Bagh Group of rocks, more popularly known as the 'Bagh Beds', in the Narmada Valley in central India provides a detailed account of sedimentation under shifting paleoecological-paleoenvironmental conditions in response to the Late Cretaceous greenhouse state and associated sea level rise. The present paper provides a review of the stratigraphic status of the Bagh Group along with a detailed account of prevalent sedimentological and paleontological information. Three distinct lithounits (of formation status) within the Bagh Group depict gradual change in depositional conditions, viz., a fluvial to fluvio-marine estuarine condition during the lowermost Nimar Sandstone (Cenomanian), followed by a restricted shallow marine platform—tidal flat during the Nodular Limestone (Turonian) and finally a relatively high-energy open shallow marine condition during topmost Coralline Limestone (Coniacian). Invertebrate body fossils of marine affinity are abundant with sporadic vertebrates (shark teeth, dinosaur bones etc.), foraminifers and trace fossils mostly within the limestone units. Amongst the invertebrates, ammonites (mainly *Placenticeras*) and echinoids (prevalent *Hemiaster*) are quite abundant with significant numbers of bivalves (predominantly *Inoceramus*), brachiopods (*Malwirhynchia*) and bryozoans. Varied distribution and association of the invertebrates in different lithounits manifest change in paleoecolgical–paleodepositional control parameters during entire sedimentation. The prevalent transgressive sequence in the epicontinental basin signifies the effect of sea level rise under the Late Cretaceous greenhouse condition in the Narmada Valley in central India.

Keywords Bagh Group · Narmada Valley · Late Cretaceous · Greenhouse condition · Transgression · Epicontinental basin · Paleogeography

B. Bhattacharya (✉) · P. Mondal
Department of Earth Sciences, Indian Institute of Technology Roorkee, Roorkee 247667, India
e-mail: biplab.bhattacharya@es.iitr.ac.in

K. Halder · R. Ray
Department of Geology, Presidency University, Kolkata 700073, India

S. Jha
Geological Survey of India, Jabalpur 482003, India

1 Introduction

The Earth faced a major "greenhouse state" during the Cretaceous period, with consequent occurrences of significant geological phenomena, namely, the formation of Large Igneous Provinces ('LIPs', Larson 1991), the Oceanic Anoxic Events ('OAEs', Schlanger and Jenkyns 1976), the deposition of Cretaceous Oceanic Red Beds ('CORBs', Hu et al. 2005; Wang et al. 2005), and the carbonate platform drowning events (Schlager 1989). The Late Cretaceous "greenhouse" period is known for elevated atmospheric CO_2 concentrations and much higher sea levels (100–170 m higher) than the present day (Miller et al. 2005; Müller et al. 2008), which inundated vast expanse of almost all the continents. The extent and effects of such sea-level changes are recorded in various resolutions and correlated across the globe in terms of sedimentological and geochemical parameters as well as different macro- and micro-flora-fauna indices (Immenhauser 2005; Miller et al. 2005; Miller and Foote 2009; Kominz et al. 2008; Müller et al. 2008; Zorina et al. 2008; Lovell 2010; Petersen et al. 2010; Boulila et al. 2011; Haq 2014; Wagreich et al. 2014). Thus, rocks belonging to this period bear significant signatures for a better understanding of the causes and consequences of the greenhouse interval on global sea-level changes and may help predict future sea-level trends (e.g. Hay 2008, 2011; Hay and Floegel 2012; Kidder and Worsley 2012; Wagreich et al. 2014).

The transgression caused the formation of various shallow epicontinental seas in all the subcontinents of the supercontinent Gondwanaland, namely, South America, Australia, Antarctica, India and Africa. At this time, the Indian Subcontinent went through major paleogeographic changes due to the fragmentation of major cratonic blocks, followed by its northeastward movement (Prasad et al. 1998). A major part of the Indian Subcontinent, which was an island rafting northeastwards during the Late Cretaceous period, was inundated with formation of several pericratonic basins (Chakraborty et al. 2019 and references therein). Consequently, thick sedimentary successions with rich fossiliferous intervals were deposited in marine to estuarine, paralic and freshwater depositional conditions in these basins. Besides the marginal areas, sea encroached well within the continents, particularly across a narrow stretch along the Narmada Valley in central India, resulting in rich siliciclastic-carbonate rock succession, popularly known as the Bagh Beds.

The Narmada Valley is a linear mega-rift zone (Biswas 1987) extending across the states of Gujarat and Madhya Pradesh in central India (Fig. 1). A short-term marine encroachment by an arm of the Tethys Sea is envisaged to result in a shallow epicontinental sea (Chiplonkar and Badve 1972a). Sedimentation took place in this basin during the Late Cretaceous (Cenomanian-Coniacian) in a mixed, cyclic continental and marine environment with the accumulation of marine and terrestrial fauna and flora. This fossil assemblage serves as an archive of biotic responses to climatic and environmental changes and development of varied ecosystems (Singh and Srivastava 1981; Khosla et al. 2003; Jaitly and Ajane 2013). A major event of the Deccan Trap volcanism occurred towards the end of the Cretaceous, resulting in the outpouring of fissure-type flood basalts, which covered most part of this sediment succession.
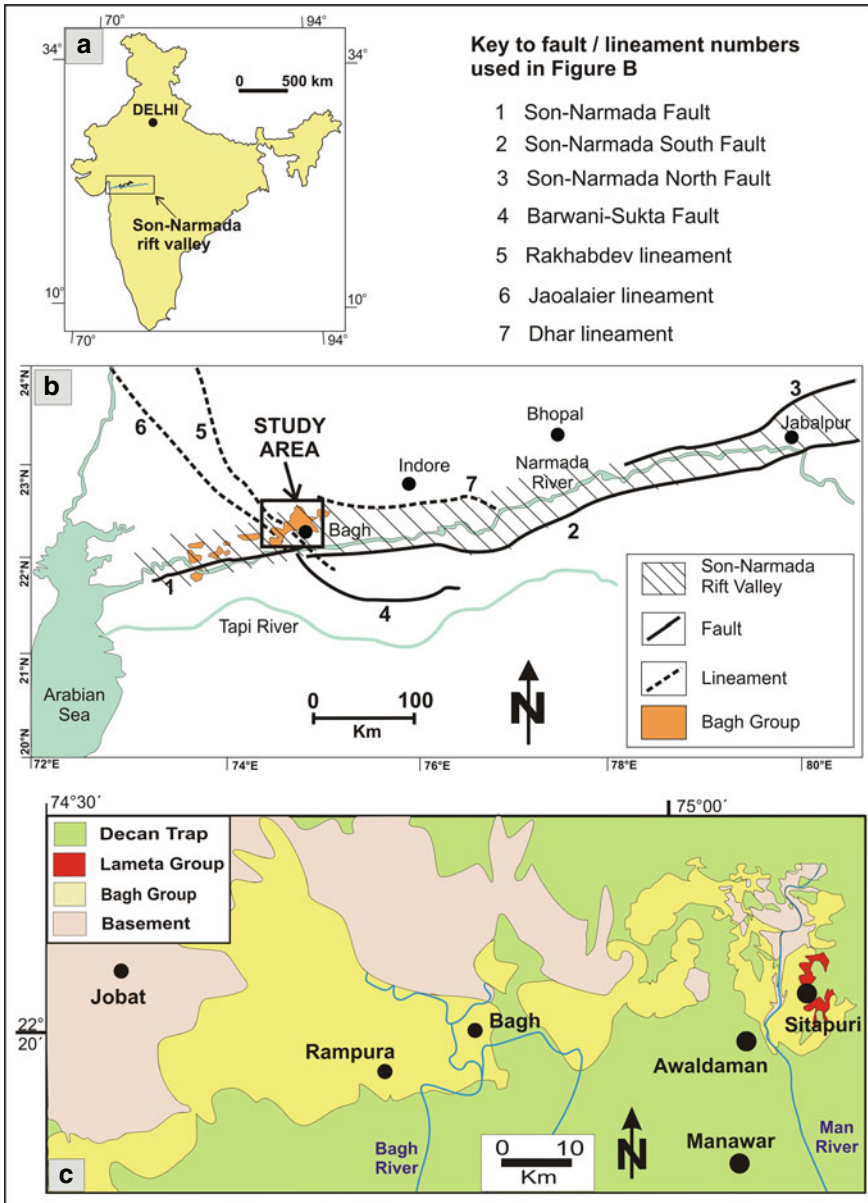
Fig. 1 **a** Map of India showing the location of the Narmada Valley. **b** Generalized geological map of part of the Narmada Valley (adapted from Abdul Azeez et al. 2013) showing the distribution of major faults and lineaments (1–7). Note the occurrence of the Bagh Group of rocks. The study area is marked on the map. **c** Geological map of the study area (modified after Jha et al. 2017), showing distribution of the Bagh Group of rocks

The Late Cretaceous Bagh Beds (now re-designated as the Bagh Group) in the Narmada Valley (Fig. 1) show a non-conformable contact with the underlying basement rocks, viz. the Proterozoic Bijawar Group of rocks. The sedimentary succession records a shift in the depositional environment from the initial fluvial to a transgressive tide-wave influenced estuarine and more open shallow marine settings, which implies significant tectono-sedimentary changes (Bhattacharya and Jha 2014; Jha et al. 2017; Bansal et al. 2019a). The Cretaceous marine transgression in the Bagh Group is established from the sedimentological, and the paleontological data (Singh and Srivastava 1981; Khosla et al. 2003; Jaitly and Ajane 2013; Bhattacharya and Jha 2014; Jha et al. 2017; Ruidas et al. 2018; Bhattacharya et al. 2020).

Important tectono-sedimentary and climatic changes are inscribed in the rocks of the Bagh Group. It stands witness to a very interesting time of the geology of India and the world. This study reviews sedimentological, paleontological and stratigraphical aspects of the Bagh Group of rocks with an aim to comprehend the present level of understanding in the light of the Late Cretaceous climatic and sea level fluctuations. In this paper, we document the up-to-date stratigraphic status of the Bagh Group with a detailed account of the sedimentological and the paleontological attributes of its individual units.

2 The Stratigraphy of the Bagh Group—Present Status

Geologically the Bagh Group of rocks were first studied by Dangerfield (1818), followed by Stewart (1821), who published a note on the geology of the Bagh area. The first fossil from the 'Bagh Beds' was discovered by Keatinge (1856), followed by a report of invertebrate body fossils and their community by Oldham (1858) from the Chirakhan area. These studies suggested the Neocomian age for the Bagh succession. Since then, the abundance of invertebrate and vertebrate body fossils within the Bagh sediments fascinated researchers, resulting in rich records of various invertebrate body fossils like ammonites, bivalves, brachiopods, echinoids, and bryozoans (Duncan 1887; Vredenburg 1907; Fourteau 1918; Chiplonkar 1939a; Guha and Ghosh 1970; Chiplonkar and Ghare 1975, 1976; Badve and Ghare 1978; Barron 1987; Funnell 1990; Ganguly and Bardhan 1993; Gangopadhyay and Bardhan 1998, 2000, 2007; Smith 2010), shark teeth (Naik 2013; Prasad et al. 2017) bone and egg shells of dinosaurs (Huene and Matley 1933; Khosla and Sahni 1995; Khosla et al. 2003), various plant fossils (Murty et al. 1963), nanoplanktons (Jafar 1982), microorganisms like foraminifera (Nayak 1987), algae (Kundal and Sanganwar 1998a) and trace fossils (Chiplonkar and Badve 1969a, b, 1970, 1972a, b; Chiplonkar and Ghare 1975; Kundal and Sanganwar 1998b; Patel et al. 2018). In contrast, the sedimentological aspect was in the slow gear with only a few attempts to understand the actual depositional condition (Pascoe 1959; Robinson 1967; Sarkar 1973; Raiverman 1975; Singh and Srivastava 1981; Bose and Das 1986; Bhattacharya et al. 1997; Bhattacharya and Jha 2014; Jha et al. 2017).

However, even after these studies, the stratigraphy of the Bagh Group was controversial without a proper age constraint. Several researchers proposed different stratigraphic successions for the Bagh Group. The first generalized stratigraphic succession was given by Blanford (1869) from Chirakhan (Table 1). Bose (1884) resurveyed the area and gave a more detailed stratigraphic succession (Table 2). With time, several modifications in the stratigraphic succession were made by various workers. Rode and Chiplonkar (1935) made some changes to that proposed by Bose (1884). They divided the Coralline Limestone into the lower and the upper units, separated by the Deola-Chirakhan Marl (Table 3).

Roy Chowdhury and Sastri (1962) mapped the area and gave a general description of each stratigraphic unit. They considered that the Deola-Chirakhan Marl was the weathered part of the Nodular Limestone; and do not bear the status of a separate stratigraphic unit, as mentioned by Bose (1884). Ramaswami and Madhavraju (1993) classified the Bagh Group into three lithounits, namely, the Nimar Sandstone, the Karondia Limestone and the Bryozoan Limestone. They clubbed the Nodular Limestone and the Deola-Chirakhan Marl into a single lithounit, the Karondia Limestone. Several modified classifications of the Bagh Group in central India were proposed by later workers (Murty et al. 1963; Poddar 1964; Sahni and Jain 1966; Verma 1968; Sastry and Mamgain 1971; Dassarma and Sinha 1975; Gupta 1975; Guha 1976; Smith 2010; Gangopadhyay and Maiti 2012 and many others), which led to utter confusions in comprehending its stratigraphy. Varied stratigraphic status has been assigned to the Bagh rocks from time to time. Most of the classifications did not assign any proper status to these sequences. Poddar (1964) referred to the succession

Table 1 Stratigraphic succession of the 'Bagh Beds' by Blanford (1869)

Deccan Trap
Coralline Limestone
Fossiliferous argillaceous limestone abounding in echinoderms (Hemiaster)
Unfossiliferous Nodular Limestone
Sandstone and conglomerate
Archean metamorphic

Table 2 Stratigraphic succession of the 'Bagh Beds' by Bose (1884)

Deccan Trap	
Upper Cretaceous	Lameta (lacustrine)
	Coralline Limestone
	Deola-Chirkhan Marl
	Nodular Limestone
Lower Cretaceous (Neocomian)	Nimar Sandstone
Jurassic	Mahadeva
Proterozoic	Vindhyans
Archean	Bijawars, metamorphic

Table 3 Stratigraphy of the 'Bagh Beds' after Rode and Chiplonkar (1935)

Upper Cretaceous		Deccan Trap—Fossil wood and Breccia zone
Lower Cretaceous	Bagh Beds	Upper Coralline Limestone
		Deola-Chirakhan Marl
		Lower Coralline Limestone
		Nodular Limestone
		Nimar Sandstone
Proterozoic		Basement

Table 4 Generalised lithostratigraphy of the Bagh Group as proposed by Guha (1976)

Group	Formations
Bagh Group	Deccan Traps/unclassified sedimentaries
	Chirakhan limestone
	Karondia limestone
	Nimar sandstone
	Metamorphics

both as group and formation. Gupta (1975) assigned these rocks to the Bagh Formation, consisting of four stratigraphic units of no definite status. However, a formal group status was first assigned to these rocks by Guha (1976) with three distinct formations (Table 4).

The stratigraphy proposed by Guha (1976) introduced new names—the "Karondia limestone" for the Nodular Limestone and the "Chirakhan Limestone" to include the Deola-Chirakhan Marl and the Coralline limestone of Bose (1884). Later, the dispute on the proper status of the Deola-Chirakhan Marl was discussed and fixed by Jaitly and Ajane (2013), where they delineated a three-fold classification of the Bagh Group (Table 5). However, the name of the topmost unit, the Coralline Limestone was renamed as Bryozoan Limestone by Taylor and Badve (1995) and later supported by Ruidas et al. (2018, 2020) due to the abundance of coral-like bryozoans and the absence of corals in this formation.

3   Sedimentology of the Bagh group—An Update

The Bagh Group of sediments is a window to the Late Cretaceous world in the Indian subcontinent. They potentially reveal the Late Cretaceous history in terms of paleoclimatic condition, basinal morphology and the depositional environment as the effect of global sea level rise in this part of the world (Tandon 2000; Jha et al. 2017). Following is a summary of the sedimentological work carried out so far on the Bagh Group.

Table 5 Generalized lithostratigraphy of the Bagh Group (after Jaitly and Ajane 2013)

	Age	Group	Formation	Member
Late Cretaceous	Maastrichtian	Deccan Trap		
		Lameta Group		
	Coniacian	Bagh	Coralline Limestone	
	Turonian		Nodular Limestone	Chirakhan
				Karondia
	Cenomanian		Nimar Sandstone	

Unconformity/fault

Precambrian Gneisses, granodiorites and crystalline rocks of Bijawar Supergroup
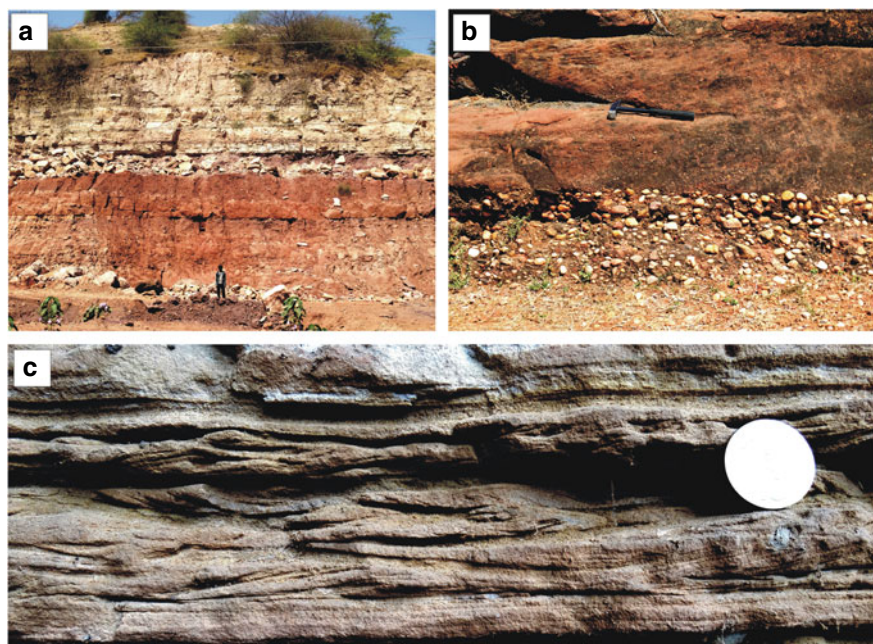
Fig. 2 a Thick succession of Nimar Sandstone exposed near Bagh town. **b** Matrix-supported conglomerate is overlain by cross-stratified sandstone within the fluvial facies association of the Nimar Sandstone. Length of the hammer is 30.5 cm. **c** Tidal strata bundles with apparent bi-directionality of the ripple forms and foresets, Nimar Sandstone succession, Bagh Cave. Diameter of the coin is 2.8 cm

3.1 Nimar Sandstone

The Cenomanian Nimar Sandstone succession (Fig. 2a) in the Narmada Valley is represented by an association of conglomerates, sandstones and mudstones of fluvial to fluvio-marine origin (Singh and Srivastava 1981; Bose and Das 1986; Bhattacharya and Jha 2014; Jha et al. 2017). Initially, Pascoe (1959) interpreted the depositional setting of the Nimar Sandstone as fluvial based on primary sedimentary structure and lithology. Later, the lower part of the Nimar Sandstone was interpreted as freshwater, whereas the top part as marine in nature (Robinson 1967; Singh and Ghose 1977). Singh and Srivastava (1981) inferred that Nimar sedimentation took place in freshwater to shallow marine intertidal to subtidal depositional setting. Bose and Das (1986) described five major facies variations within the Nimar Sandstone, indicating a transgressive marine shelf sequence. However, Bhattacharya et al. (1997), based on the carbon isotopic signature of the Nimar Sandstone, depicted a freshwater depositional setting.

Detailed sedimentological study of the Nimar Sandstone succession depicts varied facies types, which are grouped into three major facies associations, viz. (a) a fluvial facies association, (b) a fluvial-tidal mixed facies association and (c) a shoreface facies association (Bhattacharya and Jha 2014; Jha et al. 2017; Bhattacharya et al. 2020).

The fluvial facies association, mostly occurring at the basal part of the succession, is characterized by lenticular clast-supported and matrix-supported conglomerate facies (Fig. 2b), pebbly sandstone facies, sandstone–mudstone interbedded facies and pebbly trough cross-stratified sandstone facies. This facies association conforms to the broad channel filling pattern. Large- to small-scale cross-strata are common with very low mud content in most of the facies. Overall, the channel filling, lenticular morphology of the conglomerate and sandstone bodies and abundant trough cross-strata suggest deposition in fluvial channel system, with deposition of thin sandstone–mudstone heteroliths in the overbank/floodplain areas in between the channels.

The overlying fluvial–tidal mixed (estuarine) facies association is most prevalent and widespread in the Nimar succession. Within this facies association, a trough cross-stratified coarse-grained sandstone facies, a planar cross-stratified medium-grained sandstone facies and a planar laminated medium-grained sandstone facies show broad channel-filling geometry with locally preserved basal lag pebbles and lateral accretion of cross-strata sets indicating point bar settings in a meandering channel system. This facies sequence alternates with a laterally pervasive sandstone–mudstone heterolithic facies with abundant tidal bundles, flaser/wavy/lenticular beddings, reactivation surfaces, tidal rhythmites, various ripples showing apparent bi-directionality in foreset orientations (Fig. 2c), wave ripples and wave-generated tidal bundles. Details of the tidal bundles and the tidal rhythmites from this facies are described by Bhattacharya and Jha (2014). A yellow- to green- mudstone facies often intervenes this facies sequence. Repetitive stacking of the wave–tide-interactive sedimentary units on the fluvial units (see Bhattacharya and Jha 2014), producing multiple small-scale fining-up (retrograding) sequences signifies several short-term

transgressive phases. Such stacked retrograding sequences indicate a lateral shift from wave-dominant open coastal to a more tide-dominant, sheltered estuarine mouth transgressing over the fluvial depositional system, with significant backstepping of the strandline due to west-eastward marine incursion (Jha et al. 2017; Bhattacharya et al. 2020).

The overlying shoreface facies association is characterized by fossil-bearing (*Ostrea* and *Turritella*) wave-rippled sandstone facies, trace fossil-bearing (*Thalassinoides-Ophiomorpha*) thinly laminated sandstone/mudstone facies, thick massive mudstone facies and trough cross-stratified sandstone facies. This facies association manifests the predominance of marine trace fossils and body fossils with increasing mud content in upsection direction and also from east to west. Trace fossils are numerous and varied in the Nimar Sandstone (Chiplonkar and Badve 1969a, b, 1970; Chiplonkar and Ghare 1975, 1976; Singh and Dayal 1979; Kundal and Sanganwar 1998b). The assemblage is dominated by deposit feeding traces (fodinichnia) and dwelling traces (domichnia) (Kundal and Sanganwar 1998b), including *Annetuba*, *Planolites*, *Thallassinoides*, *Rosselia*, *Cylindrichnus*, *Granularia*, *Gyrochorte Palaeophycus* etc. (Chiplonkar and Badve 1969a, b; Ghare and Badve 1980; Badve 1987; Kundal and Sanganwar 1998b). The overall facies architecture reveals onlapping of the shoreface facies association on the underlying sediments (Jha et al. 2017; Bhattacharya et al. 2020). This facies association constitutes the top part of the Nimar Sandstone succession and is conformably overlain by the Nodular Limestone (Fig. 3a).

3.2   Nodular Limestone

Kumar et al. (2018) assigned a Turonian age to the Nodular Limestone. The Nodular Limestone is represented by nodular, thinly bedded, white to purple and light brown limestones (Fig. 3a, b) with abundant marine invertebrate fossils (Jafar 1982; Badve and Nayak 1984; Taylor and Badve 1995; Kundal and Sanganwar 1998a), alternating with marly shale horizons. The thickness of the marl beds increases upward. Earlier, the topmost thick, grey, argillaceous marl bed with sparsely distributed calcareous nodules was designated as the Deola-Chirakhan Marl (Schurrenberger et al. 2003). Guha (1976) earlier proposed the Karondia Limestone to replace the Nodular Limestone, which was followed later by Akhtar and Khan (1997). Consequently, Tripathi (2006) re-classified the Nodular Limestone into two units—the lower Karondia Member (represented by nodular limestone) and upper Chirakhan Member (characterized by bioturbated limestone). The Deola-Chirkhan Marl was considered a part of the upper unit. These two major lithounits are separated by a hardground at the top of the lower unit. However, in terms of fossil faunal assemblages, the Nodular Limestone and the Deola-Chirakhan Marl are similar in nature. Roy Chowdhury and Sastri (1962) and Sahni and Jain (1966) considered the Deola-Chirakhan Marl as a weathering product within the Nodular Limestone.
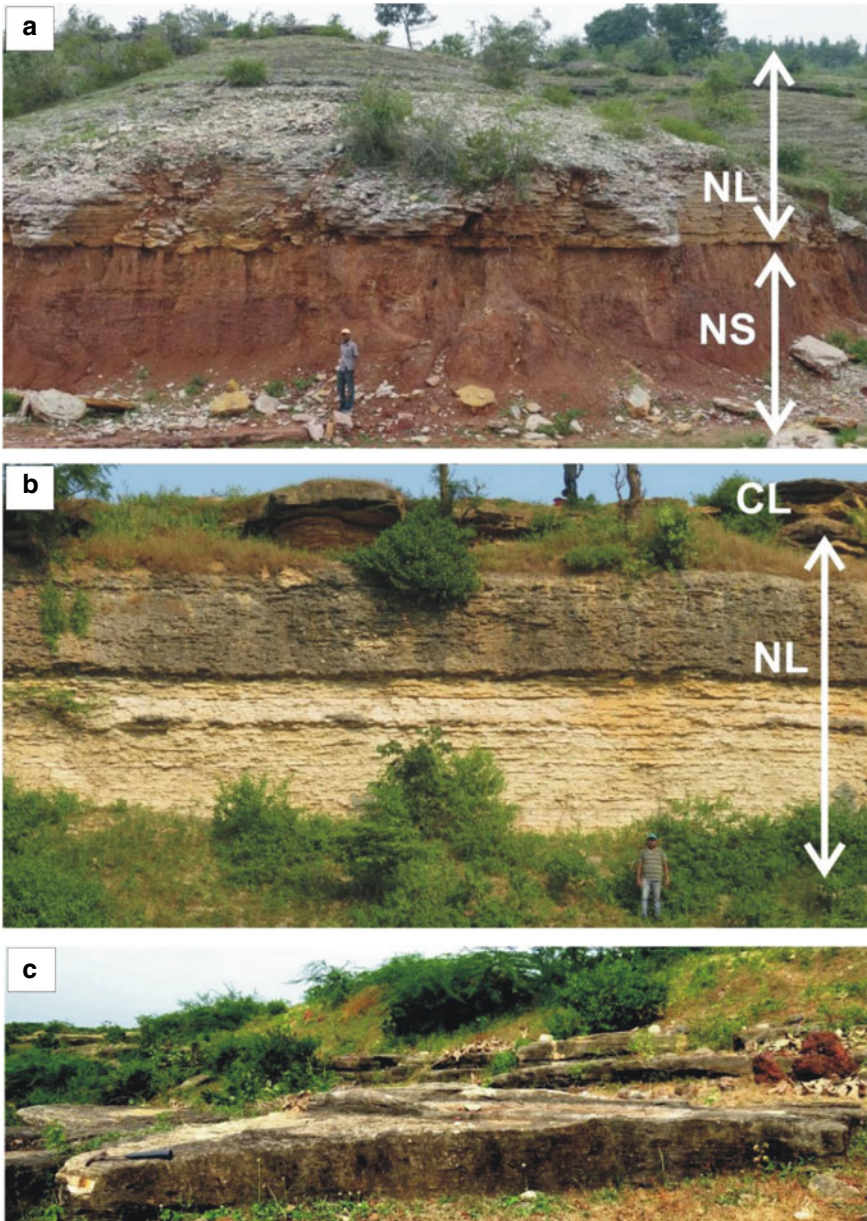
Fig. 3 a Thick succession of Nodular Limestone (NL) comformably overlies the succession of the Nimar Sandstone (NS), near Sitapuri. **b** Thick succesion of Nodular Limestone (NL), overlain by Coralline Limestone (CL) near Baria. **c** Coralline Limestone with well-developed cross-stratification. Length of the hammer is 30.5 cm

Lithologically, the Nodular Limestone is represented by three major facies, viz. a limestone (wackestone)–mudstone alternation, a nodular limestone (wackestone) and a poorly bedded limestone (wackestone), commonly devoid of primary sedimentary structures. The limestone (wackestone)-mudstone facies are characterized by planar and wavy bedded, tabular wackestone with diffused planar laminae, alternating with mudstone with desiccation cracks. The overlying nodular limestone (wackestone) facies comprises abundant calcareous to cherty nodules with desiccation cracks. Invertebrate borings and *Thallassinoides* burrows are preserved near the top of the facies. The uppermost facies of the Nodular Limestone consist of limestone (wackestone) with thin mudstone interbeds. Fossil shells of ammonites, echinoderms, bivalves etc. are scattered in all the types throughout the succession.

The predominance of fine-grained argillaceous carbonate rocks with moderately sorted intact bioclasts, alternating with marl, indicates a restricted shallow marine platform–tidal flat depositional condition for the entire Nodular Limestone (Gangopadhyay and Maiti 2012; Ruidas et al. 2018, 2020; Bansal et al. 2019a).

3.3 Coralline Limstone

The name Coralline Limestone was assigned for the abundance of coral-like bryozoans and is often alternatively referred to as the Bryozoan Limestone (Ruidas et al. 2018, 2020; Bansal et al. 2019a). It overlies the Nodular Limestone (Fig. 3b) in the Narmada Valley. The Coralline Limestone is a yellow to brown coloured, fine-grained, compact and fossiliferous limestone with fragmented shells of bryozoans, echinoids, gastropods, bivalves, brachiopods and corals (Guha 1976; Taylor and Badve 1995).

The Coralline Limestone is represented by three distinct facies, namely, a cross-stratified limestone facies (Fig. 3c), a planar laminated limestone facies and a faintly laminated limestone facies. The cross-stratified limestone facies consist of reddish brown rudstone with reworked fossil fragments of bryozoans, bivalves, echinoids, gastropods and brachiopods. Tabular cross-beds with reactivation surfaces are common. The overlying planar laminated limestone facies is classified as rudstone and is characterized by relatively higher (avg. ~50%) content of siliciclastics (quartz, feldspars, mudstone fragments, etc.), with the allochems consisting of finer fossil fragments. An oyster-bearing bed is present near the top of the facies. The faintly laminated limestone is packstone in nature and interlayered with the planar laminated limestone facies. A thick glauconite-bearing unit occurs near the top part of the Coralline Limestone (Bansal et al. 2019a). The Coralline Limestone is overlain by prograding Lameta Formation, which shows a significant increase in the siliciclastics content (Tandon 2000; Bansal et al. 2019a; Ruidas et al. 2020).

4 Paleontological Attributes of the Bagh Group

4.1 Taxonomic Outline

The rocks of the Bagh Group, especially the carbonate dominated two upper formations, yielded a lot of marine fossils. The common fossils include ammonites, bivalves, echinoids, brachiopods and bryozoans. Their taxonomic study has been going on for more than 150 years. Echinoids were the first to get detailed taxonomic treatment by Duncan (1865, 1887). Other fossil groups started to get taxonomic attention much later (Vredenburg 1907; Chiplonkar 1937, 1938, 1939a, b, 1941). A checklist of taxa reported from the Bagh Group is provided in Table 6.

The most abundant ammonite (Mollusca, Cephalopoda) genus is *Placenticeras*, which comes from the Nodular Limestone. Earlier studies on ammonites of the Bagh Group followed conventions prevalent at those times and tended to report new species based on minor morphological differences (e.g. Vredenburg 1907; Chiplonkar and Ghare 1976, 1977). They failed to appreciate large intraspecific variability and sexual dimorphism (Gangopadhyay and Bardhan 2007; Kennedy et al. 2003). Sexual dimorphism is almost omnipresent in the Mesozoic ammonite lineages (Davis et al. 1996) and has been reported in Bagh ammonites (Ganguly and Bardhan 1993; Gangopadhyay and Bardhan 2000). Ornamental polymorphism, i.e., wide discontinuous variation in ornamental pattern, has been reported in *Placenticeras kaffrarium* (Gangopadhyay and Bardhan 2007). Gangopadhyay and Bardhan (op. cit.) worked out the entire lineage of *Placenticeras* based on the stratigraphic and geographic distribution of its representative species and discussed about the importance of ornamental polymorphism in its evolution. However, doubts regarding the specific identity of ammonites are yet to be resolved. Jaitly and Ajane (2013) observed that *P. mintoi* is the dominant form in the Nodular Limestone and is characterised by wide morphological variability. They doubted the presence of *P. kaffrarium* there. Ruidas et al. (2018) found that this observation bears sense.

Bivalves are common in the Nodular Limestone and are represented mainly by several species of *Inoceramus* (Chiplonkar 1939a; Chiplonkar and Badve 1976a). Only a few other forms have been reported. Oysters are abundant at certain horizons (Chiplonkar and Badve 1976b, 1978). The upper part of the Nimar Sandstone yielded some non-inoceramid bivalves (Chiplonkar and Badve 1972b; Jha et al. 2017). Ammonites and bivalves, among molluscs, constitute a large portion of the macro-invertebrate community whereas gastropods are relatively rare. Representatives of the family Turitellidae and some other turreted gastropods are locally present at certain horizons quite abundantly, such as the top part of the Nimar Sandstone (Jha et al. 2017; Bhattacharya et al. 2020) and the lower-middle part of the Nodular Limestone (Chiplonkar and Badve 1972c; Khosla et al. 2003; Gangopadhyay and Maiti 2012).

Brachiopods and bryozoans are mainly studied by Chiplonkar (1938, 1939b) along with his co-workers (Chiplonkar and Ghare 1976). Brachiopods are represented by a low diversity fauna of three species belonging to *Malwirhynchia* that come from

Table 6 Checklist of fossils reported from Bagh Group of rocks

Taxon	Lithostratigraphy	Reference
Fossil type: algae		
Neomeris sp.	Bagh Group	Singh 1950
Cayeuxia fructilosa	Coralline Limestone; Deola Marl	Ghosh and Pal 1968
Cayeuxia frollo, *Distichoplaxpia* sp., *Lithoporellafoslie* sp., *Gymnocodiacean* sp., *Arabicodium* sp., *Boucian* sp.	Top of the Nimar Sandstone	Pal 1969, 1970a, b, 1971
Halimeda sp.	Nimar Sandstone, Jhabua	Badve and Nayak 1983
Dasycladacean sp.	Nimar Sandstone, Jhabua	Badve and Nayak 1984
Lenticulina exarata var. *anubisna*, *Ticinella albiana*, *Ticinella coronae*, *Hedbergella amabilis*	Top of the Nimar Sandstone	Nayak 1987
Archaeolithothamnium flexuosa, *A. liberum*, *A. lugeoni*, *A. turonicum*, *Lithothamnium bonyense*, *L. grahmi*, *L. lacroixi*, *Lithophyllum* sp., *Mesophyllum badvei*, *Mpacificu* sp.	Top of the Nimar Sandstone, Pipaldehla, Jhabua District	Sanganwar and Kundal 1996
Fossil type: bryozoa		
Eschara sp., *Escharina* sp.	Deola-Chirakhan Marl	Duncan 1865
Idmonea biserialis, *Ceriopora dimorphopora*, *C. conoformis*, *C. ellipsopora*, *Ceriocava micropora*, *Membranipora mathur*, *M. pseudonormaniana*, *Eschara chirakhanensis*, *E. regularis*, *E. holkari*	Coralline Limestone	Chiplonkar 1939a, b, c

Table 6 (continued)

Taxon	Lithostratigraphy	Reference
Ceriopora dispar	Coralline Limestone	Guha 1978
Fossil type: Elasmobranch		
Scapanorhynchus baghensis, *S. subulata Lamna appendiculata* var. *mongraensis*, *L. marginata*, *L. nana*, *L. basalis*, *L. libyca*, *Oxyrhina hastalis*, *Corax pristodontus*, *Ginglymostoma sokotense*, *Carcharias (Prionodon) egertoni*, *C. (Prionodon) ambadongarensis*	Top of the Nimar Sandstone, Baroda District, Gujarat	Verma 1965
Lamna divergens, *Scapanorhynchus raphiodon*	Top of the Nimar Sandstone, south of Bagh town, Amlipura, Ajantar	Dassarma and Sinha 1968
Ptychodus sp., *Scapanorhynchus* sp., *S. raphiodon*, *Cretodus* sp., *C. crassidens*, *Cretalamna* sp., *Squalicorax falcatus*	Green sandstone at the top of the Coralline Limestone, Ratitalai area	Prasad et al. 2017
Fossil type: ostracod		
Cypris sp., *Cytheris* sp., *Cytherelloidea* sp., *Cytheropteron* sp.	Bagh Beds	Roy Chowdhury and Sastri 1962

(continued)

middle to upper part of the Nodular Limestone. Chielostome bryozoans dominate the bryozoan fauna and are the major component of the Coralline Limestone.

Echinoids are a common faunal component of the Nodular Limestone. The infaunal echinoid genus *Hemiaster* is represented by maximum species diversity (Chiplonkar 1937, 1939c; Chiplonkar and Badve 1972d). The trajectory of morphological changes found in the echinoid lineage of *Hemiaster* spp. from the Nodular Limestone led Chiplonkar (1987) to believe it as the ancestral stock of the Cenozoic genus *Opisaster*.

The Bagh Group fauna is primarily an assemblage of marine invertebrates. However, a few vertebrates have also been reported from this succession. Several

Table 6 (continued)

Taxon	Lithostratigraphy	Reference
Cytherella austinensis, *Cytherella* sp. *A,* *Cytherelloidea khosalai,* *C. oudiapurensis,* *C. raoi,* *C. subgranulosa,* *C. thuatiensis,* *Bairdia* sp., *Bythocypris* sp., *Paracypris jonesi,* *Paracypris* sp. indet., *Pontocyprella*? sp. indet., *Brachycythere angulate,* *Monoceratina bugensis,* *Monoceratina tewarri,* *Protojonesia bolliaformis,* *Acuticytheretta baghensis,* *Krithe oudiapurensis,* *Neocytherides reymanti,* *Semicytherura*? sp. indet., *Sphaerolebris*? *chiplonkeri,* *Sphaerolebrisl howei,* *Crufsina derooi,* *C. thuatiensis,* *Cytheris raoi,* *Linocytherel thuatiensis,* *Planilebrisl* sp. indet	Upper Bagh Formation	Jain 1961, 1975
Bairdia sp., *Bythocypris* sp., *Paracypris gracilis,* *P. monmouthensis,* *P. jonesi,* *Brachycythere* sp. *A,* *Haplocytheridea* sp., *Cythereis* sp., *Cytherella contracta,* *Cytherelloidea ozanana,* *C. tombigbiensis*	Bagh Beds	Guha and Ghosh 1970
Paracypris jonesi, *Monoceratina bugensis,* *Cytheraloidea khosalai,* *Brachycythere batai,* *Crufsina thuatiensis,* *Semicytherual* sp.	Deoal-Chirakhan Marl	Kulsherstha 1995

Table 6 (continued)

Taxon	Lithostratigraphy	Reference
Cytherelloidea sp., *Rostrocytheridea* sp., *Makatinella* sp., *Majungaella* sp., *Sapucariella* sp., *Haughtonileberis* sp., *Nigeroloxoconcha* sp., *Veeniacythereis* sp.	Upper Bagh Formation	Chaudhary and Nagori 2017
Fossil type: gastropod		
Natica sp.	Nimar Sandstone	Bose 1884
Turritella (Zaria) multistriata Reuss, *Auriculid pulmonata*, *Melania* sp., *Haustator* cf. *meadi*	Nimar Sandstone	Mukherjee 1938
Natica cf. *sauchaensis*, *Turritella* sp. *A*, *Turritella* sp. *B*, *Alaria* sp., *Cypracea* sp., *Fasciolaria* sp., *Volutoderma* sp.	Nimar Sandstone	Chiplonkar 1942
Cerithium sp., *Fulguraria* sp., *Gyrodes tenellus*	Nimar Sandstone	Sinha and Dassarma 1965
Fulguraria elongata (d' Orbigny), *Lvria granulosa*, *Fasciolaria rigida*, *Turritella* s., *Triton* sp., *Natica* sp., *Neptunia excavate*	Nimar Sandstone and Nodular Limestone	Verma 1968
Turritella chikliensis, *T*. *sitapuriensis*	Nimar Sandstone and Nodular Limestone	Badve 1972
Gyrodoma sp.	Nodular Limestone, Chakrud	Naik 2013
Fossil type: ammonites		
Placenticeras mintoi, *Nomadoceras scindiae*, *Nomadoceras bosei*	Bagh Beds	Vredenburg 1907
Knemiceras mintoi, *Namadoceras scindice*, *Namadoceras bosei*		Chiplonkar 1941
Propiacenticeras stantoni		Jain 1969

(continued)

Table 6 (continued)

Taxon	Lithostratigraphy	Reference
Barroisiceras subtuberculatum, Subbarroisiceras mahafalense, Barroisiceras onilahyense, Barroisiceras inornatum	Bryozoan Limestone	Gangopadhyay and Bardhan 2000
Prionocyclus germari	Upper Nodular Limestone, Hatni River near Kukshi	Kennedy et al. 2003
Paraspideceras sp., *Peltoceras* sp., *Metapeltoceras* sp., *Peltomorphites* sp., *Placenticerus mintoi, Placenticerus* sp.	Nodular Limestone, Deola Marl and Coralline Limestone, Awlda, Chakrud, Bariha	Naik 2013
Namedoceras mintoi, Knemiceras mintoi, Hypengonoceras vredenburgi, Placenteceras baghensis, Parastantonoceras sp., *Baghiceras ambai, Baghiceras baghensis, Malwiceras variabilis, Placentoscaphites dangerfieldi, Placentoscaphites carteri, Placentoscaphites keatingei, Placentoscaphites ornatus, Placentoscaphites blanfordi, Placentoscaphites helices*	Nodular Limestone, Bagh area	Jaitly and Ajane 2013
Spathites sp., *Collignoniceras* sp., *Breistroffer* sp.	Nodular Limestone and Chirakhan Marl, Sitapuri and Rampura	Kumar et al. 2018
Fossil type: nautiloids		
Eutrephoceras sp.	Nodular Limestone	Gangopadhyay and Halder 1996

(continued)

shark (Chondrichthyes) teeth were reported from the top part of the Nimar Sandstone (Verma 1965; Dassarma and Sinha 1968). Khosla et al. (2003) reported some sauropod dinosaur bones from the lower and the upper parts of the Nimar Sandstone. Recently, Prasad et al. (2017) described a new assemblage of shark teeth in association with oysters from a bed lying just above the Coralline Limestone. The stratigraphic position of this bed is equivocal. Prasad et al. (2017) placed it within the Bagh Group because of its conformable boundary and marine origin.

Table 6 (continued)

Taxon	Lithostratigraphy	Reference
Fossil type: bivalves		
Pinna mathuri, *Inoceramus pseudo-latus,* *I. lamarcki* var. *indices,* *Inoceramus* sp. *A.,* *Inoceramus* sp. B., *Pecten quinque-costatus,* *Janira morrisi,* *Vola morrisi,* *Pecten (Neithea) morrisi,* *Plicatula spini-costata,* *Plicatula batnensi Modiola* *inflate,* *Modiola minor,* *Opis corniformis,* *Anthonya tumida,* *Protocardia pusilla,* *Isocardia* aff. *neglecta,* *Callista* sp., *Anisodonta* sp.	Nodular Limestone and Deola Chirakhan Marl	Chiplonkar 1939a, b, c
Pholadomya cf. *elliptica,* *Phaladodomya* cf. *indica*	Nodular Limestone	Jain 1963
Turkostrea sp., *Aviculolima* sp., *Limatulella* sp., *Regalilima* sp., *Anthracosphaerium* sp., *Actinodontophora* sp., *Flemingostrea* sp., *Burmirhynchia* sp., *Gibbirhynchia* sp., *Kallirhynchia* sp.	Nodular Limestone and Coralline Limestone, Bariha, Sitapuri, Chakrud, Awalda	Naik 2013
Acesta obliquistriata, *Pseudolimea interplicosa* *Lima* cf. *granulicostata,* *Lima scaberrima*	Nodular Limestone	Kumar et al. 2018
Barbatia (Cucullaearca) cf. *clellandi,* *Breviarca baghensis,* *Glycymeris* sp., *Trigonarca camerunensis,* *T. galdrina,* *Grammatodon* cf. *japeticum*	Nodular Limestone, Chakrud, Sitapuri, Rampura, Kosdana, Karondia	Kumar et al. 2016

(continued)

Table 6 (continued)

Taxon	Lithostratigraphy	Reference
Inoceramus hobetsensis, *I. teshioensis,* *I. tenuistriatus,* *I. apicalis,* *I. prefragilis,* *I. niger,* *I. albertensis,* *I. lamarcki geinitzi,* *I. lamarcki* var. *baghensis* n. var., *Mytiloides labiatus* Sclotheim, *Mytiloides* aff. *Subhercynicus,* *Mytiloides* cf. Lamarcki var. *cuvieri,* *Mytiloides* sp., *Mytiloides duplex,* *M.* cf. *labiatoidiformis,* *M. striatoconcentricus*	Nodular Limestone, Sitapuri, Ramapura, Khanwara, Kosdana and Karondia	Kumar et al. 2017
Pressastarte clavertensis, *P. senecta,* *P. lincolnshirensis P. pressula*	Nodular Limestone	Jaitly et al. 2015
Fossil type: brachiopod		
Malwirhynchia transversalis M. sub-pentogonalis, *M. trigonalis*	Deola Chirakhan Marl and Coralline Limestone	Chiplonkar 1938
Burmirhynchia sp., *Gibbirhynchia* sp., *Kallirhynchia* sp.	Nodular Limestone and Coralline Limestone	Naik 2013

4.2   Age of the Bagh Group

The majority of the paleontological studies commented on the age of the Bagh Group. This is also the issue on which maximum diverse views exist. The views vary from the Late Jurassic for the initiation of sedimentation in this basin (Murty et al. 1963) to the Maastrichtian for the close of marine deposition of the Bagh Group (Bose 1884; Mukherjee 1938). Chiplonkar, who has pioneered and done taxonomic studies on most of the invertebrate groups and ichnofossils, preferred a Cenomanian age for the Bagh Group of rocks in his early studies (Chiplonkar 1937, 1938, 1939a, b, c, 1941). Later, with further collection and resumption of studies along with his co-researchers, he observed that the age of the deposition should be constrained between

Table 6 (continued)

Taxon	Lithostratigraphy	Reference
Fossil type: echinoid		
Cidaris namadiscus, *Solenia mathuri*, *Polydiadema bosei*, *Phymosoma mongraensis*, *P. namadicum*, *Nucleolites elongates*, *N. rajnathi*, *N. chirakhanensis*, *N. malwaensis*, *Hemiaster holoambitatus*, *H. sub-similis*, *H.* (*Mecaster*) *rarus*, *H.* (*Mecaster*) *chirakhanensis*, *H.* (*Mecaster*) *fourtaui H.* (*Mecaster*) *heberti*, *H.* (*Mecaster*) *meslei*	Deola-Chirakhan Marl, Badia, Chirakhan, Sitapuri; Nodular Limestone, Mongra, Guneri, Khadlu, Walpur, Rampura, Bagh; Upper Coralline Limestone Chirakhan, Zirabad, Badia, Bowada, Sitapuri	Chiplonkar and Badve 1978
Nucleopygus sp.	Nodular Limestone, Zirabad	Sharma et al. 2006
Hemiaster sp.	Nodular Limestone and Coralline Limestone	Naik 2013
Cyphosoma namadicum	Nodular Limestone, Khandlai-Rampura	Khatri et al. 2013
Fossil type: polychaetes/worms		
Serpula sp., *Sarcinella* sp., *Omasaria* sp., *Proliserpula* sp., *Ditrupa* sp., *Hamlus* sp., *Fissurituba* sp.	Deola-Chirakhan Marl, Nodular Limestone	Verma 1969, Chiplonkar and Ghare 1976
Fossil type: foraminifera		
Rhizopora sp.	Upper parts of the Nimar Sandstone	Khosla et al. 2003
Quinqueloculina sp., *Triloculina* sp., *Discorbis* sp., *Cibicides* sp., *Neobulimina* sp., *Lenticulina* sp., *Planularia* sp., *Frondicularia* sp., *Nodosaria* sp., *Marginulina* sp., *Palmula* sp., *Globegerina* sp., *Globorotalia* sp.	Bagh Beds	Jain 1961

Table 6 (continued)

Taxon	Lithostratigraphy	Reference
Hyplophragmoides sp., *Ammobaculites* sp., *Triloculina* sp., *Quinqueloculina* sp., *Spiroloculina* sp., *Dentalina* sp., *Cibicides* sp.	Bagh Beds	Roy Chowdhury and Sastri 1962
Heterohelix globulosa (Ehrenberg), *H.* cf. *reussi*, *H.* sp., *Hedbregella ambilis*, *H. bomholmensis*, *H. delrioensis*, *H. kingi*, *Ticinella* sp. *A*, *Ticinella* sp. *B*	Bagh Beds	Sharma 1976
Ahmuellerella octoradiata, *Braarudosphaera bigelowi*, *Broinsonia enormis*, *Chiastozygus litterarius*, *Corollithion signum*, *Cretarhabdus crenulatus*, *Eiffellithus eximius*, *E. trabeculatus*, *E. turriseiffeli*, *Garinerago obliquum*, *Lithastrinus floralis*, *Lithraphidites helicoideus*, *Loxolithus armilla*, *Lucianorhabdus cayeuxii*, *Markalius circumradiatus*, *Microrhabdulus belgicus*, *Parhabdolithus bitraversus*, *Podorhabdus albianus*, *Prediscosphaera columnata*, *P. cretacea*, *P. spinose*, *Quadrum gartneri*, *Scapholithus fossilis*, *Tranolithus exiguous*, *T. orionatus*, *Vagalapillo motalosa*, *Watznaueria barnesae*, *W. ovate*, *Zygodiscus diplogrammus*, *Z. spirolis*, *Z. xenotus*	Top of the Nimar Sandstone, Baria Nala, Chikli	Jafar 1982

Table 6 (continued)

Taxon	Lithostratigraphy	Reference
Heterohelix cf. *Americana*, *H. bejaouvensis*, *H. glabrans*, *H. globulosa*, *H. reussi*, *H. striata*, *H. srinivani*, *H. sastrii*	Top of the Upper Coralline Limestone, Baria	Rajshekhar 1982
H. chiplonkari, *Platystaphyla brazoensis*, *Guembilitria cenomana*,? *Planoglobulina* sp., *Psamminopetta subcircularis*	Upper Coralline Limestone, Baria River	Rajshekhar 1984
Miliammim awunensis, *M. manitobensis*, *Ammobaculites advenus*, *Textularia angalica*, *Pseudobolivina* sp. indet., *Quinqueloculina* sp., *Leruiculina* sp., *Discorbis correcta*, *Discorbis* sp. *A*, *Discorbis* sp. *B*, *Gavelinella plummerae*, *Patellina subcretacea*	Top of the Nimar Sandstone	Rajshekhar 1987
Saccammindae, *Hormosinidae*, *Rzchakinidae*, *Haplophragmoididae*, *Lituolidae*, *Haplopragmiidae*, *Spiroplectamminidae*, *Tritaxiidae*, *Spiroloculinidae*, *Hauerinidae*, *Nodosariidae*, *Vaginulinidae*, *Turrilinidae*, *Bolivinidae*, *Siphogerinoididae*, *Discorbidae*, *Nonionidae*, *Rugoglobigerina (Archaeglobigerina)* sp.	Nodular Limestone	Rajshekhar 1991

Table 6 (continued)

Taxon	Lithostratigraphy	Reference
Quinqueloculina semiplana Reuss, *Q.* sp. Indet, *Miliola saxorum*, *Lenticulina arcuate*, *L. sublaevis*, *L. exarata var. danubiana*, *Pararotalia* sp. indet., *Hedbregella ambilis*, *Ticinella albania*, *T. caronae*, *Albamina* sp. indet., *Gavelinella* cf. *velascoensis*	Nimar Sandstone	Nayak 1987
Tritaxia arcuate, *Planularia sitapuriensis*, *Heterohelix globulosa*, *H. reussi*, *Planoglobulina brazoensis*, *Ammobaculites coprolithiformis*, *A. mosbyensis*, *H. calcula*, *H. glabra*, *Milliammina manitobensis*, *Tritaxia pyramidata*, *Quinqueloculina moremani*, *Q. anriqua*, *Spiroloculina cretacea*, *Vaginulina recta*, *Nodosaria* sp., *Neobulimina albertensis*, *Praebulimina reussi*, *Nonionella austianana*, *Citharina kochii*, *Epistomaroides (Anomalina) tennessenis*, *Heterohelix reusii*, *H. globulosa Planoglobulina brazoensis*	Nimar Sandstone, Deola-Chirakhan Marl, middle of the Nodular Limestone	Kulsherstha 1995
Biscutum sp., *Watznaueria* sp., *Polycyclolithaceae* sp., *Nodosaria inornatus*, *N. steinmannii*, *N. truittii*	Nimar Sandstone, Baria Nala	Rai et al. 2014

(continued)

Table 6 (continued)

Taxon	Lithostratigraphy	Reference
Fossil type: plant fossils (palynomorphs and woods)		
Cyathidites australis, *C.s minor*, *Haradisporites mineri*, *Stereisporites* sp., *Cingutriletes* sp. *Callialisporites dampieri*, *C. trilobatus*, *Klausipollenites* sp., *Alisporites ovalis*, *Abiespollenites triangularis*, *Podocarpidites ellipticus*, *P. multesimus*, *Araucariacites australis*, *Cycadopites gracilis*, *C. sakrigaliensis*, *Striatites* sp.	Lower part of the Nimar Sandstone, Umrali village, Jhabua District	Murty et al. 1963, Kumar 1994
Rhizopora	Upper parts of the Nimar Sandstone	Khosla et al. 2003
Fossil type: dinosaur		
Sauropoda (Incertae sedis)	Nimar Sandstone	Khosla et al. 2003
Theropoda tooth, *Abelisauridae gen. et* sp. indet.*(Majungasaurus and Indosuchus)*, *Archosauria* indet	Green sandstone bed overlying the Coralline Limestone	Prasad et al. 2017
Fossil type: trace fossils		

(continued)

the Albian and the Turonian (Chiplonkar 1987 and references therein). Rajshekhar (1995) observed that most of the members of the foraminiferal community are long-ranging with the dominance of Turonian components.

In recent times, the emphasis has been placed on ammonites for fine-tuning the age of deposition. Kennedy et al. (2003) recorded *Prionocyclus germeri*, an index of the Late Turonian from the middle part of the Nodular Limestone. This part is the most fossil-rich portion of the succession and also yielded *Placenticeras mintoi*, which also indicates a Late Turonian age (Jaitly and Ajane 2013). The report of *Barroisiceras onilahyense* from the overlying Coralline Limestone helps in placing this unit in the Coniancian (Gangopadhyay and Bardhan 2000; Jaitly and Ajane 2013). The age assignment of the lowermost formation, the Nimar Sandstone, is difficult because of its low fossil content and absence of any time-diagnostic ammonite. Jafar (1982), based on calcareous nannoplankton assemblage, assigned a Turonian

Table 6 (continued)

Taxon	Lithostratigraphy	Reference
Ichnotaxon	Lithostratigraphy	Reference
Arthropodiscus indicus, *Diplopodomorpha cretacea*, *Dreginozown orientale*, *Nereites malwaensis*, *Oniscoidichnus communis*, *Oniscoidiscus ampla*, *Onicoidiscus elegans*, *Onicoidichnus robustus*, *Premichnium bosei*, *Taphrhelminthosis subauricularis*, *Tasmanadia* sp., *Asterosoma spatulata*, *Biformites* cf. *insolitus Vassoievitch* sp., *Fucuopsis* cf. *angulatus*, *Vassoievitch* sp., *Laevicyclus mongraensis*, *Phycodes gregarious*, *P. mongraensis*, *Spongeliomorpha iberica*, *S. reticulate*, *Syringomorpha* sp., *Merostomichnites strandi*, *Protovirgularia mongraensis*, *Discontomaculum variabilis*, *Eophyton cretacea*, *Kinneyia simulans*, *Rivularities regularis*, *Arhrophycus maberry*, *Paleodictyon* sp., *Pennatulites longispicata*, *Cosmorphaphe*, *Pelecypodichnus chikliensis*, *Rhizocorallium mongraensis*, *Ophiomorpha nodosa*, *Arthrotelsonichnus hamadiscus*, *Cylindricum curvosus*, *Saportia striata*, *Eoclathrus subramanyami*, *Hirmeria khadluensis*, *Granularia ocliqua*, *Rectogloma* sp.	Silty shale and fine sandstone from Nimar Sandstone and from Nodular Limestone, Amba Dongar, Phata and Barwah	Chiplonkar and Badve 1969a, b, 1970, Chiplonkar and Ghare 1975

Table 6 (continued)

Taxon	Lithostratigraphy	Reference
Annetuba chapdiensis, *Cylindrichnus* sp., *Granularia yelamensis,* *Gyrochorte comosa,* *Imponoglyphus kevadiensis,* *Keckia annulata,* *Laeviyclus mongraensis,* *Palaeophycus heberti,* *P. intermediats,* *P. tulubaris,* *Planolites annularis,* *P. beverleyensis,* *P. montanus,* *Rosselia socialis,* *Thalassinoids paradoxicus,* *T. suevicus*	Upper Nimar Sandstone, Sewariya, Hardaspur and Umri	Kundal and Sanganwar 1998a
Thalassinoides sp., *Striatolites bariaensis*	Upper and middle part of the Nimar Sandstone, Bagh, Sitapuri, Baria Nadi	Singh and Dayal 1979
Aulichnites sp., *Corophioides luniformis,* *Cylindrichnus karondiaensis,* *Palaeophycus striatus*	Top of the Nimar Sandstone	Kundal and Sanganwar 2000
Conichnus conicus, *Conostichus broadheadi,* *Conostichus stouti*	Bagh Group, Narmada District, Gujarat	Patel et al. 2018
Ptychoplasma excelsum, *Ptychoplasma vagans,* *Dendroidichnites irregular,* *Ctenopholeus kutcheri,* *Bergaueria hemishperica,* *Protovirgularia isp*	Silty limestone, Bagh Formation of Katipani, Mainland Gujarat	Bhosle et al. 2019

age to the upper calcareous part of the formation. Most other types of fossils indicate a broad affinity to faunas from the Ceomanian-Turonian. The only paleomagnetic study on the Bagh Group indicated a range from the Aptian to the Santonian (Prasad et al. 1998). Hence, based on the fossil composition, the Nimar Sandstone can be broadly referred to the Cenomanian-Turonian, the Nodular Limestone to the Turonian and the Coralline Limestone to the Coniacian (see also Jaitly and Ajane 2013). Kumar et al. (2018) supported Cenomanian, Turonian and Coniacian ages for the Nimar Sandstone, the Nodular Limestone and the Coralline Limestone, respectively, the stratigraphy assigned by Jaitly and Ajane (2013). They were also able to designate three substages—Lower, Middle and Upper Turonian—within the Nodular Limestone based on index ammonites and inoceramid bivalves.

5 Discussion and Conclusions

Three major sub-environments within the fluvio-marine Nimar Sandstone are as follows.

(i) a fluvial-dominated zone initially, with the transition from fluvial channels to floodplains, having few tide-affected fluvial deposits in the basal part of the succession,

(ii) a mixed energy central estuary zone in the middle-upper part of the succession, which consists of transitional fluvio-tidal channels, tidal flats, associated with tidal channels and bars, followed by,

(iii) a wave-dominated shore environment in the outer estuary zone occupying the upper part of the succession.

Distinct cycles indicate repeated changes in the water-depth over short intervals under a tide-wave interactive system as a product of periodic marine inundation and intercalations. Such repetitive cycles with a fining-up sequence indicate inundation of the fluvio-tidal channel by marine water within a tide-dominated wave- influenced estuarine setting (Jha et al. 2017).

The deposition of overlying carbonate units signifies restricted and/or paused clastic supply in the post-Nimar transgressive depositional system. The predominance of fine-grained carbonates and mud with preservation of small intact body fossils indicates that the Nodular Limestone was deposited in a low-energy, restricted shallow marine platform-tidal flat system with evidence of periodic subaerial exposures in certain time intervals (Gangopadhyay and Halder 1996; Akhtar and Khan 1997; Gangopadhyay and Bardhan 2000; Jaitly and Ajane 2013; Ruidas et al. 2018, 2020). On the other hand, the Coralline/Bryozoan Limestone with abundant cross-stratified/plane-laminated rudstone with siliciclastics, rare mud content and well sorting of bioclasts attests to a high-energy, shallow marine depositional environment. Bansal et al. (2019a, b) interpreted a low-oxygeneted 'glauconitic sea' under the prevailing greenhouse condition.

Overall facies architecture within the Bagh Group reveals the initiation and the early phase of transgression in the lower Nimar Sandstone. The transgression reached its peak during the transition from Nimar Sandstone to the overlying Nodular Limestone. The Nodular Limestone indicates sustained transgression with aggradation, while the uppermost Coralline Limestone demarcates the end of the transgression and initiation of regression. However, many minor cyclicities and higher frequency transgression-regression cycles can be identified within all these sedimentary units, which may be understood after a further detailed analysis of the sediments, preserved organisms and the nature of sediment-organism interactions.

Paleobiogeographically the fauna from the Bagh Group was considered to have a strong affinity only to the Tethyan part of Europe, i.e. the Indo-Mediterranean Region (Duncan 1865; Vredenburg 1907; Chiplonkar 1987 and references therein). However, several other authors found that the fauna shows a mixture of characters from Madagascar, South India and South Africa (e.g. Dassarma and Sinha 1975).

This basin was considered as a part of the Indo-Madagascan Faunal Province based on ammonites (Kennedy et al. 2003; Gangopadhyay and Bardhan 2007).

A detailed paleobiogeographic analysis of the entire fauna would throw light on its affinity to the existing paleobiogeographic units and evolution of such relationships. A detailed analysis of the faunal assemblage, including numerical analysis of the faunal diversity and abundance, functional morphologic analyses and detailed taphonomic analysis would aid in the reconstruction of more detailed paleoecology and depositional environment. Thus, a comprehensive review based on the entire gamut of the sedimentological and the paleontological evidence with detailed documentation of all major and minor changes that occurred spatially and temporally through the Bagh Group of rocks would provide definite clues to understand the basin evolution pattern in the light of the Late Cretaceous global sea level fluctuations and climatic changes.

Thus, analysis of the stratigraphy, the sedimentology and the paleontology of the Late Cretaceous Bagh Group of rocks of the Narmada Valley reveals following conclusions.

(a) The stratigraphy of the Late Cretaceous Bagh Group has evolved through time and consists of three distinct lithounits of formation status, viz., the siliciclastic Nimar Sandstone (Cenomanian–Turonian), the middle fossil-bearing Nodular Limestone (Turonian) and the uppermost fossiliferous Coralline Limestone (Coniacian). The entire sequence is covered by thick, extensive Deccan lava flows.

(b) The sedimentary facies architecture of all three lithounits manifests a gradual change in the paleo-depositional condition from—(i) an initial fluvial to a tide-wave influenced estuarine condition, changing to (ii) a restricted, low-oxygenated, platform-tidal flat setting, and finally (iii) a high energy open shallow marine setting, which signifies an overall transgressive sequence in the Narmada Valley during the Late Cretaceous.

(c) Fossil records are very rich and varied in nature. Particularly, the nature and distribution of marine invertebrate bioclasts and microorganisms corroborate similar paleogeographic changes.

(d) Such transgression reflects the effect of very high global sea level rise in the epicontinental sea as a consequence of extreme high ocean water temperatures during the Cenomanian–Turonian major greenhouse phase.

References

Abdul Azeez KK, Unsworth MJ, Patro PK, Harinarayana Y, Sastry RS (2013) Resistivity structure of the Central Indian tectonic zone (CITZ) from multiple magnetotelluric (MT) profile and tectonic implications. Pure Appl Geophys 170:2231–2256

Akhtar K, Khan DA (1997) A tidal island model for carbonate sedimentation: Karondia Limestone of Cretaceous Narmada basin. J Geol Soc India 50:481–490

Badve RM (1972) Stratigraphy and palaeontology of the Bagh Beds of Narbada Valley. PhD thesis, University of Poona

Badve RM (1987) A reassessment of stratigraphy of Bagh Beds, Barwah area, Madhya Pradesh, with description of trace fossils. J Geol Soc India 30:106–120

Badve RM, Ghare MA (1978) Palaeontological aspect of Bagh Beds, India. Recent Res Geol 4:388–402

Badve RM, Nayak KK (1983) Occurrence and significance of the algae genus Hallmeda from Nimar sandstone, Bagh beds, Jhabua, M.P. Biovigyanam 9:137–148

Badve RM, Nayak KK (1984) Some additional fossils algae from Nimar Sandstone, Bagh Beds, M.P., India. In: Proc X Coll Micropal Strati, pp 185–196

Bansal U, Banerjee S, Pande K, Das DK (2019a) Unusual seawater composition of the Late Cretaceous Tethysimprinted in glauconite of Narmada basin, central India. Geol Mag 157:233–247

Bansal U, Pande K, Banerjee S, Nagendra R, Jagadeesan KC (2019b) The timing of oceanic anoxic events in the Cretaceous succession of Cauvery Basin: constraints from 40Ar/39Ar ages of glauconite in the Karai Shale Formation. Geol J 54:308–315. https://doi.org/10.1002/gj.3177

Barron EJ (1987) Global cretaceous palaeogeography—international geologic correlation program project-191. Palaeogeogr Palaeoclim Palaeoecol 59:207–214

Bhattacharya B, Jha S (2014) Late Cretaceous diurnal tidal system: a study from Nimar Sandstone, Bagh Group, Narmada Valley, Central India. Curr Sci 107:1032–1037

Bhattacharya SK, Jain RA, Tripathi SC, Lahiri TC (1997) Carbon and oxygen isotopic compositions of Infratrappen limestones from central and western India and their depositional environment. J Geol Soc India 50:289–296

Bhattacharya B, Jha S, Mondal P (2020) Palaeogeographic reconstruction of a fluvio-marine transitional system in intra-cratonic rift basin—implications on Late Cretaceous global sea-level rise. J Palaeogeogr. https://doi.org/10.1186/s42501-020-00078-6

Bhosle B, Johnson C, Vaghela S, Schultz DJ, Dholakia V (2019) First report: trace fossil assemblage *Ptychoplasma* (*P. excelsum*, *P. vagans*), *Dendroidichnites* (*D. irregulare*), *Ctenopholeus* (?*C. kutcheri*) and *Bergaueri*a (*B. hemispherica*) in the Cretaceous Rocks of Bagh Formation, Mainland Gujarat, India. Ichnos 1–10

Biswas SK (1987) Regional tectonic framework structure and evolution of western marginal basins of India. Tectonophysics 135:307–327

Blanford WT (1869) Geology of Western Sind. Mem Geol Surv India XVII (1)

Bose PK, Das NG (1986) A transgressive storm and fair weather wave dominated shelf sequence: Cretaceous-Nimar Formation, Chakrud. M.P., India. Sediment Geol 46:147–167

Bose PN (1884) Geology of the lower Narmada valley between Nimawar and Kawant. Mem Geol Surv India 21:1–72

Boulila S, Galbrun B, Miller KG, Pekar SF, Browning JV, Laskar J, Wright JD (2011) On the origin of Cenozoic and Mesozoic "third-order" eustatic sequences. Earth Sci Rev 109:94–112

Chakraborty PP, Tandon SK, Saha S (2019) Development of Phanerozoic sedimentary basins of India. J Asian Earth Sci 184:103991. https://doi.org/10.1016/j.jseaes.2019.103991

Chaudhary M, Nagori ML (2017) Palaeobiogeographic implications of Ostracoda: a case study from Bagh Formation (Upper Cretaceous) of Narbada valley, Madhya Pradesh and Gujarat. Indian J Appl Res 7:316–319

Chiplonkar GW (1937) Echinoids from the Bagh Beds. Proc Indian Acad Sci 6:60–71

Chiplonkar GW (1938) Rhynchonelles from the Bagh Beds. Proc Indian Acad Sci 7:300–316

Chiplonkar GW (1939a) Lamellibranch from the Bagh Beds. Proc Acad Indian Sci 10:255–274

Chiplonkar GW (1939b) Bryozoa from the Bagh Beds. Proc Indian Acad Sci 10B:98–109

Chiplonkar GW (1939c) Echinoids from the Bagh Beds. Pt. II. Proc Indian Acad Sci 9B:236–246

Chiplonkar GW (1941) Ammonites from the Bagh Beds. Proc Indian Acad Sci 14B:271–276

Chiplonkar GW (1942) Age and affinities of the Bagh fauna. Proc Indian Acad Sci 15B:148–152

Chiplonkar GW (1987) Three decades of invertebrate palaeontology and biostratigraphy of marine Cretaceous rocks of India. Geol Surv India Spec Publ 11:305–339

Chiplonkar GW, Badve RM (1969a) A preliminary note on the trace fossils from the Bagh Beds of Narbada valley. Curr Sci 38:394

Chiplonkar GW, Badve RM (1969b) Trace fossils from the Bagh Beds. J Palaeontol Soc India 15:1–5

Chiplonkar GW, Badve RM (1970) Trace fossils from the Bagh Beds. J Palaeontol Soc India 14:1–10

Chiplonkar GW, Badve RM (1972a) Newer observations on the stratigraphy of the Bagh Beds. J Geol Soc India 92–95

Chiplonkar GW, Badve RM (1972) Palaeontology of the Bagh Beds-I Bivalvia (excluding Inoceramidae and Ostracea). J Palaeontol Soc India 17:67–114

Chiplonkar GW, Badve RM (1972) Palaeontology of the Bagh Beds. Pt. III - Gastropoda. Bull Earth Sci 1:41–50

Chiplonkar GW, Badve RM (1972) Palaeontology of the Bagh Beds-II: Echinoidea. Proc Indian Acad Sci 76B:133–152

Chiplonkar GW, Badve RM (1976) Palaeontology of the Bagh Beds. Pt. IV - Inoceramidae. J Palaeontol Soc India 18:1–12

Chiplonkar GW, Badve RM (1976) Palaeontology of the Bagh Beds. Pt. V - Ostreiane (i). Proc Indian Acad Sci 83B:244–256

Chiplonkar GW, Badve RM (1978) Palaeontology of the Bagh Beds. Pt. V - Ostreina (ii). Proc Indian Acad Sci 87B:105–117

Chiplonkar GW, Ghare MA (1975) Some additional trace fossils from the Bagh Beds. Bull Indian Geol Assoc 8:71–84

Chiplonkar GW, Ghare MA (1976) Palaeontology of the Bagh Beds – Bryozoa, Part VI. Biovigyanam 2:59–67

Chiplonkar GW, Ghare MA (1977) Ammonoids from the Bagh Beds of Narmada valley. Indian J Earth Sci 4:109–116

Dangerfield F (1818) Some accounts of caves near Bagh called Panch Pandoo. Trans Lit Soc Bombay 2:194–204

Dassarma DC, Sinha NK (1968) On the occurrence of shark teeth and other marine fossils in the Nimar Sandstone horizon of the Bagh Beds. Indian Min 20:110

Dassarma DC, Sinha NK (1975) Marine Cretaceous formations of Narmada valley (Bagh Beds), Madhya Pradesh and Gujarat. Mem Geol Soc India Palaeontol Indica Ser 42:1–123

Davis RA, Landman NH, Dommergues JL, Marchand D, Bucher H (1996) Mature modifications and dimorphism in ammonoid cephalopods. In: Landman NH, Tanabe K, Davis RA (eds) Ammonoid paleobiology. Plenum Press, New York, pp 464–539

Duncan PM (1865) Description of the Echinodermata from the strata on the South coast of Arabia and at Bagh on the Narbada in collection of Geological Society, London. Q J Geol Soc London 30:349–363

Duncan PM (1887) Notes on Echinoidea of the Cretaceous series of the Lower Narbada valley with remarks upon their geological age. Recent Geol Surv India 20:81–92

Fourteau R (1918) Les Echinides des Bagh Beds. Recent Geol Surv India 49:34–53

Funnell BM (1990) Global and European Cretaceous Shorelines, stage by stage. In: Ginsburg RN, Beaudoin B (eds) Cretaceous resources, events and rhythms. Kulwer, The Netherlands, pp 221–235

Gangopadhyay TK, Bardhan S (1998) Apertural modifications and jaw structures of placenticeratid ammonites from the Upper Cretaceous Bagh Group, central India. Neues Jahr Geol Pal Monatshefte 4:193–202

Gangopadhyay TK, Bardhan S (2000) Dimorphism and a new record of *Barroisiceras* de Grossouvre (Ammonoidea) from the Coniacian of Bagh, central India. Can J Earth Sci 37:1377–1387

Gangopadhyay TK, Bardhan S (2007) Ornamental Polymorphism in *Placenticeras kaffrarium* (Ammonoidea; Upper Cretaceous of India): evolutionary implications. In: Landman NH, Davis RA, Mapes RH (eds) Cephalopods present and past: new insights and fresh perspectives. Springer, Dordrecht, pp 97–120

Gangopadhyay TK, Halder K (1996) Significance of the first record of nautiloid from the Upper Cretaceous Bagh Group of rocks. Curr Sci 70:462–465

Gangopadhyay TK, Maiti M (2012) Geological implication of a turreted gastropod and astartid pelecypod bearing horizon in the nodular limestone of Sukar Nala Section near Zirabad of Bagh, Dhar District, M.P., India. J Sci Tech MSU 31:45–50

Ganguly T, Bardhan S (1993) Dimorphism in *Placenticeras mintoi* from the Upper Cretaceous Bagh Beds, Central India. Cretaceous Res 14:757–756

Ghare MA, Badve RM (1980) Significance of trace fossils in sedimentation of Bagh Beds. In: Proc 3rd Indian Geol Cong Poona, pp 375–387

Ghosh AK, Pal AK (1968) Cayeuxia fructilosa Johnson from the Bagh Beds, Madhya Pradesh. Curr Sci 19:561–562

Guha AK (1976) Lithostratigraphic classification of Bagh Group (Beds), Madhya Pradesh. In: Proc IV Colloq Micropal Strat, Dehradun, pp 209–216

Guha AK (1978) Study of Ceriopores (Bryozoa) from upper Cretaceous sediments of the Bagh Group (Madhya Pradesh) and the Ariyalur Group (TamilNadu). J Palaeontol Soc India 23:30–35

Guha AK, Ghosh BK (1970) Palaeoecology and Palaeogeography of Bagh Beds Upper Cretaceous. In: Proc. Indian Sci Cong 51st Session

Gupta VJ (1975) Indian mesozoic stratigraphy. Indian stratigraphy, vol 2. Hindustan Publishing Corporation, Delhi

Haq BU (2014) Cretaceous eustasy revisited. Glob Planet Chang 113:44–58

Hay WW (2008) Evolving ideas about the Cretaceous climate and ocean circulation. Cretaceous Res 29:725–753

Hay WW (2011) Can humans force a return to a "Cretaceous" climate? Sediment Geol 235:5–26

Hay WW, Floegel S (2012) New thoughts about the Cretaceous climate and oceans. Earth Sci Rev 115:262–272

Hu X, Jansa L, Wang C, Sarti M, Bak K, Wagreich M, Michalik J, Andsotak J (2005) Upper Cretaceous oceanic red beds (CORBs) in the Tethys: occurrences, lithofacies, age, and environments. Cretaceous Res 26:3–20

Huene FV, Matley AA (1933) The Cretaceous Saurischia and Ornithischia of the Central Provinces of India. Palaenontol Indica 21:1–74

Immenhauser A (2005) High-rate sea-level change during the Mesozoic: new approaches to an old problem. Sediment Geol 175:277–296

Jafar SA (1982) Nannoplankton evidence of Turonian transgression along Narmada valley, India and Turonian-Coniacian boundary problem. J Palaeontol Soc India 27:17–30

Jain SP (1961) Discovery of ostracods and smaller foraminifers from the Upper Cretaceous Bagh Beds, Madhya Pradesh. Curr Sci 30:341–342

Jain SP (1963) On the occurrence of Pholadomya cf. elliptica Munster and Pholadomya cf. indica Noetling from the Bagh Beds of Madhya Pradesh. Curr Sci 32:506–507

Jain SP (1969) Taxonomic comments on the Ammonites from the Bagh Beds, Madhya Pradesh with remarks on the age of these beds. Bull Indian Geol Ass 2:45–48

Jain SP (1975) Ostracoda from the Bagh Beds (Upper Cretaceous) of Madhya Pradesh. Geophytology 5:88–212

Jaitly AK, Ajane R (2013) Comments on Placenticeras mintoi (Vredenburg, 1906) from the Bagh Beds (Late Cretaceous), Central India with special reference to Turonian Nodular Limestone horizon. J Geol Soc India 81:565–574

Jaitly AK, Kumar S, Pandey B (2015) First record of Pressastarte zakharov and Pinguiastarte kelly (mollusca: Bivalvia) from the turonian (upper cretaceous) of the bagh beds, central India. J Palaeontol Soc India 60:21–26

Jha S, Bhattacharya B, Nandwani S (2017) Significance of seismites in the Late Cretaceous transgressive Nimar Sandstone succession, Son-Narmada rift valley, central India. Geol J 52:768–783

Keatinge RH (1856) On Neocomian fossils from Bagh and its neighbourhood. J Bombay Branch R Asiatic Soc India 5:621–625

Kennedy WJ, Phansalkar VG, Walaszczyk I (2003) Prionocyclus germari (Reuss, 1845), a Late Turonian marker fossil from the Bagh Beds of central India. Cretaceous Res 24:433–438

Khatri A, Pathrade M, Lakhani L (2013) Occurrence of regular echinoid from Bagh Beds, MP, India. Int Res J Biol Sci 2:86–88

Khosla A, Kapur VV, Sereno C, Wilson JA, Wilson GP, Dutheil D, Sahni A, Singh MP, Kumar S, Rana RS (2003) First dinosaur remains from the Cenomanian-Turonian Nimar Sandstone (Bagh Beds), District Dhar, Madhya Pradesh, India. J Palaeontol Soc India 48:115–127

Khosla A, Sahni A (1995) Parataxonomic classification of Late Cretaceous dinosaur eggshells from India. J Palaeontol Soc India 40:87–102

Kidder DL, Worsley TR (2012) A human-induced hothouse climate? GSA Today 22:4–11

Kominz MA, Browning JV, Miller KG, Sugarman PJ, Misintseva S, Scotese CR (2008) Late Cretaceous to Miocene sea-level estimates from the New Jersey and Delaware coastal plain coreholes: an error analysis. Basin Res 20:211–226

Kulsherstha SK (1995) Micropalaeontological assessment of Bagh Beds in the type area. Unpublished PhD thesis. Panjab University, Chandigarh

Kumar P (1994) Palynology ofCarbonaceous clays on Nimar Formation, Jhabua Distt. Madhya Pradesh, India. J Geol Soc India 44:671–674

Kumar S, Jaitly AK, Pandey B, Pathak DB, Gautam JP (2017) Turonian inoceramid bivalves from the Nodular Limestone Formation (Bagh Group) of the Narmada Basin, Central India and their biostratigraphic implications. In: 10th Int Conference Cretaceous, Berichte der Geologischen Bundesanstalt, Band 120

Kumar S, Gautam JP, Pandey B, Pathak DB, Jaitly AK (2016) Some unknown arcid bivalves from the Turonian (Late Cretaceous) of Central India. Int J Sci Res 5. doi:https://doi.org/10.21275/v5i3.nov162177

Kumar S, Pathak DB, Pandey B, Jaitly AK, Gautam JP (2018) The age of the Nodular Limestone Formation (Late Cretaceous), Narmada Basin, central India. J Earth Sys Sci 127:109. https://doi.org/10.1007/s12040-018-1017-1

Kundal P, Sanganwar BN (1998) Stratigraphical, palaeogeographical and palaeoenvironmental significance of fossil calcareous algae from Nimar Sandstone Formation, Bagh Group (Cenomanian-Turonian) of Pipaldehla, Jhabua District, MP. Curr Sci 75:702–703

Kundal P, Sanganwar BN (1998) Stratigraphy and palichnology of Nimar Sandstone, Bagh Beds of Jobat area, Jhabua district, Madhya Pradesh. J Geol Soc India 51:619–634

Kundal P, Sanganwar BN (2000) Ichnofossils from Nimar Sandstone formation, Bagh Group of Manawar Area, Dhar District, Madhya Pradesh. Mem Geol Soc India 46:229–243

Larson RL (1991) Geological consequences of superplumes. Geology 19:963–966

Lovell B (2010) A pulse of the planet: regional control of high-frequency changes in relative sea level by mantle convection. J Geol Soc 167:637–648

Miller AI, Foote M (2009) Epicontinental seas versus open-ocean settings: the kinetics of mass extinction and origination. Science 326:1106–1109

Miller KG, Kominz MA, Browning JV, Wright JD, Mountain GS, Katz ME, Sugarman PJ, Cramer BS, Christie-Blick N, Pekar SF (2005) The Phanerozoic record of global sea-level change. Science 310:1293–1298

Mukherjee PN (1938) Geology of Gujarat and Southern Rajputana. Rec Geol Surv India 73:163–208

Müller RD, Sdrolias M, Gaina C, Steinberger B, Heine C (2008) Long-term sea-level fluctuations driven by ocean basin dynamics. Science 319:1357

Murty KN, Dhokarikar BG, Verma GP (1963) Plat fossils in Nimar Sandstone near Umrali, M.P. Curr Sci 32:21–22

Naik MK (2013) On some megainvertebrate (mollusca, echinodermata and brachiopoda) fossils from Bagh beds, Madhya Pradesh. Rec Zool Surv India 113:137–144

Nayak KK (1987) Foraminifera from Nimar Sandstone of Bagh Beds, Jhabua District, Madhya Pradesh. Biovigyanam 13:30–39

Oldham T (1858) On some additions to the knowledge of the Cretaceous rocks of India. J Asiatic Soc Bengal 27:112–128

Pal AK (1969) On a species of Lithoporella foslie (Calcareous algae) from the Bagh Beds of M.P. Curr Sci 38:465–466

Pal AK (1970) Onsome condiacean algae from the Bagh Beds of M.P. In: Proceeding 57th Indian Science Congress part III, Section 6, pp 326–327

Pal AK (1970b) Gymnocodiacean algae in the Bagh Group of M.P. In: Symposium on Geology and Mineral Resources M.P. Abstract, p 35

Pal AK (1971) On the algal genera Arabicodium, Boucina and Halimeda (Codiacean algae) in the Bagh Group of M.P. Q J Geol Min Metal Soc India 43:131–132

Pascoe EH (1959) A manual of the geology of India and Burma, vol 2. Government of India Press, Calcutta, pp 485–1343

Patel SJ, Shitole AD, Joseph JK (2018) Plug shaped burrows Conichnus-Conostichus from the Late Cretaceous of Bagh Group, Gujarat, Western India. J Geol Soc India 91:41–46

Petersen HI, Nytoft HP, Vosgerau H, Andersen C, Bojesen-Koefoed JA, Mathiesen A (2010) Source rock quality and maturity and oil types in the NW Danish Central Graben: implications for petroleum prospectivity evaluation in Upper Jurassic sandstone play area. Vining BA, Pickering SC (eds) Petroleum Geology: from Mature Basins to New Frontiers. In: Proceedings of the 7th Petroleum Geology Conference, pp 95–111

Poddar MC (1964) Mesozoics of western India—their geology and oil possibilities. In: 22nd International Geological Congress, vol 1. New Delhi, pp 127–143

Prasad GVR, Verma V, Sahni A, Lourembam RS, Rajkumari P (2017) Elasmobranch fauna from the upper most part of the Cretaceous Bagh Group, Narmada valley, India. Island Arc 26:e12200. https://doi.org/10.1111/iar.12200

Prasad JN, Patil SK, Venkateshwarlu M, Saraf PD, Tripathi SC, Rao DRK (1998) Palaeomagnetic results from the Cretaceous Bagh Group in the Narmada Basin, central India: evidence of pervasive Deccan remagnetization and its implications for Deccan volcanism. Geophys J Int 133:519–528

Rai J, Garg R, Singh A, Garg S, Bajpai S, Kapur VV, Agarwal S, Tripathi SC (2014) Late Cretaceous calcareous nannofossils from Nimar Sandstone, Bagh area, central peninsular India. Bitotic Evolution: Asian and western Pacific fauna and flora II – Micro flora. In: Cretaceous Ecosystems and Their Responses to Palaeoenvironmental Changes in Asia and the Western Pacific (IGCP-608), pp 41–44

Raiverman V (1975) Facies transition among Nimar, Bagh and Lameta beds. Recent Res Geol 2:123–139

Rajshekhar C (1982) Foraminifera from Bagh Beds, Madhya Pradesh. Biovigyanam 8:163–170

Rajshekhar C (1984) Planktonic Foraminifera from the Bagh beds, Madhya Pradesh. In: Proc. X Indian Colloq. Micropal Strut Pune, pp 217–222.

Rajshekhar C (1987) Foraminifera from the Nimar Sandstone, Bagh Beds. Madhya Pradesh, India. Biovigyanam 13:89–97

Rajshekhar C (1991) Foraminifera from the Nodular Limestone, Bagh Beds, Madhya Pradesh, India. J Geol Soc India 42:151–168

Rajshekhar C (1995) Foraminifera from the Bagh Group, Narmada Basin, India. J Geol Soc India 46:413–428

Ramaswami S, Madhavraju J (1993) Petrographic studies of the Bagh Beds along the Narmada Valley in Madhya Pradesh, India. Gondwana Geol Mag 4:65–79

Robinson PL (1967) The Indian Gondwana Formations—a review. In: IUGS 1st Symp. Gondwana Stratigraphy Buenos Aires, pp 208–268

Rode KP, Chiplonkar GW (1935) A contribution to stratigraphy of the Bagh beds. Curr Sci 4:322–323

Roy Chowdhury MK, Sastri VV (1962) On the Revised classification of the Cretaceous and the associated rocks of the Man river section of the Narbada Valley. Rec Geol Surv India 91:283–304

Ruidas DK, Paul S, Gangopadhyay TK (2018) A reappraisal of stratigraphy of Bagh Group of rocks in Dhar District, Madhya Pradesh with an outline of origin of nodularity of Nodular Limestone Formation. J Geol Soc India 92:19–26

Ruidas DK, Pomoni-Papaioannou FA, Banerjee S, Gangopadhyay TK (2020) Petrographical and geochemical constraints on carbonate diagenesis XE "Diagenesis" in an epeiric platform deposit: Late Cretaceous Bagh Group in central India. Carbonates Evaporites 35:94. https://doi.org/10.1007/s13146-020-00624-2

Sahni MR, Jain SP (1966) Note on a revised classification of the Bagh Beds, Madhya Pradesh. J Palaeontol Soc India 11:24–25

Sanganwar BN, Kundal P (1996) Melobesioidean algae from the Nimar Sandstone, Bagh Beds (Cenomanian-Turonian) of Pipaldehla, Jhabua District, Madhya Pradesh. In: Proc XV col Micropal Stratigra, pp 711–718

Sarkar SK (1973) Sedimentology of the Nimar-Bagh-Lameta Complex around Awaldaman and Bagh areas, Dhar District, Central India. Unpublished PhD thesis, Jadavpur University, Kolkata

Sastry MVA, Mamgain VD (1971) The marine Mesozoic Formations of India—A review. Rec Geol Surv India 101:162–177

Schlager W (1989) Drowning unconformities on carbonate platforms. In: Crevello PD, Wilson JL, Sarg JF, Read JF (eds) Controls of carbonate platform and basin development, vol 44. SEPM Spec Publ pp 15–27

Schlanger SO, Jenkyns HC (1976) Cretaceous oceanic anoxic events: causes and consequences. Geol Mijnbouw 55:179–184

Schurrenberger D, Russell J, Kerry K (2003) Classification of lacustrine sediments based on sedimentary components. J Paleolimnol 29:141–154

Sharma A, Sharma VK, Parwar R, Joshi N, Prakash MM, Nirmala M, Verma V (2006) Morphological details of new irregular Echinoid fossil from Zirabad, India. Environ Conserv J 7:107–111

Sharma V (1976) Planktonic foraminifera from the Bagh Beds, M.P. In: Proc. VI Indian Colloq Micropal Strat Varanasi, pp 235–244

Singh G, Ghose RN (1977) Nimar Sandstone. In: lexicon of Gondwana Formation of India, vol 36. Geol Surv India Misc Publ, pp 62–63

Singh IB, Srivastava HK (1981) Lithostratigraphy of Bagh beds and its correlation with Lameta Beds. J Palaeontol Soc India 26:77–85

Singh SK, Dayal RM (1979) Trace fossils and environment of deposition of Nimar Sandstone, Bagh Beds. J Geol Soc India 20:234–239

Singh SN (1950) Microfossils from the Bagh Beds of Barwaha near Indore. Curr Sci 19:174–175

Sinha NK, Dassarma DC (1965) Coilopoceratidae from the Oyster Bed horizon of the Bagh Beds, vol 20. Indian Min, p 111

Smith AB (2010) The Cretaceous Bagh Formation, India: a Gondwana Window onto Turonian shallow water echinoid faunas. Cretaceous Res 31:368–386

Stewart J (1821) Geological notes on the strata between Malwa and Guzerat. Trans Lit Soc Bombay 3:538–541

Tandon SK (2000) Spatio-temporal patterns of environmental changes in Late Cretaceous sequences of Central India. In: Okada H, Mateer NJ (eds) Cretaceous Environments of Asia. Elsevier, Amsterdam, pp 225–241

Taylor P, Badve RM (1995) A new cheilostome bryzoan from the Cretaceous of India and Europe: a cyclostome homeomorph. Palaeontology 38:627–657

Tripathi SC (2006) Geology and evolution of the Cretaceous Infratrappean Basins of Lower Narmada Valley, Western India. J Geol Soc India 67:459–468

Verma KK (1965) On fossil shark teeth from the Bagh beds of Amba Dongar area, Gujarat State. Curr Sci 34:289–290

Verma KK (1968) Seminar on Cretaceous Tertiary Formations of South India, vol 2. Mem Geol Soc India, pp 239–247

Verma KK (1969) Critical review of the Bagh Beds of India. J Indian Geos Assoc 10:45–54

Vredenburg HW (1907) The ammonites of the Bagh Beds, vol 36. Rec Geol Surv India, pp 109–125

Wagreich M, Lein R, Sames B (2014) Eustasy, its controlling factors, and the limnoeustatic hypothesis—concepts inspired by Eduard Suess. Austrian J Earth Sci 107:115–131

Wang C, Hu X, Sarti M, Scott RW, Li X (2005) Upper Cretaceous oceanic red beds in southern Tibet: a major change from anoxic to oxic, deep-sea environments. Cretaceous Res 26:21–32

Zorina SO, Dzyuba OS, Shurygin BN, Ruban DA (2008) How global are the Jurassic-Cretaceous XE "Cretaceous" unconformities? Terra Nova 20:341–346

Fluvial Architecture Modulation in Course of Aeolian Dominance: Upper Terrestrial Member, Bhuj Formation, Kutch

Amlan Koner, Subir Sarkar, Anudeb Mandal, and Sunipa Mandal

Abstract Aeolian deposits make the paleogeographic spectrum of the Early Cretaceous Bhuj Formation in Kutch Mainland basin wider than ever contemplated. The fluvial succession of the Upper Terrestrial Member that rests on Marine Member, passes up into a substantially thick aeolian succession. Fluvial architectural elements divide the fluvial succession in four vertically juxtaposed channel belts. While the second from the base belonged to a meandering system, the rest belonged to braided systems. The meandering river system had a comparatively steeper gradient and shorter length. However, paleohydraulic parameters indicate the progressive dwindling of rivers of multiple generations. The imperative is a progressive drop in base profile. The same temporal trend is reflected in the aeolian facies succession. An attempt has been made to recognize the cause of the overall drying-up trend considering the calculated paleohydraulic parameters and the observed aeolian deformation structures.

Keywords Fluvial architecture · Bhuj Formation · Kutch basin · Facies classification · Paleohydraulic parameters · Aeolian environment

1 Introduction

Sedimentary facies classification on the basis of lithology and structure is an objective procedure, but facies interpretation is subjective (Tabor and Myers 2015). The reason is that the criteria can be shared by different paleoenvironments. Further consideration of internal details of sedimentary structures, their spatial relationship, sedimentary body geometry, stratal organization, stratigraphic architecture and paleocurrent pattern can provide better insight and lead to greater success. In the face of diagonally opposite interpretations of the paleogeography of the Early Cretaceous

A. Koner · S. Sarkar (✉) · S. Mandal
Department of Geological Sciences, Jadavpur University, Kolkata 700032, India
e-mail: jugeoss@gmail.com

A. Mandal
Department of Geology, Presidency University, Kolkata 700073, India
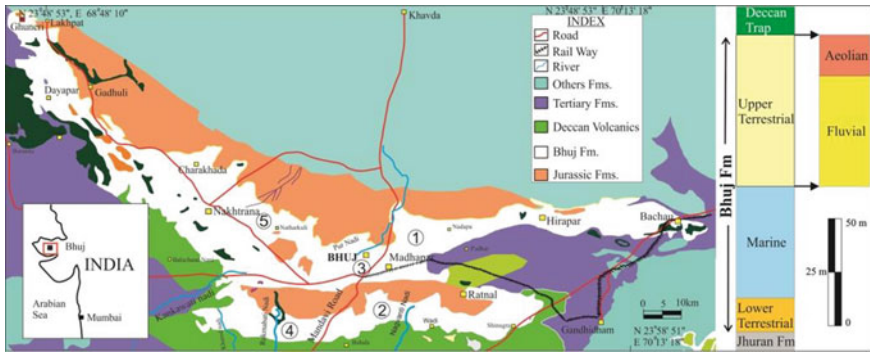
Fig. 1 Geological map of the Bhuj Formation (part of the western India map within inset, red rectangle to the left indicates the study). The numbered circles indicate the positions of the measured sections. On the right the litholog represent the distribution of constituting Members of Bhuj Formation rest on top of the Jhuran Formation in location 4. Note the division of Upper Terrestrial (UT) Member

Bhuj Formation, Kutch Mainland (Fig. 1), Mandal et al. (2016) adopted a multi-faceted approach and established that it had been neither entirely marine (Krishna et al. 1983; Howard and Singh 1985; Shukla and Singh 1990; Singh and Shukla 1991), nor almost entirely fluvial (Biswas 1977, 1981, 1983, 1991), but a fair combination of both: a marine member is encased between two fluvial members. Further extension of the study in space with a similar holistic approach reveals that the Upper Fluvial of the Bhuj Formation transits upward into an aeolian paleogeography. Temporal changes in river channel patterns, their architectural elements and paleohydraulic parameters do not reflect increasing aridity to justify the further transition to the observed transition to the late-stage aeolian dominance, even though the Aeolian facies tract indicates a drying-up trend. As an alternative to paleoclimatic trend as the causal factor of the latter change, the role of tectonism is tested with the help of soft sediment deformation structures in the Aeolian succession. The new revelations prompted renaming of the marine-encasing members in Mandal et al.'s (2016) classification as the Lower Terrestrial and the Upper Terrestrial (Fig. 1). The intention of this paper is to highlight the importance of non-trivial robust holistic programme for interpretation of paleogeography/paleoenvironment as has been carried out here within the UT Member.

2 Geological Setting

The measured thickness of the Upper Terrestrial (UT) Member of the entirely siliciclastic Early Cretaceous Bhuj Formation is around 70 m in the Kutch Mainland basin, India, where the present study was carried out (Fig. 1). Deposition of the Formation took place at the penultimate stage of evolution of a pericratonic rift basin

that opened during the Late Triassic event of Gondwana Supercontinent break-up (Biswas 1977, 1987, 2005). The syn-rift sedimentation took place throughout the Jurassic and continued till the onset of the Early Cretaceous as the Indian plate separated from Africa and drifted northward (Biswas 1982, 1987, 2016a; Arora et al. 2015, 2017; Bansal et al. 2017; Chaudhuri et al. 2018, 2020a, b, c, d). During the rest of the Early Cretaceous period, the rifting probably ceased, but crustal readjustment went on almost as long as the basin-filling continued (Biswas 1991, 2016a). Lithology of the entire Formation is sandstone and subordinate shale, although autoclastic conglomerates are present at the base of both the Lower Terrestrial (LT) and Upper Terrestrial Members of the Formation. A marine Member that intervenes between these two Terrestrial Members wedges eastward, i.e. towards land (Mandal et al. 2016). The base of the UT is well demarcated by an autoclastic conglomerate in form of a blanket, almost uniform in thickness. The UT terminates at top against either Deccan trap or a Tertiary succession (Biswas 1977; Mandal et al. 2016). A group of workers considered the entire Bhuj Formation fluvial or fluvio-deltaic (e.g. Biswas 1981, 1983, 2016b), while others considered it as entirely marine (Casshyap et al. 1983; Krishna et al. 1983; Howard and Singh 1985; Shukla and Singh 1990; Rai 2006). Mandal et al. (2016), nevertheless, reconciled the controversy in a holistic analysis suggesting an intervention of marine inundation between the two phases of fluvial sedimentation. The frequent occurrence of paleosols in the LT and the UT, discussed elsewhere, are consistent with the terrestrial origin of the LT and the UT.

3 Materials and Methods

The paper is based entirely on field observations and measurements. Usual field equipment like Brunton compus, Clinometer, GPS, Measuring Tape, Hammer and Diagonal Scale had been the mainstay of this study. Trough cross-set thicknesses within the channel-forms constitute the basic data to calculate the mean river channel depth from an empirical formula; all other paleohydrological parameters are therefrom. Bankfull channel depth has also been approximated from the thicknesses of a few completely preserved bars and channel-fills which are not truncated and buried under inferred overbank deposit (Bridge and Tye 2000; Mukhopadhyay et al. 2014). To satisfy the precondition of uniformity, troughs of different channel-belts are collected and analyzed separately. Heights of well-preserved bars are utilized for cross-checking of the equation-derived values (Bridge 1997; Leclair et al. 1997). The basic formulae from which the paleohydraulic parameters of the channel-belts have been calculated are as below:

The **mean channel depth** is calculated based on the following equation:

$$h = 0.086(d_m)^{1.19} \tag{1}$$

where d_m = mean channel depth and h = mean set thickness in meters (Allen 1968).

The **mean channel width** can be calculated from following equation:

$$w_m = 8.88d_m^{1.82} \qquad (2)$$

where d_m = mean channel depth and w_m = mean channel width in meters (Bridge and Mackey 1993a, b; Ito et al. 2006).

According to Williams (1984) and Ito et al. (2006)

$$Q_m = 0.06(w_m)^{1.66} \qquad (3)$$

where Q_m is **mean annual discharge** in m^3/s

Osterkamp and Hedman (1982) further proposed an equation

$$Q_m = 0.027(w_b)^{1.71}$$

or

$$w_b = \{(Q_m)/0.027\}^{0.58} \qquad (4)$$

where w_b is **bankfull channel width** in meters.

On the other hand, the **bankfull channel depth** (d_b) can be estimated by

$$w_b = 8.9d_b^{1.4} \ \text{(Leeder 1978)}$$

or

$$d_b = \{(w_b)/8.9\}0.71 \qquad (5)$$

where d_b is bankfull channel depth in meters.

On the basis of above-mentioned variables the **paleoslope** (S) can be estimated from following equations proposed by Schumm (1972):

$$S = 30\{F^{0.95}/(w_m)^{0.98}\}/1000 \qquad (6)$$

where S is paleoslope in m/m and F is channel width/depth ratio (Schumm 1972).

$$F = w_m/d_m \quad \text{(Schumm 1968)}$$

According to Williams (1978) the **bankfull water discharge** is estimated by following equation:

$$Q_b = 4(A_b)^{1.21}(S)^{0.28} \qquad (7)$$

where Q_b is bankfull channel discharge in m^3/s and A_b is the bank-full cross-sectional area represented by $(w_b \times d_b)$.

Based on the relationship between bankfull water discharge (Q_b) and the drainage area $(A_d$ in km$^2)$ is calculated by the following equation:

$$(A_d)^{0.75} = Q_b (\text{Leopold et al.} 1964)$$

or

$$A_d = (Q_b)^{1.33} \tag{8}$$

Finally, the **principal stream length** is approximated from the following equation:

$$L = 1.4(A_d)^{0.6} \tag{9}$$

where L is the principal stream length in km (Leopold et al. 1964).

The mean **channel belt width** (*cbw* in m) has been calculated from its relationships with d$_m$ expressed as following equation (Bridge and Tye 2000; Ito et al. 2006):

$$Cbw = 192(d_m)^{1.37} \tag{10}$$

4   Fluvial Architecture and Paleocurrent Dispersion

The Upper Terrestrial (UT) Member of the Bhuj Formation rests sharply on the Marine Member (Mandal et al. 2016). The autoclastic and generally clast-supported conglomerate blanket of, more or less, uniform thickness, at the boundary between these two Members is made predominantly of brick-coloured sandy mud clasts of varied shapes and diameter around 4 cm (Fig. 2a). More often than not, these clasts are oval-shaped instead of being flat and have their surfaces bumpy with protruding rootlets (Fig. 2b). The 70 m-thick terrigenous succession built up on this blanket is

Fig. 2   a Rhizoconcretionary conglomeratic blanket marks the contact between Marine and UT Member. Note the dominance of brick colored mud-clast; **b** rootlets showing protruding nature (scale bar = 10 cm)

overall fining upward. The predominant lithology of this UT succession is dominated by sandstones. These sandstone bodies are generally characterized externally by lenticular geometry and internally by trough cross-strata and poor grain sorting. Its middle part also includes substantially large bodies of reddish and greyish coloured shales before transiting into well sorted sandstone in the top part. Excellent three-dimensional exposure of the lower two sub-divisions allows us to carry out a thorough analysis of its constituent architectural elements. These elements of two lower sub-divisions have already been interpreted by Mandal et al. (2016) as fluvial, though not in details. Lateral facies change in river deposits is too frequent both along and across the channel axis to realize the full potential of facies analysis in reconstruction of the past river systems (Rădoane et al. 2008; Miall 1985; Rust 1972). Architectural elements with their three-dimensional geometry thus offer a better alternative (Miall 1985, 1996, 2006, 2014; Long 2011; Willis 1997; Yu et al. 2002; Bridge 2003; Miall and Jones 2003; Ethridge et al. 2005; Alexander and Fielding 2006; Long 2006, 2011; Labourdette and Jones 2007; Bose et al. 2008; Sarkar et al. 2012). Taking cognizance of a marked spatial change in their association, the fluvial architectural elements of the UT are described and interpreted below in two separate associations and the paleocurrent dispersions of these two associations are also presented separately. The elements within each of the associations are presented below according to their frequency of occurrence.

4.1 Association I

4.1.1 Channel Element (CHE1)

This element is represented by coarse-grained sandstone bodies having sharp erosional bases, often well demarcated by mud-clasts concentration where the bodies attain maximum thickness (Fig. 3a). The maximum measured thickness of these
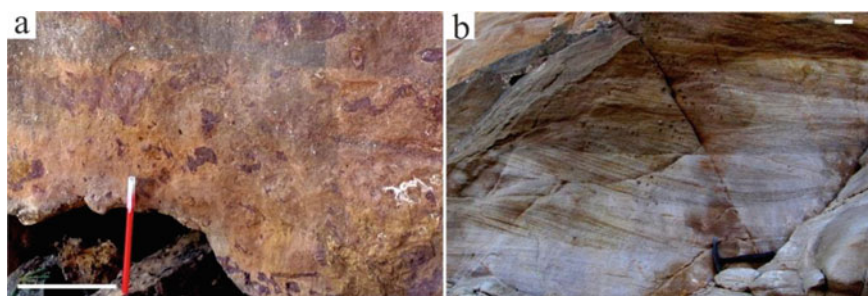
Fig. 3 **a** Mud-clasts concentration at the base of channel indicates high energy condition deposition; **b** trough cross-strata constituting the channel element (CHE1). Note the cross-set thickness within coset discernibly decreasing upward (scale bar = 10 cm)
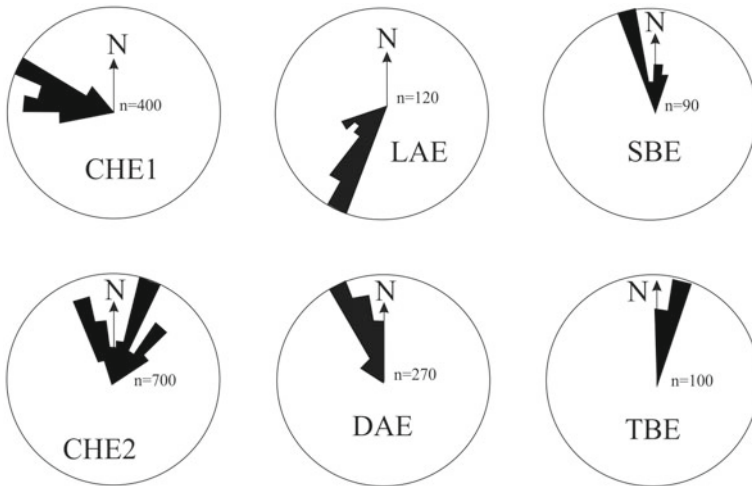
Fig. 4 Summarization of paleocurrent data of six architectural elements present within fluvial system. CHE1 data reflect the unidirectional nature of the meandering stream. LAE is at high angle to the CHE1 strengthen to conclude point bar origin in meandering system, while an acute relationship between CHE1 and SBE supports the deposition of bank attached bar. CHE2 documents the braided river course gets slightly more northward with respect to CHE1. Parallel relationship of CHE2 and DAE infer the DAE to be product of mid-channel bar. The paleocurrent orientation of TBE is also parallel to CHE2 suits well with transverse bar interpretation

bodies is around 2.5 m. The geometry of these sandstone bodies, in general, is more tabular than lenticular. However, being bounded between two master erosion surfaces below and above, they often acquire wedge-shaped geometry. Grain-size rapidly decreases from the bottom upward. Internally the sandstone bodies are sculpted with trough cosets (Fig. 3b). The cosets vary between 90 cm and 2.5 m in thicknesses, while the average cross-set thickness is 18 cm. Within individual cosets, cross-set thickness decreases upward discernibly. The dispersion of orientation of the troughs is rather high, but they still maintain unidirectionality (Fig. 4).

4.1.2 Lateral Accretion Element (LAE)

This element is heterolithic: predominantly sandstone, comparatively finer with respect to the CH1 element, but intermittently intercepted by thin sigmoidal mudstone laminae (Fig. 5a). Successive mudstone laminae bind trough cosets below and above. The cosets have thickness shorter than those of the preceding element that range up to 90 cm and their constituent cross-sets are slightly larger than CHE1, i.e. around 25 cm. The troughs are oriented parallel to their counterparts in the preceding element, but the mud laminae dip at a high angle (Fig. 4). This element laterally grades into the CH1 element.
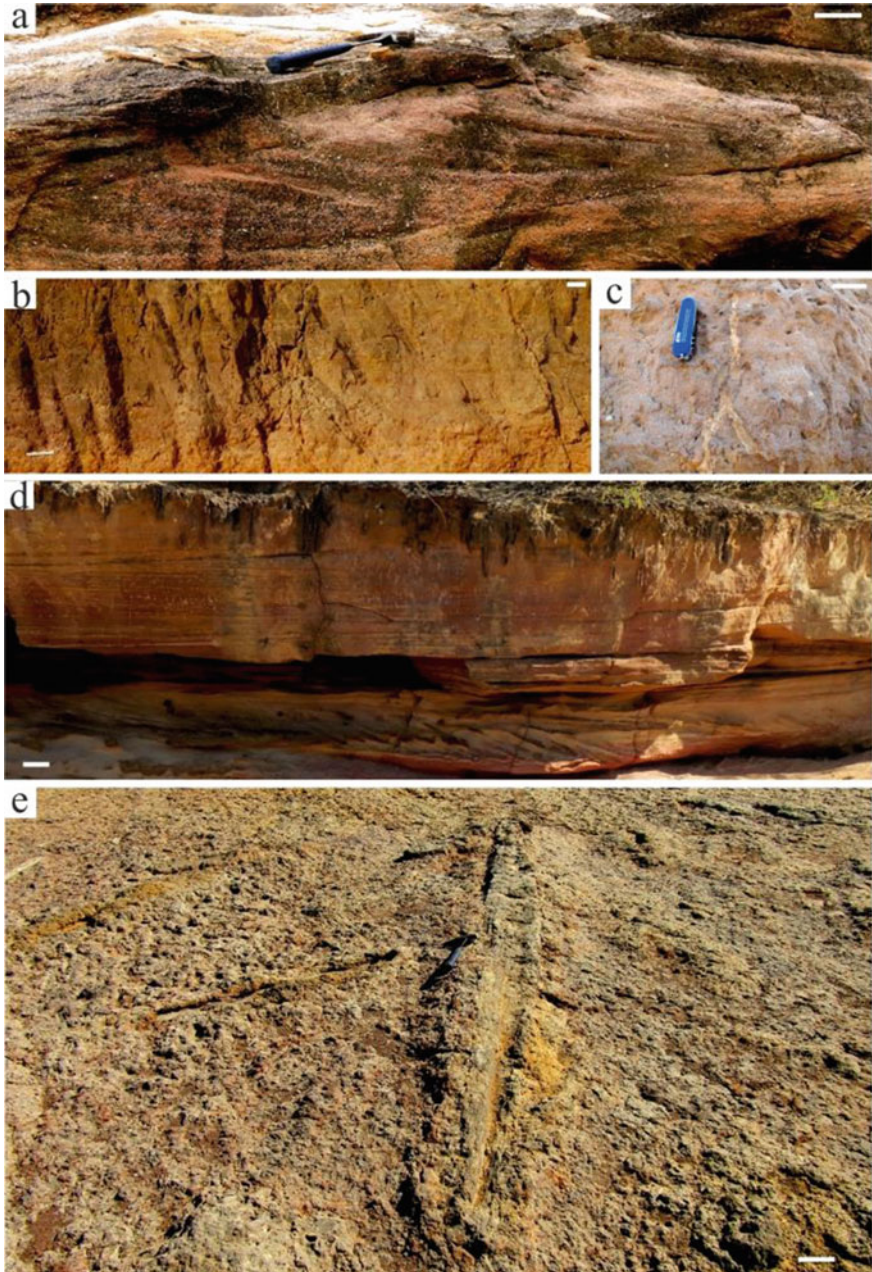
Fig. 5 a LAE with accretionary mud laminae; **b** considerable thick levee deposit (SE), planar laminated sandstone separated by gently inclined mud laminae; **c** downward bifurcated rootlet; **d** planar laminated sandstone sheets constituting the crevasse splay deposits (LSE1). Note the burrows, hanging from top and the cross-stratified sandstone body with concave-up base at the basal part infers to be the typical product of crevasse channel; **e** haphazard orientation of tree logs on top of crevasse splay deposit (scale bar = 10 cm)

4.1.3 Sandy-Sheet Element (SE)

This element is made of fine-grained sandstone and characterized by sheet-like geometry in a section parallel to the troughs (CHE1) on which it overlies but rapidly wedges out in orthogonal section. Internally the sandstone body displays fine planar or low-angle laminae divided into separate sets by thin inclined mudstone laminae (Fig. 5b). The base of the element is distinctly planar. The maximum thickness of the element measures up to 1.8 m because those sheets are amalgamated in most case. Some of these elements bear rootlets (Fig. 5c).

4.1.4 Laminated Sand-Sheet Element (LSE1)

This element is composed of medium- to fine-grained sandstone that is internally planar laminated and these laminae are not interrupted by inclined mud laminae, as in the preceding element (Fig. 5d). Unlike the preceding element, this element maintains sheet-like geometry in orthogonal sections. Both the bounding surfaces of these sheets are generally planar, but the top surface is corrugated when rippled. The ripples are strongly asymmetric and, have height and spacing around 3.6 cm and 7 cm, respectively. The average thickness of these elements is around 50 cm. However, this facies may locally rest on cross-stratified sandstone in which the laminae gradually get flattened to plane lamination. Top surfaces of some over-thickened and comparatively coarser sand sheets are strewn with tree trunks and twigs of widely variable length and diameter. Notably, these tree logs are variably oriented (Fig. 5e). These coarser and thicker sand sheets also contain brick-red nodules with central holes filled by white kaolinitic clay. This element overlies Overbank Element described below.

4.1.5 Sandy Bedform Element (SBE)

This element is made up of medium-grained sandstone, comparatively finer than the CHE1. It is linear ridge-like in geometry, as it appears discernibly wedging in one section and convex-up in section right angle to it (Fig. 6a). The base of the element is invariably flat. On the taller end its height measures up to 1.5 m and its minimum height measured is around 45 cm. Internally the element is characterized by solitary set of tabular cross-strata oriented at an acute angle to trough direction in CHE1 and orientation of the sigmoidal cross-strata in LAE (Fig. 4). Another of its remarkable feature is the presence of thin mud at the base of foresets. This element rests on CHE1. The lateral and vertical continuation of associated elements is documented in someplace else (Fig. 6b).

Fig. 6 **a** Solitary sets of tabular cross-strata belonging to bank attached bar (SBE); **b** spatial and vertical arrangement of different architectural element showing the angular relationship with respect to CHE1; **c** record of rootlet in the floodplain deposit (OFE). See the root holes are filled with yellowish clay and development of fissility planes (scale bar = 10 cm)
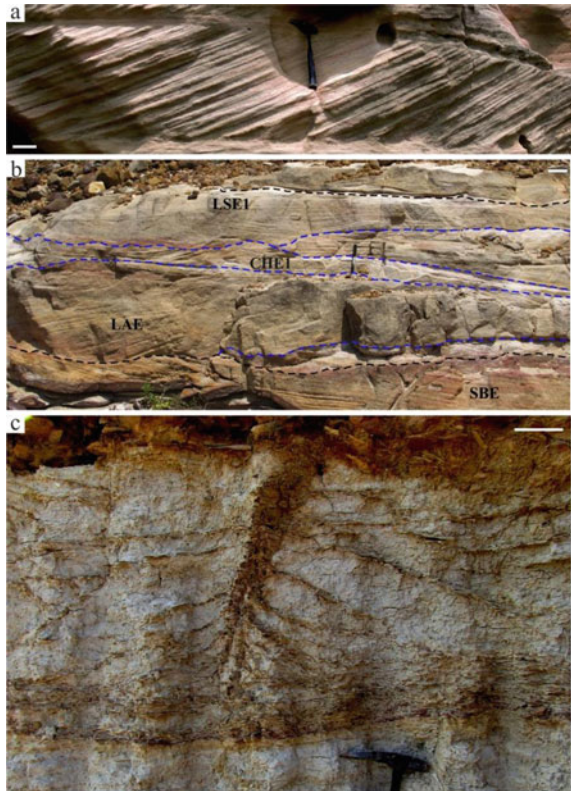
4.1.6 Overbank Fine Element (OFE)

This element, mainly shaley in lithology, form tabular bodies. The shales, when reddish in color, are comparatively sandy and are generally penetrated by burrow and root-holes filled by light-colored yellowish clay (Fig. 6c). When grey in color, the shales bear well developed fissility planes. Root-holes in them have rust-brown ferruginous coating on their walls. The shale bodies have widely variable thickness; the reddish shales are generally thinner, but the grey shales may attain thickness in decimeter scale.

4.1.7 Hollow Scour Element (HOE1)

This lenticular, asymmetric element is composed of medium- to fine-grained sandstone. The infilling sediment displays multiple sets of cross-laminae that tend to conform the geometry of the concave-up base of the element (Fig. 7a). The cross-laminae are normally graded. The exposure width of the element and its depth are 16 and 9 cm, on average. This element is closely associated with the heterolithic LAE.

Fig. 7 **a** Scoop shaped scour generation (HOE1, marked by white arrow) on top of point bar (LAE, yellow arrow); **b** concave-up erosional base later filled by planar laminated sandstone (IPSE) (scale bar = 10 cm)

4.1.8 Incised Planar-Laminated Sandstone Element (IPSE)

This element is the rarest and encountered only once on top of a heterolithic LAE. This element is channel-form with a concave-up erosional base and flat top (Fig. 7b). It is made of sandstone comparatively finer-grained and better sorted and internally planar laminated. The completely preserved channel-form has width and depth 1 m and 30 cm respectively.

4.1.9 Interpretations

Overlying a master erosion surface, the trough cross-strata in the coarsest sand grain fraction of poor sorting within the CHE1, might have formed due to the migration of dunes along the channel floor (Miall 1985, 1996; Bose et al. 2008; Long 2011; Sarkar et al. 2012). Mud-clast concentration under the thickest parts of CHE1 bodies suggests deposition in channel thalweg where depositional energy had been the highest. Tabular geometry dominating over lenticularity, the sandstone bodies presumably belonged to gradually shifting fixed channels (Friend et al. 1979, Friend 1983). Therefore, the simultaneous upward decline in grain-size and cross-set thickness within the trough cosets can be attributed to progressive lateral migration of channel thalweg and consequent decline in depositional energy (Allen 1984; Bridge 2003).

A comparative decrease in grain-size and shorter thickness of trough cross-sets with respect to those of the CHE1, suggests a bank-ward position for the LAE. The sigmoidal mud laminae inclined at a high angle to the trough cross-strata identifies the LAE deposits as lateral accretion deposits on river banks, giving rise to point bars (Allen 1963; Puigdefábregas 1973; Jackson 1976; Cant and Walker 1978; Blodgett and Stanley 1980; Best et al. 2003; Currie et al. 2009). The mud laminae presumably formed during successive floods (Chakraborty et al. 2017). Upward reduction of

cross-set thickness within the trough cosets encased by mud laminae indicates gradual shallowing of the depositional surface with a concomitant decline in the flow velocity as the channel gradually moved away.

Small ridge-like geometry of the SE is manifested in considerable lateral persistence in channel-parallel direction and short wedge-like cross-section in channel-perpendicular direction collectively resembles levees (Friend 1983; Brierley et al. 1997; Bridge 2003; Mack et al. 2003; Posamentier 2003; Arnott, 2007; Sarkar et al. 2012). The inclined mud laminae possibly formed during successive floods (Durkin et al. 2015; Chakraborty et al. 2017). The presence of rootlets suggests usual emergence after the retreat of floodwater. Position of the SE on top of the CHE1 and distinctly smaller grain composition are consistent with the levee interpretation of the former.

Planar laminated LSE1 clearly manifests a high flow regime for its fine-grained sand composition (Smith 1972; Sarkar et al. 2012). Successive occurrences of planar lamination are an indication of aggradation (Bristow et al. 1999). This might be interpreted as crevasse-splay formed on breach of the levee during the flood. In accord to an advent of crevasse splay association, cross-stratification style makes it perfect to be a crevasse channel. Uprooted tree trunks and twigs in the sediment clearly manifest vigorous flood. The diverse orientation of the long plant segments documents their rotation before final settling when the floodwater drained out. The degree of rotation after initial grounding presumably depended mostly on the respective weight and length of the plant segments and anchoring capability of the twisted twigs.

The SBE, in the given association, appears to represent a bar within the river channel, but close to the bank where comparatively diminutive flow regime permitted the formation of only straight-crested bedform (Harms et al. 1982; Collinson and Thompson 1989). It will not then be unwise to consider the element as a bank-attached bar (Miall 1985; Todd and Went 1991; Mazumder and Sarkar 2004; Yu et al. 2002; Ghosh et al. 2006). Angular relation of its cross-strata orientation with the trough and sigmoidal cross-strata in CHE 1 and LAE respectively help to identify the bar as diagonal, formed at an angle to the river bank and extended into the river channel. The intermittently occurring mud laminae at the toe of some of the foresets, probably owe their origin to successive floods.

The muddy lithology of the OFE indicates deposition in a very low energy set-up farthest from the channel thalweg (Long 2011; Sarkar et al. 2012, Mandal et al. 2016). Sediment accretion supposedly took place mostly during the flood and its immediate aftermath (Nanson 1986; Walling and Bradley 1989; Wright and Marriott 1993). Preservation of OFE arguably required a relatively higher position of the river base profile with respect to the channel-floor (Bridge 2006).

The HOE1 appears to be a scour-and-fill structure incised on a fine-grained heterolithic point bar (Durkin et al. 2015). Its disharmonic filling suggests side-filling of the scour; formation of a scour and its filling might not have taken place simultaneously (Salter 1993; Long 2011). The multiple sets of filling make discontinuities in the process, however minor, apparent. The superimposition of multi-generation scours further highlights the repetition of alternate scour and fill (Bridge 2006).

We could not find any equivalence of the IPSE in any ancient formation described in the literature. It is apparent that a small channel was incised on non-cohesive comparatively coarser sandstone during a spurt of flow intensity. The channel was filled immediately afterward so that its shape could be retained intact. The filling required a fall in the flow velocity sufficient enough to initiate sand deposition. Planar laminae within the channel-fill, nonetheless, indicate that the flow regime had still been high. Presumably, the cut and fill had been completed almost instantaneously during a flood event. Possibly the channel represents a chute cut-off joining two concave cut banks during a rush of heightened flow. Between the two cut banks presumably lay a point bar that had been incised by the flow, as is documented here.

The river channels with inferred levees and crevasse-splays appear as meandering. The wide span of the orientation of the directional attributes of the deposits further corroborates the meandering geometry of the river channels addressed herein.

4.2 Association II

4.2.1 Channel Element (CHE2)

Coarse- to medium-grained and poorly sorted sandstone constitutes this element that flaunts lenticular geometry, typically with concave upward base and flat top. Internally the sandstone is characterized typically by trough cosets (Fig. 8a). Their erosional bases are demarcated by mud clast concentrations in the basal part of the UT section. A general upward decline in grain-size attended by a decrease in thickness of the constituent cross-sets is noted within each of such bodies. The width of these sandstone bodies is indeterminable, certainly larger than several decameters and their thickness measures up to 3.2 m. Their internal cross-sets range from 15 to 38 cm in thickness. This element often passes laterally into the next element described below

Fig. 8 a Concave-up base and flat top trough cross-stratified sandstone from braided stream (CHE2); **b** association of four architectural elements within the channel fill; **c** compound cross-stratified sandstone. Note both the larger (red arrow) and smaller cross-strata (sky blue) enclosed within the larger one showing same downcurrent direction (DAE) (scale bar = 10 cm)
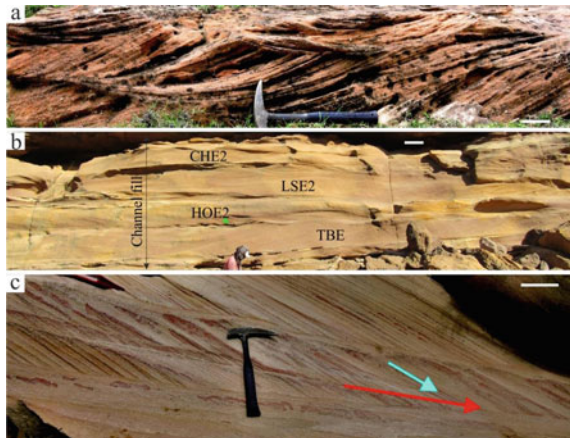
(Fig. 8b). The trough cross-strata orientation in this element is fairly consistent, the mean direction being almost northward (Fig. 4).

4.2.2 Downstream Accretion Element (DAE)

Coarse to medium-grained sandstone, comparatively coarser than the preceding element in which it laterally passes into, makes up this element that rests on a master erosion surface with a flat base and possesses convex-up geometry (Fig. 8c). Internally it is characterized by compound cross-strata in which low angle large-scale cross-strata confine between themselves small-scale steeper cross-strata, both the types of cross-strata being oriented in the same direction that parallels the trough orientation in the preceding element (Fig. 4). The convex-up geometry of this element is best discernible in the section at a right angle to the cross-strata orientation. The maximum thickness of this element measures up to 1.2 m and its exposure width has been traced up to 4 m.

4.2.3 Transverse Bar Element (TBE)

This element is made of medium- to coarse-grained and poorly sorted sandstone that forms convex-upward lenticular bodies resting on flat master erosion surfaces (Fig. 9a). Internally the element is characterized by a single set of tabular cross-strata that measure up to 55 cm in thickness. They are oriented roughly parallel to the troughs in the CHE2 (Fig. 4). In contrast to SBE in the preceding association, this element is larger in dimensions, does not shows the tendency for lateral wedging, does not have mud layers at the base of foresets and the cross-sets are almost parallel to the associated troughs.

4.2.4 Laminated Sand-Sheet Element (LSE2)

This laminar sand-sheet element is comprised of slightly coarser sandstone than the TBE on which it overlies and internally bears crude planar laminae (Fig. 9b). As its designation suggests, this element is sheet-like in geometry but laterally discontinuous. The thickness of this element measures up to 50 cm. Rare though, rootlets are locally observed on top of this element.

4.2.5 Hollow Scour Element (HOE2)

This element is an asymmetric scour encased by the TBE below and the LSE2 above and filled by curved cross-strata with a scalloped base (Fig. 9c). The exposure width of the element is about 80 cm and depth about 25 cm. All the three elements, juxtaposed together, are made of coarse-grained sandstone.

Fig. 9 **a** Large scale tabular cross-stratified sandstone typified as transverse bar (TBE); **b** planar laminated sandstone sheet on top of TBE indicate high flow shear condition (LSE2); **c** scour on top of TBE (HOE2) and successively overlain by LSE2 deposit (scale bar = 10 cm)
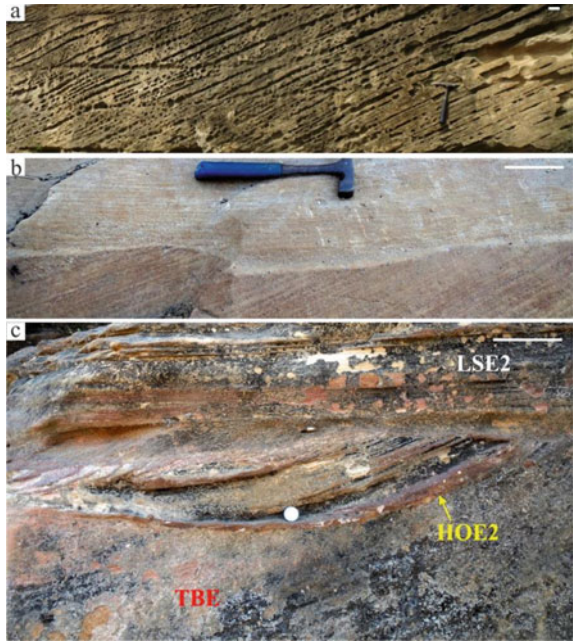
4.2.6 Upstream Accretion Element (UAE)

Flat-based and convex-up, coarse-grained and poorly sorted sandstone bodies fairly similar to the DAE in terms of lithology represent this element. In this element too large-scale cross-strata encase small-scale cross-strata, but they are inclined in the opposite direction; the smaller scale cross-strata move up the larger-scale ones (Fig. 10a). However, this element has a very limited occurrence. Nevertheless, the orientation of the smaller scale cross-strata matches well in orientation between the DAE and the UAE.

4.2.7 Downstream Lateral Accretion Element (DLAE)

This element is characterized by tabular cross-stratified sandstone in which the cross-strata orientation is at a high angle to cross-strata in CHE2 and TBE. Locally these cross-strata are found reclining on DAE and comparatively finer-grained than that on which they recline (Fig. 10b). The cross-sets in this element are around 1.2 m in thickness.

Fig. 10 a The larger
cross-strata shows opposite
direction compare to that of
smaller one (UAE);
b accretionary tabular
cross-strata (yellow)
reclining on either flank of
mid channel bar (DLAE),
deposited during retreat of
flood water. Green arrow
depicts the migration
direction of mid-channel bar
(scale bar = 10 cm)

4.2.8 Interpretations

The lenticular geometry of CHE 2, with concave-up base and flat top in the trans-verse section, is an indication of channel deposition (Miall 1977, 1996). Trough cross-strata within it clearly attest to dune migration along the channel (Miall 1985, 1988; Collinson and Thompson 1989; Smith and Rogers 1999; Eriksson et al. 2006; Smith et al. 2006, Sarkar et al. 2012). Initially, the flow strength had been enough to erode the mud clasts from the older deposits. The coarsest fraction of the sediment, including the clasts, is envisaged to have accumulated at the channel thalweg. Filling of the channels by single cosets of troughs indicates a flow continuum. Overall fining upward trend and gradual diminution of cross-set thickness in the coset attests gradual decline in flow intensity because of gradual blocking of the upstream entry into the channel (Harms et al. 1975; Allen 1983a, b; Haszeldine 1983a, b; Bridge 1997; Bose et al. 2008; Sarkar et al. 2012). Alternatively, the fining upward trend also satisfies the aggrading trend that is simply related to deposition under fixed accom-modation or rate of deposition exceeding the rate of accommodation space creation (Bridge 1997). However, the common cause is likely to be a temporal decrease in the discharge of water through the channel (Bridge 1993; Sarkar et al. 2012).

Formation of compound trough cross-strata in DAE is indicative of migration of small bedform across crests of larger bedforms having gentle lee slopes (Collinson and Thompson 1989; Smith and Rogers 1999; Eriksson et al. 2006; Bose et al. 2008). Smaller bedforms apparently traversed from stoss across the crest and then along the low angle downcurrent face of those large bedforms (Bose and Chakraborty 1994; Bose et al. 2008; Sambrook Smith et al. 2009; Sarkar et al. 2012). Being flanked by CHE2 this element represents mid-channel longitudinal bars (Long 2011).

In case of TBE planar horizontal traces of cross-strata in a section at a right angle to their dip direction clearly depicts the straight-crested nature of the bedform (Collinson and Thompson 1989). The appearance of these bedforms directly on the master erosion surfaces indicates that the bedforms developed directly on the channel floor. Cross-strata orientation parallel to channel orientation indicates that these bedforms are transverse in orientation to the channel axis (Smith 1970, 1971; Olsen 1988; Reading 1996; Best et al. 2003; Labourdette and Jones 2007; Sarkar et al. 2012).

The LSE2 on top of transverse bars possibly developed under enhanced flow shear (Harms et al. 1975; Miall 1996; Bose et al. 2008). Such strong shear likely developed on a bar-top during the falling water stage. Presence of rootlets on top of this element indicates exposure and thereby corroborates the contention of falling water stage in relation to the formation of the LSE2. Apparently, finer fraction of the reworked bar-top sediment was winnowed out, leaving a lag of coarser sand.

Placement of the HOE2 indicates its formation on top of a transverse bar during the falling water stage but before the formation the LSE2. Apparently, as the river level dropped, the scour was excavated by a highly turbulent flow (Best and Andashworth 1997). The scalloped base of the cross-strata records vacillation in the orientation of the shallow flow. The intense turbulence in the flow developed before the generation of the sheet flow and the following exposure.

The UAE appears to have formed on the upstream flank of longitudinal bars (Long 2011; Mandal et al. 2016). The upward migration of sets of ripples suggests sediment accretion on the stoss slope of the longitudinal bedforms under an enhanced rate of sediment delivery.

The DLAE oriented perpendicular to the channel flow direction must have formed under the influence of a secondary flow. Reclining against longitudinal bars, this element appears to have formed because of sand avalanching on the bar flanks during flooding (Long 2011; Mandal et al. 2016).

4.3   Association III

4.3.1   Crinkly Laminated Sandstone, IIIA

This facies in fine-grained sandstone is sheet-like in geometry and internally characterized by mm-scale crinkles arranged in crude planar laminae (Fig. 11a). The crinkled appearance owes to rough globular forms of sand grains. The sandstone beds are, however, not laterally continuous but passes into OFE of the previous association or other facies of this association described below. The measured thickness of this sandstone body attains up to 1.2 m. Some mm to cm-thick brick-red mud laminae are found to intercalate with this facies at places.
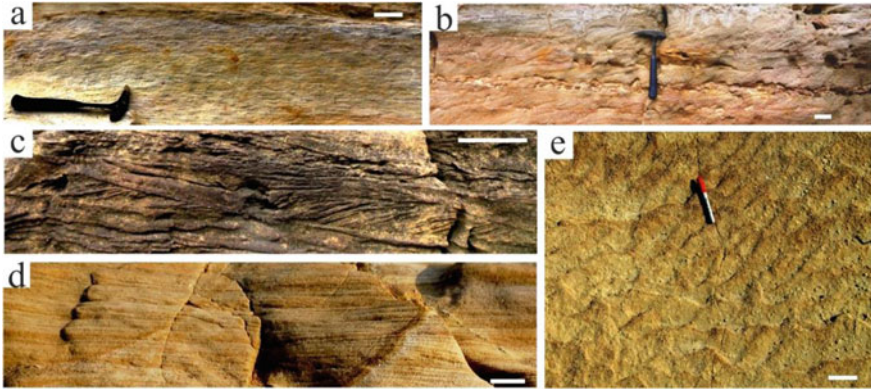
Fig. 11 **a** Crinkly laminated fine grained sandstone suggest the coagulation of dry sand grains on wet sand; **b** alternate grainflow-grainfall laminae within the rippled facies. Note the yellowish mud-clasts concentrate on fixed level, defining bed surfaces; **c** ripple drift sandstone facies showing transition from sub-critical to super-critical nature; **d** inversely graded translatent strata; **e** impact ripple. Note the coarse grain concentration along crest (scale bar = 10 cm)

Interpretations

The rough globules resemble the little lumps of sand that form on coagulation of grains together when a dry bed of sand is sprinkled with water (Kocurek and Fielder 1982; Chakraborty and Chaudhuri 1993). Multiple sand grains adhere together with water films in between them. The structure that forms thereby is thus termed adhesion structure and is interpreted here to have formed when wind-deflated sand grains accumulated on a wet surface. Perhaps aggradation of the wind-blown sediment can form a thick succession (Anderson 1988, 1990; Hunter 1977). Sinuous to planar adhesion laminae transition could be possibly formed at a lower moisture content of substrata and significant wind speed at the depositional area enhanced the adhesion ripple to be planar in nature (Hunter 1980; Kocurek 1981; Kocurek and Fielder 1982; Olsen 1989). This facies is interpreted as of interdune origin.

4.3.2 Rippled Facies, IIIB

This sandstone is dominated by ripples, but they are interlayered with subordinate sets of concave-up parallel laminae filling broad, shallow scours, and rows of small, laterally detached yellowish mud-clasts defining bedsurfaces (Fig. 11b). The top of the facies unit is, at places, rugged and uneven with bioturbation. The ripples are internally characterized by alternate dark and light-coloured cross-laminae. The dark-coloured cross-laminae are made of comparatively coarser grain fraction and distinctly wedge out downslope. The light-colored cross-laminae, however, do not show any such tendency, though thinning upslope. The concave-up parallel laminae are dominated by the comparatively light-colored sediment fraction. The parallel

lamina sets are, on average, 2.7 cm thick. The exposure width of the scours ranges up to 4 cm. The vertical bioturbation structures on top of this facies unit are mostly filled by whitish kaolinite. A few others are filled with brown colored sand and upward bifurcated.

Interpretations

The facies documents frequent changes in paleoenvironmental condition. Within the ripples, the coarser-grained laminae wedging downslope make avalanching evident and reverse grading within these laminae suggests the operation of grain-flow process (Middleton 1976; Kleinhans 2004). On contrary, the fine-grained laminae are likely products of suspension fall-out, and can thus be designated as grain-fall (Anderson 1988). Regular alternations of grain-flow and grain-fall bear clear fingerprints of aeolian action (Cooper 1958; McKee and Bigarella 1972; Hunter 1977). The broad scours were formed presumably when sediment concentration in the air dropped, but the wind velocity remained roughly the same. A slight fall in wind velocity thereafter allowed grain-fall filling the scours. The presumed decline in sediment concentration within the air-flow could have taken place either due to the wetting of the sediment source or subtle change in wind direction. The mud-clasts forming single layers terminating the scour-and-fill structures as well as the ripples under them apparently make the flooding of the depositional surface apparent. Since there is no overlapping between the clasts and the distance between them is, more or less, uniform, it seems that mud layers deposited during flood suffered shrinkage during desiccation on the recession of the flood. Upward passage of these mud-clast layers to aeolian ripples again indicates the resumption of air-flow. We thus favor intermittent shallow flooding in lieu of any assumption of wind direction variation in the course of vertical repetition of this assemblage of structural elements. This facies dominates the interdune areas.

4.3.3 Fine-Grained Ripple-Drift Sandstone, IIIC

This facies is of fine-grained sandstone characterized by ripple-drift. However, there are localized sets of parallel laminae too. Remarkably ripple climb angles are frequently and widely variable (Fig. 11c). Consequently, (i) the pseudobeds confined between successive climb planes are laterally variable in thickness, (ii) ripple climb varies from subcritical to supercritical to even sinusoidal form and (iii) there is no order in this change, or, in other words, this change takes place within a single pseudobed repeatedly. The supercritically climbing parts indicate that the ripples had heights of about 4.5 cm.

Interpretations

This facies is interpreted as aeolian primarily because of its association with other sediments bearing hallmarks of an aeolian environment. The extreme flow-unsteadiness recorded in this case is, nonetheless, in perfect agreement with unconfined and slope-defying air-flow. The transition from subcritical to supercritical ripple climb indicates increase in the rate of suspension fall-out and vice versa (Walker 1963, 1969; Jopling and Walker 1968). The sinusoidal form is indicative of simple vertical aggradation of ripples under vertical settling of grains, without lateral migration. Jopling and Walker (1968), however, had mud in their experimental system as the main bulk of suspension load. In the absence of mud in our depositional system, the climb features are to be explained by variation in the balance between velocity and sand concentration in the wind. The unconfined air-flow velocity is laterally variable, and thus, wind blows in gusts. With a given sand-size, sediment concentration in an air-flow is primarily dependent on wind velocity in case of steady supply from the source. When the wind vacillates and changes its flow path, the sand load does not shift immediately. Sediment concentration, therefore, momentarily increases with respect to the balance with wind velocity it achieved a moment ago. Suspension fall-out rate would thus be enhanced immediately. We accordingly conclude that the erratic transitions between subcritical and supercritical ripple climb, as observed in the UT Member, is as diagnostic of aeolian deposition as those recorded by Hunter (1977) and Rubin and Hunter (1982). Apparently, this facies dominates the interdune area.

4.3.4   Sandstone with Inversely Graded Low-Angle Laminae, IIID

This facies is represented by tabular body of well-sorted and fine-grained sandstone that is internally characterized by centimeter/decimeter-scale cross-laminae, often at such low angle that they may be deceptive of planar laminae (Fig. 11d). In contrast to the latter, these laminae enclose a steeper subset of cross-laminae in submillimeter-scale, albeit recognizable only here and there, and overall reverse grading across them. The fine-gained part in the basal part of each of these laminae, itself is discernibly normally graded at places, although generally looks massive. The measured outcrop width of this facies bodies ranges from 2.2 to 5.4 m. Facies thickness is widely variable and may attain tens of centimeters. The ripples on the bed surfaces have crests straight or broadly sinuous and have spacing: height ratio >12 (Fig. 11e). Coarse grains concentrate along the crests of these ripples.

Interpretations

The structural element perfectly resembles translatent strata, a distinctive constituent of many modern and ancient aeolian deposits around the globe (Fryberger et al. 1979, 1983; Pulvertaft 1985; Kocurek and Nielson 1986; Langford and Chan 1989;

Clemmensen et al. 1989; Nickling and Wolfe 1994). They are traditionally interpreted as products of subcritical climb of impact ripples with mm-scale height with very wide spacing (Hunter 1973; Ahlbrandt and Fryberger 1981; Kocurek 1981; Kocurek et al. 1992). The ripples present on the top surface of this facies, at places, exactly match the description. The density of air is about 800 times lesser than that of water and thus its lift power is comparatively very low. It is thus conceivable that once lifted up in the flow sand grains would be dragged a long way before landing on the ground as the thin air medium put little resistance to their movement. The low incidence angle of grain trajectory had not allowed these ripples to stand tall. In consequence, the ripple stoss slope turned very gentle. Subcritical climb planes of ripples were even gentler and the truncated lamina sets between them thus turned merely submillimeter-thick (Hunter 1977). As a saltating grain had impinged the ground, multiple coarser grains, those could not be lifted up, were nudged ahead. The force was transmitted to hundreds of adjacent grains as the air-film between them offered little resistance. Hence it can be envisaged that every impacting grain had set hundreds of coarser grains rolling in the wind direction. This coarser load gradually crept up the stoss of the ripples and accumulated on the crests of the ripples till the lee slopes of the ripples exceeded the angle of repose. The coarser load thus avalanched intermittently in the form of grain-flow. The fine-grain load, in contrast, was deposited from suspension in a slow continuous process. The inverse grading thus resulted after every event of grain-flow. That is the likely reason for the concentration of coarser grain fraction along the crests of the ripples on bed tops. Counterparts of this facies are found in modern aeolian interdune areas and on dune flanks.

4.3.5   Small-Scale Trough Cross-Stratified Sandstone, IIIE

This facies in finer-grained sandstone is characterized by medium-scale cross-strata that are typically long-toed (Fig. 12a). Some of them deviate considerably from their general orientation. Their set-thickness, bound by frequently repeated omission surfaces, varies laterally and vertically between 7 cm and 20 cm, respectively. Concave-up trough shape has readily been recognized in orthogonal section (Fig. 12b). The omission surfaces are mantled by thin layers of slightly coarser and darker colored grains (Fig. 12c). Steeper, darker colored and down-slope wedging cross-strata, locally seen, are very short and remain confined to the crestal part of the parental bedforms. At their toe-end the cross-strata are partially erased out by oppositely moving ripples. At places, long solitary ripple lamina sets move up the toe of the larger bedforms. Crests of these ripples are locally preserved. The ripple lamina-sets, however, do not reduce in thickness upslope. Alternate grainflow-grainfall cross-laminae are comparatively more pronounced within these smaller sets. This facies is in close association with the next facies described below.

Fig. 12 **a** Fine grained sandstone showing long toed cross stratification. Note the coarser grains mantling the bed surfaces are darker in color; **b** aerodynamic ripple; **c** dark red colored layer point to Fe encrusted omission surface, predicted to be developed due to lichen growth when exposed (scale bar = 10 cm)

Interpretations

The concave-up cross-lamina sets presumably formed because of the migration of curve-crested aerodynamic ripples of comparatively greater height than the impact ripples described in facies IIID (Hunter 1973; Kocurek et al. 1992). Evidently, relatively finer grain fraction dominated the sand load of this facies. This observation possibly implies that the sand-load was derived from a moist area that allowed little more than deflation of finer grain fraction under the prevailing wind. Since the finer grains could be lifted a little bit more, the aerodynamic ripples could gain height up to about 2.5 cm, measured from where the ripple crests are preserved. The omission surfaces were apparently created frequently in the intervals when sand supply dwindled, possibly because of enhanced moisture in the source area. The air still blowing unhindered winnowed out a comparatively finer fraction from the depositional surface. Darker color of the coarser lag possibly owes to the growth of lichen during the omissions (Oostra 2006). Local toe-end reworking of the medium-scale cross-strata suggests momentary changes in wind direction. Isolated mm-thick sets of cross-laminae moving up the medium-scale foresets may belong to strong backflows. However, there are a few caveats to the scenario proposed hereby. First, during migration of ripples with long toes generation of strong backflow is highly unlikely. Second, the cross-lamina-thickness does not decrease upslope, as it happens in case of backflow ripples. Thirdly, with well pronounced grainflow-grainfall lamina alternations the small-scale impact ripples appear to have comparatively coarser grain-size than the aerodynamic ripples (Cooper 1958; McKee and Bigarella 1972; Middleton and Hampton 1976; Hunter 1977). It is thus reasonable to assume that wind from

almost opposite direction drifted sand from a different source, presumably a drier one. Apparently wind direction did change in different frequencies. As we experience in modern days, wind direction drastically changes seasonally and also in both shorter as well as longer cycles. This facies presumably developed at the foot region of aeolian dunes dealt with later.

4.3.6 Medium to Large-Scale Tabular Cross-Stratified Facies, IIIF

This sandstone facies is coarser than the preceding ones and internally characterized by medium to large-scale tabular cross-strata. Every foreset is divided into a basal lighter part and an upper darker reddish-brown part. The lighter part is finer-grained and discernibly normally graded at places, although generally appear massive. However, the darker part more often reveals inverse grading (Fig. 12a, top part). It is downslope wedging and commonly fails to reach the base (Fig. 13a). The preserved set thickness measures between 18 cm and 90 cm. Exposed foreset surfaces locally reveal straight-crested and strongly asymmetric ripples that extend downslope (Fig. 13b). The ripples are, on average, 0.8 cm high and 10 cm apart from each other from crest to crest and rarely get bifurcated (Fig. 13c). The tabular cross-strata are, at places, arranged in climbing sets. In some of them the climb angle discernibly changes, increasing upward in the example illustrated (Fig. 13d).

Interpretations

The cross-sets presumably formed by migration of straight-crested dunes. The coarse-grained and wedge-shaped layers presumably formed because of avalanching. On the other hand, the finer-grained layer, in contrast, formed through the settling of grains from the suspension; normal grading of grain-size distribution suggests comparatively coarser grains settled first. The reverse grading in the avalanching fraction possibly owes to kinetic sieving (Middleton 1970; Gray 2018). Grain-flow is the likely depositional mechanism. Reddish color of this deposit is possibly attributable to the growth of lichen (Oostra 2006). The regular alternations between grain-fall and grain-flow clearly indicate that the bedforms were driven by wind. The ripple migration along the dune surfaces had evidently been at a right angle to the direction of dune migration. The existence of a secondary flow was an obvious prerequisite. Its passage was presumably provided by the space between the mutually parallel straight-crested dunes on the train. The climbing dunes indicate that composite dunes of very large dimensions used to form, although their preservation would, understandably be very limited (Allen 1971, 1973). The vertical change in the climb angle is likely to reflect temporal variation in the sediment budget. In the illustrated example (Fig. 13d), the increasing steepness of the climb angle or, in other words, greater preservation of dune lee face would imply an increase in the rate of sand accretion through time exceeding the rate of sand drift away from the depositional site.
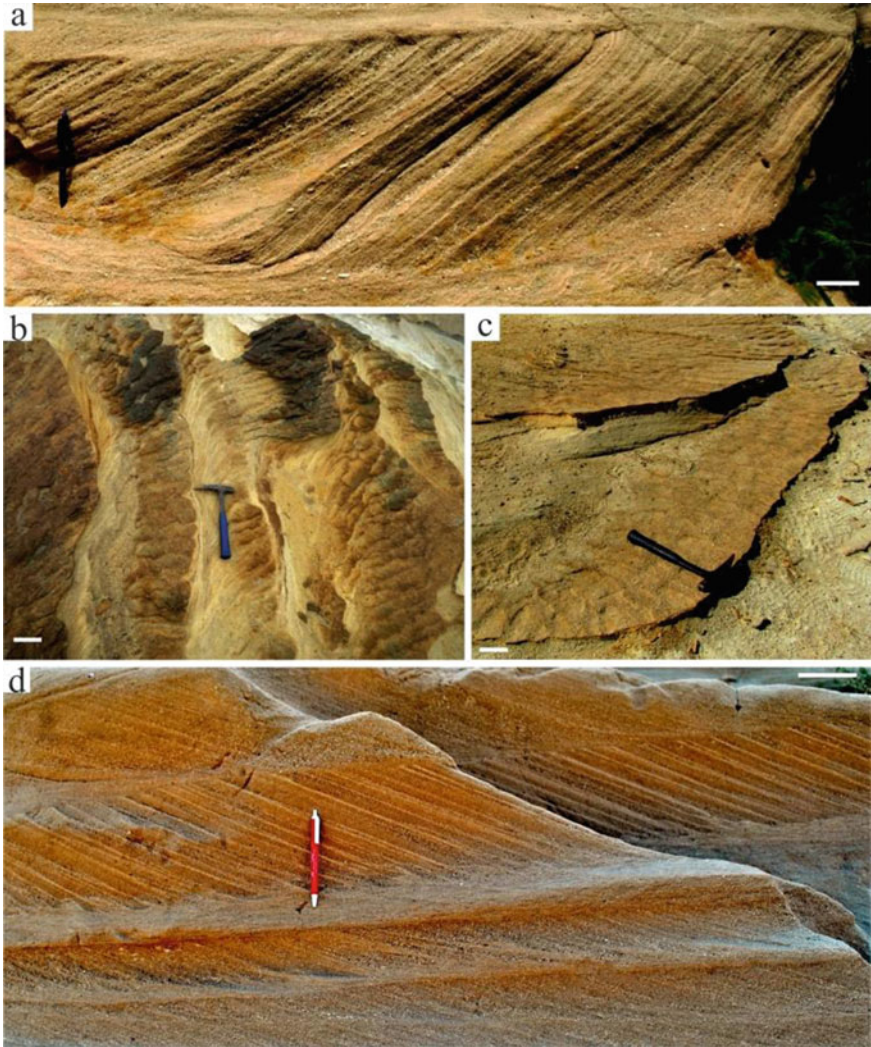
Fig. 13 **a** Medium to large-scale tabular cross-strata showing wedge shaped alternate grainflow grainfall lamina; **b** straight crested ripples; **c** bifurcated ripples; **d** tabular cross strata showing change in climb angle. Note the regular alternations of light-coloured grain-fall, and darker colored and coarser grain-flow layers (scale bar = 10 cm)

4.3.7 Medium to Large-Scale Trough Cross-Stratified Facies, IIIG

This facies is the coarsest sandstone facies in the Association III and internally characterized by medium to large-scale trough cross-sets, arranged in subcritical climb fashion (Fig. 14a). The preserved thickness of individual cross-sets varies from 15 to 40 cm. They climb one above another, understandably formed composite bedforms

of great height that is now indeterminable (Fig. 14b). Every cross-set is essentially characterized by alternate light-coloured and finer-grained at the base and dark-coloured and distinctly coarser-grained at top. Each of the foresets is overall inversely graded as the contact between these two layers within a foreset is gradational. The light-coloured layers, at places, display discernible normal grading, while the darker layers within themselves display inverse grading. The coarse reddish-brown layers are distinctly downslope wedging and in many cases, do not reach toe of the bedforms.

Interpretations

The normal grading within the distinctly finer grain fraction of the light-coloured layers indicates grain-fall from the suspension cloud; comparatively coarser grains within the cloud settled first. On the other hand, the inverse grading within the upper coarser and reddish-brown layers suggests grain-flow. Kinetic sieving in dry sand allowed the comparatively finer fraction of grains to move downward through the space between the jostling coarser grains, and that result into the inverse grading within the grain-flows (Middleton and Hampton 1976; Middleton 1976). The reddish color of the coarser layers possibly developed because of lichen growth. The trough cross-strata were presumably generated by movement of curve-crested dunes and their climbs indicate that the rate of sand supply exceeded the rate of sand transport along the depositional substratum (Hunter 1973, 1977; Rubin and Hunter 1982; Kocurek and Feilder 1982; Sarkar et al. 2012). A very dry paleoenvironmental setting is implied.

In some examples, concave-up foresets pass upward into planar strata to depict overall increase in flow velocity through time (Fig. 15). In the mid-way of this transition, brink point appears below the bedform crest and then moves up obliquely, distancing itself more and more from the bedform crest and reducing in amplitude in the course of event. The cross-strata turn convex-up and eventually pass gradually into planar strata. The brink point arises where the sand-driving flow detaches itself from the bedform surface. Migration of brink point down the bedform lee, as depicted
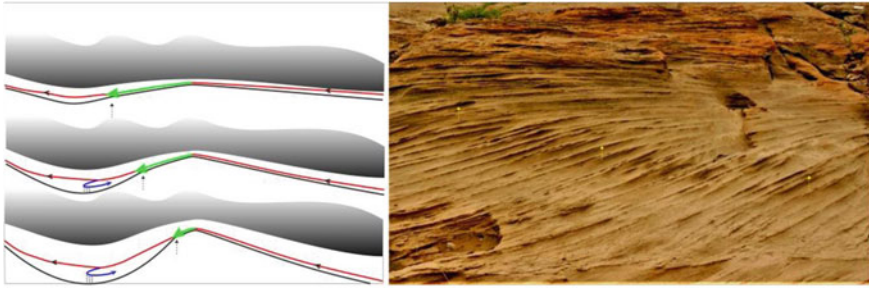
Fig. 15 Gradual disappearance of stationary asymmetric bedform under gradually descending suspension cloud. Note gradual lengthening of the tangential flow (red arrow, in the series of sketches 1–3), shortening of detached flow (green arrow), downstepping of the brink point (dashed arrow), suspension load settling from backflow at toe of the bedform and gradual burial of the bedform (scale bar = 10 cm)

in the example, indicates that the flow remained tangential, without detaching itself from the bedform surface, over an increasingly greater part of the bedform-lee. It would mean the suppression of turbulence (Lowe 1988). The turbulence in the flow can be suppressed by a suspension cloud overhanging close to the bedform crest (Kreisa and Moiola 1986; Bose et al. 1997). That would probably mean the onset of a storm. Obliquely forward movement of the brink point and decrease in its amplitude suggests that the suspension cloud became denser and descended gradually downward. Gradual picking up of the storm is a possible implication. Eventually, the brink point disappeared altogether and cross-strata turned broadly convex-up, implying that the flow did not detach at all. The rate of suspension fall-out increasing towards the bedform-toe, each of the convex-up laminae thickened toe-ward and consequently turned planar and the bedform eventually got completely buried.

5 Aeolian Facies Tract

This section focuses upon five selected transects that cover the entire preserved thickness of the UT and straddle across the contact between the fluvial part to the aeolian part overlying it. The fence diagram (Fig. 16), reconstructed on the basis of regional correlation of aeolian succession of all the five studied sections, where the features are well exposed in the eastern part of Bhuj Formation. The Aeolian facies recorded thereby depicts an overall drying-up trend. At the very base of the aeolian succession, the desiccated mud drapes indicate intermittent, perhaps seasonal wetting. This is followed by adhesion laminae that indicate the deposition within groundwater capillary zone. Successively detached sediment-starved ripples infer sediment input less than sediment output. Iron encrusted omission surface supports the contention with sediment bypass or wind diversion. Further upward, the appearance of continuous

Fig. 16 Fence diagram depicting lateral and vertical variations in aeolian facies tract resting on fluvial deposit in the UT. The numbers refer to the locations marked in Fig. 1
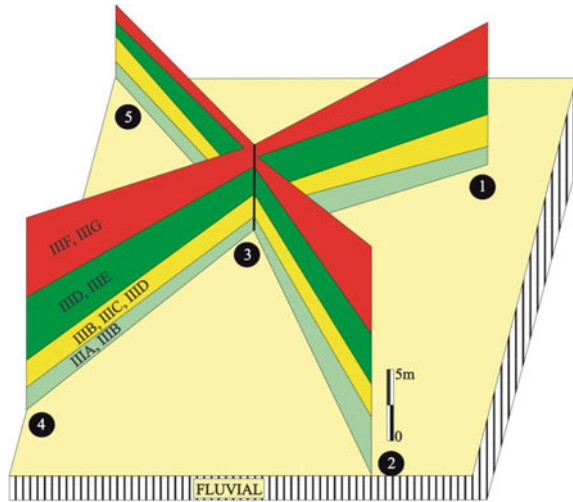
ripple trains bespeaks sediment input almost equal to sediment output. In consequence presence of translatent strata as well as small-scale cross-strata can be correlated to the sediment input slightly higher than the sediment output. Finally, the bedform culminating into climbing dune with alternate grainflow-grainfall cross-strata of larger bedform origin, either tabular or trough, that in turn, reflects the strong wind activity induced by pronounced drying-up scenario. Aggradation of aeolian sediments needs a positive sedimentation budget. Common evidence of bedform climb corroborates this contention. The river system of the past might have dried up because of the increase in the rigor of the paleoclimate or shifted away because of tectonic uplift. Both processes can manipulate the position of the groundwater table in favour of drying-up.

6 Causal Factor

Graphic depiction (Fig. 17) of the paleohydraulic parameters recorded in Table 1 indicates overall narrowing and shallowing of the channels through time, through the four vertically juxtaposed river systems, with least regard to the variations in their channel geometry. Shallowing of river channels through time is readily attributable to silting up, but simultaneous narrowing would require a decline in discharge rate, as is, indeed, also depicted. Secular reduction in bankfull width and depth further corroborates the contention that the whole fluvial system dwindled through time. Their respective bankfull area and discharge areas reduced in consequence. The reason could be climatic or tectonic or both. Both can induce downward migration of the water table of the river systems. The upward transition from initial braided to the meandering system was apparently accompanied by an increase in slope. It is not
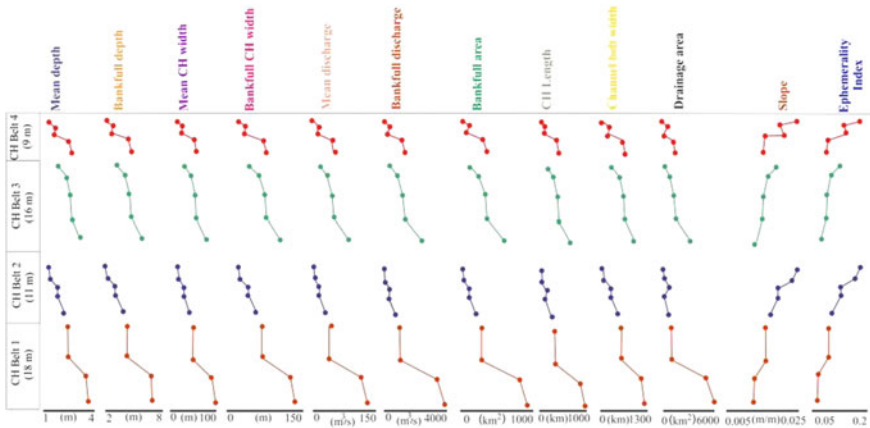
Fig. 17 Graphical representation of secular changes in paleohydraulic parameters in the fluvial part of the UT. Note the overall trend of upward decline in the parameters except last two

only mechanistically justified (Miall 2006), but also justifies drastic shortening of channel length and consequential reduction in all aspects related to water discharge. Further, the slope change tilts the balance in favors of tectonism than of paleoclimate as the ultimate cause for the secular changes in paleohydraulic parameters in the UT. Anyway, whatever the ultimate cause, the channel belt thicknesses are directly related to the position of the river base profile with respect to the river beds. The successive braided channel belts, leaving out the meandering belt, reduce in thickness upward. A progressive reduction in the vertical distance between the river bed and the base profile above it or, in other words, the accommodation space, is implied. The implied shallowing of river valleys suggests overall aggradation (Postma 1995). The secular enhancement in the calculated degree of ephemerality of the rivers is in sync with this aggradation and appears as a prelude to establishment of the aeolian regime. If indeed, the tectonic factor manipulated the observed upward transition from fluvial to aeolian drying-up setting, one would expect tell-tale deformation features. The potential examples we came across are presented below for readers' perusal:

In places the lower bed is thoroughly homogenized sandstone studded with clasts of maximum length around, while the upper laminated bed is plastically deformed but not penetrated. The contact between these two beds is strongly sheared. It appears that the source of the deformative force had originated subsurface, but that could not penetrate the shear plane. No doubt, the force could be seismic. Deformation pockets are separated by laminated sandstone. The deformation bears evidence of simultaneous liquefaction and fluidization. While the degree of deformation is intricate within the deformation pockets, the intervening layer is only upheaved and lack evidence of internal deformation. Evidently, the deformation took place repeatedly under the surface as it happens in case of seismic aftershocks. Well-sorted sandstone of massive grainfall alternates with thin and coarser grainflow layers, and a mild

Table 1 Paleohydraulic parameters in the measured fluvial tract from the base of the UT to the base of the Aeolian section

Channel belt nos.	Successive channel (CH) thickness (m)	Avg cross-set thick-ness h (m)	Mean CH depth d_m (m)	Mean CH width W_m (m)	Mean discharge Q_m (m³/s)	Bankfull CH width W_b (m)	Bankfull CH depth d_b (m)	Width/depth F	Slope S (m/m)	Bankfull area A_b (m²)	Bankfull CH discharge Q_b (m³/s)	Drainage area A_d (km²)	Principal CH length L (km)	Mean CH belt width, cb_w (m)	Ephimera-lity index, EI
CB 4 (9 m)	0.5 (n = 32)	0.14	1.46	17.70	7.07	25.27	2.10	12.12	0.019	53.02	161.43	864.2	80.93	322.67	0.18
	0.9 (n = 28)	0.18	1.86	27.48	14.69	38.60	2.83	14.77	0.015	109.41	362.33	2532.9	154.27	449.36	0.14
	0.8 (n = 28)	0.17	1.81	26.16	13.53	36.81	2.74	14.45	0.015	100.87	330.93	2245.1	143.51	432.98	0.14
	1.4 (n = 28)	0.28	2.68	53.52	44.41	73.34	4.47	19.95	0.010	327.86	1233.38	12916.9	410.04	742.20	0.09
	1.6 (n = 36)	0.29	2.81	58.04	50.81	79.29	4.72	20.69	0.010	374.65	1431.43	15746.2	461.78	788.89	0.09
CB 3 (16 m)	1.2 (n = 28)	0.20	2.04	32.64	19.54	45.56	3.19	15.96	0.014	145.23	497.04	3856.6	198.54	511.49	0.12
	2.3 (n = 24)	0.26	2.49	46.81	35.56	64.47	4.08	18.78	0.011	262.99	964.34	9311.6	336.93	671.03	0.10
	2.8 (n = 28)	0.29	2.74	55.71	47.46	76.22	4.59	20.31	0.010	350.19	1327.52	14244.4	434.83	764.90	0.09
	2.5 (n = 32)	0.30	2.82	58.50	51.48	79.90	4.75	20.76	0.010	379.56	1452.37	16053.3	467.16	793.59	0.09
	3.4 (n = 36)	0.36	3.31	78.49	83.85	106.03	5.81	23.70	0.008	615.80	2492.55	32925.9	718.87	990.12	0.07

(continued)

Table 1 (continued)

Channel belt nos.	Successive channel (CH) thickness (m)	Avg cross-set thick-ness h (m)	Mean CH depth d_m (m)	Mean CH width W_m (m)	Mean discharge Q_m (m³/s)	Bankfull CH width W_b (m)	Bankfull CH depth d_b (m)	Width/depth F	Slope S (m/m)	Bankfull area A_b (m²)	Bankfull CH discharge Q_b (m³/s)	Drainage area A_d (km²)	Principal CH length L (km)	Mean CH belt width, cb_w (m)	Ephemera-lity index, EI
CB 2 (11 m)	1.3 (n = 64)	0.13	1.46	17.57	6.99	25.10	2.09	12.08	0.019	52.40	159.34	849.3	80.09	320.95	0.18
	1.1 (n = 32)	0.15	1.57	20.26	8.86	28.79	2.30	12.88	0.018	66.27	207.04	1203.3	98.71	357.30	0.16
	0.9 (n = 32)	0.20	2.00	31.36	18.29	43.84	3.10	15.68	0.014	136.01	461.96	3498.8	187.27	496.38	0.13
	2.2 (n = 56)	0.20	1.99	31.06	18.00	43.43	3.08	15.61	0.014	133.84	453.73	3416.2	184.61	492.74	0.13
	1.5 (n = 32)	0.25	2.41	43.97	32.04	60.69	3.91	18.26	0.012	237.20	859.41	7988.8	307.34	640.10	0.10
CB 1 (18 m)	3.8 (n = 64)	0.27	2.60	50.55	40.39	69.42	4.30	19.44	0.011	298.42	1110.43	11233.1	377.08	710.95	0.10
	2.2 (n = 36)	0.27	2.62	51.09	41.11	70.13	4.33	19.53	0.011	303.70	1132.39	11529.6	383.02	716.68	0.09
	3 (n = 52)	0.4	3.64	93.19	111.52	125.10	6.53	25.61	0.008	817.06	3417.60	50101.3	924.78	1126.78	0.07
	5 (n = 68)	0.42	3.79	100.31	126.00	134.29	6.87	26.47	0.007	922.29	3912.40	59972.2	1030.14	1190.95	0.06

deformation is restricted to the latter. Evidently, the grainflow layers were comparatively more cohesive, despite being coarser, presumably because of lichen growth (Oostra 2006). It is apparent that the deformation was induced by pore fluid pressure readjustment and seismicity is not the only mechanism to induce such deformation. Even rainfall can induce such or more pronounced slump. In places, the interdune deposit is overlain by a tabular cross-stratified dune deposit and the deformation gradually die out downward from the contact between them. The asymmetric fold at the bed contact turns downward merely into a kink that tightens up before disappearing into broad undulation. This deformation can perhaps be explained by Horowitz's (1982) model for deformation created by overloading created by an advancing dune.

It is apparent that more dedicated research is needed for identifying the principal factor controlling the groundwater table at the penultimate stage of development of the Bhuj Formation. Perhaps a thorough inventory of paleosol properties, physical and chemical, within both the fluvial and aeolian parts of the UT would be beneficial in this regard. A more thorough study of the stratigraphic layout of the UT and of the penecontemporaneous deformation structures therein may yield high dividend.

7 Conclusions

The early Cretaceous Upper Terrestrial Member of the Bhuj Formation in the Kutch Mainland basin evolved, at last, into an aeolian section that evaded recognition for so long. Even though the initial fluvial channel system changed through time in pattern and in paleohydraulic parameters, the overall stratigraphic trend had been drying-up. The same trend was maintained in the evolution of the aeolian part: dominance of facies belonging to the interdune area give way upward to the dominance of dune facies of varied kinds. The implied downward migration of the groundwater table might have been induced by increasing rigor of paleoclimate or tectonic upheaval or both: the paleohydraulic parameters and the penecontemporaneous deformation structures encountered within the aeolian section remain non-committal about the matter.

References

Ahlbrandt TS, Fryberger SG (1981) Sedimentary features and significance of interdune deposits, vol 31. SEPM Special Publication, pp 293–314

Alexander J, Fielding CR (2006) Coarse-grained floodplain deposits in the seasonal tropics: towards a better facies model. J Sed Res 76:539–556

Allen JRL (1963) The classification of cross-stratified units with notes on their origin. Sedimentology 2:93–114

Allen JRL (1968) Current ripples. North-Holland Publishing Co, Amsterdam

Allen JRL (1971) Instantaneous sediment deposition rates deduced from climbing-ripple cross-lamination. J Geol Soc 127:553–561

Allen JRL (1973) A classification of climbing-ripple cross-lamination. J Geol Soc 129:537–541

Allen JRL (1983a) River bedforms: progress and problems. In: Collinson JD, Lewin J (eds) Modern and ancient fluvial systems. IAS Spec Pub 6:19–33

Allen JRL (1983b) Studies in fluviatile sedimentation: Bar, bar complexes and sandstone sheets (low-sinuosity braided streams) in the Brownstones (L. Devonian), Welsh Borders. Sediment Geol 33:237–293

Allen JRL (1984) Sedimentary structures: their character and physical basis. Developments in sedimentology, Elsevier, Amsterdam

Anderson RS (1988) The pattern of grainfall deposition in the lee of aeolian dunes. Sedimentology 35:175–188

Anderson RS (1990) Eolian ripples as examples of self-organization in geomorphological systems. Earth Sci Rev 29:77–96

Arnott RWC (2007) Stratal architecture and origin of lateral accretion deposits (LADs) and conterminuous inner-bank levee deposits in a base-of-slope sinuous channel, lower Isaac Formation (Neoproterozoic), East-Central British Columbia, Canada. Mar Pet Geol 24:515–528

Arora A, Banerjee S, Dutta S (2015) Black shale in late Jurassic Jhuran Formation of Kutch: possible indicator of oceanic anoxic event? J Geol Soc India 85:265–278

Arora A, Dutta S, Gogoi B, Banerjee S (2017) The effects of igneous dike intrusion on organic geochemistry of black shale and its implications: Late Jurassic Jhuran Formation, India. Int J Coal Geol 178:84–99

Bansal U, Banerjee S, Pande K, Arora A, Meena SS (2017) The distinctive compositional evolution of glauconite in the Cretaceous Ukra Hill Member (Kutch basin, India) and its implications. Mar Pet Geol 82:97–117

Best JL, Andashworth PJ (1997) Scour in large braided rivers and the recognition of sequence stratigraphic boundaries. Nature 387:275–277

Best JL, Ashworth PJ, Bristow CS, Roden J (2003) Three-dimensional sedimentary architecture of a large, mid-channel sand braid bar, Jamuna River, Bangladesh. J Sed Res 73:516–530

Biswas SK (1977) Mesozoic rock-stratigraphy of Kutch, Gujrat. Quart J Geol Min Met Soc India 49:1–2

Biswas SK (1981) Basin framework, palaeo-environment and depositional history of the Mesozoic sediments of Kutch, Western India. Quart J Geol Min Met Soc India 53:56–85

Biswas SK (1982) Rift basins in western margin of India and their hydrocarbon prospects with special reference to Kutch basin. AAPG Bull 66:1497–1513

Biswas SK (1983) Cretaceous of Kutch-Kathiawar region. In: Proceedings of symposium Cretaceous of India palaeoecology, palaeogeography and time boundaries. Indian Ass Palynostrat, pp 40–65

Biswas SK (1987) Regional tectonic framework, structure and evolution of the western marginal basins of India. Tectonophys 135:307–327

Biswas SK (1991) Stratigraphy and sedimentary evolution of the Mesozoic basin of Kutch, western India. In: Tandon SK (ed) Stratigraphy and sedimentary evolution of western India, pp 54–103

Biswas SK (2005) A review of structure and tectonics of Kutch basin, western India, with special reference to earthquakes. Curr Sci 88:1592–1600

Biswas SK (2016a) Tectonic framework, structure and tectonic evolution of Kutch Basin, western India, vol 6. Geological Soceity of India Special Publication, pp 129–150

Biswas SK (2016b) Mesozoic and Tertiary stratigraphy of Kutch* (Kachchh): a review, vol 6. Geological Soceity of India Special Publication, pp 1–24

Blodgett RH, Stanley KO (1980) Stratification, bedforms, and discharge relations of the Platte braided river system, Nebraska. J Sed Res 50:139–148

Bose PK, Chakraborty PP (1994) Marine to fluvial transition: Proterozoic Upper Rewa Sandstone, Maihar, India. Sediment Geol 89:285–302

Bose PK, Mazumder RK, Sarkar S (1997) Tidal sandwaves and related storm deposit in the transgressive Proto-Proterozoic Chaibasa Formation, India. Precam Res 84:63–81

Bose PK, Sarkar S, Mukhopadhyay S, Saha B, Eriksson P (2008) Precambrian basin margin fan deposits: Mesoproterozoic Bagalkot Group, India. Precam Res 162:264–283

Bridge JS (1993) The interaction between channel geometry, water flow, sediment transport and deposition in braided rivers. In: Best JL, Bristow CS (eds) Braided rivers. Geol Soc London Spec Pub 75:13–71

Bridge JS, Mackey SD (1993a) A theoretical study of fluvial sandstone body dimensions. In: Flint SS, Bryant ID (eds) Geological modelling of hydrocarbon reservoirs, vol 15. IAS IAS Special Publications, pp 213–236

Bridge JS, Mackey SD (1993b) A revised alluvial stratigraphy model. In: Marzo M, Puigdefabregas C (eds) Alluvial sedimentation, vol 17. IAS Special Publications, pp 319–336

Bridge JS (1997) Thickness of sets of cross strata and planar strata as a function of formative bed-wave geometrical migration. Geology 25:971–974

Bridge JS, Tye RS (2000) Interpreting the dimensions of ancient fluvial channel bars, channels, and channel belts from wireline-logs and cores. AAPG Bull 84:1205–1228

Bridge JS (2003) Rivers and floodplains: forms, processes and sedimentary records. Blackwell Science, Oxford

Bridge JS (2006) Fluvial facies models. In: Posamentier H, Walker RG (eds) Facies models revisited, vol 84. SEPM Special Publications, pp 85–170

Brierley GJ, Ferguson RJ, Woolfe KJ (1997) What is a fluvial levee? Sediment Geol 114:1–9

Bristow CS, Skelly RL, Ethridge FG (1999) Crevasse splays from the rapidly aggrading, sand-bed, braided Niobrara River, Nebraska: effect of base-level rise. Sedimentology 46:1029–1048

Cant DJ, Walker RG (1978) Fluvial processes and facies sequences in the sandy braided South Saskatchewan River, Canada. Sedimentology 25:625–648

Casshyap SM, Dev P, Tewari RC, Raghuvanshi AKS (1983) Ichnofossils from Bhuj Formation (Cretaceous) as palaeoenvironmental parameters. Curr Sci 52:73–74

Chakraborty T, Chaudhuri AK (1993) Fluvial-aeolian interactions in a Proterozoic alluvial plain: example from the Mancheral Quartzite, Sullavai Group, Pranhita-Godavari Valley, India. Geol Soc London Spec Pub 72:127–141

Chakraborty N, Sarkar S, Mandal A, Mejiama W, Tawfik HA, Nagendra R, Bose PK, Eriksson PG (2017) Physico-Chemical characteristics of the Barremian-Aptian siliciclastic rocks in the Pondicherry embryonic rift sub-basin, India. In: Mazumder R (ed) Sediment provenance: influences on compositional change from source to sink. Elsevier, pp 85–121

Chaudhuri A, Banerjee S, Le Pera E (2018) Petrography of Middle Jurassic to Early Cretaceous sandstones in the Kutch Basin, western India: implications on provenance and basin evolution. J Palaeogeogr 7:2–14

Chaudhuri A, Banerjee S, Chauhan G (2020a) Compositional evolution of siliciclastic sediments recording the tectonic stability of a pericratonic rift: Mesozoic Kutch Basin, western India. Mar Petrol Geol 111:476–495

Chaudhuri A, Das K, Banerjee S, Fitzsimons ICW (2020b) Detrital zircon and monazite track the source of Mesozoic sediments in Kutch to rocks of Late Neoproterozoic and Early Palaeozoic orogenies in northern India. Gond Res 80:188–201

Chaudhuri A, Chatterjee A, Banerjee S, Ray JS (2020c) Tracing multiple sources of sediments using trace element and Nd isotope geochemistry: provenance of the Mesozoic succession in the Kutch Basin, western India. Geol Mag. https://doi.org/10.1017/S0016756820000539

Chaudhuri A, Banerjee S, Prabhakar N, Das A (2020d) The use of heavy mineral chemistry in reconstructing provenance: a case study from Mesozoic sandstones of Kutch Basin (India). Geol J. https://doi.org/10.1002/gj.3922

Clemmensen LB, Olsen H, Blakey RC (1989) Erg-margin deposits in the Lower Jurassic Moenave Formation and Wingate Sandstone, southern Utah. GSA Bull 101:759–773

Collinson JD, Thompson DB (1989) Sedimentary structures, 2nd edn. Unwin-Hyman, London

Cooper W (1958) Coastal sand dunes of Oregon and Washington. GSA Mem 72:1–169

Currie BS, Colombi CE, Tabor NJ, Shipman TC, Montañez IP (2009) Stratigraphy and architecture of the Upper Triassic Ischigualasto Formation, Ischigualasto Provincial Park, San Juan, Argentina. J South Am Earth Sci 27:74–87

Durkin PR, Hnbbard SM, Boyd RL, Leckie DA (2015) Stratigraphic expression of Intra-Point-Bar erosion and rotation. J Sed Res 85:1238–1257

Eriksson PG, Bumby AJ, Brümer JJ, Van der Neut M (2006) Precambrian fluvial deposits: enigmatic palaeohydrological data from the c. 2–1.9 Ga Waterberg Group, South Africa. Sediment Geol 190:25–46

Ethridge FG, Germanoski D, Schumm SA, Wood LJ (2005) The morphological and stratigraphical effects of base-level change; a review of experimental studies, vol 35. IAS Special Publications, pp 213–243

Fryberger SG, Ahlbrandt TS, Andrews S (1979) Origin, sedimentary features of low-angle eolian 'sand sheet' deposits, Great Sand Dunes National Monument and vicinity, Colorado. J Sed Pet 49:733–746

Fryberger SG, Al-Sari AM, Clisham TJ (1983) Eolian dune, interdune, sand sheet, and siliciclastic sabkha sediments of an offshore prograding sand sea, Dhahran area, Saudi Arabia. AAPG Bull 67:280–312

Friend PF, Slater MJ, Williams RC (1979) Vertical and lateral building of river sandstone bodies, Ebro Basin, Spain. J Geol Soc 136:39–46

Friend PF (1983) Towards the field classification of alluvial architecture or sequence. In: Collinson J, Lewis J (eds) Modern and ancient fluvial systems, vol 6. IAS Special Publications, pp 345–354

Ghosh P, Sarkar S, Maulik P (2006) Sedimentology of a muddy alluvial deposit: Triassic Denwa Formation, India. Sediment Geol 191:3–36

Gray JMNT (2018) Particle segregation in dense granular flows. Ann Rev Fluid Mech 50:407–433

Harms JC, Southard JB, Spearing DR, Walker RG (1975) Depositional environments as interpreted from primary sedimentary structures and stratification sequences, vol 2. Dallas. SEPM Short Course

Harms JC, Southard JB, Walker RG (1982) Structures and sequences in clastic rocks, vol 9. SEPM Short Course

Haszeldine R (1983a) Fluvial bars reconstructed from a deep, straight channel, Upper Carboniferous coalfield of northeast England. J Sed Pet 53:1233–1247

Haszeldine RS (1983b) Descending tabular cross-bed sets and bounding surfaces from a fluvial channel in the Upper Carboniferous coalfield of north-east England. In: Collinson JD, Lewin J (eds) Modern and ancient fluvial systems. IAS Spec Pub 6:449–456

Horowitz DH (1982) Geometry and origin of large-scale deformation structures in some ancient wind-blown sand deposits. Sedimentology 2:155–180

Howard JD, Singh IB (1985) Trace fossils in the Mesozoic sediments of Kachchh, western India. Palaeo Palaeo Palaeo 52:99–121

Hunter RE (1973) Pseudo-cross lamination formed by climbing adhesion ripples. J Sed Pet 43:1125–1127

Hunter RE (1977) Basic types of stratification in small eolian dunes. Sedimentology 24:429–454

Hunter RE (1980) Quasi-planar adhesion stratification-an eolian structure formed in wet sand. J Sed Pet 50:263–266

Ito M, Matsukawa M, Saito T, Nichols DL (2006) Facies architecture and palaeohydrology of a synrift succession in the Early Cretaceous Choyr Basin, southeastern Mongolia. Cret Res 27:226–240

Jackson RG (1976) Depositional model of point bars in the lower Wabash River. J Sed Res 46:579–594

Jopling AV, Walker RG (1968) Morphology and origin of ripple drift cross-lamination, with examples from the Pleistocene of Massachusetts. J Sed Pet 38:971–984

Kocurek G (1981) Significance of interdune deposits and bounding surfaces in eolian dune sands. Sedimentology 28:753–780

Kocurek G, Feilder G (1982) Adhesion structures. J Sed Pet 52:1229–1241

Kocurek G, Nielson J (1986) Conditions favourable for the formation of warm-climate aeolian sand sheets. Sedimentology 33:795–816

Kocurek G, Townsley M, Yeh E, Havholm KG, Sweet ML (1992) Dune and dune-field development on Padre Island, Texas, with implications for interdune deposition and water-table-controlled accumulation. J Sed Res 62:622–635

Kleinhans MG (2004) Sorting in grain flows at the lee side of dunes. Earth-Sci Rev 65:75–102

Kreisa RD, Moiola RJ (1986) Sigmoidal tidal bundles and other tide-generated sedimentary structures of the Curtis Formation, Utah. GSA Bull 97:381–387

Krishna J, Singh IB, Howard JD, Jafar SA (1983) Implications of New data on the Mesozoic rocks of Kachchh, Western India. Nature 305:790–792

Labourdette R, Jones RR (2007) Characterization of fluvial architectural elements using a three-dimensional outcrop dataset: Escanilla braided system, South-Central Pyrenees, Spain. Geosphere 3:422–434

Langford RP, Chan MA (1989) Fluvial-aeolian interactions: part II, ancient systems. Sedimentology 36:1037–1051

Long DGF (2006) Architecture of pre-vegetation sandy-braided perennial and ephemeral river deposits in the Paleoproterozoic Athabasca Group, northern Saskatchewan, Canada as indicators of Precambrian fluvial style. Sediment Geol 190:71–95

Long DGF (2011) Architecture and depositional style of fluvial systems before land plants: a comparison of Precambrian, early Paleozoic and modern river deposits. From river to rock record: the preservation of fluvial sediments and their subsequent interpretation. SEPM Spec Pub 97:37–61

Leclair SF, Bridge JS, Wang F (1997) Preservation of cross-strata due to migration of subaqueous dunes over aggrading and non-aggrading beds: comparison of experimental data with theory. Geosci Canada 24:55–66

Leeder MR (1978) A quantitative stratigraphic model for alluvium, with special reference to channel deposit density and interconnectedness. In: Miall AD (ed) Fluvial sedimentology. Can Soc Pet Geol Mem 5, pp 587–596

Leopold LB, Wolman GM, Miller JP (1964) Fluvial processes in River Geomorphology. Freeman, San Francisco

Lowe DR (1988) Suspended-load fallout rate as an independent variable in the analysis of current structures. Sedimentology 35:765–776

Mack GH, Leeder M, Perez-Arlucea M, Bailey BDJ (2003) Early Permian silt-bed fluvial sedimentation in the Orogrande basin of the Ancestral Rocky Mountains, New Mexico, USA. Sed Geol 160:159–1781

Mandal A, Koner A, Sarkar S, Tawfik HA, Chakraborty N, Bhakta S, Bose PK (2016) Physico-chemical tuning of palaeogeographic shifts: Bhuj Formation, Kutch, India. Mar Pet Geol 78:474–492

Mazumder R, Sarkar S (2004) Sedimentation history of the Palaeoproterozoic Dhanjori Formation, Singhbhum, eastern India. Precam Res 130:267–287

McKee ED, Bigarella JJ (1972) Deformational structures in Brazilian coastal dunes. J Sed Res 42:670–681

Miall AD (1977) Lithofacies types and vertical profile models in braided river deposits: a summary. In: Miall AD (ed) Fluvial sedimentology. Can Soc Pet Geol, pp 597–604

Miall AD (1985) Architectural-element analysis: a new method of facies analysis applied to fluvial deposits. Earth-Sci Rev 22:261–308

Miall AD (1988) Facies architecture in clastic sedimentary basins. In: Kleinspehn K, Paola C (eds) New perspective in basin analysis. Springer, Berlin, Heidelberg, New York, pp 67–81

Miall AD (1996) The geology of fluvial deposits: sedimentary facies, basin analysis and petroleum geology. Springer, Heidelberg

Miall AD, Jones B (2003) Fluvial architecture of the Hawkesbury Sandstone (Triassic), near Sydney, Australia. J Sed Res 73:531–545

Miall AD (2006) The geology of fluvial deposits: sedimentary facies, basin analysis and petroleum geology. Springer, Berlin

Miall AD (2014) The facies and architecture of fluvial systems. In: Fluvial depositional systems. Springer International Publishing, pp 9–68

Middleton GV (1970) Experimental studies related to problems of flysch sedimentation. In: Lajoie J (ed) Flysch sedimentology in North America. Bus Econ Sci Ltd Toronto, pp 253–272

Middleton GV (1976) Hydraulic interpretation of sand size distributions. J Geol 84:405–426

Middleton GV, Hampton MA (1976) subaqueous sediment transport and deposition by sediment gravity flows. In: Stanley DJ, Swift DJP (eds) Marine sediment transport and environmental management, pp 197–218

Mukhopadhyay S, Choudhuri A, Samanta P, Sarkar S, Bose PK (2014) Were the hydraulic parameters of Precambrian rivers different? J Asian Earth Sci 91:289–297

Nanson GC (1986) Episodes of vertical accretion and catastrophic stripping: a model of disequilibrium floodplain development. GSA Bull 97:1467–1475

Nickling WG, Wolfe SA (1994) The morphology and origin of Nabkhas, region of Mopti, Mali, West Africa. J Arid Env 28:13–30

Olsen H (1988) The architecture of a sandy braided-meandering river system: an example from the Lower Triassic Soiling Formation (M. Buntsandstein) in W-Germany. Geol Runds 77:797–814

Olsen H (1989) Sandstone-body structures and ephemeral stream processes in the Dinosaur Canyon Member, Moenave Formation (Lower Jurassic), Utah, USA. Sediment Geol 61:207–221

Oostra HGM (2006) Lichen rich coastal and inland sand dunes (corynephorion) in the Netherlands: vegetation dynamics and nature management. PhD Thesis, Wageningen University and Research Centre

Osterkamp WR, Hedman ER (1982) Perennial stream flow characteristics related to channel geometry and sediment in the Missouri River Basin. USGS Prof Pap 1242:1–37

Posamentier HW (2003) Depositional elements associated with a basin floor channel-levee system: case study from the Gulf of Mexico. Mar Pet Geol 20:677–690

Postma G (1995) Sea-level-related architectural trends in coarse-grained delta complexes. Sediment Geol 98:3–12

Puigdefábregas C (1973) Miocene point-bar deposits in the Ebro Basin, northern Spain. Sedimentology 20:133–144

Pulvertaft TCR (1985) Aeolian dune and wet interdune sedimentation in the Middle Proterozoic Dala Sandstone, Sweden. Sediment Geol 44:93–111

Rădoane M, Rădoane N, Dumitriu D, Miclăuş C (2008) Downstream variation in bed sediment size along the East Carpathian Rivers: evidence of the role of sediment sources. Earth Sur Proc Land 33:674–694

Rai J (2006) Discovery of nannofossils in a plant bed of the Bhuj Member, Kutch and its significance. Curr Sci 91:519–526

Reading HG (1996) Sedimentary environments: processes, facies and stratigraphy. Blackwell Science, Oxford

Rubin DM, Hunter RR (1982) Bedform climbing in theory and in nature. Sedimentology 21:121–138

Rust BR (1972) Structure and process in a braided river. Sedimentology 18:221–245

Salter T (1993) Fluvial scour and incision: models for their influence on the development of realistic reservoir geometries. In: North CP, Prosser DJ (eds) Characterization of fluvial and aeolian reservoirs, vol 73. Geological Soceity Special Publications, London, pp 33–51

Sambrook Smith GH, Ashworth PJ, Best JL, Lunt IA, Orfeo O, Parsons DR (2009) The sedimentology and alluvial architecture of a large braid bar, Rio Parana, Argentina. J Sed Res 79:629–642

Sarkar S, Samanta P, Mukhopadhyay S, Bose PK (2012) Stratigraphic architecture of the Sonia Fluvial interval, India in its Precambrian context. Precam Res 214:210–226

Schumm SA (1968a) River adjustment to altered hydrologic regimen, Murrumbidgee River and paleochannels, Australia. US Gov Printing Office 598, pp 1–65

Schumm SA (1972) Fluvial palaeochannels. In: Rigby JK, Hamblin WK (eds) Recognition of ancient sedimentary environments. SEPM Spec Pub 16:98–107

Shukla UK, Singh IB (1990) Facies analysis of Bhuj sandstone (Lower cretaceous) Bhuj area, Kachchh. J Palaeontol Soc India 35:189–196

Singh IB, Shukla UK (1991) Significance of trace fossils in the Bhuj sandstone (Lower Cretaceous), Bhujarea, Kachchh. J Palaeontol Soc India 36:121–126

Smith ND (1970) The braided stream depositional environment: comparison of the Platte River with some Silurian clastic rocks, North Central Appalachians. GSA Bull 81:2993–3014

Smith ND (1971) Transverse bars and braiding in the lower Platte River, Nebraska. GSA Bull 82:3407–3420

Smith ND (1972) Some sedimentological aspects of planar cross-stratification in a sandy braided river. J Sed Res 42:624–634

Smith ND, Rogers J (1999) Fluvial sedimentology. Blackwell Science

Smith GHS, Ashworth PJ, Best JL, Woodward J, Simpson CJ (2006) The sedimentology and alluvial architecture of the sandy braided South Saskatchewan River, Canada. Sedimentology 53:413–434

Tabor NJ, Myers TS (2015) Paleosols as indicators of paleoenvironment and paleoclimate. Ann Rev Earth Planet Sci 43:333–361

Todd SP, Went DJ (1991) Lateral migration of sand-bed rivers: examples from the Devonian Glashabeg Formation, SW Ireland and the Cambrian Alderney Sandstone Formation, Channel Islands. Sedimentology 38:997–1020

Walker RG (1963) Distinctive types of ripple-drift cross-lamination. Sedimentology 2:173–188

Walker RG (1969) Geometrical analysis of ripple-drift cross-lamination. J Earth Sci Canada 6:383–391

Williams GP (1978) Bank-full discharge of rivers. Water Resour Res 14:1141–1154

Williams GP (1984) Palaeohydrologic equations for rivers. In: Costa JE, Fleisher PJ (eds) Development and application of geomorphology. Springer, Berlin, pp 343–367

Walling DE, Bradley SB (1989) Rates and patterns of contemporary floodplain sedimentation: a case study of the River Culm, Devon, UK. GeoJournal 19:53–62

Willis BJ (1997) Architecture of fluvial-dominated valley-fill deposits in the Cretaceous Fall River Formation. Sedimentology 44:735–757

Wright VP, Marriott SB (1993) The sequence stratigraphy of fluvial depositional systems: the role of floodplain sediment storage. Sediment Geol 86:203–221

Yu X, Ma X, Quing H (2002) Sedimentology and reservoir characteristics of a Middle Jurassic fluvial system, Datong Basin, Northern China. Canadian Pet Geol Bull 50:105–117

Mineralogical and Textural Characteristics of Red Boles of Western Deccan Volcanic Province, India: Genetic and Paleoenvironmental Implications

Pragya Singh, Emilia Le Pera, Satadru Bhattacharya, Kanchan Pande, and Santanu Banerjee

Abstract This study presents physical, petrographical and mineralogical investigation of interbasaltic red bole within the late Cretaceous Deccan lava flows in Pune and Mahabaleshwar areas (India) to understand depositional and weathering conditions. The micromorphological study of red boles reveals two genetic types characterized by distinct features. The first variety, with general sharp lower and upper contacts, consisting predominantly of altered basaltic fragments and volcanic glasses along with hematite, plagioclase, pyroxene (mainly augite), accessory olivine replaced by iddingsite, zircon, quartz, Fe–Ti opaque phases (ilmenite and magnetite), represents a volcaniclastic bole bed. The second variety of red bole, with gradational lower contact and sharp upper contact, containing basaltic clasts, alteromorphs/iddingsite, abundant zeolite and glaebules in groundmass of homogeneous, red, ferruginous clay, is classified as a volcanic paleosol. They are devoid of olivine and pyroxene, with rare alteromorphs of glass. The clay mineral content of red boles was investigated using XRD and VNIR. The presence of 2.21, 2.24 and 2.29 μm absorption features in reflectance spectra of VNIR spectroscopy indicates a mixture of Al-smectite (montmorillonite) and Fe-smectite as the clay mineral constituents, which is confirmed by the XRD data. The presence of smectite and hematite in both types of red boles suggest their formation under near-neutral pH, poorly-drained and moderate weathering condition. Hematite in the red bole suggests a combination of oxidative weathering and the effect of post-burial diagenesis. The volcaniclastic red boles with partially to unaltered mafic minerals and glass shards possibly indicates limited subaerial/subaqueous alteration under oxic condition. The paleosol type red boles with pedogenic features indicate prolonged sub-aerial weathering of flow top

P. Singh · K. Pande · S. Banerjee (✉)
Department of Earth Sciences, Indian Institute of Technology Bombay, Powai, Mumbai 400076, India
e-mail: santanu@iitb.ac.in

E. Le Pera
Dipartimento di Biologia, Ecologia e Scienze della Terra, Università della Calabria, 87036 Rende, Cosenza, Italy

S. Bhattacharya
Space Applications Centre, Indian Space Research Organization, Ahmedabad 380 015, India

basalt, indicating significant hiatus in Deccan volcanism. Zeolite and other alteration products possibly indicate hydrothermal alteration on red bole.

1 Introduction

The bole beds within Deccan traps are very conspicuous in the field by their distinctive red or green coloration and clay-dominated fabric. The bole beds mark a volcanic quiescence in late Cretaceous Deccan volcanism (Widdowson et al. 1997; Chenet et al. 2008; Srivastava et al. 2012). As colours of the bole beds are variable, some authors name them separately as red, brown and green boles (Widdowson et al. 1997). They also exhibit variable geometry (Walker 1999; Chenet et al. 2008; Srivastava et al. 2012), clay mineralogy and magnetic signatures (based on colour) (Gavin et al. 2011; Srivastava et al. 2012). The origin of the red boles is controversial. In fact, these bole beds are variously considered as (a) products of baking of weathered basalt-derived sediments from overlying flow at ~400–500 °C (Gavin et al. 2010, 2011; Louime et al. 2011; Srivastava et al. 2015), (b) as a state of hydrothermal and deuteric alteration (Singer and Ben-Dor 1987; Gérard et al. 2006; Chenet et al. 2008), (c) a mixing of basaltic derivatives and volcanic ash (Wilkins et al. 1994; Emeleus et al. 1996) (d) reworked weathered sediments (Srivastava et al. 2012), (e) products related to a weathering-limited erosion regime with a short-term pedogenesis (Sayyed and Hundekari 2006), (f) result of groundwater ingression through flow bottom breccia (Duraiswami et al. 2020).

Several authors have highlighted geochemistry (Wilkins et al. 1994; Sayyed and Hundekari 2006; Sayyed at el. 2014), clay mineralogy (Widdowson et al. 1997; Ahmad and Shrivastava 2008) and reflectance spectroscopy (DRS) (Srivastava et al. 2012) for the characterization of the bole beds in Pune and nearby area. However, petrographical characterization of these bole beds has not been attempted even though textural and mineralogical characterization of bole beds could be useful to infer the origin and paleoenvironmental conditions of their formation. The composition of clays and other volcaniclastic particles provide an idea of the degree of alteration of the original minerals and glassy particles under surface/subsurface conditions. In fact, volcanic paleosol is expected to form under humid conditions in case of a prolonged eruption-free interval (Sayyed and Hundekari 2006; Srivastava et al. 2012). Moreover, the model proposed by the bole beds study is significant as the clayey constituents serve as an analogue to explain, for instance, Martian phyllosilicates formation (Gavin et al. 2010; Greenberger et al. 2012; Shukla et al. 2014). In this paper, we have documented physical, petrographical and mineralogical characterization of red boles in Pune and Mahabaleshwar region, India. The objective of this paper is to highlight the texture and mineralogy of red boles to identify any

characteristics that might help to reveal interesting insights into their genesis and paleoenvironmental history.

2 Geological Background

The interbasaltic bole horizon is extensively reported from Pune and Mahabaleshwar sections of the western sub-province of Deccan Volcanic Province (DVP), India (Fig. 1). The Deccan Volcanic Province is one of the larger and better-preserved mafic continental flood basalt provinces of the world, with a present-day areal extent of ~0.5×10^6 km^2 and an estimated original area of at least 1.5×10^6 km^2 (e.g. Sheth 2005; Vaidyanadhan and Ramakrishnan 2008; Valdiya 2016; Kale et al. 2019, 2020; Verma and Khosla 2019; Duraiswami et al. 2020). Based on significant variation in geochemical parameters like major elements, minor and trace elements, their ratios, as well as Sr^{86}/Sr^{87} ratio and REE etc., the Western Deccan volcanic province, has been classified into three major subgroups: Kalsubai (~2000 m), Lonavala (~525 m),
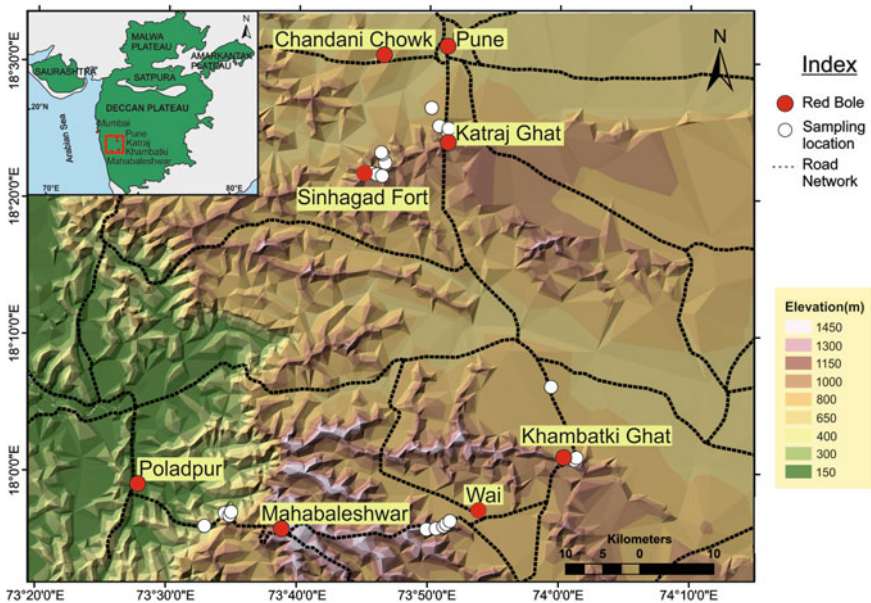
Fig. 1 Outline of the Major geographic sectors and different sub-provinces of the Deccan Volcanic Province (DVP), India (modified after Kale et al. 2020; Sheth et al. 2019). The DVP is divided into four distinct geographical sub-provinces, namely Mandla, Malwa, Central, and Western sub-provinces, which is further subdivided into the Amarkantak, Malwa, Satpura, and Sahyadri groups respectively (sampling locations at Sinhagad Fort, Katraj Ghat, Khambatki Ghat and Wai-Mahabaleshwar-Poladpur section are indicated in Digital Elevation Model using white circles; red circles mark important cities)

Table 1 Chemostratigraphic units of the western parts of the Deccan Volcanic Province (after Subbarao and Hooper 1988). Giant plagioclase basalt (GPB) flows separates different formations

Chemostratigraphy (After Subbarao and Hooper 1988)		
Group	Subgroup	Formation
Deccan trap	Wai	Desur
		Panhala
		Mahabaleshwar
		Ambenali
		Poladpur
	Lonavala	Bushe
		Khandala
	Kalsubai	– Giravali GPB –
		Bhimashankar
		– Manchar GPB –
		Thakurwadi
		– Tunnel 5 GPB –
		Neral
		– Kashele GPB –
		Igatpuri
		– Thalghat GPB –
		Jawhar

and Wai Subgroups (~1100 m) and 12 stratigraphic units (Formations) (Table 1) (Beane et al. 1986; Subbarao and Hooper 1988; Subbarao et al. 1994; Sheth et al. 2019). However, many workers disagree with the chemostratigraphy because of the multi-vent, fissure type eruptive history, fed by magma having diverse contaminants in the form of differing sub-trappean crusts (e.g. Kale et al. 2019, 2020). In this paper, however, we have retained the formation name for describing field occurrence of the red bole beds. The stratigraphy of the samples is presented in the log of Fig. 2.

Red boles are unevenly distributed within the Deccan volcanics. They are relatively abundant in areas dominated by simple lava flow rather than compound lava flows (e.g. Mahabaleshwar section and southeastern Deccan) (Wilkins et al. 1994; Chenet et al. 2008; Vijaya et al. 2010). Numerous occurrences of red boles have been reported from the Wai subgroup, which could be due to highly episodic eruptions in the youngest phase of DVP (Cox and Hawkesworth 1985; Widdowson et al. 1997; Renne et al. 2015). The age of Wai subgroup (i.e. Poladpur, Ambenali and Mahabaleshwar formations) ranges from late Maastrichtian to early Danian (Schoene et al. 2019). This study includes detailed observations of several outcrops near Pune and Mahabaleshwar, including red boles in Sinhagad fort section, Katraj Ghat, Khambatki Ghat (Wai Taluka) and Mahabaleshwar Plateau (Fig. 1, 2).
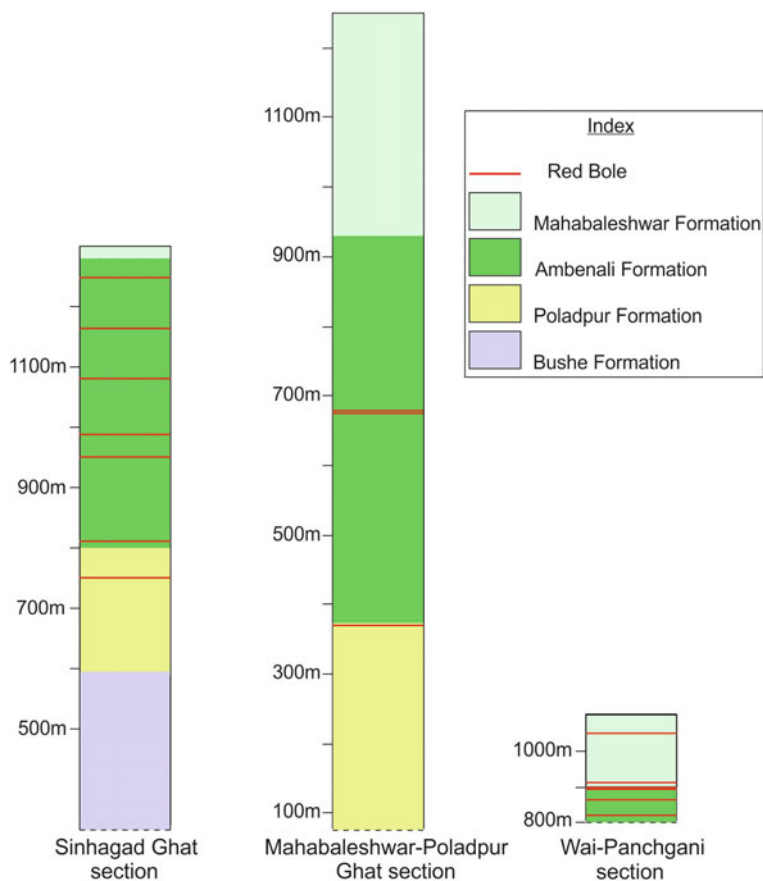
Fig. 2 Log showing stratigraphic height or vertical occurrence of sampled red bole beds at Sinhagad Ghat section, Mahabaleshwar–Poladpur Ghat section and Wai–Panchgani section. The formations are demarcated based on available data (Beane et al. 1986; Schoene et al. 2019; Chenet et al. 2008)

3　Sampling and Methods

The red bole samples for the present study were collected from the following locations in Pune and Mahabaleshwar area.

Sinhagad Fort Section

This ~700 m thick Ghat section is located ~20 km southwest of Pune (Fig. 1). It begins with lower Poladpur Formation and continues up to the base of the Mahabaleshwar Formation, with nicely exposed Ambenali Formation (Schoene et al. 2015, 2019). Six red bole samples were collected along this section (Figs. 3A; 4E, F).

Katraj Ghat

Fig. 3 Field photographs of red bole **A** ~1 m, thick homogeneous indurated red bole (yellow arrow) exposed at Sinhagad Ghat section (Pune); **B** ~40 cm thick fissile, finely laminated red bole overlying clast supported breccia fill type deposit, Khambatki Ghat. The amygdaloidal basaltic clasts lying below red bole are subangular to subrounded and with variable size; **C** Close-up view of red bole of Fig. B; **D** Flow top breccia with red matrix infilling exposed along Wai–Panchgani section; **E** ~27 cm thick orange coloured bole bed with subangular blocky structure exposed on Mahabaleshwar–Poladpur section; **F** Bole bed with an orange tint, overlying highly weathered amygdaloidal basalt, exposed near Poladpur; **G** ~50 cm thick, massive structureless red bole showing sharp contact with upper basalt, lower contact not exposed; **H** ~130 cm thick red bole mixed with basalt (white arrow), unlike other red boles it shows slight inclination (yellow arrow) (Length of hammer = 38 cm)
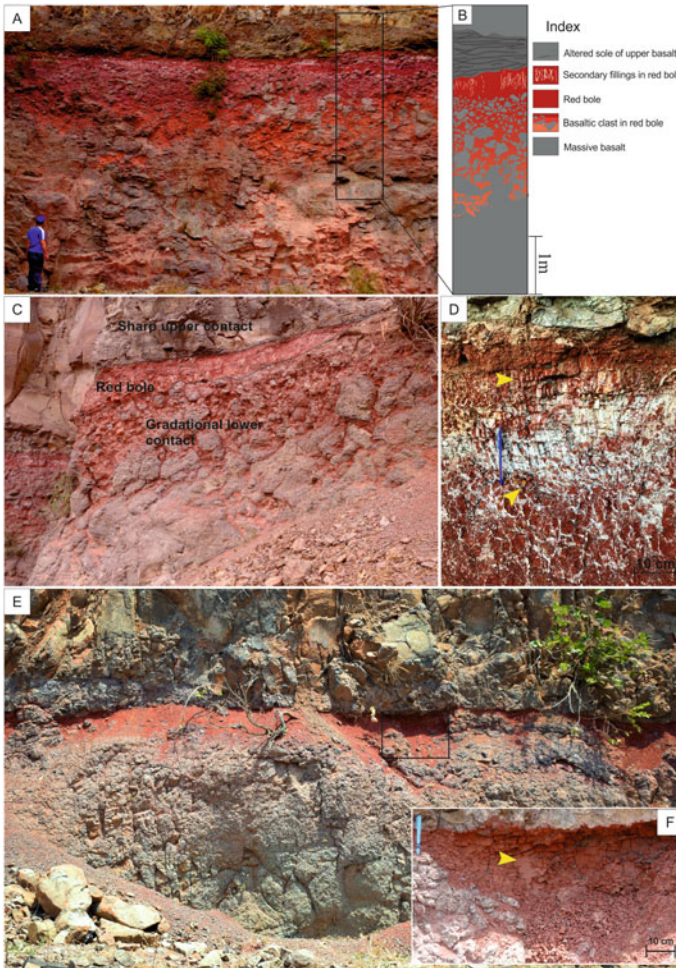
Fig. 4 **A** ~2 m thick prominent red bole having sharp contact with the overlying basalt and gradational contact with underlying weathered amygdaloidal basalt, ~50 cm thick red fragile bole with extensive white secondary filling; **B** Pictorial representation of red boles at the south of Jambhulwadi lake, behind Indian Oil Petrol pump, north of New Katraj Tunnel, Pune; **C** Basaltic clast with red matrix in between, increases in size downward towards lower basalt; **D** Extensive white secondary filling and "pencil" columnar joints (yellow arrow) in red bole of Katraj Ghat section; **E** Red bole at Sinhagad Fort section showing sharp contact with both overlying and underlying basalt. The red bole thickness varies laterally with maximum thickness at local depressions on underlying basalt, indicated by yellow arrow (**F**)

This section crops out south of Pune on state highway 114 (Fig. 1). The base of section marks the boundary between Bushe and Poladpur formations contact, whereas the boundary between Poladpur and Ambenali formations occur at ~700 m elevation (Schoene et al. 2019). Three red bole samples were collected from Katraj Ghat, which includes a prominent red bole to the north of New Katraj Tunnel (Fig. 4A–D).

Khambatki Ghat (Wai Taluka)

This section occurs to the south of Pune on highway NH4 (Surur-Pune road) (Fig. 1). The Poladpur-Ambenali formations transition lies near the base of the Ghat. The contact between Ambenali and Mahabaleshwar formations is located at the top part of the Ghat section (Subbarao et al. 2000; Schoene et al. 2019). Three red boles were collected along this section (Fig. 3B, C).

Mahabaleshwar-Poladpur/Ambenali Ghat section

Mahabaleshwar-Poladpur Ghat section has a thickness of 1200 m, which corresponds to approximately one-third of the total trap thickness (Subbarao et al. 2000). Five red boles with orange tint were collected at different elevations along this section (Fig. 3E, F).

Wai-Panchgani Section

This section is ~300 m thick (Chenet et al. 2008). Samples were collected from five red boles on Wai-Panchgani road between Siddhanath wadi Rural and Dandeghar (Fig. 3D, G, H).

The red bole samples were collected from Pune and Mahabaleshwar areas. Thin sections of red bole samples were prepared with utmost care because of their soft and fragile nature. Each sample was impregnated in resin (1:1 ratio of epoxy and hardener) before cutting and grinding to avoid disintegration. They were kept in the oven overnight at 50 °C for hardening. The hard samples were sliced, ground, and mounted on a glass slide using a mixture of Buehler® Epothin 2 Epoxy resin and Buehler® Epothin 2 Epoxy hardener (2:1 ratio). Thin sections were prepared from the hardened samples by dry grinding and polishing using silicon carbide polishing paper and alumina powder, respectively. A detailed petrographical investigation was carried out using Leica DM 4500P polarizing microscope, and the images were taken using Leica DFC420 camera and Leica Image Analysis software (LAS- v4.6) attached to it at the Department of Earth Sciences, Indian Institute of Technology Bombay. Mineral species of zeolite, plagioclase and pyroxenes were identified by using Electron probe micro analyzer (EPMA) at the Department of Earth Sciences, Indian Institute of Technology Bombay.

Bulk mineralogy of red bole samples was determined by X-ray diffraction with a randomly oriented powder mount, using nickel filter copper radiation at a scan speed of 96 s/step in an Empyrean X-ray Diffractometer with Pixel 3D detector at the Department of Earth Sciences, Indian Institute of Technology Bombay. The powdered samples were scanned from 1° to 70° (step size 0.026° 2θ). For clay-mineral identification, the clay fractions were separated from the bulk sample by centrifugation or decantation and mounted as an oriented aggregate on glass slides. The oriented

clay samples were then scanned from 1° to 30°. These samples were examined under three different modes of scanning, viz., air-dried, after ethylene glycol treatment, and after heating at 400 °C and 550 °C, maintaining the same instrumental settings. Qualitative and semi-quantitative identification of mineral phases were carried out using High-score Plus software.

A FieldSpec®4 Hi-Res spectroradiometer (Analytical Spectral Devices, Boulder, CO, USA) was used for measuring the reflectance of different size fractions of red bole over 0.35–2.5 µm, i.e., visible-near infrared (VNIR) wavelength range of the electromagnetic (EM) spectrum. A contact probe equipped with a high-intensity light source, provided with the Field Spec®4 Hi-Res instrument, was used to collect the spectra in laboratory conditions. The contact probe contains a 100 W halogen reflectorized lamp, with a fibre-optic input socket. An angle of 30° was maintained between the halogen lamp and the fibre-optic input socket for better results (Naveen et al. 2018; Bhattacharya et al. 2016).

4 Results

4.1 Physical Characterization

The red boles are widespread in Pune and Mahabaleshwar areas. The colour of red boles varies in different sampling locations ranging from shades of red, orange to brown colour. The bole may be either massive or bedded, and they exhibit variable geometry, i.e., bedded, lenticular, laterally pinching and lenses. Grain size and the degree of fissility and friability of bole beds are variable. Based on colour, thickness, lateral dimensions, contact relationships and macro-morphology, two types of bole beds are identified.

(a)   Red bole horizon with sharp lower contact

These boles show sharp contact with both underlying and overlying basalt (Fig. 4E). The red bole on breaking shows subrounded-subangular blocky structure, depending on the degree of friability. The thickness of bole bed varies laterally from a few cm to ~30 cm, and the maximum thickness is noted at local depressions on lower amygdaloidal basalt (Fig. 4E, F).

(b)   Red bole horizon with gradational lower contact

This type of red boles lies above flow top breccia. They show gradational contact with the underlying basalt and sharp contact with the overlying basaltic flow. The nature of red bole lying above flow top breccia varies from well-developed red bole to thinly laminated fissile bole. In a few sections, red bole occurring above flow top breccia, exhibit well-developed weathering profiles with decreasing size of basaltic clasts and an increasing effect of alteration from the base to the top (Fig. 4A–C). These

red boles are mostly devoid of sedimentary structures but show poor lamination in places. They exhibit an extensive network of secondary zeolite fillings (Fig. 4A, D) and pencil columnar joints (Fig. 4D). In places, the bole beds occurring above flow top basalt, showing gradational contact with lower basalt, occur as thin laminated, fissile layers. These fissile red boles laterally terminate into breccia fill bed with red matrix in-between (Fig. 3B, C).

4.2 Petrography

Petrographical analysis of the bole beds reveals the presence of altered volcanic lithic fragments and monomineralic grains as phenocrysts set in a groundmass of fine-grained, altered and oxidized fragments, clays and other secondary minerals. The proportion of these constituents vary among the different variety of bole beds. The petrography of the sampled red boles, has been conducted through the examination of thin sections under the polarizing microscope. The most prominent compositional characteristics can be summarized as follows:

(a)   Red bole horizon with dominance of volcaniclastic constituents

The mineralogy and texture classification of the various volcanic lithic grain types of the bole beds samples are all maficlastic (e.g. Critelli et al. 2003) were determined according to the terminology of operational categories used for the volcanic lithic fragments, namely the Lv categories, of Dickinson (1970) that have been developed later by Marsaglia (1992, 1993). According to these categories, the average size of the Lv particles in red boles, ranges from medium sand to coarse silt size with only a few grains ranging from coarse to very coarse sand size. Volcanic lithic fragments in these red boles belong to lathwork (Lvl), microlitic (Lvmi) and vitric (Lvv) types. Volcanic fragments with microlitic texture (Lvmi) contain silt-sized microlites of plagioclase and opaques, set in altered and opaque groundmass (Fig. 5A). Lathwork volcanic fragments (Lvl) include sand-sized partly to completely altered euhedral to subhedral plagioclase, opaque phenocrysts with intersertal brown, black and altered/devitrified glass (Figs. 6A; 7A, B) (e.g. Dickinson 1970). Volcanic vitric fragments (Lvv) mainly occur either as coarse to medium sand size scoria (Fig. 7H) or as very fine to medium sand size glass and glass shards (Figs. 5A, B, G; 6B, D). These fragments are partially to completely altered to clay minerals, iron oxide and opaque products (Fig. 5E). Black (non-vesicular; tachylite) (Fig. 6A), brown (Fig. 6B) (sideromelane), colourless and yellow-orange (palagonite, Pal) glassy particles, with variable vesicularity (Figs. 5A, B, E, G; 6B, D) characterize the red bole. These fragments are devoid of both microlites and sand-sized phenocrystals. Few glass shards show flow-like structure (Fig. 5G). The dominant vitric fragments in the red bole belong to yellow-orange (palagonite) and brown glass types.

Variably altered plagioclase (with labradorite, bytownite and andesine compositions), pyroxene such as augite and olivine are common monomineralic grains
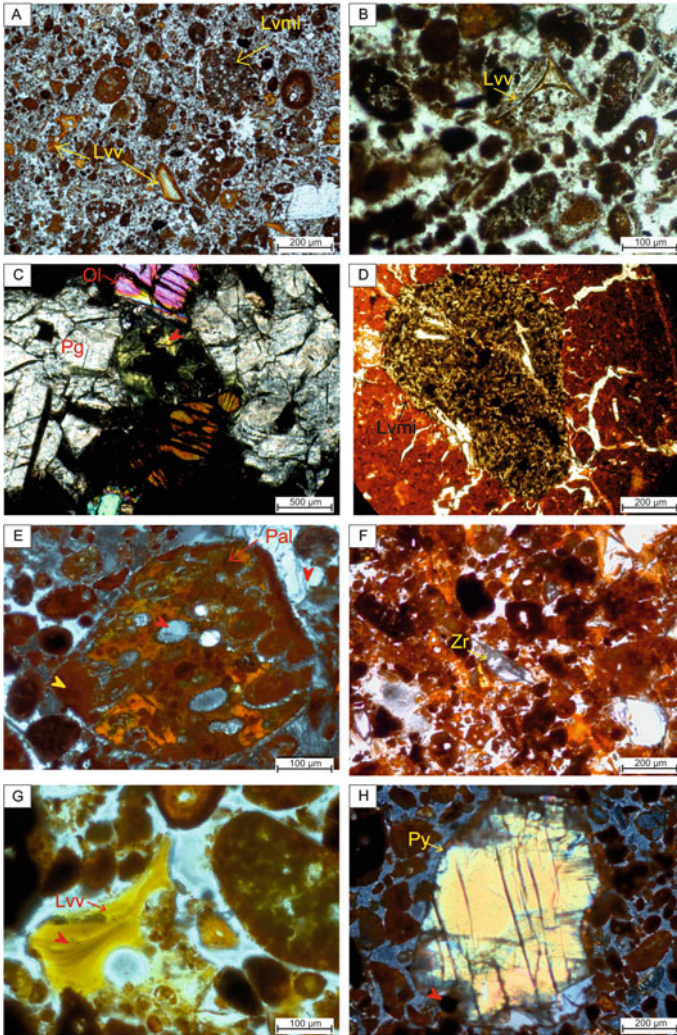
Fig. 5 Photomicrographs under plane polarized light showing **A** vesicular and non-vesicular cuspate and platy glass shards (Lvv) respectively, volcanic fragment with microlitic texture (Lvmi) and oxidized or weathered fragments of variable size in poorly sorted red bole; **B** bubble junction glass shards (Lvv) in red bole; **C** glomeroporphyritic cluster of replaced/altered plagioclase laths (Pg), olivine (Ol) and brown amphibole set in altered black groundmass of lower basalt under cross polarized light; **D** volcanic lithic fragment with microlitic texture (Lvmi) surrounded by fine grained red, clayey homogeneous groundmass of possible illuvial clay in red bole; **E** Sideromelane scoria altered to palagonite (palagonite, Pal), vesicles filled with alteration product (clay mineral) (indicated by yellow arrow) and zeolite (filling vesicles and intergranular spaces, indicated by red arrow), surrounded by rounded altered fragments, under cross polarized light; **F** subhedral, fine sand sized zircon (Zr); **G** yellow glass shards (red arrow) showing flow like structure; **H** pyroxene indicated by yellow arrow and opaque mineral (red arrow) in red bole, under cross polarized light
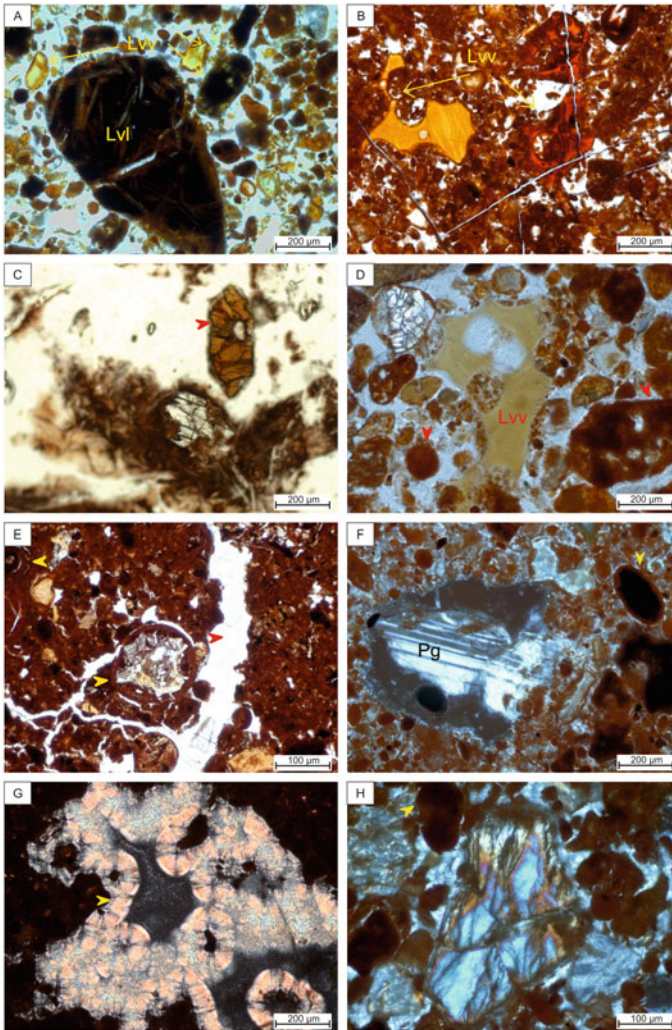
Fig. 6 Photomicrographs illustrating **A** lathwork volcanic lithic fragments (Lvl) with plagioclase laths present in black, altered groundmass and yellow and black non-vesicular glass (Lvv) under plane-polarized light; **B** yellow and brown oversized (sideromelane) glass shards (Lvv) surrounded by finer oxidized matrix under plane-polarized light; **C** brown alteromorph, indicated by red arrow, replacing mafic mineral under plane-polarized light; **D** yellow glass shard (Lvv) and weathered rounded fragments (red arrow); **E** rounded pisolite like structure surrounded by zeolites veins in homogenized brown groundmass, under plane-polarized light; **F** partially replaced plagioclase (Pg) and oxidized fragments (yellow arrow) under cross-polar; **G** microlayers of alternating zeolite and clay (yellow arrow) occurring as cavity filling, under cross-polar; **H** medium sand-sized olivine and oxidized fragment (yellow arrow) under cross polars
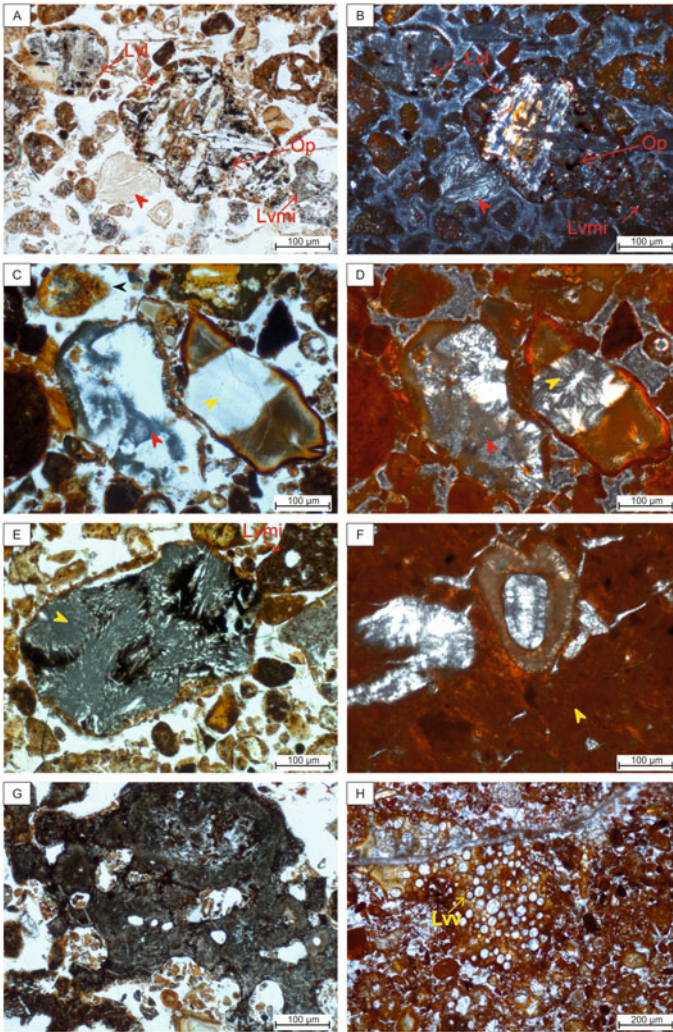
Fig. 7 Photomicrographs showing **A** Volcanic lithic fragment with lathwork texture (Lvl) having phenocrysts of plagioclase and opaques (Op) set in black glass, volcanic fragment with microlitic texture (Lvmi) under plane polarized light, red arrow at bottom indicates formation of secondary mineral; **B** The same view of Fig. A under crossed polars; **C** zeolite (yellow arrow) (replacing former phenocrystals) and grey coloured authigenic clay mineral (red arrow), at top the black arrow indicates altered/palagonite glass; **D** The same view of Fig. C under crossed polars; **E** clay mineral (yellow arrow) replacing the primary grain and neoformed ferruginous products, of a former Lvl volcanic grains, under plane polarized light; **F** zeolite (white-grey mineral) filling cavities, surrounded by iron-rich fine-grained homogeneous groundmass under cross polars; **G** altered/devitrified vesicular glass (Lvv) under plane polarized light; **H** medium sand-sized palagonized scoria (Lvv with orange glass) under plane-polarized light

(Figs. 5H; 6F). Minor constituents include zircon (Fig. 5F), quartz and Fe–Ti opaque phases like ilmenite and magnetite (Figs. 5H, 7A). The olivine grains are partially to wholly altered to subhedral to euhedral brown iddingsite/alteromorphs in most of the red boles (Fig. 6C). Zeolite (heulandite variety) commonly occurs as fine-grained void- and vein-filling and as a replacement of former volcanic lathwork grains, glass shards and sand-sized phenocrystals of plagioclase (Fig. 7C, D).

(b)   Red bole horizon with pedogenic features

Thin section study reveals the presence of highly weathered/altered basaltic clasts of size from 100 μm to 5 mm with recognizable needle-like plagioclase microlites (Fig. 5D), iron glaebules (Fig. 6E), iddingsite/alteromorph and oxidized/opaque fragments set in groundmass of homogeneous red, ferruginous, clayey material (Fig. 7F). This variety of bole bed has undergone extensive zeolitization, occurring as veins- and voids-filling (Figs. 5D, 6E, 7F). The zeolite fillings sometimes occur as alternate microlamination with clay minerals (Fig. 6G).

4.3 *Mineralogical Characterization*

The XRD pattern of air-dried randomly oriented powder mounts of a few selected red bole samples reveal the mineralogy of clay minerals (Fig. 8). An oriented aggregate mounts of separated clay-mineral shows basal reflections at (001) ~15 Å, (003) 5.0 Å, (005) 3.0 Å and (060) 1.50 Å in air-dried condition. The 001 peak shifts to ~16.9 Å on treatment with ethylene glycol and collapses to ~10 Å on heating to 400 and 550 °C for half an hour, producing a diffraction pattern similar to illite.

The basal reflections (001), (003) and (060) at ~15, 5.0 and 1.508 Å indicate the presence of 2:1 clay, i.e., smectite mineral (montmorillonite). A slight shift in (060) reflections from 1.50 to 1.51 Å indicates the dioctahedral clay to be Fe containing in some bole beds. Low quartz is identified by reflection at 3.35 Å (001), 4.26 Å (100) and 1.54 Å (211), hematite is identified by reflection at 2.69 Å (104), 2.52 Å (110), 1.69 Å (116), anorthite 4.04 Å ($\bar{2}$01), 3.33 Å, 3.18 Å (002), albite is identified by 3.19 Å (002), 4.03 Å ($\bar{2}$01), 3.68 Å (130), and pyroxene shows d-spacing of 2.99 Å ($\bar{2}$21), 2.94 Å (310) and 3.23 Å (220). Zeolite (heulandite) is identified by sharp reflection in clay mineral range, i.e., 8.95 Å (020), 7.96 Å (200), 5.26 Å ($\bar{3}$ 11) (Moore and Reynolds 1989).

4.4 *Spectral Characterization*

Characteristic absorption bands in reflectance spectra of powdered sample of red bole have been studied using visible-near infrared spectroscopy for the determination of clay mineralogy. Spectra of red bole show broad and shallow absorption bands near
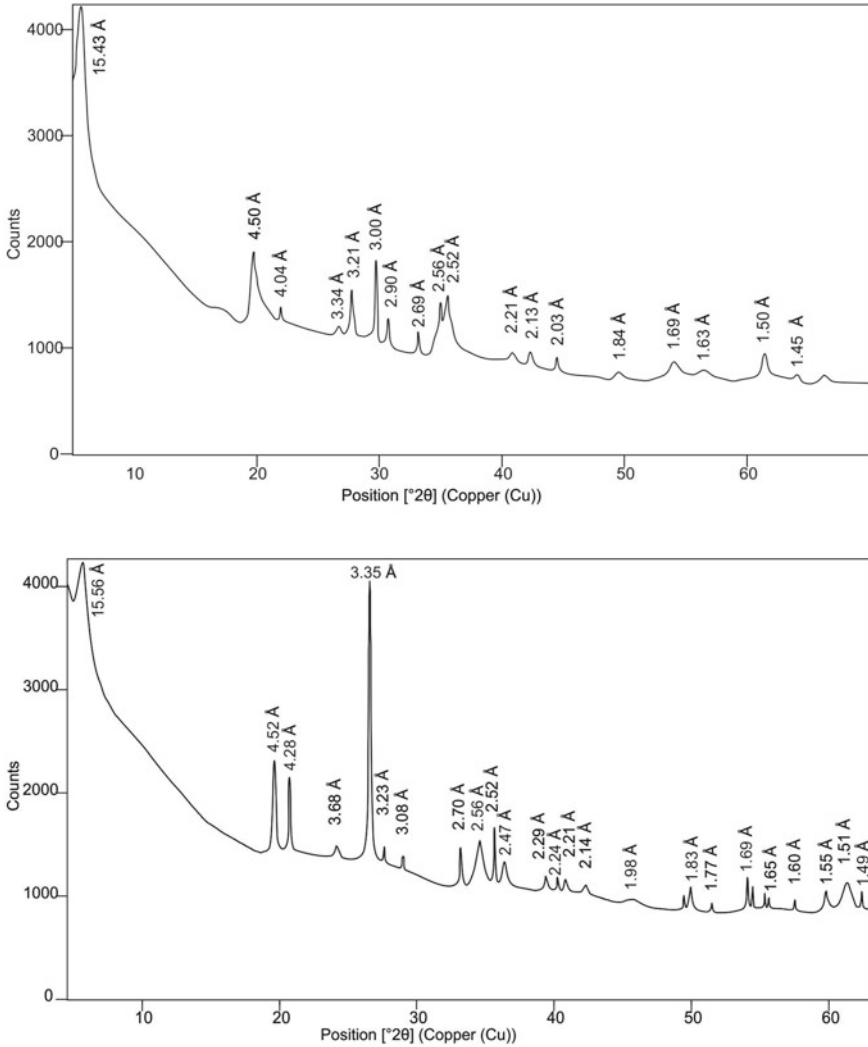
Fig. 8 XRD Diffraction pattern of air-dried randomly oriented powder mounts of red bole

~0.51, ~0.65 and ~0.86 µm; a sharp and deep band with shoulder near 1.418 and 1.914 µm, and shallow and broad peaks between 2.1 and 2.3 µm (Fig. 9).

The visible-near infrared spectroscopy of red boles reveals the presence of a broad absorption feature near 0.86 µm, which is due to Laporte-forbidden transition of Fe^{3+} in the crystal lattice (Hunt and Ashley 1979; Morris et al. 1985; Sherman and Waite 1985; Bishop and Murad 2005; Bhattacharya et al. 2016). The data indicates the presence of iron oxide, i.e. hematite. A sharp and deep band at ~1.4 and ~1.9 µm with shoulders on the right of both bands indicate OH stretching overtone and H_2O
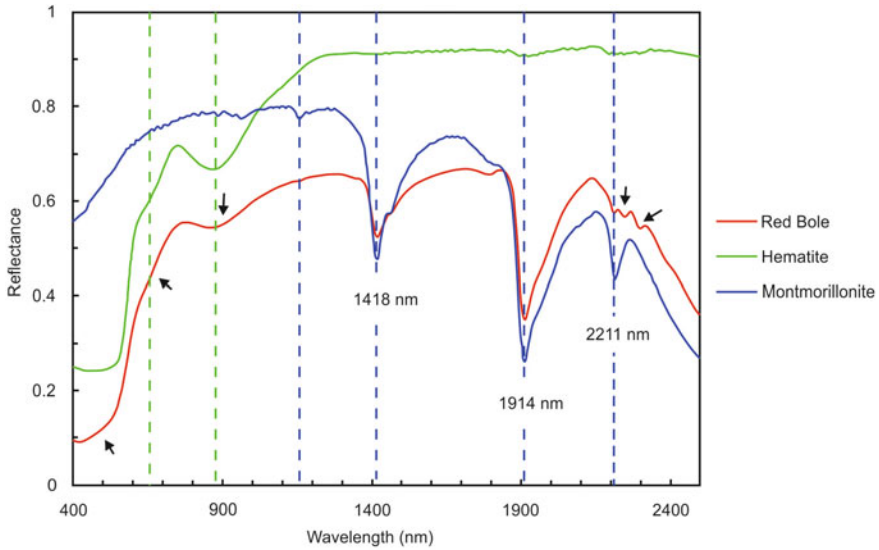
Fig. 9 Reflectance spectra of powdered red bole sample, taken in laboratory condition. The red spectral curve is of red bole sample and the blue and green spectral curves are of montmorillonite and hematite respectively taken from USGS mineral spectral library. The coloured dash line represents matching peaks of that particular mineral with red bole peaks. Black arrow indicating doublet feature near 2.20 μm may infer the presence of an additional component (e.g. Fe–OH site) mixed with the Al-phyllosilicate (Bishop et al. 2013) whereas the black arrow indicating weaker absorption features at lower wavelength and broad, shallow feature near 0.9 μm indicates presence of iron oxide probably hematite

combination, respectively. This overtone band occurs at 1.43 μm for 2Fe–OH (Bishop et al. 2002a, b; Frost et al. 2002), at 1.41 μm for 2Al–OH (Bishop et al. 2002a, b), and at 1.38–1.39 μm for 3 Mg–OH (Clark et al. 1990; Bishop et al. 1994, 2002a, b; Ehlmann et al. 2009). The depth of the ~1.9 μm absorption band is related to the amount of H_2O content in hydrous minerals (i.e. interlayers of clay mineral, in zeolite extra framework sites, and as surface hydration) (Bishop et al. 1994).

Metal-OH combination bands occur from 2.20 to 2.35 μm depending on the metal present on the octahedral position of phyllosilicate structure (Clark et al. 1990). In smectite, these Metal-OH combination bands occur near 2.20 μm for 2Al–OH bonds, 2.24–2.26 μm for $AlFe^{3+}$–OH, 2.29 μm from Fe^{3+}–OH, and 2.30–2.34 μm for Mg–OH (Clark et al. 1990; Bishop et al. 2008; Greenberger et al. 2012; Andrieux and Petit 2010). Absorption feature centered at 2.21 μm in reflectance spectra of red bole infers the 2Al–OH combination band (stretching and bending vibrations). Doublet feature near 2.20 μm, i.e., 2.21 and 2.24 μm and a slight shift of 1.4 μm band towards higher reflectance possibly reveal the presence of an additional component (Fe–OH site) mixed with the Al-phyllosilicate (Greenberger et al. 2012; Bishop et al. 2013). 2.29 μm absorption feature (marked by black arrow in Fig. 9) indicates the presence of Fe^{3+} at the structural site, which possibly means the presence of Fe-smectite. The

sharp and deep band at ~1.4 and ~1.9 µm and a metal-OH combination band indicate the presence of hydrated minerals like zeolites and phyllosilicates.

5 Discussion

Bole beds occur at multiple stratigraphic intervals within the Deccan basalt. Within the sampled locations in Pune and Mahabaleshwar, as per the chemostratigraphic classification of Deccan volcanics, the majority of red boles occurs in the Ambenali Formation, followed by Poladpur and Mahabaleshwar formations of the Wai subgroup. The XRD data and VNIR reflectance spectra, along with petrographic study, reveals a mixture of smectites (Fe/Al-smectites), iron oxides (hematite, magnetite), plagioclase, pyroxene and zeolites (Ca-zeolite, i.e. heulandite) as main constituents of the red bole.

Physical attributes and lower and upper contacts of red boles are variable. The first variety of red bole mainly shows sharp contact with lower basalt in the study area. But they can also occur locally above flow top basalt with gradational contact. In the latter case, red bole occurs as matrix between basaltic clasts. This type of red bole usually shows thin bed/laminations and occur in local depressions above lower basalt or flow top breccia. The laminations could be the result of the transportation of volcaniclastic particles. The second variety of red boles occur as weathering progression with gradational contact with lower basalt. This exhibits extensive zeolitization and small-scale "pencil" columnar joints. Small pencil columnar joint in red boles could be the result of thermal contraction followed by heating by the overlying lava flow (cf. Sarkar et al. 2000).

The first variety of red boles, as per the field description, shows dominance of volcanic lithic fragments and basaltic clasts along with monomineralic grains and accessory phases like opaque phase (ilmenite, magnetite), zircon and quartz. Zeolites and clays occur as secondary minerals. These boles are poorly sorted based on the variation in grain size. The weathered volcaniclastic boles exhibit the presence of lathwork and microlitic grains, suggesting derivation of the constituents from basaltic lava flows and pyroclastic rocks (Dickinson 1970; Marsaglia 1992, 1993; Morrone et al. 2017, 2020; Affolter and Ingersoll 2019; Le Pera and Morrone 2020). Accessory unstable heavy minerals such as pyroxene-amphibole-opaques, though altered, allowed a provenance diagnosis, too (e.g. Andò et al. 2012; Le Pera and Morrone 2018). Volcanic lithic fragments variably alter to clay minerals and zeolites, and some exhibit devitrification textures. The presence of bubble wall, platy and cuspate glass shards, along with scoria and variably vesicular glass, further suggests a pyroclastic input in these bole beds (Fisher and Schmincke 1994). Lithic fragments, described as glassy basalts, are dominant in the red bole. These glassy groundmasses were divided into orange-yellow and brown colour, with a minor amount of black and colourless glass, because these subdivisions of volcanic glass provide a direct means of assessing magmatic affinities of the source terrane (e.g. Cawood 1991), and, also, glass colour is thought to be a function of magma composition

and cooling rate (e.g. Schmincke 1981; Marsaglia 1992, 1993). The occurrence of brown glass (sideromelane) in some red bole possibly suggests their formation under rapid quenching in contact with water (e.g. Peacock and Fuller 1928; Critelli and Ingersoll 1995). The black glass forms in both subaerial or subaqueous conditions, with slower cooling rates (Fisher and Schmincke 1984, 1994; Cas and Wright 1987; Marsaglia 1993). Orange glassy fragments possibly represent either oxidation during weathering, hydrothermal palagonitization (e.g. Marsaglia 1993) or palagonitization during burial diagenesis (e.g. Stroncik and Schmincke 2002; Pauly et al. 2011). As expected, these grains, exhibiting lathwork textures with brown and black glass, and lacking colourless glass (e.g. Lunderg 1991), coherently are sensitive indicators of the parental basaltic rock (e.g. Morrone et al. 2017, 2020). Moreover, in association with concurrent precipitation of zeolites, also palagonitization, suggested by orange glassy lithic fragments, characterizes the red boles. The palagonitization process has the potential to stabilize and cement volcanic piles within several years after cessation of volcanism (e.g. Jacobsson 1978; Jacobsson and Moore 1980; Schipper et al. 2015). Thus, this palagonitic facies could be considered as a diagnostic paleoenvironmental condition of quiescence within the basaltic Deccan province in India. Few glass shards, showing flow-like structure, possibly are replaced by neoformed clays (Fedoroff et al. 2010). The glassy components alter to palagonite and authigenic phases (clay and zeolites) (Berger et al. 1987; Crovisier et al. 1987; Zhou and Fyfe 1989).

The partial to complete alteration of olivine to the alteromorphs/brown iddingsite indicates oxidative weathering as a result of deuteric alteration or hydrothermal process (Wilshire 1958; Smith et al. 1987; Velbel 2009, 2014). However, the presence of slightly altered or fresh olivine in a few samples suggests very limited subaerial exposure of these volcanogenic deposits. Pyroxene alters partially along grain edge and cleavage planes into opaque phases/smectite and iron oxide/hydroxide (e.g. Wilson 2004). Alteration of pyroxenes into hematite is common under the tropical conditions in weathered basalt (Glasmann and Simonson 1985; Schott and Berner 1985). The presence of iron oxide mineral, i.e. hematite, suggests a higher concentration of Fe^{3+} in red bole, which in turn indicates weathering under oxidative environment i.e. the concentration of $O_2 \geq 10^{-6}$. The presence of hematite could be the reason for red colour of bole bed. Hematite in red bole might have formed by either dehydration of iron oxyhydroxides (e.g. goethite) on burial (Retallack 1991, 2001; Spinola et al. 2017) or by post formational heating by upper lava flow under subaerial arid condition, favouring oxidation of Fe^{2+} into Fe^{3+} (Singer 1970; Velde 1995; Srivastava et al. 2015, 2018) or by a combination of both processes. The presence of <150 μm subhedral zircon in a few red boles samples of Wai-Panchgani and Mahabaleshwar-Poladpur sections is intriguing. The source of zircon and quartz could indicate a more felsic volcanism, contemporaneous with Deccan mafic volcanism (cf. Schoene et al. 2015).

Secondary phases present in red bole include Ca-zeolite (commonly heulandite), clay (smectite) and iron oxide/hydroxide. These minerals occur as intergranular and intragranular pores space-filling and as replacement of both monomineralic species and polymineralic grains. Hydration and weathering of volcanogenic

deposit and basaltic fragments containing fine-grained volcanic glasses and abundant unstable minerals (olivine, pyroxene and plagioclase) are considered factors controlling neoformation of smectite and zeolite during burial diagenesis (Hay 1966; Lee and Klein 1986; Velbel 1993; Chipera et al. 2008; Zhu et al. 2012). However, some very coarse-grained zeolites, filling veins and vugs, indicates a dominant hydrothermal influence (Gottardi 1989). The genesis of heulandite, which has high Si/Al ratios, would have occurred under neutral to moderate pH (7–9) condition, and, in buried volcaniclastic sediments, it precipitates at a temperature around ~100 °C (Iijima 1986; Gottardi 1989; Howie et al. 1992).

Smectite reported in red bole occurs as replacement product or pore-lining or grain coatings suggests an early diagenetic origin (García et al. 2005). Smectite formation would have occurred under an oxidizing environment with slightly alkaline pH ~ 8 at low temperatures (Harder 1972; Srivastava et al. 2018). The presence of smectite and the absence of kaolinite in red bole indicates moderate weathering conditions and a poorly drained environment with above neutral pH conditions (Smith 1962; Velde 1995, 2000).

The other types of red bole have been attributed to a volcanic paleosol horizon. It contains weathered basaltic fragment (~up to 5 mm size), alteromorphs/brown iddingsite, glaebules within a groundmass of homogeneous, red, ferruginous, clayey material probably illuvial clay (referred to as illuvial argillans in volcanic paleosols by Singer et al. 1994). Extensive zeolitization and secondary mineral occur as vein- and void-filling, this process being compatible with a rapid formation taking place in alkaline soils (e.g. Renaut 1993). These horizons, interpreted as paleosols, contain sporadic altered glass shards, whereas the lack of olivine and pyroxene could suggest a selective dissolution and final disappearance of these unstable species (e.g. Andò et al. 2012).

The illuvial clay in paleosol type red bole could be the result of the remobilization of clay in the uppermost part of the alteration zone. The occurrence of illuvial argillans provides a clue to the pedogenic origin of the material (Singer et al. 1994; Stoops and Schaefer 2018). Red colour of groundmass could be related to the presence of fine-grained hematite (Stoops and Marcelino 2018). The occurrence of iron glaebules/nodules suggests periodic conditions of low redox potential, probably resulting from seasonally deficient drainage (Singer et al. 1994). The occurrence of zeolite in pores confirms that they are formed from solution rather than the direct transformation from clay minerals in the groundmass (Renaut 1993). The presence of these pedogenic features in red bole indicates that they developed as a result of subaerial weathering of basaltic flow during a period of volcanic quiescence in Deccan volcanism.

The red boles in the study area have been ascribed to two genetic types. The first variety having dominance of volcaniclastic constituents is classified as volcaniclastic type red bole and the second variety having pedogenic features is identified as a volcanic paleosol. Both varieties of red bole contain smectite and hematite, which suggest their formation under poor drainage and subaerial weathering condition with moderate intensity. The presence of hematite supports oxidative weathering and effect of post-burial diagenesis. The presence of pedogenic features in paleosol

type bole suggests prolonged subaerial weathering of flow top basalt, indicating significant post-eruption quiescence of Deccan volcanism. The volcaniclastic red boles, with partially to unaltered mafic minerals and glass shards, possibly indicates limited subaerial exposure and/or subaqueous alteration. Zeolite and other alteration products possibly indicate hydrothermal influence on red bole. The present study, therefore, indicates that red bole above flow top breccia may not indicate a significant break in Deccan volcanism (cf. Duraiswami et al. 2020).

The basalt-derived clay mineral in red bole is not only crucial for paleoenvironmental interpretation but is also an analogue to Martian phyllosilicates (Gavin et al. 2010; Greenberger et al. 2012; Shukla et al. 2014). Al and Fe/Mg smectite are typically restricted to the oldest Noachian crust of Mars, indicating a distinctive set of processes involving water-rock interaction, prevalent in early Mars history. The exact mechanisms and physico-chemical conditions in the formation of these hydrous clay minerals of Mars is still a controversial topic (Chevrier et al. 2007; Ehlmann et al. 2013). A clear understanding of the genesis of clay minerals in red bole and variation in its chemistry in the vertical profile of red bole would be useful for understanding the processes active during early Noachian on Mars.

6 Conclusions

Results of red boles study of the Deccan volcanic province have demonstrated that the integration of sedimentology, stratigraphy and petrology, provides an effective means for interpreting complex processes in response to volcanic inactivity of the Cretaceous Deccan Trap. Major conclusions of the study are as follows.

(a) The presence of volcanic lithic fragments and glass shards along with scoria, with lathwork (Lvl), microlitic (Lvmi) and vitric (Lvv) textures in many of the red boles suggest the predominant derivation of constituents of red boles from basaltic lava flows and pyroclastic rocks. These *source-sensitive* lithic fragments testify the genetic link with the chemistry, mineralogy and tectono-stratigraphic level of the parental basaltic bedrock.

(b) The dominance of orange-yellow and brown coloured glass, along with a minor amount of black and colourless glass in volcaniclastic bole suggests their formation under subaerial or subaqueous condition. Orange glass particles indicate either oxidation during subaerial weathering or palagonitization processes.

(c) Altered olivine and brown iddingsite are related to oxidative weathering or hydrothermal processes. However, a minor amount of slightly altered or fresh olivine in a few samples suggests very limited subaerial exposure, indicating a possible different intensity and duration of the weathering process.

(d) The absence of kaolinite and the presence of smectite in red boles indicates moderate weathering conditions. Formation of smectite (montmorillonite) and hematite in red boles occurs in an oxidative environment, at near-neutral pH

(~5.5–8) conditions, in a poorly drained environment. In addition, heulandite, in the studied volcanic system, cause major modifications of both red boles horizons original textures, making relationships between these not easily discernible.

(e) Field observations, along with mineralogical and micromorphological investigation broadly categories red bole into two genetic types i.e. weathered volcaniclastic deposit and volcanic paleosol. The volcaniclastic red boles, having partially altered to unaltered mafic mineral phases and basaltic glass shards, are the result of limited subaerial/subaqueous alteration in oxic conditions along with hydrothermal influence. The occurrence of distinct pedogenic features like illuviation argillans, glaebules, iddingsite and weathered basaltic clasts in paleosol type of red bole implies sub-aerial, oxidative weathering, indicating prolonged lull in Deccan eruption.

References

Affolter MD, Ingersoll RV (2019) Quantitative analysis of volcanic lithic fragments. J Sed Res 89:479–486

Andò S, Garzanti E, Padoan M, Limonta M (2012) Corrosion of heavy minerals during weathering and: a catalogue for optical analysis. Sediment Geol 280:165–178

Andrieux P, Petit S (2010) Hydrothermal synthesis of dioctahedral smectites: the Al–Fe^{3+} chemical series: Part I: influence of experimental conditions. App Clay Sci 48:5–17

Ahmad M, Shrivastava JP (2008) Compositional studies on clays associated with the intra-volcanic bole horizons from the Eastern: palaeoenvironmental implications. Mem Geol Soc India 74:299–321

Beane JE, Turner CA, Hooper PR, Subbarao KV, Walsh JN (1986) Stratigraphy, composition and form of the Deccan basalts, Western Ghats, India. Bull Volcanol 48:61–83

Berger G, Schott J, Loubet M (1987) Fundamental processes controlling the first stage of alteration of a basalt glass by seawater: an experimental study between 200 and 320 C. Earth Planet Sci Lett 84:431–445

Bhattacharya S, Mitra S, Gupta S, Jain N, Chauhan P, Parthasarathy G (2016) Jarosite occurrence in the Deccan Volcanic Province of Kachchh, western India: Spectroscopic studies on a Martian analog locality. J Geophys Res 121:402–431

Bishop JL, Lane MD, Dyar MD, Brown AJ (2008) Reflectance and emission spectroscopy study of four groups of phyllosilicates: smectites, kaolinite-serpentines, chlorites and micas. Clay Miner 43:35–54

Bishop JL, Loizeau D, McKeown NK, Saper L, Dyar MD, Des Marais DJ, Parente M, Murchie SL (2013) What the ancient phyllosilicates at Mawrth Vallis can tell us about possible habitability on early Mars. Planet Space Sci 86:130–149

Bishop J, Madejova J, Komadel P, Froschl H (2002a) The influence of structural Fe, Al, and Mg on the infrared OH bands in spectra of dioctahedral smectites. Clay Miner 37:607–616

Bishop JL, Murad E (2005) The visible and infrared spectral properties of jarosite and alunite. Am Miner 90:1100–1107

Bishop JL, Murad E, Dyar MD (2002b) The influence of octahedral and tetrahedral cation substitution on the structure of smectites and serpentines as observed through infrared spectroscopy. Clay Mineral 37:617–628

Bishop JL, Pieters CM, Edwards JO (1994) Infrared spectroscopic analyses on the nature of water in montmorillonite. Clays Clay Miner 42:702–716

Cas RA, Wright JV (1987) Volcanic successions: modern and ancient: a geological approach to processes. Products and Successions, Allen and Unwin, London

Cawood PA (1991) Nature and record of igneous activity in the Tonga Arc, SW Pacific, deduced from the phase chemistry of derived detrital grains. In: Morton AC, Todd SP, Haughton PDW (eds) Developments in sedimentary provenance studies. Geol Soc Spec Publ 57:305–21

Chenet AL, Fluteau F, Courtillot V, Gérard M, Subbarao KV (2008) Determination of rapid Deccan eruptions across the Cretaceous-Tertiary boundary using paleomagnetic secular variation: Results from a 1200 m-thick section in the Mahabaleshwar escarpment. J Geophys Res 113:B04101. https://doi.org/10.1029/2006JB004635

Chevrier V, Poulet F, Bibring JP (2007) Early geochemical environment of Mars as determined from thermodynamics of phyllosilicates. Nature 448:60–63

Chipera SJ, Goff F, Goff CJ, Fittipaldo M (2008) Zeolitization of intracaldera sediments and rhyolitic rocks in the 1.25 Ma lake of Valles caldera, New Mexico, USA. J Volcanol Geotherm Res 178:317–330

Clark RN, King VVT, Klejwa M, Swayze GA, Vergo N (1990) High spectral resolution reflectance spectroscopy of minerals. J Geophys Res 95:12653–12680

Cox KG, Hawkesworth CJ (1985) Geochemical stratigraphy of the Deccan Traps at Mahabaleshwar, Western Ghats, India, with implications for open system magmatic processes. J Petrol 26:355–377

Critelli S, Arribas J, Le Pera E, Tortosa A, Marsaglia KM, Latter KK (2003) The recycled orogenic sand provenance from an uplifted thrust belt, Betic Cordillera, Southern Spain. J Sed Res 73:72–81

Critelli S, Ingersoll RV (1995) Interpretation of neovolcanic versus palaeovolcanic sand grains: an example from miocene deep-marine sandstone of the Topanga Group (southern California). Sedimentol 42:783–804

Crovisier JL, Honnorez J, Eberhart Jp (1987) Dissolution of basaltic glass in seawater: mechanism and rate. Geochim Cosmochim Acta 51:2977–2990

Dickinson WR (1970) Interpreting detrital modes of greywacke and arkose. J Sed Pet 40:695–707

Duraiswami RA, Sheth H, Gadpallu P, Youbi N, Chellai EH (2020) A simple recipe for red bole formation in continental flood basalt provinces: weathering of flow-top and flow-bottom breccias. Arab J Geosci 13:1–14

Ehlmann BL, Berger G, Mangold N, Michalski JR, Catling DC, Ruff SW, Chassefière E, Niles PB, Chevrier V, Poulet F (2013) Geochemical consequences of widespread clay mineral formation in Mars' ancient crust. Space Sci Rev 174:329–364

Ehlmann BL, Mustard JF, Swayze GA, Clark RN, Bishop JL, Poulet F, Des Marais DJ, Roach LH, Milliken RE, Wray JJ, Barnouin-Jha O, Murchie SL (2009) Identification of hydrated silicate minerals on Mars using MRO CRISM: geologic context near Nili Fossae and implications for aqueous alteration. J Geophys Res E: Planets 114. https://doi.org/10.1029/2009JE003339

Emeleus CH, Allwright EA, Kerr AC, Williamson IT (1996) Red tuffs in the palaeocene lava successions of the inner hebrides. Scottish J Geol 32:83–89

Fedoroff N, Courty MA, Guo Z (2010) Palaeosoils and relict soils. In: Stoops G, Marcelino V, Mees F (eds) Interpretation of micromorphological features of soils and regoliths. Elsevier, Amsterdam, pp 623–662

Fisher RV, Schmincke H-U (1984) Pyroclastic rocks. Springer-Verlag, Berlin

Fisher RV, Schmincke HU (1994) Volcaniclastic sediment transport and deposition. In: Pye K (eds) Sediment transport and depositional processes. Blackwell Scientific Publications, pp 351–388

Frost RL, Kloprogge JT, Ding Z (2002) Near-infrared spectroscopic study of nontronites and ferruginous smectite. Spectrochim Acta A Mol Biomol Spectrosc 58:1657–1668

García-Romero E, Vegas J, Baldonedo JL, Marfil R (2005) Clay minerals as alteration products in basaltic volcaniclastic deposits of La Palma (Canary Islands, Spain). Sediment Geol 174:237–253

Gavin P, Chevrier V, Sayyed MRG, Islam R (2010) Spectral analysis of Deccan paleosols, India: Analog for phyllosilicates on Mars. In: 41st Lunar planet science conference, p 1904

Gavin P, El Senousy A, Chevrier V, Sayyed MRG and Islam R (2011) Spectral properties of Deccan paleosols, India: implications for thermally altered phyllosilicates on Mars. In: 42nd Lunar planet science conference, p 1905

Gérard M, Caquineau S, Chenet AL, Fluteau F, Courtillot V, Subbarao KV (2006) Red boles in the Deccan traps: time constraints from alteration processes. Geophys Res Abstr 8:07092

Glasmann JR, Simonson GH (1985) Alteration of basalt in soils of Western Oregon. Soil Sci Soc America 49:262–273

Gottardi G (1989) The genesis of zeolites. Eur J Mineral 1:479–488

Greenberger RN, Mustard JF, Kumar PS, Dyar MD, Breves EA, Sklute EC (2012) Low temperature aqueous alteration of basalt: mineral assemblages of Deccan basalts and implications for Mars. J Geophys Res 117:E00J12. https://doi.org/10.1029/2012je004127

Harder H (1972) The role of magnesium in the formation of smectite minerals. Chem Geol 10:31–39

Hay RL (1966) Zeolites and zeolitic reactions in sedimentary rocks. GSA Spec Pap 85:1–130

Howie RA, Zussman J, Deer W (1992) An introduction to the rock-forming minerals. Longman

Hunt GR, Ashley RP (1979) Spectra of altered rocks in the visible and near infrared. Econ Geol 74:1613–1629

Iijima A (1986) Occurrence of natural zeolites. J Clay Sci Soc Jpn 26:90–103

Jacobsson SP (1978) Environmental factors controlling the palagonitisation of the Surtsey tephra, Iceland. Bull Geol Soc Denmark 27:91–105

Jacobsson SP, Moore JG (1980) Through Surtsey. Unique hole shows how volcano grew. Geotimes 25:14–16

Kale VS, Bodas M, Chatterjee P, Pande K (2020) Emplacement history and evolution of the Deccan Volcanic Province, India. Episodes 43:278–299

Kale VS, Dole G, Shandilya P, Pande K (2019) Stratigraphy and correlations in Deccan Volcanic Province, India: Quo vadis? GSA Bull 132:588–607

Le Pera E, Morrone C (2018) Heavy minerals distribution and provenance in modern beach sands of Campania, Italy. Rendiconti Online Soc Geol Ital 45:136–140

Le Pera E, Morrone C (2020) The use of mineral interfaces in sand-sized volcanic rock fragments to infer mechanical durability. J Palaeogeogr 9:21. https://doi.org/10.1186/s42501-020-00068-8

Lee YI, Klein GD (1986) Diagenesis of sandstones in the back-arc basins of the Western Pacific Ocean. Sedimentol 33:651–675

Louime C, Onokpise O, Vasanthaiah H (2011) Deformed and dragged red bole horizon near Pune, Maharashtra. Curr Sci 100:1488

Lundberg N (1991) Detrital record of the early Central American magmatic arc: Petrography of intraoceanic forearc sandstones, Nicoya Peninsula, Costa Rica. GSA Bull 103:905–915

Marsaglia KM (1992) Petrography, provenance of volcaniclastic sands recovered from the Izu-Bonin Arc, Leg 126: Proc Ocean Drill Program. Sci Res 126:139–54

Marsaglia K (1993) Basaltic island sand provenance. In: Johnsson MJ, Basu A (eds) Processes controlling the composition of clastic sediments. GSA Spec Pap 284:41–65

Moore DM, Reynolds Jr RC (1989) X-ray diffraction and the identification and analysis of clay minerals. Oxford University Press (OUP), Oxford

Morris RV, JrHV Lauer, Lawson CA, JrEK Gibson, Nace GA, Stewart C (1985) Spectral and other physicochemical properties of submicron powders of hematite (α-Fe2O3), maghemite (γ-Fe2O3), magnetite (Fe3O4), goethite (α-FeOOH), lepidocrocite (γ-FeOOH). J Geophys Res 90:3126–3144

Morrone C, De Rosa R, Le Pera E, Marsaglia KM (2017) Provenance of volcaniclastic beach sand in a magmatic-arc setting: an example from Lipari island (Aeolian archipelago, Tyrrhenian Sea). Geol Mag 154:804–828

Morrone C, Le Pera E, Marsaglia KM, De Rosa R (2020) Compositional and textural study of modern beach sands in the active volcanic area of the Campania region (southern Italy). Sediment Geol 396:105567

Naveen Sarkar S, Kumar TN, Ray D, Bhattacharya S, Shukla AD, Moitra H, Dagar A, Chauhan P, Sen K, Das S (2018) Mineralogy and spectroscopy (VIS near infrared and micro-Raman) of chromite from Nidar ophiolite complex, SE Ladakh, India: implications for future planetary exploration. Planet Space Sci 165:1–9

Pauly BD, Schiffman P, Zierenberg RA, Clague DA (2011) Environmental and chemical controls on palagonitization. Geochem Geophys Geosys 12:1–26

Peacock MA, Fuller RE (1928) Chlorophaeite, sideromelane and palagonite from the Columbia River Plateau. Am Miner 13:360–383

Renaut RW (1993) Zeolitic diagenesis of late Quaternary fluviolacustrine sediments and associated calcrete formation in the Lake Bogoria Basin, Kenya Rift Valley. Sedimentol 40:271–301

Renne PR, Sprain CJ, Richards MA, Self S, Vanderkluysen L, Pande K (2015) State shift in Deccan volcanism at the Cretaceous-Paleogene boundary, possibly induced by impact. Science 350:76–78

Retallack GJ (1991) Untangling the effects of burial alteration and ancient soil formation. Ann Rev Earth Planet Sci 19:183–206

Retallack GJ (2001) Soils of the past: an introduction to paleopedology, 2nd edn. Blackwell Science, United Kingdom

Sarkar PK, Chakranarayan AB, Deshwandikar AK, Fernandes MR, Raut SD (2000) Development of pencil joints in a red bole bed at Dighi, Raigad district, Maharashtra, India. Curr Sci 79:1422–1423

Sayyed MRG, Hundekari SM (2006) Preliminary comparison of ancient bole beds and modern soils developed upon the Deccan volcanic basalts around Pune (India): Potential for palaeoenvironmental reconstruction. Quat Int 156:189–199

Sayyed MRG, Pardeshi RG, Islam R (2014) Palaeoweathering characteristics of an intrabasaltic red bole of the Deccan Flood Basalts near Shrivardhan of Western coast of India. J Earth Sys Sci 123:1717–1728

Schipper CI, Jakobsson SP, White JD, Palin JM, Bush-Marcinowski T (2015) The Surtsey magma series. Sci Rep 5:11498. https://doi.org/10.1038/srep11498

Schmincke HU (1981) Ash from vitric muds in deep sea cores from the Mariana Trough and fore-arc region (South Philippine Sea) (Sites 453, 454, 455, 458, 459 and SP), Deep Sea Drilling Project, Leg 60. In: Hussong DM, Uyeda S (eds) Initial reports of the deep-sea drilling project, Washington DC: US Government Printing Office, vol 60, pp 473–481

Schoene B, Samperton KM, Eddy MP, Keller G, Adatte T, Bowring SA, Khadri SFR, Gertsch B (2015) U-Pb geochronology of the Deccan Traps and relation to the end-Cretaceous mass extinction. Science 384:182–184

Schoene B, Eddy MP, Samperton KM, Keller CB, Keller G, Adatte T, Khadri SFR (2019) U-Pb constraints on pulsed eruption of the Deccan Traps across the end-Cretaceous mass extinction. Science 363:862–866

Schott J, Berner RA (1985) Dissolution mechanisms of pyroxenes and olivines during weathering. In: Drever JI (ed) The chemistry of weathering. Springer, Dordrecht, pp 35–53

Sherman DM, Waite TD (1985) Electronic spectra of Fe^{3+} oxides and oxide hydroxides in the near IR to near UV. Am Miner 70:1262–1269

Sheth HC (2005) From Deccan to Reunion: no trace of a mantle plume. In: Foulger GR, Natland JB, Presnall DC, Anderson DL (eds) Plates, plumes, and paradigm. GSA Spec Pap 388:477–501

Sheth H, Vanderkluysen L, Demonterova EI, Ivanov AV, Savatenkov VM (2019) $^{40}Ar/^{39}Ar$ of the Nandurbar Dhule mafic dyke swarm: Dyke sill flow correlations and stratigraphic development across the Deccan flood basalt province. Geol J 54:157–176

Shukla AD, Ray D, Pande K, Shukla PN (2014) Formation of paleosol (fossil soil) in Deccan continental flood basalt: alteration style and implications towards aqueous environments of early Mars. In: Eighth international conference on mars. Pasadena, California, pp 1194

Singer A (1970) Edaphoids and paleosols of basaltic origin in the Galilee, Israel. J Soil Sci 21:290–296

Singer A, Ben-Dor E (1987) Origin of red clay layers interbedded with basalts of the Golan Heights. Geoderma 39:293–306

Singer A, Wieder M, Gvirtzman G (1994) Paleoclimate deduced from some early Jurassic basalt-derived paleosols from Northern Israel. Palaeo Palaeo Palaeo 111:73–82

Smith KL, Milnes AR, Eggleton RA (1987) Weathering of basalt: formation of iddingsite. Clays Clay Miner 35:418–428

Smith WW (1962) Weathering of some Scottish basic igneous rocks with reference to soil formation. J Soil Sci 13:202–215

Spinola DN, de Castro Portes R, Schaefer CEGR, Solleiro-Rebolledo E, Pi-Puig T, Kühn P (2017) Eocene paleosols on King George Island, Maritime Antarctica: macromorphology, micromorphology and mineralogy. CATENA 152:69–81

Srivastava P, Sangode SJ, Meshram DC, Gudadhe SS, Venkateshwarlu M (2012) Palaeoweathering and depositional conditions in the interflow sediment units (bole beds) of Deccan Volcanic Province, India: a mineral magnetic approach. Geoderma 177(178):90–109

Srivastava P, Sangode SJ, Torrent J (2015) Mineral magnetic and diffuse reflectance spectroscopy characteristics of the Deccan Volcanic bole beds: implications to genesis and transformations of iron oxides. Geoderma 239:317–330

Srivastava P, Siva Siddaiah N, Sangode SJ, Meshram DC (2018) Mineralogy and geochemistry of various coloured boles from the Deccan volcanic province: implications for palaeoweathering and palaeoenvironmental conditions. CATENA 167:44–59

Stroncik NA, Schmincke HU (2002) Palagonite—a review. Int J Earth Sci 91:680–697

Stoops G, Marcelino V (2018) Lateritic and bauxitic materials. In: Stoops G, Marcelino V, Mees F (eds) Interpretation of micromorphological features of soils and regoliths. Elsevier, Amsterdam, pp 691–720

Stoops G, Schaefer CEGR (2018) Pedoplasmation: formation of soil material. In: Stoops G, Marcelino V, Mees F (eds) Interpretation of micromorphological features of soils and regoliths. Elsevier, Amsterdam, pp 59–74

Subbarao KV, Bodas MS, Khadri SFR, Beane JE (2000) The Western Deccan Basalt Province. Penrose Deccan 2000 field excursion guide. Geol Soc India 1–243

Subbarao KV, Chandrasekharam D, Navaneethakrishnan P, Hooper PR (1994) Stratigraphy and structure of parts of the Central Deccan Basalt Province: eruptive models. In: Subbarao KV (ed) Volcanism. Wiley Eastern Ltd, New Delhi, India, pp 321–332

Subbarao KV, Hooper PR (1988) Reconnaissance map of the Deccan Basalt Group in the Western Ghats, India Scale 1: 1,000,000. In: Subbarao KV (ed) Deccan flood basalts. Geol Soc India Mem 10

Vaidyanadhan R, Ramakrishan M (2008) Geology of India, vol 2. Geol Soc India, Bangalore

Valdiya KS (2016) The making of India: geodynamic evolution, 2nd ed. Springer International

Velbel MA (1993) Formation of protective surface layers during silicate-mineral weathering under well-leached, oxidising conditions. Am Miner 78:408–417

Velbel MA (2009) Dissolution of olivine during natural weathering. Geochim Cosmochim Acta 73:6098–6113

Velbel MA (2014) Etch-pit size, dissolution rate, and time in the experimental dissolution of olivine: implications for estimating olivine lifetime at the surface of Mars. Am Miner 99:2227–2233

Velde B (1995) Composition and mineralogy of clay minerals. In: Vede B (ed) Origin and mineralogy of clays. Springer, Berlin, Heidelberg, pp 8–42

Velde B (2000) Clay minerals: a physico-chemical explanation of their occurrence. Elsevier, Amsterdam

Verma O, Khosla A (2019) Developments in the stratigraphy of the Deccan Volcanic Province, peninsular India. C R Geosci 351:461–476

Vijaya Kumar K, Chavan C, Sawant S, Naga Raju K, Kanakdande P, Patode S, Deshpande K, Krishnamacharyulu SKG, Vaideswaran T, Balaram V (2010) Geochemical investigation of a semi-continuous extrusive basaltic section from the Deccan volcanic province, India: implications for the mantle and magma chamber processes. Contrib Miner Petrol 159:839–862

Walker GPL (1999) Some observations and interpretations on the Deccan Traps. Geol Soc India Mem 43:367–395

Widdowson M, Walsh JN, Subbarao KV (1997) The geochemistry of Indian bole horizons: palaeoenvironmental implications of Deccan intravolcanic palaeosurfaces: recognition, reconstruction and palaeoenvironmental interpretation. Geol Soc Lond Spec Publ 120:269–281

Wilkins A, Subbarao KV, Ingram G, Walsh JN (1994) Weathering regimes within the Deccan basalts. In: Subbarao KV (ed) Volcanism. Wiley Eastern, New Delhi, pp 217–223

Wilshire HG (1958) Alteration of olivine and orthopyroxene in basic lavas and shallow intrusions. Am Miner 43:120–147

Wilson MJ (2004) Weathering of the primary rock-forming minerals: processes, products and rates. Clay Miner 39:233–266

Zhou Z, Fyfe WS (1989) Palagonitization of basaltic glass from DSDP Site 335, Leg 37; textures, chemical composition, and mechanism of formation. Am Miner 74:1045–1053

Zhu S, Zhu X, Wang X, Liu Z (2012) diagenesis and its control on petroleum of Permian in northwestern margin of Junggar Basin, China. Sci China Earth Sci 55:386–396

Correction to: Mesozoic Stratigraphy of India

Santanu Banerjee and **Subir Sarkar**

Correction to:
S. Banerjee and S. Sarkar (eds.),
***Mesozoic Stratigraphy of India*, Society of Earth Scientists**
Series, https://doi.org/10.1007/978-3-030-71370-6

In the original version of the book, belated corrections are updated for the following chapters:

Chapter "Nautiloid Biostratigraphy of the Jurassic of Kutch, India: An Exploration of Bio- and Chrono-stratigraphic Potential of Nautiloids"

The Table 1 has been formatted correctly

Chapter "Biostratigraphic Implications of the Calcareous Nannofossils from the Spiti Formation at Langza, Spiti Valley":

The affiliation "Department of Geology, School of Earth, Biological and Environmental Science, Central University of South Bihar, Gaya 824236, Bihar, India" of the author "Nazim Deori" has been changed to "Department of Earth and Environmental Sciences, K.S.K.V. Kachchh University, Bhuj, Gujarat, India".

The correction chapters and book have been updated with the changes.

Index